MODERN ENGINEERING FOR DESIGN OF LIQUID-PROPELLANT ROCKET ENGINES

Dieter K. Huzel and David H. Huang

— REVISED, UPDATED, AND ENLARGED BY —

Harry Arbit
William R. Bissell
Richard Brewster
Mary P. Cardenas
Elden H. Cross
Kenny C. Gaspar
William Gillon
Eugene D. Jackson III
Al Martinez
John G. Perry
William M. Stanley
Ronald Urquidi

*

Rocketdyne Division of Rockwell International

Volume 147
PROGRESS IN
ASTRONAUTICS AND AERONAUTICS

A. Richard Seebass, Editor-in-Chief

Sponsored by the Rocketdyne
Division of Rockwell International

All royalties devoted to the
AIAA Student Scholarship Fund

AIAA

Published by the American Institute of Aeronautics and Astronautics
370 L'Enfant Promenade, SW, Washington DC, 20024-2518

American Institute of Aeronautics and Astronautics, Inc.
370 L'Enfant Promenade, SW, Washington, DC 20024

ISBN 1-56347-013-6

ISSN 0079-6050

Progress in Astronautics and Aeronautics

FOREWORD

When Dave Huang and I set out to write the first edition of this book, we were motivated, among other things, by our observation that no textbook was available that we could hand to a newly hired young engineer and say: "Here, study this and then we will talk about your specific assignments in our rocket-engine business". Instead, as supervisors, we and our lead engineers had to spend many hours explaining what actually should have been documented, to serve as an introduction, but also as a reference to provide answers to letter questions. Thus we went to work.

I was fortunate to have in Dave a coauthor of such superior abilities. In his "Author's Guide," a commercial publisher observes (after discussing the problems with multiple authorships): "(We hope) you'll still be speaking to one another after the book has been published." I am happy to say that we, (Dave now holds a high government position in the Republic of China, (Taiwan)), do indeed still speak to each other.

A few years ago, Martin Summerfield, President of the Princeton Combustion Research Laboratories, and then Editor-in-Chief of the Progress in Astronautics and Aeronautics technical-monograph series of the American Institute of Aeronautics and Astronautics (AIAA) suggested that our book should be re-issued, but only after an update of all areas where technology has seen major advances since publication of the first edition. Fortunately, the Rocketdyne Division of Rockwell International agreed to sponsor the needed effort. A team of specialized staff members was formed and began the work. The results are before you.

In the "Commentary" column of AIAA's March 1988 *Aerospace America* magazine, J.R. Thompson, NASA Deputy Administrator, emphasizes the need to "take advantage of this nation's substantial Shuttle investment... by adapting available hardware as it proves itself in service." Although this comment was contained in a discussion of the Advanced Launch System (ALS), it can be readily applied to any other future propulsion system, perhaps with the addition of "and available know-how, practices, and experiences." It is hoped that this book will contribute to all efforts responsive to the quoted exhortation.

Reliable rocket-engine systems do not come about by happenstance. They are the result of the work of a dedicated team of professionals—engineers, materials specialists, production workers, and numerous other disciplines. These skilled people are found not only in the plants of major rocket-engine producers, such as Rocketdyne, Aerojet, and Pratt & Whitney, or in specialized centers of NASA and the branches of the U.S. Armed Forces, but also and equally important—in the plants of the "suppliers," the hundreds of smaller companies that produce many of a rocket engine's highly specialized parts. It is the dedication, skill, and pride of workmanship of these people that made possible this nation's many space successes—manned or unmanned. Future projects depend on them just as much. For them too, this book is intended.

Special emphasis has been placed here on engine flight applications to stimulate engine systems and subsystem designers to think in these terms *from the outset.* In addition to filling the needs of the young engineer entering the rocket-propulsion field and practicing designer seeking wider knowledge, we always intended "Design of Liquid Propellant Rocket Engines" as a textbook, with specific consideration of the teacher without industry experience. I hope it will also stimulate those desiring to specialize in a rocket-engine subsystem by supplying adequate information to enable them to benefit fully from the specialized literature.

Wernher von Braun, then Director of NASA Marshall Space Flight Center graciously provided the forward for the first edition of this book, which was published in restricted form in 1967 by the NASA Office of Technology Utilization (SP-125). Because of the foreward's significance I quote it here"

> "Success in space demands perfection. Many of the brilliant achievements made in this vast, austere environment seem almost miraculous. Behind each apparent miracle, however, stands the flawless performance of numerous highly complex systems. All are important. The failure of only one portion of a launch vehicle or spacecraft may cause failure of an entire mission. But the first to feel this awesome imperative for perfection are the propulsion systems, especially the engines. Unless they operate flawlessly first, none of the other systems will get a chance to perform in space."
>
> "Perfection begins in the design of space hardware. This book emphasizes quality and reliability in the design of propulsion and engine systems. It draws deeply from the vast know-how and experience which have been the essence of several well-designed, reliable systems of the past and present. And, with a thoroughness and completeness not previously available, it tells how the present high state of reliability, gained through years of research and testing, can be maintained, and perhaps improved, in engines of the future."
>
> "As man ventures deeper into space to explore the planets, the search for perfection in the design of propulsion systems will continue. This book will aid materially in achieving this goal."
>
> Wernher Von Braun
> Director
> Marshall Space Flight Center, NASA

I want to thank the many professionals in the various design, development, test, graphics and publications

departments who helped make this book possible. Special recognition goes to R.E. Grate, C.A. Macgregor, H.M. Alexander, S.B. Maculuso, and T. Holwager of the Rocketdyne Division of Rockwell International, who all ably assisted us with the original manuscript. This updated version was accomplished largely by members of the technical staff of Rocketdyne: Harry Arbit, William W. Bissell, Richard Brewster, Mary P. Cardenas, Elden H. Cross, William Gillon, Stanley V. Gunn, Eugene D. Jackson III, Al Martinez, John G. Perry, A.H. Sobin, William M. Stanley, and Ronald Urquidi, together with general editors Joanne Bergeuer, Nancy Derr, and Noel Thorp.

Last and most important, thanks are due the manifold support the book's original writing and its update received from Rockwell International and its divisions. Rocketdyne engine technology has provided a major foundation for the book, its management the drivers in its updating.

Dieter K. Huzel
Thousand Oaks, CA

PREFACE

Over the quarter-century since publication of the original text of this book, astronauts have landed on the Moon and deep-space probes have visited all of the planets of our solar system. All of these undertakings depended entirely on rocket power. So will future space projects of many kinds, such as the Space Station Freedom, communications and exploration satellites, space ferries and shuttles, space probes, and, in the more distant future, Moon settlements.

Throughout the decades since Robert Goddard made his first lp-rocket launching in 1926, these thrust-producing devices, both turbopump-fed and pressure-fed, have assumed various shapes, sizes, configurations, and "cycles," depending on application, chosen thrust level, propellant type, and several other, often special, factors. One aspect has not changed: the basic physical and design principles.

In the context of practical design experience, this book introduces the reader to these basic principles; but more to the purpose, it supplies the bridge for the student and the young engineer from rocket propulsion fundamentals (otherwise well covered in the literature) to actual rocket-engine design and development work as done in industry (very little, if at all, covered in the literature). The book emphasizes realistic application of rocket propulsion theories, and this should help avoid, or at least reduce, time- and money-consuming errors and disappointments. In so doing, it consolidates numerous closely related subjects, hitherto often treated separately, bringing them up to date at the same time.

This book was written "on the job" for use by advanced students and engineers active in all phases of engine systems design, development, and application, in industry and government agencies. It presents sufficient detail to familiarize and educate those responsible for various aspects of liquid-propellant rocketry, including engine systems design, engine development, and flight-vehicle application. It should enable the rocket engineer independently to make preliminary detail designs for complete or partial engine systems and to understand and judge the problems, limitations, and "facts of life" of the various subsystems making up a complete engine system. It also aims to educate those ultimately interested in specialized subsystems and component design (thrust chamber, turbopump, control valves, etc.) about their own as well as neighboring subsystems and about the complete engine system. This should enable the beginner to prepare realistic analytical calculations and design layouts with a long head-start toward the final specialized design for subsystem production release.

This book addresses the young in a special way. Many of us who contributed to past projects are now retired or are about to retire. Some experienced hands have passed away. It is immensely important that the skills, experience, and know-how of this earlier generation be preserved and passed on to a younger generation—clearly, completely, and effectively. Losses would be costly. There must not be a gap. The managers of the many companies that form the rocket-engine industry and the pertinent government agencies are quite aware of this danger, and are employing various "in-house" programs to meet it.

This book makes a valuable contribution to that goal. The original authors stood among the forefront of design and development teams of larger propulsion systems, and Dieter Huzel spent several years in "long-life technology" work. David Huang for many years directed advanced rocket-engine design and development.

I am confident that the commendable efforts of the American Institute of Aeronautics and Astronautics to update, enlarge, and publish this book and to make it available to the field will greatly help to preserve and advance U.S.rocket-engine technology.

William F. Ezell
Vice President, Engineering
Rocketdyne Division,
Rockwell International

Table of Contents

Introduction To Liquid-Propellant Rocket Engines

Since World War II, rocket jet-propulsion has evolved from a rudimentary science to a refined engineering art. Today, a select number of aerospace companies in the U.S. and abroad produce a large number of sophisticated liquid-propellant rocket-engine power plants capable of propelling scientific, commercial, and military vehicles to low and high Earth orbit and to the planets in our solar system. Typical of the postwar evolution of liquid-propellant rocket power plants has been the family tree of Rocketdyne engines deriving from the Navaho and Redstone precursor engines of the early 1950s depicted in Fig. 1-1. Eight of these engine models have been used in NASA, U.S. Air Force, and commercial launches for missions ranging from near-Earth orbit to manned lunar missions. Approximately 3300 engine production units have been delivered since 1956 to power Redstone, Jupiter, Thor, Delta, Atlas, Saturn, and Shuttle systems for these missions. Three of these engines remain in production today: the RS-27 used for the Delta vehicle, the MA-5 used for the Atlas vehicle, and the Space Shuttle Main Engine (SSME). The SSME embodies the culmination of state-of-the-art technologies from 30 years of liquid hydrogen/liquid oxygen rocket engine component design, fabrication, development, and qualification testing. The reusable SSME (see Fig. 1-2) operates with liquid hydrogen/liquid oxygen propellants, and delivers a vacuum thrust of 470,000 lb using a chamber pressure of 3028 psia with a propulsion system weight of 6862 lb.

A similar evolutionary period at Aerojet TechSystems of GenCorp has produced a highly successful line of storable liquid-propellant rocket engines for the Air Force's Titan series of vehicles. The first-stage rocket engine (LR87-AJ-11) for the Titan III combines two identical 220,000-lb sea-level thrust engines attached to a steel frame which mounts onto the launch vehicle as depicted in Fig. 1-3. The storable nature of the propellants provides the Titan III with enhanced launch readiness for accomplishing Air Force missions. A lower-thrust engine, the LR91-AJ-11, with an altitude thrust of 100,000 lb, provides second-stage propulsion power for the Titan III C vehicle. The propellants for both the LR87-AJ-11 and the LR91-AJ-11 are fed to the engine by a powerful set of turbopumps. A set of two AJ10-138 engines completes the three-stage Titan III C vehicle propulsion. These tank-pressure-fed storable propellant engines deliver a total upper-

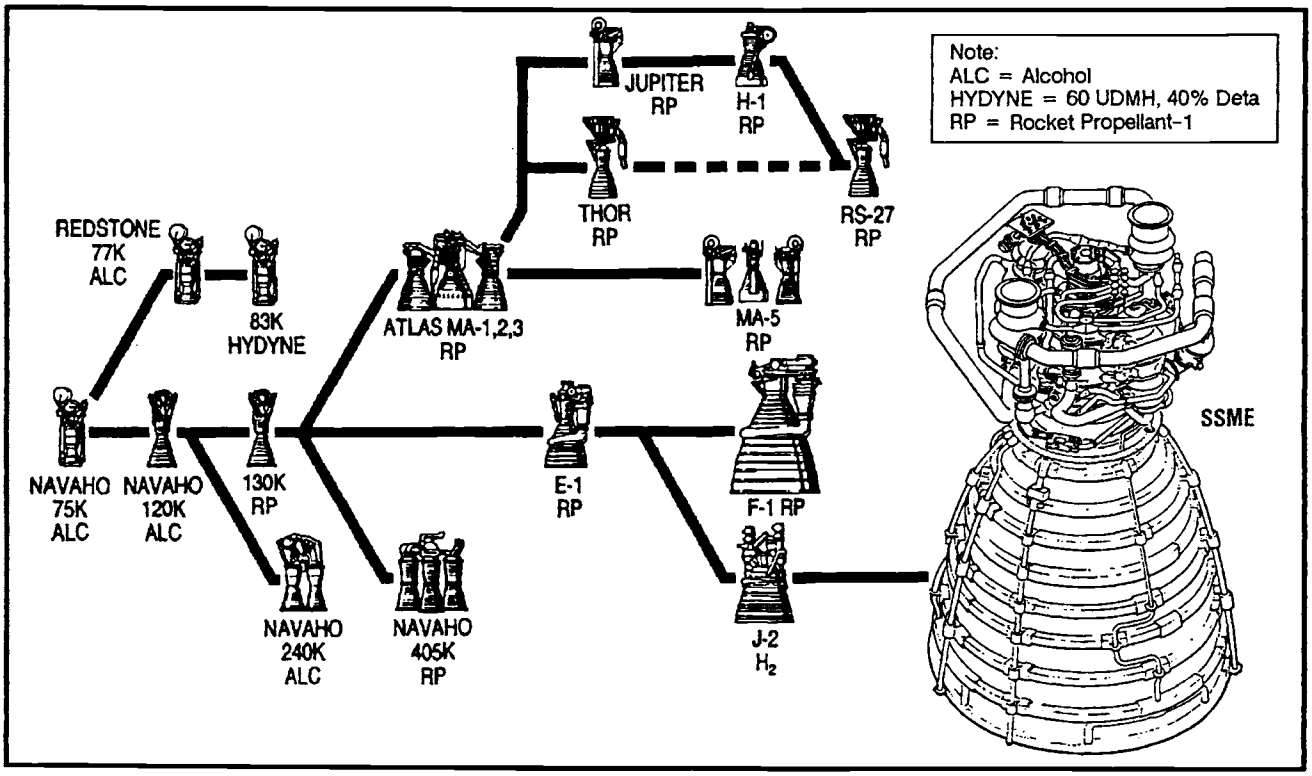

Fig. 1-1 Evolution of modern cryogenic-liquid-propellant rocket engines at Rocketdyne.

stage thrust of 16,000 lb. The engines are designed for multiple zero-gravity restarts and give the upper-stage vehicle the ability to reach higher orbits, modify the existing orbit, or rendezvous with other space vehicles. The Titan III C vehicle, assembled by Martin Marietta Corp., had flown 136 missions for the U.S. Air Force through March 1982. The highly reliable high-performance engines and vehicle ensure their combined use well into the 1990s.

The two Titan III E lower stages have been used to place in orbit General Dynamics' cryogenic Centaur upper-stage vehicle. The Centaur vehicle is powered by the RL-10, a cryogenic liquid propellant (liquid hydrogen, liquid oxygen) upper-stage rocket engine developed by Pratt & Whitney, a division of United Technologies. The RL-10 was initially developed in the period 1959-1963 and through 1974 had seen more than 10,000 firings. The engine is capable of self-conditioning in orbit with subsequent restarts. Through a series of ground-directed engine firings it has been used to propel the Centaur and such cargo as the Viking Spacecraft to Mars and the Voyager Spacecraft to Jupiter, Saturn, and Uranus. Through 1986, 172 engines had been fired in space, accumulating 278 space firings and 20+ hours of run time in space. Product improvement of the original RL-10 has led to the highly reliable RL-10-3-3-A (Fig. 1-4) and to a series of RL-10 derivative designs of greater sophistication.

These are but a few examples of the liquid-propellant rocket engines in current use and their continued application in gaining access to the inner frontiers of our solar system. It is the purpose of this book to introduce the reader to the design of the liquid-propellant rocket engine components that so effectively convert the chemical energy of suitable liquids into propulsive power, and to the design principles that are used to assemble these sub-assemblies into efficient, reliable, and cost-effective liquid-propellant rocket engine systems.

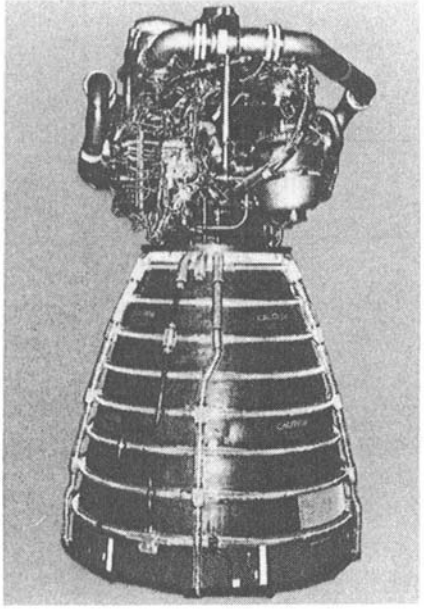

Fig. 1-2 Space Shuttle Main Engine (SSME).

1.1 BASIC ELEMENTS OF A LIQUID-PROPELLANT ROCKET ENGINE

Seven major subsystems comprise a liquid-propellant rocket engine system: thrust-chamber assembly, propellant feed system, turbine-drive system (gas generator, preburner, etc.), propellant-control system, electric and pneumatic controller systems, thrust-vector control (TVC) system, interconnect components and mounts. Six of these (except for the TVC system) are depicted in Fig. 1-5 for the RL-10-3-3-A engine.

The thrust-chamber assembly generates power by combusting liquid propellants raised to the required

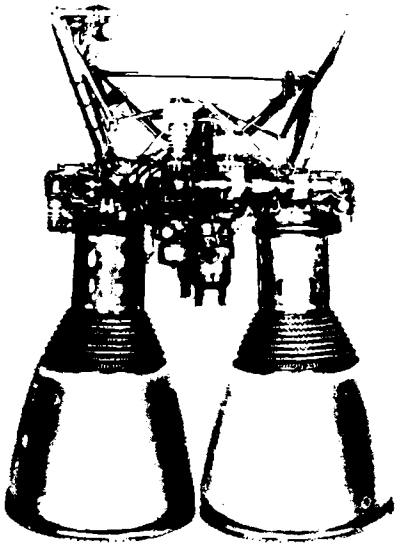

Fig. 1-3 Titan III First-Stage booster engines—Aerojet's LR87-AJ-11.

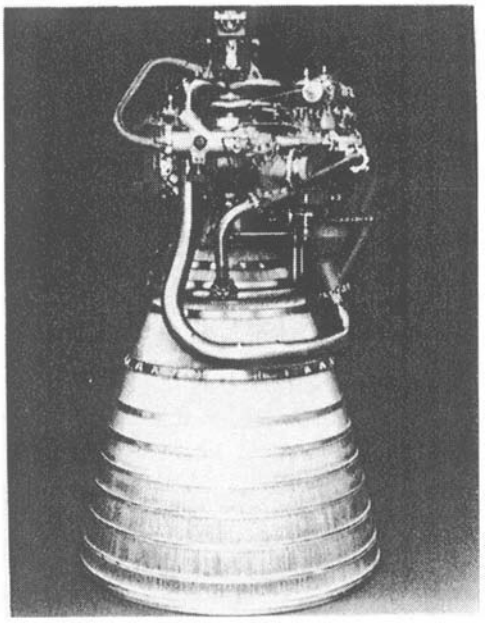

Fig. 1-4 Centaur's main propulsion engines—the Pratt & Whitney RL-10-3-3-A.

combustion pressure by the propellant feed system. The thrust chamber houses the main injector; it atomizes, mixes, ignites, and ultimately promotes the complete combustion of the liquid propellants. The combustion products are discharged through a converging-diverging nozzle to achieve high gas velocities and thrust. Depending on the application and simplicity desired, the propellant feed system will consist of propellant tanks, lines, and turbopumps; propellant turbopumps and lines; and in the case of a pressure-fed engine system, simple propellant tanks and lines.

The turbines are (in most cases) driven by energetic high-temperature gases produced in gas generators, preburners, heat exchangers heated by the main thrust-chamber combustion products, or gases tapped directly from the main combustion chamber. Occasionally low-power turbines are driven hydraulically by high-pressure propellants in the system.

In each of the three cases above, a set of propellant valves in the propellant-control system meters the two propellants flowing to the injector controlling both total amount and relative amount. Total amount is used in thrust control while the relative amount is used in control of propellant mixture ratio. The valves also perform the task of starting and shutting down the engine through proper sequencing and regulation of propellant flowrates.

These final control elements (valves) are electrically or pneumatically controlled. The controllers receive command signals from the vehicle or previously stored electric commands in the controller memory to effect valve control during engine operation (to yield desired thrust and mixture-ratio variation or propellant consumption during flight). The TVC system effects directional changes of the vehicle.

Depending on the method of propellant feed, there are two basic types of liquid-propellant rocket engines: those having propellants directly fed from pressurized tanks to the thrust chamber and those having the propellants fed to the thrust chamber by a set of turbopumps. In the first case, the tank pressures may typically be a few hundred pounds per square inch. In the second instance, the propellants are supplied from the tanks to the inlets of turbopumps at relatively low pressures, typically 30 to 100 psig. The turbopumps then raise these inlet pressures to high levels, which in modern engines like the SSME may reach 8,000 psig or more. In the case of the SSME, low-pressure propellant pumps provide an intermediate pumping stage between tank

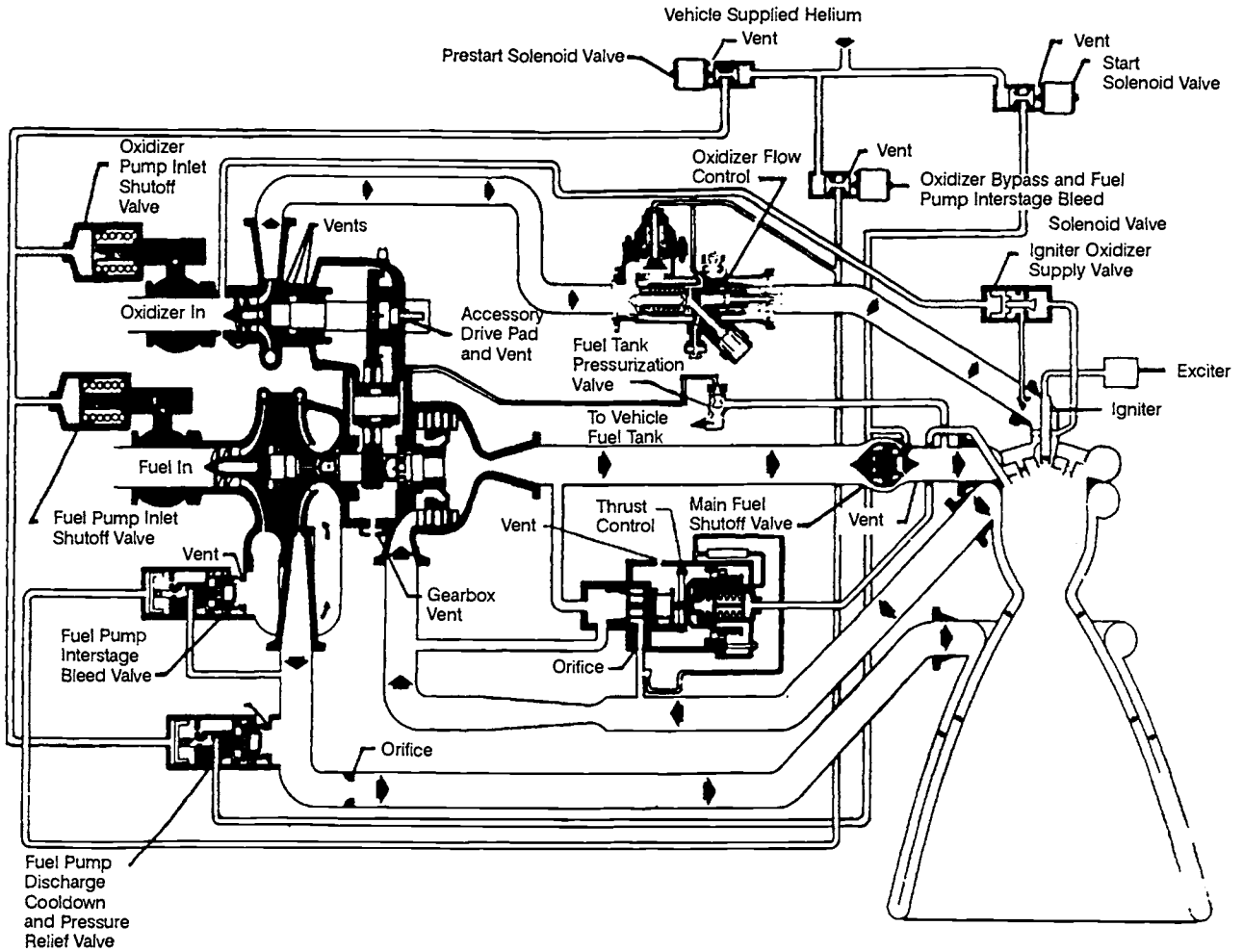

Fig. 1-5 Engine schematic for Pratt & Whitney RL-10-3-3-A, depicting major subsystems.

and main turbopumps. Because of tank weight considerations, pressure feed will be limited to propulsion-system sizes that deliver relatively low stage velocity increments. Many modern liquid-propellant rocket engines use turbopump feed because it lowers the total weight of inert parts per stage.

A schematic diagram of a turbopump-fed system, which uses heated helium for tank pressurization, is shown in Fig. 1-6. The major components of both the pressure-fed and pump-fed systems are called out in the figure. Subsequent chapters of this book discuss in detail each of these components and the design philosophies for them.

Although the two engine types differ significantly in a number of respects, they have one major component in common: the thrust chamber. Because of the importance of understanding the chemical and gas-dynamic processes in the thrust chamber, the following sections summarize the equations that govern these processes, and point out the significance of them to achieving optimum engine performance.

1.2 GENERATION OF THRUST

The thrust of a rocket is the reaction experienced by its structure due to the ejection of high-velocity matter—the same phenomenon that makes a gun recoil. In the latter case the forward momentum (mass x velocity) of the bullet and the "powder charge" equals the rearward momentum (recoil) of the gun proper.

All self-propelled means of transportation within a liquid or gaseous medium obtain driving force on the basis of exchange of momentum. Ship propellers, airplane propellers, water wheels, oars, and the like generate forward "push" at the expense of the momentum of water or air masses accelerated rearward. Rocket propulsion differs from these devices only in the relative magnitude of the accelerated masses and the velocities. While, hitherto, large masses were thrown back at low velocities, in rocket propulsion only relatively small masses of gas are used, which are carried within the vehicle and ejected at a very high velocity.

The efflux of hot gas from a rocket vehicle can basically be regarded as the ejection of small masses such as Δm (the molecules of gas) at a high relative velocity v_e with respect to the vehicle, which has a mass m_v and is moving at the velocity u. The force, the momentum, and the velocity are vector quantities. Consider a simplified system where only one particle Δm is being ejected at any one time. (The discussion through Eq. 1-8 emulates G.P. Sutton in his *Rocket Propulsion Elements*, 5th Ed., Wiley, New York 1986.) The net momentum of this system M is—

$$M = m_v u = \Delta m(u - v_e) \qquad (1\text{-}1)$$

Differentiating with respect to time yields $dM/dt = 0$ (no external momentum change). The $d(\Delta m)/dt$ approaches $-dm/dt$ for a continuously flowing gas. This equals the rate of decrease of the vehicle mass m_v. The exhaust velocity v_e is constant and thus its

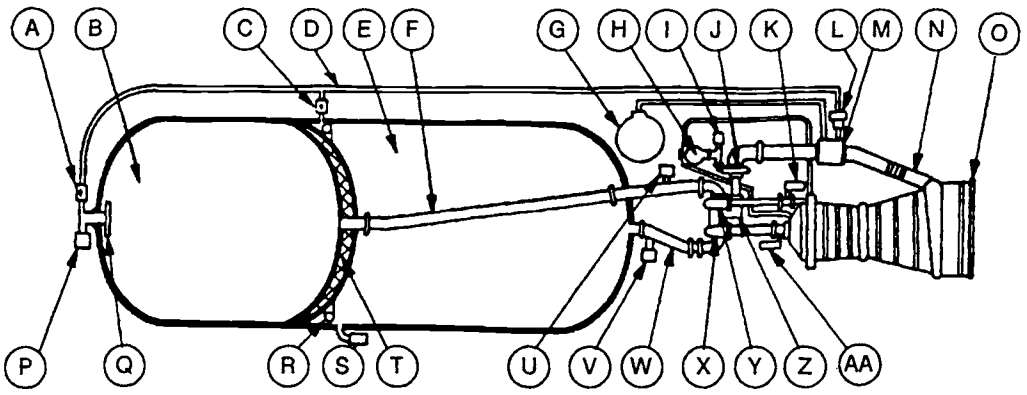

A Check Valve
B Fuel Tank
C Check Valve
D Pressurizing Gas Line
E Oxidizer Tank
F Fuel Duct
G High Pressure Helium Bottle
H Gas Generator and Valve Assembly
I Turbine Starting Spinner
J Gas Turbine
K Main Fuel Valve
L Pressure Regulator
M Heat Exchanger
N Turbine Exhaust Duct
O Thrust Chamber Assembly
P Fuel Tank Vent and Relief Valve
Q Pressurizing Gas Diffuser
R Pressuring Gas Diffuser
S Oxidizer Tank Vent and Relief Valve
T Intertank Insulation (required for cryogenic and noncryogenic propellant combination)
U Fuel Tank Fill and Drain Valve
V Oxidizer Tank Fill and Drain Valve
W Oxidizer Duct
X Oxidizer Pump
Y Fuel Pump
Z Gear Box
AA Main Oxidizer Valve

Fig. 1-6 Typical turbopump-fed liquid-propellant rocket engine system.

time derivative is equal to 0. Also, Δm is very small and approaches 0 as its limit. Thus one obtains—

$$m_v \frac{du}{dt} = -\frac{dm}{dt} v_e \qquad (1\text{-}2)$$

The left-hand term equals the net force (N_f) acting on the fluid element which when integrated over the control surface as in Fig. 1-6 becomes—

$$N_f = -\frac{dm}{dt} v_e = m v_e = \frac{w}{g} v_e \qquad (1\text{-}3)$$

This net force obtains for any true rocket engine in a vacuum. It assumes a uniform exhaust velocity that does not vary across the area of the jet. The minus sign in Eq. (1-2) indicates a decrease in the mass of the vehicle or reflects the velocity v_e being opposite in direction to the net force. The propellant mass flow rate $\dot{m}$ is used instead of -dm/dt in the remainder of the book, and the weight flow rate w, usually a measured quantity, when divided by the acceleration of gravity *g*, again represents mass flow rate. The preceding equation shows that, in a vacuum, the force is proportional to the propellant flow rate and exhaust velocity.

The pressure of the environment—air ambient pressure for a rocket in flight—has an influence on the magnitude of the net force. Figure 1-7 shows schematically the external pressure acting uniformly on the outer surface of a rocket chamber and the gas pressures on the inside of a typical chemical or nuclear rocket engine. The size of the arrows indicates the relative magnitude of the pressure forces. The axial net force can be determined by integrating all the pressures acting on areas that can be projected on a plane normal to the nozzle axis. The forces acting radially outward are appreciable but do not contribute to the net axial force, because the rocket is axially symmetrical.

By inspection it can be seen (and this can be proven) that at the exit area Ae of the engine's gas exhaust there is an unbalance of the external environmental or atmospheric pressure Pa and the local pressure Pe of the hot gas jet at the exit plane of the nozzle. For a rocket engine flying in a homogeneous atmosphere (neglecting localized boundary-layer effects), the net axial force through integration of all pressures in the control volume takes the following form:

$$N_f = \int_{A_{tc}}^{o} P_{tc}\, dA - A_e P_e + A_e P_a = \frac{\dot{w}}{g} V_e \qquad (1\text{-}4)$$

From this equation it follows that the net external axial force acting on the rocket will be as follows:

$$F = \frac{\dot{w}}{g} V_e + A_e (P_e - P_a) \qquad (1\text{-}5)$$

This external force—the thrust acting on the vehicle—combines two terms: momentum thrust (product of the propellant mass flow rate and the exhaust velocity relative to the vehicle) and pressure thrust (product of the cross-sectional area of the exhaust jet leaving the vehicle and the difference between the exhaust pressure and the fluid pressure). For exhaust pressure less than the surrounding fluid pressure, pressure thrust will be negative. This condition gives a lower thrust and is undesirable.

When the fluid pressure equals the exhaust pressure, the pressure thrust term becomes zero, and

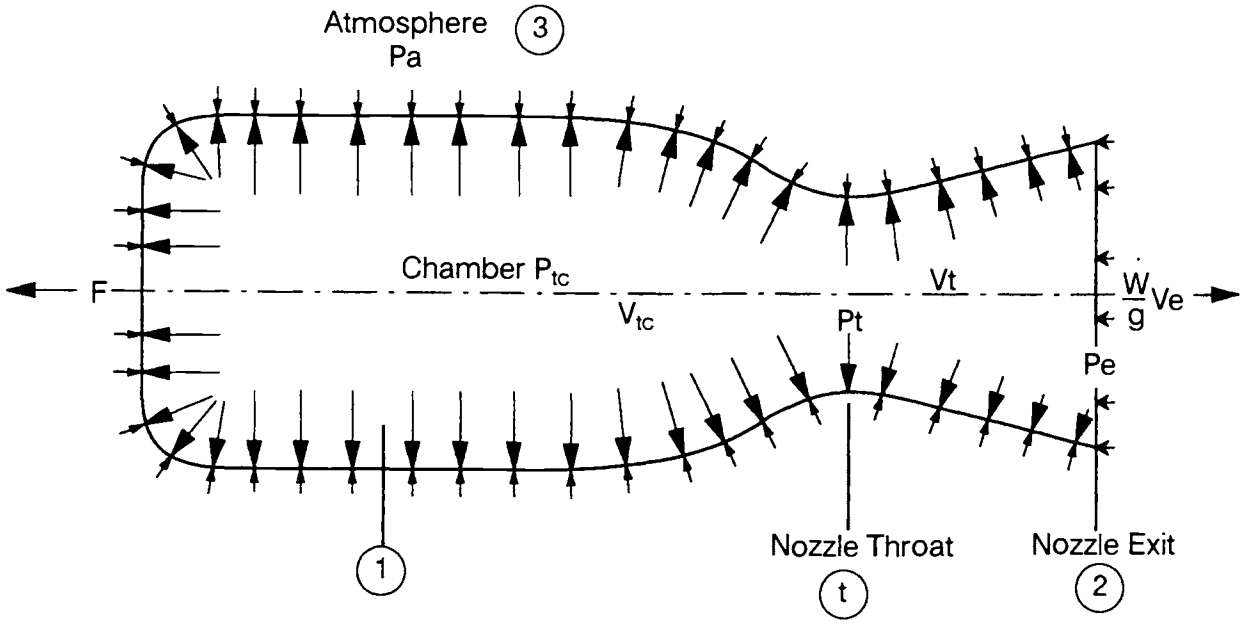

Note: (Internal gas pressure is highest inside the chamber and decreases steadily in the nozzle; external atmospheric pressure is uniform.)

Fig. 1-7 Pressure balance on the chamber and nozzle wall.

the thrust can be expressed as—

$$F = \frac{\dot{w}}{g} V_e \qquad (1\text{-}6)$$

This condition gives a maximum thrust (for a given atmospheric pressure) for a given propellant and chamber pressure. The rocket nozzle design that permits expansion of the propellant products to the same pressure of the surrounding fluid has what is called *optimum expansion ratio.*

Equation (1-5) shows that the thrust of a rocket is independent of flight velocity. Because changes in the fluid pressure affect the pressure thrust, the rocket thrust rises with increasing altitude. The change in pressure thrust with altitude can amount to 10 to 30% of the overall thrust. Figure 1-8 shows the variation of thrust and specific impulse with altitude for a typical rocket engine.

Equation (1-5) is often expressed as follows:

$$F = c\frac{\dot{W}}{g} \qquad (1\text{-}7)$$

where c is defined as the effective exhaust velocity (ft/s) and comprises—

$$c = v_e + A_e(p_e - p_a)(g/\dot{W}) \qquad (1\text{-}8)$$

The effective exhaust velocity is not the actual gas velocity except when $p_e = p_a$ where c becomes equal to v_e. As explained with Eq. (1-5), the presence of a term $A_e(p_e - p_a)$ (g/W) indicates that optimum v_e is not optimum for that altitude of operation.

Sample Calculation 1-1

The following data describe a liquid-propellant rocket engine: thrust F = 100,000 lb at sea level; propellant consumption rate W = 369.3 lb/s; thrust chamber exit area A_e = 760.8 in.^{2}; gas exit average static pressure p_e = 10.7 psia; ambient pressure p_a = 14.7 psia (sea level); gravitational constant g = 32.2 ft/s^2. The exit pressure across the exit of a nozzle has a sinusoidal profile, with the value at the wall being approximately twice the average and the value at the axis of the nozzle being of the order of 10% of the wall pressure. The average exit pressure p_e then takes the place of the one-dimensional exit pressure required by Eq. (1-5).

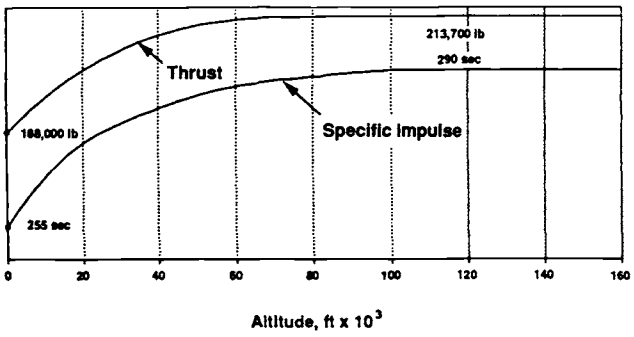

Fig. 1-8 Altitude performances of the H-1 liquid-propellant rocket engine.

Problem

From the equation above, determine (a) gas exhaust velocity, (b) engine thrust in vacuum, and (c) the effective exhaust velocities at sea level and in vacuum.

Solution 1-1

(a) From Eq. (1-5) the gas exhaust velocity will be as follows:

$$\begin{aligned} v_e &= [F - A_e(p_e - p_a)](g/W) \\ &= [100{,}000 - 760.8(10.7 - 14.7)](32.2/369.3) \\ &= 9040 \text{ ft/s} \end{aligned}$$

Although the average exit pressure (10.7 psia) is below the sea-level ambient pressure (14.7 psia), no separation of the flow will occur in this nozzle (an undesirable phenomena associated with erratic side-loads). Separation will occur in a nozzle when the wall pressure runs some 25-35% of the ambient pressure, this value varying with propellant combination and nozzle exit flow angle. In the subject example, the wall pressure will be approximately 21.4 psia (2 x 10.7), a value considerably larger than sea-level ambient pressure. Therefore, there should be no concern about nozzle flow separation at this point.

(b) Inspection of Eq. (1-5) will show that the difference in thrust between vacuum and sea level equals $A_e p_a$. This thrust increase $A_e p_a$ is realized gradually as the rocket ascends, in two distinct steps, first by reduction of the negative thrust term $A_e(p_e - p_a)$ to zero. This will occur when $p_e = p_a$—that is, when the rising vehicle reaches an altitude where p_a = 10.7 psia—in this specific case, the ideal expansion! As the vehicle continues to ascend and eventually reaches vacuum where p_a = 0, the increase of the positive term $A_e(p_e - p_a)$ raises the thrust level further. The combined effect of the two steps simply eliminates $A_e - p_a$. Thus we obtain engine thrust in space:

$$F = 100{,}000 + 760.8 \times 14.7 = 111{,}183.8 \text{ lb}$$

(c) Equation (1-8) then yields the effective exhaust velocity at sea level:

$$\begin{aligned} c &= v_e + A_e(p_e - p_a)(g/W) \\ &= 9040 + 760.8 \times (10.7 - 14.7) \times (32.2/369.3) \\ &= 8772 \text{ ft/s} \end{aligned}$$

and in vacuum:

$$\begin{aligned} c &= v_e + A_e p_e (g/W) \\ &= 9040 + 760.8 \times 10.7 \times (32.2/369.3) \\ &= 9750 \text{ ft/s} \end{aligned}$$

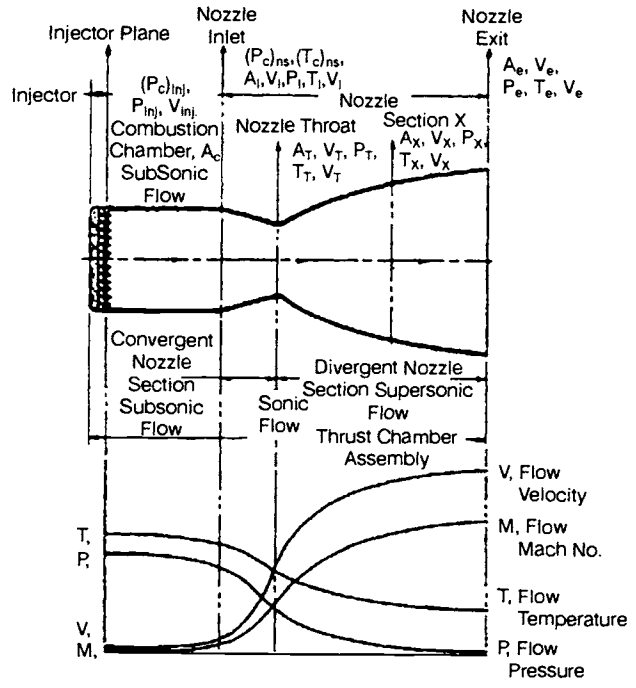

Fig. 1-9 Gas flow within liquid-propellant-rocket thrust chamber.

1.3 GAS-FLOW PROCESSES IN THE COMBUSTION CHAMBER AND NOZZLE

Since the analytical treatment of compressible fluids flowing through cylindrical ducts and nozzles can be found in standard aerodynamic and thermodynamic textbooks, no attempt will be made here to derive basic equations governing gas flows. Rather, significant applications of equations used in actual rocket design will be presented. The parameters and terms applicable to gas flows in a liquid-propellant rocket thrust chamber are shown in Fig. 1-9 and Table 1-1. These parameters serve to define the characteristics of gas flow at various points within the thrust chamber. Gas-flow calculations for rocket thrust-chamber design usually assume the following ideal conditions:

- Homogeneous gas composition.
- Perfect gas.
- No heat transfer through the motor walls in either direction (i.e., adiabatic processes). If no increase in entropy occurs, i.e., if the process is considered reversible, it is called an isentropic process.
- No friction.
- Steady flow rate.
- One-dimensional flow (all gas molecules move on parallel lines).
- Velocity uniformity across any section normal to chamber axis.
- Chemical equilibrium established within the combustion chamber and remaining constant in the nozzle.

Table 1-1 Terms used in calculating gas flows.

a_c, a_t : Local velocity of sound in chamber and at nozzle throat (ft/s); ($at=\sqrt{RTt}$).
Ac : Cylindrical cross section of chamber ($in.^2$).
Ai, At, Ae Ax : Flow areas at nozzle inlet, throat, exit and any section X normal to axis ($in.^2$).
Cp, Cv : Specific heats for constant pressure and for constant volume (Btu/lb°F).
g : Gravitational constant (32.2 ft/s^2 at sea level).
J : Energy conversion factor (778 ft-lb/Btu).
Mc, Mi, Mt, Me, Mx : Flow Mach number (via) at chamber; nozzle inlet, throat and exit; and at any section X normal to axis.
M : Molecular weight of combustion products.
(Pc)inj : Chamber total pressure at injector end ($lb/in.^2$). Because of the relatively low propellant-injection flow velocities V_{inj}, the measurable static pressure at this station is generally treated as equivalent to the total pressure.
(Pc)ns : Nozzle stagnation pressure or chamber total pressure at nozzle inlet ($lb/in.^2$); $(Pc)ns = Pi[1 + 1/2\ (\gamma-1)M^2i]^{\gamma/\gamma-1}$.
Pi, Pt, Pe, Px : Flow static pressures at nozzle inlet, throat and exit and at any section X normal to axis ($lb/in.^2$).
R : Gas constant (1544 M) (ft/°R)
(Tc)ns : Nozzle stagnation temperature or chamber total temperature [(0(t)]: $(Tc)ns = Ti[1+ 1/2(\gamma-1(M^2i]$.
Ti, Tt,Te, Tx : Flow temperature at nozzle inlet, throat, and exit; and at any section normal to axis (°R).
Vinj : Injector flow velocity = 0 (by assumption).
vi, vt, ve, vx : Flow velocities at nozzle inlet, throat, and exit and at any section X normal to axis (ft/s).
Vi, Vt, Ve, Vx : Flow specific volumes at nozzle inlet, throat, exit and at any section X normal to axis (ft^3/lb).
W : Steady weight flow rate (lb/s).
ε : Nozzle expansion area ratio (A_e/A_t).
εc : Nozzle contraction area ratio (A_c/A_t).
γ : Specific heat ratio (C_p/C_v).

In the actual design of a rocket and for the prediction of its behavior, certain correction factors, usually empirically obtained, will be applied to the results derived from these ideal assumptions.

The Perfect Gas Law

At any section X the perfect gas law states:

$$144\ p_x V_x = RT_x \qquad (1\text{-}9)$$

Principle of Conservation of Energy

In an adiabatic process, the increase in kinetic energy of the flowing gases between any two points equals the decrease in enthalpy. Applied to a nozzle,

this yields the following expression for a unit weight of gas flow:

$$\frac{1}{2gJ}(v_x^2 - v_i^2) = C_p(T_i - T_x) \qquad (1\text{-}10)$$

Principle of Conservation of Matter

$$\dot{W} = \frac{A_i v_i}{144 V_i} = \frac{A_x V_x}{144 V_x} = \text{constant} \qquad (1\text{-}11)$$

The Isentropic-Flow Process

For any isentropic-flow process the following relations hold between any two points:

$$p_i V_i^{\gamma} = p_x V_x^{\gamma} = \text{constant} \qquad (1\text{-}12)$$

and

$$T_i/T_x = (p_i/p_x)^{(\gamma-1)/\gamma} = (V_x/V_i)^{\gamma-1} \qquad (1\text{-}13)$$

Gas Flow Through Liquid-Propellant Rocket Combustion Chambers

A liquid-rocket combustion chamber converts propellants into high-temperature, high-pressure gas through combustion, which releases the chemical energy of the propellant, resulting in an increase in internal energy of the gas. Combustion chambers have been generally of tubular construction, as shown in Fig. 1-9. The liquid propellants are injected at the injection plane with a small axial velocity which is assumed to be zero in gas-flow calculations. The combustion process proceeds throughout the length of the chamber and is expected to be completed at the nozzle entrance. Heat liberated between injection plane and nozzle inlet increases the specific volume of the gas. To satisfy the conditions of constant mass flow, the gas must be accelerated toward the nozzle inlet with some drop of pressure. In brief, the following takes place.

The gas-flow process within the combustion chamber, that is, within the volume upstream of the nozzle entrance, is not entirely isentropic but rather is a partly irreversible, adiabatic expansion. Although the stagnation temperature, or total temperature, remains constant, the stagnation pressure, or total pressure, will decrease. This causes permanent energy losses, which are a function of the gas properties as expressed by and of the nozzle contraction area ratio ε_C (A_C/A_t). Wherever the acceleration of gases is largely affected by expansion due to heat release, rather than by a change of area, as in a nozzle, the stated losses occur. The greater the contribution of the nozzle to overall thrust, the more efficient will be the gas acceleration. Conversely, with no nozzle attached, the losses are maximum. The great importance of ε_C to the thrust-chamber design becomes apparent. It will be discussed further in Chapter 4.

Figure 1-10 shows the loss of total pressure for two typical specific heat ratio (γ) values as a function of the nozzle contraction area ratio ε_C. Generally used in rocket design, these data are calculated from the Rayleigh flow process.

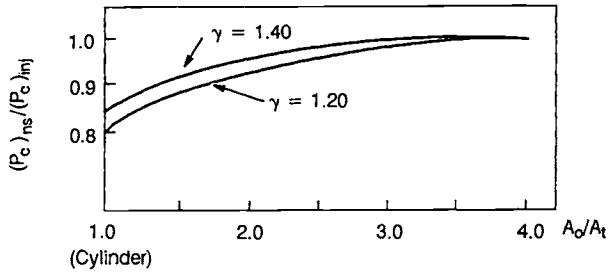

Fig. 1-10 Loss of total pressure for two typical values as a function of the nozzle contraction area ratio *c*.

Neglecting the flow velocity at the injecting end—i.e., assuming $v_{inj}=0$ and $(p_C)_{inj}=p_{inj}$—the total pressure ratio $(p_C)_{inj}/(p_C)_{ns}$ can also be expressed in terms of flow Mach number M_i at the nozzle inlet and of the specific heat ratio γ:

$$(p_c)_{inj}/(p_c)_{ns} = (1 + \gamma M_i^2)/\left(1 + \frac{\gamma - 1}{2} M_i^2\right)^{\gamma/(\gamma-1)} \qquad (1\text{-}14)$$

For the reasons mentioned above, it is desirable that the Mach number at the nozzle entrance be small. A thrust chamber with a contraction area ratio of $A_C/A_i = 2$ will typically have a value of $M_i=0.31(\gamma = 1.2)$. For the static pressure ratio, the expression simplifies to—

$$p_{inj}/p_i = 1 + \gamma M_i^2 \qquad (1\text{-}15)$$

Gas Flow Through Rocket Nozzles

The prime function of a rocket nozzle is to convert efficiently the enthalpy of the combustion gases into kinetic energy and thus create high exhaust velocity of the gas. The nozzle is the most efficient device for accelerating gases to supersonic velocities. Rocket nozzles are conventionally of the converging-diverging De Laval type, with the cross-sectional area decreasing to a minimum at the throat and then increasing to the exit area, as shown in Fig. 1-9. The flow velocity through a nozzle increases to sonic velocity at the throat and then increases further supersonically in the diverging section.

In practice, for one-dimensional isentropic expansion, (ODE) calculations, it is assumed that the gas flow through the nozzle will be an isentropic expansion, and that both the total temperature and the total pressure will remain constant throughout the nozzle. The pressure ratio $pt/(Pc)_{ns}$ between the throat and chamber is called the *critical pressure ratio* and is solely a function of specific heat ratio:

$$p_t/(p_C)_{ns} = [2/(\gamma+1)]^{\gamma/(\gamma-1)} \qquad (1\text{-}16)$$

The static pressure Pt at a nozzle throat with sonic flow, where the maximum weight flow per unit

area occurs, is defined as *critical pressure*. The velocity of sound is equal to the velocity of propagation of a pressure wave within a medium. It is therefore impossible for a pressure disturbance downstream of the nozzle throat to influence the flow at the throat or upstream of the throat, provided that this disturbance will not create a higher throat pressure than the critical pressure.

It is one of the characteristic features of an attached diverging or De Laval nozzle, however, that sonic velocity in the nozzle throat is maintained even if the back pressure (ambient pressure) at the nozzle exit is greater than the pressure required at the throat for sonic velocity. As a result, a pressure adjustment (recovery) must take place between the throat and the nozzle exit (ambient pressure). This adjustment may take place through subsonic deceleration (isentropic) or by way of non-isentropic discontinuities called shock waves, or a combination of both. Figure 1-11a presents several of the possible conditions that may occur in an overexpanded nozzle. The situations shown represent cases of an over-expanded nozzle.

In short, pressures lower than ambient may be present in a supersonic nozzle. The higher ambient pressure cannot advance upstream within the nozzle, since the gases are flowing with supersonic velocity. An exception to this is in the region of the flow along the nozzle walls, where, due to friction, a boundary layer of slow-moving gases may exist. In this subsonic boundary layer, ambient pressure may advance for a distance, forcing the low-pressure center jet away from the walls. It might be expected that the point of separation will be at the point of optimum expansion, but separation usually occurs further down-stream. In fact, it rarely occurs at all in conventional rocket nozzles within the designed region of operation, unless an extreme case of overexpansion exists or unless excessive nozzle divergence angles are chosen. Thus, in many cases it is correct to base all nozzle calculations on the assumption that no separation occurs, i.e., that the nozzle is filled at all stations (see Fig. 1-11b).

Some useful relations for ideal gas flow through a rocket nozzle take the following form:

Theoretical exit velocity:

$$v_e = \sqrt{\frac{2g\gamma}{\gamma - 1} RT_i \left[1 - \left(\frac{p_e}{p_i} \right)^{\frac{\gamma - 1}{\gamma}} \right] + v_i^2} \qquad (1\text{-}17)$$

$$v_e = \sqrt{\frac{2g\gamma}{\gamma - 1} R(T_c)_{ns} \left[1 - \left(\frac{p_e}{(p_c)_{ns}} \right)^{\frac{\gamma - 1}{\gamma}} \right]} \qquad (1\text{-}18)$$

Theoretical gas weight flow rate:

$$\dot{W} = A_t (p_c)_{ns} \sqrt{\frac{g\gamma [2/(\gamma + 1)]^{\frac{\gamma + 1}{\gamma - 1}}}{R(T_c)_{ns}}} \qquad (1\text{-}19)$$

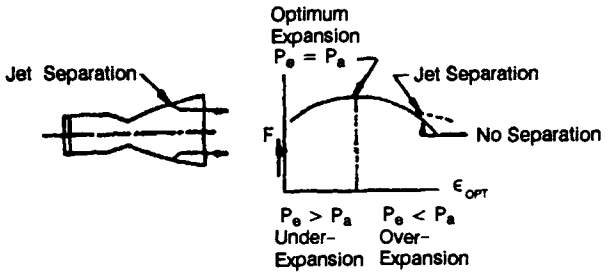

a) Effect of Non-optimum Nozzle Length and of Jet Separation on Thrust F

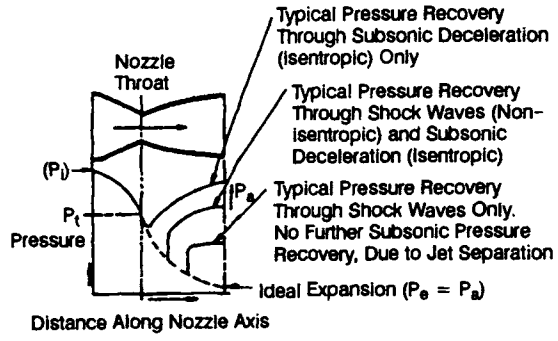

b) Pressure Distribution in an Overexpanded De Laval Nozzle

Fig. 1-11 Thrust and pressure distribution in an overexpanded De Laval nozzle.

Theoretical nozzle expansion ratio:

$$\epsilon = \frac{A_e}{A_t} = \frac{\left(\frac{2}{\gamma + 1} \right)^{\frac{1}{\gamma - 1}} \left[\frac{(p_c)_{ns}}{p_e} \right]^{\frac{1}{\gamma}}}{\sqrt{\frac{\gamma + 1}{\gamma - 1} \left[1 - \left(\frac{p_e}{(p_c)_{ns}} \right)^{\frac{\gamma - 1}{\gamma}} \right]}} \qquad (1\text{-}20)$$

At the throat:

$$p_t = (p_c)_{ns} \left[\frac{2}{\gamma + 1} \right]^{\frac{\gamma}{\gamma - 1}} \qquad (1\text{-}21)$$

$$v_t = \sqrt{\frac{2g\gamma}{\gamma + 1} R(T_c)_{ns}} \qquad (1\text{-}22)$$

At any section X between nozzle inlet and nozzle exit:

$$\frac{A_x}{A_t} = \frac{1}{M_x} \sqrt{\left[\frac{1 + \frac{\gamma - 1}{2} M_x}{\frac{\gamma + 1}{2}} \right]^{\frac{\gamma + 1}{\gamma - 1}}} \qquad (1\text{-}23)$$

At any section X between the nozzle inlet and nozzle throat:

$$\frac{A_x}{A_t} = \frac{\left[\frac{2}{\gamma + 1} \left(\frac{(p_c)_{ns}}{p_x} \right)^{\frac{\gamma - 1}{\gamma}} \right]^{\frac{\gamma + 1}{2(\gamma - 1)}}}{\sqrt{\frac{2}{\gamma - 1} \left[\left(\frac{(p_c)_{ns}}{p_x} \right)^{\frac{\gamma - 1}{\gamma}} - 1 \right]}} \qquad (1\text{-}24)$$

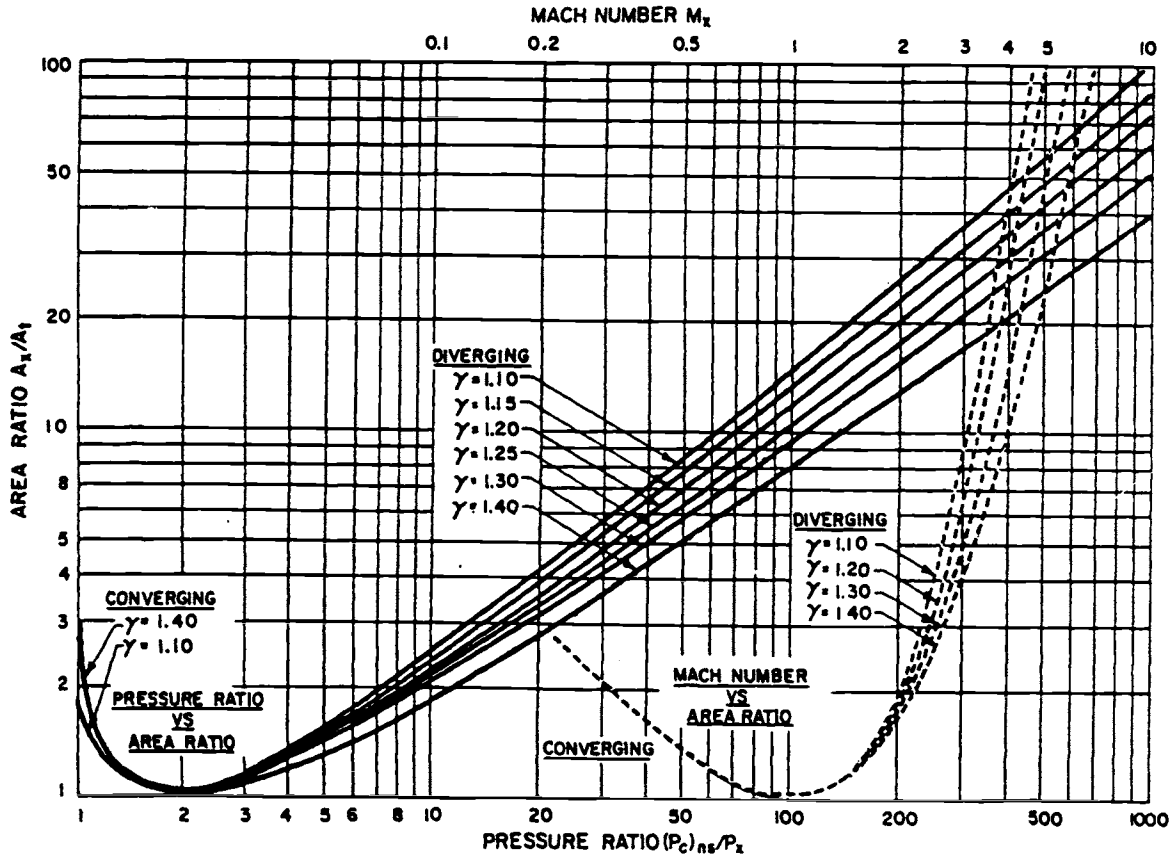

Fig. 1-12 Variations of isentropic pressure ratio and Mach number with area ratio in converging and diverging sections of De Laval nozzle.

At any section X between the nozzle throat and nozzle exit:

$$\frac{A_x}{A_t} = \frac{\left(\frac{2}{\gamma+1}\right)^{\frac{1}{\gamma-1}}\left(\frac{(p_c)_{ns}}{p_x}\right)^{\frac{1}{\gamma}}}{\sqrt{\frac{\gamma+1}{\gamma-1}\left[1-\left(\frac{p_x}{(p_c)_{ns}}\right)^{\frac{\gamma-1}{\gamma}}\right]}} \qquad (1\text{-}25)$$

$$v_x = \sqrt{\frac{2g\gamma}{\gamma-1}R(T_c)_{ns}\left[1-\left(\frac{p_x}{(p_c)_{ns}}\right)^{\frac{\gamma-1}{\gamma}}\right]} \qquad (1\text{-}26)$$

$$\frac{v_x}{v_t} = \sqrt{\frac{\gamma+1}{\gamma-1}\left[1-\left(\frac{p_x}{(p_c)_{ns}}\right)^{\frac{\gamma-1}{\gamma}}\right]} \qquad (1\text{-}27)$$

Variations of isentropic pressure ratio and Mach number with the area ratio in the convergent and divergent sections of a De Laval nozzle are shown in Fig. 1-12. Useful values of functions of the specific heat ratio γ are listed in Table 1-2.

Table 1-2 Useful values of functions of the specific heat ratio γ.

γ	$\sqrt{\frac{2g\gamma}{\gamma-1}}$	$\frac{\gamma-1}{\gamma}$	$\left(\frac{2}{\gamma+1}\right)^{\gamma/(\gamma-1)}$	$\gamma\sqrt{\left(\frac{2}{\gamma+1}\right)^{(\gamma+1)/(\gamma-1)}}$
1.10	26.61	0.0909	0.5847	0.6590
1.15	22.21	0.1304	0.5744	0.6848
1.20	19.65	0.1667	0.5645	0.7104
1.21	19.26	0.1736	0.5626	0.7155
1.22	18.89	0.1803	0.5607	0.7205
1.23	18.55	0.1870	0.5588	0.7257
1.24	18.23	0.1936	0.5569	0.7307
1.25	17.94	0.2000	0.5549	0.7356
1.26	17.66	0.2064	0.5532	0.7408
1.27	17.40	0.2126	0.5513	0.7457
1.28	17.15	0.2188	0.5494	0.7508
1.29	16.92	0.2248	0.5475	0.7558
1.30	16.70	0.2308	0.5457	0.7608
1.33	16.10	0.2481	0.5405	0.7757
1.36	15.59	0.2647	0.5352	0.7906
1.40	15.01	0.2857	0.5283	0.8102
1.50	13.89	0.3333	0.5120	0.8586
1.60	13.10	0.3750	0.4968	0.9062

Sample Calculation 1-2

The following data describe the thrust chamber of an ideal liquid-propellant rocket engine: thrust chamber propellant flow rate W_{tc} = 360.7 lb/s; nozzle stagnation pressure $(p_c)_{ns}$ = 1000 psia; chamber total temperature $(T_c)_{ns}$ = 6540°R; product-gas molecular weight M = 22.67; gas specific heat ratio γ = 1.20; nozzle expansion area ratio ε = 12. The following conditions are also assumed: flow Mach number at injecting plane, M_{inj} = 0; flow Mach number at the

nozzle inlet, M_i=0.4. (In practice, thrust chamber design values for M_i range from 0.15 to 0.45.)

Problem

Determine the following: (a) flow static pressures: p_{inj}, p_i, p_t, p_x at $A_x/A_t = 4$ and pe; (b) flow temperatures: T_{inj}, T_i, T_t, T_x, T_e; (c) flow specific volumes: V_{inj}, V_i, V_t, V_x, V_e; (d) flow velocities: v_i, v_t, v_x, v;; flow Mach numbers: M_x, M_e; (f) flow areas: A_c, A_i, A_t, A_x, A_e.

Solution 1-2

(a) Flow static pressures:
From Eq. (1-14)—

$$(p_c)_{inj} = (p_c)_{ns}(1 + \gamma M_i^2)/\left(1 + \frac{\gamma - 1}{2} M_i^2\right)^{\frac{\gamma}{\gamma - 1}}$$

$$= 1000 \times \frac{(1 + 0.16 \times 1.20)}{\left(1 + \frac{0.2}{2} \times 0.16\right)^6}$$

$$= \frac{1.192}{1.1} = 1082 \text{ psia}$$

Since, by assumption, M_{inj}=0—

$$p_{inj} = (p_c)_{inj} = 1{,}082 \text{ psia}$$

From Eq. (1-15)—

$$p_i = p_{inj}/(1 + \gamma M_i^2) = \frac{1082}{1 + 0.16 \times 1.20}$$

$$= \frac{1082}{1.192} = 909 \text{ psia}$$

From Eq. (1-21)—

$$p_t = (p_c)_{ns}\left[\frac{2}{\gamma + 1}\right]^{\frac{\gamma}{\gamma - 1}} = 1000 \times 0.564 = 564 \text{ psia}$$

From Fig. 1-12 or Eq. (1-25) at
$A_x/A_t = 4$—

$$p_x = (p_c)_{ns} \times \frac{1}{23} = \frac{1000}{23} = 43.5 \text{ psia}$$

From Fig. 1-12 or Eq. (1-20)—

$$p_e = \frac{(p_c)_{ns}}{101.5} = \frac{1000}{101.5} = 9.85 \text{ psia}$$

(b) Flow temperatures:
Since $(T_c)_{inj}$-$(T_c)_{ns}$ = constant and
M_{inj} = 0—

$T_{inj} = (T_c)_{inj} = (T_c)_{ns} = 6540°R.$

By definition—

$$T_i = \frac{(T_c)_{ns}}{[1 + \frac{1}{2}(\gamma - 1)M_i^2]}$$

$$= \frac{6540}{1 + 0.1 \times 0.16} = \frac{6540}{1.016} = 6440° \text{ F}$$

From Eq. (1-13)—

$$T_t = (T_c)_{ns}\left[\frac{p_t}{(p_c)_{ns}}\right]^{\frac{\gamma - 1}{\gamma}} = 6540 \times 0.909 = 5945° \text{ R}$$

$$T_x = (T_c)_{ns}\left[\frac{p_x}{(p_c)_{ns}}\right]^{\frac{\gamma - 1}{\gamma}} = 6540 \times \frac{1}{1.686} = 3880° \text{ R}$$

$$T_e = (T_c)_{ns}\left[\frac{p_e}{(p_c)_{ns}}\right]^{\frac{\gamma - 1}{\gamma}} = 6540 \times \frac{1}{2.16} = 3025° \text{ R}$$

(c) Flow specific volumes:

$$R = \frac{1544}{\mathfrak{M}} = \frac{1544}{22.67} = 68$$

From Eq. (1-9)—

$$V_{inj} = \frac{RT_{inj}}{144\ p_{inj}} = 68 \times 6540144 \times 1082 = 2.846 \text{ ft}^3/\text{lb}$$

$$V_i = \frac{RT_i}{144\ p_i} = \frac{68 \times 6440}{144 \times 909} = 3.34 \text{ ft}^3/\text{lb}$$

$$V_t = \frac{RT_t}{144\ p_t} = \frac{68 \times 5945}{144 \times 564} = 4.97 \text{ ft}^3/\text{lb}$$

$$V_x = \frac{RT_x}{144\ p_x} = \frac{68 \times 3880}{144 \times 43.5} = 42.1 \text{ ft}^3/\text{lb}$$

$$V_e = \frac{RT_x}{144\ p_x} = \frac{68 \times 3025}{144 \times 9.85} = 145.1 \text{ ft}^3/\text{lb}$$

(d) Flow velocities: ($a_i = \sqrt{g\gamma\ RTi}$):

$v_i = M_i a_i = 0.4 \times 32.2 \times 1.2 \times 68 \times 6440$
$= 0.4 \times 4110 = 1646$ ft/s

$v_t = M_t a_t = 1 \times 32.2 \times 1.2 \times 68 \times 5945$
$= 3958$ ft/s

From Eq. (1-26)—

$$v_x = \sqrt{\frac{2g\gamma}{\gamma - 1} R(T_c)_{ns}\left[1 - \left(\frac{p_x}{(p_c)_{ns}}\right)^{\frac{\gamma - 1}{\gamma}}\right]}$$

$$= \sqrt{6540 \times 64.4 \times 6 \times 68 \times [1 - 0.593]}$$

$$= \sqrt{64.4 \times 6 \times 68 \times 0.407 \times 6540}$$

$$= 8360 \text{ ft/s}$$

From Eq. (1-18)—

$$v_e = \sqrt{\frac{2g\gamma}{\gamma - 1} R(T_c)_{ns} \left[1 - \left(\frac{p_e}{(p_c)_{ns}} \right)^{\frac{\gamma - 1}{\gamma}} \right]}$$

$$= \sqrt{64.4 \times 6 \times 68 \times 6540 \times 0.543} = 9760 \text{ ft/s}$$

(e) Flow Mach numbers:
Since—

$$a_x = \sqrt{g\gamma RT_x} = \sqrt{32.2 \times 1.2 \times 68 \times 3880} = 3226 \text{ ft/s}$$

$$M_x = \frac{v_x}{a_x} = \frac{8360}{3226} = 2.59$$

$$a_e = \sqrt{g\gamma RT_e} = \sqrt{32.2 \times 1.2 \times 68 \times 3025} = 2820 \text{ ft/s}$$

$$M_e = \frac{v_e}{a_e} = \frac{9620}{2820} = 3.43$$

(f) Flow areas:
From Eq. (1-11)—

$$A_i = \frac{144\dot{W}_{tc}V_i}{v_i} = \frac{144 \times 360.7 \times 3.34}{1646} = 105.4 \text{ in.}^2$$

$$A_c = A_i = 105.4 \text{ in.}^2$$

$$A_t = \frac{144\dot{W}_{tc}V_t}{v_t} = \frac{144 \times 360.7 \times 4.97}{3958} = 65.4 \text{ in.}^2$$

$$A_x = \frac{144\dot{W}_{tc}V_x}{v_x} = \frac{144 \times 360.7 \times 42.1}{8360} = 261.8 \text{ in.}^2$$

or

$$A_x = 4 \times A_t = 261.8 \text{ in.}^2$$

$$A_e = \frac{144\dot{W}_{tc}V_e}{v_e} = \frac{144 \times 360.7 \times 145.1}{9670} = 782 \text{ in.}^2$$

or

$$A_e = 12 \times A_t = 782 \text{ in.}^2$$

1.4 PERFORMANCE PARAMETERS OF A LIQUID-PROPELLANT ROCKET ENGINE

The performance of a rocket engine can be expressed by a quantity commonly called "specific impulse" I_S. If impulse imparted to the vehicle and propellant weight consumption were measured during a given interval, I_S would have the dimension lb-sec/lb. In practice, thrust is usually measured in conjunction with propellant-weight-flow-rate measurements. This yields the same dimension: lb/(lb/sec). I_S may thus be expressed as—

$$I_S = F/\dot{W} \qquad (1\text{-}28)$$

Since weight is the force exerted by a mass on its rigid support under the influence of gravitation (by convention at sea level on Earth), it has become accepted practice to measure I_S in "seconds," by canceling out the terms for the forces. Obviously, the expression does not denote a time, but rather a magnitude akin to efficiency. Specific impulse directly contributes to the final velocity of the vehicle at burnout and thus has a pronounced effect on range or size of payload, or both. This will be shown further in connection with Eq. (1-30).

It is important to state whether a specific impulse quoted refers to the thrust-chamber assembly only (I_S)tc or to the overall engine system (I_S)oa. Often the distinction may not be self-evident. It is important, therefore, to state accurately to what system the quoted specific impulse refers. In a turbopump-fed system, for instance, overall engine specific impulse may include turbine power requirements, vernier, and attitude-control devices. All of these may be fed from one or all of a given vehicle's propellant tanks. If they are properly considered, the user, in this case the vehicle builder, will obtain the correct value for his own optimization studies, which include propellant tank sizes, payload weight, and range, among other parameters.

In many instances, specific impulse (I_S)tc for the thrust chamber only may be significant, such as during the component-development period of this subassembly. The specific impulse stated (I_S)tc will be higher than for a complete system, by 1 to 2 percent, as a rule. The specific impulse thus stated would be too high for the vehicle builder, who must consider the supply of propellants for turbine power and to the auxiliary devices mentioned above as well.

The engine specific impulse, along with the vehicle mass ratio, determines the performance of a space vehicle. Mass ratio R is defined by—

$$R = \text{Initial vehicle weight/burnout weight} \qquad (1\text{-}29)$$

where the initial weight is the total gross weight when the engine ignites and the burnout weight is the initial weight minus the propellant consumed. This value is then used in the "rocket equation" to calculate the ideal delta-v:

$$\Delta V = g \times Is \times \ln(R) \qquad (1\text{-}30)$$

The ideal delta-v is the velocity increment that would be added to a vehicle in free space with the engine firing axially. In most real appli-cations the actual velocity increase will be less than the ideal value. A launch vehicle flying from Earth's surface to low orbit will experience velocity losses due to atmospheric drag, gravitation, and non-axial thrust (due to engine gimballing to provide steering). For example, the velocity required to maintain a circular orbit at an altitude of 100 n. mi. is about 25,600 ft/s; a launch vehicle, however, must typically provide an ideal delta-v of about 30,000 ft/s to attain this orbit. For a multistage vehicle, Eq. (1-29) and (1-30) must be applied to each stage individually. The burnout

weight of each stage will be reduced by the stage inert weight to get the initial weight of the next stage. The total delta-v is then obtained by adding the values for each stage.

Thrust-Chamber Specific Impulse $(I_s)_{tc}$

The overall performance of the liquid-propellant thrust chamber is a direct function of the propellant combination, the combustion efficiency of propellants in the chamber, and the product gas expansion performance in the nozzle. The expression for $(I_s)_{tc}$ may be obtained in several ways. From Eq. (1-28):

$$(I_s)_{tc} = \frac{F}{\dot{W}_{tc}} \tag{1-31}$$

Combining Eq. (1-31) and (1-7):

$$(I_s)_{tc} = \frac{c}{g} \tag{1-31a}$$

The effective exhaust velocity c may be further defined as the product of two convenient parameters, c* and C_f:

$$c = c^* C_f \tag{1-31b}$$

where the *characteristic velocity* c* in feet per second (commonly pronounced "cee-star") is a parameter primarily used to rate the propellant combustion performance. The *thrust coefficient* C_f is a dimensionless parameter used to measure the gas expansion performance through the nozzle. Combining Eq. (1-31a) and (1-3lb):

$$(I_s)_{tc} = \frac{c^* C_f}{g} \tag{1-31c}$$

I_s and R will be of ultimate importance to the missile or space-vehicle builder, but both c* and C_f are of great and early importance to the engine and thrust-chamber designer and developer.

Characteristic Velocity c*

In a system with sonic velocity at the throat, the quantity c* reflects the effective energy level of the propellants and the design quality of injector and combustion chamber. It may be defined by the following expression:

$$c^* = \frac{(p_c)_{ns} A_t g}{\dot{W}_{tc}} \tag{1-32}$$

This form shows that c* measures combustion performance in a given thrust chamber by indicating how many pounds per second of propellant must be burned to maintain the required nozzle stagnation pressure. A lower value of propellant consumption W under the given condition indicates a combustion process of higher energy and efficiency and gives a correspondingly higher value of c*. By substituting W_{tc} with Eq. (1-19) in Eq. (1-32), the equation for theoretical c* may be rewritten in the following form:

$$c^* = \frac{\sqrt{g\gamma R (T_c)_{ns}}}{\gamma \sqrt{\left[\frac{2}{\gamma+1}\right]^{\frac{\gamma+1}{\gamma-1}}}} \tag{1-32a}$$

This form shows that c* is a function of the properties of the product gas at the exit of the combustion chamber (i.e., at the nozzle inlet), namely, specific heat ratio γ, gas constant R, and temperature $(T_c)_{ns}$.

Thrust Coefficient C_f

The quantity C_f reflects the product-gas expansion properties and design quality of the nozzle. Combining Eq. (1-31), (1-31c), and (1-32), the expression for theoretical C_f may be written as follows:

$$C_f = \frac{F}{A_t (p_c)_{ns}} \tag{1-33}$$

This form shows that C_f measures the force augmented by the gas expansion through the nozzle, as compared to the force which would be generated if the chamber pressure acted over the throat area only. By combining Eq. (1-6), (1-18), (1-19), and (1-33), the equation for theoretical C_f at any altitude may be rewritten in the following form:

$$C_f = \sqrt{\frac{2\gamma^2}{\gamma-1}\left[\frac{2}{\gamma+1}\right]^{\frac{\gamma+1}{\gamma-1}}\left[1 - \left(\frac{p_e}{(p_c)_{ns}}\right)^{\frac{\gamma-1}{\gamma}}\right]} + \epsilon\left[\frac{p_e - p_a}{(p_c)_{ns}}\right] \tag{1-33a}$$

Equation 1-33a shows that C_f is a function of specific heat ratio γ, chamber pressure p_c, ambient pressure p_a, and nozzle area expansion ratio ε .

As will be noted, the throat stagnation pressure $(p_c)_{ns}$ has been used in Eq. (1-32) and (1-33). This has been the practice in industry and in most of the literature. Briefly, the reason is that $(p_c)_{ns}$ reflects the true theoretical gas property at the nozzle inlet, and gives a more logical value to c* and C_f. In actual operation the true value of $(p_c)_{ns}$ can not be measured. The $(p_c)_{ns}$ is mathematically converted from the measured value of the gas static pressure at the injector, p_{inj}. The accuracy of this calculated value has to be verified by the test results. Likewise, the gas properties, and thus the specific heat ratio γ, which additionally changes along the chamber axis, affect the true values of c* and C_f. This also must be verified by actual test results.

To understand better the nature of C_f and the design parameters that influence it, first rearrange Eq. (1-33) as follows:

$$F = (p_c)_{ns} \bullet At \bullet C_f \tag{1-34}$$

The formula says that the thrust generated by a thrust chamber (the effect) is produced by pressure (the

cause) as a function of the physical properties of the chamber itself. The relationships and effects of the principal design parameters become clearer through the following steps.

Assume a wish to generate a certain thrust F. The chamber being a straight cylinder (Fig. 1-13), its pressure has a very small effect on the cylindrical wall (the forces normal to the chamber axis will cancel each other), except for effects of friction, which we neglect. There is no part of the chamber for the pressure to act upon at the exit. The only chamber area upon which the pressure can act is the injector plate. Since, for the cylindrical chamber, the injector area A_i equals A_t, we can write—

$$F_{cyl} = p_{inj} \cdot A_t \qquad (1\text{-}35)$$

For the reasons explained [see Eq. (1-34)], Eq. (1.-35) can be rewritten to include $(p_c)_{ns}$:

$$F_{cyl} = (p_c)_{ns} \cdot A_t \cdot C_{f_1} \qquad (1\text{-}36)$$

Because $(p_c)_{ns}$ is smaller than p_{inj} (Fig. 1-10), the coefficient C_{f_1} is introduced to correct for this fact. For instance, if the ratio $(p_c)_{ns}/p_{inj}$ was found to be 0.8 from Fig. 1-10, C_{f_1} would have to be 1.25 to offset the introduction of $(p_c)_{ns}$. The use of a thrust coefficient of 1.25 in a straight cylinder thrust chamber for which $(p_c)_{ns}/p_{inj}$ is 0.8 is merely part of a mathematical rearrangement, but does not signify an increase in thrust for a given p_{inj}.

The combustion chamber including the injector will have to produce the required pressure $(p_c)_{ns}$ with a flow rate (magnitude determined by c* and throat area A_t). Transformation of Eq. (1-32) shows the relationship:

$$(p_c)_{ns} = \dot{W}_{tc} \cdot c^* \cdot \frac{1}{A_t \cdot g} \qquad (1\text{-}37)$$

In actual practice, the value of c* for a given propellant combination and thrust chamber design will be arrived at tentatively from existing experience and be refined during developmental testing.

Now redesign the cylindrical thrust chamber as shown in Fig. 1-14. Maintaining the same throat area A_t=A_e, enlarge the combustion chamber including injector to a diameter somewhat larger than that of A_t. The flow rate remains W_{tc}.

In the straight cylindrical chamber (Fig. 1-13), the gas velocity was sonic at the end of the cylindrical chamber portion, which coincided with A_t and A_e. From earlier discussions (see section 1-2), we know that expansion (acceleration) is nonisentropic in that case. In the redesigned chamber (Fig. 1-14) by contrast, gas velocities are still well below sonic velocity at the end of the cylindrical portion. Most of the acceleration to sonic velocity will now occur in the added convergent nozzle. Since we can make the assumption that the combustion process is complete at the end of the cylindrical chamber portion, the subsequent expansion (acceler-ation) in the con-vergent nozzle is assumed to be isentropic; i.e., to occur without further total pressure losses. Since we keep W_{tc} and A_t constant and assume that c* remains unchanged, the nozzle stagnation pressure $(p_c)_{ns}$ will also retain the same value as the straight cylindrical chamber. However, the required total pressure at the injector end will definitely be lower because of the reduced pressure losses in the combustion chamber. The result is a favorable redesign because slightly lighter tanks can be used in pressurized systems because the same propellant flow rate can be sustained with lower tank pressures.

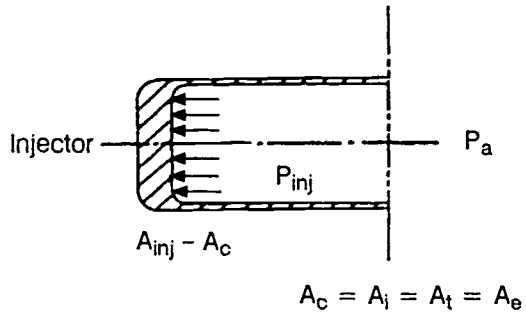

Fig. 1-13 Straight cylindrical thrust-chamber.

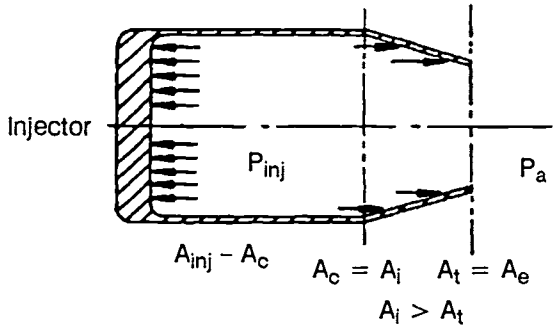

Fig. 1-14 Cylindrical thrust chamber with convergent nozzle.

In turbopump-fed systems, the required turbopump horsepower will decrease. However, the forces acting upon the thrust chamber, and thus the developed thrust, can be assumed to have remained unchanged because lower pressure acts upon the larger injector and opposing forces are present at the converging nozzle, cancelling each other out.

In short, the redesign (Fig. 1-14) reduces demands on the propellant feed system for the same W_{tc} and the same thrust level.

Further redesign of the chamber can include a divergent nozzle section, as in Fig. 1-15. Up to the throat area, nothing changes over the preceding configuration, which includes a convergent nozzle only. Since the gas velocity in the throat area is always sonic (except for very low, subcritical chamber pressures), the attachment of the divergent nozzle section will have no effect on the previously described gas processes and the pressures upstream of the throat. However, conditions downstream from the throat will now be different.

With the cylindrical chamber, and the chamber with convergent nozzle, the static pressure energy

available at the throat is dissipated by expansion to atmospheric pressure, flowing freely in all directions. Attaching a divergent nozzle prevents the gases from dissipating at random and further accelerates the gases in one preferred direction only. Since this process takes place in the divergent part of the thrust chamber, the static pressures of the expanding gases produce a force on the chamber, as indicated by arrows in Fig. 1-15. Expression of the thrust for the complete thrust chamber with convergent-divergent nozzle can now be written as follows:

$$F_{tc} = \int_0^{A_t} pdA + \int_{A_t}^{A_{inj}} pdA - \int_{A_t}^{A_i} pdA + \int_{A_t}^{A_c} pdA \quad (1\text{-}38)$$

The last expression in the equation represents the gain realized from attaching the divergent nozzle to the throat. Combining all gains into a single coefficient C_f (see Eq. 1-33) again yields Eq. (1-34):

$$F = (p_c)_{ns} \bullet A_t \bullet C_f$$

In brief, it may be stated that the redesign (Fig. 1-15) produces thrust for the same W_{tc} and the same feed-system configuration.

Summary of the Influences of p_a, ε, γ, R, and $(p_c)_{ns}$ on Engine Performance

Effect of p_a. An ambient pressure p_a reduces the vacuum thrust F of an engine by the amount $p_a \bullet A_e$ [see Eq. (1-5)]; C_f will be similarly affected by the amount $\varepsilon \bullet p_a/(p_c)_{ns}$, as shown in Eq. (1-33a). This may be rewritten as $C_f = (C_f)_{vac} - \varepsilon p_a/(p_c)_{ns}$. The lower the ambient pressure, the higher will be thrust and performance. Maximum values are obtained in vacuum.

Effect of ε. Optimum thrust for a given ambient pressure is obtained when the nozzle expansion area ratio $\varepsilon = A_e/A_t$ is such that $p_e = p_a$. This may be seen from Fig. 1-16. If the divergent nozzle section is extended in the region where $p_e > p_a$, thrust will increase; however, where $p_e < p_a$, lengthening the nozzle will decrease thrust. Therefore, it would be beneficial to design the nozzle to yield $p_e = p_a$ to reach an optimum value for the thrust coefficient. The ε for this condition is called *optimum nozzle expansion area ratio.* Unfortunately, because of changing ambient pressure during flight, no one ε *is* optimum. Trajectory and payload optimization studies usually determine the best compromise. Such a study is not required (except for weight and size considerations) for rockets which start and stop at the same altitude (same ambient pressure), such as upper stages, where ambient pressure is zero or near zero at all times. For the special case of $p_a = 0$ (vacuum conditions), ε would become infinity to satisfy "ideal expansion." An increase in nozzle expansion area ratio increases specific impulse but at the same time increases weight. A payload optimization trading the effects of engine performance and engine weight on payload leads to selection of engine nozzle expansion ratio. For a space engine,

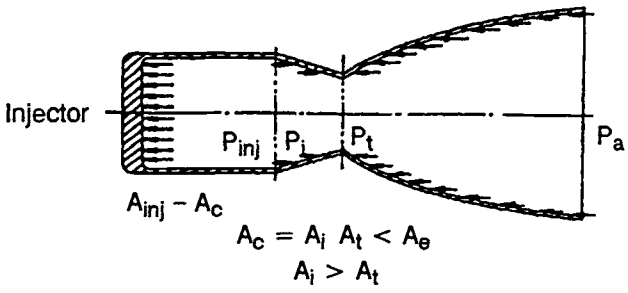

Fig. 1-15 Redesign of thrust chamber with divergent nozzle section.

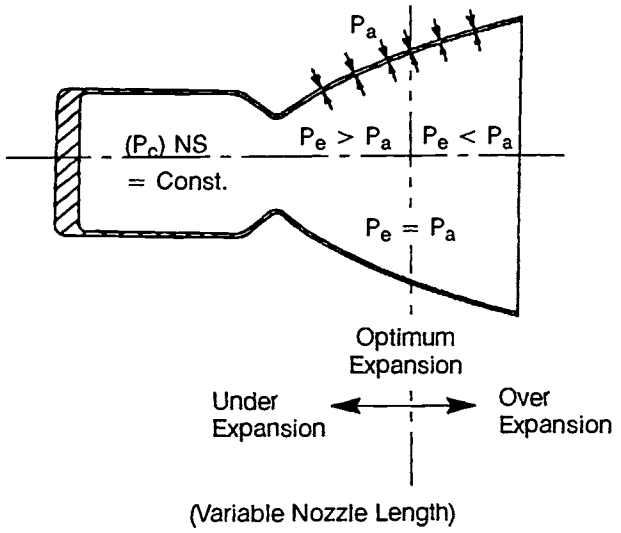

Fig. 1-16 Effect of ε on engine performance.

the diminishing returns in payload as expansion area ratio increases can be used to limit expansion area ratio to values less than 400.

Effect of γ. The specific heat ratio indicates the energy-storing capacity of the gas molecule. A smaller value of γ indicates a higher energy storing capability, and in turn gives higher engine performance. As shown in Eq. (1-32a) and (1-33a), a smaller γ will yield a higher value for both, c^* and C_f.

Effect of R(R = 1544/M). For constant $(T_c)_{ns}$ Eq. (1-32a) shows that c^* will increase if the gas constant R increases; i.e., the gas molecular weight decreases. Thus, a higher value of R will yield a higher engine performance.

Effect of $(p_c)_{ns}$. The effective chamber pressure or nozzle stagnation pressure $(p_c)_{ns}$ appears in Eq. (1-33a) for C_f in the form of two pressure ratios, $p_e/(p_c)_{ns}$ and $p_a/(p_c)_{ns}$. As is evident from Eq. (1-20), the ratio $p_e/(p_c)_{ns}$ has a singular value for a given ε and γ $(p_c)_{ns}$ in Eq. (1-33), and therefore influences C_f only through the negative term, $p_a/(p_c)_{ns}$. An increase in $(p_c)_{ns}$ decreases this negative term and hence increases C_f. This effect is more pronounced when p_a is high. Since the thrust is proportional to both $(p_c)_{ns}$ and C_f, an increase in

$(p_c)_{ns}$ in a given thrust chamber will increase the thrust. The $(p_c)_{ns}$ also has some effect on the combustion process. Increasing $(p_c)_{ns}$ tends to increase $(T_c)_{ns}$ and to reduce γ and R. The overall result is usually an increase in c*.

Correction Factors and Magnitudes of Engine Performance Parameters

The actual performance of a liquid-propellant rocket engine differs from that of an ideal one because of friction effects, heat transfer, nonperfect gases, nonaxial flow, nonuniformity of the working fluid, flow distribution, and shifting gas composition. The latter refers to the fact that the gas properties (γ, M, R) are not truly constant along the nozzle axis, as the isentropic treatment of the processes assumes. Correction factors must therefore be applied to the performance parameters derived from theoretical assumptions. Some important correction factors follow:

Correction factor for thrust and the thrust coefficient:

$$\eta_f = \frac{\text{Actual thrust coefficient}}{\text{Ideal thrust coefficient}} = \frac{\text{Actual thrust}}{\text{Ideal thrust}} \qquad (1\text{-}39)$$

The values for η_f range from 0.92 to 1.00.

Correction factor for effective exhaust velocity and specific impulse:

$$\eta_v = \frac{\text{Actual effective exhaust velocity}}{\text{Ideal effective exhaust velocity}} = \frac{\text{Actual specific impulse}}{\text{Ideal specific impulse}} \qquad (1\text{-}40)$$

The values for range from 0.85 to 0.98.

Correction factor for characteristic velocity:

$$\eta_v^* = \frac{\text{Actual characteristic velocity}}{\text{Ideal characteristic velocity}} \qquad (1\text{-}41)$$

The values for ηv^* range from 0.87 to 1.03.

Correction factor for propellant mass flow rate:

$$\eta_w = \frac{\text{Actual propellant mass flow rate}}{\text{Ideal propellant mass flow rate}} \qquad (1\text{-}42)$$

The values for η_w range from 0.98 to 1.15.

The relation among correction factors may be expressed as follows:

$$\eta_v = \eta_v^* \cdot \eta_f \qquad (1\text{-}43)$$

$$\eta_v = 1/\eta_w \qquad (1\text{-}44)$$

Actual ranges of liquid-propellant rocket engine parameters are listed in Table 1-3. Values of the vacuum or altitude thrust coefficient $(C_f)_{vac}$ plotted as functions of nozzle expansion area ratio ε and gas specific heat ratio γ are shown in Fig. 1-17.

Table 1-3 Actual ranges of liquid-propellant rocket engine parameters.

Gas temperature T, R°	4000 to 7000
Nozzle stagnation pressure Pc_{ns}, psia	10-2500
Molecular weight M	.2 to 30
Gas constant R	51.5 to 772
Gas flow Mach number M	.0 to 4.5
Specific heat ratio γ	1.13 to 1.66
Nozzle expansion area ratio ε	3.5 to 100
Nozzle contraction area ratio εc	1.3 to 6
Thrust coefficient C_f	1.3 to 2.0
Characteristic velocity c*, ft/s	3000-8000
Effective exhaust velocity c, ft/s	4000-12,000
Specific impulse (vacuum) $I_{s,\ s}$	150-480

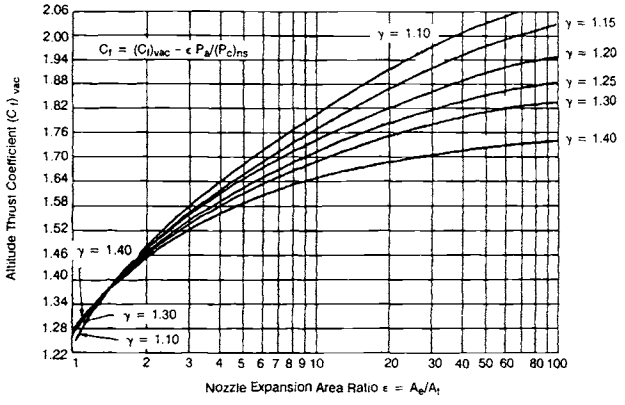

Fig. 1-17 Altitude thrust coefficient as function of area ratio and specific heat ratio.

During the 1970s, the joint Army, Navy, and Air Force (JANNAF) committee on rocket-engine performance developed analytical procedures anchored on test data to calculate the performance-correction parameters in a rigorous manner. Because of the extensive nature of the subject and the fact that examples throughout this book are based on coefficients defined by Eq. (1-39) through (1-44), no detailed discussions of the JANNAF rigorous analysis procedures will be made here. The JANNAF *Rocket Engine Performance Prediction and Evaluation Manual* (CPIA Publication 246, April 1975) gives further information on performance procedures. Simplified JANNAF performance coefficients have been defined that characterize the principal physical processes occurring in the thrust chamber: propellant atomization, mixing, evaporation, chemical reaction, gas expansion; and effects such as chemical reaction rates and boundary-layer and streamline and velocity-vector divergence in the converging and diverging nozzles.

Sample Calculation 1-3

Assume a thrust chamber for the same ideal liquid propellant rocket engine as given in Sample Calculation 1-2, in which W_{tc} = 360.7 lb/s; $(P_c)_{ns}$=1000 psia; $(T_c)_{ns}$=6540°R; M = 22.67; γ =1.20; and ε =12.

Problem

Determine the following: (a) Theoretical c*; (b) theoretical C_f at sea level and in space; (c) theoretical $(I_s)_{tc}$ at sea level and in space; (d) actual c*, if c* correction factor ηv^*=0.97; (e) actual C_f at sea level and in space, if sea-level C_f correction factor n_f = 0.983; (f) actual $(I_s)_{tc}$ at sea level and in space; (g) $(I_s)_{tc}$ correction factor at sea level; (h) thrust at sea level and in space; and (i) actual A_t and A_e.

Solution 1-3

(a) From Eq. (1-32a):

$$\text{Theoretical } c^* = \frac{\sqrt{g\gamma R(T_c)_{ns}}}{\gamma\sqrt{\left(\frac{2}{\gamma+1}\right)^{\frac{\gamma+1}{\gamma-1}}}}$$

$$= \frac{\sqrt{32.2 \times 1.2 \times \frac{1544}{22.67} \times 6540}}{0.7104}$$

$$= 5830 \text{ ft/s}$$

(b) From Eq. (1-33a):

$$\text{Theoretical } C_f = \sqrt{\frac{2\gamma^2}{\gamma-1}\left(\frac{2}{\gamma+1}\right)^{\frac{\gamma+1}{\gamma-1}}\left[1-\left(\frac{p_e}{(p_c)_{ns}}\right)^{\frac{\gamma-1}{\gamma}}+\epsilon\frac{p_e-p_a}{(p_c)_{ns}}\right]}$$

From Sample Calculation 1-2: Pe=9.85 psia

At sea level Pa=14.7 psia:

$$\text{Theoretical } C_f = 2.247 \times \sqrt{1-\left(\frac{9.85}{1000}\right)^{1/6}} + 12 \times \frac{9.85-14.7}{1000}$$

$$= 2.247 \times \sqrt{1-0.4625} - \frac{4.85 \times 12}{1000}$$

$$= 2.247 \times 0.734 \times 0.0582$$

$$= 1.65 - 0.0582$$

$$= 1.5918$$

In space:

$$\text{Theoretical } C_f = 1.5918 + 12 \times \frac{14.7}{1000}$$

$$= 1.5918 + 0.1764$$

$$= 1.7682$$

(c) From Eq. (1-31):

$$\text{Theoretical } I_s = \frac{c^* \cdot C_f}{g}$$

At sea level:

$$\text{Theoretical } (I_s)_{tc} = \frac{5830 \times 1.5918}{32.2} = 288.4 \text{ lb s/lb}$$

In space:

$$\text{Theoretical } (I_s)_{tc} = \frac{5830 \times 1.7682}{32.2} = 319.6 \text{ lb s/lb}$$

(d) From Eq. (1-41):

$$\text{Actual } c^* = \eta_v{}^* \cdot \text{theoretical } c^*$$

$$= 0.97 \times 5830 = 5650 \text{ ft/s}$$

(e) From Eq. (1-39):

$$\text{Actual } C_f = \eta_f \cdot \text{theoretical } C_f$$

At sea level:

$$\text{Actual } C_f = 0.983 \times 1.5918 = 1.566$$

In space:

$$\text{Actual } C_f = 1.566 + 12 \times \frac{14.7}{1000}$$

$$= 1.566 + 0.1764 = 1.7424$$

(f) At sea level:

$$\text{Actual } (I_s)_{tc} = \frac{5650 \times 1.566}{32.2} = 275 \text{ lb s/lb}$$

In space:

$$\text{Actual } (I_s)_{tc} = \frac{5650 \times 1.7424}{32.2} = 306 \text{ lb s/lb}$$

(g) From Eq. (1-40):

$$\underset{\eta_v \text{ at sea level}}{(I_s)_{tc} \text{ correction factor}} = \frac{\text{Actual } (I_s)_{tc} \text{ at sea level}}{\text{Theoretical } (I_s)_{tc} \text{ at sea level}}$$

$$= \frac{275}{288.4} - 0.954$$

Or from Eq. (1-43):

$$\eta_v = \eta_v^* \cdot \eta_f = 0.97 \times 0.983 = 0.954$$

(h) From Eq. (1-31):

$$\text{Thrust F at sea level} = \dot{W}_{tc} \cdot (I_s)_{tc} \text{ at sea level}$$

$$= 360.7 \times 275 = 99{,}200 \text{ lb}$$

$$\text{Thrust F in space} = \dot{W}_{tc} \cdot (I_s)_{tc} \text{ in space}$$

$$= 360.7 \times 306 = 108{,}500 \text{ lb}$$

(i) From Eq. (1-33):

$$A_t = \frac{F}{C_f \cdot (p_c)_{ns}} = \frac{99{,}200}{1.566 \times 1{,}000} = 63.4 \text{ in.}^2$$

$$A_e = \epsilon \cdot A_t = 12 \times 63.4 = 760.8 \text{ in.}^2$$

1.5 LIQUID PROPELLANTS

The term "liquid propellant" covers both liquid oxidizers (liquid oxygen, liquid fluorine, nitric acid, etc.) and liquid fuels (RP-1, alcohol, liquid hydrogen, etc.). In some cases, additives are used (water, ferric chloride, etc.). The propellants furnish the energy and the working fluid for the rocket engines. The selection of the propellants is one of the most important steps in the design of an engine. It greatly affects overall engine system performance as well as the design criteria for each engine component. The propellant selection in turn is influenced by price, supply, handling, and storage considerations.

Monopropellants

Liquid monopropellants may be either a mixture of oxidizer and combustible matter or a single compound that can be decomposed with attendant heat release and gasification. A rocket monopropellant must be stable in a natural or controlled environment, yet should produce hot combustion or decomposition gases when pressurized, heated, or fed through a catalyst. A liquid-monopropellant engine system usually does have the advantage of simplicity of tankage, feed plumbing, flow control, and injection. Unfortunately, most of the practical mono-propellants, such as hydrogen peroxide (H_2O_2), have a relatively low performance. Therefore they are mainly used as secondary power sources in rocket engine systems, such as for turbopump gas generators, auxiliary power drives, and attitude and roll-control jets. Certain high-performance monopropellants, such as methyl nitrate(CH_3NO_3), are rather unstable and are considered unsafe for rocket applications. However, some monopropellants that promise relatively high-performance and safer operational characteristics have been under development recently. If successful, these may effect wider application of liquid-monopropellant engines.

Bipropellants

A liquid-bipropellant system employs two different propellants, usually an oxidizer and a fuel. Separate tanks hold oxidizer and fuel, which are not mixed until they reach the combustion chamber. Present-day liquid-propellant rocket engines use bipropellants almost exclusively because they offer higher performance and safer operation.

Many bipropellant combinations employ ignition devices such as (a) chemical pyro-technic igniters, (b) electric spark plugs, (c) injection of a spontaneously ignitable liquid fuel or oxidizer ("pyrophoric fluid") ahead of the propellant proper, or (d) a small combustor wherein ignition is started by devices (a) or (b), in turn starting the main chamber by the hot gas produced.

Other bipropellant combinations, called *hypergolics*, ignite spontaneously upon mixing and thus permit greatly simplified ignition, but also pose certain hazards. For instance, accidental mixing of the fuel and oxidizer due to tank or other hardware failures could cause a violent explosion. These hazards must be considered when designing an engine system using hypergolics.

Cryogenic Propellants

Some liquid propellants are liquefied gases of very low boiling point (-230 to -430°F) at ambient pressure and low critical temperature (10 to -400°F). These propellants are defined as *cryogenics*. The most common cryogenic propellants for rocket applications are liquid oxygen (O_2), liquid hydrogen (H_2), liquid fluorine (F_2), oxygen difluoride (OF_2), or mixtures of some of them. Cryogenic propellants pose storage and handling problems. Elaborate insulation must minimize losses due to boiloff; the complexity of the insulation will depend on storage period and type of cryogenic. Recently, novel insulating techniques have been under development that should greatly reduce boiloff losses. Adequate venting systems are needed for the developed gases. Storage and handling equipment and components are extremely sensitive to atmospheric or other moisture; even minute quantities may cause a jamming of, for instance, a valve. The design criteria, including materials selection for engine systems using cryogenic propellants, must consider the very low temperatures involved. The mechanical design of engine components for cryogenic-propellant applications will be discussed in subsequent chapters.

Storable Liquid Propellants

In contrast to the cryogenics, certain other liquid propellants are stable over a reasonable range of temperature and pressure, and are sufficiently non-reactive with construction materials to permit storage in closed containers for periods of a year or more. These propellants are defined as *storables*. Storable liquid propellants permit almost instant readiness of the rocket engine and may result in greater reliability due to the absence of extremely low temperatures

and the need to dispose of boiloff vapors. Application of storables to military vehicles as well as to the upper stages of space vehicles has increased in recent years. The mechanical design of storable-propellant engine components will be further discussed in subsequent chapters.

Additives for Liquid Propellants

Sometimes additives are mixed into liquid propellants to improve cooling characteristics, to depress freezing point, to reduce corrosive effects, to facilitate ignition, and to stabilize combustion.

Optimum Mixture Ratio

A certain ratio of oxidizer weight to fuel weight in a bipropellant combustion chamber will usually yield a maximum performance value called the *optimum mixture ratio*. As a rule, the optimum mixture ratio is richer in fuel than the stoichiometric mixture ratio and theoretically will see all the fuel completely oxidized and the flame temperature at a maximum. This is because a gas slightly richer in fuel tends to have a lower molecular weight, which results in higher overall engine system performance. The optimum mixture ratio of some propellant combinations shifts slightly with changes in chamber pressure. Also, in actual application the mixture ratio may be shifted away from the optimum value for one of the following reasons: lower chamber temperature to stay within the temperature limitations of chamber construction material, required coolant flow, or better combustion stability.

Density Impulse

In addition to the overall system-oriented specific impulse, as discussed in section 1-3, an important propellant-performance parameter called *density impulse* expresses the total impulse delivered per unit volume of the propellant. It is defined as follows:

$$\text{Density impulse} = I_s \bullet d \text{ (s)} \qquad (1\text{-}45)$$

where d = bulk density or the propellant combination's specific weight:

$$d = \frac{(r_w - 1)}{\frac{r_w}{d_o} + \frac{1}{d_f}} \qquad (1\text{-}46)$$

r_w = (oxidizer/fuel) weight mixture ratio
d_o = bulk density of the oxidizer, specific weight
d_f = bulk density of the fuel, specific weight

Selection of Liquid Propellants

When selecting a propellant or propellant combination for a specific application, it is well to realize that most propellants, in addition to their advantages, may have certain disadvantages. Thus, propellant selection usually includes some compromises. The more important and desirable propellant features are listed here; order of importance may vary as a function of application:

- High energy release per unit of propellant mass, combined with low molecular weight of the combustion or decomposition gases, for high specific impulse.
- Ease of ignition.
- Stable combustion.
- High density or high density impulse to minimize the size and weight of propellant tanks and feed systems.
- Ability to serve as an effective coolant for the thrust chamber (optimum combination of high specific heat, high thermal conductivity, and high critical temperature).
- Reasonably low vapor pressure at 160°F (a frequent specification value for military applications) for low tank weight and low net positive pump suction head requirement.
- Low freezing point (preferably less than -65°F) to facilitate engine operation at low temperature.
- Absence of corrosive effects; compatibility with engine construction materials.
- For storables: good storability as assisted by a high boiling point (preferably above 160°F) and by the resistance to deterioration during storage.
- Low viscosity (preferably less than 10 cp down to -65°F) to minimize pressure drops through feed system and injector.
- High thermal and shock stability to minimize explosion and fire hazard.
- Low toxicity of raw propellants, their fumes, and their combustion products.
- Low cost.
- Availability.

Liquid-Propellant Performance and Physical Properties

Detailed methods to calculate the performance for any given liquid propellant or propellant combination can be found in the One-Dimensional Equilibrium (ODE) and Two-Dimensional Kinetics (TDK) methodologies developed by NASA for government and industry use and documented in NASA SP-273, *One-Dimensional Equilibrium*, Mar 1976; NAS 9-12652 *Two-Dimensional Kinetic (TDK) Reference Computer Program*, Dec 1973. For the theoretical calculations, it is generally assumed that the ideal conditions exist as described in section 1.3 (Gas Flow Processes) of this chapter. The prime objective of propellant performance calculations is to derive the quantities c^*, C_f, and I_s. These are obtained from evaluation of the flame or chamber temperature $(Tc)_{ns}$, the gas mean molecular weight M, and the specific heat ratio γ for a given $(Pc)_{ns}$, Pe and Pa. The chamber temperature is calculated in the ODE methodology from the heat of the chemical reaction of the propellants and from the specific heat of the gases.

Inputs to the theoretical ODE and TDK programs include propellant formulation, state of the

Table 1-4 Theoretical performance of rocket propellant combinations (prepared by Rocketdyne Chemical and Material Technology).

Conditions	Symbols and Units	Propellants
Adiabatic combustion	I Theoretical maximum specific impulse, s	JANAF thermochemical data used throughout
Isentropic expansion	r Mixture ratio-mass oxidizer/mass fuel	■ EARTH-STORABLE: at room temperature, 77°F
One-dimensional expansion	d Bulk density $\Sigma M/\Sigma V$, g/cm³	▲ SPACE-STORABLE: arbitrarily, NBP > -238°F
Shifting equilibrium	T_c Chamber temperature, F	★ CRYOGENIC
	C* Characteristic velocity, ft/s	

To Approximate I_{opt} at Other Pressures	
Pressures	Multiply by
1,000	1.00
900	0.99
800	0.98
700	0.97
600	0.95
500	0.93
400	0.91
300	0.88

Optimum Expansion, P_c = 1,000 psia → P_e = 14.7 psia

Oxidizer	Fuel	I_{opt}	r	T_c	d	C*
LOX ★	★ H_2	389.4	4.13	4964	0.29	7927
	★ H_2-Be 49/51 ■	459.0	0.87	4636	0.23	9293
	★ CH_4	309.6	3.21	5900	0.82	6091
	▲ C_2H_6	306.7	2.89	6008	0.90	6038
	▲ C_2H_4	311.5	2.38	6307	0.88	6150
	■ RP-1	300.1	2.58	6157	1.03	5902
	■ N_2H_4	312.8	0.92	5669	1.07	6207
	■ B_5H_9	318.8	2.12	6933	0.92	6218
	▲ B_2H_6	341.9	1.96	6312	0.74	6696
	★ CH_4/H_2 92.6/7.4	319.0	3.36	5873	0.71	6298
GOX ★	■ GH_2	407.9	3.29	4669	-	8366
F_2 ★	★ H_2	411.8	7.94	6672	0.46	8385
	★ H_2-Li 65.2/34.0 ■	434.3	0.96	3326	0.19	8792
	★ CH_4	348.4	4.53	7084	1.03	6786
	■ C_2H_6	340.3	3.68	7077	1.09	6624
	■ MMH	348.3	2.39	7365	1.24	6769
	■ N_2H_4	365.3	2.32	8062	1.31	7281
	■ NH_3	360.3	3.32	7839	1.12	7199
	■ B_5H_9	357.3	5.14	9122	1.23	7045
OF_2 ▲	★ H_2	409.6	5.92	5992	0.39	8341
	★ CH_4	355.6	4.94	7515	1.06	7085
	▲ C_2H_6	358.3	3.87	8202	1.13	7140
	■ RP-1	349.4	3.87	8017	1.28	6994
	■ MMH	349.7	2.28	7367	1.24	6952
	■ N_2H_4	345.0	1.51	6816	1.26	6848
	■ BA1185	335.3	1.75	6739	1.24	6843
	▲ B_2H_6	372.8	3.95	8094	1.01	7363
	■ B_5H_9	361.1	4.16	8717	1.20	7096
FLOX ★ 30/70	★ H_2	395.0	4.80	5349	0.32	8049
FLOX ■ 30/70	■ RP-1	316.6	3.01	6629	1.09	6260
FLOX ■ 70/30	■ RP-1	344.6	3.84	7882	1.20	6910
FLOX ■ 87.8/12.2	■ MMH	359.7	2.82	8049	1.24	7188
N_2F_4 ▲	★ CH_4	319.1	6.44	6701	1.15	6289
	▲ C_2H_4	309.7	3.67	6766	1.13	6051
	■ MMH	322.8	3.35	6906	1.32	6325
	■ N_2H_4	335.0	3.22	7617	1.38	6755
	■ NH_3	326.9	4.58	7344	1.22	6627
	■ B_5H_9	332.5	7.76	8656	1.34	6551
CLF_5 ■	■ MMH	302.2	2.82	6470	1.40	6027
	■ N_2H_4	313.2	2.66	7041	1.47	6350
	■ MHF_3	303.2	2.78	6467	1.41	6049
	■ MHF_5	305.0	2.46	6723	1.46	6114
CLF_3 ■	■ MMH	284.6	2.97	6165	1.42	5706
	■ N_2H_4	294.4	2.81	6602	1.49	5985
N_2O_4 ■	■ MMH	288.5	2.17	5652	1.19	5726
	■ MMH-BE 76.6/29.4	316.9	0.99	5779	1.17	6096
	■ MMH-AL 63.0/27.0	295.0	0.85	5961	1.27	5855
	■ N_2H_4	292.0	1.36	5418	1.21	5843
	■ N_2H_4-UDMH 50/50	288.9	1.98	5603	1.12	5731
	■ N_2H_4-BE 80/20	327.4	0.51	5500	1.20	6293
	■ B_5H_9	298.7	3.18	6653	1.11	5848
MON-25 ■	■ MMH	289.7	2.28	5707	1.17	5751
	■ N_2H_4	293.1	1.43	5473	1.19	5862
IRFNA (III-A) ■	■ Hydyne	269.2	3.26	5158	1.30	5339
	■ MMH	274.5	2.59	5160	1.27	5464
	■ UDMH	272.2	3.13	5205	1.26	5406
IRFNA (IV, HDA) ■	■ Hydyne	274.4	3.06	5358	1.32	5432
	■ MMH	279.8	2.43	5347	1.29	5563
	■ UDMH	277.4	2.95	5401	1.28	5498
H_2O_2 ■	■ MMH	284.7	3.46	4928	1.24	5663
	■ N_2H_4	286.7	2.05	4804	1.24	5745
	■ N_2H_4-Be 74.5/25.5	335.6	0.48	5279	1.21	6375
	■ B5H9	307.8	2.20	4833	1.02	5996
N_2H_4 ■	★ B_2H_6	341.0	1.16	4048	0.63	6823
	■ B_5H_9	326.9	1.27	4426	0.80	6432

Vacuum Expansion, P_c = 1,000 psia → ε = 40

Oxidizer	Fuel	I_{vac}	r	T_c	d	C*
LOX ★	★ H_2	455.3	4.83	5392	0.32	7828
	★ H_2-Be 49/51 ■	540.3	0.91	4692	0.24	9350
	★ CH_4	368.9	3.45	5954	0.83	6030
	▲ C_2H_6	365.7	3.10	6064	0.91	5986
	▲ C_2H_4	370.9	2.59	6370	0.89	6085
	■ RP-1	358.2	2.77	6202	1.03	5850
	■ N_2H_4	353.1	0.98	5695	1.07	6162
	■ B_5H_9	383.5	2.16	6985	0.92	6215
	▲ B_2H_6	409.8	2.06	6445	0.75	6689
	★ CH_4/H_2 92.6/7.4	379.5	3.63	5949	0.72	6224
GOX ★	■ GH_2	457.7	3.92	5184	-	8263
F_2 ★	★ H_2	479.3	9.74	7205	0.52	8301
	★ H_2-Li 60.7/39.3 ■	515.3	1.08	3585	0.21	8714
	★ CH_4	415.8	4.74	7111	1.04	6773
	■ C_2H_6	406.8	3.78	7093	1.10	6607
	■ MMH	415.4	2.47	7396	1.24	6520
	■ N_2H_4	430.1	2.37	8074	1.31	6963
	■ NH_3	422.8	3.35	7846	1.12	7196
	■ B_5H_9	427.7	5.58	9181	1.25	7020
OF_2 ▲	★ H_2	477.4	7.37	6489	0.44	8198
	★ CH_4	421.5	5.58	7605	1.09	7017
	▲ C_2H_6	422.1	3.86	8200	1.13	7139
	■ RP-1	410.3	3.85	8010	1.28	6989
	■ MMH	415.0	2.58	7471	1.26	6909
	■ N_2H_4	409.0	1.65	6897	1.27	6828
	■ BA1185	398.8	1.92	6816	1.25	6621
	▲ B_2H_6	445.6	3.98	8107	1.02	7109
	■ B_5H_9	432.5	4.30	8751	1.21	7090
FLOX ★ 30/70	★ H_2	461.2	5.70	5783	0.36	7930
FLOX ■ 30/70	■ RP-1	377.2	3.30	6677	1.10	6198
FLOX ■ 70/30	■ RP-1	403.6	3.84	7881	1.20	6904
FLOX ■ 87.5/12.5	■ MMH	423.3	2.83	8047	1.23	7172
N_2F_4 ▲	★ CH_4	376.7	6.51	6705	1.15	6282
	▲ C_2H_4	368.6	3.71	6769	1.14	6046
	■ MMH	380.6	3.39	6913	1.32	6318
	■ H_2H_4	390.5	3.25	7621	1.38	6751
	■ NH_3	379.9	4.58	7343	1.22	6629
	■ B_5H_9	397.8	8.31	8677	1.35	6535
CLF_5 ■	■ MMH	355.9	2.83	6474	1.40	6027
	■ N_2H_4	365.3	2.71	7061	1.47	6346
	■ MHF_3	356.9	2.81	6474	1.41	6050
	■ MHF_5	357.1	2.49	6732	1.46	6112
CLF_3 ■	■ MMH	334.1	3.01	6175	1.42	5706
	■ N_2H_4	342.4	2.89	6631	1.50	5977
N_2O_4 ■	■ MMH	341.5	2.37	5657	1.20	5657
	■ MMH-Be 70.8/29.2	379.6	1.10	6244	1.21	6066
	■ MMH-AL 58/42	353.1	0.87	6242	1.31	5810
	■ N_2H_4	343.8	1.42	5419	1.22	5808
	■ N_2H_4-UDMH 50/50	341.7	2.15	5605	1.20	5679
	■ N_2H_4-Be 76.6/23.4	392.8	0.60	5846	1.22	6277
	■ B_5H_9	358.5	3.26	6703	1.11	5842
MON-25 ■	■ MMH	342.9	2.50	5716	1.18	5682
	■ N_2H_4	345.0	1.51	5479	1.20	5825
IRFNA (III-A) ■	■ Hydyne	318.7	3.41	5142	1.31	5304
	■ MMH	324.3	2.71	5145	1.28	5429
	■ UDMH	322.1	3.31	5187	1.27	5361
IRFNA (IV, HDA) ■	■ HYDYNE	325.2	3.25	5344	1.33	5385
	■ MMH	330.8	2.58	5337	1.31	5512
	■ UDMH	328.6	3.12	5391	1.29	5452
H_2O_2 ■	■ MMH	336.8	3.69	4905	1.24	5623
	■ N_2H_4	337.6	2.12	4793	1.25	5723
	■ N_2H_4-Be	403.5	0.57	5608	1.24	6364
	■ B_5H_9	371.6	2.09	4707	1.01	5961
N_2H_4 ■	★ B_2H_6	403.4	1.16	4048	0.63	6823
	■ B_2H_9	389.7	1.27	4426	0.80	6431

BA1185: 50.5% MMH, 29.8% N_2H_4, 19.7% H_2O
MHF-3: 86% MMH, 14% N_2H_4
MHF-5: 55% MMH, 26% N_2H_4, 19% $N_2H_5NO_3$
MON-25: 25% NO, 75% N_2O_4

HYDYNE: 60% UDMH, 40% DETA
IRFNA III-A: 83.4% HNO_3, 14% NO_2, 2% H_2O, 0.6% HF
IRFNA IV HDA: 54.3% HNO_3, 44% NO_2, 1% H_2O, 0.7% HF
RP-1: MIL-P-25576C

5245-422

Table 1-5 General data on some storable liquid rocket propellants.

Propellant	Formula	Use	Mol. (wt)	Freezing Point (°F)	Boiling Point (°F)	Vapor Pressure (psia)	Density gm/cc	Stability	Handling Hazard	Storability	Materials Compatibility
Aniline	$C_6H_5NH_2$	Fuel, coolant	93.2	21	364	0.25 at 160°F	1.022 at 68°F	Good	Good	Good	Al., steel, Teflon, Kel-F
Bromine pentafluoride	BrF_5	Oxid., coolant	174.9	-80.5	104.5	41 at 160°F	2.48 at 68°F	Up to 800°F	Reacts with fuel	Good	Al., alloy, 18-8 stainless steel, nickel alloy, copper, Teflon
Chlorine trifluoride	ClF_3	Oxid.	92.5	-105.4	53.15	80 at 140°F	1.825 at 68°F	Up to 600°F	Toxic	Good below 140°F	Al., alloy, 18-8 stainless steel, nickel alloy, copper, Teflon
92.5% E.A. (ethyl alcohol)	C_2H_5OH	Fuel, coolant	41.25	-189	172	13 at 160°F	0.81 at 60°F	Good	Flammable	Good below 130°F	Al., steel, nickel alloy, Teflon, Kel-F, polyethylene
Hydrazine	N_2H_4	Fuel, oxid., coolant	32.05	34.5	235.4	2.8 at 160°F	1.01 at 68°F	Up to 300°F	Toxic, flammable	Good	Al., 304.307 stainless steel, Teflon, Kel-F, polyethylene
95% hydrogen peroxide	H_2O_2	Monoprop., oxid., coolant	32.57	21.9	294.8	0.05 at 77°F	1.414 at 77°F	Unstable decomposition at 285°F	Hazardous skin contact, flammable	Deteriorates at 1%/yr	Al., stainless steel, Teflon, Kel-F
98% hydrogen peroxide	H_2O_2	Same as above	33.42	27.5	299.2	0.043 at 77°F	1.432 at 77°F	Same as above	Same as above	Same as above	Same as above
Hydyne (40% "Deta" 60% "UDMH")	$NH(C_2H_4NH_2)_2$, $(CH_3)_2NNH_2$	Fuel, coolant	72.15	-65	140 to 400	16.5 at 60°F	0.855 at 60°F	Good	Toxic	Good	Al., stainless steel, Teflon, Kel-F
IFRNA (inhibited red fuming nitric acid)	82% HNO_3, 15% NO_2, 2% H_2O, 1% HF	Oxid., coolant	55.9	-57	150	17.3 at 160°F	1.57 at 68°F	Good	Toxic, hazardous skin contact	Good	Al., stainless steel, Teflon, Kel-F, polyethylene
JP-4 (jet propulsion fuel)	$C_{9.66}H_{19}$	Fuel, coolant	128	-76	270 to 470	7.2 at 160°F	0.747 to 0.825 at 60°F	Good	Vapor explosive	Good	Al., steel, nickel alloy, neoprene, Teflon, Kel-F
MMH (monomethylhydrazine)	$CH_3NH\text{-}NH_2$	Fuel, coolant	46.08	-63	187	8.8 at 160°F	0.878 at 68°F	Good	Toxic	Good	Al., 304.307 stainless steel, Teflon, Kel-F, polyethylene
Nitrogen tetroxide	N_2O_4	Oxid.	92.02	11	70	111 at 160°F	1.44 at 68°F	Function of temp.	Very toxic, hazardous skin contact	Good when dry	Al., stainless steel, nickel alloy, Teflon
Pentaborane	B_5H_9	Fuel	63.17	-52.28	140.11	19 at 160°F	0.61 at 68°F	Good	Explosive on exposure to air, very toxic	Good	Al., steel, copper, Teflon, Kel-F, Viton A
Propyl nitrate	$C_5H_7NO_3$	Fuel, coolant	105.09	-130.9	231	3.7 at 160°F	1.06 at 68°F	Fair	Sensitive to shock	Good	Al., stainless steel, Teflon, Kel-F
RP-1 (rocket propellant)	Mil-Spec-F25576B	Fuel, coolant	165 to 195	-47 to -64	342 to 507	0.33 at 160°F	0.8 to 0.82 at 68°F	Auto. ignition at 470°F	Flammable	Good	Al., steel, nickel alloy, copper, Teflon, Kel-F, Neoprene
TEA (triethylaluminum)	$(C_2H_5)_3Al$	Fuel, start compound	114.15	-49.9	381	0.40 at 160°F	0.836 at 68°F	Decomp. over 400°F	Ignites on contact with air	Good	Al., steel, copper, Teflon
TMA (trimethylamine)	$(CH_3)_3N$	Fuel	59.11	-179	37	108 at 160°F	0.603 at 68°F	Good	Good	Good	Al., steel, copper, Teflon
TMB-1, 3-D (NNN'-N'-tetramethylbutane-1, 3-diamine)	$(CH_3)_2N\text{-}CH_2CH_2\text{-}CH\text{-}N(CH_3)_2CH_3$	Fuel, coolant	144.2	-131	320	1.32 at 160°F	0.795 at 68°F	Stable 1 h at 500°F	--	Good	Al., 347 stainless steel, polyethylene
TNM (tetranitromethane)	$C(NO_2)_4$	Oxid.	196.04	57.3	259	2.38 at 165°F	1.64 at 68°F	Thermal unstable	Shock sensitive	Good below 100°F	Al., mild steel, Teflon, Kel-F
UDMH (unsymmetrical dimethylhydrazine)	$(CH_3)_2NNH_2$	Fuel, coolant	60.08	-72	146	17.6 at 160°F	0.789 at 68°F	Good	Toxic	Good	Al., stainless steel, Teflon, Kel-F
WFNA (white fuming nitric acid)	97.5% HNO, 2% H_2O, 0.5% NO_2	Oxid., coolant	59.9	-45	186	9.09 at 160°F	1.46 to 1.52 at 68°F	Decomp. above 100°F	Toxic, hazardous skin contact	Fair	Al., stainless steel, Teflon, Kel-F, polyethylene

Table 1-6 General data on some cryogenic liquid rocket propellants.

Propellants	Formula	Use	Mol. wt.	Freezing Point, °F	Boiling Point, °F	Critical Press., psia	Critical Temp., °F	Density at Boiling Point bm/cc	Stability	Handle Hazard	Materials Compatibility
Ammonia	NH_3	Fuel, coolant	17.03	-108	-28			0.683	Good	Toxic, flammable	Al., steel, lead, Teflon, Kel-F, Vitron A
Liquid fluorine	F_2	Oxid.	38.00	-364	-307	808	-200.5	1.509	Good	Very toxic, flammable	Al.m, 300 series stainless steel, nickel alloy, brasses
Liquid hydrogen	H_2	Fuel, coolant	2.016	-434.6	-422.9	187.8	-400.3	0.071	Good	Flammable	Stainless steel, nickel alloy, Al. alloy, Kel-F
Liquid oxygen	O_2	Oxid.	32.00	-362	-297 4	735	-182	1.142	Good	Good	Al., stainless steel, nickel alloy, copper, Teflon, Kel-F
Oxygen difluoride	OF_2	Oxid.	54.00		-299	719	-72.3	1.521	Good	Very toxic, flammable	Al., 300 series stainless steel, nickel alloy, brass
Ozone	O_3	Oxid	48.00	-420	-168	804	10.2	1.460	Above 20% explosive	Very toxic, flammable	Al., 300 series stainless steel, Teflon, Kel-F

propellant (liquid, gas or solid), temperature at which energy level is calculated (heat of formation), chamber pressure, and mixture ratio.

Computed-program outputs include the following data for both combustion chamber and expansion nozzle: pressure, temperature, molecular weight, gas specific heat ratio, Mach number, enthalpy, entropy, density, sonic velocity, area ratio, species list and concentrations, and C*, C_f and I_s.

Three approaches are taken to describe the theoretical gas-expansion characteristics within the chamber and expanding nozzle: frozen, equilibrium, and kinetics.

The flow process is considered to be "frozen" when the gas composition does not change from the chamber to the nozzle exit. The flow process is considered to be in "equilibrium" if the gas composition does change between the chamber and nozzle exit. Equilibrium expansion represents the highest level for energy release. Equilibrium performance is calculated to be a higher value because the reactions are reversible. The energy-consuming dissociated species recombine in the nozzle and add to the chemical energy release for the system.

Real-gas expansion is controlled by finite-rate chemistry. A shift occurs in the equilibrium process during expansion, the amount of shift governed by residence time, temperature, and pressure for the expanding gases. Kinetic performance losses occur because the chemical reactions are not fully reversible. A lesser amount of recombination occurs in the nozzle. Special computer programs are used to deter-mine the "kinetic" maximum for performance. They are part of the TDK package.

The delivered values for C*, C_f and I_s are reduced from the theoretical values owing to the losses described in the JANNAF performance section, in the following degrees: incomplete combustion (0-5%), reaction kinetics losses (0-8%), nozzle-divergence losses (0-5 %), and boundary-layer drag losses (0-3 %). In practice it has been found that actual test results for total delivered I_s is usually 3-12% lower than the theoretical values, depending on thrust, chamber-pressure, and propellant combination. Table 1-4 shows the relative performance of a large number of propellant combinations. Physical properties of important liquid monopropellants and bipropellants are given in Tables 1-5 and 1-6.

Engine Requirements and Preliminary Design Analyses

2.1 INTRODUCTION

A liquid-propellant rocket engine converts the chemical energy contained in tanks into a propulsive force that will propel the vehicle and payload from one place to another. The most encompassing design goal for the rocket engine(s) is to meet all of the mission requirements at the least mission life-cycle cost. Desired characteristics of a rocket engine include high thrust-to-weight ratio and high thrust per unit of flowrate (specific impulse, I_S). High specific impulse and high thrust-to-weight can lead to lower cost per pound of payload in orbit. Simplicity, robustness, and reliability of the power-cycle components are important links in establishing overall vehicle reliability, maintenance, and life (which have a direct effect on system life-cycle cost). Besides high performance (specific impulse and weight)—a requirement of paramount importance for attainment of mission goals—they too will be very desirable requirements for the engine system and its components.

The tasks of engine preliminary design and optimization are the judicious selection of components and component arrangements so that all the desired qualities enumerated above can be fully refined and mission goals satisfied with minimum investment and risk. This process begins with an initial optimization of an engine cycle configuration that meets a set of vehicle/engine requirements outlined by the customer. Component specifications established from this initial process are then scrutinized by specialists. The succeeding optimizations and refinements aim to endow the engine system with all the desired characteristics.

In the first step of preliminary design (Fig. 2-1), the vehicle requirements are used to establish a large number of the engine requirements. These, together with candidate component definitions, are then used to scope possible engines within reasonable technology limitations. With an approach decided upon, the preliminary design process can begin in earnest, first on the engine and then including the components that make it up. This requires some iteration and feedback because the engine is needed to define the components but, at the same time, it is made up of the components. A reasonable guess of the component characteristics will be needed in the beginning to describe the engine preliminary design so that its characteristics may be obtained. From these, the component characteristics are refined through a process of optimization and iteration. Detailed component design then follows.

The following discussion presents the sequence of considerations in preliminary design process. First, the major rocket-engine design parameters that are typically required by the vehicle are defined. Next, the requirements of various missions are discussed. These requirements dictate the features and goals that are to be emphasized during the design process. This leads into typical optimizations to meet mission requirements. Next comes selection of the optimum engine components. Some advanced engine component concepts will be discussed, and then some of the procedures used to optimize them reviewed. The section concludes with discussion of design philosophy and considerations to be kept in mind during the entire design process. This leads into the sample engine concepts and designs presented in Chapter 3 and the component concepts, designs, and integration presented in the remainder of the text.

2.2 MAJOR ROCKET-ENGINE DESIGN PARAMETERS

To configure the engine system properly with a vehicle, design and development specifications will have to cover the following parameters above all: thrust level, performance (specific impulse), run duration, propellant mixture ratio, weight of engine system at burnout, envelope (size), reliability, cost, and availability (time table-schedule).

As the design progresses, numerous additional parameters will have to be considered. Before turning to them, we briefly review and discuss those listed above. It should be noted that the last five items are closely interdependent. For instance, making an engine available in the shortest possible time

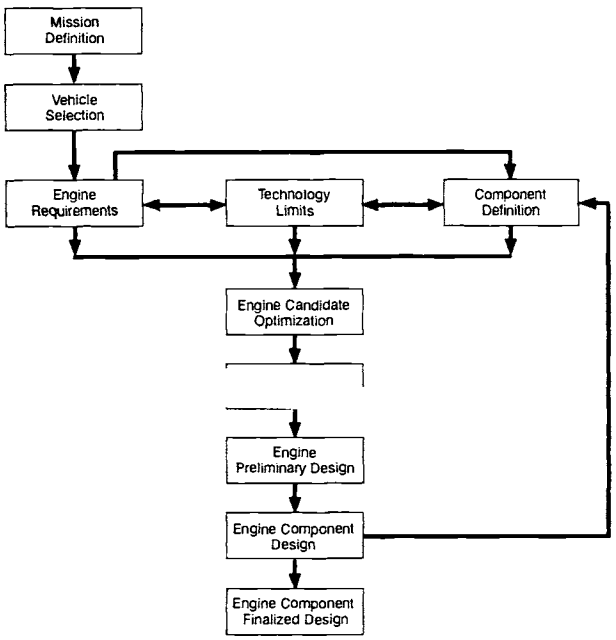

Fig. 2-1 Flowchart for rocket-engine preliminary design.

("crash program") will raise the cost and will unfavorably affect reliability. A longer design and development period may not necessarily reduce cost, but it will offer higher values in exchange for the dollar—higher reliability, refined (lower) weight, and an optimized (smaller) envelope.

Thrust Level

This engine parameter, a basic one, similar to the power rating of a gasoline engine or electric motor, will affect most of the other engine parameters and many of the development considerations.

The total thrust required of a rocket-propelled vehicle will predominantly be governed by the total takeoff weight of the vehicle (including engine) and the minimum and maximum accelerations permissible. The number of engines to be used decides the proper engine thrust level. This decision is often strongly influenced by the availability of already existing engines, which would eliminate, or at least drastically reduce, the design and development cost for the propulsion system. The selection of individual engine thrust level also is–or at least should be–influenced by the general state of the art, particularly if sizes substantially larger than previously developed are considered.

More recently, largely as a result of the advent of manned rocket flight and of the high cost of very large vehicle systems, the decision to use a many-engined (clustered) propulsion system has been additionally affected by safety considerations, to permit mission completion, or at least safe return of the crew, in case of an engine failure. This "engine out" principle is analogous to the consideration of multiple- vs. single-engine airplanes. Extensive studies have been conducted on rocket vehicles to establish the "break-even" point regarding the minimum and maximum number of engines profitably employed in a cluster. Failure of single-engined rocket vehicles not only might destroy the vehicles but also could cause severe damage to expensive ground facilities. This explains the great emphasis placed on thrust subdivision.

Thrust levels for first-stage booster engines, which start at or near sea-level altitude and stop at a specified higher altitude, are usually quoted for sea-level conditions. Additionally, the specifications may contain information on thrust level at altitudes above sea level, frequently in the form of a graph (see Fig. 2-2). The nominal thrust of engines in stages starting and operating at or near vacuum conditions is quoted for that environment. Most engines are designed for a single nominal thrust (sea level or altitude), for which they are calibrated by means of propellant-line orifices or, less frequently, with the aid of regulators. Engines designed for variable thrust (throttling) always require some type of regulator. This will be discussed further in Chapter 7.

Performance

Although the general term "performance" of a rocket engine in the strict sense covers a number of parameters (I_S, c^*, C_f, etc.), specific impulse (I_S) is considered the prime performance parameter. As was seen in Chapter 1, specific impulse, also referred to as specific thrust, is measured in "seconds" (not the dimension of time, but an abbreviation of the dimension lb-s/lb; lb/(lb/s) means (specific thrust). It is important to state whether a specified value of I_S refers to the complete engine system or to the thrust chamber only. Frequently, by stating a percentage an "actual" or "practical" value of I_S is linked to the maximum value theoretically possible. The theoretical values for the better-known propellant combinations are well established, and as a result practical values have become quite predictable. Combinations less well-known have often produced disappointments. Great caution should be exercised in the use of theoretical values that have not been verified in tests.

In recent years, the performance of a rocket engine, as expressed by its specific impulse, has received considerable attention, far beyond its true significance. In June 1959, Theodore von Karman observed:

> *It is my personal belief that the length of the period of attaining reasonable reliability in the development process could be essentially reduced if simple design were emphasized as a leading principle, even if we had to make some sacrifice in the quantitative measure of "efficiency." Essential elements have to be designed as simply as possible, even if this means a reduction in quantitative efficiency and a certain increase of bulkiness and/or weight.*

Undoubtedly, his observations were prompted by a noticeable trend on the part of both the engine builder and the customer to sacrifice, or at least to compromise, nearly all other capabilities of a rocket propulsion system for I_S increases, which sometimes amounted to less than one percent.

Frequently, increasing emphasis on I_S during the life of a project can be traced to marginal engineering reserves in the initial vehicle design, especially with weight assumptions and tank capacities. The need for competitive bidding may have contributed to this situation.

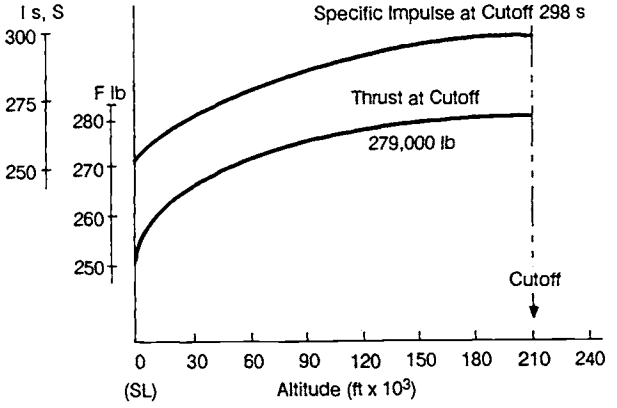

Fig. 2-2 Typical rocket-engine performance vs. altitude.

On the other hand, the highest I_s that can be obtained *without compromise* will pay off substantially. For instance, in the case of a typical medium-range ballistic missile, an increase of one second in I_s will increase range approximately 15 n. mi. In other terms, an I_s increase of less than one-half percent will increase range one percent. As impressive as these figures for increased flight range are, it should be kept in mind that I_s should not compromise other engine properties that will determine whether the vehicle will fly at all .

Moreover, I_s will prove more critical in some applications than others. In a three-stage vehicle, for example, I_s is more critical for the third stage than the second, and it is more critical for the second than for the first. A pound of propellant in the third stage is a pound of *payload* for the second stage, and therefore requires additional second-stage propellant to lift it, and so on. (This weight multiplication with stage number is discussed in more detail later.) The result: more will be gained by maximizing I_s for an upper stage than for a lower. Likewise, there is more benefit in maximizing I_s for a high-velocity mission than for a low-velocity one.

Duration

Because, by definition, a rocket vehicle carries its own propellant supply, including the oxidizer, its run duration will reflect an optimized balance among takeoff weight, trajectory, thrust level, and minimum and maximum accelerations. Consequently, run-duration times of most large liquid-propellant rocket engines fall into a relatively narrow band, about 50 to 400 s (except for the Space Shuttle Main Engine, which operates for 500 s, over both the periods of solid-propellant booster operation and the period to orbit after booster separation).

User specifications include formal demonstration (such as preliminary flight rating tests [PFRT] and qualification tests) requiring accumulated engine firing times, without breakdown, of many times the comparatively short-rated flight duration. These specifications therefore govern most engine design considerations, with the exception of the following areas, which for weight considerations are tailored to the flight-run duration:

- Auxiliary tank capacity, for systems which employ a separate turbine power supply.
- Propellant-tank pressurization supply, if it is part of the engine system.
- Lube-oil tank capacity, if applicable.
- Temperature nonequilibria, such as those of uncooled nozzles.

Closely related to the run duration are the start and shutdown characteristics of an engine system, the requirements for both of which may be very stringent in a given vehicle system. The characteristics and the quality of the "start," or "thrust buildup," of a liquid-propellant rocket engine are judged by the following factors:

- Compliance with specified thrust-vs.-time characteristics.
- Maximum rate of increase at any time during buildup.
- Freedom from surges and thrust overshoots.
- Smoothness (freedom from damaging oscillations).
- Repeatability from run to run and from engine to engine.

These characteristics will be discussed in greater detail in Chapter 10, "Engine Systems Design Integration." Suffice it to state at this point that a rocket engine is not easy to adapt to special thrust-buildup requirements. Difficulties in this area can arise from inadequate communication between vehicle and the engine contractors. Both must thoroughly understand the problems.

The characteristics of engine "shutdown" or "thrust decay" are predominantly influenced by guidance considerations. To understand this better, consider the case of a single-stage, ground-to-ground ballistic missile. As the term "ballistic" implies, the missile imparts a desired speed to a known payload, in a desired direction from a desired point, after which the payload coasts freely to the target. This is analogous to a cannon, where muzzle exit velocity of the projectile, gun-barrel attitude, and location of the gun emplacement will determine the point of impact (neglecting environmental influences such as wind). With a ballistic rocket, the gun barrel is literally replaced by the guidance system, the intricate components of which not only predetermine the three basic parameters mentioned but also have the ability to compensate for deviations of any or all of them. If, for instance, the trajectory angle near the point of cutoff is too steep, the guidance system will compensate accordingly, by calling for a higher final velocity, by slightly delaying the cutoff signal, simultaneously considering the distance over ground already covered.

It is obvious that a prompt and repeatable execution of the cutoff signal is imperative. For several reasons, however, it is impossible to effect an instantaneous thrust cessation: time is required to sense and then transmit the cutoff signal; closing of valves requires a finite time; structural (hydraulic-hammer) considerations are superimposed; residual propellants below the valves have an effect. Figure 2-3 shows a typical thrust-decay diagram. Recall this expression:

$$Ft = m\Delta v \tag{2-1}$$

Thrust multiplied by time equals mass times velocity increase:

$$\Delta v = \frac{Ft}{m} \tag{2-2}$$

The velocity increase following cutoff signal is a function of the residual thrust acting on the vehicle mass m, and is integrated over the time from cutoff signal to thrust cessation; this integral is commonly

referred to as the "cutoff impulse." A typical value for a well-known earlier rocket (Redstone) was 16,000 lb-s ±2500 lb-s. Note the tolerance. This deviation will obviously influence missile accuracy. Reduction of the tolerance is thus an important design and development goal.

It might be concluded that a substantial reduction of the tolerance is the principal task, zero deviation being the optimum. This is unfortunately not so because the final vehicle mass m, on which the decaying thrust force acts, is unpredictable within certain limits, due to weighing tolerances of the initial vehicle mass and to flow-rate and mixture-ratio tolerances. The engine designer and developer will have to concentrate on reducing both: base value and tolerance.

A glance at Fig. 2-3 will show that the area under the thrust curve is a function of not only decay time but also of main-stage thrust level. In fact, the major portion of the shaded area is accumulated before the beginning of thrust decay. This observation has led to the utilization of vernier thrust systems. A vernier cutoff system is characterized by a substantial thrust reduction before cutoff. This can be accomplished by thrust reduction, for a few seconds, of the main engine itself (V-2 fashion) or by shutdown of the main engines, while much smaller engines continue for a brief period (typical: 0-25 s, depending on final ΔV required).

It should be emphasized that any components that must be added to improve cutoff characteristics are basically undesirable; for they will drastically increase engine complexity. The addition of such components should be avoided at all costs. Here again, close coordination becomes vital between the vehicle (guidance) designer and engine designer; thorough understanding of their common problems will be vital.

Mixture ratio

Stoichiometric mixture ratio depends on the type of propellant used. Theoretical temperature and heat release are maximum at this ratio. In rocket engines,

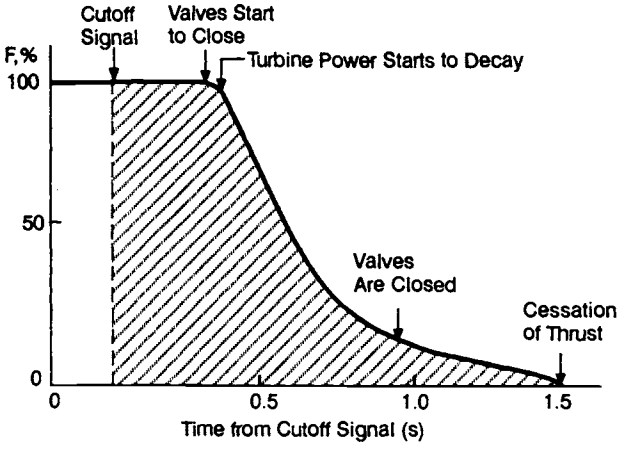

Fig. 2-3 Typical thrust-decay diagram.

however, where the highest possible exhaust velocity is desired, optimum conditions often prevail at other than stoichiometric ratios. Equation (1-18) indicates that the gas properties strongly affect exhaust velocity. The expression for the specific gas constant R in Eq. (1-18) may be rewritten as follows:

$$R = \frac{R'}{M} \tag{2-3}$$

where R' is the universal gas constant and M is the molecular weight of the gas (see Table 1-1). The lower the molecular weight, the higher the exhaust velocity, other things being equal. Analytical and experimental investigations will determine the optimum balance between energy release (heat) and composition (molecular weight) of the gas, a portion of which will consist of gasified but unburnt propellants. The optimum point may also be affected by the following:

- *Stay time of the burning gas in the combustion chamber.* Stay time is a function of combustion-chamber volume and of gas volumetric flow rate. Complete combustion, even though desirable, requires a finite time, which will not be available unless the chamber is relatively large, and correspondingly heavy. A compromise in chamber size, therefore, is often made. This leaves unburned a small percentage even of the propellants entering the nozzle, propellants which could have burned given sufficient time (chamber volume). This percentage must be considered for accurate determination and optimization of the composition of the combustion gases and when optimizing the gas properties with energy release and system weight.

- *Cooling considerations.* The temperatures resulting from stoichiometric or near-stoichiometric mixture ratios, dependent on propellant type, may impose severe demands on the chamber-wall cooling system. A lower temperature may therefore be desired, and can be obtained by selecting a suitable ratio.

- *Propellant density.* Propellant density can make it profitable to deviate from the mixture ratio that yields optimum specific impulse. For example, in the case of the LOX/LH_2 propellant combination, where the density of the oxidizer is 16 times that of the fuel, vehicle manufacturers prefer to sacrifice some engine performance to obtain smaller tanks, and thus lower overall system weight. Typically, an engine mixture ratio of 6 is used for LOX/LH_2, rather than the optimum I_S mixture ratio of approximately 4.5.

Once the optimum mixture ratio has been determined for a given engine system, based on the major factors just discussed, it is obvious that deviations from it will penalize engine performance. Since the vehicle powered by an engine will have been sized and tanked to conform with the specified

engine mixture-ratio, it is important to know that deviations will also lower vehicle performance—cut run time, owing to premature exhaustion of one of the propellants, and reduce mass ratio, owing to excessive residual amounts of the other propellant (increased burnout weight). Since the relationship between engine performance (I_s) and mixture ratio for many systems is usually relatively flat near the optimum point (Fig. 2-4), the effects from duration and burnout weight may well be the most influential ones for vehicle range.

The effects of even minor discrepancies in mixture ratio during the rocket-engine operating time (propellant utilization) are substantial. In a typical single-stage medium-range ballistic missile, for example, each pound of excess burnout weight will decrease range approximately 0.2 n. mi. For long-range vehicles, the penalty is still higher. Active mixture-ratio-control systems have been utilized on systems such as the Atlas that are highly sensitive to residual-propellant effects.

Weight

The parameter of weight, as no other, dominates the thinking of rocket engineers. Success is often gaged directly in pounds of payload flown per dollar spent. The importance weight rightfully carries does not necessarily mean that it is all-important. For instance, a somewhat smaller payload placed into orbit more reliably, or at a lower cost per pound, may be preferred.

As we have seen earlier, a vehicle's final velocity is a function of, among other parameters, its mass ratio. The smaller the final mass, the higher the final velocity. However, since payload mass should be as high as possible, the weight squeeze is applied to all vehicle components which are not payload. This includes the engine.

To isolate the influence of vehicle structural weight, engineers use a parameter called "propellant fraction." This factor expresses the ratio of the total propellant weight to the fueled vehicle weight without payload. Typical values are 0.94 for turbopump-fed systems and 0.89 for pressure-fed systems. For turbopump-fed engines, the ratio of thrust to engine weight is another useful yardstick. Larger modern liquid-propellant rocket engines may fall into a range from 75 to 125 lb of thrust per pound of engine weight. These figures represent a substantial progress over the past (see Fig. 2-5).

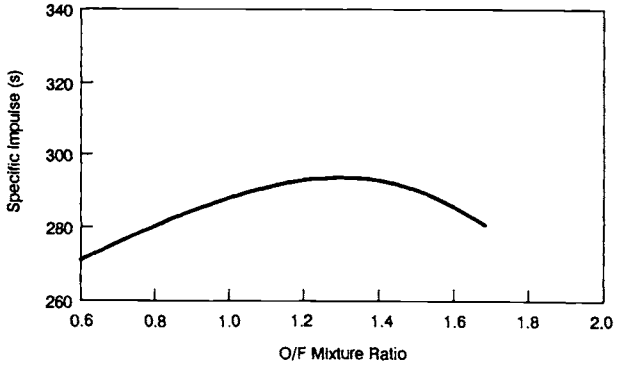

Fig. 2-4 Theoretical thrust-chamber performance vs. mixture ratio for N_2O_4/N_2H_4. At pc - 1000 psia shifting equilibrium and optimum sea-level expansion.

Appendix A presents a more detailed discussion of the various facets of rocket-engine weight and its interaction with the vehicle. Included are considerations of dry weight, wet weight, propellant weight, residual-propellant weight, and payload weight as well as the influence of structural weight on propellant weight, and the tradeoffs between weight and burnout velocity and between weight and required performance.

Envelope (size)

The linear dimensions of liquid-propellant rocket engines require relatively elaborate description and frequently cannot be made clear without a drawing. When only approximate values are required for comparison or for overall estimates, engineers use the term "envelope". For instance, definition of a hypothetical smallest cylinder, cube, or sphere into which the engine would fit conveys a good feeling of engine size or bulkiness.

Obviously, engine size directly affects engine weight (Fig. 2-5). Increasing engine size also directly affects numerous other areas, such as these:

- The vehicle structure becomes heavier, especially with upper stages. Engine size directly affects the size and thus weight of the aft end and/or interstage structure.
- Handling equipment and procedures become more costly.
- Servicing becomes more difficult.
- Manufacturing machinery becomes larger.
- Storage and transportation means become more bulky.

Several of these areas present a definite upper limit, such as railroad tunnel sizes, clearances on bridges and underpasses, and available machine tools.

For a given chamber pressure, thrust-chamber expansion area ratio has a very pronounced effect on engine envelope. When optimizing the thrust-chamber expansion area ratio, which is also influenced by performance, weight, pressure drop, heat transfer, and other considerations, its effect on envelope, and thus on other vehicle systems, must be considered.

Reliability

Reliability has become almost a branch of science by itself, engaging, in addition to the designer, development engineer, and user, mathematicians, statisticians, and "human factor" and "man-rating" specialists. Numerous books have been written on the subject and manufacturers maintain entire groups to predict, monitor, tabulate, and evaluate the reliability of their products. The advent of manned space flight

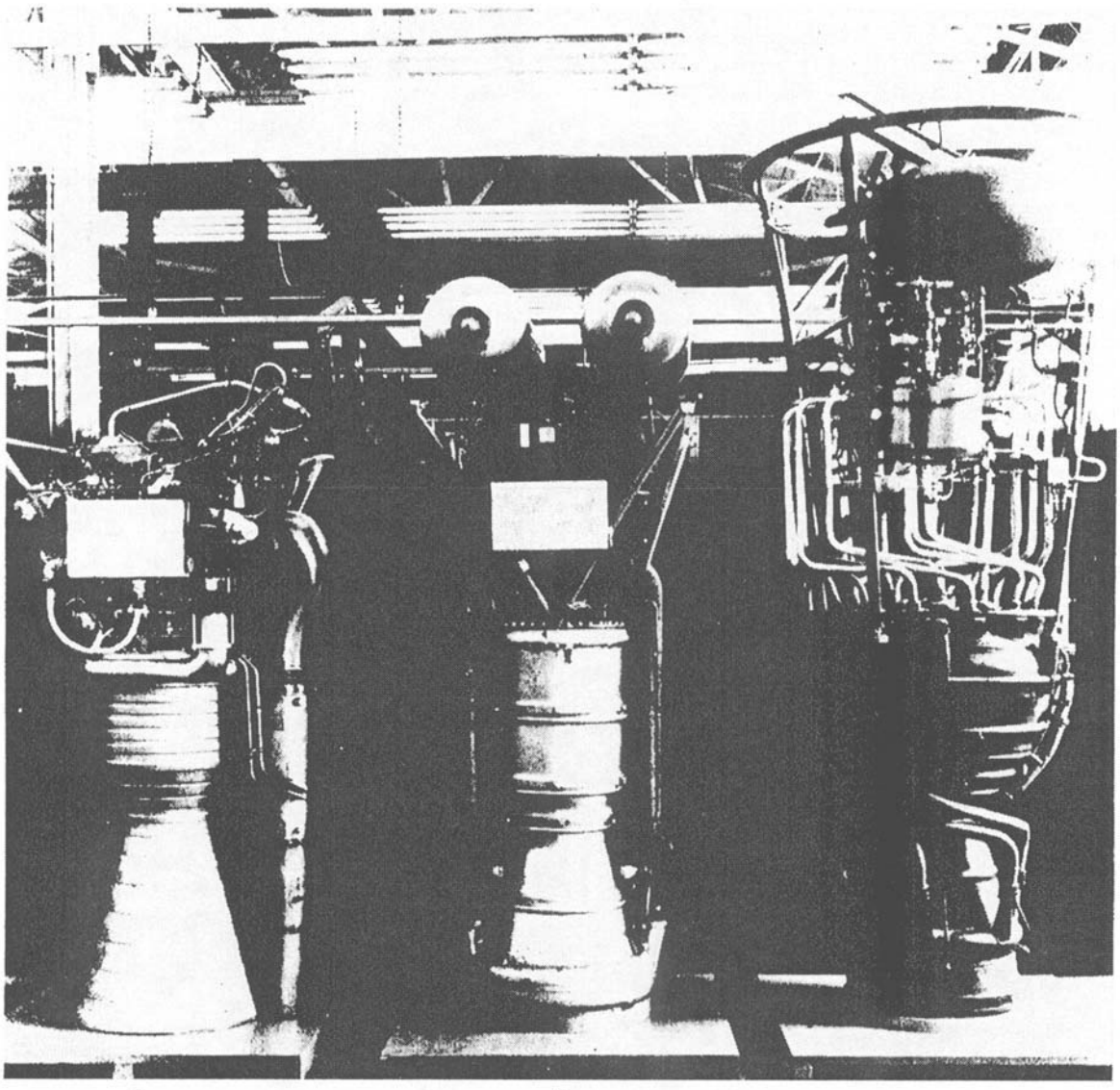

a)

Early Navaho Engine
(Rocketdyne 1953)
Thrust:$_{SL}$: 120,000 lb
Dry Weight: 1,230 lb
$I_{s_{SL}}$ = 230 s
$\frac{F}{W}$ = 97.5

b)

Early Redstone Engine
(Rocketdyne 1952)
Thrust:$_{SL}$: 75,000 lb
Dry Weight: 1,475 lb
$I_{s_{SL}}$ = 215 s
$\frac{F}{W}$ = 50.8

c)

German V-2 Engine
(1942)
Thrust:$_{SL}$: 56,000 lb
Dry Weight: 2,484 lb
$I_{s_{SL}}$ = 199 s
$\frac{F}{W}$ = 22.5

Fig. 2-5 Early progress in ratio of thrust to engine weight.

has placed even greater emphasis on rocket-engine reliability.

Reliability may be defined as the ability of the engine to perform according to specifications, whenever "the button is pushed." The degree to which it will meet specs can be expressed in figures and graphs. If the evaluation is made following a test series, reliability can be expressed simply as the ratio of success to failure, say, 98% (2 failures and 98 successes in 100 runs). As there is no guarantee, however, that the system under test will perform identically in subsequent tests, reliability predictions will be made, the accuracy ("confidence level") of which will increase with the amount of information available. Statisticians interpret the interrelation of reliability and its confidence level..

What can the rocket-engine designer do to achieve the highest possible reliability, as early as possible? Appendix B compiles pointers and thoughts which have proven valuable, followed by specific details for the implementation of a reliability-assurance program.

Cost

Cost considerations should enter a design at the very beginning, not only from the viewpoint of competitive bidding and narrow profit-margins, but also

in terms of available or developed national resources. A major rocket program may tax the resources of certain materials, facilities, and services to the limit. Moreover, it should be ascertained that the program does not rely on facilities and on supply of materials and of propellants that may not become available for several years. The rocket engine under design may well be for a project costing hundreds of millions of dollars. Savings of even fractions of a percent can therefore amount to millions.

Cost, as far as the designer is concerned, will be affected by the selection of materials, by the machinery required to make the parts, by the time and skill required to make them, by the difficulty of assembling, testing, and servicing the parts, and last, but not least, by the experience of the people making the design.

Availability (Scheduling)

The best design, the most perfect device, may be useless if it is not available when needed. In a way, the *design* (in our case) of a rocket engine is a product by itself. It must be planned, prepared, and made. It generates physical products: drawings, written instructions, and procedures, which all must be faultless and available when needed. Delays in the release of drawings can become very costly indeed. In a manufacturer's overall plan of action, the design will be timed and synchronized with other activities. If the drawings are not available on schedule, sizable portions of a machine shop or an assembly plant may be forced to stand idle.

2.3 MISSION REQUIREMENTS

A multitude of missions engender rocket-engine designs, and each mission has distinctive requirements. Some of these missions will be discussed here along with associated engine design requirements and optimization approaches.

Typical Mission Goals

Many missions require multiple stages to reduce overall vehicle size and propellant consumption. A basic stage consists of engines, propellant tanks, and the required support structure. As the tanks empty, the weight that no longer performs a function becomes dead-weight, and it is more efficient (i.e., requires less propellant) to get rid of it by dropping off the entire stage, and then starting the engines in the next stage, which has full propellant tanks. This technique was used for the Saturn rocket (Fig. 2-6) that launched the Apollo Mission to the moon. Saturn used three pump-fed liquid-propellant rocket stages to get into orbit around Earth and to initiate the flight from Earth to lunar orbit. The staging sequence is illustrated in Fig. 2-7 for the Apollo 10 flight: a "series burn" because the stages burn in series, i.e., fire consecutively rather than simultaneously.

The current Space Shuttle uses a parallel-burn arrangement. The first-stage booster engines, which use solid propellant, and the core-stage engines, which use LOX and LH_2, start simultaneously and lift the vehicle off. First-stage propellant exhausted, the solid boosters drop off and the core engines continue to burn. Propellants for the core engines exhausted, the core external tank drops off. The core engines remain attached to the Orbiter for recovery. Parallel burn sacrifices some of the payload capacity of series burn to recover the main engines.

Saturn and Space Shuttle will illustrate how the mission and vehicle requirements lead to engine type.

Saturn vehicle for the Apollo Mission. F-1 engines were used in the first stage of the Saturn vehicle. Because they initially exhausted to atmospheric pressure, they had a relatively high chamber pressure to obtain the higher nozzle area ratio required to obtain high specific impulse. To obtain high chamber pressures without excessive tank weight, they were pump-fed; and because they spent much of the flight in the atmosphere, they used dense fuel (rather than liquid hydrogen) to minimize tank size, stage inert weight, and aerodynamic drag. Because they were expendable (flew only once), development emphasized the 150-s operating duration. For these reasons, the F-1 engine had the very high thrust of 1.5-million pounds, a high (at that time) chamber pressure of 1000 psia, a dense fuel (RP-1), and, to minimize development costs, a gas-generator turbine drive.

J-2 engines powered the second and third stages of Saturn, five in the second stage and one in the third. These engines had a higher premium on performance because every pound of propellant in an upper stage is a dead weight that must be lifted by the lower stages. Also, upper-stage engines generally exhaust to a vacuum, and therefore do not have to have a high chamber pressure to obtain a high nozzle area ratio. However, the J-2 engine was tested at sea-level conditions. Its area ratio of 27 was selected based on full nozzle flow without the use of an exhaust diffuser. As a result, the J-2 engine, using liquid hydrogen for fuel, had a larger nozzle area ratio with a chamber pressure that was less than that for the F-1. Also, it was designed for lower thrust than the F-1 engine because it did not have to lift as much: 225,000 lb at a chamber pressure of 787 psia. Because it also was expendable, the J-2 also used the gas-generator cycle to minimize development cost.

Space Shuttle. "Core" engines combine the requirements of booster and upper-stage engines, and operate during both booster and upper stage flight. Because they burn longer than booster engines, core engines have a higher premium on performance. Unfortunately, they have a limited nozzle area ratio because they must also operate at sea level, where the exhaust pressure is relatively high. Consequently, they have an even higher premium on chamber pressure than booster engines.

The Space Shuttle Main Engine (SSME), an example of such an engine, has the very high chamber pressure of 3000 psia. To maximize performance at this high chamber pressure, it utilizes a staged combustion cycle in which all of the propellants burn in the thrust chamber at high pressure. To minimize the weight of the resulting

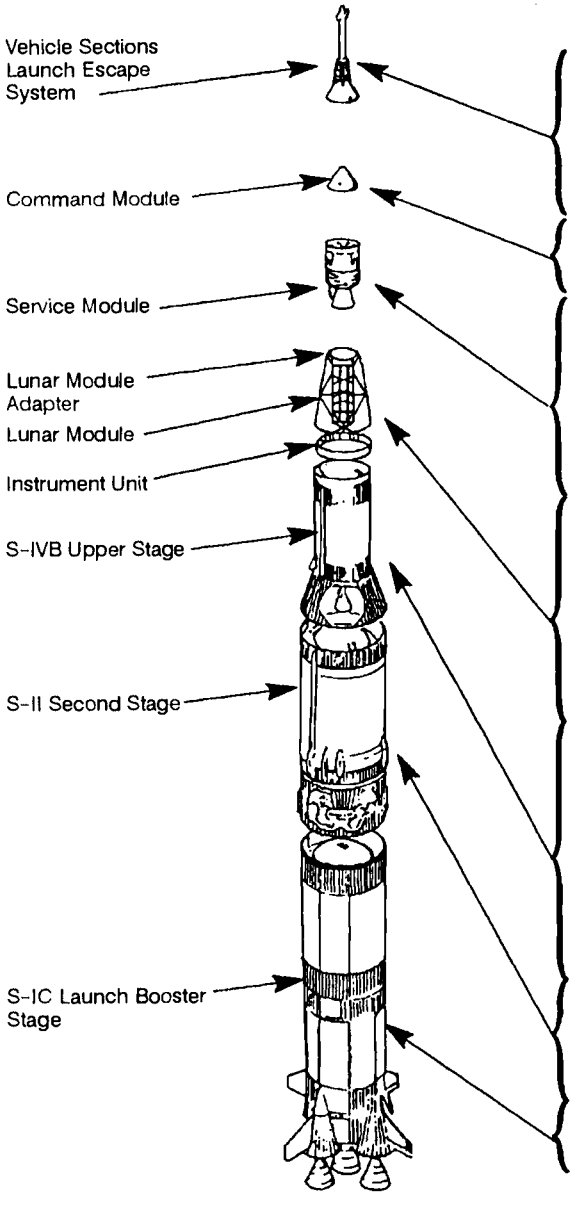

Number and Model of Propulsion System	Propellants, Starts, Burn Time	Thrust (lb)	Usage or Missions
1 4-Nozzle	Solid 1 burn, 8 s	147,000	Payload emergency separation from vehicle during early flight
1	Solid 1 burn, 0.5 s	2,400	Pitch control during emergency separation
1 TE-380	Solid 1 burn, <1 s	31,500	Normal (no emergency) separation of entire tower at +180 s or in emergency separation, after tower and spacecraft have been carried safe distance (1 mil) from vehicle, will pull tower from spacecraft
12 SE-8 (6 redundant)	NTO/MMH Multiburns (230 s max)	(93 each)	Reaction control of command module during reentry
16 R4D-1	NTO/50% UDMH and hydrazine Multiburns	(100 each)	Reaction control, propellant settling, lunar module docking adjustments, minor velocity corrections, and last separation of command and service modules upon reentry
1 AJ10-137	NTO/50% UDMH and hydrazine Multiburns (12.5 min max)	21,900	Payload emergency separation from vehicle after escape tower jettison; deceleration during earth-orbit missions; midcourse velocity correction during translunar coast; plane changes; spacecraft insertion into lunar orbit and transearth orbit
16 R4D-2	NTO/50% UDMH and hydrazine Multiburns	(100 each)	Reaction control system for lunar module and aid in rendezvous/docking with spacecraft after return from lunar surface (in ascent section of lunar module)
1 8258	NTO/50% UDMH and hydrazine 2 burns (5 min max)	3,500	Ascent power from lunar surface to lunar orbit and rendezvous/docking with spacecraft
1 10,500	NTO/50% UDMH and hydrazine Multiburns (16 min max)	1,050→10,500 (throttlable)	Deceleration, midcourse correction, descent thrusting, and hover to lunar landing; also can return lunar module to lunar orbit if emergency arises
6	NTO/NMH Pulsefired (20 min max)	(150 each)	Reaction control during 4 h coast period after first J-2 burn and during translunar maneuvers
2 SE-7-1	NTO/MMH 2 burns (425 sec max)	144	Propellant settling after first J-2 burn and during restart chilldown prior to second J-2 burn
1 J-2	LOX/Liquid hydrogen 2 burns (8.5 min max)	230,000	Final vehicle boost into earth orbit (142 s) and after 4 h coast period, reignite (at apogee or earth orbit) to insert payload (360 s) into translunar trajectory
2 TX-280	Solid 1 burn (3.9 s)	6,780	Propellant settling prior to J-2 first burn
4 TE-29-1B	Solid 1 burn (1.5 s)	140,000	Separation by deceleration of S-II stage; four retros mounted on aft interstage assembly facing upward
5 J-2	LOX/Liquid hydrogen 1 burn (400 s)	1,150,000	Boosters
8	Solid 1 burn (0.67 s)	704,000	Separation retros
5 F-1	LOX/RP-1 1 burn (150 s)	7,610,000	Boosters

Fig. 2-6 Propulsion systems for Saturn V-Apollo lunar-landing mission.

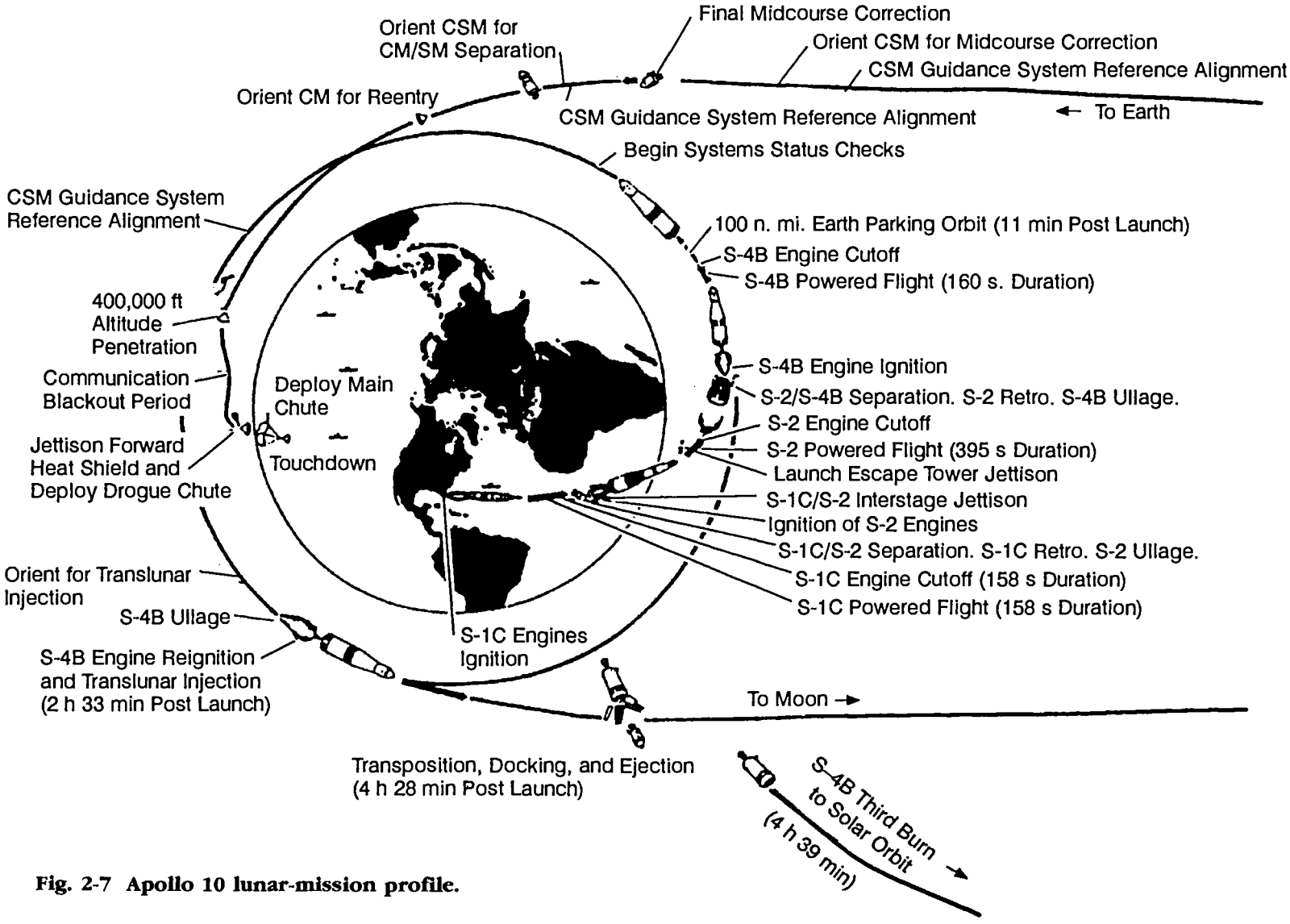

Fig. 2-7 Apollo 10 lunar-mission profile.

high-power turbomachinery, the SSME utilizes boost pumps to allow the main pumps to operate at high speed without cavitation. These same high speeds require the use of high-speed bearings, seals, turbines in the main turbopumps. Because of these features, the SSME has pushed technology further than any other rocket engine.

Attitude control and orbit-maneuvering engines. Attitude-control and orbit-maneuvering engines have low thrust compared to the engine types just discussed for obvious reasons. Also, their operating durations are usually shorter, ranging from a few milliseconds to a few seconds. Because of these two factors, small size and short duration, turbopumps are not always practical (unless accumulators are used) and, as a result, these engine types are very often pressure-fed. For similar reasons, standard regenerative cooling is often replaced with radiation, ablative, and inter-regen cooling (a combination of film cooling augmented by conduction back to the injector). Also, because attitude-control engines often must be operational over a long period of time in orbit, they often use storable propellants.

Missile. Missile main-propulsion engines can have thrust ranging from the orbit-maneuvering engine (OME) type to the levels of the larger engines discussed above; and they have operating durations between those of the attitude-control engines and the others. Although having short operating durations, they must be storable for long periods because they are generally used only during times of conflict. They are mass-produced and expendable for obvious reasons. This combination of requirements results in features that are similar to those for attitude-control and orbit-maneuvering engines; i.e., pressure-feed, modest chamber pressure, storable propellants, and non-regenerative cooling. Because they operate for a relatively long time as compared to attitude-control engines, pure radiation cooling would be inadequate. However, the other cooling options (ablative and inter-regen) would be applicable.

Manned. A manned vehicle creates a premium on reliability and crew safety. Those factors make manned vehicles much more costly to build and to operate. Of the engine applications discussed above, all but the missile could be man-rated by utilizing a carefully structured design, development, and testing program.

Expendable. An expendable engine will not be recovered once it has completed its mission. The engines in the Saturn vehicle were expendable, while the engines in the Space Shuttle are reusable. This has a significant impact on the technology level used for an engine. An expendable engine may use a lower technology and a less stringent development program.

Reusable. A reusable engine can afford a higher technology because the added cost of design, development, and testing will be amortized over a number of flights.

Storable systems. Systems using storable propellants (liquid at normal conditions--either at sea level or for satellite or space-transfer applications) require careful attention to issues such as material compatibility and life of components such as seals that are in contact with propellants for an extended period of time. Typical propellants for these applications include nitrogen tetroxide (NTO) and hydrazine derivatives such as monomethylhydrazine (MMH). Engines of this type include the Titan engines that propel missiles that are stored for long times in silos and the XLR-132, a small engine (3750-lb thrust) intended for use in orbit transfer. (The XLR-132 was designed to be earth/space storable for on-demand use over a three-year period.)

Typical Vehicle-Requirement Optimization

A Boeing analysis (Fig. 2-8) of a single-stage-to-orbit (SSTO) vehicle illustrates a typical optimization in which engine design parameters are selected based on their impact on vehicle capabilities. For this horizontal-takeoff vehicle launched from a rocket-propelled sled, parametric engine thrust, weight, and performance data were supplied by the engine manufacturer to Boeing, and it then used the data to predict the impact on vehicle gross weight and payload. Three separate engine parameters—thrust, nozzle area ratio, and chamber pressure—were optimized.

Thrust. Figure 2-8c shows vehicle gross liftoff weight (GLOW) as a function of thrust per engine and number of engines. As indicated, vehicle payload was held constant at 65,000 lb. For each curve, each of which is for a fixed number of engines, GLOW reaches a minimum. For engine thrust below this minimum, vehicle accelerations and velocities are low. That causes inefficient propellant consumption, because it is best to accelerate to a high velocity early in the vehicle trajectory to minimize the amount of propellant that has to be carried to a higher altitude. The inefficient propellant consumption results in a larger GLOW due to a larger propellant load, despite the fact that engine weight and vehicle aerodynamic drag are lower. For engine thrust above the minimum, the reverse happens; a high velocity is attained early in the trajectory, but the engine weight and the vehicle aerodynamic drag are up, and the latter two dominate. Consequently, any given number of engines will have a design (engine) thrust that minimizes gross liftoff weight of the vehicle. This minimum GLOW should correlate with minimum cost.

Figure 2-8c also shows that GLOW increases with number of engines; support structure for the engines lowers thrust-to-weight ratio (T/W). This has to be balanced, however, against the greater reliability of the greater number of engines. If an engine goes out, the remaining engines may be able to complete the mission if the failure occurs late in the burn. If it occurs early in the burn, the remaining engines increase the chances of a safe abort.

Figure 2-8d leads to similar conclusions from a perspective of maximizing payload for a constant GLOW. The analysis shown in Fig. 2-8c would be the initial study conducted to define the vehicle when little is known about it. The vehicle defined to some extent, its payload capabilities can be analyzed as illustrated in Fig. 2-8d, which also shows that the

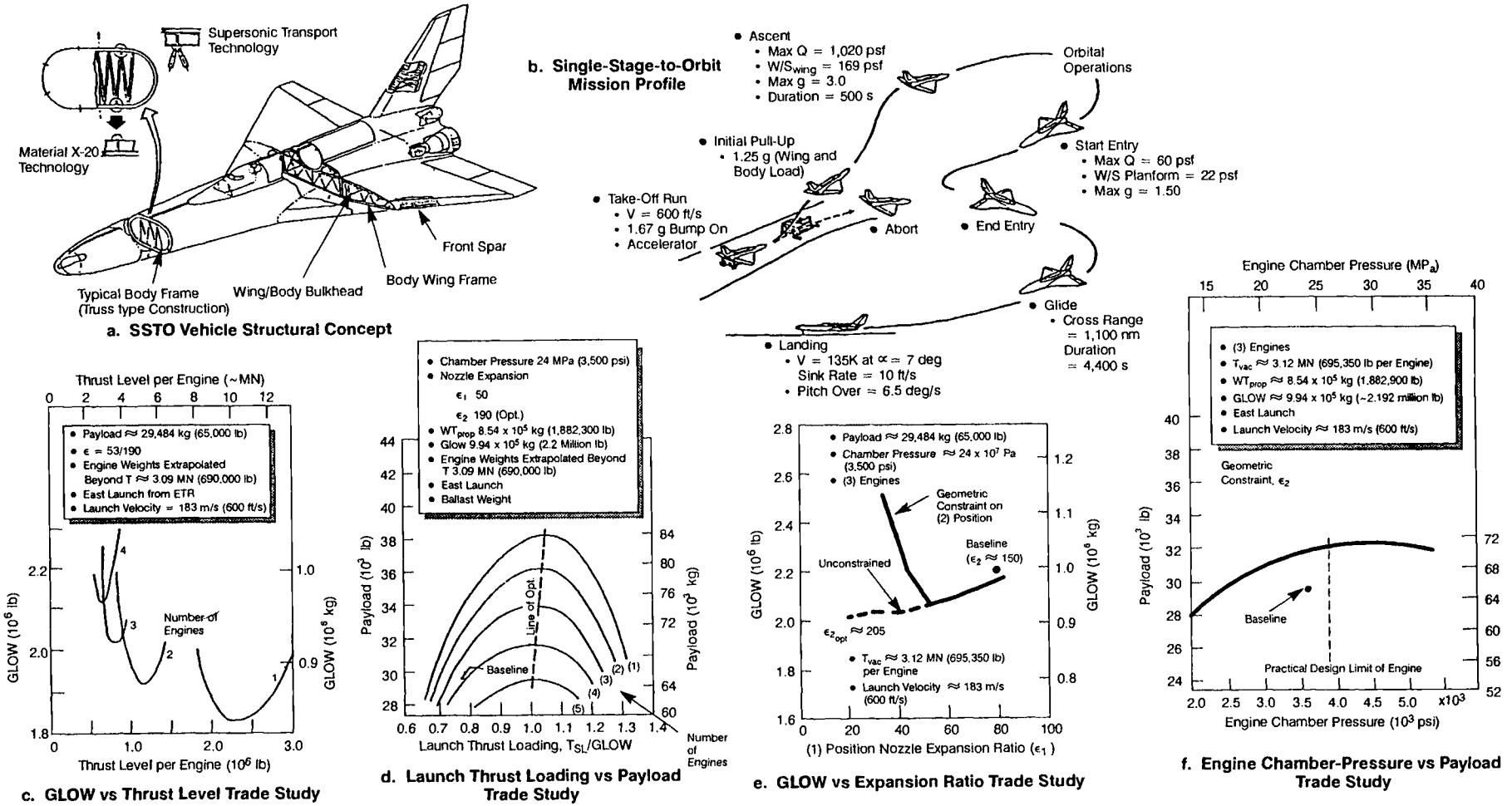

Fig. 2-8 Typical single-stage-to-orbit vehicle, mission-profile and trade-study results. Courtesy of Boeing Aerospace Co.

optimum total thrust for this type of vehicle lies between 1.00 and 1.05 times GLOW.

Nozzle area ratio. Figure 2-8e illustrates the optimization of the area ratio of a dual-position nozzle for the engines. As the area ratio in the retracted skirt position (position 1, which is used at takeoff when the ambient pressure is highest) drops below the baseline, the GLOW initially decreases because the performance at low altitude is improving. However, at a position 1 area ratio of 50, the nozzle skirt, which is the retracting part of the nozzle, can no longer be retracted around the engine because its minimum diameter is smaller than the envelope of the engine-power head. This makes it necessary to change to a heavier nozzle-retraction device for position-1 area ratios less than 50. As a result, a position-1 nozzle area ratio of 50 would be the optimum from a minimum-GLOW standpoint.

Chamber pressure. A staged combustion cycle was selected to meet the high engine-performance requirements of SSTO vehicles. For that type of engine cycle, two factors cause an optimum: sea-level performance and engine weight. Sea-level performance increases with chamber pressure because increasing the chamber pressure increases the allowable nozzle area ratio in the retracted position. This causes payload to increase with chamber pressure. The other factor is engine weight. Thrust chambers are heavy at low chamber pressures and turbopumps are heavy at high chamber pressures, a situation that generally results in a minimum total engine weight occurring at about 2500-psia chamber pressure. For the vehicle under consideration, these two factors produce an optimum payload near 4500-psia chamber pressure, as shown in Fig. 2-8f. Because the curve is relatively flat in the vicinity of the optimum, and because a further increase in chamber pressure would increase the number of stages in the hydrogen fuel pump, it was concluded that a baseline chamber pressure of 3500 psia would be appropriate.

2.4 ENGINE PRELIMINARY DESIGN

The next step in the design process, determining the engine and engine-component parameters that meet the requirements of the mission and vehicle, begins with selecting candidate concepts. Then optimizing them yields a preferred concept, together with the preliminary design parameters that are used (as discussed in later chapters) to initiate detailed design of the components.

Engine System and Component Concepts

For the application at hand, engine candidates are synthesized from a known stock of system and subsystem concepts. Typical advanced engine and engine-subsystem concepts for a SSTO vehicle are summarized below under the major headings of system configuration, nozzles, thrust chambers, and turbomachinery. A high-pressure pump-fed engine is assumed due to the performance and thrust requirements of the typical application studied. The list includes both current-technology and advanced-technology concepts.

It is apparent that there must be some interplay between the concept selection and the vehicle requirement optimization discussed above, because some of the assumptions used in the vehicle optimizations are the subsystem concepts and components. For example, the engine cycle was assumed in the vehicle requirement optimization and, at the same time, the engine cycle is one of the engine concept variables in Table 2-1.

Engine System Configuration. The top three concepts in Table 2-1 are the most common turbine-drive cycles for pump-fed liquid-propellant rocket engines. The schematic flow paths for these cycles are illustrated in Fig. 2-9. As indicated, all are fuel-cooled. Also, the single-shaft turbopump arrangement (i.e., one turbine driving both the fuel pump and the oxidizer pump that are mounted on the same shaft) is shown for the basic cycles in Fig. 2-9 to keep the schematics as simple as possible. More-complex concepts are discussed later.

The gas-generator cycle (Fig. 2-9a) is the only one of the three that has the turbine flow-path in parallel with the thrust chamber flow-path. This largely separates the two functions and makes the gas-generator engine much easier to develop and operate. It does have a performance penalty, however, due to three facts: 1) the turbine-drive gases are not fully expanded as in the thrust chamber, 2) the turbine gases are not fully combusted to the mixture ratio of the thrust chamber, and 3) there is a mixture-ratio shift (away from optimum) created in the main thrust chamber when flow is taken from the system to supply the gas generator. The inherent simplicity of this type of engine makes it a prime candidate for both booster and space engines. The F-1 and J-2 engines used for the booster and upper stages, respectively, for the Saturn launch vehicle used this type of cycle.

The expander cycle (Fig. 2-9b) avoids the turbine-drive gas losses of the gas-generator cycle by placing the turbine in series with the thrust chamber, exhausting directly into it. This cycle differs from the other two in that there is no combustion upstream of the turbine; the turbine-drive gas is the fuel after it has been heated in the thrust-chamber cooling jacket. This limits the turbine inlet temperature, which, in turn, limits the attainable chamber pressure. As a result, this engine is primarily a space engine where it can exhaust to a vacuum and, consequently, can have a very high nozzle area ratio in spite of its lower chamber pressure. The RL-10 engine for the Centaur vehicle uses this type of cycle.

The staged combustion cycle (Fig. 2-9c) resembles the expander cycle in that it has the turbine exhausting directly into the thrust chamber, and is similar to the gas-generator cycle in that it has combustion upstream of the turbine. For booster applications, this engine can perform better than the gas-generator cycle because it has no secondary-flow losses, and can perform better than the expander cycle because the higher turbine-inlet temperature allows it to have a higher chamber pressure and, consequently, a larger nozzle area ratio. As a space engine, it has an advantage over the expander cycle in that, due to its higher chamber pressure, it can

Table 2-1 Candidate advanced-engine-system cycles, configuration concepts, and components.

Concept	Performance	Life	Wt	Potential Benefits	Potential Drawbacks	Features
Staged combustion cycle	x			High P_c, high performance	Higher development cost	Maximum performance; eliminates secondary flow losses; maximum energy available to turbines; severe turbine environment; high pump pressures
Gas generator cycle		x	x	Simplicity, lower development cost	Lower performance	Simple system; components independent; parallel turbine and chamber flows; easy to develop/test
Expander cycle	x	x		Good performance, good turbine environment	Power limited	Benign turbine environment; topping cycle for high performance; no secondary flow stream; limited to relatively low thrust levels unless multiple chambers used
Hybrid cycle	x			High P_c, low turbine temperatures	Requires validation	Fuel side staged combustion cycle; oxidant side expander cycle; reduced turbine hot-gas temperature due to hydrogen mixing
Oxidizer-rich preburners (for oxidizer pump)	x			High P_c, less interpropellant sealing problem, increased turbine flow	Possible turbine overtemperature	Increased turbine flow rates; material compatibility issues
Dual expander	x			Better altitude I_{sp}, better propellant density	Complexity, possible cooling problems, heavy	Dual thrust chambers; dual staged-combustion cycles; altitude compensation; increased turbine energy; eliminates purge test requirement
Dual throat	x			Increased altitude I_{sp}	Weight, cooling	Tripropellant system; central and annular thrust chambers; conventional bell nozzle; separate or simultaneous chamber operation; acts like E-D nozzle at altitude; base bleed at altitude in central combustor
Optimum mixture ratio	x			Optimum I_{sp}		Operate engine at peak Isp mixture ratio; operate engine at peak payload mixture ratio; variable mixture ratio for high-density impulse
Slush H_2	x			Better bulk density of propellants	Cost; operational difficulties	Increased propellant bulk density; smaller tanks; potential payload benefits

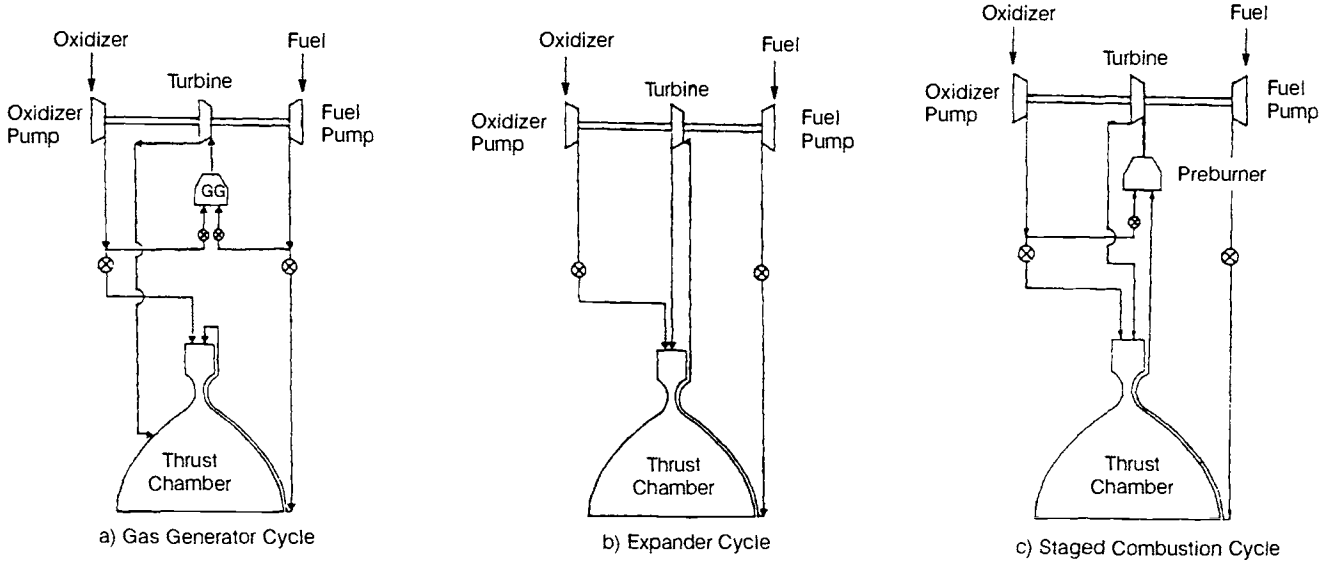

Fig. 2-9 Basic cycles for pump-fed liquid-propellant engines.

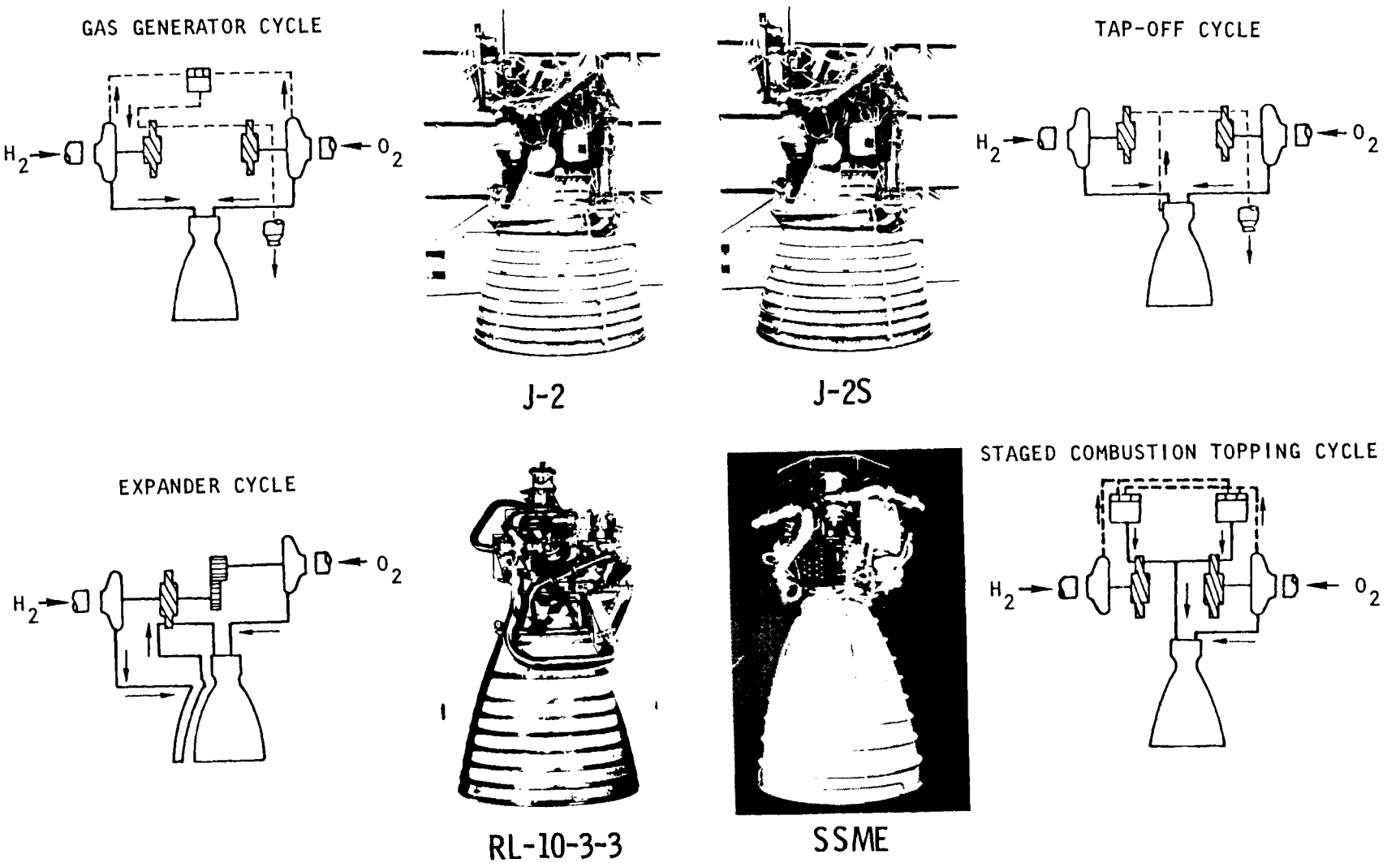

Fig. 2-10 Power cycles of pump-fed liquid-propellant engines.

attain the same performance with a smaller nozzle. However, relative to the other two cycles, the staged combustion cycle has the highest performance but it is more complex, more difficult to develop, and heavier. The SSME uses this type of cycle.

In actual practice, most of these engines do not use the single-shaft turbopump arrangement, as shown in Fig. 2-10. The J-2 and the SSME use a separate turbopump for each propellant (dual shaft), and the in RL-10 a gear drives the LOX pump off the LH_2 turbopump drive shaft. Figure 2-10 shows the J-2S engine, a modified form of the J-2. The J-2S obtains its turbine-drive gas by tapping the main combustion chamber.

Other engine-cycle concepts are basically derivatives, combinations, or variations of those in Fig. 2-9. Some of them are summarized in Table 2-2.

The hybrid staged-combustion cycle (Table 2-2d) represents a compromise between the high performance of conventional staged combustion (Fig. 2-9c and Table 2-2a) and the simplicity of the expander (Fig. 2-9d). It uses the staged combustion cycle to drive the fuel turbopump and the expander cycle to drive the oxidizer turbopump. In this manner, lower

Table 2-2 Engine-cycle concepts and relative evaluation.

Engine Cycle Concept	Configuration Features	Relative Performance Potential	Relative Weight Comparison	Reliability Considerations	Technology Assessment Summary
(A) Conventional Staged Combustion 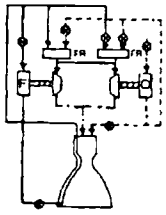	Conventional staged combustion cycle as used in SSME engine. Fuel-rich preburner is used to generate turbine drive gas, remaining oxygen is combusted with turbine drive gas in main combustion chamber. Single or dual preburners can be used for turbine drive gas. Fuel regenerative cooling is used for the main combustion chamber.	High delivered specific impulse (no turbine exhaust losses) since all propellants are combusted at high pressure and expanded through high area ratio nozzle. High pressure (3,000 psi and above) provide high area ratio (90 to 120) and high delivered specific impulse.	Thrust chamber weight decreases with chamber pressure, required pump power increases substantially with increasing chamber pressure due to interdependency of flow circuits. Turbopump and powerhead weight increases more rapidly with chamber pressure than for gas generator cycle.	Development of the SSME has shown that careful attention must be paid to engine start transient operating conditions to avoid turbine over-temperatures. Also mechanical and structural design of turbopump are key engine reliability drivers.	Development of SSME gives strong technical base for development of staged-combustion engines having different design point thrust and chamber pressure. Regenerative cooling of thrust chamber feasible at 130 to 200K vacuum thrust level at chamber pressures up to 4,500 psia.
(B) Mixed-Preburner Staged Combustion 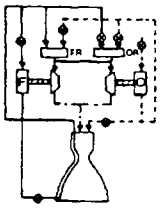	Staged combustion cycle with oxidizer-rich preburner to drive the LOX turbomachinery and a fuel-rich preburner to drive the fuel turbomachinery. All oxygen is combusted in the preburners so there is more turbine drive gas than in conventional staged-combustion cycle. Fuel regenerative cooling is used for the main combustion chamber.	High delivered specific impulse (no turbine exhaust losses) since all propellants are combusted at high pressure and expanded through high area ratio nozzle. Chamber pressure capability higher than conventional staged-combustion cycle, higher specific impulse, higher area ratio.	As with conventional staged-combustion cycle, thrust chamber weight decreases with chamber pressure. Required pump power increases substantially with increasing chamber pressure due to interdependency of flow circuits. Turbopump and powerhead weight increases more rapidly with chamber pressure than for gas generator cycle.	Development of the SSME has shown that careful attention must be paid to engine start transient operating conditions to avoid turbine over-temperatures. Also mechanical and structural design of turbopump are key engine reliability drivers. The oxidizer-rich environment is a reliability area that needs to be assessed with both advantages and disadvantages existing.	Development of SSME gives strong technical base for development of the mixed preburner staged-combustion engine. Regenerative cooling of thrust chamber feasible at 130 to 600K vacuum thrust level at chamber pressures up to 6,000 psia. The oxidizer-rich turbine drive technology needs to be developed and risks need to be assessed.
(C) Dual Expander 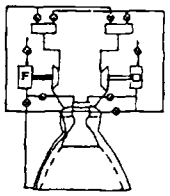	The dual-expander engine uses an arrangement of concentric combustion chambers to obtain lower area ratio performance with both combustors firing and high area ratio performance with only outer combustor firing. This arrangement requires a more complex cooling and propellant injection scheme.	The dual-expander engine achieves an increase in specific impulse when the outer combustor is firing with the inner shut down. This can be advantageous for launch vehicles which must first operate from within the atmosphere and then in vacuum conditions.	The increased complexity of the thrust chamber design will result in a heavier thrust chamber and injector configuration. Also there are an increased number of control valves on the engine.	The more advanced nature of this configuration points to a lower initial system reliability. The chamber configuration and adequate cooling during both modes of operation will largely determine overall engine reliaiblity.	Technology is required in the basic thrust chamber to determine configuration and the proper contour. This can be done in a cold-flow diagram. The proper cooling method (transpiration/regenerative) must be demonstrated for a long life chamber.
(D) Hybrid Staged Combustion 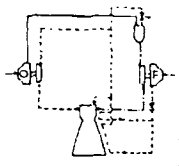	The hybrid staged combustion cycle is a variation of the conventional staged combustion cycle. In this cycle fuel turbine is driven by a fuel-rich preburner and the oxidizer turbine is driven by heated hydrogen supplied by heat exchange in a portion of the nozzle.	The chamber pressure delivery and performance of this cycle is lower than the conventional staged-combustion cycle.	There is some weight difference due to the removal of the oxygen preburner. Heated hydrogen is the turbine working fluid and results in a larger oxygen turbine.	The main attribute of this cycle is the use of lower temperature turbine drive fluids with attendant benefits in reliability and life.	Advanced technology is required to raise chamber pressure to higher levels than currently delivered by SSME. Areas for technology advancement are the pump staging, crossovers, and bearings.
(E) Gas Generator 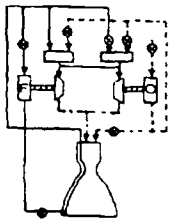	Conventional gas generator cycle used in Saturn-Apollo J-2 engine with a series turbine drive configuration. Turbine exhaust gas is introduced back into expansion section of nozzle to regain performance. Pump pressure needs only to supply system pressure drops and does not depend upon turbomachinery efficiencies.	Performance of the gas generator is lowered by two factors: (1) the lower specific impulse of the turbine exhaust gases due to their lower temperatures, and (2) the shift in thrust chamber mixture ratio necessary to balance the effect of the fuel-rich turbine exhaust gases. This causes a substantial performance penalty (-10 to 12 s) in specific impulse at 3,000 psia.	The weight of the gas generator cycle is less than that of closed cycles such as the staged-combustion cycle. Gas generator cycles are usually run at moderate pressure to avoid the higher loss associated with high pressure designs.	The reliability of gas generator engines has been high with the flight history showing very few propulsion system flight failures.	The technology requirements for gas generator cycle engines are moderate due to the large amount of development work previously accomplished on this system.

turbine-drive temperatures can be realized together with a gain in reliability and life, for only a small penalty in performance.

The mixed-preburner staged combustion cycle (Table 2-2b) uses an oxidizer-rich preburner to drive the oxidizer pump so as to maximize the power available to drive the turbomachinery, thereby yielding the cycle with the highest chamber pressure.

The dual-expander (meaning dual-thrust-chamber expansion) cycle (Table 2-2c) uses dual combustion chambers arranged concentrically to yield a dual nozzle area ratio, which improves performance by allowing the nozzle area ratio to be larger at high altitudes.

Other system concepts in Table 2-1 include propellant-related options such as optimum mixture ratio and the use of slush hydrogen. Optimum mixture ratio refers to variable engine mixture ratio with the LOX/LH_2 propellant combination. To do this, high engine mixture ratios (up to 12 to 16) are used for the booster operating mode and low engine mixture ratios (4 to 6) are used for the space operating mode. In the booster mode, high mixture ratio yields the high propellant bulk densities desired to minimize both tank sizes and vehicle aerodynamic drag when traveling in the atmosphere and, in the space-engine mode, where there are few factors to compromise performance, low mixture ratio yields high performance to minimize total propellant consumption and, consequently, total weight. The net benefit of this concept is a smaller total tank size. This has to be traded off against greater system complexity and a greater total propellant weight.

The last system in Table 2-1, a slush-hydrogen engine, employs partially frozen hydrogen to increase the propellant density, thereby reducing tank size. This has to be traded off against the higher cost of obtaining and maintaining hydrogen in a slush condition.

Nozzles. The standard nozzle for rocket engines, the bell (Fig. 2-11A) nozzle, has a bell shape for the portion downstream of the throat. For high-pressure pump-fed engines, bell nozzles are generally regeneratively cooled by the fuel. They are very efficient for the altitude for which they are designed. However, their area ratio is fixed and, as a result, booster engines with this type of nozzle operate off-

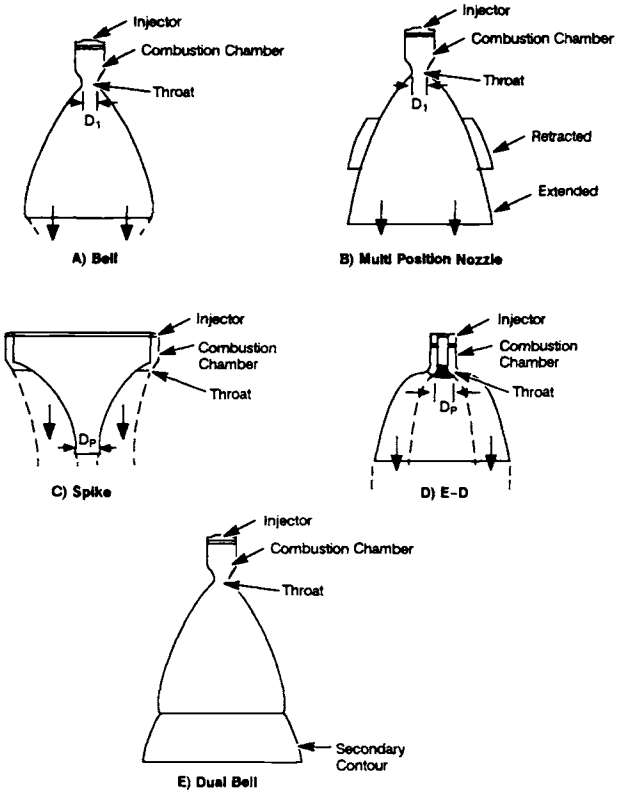

Fig. 2-11 Thrust-chamber nozzle concepts.

Table 2-3 Candidate advanced nozzle concepts.

Concept	Potential Benefits	Potential Drawbacks	Features
Multiposition nozzle	Altitude compensation higher I_{sp}	Complexity, weight	One or more translating or movable nozzle segments; altitude compensation
Variable position nozzle	Altitude compensation optimum at all altitudes	Complexity, weight, unproven concept	Continuously varying nozzle position; maintains optimum I_{sp} at all altitudes
Aerospike	Good altitude compensation	Weight, cooling difficulties	Good altitude compensation; short length; high diameter
E-D (expansion-deflection)	Altitude compensation	Weight, cooling	Outwardly directed annular throat; outer wall contour deflects exhaust gases axially; shorter than conventional bell for same thrust; larger diameter than conventional bell; altitude compensating
Dual bell	Altitude compensation	Weight, cooling	Fixed nozzle with double bell contours; contour transition at area ratio that optimizes sea-level performance; exhaust attaches to second contour at altitude; performance similar to multiposition nozzle; lightweight due to absence of extension mechanism

design for all but that moment when they pass through the nozzle design altitude. The nozzle concepts summarized in Table 2-3 are all designed to provide some degree of altitude compensation, thereby alleviating the performance penalties of the fixed nozzle. As shown in Table 2-3, the degree of compensation ranges from optimum performance at two altitudes up to optimum performance at all altitudes (up to the area-ratio limit of that nozzle). Some achieve this capability mechanically, and some achieve it aerodynamically. All achieve it at the expense of weight and complexity. The final selection would be based on a tradeoff between the benefits of improved performance and the penalties of increased weight and greater complexity.

The first concept in Table 2-3, the multiposition nozzle shown in Fig. 2-11B, usually consists of the basic bell, with one or more movable extension segments that can be moved into position to increase the overall nozzle area ratio to match the reduced ambient pressure that occurs as the vehicle gains altitude. The result is optimum performance at two or more altitudes, depending on the number of movable segments.

The variable-position nozzle can yield optimum performance continuously. An example, the overlapping-petal arrangement used in turbojets, may be very heavy and very complex, particularly if used in combination with regenerative cooling. As indicated in the table, this type of nozzle has not been used for rockets.

A candidate that also offers continuous altitude compensation, the aerospike (Fig. 2-11C), has an annular throat with expansion along the spike wall. Because there is no outer wall, the outer plume is free to adjust with altitude. The resulting excellent altitude compensation must be balanced against the weight of the large annular combustion chamber and the associated cooling of the large surface area.

The expansion-deflection nozzle (E-D, in Fig. 2-11D) avoids some of the combustion-chamber weight and cooling problems of the aerospike by essentially reversing the flow path of the aerospike nozzle. The flow is directed radially outward through the annular throat, thereby resulting in a more conventionally sized combustion chamber. Also, the annulus diameter is much less, thereby greatly reducing the cooling area in the region of the throat, where the cooling problem is the most critical. The altitude compensation occurs by having the plume in the center of the nozzle vary with altitude. As with the aerospike, some flow through the base region is desirable to increase base pressure and improve nozzle performance.

The dual bell (Fig. 2-11E) steps the nozzle contour so that the plume separates from the nozzle wall at the step during low-altitude operation, and follows the contour below the step during high-altitude operation. This yields optimum performance at two altitudes (assuming one step), similar to the multiposition nozzle with one translating segment. Relative to the multiposition nozzle, it has the advantage of not requiring a heavy translating mechanism, but has the disadvantage of a larger volume.

Thrust Chambers. As shown in Table 2-4, four of the advanced thrust-chamber concepts involve cooling-jacket options to improve chamber life. Two of the four achieve longer life by cooling the chamber wall at the expense of engine performance. The other two achieve longer life by using high-temperature low-conductivity thermal barriers that require development. In assessing these four cooling-jacket options, the first two involve a tradeoff between life and performance, and the second two involve a tradeoff between life and the cost of development and fabrication.

Transpiration cooling utilizes a porous thrust-chamber wall through which coolant seeps. The resultant evaporation on the wall surface and the concentration of coolant along the wall both keep the wall cooler than with purely regenerative cooling.

Table 2-4 Candidate advanced thrust-chamber concepts.

Concept	Performance	Life	Potential Benefits	Potential Drawbacks	Features
Transpiration cooling	x		Improved chamber life	Reduced performance	Transpiration cooling of chamber wall results in better cycle life; performance penalty due to mixture ratio maldistribution
Film cooling	x		Improved chamber life	Reduced performance	Similar to transpiration cooling; fuel-rich film on chamber wall; lower wall temperatures
Refractory liner	x	x	Thermal barrier reduces heat flux at high P_c	Requires development	High-temperature, low conductivity thermal barrier; near-adiabatic chamber; slight performance gain (reduced boundary-layer loss); life gain due to reduced heat flux
Rhenium liner	x	x	Thermal barrier reduced heat flux at high P_c	Fabrication difficult, costly	Same as above
Baffleless injector		x	More effective propellant injection	Risk of instability	Elimination of injector baffles; improved injection efficiency

For a given chamber pressure, this increases the chamber life, and for a given life it can increase the attainable chamber pressure. However, the concentration of coolant along the wall results in less propellant being fully combusted at the entrance to the thrust chamber, which results in less propellant being fully expanded in the nozzle. This constitutes a loss, which must be traded against the advantages discussed above.

Film cooling obtains a similar result by introducing coolant through passages in the combustion-chamber wall. That flow is introduced through small passages, rather than through the porous wall used in transpiration cooling. The coolant then helps cool the downstream wall by flowing along the wall surface. The film can also be introduced at the injector face by concentrating some of the fuel injector elements along the wall. As with the transpiration cooling, a loss due to incomplete combustion and expansion of the film coolant occurs.

The next two candidates in Table 2-4, refractory and rhenium liners, are high-temperature, low-conductivity thermal barriers applied to the hot-gas side of the thrust chamber. These barriers reduce the heat flux and the temperature of the thrust-chamber wall. As above, this can either increase the life of the thrust chamber for a given chamber pressure or increase the chamber pressure for a given life. An additional benefit of these candidates is that they can permit operation at high chamber pressures. As major disadvantages, both liner candidates need development to ensure that they have the ability to meet the rocket-engine life requirements.

The last thrust-chamber concept involves the use of injectors without baffles. This concept involves a slight risk of instability. However, experience with the SSME has indicated that this risk is very low with LOX/LH_2. Removal of baffles to improve performance is probably advisable. In this case, the tradeoff is between the penalty of a slightly greater risk of instability and the benefits of better performance, reduced weight, and reduced cost.

Turbomachinery. The nine turbomachinery options in Table 2-5 potentially can increase efficiency, decrease weight, increase life, or do some combination of the three. These options are discussed individually below in the order of presentation in Table 2-5.

Increasing the number of pump stages generally increases efficiency, throttleability, and margin

Table 2-5 Candidate advanced engine-turbomachinery concepts and components.

Concept	Performance	Life	Wt	Potential Benefits	Potential Drawbacks	Features
Increased number of pump stages	x			Higher P_c leading to higher I_{sp}	Increased weight and complexity	Improved pump efficiency; reduced head per stage; increased stage specific speed
High-speed turbopumps	x			Higher pump efficiency, reduced weight	Possible life impact	Improved pump efficiency; increased stage specific speed; required high-strength materials
Hydrostatic bearings		x		Reduced weight, simplicity	Requires validation	
Magnetic bearings		x		Frequency control	Small radial load capacity	
High-velocity crossovers	x			Improved pump efficiency		Improved pump efficiency
Multistage partial admission turbines	x			Higher turbine efficiency		
Jet pumps for low-pressure boost		x	x	Lightweight, no moving parts	Requires validation	No moving parts; high reliability
Increased turbine inlet temperatures	x			Higher P_c and I_{sp}	Possible life and reliability impact	Higher energy available to turbopumps; requires advanced materials
Cooled turbines	x	x		Improved blade environment	Increases complexity	Longer life at current temperatures; increased turbine temperatures at same life
Ceramic turbine blades	x	x	x	Strong, lightweight, high temperature capability	Brittle, fragile	Preloaded blades in compression; high temperature operation; brittle, subject to thermal shock

relative to the impeller tip-speed limit. Also, it decreases pump diameter at the expense of increased pump length. However, it increases complexity and cost. The net impact on the engine is improved performance and throttleability. The impeller life may be extended, but the life of the shaft-support system may be compromised by critical speed. Cost and complex-ity would increase for the engine just as for the pump. In general, the number of pump stages is minimized within the tip-speed limits if the stage specific speed is over 700, which is sufficient to yield a reasonable efficiency.

Designing turbopumps for high rotational speed tends to increase the efficiency of the pump, may increase the efficiency of the turbine, and definitely decreases the weight of the entire turbopump. If the speed is too high, however, the lives of the bearings and seals can be compromised, cavitation damage and/or insufficient pressure rise can occur in the pump impeller if not enough inlet pressure is supplied, and the turbine blades can be overstressed. In general, the design rotational speed needs to be maximized within component limits that provide reasonable operating margins for the components.

Hydrostatic bearings eliminate the bearing rotational-speed limits by eliminating the rolling elements in the bearings. This also theoretically eliminates the bearing life limits as long as metal-to-metal contact is avoided. Disadvantages are a decrease in pump efficiency due to an increase in flow leakage and an increase in development cost due to the lack of a broad base of experience with this type of bearing. In general, hydrostatic bearings are now being recommended for long-life and high-performance rocket engine applications.

Magnetic bearings achieve the same objective as hydrostatic bearings by supporting the shaft by magnetic rather than hydrostatic forces. They have an additional advantage of being able to compensate for shaft oscillations by varying the strength and frequency of the magnetic forces. At present, however, practical magnets are too weak to support the shaft with any reasonable size of bearing. The state-of-the-art for this type of bearing is still in its infancy.

High-velocity crossover passages from the exit of one centrifugal-pump stage to the entrance to the next tend to improve the efficiency and decrease the size and weight of multistage centrifugal pumps. In general, they are used for high-pressure liquid-hydrogen pumps.

For small pump-fed rocket engines (thrust levels less than 30,000 lb), multistage partial-admission turbines can be used to obtain reasonable blade heights at the high-pitch-line velocities that yield high turbine efficiencies. The net impact on the engine is a higher chamber pressure, which can be used to reduce engine size and weight for a given performance or to obtain higher performance from a given engine size and weight.

Jet pumps are very simple units that can be used for boost pumps. They utilize high-pressure flow that is recirculated from the main pump discharge to pressurize the low-pressure incoming flow. This is done in an ejector, and therefore the jet pump has no moving parts. Using this type of pump in this application yields the benefits of a boost pump (higher efficiency and lighter weight for the main turbopump) with very little increase in either complexity or cost. As its major drawback, the jet pump has very low efficiency. When selecting a boost pump, therefore, the tradeoff is between the simplicity of the jet pump and the higher efficiency of a conventional low-pressure rotating pump and drive.

High turbine-inlet temperatures are very desirable for engine cycles because they increase the amount of energy available per unit flowrate to drive the turbomachinery. This increases the pump pressure rise per unit turbine flowrate, which, in turn, increases the chamber pressure attainable for a given turbine flowrate. This increased chamber pressure can be used in one of several ways, such as to increase the nozzle area ratio and the performance or to decrease the engine size and weight for a given nozzle area ratio. In any event, high turbine-inlet temperatures are beneficial. Any turbine material that has a higher-temperature capability is desirable. This capability can also be used to increase the operating margin relative to the ultimate limit, which, for a given turbine-inlet temperature, will increase life and reliability.

An alternative method for raising the turbine-inlet temperature—using a portion of the propellant to cool the blades and/or the rotor—can increase the operating stress level for a given hot-gas temperature, thereby allowing either a higher rotational speed (higher blade stress) to yield a lighter-weight turbopump or a higher pitch-line velocity (higher disc stress) to yield higher efficiency. In addition, it can simply be used to increase the life and reliability of an existing unit under its existing operating conditions. As a disadvantage, cooling usually requires additional propellant consumption, a performance penalty. To be beneficial, the advantages of turbine cooling have to outweigh the performance penalty.

A material and design option that has the potential of allowing higher turbine-inlet temperatures, the use of hollow ceramic blades held in compression by a metal fixture that passes through the hollow portion, requires considerable development effort to ensure that the attachment eliminates the brittleness associated with ceramics.

Preliminary Design Optimization

Once a set of candidate components has been selected, the engine must be optimized to yield the design parameters for the components. As discussed earlier, the basic overall goal will usually be minimum vehicle life-cycle cost per unit of payload. Because this cost is the total cost related to the engine during its operating life, the optimization analysis must include consideration of such factors as performance, weight, development, design, fabrication, maintenance, servicing, and operations, as well as propellant selection. In general, maximizing performance and minimizing weight within reasonable technology limits will contribute to minimizing many of these costs. Performance and weight are

much easier than the other factors to quantify early in the design process. Therefore, maximizing performance and minimizing weight are usually the initial design goals, which are then tempered by cost considerations.

In the optimization process, the various components are characterized basically as a function of chamber pressure, and the chamber pressure is varied to yield engine performance and weight as a function of it. The design is not permitted to exceed any of the component limits that are specified to keep the engine within a safe design region. These limits may fall into the category of envelope (maximum length and diameter allowed by the installation in the vehicle), interface (minimum pump-inlet and nozzle-exit pressures allowed by the vehicle), stress (pump impeller tip speeds, turbine-blade stresses, bearing speed), or fluid-mechanical factors (cavitation in the pumps). In the discussion below, the performance and weight optimization processes are discussed individually.

Performance. Thrust-chamber performance usually increases with chamber pressure. High pressure reduces performance losses, such as those due to reaction kinetics. Thus high pressure and high area ratios can be permitted. In addition, there is usually some limit on the nozzle-exit conditions, such as minimum exit static pressure for a booster engine or maximum nozzle-exit size for an upper-stage engine, which limits expansion area ratio. As a result, increasing chamber pressure increases maximum permissible nozzle area ratio and thrust-chamber performance. This thrust-chamber performance trend with chamber pressure is shown by the dashed curve in Fig. 2-12. For staged-combustion and expander cycles, the engine performance equals the thrust-chamber performance. As a result, simply maximizing chamber pressure maximizes engine performance. That issue is discussed in more detail below. For the gas-generator cycle, the secondary-flow losses (due to the turbine-drive gas path being in parallel with the thrust chamber) are proportional to pump pressure rise, which, in turn, is roughly proportional to chamber pressure. When these losses are deducted from the thrust-chamber performance, the resulting curve of engine performance vs. chamber pressure has a definite maximum, as shown in Fig. 2-12. The procedure used to optimize gas-generator-cycle performance finds that maximum.

As discussed above, the performance for staged-combustion and expander cycles will be optimized by maximizing chamber pressure within other constraints. That procedure is illustrated by Fig. 2-13, which shows the relationship between turbine pressure ratio, chamber pressure, and turbopump efficiency (product of pump and turbine efficiencies). For a given value of turbopump efficiency, the curve of pressure ratio vs. chamber pressure curves upward, eventually reaches infinite slope, and then curves backward as the increase in required turbine pressure drop begins to exceed the corresponding increase in pump pressure rise. For a given turbopump efficiency, there will be a maximum chamber pressure and, in turn, a maximum performance; but, for a given number of pump and turbine stages, turbopump efficiency declines as pump pressure rises and the corresponding turbine pressure ratio increases. This results in a fixed staging optimum that occurs at lower values of turbine pressure ratio and pump pressure rise than the fixed efficiency optimum, as also shown in Fig. 2-13. Therefore, the procedure used to optimize staged combustion and expander

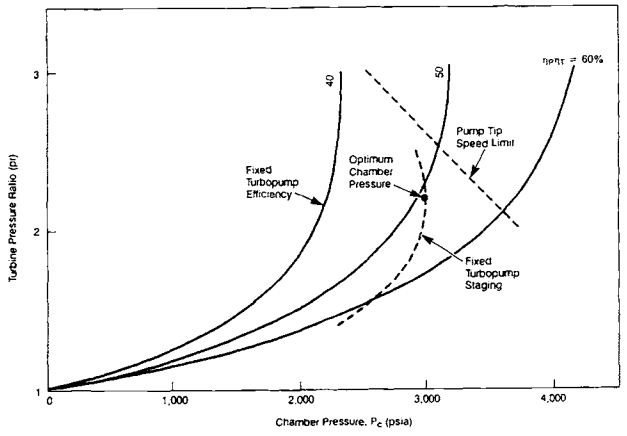

Fig. 2-13 Staged-combustion-cycle performance optimization.

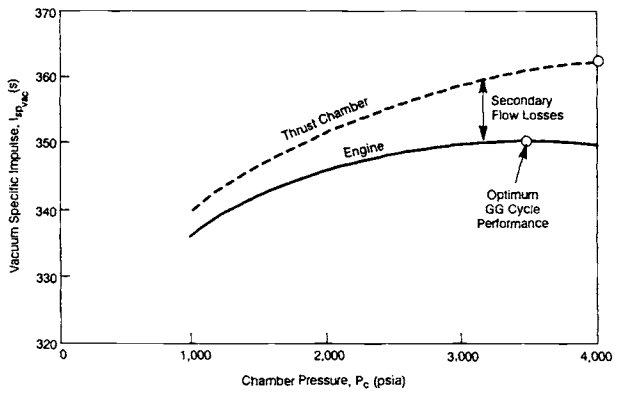

Fig. 2-12 Gas-Generated (GG)-cycle performance optimization.

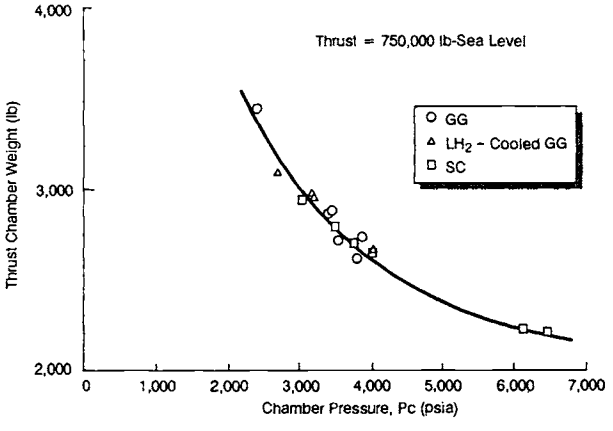

Fig. 2-14 Thrust-chamber weight trends.

cycle engines will determine the optimum chamber pressure on the appropriate fixed turbopump staging curve. This has to be done within the engine-component technology limits, such as pump-impeller tip speed. The optimum shown in Fig. 2-13 is satisfactory in that it occurs at a pump-impeller tip speed below the technology limit.

Weight. Rocket-engine component weight trends with chamber pressure are shown for LOX/hydrocarbon engine candidates in Fig. 2-14 through 2-19. For a fixed thrust, thrust-chamber weight decreases with increasing chamber pressure (Fig. 2-14) because the thrust-chamber size decreases. On the other hand, turbopump weight increases with chamber pressure (Fig. 2-15) because horsepower is proportional to pressure rise, which, in turn, is roughly proportional to chamber pressure. Ducting and pressurization system weights also increase with chamber pressure (Fig. 2-16) because increased internal pressures increase the wall thickness of ducts and pressure vessels. Other components show little impact of chamber pressure (Fig. 2-17). As the end result of these trends, engine weights reach minimums at chamber pressures between 2000 and 3000 (Fig. 2-18 and 2-19). This is typical for pump-fed liquid-propellant rocket engines.

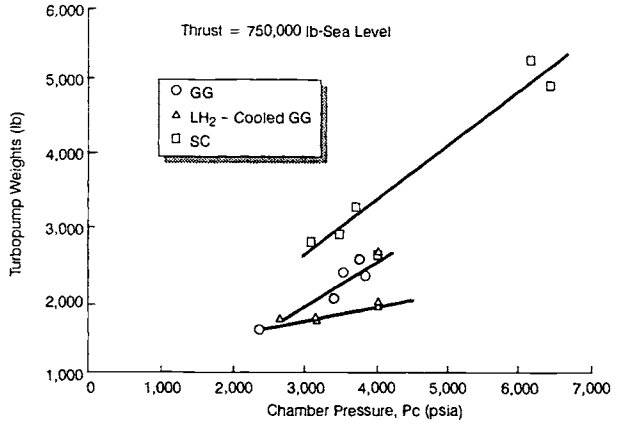

Fig. 2-15 Turbopump weight trends.

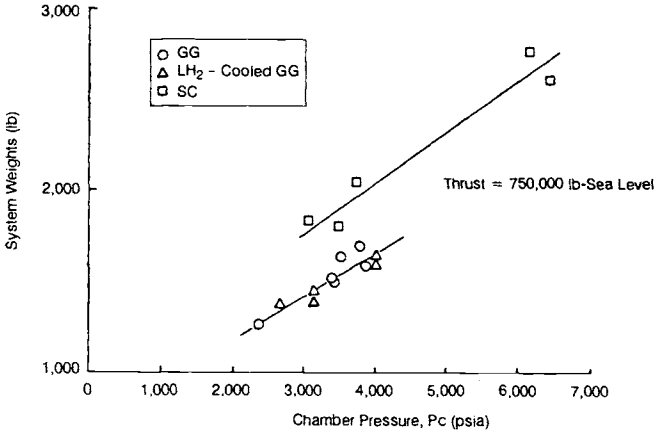

Fig. 2-16 System (ducting, pressurization, etc.) weight trends.

As shown in Fig. 2-18, staged-combustion-cycle engines are considerably heavier than gas-generator-cycle engines, because staged turbines are in series with the thrust chamber, whereas gas-generator turbines are in parallel. The series arrangement produces much higher pump pressure rises for the staged combustion cycle, which, in turn, results in heavier turbopumps (Fig. 2-15), heavier ducts (Fig. 2-16), and heavier valves, preburners, and manifolds (Fig. 2-17). The only major component that is not significantly affected by this cycle difference is the thrust chamber (Fig. 2-18).

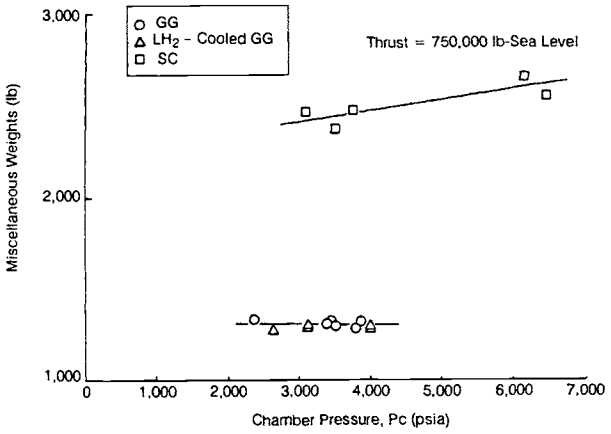

Fig. 2-17 Miscellaneous (valves, controls, GGs, PBs, manifolds) weight trends.

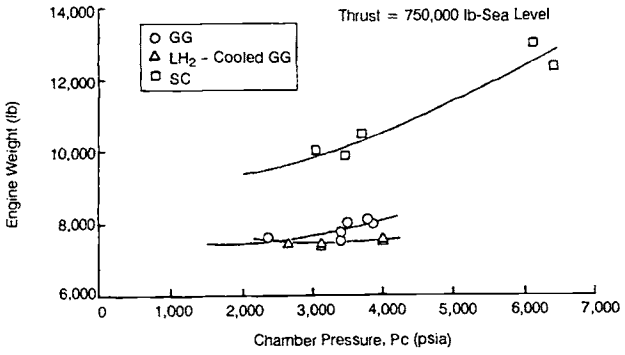

Fig. 2-18 Engine weight trends.

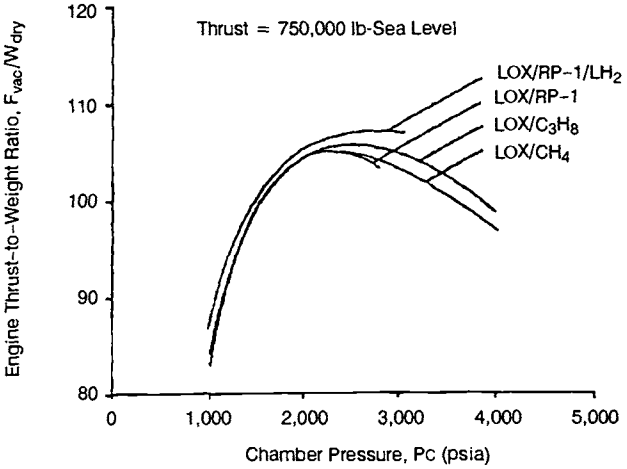

Fig. 2-19 Thrust-to-weight ratios for GG cycles.

2.5 DESIGN PHILOSOPHY

Once the overall engine concept has been defined, the design process can begin. Several factors must be kept in mind. Design quality must be ensured, and a procedure to maintain it throughout the design process must be established. The tasks used to conduct the systems analysis and generate the design layout must occur in the proper sequence and must complement one another. Finally, thorough stress analyses and material selections must be made throughout the design process in order to be able to meet the stringent reliability and weight requirements.

The Importance of Design Quality

Even today, many people regard the design of technical objects as not much more than the act of putting pencil lines on large pieces of paper. The general concept of design is much broader. Many a designer may not even occupy a drawing board, since he may be completely devoted to the creation of basic ideas and solutions, to the numerical checking of their validity, or to the planning, direction, and integration of a design team. On the other hand, many of the most successful designers always retain their board—their most valuable tool of creation—however advanced their position in the organization may be.

It is commonplace to state that a technical project will stand or fall with the quality of its design. Obviously, no device can be built, tested, or used until and unless it has been specified first how to build, test, and operate it. With this in mind, a completed design can be considered a set of instructions for shop actions to follow. For instance, final drawings are only the end product of an extensive, diversified effort which preceded their release. All this is well known, yet sometimes forgotten in the daily grind of a project. Suffice it to state that the design and the designer are principal links of the chain in a project.

This book attempts to supply some of the necessary special tools required to arrive at a detailed "set of instructions" to the shop foreman, from which an engine could be actually built and prepared for test. The following chapters are devoted to the necessary technical detail, based on the latest state of the art in the field of liquid-propellant rocket engines.

The numerous areas that the designer should consider early and keep in mind at all times, for overall increase of quality and reliability and for reduction of cost, include the following:

- Experience, reliability, and reputation of subcontractors and their products.
- Adequate receiving inspection.
- Clear and complete instructions for inspection and quality control.
- Full use of the experience of others in plant and out of plant.
- Use of suitable existing designs, from small parts to subsystems.

Table 2-6 Engine-design checkoff sheet.

Project: _____

Subsystem: _____

Item

1. Have designs for similar earlier projects been thoroughly reviewed and understood?
2. Have principal participants in those projects been contacted? Has their advice been solicited?
3. Has a list been prepared of all problems which were encountered in previous, related projects, including their solutions?
4. Has the new engine system schematic diagram been reviewed for hidden "won't works?"
5. Has the number of components and their complexity been reduced to a minimum, without loss in flexibility and serviceability, for maximum reliability? (in particular: has minimum of moving parts been achieved?)
6. Has a thorough malfunction analysis been made? (Assessment of malfunction effects of each component on all other parts and on the complete system. Include external systems, such as the vehicle and GSE.)
7. Have all existing detail designs been reviewed for possible inclusion and/or adaptation to the new design?
8. Have standard parts been used wherever possible, permissible, or as prescribed by customer specifications?
9. Has the number of external connections ("customer connections") been held to a minimum?
10. Has the location and type of customer connections been chosen in the best interest of the customer? Has he been consulted?
11. Has the need for ground support equipment (GSE) been reduced to a minimum, by number as well as by complexity?
12. Are there good reasons if support equipment used during R&D is different from the one supplied to the field?
13. Have all environmental conditions been considered, including those not likely but possible to occur? (Salt spray, sand, fungus, humidity, temperature, etc.)
14. Has resistance to vibration and shock effects been considered? In all planes? Including improper handling?
15. Have acceleration effects been considered? In all planes?
16. Has the use of critical materials been held to a minimum? (Chromium, molybdenum, tungsten, cobalt, etc.)
17. Has it been made absolutely certain that no cheaper materials will do?
18. Has it been assured that no electrolytic action can occur due to attachment of dissimilar metals?
19. Can the engines be gimballed according to specifications?
20. Can the engine be clustered, if necessary?
21. Can the engine be attached to air frames other than the one presently contemplated?
22. Has it been confirmed that all parts can be made?
23. Has it been confirmed that there is no cheaper way of making these parts?
24. Can the parts readily be assembled, with a minimum of special tools?
25. Has it been made impossible to incorrectly assemble and install any part? (Or incorrectly reassemble and reinstall them in the field?)
26. Will all parts requiring service be readily accessible, prior to and following mating of the engine with the vehicle?
27. Have all markings been called out completely and correctly?
28. Do instructions for inspection and quality control leave no gap?
29. Has it been ascertained that (without penalty) the design cannot save further weight?
30. Is the envelope the smallest possible?
31. Can the system be drained, readily and completely? (Avoidance of traps, low spots, etc.)
32. Have engine propellant feed system components, including pumps and thrust chamber, been designed for minimum trapped propellants after cutoff? (Minimum wet weight)
33. Has the purchasing department been appraised of the significance of mandatory (proven) sources, where applicable?
34. Can it be transported? In one or several pieces?

- Availability and application of an effective failure analysis and correction system.
- Last, but not least, the experience, knowledge, analytical capabilities and judgment of the designer himself.

Time-proven tools available to the designer to optimize his design and the end product it describes include the following:

- Design-checkoff sheets. Checkoff sheets force the designer to check his design systematically from all imaginable angles, before release. A sample sheet is shown in Table 2-6.

Table 2-7 Engine-design-change checkoff sheet.

Project:
Change No.:_____

Supervisor:

Assuming that it has been ascertained beyond doubt (has it?) that a design change must be made, check that the effect of this change is fully understood and implemented in the following areas:

1. Interchangeability of changed parts.
2. "Chain Reaction" to other parts and systems, including vehicle, test facilities, and GSE.
3. Engine start and stop sequence.
4. Engine performance, including gain factors.
5. Conformance with all specifications.
6. Weight, envelope, c.g., moments of inertia, loads.
7. Reliability.
8. Instrumentation, data recording, telemetry.
9. Packaging, shipping, storage.
10. Development and qualification.
11. Human factors: skills, training, notification of persons concerned.
12. Field service equipment and procedures.
13. Handbooks and other user documents.
14. Logistics (spare parts maintenance).
15. Manufacturing tooling and processes.
16. Purchased materials.
17. Subcontractor-supplied parts.
18. Funding.
19. Agreed-to delivery dates.
20. Customer notification and approval.

- Design-change checkoff sheets. Used for systematic evaluation of design changes on all potentially affected systems, including the user and the vehicle. A sample sheet is shown in Table 2-7.
- Failure report. The feedback to the designer of failures of his product in the field, for immediate corrective action.
- Change control. A project-wide effort to scrutinize and minimize proposed changes; and to establish and monitor implementation by engine serial number, if the change must be made.
- Specifications. Detailed specifications, often based on applicable government specifications, to establish the exact execution of all manufacturing processes, materials used, parts purchased, tests to be performed, and so on.

Systems Analysis and Design Layout

So far, numerous important basic considerations for rocket-engine design have been discussed. The detailed engine-design procedures and the treatment of typical examples as they may occur in practice will now follow. The questions are where to start, how to proceed, and what are the expected results.

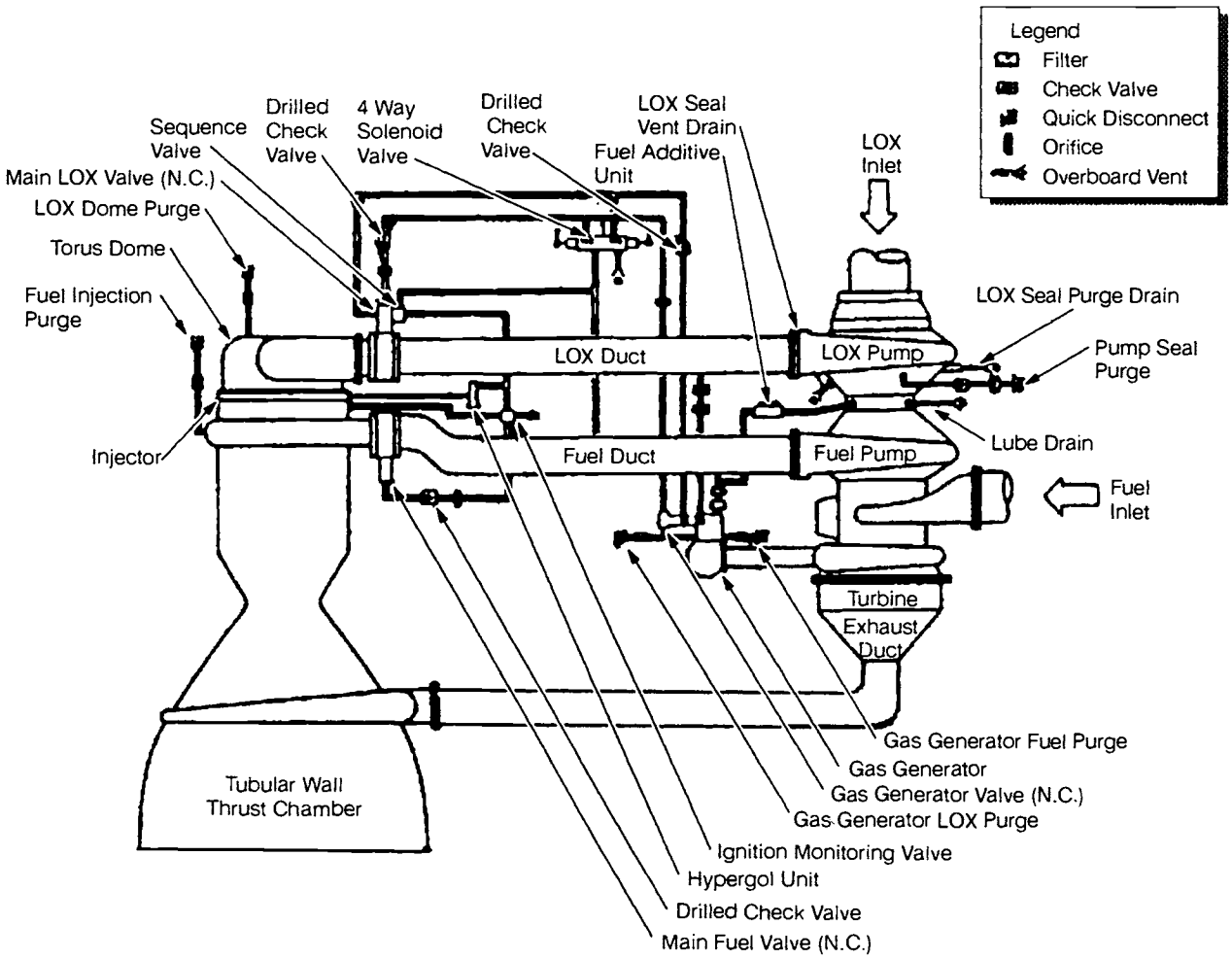

Fig. 2-20 Typical engine-system schematic diagram.

It would be beyond the scope of this book to describe the detailed mechanics of the generation of design drawings, their breakdown, their execution, and the system for their release. The young engineer, who uses this book and already works in industry, knows. The student reader can be assured that the future employer has a manual (usually voluminous) covering this subject exhaustively, and slanted to his specific needs. The following are specific design techniques as they are used in liquid-propellant engine design. Many of these techniques will be applied in subsequent chapters, in connection with the discussion and demonstration of various component designs.

The activities discussed below are not clearly separated phases, following one another in a rigid sequence. Rather, they overlap, frequently occur in parallel, and are tightly interwoven. One of the first drawings the liquid-rocket designer will most likely prepare is a schematic diagram of the engine system. A typical example (Fig. 2-20) shows how the principal components are linked together. The schematic may be accompanied by a sequence diagram, showing the operation of each component in relation to the other as a function of time (Fig. 2-21).

Concurrently, analyses will have been conducted to establish preliminary engine-performance parameters and operating characteristics, as well as individual component configurations and operating principles. Figure 3-1 shows a typical example of a performance diagram. Engine and component starting and operating characteristics can be analytically predicted with a high degree of accuracy by computers. Thus, important knowledge required for optimum design is obtained long before the part is actually built and tested. Savings in time and cost are substantial. These analyses and computer programs will draw heavily upon experience with earlier systems and on advanced design studies.

Once the prototype schematic diagram is considered completed, and performance parameters have been established by the analysis, the first actual "engine picture" will be drawn. This very likely will be a general, in-scale preliminary layout of the engine system and components. Figure 3-2 shows a typical example of a preliminary layout.

Through continued analyses, calculations, consultations, and joint reviews by all participants, the layout will gradually take final shape. In this process, nothing should be left to chance. Consultations with specialists in their fields and rigorous calculations, double-checked for accuracy and presented in a readily understood form, will contribute materially. Layout drawings should be made accurately and to true scale. In this manner, all components of the engine system will have been designed and optimized for one another, rather than "hung on a mounting frame in Christmas-tree fashion."

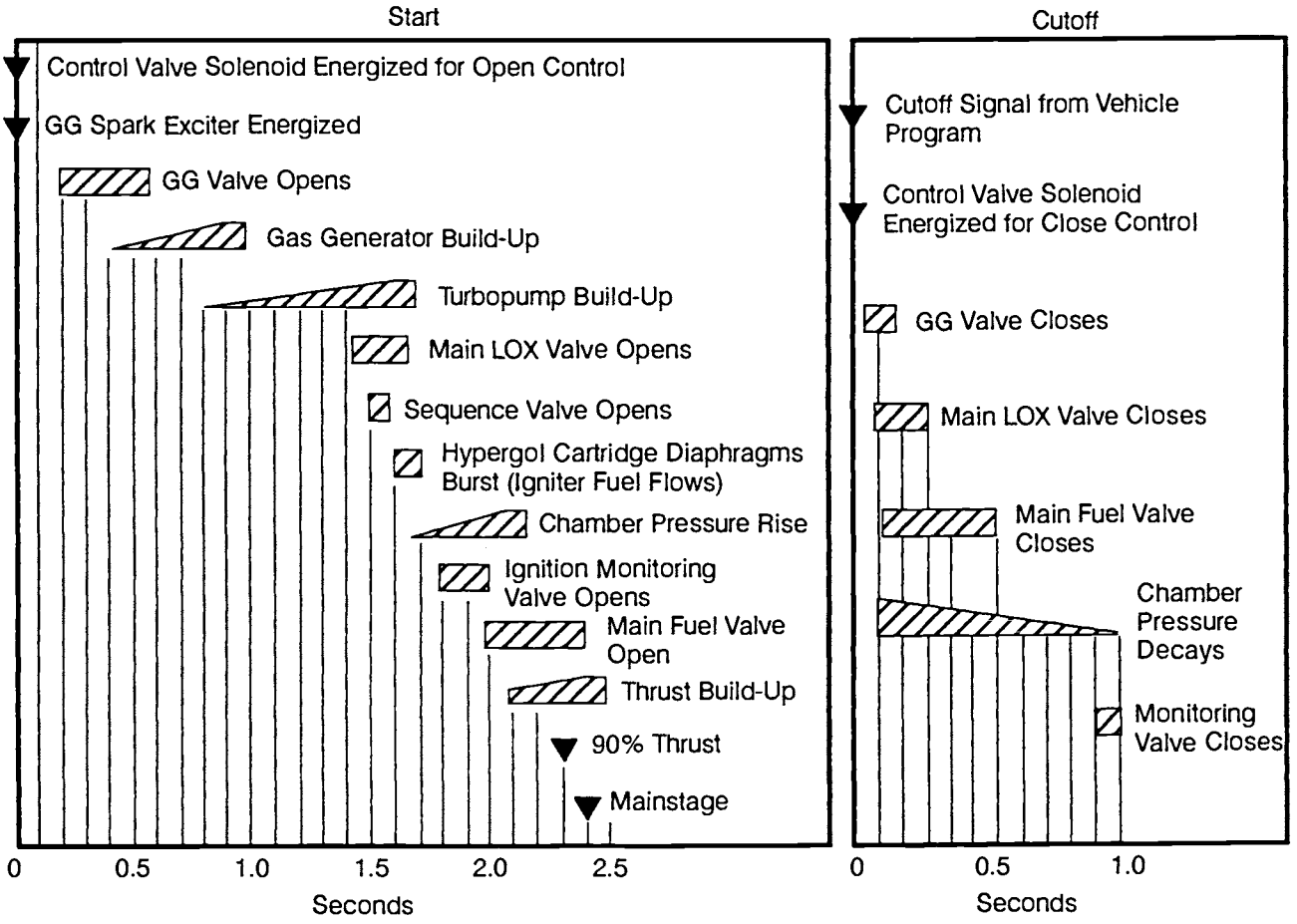

Fig. 2-21 Typical engine-system sequence diagram.

Before working drawings are made from the layouts, they should again be reviewed and revised as necessary, taking into consideration all design aspects, the basic considerations, and the reliability-assurance aspectsthat were discussed here.

Stress Analysis

Stringent reliability and weight requirements call for rigorous and complete stress analyses during the mechanical design of engine components. Stress analyses predict the manner in which a mechanical part will likely fail under anticipated working conditions. They also generate means to prevent failure. The goal is to design a part with sufficient, but not excessive, strength in every detail.

In conjunction with the engine design layouts, the approximate shape of the parts will be established, based on functional requirements and on similar satisfactory designs of the past.

First, a preliminary design sketch is made. Subsequently, probable working loads, environmental effects, deflections, stresses, and final dimensions will be determined, step by step, together with the selection of materials. The following steps are typical for stress analyses:

- Analyze and determine the loads and environmental effects to be expected during the useful life of the part.
- Evaluate the various possible modes of part failure from stress and strain induced within the part by the working loads and from other effects.
- Select the materials and establish their mechanical properties under anticipated working conditions. Applying a likely theory of failure, arrive at the final dimensions of the part.
- Apply experimental stress analyses to refine the above procedure. Redesign the part if necessary.

In certain cases, such as with highly stressed lightweight members, further stress-analysis refinement must be obtained. The greater the refinement desired, the more nearly the methods of stress analysis must indicate the true strength of the member. This requires consideration of complex states of stress, residual stresses, stress concentrations, dynamic effects, inelastic effects, and other influences which determine the true stresses within the member. Here follows discussion of the four steps of stress analysis just enumerated.

Working Loads and Environmental Effects. In stress analyses for mechanical design, working loads and environmental effects should be considered jointly. Stresses and strains induced in mechanical parts by external forces, which we will call "loads," are affected significantly by environmental effects such as temperature, chemical reactions, corrosion, etc. Furthermore, the mechanical properties of most materials are affected by temperature. Sometimes, thermal stresses are induced as a result of temperature gradients within the part. Chemical reactions or corrosion can change the mechanical properties of the material, as well as the size and shape of the part. For the analysis of working loads and environmental effects, the following must be determined:

- The type of load: constant, impact, or repeated.
- The maximum value and duration of a constant load; the maximum and the minimum value for repeated or varying loads.
- The nature of load application: concentrated or uniform; rate per unit of time; and, for repeated loads, total number of working cycles.
- Vibration-load effects.
- Load effects with respect to the nature of material: ductile or brittle.
- Load effects with respect to the shape of a part: effect of geometry on stress concentration.
- Temperature effects: thermal stresses, high-temperature creep and reduction of strength, low-temperature embrittlement.
- Chemical reaction or corrosion effects: embrittlement, stress concentration.

A part will have a proper margin of safety if it is designed with a design limit load larger than the maximum expected working load. The design limit load in turn should be smaller than the calculated damaging loads because of the uncertainty and inaccuracy involved in stress analyses. Damaging loads include endurance limit load, yield load, and ultimate load. The more accurate the analysis, the smaller the allowable margin between the design limit loads and damaging loads. Typical recommended criteria for the working loads, the design limit loads, and the damaging loads (yield and ultimate loads), plus proof-testing loads applied to component design, can be defined as follows:

- Design limit load; select the largest of the following:

$$\begin{matrix} 1.2 \times \text{load (A)} \\ 1.2 \times \text{load (B)} \\ 1.1 \times \text{load (C)} \\ 1.0 \times \text{load (D)} \end{matrix} \qquad (2\text{-}4)$$

where—

Load (A) = Working load under normal steady operating conditions.

Load (B) = Working load under normal transient operating conditions, such as during normal engine start and stop.

Load (C) = Working load under occasional transient operating conditions, such as load during irregular starts.

Load (D) = Mandatory malfunction load that must be taken into account. For example, in a clustered engine configuration, certain mount members may carry the greatest load when one engine ceases to fire while the others are still operating (engine-out capability). In certain instances it is mandatory that an individual rocket engine continue to operate when a given component fails. If this causes significant

structural loads, they are considered mandatory malfunction loads.

- *Yield load*: the load that will induce a stress equal to the yield strength of the material used under rated ambient conditions.
  Yield load = 1.1 design limit load (2-5)

- *Ultimate load*: the load that will induce a stress equal to the ultimate strength of the material used under rated ambient conditions.
  Ultimate load = 1.5 x design limit load (2-6)

- *Proof-test load*: the load applied to test the part during the acceptance inspection. Its value can be adjusted for material properties if the rated ambient conditions cannot be duplicated for the test.

  Proof-test load = 1.0 x design-limit load (2-7)

When a part is subjected to an indefinite number of cycles during service life, such as in rotating machinery, the endurance limit of a material should be applied instead of the ultimate strength. The endurance limit is the stress which can be repeated an infinite number of times without causing failure of the material from progressive fracture or fatigue. The endurance limit of metals, depending largely on range of stress variation, runs as low as 20-60% of ultimate strength in tension. An additional design margin of safety should also be allowed for dynamic-impact loads. When the shape of a part changes abruptly, as with a groove, a notch, a hole, or small section joining a large one, the value of unit stress at points close to the abrupt change or discontinuity increases steeply. Stress increase generally ranges from 100 to 300% of the mean stress in the section.

Sample Calculation 2-1

The hydraulic accumulator of a large liquid-propellant rocket engine has the following design parameters: (a) required volume (fluid capacity), 7238 cu in.; (b) working pressure (load) under normal steady and transient operating conditions, 2000 psia; (c) occasional surge pressure, 2200 psia; (d) mandatory malfunction pressure, 2450 psia; (e) maximum ambient temperature, 3000°F; (f) material selected, AISI 4340 H.T.-180 (strength at room temperature: ultimate, 185,000 psi; yield, 170,000 psi. strength at 300°F: ultimate, 178,000 psi; yield, 150,000 psia).

Problem

Determine the following: (a) lightest possible configuration and resulting dimensions; (b) required proof-test pressure at room temperature.

Solution 2-1

(a) A sphere will be used because it is the lightest pressure vessel for a given volume and pressure. For a 7238-in.^{3} volume:

Required inside diameter of the sphere—

$$= \sqrt[3]{\frac{6}{\pi}\text{volume}} = \sqrt[3]{\frac{6}{\pi} \times 7238}$$

$$= 24 \text{ in.} \qquad (2\text{-}8)$$

From Eq. (2-4), design-limit pressure = largest of the following:

1.2 x 2000 = 2400 psia;
1.1 x 2200 = 2420 psia;
1.0 x 2450 = 2450 psia
Selected: 2450 psia

From Eq. (2-5), yield pressure = 1.1 x 2450 = 2695 psia.

Thickness of sphere wall—

$$= \frac{\text{Yield pressure} \times \text{diameter of sphere}}{4 \times \text{yield strength at } 300^\circ \text{ F}}$$

$$= \frac{2{,}695 \times 24}{4 \times 150{,}000} = 0.108 \text{ in.} \qquad (2\text{-}9)$$

or from Eq. (2-6), with ultimate pressure = 1.5 x 2450 = 3675 psia, thickness of sphere wall—

$$= \frac{\text{Ultimate pressure} \times \text{diameter of sphere}}{4 \times \text{ultimate strength at } 300^\circ \text{ F}}$$

$$= \frac{3{,}675 \times 24}{4 \times 178{,}000} = 0.124 \text{ in.} \qquad (2\text{-}10)$$

Use the higher value, 0.124 in. Therefore, the sphere dimensions will be 24-in. in inside diameter (ID) x 0.124-in. in wall thickness.

(b) From Eq. (2-7), nominal proof-test pressure at 300°F will be—

$$= \text{Design limit pressure}$$

$$= 2{,}450 \text{ psia} \qquad (2\text{-}11)$$

Proof-test pressure corrected for room temperature conditions will be—

$$= 2{,}450 \times \frac{\text{Yield strength at room temperature}}{\text{Yield strength at } 300^\circ \text{ F}}$$

$$= 2{,}450 \times \frac{170{,}000}{150{,}000} = 2{,}780 \text{ psia} \qquad (2\text{-}12)$$

Evaluation of failure modes. There are three basic types of failure mode: elastic deflection, permanent plastic deformation, and fracture. Although not a material failure, elastic deflection may cause a part to perform improperly, resulting in malfunction of a component or system. The other two—plastic deformation and fracture—are material failures influenced by material properties, load and

environmental conditions, and by the shape of the part.

Each of the three failure modes is characterized by certain criteria. For elastic deflection, strain; for plastic deformation and fracture, stress. In the process of stress analyses, following load determination, the possible modes of failure of the part can be established in relation to the criteria induced by the loads. Failure cause can thus be determined, and the failure prevented through design changes. Some of the possible combinations of failure modes and criteria are listed in Table 2-8 together with suggested design remedies.

Selection of Materials and Dimensions. For the process of finalizing the dimensions of a part to endure all working loads and environmental conditions without failure, the strength or ability of the selected material to withstand these loads must be known. Material properties are determined through tests of specimens. In these tests, all conceivable loads, such as tension, compression, torsion, and shear, are applied often with simultaneous application of temperature, vibration, or chemical environment. The results are compiled in graphs and tables. From these tables, materials with properties most suitable for a particular application can be selected.

Experimental Stress Analyses. A rocket-engine part may be of such shape, or may be loaded in such a way, that design based on theoretical analysis alone proves difficult and unreliable. Then experimental stress analyses can supplement the theoretical methods. Many recent advances in stress analysis can be attributed to the development of effective experimental methods. Measurements of strains and stresses will be made while applying loads simulating as closely as possible the ones expected in actual use. These loads can be applied to full-size prototype parts, to scale models made from the real material or from special plastic material, or to portions of full-scale parts. Not infrequently, applied loads are intentionally increased beyond rated levels, until failure of the part occurs. These "tests to failure" can establish the actual margin of safety achieved in the design. The tools used in experimental stress analysis include electrical, mechanical, and optical strain gages and photoelastic plastic models, lacquers, and paints.

Selection of Materials

Selection of materials for liquid-propellant rocket engines is complicated by the extreme environmental conditions these materials must withstand.

Table 2-8 Failure modes and criteria.

Failure Mode	Conditions	Criteria	Design Remedies
1. Elastic deflection:			
a. Stable equilibrium	Load within elastic limits	Strain; linear or angular displacement (stretch or bending)	Change of shape or dimensions (stiffening); material selection
b. Unstable equilibrium	Loads within elastic limits	Buckling; ratio of applied vs critical load	Change of shape or dimensions
c. Vibration	Within elastic limits; abrupt changes of loads; repeated application of load at or near natural frequency	Amplitude, frequency transmissivity, resonance	Stiffening; change of natural frequency; damping
2. Plastic deformation:			
a. Yield	Loads exceed elastic limits	Stress; permanent set	Change of dimensions and/or material
b. Creep	Loads may or may not exceed elastic limits; elevated temperatures	Stress; slow permanent set	Change of dimensions and/or material
3. Fracture:			
a. Overload	Load increase beyond yield point to ultimate strength	Stress; elongation; area reduction; rupture	Change of dimensions and/or material
b. Brittleness	Load above ultimate strength	Stress; rupture with little or no yield	Change of dimensions and/or material; change of heat treatment; change of contour
c. Impact or shock	Abrupt load application to ductile materials	Stress; behavior like brittle materials	Selection of most ductile material; increased margin of safety
d. Fatigue	Many repeated load applications within elastic limits	Stress; number of load applications	Change of shape and dimensions; change of material; increase of endurance limits

Table 2-9 Examples of materials usage in rocket engines.

Material	Examples	Applications	Useful Temp Range	Comments
Austenitic stainless steels	316, 321, 347, 21-6-9, 16-25-6	Nozzle tubing, ducts, bolts, bellows, hydraulic tubing, ducts, washers, shims, turbine discs, injectors	-423°F to 600°F	Susceptible to pitting and stress corrosion
Martensitic stainless steels	440C	Bearings – balls, races	-423°F to 300°F	Susceptible to all forms of corrosion
PH stainless steels	17-4 PH, 17-7 PH, 15-5 PH	Valve parts – stems, poppets	-110°F to 200°F	Susceptible to hydrogen environment embrittlement. Stress corrodes in high strength tempers, marginal for cryogenic applications
Nickel-base superalloys	718, 625, WASPALOY® MAR-M-246 & 247® HASTELLOY-C®	Impellers, inducers, pump housings, valves, ducts,manifolds, bolts, turbine blades, turbine discs, shafts, bellows, stators, injectors	-423°F to 1500°F	Susceptible to hydrogen environment embrittlement
Iron-base superalloys	903, 909, A286	Struts, ducts, bellows, bolts, turbine discs	-423°F to 1100°F	Resistant to hydrogen environment embrittlement
Aluminum alloys	A356, A357, 6061, 7075, T73, 2219	Pump housings, impellers, injectors, gear cases, brackets, valve bodies	-423°F to 200°F	Often used as castings
Copper alloys	OFHC Cu, NARloy-Z, NARloy-A	Thrust chambers, injector rings, baffles	-423°F to 1000°F	High oxygen grades susceptible to hydrogen reaction embrittlement
Titanium alloys	Ti-5Al-2.5 Sn ELI, Ti-6Al-4V ELI Ti-6Al-6V-2Sn Ti-10Y-2Fe-3 Al	Impellers, inducers, pump housings, valve bodies, ducts, gimbal blocks, pressure bottles, hydraulic tubing	-423°F to 600°F	Pyrophoric reaction in LOX, pure GOX, red fuming nitric acid. May absorb hydrogen above -110°F
Beryllium	Be-98, BeO-1.5	Small thrust chambers	70°F to 1200°F	Brittle, avoid all notches in design. Hazardous material, not weldable
Cobolt alloys	HAYNES 188®, L-605, ELGILOY®, MP 3Sn, STELLITE 21®	Injector posts, ducts, springs, turbine blades	-320°F to 2100°F	Vary in susceptibility to hydrogen environment embrittlement
Low alloy steels	4130, 4340, 9310, 52100	Thrust mounts, frames, reinforcing bands, gears, shafts, bolts, bearings	70°F to 300°F	Susceptible to corrosion, marginal for cryogenic applications
Fluorocarbon polymers	Kel-F, PTFE, FEP	Seals, coatings, rub rings, electrical insulation	-423°F to 200°F	Generally compatible with liquid oxygen
Elastomers	Nitrile rubber, silicone rubber, chloroprene rubber, butyl rubber, fluorocarbon rubber	O-rings, gaskets, sealants, electrical insulation, adhesives	70°F to 300°F	Not compatible with liquid oxygen
Nickel	Nickel-200 Electrodeposited Ni	Nozzle tubing, electrodeposited close-outs of coolant channels for combustion chambers	-423°F to 1000°F	Susceptible to hydrogen environment embrittlement
Carbon	P5N, P692	Combustion chamber throat inserts, dynamic turbine seals	-423°F to 600°F	Brittle material
Ceramics	Al_2O_3, ZrO, WC, SiO_2	Protective coatings on turbine blades, nozzles, thrust chambers, thermal insulation, valve seat, and poppet coatings	-423°F to 1500°F	High temperatures, brittle materials

Caution: This table is not to be used for materials selection.

The low temperatures encountered when in contact with cryogenic liquids introduce severe toughness and ductility problems with metals and non-metals alike. On the other hand, metals which contact the hot exhaust gases must be capable of resisting creep and stress rupture at elevated temperatures. Table 2-9 summarizes some examples of materials and their usage.

Both hydrogen and oxygen can precipitate catastrophic failures of many materials. Hydrogen environment embrittlement (HEE) will occur when a susceptible metal undergoes strain in the presence of gaseous hydrogen. Most metals suffer greatest susceptibility near ambient temperature; below 200°F most metals become immune to HEE. However, consideration must be given to start-up and shut-down conditions because even a short-term exposure to warm hydrogen could cause embrittlement. Metals which are most susceptible to HEE include martensitic steels, nickel and nickel alloys, and titanium alloys.

Contact of many metals and nonmetals with oxygen can result in spontaneous ignition. Metals which cannot be used with liquid or gaseous oxygen include titanium and magnesium. Caution must be exercised when using aluminum in high-pressure oxygen (LOX or GOX), particularly in applications when rubbing or particle impingement may occur. Most nonmetallics are not compatible with oxygen systems. Fluorocarbons such as Teflon and Kel-F exhibit limited compatibility but must be batch-tested before use.

Corrosion and stress corrosion cracking (SCC) must be considered when selecting materials for liquid-propellant rocket engines. Many propellants and exhaust gases are corrosive to metals, therefore compatibilities must be determined on an individual, case-by-case basis. Also, metals must withstand severe ambient environments during storage. Alloy steels, magnesium alloys, and high-strength aluminum alloys are generally unsuitable *unless* they are protected from the environment. Likewise, SCC must be considered when selecting metals for engine application. Alloys with low resistance to SCC include alloy steels heat-treated to high strength, precipitation-hardening stainless steels in high-strength conditions, and high-strength aluminum alloys in the-T6 temper.

Finally, the behavior of metals under the vacuum conditions in space must be considered. Metals with low vapor pressure, such as cadmium, will vaporize and could redeposit on other surfaces. Also, metal whiskers can grow on many metals, causing "shorting" of electronic components and switches.

The materials most commonly used in liquid-propellant rocket engines, and their abilities to withstand the aforementioned environmental conditions, are described in more detail in Appendix C.

Introduction to Sample Calculations

3.1 APPROACH

A primary goal of this book—to familiarize the reader with the detailed techniques used by industry in liquid-propellant rocket engine systems and component design—has engendered a set of realistic sample calculations. To promote an understanding of the interrelationship among major subsystems, principal calculations have been made for the engines of a hypothetical multistage space vehicle. These calculations and their associated designs were especially prepared for this book and are not related to existing or planned engines. Because the various subsystems of liquid-propellant rocket engines will be discussed in subsequent chapters, most of the supporting sample calculations throughout the book, will be for the engines of the assumed vehicle. For simplicity of reference, the space vehicle will be called *Alpha*. It will be composed of four stages: A-1, A-2, A-3, and A-4. Table 3-1 lists the major parameters of the *Alpha*.

The *Alpha* vehicle combines realistic designs, even though not necessarily optimized. For instance, a different propellant combination has been chosen for each stage to permit sample calculations and designs for a number of typical propellant combinations, feed systems, and thrust levels. To permit multiple use of parts, fewer combinations would be chosen. In fact, the student and the teacher using this book may find it interesting and instructive to modify the designs chosen. For instance, the student may wish to determine what engine-design parameters would result if Stages A-2 and A-3 were to use the same propellant combination; or what design parameters would be obtained if Stages A-3 and A-4 were combined into one stage, capable of restart and throttling to 30% nominal thrust.

It is not our intent to fix a specific mission for *Alpha*. However, a "primary mission" for it could be the landing of an unmanned scientific payload on the Moon to gather samples and return them to Earth. The staging sequence might then be as follows:

Stage A-1: Boost to 250,000-ft altitude.
Stage A-2: Boost to 300-n.mi altitude and inject into Earth parking orbit.
Stage A-3: Accelerate to escape velocity and inject into a translunar trajectory.
Stage A-4: First start—deceleration for lunar orbit and soft Moon landing of scientific payload; second start—Moon takeoff for return to Earth. In addition to its main power plant, Stage A-4 will require very low-thrust attitude control jets.

Even if designed for a given "primary mission," a vehicle combination retains a certain degree of flexibility. Within the limits of existing propellant-tank configurations, the following principal possibilities of modification exist:

- Omission of the upper two stages for Earth-orbital tankers, shuttle vehicles, space-station assembly, and supply ships.
- Omission of Stage A-4 for unmanned deep-space-probe assignments, with no return intended.
- Off-nominal tanking of one or more stages. This modification may yield some overall performance gains for special missions.

Most emphatically, it is not our intent to say that the stated modifications can be made a few days before launch. Rather, the stages and certain of their subsystems — in particular, the engines — should be regarded as building blocks. Their availability can permit meeting a new requirement, for example, within a year, as compared to several years when "starting from scratch." In such ways, substantial gains have been obtained in practice. The earlier Thor, Redstone, and Atlas Mercury boosters are well-known cases.

Brief mention should be made here of experimental engine systems, sometimes referred to as "breadboard" engines. Because of time and funding limitations, the design and development of liquid-propellant rocket engines for a given mission rarely permit the investigation of novel ideas and principles. New ideas must then be tried independently, detached from rigid schedules. Here, the test effort can be conducted with full awareness that many of the principles under investigation will not "make the grade." However, although those that succeed can be applied to advanced operational systems, the marginal ones are just as valuable, because they were prevented from finding their way into operational engines. If experimentally verified advances are selected for operational use with strong emphasis on vehicle application, true progress will have been

Table 3-1 Four-stage *Alpha* space vehicle.

Takeoff weight, 2,100,000 lb;
Payload[a] for 300-n.mi. orbit, 109,500 lb

Stage	Stage Thrust, lb	Number of Engines	Engine Thrust, lb	Propellant
A-1	3,000,000	4	750,000	LO_2/RP-1
A-2	600,000	4	150,000	LO_2/LH_2
A-3	48,000	3	16,000	LF_2/LH_2
A-4	15,000	2	7,500	N_2O_4/N_2H_4

[a]Consisting of stages 3 and 4 and of the mission payload

made. The major U.S. liquid-propellant engine manufacturers conducted experimental engine programs with excellent results for a number of years.

The reader will now become acquainted with some of the characteristics of the engines which have been selected for the different stages of the *Alpha* vehicle. The summarizing descriptions can serve as a guide and reference throughout the book.

3.2 A-1 STAGE ENGINE

Four engines, each with 750,000-lb thrust, were selected for a combined thrust of 3-million lb, as a compromise between the number of engine systems, and thus complexity, on the one hand, and flexibility, on the other. Flexibility can be gained in different ways, such as including engine-out capabilities using

Table 3-2 A-1 Stage engine operating parameters for sea-level conditions.

Engine (turbopump feed):		
Thrust	lb	750,000
Nominal single-firing duration	s	165
Specific impulse	s	262.4
Oxidizer LO_2:		
Flow rate	lb/s	1,967.7
Density	lb/ft^3	71.38
Fuel RP-1:		
Flow rate	lb/s	892.3
Density	lb/ft^3	50.45
Mixture ratio	O/F	2.20
Thrust chamber (tubular wall construction regeneratively cooled by fuel):		
Thrust	lb	747,000
Specific impulse	s	270
Injector end pressure	psia	1,095
Nozzle stagnation pressure	psia	1,000
Oxidizer flow rate	lb/s	1,941
Fuel flow rate	lb/s	827
Mixture ratio	O/F	2.35
c^* efficiency	%	97.5
c^*	ft/s	5,660
C_f efficiency	%	98
C_f		1.532
Contraction ratio	A_c/A_t	1.6
Expansion ratio	A_e/A_t	14
Throat area A_t	in2	487
L^*	in.	45
Nozzle contour		80% bell
Oxidizer side:		
Injector pressure drop	psi	200
Torus dome pressure drop	psi	150
Line pressure drop	psi	25
Main valve pressure drop	psi	35
Pump inlet pressure	psia	55
Pump discharge pressure	psia	1,505
Developed pump head	ft	2,930
Pump:		
Flow rate	lb/s	1,971
Shaft power	bhp	14,850
Efficiency	%	70.7
Shaft speed	rpm	7,000
Heat exchanger	lb/s	3
Fuel side:		
Injector pressure drop	psi	200
Jacket and manifold pressure drop	psi	270
Line pressure drop	psi	10
Main valve pressure	psi	15
Calibration orifice pressure drop	psi	110
Pump:		
Inlet pressure	psia	45
Discharge pressure	psia	1,720
Developed pump head	ft	4,790
Pump:		
Flow rate	lb/s	892
Shaft power	bhp	11,790
Efficiency	%	65.8
Shaft speed	rpm	7,000
Turbine:		
Inlet pressure	psia	640
Inlet temperature	°F	1400
Pressure ratio		23.7
Gas flow rate	lb/s	92
Shaft power	bhp	27,140
Efficiency	%	58.2
Shaft speed	rpm	7,000
Shaft torque	in-lb	20,380
Auxiliary drive:		
Shaft power	bhp	500
Gas generator system:		
Oxidizer side:		
Flow rate	lb/s	26.7
Entrance loss	psi	25
Line pressure drop	psi	25
Control-orifice pressure drop	psi	615
Valve pressure drop	psi	10
Injector pressure drop	psi	120
Fuel side:		
Flow rate	lb/s	65.3
Entrance loss	psi	25
Line pressure drop	psi	25
Control-orifice pressure drop	psi	800
Valve pressure drop	psi	20
Injector pressure drop	psi	140
Gas generator:		
Mixture ratio	O/F	0.408
Injector end pressure	psia	710
Combustor pressure drop	psi	70
Thrust vector control:		
Minimum acceleration	rad/s2	1
Maximum velocity	deg/s	10
Displacement	deg	±14

smaller systems or designs already in existence and implementing various guidance (gimballing) and packaging considerations.

The propellant combination of liquid oxygen (LOX) and kerosene-type RP-1 fuel was selected for the A-1 engine, principally because high performance will not be as critical for booster first stages as for upper stages. Moreover, both propellants are abundantly available and comparatively inexpensive; the fluids and their combustion products are "docile"; their corrosivity is nil. Both fluids are relatively dense. Liquid-propellant rocket engine systems using these propellants are well developed and reliable, and thus many "off the shelf" components and designs are available for them.

General Engine-System Description

The A-1 engine is a single-start, fixed-thrust, gimballed, bipropellant system. The fuel, RP-1, is also used as the turbopump lubricant and as the engine-control-system actuating fluid. The major components of the A-1 engine are a regeneratively-fuel-cooled, double-pass, tubular-wall thrust chamber with bolt-on injector; a direct-drive turbopump consisting of two centrifugal pumps and a single-stage, two-wheel turbine; an uncooled gas generator with a dual-ball valve; butterfly main valves; and the required controls. The gas generator uses the same propellant combination as the thrust chamber. Table 3-2 presents all necessary operating parameters on which engine component designs will be based for the A-1 engine system.

Figure 3-1 shows the A-1 engine schematic, which identifies clearly all major engine components and their interconnecting plumbing. For the various phases of engine design and development, it has been found useful to work from an "engine-performance diagram," a combination of the basic engine schematic and the principal performance parameters. The A-1 engine diagram is shown in Fig. 3-1. (We suggest that the readers prepare their own performance diagrams for the other three stages.)

For compactness and simplicity of mounting, the turbopump is attached directly to the thrust chamber. All other components either are mounted on these two assemblies or are located in the plumbing system between them. This arrangement permits engine gimballing without pump-discharged, high-pressure propellant-duct flexure. Instead, thrust-vector control is achieved by gimballing the entire engine. The engine weighs approximately 7500 lb dry, 7900 lb wet, and 7830 lb at burnout. The preliminary design layout of the A-1 engine system and its overall dimensions are presented in Fig. 3-2.

System Operation

For starting, the A-1 engine employs a "main-tank-head start" approach, combined with a pressure-ladder sequence. Propellants are used under vehicle tank-head pressures to initiate gas-generator operation. As the turbopump starts to accelerate, main propellant pressures "bootstrap" the system to mainstage level.

Starting sequence. As shown in Figs. 2-20 and 2-21 (pages 45 and 46), launch preparations completed and the main propellant tanks pressurized, the gas-generator's dual spark plugs are activated upon a given signal, and the engine four-way control valve is energized to open. The closing side is vented, and fuel-pump outlet pressure (50 psia from tank head) is admitted to the opening side of the main oxidizer and the gas-generator valve actuators. The gas-generator valves open and admit both propellants to the gas-generator combustor, where they are ignited by the spark plugs. At this point, the main oxidizer valve remains closed; the valve spring prevents it from opening until later in the sequence, when substantially higher actuating fuel pressures are developed by the pump.

The initial, low power level of the gas generator is sufficient to start and accelerate the turbopump. This acceleration, in turn, increases the propellant pressures available to the gas generator, which is connected upstream of the still-closed main fuel and oxidizer valves. As a result, the gas-generator turbine system "bootstraps" itself.

At a predetermined fuel-pump outlet pressure (valve-spring rate selection), the main oxidizer valve opens. During the oxidizer-valve stroke, an integral and mechanically linked igniter fuel-sequence valve is actuated. The sequence valve then admits pressurized fuel to a hypergol igniter cartridge, rupturing its diaphragms. Hypergol (such as triethylaluminum) enters the combustion-chamber igniter elements and ignites with the oxidizer (which is just being admitted by the main oxidizer valve). The fuel following the hypergol sustains the igniter flame.

The chamber pressure which results from igniter combustion is sufficient to actuate the ignition-monitor valve. This valve admits fuel pressure to the actuator that opens the main fuel valve, the last step in the sequence. As the main fuel enters the combustion chamber, the chamber pressure and thrust climb to the rated level.

Cutoff sequence. As shown in Figs. 2-20 and 2-21, a cutoff signal de-energizes, and thus closes the engine four-way control valve. The opening pressures of all valves vent; the valves close. Turbine power and main-chamber pressure decay. While the main propellant tanks vent, all valves are held in the closed position by springs. Note that the gas-generator valve and the main oxidizer valve are closed by admitting actuation pressure to their closing port, but the main fuel valve is closed by spring force only. Experience has shown that cutoff precision is largely influenced by turbopump decay characteristics and by cessation of the propellant flow that has the smallest duct volume below the valve — in this case, the oxidizer (with no cooling jacket). The fast-closing valves need some timing, however, to control pressures caused by waterhammer effects.

3.3 A-2 STAGE ENGINE

For the same reasons as with the first stage, the A-2 will have clustered (four) engines, delivering vacuum thrust of 600,000 lb (150,000 lb per engine). Because

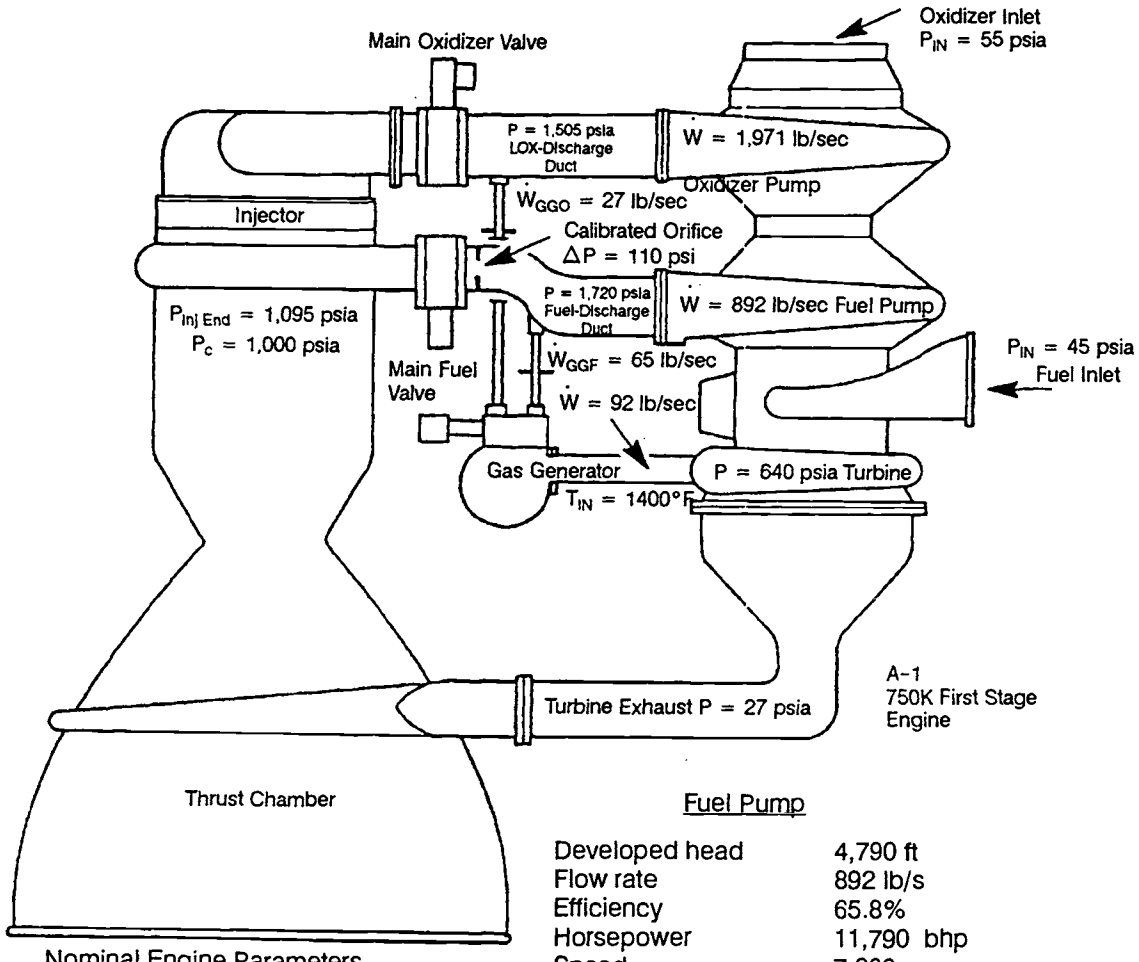

Nominal Engine Parameters

Propellants:	
Liquid oxygen density	71.38 lb/ft^3
RP-1 density	50.45 lb/ft^3
Thrust (sea level)	750,000 lb
Specific impulse	262.4 s
Mixture ratio	2.20

Thrust Chamber

Expansion area ratio	14
Throat area	487 in^2
Thrust	747,000 lb
Specific impulse	270 s
Mixture ratio	2.35
Flow rates:	
Oxidizer	1,941 lb/s
Fuel	827 lb/s

Fuel Pump

Developed head	4,790 ft
Flow rate	892 lb/s
Efficiency	65.8%
Horsepower	11,790 bhp
Speed	7,000 rpm

Oxidizer Pump

Developed head	2,930 ft
Flow rate	1,971 lb/s
Efficiency	70.7%
Horsepower	14,850 bhp
Speed	7,000 rpm

Turbine

P_{in}	640 psia
Pressure ratio	23.7
$Temp_{in}$	1400°F
Efficiency	58.2%
Horsepower	27,140 bhp
Exhaust thrust	3,000 lb

Fig. 3-1 A-1 engine performance diagram.

of the substantial performance gains obtainable through the use of high-energy propellants in upper stages, liquid oxygen/liquid hydrogen (LOX/LH_2) have been selected as propellants.

Over the years, the production and handling of the cryogenics liquid oxygen and liquid hydrogen have become routine; and the price has come down considerably. Both elements are abundantly available. Their combustion product — water vapor — is the most harmless of all propellant exhausts, solid or liquid. Telemetry engineers like it because of its low attenuation of RF signals, an important aspect for vehicle guidance and telemetry. Most important, the yield in specific impulse of this combination approaches theoretical maximum for chemical reactions. Only certain fluorine/hydrogen combinations are slightly higher (approximately 4%). (The extreme toxicity of fluorine and fluorine compounds, both as liquids and as components of combustion products, makes fluorine less attractive for operational use.) By building the A-1 and A-2 stages a little larger, the same payload that fluorine offers can be obtained.

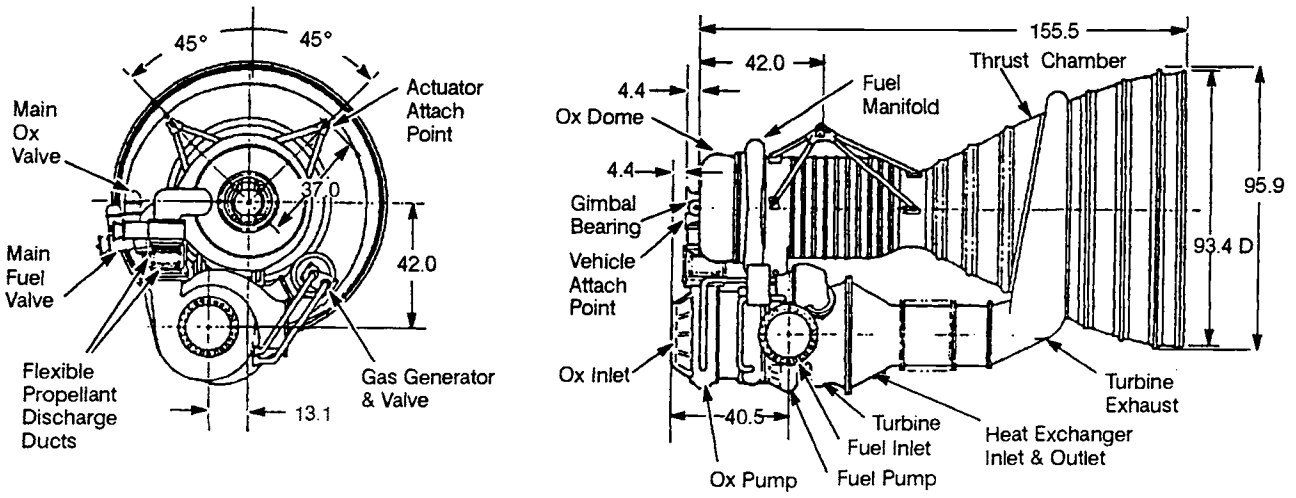

Fig. 3-2 Preliminary layout of A-1 first-stage engine system.

Moreover, all the advantages of LOX/LH_2 are retained, including the extensive past experience with them.

Even so, hydrogen does have its drawbacks, the principal one being its low density, resulting in rather bulky tanks, which make it an unattractive candidate for first-stage/booster applications in most cases. For a typical oxygen-to-hydrogen mixture ratio of 5:1, the corresponding volume ratio is inversed: 1:5. This disadvantage, however, will be offset for upper stages by the high-energy yield (I_S). The improved state of the art of ultralightweight vehicle and tank constructions will further increase the superiority of hydrogen for upper stages.

Low density also creates a high boiloff rate, unless tanks and lines are properly insulated. Because of the low density and the resulting large surface area of the containers, the heat input per unit of hydrogen mass is high. Furthermore, the temperature of liquid hydrogen is sufficiently low to liquefy air on tank surfaces. This liquefaction sharply increases heat-transfer rates, resulting in extreme boiloff rates. Tank-and-line insulation, therefore, is vital. Although the techniques of rocket-vehicle insulation are highly developed, the necessary insulation does impose some weight penalties.

Overall, however, hydrogen produces a substantial net performance gain for upper stages.

General Engine-System Description

The A-2 engine is a single-start, fixed-thrust, gimballed, bipropellant system. The thrust chamber features a combination of fuel regenerative cooling and film cooling with turbine exhaust gas. The chamber assembly is fed by two independent, direct-drive centrifugal turbopumps. For the fuel, an alternative axial pump may be chosen. Each operates at optimum speed. Hot gases are tapped off the main combustion chamber to power the turbines. A hot-gas orifice in the tapoff duct controls the engine thrust level. The turbines, gas-coupled in parallel, exhaust to the thrust chamber, being injected in the 30:1-expansion-area-ratio plane. Thus, the gases provide film cooling for the nozzle portion and from there to the 40:1-area-ratio plane. The remainder of the chamber, upstream of the 30:1 plane, is regeneratively cooled (1 1/2 pass). Helium gas actuates the controls. No lubricants and no fluids that could freeze at low temperatures are used. Hot gases generated by a solid-propellant turbine spinner start the engine. Chlorine trifluoride (ClF_3), hypergolic with LH_2, ignites the combustion chamber. The turbine spinner and igniter fluid are both insulated and temperature-conditioned electrically from a ground source until first-stage takeoff. Gaseous hydrogen bled from the thrust-chamber coolant passage pressurizes the main-fuel tank. A small portion of liquid oxygen, bled from the oxidizer-pump discharge and heated in a heat exchanger, pressurizes the main oxidizer tank .

Table 3-3 lists the A-2 engine operating parameters. The engine schematic diagram appears in Fig. 3-3. Note that engine parameters are based on *vacuum* conditions—because A-2 starts and operates in a vacuum for its entire duration. In the case of the A-2 Stage, the starting altitude of 250,000 ft can be considered absolute vacuum, for all practical purposes.

Gimballing the entire engine applies TVC. The engine weighs approximately 2181 lb dry, 2317 lb wet, and 2292 lb at burnout. The overall dimensions and the preliminary design layout of the A-2 engine are shown in Fig. 3-4.

System Operation

The A-2 engine (Fig. 3-3 and 3-5) employs a "turbine spin start" for very fast buildup (less than 2 s from start signal to main stage). Starting power is furnished by a turbine spinner. Chamber tapoff gases then bootstrap the turbine.

Starting Sequence

As part of the separation and staging sequence, a vehicle programmer furnishes a start signal (to the engine) that ignites the turbine spinner, which supplies gases at 2000°F to the turbines and combustion chamber. This signal also energizes the solenoid of the engine control valve that vents the closing side of both main propellant-valve actuators and

Table 3-3 A-2 Stage engine operating parameters for vacuum conditions.

Engine (turbopump feed):		
Thrust	lb	150,000
Nominal single-firing duration	s	250
Specific impulse	s	434
Oxidizer LO_2:		
Flow rate	lb/s	288
Density	lb/ft^3	71.38
Fuel LH_2:		
Flow rate	lb/s	57.6
Density	lb/ft^3	4.42
Mixture ratio	O/F	5
Thrust chamber (tubular wall construction regeneratively cooled by fuel. Nozzle extension film cooled by turbine exhaust gas):		
Thrust	lb	149,500
Specific impulse	s	440
Injector end pressure	psia	875
Nozzle stagnation pressure	psia	800
Oxidizer flow rate	lb/s	285.2
Fuel flow rate	lb/s	54.5
Mixture ratio	O/F	5.22
c* efficiency	%	97.5
c*	ft/s	7,480
C_f efficiency	%	101
C_f		1.895
Contraction ratio	A_c/A_t	1.60
Expansion ratio	A_e/A_t	40
Throat area A_t	in^2	98.6
L*	in.	26
Nozzle contour		75% bell
Oxidizer side:		
Injector pressure drop	psi	160
Torus dome pressure drop	psi	40
Line pressure drop	psi	20
Main valve pressure drop	psi	20
Calibration orifice pressure drop	psi	60
Pump inlet pressure	psia	35
Pump discharge pressure	psia	1,175
Developed pump head	ft	2,305
Pump weight flow rate	lb/s	290.5
Pump volumetric flow rate	gpm	1,830
Heat exchanger bleed (oxidizer tank pressurization)	lb/s	2.5
Pump:		
Shaft power	bhp	1,910
Efficiency	%	64
Shaft speed	rpm	8,600
Turbine:		
Inlet pressure	psia	700
Inlet temperature	°F	1200
Pressure ratio		16
Gas flow rate	lb/s	1.58
Shaft power	bhp	1,940
Efficiency	%	54.3
Shaft speed	rpm	8,600
Shaft torque	in-lb	14,200
Fuel side:		
Injector pressure drop	psi	100
Jacket and manifold pressure drop	psi	325
Line pressure drop	psi	20
Main valve pressure drop	psi	20
Calibration orifice pressure drop	psi	60
Pump inlet pressure	psia	25
Pump discharge pressure	psia	1,400
Developed pump head	ft	44,800
Pump weight flow rate	lb/s	59.8
Pump volumetric flow rate	gpm	6,080
Heat exchanger bleed	lb/s	2.2
Pump:		
Shaft power	bhp	6,100
Efficiency	%	80
Shaft speed	rpm	27,000
Chamber coolant passage bleed for fuel tank pressurization	lb/s	2.2
Turbine:		
Inlet pressure	psia	700
Inlet temperature	°F	1200
Pressure ratio		16
Gas flow rate	lb/s	4.32
Shaft power	bhp	6,100
Efficiency	%	62.5
Shaft speed	rpm	27,000
Shaft torque	in-lb	14,250
Tapoff gas from thrust chamber for turbine drive:		
Pressure	lb/in^2	750
Temperature	°F	1200
Weight flow rate	lb/s	5.9
Mixture ratio	O/F	0.90
Thrust vector control:		
Minimum acceleration	rad/s^2	2
Maximum velocity	deg/s	15
Displacement	deg	±6

pressurizes the opening side of the fuel-valve actuator with helium gas. Simultaneously, the hypergol-sequence valve (mechanically linked to the main fuel valve), is opened and the actuator of the (normally open) fuel-bleed valve is pressurized closed. The fuel flows through the chamber cooling jacket under increasing pump-discharge pressure and injects into the combustion chamber. Ignition is achieved by the hypergolic reaction between hydrogen and the slug of chlorine trifluoride forced into the chamber by increased oxidizer-pump discharge pressure.

When the main fuel valve reaches the 90%-open position, ports open that are integral with the actuating piston and permit helium gas to flow through the hypergol-monitor valve and to pressurize the open side of the main oxidizer-valve actuator. The main oxidizer valve opens, admitting oxidizer to the chamber where pressure builds up rapidly. Chamber tapoff gases bootstrap the turbines to mainstage operation. The spinner burns for about 1.2 s. After the main stage level is achieved, the propel-lant-utilization servo system begins to function.

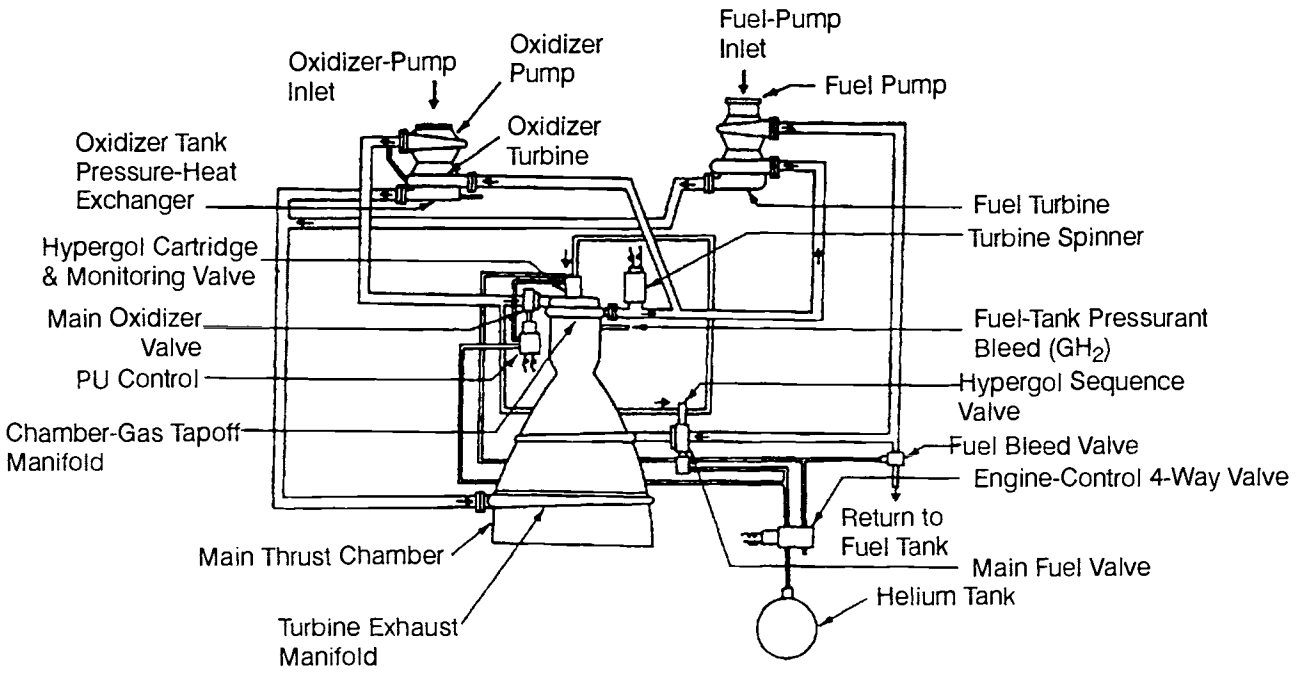

Fig. 3-3 A-2 Stage engine-system schematic diagram.

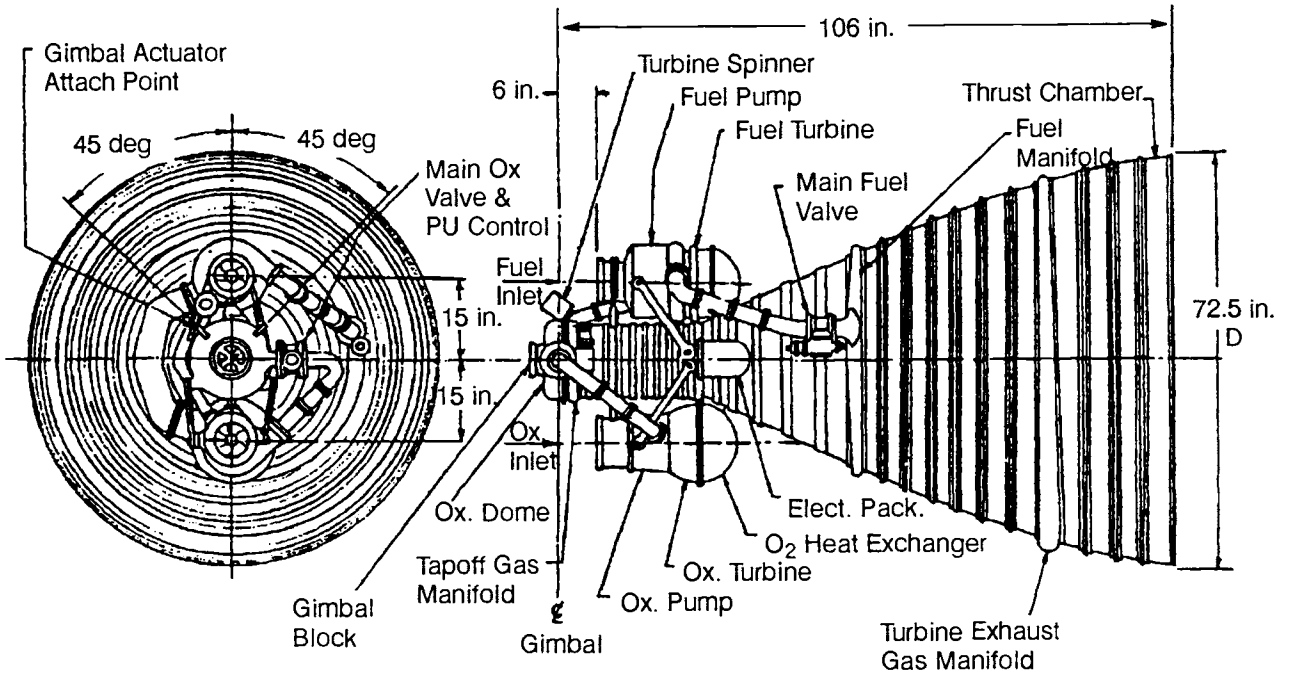

Fig. 3-4 Preliminary layout of A-2 Stage engine system.

Cutoff Sequence

The cutoff signal, received from the vehicle programmer, de-energizes the engine-control valve causing it to close. This closure vents the open side and pressurizes the closing side of the main propellant-valve actuators. By proper orificing of the helium lines, the main oxidizer valve is made to close faster than the main fuel valve, to ensure a fuel-rich cutoff. The valve closure causes engine thrust to decay. The fuel bleed valve opens after venting of the helium pressure in its actuator.

3.4 A-3 STAGE ENGINE

Three engines of 16,000-lb thrust each power the A-3 Stage. They employ liquid fluorine and liquid hydrogen as propellants to gain the very high performance required of upper stages. To date, there have been almost no applications of fluorine as a propellant except on an experimental basis. Fluorine has vigorous and reliable hypergolic ignition and superior specific impulse with most fuels. The high density of liquid fluorine, combined with high performance with liquid hydrogen, results in maximum payloads. It

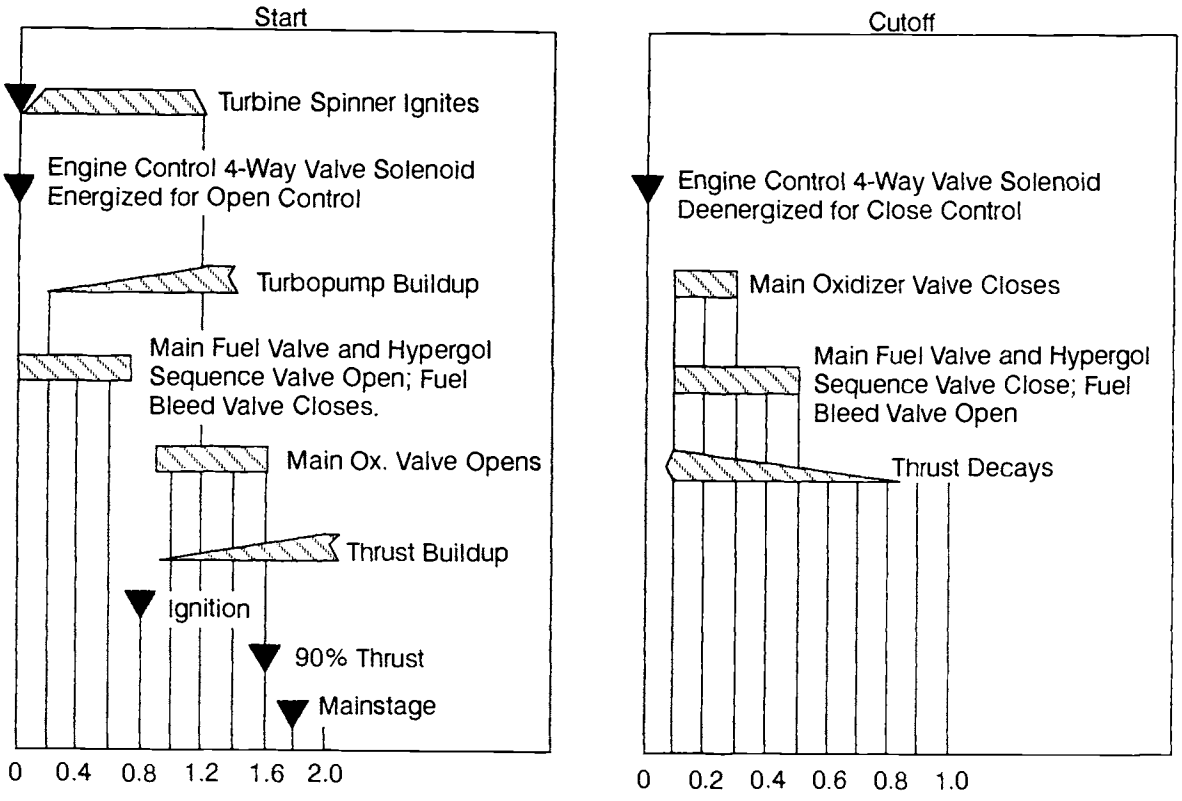

Fig. 3-5 A-2 Stage engine-system sequence diagram.

has been thought that as mis-sion requirements become more ambitious, payload advantages from the fluorine-oxidized propellant combination might compensate for handling problems caused by fluorine toxicity and corrosiveness.

General Engine-System Description

The A-3 engine is a multiple-start, gimballed, bipropellant system. The thrust chamber uses a combination of fuel-film (LH_2) and radiation cooling. The propellants are fed directly from pressurized propellant tanks, through main propellant valves, to thrust-chamber inlets. The propellant tanks and their gas pressurization system are considered part of the engine propellant-feed system. Gaseous helium, supplied from a high-pressure helium bottle located inside the main fuel tank, pressurizes the main oxidizer tank. The main fuel tank is pressurized by gaseous hydrogen, supplied from a liquid-hydrogen bottle pressurized by helium; it is located inside the main fuel tank. Both pressurants are heated in heat exchangers, located at the thrust-chamber nozzle extensions, before being expanded through pressure regulators and transferred to the propellant tanks. Helium gas operates the main valves and the gimbal actuators and purges the propellant manifolds during the hypergolic start.

Table 3-4 lists A-3 engine operating parameters for vacuum conditions. Figure 3-6 shows the propulsion system schematic diagram.

The highly reactive and toxic nature of fluorine forces simplicity and a minimum number of components in design of the entire propulsion system. Welded joints are used extensively. No rotating seals are employed; sliding seals, the metal-bellows type.

A preliminary design layout of the A-3 propulsion system and its dimensions are depicted in Fig. 3-7. The fuel tank is pressure- rather than mechanically stabilized. The thrust loads are transmitted to the payload through the fuel tank. Both tanks are insulated, along with the ducts between tanks and engine systems. Gimballing the thrust chambers applies TVC. Each basic engine weighs approximately 330 lb dry and 365 lb at burnout. Each has a cylindrical space envelope of 5 ft 4 in. in diam by 7 ft 6 in. in length. The propulsion system (including the three engines and the tankage) weighs approximately 5130 lb dry, 37,900 lb wet, and 5530 lb at burnout.

System Operation

The A-3 propulsion system is designed for automatic start on receiving a signal from the guidance system. A similar signal starts automatic engine shutdown. One or more restarts can be made by merely sending additional start/shutdown signals to the propulsion system. Figure 3-8 shows the operational sequence of the A-3 engine stage. In conjunction with Fig. 3-6, this figure illustrates the startup and shutdown of the system.

3.5 A-4 STAGE ENGINE

The A-4 stage employs two engines, each of 7500-lb thrust, to achieve a desired thrust of 15,000 lb. It is as-

sumed that the mission assigned to this fourth (and last) stage of the space vehicle may require prolonged cruising periods before ignition and possibly even longer waiting periods before re-ignition. Although it would be desirable to utilize the high-energy propellants of the second and third stages, the fact that they are cryogenics poses some problems. Cryogenic propellants could probably be used with refined insulation techniques, but they were not selected because the increase in complexity (resulting from the insulation techniques) was deemed inappropriate for a vehicle of this size. Solid propellants were also ruled out because of the requirement for repeated starts and throttling.

Storable hypergolics possess certain characteristics that contribute to high reliability—such as simplicity of ignition and ease of propellant maintenance (because the propellants can be contained in closed vessels over reasonable temperature ranges for considerable periods of time without developing excessively high pressures or undergoing unacceptable changes in composition). Applicable storables with high performance include chlorine trifluoride (ClF_3)/hydrazine (N_2H_4) and nitrogen tetroxide (N_2O_4)/N_2H_4. As a monopropellant, hydrazine is prone to explosive thermal decomposition, but this condition can be remedied by certain additives. The ClF_3/N_2H_4 produces slightly higher performance

Table 3-4 A-3 Stage engine operating parameters for vacuum conditions.

Engine (pressurized gas-feed):		
Thrust	lb	16,000
Nominal total multiple-firing duration	s	300
Specific impulse	s	446
Oxidizer LF_2:		
Density	lb/ft^3	94.16
Flow rate	lb/s	30.78
Fuel LH_2:		
Density	lb/ft^3	4.42
Flow rate	lb/s	5.13
Mixture ratio	O/F	6
Thrust chamber (solid wall film cooled by fuel and radiation cooled on nozzle extension):		
Thrust	lb	16,000
Specific impulse	s	446
Injector end pressure	psia	110
Nozzle stagnation pressure	psia	100
Oxidizer flow rate	lb/s	30.78
Fuel flow rate	lb/s	5.13
Mixture ratio	O/F	6
c* efficiency	%	98
c*	ft/s	7,910
C_f efficiency	%	102
C_f		1.817
Contraction ratio	A_c/A_t	2
Expansion ratio	A_e/A_t	35
Throat area A_t	in^2	88
L*	in.	28
Nozzle contour		70% bell
Thrust vector control:		
Minimum acceleration	rad/s^2	2
Maximum velocity	deg/s	15
Displacement	deg	±7
Oxidizer side (pressurized by heated helium):		
Injector pressure drop	psi	25
Oxidizer dome pressure drop	psi	5
Main valve pressure drop	psi	8
Line pressure drop	psi	5
Calibration orifice pressure drop	psi	17
Oxidizer tank pressure	psia	170
Total oxidizer weight (300 s duration for 3 engines, plus 1% residual)	lb	27,950
Oxidizer tank volume (including 3% ullage volume)	ft^3	305
Pressurant (helium) flow rate (assuming tank gas temperature 400°R)	lb/s	0.1555
Total pressurant weight (including other requirements in the system) (assume storage bottle final pressure 350 psi, plus 2% reserve)	lb	60
Pressurant storage tank, volume (assume 200°R storage temperature, including 3% ullage volume)	ft^3	7.35
Pressurant storage tank, initial pressure	psia	4,500
Fuel side (pressurized by heated hydrogen)		
Injector pressure drop	psi	25
Inlet manifold pressure drop	psi	10
Main valve pressure drop	psi	10
Line pressure drop	psi	5
Fuel tank pressure	psia	160
Total fuel weight (300 s duration for 3 engines, plus 1% residual)	lb	4,660
Fuel tank volume (including 3% ullage volume)	ft^3	1,087
Pressurant (hydrogen) flow rate (assuming tank vapor temperature 300°R)	lb/s	0.346
Total pressurant weight (assuming storage bottle final pressure 350 psia, plus 4% reserve)	lb	108
Pressurant storage tank, volume (liquid hydrogen including 3% ullage volume)	ft^3	25.2
Pressurant storage tank, pressure	psia	350

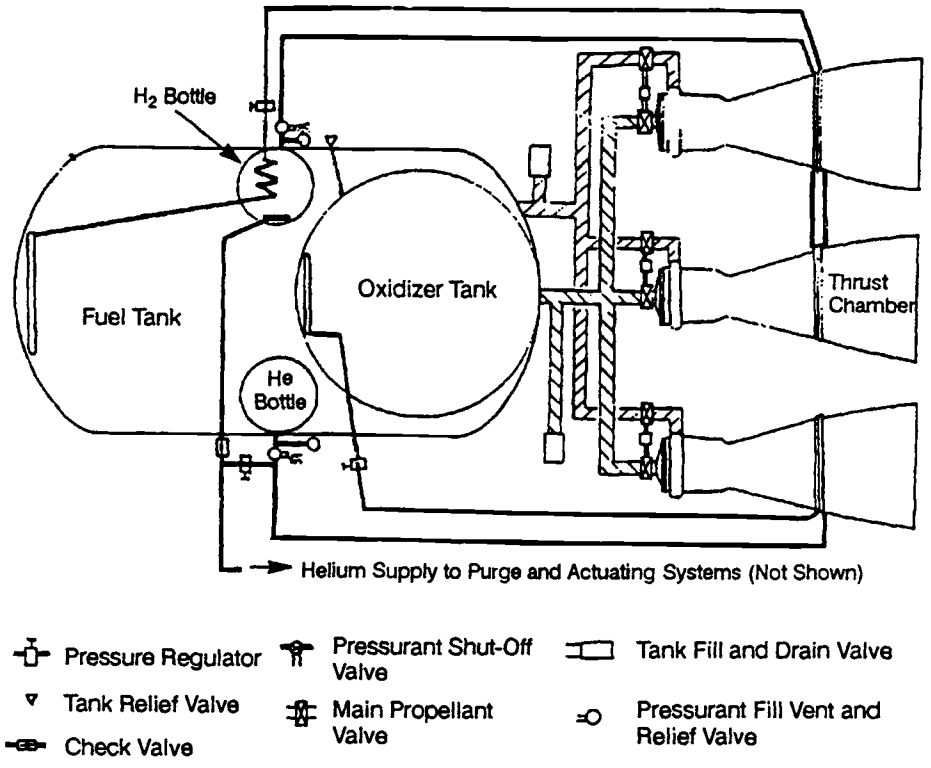

Fig. 3-6 A-3 Stage engine-system schematic diagram.

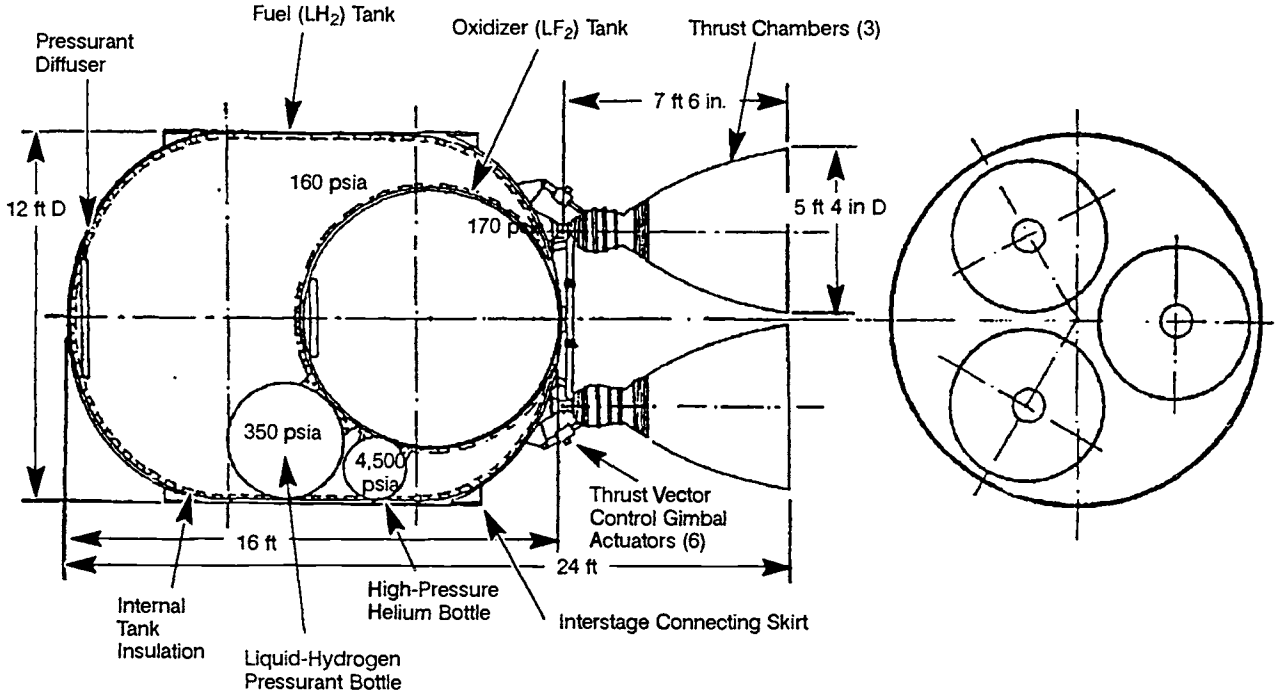

Fig. 3-7 Preliminary layout of A-3 Stage propulsion system.

Table 3-5 A-4 Stage engine operating parameters for vacuum conditions.

Engine (pressurized gas-feed) and throttleable:		
Thrust	lb	7,500
Nominal total multiple-firing duration at full thrust	s	410
Specific impulse	s	320
Oxidizer N_2O_4:		
Density	lb/ft^3	90.88
Flow rate	lb/s	12.78
Fuel N_2H_4:		
Density	lb/ft^3	63.25
Flow rate	lb/s	10.65
Mixture ratio	O/F	1.2
Thrust chamber (ablatively cooled and radiation cooled on nozzle extension):		
Thrust	lb	7,500
Specific impulse	s	320
Injector end pressure	psia	110
Nozzle stagnation pressure	psia	100
Oxidizer flow	lb/s	12.78
Fuel flow	lb/s	10.65
Mixture ratio	O/F	1.2
c* efficiency	%	98
c*	ft/s	5,540
C_f efficiency	%	101
C_f		1.858
Contraction ratio	A_c/A_t	2
Expansion ratio	A_e/A_t	35
Throat area, A_t	in^2	40.4
L*	in.	32
Nozzle contour		70% bell
Thrust vector control:		
Minimum acceleration	rad/s^2	2
Maximum velocity	deg/s	15
Displacement	deg	±7
Oxidizer side (pressurized by heated helium):		
Injector pressure drop	psi	25
Oxidizer dome pressure drop	psi	3
Line pressure drop	psi	5
Main valve pressure drop	psi	4
Calibration orifice pressure drop	psi	8
Mixture ratio control reserve	psi	10
Oxidizer tank pressure	psia	165
Total oxidizer weight (410 s full thrust duration for 2 engines, plus 0.8% residual)	lb	10,560
Oxidizer tank volume (including 2.5% ullage volume)	ft^3	120
Nominal pressurant (helium) flow rate (assuming tank ullage temperature 700°R)	lb/s	0.0225
Total pressurant weight (assuming storage bottle final temperature 191°R, pressure 400 psia, plus 2% reserve)	lb	12.95
Pressurant storage tank:		
Volume	ft^3	4.3
Pressure	psia	4,500
Temperature	°R	560 max
Fuel side (pressurized by heated helium):		
Injector pressure drop	psi	25
Inlet manifold pressure drop	psi	4
Line pressure drop	psi	4
Main valve pressure drop	psi	4
Calibration orifice pressure drop	psi	8
Fuel tank pressure	psi	155
Total fuel weight (410 s full thrust duration for 2 engines, plus 1.2% residual)	lb	8,840
Fuel tank volume (including 2.5 ullage volume)	ft^3	143.5
Nominal pressurant (helium) flow rate (assuming tank ullage temperature 700°R)	lb/s	0.025
Total pressurant weight (assuming storage bottle final temperature 191°R, pressure 400 psia, plus 2% reserve)	lb	14.4
Pressurant storage tank:		
Volume	ft^3	4.77
Pressure	psia	4,500
Temperature	°R	560 max

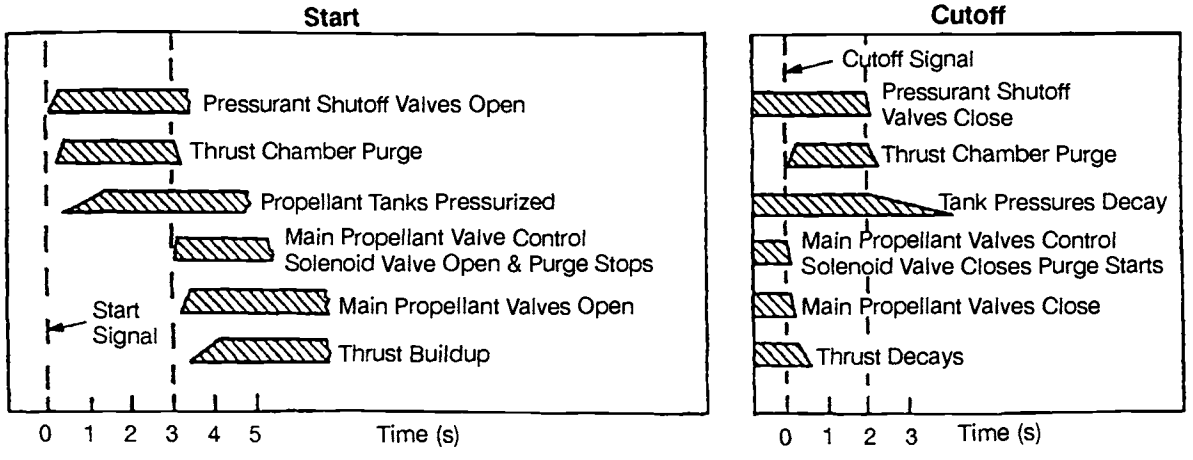

Fig. 3-8 A-3 Stage engine and propulsion system operational sequence.

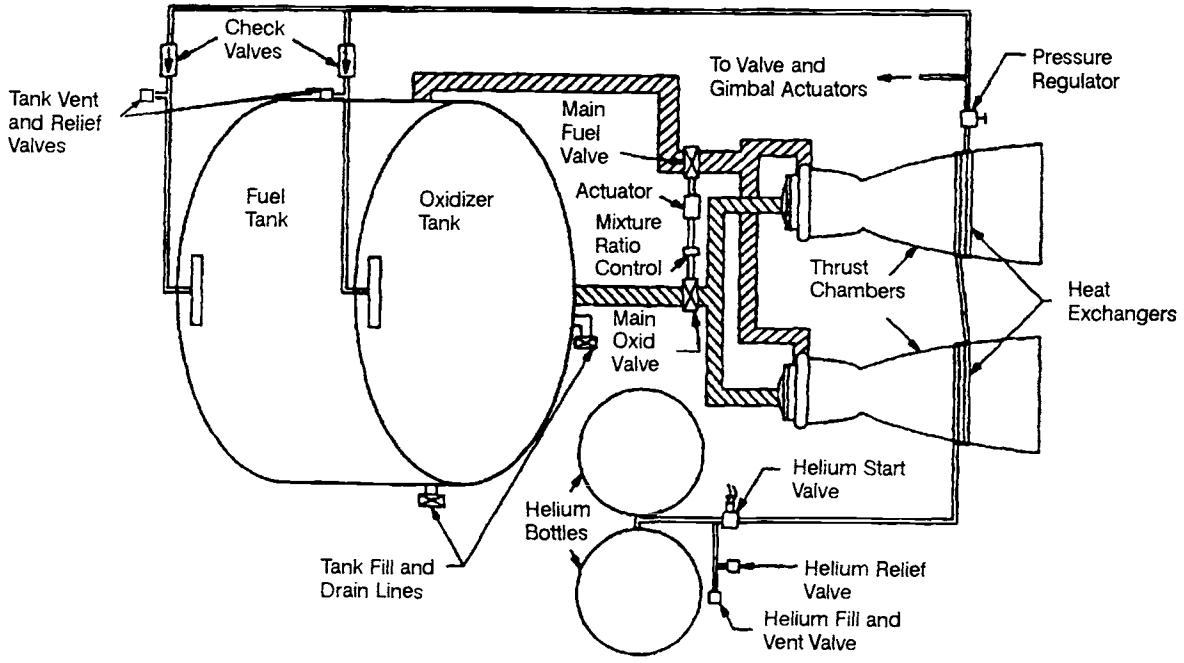

Fig. 3-9 A-4 Stage engine and propulsion system schematic diagram.

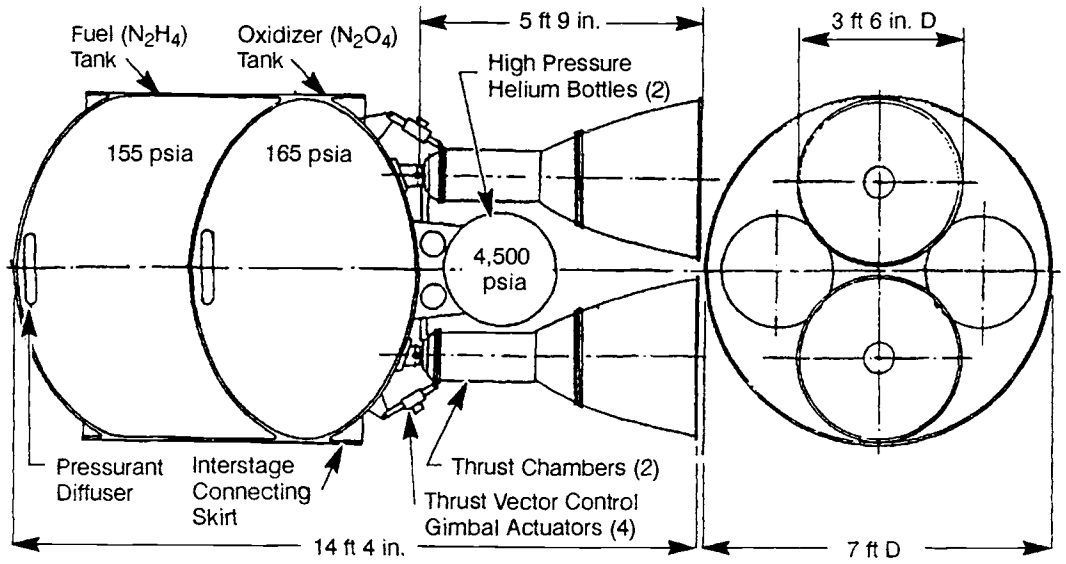

Fig. 3-10 Preliminary layout of A-4 Stage propulsion system.

than N_2O_4/N_2H_4, but ClF_3 requires special design provisions for handling because of its thermal characteristics. For this reason, N_2O_4/N_2H_4 was chosen for the A-4 engine. N_2O_4/N_2H_4 has performance comparable to LO_2/RP-1's.

Teflon and Teflon 100X can be used as seal material in the A-4 engine system. Although Kel-F is a satisfactory material for use with N_2H_4, it degrades after short-term service in N_2O_4. Most series 300 stainless steels, aluminum alloys, nickel, and nickel-base brazing alloys can be used as construction materials.

General Engine System

The A-4 engine is a multiple-start, variable-thrust, gimballed, bipropellant system. The thrust-chamber assembly employs ablative and radiation cooling and undergoes hypergolic ignition. This engine system links two thrust chambers to one propellant-feed system and one set of propellant controls. The propellants are fed by pressurants directly from the propellant tanks through the main propellant valves to thrust-chamber inlets. Gaseous helium supplied from high-pressure bottles pressurizes both tanks. The pressurant is heated in heat exchangers, located at the thrust-chamber nozzle extensions before expansion through a pressure regulator and transferred to the propellant tanks. Helium gas also operates the main valves and the gimbal actuators.

Table 3-5 gives A-4 engine operating parameters at vacuum condition. Figure 3-9 shows an engine and propulsion system schematic diagram.

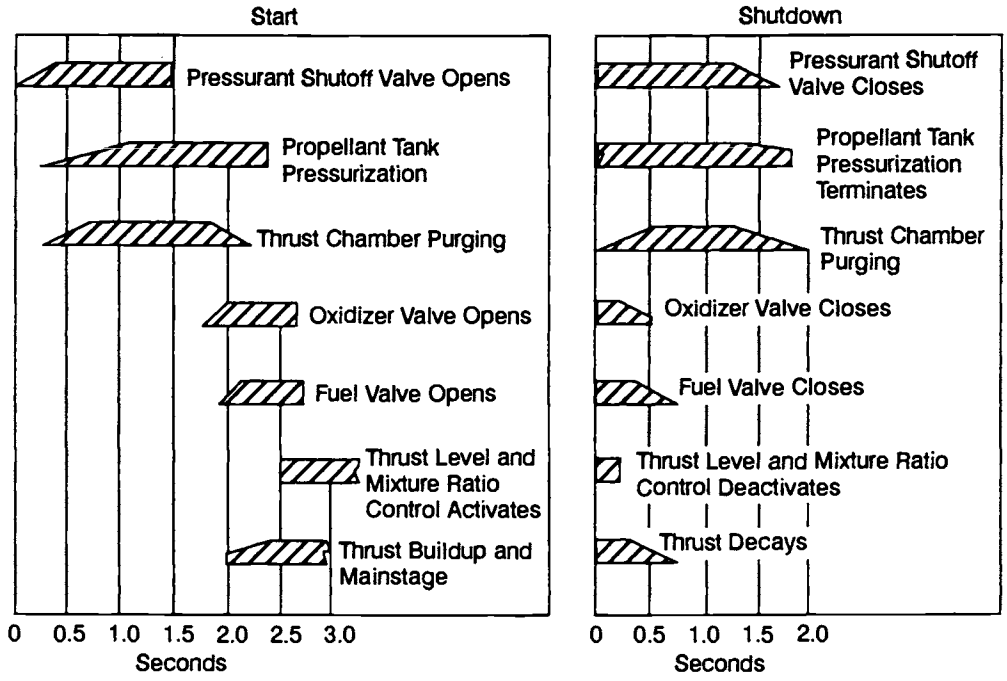

Fig. 3-11 A-4 Stage engine operational sequence.

The engine gimbal blocks are fastened to thrust mounts attached to the aft end of the oxidizer tank. The fuel tank is attached forward of the oxidizer tank to form an integral vehicle structure. As in the A-3 system, the thrust loads are transmitted to the payload through the pressure-stabilized tank assembly. The propellant ducts between fuel tank and engine systems are routed outboard and covered by fairings for protection against aerodynamic heating and for lower air resistance during first-stage boost.

Both throttling and propellant-utilization control are achieved by varying the degree of opening of both propellant valves. The positions of valves are controlled by the vehicle guidance system in conjunction with a vehicle propellant-quantity measuring system. Gimballing the thrust chambers applies TVC. The basic single engine weighs approximately 150 lb dry and 170 lb at burnout. It has a cylindrical space envelope of 3 ft 6 in. in diam by 5 ft 9 in. in length. The complete propulsion system (including the two engines and the tanks) weighs approximately 725 lb dry, 19,649 lb wet, and 795 lb at burnout. Figure 3-10 shows the preliminary design layout of the A-4 propulsion system.

Note that for the A-3 and A-4 engines, a slightly smaller nozzle expansion area ratio has been specified than for the A-2. Although all three upper stages operate in vacuum and can use the largest practical expansion area ratio for best performance, other considerations influence the ratio actually chosen.

System Operation

The propulsion system has been designed to start automatically upon a signal from the guidance system. During main-stage operation, engine's thrust level and mixture ratio will be controlled continuously through the engine-control package by the guidance and propellant-utilization systems. A guidance signal shuts the engine down. The propulsion system can restart an indefinite number of times. It can be operated at any level between 10% and full thrust. Figure 3-11 shows the operational sequence of the A-4 Stage engine.

Design of Thrust Chambers and Other Combustion Devices

While each of the proud designers of the various subsystems of a rocket engine considers his product as "the heart of the engine," the thrust-chamber assembly undeniably embodies the essence of rocket propulsion: the acceleration and ejection of matter, the reaction to which imparts propulsive force to the vehicle. The designer aims to achieve this with a device of maximum performance, stability, and durability and minimum size, weight, and cost.

The design of a thrust chamber presents one of the more complex tasks in the field of liquid-propellant rocket engineering, primarily because the basic processes, especially the combustion within the thrust chamber, are imperfectly understood. This makes analyses difficult and imprecise. Thus, during most engine-development programs, a major effort must be expended on design and development of the thrust chamber.

4.1 BASIC THRUST-CHAMBER ELEMENTS

The thermodynamic processes governing the generation of thrust within a chamber have been treated in Chapter 1. In a liquid-bipropellant rocket engine, the following basic steps characterize the conversion of the energy of propellants into thrust:

1) The liquid propellants, at proper oxidizer/fuel mixture ratio (O/F), are injected into the combustion chamber and atomized into droplets.

2) The droplets are subsequently vaporized by heat transfer from the surrounding gas. The size and velocity of the droplets change continuously during their entrainment in the combustion-gas flow.

3) The vaporized propellants are mixed rapidly, further heated, and promptly react, thus continuously increasing gaseous mass flowrate within the combustion chamber. This gas-phase reaction is aided by high-speed diffusion of active molecules and atoms. Combustion will essentially be complete upstream of the chamber throat, when all liquid droplets have been vaporized. Under certain conditions, shock and detonation waves may be generated by local disturbances in the chamber, possibly caused by fluctuations in mixing or propellant flow. These may trigger pressure oscillations that are amplified and maintained by the combustion processes. Such high-amplitude waves—referred to as "combustion instability"—produce high levels of vibration and heat flux that can be very destructive. A major portion of the design and development effort therefore concerns stable combustion.

4) As the gaseous products of the combustion process pass toward and through the throat, they are accelerated to sonic, and then to supersonic, velocity within the diverging nozzle section, and are finally ejected.

The basic elements of a thrust chamber include a combustion chamber, expansion nozzle, injector, ignition device (for nonhypergolic propellants), propellant inlet and distribution manifolds, and appropriate surfaces and structures for component mounting and for carrying the thrust forces to the vehicle.

Figures 4-1 and 4-2 illustrate a thrust-chamber assembly that typifies those employed for relatively low chamber pressure (<1000 psia) and liquid oxygen/RP-1 propellants. This assembly has three major subassemblies: thrust-chamber body (which includes the expansion nozzle), injector, and igniter. In some cases, particularly for larger engines, the nozzle may be a separate piece that attaches to the thrust-chamber body at some small distance beyond the throat.

The thrust-chamber body subassembly, a venturi shape, consists of a cylindrical section in which the combustion occurs, a section narrowing toward a throat, and a bell-shaped, expanding nozzle section through which the combustion gases are expelled. The wall of this chamber is constructed of nickel tubes running longitudinally, joined by silver brazing, and retained by external tension bands. The tubes, of 0.012-in. wall thickness, have rectangular cross section of varying area, to conform to the thrust-chamber shape. This construction permits simple thrust-chamber cooling by flowing fuel through the tubes of the chamber wall. The fuel, under pressure, enters the thrust-chamber body at the fuel-manifold

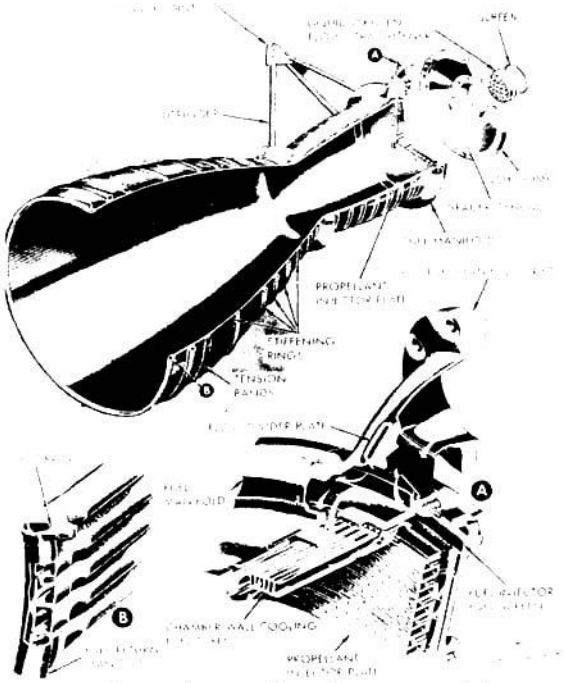

Fig. 4-1 Thrust-chamber assembly.

inlet and is distributed to alternate thrust-chamber tubes. It then moves down toward the nozzle exit where the fuel-return manifold reverses the flow into the return tubes. The fuel then flows through an injector fuel screen, and into the injector. To meet conditions of high heat flux (e.g., LOX/hydrogen combustion at high chamber pressure), the chamber will usually be constructed from a single solid piece of highly conductive material containing many small slots (coolant-flow passages) within the wall, instead of tubes.

Following are the operating characteristics and principal dimensions of a hypothetical thrust chamber similar to the one shown in Fig. 4-1:

Propellants	LOX/RP-1
O/F mixture ratio	2.30
Characteristic velocity c*, ft/s	5400
Thrust coefficient C_f (sea level)	1.489
Specific impulse $(I_s)_{tc}$ (sea level), s	249
Total propellant flowrate, lb/s	402
Thrust (sea level), lb	100,000
Chamber pressure (injector end), psia	520
Chamber pressure (nozzle stagnation), psia	480
Average gas specific-heat ratio	1.233
Combustion-chamber cross-section area, $in.^2$	244
Throat area, $in.^2$	140
Nozzle exit area, $in.^2$	1120
Combustion-chamber volume (above throat), in^3	5320
Combustion-chamber length (to throat), in.	28.5
Characteristic chamber length L*, in.	38
Overall thrust-chamber length, in.	73
Design contraction area ratio	1.60
Design expansion area ratio	8

High-strength bolts hold the thrust-chamber injector (Fig. 4-2)—a round plate honeycombed with circular and radial inner passages which lead to drilled injection orifices—in position at the fuel manifold, below the liquid-oxygen dome. The seals between the injector and thrust-chamber bodies are of the O-ring type, made of material selected for compatibility with the fuel. A mount in the center of the injector permits installation of a pyrotechnic igniter. The injector has 20 circular concentric copper rings that contain the injection orifices. Fuel and oxidizer are kept separate by an elaborate distribution system feeding alternate rings. Fuel flows through the outermost ring, through each alternate inner ring, and through a central fuel disk separately fed from an igniter fuel valve through an ignition fuel-inlet port. Liquid oxygen is supplied to the remaining rings. The injection orifices are angled so that the propellant streams impinge upon each other in the thrust chamber, in a like-on-like pattern (i.e., LOX on LOX and fuel on fuel). The primary orifices are arranged in pairs, with 0.416 in. between center lines and a 40-deg included impingement angle, for both propellants.

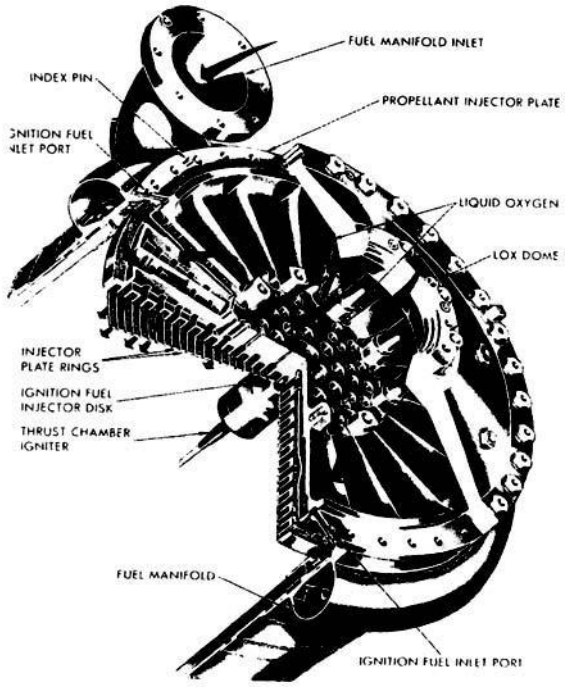

Fig. 4-2 Thrust-chamber injector.

The liquid-oxygen dome provides the inlet for the liquid oxygen. It also serves as the thrust-chamber-to-vehicle attachment interface. The electrically fired pyrotechnic igniter is mounted at the center of the injector.

Injector design, particularly selection of the number, size, and location of orifices, will be crucially important to the performance and stability (and often thrust-chamber-wall heat flux) of the engine. In addition to the like-impinging doublet elements described above, the injector may also employ unlike impingement and multiple (more than two) stream impingements. Finally, liquid/gas propellant combinations will usually employ coaxial injection elements in which the gaseous fuel (e.g., hydrogen or methane) in the annulus atomizes the liquid (e.g., LOX) in the central stream.

4.2 THRUST-CHAMBER PERFORMANCE PARAMETERS

The significance of the parameters that express or influence the efficiency of thrust-chamber operation has been discussed in section 1.3 of Chapter 1. Before discussing the details of actual thrust-chamber design, the parameters will be summarized here and their use illustrated for design calculations, by applying them to the engine systems of the *Alpha* vehicle discussed in Chapter 3.

Specific Impulse I_S (s)

From Eq. 1-31 and 1-31c:

$$(I_s)_{tc} = \frac{F}{\dot{W}_{tc}} = \frac{c^* C_f}{g}$$

The I_S figure indicates the overall quality of the thrust-chamber design, showing the level of thrust generated per "running propellant expenditure."

Characteristic Velocity c^* (ft/s)

From Eq. 1-32a:

$$c^* = f(\gamma, R, (T_c)_{ns}) \qquad (4\text{-}1)$$

Assuming that the propellant and mixture-ratio selections have been made, it can be expected that the gas properties (γ,R) will fall into a known band. From there on, c^* almost entirely depends on the temperature of the gases. Obviously, this temperature has a theoretical maximum for a selected propellant combination. How close to this maximum the chamber will operate depends on influences discussed for mixture ratio in Chapter 2. Figures 4-3, 4-4, 4-5, and 4-6 illustrate this. The c^* peaks at combustion temperatures somewhat lower than maximum. Other considerations, such as bulk densities, which affect vehicle tank sizes, may cause further adjustments of the mixture ratio to gain optimum overall vehicle performance. Within these boundaries, the quality of the combustion process greatly depends on the design efficiency of the thrust-chamber assembly, in particular, the injector.

Thrust Coefficient C_f (dimensionless)

From Eq. 1-33a:

$$C_f = f(\gamma, \epsilon, p_a) \qquad (4\text{-}2)$$

Assume that the performance efficiency of energy generation through the combustion process, the effects of which have just been summarized for c^*, has been determined. Then, with a given gas property γ, the performance efficiency of the remaining thrust-generating functions of the thrust chamber, essentially those of the divergent nozzle, will depend on the nozzle geometry (mainly ϵ, which determines the pressure ratio $p_e/(p_c)ns$ and the ambient pressure (p_a).

Performance Calculation

In design practice, the calculation of thrust-chamber performance is based on theoretical propellant combustion data and the application of certain correction factors, as explained in Chapter 1. The theoretical propellant combustion data are derived from thermochemical computations which equate the heat of reaction of the propellant combination to the rise in enthalpy of the combustion gases. Typical propellant combustion data at frozen composition are presented in Fig. 4-3 through 4-6. For given propellant combinations and chamber-nozzle stagnation pressures $(P_c)_{ns}$, the values of the combustion gas temperature $(T_c)_{ns}$, molecular weight M, and specific heat ratio γ are plotted against the O/F mixture ratio r_w. Performance correction factors are determined by the theoretical assumptions and from test data, as well as from the chosen design configurations. Typical performance calculation methods have been demonstrated earlier by sample calculation (1-3). The following sample calculations illustrate more specific approaches. Although the frozen composition curves in Fig. 4.3 to 4.6 are used in these examples, the corresponding equilibrium composition curves are now generally employed.

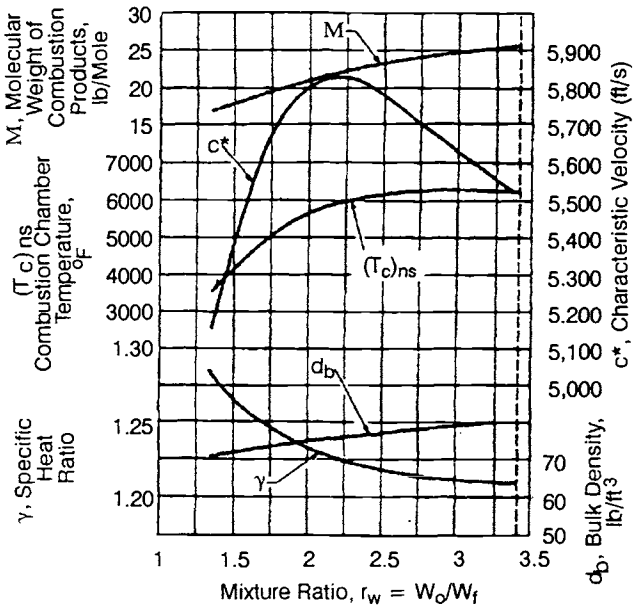

Fig. 4-3 Theoretical O_2/RP-2 combustion data. Frozen composition; $(p_c)_{ns}$ = 1000 psia.

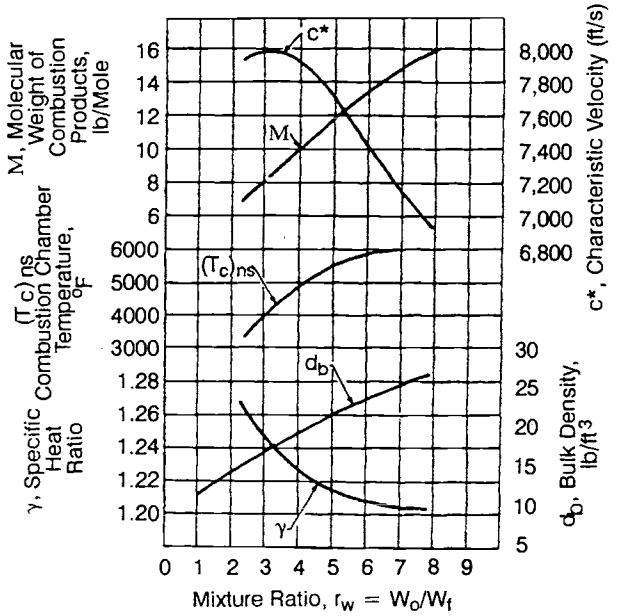

Fig. 4-4 Theoretical O_2/H_2 combustion data. Frozen composition; $(p_c)_{ns}$ = 800 psia.

Sample Calculation 4-1

Problem

Determine the design values of c^*, C_f, and $(I_s)_{tc}$ for the engine thrust chambers of the stages of the hypothetical *Alpha* vehicle, with the following assumed design parameters:

(a) *750K A-1 Stage Engine:* Propellants, LO_2/RP-1; thrust chamber O/F mixture ratio, 2.35; $(P_c)_{ns}$, 1000 psia; propellant combustion data, Fig. 4-3; nozzle expansion area ratio $\varepsilon = 14$.

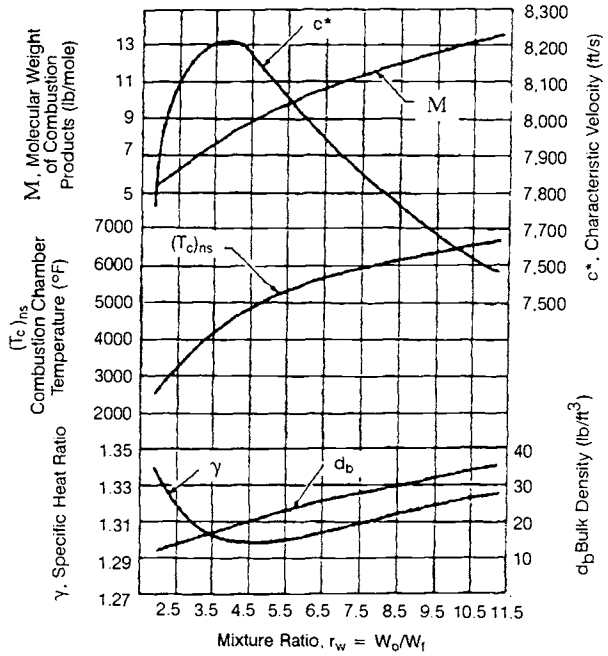

Fig. 4-5 Theoretical F_2/H_2 combustion data. Frozen composition; $(p_c)_{ns}$ = 100 psia.

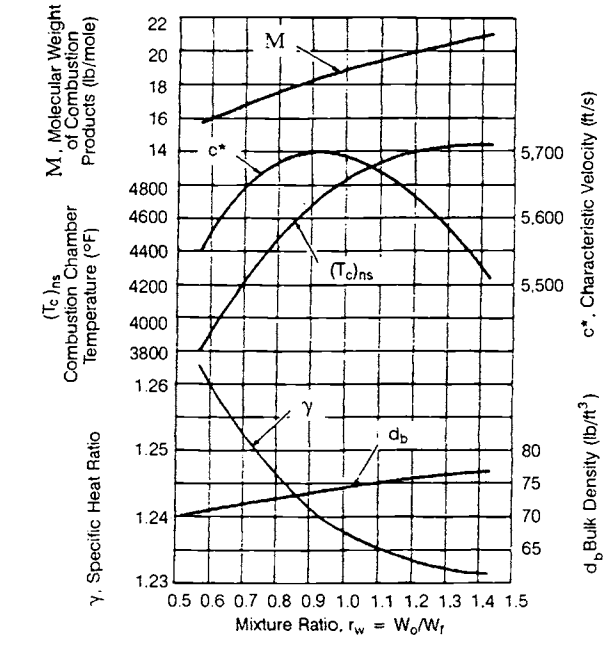

Fig. 4-6 Theoretical N_2O_3/N_2H_4 combustion data. Frozen composition; $(p_c)_{ns}$ = 100 psia.

(b) *150K A-2 Stage Engine:* Propellants, LO_2/LH_2; thrust chamber O/F mixture ratio, 5.22; $(P_c)_{ns}$, 800 psia; propellant combustion data, Fig. 4-4; nozzle expansion area ratio $\varepsilon = 40$.

Solution 4-1

(a) From Fig. 4-3 for LO_2/RP-1 at $(P_c)_{ns}$ = 1000 psia and a mixture ratio of 2.35, the following values are derived for the chamber product gases:

$(T_c)_{ns}$ = 6000°F or 6460°R, M = 22.5 lb/mol, γ = 1.222

Substitute into Eq. (1-32a):

$$\text{Theoretical } c^* = \sqrt{\frac{32.2 \times 1.222 \times 6{,}460 \times 1{,}544/22.5}{0.7215}}$$

$$= 5810 \text{ ft/s}$$

This value for c^* can also be derived from Fig. 4-3. For a good combustion chamber and injector design, the c^* correction factor for LO_2/RP-1 and frozen composition will be about 0.975.

$$\text{Design } c^* = 5810 \times 0.975 = 5660 \text{ ft/s}$$

For $\gamma = 1.222$, $\varepsilon = 14$, a theoretical vacuum C_f value of 1.768 can be derived from Fig. 1.11:

$$\text{Theoretical } C_f \text{ at sea level} = (C_f)_{vac} - \frac{\varepsilon p_a}{(P_c)_{ns}}$$

$$= 1.768 - \frac{14 \times 14.7}{1{,}000}$$

$$= 1.562$$

Sea level C_f can also be calculated using Eq. (1-33a), with the aid of Eq. (1-20). With effective nozzle-contour design, an overall C_f correction factor of 0.98 for LO_2/RP-1 frozen composition can be used. Design sea level $C_f = 1.562 \times 0.98 = 1.531$.

From Eq. (1-31c):

$$\text{Design sea level } (I_s)_{tc} = \frac{5660 \times 1.531}{32.2} = 270 \text{ s}$$

(b) A-2 Stage engine: From Fig. 4-4 for LO_2/LH_2 at $(P_c)_{ns}$ = 800 psia and a O/F mixture ratio of 5.22, the following values are derived for the chamber product gases:

$(T_c)_{ns}$ = 5580°F or 6040°R, M = 12 lb/mol, γ = 1.213

Substitute into Eq. (1-32a):

$$\text{Theoretical } c^* = \sqrt{\frac{32.2 \times 1.213 \times 6{,}040 \times 1{,}544/12}{0.717}}$$

$$= 7670 \text{ ft/s}$$

Based on experimental data, a c^* correction factor can be assumed for the LO_2/LH_2 frozen-composition data of about 0.975.

$$\text{Design } c^* = 7670 \times 0.975 = 7480 \text{ ft/s}$$

For $\gamma = 1.213$ and $\varepsilon = 40$, a theoretical vacuum C_f value of 1.876 can be derived from Fig. 1-17. C_f can also be calculated using equations (1-33a) and (1-20). With effective nozzle-contour design, an overall C_f correction factor value of 1.01 can be used for LO_2/LH_2 frozen-composition data:

$$\text{Design vacuum } C_f = 1.876 \times 1.01 = 1.895$$

From Eq. (1-31c):

$$\text{Design vacuum } (I_s)_{tc} = \frac{7480 \times 1.895}{32.2} = 440 \text{ s}$$

The reader should perform his own calculations for the A-3 and the A-4 engines, with the aid of Tables 3-4 and 3-5 and Fig. 4-5 and 4-6.

4.3 THRUST-CHAMBER CONFIGURATION LAYOUT

After major thrust-chamber operating parameters such as type of propellant, thrust level, chamber pressure, C_f, c^*, and I_s have been established from engine system requirements and performance calculations, one of the fundamental dimensions of the thrust chamber, the throat area, can be readily derived (Eq. 1-33). The throat area is usually the starting point of a thrust-chamber configuration layout. The combustion chamber and nozzle section are commonly designed as an integral thrust-chamber body. For light weight and ease of manufacture, a thrust chamber will have the general shape of a pressure vessel with wall surfaces of rotation and smooth contours.

Combustion-Chamber Volume

The combustion chamber serves as an envelope to retain the propellants for a sufficient period ("stay time") to ensure complete mixing and combustion. The required stay time, or combustion residence time, is a function of many parameters. The rate of combustion is determined by the propellant combination, the injected conditions of the propellants (liquid, gas, gel), combustor geometry (contraction ratio, Mach number, turbulence level), and injector design. Rate-limiting factors are vaporization rates for liquid propellants (or surface-regression rates for injected solids), mixing time, and the (seldom limiting) kinetic rates of the reactions. Larger engines, with their typically larger injection elements, will produce larger drop sizes, extending the time required for combustion completion. Combustor volume thus has a definite effect on combustion efficiency. The theoretically required combustion-chamber volume is a function of the mass flowrate of the propellants, the average density of the combustion products, and the stay time needed for efficient combustion. This relationship can be expressed by the following equation:

$$V_c = \dot{W}_{tc} V t_s \qquad (4\text{-}3)$$

where V_c = chamber volume, ft^3; $\dot{W}_{tc}$ = propellant mass flowrate, lb/s; V = average specific volume, ft^3/lb; and t_s = propellant stay-time, s.

A useful parameter relative to chamber volume and residence time is the "characteristic length" (L*, pronounced "L-star")—the chamber volume (in cubic inches) divided by the nozzle sonic throat area (in square inches):

$$L^* = \frac{V_c}{A_t} = \frac{\dot{W}_{tc} V t_s}{A_t} \qquad (4\text{-}4)$$

The L* concept is much easier to visualize than the more elusive "combustion residence time," expressed in small fractions of a second. Since the value of A_t is in nearly direct proportion to the product of $\dot{W}_{tc}$ and V, L^* is essentially a function of t_s. The effect of L^* on c^* in an experimental combustion chamber is shown in Fig.4-7. The c^* value increases with L^* to an asymptotic maximum. Increasing L^* beyond a certain point tends to decrease overall engine system performance because of the following:

- Larger L* results in higher thrust-chamber volume and weight.
- Larger L* creates more surface area in need of cooling and may increase thermal losses.
- Larger L* increases the frictional losses in the combustion chamber, reducing nozzle stagnation pressure and resultant thrust.

The customary method of establishing the L* of a new thrust-chamber design largely relies on past experience with similar propellants and engine size. Various computer programs for combustion modeling have provided assistance and guidelines to verify the size selection. Most of these models are based on estimated or assumed propellant drop size; they

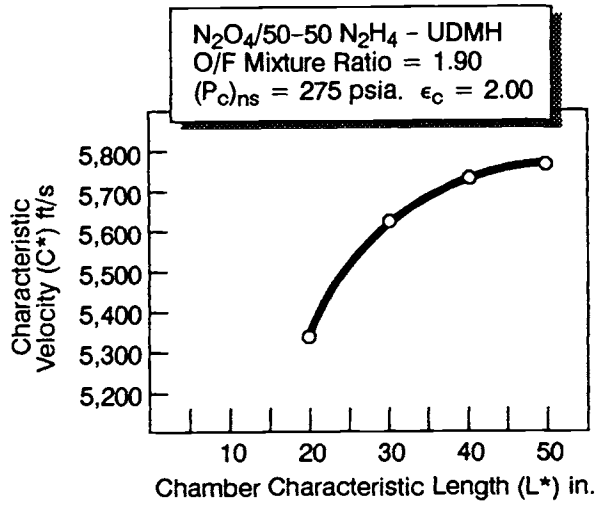

Fig. 4-7 Effect of L* on c* value of experimental thrust chamber.

include expressions for the rate of vaporization in the combustion environment and predict the rate and degree of combustion completeness. Some of these models have expressions for prediction of mixing effects, but the predictions will be much less reliable than the vaporization/combustion values.

Under a given set of operating conditions, such as type of propellant, mixture ratio, chamber pressure, injector design, and chamber geometry, the value of the minimum required L* can only be evaluated by actual firings of experimental thrust chambers. L* values of about 15 to 120 in. for corresponding propellant stay times of 0.002 to 0.040 s have been used in various thrust-chamber designs. Typical L* values for various propellants are shown in Table 4-1. With throat area and minimum required L* established, the chamber volume can be calculated by Eq. (4-4).

Combustion-Chamber Shape

As can be seen from Eq. (4-3), the stay time is theoretically independent of combustion-chamber geometry. On this purely mathematical basis, for a given required volume, the chamber can have any shape. In actual design, however, the choice of combustion chamber configuration is limited. A long chamber with a small cross section entails high nonisentropic pressure losses, as explained in Chapter 1. Long chambers also dictate a longer thrust-chamber envelope and impose space limitations on the injector design to accommodate the desired number of injection elements. With a short chamber of large cross section, the propellant atomization and vaporization zone occupies a relatively large portion of the chamber volume, while the mixing and combustion zone becomes too short for efficient combustion. Other factors, such as heat transfer, combustion stability, weight, and ease of manufacturing, must also be considered in determining the final combustion-chamber configuration.

Three geometrical shapes that have been used in combustion-chamber design are shown in Fig. 4-8.

Table 4-1 Typical combustion chamber characteristic length (L*) for various propellant combinations.

Propellant Combination	Combustion Chamber Characteristic Length (L*), in.
Chlorine trifluoride/hydrazine-base fuel	20-35
Liquid fluorine/hydrazine	24-28
Liquid flourine/liquid hydrogen (GH_2 injection)	22-26
Liquid fluorine/liquid hydrogen (LH_2 injection)	25-30
Hydrogen peroxide/RP-1 (including catalyst bed)	60-70
Nitric acid/hydrazine-base fuel	30-35
Nitrogen tetroxide/hydrazine-base fuel	30-35
Liquid oxygen/ammonia	30-40
Liquid oxygen/liquid hydrogen (GH_2 injection)	22-28
Liquid oxygen/liquid hydrogen (LH_2 injection)	30-40
Liquid oxygen/RP-1	40-50

While spherical and near-spherical chambers were used in early European designs, the cylindrical chamber has been employed most frequently in the United States. Compared to a cylindrical chamber of the same volume, a spherical or near-spherical chamber offers the advantage of less cooling surface and weight. A sphere has the best surface-to-volume ratio of all the geometric choices, and for the same material strength and chamber pressure, the minimum wall thickness required for pressure loads is about half that of a cylinder. However, the spherical chamber is more difficult to manufacture and has provided poorer performance in other respects.

Selecting the proportions and size of a new thrust-chamber assembly for specified thrust and chamber pressure usually appears to be a rather arbitrary process. The operating regime (sea level, vacuum), chamber pressure, and thrust level provide the desired nozzle area ratio and thrust coefficient for the approximate nozzle, which sets the throat area for the selected engine. The largest remaining gray area thus becomes combustion-chamber sizing. The total combustion process, from injection of the reactants until completion of the chemical reactions and conversion of the products into hot gases, requires finite amounts of time and volume, as expressed by the characteristic length L*. The value of this factor is significantly greater than the linear length between injector face and the throat plane. The contraction ratio, which is defined as the major cross-sectional area of the combustor (typically in the cylindrical portion near the injector face) divided by the throat area, is basically related to the mean Mach number of the combustion gas.

Typically, large engines are constructed with a low contraction ratio and a comparatively long length; and smaller chambers employ a large contraction ratio with a shorter length, while still providing sufficient L* for adequate vaporization and combustion dwell-time. A look at some extreme examples gives insight into the reasons for this tendency. In general, the combustion process is not scaleable. Thus, if it is decided to scale down the F-1 engine from 1,500,000 lb of thrust to 100 lb while maintaining the same length and contraction ratio, the 39-in.-long combustor, which is about 40 in. in diam. in the F-1, would be less than 1/8 in. in diam. in the 100-lb engine. The converse approach, scaling a 100-lb-thrust engine to the F-1 thrust level, would result in an equally grotesque configuration. A small, 100-lb-thrust attitude-controll engine typically has a combustor about 1 in. in diam. and about 4 in. or less in length. Increasing the chamber area to the F-1 thrust level would produce a diameter of about 10 ft; convergence to the throat diameter in 4 in. of chamber length would be nearly impossible.

As a good place to start, the process of sizing a new thrust chamber examines the dimensions of previously successful designs in the same size class and plotting such data in a rational manner. As shown above, the throat size of a new engine can be generated with a fair degree of confidence, so it makes sense to plot the data from historical sources in relation to throat diameter. Figures 4-9 and 4-10 plot contraction ratio and chamber length, respec-

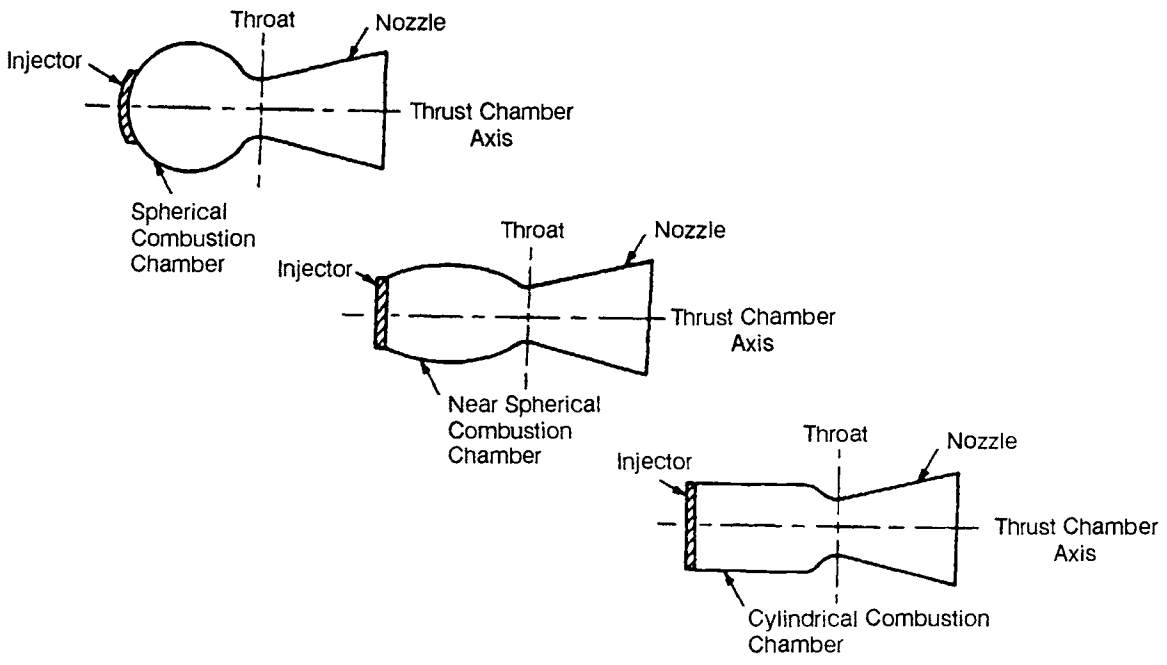

Fig. 4-8 Frequently used geometrical shapes for combustion chambers.

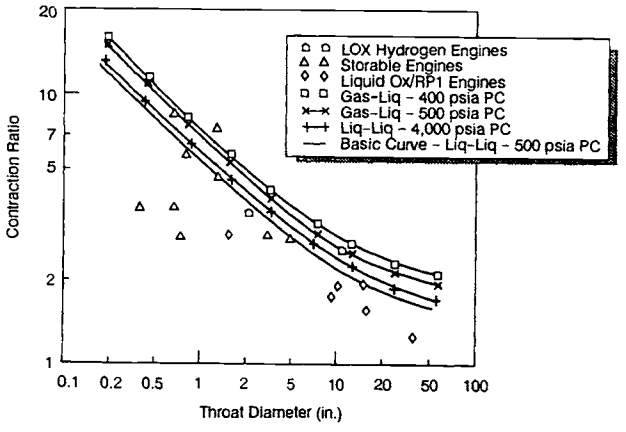

Fig. 4-9 Contraction ratio relationships used in scaling program.

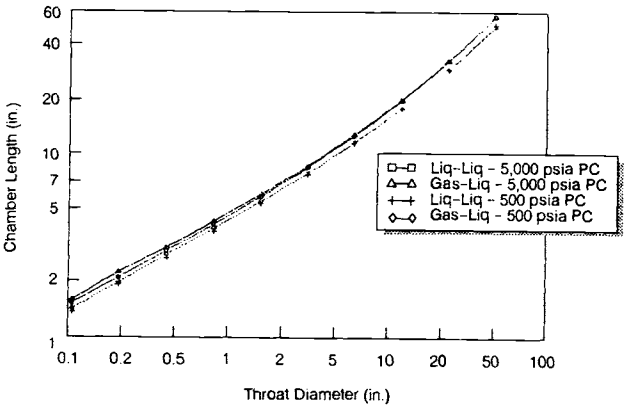

Fig. 4-10 Chamber length relationships used in scaling program.

tively, as functions of throat diameter. It is important that the output of any modeling program not be slavishly applied, but be considered a logical starting point for specific engine sizing.

Throat size is not the only driving force in chamber sizing. Since the primary purpose of the combustion chamber is the effective reaction of the propellants, the forces which govern and limit these reactions are major drivers. The conditions of the injected reactants are significant parameters. The form of the propellants—gases, liquids, gels, or even solids—has major impact on reaction times and the resultant chamber volume required for adequate dwell time. Obviously, a gas/gas reaction takes minimum volume or distance in the chamber, since it requires no atomization/vaporization mechanisms. This characteristic has been verified in some combustors that have provided very good performance when only 1/2 in. long. The converse of this experience has been with liquid-propellant rocket engines with large injection elements; these have shown poor performance even when combustion-chamber lengths have been increased to 100 in. Propellants containing solid materials have evidenced even greater resistance to efficient combustion. The high chamber pressures used in advanced booster engines also have combustion problems related to high injection density levels. The high flowrates per square inch of injector face area lead to large orifices, with resultant large droplets, and the elevated pressure also slows vaporization rates. Any model or sizing approach must make provisions for these effects, or the designer using the procedure must modify the results in response to these requirements.

Although a rocket combustion chamber might properly have proportions which approach a sphere, the combustor requires a certain volume to accom-

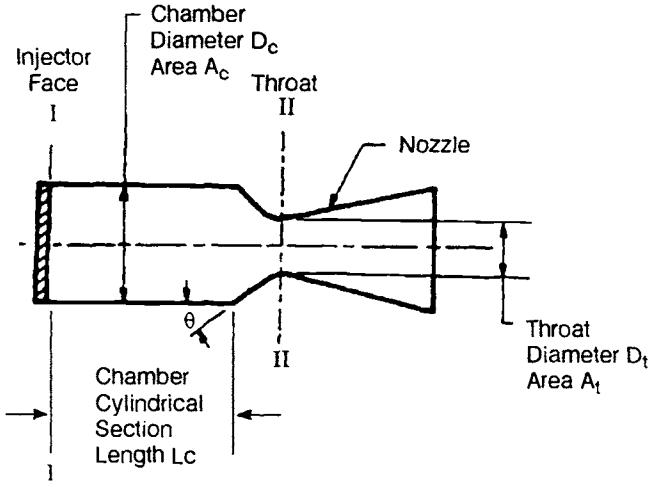

$$\text{Chamber Contraction Area Ratio} \quad \epsilon_c = \frac{A_c}{A_t}$$

Fig. 4-11 Elements of basic cylindrical combustion chamber.

plish the vaporization and reaction and it is assuredly a pressure vessel. The total surface area is a design factor for both structural strength and weight as well as for the total amount of heat rejected to the structure. The suggested design approach tends to keep the proportions of the combustor neither too long and thin nor too short and fat, but does not force it to spherical proportions. Other design factors in chamber construction and injector placement tend to favor a more cylindrical chamber. Keeping the combustor somewhat smaller in diameter and a little longer helps provide turbulence for mixing and reaction; also, the smaller diameters are more conducive to combustion stability.

Other factors, such as packaging and cost-vs-complexity trades, enter into the final sizing of a rocket engine. A sophisticated injection pattern can provide the required level of performance in a shorter, more compact combustor than a coarse, simplified pattern. In some engine configurations, cooling limitations can dictate a shorter combustion chamber, in spite of potential loss of performance. A limited-volume packaging problem can also force less chamber size, with a calculated performance tradeoff. In the other direction, engines using cooling enthalpy as the energy source for pumping work (expander or topping cycles) may require greater chamber length to provide the needed heat input to the working fluid.

The basic elements of a cylindrical thrust-chamber are identified in Fig. 4-11. In design practice, it has been arbitrarily defined that the combustion-chamber volume includes the space between the injector face I-I and the nozzle throat plane II-II. The approximate volume of the combustion chamber can be expressed by the following equation:

$$V_c = A_t\left[L_c\epsilon_c + \frac{1}{3}\sqrt{\frac{A_t}{\pi}}\cot\theta(\epsilon_c^{1/3} - 1)\right] \qquad (4\text{-}5)$$

The total surface area of the combustion-chamber walls, excluding the injector face, can be approximated by the following expression:

$$\text{Total area} = 2L_c\sqrt{\pi\epsilon_c A_t} + \csc\theta(\epsilon_c - a)A_t \qquad (4\text{-}6)$$

As a practical matter, both chamber volume and surface area can be more easily and accurately determined by a numerical-integration computer program that can include effects of wall radius and approach angles and also provide information on local gas velocities, etc.

Nozzle Expansion Area Ratio

With all other parameters fixed, particularly chamber pressure, there is only one optimum nozzle expansion area ratio for a given altitude. Except for systems that start in vacuum, ambient pressure must be considered. This is especially true for boosters that start at or near sea-level, for which ambient pressure will not be constant. It is therefore important to know the trajectory of the vehicle to be propelled or, more specifically, its altitude-vs-time characteristics. With this information, the designer is in a position to make a first optimizing selection of a nozzle expansion area ratio for best results throughout the entire trajectory. The optimization for ambient pressure then is essentially an averaging process.

A first-stage booster engine presents an extreme case of such compromise in nozzle expansion ratio. A nozzle optimized for the pressure ratio at sea-level ambient pressure will soon be underexpanded and wasteful of potential thrust as the vehicle gains altitude. For this reason, booster-engine expansion ratios are typically based on the expected limit of attached nozzle flow. A classic bell nozzle operates with full exit-plane flow at an expanded pressure significantly below ambient pressure. This is definitely not an optimized operating point at this altitude for this nozzle area ratio, since a large portion of the expansion wall area is at a static pressure below ambient and is contributing negative thrust. As the vehicle gains altitude, however, the thrust coefficient improves and is soon higher than it would be for an expansion ratio sized for the sea-level pressure ratio; there is usually significant gain in overall delivered specific impulse for the mission.

This overexpansion presents various mechanical and structural problems caused by the loads on sections of the wall below ambient pressure. An even worse structural problem can exist at a lower pressure than this design point (such as during pressure rise in start-up), when the nozzle flow can alternately attach and detach from the wall. This condition is typically a cyclic phenomenon and generally couples with a structural resonant distortion mode of the nozzle skirt. For these reasons, the nozzle structure should be as rigid as possible within the weight constraints, and extended operation at these transient pressure-ratio points must be avoided. In some cases, temporary restraining structures are provided during start transients; they disconnect after start to minimize

system flight-weight. A typical mainstage exit static pressure being used for current booster design is 6 psia, and the expansion ratio is selected on this basis.

The limit on booster expansion ratio because of these factors is the reason that high chamber pressure is desirable for booster engines. The chamber pressure and resultant expansion-ratio limit have large impact on the maximum specific impulse available.

Other considerations can cause the designer to deviate from the "paper optimum" for the nozzle expansion area ratio. Some of the most common considerations are weight, size, ease of manufacturing, handling, and cooling (heat-transfer) requirements.

Nozzle Shape

Most rocket nozzles are of the converging-diverging De Laval type. Since the flow velocity of the gases in the converging section of rocket nozzle is relatively low, any smooth and well-rounded convergent nozzle section will have very low energy losses. By contrast, the contour of the diverging nozzle section is very important to performance, because of the very high flow velocities involved. The selection of an optimum nozzle shape for a given expansion area ratio is generally influenced by the following design considerations and goals:

- Uniform, parallel, axial gas flow at the nozzle exit for maximum momentum vector.
- Minimum separation and turbulence losses within the nozzle.
- Shortest possible nozzle length for minimum space envelope, weight, wall friction losses, and cooling requirements.
- Ease of manufacturing.

Any abrupt change or discontinuity in the nozzle wall contour should be avoided to prevent the possibility of shock waves or turbulence losses. Theoretically, the nozzle throat is simply the unique plane of minimum cross-sectional area. In practice, a well-rounded throat section is employed. Only the nozzle exit plane has a sharp edge, because a rounded one would permit over-expansion and flow separation.

Conical nozzle. In early rocket-engine applications, the conical nozzle, which proved satisfactory in most respects, was used almost exclusively. A conical nozzle allows ease of manufacture and flexibility in converting an existing design to higher or lower expansion area ratio without major redesign.

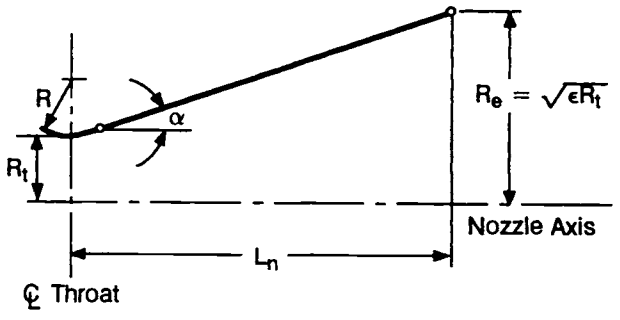

Fig. 4-12 Conical nozzle contour.

The configuration of a typical conical nozzle is shown in Fig. 4-12. The nozzle throat section has the contour of a circular arc with a radius, R, ranging from 0.5 to 1.5 times the throat radius R_t. The half-angle of the nozzle convergent cone section can range from 20 to 45 deg. The divergent cone half-angle α varies from approximately 12 to 18 deg. The length of the conical nozzle section can be expressed by the following equation:

$$L_n = \frac{R_t(\sqrt{\epsilon} - 1) + R(\sec \alpha - 1)}{\tan a} \qquad (4\text{-}7)$$

The conical nozzle with a 15-deg divergent half-angle has become almost a standard because it is a good compromise on the basis of weight, length, and performance.

Since certain performance losses occur in a conical nozzle as a result of the nonaxial component of the exhaust gas velocity, a correction factor, λ , is applied in the calculation of the exit-gas momentum. This factor (thrust efficiency) is the ratio between the exit-gas momentum of the conical nozzle and that of an ideal nozzle with uniform, parallel, axial gas-flow. The value of λ can be expressed by the following equation:

$$\lambda = \tfrac{1}{2}(1 + \cos \alpha) \qquad (4\text{-}8)$$

where α = half-angle of the conical nozzle.

For an ideal nozzle, λ is unity. For a conical nozzle with α = 15 deg and λ = 0.983, the exit-gas velocity will be 98.3% of the ideal nozzle-exit velocity calculated by Eq. (1-18). The vacuum-thrust coefficient of a nozzle is directly proportional to the thrust or to the nozzle-exit gas velocity. Therefore, the theoretical vacuum thrust coefficient (neglecting friction and other flow losses) of a conical nozzle with 15-deg half-angle will be 98.3% of the ideal nozzle thrust coefficient calculated by Eq. (1-33a).

Bell nozzle. To gain higher performance and shorter length, engineers developed the bell-shaped nozzle. It employs a fast-expansion (radial-flow) section in the initial divergent region, which leads to a uniform, axially directed flow at the nozzle exit. The wall contour is changed gradually enough to prevent oblique shocks.

Figure 4-13 shows the contour of a bell nozzle. A circular arc of selected radius R_1 is chosen for the nozzle contour MT upstream of the throat. Contour TNE is the diverging portion of the nozzle. The initial expansion occurs along contour TN; contour NE turns the flow over to a direction nearer to axial. For design convenience, the contour TN is also a circular arc, with a smaller radius R_2.

Using transonic-flow analysis, a constant-Mach-number line TO can be defined at the throat. Given the flow condition along TO and the solid boundary TN, a kernel flow field TNKO can be generated by the method of characteristics. The kernel of the rocket-nozzle contour is defined as that portion of the supersonic flow field determined entirely by throat

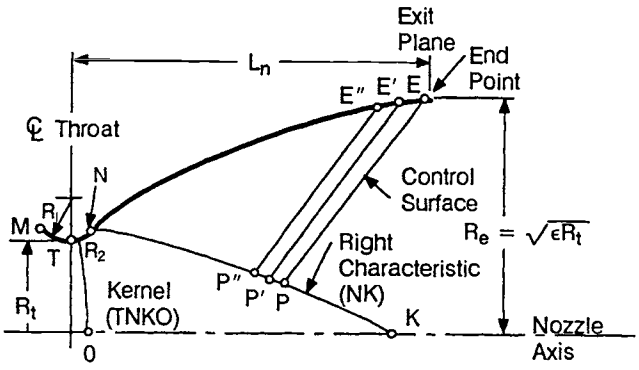

Fig. 4-13 Bell nozzle contour.

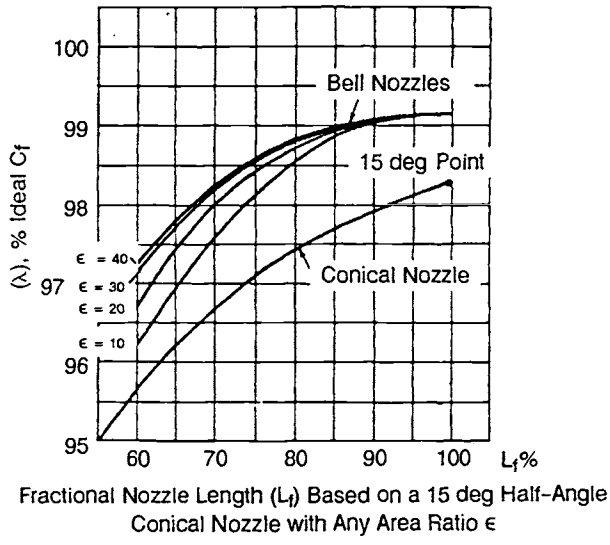

Fig. 4-14 Thrust efficiency vs bell nozzle length.

conditions. The last right characteristic line NK of kernel TNKO, and thus the location of the point N along contour TN, is determined by specific design criteria.

The location of the end-point E along contour NE is defined by the given nozzle expansion area ratio and nozzle length (distance between throat and exit plane). Then the right characteristic line NK can be determined by satisfying the following conditions concurrently:

1) A control surface PE can be generated between the point E and a selected point P along the line NK.
2) Mass flow across PE equals the mass flow across NP.
3) Maximum thrust by the nozzle is attained.

By selecting points P', P", etc. along line NK, a series of control surfaces P'E', P"E", etc. can be generated to define points E', E", etc. along the contour NE. Calculations for the nozzle contour can be effectively performed by a computer.

An equivalent 15-deg-half-angle conical nozzle is commonly used as a standard to specify bell nozzles. For instance, the length of an 80% bell nozzle (distance between throat and exit plane) is 80% of that of a 15-deg-half-angle conical nozzle having the same throat area, radius below the throat, and area expansion ratio.

Figure 4-14 shows the thrust efficiency, γ, versus fractional nozzle length, L_f, for conical and bell nozzles.

Bell-nozzle lengths beyond approximately 80% do not significantly contribute to performance, especially when weight penalties are considered. However, bell nozzle lengths up to 100% can be optimum for applications stressing very high performance.

Parabolic approximation of the bell nozzle. One convenient way of designing a near-optimum-thrust bell nozzle contour uses the parabolic approximation procedures suggested by G. V. R. Rao. The design configuration of a parabolic approximation bell nozzle is shown in Fig. 4-15. The nozzle contour immediately upstream of the throat T is a circular arc with a radius of 1.5 R_t. The divergent-section nozzle contour is made up of a circular entrance section with a radius of 0.382 R_t from the

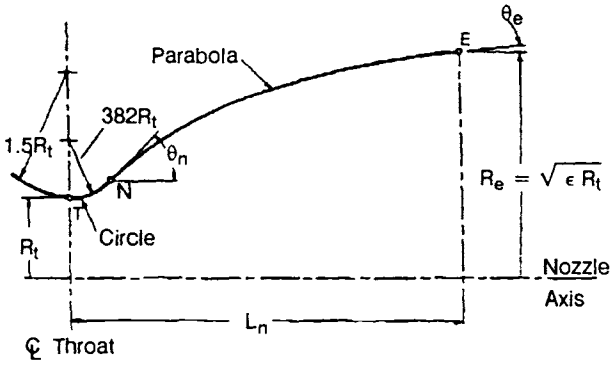

Fig. 4-15 Parabolic approximation of bell nozzle contour.

throat T to the point N and parabola from there to the exit E.

Design of a specific nozzle requires the following data: throat diameter D_t, in.; axial length of the nozzle from throat to exit plane, L_n, in. (or the desired fractional length, L_f, based on a 15-deg conical nozzle); expansion area ratio ε; initial wall angle of the parabola θ_n, deg; and nozzle-exit wall angle θ_e, deg.

The wall angles θ_n and θ_e are shown in Fig. 4-16 as a function of the expansion area ratio ε. Optimum nozzle contours can be approximated very accurately by selecting the proper inputs. Although no allowance is made for different propellant combinations, experience has shown only small effect of the specific heat ratio γ upon the contour.

Annular nozzles. For ideal expansion, the thrust generated by a thrust chamber depends only upon the mass-flow conditions (velocity and direction) at the nozzle exit. In some nozzle designs,

such as annular nozzles, the gas at the throat does not necessarily flow parallel to the axis, but the exit flow is similar to that of a conical or bell nozzle and thus produces the same thrust results.

There are two basic types of annular nozzles: radial-inflow (spike nozzle) and radial-outflow [Expansion-Deflection (E-D), Reverse-Flow (R-F), and Horizontal-Flow (H-F)]. They are shown in Fig. 4-17, together with conventional conical and bell nozzles. For comparison of the effect of nozzle type on size, all nozzles shown are scaled to the same thrust level, nozzle expansion area ratio, and theoretical nozzle efficiency. These nozzles show potential for adapting their geometry to space-vehicle applications, because short-ended nozzles reduce interstage structural weight and permit an increase in payload through increased performance for a given length.

The nozzle expansion area ratio ϵ for an annular nozzle is defined by Eq. (4-9), as follows:

$$\epsilon = \frac{\text{Projected area of the contoured nozzle wall}}{\text{Throat area}} = \frac{A_e - A_p}{A_t} \qquad (4\text{-}9)$$

where the projected area of the contoured nozzle wall equals nozzle-exit-plane area A_e less the center-body projected area A_p. Another convenient design parameter for annular nozzles is the annular diameter ratio D_p/D_t, where D_t is the throat diameter of an equivalent circular throat and D_p is the centerbody diameter. The parameter D_p/D_t is an index of the annular-nozzle-design geometry as compared to a conventional nozzle. The contour-calculating methods for annular nozzles are similar to those for bell nozzles.

In a conical or bell nozzle, the gases may expand to pressures well below the ambient (sea level or low-altitude operation) before flow separation from the nozzle wall occurs. As explained in Chapter 1, for nozzles with large area ratios this over-expansion reduces thrust at low altitudes. Annular nozzles, because of their special characteristics, are not subject to these losses. As shown in Fig. 4-18 for an E-D nozzle (and equally applicable to other annular nozzles), the back pressure P_b at the back face of the centerbody plays an important role in regulating the nozzle flow. The value of P_b is a function of the ambient pressure and generally is lower than am-

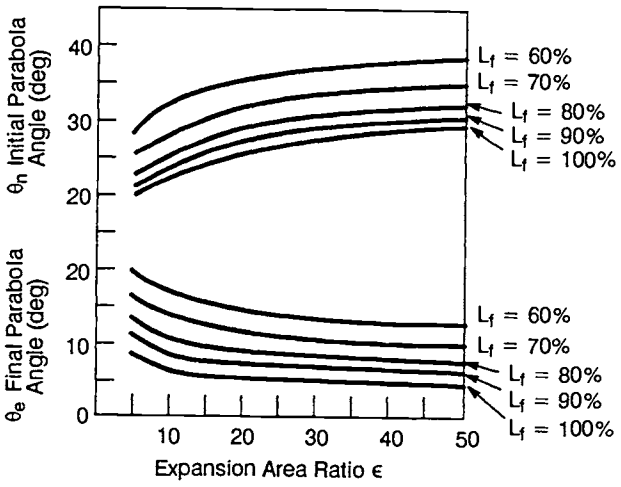

Fig. 4-16 Θ_n and Θ_e as function of expansion area ratio.

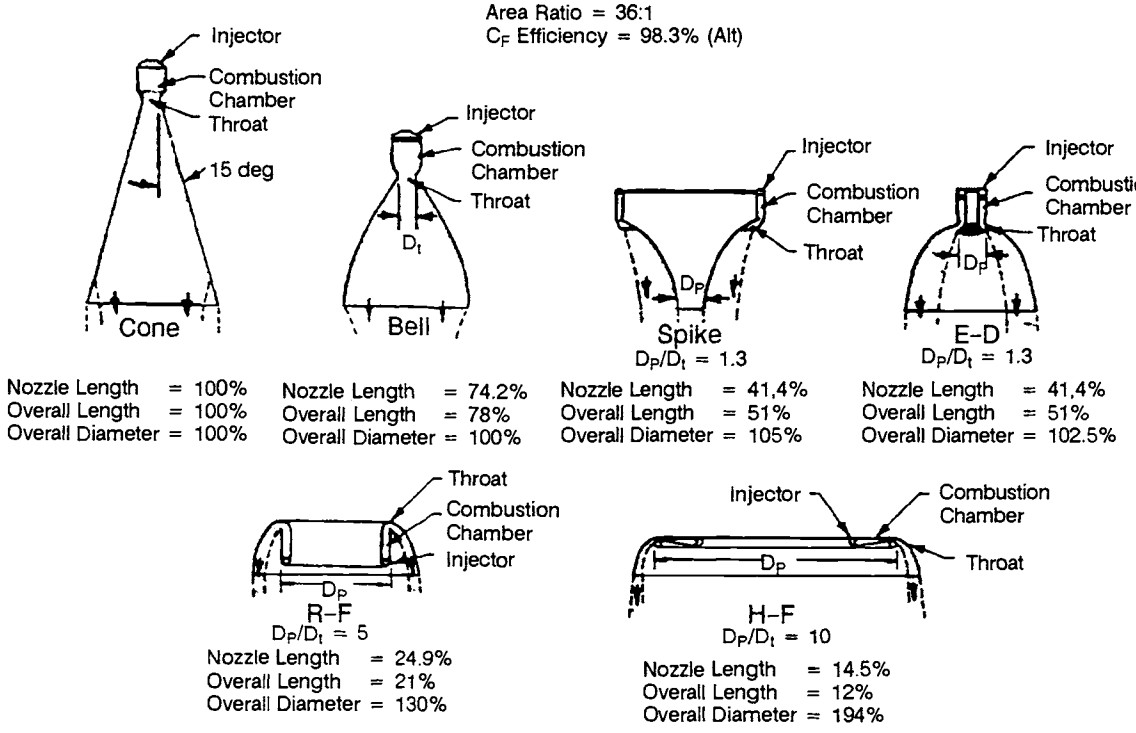

Fig. 4-17 comparison of nozzle shapes.

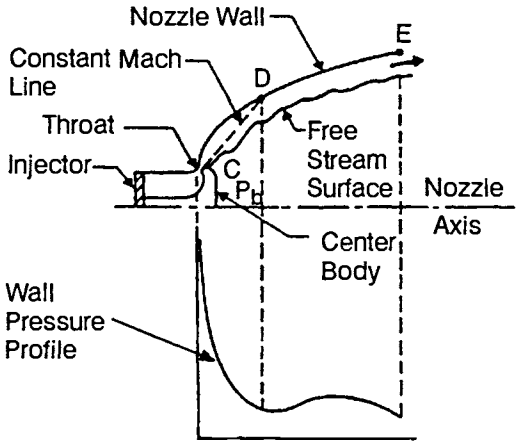

Fig. 4-18 E-D nozzle at low altitude operation.

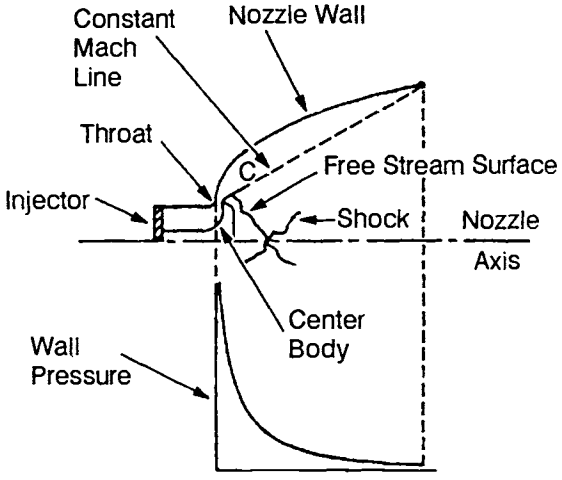

Fig. 4-19 E-D nozzle at high altitude operation.

bient. Downstream of the throat, the expansion of the gases around the centerbody shoulder C will continue unaffected until this base pressure is reached. After the initial gas expansion through the constant-Mach line CD, the downstream flow of gases is controlled by two boundary conditions: 1) The nozzle wall contour DE, which turns the gases to near-axial flow, and 2) the base pressure P_b, which influences the free-stream surface of the inner jet boundary.

Because of the curved wall contour, the gases are deflected, which leads to some compression and local increases in wall pressure. A typical nozzle-wall pressure distribution for low-altitude operation is shown in Fig. 4-18. This compressive turning at the nozzle wall, which is also typical of the spike nozzle, improves nozzle performance at low altitude. Because of the selfadjusting nature of the inner jet boundary, there is no flow separation from the nozzle wall, as in the case of a conventional nozzle.

In high-altitude operation, the base pressure P_b becomes so low that the nozzle flow converges behind the centerbody, as shown in Fig. 4-19. Since the flow at the closure point must be axial, a shock wave may occur, depending on the flow conditions. However, the expansion of the gases may continue unaffected up to the end of the nozzle. Nozzle-wall pressure distribution under this condition is also shown in Fig. 4-19.

An improved spike-nozzle concept , the *aerodynamic spike nozzle* has a truncated annular spike (radial-inflow type) that utilizes a small amount of secondary flow introduced into the nozzle base region. Performance of the aerodynamic spike nozzle reflects various geometric parameters, the amount of secondary flow, the manner in which this secondary flow is introduced, and the relative energy between the primary and secondary streams. To describe the flow field and the interrelated effect of truncating the spike nozzle, the base pressure and the base-pressure increase achieved through the secondary-flow addition require a lengthy, detailed discussion; only the basic operation can be presented here.

The primary flow (high-pressure gases), which produces the major portion of the engine thrust, is exhausted from an annular-type combustion chamber and expands against the metal surface of the center truncated-spike nozzle (Fig. 4-20). The characteristics of the primary flow field upstream of the base, shown as region 1 in Fig. 4-20, are determined by the annular throat geometry, the nozzle wall contour, and the ambient pressure. The annular primary flow continues to expand beyond the nozzle surface and encloses a subsonic, recirculating flow field in the base region (region 2). The pressure acting on the nozzle base contributes additional thrust to the nozzle.

Introducing a small amount of secondary flow into the base (added to the recirculating flow) further increases the base pressure. As the secondary flow is increased, the overall nozzle efficiency (considering the additional flow) increases because of this increase in base pressure. There is a limit to this gain in efficiency, and an optimum secondary flow exists for each configuration.

The outer surface of the annular primary flow is a free-jet boundary, influenced by ambient pressure. This influence endows this type of nozzle with altitude compensation. In operation at high-pressure ratios (i.e., altitude conditions) the outer free-jet boundary of the primary flow expands outward, governed by the Prandtl-Meyer turning angle at the throat. At low pressure ratios (i.e., sea-level operation) the relatively higher ambient pressure compresses the outer free-jet boundary of the primary flow field. This compression increases the static pressure on the nozzle wall and partially offsets the negative effect of the higher ambient pressure on the back side of the nozzle. The base pressure also is increased with the higher ambient, because the compressed primary flow field, which influences the base pressure, has higher static pressure. This combination of flow-field effects imparts the altitude compensation inherent to the aerodynamic spike nozzle.

Figure 4-21 compares performance of various nozzle designs. It shows the nozzle thrust coefficient C_f for an ideal nozzle (i.e., a variable-area-ratio nozzle having the optimum expansion for each chamber pressure to ambient pressure ratio p_c/p_a), together

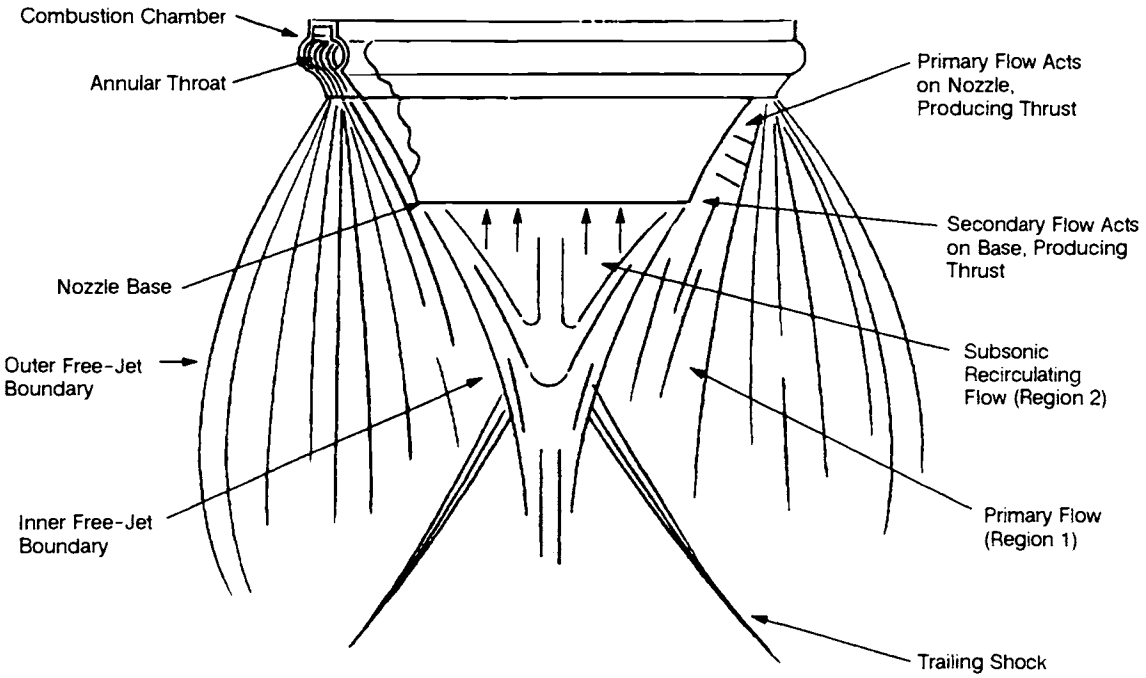

Fig. 4-20 Aerodynamic spike flow field illustrated under altitude conditions.

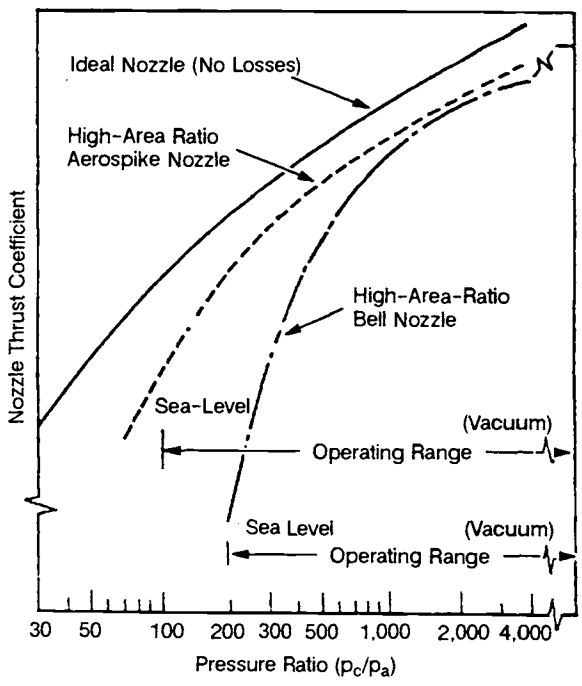

Fig. 4-21 Nozzle performance comparison.

with those of the high-area-ratio aerodynamic spike and bell nozzles. The C_f curve of the aerodynamic spike follows ideal nozzle performance (altitude compensation), rather than dropping off rapidly like bell design at low p_c/p_a (i. e., sea-level) operating points. All nozzles have a higher C_f at a high p_c/p_a (i. e., vacuum).

The development of the annular-nozzle concept may influence the design of rocket vehicles, especially in boattail-structure and staging optimization.

The advantages and disadvantages of annular nozzles may be summarized as follows:

Advantages

1) Shortened nozzle length for the same performance, or increased performance (higher expansion area ratios) for a given length.
2) Improved performance at sea level or low altitudes. (Annular nozzles with high expansion area ratios can be used for a single-stage sea-level to vacuum mission.)
3) The relatively stagnant region in the center of the nozzle can possibly be used for installation of gas generators, turbopumps, tanks, and auxiliary equipment and for turbine gas discharges.
4) A segmented-combustion-chamber design can be used, easing development effort (individual segments can be built and tested during the early phases) and improving combustion stability.

Disadvantages

1) Relatively high cooling requirements, because of higher heat fluxes and greater surface areas to be cooled.
2) Heavier structural construction in some applications.
3) Manufacturing difficulties.

Clustered-Nozzle Concepts

Two-dimensional, or cluster-type, nozzles (Fig. 4-22) are special cases related to the annular-nozzle family. An engine assembly with a two-dimensional nozzle, using a two-dimensional centerbody expansion

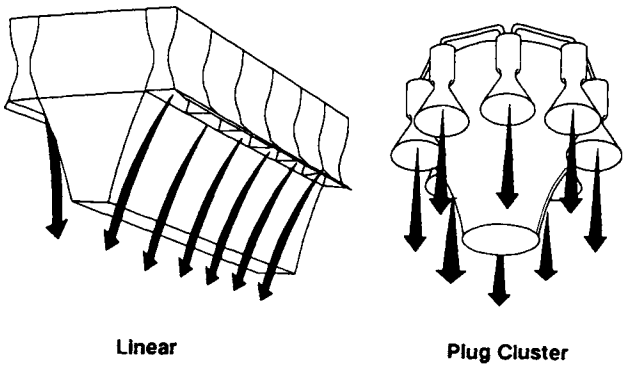

Fig. 4-22 Cluster nozzle concepts.

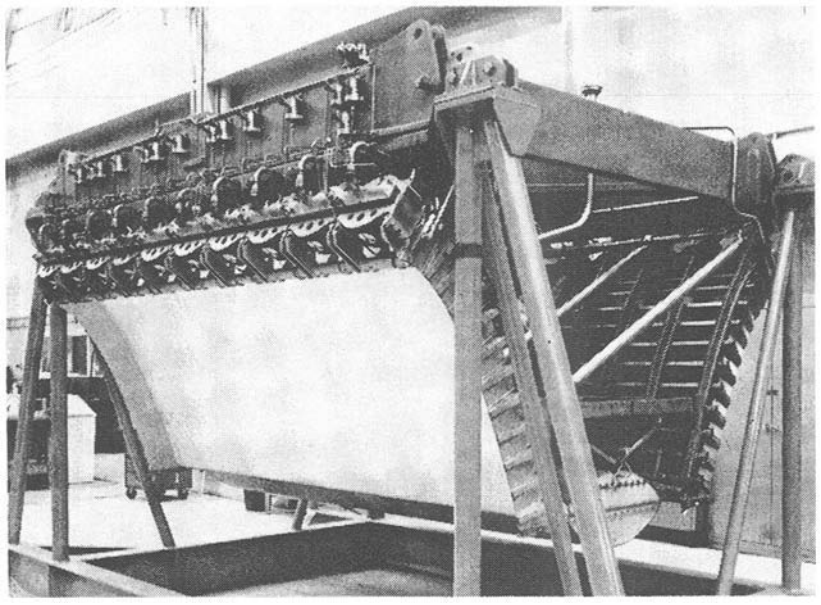

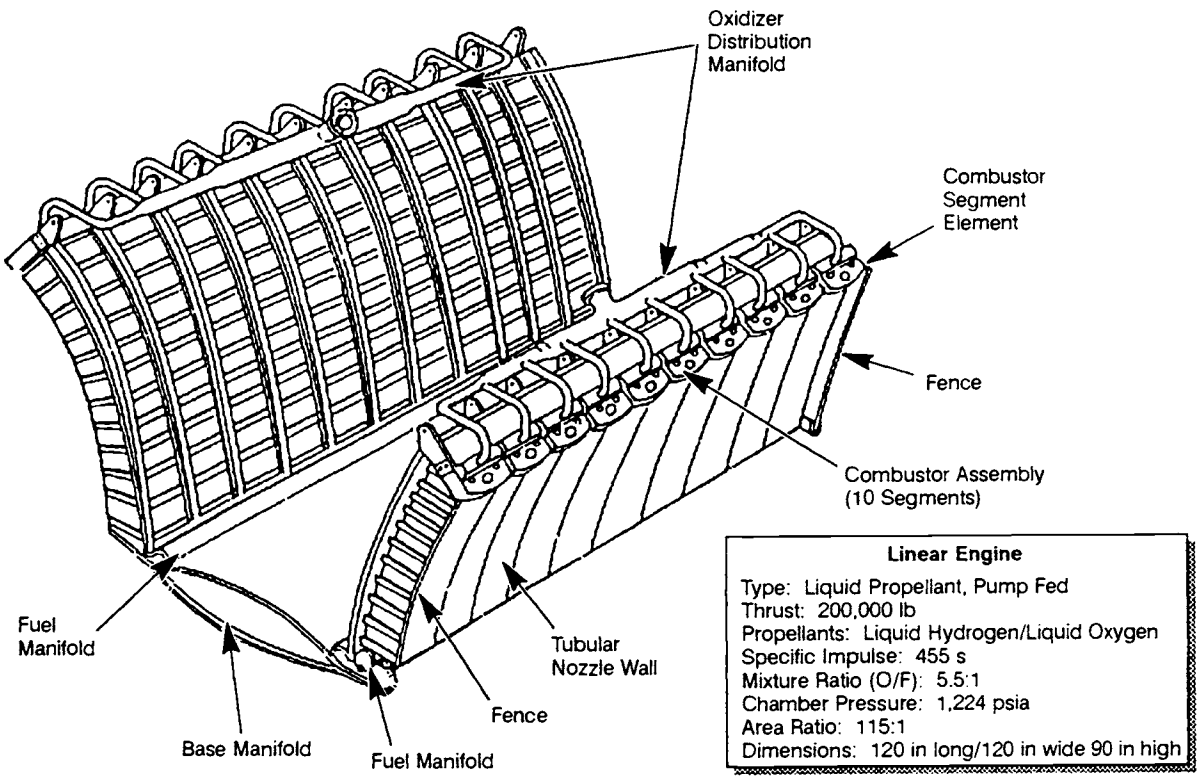

Fig. 4-23 Linear engine.

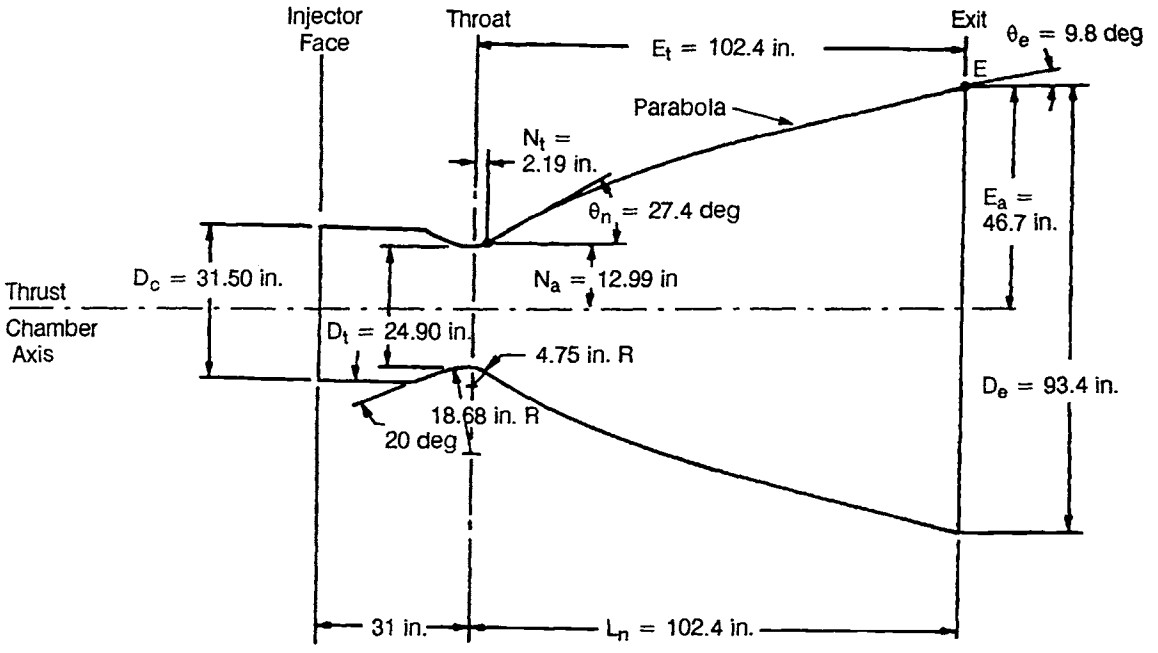

Fig. 4-24 A-1 Stage engine thrust chamber, internal configuration layout: ε = 14, 80% bell, L^* = 45 in., ε_c = 1.6.

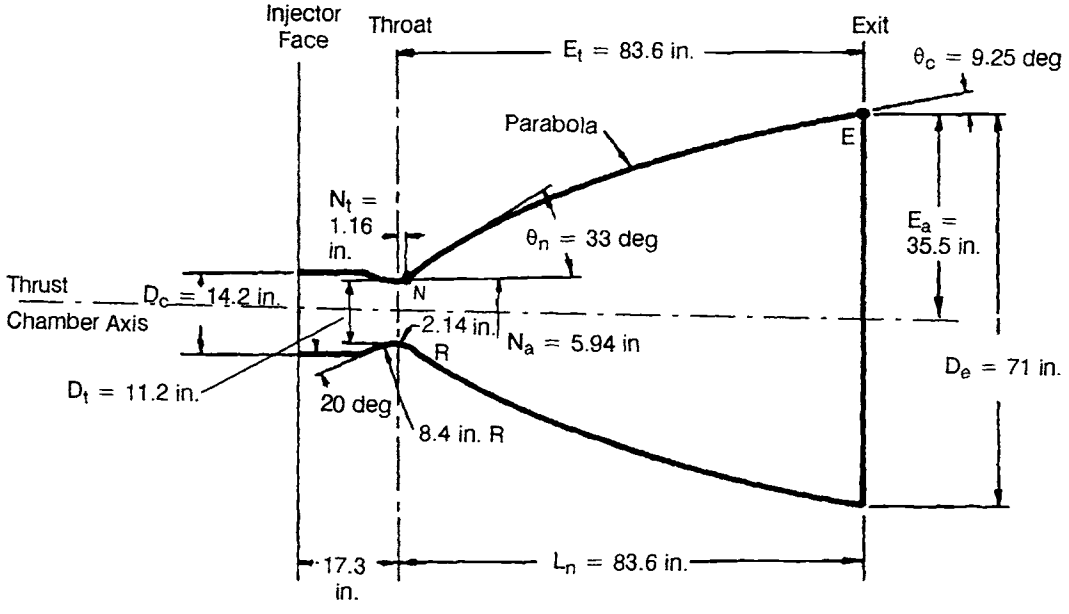

Fig. 4-25 A-2 Stage engine thrust chamber, internal configuration layout: ε = 40, 75% bell, L^* = 26 in., ε_c = 1.6.

surface, was demonstrated in hot firing on the "J-2 Linear" engine (Fig. 4-23). It appeared to have merit for special applications. Clusters of conventional, bell-nozzle chambers have also been proposed, and some wind-tunnel data have been obtained, although there is little hot-fire experience. This configuration offers the compact packaging and some of the altitude-correcting characteristics of the more classic annular nozzles.

Sample Calculation 4-2

Problem

Lay out the thrust-chamber internal configuration (cylindrical combustion chamber with bell nozzle) for the engines on the *Alpha* vehicle with the data derived from Sample Calculation (4-1) and the following required chamber thrusts F_{tc}:

- **A.** A-1 Stage engine: F_{tc_1} = 747,000 lb at sea-level
- **B.** A-2 Stage engine: F_{tc_2} = 149,500 lb at altitude
- **C.** A-3 Stage engine: F_{tc_3} = 16,000 lb at altitude
- **D.** A-4 Stage engine: F_{tc_4} = 7500 lb at altitude

The detailed calculations and results are presented below for the first-stage engine only (Fig. 4-24). For the other stages the calculation results are summarized in Fig. 4-25 to 4-27. The reader is urged

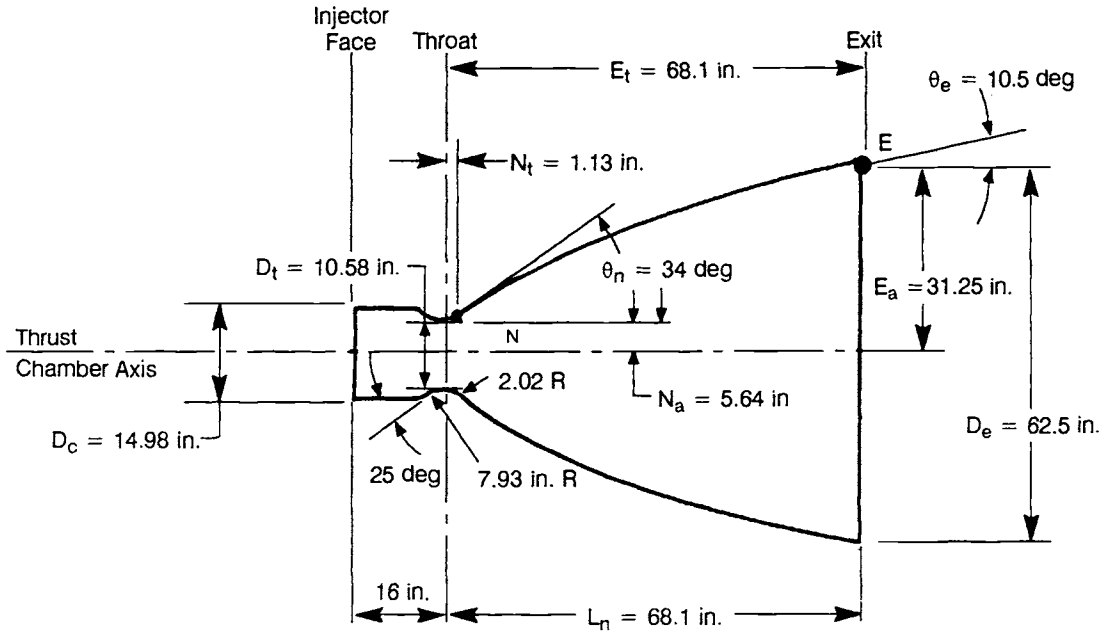

Fig. 4-26 A-3 Stage engine thrust chamber, internal configuration layout: ε = 35, 70% bell, L* = 28 in., ε_c = 2.

to make his own calculations, using the first stage as a guide, and to compare his results with those shown.

Solution

A-1 Stage engine:

From sample calculation (4-1): Design sea level $C_f = 1.531$; $(p_c)_{ns} = 1{,}000$ psia; $\epsilon = 14$

Substitute into equation (1-33):

Throat area: $$A_t = \frac{747{,}000}{1.531 \times 1{,}000} = 487 \text{ in.}^2$$

Throat diameter: $$D_t = \sqrt{\frac{4}{\pi} \times 487} = 24.9 \text{ in.}$$

$$R_t = \frac{24.9}{2} = 12.45 \text{ in.}$$

Exit diameter: $$D_e = \sqrt{14} \times 24.9 = 93.4 \text{ in.}$$

$$R_e = \frac{93.4}{2} = 46.7 \text{ in.}$$

Use a combustion chamber L* of 45 in. for LO_2/RP-1 application and substitute into Eq. (4-4):

Chamber volume: $V_C = 487 \times 45 = 21{,}915$ in.

Use a nozzle convergent half-angle of 20 deg, a contraction area ratio $\varepsilon_C = 1.6$, and a circular arc of radius $R = 1.5\ R_t$, or 18.68 in., for nozzle contour upstream of the throat, as follows:

Chamber diameter: $$D_c = \sqrt{1.6} \times 24.9 = 31.5 \text{ in.}$$

$$R_c = \frac{31.5}{2} = 15.75 \text{ in.}$$

Use Eq. (4-7) to calculate the chamber convergent cone length:

Convergent cone length

$$= \frac{12.45(\sqrt{1.6} - 1) + 18.68 \text{ (sec 20 deg} - 1)}{\tan 20 \text{ deg}}$$

$$= \frac{4.515}{0.364} = 12.4 \text{ in.}$$

Using the cone-frustum-volume equation and neglecting the slight rounding of the throat, the approximate convergent cone volume can be obtained as follows:

$$\text{Volume} = \frac{\pi}{3} \times 12.4[(15.75)^2 + (12.45)^2 + 15.75 \times 12.45]$$

$$= 7{,}760 \text{ in.}^3$$

Required volume for cylindrical chamber section

$$= 21{,}915 - 7{,}760 = 14{,}155 \text{ in.}^3$$

Required length for cylindrical chamber section

$$14{,}155/1.6\ A_t = 18.17 \text{ in.}$$

Distance from injector face to throat

$$= 18.17 + 12.40 = 30.57, \text{ say } 31 \text{ in.}$$

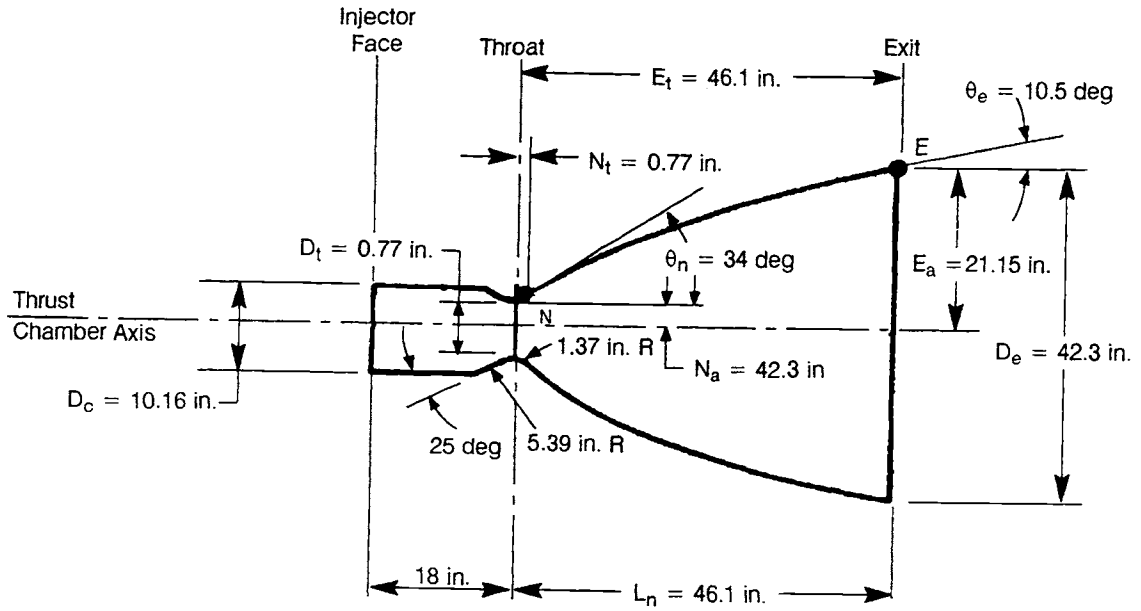

Fig. 4-27 A-4 Stage engine thrust chamber, internal configuration layout: ε = 35, 70% bell, L^* = 32 in., ε_c = 2.

Now design an "80% bell" nozzle configuration using the parabolic approximation procedure. The nozzle contour downstream of the throat will be a circular arc of radius 0.382 R_t, or 4.75 in. By definition, the nozzle length L_n will be 80% of the length of an equivalent 15-deg-half-angle conical nozzle. Substitute into Eq. (4-7):

$$L_n = 0.8 \times \left[\frac{12.45(\sqrt{14} - 1) + 4.75(\sec 15 \text{ deg} - 1)}{\tan 15 \text{ deg}}\right]$$

$$= 0.8 \times 128 = 102.4 \text{ in.}$$

The parabolic-contour wall angles θ_n and θ_e can be derived from Fig. 4-16 for ε = 14 and L_f = 0.8, θ_n = 27.4 deg, and θ_e = 9.8 deg. The location of N and E along the nozzle contour, with respect to throat and nozzle axis, can be calculated as follows:

$N_t = 0.382\, R_t \sin \theta_n = 2.19$ in.
$N_a = R_t + 0.382\, R_t (1\text{-}\cos \theta_n) = 12.99$ in.
$E_t = L_n = 102.4$ in.
$E_a = R_e = 46.7$ in.

With the aid of the established coordinates for points N and E and the angles θ_n and θ_e, a parabola can be fitted to complete the contour. Figure 4-24 shows the general layout of the A-1 Stage engine thrust chamber. More-accurate calculations of the divergent nozzle contour can be made with a computer program using the method of characteristics.

Since the calculations for the thrust-chamber configuration are based on the calculated design C_f value, which has to be verified by subsequent testing, a slight change of chamber pressure is usually allowed to compensate for C_f deviations in order to meet the required thrust.

Table 4-2 Comparison of sample combustion chamber sizing.

	Sample Calculation (4-2)	Curve-Fit Expression
A-1		
Contraction ratio	1.6	1.9
Chamber diameter, in.	31.5	34.6
Chamber length, in.	31.0	27.7
Characteristic length, in.	45.0	50.6
A-2		
Contraction ratio	1.6	2.7
Chamber diameter, in.	14.2	18.5
Chamber length, in.	17.3	16.6
Characteristic length, in.	16.0	41.0
A-3		
Contraction ratio	2.0	2.7
Chamber diameter, in.	15.0	17.5
Chamber length, in.	16.0	15.1
Characteristic length, in.	28.0	37.2
A-4		
Contraction ratio	2.0	2.6
Chamber diameter, in.	10.2	11.5
Chamber length, in.	18.0	12.1
Characteristic length, in.	32.0	28.6

Alternate Solution

The alternative chamber-sizing method based on experience with existing engines and on rational scaling criteria, can be used to lay out the internal dimensions of the A-1, A-2, A-3, and A-4 thrust chambers. Application of Fig. 4-9 and 4-10 gives the contraction ratios and chamber lengths based on the

throat diameters calculated above. Comparisons of the results obtained by both techniques are given in Table 4-2. The curve-fit method is considered to be the more reliable.

4.4 THRUST-CHAMBER COOLING

Cooling Techniques, and Selection

Because of high combustion temperatures (4000 to >6000°F) and high heat-transfer rates from the hot gases to the chamber wall (0.5 to over 100 Btu/in.^{2}-s), thrust-chamber cooling will be a major design consideration. For short-duration operation (up to a few seconds) uncooled chambers may sometimes be used; the heat will be absorbed by a heavy chamber wall acting as a heat sink, until the wall temperature approaches the failure level; but for most long-duration applications a steady-state chamber cooling system must be employed. One or a combination of the following chamber-cooling techniques will typically be used:

1. *Regenerative cooling*. Regenerative cooling, the most widely applied method, utilizes one or possibly both of the propellants fed through passages in the thrust-chamber wall for cooling, before being injected into the combustion chamber. (See section 4.1 and Fig. 4-1.)
2. *Dump cooling*. With this principle, a small percentage of the propellant, such as the hydrogen in a LO_2/LH_2 engine, is fed through passages in the thrust chamber wall for cooling and is subsequently dumped overboard through openings at the rear end of the nozzle skirt. Because of inherent problems, such as performance losses, this method has only limited application.
3. *Film cooling*. Here, exposed chamber-wall surfaces are protected from excessive heat by a thin film of coolant or propellant introduced through orifices around the injector periphery or through manifolded orifices in the chamber wall near the injector and sometimes in several more planes toward the throat. The method has been used, particularly for high heat fluxes, either alone or in combination with regenerative cooling.
4. *Transpiration cooling*. Transpiration cooling introduces a coolant (either gaseous or liquid propellant) through porous chamber walls at a rate sufficient to maintain the desired temperature of the combustion-gas-side chamber wall. This method is essentially a special type of film cooling.
5. *Ablative cooling*. In this process, combustion-gas-side wall material is sacrificed by melting, vaporization, and chemical changes to dissipate heat. As a result, relatively cool gases flow over the wall surface, thus lowering the boundary-layer temperature and assisting the cooling process. In addition, the ablative material is usually a good thermal insulator, keeping to a minimum the heat transmitted to the outer structure. Ablative cooling has been used in numerous designs, initially mainly for solid-propellant systems, but later, equally successfully, for short-duration and/or low-P_c liquid systems.
6. *Radiation cooling*. With this method, heat is radiated away from the surface of the outer thrust-chamber wall. It has been successfully applied to very small, high-temperature-material combustion chambers and to low-heat-flux regions, such as nozzle extensions.

Selection of the best cooling method for a given thrust chamber depends on many considerations. There are no simple-and-fast rules. However, the main factors that influence the selected design approaches will be the following:

1. *Propellants*. The properties of the combustion products, such as temperature, specific heat, specific weight, viscosity, etc., have a direct bearing on the heat-transfer rate and thus affect chamber cooling requirements and methods. The properties and flowrates of the propellants determine whether they are suitable or sufficient for regenerative, transpiration, dump, or film cooling. Consequently, the propellants involved will be a primary consideration in the design of a chamber cooling system.
2. *Chamber pressure*. Higher chamber pressures are linked with higher combustion-gas mass flowrates per unit area of chamber cross section and therefore with higher heat-transfer rates. Regenerative- and film-cooling methods are usually combined to meet the stringent requirements of high-chamber-pressure applications.
3. *Propellant-feed system*. The type of propellant feed used in an engine system determines its pressure budget. In a turbopump-fed engine, more pressure drop is usually available for chamber cooling. The availability of this pressure drop permits the use of regenerative cooling, which requires sufficient pressure to force the coolant through the cooling passages before entering the injector. A pressure-fed engine usually has more stringent pressure limitations and operates at relatively lower chamber pressures. This suggests the application of film, ablative, or radiation cooling or combinations of these techniques.
4. *Thrust-chamber configuration*. The geometric shape of the chamber affects local combustion-gas mass flowrates and wall surface areas to be cooled. This influences the choice of cooling method.
5. *Thrust-chamber construction material*. The properties of the thrust-chamber materials will profoundly affect the cooling-system design. Strength at elevated temperature and thermal conductivity will determine the suitability of a given material for regenerative cooling. For film-cooled chambers, higher

allowable material working-temperatures are desired, for lower film-coolant flowrates. The application of radiation cooling to a chamber depends largely on the availability of high-temperature (3000°F and up) materials. The success of ablative cooling depends entirely on the availability of suitable materials.

In practice, the design of the thrust-chamber cooling system is a major link in the complete engine design. It cannot be treated independently, without consideration of other engine system aspects. For instance, optimization of the chamber pressure of a high-performance engine may be largely limited by the capacity and efficiency of the chamber-cooling system. In turn, chamber pressure affects other design parameters, such as the nozzle expansion ratio, propellant feed pressure, and weight. Because of the complex interrelations between these factors, the complete analysis of chamber-cooling systems is a specialized field, requiring thorough knowledge of heat transfer, fluid mechanics, thermodynamics, materials, and structures. The engine system designer should therefore enlist the services of competent specialists in these fields.

Gas-Side Heat Transfer

A primary step in the design of a thrust-chamber cooling system analizes heat transfer from the combustion gases to the chamber walls (gas-side heat transfer), which occurs by forced convection. Before the gases can transfer heat to the wall, the heat energy must pass through a layer of stagnant gas along the wall, the boundary layer. The basic correlation for this complicated convective heat transfer can be expressed by the following equation:

$$q = h_g(T_{aw} - T_{wg}) \qquad (4\text{-}10)$$

where

- q = Heat flux, or heat transferred across the stagnant gas film per unit surface area per unit time, Btu/in.^{2}-s
- h_g = Gas-side-heat transfer coefficient, Btu/in.^{2}-s-°R
- T_{aw} = Adiabatic wall temperature of the gas, °R
- T_{wg} = Hot-gas-side local chamber-wall temperature., °R

The adiabatic wall temperature of the combustion gas at a given location in the thrust chamber may be obtained from the following expression:

$$T_{aw} = (T_c)_{ns}\left[\frac{1 + r\left(\frac{\gamma - 1}{2}\right)M_x^2}{1 + \left(\frac{\gamma - 1}{2}\right)M_x^2}\right]$$

$$= (T_c)_{ns}R \qquad (4\text{-}10\text{-}a)$$

where

- $(T_c)_{ns}$ = Nozzle stagnation temperature (or chamber total temperature), °R
- M_x = Local Mach number
- r = Local recovery factor
- R = Effective recovery factor (from 0.90 to 0.98)

The local recovery factor represents the ratio of the frictional temperature increase to the increase caused by adiabatic compression. It may be determined experimentally or estimated from the following simplified correlations based on the Prandtl number:

$$r = (Pr)^{0.5} \text{ Laminar flow}$$
$$r = (Pr)^{0.33} \text{ Turbulent flow}$$

Determination of the gas-side heat transfer coefficient h_g presents a rather complex problem. Comparisons of analytical results with experimental heat-transfer data obtained on rocket thrust chambers have often shown disagreement. The differences are largely attributed to the initial assumptions for analytical calculations. The boundary layer that controls the heat-transfer rate to the wall will be greatly affected by the turbulent combustion process and the local gas composition and temperature. Also, each injector configuration produces different combustion characteristics (turbulence and localized gas properties). This results in deviations from calculations based on the assumption of homogeneous product gases. However, it has been established by experiment that the heat-transfer coefficient is predominantly influenced by the mass velocity or the mass flowrate per unit area of the gas, subject to the exponent 0.8. In comparison, all other factors are relatively minor. A rough approximation of h_g can thus be expressed by the following equation:

$$h_g \approx (\rho' V)^{0.8} \qquad (4\text{-}11)$$

where

- ρ' = free-stream local gas density, lb/ in.^{3}
- V = free-stream value of local gas velocity, in./s

Thus, under normal circumstances, the heat-transfer coefficient varies with the chamber pressure to the 0.8 power and throughout a given chamber inversely with the local chamber diameter to an exponent of 1.6.

Based on experience with turbulent boundary layers, some relatively simple correlations for the calculation of the gas-side heat-transfer coefficient have been developed. The following form (credited to Colburn) has been much used:

$$Nu = C\ Re^{0.8}Pr^{0.34} \qquad (4\text{-}12)$$

where

- Nu = Nusselt number = $h_g D/k$
- C = Dimensionless constant
- Re = Reynolds number= $\rho' VD/\mu$
- V = Free stream velocity, in./s

Pr = Prandtl number = $\mu C_p/k$
D = Hydraulic diameter, in.
k = Gas thermal conductivity, Btu/s-in.^{2}-°F/in.
μ = Viscosity, lb/in.-s
C_p = Specific heat at constant pressure, Btu/lb-°F

Bartz developed the following correlation from Eq. (4-12) primarily for nozzle heat transfer:

$$h_g = \left[\frac{0.026}{D_t^{0.2}}\left(\frac{\mu^{0.2}C_p}{Pr^{0.6}}\right)_{ns}\left(\frac{(p_c)_{ns}g}{c^*}\right)^{0.8}\left(\frac{Dt}{R}\right)^{0.1}\right] \times \left(\frac{A_t}{A}\right)^{0.9}\sigma \qquad (4\text{-}13)$$

where
R = Nozzle radius of curvature at throat, in.
σ = Correction factor for property variations across the boundary layer
A = Area along chamber axis, in.^{2}

The value of σ can be established in terms of nozzle stagnation temperature, local gas-side chamber wall temperature, and local Mach number, as follows:

$$\sigma = \frac{1}{\left[\frac{1}{2}\frac{T_{wg}}{(T_c)_{ns}}\left(1+\frac{\gamma-1}{2}M^2\right)+\frac{1}{2}\right]^{0.68}\left[1+\frac{\gamma-1}{2}M^2\right]^{0.12}} \qquad (4\text{-}14)$$

Values of σ as a function of $T_{wg}/(T_c)_{ns}$ and γ, as computed by Bartz, are shown in Fig. 4-28.

If Pr and μ data are not available for particular combustion-gas mixtures, the following equations may be used for approximate results:

$$Pr = \frac{4\gamma}{9\gamma - 5} \qquad (4\text{-}15)$$

$$\mu = (46.6 \times 10^{-10})M^{0.5}T^{0.6} \qquad (4\text{-}16)$$

where T = temperature of gas mixture, °R; M = molecular weight, lb/mol; and μ = viscosity, lb/in.-s.

Equations (4-13), (4-14), (4-15), and (4-16) can be used to calculate approximate h_g values along the thrust-chamber walls. However, the calculated values should be expected to be lower than the actual ones if the following conditions exist:

1) Substantial fraction of the combustion gases are strong radiators.
2) Substantial dissociation, with subsequent recombination near the wall.
3) Strong, high-frequency, flow instabilities.

On the other hand, the calculated values may be higher than actual ones, because of the following:

1) The combustion reactions may not be completed in the chamber.

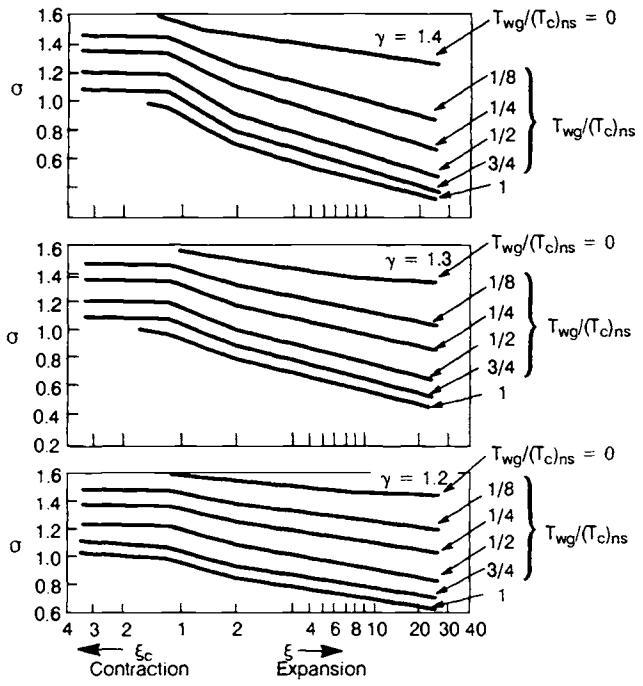

Fig. 4-28 Values of correction factor σ for property variation across boundary layer.

2) The combustion gases may deposit solids on the chamber walls, that act as insulators.
3) Boundary-layer cooling may be used.

With certain propellant combinations, the combustion products contain small amounts of solid particles. These solids tend to deposit on the chamber walls and form a rather effective insulating layer. Quantitative evaluations of the insulation effectiveness of such layers, which are necessary for correct heat-transfer calculations, have been made experimentally.

In the case of the LO_2/RP-1 combination (at chamber pressures below about 1500 psi), carbon solids are deposited on the chamber walls. After a firing, the carbon gives the interior of the thrust chamber the appearance of being freshly painted black. The outer surface of the carbon appears sooty and can easily be removed by light rubbing. Underneath the exterior soot layer may be a harder, graphite-like layer that can also be removed but is more tenacious. This carbon deposit significantly increases the gas-side thermal resistance. The temperature of the carbon deposit at the hot-gas-side interface approaches the gas temperature as the carbon thickness increases.

Values of the thermal resistance of the carbon deposit at the indicated test conditions, based on experimental results obtained with a LO_2/RP-1 thrust chamber, are shown in Fig. 4-29. For calculations of gas-side heat transfer with the solid deposit on the chamber walls, the following equations can be used:

$$q = h_{gc}(T_{aw} - T_{wg}) \qquad (4\text{-}17)$$

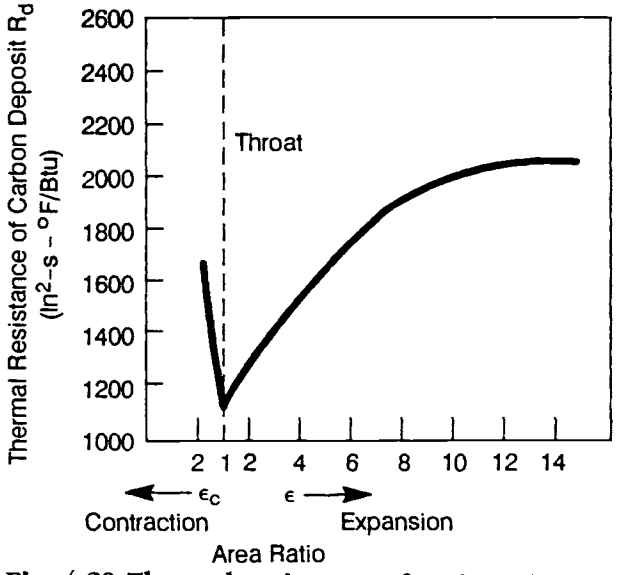

Fig. 4-29 Thermal resistance of carbon deposit on chamber walls LO_2/RP-1, mixture ratio = 2.35, $(p_c)_{ns}$ = 1,000 psia.

where h_{gc} = overall gas-side thermal conductance, Btu/in.^{2}-s-°R

and

$$h_{gc} = \frac{1}{\frac{1}{h_g} + R_d} \qquad (4\text{-}18)$$

where R_d = thermal resistance caused by the solid deposit, in.^{2}-s-°R/Btu. When there is no solid deposit, $R_d = 0$, $h_{gc} = h_g$, and Eq. (4-10) is used for heat-transfer calculations.

Sample Calculation 4-3

Problem

Determine the approximate design gas-side overall thermal conductance h_{gc} in the combustion chamber, at the throat, and at the exit nozzle point of $\epsilon = 5$ for the regeneratively cooled thrust chambers on the A-1 and A-2 Stage engines.

Solution

(a) *A-1 Stage Engine*

First, consider Eq. (4-13). The combustion reactions are assumed to be homogeneous and complete. From Fig. 4-3 the following values can be derived for the chamber product gases, for LO_2/RP-1 at $(P_c)_{ns}$ = 1000 psia and a mixture ratio of 2.35:

$(T_c)_{ns}$ = 6000°F or 6460°R
M = 22.5 lb/mol
γ = 1.222

The design $(T_c)_{ns}$ = theoretical $(T_c)_{ns}$ x (c* correction factor)^2 = 6460°R x $(0.975)^2$ = 6140°R. (See Eq. 1-32a and 1-41.) From Sample Calculation 4-1: Design c* = 5660 ft/s. From Sample Calculation 4-2: D_t = 24.9 in.

Mean radius of the throat contour $= \frac{18.68 + 4.75}{2}$
$= 11.71$ in.

Then:

$$C_p = \frac{\gamma R}{(\gamma - 1)J} = \frac{1.222 \times \frac{1544}{22.5}}{(1.222 - 1) \times 778} = 0.485 \text{ Btu/lb-°R}$$

From Eq. (4-15):

$$Pr = \frac{4 \times 1.222}{(9 \times 1.222) - 5} = 0.816$$

From Eq. (4-16):

$$\mu = (46.6 \times 10^{-10}) \times (22.5)^{0.5} \times (6140)^{0.6}$$
$$= 46.6 \times 10^{-10} \times 4.76 \times 188$$
$$= 4.18 \times 10^{-6} \text{ lb/in.-s}$$

From Eq. (4-13):

$$h_g = \left[\frac{0.026}{24.9^{0.2}} \times \left(\frac{(4.18 \times 10^{-6})^{0.2} \times 0.485}{0.816^{0.6}}\right) \times \left(\frac{1000 \times 32.2}{5660}\right)^{0.8} \times \left(\frac{24.9}{11.71}\right)^{0.1}\right] \left(\frac{A_t}{A}\right)^{0.9} \sigma$$

$$= 0.01366 \times 0.046 \times 4.02 \times 1.078 \times \left(\frac{A_t}{A}\right)^{0.9} \sigma$$

$$= 0.0027 \times \left(\frac{A_t}{A}\right)^{0.9} \sigma$$

Since the carbon-deposit temperature approached the gas temperature, a $(T_{wg}/(T_c)_{ns}$ value of 0.8 is used to determine the σ values from Fig. 4-24 ($\gamma \cong 1.2$). At the combustion chamber:

$$\left(\frac{A_t}{A}\right)^{0.9} = \left(\frac{1}{1.6}\right)^{0.9} = 0.655, \ \sigma = 1.05$$

$$h_g = 0.0027 \times 0.655 \times 1.05$$
$$= 0.00185 \text{ Btu/in.}^2\text{-s F}$$

At the throat:

$$\left(\frac{A_t}{A}\right)^{0.9} = 1, \ \sigma = 1$$

$$h_g = 0.0027 \times 1 \times 1 = 0.0027 \text{ Btu/in.}^2\text{-s F}$$

At the exit nozzle point of

$$\epsilon = 5, \quad \left(\frac{A_t}{A}\right)^{0.9} = \left(\frac{1}{5}\right)^{0.9} = 0.235, \ \sigma = 0.8$$

$$h_g = 0.0027 \times 0.235 \times 0.8$$
$$= 0.000507 \text{ Btu/in.}^2\text{-s F}$$

The experimental data of Fig. 4-29 can be used to determine the values of thermal resistance R_d for the carbon deposit. The thermal resistances are

$$1670\frac{\text{in.}^2\text{s}^\circ\text{F}}{\text{Btu}},\ 1125\frac{\text{in.}^2\text{s}^\circ\text{F}}{\text{Btu}},\ \text{and}\ 1645\frac{\text{in.}^2\text{s}^\circ\text{F}}{\text{Btu}},$$

for points at the combustion chamber, the throat, and the nozzle exit area ratio of 5. Substituting into Eq. (4-18), at the combustion chamber

$$h_{gc} = \frac{1}{\frac{1}{0.00185} + 1670} = 0.00045\ \text{Btu/in.}^2\text{-s-}^\circ\text{F}$$

At the throat

$$h_{gc} = \frac{1}{\frac{1}{0.0027} + 1125} = 0.00067\ \text{Btu/in.}^2\text{-s-}^\circ\text{F}$$

At the exit nozzle of $\varepsilon = 5$

$$h_{gc} = \frac{1}{\frac{1}{0.000507} + 1645} = 0.000276\ \text{Btu/in.}^2\text{-s-}^\circ\text{F}$$

(b) *A-2 Stage Engine*

Again, the combustion reactions are assumed to be homogeneous and complete. From Fig. 4-4, the following values are derived for the chamber product gases, for LO_2/LH_2 at $(P_c)_{ns}$ = 800 psia and a mixture ratio of 5.22: $(T_c)_{ns}$ = 5580°F or 6040°R, M = 12 lb/mol, γ = 1.213. The design $(T_c)_{ns}$ = theoretical $(T_c)_{ns}$ x (c* correction factor)^2 = 6040 x $(0.975)^2$ = 5740°R. From Sample Calculation 4-1: design c* = 7480 ft/s. From Fig. 4-25: D_t = 11.2 in.

Mean radius of throat contour = $\frac{8.4 + 2.14}{2}$ = 5.27 in.

Then:

$$C_p = \frac{\gamma R}{(\gamma - 1)J} = \frac{1.213 \times \frac{1544}{12}}{(1.213 - 1) \times 788} = 0.943\ \text{Btu/lb}^\circ\text{F}$$

From Eq. (4-15):

$$\text{Pr} = \frac{4 \times 1.213}{(9 \times 1.213) - 5} = 0.820$$

From Eq. (4-16):

$$\mu = (46.6 \times 10^{-10})(12)^{0.5}(5740)^{0.6}$$
$$= 46.6 \times 10^{-10} \times 3.47 \times 180$$
$$= 2.92 \times 10^{-6}\ \text{lb/in.-s}$$

From Eq. (4-13):

$$h_g = \left[\frac{0.026}{11.2^{0.2}} \times \left(\frac{(2.92 \times 10^{-6})^{0.2} \times 0.943}{0.820^{0.6}}\right) \times \left(\frac{800 \times 32.2}{7480}\right)^{0.8} \times \left(\frac{11.2}{5.27}\right)^{0.1}\right]\left(\frac{A_t}{A}\right)^{0.9}\sigma$$

$$= 0.01605 \times 0.0828 \times 2.69 \times 1.078 \times \left(\frac{A_t}{A}\right)^{0.9}\sigma$$

$$= 0.00385 \times \left(\frac{A_t}{A}\right)^{0.9}\sigma$$

Since there is no solid deposit on the chamber walls, an average gas-side wall temperature of 1500°R is assumed, and a $(T_{wg}/(T_c)_{ns})$ value of (1500/5740) or 0.26 is used to determine the σ values from Fig. 4-28. At the combustion chamber:

$$\left(\frac{A_t}{A}\right)^{0.9} = \left(\frac{1}{1.6}\right)^{0.9} = 0.655,\ \sigma = 1.38$$

$h_{gc} = h_g$ = 0.00385 x 0.655 x 1.38
= 0.00348 Btu/in.^{2}-s-°F.

At the throat:

$$\left(\frac{A_t}{A}\right)^{0.9} = 1,\ \sigma = 1.35$$

Then $h_{gc} = h_g$ = 0.00385 x 1.0 x 1.35
= 0.00520 Btu/in.^{2}-s-°F.

At the nozzle exit point, ε = 5:

$$\left(\frac{A_t}{A}\right)^{0.9} = \left(\frac{1}{5}\right)^{0.9} = 0.235,\ \sigma = 1.16$$

Then $h_{gc} = h_g$ = 0.00385 x 0.235 x 1.16
= 0.00105 Btu/in.^{2}-s-°F

Regenerative Cooling

Regenerative cooling, which sees increasing application in high-pressure, high-heat-flux thrust chambers, has several advantages over other cooling techniques, and some disadvantages. Advantages include no performance loss (thermal energy absorbed by the coolant is returned to the injector), essentially no change in wall contour as a function of time, indefinite firing duration, and relatively lightweight construction. Disadvantages include limited throttling with most coolants, reduced reliability with some coolants (e.g., hydrazine), high pressure drops required at high-heat-flux levels, and thrust levels, mixture ratios, or nozzle area ratios possibly limited by maximum allowable coolant-temperature.

Design of a regeneratively cooled thrust chamber involves consideration of gas-side heat flux, wall

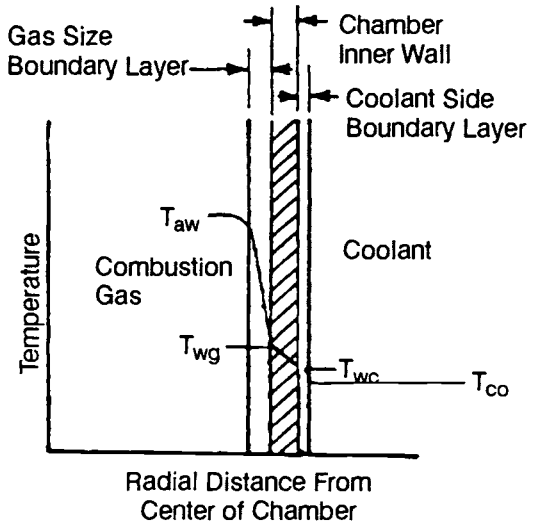

Fig. 4-30 Heat transfer schematic for regenerative cooling.

structural requirements, coolant-side heat transfer, and the effects of temperature increases on coolant properties.

Heat transfer in a regeneratively cooled chamber can be described as the heat flow between two moving fluids, through a multilayer partition. Figure 4-30 shows this process schematically. The general steady-state correlation of heat transfer from the combustion gases through the layers, which include the metal chamber walls, to the coolant can be expressed by the following equations:

$$h_{gc}(T_{aw} - T_{wg}) = q = \left(\frac{k}{t}\right)(T_{wg} - T_{wc}) \qquad (4\text{-}19)$$

$$= h_c(T_{wc} - T_{co}) \qquad (4\text{-}20)$$

$$= H(T_{aw} - T_{co}) \qquad (4\text{-}21)$$

$$H = \frac{1}{\frac{1}{h_{gc}} + \frac{t}{k} + \frac{1}{h_c}} \qquad (4\text{-}22)$$

where

- q = Heat flux, Btu/in.^{2}-s
- h_{gc} = Overall gas-side thermal conductance, Btu/in.^{2}-s-°F (see Eq. 4-18; without deposits, $h_{gc} = h_g$)
- h_c = Coolant-side heat-transfer coefficient, Btu/in.^{2}-s-°F
- k = Thermal conductivity of chamber wall, Btu/in.^{2}-s-°F/in
- t = Chamber-wall thickness, in.
- T_{aw} = Adiabatic wall temp. of the gas, °R
- T_{wg} = Gas-side wall temperature, °R
- T_{wc} = Coolant-side wall temperature, °R
- T_{co} = Coolant bulk temperature, °R
- H = Overall heat-transfer coefficient, Btu/in.^{2}- s-°F

The bulk temperature of the coolant increases from the point of entry until it leaves the cooling passages, as a function of the heat absorbed and of the coolant flowrate. Proper balance of these parameters, to maintain the chamber walls at temperatures below those at which failure might occur because of melting or stress, becomes one of the major requirements for the design of regeneratively cooled thrust chambers. For metals commonly used in thrust-chamber walls, such as stainless steel, nickel, NARloy-Z, and nickel-base superalloys, the limiting hot-gas-side wall temperature ranges from 900 to 1800°F. The resultant differences between combustion-gas temperature and wall temperature range from 2500 to 6000°F.

Assume a station in the thrust chamber with gas temperature T_{aw} and coolant bulk temperature T_{co}. Referring to Eq. 4-21, it will be seen that the heat flux q, which must be the same through all layers, is a function of the temperatures and of overall heat-transfer coefficient H. The value of H is composed of the individual coefficients for the boundary layers and the chamber metal wall (Eq. 4-22). The smaller H is, the smaller q. However, it is one of the major design goals to keep coefficient h_{gc} low, but heat-transfer coefficient h_c and conductivity t/k high, in relation to h_{gc}. Since the temperature differentials are inversely proportional to the heat-transfer coefficients of the heat-flow paths, the temperature drop will then be steepest between hot gas and inner chamber wall. The effect is analogous to voltage drops along resistors in electrical circuits.

The heat absorbed by the propellant used for regenerative cooling raises the temperature of the propellant, and thus the energy level, before it is injected into the combustion chamber. However, the effect on overall engine performance is slight, the gain usually being less than 1%. On the other hand, regenerative cooling, with attendant pressure losses requiring additional turbopump power or higher gas-pressurization levels, imposes an overall performance penalty.

Gas-side heat transfer was discussed in a preceding section of this chapter. It is a function of combustion-gas properties, chamber pressure, and chamber geometry and is transmitted in three modes which, in order of decreasing importance, are forced convection, chemical recombination, and radiation from the gas to the wall.

Coolant-Side Heat Transfer

The coolant-side heat-transfer coefficient h_c is influenced by many factors. At the high heat fluxes and temperatures encountered in thrust-chamber operation, the propellants used for cooling may become corrosive, may decompose, or may deposit impurities upon the heated surface, thereby reducing cooling effectiveness. It is impossible to calculate the h_c values under these conditions without experimental data.

The characteristics of coolant-side heat transfer depend largely on the coolant pressure and coolant-side wall temperature. Figure 4-31 plots heat flux vs.

wall temperature for a constant coolant pressure, bulk temperature, and flow velocity. Curve A indicates the behavior of heat transfer at coolant pressures below critical. Line segment A_1–A_2 represents normal forced-convection heat transfer without boiling when the wall temperature is below the saturation temperature of the coolant corresponding to the fluid pressure. As the wall temperature at A_2 exceeds the saturation temperature by a certain margin (50 to 100°F), bubbles will form within the coolant layer close to the wall. The bubbles grow continuously out into the colder liquid stream until condensation at the vapor-to-liquid surface begins to exceed the rate of vaporization at the base of the vapor bubble, whereupon the bubbles start to collapse. This process, which occurs at high frequencies, is called "nucleate boiling." It substantially increases the heat-transfer coefficient, resulting in little increase in wall temperature for a wide range of heat flux. The heat transfer with nucleate boiling is represented by line A_2–A_3. At A_3, further increase in the heat flux abruptly leads to such a dense bubble population that the bubbles combine into a vapor film with an attendant large decrease in heat-transfer coefficient. The region of heat transfer with film boiling is represented by line A_3–A_4. The resulting increase in wall temperature is so high that failure of the wall material often occurs. The heat flux at A_3 is defined as the upper limit of nucleate boiling of the coolant q_{ul}, which therefore should be used as the design limit for a regenerative cooling system.

Curve B indicates the heat-transfer behavior of a coolant above critical pressure. Since no boiling can occur, the wall temperature continually increases with increasing heat flux. Line A_1–B_2 represents the heat-transfer region, when the wall temperature is below the coolant critical temperature. The heat-transfer coefficient remains essentially constant. As the wall temperature reaches the critical temperature B_2 and higher, a gradual transition to a stable supercritical vapor-film boundary layer begins; this results in somewhat lower heat-transfer coefficients. Line B_2–B_3 represents the heat transfer in this region. Wall failure temperatures are usually reached at lower temperatures when the coolant is above the critical pressure than when it is below it. Where possible, a coolant operating pressure between 0.3 to 0.7 of critical pressure should be used to take advantage of the high heat-transfer coefficients available with nucleate boiling. In most systems, however, particularly those fed from a turbopump, the coolant pressure is supercritical. For the nonboiling subcritical temper-ature regions of both subcritical and supercritical coolant pressures (A_1–A_2 and A_1–B_2 in Fig. 4-31), the relationship between wall temperature and heat flux, which depends on the heat transfer coefficient h_c, can be predicted with sufficient accuracy for design purposes with the help of the Sieder-Tate equation (Eq. 4-23) for turbulent heat transfer to liquids flowing in channels:

$$Nu = C_1 Re^{0.8} Pr^{0.4} \left(\frac{\mu}{\mu_w}\right)^{0.14} \qquad (4\text{-}23)$$

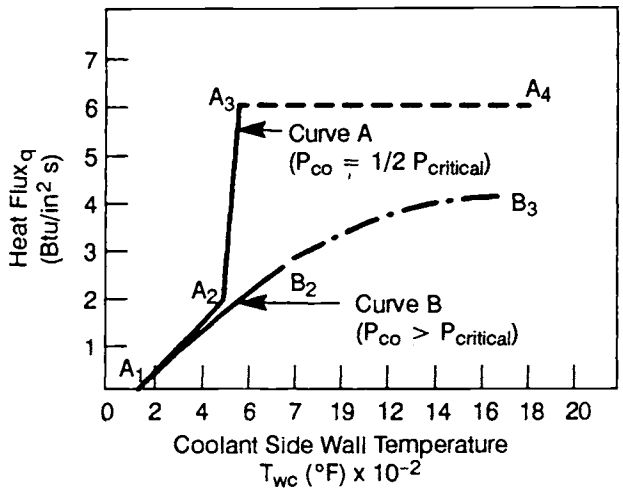

Fig. 4-31 Heat flux vs coolant side wall temperature of typical propellant in various heat transfer regions.

where—

- C_1 = Constant (different values for various coolants)
- Nu = Nusselt number = $h_c d/k$
- Re = Reynolds number = $\rho V_{co} d/\mu$
- Pr = Prandtl number = $\mu C_p/k$
- μ = Coolant viscosity at bulk temp., lb/in.-s
- μ_w = Coolant viscosity at coolant sidewall temperature, lb/in.-s
- d = Coolant passage hydraulic diameter, in.
- k = Coolant thermal conductivity, Btu/s-in.^{2}-°F/in.
- ρ = Coolant density, lb/in.^{3}
- V_{co} = Coolant velocity, in./s
- C_p = Coolant specific heat at constant pressure, Btu/lb-°F

The heat flux at the upper limit of nucleate boiling, q_{ul}, can be estimated from this relation:

$$\frac{q_{ul}}{q_{nonboiling}} = \frac{C_2 \times 10^4}{P_{co} G} \qquad (4\text{-}24)$$

where—

- C_2 = Constant, its value depending on coolant
- $q_{nonboiling}$ = Heat flux without nucleate boiling, Btu/in.^{2}-s
- P_{co} = Coolant pressure, psia
- G = Coolant maximum flowrate per unit area, lb/in.^{2}-s

When the heat is transferred through a vapor-film boundary layer (coolant at supercritical pressure and temperature, region B_2–B_3 in Fig. 4-31), the coolant-side heat-transfer coefficient can be estimated from the following expression:

$$h_c = \frac{0.029 C_p \mu^{0.2}}{Pr^{2/3}} \left(\frac{G^{0.8}}{d^{0.2}}\right) \left(\frac{T_{co}}{T_{wc}}\right)^{0.55} \qquad (4\text{-}25)$$

where—

- C_p = Coolant specific heat at constant pressure, Btu/lb-°F

μ = Coolant viscosity, lb/in.-s
Pr = Prandtl number
G = Coolant weight flowrate per unit area, lb/in.^{2}-s
d = Coolant-passage hydraulic diameter, in.
T_{co} = Coolant bulk temperature, °R
T_{wc} = Coolant-side wall temperature, °R

The bulk temperature of most coolants should be kept below the critical temperature, since the vapor-film heat-transfer coefficient would be too low to cool the wall effectively. The cooling capacity of the liquid-state regenerative coolant system can be estimated by the following:

$$Q_c = \dot{w}_c C_p (T_{cc} - T_{ci}) \qquad (4\text{-}26)$$

where

Q_c = Coolant capacity, Btu/s
$\dot{w}_c$ = Coolant mass flowrate, lb/s
Cp = Coolant specific heat at constant pressure, Btu/lb-°F
T_{cc} = Coolant critical temperature, °R
T_{ci} = Coolant inlet temperature, °R

The allowed value of gas heat-transfer rate Q for the total chamber wall should be kept below Q_c by a safe margin ($Q < Q_c$). However, there is no such limitation when hydrogen is used as a coolant. Hydrogen has excellent heat-transfer characteristics, with a reasonably high heat-transfer coefficient even in the supercritical pressure and temperature region. Usually liquid hydrogen enters the chamber coolant passage under supercritical pressure and reaches supercritical temperature a short distance from the inlet.

The coolant passage areas at various points along the chamber walls are designed to maintain the proper coolant velocity, dictated by the heat-transfer coefficients determined by the heat-transfer calculation. There are several basic design approaches for regenerative-cooled thrust chambers. Axial-flow cooling jackets, made up of tubes, are used in the design of some large thrust chambers (3000 lb of thrust and up); coaxial shells separated by helical ribs or wires generally typify smaller-thrust-chamber designs. An increasingly used regenerative cooling method for high-pressure, high-heat-flux engines employs rectangular slots or channels machined circumferentially into the chamber wall. Figure 4-1 shows a large, regeneratively cooled, tubular-wall thrust chamber. Figure 4-32 represents a typical coaxial shell design for a smaller thrust chamber. In this design, the coolant passage is defined as the rectangular area between inner and outer shells and two adjacent ribs, which are wrapped helically around the inner shell or liner. Figure 4-33 shows the combustion chamber of the Space Shuttle Main Engine, which has 390 coolant slots in the copper alloy (NARloy-Z) liner; the slots are closed out with a thin layer of electrodeposited copper (as a hydrogen barrier) and then electrodeposited nickel (for strength); and the liner is contained within an Inco-718 structural shell.

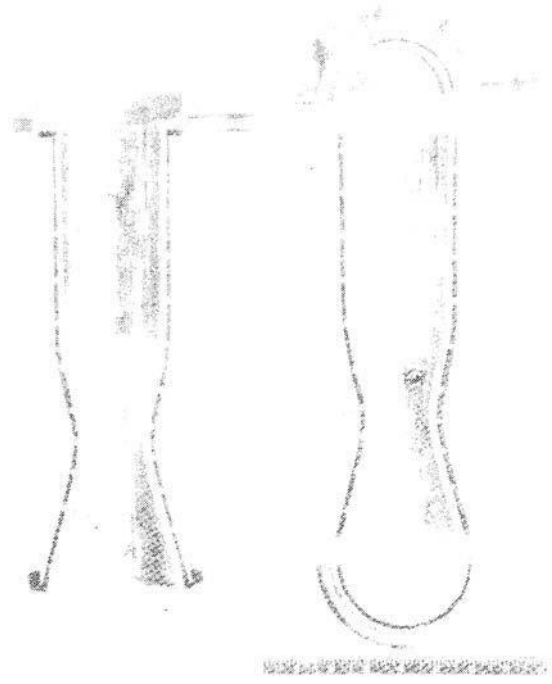

(Note: overheated and burnt-through spot on chamber wall)

Fig. 4-32 Coaxial shell thrust chamber cutaway.

Wall Design Considerations

The three most important parameters involved in the design of a regeneratively cooled chamber wall are the wall material thermal conductivity, the maximum allowable operating temperature, and the wall thickness between the hot gas and the coolant. High conductivity is desirable because it reduces the wall temperature drop for a given heat flux. If the coolant undergoes nucleate boiling or is subject to decompositon, however, high wall conductivity may not be advantageous, because of the resulting lower gas-side wall temperatures and higher heat fluxes. Wall thickness is established by structural requirements to accommodate pressure and thermal stresses as well as by fabrication feasibility limits. Further, the wall material can significantly affect coolant pressure-drop requirements, particularly at high chamber pressures.

Tubular-Wall Thrust Chamber Design

In the design of tubular-wall thrust chambers, the number of coolant tubes required is a function of the chamber geometry, the coolant weight flowrate per unit tube area, the maximum allowable tube wall stress, and fabrication considerations. The critical cooling region near the throat, where the heat flux is highest, determines the number of tubes required for a given coolant flowrate. For lower stress, tube cross-sections of circular shape are preferred, but other

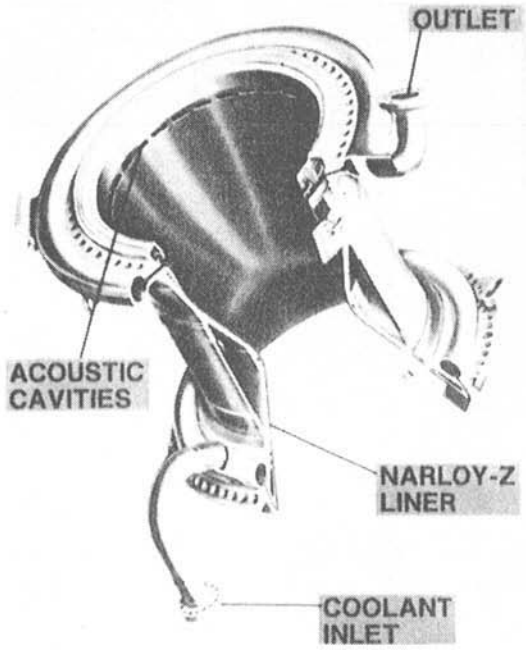

GEOMETRY

NUMBER OF SLOTS	390
NUMBER OF ACOUSTIC CAVITIES	30
INJECTOR END DIAMETER	17.74 IN.
THROAT AREA	83.41 IN.^{2}
INJECTOR END TO THROAT LENGTH	14.00 IN.
EXPANSION RATIO	5.0:1

KEY PERFORMANCE PARAMETERS

	RPL (100%)	FPL (109%)
THROAT STAGNATION PRESSURE (PSIA)	3010	3283
COOLANT INLET PRESSURE (PSIA)	5890	6600
COOLANT INLET TEMPERATURE (°R)	95	100
COOLANT EXIT PRESSURE (PSIA)	4800	5375
COOLANT EXIT TEMPERATURE (°R)	493	479
COOLANT FLOWRATE (LB/SEC)	26	30
HOT GAS WALL TEMPERATURE AT THROAT (°R)	1510	1560

Fig. 4-33 SSME main combustion chamber.

shapes are often used to meet certain flow-area requirements. The stress analysis of the tubes is based upon three primary considerations: the hoop stress caused by coolant pressure, the thermal stress caused by temperature gradients across the tube section and the wall, and the bending stress caused by distortion induced by the pressure differential between adjacent tubes (if any) or by other effects such as discontinuities. The tube design stress is based on the combined stress from these three considerations. In most designs, the maximum combined stress occurs at the throat region.

As shown in Fig. 4-34, the maximum combined tangential stresses of the circular tube will be at section A-A and can be expressed as follows:

$$S_t = \frac{(p_{co} - p_g)r}{t} + \frac{Eaqt}{2(1-v)k} + \frac{6M_A}{t^2} \qquad (4\text{-}27)$$

where

S_t = Combined tangential tensile stress, lb/in.^{2}
q = Heat flux, Btu/in.^{2}-s
r = Tube radius, in.
t = Tube wall thickness, in.
p_{co} = Coolant pressure, lb/in.^{2}
p_g = Combustion gas pressure, lb/in.^{2}
E = Modulus of elasticity of tube wall material, lb/in.^{2}
a = Thermal expansion coefficient of tube wall material, in/in.-°F
k = Thermal conductivity of tube wall material, Btu/in.^{2}-s-°F/in.
v = Poisson's ratio of tube wall material
M_A = Bending moment caused by discontinuity, in.lb-in. (no effect of pressure differential between adjacent tubes for circular-tube design)

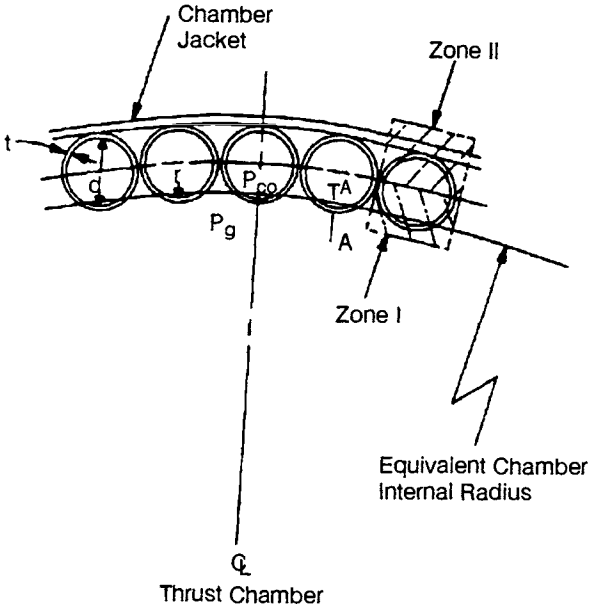

Fig. 4-34 Circular tube wall of regeneratively cooled thrust chamber.

Since the combustion-gas-side portion of the tube (zone I) has a much higher mean temperature than that of the backside tube portion and chamber outer shell (zone II), the thermal expansion of zone I will be restrained by zone II. Because of the considerably greater mass of zone II, thermal inelastic buckling will be induced under certain conditions in zone I in the longitudinal direction. The longitudinal thermal stress can be estimated by

$$S_l = Ea\Delta T \qquad (4\text{-}28)$$

where S_l = longitudinal thermal stress, lb/in.^{2}, and ΔT = mean temp. difference between zone I and zone

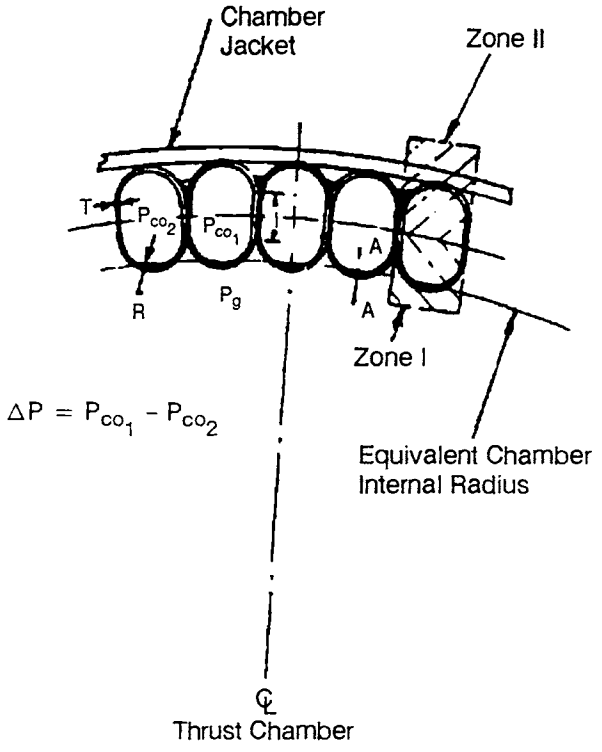

Fig. 4-35 Elongated tube wall of regeneratively cooled thrust chamber.

II, °F. S_1 should be kept at a level not higher than 0.9 S_c, below.

The critical stress for longitudinal inelastic buckling on zone I can be estimated by—

$$S_c = \frac{4E_t E_c t}{(\sqrt{E_t}\sqrt{E_c})^2\sqrt{3(1-v^2)}r} \qquad (4\text{-}29)$$

where

S_c = Critical stress for longitudinal inelastic buckling in zone I, lb/in.^{2}
E_t = Tangential modulus of elasticity at wall temperature, lb/in.^{2}
E_c = Tangential modulus of elasticity from compression stress-strain curve, at wall temperature, lb/in.^{2}

Stresses from an elongated-cross-section tube design, as shown in Fig. 4-35, can be calculated from Eq. (4-27), (4-28), and (4-29). Here, again, the maximum combined stress is at section A. The bending moment at section A, M'_A, should take into consideration the pressure differential (if any) between adjacent tubes:

$$M'_A = M_A + K_A\frac{I\Delta p}{2} \qquad (4\text{-}30)$$

where

M'_A = Combined bending moment at section A, in.-lb/in.
M_A = Bending moment due to discontinuity, in.-lb/in.
K_A = Dimensionless design constant based on test results (range 0.3–0.5)
I = Length of flat portion on tube wall, in.
Δp = Pressure differential between adjacent tubes, lb/in.^{2}

Maximum stress of the elongated tube can be calculated by substituting Eq. (4-30) into Eq. (4-27).

The working loads induced in a regenerative tubular-wall chamber by the chamber pressure are designed to be absorbed by a chamber jacket or tension bands wrapped around the tube bundle.

Coaxial-Shell Thrust Chamber Design

In a coaxial shell-type thrust chamber, as shown in Fig. 4-32, the outer shell is subjected only to the hoop stress induced by the coolant pressure. The inner shell, however, undergoes a combination of compressive stress, caused by the pressure differential between the coolant and combustion gases, and the thermal stress caused by the temperature gradient across the wall. The maximum stress occurs at the inner-wall surface of the inner shell and can be calculated from this equation:

$$S_c = \frac{(p_{co} - p_g)R}{t} + \frac{Eaqt}{2(1-v)k} \qquad (4\text{-}31)$$

where

S_c = Max. combined compressive stress, lb/in.^{2}
q = Heat flux, Btu/in.^{2}-s
R = Radius of the inner shell, in.
t = Thickness of the inner shell, in.
p_{co} = Coolant pressure, lb/in.^{2}
p_g = Combustion-gas pressure, lb/in.^{2}
E = Modulus of elasticity of inner-shell material, lb/in.^{2}
a = Thermal expansion coefficient of inner-shell material, in./in.-°F
k = Thermal conductivity of inner-shell material, Btu/in.^{2}-s-°F/in
v = Poisson's ratio of inner-shell material

Pressure Drop in Cooling Passages

It is desirable to design a cooling passage with minimum pressure drop. Abrupt change of flow direction and sudden expansion or contraction of flow areas should be avoided. The inner surface of cooling passages should be smooth and clean. A cooling passage can be treated as a hydraulic conduit and the pressure drop calculated accordingly, as follows:

$$\Delta p = f\frac{L}{d}\frac{\rho V_{co}^2}{2g} \qquad (4\text{-}32)$$

where

Δp = Coolant pressure drop through the portion of cooling passage under consideration, lb/in.^{2}
L = Length of that portion, in.

d = Equivalent average diameter of that portion, in.
ρ = Average density of the coolant, lb/in.^{3}
V_{co} = Average coolant flow velocity, in./s
g = Mass conversion factor, equal to gravitational constant, 32.2 x 12 in./s^2
f = Friction loss coefficient, a function of the Reynolds number and of cooling passage conditions such as surface smoothness, geometric shape, etc.: can be determined only experimentally.

Sample Calculation 4-4

Determine the cooling passage and the tube design at the throat for the thrust chambers of the A-1 and A-2 Stage engines.

Solution

(a) *A-1 Stage Engine*

The fuel RP-1 will be the coolant. Since the cooling requirement is most stringent at the throat, the tube design for this station will serve as the starting point for the entire chamber. For its high strength, Alloy X-750 will be the tube material. Based on experimental test results that showed good solid-carbon deposits, design values not exceeding 1460°R may be permitted for gas-side tube-wall temperature. Specifically, the throat region will be given a T_{wg} value of 1188°R. Using the results of Sample Calculation 4-3, the value of the adiabatic wall temperature T_{aw} can be calculated by multiplying $(T_c)_{ns}$ by the estimated stagnation recovery factor of 0.923, or T_{aw} = 6140 x 0.923 = 5667°R. From the same calculation, the overall gas-side thermal conductance at the throat region will be h_{gc} = 0.00067 Btu/in.^{2}-s-°F. Substituting into Eq. (4-10), yields the heat flux at the throat:

$$q = (5667\text{-}1188) \times 0.00067 = 3.00 \text{ Btu/in.}^2\text{-s}$$

Material-property data list the following average values for Alloy X-750 at 1000-1200°R: coefficient of thermal expansion, a = 8 x 10^{-6} in./in.-°F; modulus of elasticity, E = 28 x 10^6 psi; thermal conductivity, k = 3.19 x 10^{-4} Btu/in.^{2}-°F/in; Poisson's ratio v, = 0.35.

A circular-tube configuration will be used with an internal diameter d and a wall thickness of 0.020 in. The assumption for thickness must be verified by heat-transfer and stress calculations. From Eq. (4-19), the coolant-side wall temperature will be

$$T_{wc} = T_{wg} - \frac{qt}{k} = 1188 - \frac{3.00 \times 0.02}{3.19 \times 10^{-4}} \cong 1000°R$$

The design will employ a double-pass; i.e., the coolant passes down through alternating tubes and up through adjacent tubes. For an "up" tube, assume a coolant bulk temperature T_{co} = 600°R at the throat (the more severe case, since the coolant has passed the throat region before, on the way down). This temperature is well below critical and can be expected to remain so for the remainder of the passage. Total temperature increase for a typical thrust-chamber design is about 100-400°F between cooling jacket inlet and outlet. The heat-transfer coefficient required to permit the calculated heat flux for the temperature differential assumed can now be calculated from Eq. (4-20):

$$h_c = \frac{q}{T_{wc} - T_{co}} = \frac{3.00}{1000 - 600}$$
$$= 0.0075 \text{ Btu/in.}^2\text{-s-°F}$$

Equation (4-23) shows the relationship between required h_c and correct tube diameter, with experimental data for RP-1 (C_1 = 0.0214):

$$Nu = 0.0214 Re^{0.8} Pr^{0.4} \left(\frac{\mu}{\mu_w}\right)^{0.14}$$

or, substituting corresponding terms:

$$\frac{h_c d}{k} = 0.0214 \left(\frac{\rho V_{co} d}{\mu}\right)^{0.8} \left(\frac{\mu C_p}{k}\right)^{0.4} \left(\frac{\mu}{\mu_w}\right)^{0.14} \quad (a)$$

The following additional relationships exist:

$$\text{Number of tubes } N = \frac{\pi[D_t + 0.8(d + 0.04)]}{(d + 0.04)}$$
$$= \frac{(0.8d + 24.93)}{(d + 0.04)} \quad (b)$$

From Sample Calculation 4-2, D_t = 24.9 in. The factor 0.8 expresses the fact that the tube centers are located on a circle, rather than in a straight line. The double-pass design will then have the following coolant velocity:

$$V_{co} = \frac{\frac{\dot{W}_f}{\rho}}{\frac{N}{2}\frac{(\pi d^2)}{4}} = \frac{827 \times 8}{\pi N d^2 \rho} = \frac{2106}{N d^2 \rho} \quad (c)$$

From Table 3-2: $\dot{w}_f$ = 827 lb/s; ρ = local value of fluid density.

RP-1 at 600°R has the following properties: μ = 4.16 x 10^{-5} lb/in.-s; k = 1.78 x 10^{-6} Btu/in.^{2}-s-°F/in.; C_p = 0.5 Btu/lb-°F. For RP-1 at 1000 R, μ_w = 0.416 x 10^{-5} lb/in.-s. Now substitute known values and Eq. (c) into Eq. (a):

$$\frac{0.0075d}{1.78 \times 10^{-6}} = 0.0214 \times \left(\frac{\rho d \frac{2106}{N d^2 \rho}}{4.16 \times 10^{-5}}\right)^{0.8}$$
$$\times \left(\frac{0.5 \times 4.16 \times 10^{-5}}{1.78 \times 10^{-6}}\right)^{0.4} \times \left(\frac{4.16 \times 10^{-5}}{0.416 \times 10^{-5}}\right)^{0.14}$$

$$4{,}220d = 115{,}000 \left(\frac{1}{Nd}\right)^{0.8}$$

$$N = 62.4 d^{-2.25} \quad (d)$$

And substitute Eq. (d) into Eq. (b):

$$62.4d^{-2.25} = \frac{\pi(0.8d + 24.93)}{(d + 0.04)}$$

$$d = 0.85 \text{ in.}$$

Substitute (d) into Eq. (b): N = 94.5.

Since a two-pass design needs a whole, even tube number, a design value of N = 94 will be substituted into Eq. (b), yielding d = 0.855 in.

To define a new tube design, repeated calculations, with varied assumptions, will be required. An experienced designer will require fewer approaches, particularly if test results of prior, comparable designs are available. Even for complicated conditions, however, great amounts of data can be generated in a relatively short time on a computer. Proceed as follows. From Table 3-2:

$$\rho = \frac{50.45}{1728} = 0.0292 \text{ lb/in.}^3$$

Substitute into Eq. (c):

$$V_{co} = \frac{2106}{94 \times (0.855)^2 \times 0.0292}$$

$$= 1051 \text{ in./s or } 87.6 \text{ ft/s}$$

At the throat, p_{CO} = 1500 psia represents an interpolation between fuel-pump outlet pressure and injector-manifold pressure. Combustion-gas pressure at the throat will be

$$p_g = p_t = (p_c)_{ns}\left(\frac{2}{\gamma + 1}\right)^{\frac{\gamma}{\gamma - 1}} = 1000 \times 0.562 = 562 \text{ psia}$$

And γ = 1.222 from Sample Calculation 4-2; use Table 1-2. Maximum tensile stress at the inner tube-wall face can then be determined using Eq. (4-27):

$$S_t = \frac{(1500 - 562) \times 0.427}{0.020}$$

$$+ \frac{28 \times 10^6 \times 8 \times 10^{-6} \times 3.0 \times 0.2}{2 \times (1 - 0.35) \times 3.19 \times 10^{-4}} + 6\frac{M_A}{t^2}$$

$$= 20{,}000 + 35{,}500 + 15{,}000M_A$$

$$= 52{,}500 + 15{,}000M_A$$

Material property data list an F_{ty} of 82,000 for Alloy X-750 at 1000°R, which leads to the following value:

$$\text{Maximum allowable } M_A = \frac{82{,}000 - 52{,}500}{15{,}000}$$

$$= 1.97 \text{ in.-lb/in.}$$

From experience, it can be assumed that the bending moment caused by discontinuity in this case will be less than 1.97 in./lb/in. Thus the assumed 0.020-in. thickness for the tube wall is sufficient. Summarizing the tube configuration at the throat: d = 0.855 in., t = 0.020 in., N = 94.

(b) *A-2 Stage Engine*

The fuel, hydrogen, will be the coolant , and again Alloy X-750 will be the tube material. To avoid the "hot shortness" (low-ductility) properties of Alloy X-750 in the range 1200-1400°F, the mean temperature of the tube wall must be kept under 1000°F (1460°R). The adiabatic wall temperature T_{aw} of the gas can be calculated using an assumed stagnation recovery factor of 0.92: $T_{aw} = (T_c)_{ns} \times 0.92 = 5740 \times 0.92 = 5270$°R. From Sample Calculation 4-3, the overall gas-side conductance at the throat region h_{gc} = 0.00520 Btu/in.^{2}-s-°F. Substituting into Eq. (4-19) yields the heat flux at the throat:

$$q = (5270\text{-}1600) \times 0.00520 = 3670 \times 0.00520$$
$$= 19.10 \text{ Btu/in.}^2\text{-s}$$

A value of 1600°R will be used for the gas-side wall temperature T_{wg} at the throat region. The following data apply to Alloy X-750 at 1600°R (1140°F): a = 8.2 x 10^{-6} in/in.-°F; E = 24 x10^6 psi; k = 3.86 x 10^{-4} Btu/in.^{2}-s-°F/in.; v = 0.35.

A circular-tube configuration will be used with an internal diameter d and a wall thickness of 0.008 in. From Eq. (4-19) coolant-side wall temperature will be

$$T_{wc} = 1600 - \frac{19.10 \times 0.008}{3.86 \times 10^{-4}} = 1600 - 396 = 1204° \text{ R}$$

A mean value will describe the wall temperature:

$$T_{wc} = \frac{1600 + 1204}{2} = 1402° \text{ R} < 1460° \text{ R}$$

Assuming a coolant bulk temperature T_{CO} = 135 R at the throat, Eq. (4-20) then yields

$$h_c = \frac{19.10}{1204 - 135} = 0.0179 \text{ Btu/in.}^2\text{/s/°F}$$

Substituting into Eq. (4-25) gives

$$0.0179 = \frac{0.029C_p\mu^{0.2}}{P_t^{2/3}} \frac{(G^{0.8})}{(d^{0.2})} \left(\frac{T_{co}}{T_{wc}}\right)^{0.55} \qquad \text{(a)}$$

From Fig. 4-25, D_t = 11.2 in. The following relationships exist:

$$\text{Number of tubes } N = \frac{\pi[D_t + 0.8(d \times 0.016)]}{(d + 0.016)}$$

$$= \frac{\pi(0.8d + 11.213)}{(d + 0.016)} \qquad \text{(b)}$$

A 1 1/2-pass design will be used (i.e., the coolant enters the fuel manifold at the ε = 8 nozzle plane, flows to e = 30 and back, and then passes through the throat and combustion chamber zone before it enters the injector). From Table 3-3: $\dot{w}_t$ = 54.5 lb/s. Coolant weight flowrate per unit area will be:

$$G = \frac{\dot{w}_f}{N\left(\frac{\pi d^2}{4}\right)} = \frac{54.5 \times 4}{\pi N d^2} = \frac{69.3}{Nd^2} \qquad \text{(c)}$$

For hydrogen at 135°R: Pr = 0.82; C_p = 3.5 Btu/lb-°F; μ = 0.367 x 10^{-6} lb/in.-s. Substituting these values and Eq. (c) into Eq. (a) yields the following:

$$0.0179 = \frac{0.029 \times 3.5 \times (0.3657 \times 10^{-6})^{0.2}}{(0.82)^{2/3}} \times \left[\frac{\left(\frac{69.3}{Nd^2}\right)^{0.8}}{d^{0.2}} \right] \times \left(\frac{135}{1204}\right)^{0.55}$$

or $N = 3.91d^{-2.25}$. Then, substituting Eq. (d) into Eq. (b) yields

$$3.91d^{-2.25} = \frac{\pi(0.8d + 11.213)}{(d + 0.016)} \quad ; \; d = 0.185 \text{ in.}$$

Substituting into Eq. (b) gives

$$N = \frac{\pi(0.8 \times 0.185 + 11.213)}{(0.185 + 0.016)} = 178$$

Maximum tensile stress can now be checked at the inner-wall surface using Eq. (4-27). At the throat, estimated p_{co} = 1200 psia; $p_g = p_t = (p_c)_{ns}\,[2/(\gamma+1)\gamma / (\gamma-1)]$ = 800 x 0.554 = 443 psia; and γ = 1.213 from Sample Calculation 4-1. Then:

$$S_t = ((1200\text{-}443) \times 0.0925/0.008) + (24 \times 10^6 \times 8.2 \times 10^{-6} \times 19.10 \times 0.008/[2(1 - 0.035)\times 3.86 \times 10^{-4}] + 6 \frac{M_A}{(0.008)^2} = 68{,}750 + 94{,}900\, M_A$$

Material property data list an F_{ty} of 81,000 psi for Alloy X-750 at 1200°R. Then—

$$\text{Max. allowable } M_A = \frac{81000 - 68750}{93900} = 0.131 \text{ in.-lb-in.}$$

From experience, it can be assumed that the bending moment caused by discontinuity will be less than 0.131 in.-lb/in. Thus the selection of 0.008-in. tube thickness is valid. Summarizing the tube configuration at the throat: d = 0.185 in., t = 0.008 in., N = 178.

As a general design aid, Fig. 4-36 and 4-37 present construction details for a typical regeneratively-cooled, tube-wall thrust chamber. The chamber shown is very similar to the one presented in Fig. 4-1 and 4-2. Figure 4-36 shows clearly how the tube shape changes along the longitudinal axis.

In a typical manufacturing process, tubes of uniform circular cross-section are first cut to length and then swaged or tapered. The tubes are filled with wax, and then bent (preshaped) in a special fixture to the thrust-chamber contour. After wax removal, each tube is placed in a die of varying cross-sectional area. Hydraulic pressure applied to the inside of the tube forces it to align with the die and to assume final shape. A trimming process usually follows. In preparation for assembly into a chamber, the tubes are arranged on a brazing fixture (core). Proper brazing requires great care to assure even distribution of the gaps between tubes. Earlier chamber models

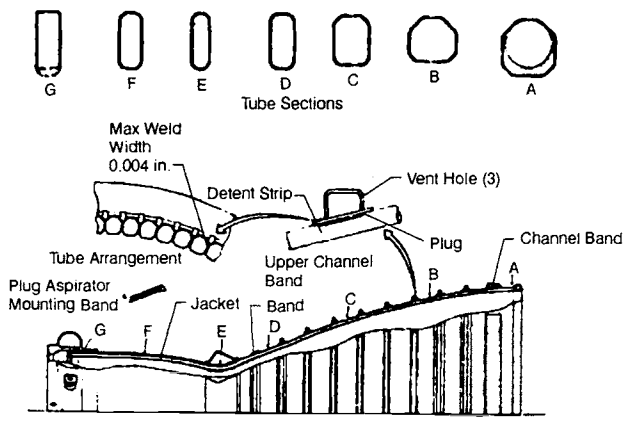

Fig. 4-36 Typical regeneratively cooled tube wall thrust chamber.

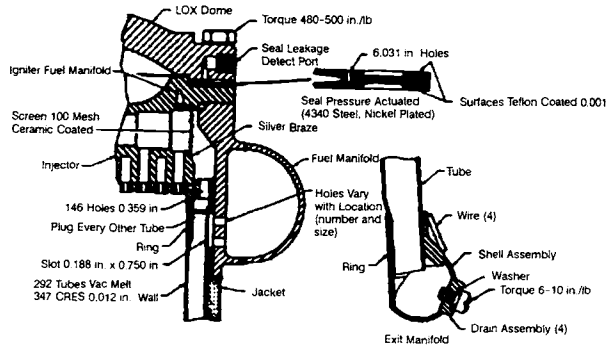

Fig. 4-37 Detail of injector manifolding and return manifold of typical regeneratively cooled tube wall thrust chamber.

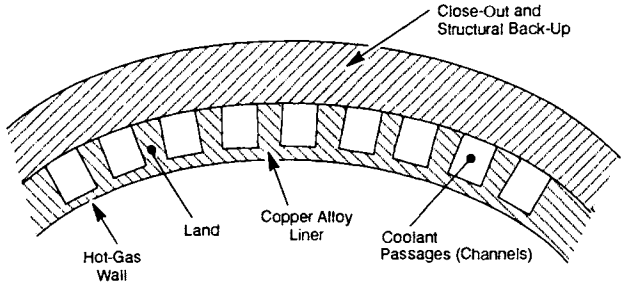

Fig. 4-38 Typical channel wall configuration.

were then hand-brazed, a process requiring many weeks and considerable skill. More recently, furnace brazing has been successfully applied, drastically cutting chamber-assembly time.

Channel-Wall Design

The preferred cooling technique for high-pressure (2000 psi or greater) thrust chambers, in which heat flux may be very high, flows the coolant through rectangular slots, or channels, machined into the chamber liner. The machined channels are closed out and the liner is enclosed in a structural support shell (Fig. 4-38). Examples of such chambers are those used in the O_2/H_2 SSME, in which cryogenic hydrogen is the coolant (Fig. 4-33) and in the NTO/MMH XLR-132 engine, in which supercritical

NTO is the coolant (Fig. 4-39). In both chambers, the inner wall containing the coolant channels is NARloy-Z, a copper-silver-zirconium alloy with significantly greater strength than pure copper but with only slightly lower thermal conductivity. For structural strength the channels are closed out by a thin layer of electrodeposited copper followed by electrodeposited nickel.

Channel-wall cooling has two major advantages for high-heat-flux applications. One is the increased wall mass available, which permits "smoothing" of any localized, extremely-high-heat-flux regions, thereby permitting the wall to survive such occurrences. The second advantage is the ability to use high-conductivity material for wall construction, such as copper, copper alloys, and nickel.

Design of a channel-wall thrust chamber begins with a contour analysis. Key parameters required for this analysis include the combustor injector-to-throat length, combustor length and diameter before start of convergence, convergence angle, and the throat radii, upstream and downstream.

A boundary-layer program is used to estimate the gas-side film coefficient profile along the combustor and nozzle. The local Stanton Number is obtained by using a semi-empirical correlation between the Stanton Number and the energy-boundary-layer thickness and between the skin-friction coefficient and the momentum-boundary-layer thickness. The convective film coefficient is then given by—

$$h_g = \rho V C_p St \qquad (4\text{-}33)$$

where ρ = gas density, lb/in.^{3}; V = velocity, in./s; C_p = heat capacity, Btu/lb-°F; and St = Stanton Number = $h_g/\rho V C_p$.

The injector-end heat-transfer coefficient can be estimated by scaling experimental data (for example, from the SSME 40K subscale chamber), using flowrate and property corrections based on the standard Nusselt Number correlation, as follows:

$$(h_g)_2 = (h_g)_1 \frac{k_2}{k_1}\left(\frac{G_2}{G_1}\frac{\mu_1}{\mu_2}\right)^{0.8}\left(\frac{Pr_2}{Pr_1}\right)^{0.4} \qquad (4\text{-}34)$$

where k = gas thermal conductivity, Btu/s-in.^{2}-°F/in.; G = mass flux, lb/s-in.^{2}; μ = viscosity, lb/in.-s; and Pr = Prandtl number. Subscript 1 : reference parameters (40K subscale test data); subscript 2 : design parameters.

The injector-end heat-transfer coefficient is blended into the axial profile derived from the boundary-layer program (Fig. 4-40), and the coolant-channel flow-area and wall-thickness requirements are then determined.

Various computer programs have been written to analyze the temperature distribution in a channel-wall configuration. In one such program, "REGEN", a two-dimensional analysis is employed in conjunction with the one-dimensional compressible-flow equations. The procedure accounts for variable coolant-side wall temperature in calculating coolant-side film coefficients. Figure 4-41 shows a sample printout of the REGEN program. The estimated temperatures are printed as a "plot" between the two axes of symmetry

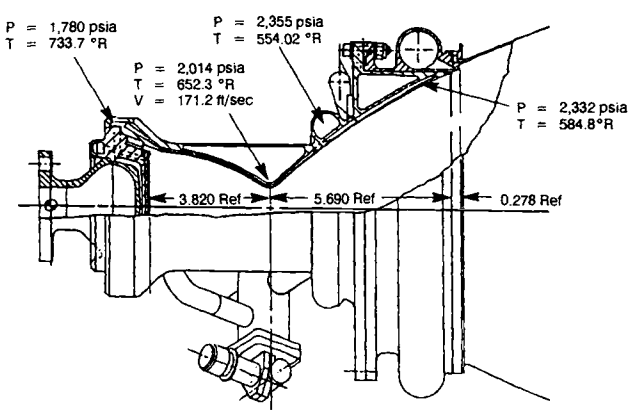

Fig. 4-39 Flightweight XLR-132 thrust chamber showing 1-1/2-pass, longitudinal, coolant channel in wall.

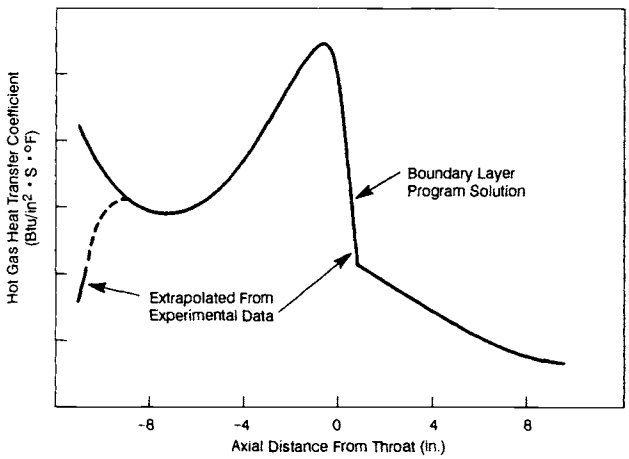

Fig. 4-40 Hot-gas heat transfer coefficient profile.

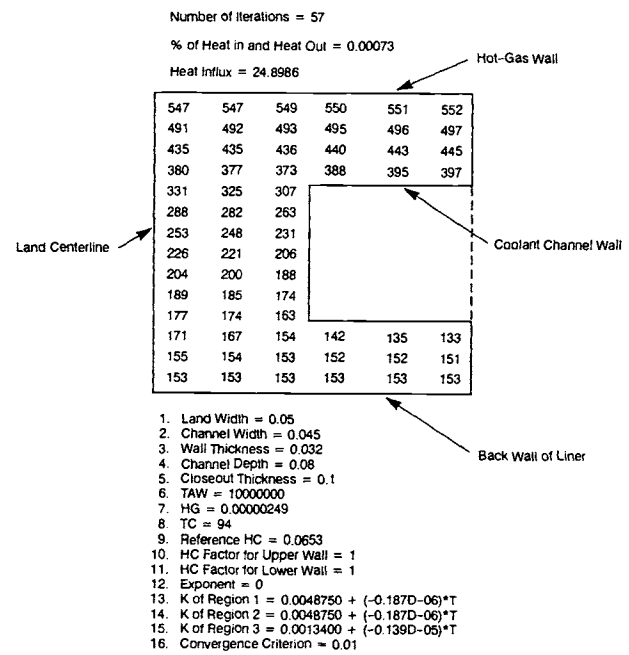

Fig. 4-41 Sample output of the REGEN computer program.

of the channel (center of the land and center of the channel). Maximum temperatures (547 and 552°F) are at the center of the land and center of the channel, respectively.

For regions in which the coolant passages curve, a cooling enhancement factor accounts for secondary-flow eddies that develop in the stream. The straight-path film coefficient is multiplied by this factor to give the local value. The coolant curvature enhancement factor, which is also applicable to tubes, is shown as a function of turning angle in Fig. 4-42.

An optimized, regeneratively-cooled thruster may combine the coolant-channel and tube-wall concepts. In the SSME, for example, the channel-wall combustor has demonstrated ability to withstand throat heat-flux levels on the order of 100 Btu/in.^{2}-s. At a nozzle expansion ratio of 5, the chamber is attached to a tubular thin-wall nozzle, which is much more weight efficient than a channel-wall configuration at the lower heat flux.

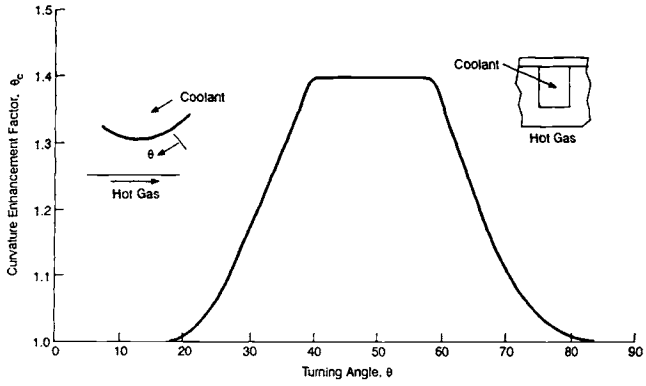

Fig. 4-42 Curvature enhancement factor profile.

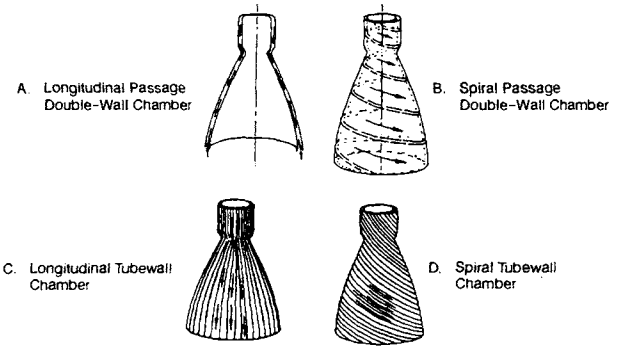

Fig. 4-43 Typical dump-cooled chamber fabrication methods.

Dump Cooling

Dump cooling may prove particularly effective in hydrogen-fueled, low-pressure systems (p_c<100 psia) or in nozzle extensions of high-pressure hydrogen systems. A small amount of the total hydrogen flow is diverted from the main fuel-feed line, passed through cooling passages, and ejected. The heat-transfer mechanism is similar to that of regenerative cooling. The coolant, however, becomes superheated as it flows toward the nozzle exit, where it is expanded overboard at reasonably high temperatures and velocities, thus contributing some thrust. Application of dump cooling is often limited, however, by various technical difficulties, such as discharge nozzle design at low coolant flowrates.

The type of coolant path for a dump-cooled thrust chamber will be selected to assure maximum overall engine system performance. Two possible paths are shown in Fig. 4-43:

1) Axial flow: a one-pass longitudinal passage, using double-wall (Fig. 4-43a) or tube-wall design (Fig. 4-43c). Both are open-ended, with provision for expansion of the dumped superheated hydrogen gas at the nozzle exit.
2) Circumferential flow: a double-wall design with a spiral flow path for the coolant and provision for expansion of the dumped superheated hydrogen gas in the axial direction (Fig. 4-43b). A spiral-wound tube design may also prove advantageous (Fig. 4-43d).

The various constructions differ considerably in complexity and fabrication cost. Selection will depend on an optimum tradeoff among reliability, performance, cost, and weight. The longitudinal-passage designs are often chosen for higher coolant flowrates, as related to the physical size of the thrust chamber. The spiral-passage designs are used for lower coolant flowrates to alleviate the difficulties of maintaining proper flow velocities and dimensional clearances in the coolant passage.

Because the hydrogen coolant gas can be discharged at relatively high temperatures (1000°R and up), overall engine system performance may not be affected appreciably by the dump-coolant flow.

Film Cooling

Porous wall materials, or slots and holes provided in thrust-chamber walls, can serve to introduce a coolant, a process commonly referred to as film cooling. Because of interaction between coolant film and combustion gases, as a result of heat and mass transfer, the effective thickness of the coolant film decreases in the direction of flow. In most cases, therefore, additional coolant is injected at one or more downstream chamber stations. Figure 4-44 shows a model of the film-cooling process. The coolant is introduced through rows of holes. The fluid introduced through row "A" will cover the wall surface between "A" and "B." Fluid from row "B" will cover the surface between "B" and "C," etc. In an optimum design, the flowrate from each row is just sufficient to cover the area to be cooled.

Although heat protection exclusively by film cooling has not been applied in the past for the major operational rocket engines, it is significant that, in practice, regenerative cooling is nearly always supplemented by some form of film cooling. In most instances, a fuel-rich gas boundary layer is

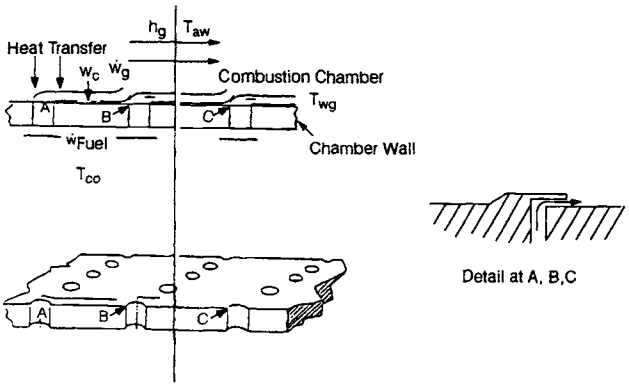

Fig. 4-44 Film-cooling model.

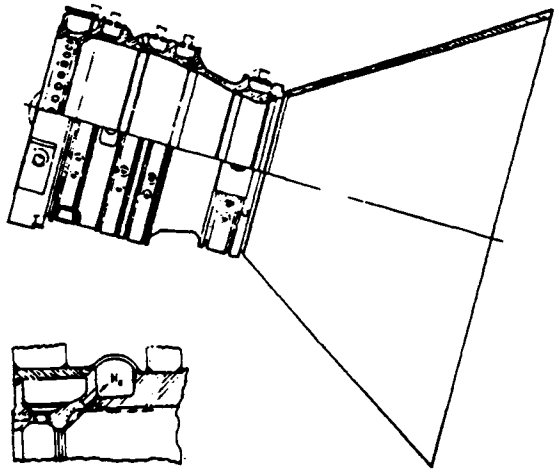

Fig. 4-45 Experimental hydrogen/oxygen, film-cooled thrust chamber.

created by the injection of fuel toward the chamber wall through peripheral orifices in the injector. An important advantage of film cooling is the fact that it reduces heat transfer through the wall. Consequently, thermal stresses become less critical. This is an important consideration, because thermal stresses may establish the feasibility limits of conventional regenerative cooling.

Liquid-Film Cooling

It has been shown experimentally that, simply to reduce heat transfer to the wall, film cooling is more effective with the coolant injected as a liquid than as a gas. Liquid coolant film behaves essentially as an isothermal heat sink as it evaporates and diffuses into the free stream. However, this process results in two-phase flow, consisting of an annular liquid coolant film and a combustion-gas core. This effect introduces coolant losses, which reduce the theoretical cooling potential. Disturbances in the form of capillary waves appear on the surface of the liquid film adjacent to the combustion gases and accelerate coolant loss. The following theoretically derived equation can be used for design calculations of liquid-film-cooled thrust chambers:

$$\frac{G_c}{G_g} = \frac{1}{\eta_c} \cdot \frac{H}{a(1 + b^{C_{pvc}/C_{pg}})} \tag{4-35}$$

where

G_c = Film-coolant weight flowrate per unit area of cooled chamber wall surface, lb/in.^{2}-s

G_g = Combustion-gas weight flowrate per unit area of chamber cross section perpendicular to flow, lb/in.^{2}-s

η_c = Film-cooling efficiency

H = Film-coolant enthalpy, Btu/lb

$$= \frac{C_{pvc}(T_{aw} - T_{wg})}{C_{plc}(T_{wg} - T_{co}) + \Delta H_{vc}}$$

C_{plc} = Average specific heat at constant pressure of the coolant in the liquid phase, Btu/lb-°F

C_{pvc} = Average specific heat at constant pressure of the coolant in the vapor phase, Btu/lb-°F

C_{pg} = Average specific heat at constant pressure of the combustion gases, Btu/lb-°F

T_{aw} = Adiabatic wall temperature of the gas, °R

T_{wg} = Gas-side wall temperature and coolant-film temperature, °R

T_{co} = Bulk temperature at manifold, °R

ΔH_{vc} = Heat of vaporization of coolant, Btu/lb

a = $2V_d/V_m f$

b = $(V_g/V_d)-1$

f = Applicable friction coefficient for the two-phase flow between combustion gases and liquid film coolant

V_d = Axial stream velocity of combustion gases at edge of boundary layer, ft/s

V_m = Average axial stream velocity of combustion gases, ft/s

V_g = Axial stream velocity of combustion gases at the center line of the thrust chamber, ft/s

In practice the theoretically determined film-coolant flowrate would be inadequate because of losses. A film-cooling efficiency η_c must be introduced to correct for this. Liquid-film cooling efficiency values range from about 30 to 70%, depending on injection geometry and flow conditions. They are determined experimentally in hot firings of a specific design or test model.

Hydrocarbon fuels have been found to be very effective liquid-film coolants, owing to their action as both film and barrier cooling-agents. As mentioned earlier, these fuels deposit carbon on the wall, which serves as an effective insulator. At chamber pressures of 2000 psi or higher, however, carbon deposition is significantly less than at lower pressures.

Gaseous-Film Cooling

With the increasing use of hydrogen, gaseous-film cooling has become important because, even if hydrogen is injected as a liquid for film-cooling purposes, the film between the combustion gases and

the chamber wall is heated to temperatures above critical within a very short distance, after which the film behaves as a gas. For design calculations of gaseous-film-cooled thrust chambers, the following theoretically derived equation can be used:

$$\frac{T_{aw} - T_{wg}}{T_{aw} - T_{co}} = e^{-\left(\frac{h_g}{G_c C_{pv} \eta_c}\right)} \qquad (4\text{-}36)$$

where

T_{aw} = Adiabatic wall temp. of the gas, °R
T_{wg} = Max. allowable gas-side wall temp., °R
T_{co} = Initial film-coolant temperature, °R
e = Base of natural logarithms, 2.718
h_g = Gas-side heat-transfer coefficient, Btu/in.^{2}-s-°F
G_c = Film-coolant weight flowrate per unit area of cooled chamber wall surface, lb/in.^{2}-s
C_{pvc} = Average specific heat at constant pressure of the gaseous film coolant, Btu/lb-°F
η_c = Film-cooling efficiency

Equation (4-36) assumes that a balance exists between heat input and coolant temperature-rise. The heat input is based upon the gas-side heat-transfer coefficient h_g and the difference between the adiabatic gas temperature at the wall and the coolant-film temperature. The heat absorbed is proportional to the heat capacity of the coolant film from initial to final temperature values. Once equilibrium is reached, no heat is transferred to the wall (adiabatic condition) and the chamber-wall surface will have achieved the film-coolant temperature corresponding to the various axial locations. Accordingly, the wall-surface temperature will range axially from the value of initial coolant temperature to a maximum allowable design wall temperature, at which point the next film-coolant injection station must be provided. It is the specific aim of film-cooled-thrust-chamber design to accomplish cooling with an optimum number of coolant-injection stations.

Figure 4-45 shows an experimental hydrogen-film-cooled thrust chamber. Cooling is provided by four film-coolant injector rings upstream and one downstream of the throat. Axial coolant injection, in the direction of combustion-gas flow, greatly improves film-cooling efficiency, whereas normal injection results in the escape, without any benefit, of large portions of the coolant into the combustion-gas stream. Typically, film-coolant flow is approximately 3 to 10% of the propellant.

Sample Calculation 4-5

Problem

The hydrogen-film-cooling system for the thrust chamber of the A-3 Stage engine has the following data properties at the throat section: h_g = 0.0011 Btu/in.^{2}-s-°F; T_{aw} = 5240°R; T_{wg} = 1900°R (max); T_{co} = 50°R; and C_{pvc} = 3.6 Btu/lb-°F (average). Assuming a value of 0.5 for film-cooling efficiency, determine the film-coolant weight flowrate per unit area of cooled chamber surface in the throat section.

Solution

Substitute the given data into Eq. (4-36):

$$\frac{5240 - 1900}{5240 - 50} = e^{-\left(\frac{0.0011}{G_c \times 3.6 \times 0.5}\right)}$$

$$1.554 = e^{\left(\frac{0.00061}{G_c}\right)}$$

$$G_c = \frac{0.00061}{\ln 1.554} = \frac{0.00061}{0.439} = 0.001392 \text{ lb/in.}^2\text{-s}$$

To calculate the heat flux for a regenerative cooling system with added film cooling, a corrected value of T_{aw} must be used in Eq. (4-10) or (4-17). This corrected adiabatic wall temperature can be determined experimentally under the specific thrust-chamber operational and film-cooling conditions. It has been found that there is practically no difference in the gas-side heat-transfer coefficient with and without film cooling. Thus, the normal gas-side heat-transfer coefficient h_g can be used in Eq. (4-10). Note that if a hydrocarbon fuel is used as the film coolant, carbon deposition must be taken into account (Eq. 4-17).

Mixture-Ratio Bias

Film cooling achieves its effect by lowering the temperature of the gas in contact with the chamber wall, thus reducing the heat flux into it. Another means of lowering the peripheral gas temperature modifies the propellant mixture ratio in this region, regardless of what other cooling technique is employed. Biasing the mixture ratio in the outer region of the injector to produce lower-temperature combustion (usually achieved by making this region more fuel-rich than the core flow) can yield substantial decreases in heat flux. This has been demonstrated, for example, in experimental firings of LOX/RP-1 at high chamber pressure (2000 psi) in a 3.5-in. workhorse combustor. A high-performance injector (95% c* efficiency), with a pattern of intersecting oxidizer and fuel circumferential fans, exhibited high-heat-flux levels in its original configuration, which had a slightly-oxidizer-rich periphery (compared to the nominal 2.8 mixture ratio). By moving the outer row of fuel orifices slightly outboard, the mixture ratio in the outer zone was changed to fuel-rich, relative to the core value. The effect of this minor modification was dramatic (Fig. 4-46). Heat flux in the cylindrical chamber section was reduced about 70% and heat flux at the throat was reduced about 30%, with no measurable performance degradation. Note, however, that a change of this magnitude is not typical; mixture-ratio bias usually has a much smaller effect on heat flux.

Transpiration Cooling

Figure 4-47 shows the principle of transpiration cooling. Coolant can be introduced through numerous drilled holes in the inner chamber wall or

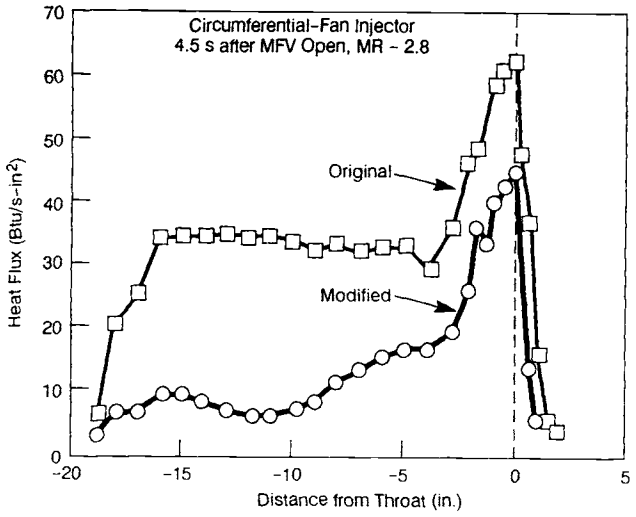

Fig. 4-46 Effect of outer zone mixture ratio bias on combustion chamber heat flux (LOX/RP-1 at 2,000 psi).

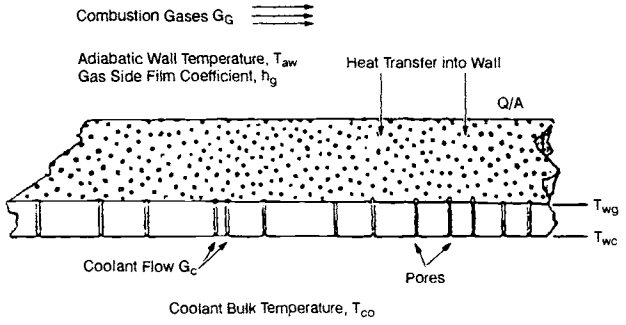

Fig. 4-47 Transpiration cooling model.

the wall can be made of porous material. In both cases, the permeable chamber inner-liner is enclosed by an outer shell (similar to Fig. 4-32), forming a jacket from which the coolant emerges. For adequate design, the total coolant-flow requirement and coolant weight flowrate per unit area of cooled chamber wall must be determined and then implemented by a practical method. Transpiration-coolant-flow requirements determined from theoretical equations are significantly lower than those for film cooling because of more efficient coolant distribution. The Rannie equation for transpiration cooling can be used to calculate the theoretical coolant-flow requirements:

$$\frac{T_{aw} - T_{co}}{T_{wg} - T_{co}} = \left[1 + \left\{1.18(Re_b)^{0.1} - 1\right\}\right.$$

$$\left.\left\{1 - e^{-37\left(\frac{G_c}{G_g}\right)(Re_b)^{0.1}}\right\}\right]$$

$$\left[e^{37\left(\frac{G_c}{G_g}\right)(Re_b)^{0.1}Pr_m}\right] \qquad (4\text{-}37)$$

where

T_{aw} = Adiabatic wall temp. of the gas, °R

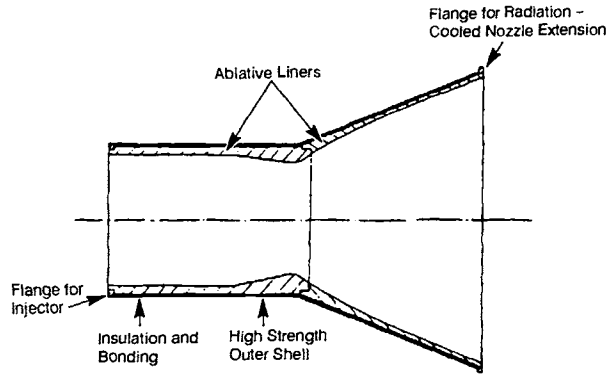

Fig. 4-48 Ablatively cooled thrust chamber.

T_{wg} = Gas-side wall temperature, °R
T_{co} = Coolant bulk temperature, (entering) °R
G_c = Transpiration-coolant weight flowrate per unit area of cooled chamber-wall surface, lb/in.²-s
G_g = Combustion gas weight flowrate per unit area of chamber cross section perpendicular to flow, lb/in.²-s
Pr_m = Mean film Prandtl number
e = Base of natural logarithms, 2.718
Re_b = Bulk combustion-gas Reynolds number

Equation (4-37) predicts coolant flows slightly lower than those required experimentally. It is recommended that an efficiency factor of approximately 0.85 be used for calculations.

The porous material used for the transpiration-cooled chamber walls must be selected and dimensioned for correct hydraulic resistance to obtain the required coolant flowrate per unit surface area. It must also be able to withstand the stresses caused by the pressure differential between coolant and combustion gases, as well as thermal stresses. These requirements impose certain limitations on the selection of materials and on construction methods. The mechanical design of the coolant distribution system, therefore, is an important factor for successful application of transpiration cooling.

Ablative Cooling

Ablatively-cooled thrust chambers offer many advantages for booster and upper-stage applications. They can be designed to meet cumulative firing durations from a few seconds to many minutes. Most designs are limited to chamber pressures of 300 psia or less. When assisted by film cooling or by throat inserts made of refractory materials, however, they have proven successful in firings up to a chamber pressure of 1000 psia. In general, ablative chamber construction can be rugged, keep exterior wall temperatures to a minimum, and have relatively low cost.

Pyrolysis of resins contained in the chamber-wall material does the cooling. The thrust-chamber construction will vary with mission requirements. As shown in Fig. 4-48, the chamber and nozzle employ an ablative liner, a thin layer of insulation, and a high-strength outer shell. The ablative liner is

fabricated from materials such as phenolic-resin-impregnated high-silica fabric or carbon/carbon composites. The structures are woven, braided (3D), or tape-wrapped and molded. Thickness is programmed as a function of chamber station to provide adequate strength, char thickness, insulation, and minimum weight for a particular mission. A wrap of oriented phenolic-impregnated asbestos or rubber covers the outer (far) surface of the ablative liner as an insulator. The high-strength outer shell may be composed of any one of a number of structural materials, such as filament-wound glass bonded with epoxy resin, carbon/carbon composites bonded with a resin, alumimum, and stainless steel.

Figure 4-49 shows an ablative-cooled thrust chamber fitted with a throat insert. Quartz/phenolic resin, 98% tungsten/2% molybdenum alloy, and pyrolytic graphite have been successfully employed as insert materials. The quartz/phenolic resin and tungsten-molybdenum alloy have given the best results. Although pyrolytic graphite has a much lower density than the tungsten alloy and therefore has a substantial weight advantage, it is vulnerable to fracture from thermal shock, making design and installation critical. The throat insert is usually installed with heavy graphite backups for better structural strength. Insert and backups are bonded to the thrust chamber's main ablative liner with epoxy adhesives. These adhesives have performed satisfactorily up to 500°F. Certain ceramic materials, such as silicon carbide, have also been used successfully as throat inserts in space engines.

When heat is transferred from the hot combustion gases to the ablative chamber wall, the resin in the ablative material decomposes or pyrolyzes into a porous carbonaceous char, with evolution of volatile gases. These gases move from the pyrolysis reaction zone, through the char, to the wall surface, where they mix with the combustion-gas boundary layer. As this process continues, the pyrolytic reaction zone recedes, leaving behind a charred region of increasing thickness. The wall surface itself may also recede if the charred material is removed by mechanical action of the flowing combustion gas.

Design of an ablative thrust chamber for a given mission depends on the accuracy of predicting the depth of char during exposure and on the soak-back temperature variation in the insulation surrounding

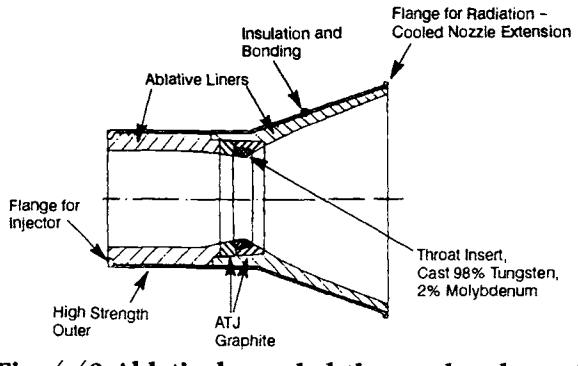

Fig. 4-49 Ablatively cooled thrust chamber with throat insert for high chamber pressure applications.

the charred portion of the thrust chamber wall during and after the hot firing. Test data from hot firings with various ablative thrust chambers indicate that the charring process in the combustion chamber (including the throat)—that is, the relation between mass pyrolyzed and heat absorbed—can be expressed by the following equation:

$$a = c\left[\frac{2kt}{R_r R_v C_p \rho} \ln\left(1 + \frac{R_r R_v C_p (T_{aw} - T_d)}{L_p}\right)\right]^{0.5} \left[\frac{(p_c)_{ns}}{100}\right]^{0.4} \quad (4\text{-}38)$$

where

- a = Char depth, in.
- c = Correction factor based on experimental data for the specific design at the throat section and on a nozzle stagnation pressure of 100 psia
- R_r = Weight fraction of resin content in the ablative material
- R_v = Weight fraction of pyrolyzed resin vs. total resin content R_r
- C_p = Heat capacity at constant pressure of pyrolysis gases, Btu/lb-°F
- ρ = Density of ablative material, lb/in.^{3}
- k = Heat conductivity of char, Btu/s-in.^{2}-°F/in
- t = Thrust-chamber firing duration, s
- L_p = Latent heat of pyrolysis, Btu/lb
- T_{aw} = Adiabatic wall temperature of the gas, °R
- T_d = Decomposition temperature of resin, °R
- $(p_c)_{ns}$ = Nozzle stagnation chamber pressure, psia

Results predicted by Eq. (4-38) agree very closely with char-depth data obtained from firings of Refrasil-filled phenolic chambers. Downstream of the throat, however, char had somewhat greater depth than predicted on the basis of the equilibrium gas temperature. Temperature recovery in the boundary layer may be one cause of the discrepancy. A modified equation is therefore used to predict char depth in the nozzle:

$$a = bt^{0.5}e^{-0.0247\epsilon} \quad (4\text{-}39)$$

where b = a constant depending upon the nature of the ablative shield (to be determined experimentally), ϵ = nozzle expansion area ratio at the investigated section, and e = base of natural logarithms, 2.718.

The char-rate analysis is based on the formation of a char layer that progresses from the heated surface toward the supporting wall. Formation of a hard carbonaceous surface of increasing thickness is vital during pyrolysis of the resin because this surface resists thermal and mechanical ablation and chemical attack. At the charring interface, which slowly travels away from the hot chamber gases, a large amount of heat energy is absorbed by pyrolysis, i.e., by the melting and vaporization of the bonding material. As gaseous pyrolysis products flow through and out of this char layer, they control the heat flux

to the walls by endothermic decompositions and by migration into the boundary layer.

The ablation processes produce no gross dimensional changes; but mechanical erosion sometimes occurs in the throat region, caused by the high prevailing shear-stresses. Chamber pressures below 150 psia usually cause less throat erosion.

The adaptation of ablative thrust-chamber technology to the special field of space engines has advanced during recent years. Approaches typical of this type of engine are discussed in Chapter 11.

Sample Calculation 4-6

Problem

The following design data characterize the ablatively-cooled thrust chamber of the A-4 Stage engine: c = 1.05; R_r = 0.3; R_V = 0.41; C_p = 0.38 Btu/lb-°F; ρ = 0.061 lb/in.^{3}; k = 9.8 x 10^{-6} Btu/in.^{2}-s-°F/in; L_p = 686 Btu/lb; T_{aw} = 5060 R; T_d = 1460 R; b = 0.0335.

Determine the char thickness at the throat and combustion-chamber section, and in the nozzle at station ε = 5, after firing for the design duration of 410 s.

Solution

From Table 3-5: $(p_c)_{ns}$ = 100 psia. Substitute this and given data into Eq. (4-38). The char thickness at the throat and combustion section will be—

$$a = 1.05\left[\frac{2 \times 9.8 \times 10^{-6} \times 410}{0.3 \times 0.41 \times 0.38 \times 0.061} \times \ln\left(1 + \frac{0.3 \times 0.41 \times 0.38(5060 - 1460)}{686}\right)\right]^{0.5} \times (1)^{0.4}$$

$$= 1.05 \times [2.82 \times \ln 1.245]^{0.5} = 0.828 \text{ in.}$$

Char thickness at nozzle station ε = 5, using Eq. (4-39), will be—

$$a = bt^{0.5}e^{-0.0247\varepsilon} = 0.0335 \times (410)^{0.5} \times (2.718)^{-0.0247 \times 5}$$

$$= 0.0335 \times 20.248 \times (2.7182)^{\frac{1}{8.1}}$$

$$= 0.599 \text{ in.}$$

Radiation Cooling

Cooling by radiation heat transfer will usually be practical for thrust-chamber nozzle extensions, where pressure stresses are lowest. Radiation cooling of very small, pyrolytic-graphite combustion chambers and throats has also been demonstrated. Assuming negligible temperature drop through the wall, the steady-state heat transfer for a radiation-cooled wall, as shown schematically in Fig. 4-50, can be expressed by the following equation:

$$h_{gc}(T_{aw} - T_{wg}) = \epsilon\sigma T_{wg}^4 \qquad (4\text{-}40)$$

where

- h_{gc} = Overall gas-side thermal conductance, Btu/in.^{2}-s-°R
- T_{aw} = Adiabatic wall temp. of the gas, °R
- T_{wg} = Gas-side wall temperature = bulk wall temperature, °R
- ε = Total emissivity of outer-wall surface
- σ = Stefan-Boltzmann radiation-heat-transfer constant, 0.3337 x 10^{-14} Btu/in.^{2}-s-(°R)^4

The design approach determines a T_{wg} value that will satisfy Eq. (4-40) within the structural strength of the wall material under operational conditions. Only materials which possess short-time strength in the temperature range of 2600-3500°R have been successfully applied to radiation cooling. Pyrolytic graphite, a molybdenum alloy containing 0.5% titanium, and a 90% tantalum-10% tungsten alloy appear to have sufficient short-time strength for use at 3500°R. Because of the low emissivity of molybdenum and also for resistance against oxidation, a coating of $MoSi_2$ must be applied to both sides of the metal. Withstanding temperature higher than the working range of bare metals may necessitate the use of insulating coatings of ceramic materials on the gas-side wall surface. Because of brittleness and coefficient of thermal expansion relative to that of the alloys, these coatings must be applied judiciously.

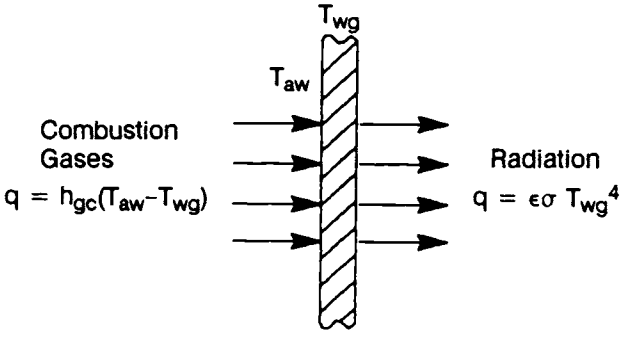

Fig. 4-50 Schematic of radiation cooling.

Sample Calculation 4-7

Problem

The following design data characterize the A-4 Stage nozzle extension at area ratio = 8: h_{gc} = 7.1 x 10^{-5} Btu/in.^{2}-s-°R; T_{aw} = 4900°R. Assuming a total emissivity of 0.95 of the outer-wall surface, determine bulk temperature and radiated heat flux.

Solution

Substitute data into Eq. (4-40):

$$7.1 \times 10^{-5} (4900-T_{wg}) = 0.95 \times 0.337 \times 10^{-14} \times (T_{wg})^4$$

$$(T_{wg})^4 = 22.4 \times 10^9 \times (4900-T_{wg})$$

$$T_{wg} = 2660°R$$

$$\text{Heat Flux} = 7.1 \times 10^{-5} (4900-2660) = 0.159 \text{ Btu/in.}^2\text{-s}$$

Heat-Sink Cooling

Because a heat-sink combustor does not reach steady-state conditions, transient conduction relations must be solved for the temperature distribution in the wall as a function of time. A changing temperature gradient exists across the wall during the firing. The following factors apply to heat-sink cooling:

1) Operating times should be short to minimize the amount of heat absorbed by the wall.
2) Values should be high for wall-material specific heat (to increase heat-absorption capacity) and conductivity (to minimize temperature gradients and thermal stresses within the wall).
3) A liner (ceramic, refractory metal, insulating paint, or an ablative) between the wall and the combustion gases should be considered to reduce heat flux.

Thin ceramic coatings (such as ZrO_2 or Al_2O_3) can provide substantial wall protection at high heat fluxes; at low heat fluxes, however, a thicker coating will be needed to reduce heat flux appreciably to the chamber wall. Three factors limit coating thickness:

1) Excessive coating thickness may result in high temperature and possibly surface melting of the coating.
2) Maximum coating temperature (and therefore maximum coating thickness) will also be limited by thermal gradients and stresses that threaten coating integrity.
3) Improper adherence between coating and wall or differential thermal expansion at the wall-coating interface may cause spalling. This may be alleviated by use of graduated coatings to match the coefficients of thermal expansion.

A refractory metal liner (such as molybdenum) may be employed to take advantage of contact resistance (a function of liner temperature and of surface roughness and hardness). The liner can be allowed to heat to high temperatures because it is not a structural member.

Film cooling on a heat-sink chamber can reduce heat flux to the wall. If the external wall temperature is sufficiently high (e.g., about 2500°F for a graphite chamber), radiation cooling may begin to have an effect.

Combined Cooling Methods

Various techniques of thrust-chamber cooling can be used in combination to provide efficient overall cooling. Combinations such as the following have been successfully employed: regenerative and film cooling, radiation and film cooling, mixture-ratio biasing and regenerative cooling, ablative and film cooling, and heat-sink and mixture-ratio biasing.

4.5 INJECTOR DESIGN

The injector, as the name implies, injects the propellants into the combustion chamber in the right proportions and the right conditions to yield an efficient, stable combustion process. Placed at the forward, or upper, end of the combustor (Fig. 4-1 and 4-2), the injector also performs the structural task of closing off the top of the combustion chamber against the high pressure and temperature it contains. The injector has been compared to the carburetor of an automobile engine; since it provides the fuel and oxidizer at the proper rates and in the correct proportions, this may be an appropriate comparison. However, the injector, located directly over the high-pressure combustion, performs many other functions related to the combustion and cooling processes and is much more important to the function of the rocket engine than the carburetor is for an automobile engine.

No other component of a rocket engine has as great an impact upon engine performance as the injector. The measure of delivered performance (specific impulse) is the number of pounds of thrust provided per pound of propellant consumed per second (see section 1.2). Each percentage-point loss in injector combustion efficiency (c^*, Eq. 1-32) means a loss of the same magnitude in overall I_s propulsive efficiency.

In various and different applications, well-designed injectors may have a fairly wide spread in combustion efficiency, and it is not uncommon for an injector with c^* efficiency as low as 92% to be considered acceptable. Small engines designed for special purposes, such as attitude control, may be optimized for response and light weight at the expense of combustion efficiency, and may be deemed very satisfactory even if efficiency falls below 90%. Since these systems burn only a small portion of the vehicle's propellant loading, their response in making precise small corrections is more important than their steady-state combustion efficiency. In general, however, recently well-designed injection systems have demonstrated c^* efficiencies so close to 100% of theoretical that the ability to measure this parameter is the limiting factor in its determination. Examples are the SSME (99.7%) and the upper-stage XLR-132 engine (99%).

High levels of combustion efficiency derive from uniform distribution of the desired mixture ratio and fine atomization of the liquid propellants. Local mixing within the injection-element spray pattern must take place at virtually a microscopic level to ensure combustion efficiencies approaching 100%.

Combustion stability is also a very important requirement for a satisfactory injector design. High performance can become secondary if the injector is easily triggered into destructive instability. At times, it may seem that the design requirements for stability are counter to those for performance, since many of the injector key parameters for high performance appear also to reduce the stability margin. Stable operation will depend in good part on the injection-element type selected and the provision for damping any oscillatory phenomena. Injection flow resistance is an example of an aid in designing for stability; this is one reason for the typical use of 15-20% of chamber pressure as an appropriate level of injector pressure drop.

Injector Design Issues

Injector design, like many engineering tasks, entails many compromises. For any new engine application, there are almost always several different approaches that could produce a satisfactory injector design, and perhaps more than one approach which would provide an outstanding injector design. The proper design starting point considers the particular application, engine size, propellant combination, and design priorities. Of course, the initial approach invokes complete optimization of all features: light weight, high performance, low cost, reliability, etc.; but that soon emphasizes priority for the really important design parameters.

Two greatly different real engines will serve to illustrate how priorities are realistically established.

The SSME requirements called for a highly sophisticated, high-performance booster/core engine using liquid-oxygen/liquid-hydrogen propellants. It was to be reusable over multiple missions in manned spacecraft, a use that dictates a higher reliability than any other application. High sophistication and very high performance did not mean inexpensive or particularly light weight. The SSME actually has three injectors: the usual main-engine injector and one injector each for the fuel and oxidizer turbine-drive preburners. Each had to be highly developed for its specific task.

In contrast, at the other end of the spectrum, a "divert" engine for a small kinetic-energy weapon ("smart bullet"), called for light weight, small size, and extremely rapid response. This engine had a firing life of only a few seconds, but had to reach thrust in a handful of milliseconds. The injector was given an unlike-impinging, 36-element pattern supplied by a manifold with short direct passages from a valve integrated into the injector body. The injector face had a diameter of only 1 inch. The engine thrust-to-weight ratio set a record high, and steady-state performance proved very good, considering the rapid response and very small combustion chamber.

Basic injector design will combine prior experience and innovation in terms of the identified problems. Type of propellants and injection condition most strongly influence selection of the injection element . For liquid oxygen and the fuel a lightweight gas, such as hydrogen, a coaxial element will be the primary candidate. For hypergolic liquids and rapid response in a small chamber, an unlike-impinging pattern will be the logical starting point.

For a large booster with LOX/RP-1 propellants, combustion stability becomes a major issue, and the density of liquid-phase injection generally rules out the use of a coaxial pattern. The element of choice in this case would probably be a like-impinging type, such as a like-doublet. The possibly better mixing from an unlike-impinging element would be outweighed by the probability of sensitivity to instabilities. The number of like-doublet elements used would depend on the engine size and would involve a tradeoff between fabrication costs and stability concerns, on the one hand, favoring fewer elements, and the performance requirements on the other, dictating more numerous elements. The placement of elements will be important in providing good mixing interaction between elements, uniform mass distribution, and possibly tailoring the mixture-ratio distribution to minimize combustor wall-heating.

Mass distribution, another important design parameter for successful injector/combustor interaction, can be difficult to achieve in truly uniform fashion across the injector face. The mechanical space requirements for the perimeter of the manifolds push the outer row of elements inward, away from the wall. In addition, the use of acoustic cavities around the injector perimeter further forces the outer row away from the wall. The result usually will be a mass-deficient zone around the injector perimeter. The initial gas generated, centered inward, will tend to fill the chamber area, causing an outward "radial wind" that carries a portion of the reacting gases against the wall. With most liquid-propellant combinations, the oxidizer vaporizes more rapidly than the fuel. The oxidizer-rich hot gases thus scrub the upper section of the chamber severely, increasing local heating and, in extreme cases, burning the inner surface of the chamber. Good injector design includes a computation of the effective mass distribution and an assessment of design adequacy in this regard.

Mixture-ratio distribution also plays an important part from the standpoint of both performance and chamber compatibility. With combustion chambers made of metals (copper, nickel, steel) that are fuels, it is important to avoid scrubbing of the chamber wall by high-temperature oxidizing streams. Most injection patterns are designed to avoid this possibility, and generally to provide an excess of fuel in these areas. Formal film cooling or boundary-layer cooling systems frequently employ fuel streams that directly impinge against the wall at a shallow angle, to spread a protective evaporating layer on the wall surface. Other systems use "barrier zone" elements, either fuel-rich or totally fuel, in the region adjacent to the wall. All these methods involve a performance penalty, since the coolant fuel mainly will be unavailable for effective combustion. It will not be completely lost from the propulsive flow, however, because it will be heated and expanded as part of the working fluid; but this is less effective than burning it in a well-mixed fashion. The performance loss for

this type of mixture-ratio unbalance varies significantly for different propellant combinations. Hydrogen entails only a very small penalty for film cooling.

Combustion Stability

Combustion stability is covered in section 4.8, but the interaction between stability and injector configuration is an important consideration in injector design. As mentioned, high performance can become secondary if the system can easily be triggered into a destructive instability, and many of the injector parameters that provide high performance appear to reduce the stability margin. All systems which release large amounts of energy have the potential for destructive oscillations, particularly if there is regenerative feedback (gain) between the combustion phenomena and the rate of energy release. This is particularly true of the combustion process, because temperature and pressure variations can directly impact the rates of vaporization and reaction. Stable operation can be achieved by either damping or detuning these processes. The injection flow resistance provides isolation between propellant flows and chamber disturbances. The characteristics of the injection element also significantly impact the stability of a particular design. In general, unlike-impinging elements are the most easily excited to instability, with like-impinging elements lower in sensitivity, and nonimpinging elements the most stable.

Manifolding, as well as other elements of the propellant-feed systems, may have frequency characteristics that can couple with chamber acoustic modes. These should also be addressed in the injector design. One example of this, the length of the central post in a coaxial injection element, can have organ-pipe modes; another, the "racetrack" mode, can exist in ring-groove manifolds. These frequencies should be considered during design, and damping devices or detuning applied where appropriate.

Injectors frequently have physical devices to aid in damping or to otherwise change frequency response. Typical of these devices are acoustic cavities and baffles. Figure 4-51 shows an example of an injector with baffles. These reduce the effective local size of the combustion area by compartmenting the injector face, thus raising the resonant frequencies to higher, more easily damped, values. The baffles operate in a high-heat-load environment, and cooling provisions, shown in the figure, are frequently required. The length of the baffles is related to energy release rates, which describe the so-called "sensitive" zone, the region most likely to initiate instability. It is desirable to make the baffles as short as practical for structural and thermal reasons, since generally the cooling provisions cause some performance loss.

Acoustic cavities are damping devices that employ tuned lengths or other open areas exposed to the reaction process (functionally similar to acoustic liners used in jet-engine afterburners). In rocket engines, they are most effective when located between the outer perimeter of the injector face and the start of the combustor wall. The usual configurations are Helmholtz resonators or quarter-wave slots. The open areas required for these devices impact injector design, influencing structural and cooling requirements, and also tend to affect adversely the outer-zone pattern provided for mass distribution and wall cooling.

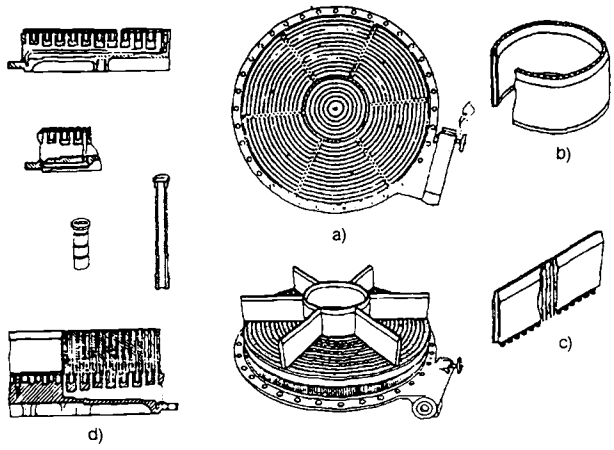

a) Placement of baffles on injector face
b) Fuel-cooled baffle hub
c) Fuel-cooled baffle spoke
d) Baffle coolant feeds

Fig. 4-51 Baffled injector.

Manifolds

Selecting injection-element types and establishing a pattern for them will be tightly interwoven with the design of a feed-system manifold—interconnecting multiple feed paths to a single supply source. The manifold must first provide passages to feed the often complex, interrelated injector orifices in the desired pattern. The pattern selection is frequently driven by the need to provide this manifolding and the limitation of available fabrication techniques. Providing all the elements with uniform flow requires a free-flowing manifold system, with minimized flow restrictions, to avoid nonuniform distribution of mass and mixture ratio across the injector face. This, in turn, dictates a large manifold volume, but other factors limit the practical size, notably, locating the physical space for the intertwined flow passages of the two propellants and establishing the so-called "dribble volume." The volume of the manifold determines the time required to prime the system and the length of time during which the vapor pressure maintains "dribbling" flow after the inlet valves have been closed. The dribbled propellants continue the combustion process at reduced pressure and poor efficiency after the initiation of engine cutoff. The thrust delivered during this time is usually referred to as "cutoff impulse." Many systems specify a maximum value for this. Rocket engines often must provide a specific amount of impulse to produce the required final velocity with a high degree of accuracy; the dribble volume very adversely affects repeatability, particularly for small attitude-control or maneuvering rockets, which are primarily com-

manded in short pulses—frequently only a few milliseconds long. The dribble volume represents a major loss in efficiency for this class of engine.

With efficient distribution requiring greater flow area and resulting volume, and cutoff requirements pulling the opposite way, there must be an engineering compromise. The most effective sizing tool has been a rational guideline for injection flow velocity. A rule of thumb which has served well in numerous design programs gives each manifold run four times the flow area of the total group of injection orifices that are fed by it. Consequently, a linear manifold feeding a row of injection orifices should be tapered, with the area decreasing as each additional orifice is fed. An alternative, which produces virtually the same result, is called the "1% rule." This rule can be applied to any branch of a flow system and does not require knowledge of the injection orifice area: velocity head (dynamic component of the total pressure) shall not exceed 1% of the local system pressure. For example, the velocity head in a feed line with a working pressure of 3000 psi should not exceed 30 psia. Velocity head in psi is readily computed from Eq. 4-41:

$$H_{vel} = \frac{2.238\dot{w}^2}{\rho A^2} \qquad (4\text{-}41)$$

where w = weight flowrate, lb/s; ρ = density, lb/ft^3; and A = flow cross-sectional area, in.^{2}. That guideline will generally keep manifold velocity-induced distribution variations below 5% in average flow (the "noise level" for most applications). In engines needing response more than steady-state performance, it is often acceptable to drop the manifold area to a two-to-one ratio to keep short-pulse efficiency as high as possible, although system pressure loss and injector flow distribution will be compromised to achieve this response.

Figure 4-52 shows the way manifold velocities impact element flow distribution. The figure shows a typical ring-shaped manifold with orifices distributed around the perimeter and a single manifold feeder. The picture represents the perimeter unwrapped, with the inlet in the center. The injection orifices directly under the inlet see the inlet velocity-head. This increases the flowrate through these elements, commensurate with the increase in effective pressure drop. As the main flow branches into the legs of each side, there is a "vena contracta" effect, and the local velocity is high, resulting in low static pressure in this portion of the manifolding. These orifices typically provide the lowest flow, since this static-pressure drop exceeds the pressure loss around the manifold. Other initial orifices are also reduced in average flow by the static-pressure drop caused by manifold velocity. As flow is bled off around the ring, the cross-velocity drops, and average flowrate per element increases slightly until, at the far side of the manifold, most of the velocity head is recovered as the velocity goes to zero; these orifices flow higher than average.

Figure 4-52 assumes orifices at right angles to the flow, without significant irregularities, or burrs. An entrance burr might act either as a scoop, to increase

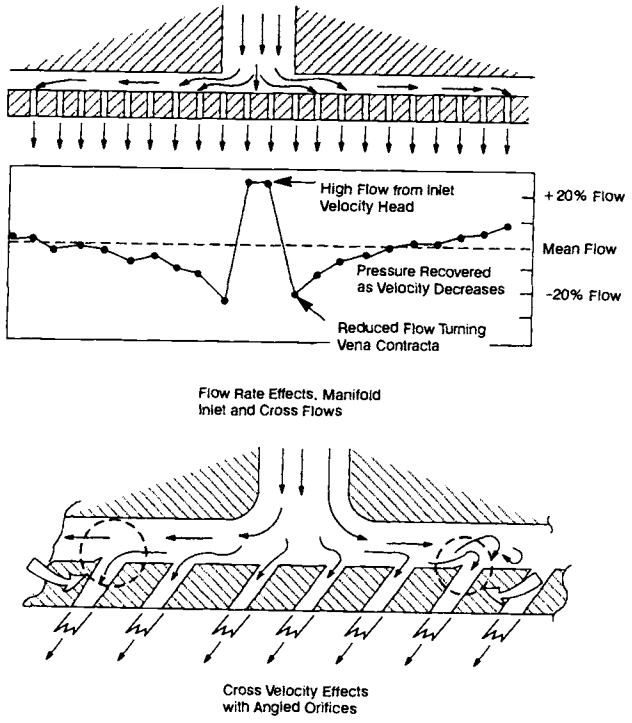

Fig. 4-52 Velocity effects in injector manifolds.

flow, or as a baffle, diverting flow. This same effect is seen when the injection orifices are drilled at an angle to the manifold flow. In that case, the flow is increased by the scoop effect and pressure recovery. The reverse effect is also true; angling the orifices away reduces the flowrate. Most of these effects can be reduced to acceptable levels by reducing the manifold velocity to the guideline values. With good design practice, the impact of manifold flows on injector flow distributions can be relatively minor.

Manifold Types

Figures 4-53, 4-54, and 4-55 show some of the more common manifold configurations used in rocket-engine design. The classic liquid/liquid propellant injector for a booster engine typically employs a "ring groove"-face manifold with a "LOX dome." Figure 4-53 illustrates the injector body of such an engine (LOX dome covering not shown). In this system, the manifold passages are typically lathe-turned as circular grooves in the face of the injector body. The injection orifices are drilled into the ring-shaped bands, which are inserted into the open face of these grooves and are attached by brazing, welding, or other means to close out and seal the face. With fuel-cooled chambers, the fuel flow is typically conducted to the outer perimeter of the injector body and ducted into the fuel rings by radial passages (drilled, milled, cast, etc.). The intersection of these radial passages with the rings are called "dog legs." The alternate oxidizer rings from the LOX dome usually feed through axial passages (between the radial fuel passages) that carry the oxidizer down to the oxidizer rings (these axial passages are frequently referred to as "downcomers").

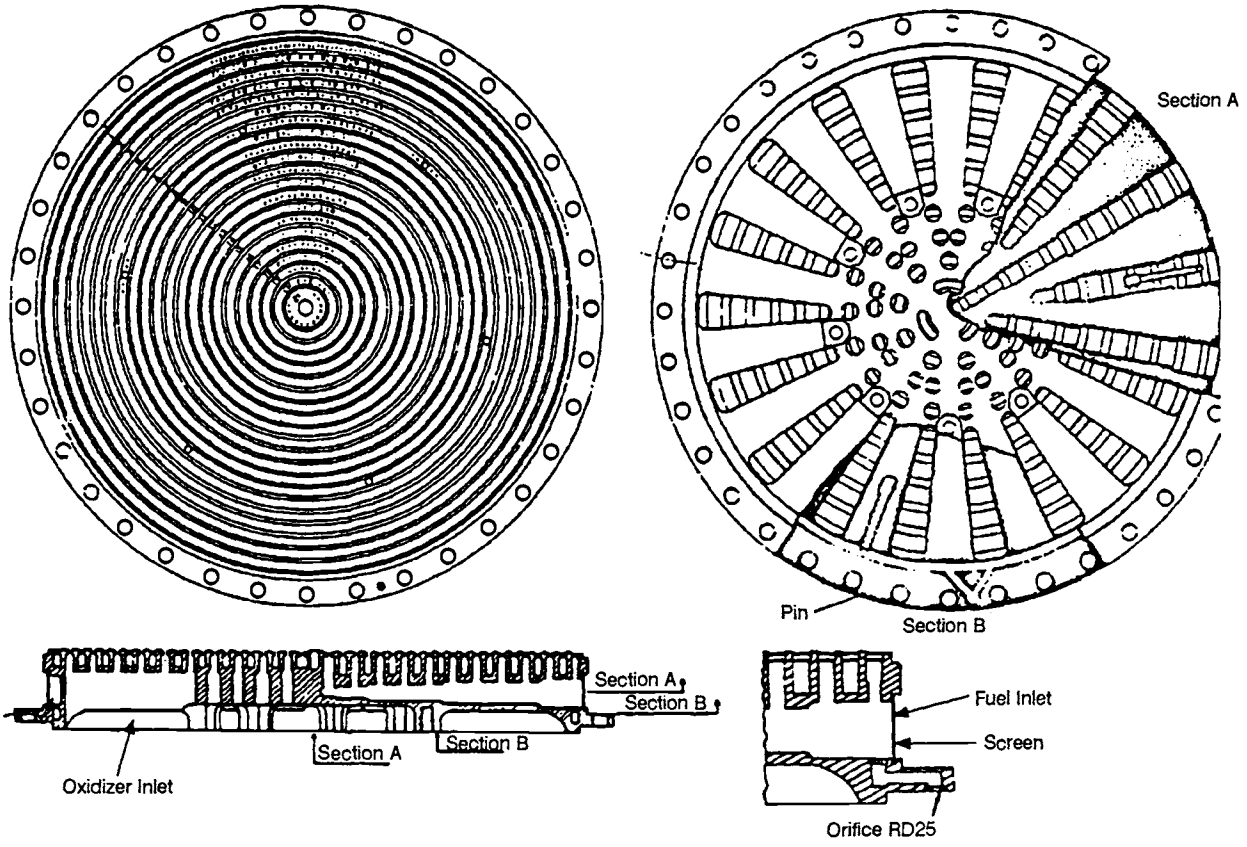

Fig. 4-53 Concentric ring injector.

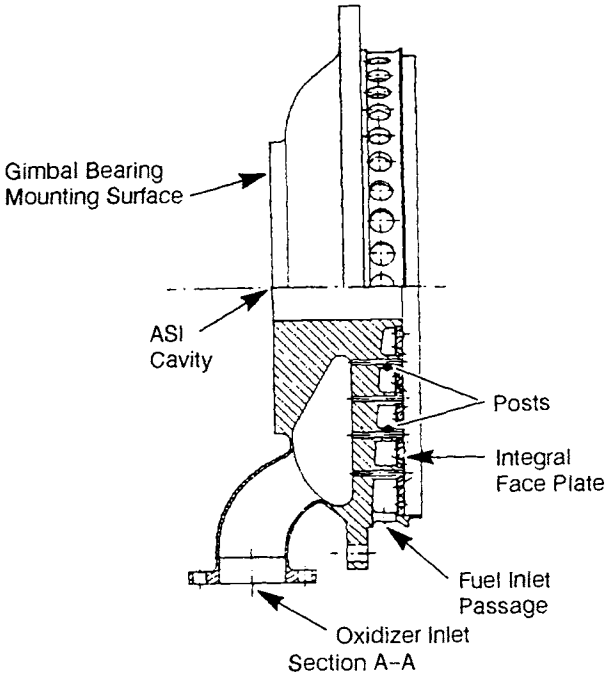

Fig. 4-54 Integral face plate injector.

In large gas/liquid injectors, such as those used for hydrogen/oxygen engines, the manifold is somewhat similar, with a roughly equivalent LOX dome, but the fuel manifold is generally another cavity "below" this dome. Figure 4-54 shows a view of one of the J-2 injectors that had this general configuration. These engines usually employ a concentric element. The central oxidizer tube of each element carries the oxidizer "down" through the fuel manifold. Fuel surrounds this post and enters into the individual element through a fuel sleeve. The injector face is supported against the manifold pressure by these element assemblies. In the J-2 configuration shown, the face plate was a transpiration-cooled, porous, stainless steel plate, mechanically attached to the LOX post structure by a mechanical flare joint. More recent engines typically use a mechanically threaded face-nut system.

With smaller injector assemblies, such as the gas-generator injector shown in Fig. 4-55, the injector manifolding can be machined directly into a homogeneous injector body. Drilled radial passages directly feed fuel; oxidizer injection orifices are drilled directly into a LOX-dome-equivalent cavity.

As mentioned, the manifold systems for small pulsing engines require very restrictive manifolding to avoid dribble volume. Such manifolding is usually a complex arrangement of intersecting drilled passages, to provide minimum volume with adequate flow area. This method also provides extremely good pressure integrity, which is valuable, since some pulse engines have experienced manifold detonations.

In some small pulse engines with relatively few elements, the manifolding has taken the form of capillary feed tubes from the valve directly to each

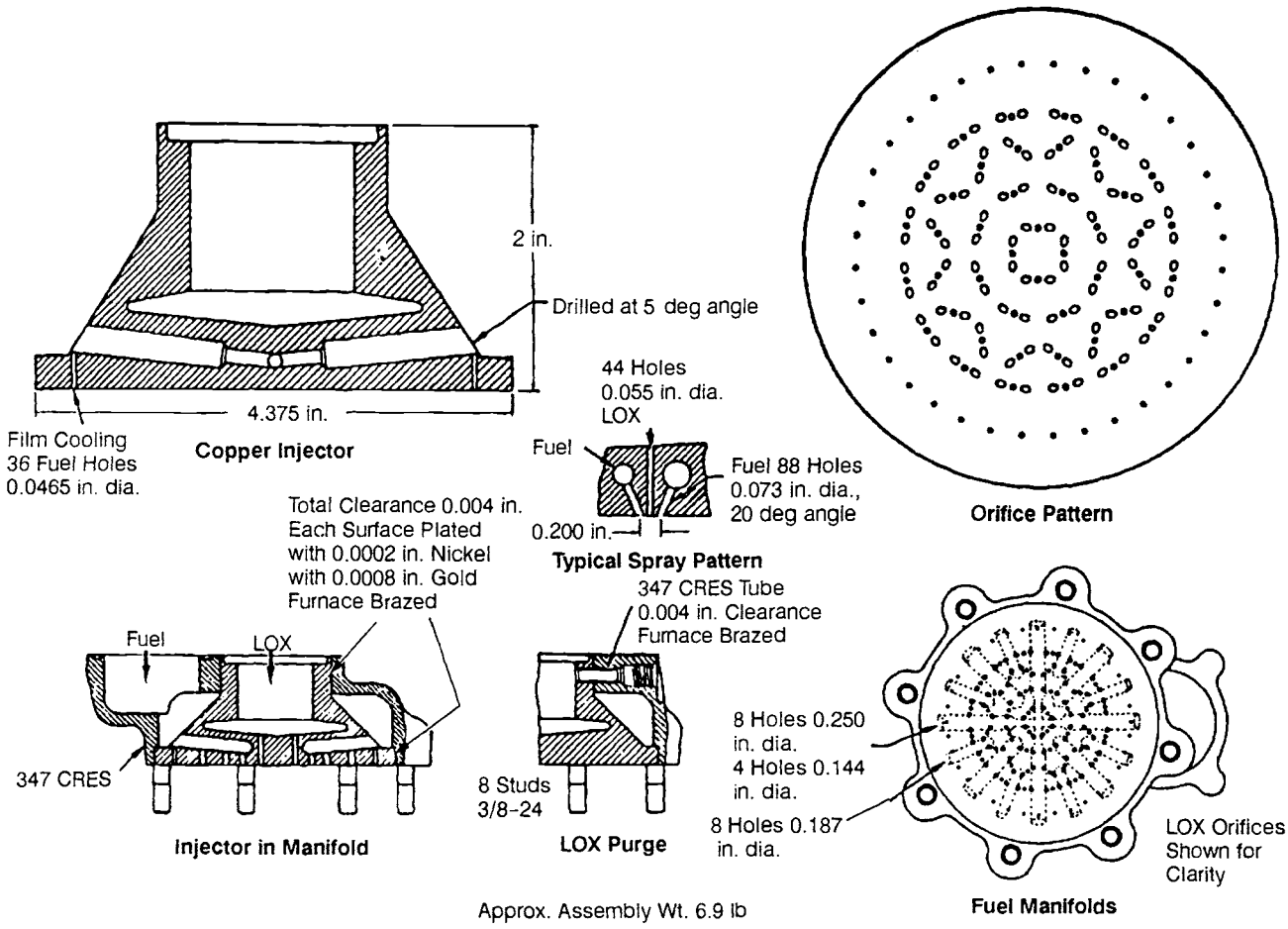

Fig. 4-55 Bipropellant gas generator injector.

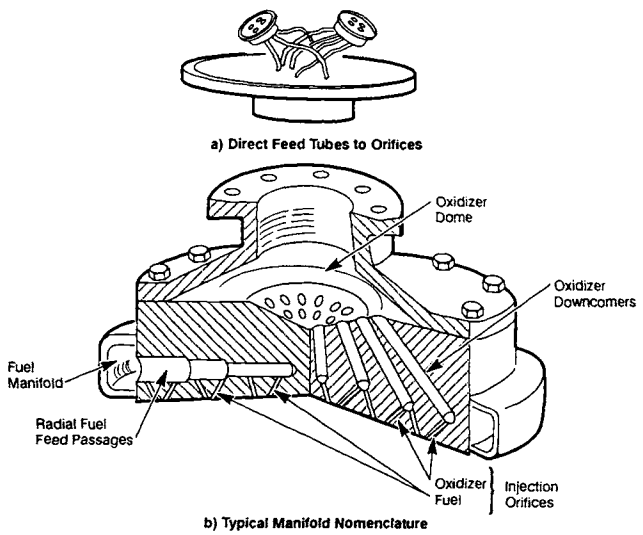

Fig. 4-56 Types of injector manifolds.

orifice entrance (Fig. 4-56). This can have the added benefit of combining thermal isolation for the heat-sensitive valve components with minimum volume and simultaneous feed to each element. Figure 4-56 also shows typical manifold nomenclature.

Injection Elements

The configuration of an injector is frequently described as being a pattern of specific injection elements. The most common types of injection elements are nonimpinging, unlike-impinging, and like-impinging (Fig. 4-57).

Nonimpinging Elements

Coaxial. The most common type of nonimpinging element, the coaxial configuration, characterizes the SSME injector and other oxygen/hydrogen engines. The coaxial, or concentric, injection element usually has a slow-moving central stream of liquid oxidizer surrounded by a high-velocity concentric sheet of gaseous fuel. Initially developed at NASA during early experiments with LOX/hydrogen, it has a well-earned reputation as a high-performance, stable injection element for gaseous fuel and liquid oxidizer. The liquid oxidizer is deliberately injected at low velocity, with the usual injection pressure-drop accomplished by an upstream metering orifice in each element, and diffused to a reduced velocity in the tubular LOX post. On the other hand, the fuel injection pressure is turned into high injection velocity in the annular gap around the LOX post. Mixing, atomization of the liquid, and mass distribution are provided by the

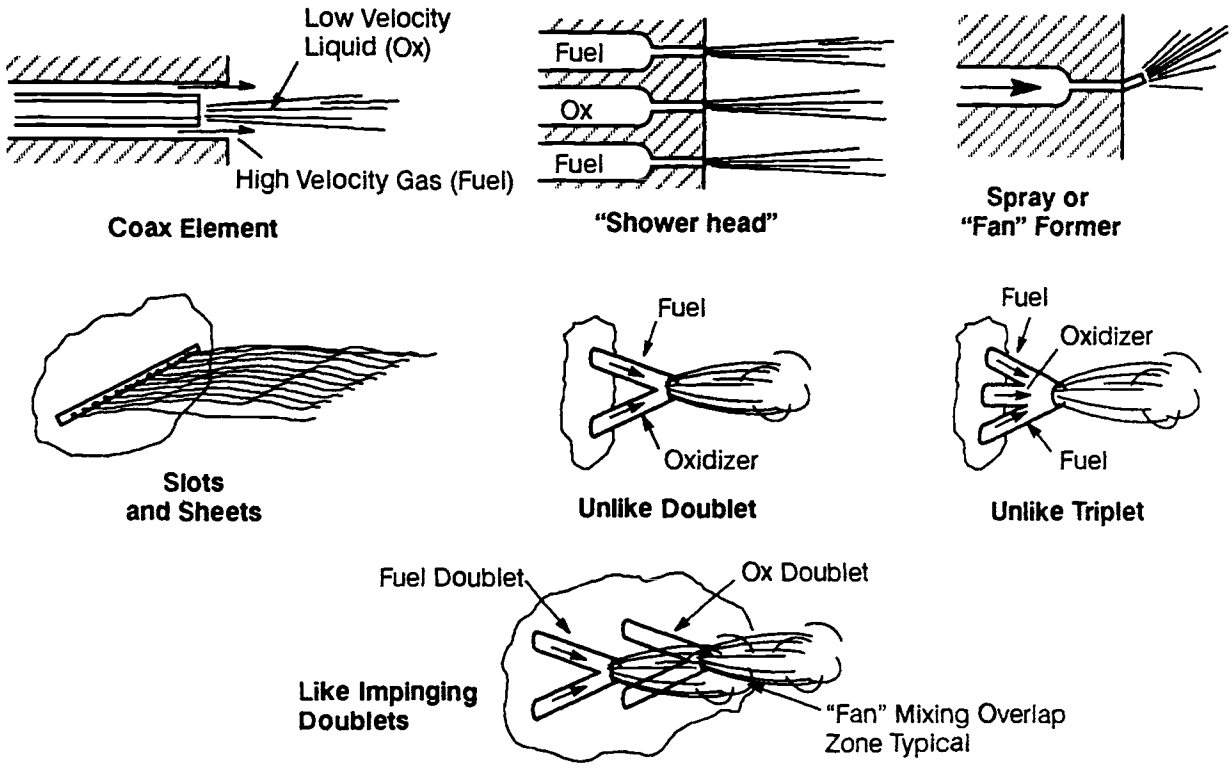

Fig. 4-57 Typical injector element types.

shearing action of the high-velocity gaseous fuel on the surface of the liquid. Typical in this application are liquid velocities of less than 100 ft/s and gaseous fuel velocities of over 1000 ft/s. The fuel surrounding the oxidizer tends to shield the combustion process, which enjoys a favorable combustor-wall heating environment, and also appears to benefit combustion stability. The coaxial element is less well suited to liquid fuels, or even very dense gaseous fuels, since the velocity relationships required to make it work well are difficult to obtain.

Showerhead. Directly axial, or near-axial, non-impinging streams of either liquid or gaseous propellants are generally referred to as "showerheads." This type of element provides very little effective atomization or mixing, and is seldom used for primary injection. It is most frequently used for fuel-film-cooling streams at the chamber wall.

Fan formers. Liquid-injection geometry that provide sprays in "cones" or "fans" are frequently used in various types of combustions systems. Such injection methods are the primary techniques in air-breathing systems with liquid fuels. Generally, these units use internal geometry employing either swirl or impingement to provide a stream which diverges in a predetermined pattern as a finely atomized spray. However, these systems have not been popular with rocket-injector designers, probably because of face-cooling problems and high total-mass-flow densities associated with rocket combustors. Limited attempts to use this type of element have not been particularly successful.

Slots and sheets. Narrow, two-dimensional slots have often been suggested to increase the surface area of propellant streams, but they have seldom been successful. Flow from slots usually has proven quite erratic, tending to ligament into large and irregular masses. Sheet flow of liquids generally requires swirl or impingement to provide the desired dispersal.

Unlike-Impinging Elements

Unlike doublets. A straightforward way of mixing two different fluid streams directs one against the other; this in essence describes the basic unlike-impinging doublet. The impact produces a fan-shaped spray made up of a mixture of the two impinging fluids. With no combustion or other chemical reactions, the combined streams form a largely two-dimensional spray in a plane basically at right angles to the plane which includes the centerlines of the impinging streams. From the impingement angles of the two streams the spray spreads at a resultant angle ("beta angle," computed from sum of momentum vectors) based on the combined momentums (Fig. 4-58):

$$\tan \beta = \frac{\dot{w}_1 V_1 \sin a_1 - \dot{w}_2 V_2 \sin a_2}{\dot{w}_1 V_1 \cos a_1 + \dot{w}_2 V_2 \cos a_2} \qquad (4\text{-}42)$$

For the impinging streams shown in Fig. 4-58, α_1 and α_2 are the respective angles between the thrust-chamber axis and the streams, $\dot{w}_1$ and $\dot{w}_2$ are the weight flowrates, and V_1 and V_2 are the injection velocities.The width of the spray fan largely reflects the included impingement angle of the two streams, the thickness to the stream diameters, and the

turbulence level. Mixing in the spray fan is not perfectly distributed, being adversely affected by any momentum and/or stream-diameter mismatch of the impinging fluids. Stream misimpingement, resulting from the fact that the stream centerlines rarely intersect at the theoretical impingement point, distorts the shape of the spray fan and produces mixing imperfections. Other effects arise when combustion processes are superimposed upon impinging-stream hydrodynamics. One such phenomenon, that affects the performance of highly-reactive, unlike-impinging reactants—"blow apart," or reactive-stream separation, or reactive demixing—occurs because hypergolic propellants usually have extremely short ignition delay and thus start generating gases before completion of the mechanical impact of the two streams. These gases add forces to the hydrodynamic ones and tend to separate the surfaces of the reactants. At high chamber pressures, there is evidence that liquid propellants not normally considered hypergolic (such as liquid oxygen/kerosene) may also exhibit this phenomenon.

Other effects of the combustion process may also modify the mixing and mass distribution of the injected sprays. Because of the turbulence near the injector face and hot-gas crossflow, "radial winds" will distort the spray and strip off the most rapidly atomizing portions of the injected propellants. This effect will be discussed in the section on mass distribution.

Unlike triplets. A mismatch in stream size and momentum between the oxidizer and the fuel in unlike doublet elements will force the spray away from the desired axial direction and distort the fan, resulting in poorer mixing. This problem may be avoided by use of a symmetrical, unlike-injection element consisting of an axial central stream of one propellant and two symmetrically-impinging outer streams of the other propellant. This unlike triplet may have either two fuel streams impinging on a central oxidizer stream (fuel-oxidizer-fuel) or the reverse (oxidizer-fuel-oxidizer). In most propellant combinations, the total oxidizer flow area will be the greater, so the O-F-O system provides a closer match of stream sizes and consequently better mixing. However, placing the oxidizer on the outside of any element configuration entails the risk of oxidizer-rich streaking. A typical triplet-spray fan will be narrower than an equivalent doublet, and the mass more concentrated as a result. Unlike-triplet injectors have demonstrated high levels of mixing and resultant combustion efficiency, but they also tend to be sensitive to stability problems.

Pentads, etc. Obviously, there are many possible combinations of unlike-impinging streams. However, an unlike impinging stream configuration seldom exceeds the use of four streams of one propellant against a center stream of the other. Properly designed pentads, or quadlets, or other groupings, can have high levels of mixing efficiency but exhibit poorer mass distribution. These elements should be considered when there are much higher mass flows of one reactant relative to the other, as in gas-generator combustors, which operate very fuel-rich. In general, these multiple-impinging configurations prove sensitive to combustion instability and are probably even worse than the triplet element.

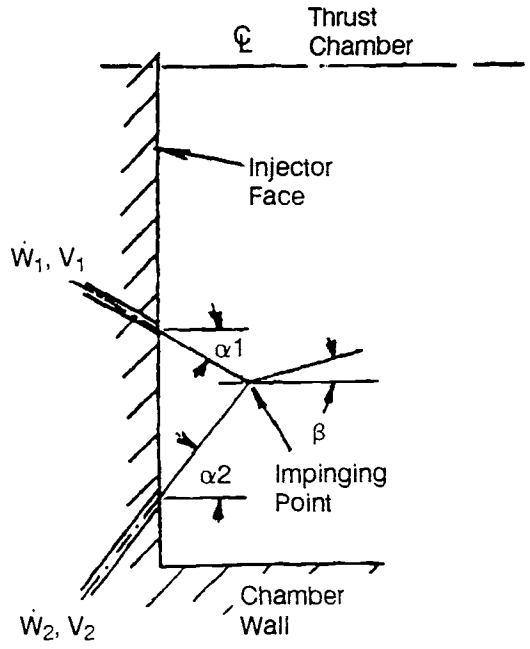

Fig. 4-58 Resultant angle of impinging streams.

Like-impinging Elements

Like doublets. Like-impinging (or self-impinging) elements impinge the injected streams (liquid or gas) directly on other streams of the same propellant. The most common of these, a doublet configuration, has two like-fluid streams angled together to an impact point, producing in a fan-shaped spray of droplets similar to that of an unlike doublet. These fans also travel in a direction determined by the resultant of the momentum vectors of the incoming streams before the impingement and are generally two-dimensional, as described for the unlike doublet. However, there is no mixing within this fan, since only one reactant is present in each. Energy dissipated by the impingement atomizes the liquids. Orientation of the initial fans for secondary impingement and overlapping of the sprays mixes the two propellants. Provision of this interaction between doublet sprays will be the key to a successful like-impinging doublet design.

Like-impinging elements are frequently used for liquid/liquid propellant systems in which reaction or heat transfer between unlike-impinging streams is undesirable. The like-impinging doublet avoids most of the reactive-stream demixing of unlike-impinging designs and better maintains combustion stability than unlike patterns. Although the initial mixing provided by the element is poorer than for the unlike-impinging case, good design practice can provide high levels of overall combustion efficiency.

Like-impinging triplets. Three streams of the same propellant can be directed to a common impingement point. This concept has been applied in some injectors requiring small holes, since more triplet elements can be packed into the same

manifold space than doublets. However, the like-impinging triplet usually produces narrower spray fans and larger drops than an equivalent doublet, resulting in an overall net loss rather than gain. The same result is obtained with self-impinging quadlets, pentads, and other multiple-orifice arrangements.

Other Element Types

Virtually any way that a liquid can be sprayed has been tried in rocket-engine injectors. Early injection patterns frequently used splash plates to break up the liquid streams and to reduce emphasis on careful control of the dimensions of impinging streams. Injectors have also been designed with swirl, or other geometric features within the injector structure, to enhance atomization and distribution of the fluids.

Platelet construction. One design concept, called "platelet construction," has effectively employed diffusion-bonded photo-etched plates for fabrication of small- to mid-sized injectors (analogous to printed-circuit-board technique in the electronics industry). It offers significant advantages in cost and in design freedom for innovative manifolding and injection elements, and has been used to provide spray formers of various configurations, often with effective stream impingement.

Premixed. It is common practice to premix fuel and oxidizer upstream of the chamber in other types of combustor design, but very rare in rocket-engine combustors. In air-breathing systems, the fuel is mixed with air and "flameholding" is provided downstream, in the combustion zone. At the high pressures and high-mass-flux conditions in a rocket engine, however, the probability of a premixed reaction travelling upstream to the mixing section is high and could be disastrous. Many rocket propellant combinations are either hypergolic or potentially detonable in the mixed condition. In spite of these limitations, some experiments have been made with premix chambers, although frequently they also become precombustion chambers with excessive thermal loads on the structure. Such special elements are useful for solving special problems, but, in general, better performance and better control of wall heating and combustion stability have been provided by more conventional injection elements.

Throttling

Many rocket engines have a requirement for variable thrust over a wide range of operating conditions. That spells special problems for injector designers. Most well-designed injector systems with reasonable pressure isolation can be throttled through a modest range of operating levels by upstream flow restriction. However, the operating range will be limited in liquid injection systems because of pressure drop/flow relationships and the need to provide a significant pressure drop across the injection elements. Liquid pressure-drop changes as the square of flowrate while chamber pressure is linear with flow. For example, starting with a maximum thrust level at 1000 psia with a propellant pressure drop of 20%, and throttling down to half thrust, chamber pressure would become 500 psia and delta pressure would be 50, 10% of chamber pressure. Further throttling would lower the injection-pressure drops to dangerously low levels. Some rocket engines have been throttled successfully by reducing upstream flow, but many have also experienced severe pressure oscillations.

Various methods were proposed to meet the Saturn/Apollo Lunar Module descent-engine requirement of a 10-to-1 throttling range. One used a system of gas entrainment in the liquid propellants to maintain atomization and flow isolation at low flowrates by in effect reducing propellant density at throttled condition. This system has the problem of a third consumable and associated control requirements but was simpler than many mechanical ones. The flight Lunar Descent engine used a pintle-type injector (Fig. 4-59). A central element had axially moving components to change the injection-flow area. This provided the desired range of thrust control with reliability and stability. A design for the sustainer section of the Lance missile used a pintle of a different configuration (Fig. 4-60) and demonstrated throttling of over 40-to-1. This system had injection orifices in the form of tapered "ramp" grooves, with area throttling by sliding piston-ring seals. This basic throttling system has been used on numerous experimental engines.

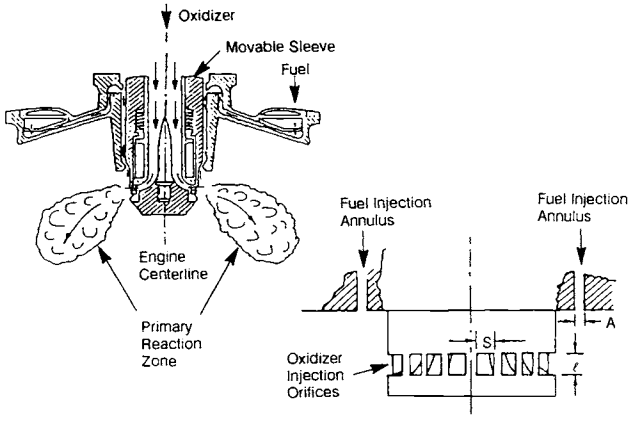

Fig. 4-59 Pintle injector.

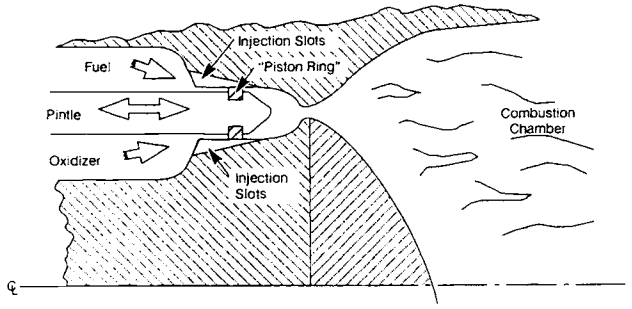

Fig. 4-60 Lance sustainer pintle injector.

Injection Pressure Drop and Orifice Sizing

A good starting point for the design level of injection flow resistance is 20% of chamber pressure. For example, if the design chamber pressure is 2000 psia, the pressure loss across the injection orifice system would be targeted at 400 psid at design flowrates and conditions. For each propellant, the total flow area of the injection orifices is based on the desired expected flowrate and the pressure drop. The differential pressure across the injection orifices imparts the injection velocity to the streams. In turn, it supplies the energy for atomization and provides mixing by controlled mass distribution. Low-velocity streams without pressure drop would just dribble weakly into the chamber and puddle into ineffective pools, with resultant poor mixing and poor combustion. Equally important, the injection-pressure drop provides isolation between a combustion disturbance and the local, instantaneous propellant flowrates. NASA specifications allow up to 5% of chamber-pressure oscillations for "stable" combustion. If there were only 5% pressure drop across the injection orifices and a local pressure disturbance of 5% of chamber pressure occurred, the local flow would stop. Hence, the local rate of reaction would fall, the pressure wave would be followed by a rarification wave, and that, in turn, would cause a temporary increase in local flowrate. If any of the system frequencies were close to these rise rates, a combustion instability would build. Even with the baseline 20% pressure drop, a 5% disturbance can cause significant flow variations. Typically, although an injection pressure drop of 20% of chamber pressure is recommended as a starting point, some applications, such as engines designed for throttling or those with stability sensitivity, may require higher values.

Injection area and orifice diameter can be computed with simple expressions based on flowrate, propellant density, and a factor for the head-loss coefficient, as follows:

$$A_{inj} = \dot{w}\sqrt{\frac{2.238K}{\rho\Delta P}} \qquad (4\text{-}43)$$

$$d_{orifice} = \left(\frac{3.627K\dot{w}^2}{\rho\Delta PN^2}\right)^{0.25} \qquad (4\text{-}44)$$

where $\dot{w}$ = flowrate, lb/s; ρ = density, lb/ft^3; ΔP = pressure drop, lb/in.^{2}; K = head-loss coefficient; N = number of orifices. A reasonable value of the head-loss coefficient would be 1.7 for a sharp-edged orifice of a typical length used in injectors, or 1.2 for a radiused-entrance orifice. (Injection orifices generally are "short tube" passages ducting flow from a manifold to the combustion chamber.)

This method of orifice sizing, using the head-loss coefficient instead of the more common flow-coefficient, sums the appropriate values for the specific orifice configuration. For example, a square-edge tubular orifice has an entrance-loss coefficient of 0.5, a running friction loss on the order of 0.2, and an exit loss of 1.0 into a near-infinite reservoir, resulting in a total K of 1.7. For impinging-injection elements, it is generally preferable to have a radius or other type of orifice entrance to reduce the head-loss coefficient. It is also desirable to turn as much of the available pressure loss as possible into injection velocity for best atomization and mixing. In addition, the directional control of a liquid stream is more consistent with a low entrance-loss. This orifice design approach is also supported by the concept that the inertia of the injected stream, like the pressure drop, helps provide stability isolation.

However, injection-orifice sizing proves a bit more complex than the preceding discussion may indicate. The total injection area is easy to compute, but orifice diameters depend on the number of elements in the injector. For maximum atomization and mixing efficiencies, the choice would be to use as many elements as feasible, or orifice sizes as small as can be fabricated. In the real world, the choices are never this simple and many factors must be considered. In addition to the difficulties of manufacturing myriads of tiny holes, there are the factors of combustion stability and contaminant plugging to be considered. Also, fine injection patterns are easier to excite in combustion-instability modes. Fortunately, large engines, which have the more serious stability concerns, tend to have longer combustion chambers, with increased residence time, and do not require very small orifices to provide high levels of combustion efficiency. Small engines, which require compact combustion chambers, are less prone to stability problems and can utilize fine injection patterns. Injection-orifice sizes have ranged from diameters as small as 0.004 in., for a 1-lb-thrust experimental engine, to nearly 0.75 in. in a pressure-fed booster application. The more usual range has been from 0.0135 in. (in the XLR-132 upper-stage storable-propellant engine) to 0.281 in. (in the Saturn F-1 booster); most injector orifices are in the range of 0.020 to 0.080 in.

Determination of the proper metering area of the LOX post in a coaxial injector is more complex than in the single-orifice case. Typically, the design velocity for the central LOX stream is low (between 50 and 100 ft/s) and the velocity head falls well below the desired degree of pressure isolation. An upstream orifice can regulate the flow and give the pressure drop required for stability. The head-loss computations give an accurate estimate of the system flow resistance. The primary pressure loss derives from the sudden expansion from the metering-orifice diameter to the post internal diameter. The entrance of the orifice is usually well rounded, to yield low loss at this point. The friction inside the LOX post and the exit pressure loss are taken at the lower velocity. The SSME LOX post represents a more special case (Fig. 4-61), since the expansion from the metering orifice is taken in two steps.

Elements with internal momentum exchange, or swirl, and diffusion-bonded "platelet" elements are special cases for flow-resistance prediction. In these cases, the only reliable approach is the use of experimental flow testing to establish rational coefficients.

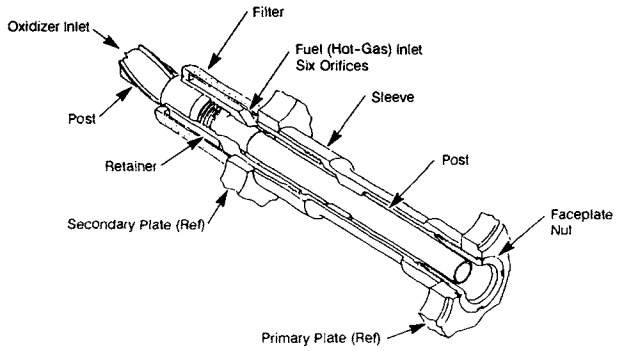

Fig. 4-61 LOX post schematic.

Combustion modeling using computer programs to predict atomization and vaporization helps select the most appropriate orifice sizes. Some computer programs provide guidelines for the degree of combustion-stability sensitivity, but previous experience with similar applications remains the best arbiter on element sizing.

Experimental Evaluation of Injector Designs

The design of an injector can be improved by proper application of experimental results obtained in nonreactive (cold-flow) and hot-fire testing. The latter is the true test of the merit of any design, but much valuable information can be obtained at considerably lower cost and risk by use of nonreactive techniques.

Cold-flow calibration tests. The most basic cold-flow tests calibrate flow resistance and visual assessment of the injected streams. These should be performed before hot-fire testing of any new injector. Flow-resistance data are required for setting inlet pressures. Agreement of measured and computed resistance values checks the computation technique or, in some cases, gives a measure of the quality of fabrication. Visual observation of flow streams complements these data, indicating any misdrilling of orifices or potential plugging or other blockage of any elements. Visual observation of the spray pattern helps identify impingement problems and gives clues to the interaction of the combustion process with the combustor wall. The appearance of the streams also gives an indication of the degree of atomization that the pattern is producing.

Ideally, the pressure-drop calibration should be done with raised downstream back pressure. Nevertheless, valid information on flow resistance can be obtained without requiring full simulated flowrate, as long as cavitation is avoided in the testing. Most injection elements will not cavitate if the back pressure is at least half the pressure drop across the test orifices. Therefore, with ambient backpressure (14.7 psia), data would be taken up to about 30 psid. Data should be obtained for several flows above and below this pressure-loss value, so that the cavitation points may possibly be determined. Plotting of flow resistance will indicate any departures associated with cavitation. The backpressure fixture can provide dual utility if designed also to be used as a backflush fixture to clean the injector assembly. Liquid or gaseous backpressure seems to be equally satisfactory for resistance calibration, although gaseous backpressure gives a truer simulation of hot-fire conditions.

Cold-flow mixing tests. Numerous techniques have been employed to predict injector performance from nonreactive flow data. Liquid/liquid patterns can be evaluated fairly well by using two nonsoluble liquids as propellant simulants and collecting the spray in a grid system. The flow from each position in the grid is collected and the mass ratio at that place determined. These tests are relatively inexpensive and the information is valuable in design. Gas/liquid nonreactive mixing tests are much more difficult to do and are subject to greater unknowns, but they may still provide useful data.

Atomization testing. The degree of atomization of the propellants strongly conditions combustion efficiency and relative sensitivity to destabilizing influences. Numerous methods of nonreactive atomization testing have been used, ranging from qualitative observations during cold-flow calibrations to sophisticated laser measurements and holographic reconstructions. Early quantitative efforts were based on the collection of frozen droplets of wax or low-melting metals. Later efforts concentrated on laser devices using doppler interference, diffraction, or other nonintrusive optical diagnostic techniques. These techniques generally suffer from obscured view at the high-mass-flux operating conditions typical of high-chamber-pressure engines. Also, high-chamber-pressure large engines with supercritical injection conditions are less sensitive to the hydraulic-atomization characteristics of the injection elements. Most engines in this class appear to be mixing-limited, rather than vaporization-limited, in performance. Consequently, some interest has shifted away from atomization measurements.

Hot-fire tests. Hot-fire testing is often applied to subscale simulations of planned larger assemblies, but final data are obtained in full-scale hardware. In either case, however, the right kind of test program will be very important in developing and proving the design. It is generally desirable to evaluate a larger operational range of flowrates, pressure, and mixture ratio than to evaluate just the specified requirements. Mixture-ratio testing can sometimes indicate momentum-related performance characteristics that can aid in the next design or rework of the existing design. Heat-flux measurements in a calorimeteric chamber also provide data that can make improvements possible. Thermal capability of the test chamber must be investigated in evaluating the injection pattern and to establish the need for, and optimization of, any film-cooling flows that may be required.

Variation of some of the physical test characteristics is often desirable, such as change in combustor length to evaluate required L*. Stability characteristics are often assessed by introducing chamber-pressure disturbances such as "bombs," "pulse guns," or rapid perturbations of propellant flowrates. The time required to damp out any

"ringing" resulting from such disturbances helps indicate stability margin in the system.

Frequently, injector modifications can be made to the hardware under test to evaluate these effects. Injection orifices can be plugged or enlarged, and orifices can be added for film cooling, for example. Obtaining valid experimental data in these tests requires appropriate instrumentation. The injector designer must take these requirements into consideration in providing suitable ports for pressure, temperature, and vibration measurements.

Analytical Models

Many analytical models have been written and used for prediction of injector/chamber performance. They are primarily vaporization and spray-path mixing models and depend on many empirically modeled mechanisms and on user skill to provide meaningful predictions. Computer models are also employed to quantify empirically the design features known to impact combustion stability, such as orifice size, chamber diameter, and chamber pressure. These parameters are fit to various expressions that provide a factor that reflects the divergence of these characteristics of a proposed design from previous successful practice. The model outputs provide general guidelines and an indication of pretest prediction of combustion stability.

Considerable effort is being expended on computational fluid dynamic (CFD) models, but none has yet been developed to the state of a truly useful injector-design tool. Rational, simple, two-dimensional flow regimes, such as airfoils and expansion nozzles, are fairly well simulated by CFD techniques, but results for rocket-engine combustors have been limited to reasonably accurate predictions of local flow fields and local droplet behavior. The multidimensional mechanisms of an impinging-stream injector are still not well enough understood to model effectively a major portion of the injection/combustion phenomena, even if the required computational power were economically available. These mechanisms, combined with the turbulence and other forces acting in the combustion chamber, put CFD techniques out of the realm of practical utilization for injector design for the present. The potential exists for improved analytical tools in this area, however, and continued effort is justified.

Sample Calculation 4-8

Using data in Tables 3-2 and 3-3, determine the injector-orifice sizes and injection velocities for the A-1 and A-2 Stage engines.

(a) *A-1 Engine*

Thrust-chamber propellant flowrates are 1941 lb/s (oxidizer) and 827 lb/s (fuel); propellant densities are 71.38 lb/ft^3 (oxidizer) and 50.45 lb/ft^3 (fuel); injector pressure drops are 200 psi for both propellants. Assume an injection pattern of 750 element sets, with one oxidizer selfimpinging and one fuel selfimpinging doublet per set, for a total of 1500 each oxidizer and fuel orifices. If the orifices have prepared entrances (at the least, an angled countersink), the head-loss coefficient will be about 1.3. From Eq. (4-43) and (4-44):

$$A_o = 1941\left(\frac{2.238 \times 1.3}{71.38 \times 200}\right)^{0.5} = 27.7 \text{ in.}^2$$

$$A_f = 827\left(\frac{2.238 \times 1.3}{50.45 \times 200}\right)^{0.5} = 14.04 \text{ in.}^2$$

$$d_o = \left(\frac{4 \times 27.7}{\pi \times 1500}\right)^{0.5} = 0.153 \text{ in.}$$

$$d_f = \left(\frac{4 \times 14.04}{\pi \times 1500}\right)^{0.5} = 0.109 \text{ in.}$$

The injection velocities will be as follows:

$$V_o = \frac{144 \times 1941}{27.7 \times 71.38} = 141 \text{ ft/s}$$

$$V_f = \frac{144 \times 827}{14.04 \times 50.45} = 168 \text{ ft/s}$$

Use of an orifice flow coefficient C_d to compute injection velocity is not recommended, because most orifices flow "full."

(b) *A-2 Engine*

From Table 3-3, the propellant flowrates for the thrust chamber are 285.2 lb/s (oxidizer) and 54.5 lb/s (fuel); the propellant densities are 71.38 lb/ft^3 (oxidizer) and 0.72 lb/ft^3 (fuel; gaseous hydrogen at 180°R). Coaxial injection elements are used; with a typical density of about two elements per square inch of injector face area (157.8 in.^{2}), a total of 300 elements can be assumed. Start with a generally accepted value of LOX velocity in the central post of 60 ft/s, as follows:

$$\text{Total post area} = \frac{144 \times 285.2}{71.38 \times 60} = 9.59 \text{ in.}^2$$

$$\text{Post I.D.} = \left(\frac{4 \times 9.59}{\pi \times 300}\right)^{0.5} = 0.20 \text{ in.}$$

The fuel-side pressure drop in coaxial injectors will generally be less sensitive to pressure oscillations than in impinging-stream configurations. In addition, the pressure loss in the cooling jacket and the difficulty of pumping liquid hydrogen force the selection of fuel-side-injection pressure drops somewhat lower than the "standard" 20% of chamber pressure. A convenient level is 15%, or 130 psi. (Values as low as 10% have been successfully used.) The fuel-side head-loss coefficient can be taken as 1.7 (typical of a sharp-edged, drilled orifice):

$$\text{Total fuel area} = 54.5\left(\frac{2.238 \times 1.7}{0.72 \times 130}\right)^{0.5} = 11.0 \text{ in.}^2$$

$$\text{Fuel area per element} = 11.0/300 = 0.0367 \text{ in.}^2$$

A LOX-post wall thickness of 0.025 in. then gives—

$$\text{Lox-post O.D.} = 0.20 + 0.05 = 0.250 \text{ in.}$$

$$\text{Total element area} = 0.0367 + [0.7854 \times (0.25)^2]$$

$$= 0.0858 \text{ in.}^2$$

$$\text{Element I.D.} = (0.0858/0.7854)^{0.5} = 0.330 \text{ in.}$$

$$\text{Fuel gap} = (0.330 - 0.250)/2 = 0.040 \text{ in.}$$

$$\text{Fuel velocity} = \frac{54.5 \times 144}{0.72 \times 11.0} = 991 \text{ ft/s}$$

$$\text{Velocity ratio} = 991/60 = 16.5$$

This velocity ratio falls within the range (10 to 20) that gives good atomization and mixing. Because the low oxidizer velocity and flow resistance might not assure stability, a metering orifice is placed at the inlet of each LOX post. Such metering orifices are designed by an iterative process because the primary flow resistance arises from the expansion loss between the orifice and the post I.D. and is difficult to predict accurately.

4.6 GAS-GENERATING DEVICES

In liquid-propellant engine systems, gases are required to power the propellant feed systems and other subsystems. Bottled compressed gases such as helium can be employed for these purposes; but the use of higher-temperature gases generated by suitable devices gives much higher overall system performance. Gases at temperatures ranging from 400 to 1000°F are used for pressurizing propellant tanks. Gases in the range from 1200 to 1700°F have been used to drive gas turbines for pump-fed systems. Wherever possible, the engine system's primary propellants are used for generating gas in the interests of overall system simplicity. In certain applications, however, such as in a pressurized gas-fed system or to start a turbopump-fed system, high-pressure propellants other than those tapped off the primary system are required for gas generation.

Most operational engine systems use special devices for gas generation. However, tapping hot gases from the main chamber has shown promise in certain applications. Design objectives for operational gas generators may be summarized as follows:

1) Ability to produce gases safely, with required properties (temperature, pressure, nonexplosive), in a compact unit at the required flowrate.
2) Ability to start and stop smoothly without abrupt temperature surges, pressure oscillations, or overflow of unburned propellants.
3) Ability to operate over a wide range of propellant flowrates and (in the case of bipropellants) mixture ratios and to respond closely to the control system.
4) Ability to maintain safe shutdown without complicated purging and draining systems.
5) Ability to restart safely (restartable engine systems only).

Additional design requirements depend on the particular engine system involved.

Gas generators can be classified according to the propellants employed: solid-propellant, liquid-monopropellant, or liquid-bipropellant.

Solid-Propellant Gas Generators

Solid-propellant gas generators are used in liquid-propellant propulsion systems for limited-duration applications, such as providing a supply of pressurized gas to power turbines for engine start or to provide gas pressurant for short-duration, pressure-fed systems. The temperature of gases generated by solid propellants generally exceed 2000°F, which is too high for uncooled components over extended durations. Diluents can be used, either incorporated into the propellant formulation or injected into the gas stream. Use of diluents increases system complexity or, in the case of coolants added to the solid propellant, reduces gas-generator efficiency and may degrade performance.

Figure 4-62 shows a typical design of a solid-propellant gas generator used to supply power to a turbine for engine start. It is built in the form of a replaceable cartridge that bolts to a flange at the liquid-propellant gas generator (shown in Fig. 4-64). This design is a disposable type, not intended to be reloaded and reused. The unit consists of three concentric cylinders of solid propellant with retainer plates, an igniter containing pyrotechnic pellets, a structural case, an outlet orifice, a burst diaphragm, and two initiators (removable). Electrically fired initiators are installed immediately before engine start to minimize the risk of inadvertent initiation.

A firing stimulus is sent to the gas generator at engine start. This fires the initiators and ignites the pellet charge. It, in turn, ignites the solid-propellant grains. Within approximately 40 ms, the generator produces gas at a rate of 4.7 lb/s and maintains this flowrate for approximately 1.0 s. The gas generator operates at a chamber pressure of 1000 psia, producing gas at 2550°F. The product gas has a characteristic velocity of 4260 ft/s.

In addition to the basic, constant-flowrate unit, gas generators can be designed with tailored flowrate profiles to meet special requirements. Gas generators with regressive flowrate-time profiles, i.e., flowrates that decrease during the burn, have been produced for operational vehicles, and progressive-burning units featuring increasing flowrate-time profiles have been designed and fabricated to power turbines for LOX /H_2 engines during start.

Current technology enables use of exploding-bridgewire, flying-plate, and laser concepts to design initiators that are resistant to inadvertent ignition. Use of such devices can support factory installation

of the initiators into the solid-propellant gas generators.

Design of solid-propellant gas generators requires the application of basic principles of internal ballistics. Propellant is contained within the case in the form of one or more geometric units, called propellant grains. The rate at which a grain produces gas is a function of the propellant formulation, the amount of surface area burning, the operating pressure at the burning surface, and the bulk temperature of the propellant. Exposed surfaces of solid propellant burn in a direction normal to the surface at a rate dependent on gas-generator chamber pressure and propellant temperature. The correlation can be expressed as follows:

$$R = k_1\left(\frac{P_c}{1000}\right)^n \tag{4-45}$$

where R = linear burning rate of the propellant, in./s; k_1 = constant representing the linear burning rate of a given propellant, at a given temperature and at a chamber pressure of 1000 psia; P_c = chamber pres sure, psia; and n = constant indicating sensitivity o the propellant burning rate to changes in pressure at a given propellant temperature.

The weight flowrate of gas produced by a solid-propellant gas generator can be calculated as follows:

$$\dot{w}_g = A_b R \rho \tag{4-46}$$

where $\dot{w}_g$ = weight flowrate produced by the gas generator, lb/s; A_b = burning-rate area, in.^{2}; and ρ = propellant density, lb/in.^{3}. A constant-flow gas generator requires a propellant design that provides constant burning area as the propellant is consumed.

Solid-propellant gas generators often have sonic outlet orifices to decouple chamber pressure from the downstream pressure, which may be changing during the start sequence. In such a choked-flow gas generator, the gas flowrate, chamber pressure, and orifice throat area are related by Eq. (1-32). The chamber pressure is given by the following expression:

$$P_c = k_2\left(\frac{A_b}{A_o}\right)^{\frac{1}{1-n}} \tag{4-47}$$

where k_2 = constant, characteristic for a given propellant at a given temperature; A_o = gas-generator orifice area, in.^{2}; A_b = burning area, in.^{2}; and n = constant.

Liquid-Monopropellant Gas Generators

Monopropellants such as hydrogen peroxide (H_2O_2) and hydrazine (N_2H_4) have been used as gas generants in many applications. They permit a simple generator system and do not require mixture-ratio adjustments. These systems are relatively easy to control and the gases are generated at predictable temperatures. Unless the monopropellant is also employed as one of the engine's main propellants, however, the generator system introduces a third propellant, often requiring special handling and tankage.

Figure 4-63 shows a schematic of a typical monopropellant gas generator using 90% hydrogen peroxide. The catalytic screen pack (bed) consists of alternate layers of stainless steel mesh and silver-plated-brass-wire screens secured by perforated end-plates or grids, which are applied with a preload of approximately 800-1000 lb/in.^{2} of bed cross-sectional area. The length of the catalytic bed generally ranges from 2 to 3 in. The allowable design throughput, that is, propellant flowrate per unit cross-sectional area of catalytic bed, is about 0.4 lb/in.^{2}-s. The propellant pressure drop across the bed can be approximated by the following:

$$\Delta P_b = \frac{C_1 G_b^{1.95}}{P_c^{0.9}} + C_2 t \tag{4-48}$$

where ΔP_b = pressure drop through the catalytic bed, psi; G_b = throughput, lb/in.^{2}-s; P_c = gas-generator chamber pressure at the end of the catalytic bed, psia; t = accumulated running time, s; and C_1, C_2 = constants determined experimentally for a given bed configuration.

Sample Calculation 4-9

A hydrogen-peroxide (monopropellant H_2O_2) gas generator attached directly to the inlet flange of a turbine has turbine-inlet pressure of 340 psia and total turbine nozzle throat area of 0.776 in.^{2} Assume

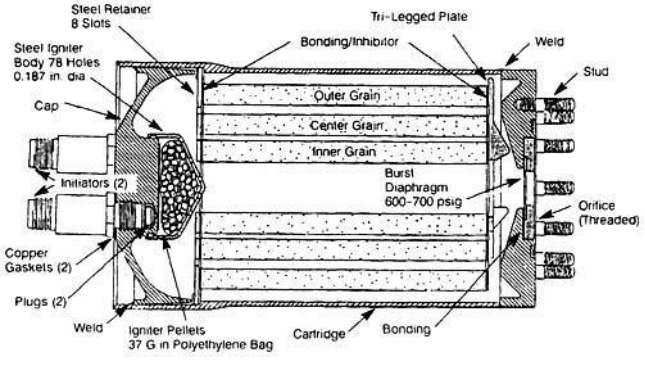

Fig. 4-62 Disposable solid propellant gas generator.

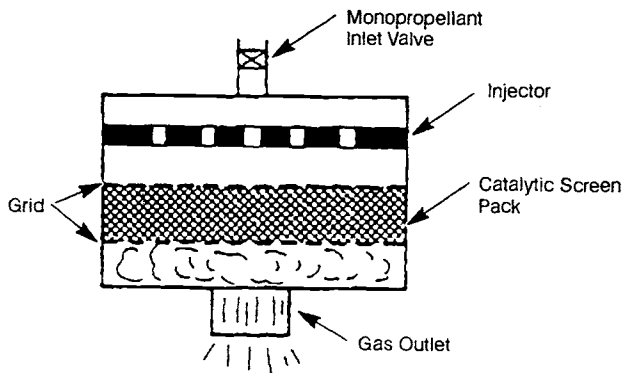

Fig. 4-63 Schematic of monopropellant gas generator.

a c^* value of 3080 ft/s for 90% H_2O_2 and the catalytic-bed design constants $C_1 = 7.2 \times 10^4$ and $C_2 = 0.021$ psi/s.

Problem

Determine the gas flowrate, catalytic-bed area, and pressure drop after 480 s of accumulated running time.

Solution

Proceed as follows. Gas-generator pressure will equal turbine-inlet pressure of 340 psia. Equivalent gas-generator throat area will equal total turbine nozzle throat area = 0.776 in.^{2}. Substituting into Eq. (1-32):

$$3080 = \frac{340 \times 0.776 \times 32.2}{\dot{w}_g}$$

Gas flowrate $\dot{w}_g = 2.76$ lb/s.

Now apply a design value for catalytic-bed throughput G_b of 0.4 lb/in.^{2}-s. Catalytic bed area will equal 2.76/0.4 = 6.9 in.^{2} Substitute given data into Eq. (4-48), as follows:

$$\text{Bed pressure drop } \Delta P_b = \frac{7.2 \times 10^4 \times (0.4)^{1.95}}{(340)^{0.9}} + 0.021 \times 480 = 63.5 + 10 = 73.5 \text{ psi}$$

Liquid-Bipropellant Gas Generators

Bipropellant gas-generator systems are used in most current large engines because they utilize the same propellants and generally provide the most flexible high-performance system. This category also includes gas-generator systems referred to as "preburners," which have a slightly different application in staged-combustion-cycle engines. Bipropellant gas generators act in the same fashion as the injector/combustor components of the main engine. They differ primarily in the selected mixture ratio to provide the desired gas temperature and chemical properties. Primarily these components provide the motive gases for turbine-driven machinery in the engine (mainly the propellant pumps). This application requires a discharge temperature that the turbine blades can accommodate. Generally, delivered temperatures have been held below 1800°F; current practice is closer to 1140°F. The highest allowable temperature is desirable, since this maximizes delivered power for the propellant weight flow diverted from the primary propulsive effort. However, temperatures that are too high have an adverse effect on the life of the turbine components.

Lower gas temperatures are usually produced by fuel-rich operation, which provides a reducing atmosphere for the downstream structural components. Low temperatures can also be produced by oxidizer-rich operating conditions, but the oxidizing nature of the combustion gases constitutes a severe environment (most metals are fuels). The oxidizer-rich case is therefore relatively rare (notable exception: a large Russian engine which uses an NTO-rich preburner in a staged combustion cycle). Another variation from fuel-rich gas generators invólves the use of a diluent, such as water, in a near-stoichiometric gas generator, as in the European Ariane system. The primary problems with fuel-rich gas generators are formation of soot and coking with carbon-bearing fuels, flammability of the exhaust gases, and performance losses in the engine cycle. Fuel-rich gas generators with hypergolic storable-propellant combinations have problems with temperature control. Since the fuels in these combinations are hydrazine-based, a monopropellant reaction process can occur that releases a great deal of heat, regardless of the mixture ratio.

Even with the more stable hydrazine fuels, such as monomethyl hydrazine, the crossover point between fuel monopropelling or just diluting the reaction mixture for a lower temperature is difficult to predict or control. The staged combustion cycle addresses many of the disadvantages of fuel-rich gas-generator operation, at the expense of system complexity. In these cycles, turbine-discharge gases are the "fuel" for the engine's primary combustion chamber. The resulting system pressures bootstrap to high levels to accomplish this, as in the SSME, in which the combustion-chamber pressure of about 3000 psi requires an upstream pump-discharge pressure of almost 8000 psi.

Figure 4-64 and Table 4-3 describe a typical liquid-bipropellant gas generator used on existing booster engines. It was designed to produce hot gases from the primary engine propellants (LO_2/RP-1) to drive the turbine of a pump-fed system. The control system consists of two normally-closed linked poppet valves which control the flow of propellants to the gas-generator injector. The valve assembly includes an oxidizer strainer, oxidizer poppet, fuel poppet, timing orifice, actuating piston, and valve main-body. The valve assembly is actuated by gas pressure, which forces the piston down on the fuel

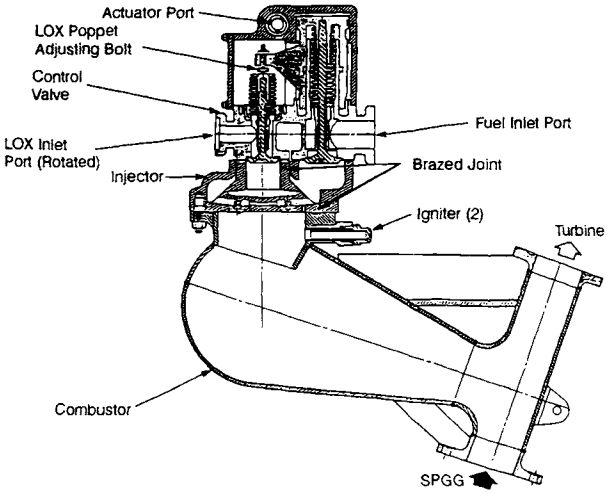

Fig. 4-64 Liquid bipropellant gas generator.

Table 4-3 Operating characteristics of a typical liquid bipropellant gas generator system.

Oxidizer	Liquid oxygen
Fuel	RP-1
Total propellant flow rate	17.34 lb/s
O/F mixture ratio	0.342
Oxidizer flow rate	4.42 lb/s
Fuel flow rate	12.92 lb/s
GG chamber pressure (injector end)	612.1 psia
GG chamber temperature	1200°F
Oxidizer side pressure drop of line, valve, and injector	114 psi
Oxidizer side pressure drop across orifice	121 psi
GG oxidizer supply line takeoff pressure (total at main oxidizer pump discharge)	846 psia
Fuel side pressure drop of line, valve, and injector	216 psi
Fuel side pressure drop across orifice	80 psi
GG fuel supply line takeoff pressure (total at main fuel pump discharge)	907 psi

side, to open the fuel poppet. A yoke integral with the piston actuates the oxidizer poppet. The valve design, through a combination of manifold volumes and LOX-poppet adjustments, effects a slight oxidizer lead to prevent detonations and a fuel-rich cutoff to avoid possible turbine burning. The propellants flow through the poppets to the injector and into the gas-generator combustor and are mixed and reacted within the inner chamber and combustor body. Two pyrotechnic igniters start the propellants. A gas duct with two opposing flanges is located at the end of the combustor body. These flanges connect with the solid-propellant gas generator's turbine spinner and the turbine-inlet duct.

Figure 4-65, a cross section through the SSME powerhead assembly, shows the two preburners used in this system. A separate injector/combustor section drives the fuel turbine, and another drives the LOX-turbopump system. Engine operating points are set and controlled primarily by changing the operating conditions of these two combustor/turbine systems. This section view also shows how the discharge of these turbines is introduced as the fuel for the primary combustion chamber.

The basic design parameters for bipropellant gas generators are virtually the same as for thrust-chamber-injector/combustor designs. The total effective throat area of the turbine-inlet nozzle system can be considered the equivalent of the throat of a thrust chamber. This can be used to calculate the combustion chamber's characteristic length (L*). In general, the effective L* of a gas generator will be about twice that of an equivalent thrust chamber and the effective contraction ratio will usually also be greater. This is based on the lower vaporization rates of liquid propellants at lower temperatures and the sensitivity of the turbine structure to relatively small levels of temperature striations ("streaks").

The primary sizing of gas generators is directed by the size of the turbine, which is dictated by the

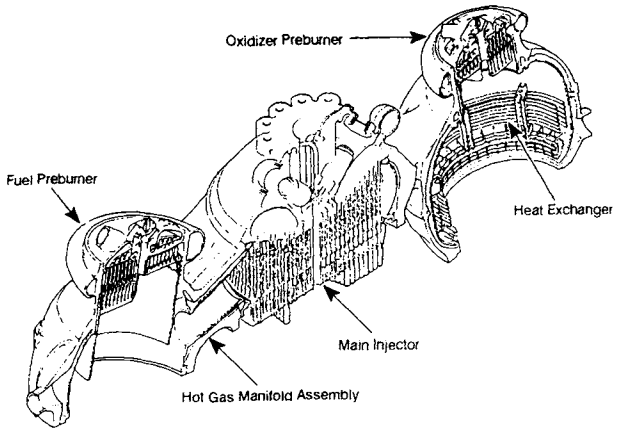

Fig. 4-65 Cross section of SSME powerhead assembly.

power requirements of the pumping system. Maximum available energy will be extracted from the generated gases when they expand isentropically through a supersonic nozzle to the available exit pressure. This available energy is given by Eq. (6-14), (6-15), and (6-16).

Because of the relatively low product-gas temperatures, gas-generator chamber designs do not usually employ cooling provisions. Exceptions are systems designed for repeated operation, in which temperature cycling might cause unacceptable levels of cracking. Even such long-life requirements call for careful study of cost trades before incorporation of active cooling systems.

Thrust-Chamber Gas-Tapoff Systems

In these systems, combustion-product gases are bled from the main thrust chamber and ducted to the turbine, where they are used as the working fluid. This arrangement eliminates the need for a separate gas generator and contributes significantly to engine system simplicity and reliability. Figure 4-66 shows a schematic of a tapoff system.

In a separate gas-generator system, gases are produced and "tailor-made" for turbine-power purposes, with the benefit of relatively high liquid-supply pressures. In a tapoff system, the bulk of the extremely hot gases of the main chamber would not

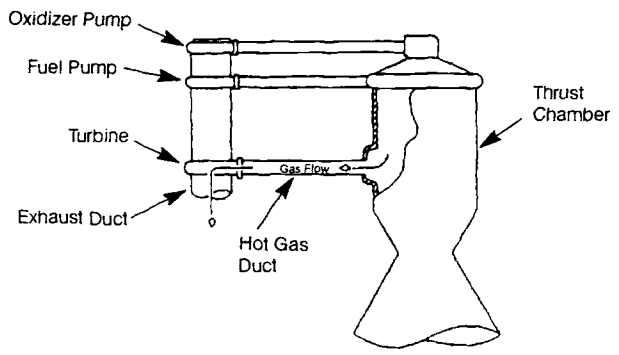

Fig. 4-66 Schematic diagram of thrust chamber gas tapoff system.

be suitable as turbine-drive fluid because of the limitations of the turbine construction materials. It has been successfully demonstrated, however, that by withdrawing chamber gases from the boundary zones only, and by proper shaping and location of the bleed ports, the desired turbine-inlet temperature (usually less than 1700°F) can be reliably and repeatably produced for a given thrust chamber and injector design.

The bleed gases thus withdrawn have been found to possess thermodynamic properties comparable to the products of a liquid-bipropellant gas generator utilizing the same propellants. Obviously, a tapoff turbine must be designed to operate at an inlet pressure lower than the thrust-chamber pressure. Furthermore, a tapoff engine system will require a simple starting device, such as a gas spinner. With the aid of a hot-gas-regulating valve placed at the turbine inlet, hydrogen-tapoff engine systems have been successfully throttled to thrust ratios of 10:1 or better.

4.7 IGNITION DEVICES

Release of chemical energy stored in liquid propellants can be initiated by a number of methods; and they have been used for both thrust chambers and gas generators. Selection of an ignition system depends on the nature and phase of the propellants (bipropellants or monopropellants), need for altitude start, need for restart, system safety, compatibility of the ignition method with overall engine design, and weight and space considerations.

All ignition methods, particularly those for bipropellant systems, have one overriding requirement in common: rapid reliable ignition of incoming propellants before accumulation of reactive material. Propellants entering the combustion chamber not promptly ignited can cause explosive mixtures to form and detonate. Assurance of satisfactory ignition depends on proper selection of the ignition method, quality of design, and integrity of the ignition-system hardware.

Igniters

Igniters are defined as devices, or assemblies, that release heat and thereby initiate reaction of the main propellants. Igniters derive power from an outside source or from a limited quantity of internally stored energy. Because of the necessity of having an ignition source available at the time of main propellant introduction, systems can be designed to provide pilot flows of main propellants to be ignited before opening the main valves. Once ignited, main propellants remain ignited, so it is not necessary to maintain an ignition source, although some ignition systems do maintain such a source throughout mainstage operation.

Pyrotechnic igniters. Pyrotechnic igniters are electrically initiated slow-burning pyrotechnic torches. They are designed with solid-propellant technology and typically incorporate one or more solid-propellant charges. Burn duration is in the range of 2 to 10 s, depending on engine requirements. Pyrotechnic igniters can be mounted to the thrust-chamber injector at the injector face (Fig. 4-2), or through the injector from the manifold side. Flame-spreading designs enhance heat distribution and ensure early ignition of incoming propellants. Injector-mounted igniters with radial flame output (Fig. 4-67) provide a sheet of flame immediately downstream of, and parallel to, the injector face. These designs were in common use in the 1950s. A more recent igniter design, for an upper stage LOX/H_2 engine, is axially mounted through the injector, with a flame tube and a deflector that splits the flow and imparts a radial component to the combustion products expelled from the igniter.

Pyrotechnic igniters for gas-generator propellant ignition have been mounted in gas-generator bosses as screw-in plugs (Fig. 4-68). The igniter propellant, typically an end-burning charge, produces a flow of hot gas and incandescent particles that are expelled into the combustor parallel to, and slightly downstream of, the GG injector. Figure 4-68 shows a pyrotechnic igniter used for GG ignition for a 1,500,000-lb thrust LOX/RP-1 engine. The same design was used to ignite turbine exhaust gases where they enter the thrust-chamber assembly. It had the following characteristics: no-fire voltage, 250 Vac; firing voltage, 500 Vac, 60 Hz; pyrotechnic, perchlorate/aluminum/boron/epoxy-rubber; flame temperature, approximately 4000°F; output flow rate, 0.25 gm/s; and operating duration, 8 s.

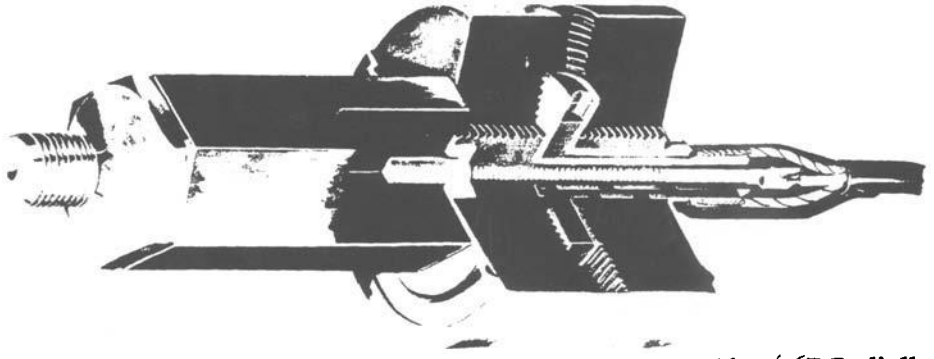

Fig. 4-67 Radially outward firing pyrotechnic igniter for center of injector mounting.

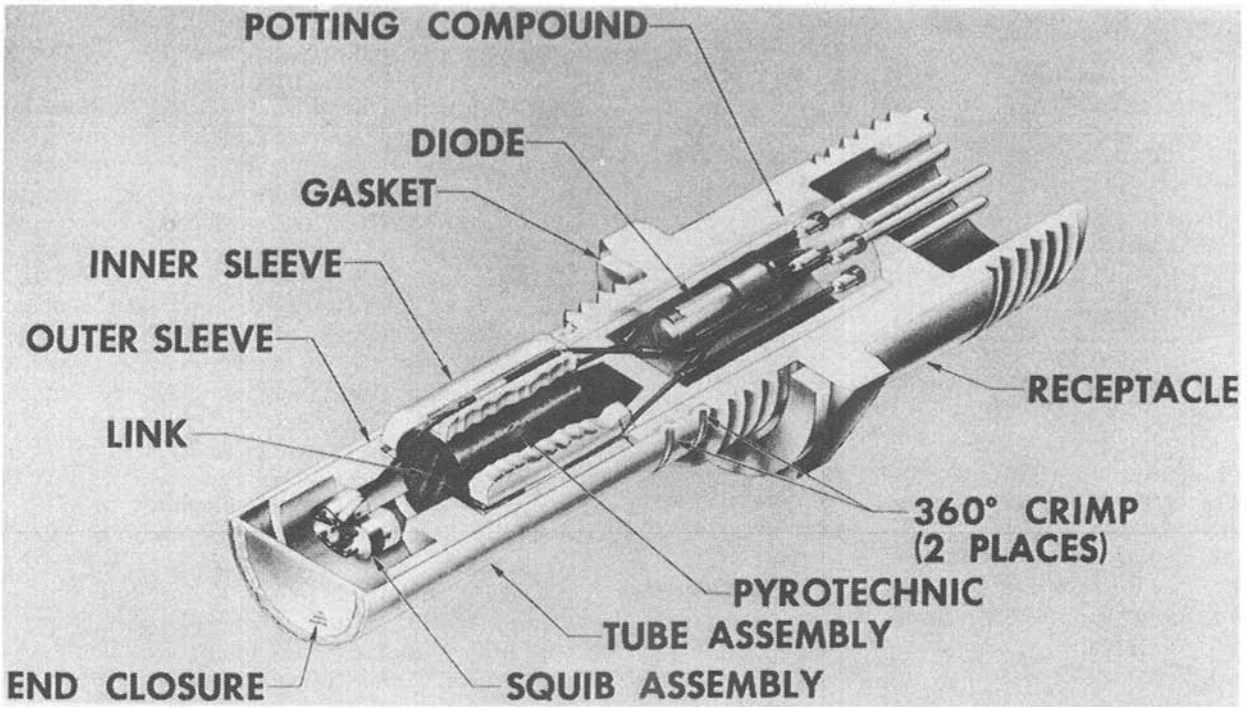

Fig. 4-68 Gas generator igniter with built-in fusible link.

Pyrotechnic igniters are initiated by electric squibs that light the igniter propellant. Early pyrotechnic igniters fired directly from 28-Vdc power sources, but more recent igniters are designed to fire from 500-Vac power supplies. High-voltage designs provide good protection against inadvertent firing, including accidental application of electric power such as direct hookup to 220-Vac power. A number of electrical firing concepts represent options in designing to required reliability and safety. Exploding-bridgewire or laser initiators provide very safe pyrotechnic devices. Igniters can also be designed to ignite from other "hot" components, such as a solid-propellant gas generator used to start the turbopumps.

Fusible-link electrical circuits, designed to provide an open circuit when the igniter is successfully fired, are commonly incorporated in pyrotechnic igniters. The fuse element is buried in the propellant column (or otherwise configured) to require propellant burning to interrupt the circuit. "Opening" of the linking wire circuit verifies that the igniter has received an adequate firing stimulus and has responded correctly.

Proper use of redundant igniters, with redundant electrical firing systems and fusible-link ignition-verification circuits, can give ignition reliability in excess of 0.9999. Pyrotechnic ignition systems were successfully used in one or more locations in the Atlas, Delta, F-1, H-1, J-2, Redstone, and Thor propulsion systems.

Although pyrotechnic igniters provide excellent ignition sources, they have not been popular in recent engine systems, for reasons such as these:

1) Electro-explosive interfaces and electrical components necessitate redundancy.
2) Many large injectors are compartmented, requiring separate ignition source(s) for each compartment.
3) Pyrotechnic devices are encumbered by stringent safety requirements that raise hardware costs.
4) Field checkout and installation of components are frequently required. Field sites must provide facilities for receiving, handling, and storing pyrotechnic devices.
5) The igniter must be installed for each engine test and for launch.

Technology is now available for design of pyrotechnic igniters with laser-pyrotechnic interfaces replacing the electro-explosive interfaces. Elimination of the electro-explosive interfaces enables design of devices insensitive to radio-frequency-induced power and electrostatic discharge. Combined with the use of through-bulkhead initiation, laser firing can provide a very safe subsystem that will reliably contain high chamber pressures without need for high-temperature, high-pressure, glass-to-metal, or ceramic-to-metal seals.

Hypergolic Igniters

The term "hypergolic" denotes a bipropellant combination that ignites spontaneously when the two

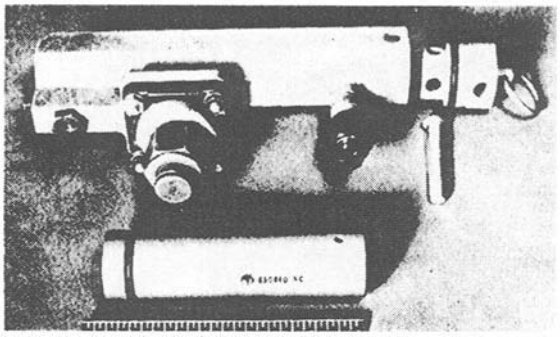

Fig. 4-69 Hypergol slug cartridge and housing.

components meet. Such a system was used as an ignition source for the German A-4 engine (later called V-2 engine), which used hydrazine-hydrate ($N_2H_4 \cdot H_2O$) and 80% hydrogen peroxide (H_2O_2). Thin tubes supported by a wooden stick were inserted into the thrust chamber from below. Upon an "ignition" signal, a ground-mounted supply unit, including remotely operated valves, fed the two components to the injection region, where they burned with a spontaneously igniting hot flame. This method may also have been used temporarily on other systems. However, its clumsiness, the frequent clogging of feed lines, and the need to eject a considerable amount of inert solid material made it undesirable. Also, adaptation to repeated starts would be complex and would require vehicle mounting, thus adding inert flight weight.

An improved technique for using the hypergolic effect for main propellant ignition employs a hypergolic slug. In this design, a small amount of fluid, hypergolic with one of the main propellants, is stored in a cylindrical cartridge that has burst diaphragms at both ends. The cartridge, in turn, is loaded into a housing forming part of a bypass line paralleling a high-pressure main-propellant-feed line (Fig. 4-69). A fluid chosen to be hypergolic with the oxidizer but neutral to the fuel would be installed in the fuel system, and vice versa. The former is the more common; a fuel-bypass line feeds an injection element in the center of the injector, or a set of elements distributed over the injector face, including at least one element in each compartment in compartmented injector designs. When the pump starts and outlet pressures rise, the oxidizer valve is opened. As pressures rise further, burst diaphragms in the hypergolic-fluid cartridge rupture and the fluid meets with oxidizer in the chamber, igniting spontaneously. The fuel following the slug sustains the ignition flame. The main fuel valve is then opened and all parameters reach mainstage level. Since the igniter elements carry fuel fed from the main propellant source after ignition, they continue to participate in the combustion, undistinguished from the remainder of the main injector.

Triethylaluminum, a room-temperature storable liquid, hypergolic with liquid oxygen, offers excellent ignition-delay characteristics. However, a major combustion product is aluminum oxide, a tenacious solid that can clog small feed passages and orifices. Triethylboron, another room-temperature-storable liquid hypergolic with oxygen, produces a softer, less-tenacious residue than triethylaluminum. However, triethylboron has demonstrated long ignition delays when injected into very cold oxygen. Mixtures of 10-15% by weight of triethylaluminum in triethylboron provide satis-factory ignition-delay characteristics with liquid oxygen, while producing an acceptable residue.

The quantity of hypergol required for start is based on the feed-system design and the start sequence. Just a fraction of a cubic inch of hypergol will cause ignition at each location. Typically, however, a branched feed system will be employed; and several cubic inches of fluid will be required to ensure that hypergol precedes fuel in all igniter-element feed passages. Hypergol volumes vary from 4 cu. in., used in small vernier engines, to 35 cu. in., used for a multicompartment injector in a 1,500,000-lb-thrust LOX/RP-1 engine.

Organometallic-hypergol slug injection—the standard technique for ignition of main propellants in LOX/RP-1 engines—has been used in the Atlas, Delta, H-1, F-1, and Thor propulsion systems with an outstanding reliability record. The hypergol-slug system has not found application for gas-generator ignition, because it generates solid particles and requires an oxidizer lead; these conditions are not compatible with most turbine-drive designs.

Reactive-oxidizer hypergols, such as gaseous fluorine and chlorine trifluoride, have proven useful for ignition in research and development combustors, but they have not been used in production systems because of the extreme reactivity and toxicity of the materials and the corrosive potential of the combustion products.

Hypergol igniters embody reactive materials that are not delivered in the engine system. Organometallic liquids are pyrophoric as well as hypergolic with oxygen. Most, if not all, hypergols are toxic. Field processing of hypergol-filled cartridges requires controlled storage and very careful handling procedures. When selecting a slug-hypergol ignition system, the designer must consider safety requirements and provide facilities and procedures for producing, testing, packaging, shipping, handling, and installing the igniters.

Spark plugs. Spark plugs and their supporting electronics have been developed to high levels of reliability for liquid-propellant rocket engines. Spark-ignition systems are well-suited for applications requiring repeat starts without servicing between starts. The plugs can be used in direct spark applications or to ignite propellants in a precombustor or torch device. The latter concept has been preferred, to ensure propellant ignition at controlled, low-flowrate conditions, to allow starting the igniter before introduction of main propellants, and to provide a controlled environment for the plug, following ignition, to protect the plug tips. Direct-spark systems, in which sparkplugs directly ignite gas-generator (GG) or main-injector propellants, are not usable for all applications and require careful design to ensure acceptable ignition without potentially damaging pressure-spikes.

Three types of spark-ignition systems and three types of sparkplugs have been used for rocket-engine ignition. High-tension and low-tension capacitive-discharge and inductive discharge ignition-exciters have been designed, fabricated, and tested. Sparkplugs have been designed with air, surface, and shunted-surface gaps. The most robust, flexible electronic systems incorporate high-tension, capacitive discharge exciters mated to recessed surface-gap plugs. A properly designed capacitor-discharge ignition system can deliver sparks into a chilled combustor at chamber pressures in excess of 300 psia. Such a system, designed for a 200,000-lb-thrust LOX/H_2 engine, was used in a spark-torch igniter for main propellant ignition and in a direct-spark application for gas-generator-propellant ignition. The ignition exciter delivered 320 millijoules per spark, with approximately 100 millijoules per spark at the plug tip (Fig. 4-70). The exciter provided a maximum ionization voltage greater than 27 kV and produced approximately 50 sparks per second. Operated from 28 Vdc, it was active for less than 10 s during the engine-start sequence. Ignition-exciter and plug high-voltage electrical components were enclosed, pressurized, and sealed to enable operation at near-vacuum condition.

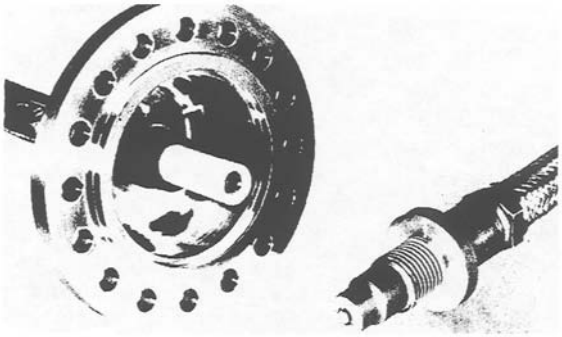

(Note: at right, screw-in spark plug; at left, cable connector)

Fig. 4-70 Spark igniter assembly.

A more recent ignition system, for a 470,000-lb-thrust LOX/H_2 engine, features an integrated exciter and plug assembly, eliminating the need for a high-voltage cable. This igniter assembly (Fig. 4-71) incorporates an inductive exciter delivering approximately 10.5 millijoules per spark at the plug tip. The igniter produces approximately 75 sparks per second. Dual, redundant igniters serve each of three ignition functions, all spark-torch applications. Although the integral-plug exciter offers benefits in size and weight, shielding radio-frequency energy, and providing a controlled environment for high-voltage electronics, the system has only limited spark energy and thus may not be suitable for systems requiring high power sparks and high-pressure-quench resistance.

The designer should provide dual, redundant plugs in all high-reliability spark applications to preclude system failure resulting from failure of a single electrical component in the ignition exciter, cable, or plug.

Spark-torch igniters. Limitations of direct-spark systems in providing a widespread ignition source (spark plasma), in withstanding spark-quenching GG pressure environments, and in surviving main combustor operating conditions led to development of spark-torch ignition systems, or augmented-spark-ignition (ASI) systems, in which small amounts of engine propellant are fed into an igniter combustor and ignited by electric sparks. The flame output is ducted to the required area and, in turn, ignites main propellants. Torch igniters may vary in size from about 1/4- to 1-in. diameter.

The igniter is built into the injector or is assembled onto the injector end of the thrust-chamber assembly, as required, to provide an ignition source at the desired place. Mounting of torch igniters on

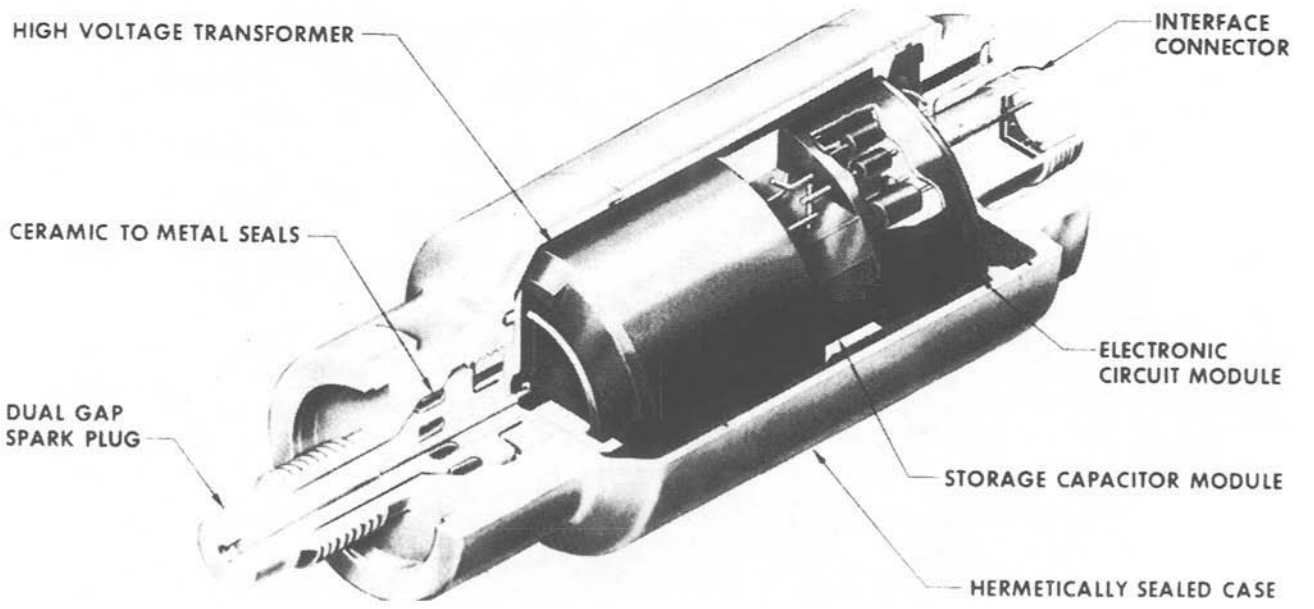

Fig. 4-71 Integral ignition exciter and spark plug assembly.

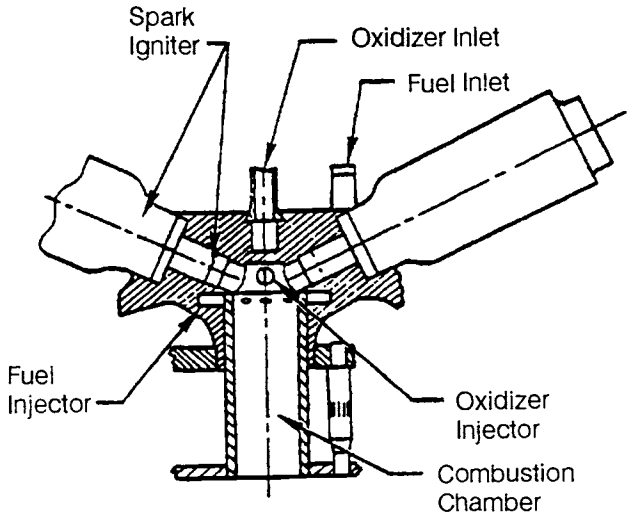

Fig. 4-72 Augmented spark igniter.

the centerline of the injector, with output directed down the center of the thrust chamber, has proven satisfactory for several large LOX/H_2 engines.

Figure 4-72 shows the principle of an augmented-spark-igniter design in an igniter featuring a like-on-like oxidizer doublet impinging at the combustor axis. Fuel is injected through multiple, tangentially-aligned orifices for igniter combustion and for cooling the combustor wall. The swirling fuel also imparts rotation to the exhaust, and the output is a swirling hot-core gas stream. Redundant sparkplugs placed upstream of the fuel-injection orifices, in a propellant-recirculation zone, enable rapid ignition and ensure a survivable environment for the plug tips. The combustion chamber may include a convergent, throatless nozzle or a straight, cylindrical output tube, depending on design constraints for the injector packaging and on the dispersion angle desired for the exhaust stream. High-thermal-conductivity materials, such as copper alloys, are typically used in fabrication of the igniter injector. The nozzle-tube assembly is manufactured from stainless steel or comparable low-thermal-conductivity material. The igniter (Fig. 4-72), originally designed to operate with LOX and RP-1, has also seen extensive service with LOX/H_2 propellants.

The torch igniter can deliver a very large number of starts, including ignition at high altitude. It can operate over wide ranges of propellant-inlet conditions, mixture ratios, and flowrates. Following ignition of igniter propellants, the spark system is turned off and the torch continues to operate during the start transients and throughout mainstage. This ensures an ignition source when required, minimizes the igniter's valve-sequence requirements, and prevents main-chamber propellants and combustion products from backing into the igniter nozzle and igniter-feed system. Igniter propellant flowrates of about 0.1- 0.3% of the main propellant flow have proven sufficient for large LOX/H_2 engines.

Spark-torch igniters can also be designed in miniature configurations for small engines. Small, hot-core, spark-torch igniters have been designed and tested that use outlet flame tubes less than 0.5 in. in diam and operate at flowrates of 0.05-0.15 lb/s.

Combustion-wave igniters. Large segmented engines and multicompartmented injectors with numerous individual compartments may require near-simultaneous ignition at many locations. Use of a large number of single-point ignition sources becomes expensive and requires a substantial amount of igniter hardware. A combustion-wave igniter with branched outputs provides multipoint ignition sources from a single precombustor.

This ignition concept (Fig. 4-73) uses a combustion wave passing through unburned, manifolded, premixed propellants to ignite bipropellant pilot elements at, or near, the injector face. An electric spark initiates combustion in the premix chamber. The resultant flame, or deflagration wave, propagates in the direction of flow. It produces compression and shock, and eventually a detonation wave develops in the unburned mixture that propagates through the manifold to the pilot locations. Combustion-wave characteristics are dependent on the propellant combination, propellant mixture ratio, premix temperature and pressure, and the manifold's internal geometry. Branched manifolds direct the combustion wave to the required pilot-ignition locations.

The ignition system consists of a precombustor with propellant-feed system, sparkplug electronics, branched distribution manifold, pilot flow-injection elements, and related propellant-control valves. Pilot-flow elements are integrated into the main injector design at the required locations. Propellant flow is established in the igniter precombustor and manifold. At about the time the igniter "primes" with gaseous propellants, pilot flow is established at the main injector pilots. The spark system is initiated and the igniter oxidizer valve is sequenced closed. Combustion is established in the precombustor and

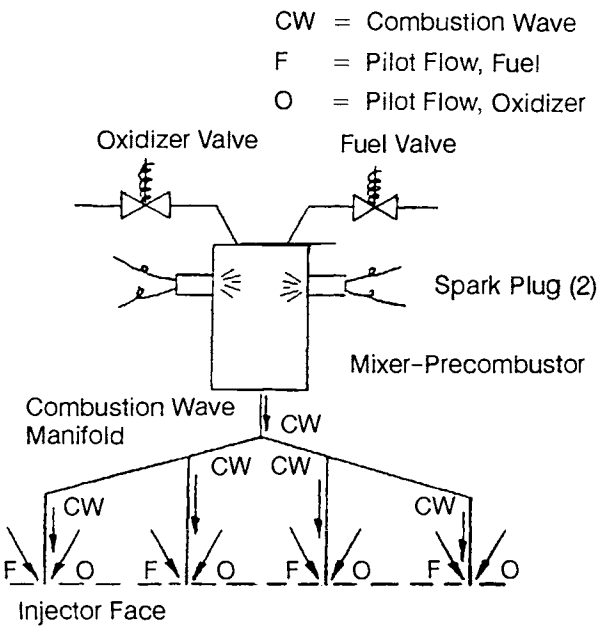

Fig. 4-73 Combustion wave ignition system.

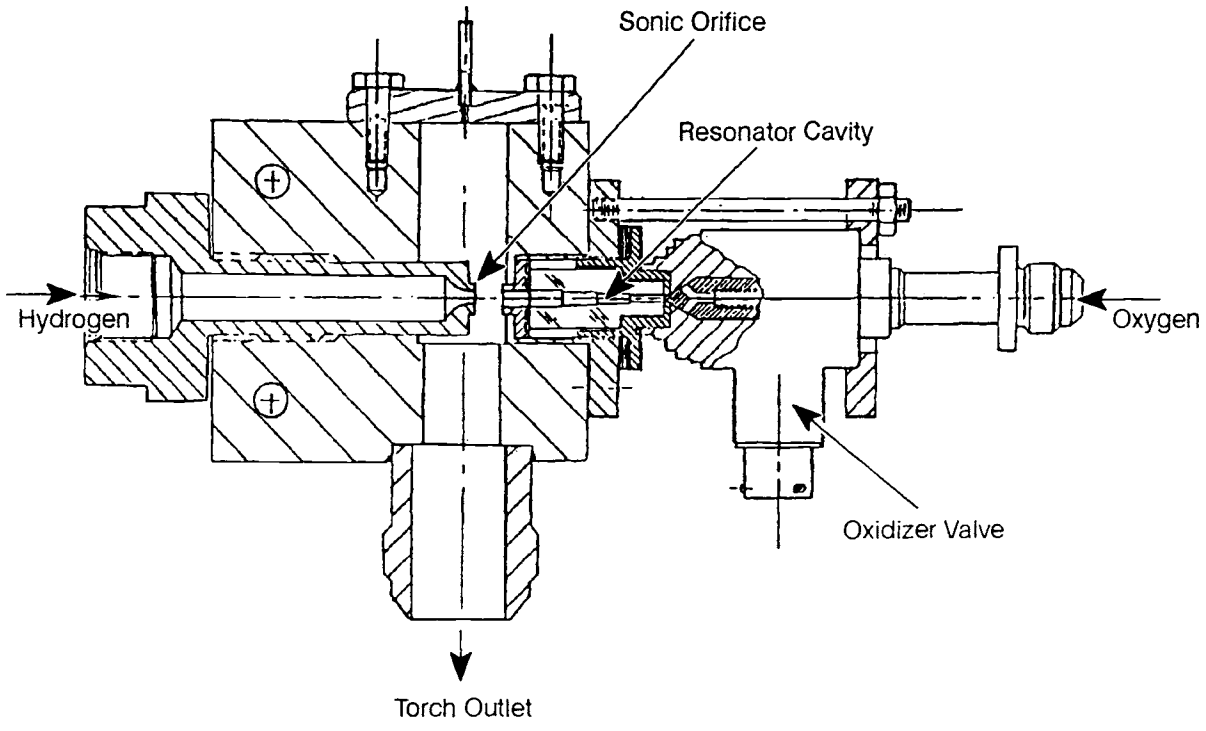

Fig. 4-74 Resonance igniter.

propagates throughout the distribution network, igniting the pilots. The pilot flames ignite the main propellants, sequenced into the chamber by the main propellant valves.

This system functions well with gaseous oxygen and gaseous hydrogen, but it is also usable with other gaseous propellants. Minimum diameter of the internal manifold passages can be as small as 0.010 in. for hydrogen/oxygen at ideal conditions. Passage lengths are theoretically unlimited. Propagation has been experimentally demonstrated in coiled tubing to lengths of about 600 ft.

The primary disadvantage of this concept is the amount of hardware required: a spark ignition system, precombustor, combustion-wave manifold, pilot elements, and significant propellant-feed hardware, including sequence-control valves. Pilot elements at the main injector must be properly designed and operated to ensure ignition by the combustion-wave pulse and to "flame-hold," ensuring the presence of an ignition source when the main valves are opened.

Resonance igniters. Resonance igniters use a flow of pressurized gaseous propellant to create resonance heating that will start the igniter propellants. Igniter exhaust, with or without oxidizer augmentation, is directed to the injector face, where it is used to ignite the main propellants as they enter the combustor.

The igniter consists of the basic elements shown in Fig. 4-74. It does not require external electrical power or catalysts. Gas introduced from an elevated pressure source upstream of the sonic nozzle expands into the mixing chamber and is directed into the resonator cavity, where it is cyclically compressed and expanded. This raises the temperature of the gas at the closed end of the cavity. An additional amount of gas spills directly into the mixing chamber and is exhausted from the igniter. Temperatures of 2000°F have been generated within 60 ms with gaseous hydrogen. After the fuel in the cavity has reached a sufficient temperature, oxidizer is introduced at the "hot" zone to effect ignition. The concept can be used with propellants other than hydrogen/oxygen, and with premixed propellant combinations. Several variations of the resonance-cavity design have been tested, including "flow-through" designs, which heat gas for subsequent injection into a combustible mixture or for injection with a second propellant to create a combustible mixture.

Special designs. To minimize the need for engine electrical inputs and to simplify engine sequencing, liquid-propellant gas generators have been designed to ignite directly from solid-propellant-gas-generator (SPGG) combustion products. In a variation of this concept, a gas generator was designed incorporating dual pyrotechnic igniters that ignited from SPGG combustion products and, in turn, ignited liquid propellants entering the gas generator. The pyrotechnic igniters could not be electrically initiated, but contained fusible-link circuits to monitor igniter ignition. The igniter-link circuits could rapidly detect inadvertent SPGG ignition and initiate a chain of events leading to safe engine shutdown.

Catalysts. In a general sense, catalysts are not igniters but initiators and sustainers of reactions, and remain unchanged during these reactions. In rocketry, catalysts have been used predominantly to initiate and sustain the decomposition of monopropellants ("monergols"), notably, hydrogen peroxide. Several operational or near-operational systems existed during World War II, such as the earlier Messerschmitt Me-163, which used hydrogen peroxide with potassium permanganate solution as the catalyst,

and the turbine steam-generating system of the V-2 ballistic missile, which employed 80% hydrogen peroxide with either potassium permanganate or sodium permanganate as catalysts.

Because they need relatively elaborate timing, valving, and interlocking devices, liquid catalysts were soon found to be cumbersome and undesirable. Development of solid catalysts was undertaken. They have been used in the Redstone rocket steam-plant and in the AR airplane super-performance rockets, which decompose hydrogen peroxide fed through a solid catalyst bed consisting of impregnated wire screens. Since the specific impulse of decomposed hydrogen peroxide alone is low (below 200 s, depending on concentration and design parameters), RP-1 fuel is injected below the decomposition chamber. Because of the high temperature of the decomposition gases (1400°F), the RP-1 ignites and burns spontaneously with the free oxygen of the decomposed H_2O_2 (Fig. 4-75). In this manner, the solid catalyst indirectly serves as an ignition system. While the specific impulse with an RP-1 afterburner is still moderate (approximately 245 s for the AR), such a system offers versatility, storability, and simplicity, including the capability of throttling to low levels and restartability.

More recently, it has been successfully demonstrated that catalytic ignition offers an alternative to augmented spark ignition for hydrogen/oxygen systems. The concept is basically simple, requiring only the feeding of a mixture of gaseous hydrogen and oxygen through a properly designed catalyst-bed. Catalysts for hydrogen-oxygen mixtures include iridium, palladium, and platinum. Component igniters have been designed and tested, and catalytic igniters have been used to start large thrust chambers. However, highly reliable and durable catalytic igniters suitable for production-engine applications have not yet been developed.

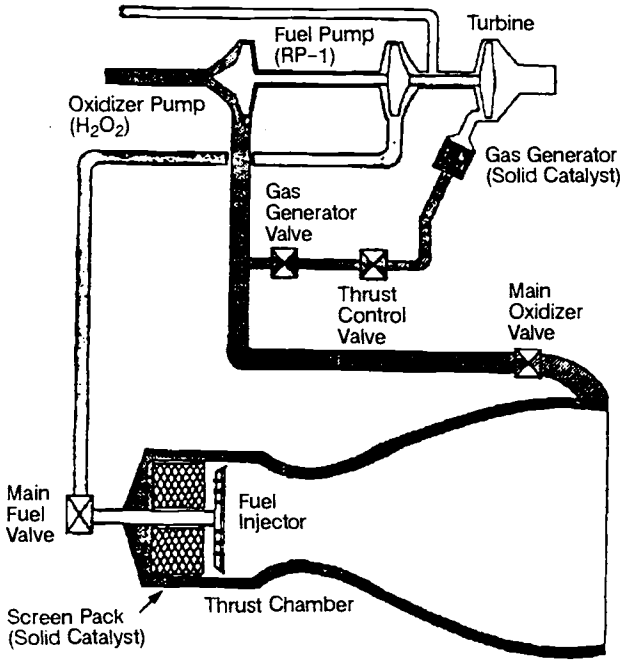

Fig. 4-75 Schematic of a Rocketdyne AR-1 superperformance rocket engine.

Ignition Detection

The potentially catastrophic consequences of ignition failure have prompted extensive investigations of means to detect reliably the presence or absence of ignition in liquid-propellant rocket engines. Ignition is a discrete event. The only verification required is that safe, damage-free ignition has been achieved. Ideally, the ignition-detection system should be capable of instantaneous, 100%-reliable ignition detection—detection so rapid that, proper ignition not achieved, the engine can be shut down safely. With such a system, the start sequence can proceed only after receipt of an "ignition OK" signal. In practice, however, ignition reliability typically exceeds the reliability of the ignition-detection system. The resultant decrease in reliability caused by combining a high-reliability ignition system with a less-reliable detection system is only acceptable for high-reliability, "ground-level" ignitions, in which an erroneous engine shutdown can be tolerated. Such systems have proven valuable for development and acceptance testing.

Ignition-detection systems are not tied into engine-start logic for upper-stage or space-based applications, where an erroneous engine shutdown would cause loss of mission. When ignition-detection systems cannot be included in operational engine sequencing, they can be used in preflight ground-test safety systems, and the "ignition OK" signal can be monitored during flight to further build a reliability database.

In one form or another, the engine designer must provide means for ignition detection. A survey follows of several which have found operational application.

Visual detection. For the V-2 and the early U. S. Redstone missiles, visual observation by the test conductor was the ignition detector. Man was the interlocking device and would initiate the next sequence step only if, in his judgment, ignition was adequate. This simple procedure was satisfactory because these early systems employed a prestage, during which the main propellants were admitted at low tank-head pressures. The resulting relatively-low flowrates were then increased by starting the turbopump after receipt of a "Prestage OK" signal.

With the increasing size of modern rocket engines, visual observation became unreliable. The type of installation of these systems in static-firing stands and on launch pads made direct observation difficult. Furthermore, improved igniters, developed to keep the ignition flame concentrated where it should be, i.e., at the injector face, resulted in little or no visible fire emerging at the chamber exit. With the disappearance of the prestage step, the visual problem increased, because the large amount of oxidizer present in full-flow ignitions shrouds the ignition flame. Means had to be found to detect ignition by other methods.

Optical detection. Ground-mounted optical devices can be moved close to the chamber exit. A number of types have been investigated, such as simple light- or infrared-sensitive cells. They were found to be subject, however, to the limitations mentioned for human observers. It is possible to mount the optical devices in the chamber wall facing toward the inside near the injector face; but the devices then become vehicle-mounted and require interfaces to ground-support equipment. Also, "windows" in the chamber wall represent undesirable discontinuities that impact heat-transfer continuity and pressure-seal integrity.

Pyrometers. Heat-sensitive pyrometers are closely related to the optical devices and are subject to the same limitations.

Fusible-wire links. For many applications, fusible-wire links prove simple and reliable devices. A wire is strung across the chamber exit, which, when fused by the ignition flame, interrupts a circuit and signals "Ignition OK." Proper selection of wire gage, material, and distance from the chamber exit and/or center, will give some quantitative judgment. The wire can be ground-mounted or chamber-mounted. It must be isolated and should have spring loading, like fuses, to ensure positive separation.

Wire links have a number of shortcomings. The fused-wire ends may touch other metal parts and thus reconnect the circuit before the relay drops out. Suitable circuitry and mounting must therefore be applied. If a pyrotechnic igniter is used, the wire can be broken by inert particles or even by a dud igniter coming out of the chamber, giving an incorrect "ignition OK" signal. This has been overcome by providing redundancy, with several wires in parallel, all of which must be broken before the sequence can proceed. In another design, the wire is mounted as a loop in a groove on a wooden or plastic stick. It is thus supported against all reasonably expected mechanical damage and adequate insulation is maintained after fusion.

Pressure-sensing devices. Because of the need to mount the fusible wires at the exit of the thrust chamber, they are subject to some of the limitations noted for visual and optical methods. It has, therefore, been attempted to sense the pressure rise in the combustion chamber resulting from the burning igniter flame. Since the pressure rise is small (a few psi at best), however, reliable discrimination is difficult. Further, the transducers must be able to withstand the much higher pressures during subsequent mainstage. Pressure-sensing devices, however, do have potential for multistart engines.

Resistance wires. Another method designed to overcome the shortcomings of fusible-wire links applies resistance wires. Constructed like a glow plug and connected to a bridge circuit, the resistance wire signals by a distinct change in resistance the presence or absence of ignition. The art is to find *the* spot in the thrust chamber or gas generator that experiences a clear temperature rise as a function of ignition, yet remains cool enough to prevent fusion of the wire. Resistance-wire sensors are ideally suited for repeatable-start engines.

Indirect methods. In conjunction with hypergolic-slug ignition, other approaches to ignition sensing have been developed. In one design, an electric contact ensures that a cartridge is actually installed. This does not ensure, however, that the cartridge is loaded or completely loaded, or that the downstream lines are not clogged, or that the diaphragms will burst. Weighing the cartridge and purging all lines must be included in the firing preparation.

In another arrangement, a switch senses pressure buildup in the igniter injection line upon rupture of the burst diaphragms of the hypergolic-fluid cartridge. The switch signal then initiates the next sequential step. A modification of the system substitutes a pressure-actuated valve for the switch with similar effects. This method does not ensure, however, that the cartridge is properly filled with the right amount of the correct fluid.

Spark igniters are monitored to verify that the plugs are sparking, based on electrical-circuit performance in the ignition exciter. Ignition-monitor circuits are commonly designed to verify spark rate at the exciter and to indicate the amount of energy being delivered by the exciter. Operation of the plug is dependent on electrode design, electronic-circuit design, and gas composition, temperature, and pressure at the tip. High chamber pressure will quench the sparks by preventing arcing at the sparkplug tip. With a properly designed monitor circuit, the health of the electronic subsystem can be checked before engine start, and the spark system can be monitored during start to verify spark quench within a predetermined chamber-pressure range.

A technique that has proven useful for ignition detection monitors the chamber pressure-to-flowrate ratio to determine when ignition occurs. Obviously, this technique is of use only in systems in which flowrates and pressures can be accurately measured during start. The method has been successfully incorporated during static testing and has proved generally useful when the necessary parameters are monitored.

The methods in the above list, which undoubtedly is not complete, are described as indirect because none of them directly and reliably detects ignition, i.e., the release of adequate heat. This is a drawback and cannot entirely be offset by weighing, certifying, and inspecting.

4.8 COMBUSTION INSTABILITY

"Combustion instability" is defined in terms of the nature of pressure fluctuations in the combustion chamber. Chamber-pressure fluctuations are always present during normal, stable operation of a rocket-engine system. They are usually quite random, showing frequency spectra that are essentially continuous in nature, with few, if any, recognizable peaks. In unstable combustion, however, large concentrations of vibratory energy appear at one or more frequencies in the spectrum and can easily be recognized against the normal random-noise background.

Stable operation is a design prerequisite for rocket-engine combustors because high-frequency combustion instabilities carry the potential for serious damage and catastrophic engine failure. Low-frequency instabilities can interfere with vehicle operation or damage instrumentation. In a few instances, vehicles have been lost due to combustion instability during flight. In most cases, combustion-stability issues will be resolved during engine development, although considerable resources may be required. Experience has shown that no engine type or propellant combination can be considered inherently stable.

Stability can be affected by the configuration of the engine-feed systems, injector, and thrust chamber as well as by operating conditions. Hence, it is important to address the issue of combustion stability, as well as engine performance, during the early stages of engine design, before any required modifications become difficult to implement. For example, combustion stability may be improved by the addition of damping devices such as baffles or cavities, but they must be integrated with the injector and the propellant manifolds. Modification of the injector pattern may enhance stability but may also affect combustion performance and combustor heat-loads.

To verify the stability margin of a given combustor design, a stability-rating test program should be conducted. Occurrences of combustion instability can be detected during engine operation by use of high-frequency pressure transducers and accelerometers. The level of disturbance significant enough to be considered a combustion instability is not well defined. CPIA Publication 247, "Guidelines for Combustion Stability Specifications and Verification Procedures for Liquid-Propellant Rocket Engines," suggests that sustained oscillations with peak-to-peak amplitudes greater than 10% of the steady-state chamber pressure are generally considered as constituting combustion instability. However, that same document also indicates that oscillations of 3-5% of chamber pressure may be unacceptable in specific engine systems. Stability-level criteria for accelerometers depend on transducer installation and the structural dynamics of the combustor and facility. Within milliseconds combustion-instability oscillations usually grow to substantial fractions or even multiples of the steady-state chamber pressure. When this occurs, the engine must be cut off promptly to minimize damage to combustor hardware.

Types of Instability

Most instability oscillations can be classified as being of one of two fundamental types: acoustic-high-frequency or low-frequency. Sometimes, intermediate-frequency, low-amplitude instabilities are distinguished as a third type, to which the term "buzz" has been applied. Buzz instabilities are feed-system coupled and are characterized by wave motion in the chamber at a frequency below that expected for an acoustic chamber mode. Such activity has been detected during transients, such as engine start, when chamber acoustic conditions are not well defined. It is possible that some occurrences of buzz may actually be high-frequency instabilities at off-design operating conditions.

For simplicity, this section will focus on low- and high-frequency instabilities, describing the influential design parameters and typical design and developmental test approaches used to gain stability. For a more detailed description of instability characteristics and analysis procedures, consult NASA SP-194, "Liquid Propellant Rocket Combustion Instability."

Acoustic-mode instabilities can be divided into two categories: the "intrinsic acoustic mode," in which the propellant-injection flow oscillations are negligibly small, and the "injection-coupled acoustic mode," in which the propellant-injection flow oscillations play an essential role. That is, intrinsic acoustic stability is determined by coupling between the propellant burning process and the chamber acoustics, while injection-coupled acoustic stability is determined by coupling between the propellant-injection process and the chamber acoustics. The frequency of acoustic oscillations in a combustion chamber is a function of the gas sound speed and the chamber geometry. Because of great differences in combustor geometry it is not appropriate to identify the mode of an instability solely on the basis of the frequency of the oscillation.

High-frequency instabilities cause acoustic modes that closely match those of a closed cylindrical volume. For proper remedial action, it will often be important to know which mode the oscillation is exhibiting. The modes can exist either as standing waves or traveling waves. The characteristic frequencies of standing waves in a cylinder can be determined from classical acoustic theory. Tangential, radial, and longitudinal oscillations can exist in a combustor as pure or combined modes. The chamber acoustic frequencies, f_{ijk}, corresponding to these modes, can be approximated by the following equation:

$$f_{ijk} = A_c[(a_{ij}/d_c)^2 + (k/2L_c)^2]^{0.5} \qquad (4\text{-}49)$$

where i, j, and k are the tangential, radial, and longitudinal mode numbers; a_{ij} is the i-j mode eigenvalue; L_C is the chamber length; A_C is the chamber acoustic velocity; and d_C is the chamber diameter. The chamber, injector, and nozzle convergence promote "closed-closed organ pipe" type of longitudinal modes. The effective length for longitudinal modes is somewhat less than the actual chamber length because of the gradual contraction in the chamber diameter near the nozzle-throat inlet. Figure 4-76 illustrates several chamber acoustic modes.

Typically, the acoustic velocity predicted by equilibrium chemistry for conditions of complete combustion is used to calculate theoretical frequencies. However, many situations can induce acoustic velocities (and hence transverse-mode frequencies) that are significantly different from those indicated by equilibrium results. Standing

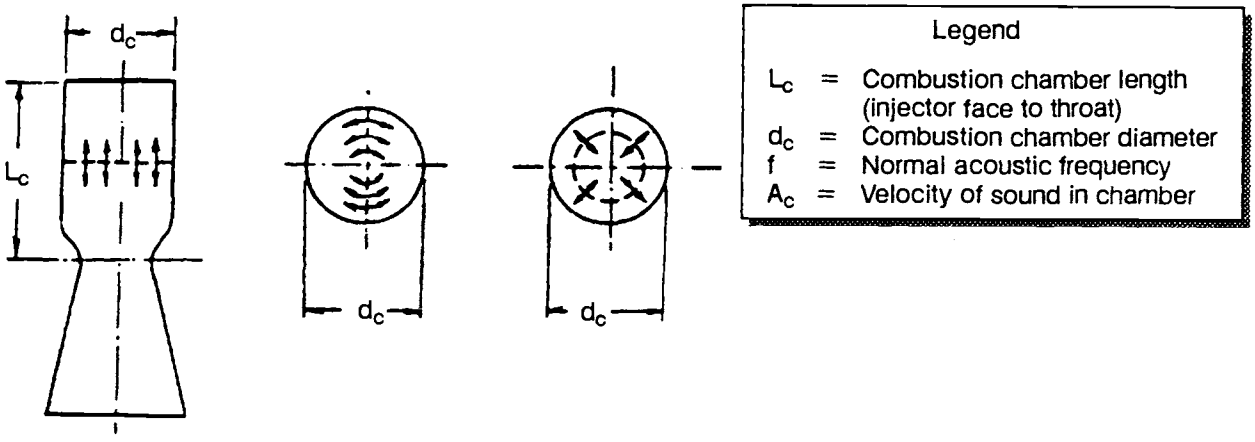

Fig. 4-76 Three modes of instability.

waves give rise to characteristic chamber-wall pressure distributions that can be used to identify the mode even when the observed frequency does not correspond to an expected value. For example, the first tangential mode produces two circumferential locations of maximum fluctuating pressure amplitude and two locations at which the pressure does not vary. High-frequency pressure instrumentation is usually installed at various circumferential locations to take advantage of this fact.

Transverse instabilities may also take the form of traveling or "spinning" waves. A spinning wave travels around the circumference of the chamber. Careful placement of multiple high-frequency pressure transducers can detect and help identify this mode.

Generally, tangential modes have been found to be the most severe with respect to damage potential. Quite often, the first tangential mode of a combustor is the critical one to be stabilized. Severe damage and catastrophic failure have been observed in tens to hundreds of milliseconds of a tangential-mode instability. Tangential modes tend to exhibit maximum pressure fluctuations in the region of the injector face. Often, when fully developed, these modes exhibit steep-fronted waves with peak-to-peak amplitudes equivalent to a large fraction of the chamber pressure. Longitudinal waves are characteristically much less damaging. Test combustors are usually equipped with "rough-combustion cutoff devices" that sense the amplitude and duration of the oscillations and cut the test promptly when preset criteria are exceeded.

As indicated earlier, liquid-propellant-engine combustion instability can also occur in nonacoustic (low-frequency) modes. These modes exhibit uniform chamber-pressure oscillations, without acoustic-wave effects, and are usually referred to as "chugging" modes. Chugging instability is characterized by coupling between the propellant-feed system and injection flow oscillations and the lumped chamber-pressure oscillations.

There are two general methods by which combustion instability may be avoided: alter the basic design of the combustor to eliminate any coupling mechanisms that might cause an instability, and install damping devices in the combustion chamber to inhibit unstable combustion.

Intrinsic Acoustic Instabilities

The combustion process is controlled by liquid-propellant atomization, vaporization, mixing, and chemical kinetics. The combination of these processes defines the rate-controlling mechanism of an intrinsic instability. In rate control, one of the processes may require a significantly longer time to complete relative to the others. The Rayleigh criterion states that if energy is added to an oscillation during the high-pressure phase of the cycle, the wave will be reinforced and grow. Therefore, the burning rate controls the phasing between the mass production of product gas and the low-amplitude white noise that always exists in a combustor. Just the right phasing may cause an instability.

Although the mechanisms involved in the combustion process are well defined, the physical processes are complex. The problem is further complicated when wave-induced mixing and droplet deformation and drag are included. There are, however, trends associated with combustor design and operating conditions that should be considered during the design process. First is the injector type, which is usually a concentric tube (coax) or an impinging element. The combustion process of the coax element tends to be distributed more throughout the chamber relative to most impinging injectors. Such distributed energy release has a stabilizing effect. Intrinsic stability is also affected by the mass-flux distribution, which is a function of the injection pattern.

The atomization process strongly depends on injection-element design in both coax and impinging injectors. The atomization process of a coax element

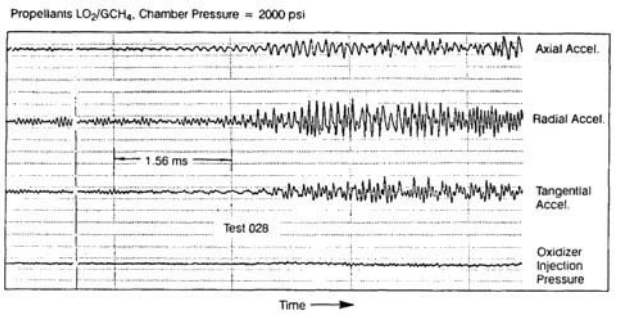

Fig. 4-77 Injection-coupled acoustic instability.

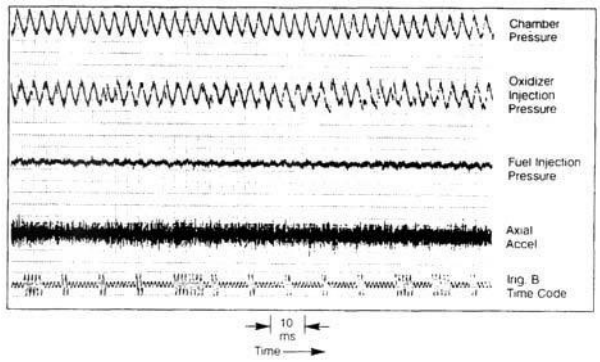

Fig. 4-78 Typical chug instability.

is enhanced as the velocity difference between the gaseous fuel and liquid oxidizer jet is increased, but some data suggest that the degree of atomization may degrade if the velocity difference becomes very large. The atomization process of an impinging element strongly depends on the liquid-stream diameters, the kinetic energy of the propellant streams, and the impingement angle. Consequently, orifice size and injection velocity can greatly affect the atomization rate. Liquid-propellant vaporization rates are strong functions of chamber pressure, increasing with increasing chamber pressure. Interelement mixing is more significant with a like-impinging element than with a coax element.

As the overall burning rate increases, a decrease typically will be seen in the stability margin of a combustor. Unstable combustion is usually associated with high performance, but this is not universally true.

Injection-Coupled Acoustic Instability

Injection-coupled acoustic instability is typically characteristic of a coax element for acoustic modes. Both impinging and coaxial injectors may exhibit low-frequency (nonacoustic), injection-coupled instabilities. The rate-controlling processes of an injection-coupled instability are the pressure and flow oscillations in the feed system due to hydraulic resonance. The center tube of a coax element is prone to organ-pipe resonance. If the resonant frequency of the element coincides with an acoustical-chamber mode, an instability may occur. The combustion process is important in this case, since coupling must occur, but the dominant rate-controlling process is the feed-system oscillation. This instability can be minimized by designing the injector so that feed-system flow resonances do not coincide with chamber resonant modes. If this cannot be accomplished, the feed-system gain should be reduced by increasing the feed-system pressure drop.

Pressures and acceleration levels of an acoustic instability attributed to injection coupling are shown in Fig. 4-77 for a coax-element injector with LO_2/GCH_4 propellants at 2000-psi chamber pressure. As shown in the figure, the instability produces a complex waveform, with the dominant mode being the first tangential. Also as shown in the figure , the accelerometers respond to the instability, but close examination is required to determine the frequency content. Typically, the accelerometers are used as rough combustion transducers. The final parameter shown in Fig. 4-77 is the oxidizer-manifold pressure, which also responds to the unstable combustion.

Low-Frequency Instabilities

Chugging has often been associated with the quality and promptness of ignition of the entering propellants. Ignition processes include "flame-holding characteristics," "combustion lag-times," and "flame-propagation velocity." These processes are related to an excessive accumulation of unburned fuel, with subsequent detonation or cyclic higher-rate combustion. The resulting chamber-pressure spikes cause a reduction, or even reversal, of the propellant flows and a consequent rapid collapse of chamber pressure, allowing propellants to rush in and repeat the cycle. The physical dimensions of the combustion chamber and propellant ducts and the magnitude of the propellant flowrates and their mixture ratio play critical roles in the phenomena of low-frequency system oscillations.

Pressure and acceleration levels of a typical chug are displayed in Fig. 4-78. Note that the chamber and feed-system pressure oscillations are at the same frequency and show a constant phase difference that is indicative of the combustion lag-time.

Chugging occurs most frequently during start or shutdown of an engine system or at off-rated operating conditions. Also, thrust levels too high or (particularly) too low may lead to chugging. The latter is important in systems requiring throttling to a lower-than-rated thrust level during flight; for them chugging may occur when the resistances drop between the propellant manifolds and the combustion chamber. If sustained, chugging can cause performance losses attributable to widely fluctuating mixture ratios. Another phenomenon involves the transition of a chug instability to an acoustic mode. Although a chug instability may damp with increasing chamber pressure, it still may excite an acoustic instability. Short pressure-ramp times during engine operation may eliminate this problem.

Prevention of Triggering Mechanisms

The best method of controlling instability is to prevent the occurrence of the physical or chemical processes which trigger and sustain the instability. While a great number of studies have been carried out in which different parameters were varied systematically, the results have failed to yield truly generalized design criteria. This can be traced to the fact that the basic processes that trigger and sustain the various types of instability are complex and highly coupled. Thus, although a design parameter or criterion which controls one type of instability may have been established, this same parameter may enhance another type of instability.

Propellant-Feed-System Design

As indicated in the foregoing discussion, certain combustion instabilities are sustained through an interaction between feed-system and combustion dynamics. Since hydraulic resonances are a major factor in sustaining this type of instability, it is necessary to design a feed system with hydraulic characteristics that will not trigger the interaction with the combustion process. In particular, for coaxial injectors, the center tube must be designed so that its longitudinal modes do not coincide with chamber acoustic modes. The feed-system hydraulic resonances must be determined and must not coincide with chamber resonances. For acoustic and low-frequency (chug) stability, the stability margin increases with increasing injection pressure drop. Also, for low-frequency stability, reduced manifold volume tends to improve stability.

Combustion-Chamber Design

Analytical studies and experimental results have indicated that the geometrical configuration of the combustion chamber governs the frequencies of acoustic modes of instability. Chambers with large length-to-diameter ratios appear to be more prone to large-amplitude longitudinal instability than shorter-length chambers. On the other hand, chambers with small length-to-diameter ratios appear to be more sensitive to the transverse modes, relative to the longitudinal modes of the combustor. Also, with a given injector-element pattern, small-diameter chambers are more stable than large-diameter chambers. Damping devices will be required if the inherent damping of the chamber can not overcome the associated gain of the combustion process,.

Injector Design

Injector design is a most critical factor governing the mechanisms associated with instability. In turn, it offers great potential for controlling instability-triggering processes through variation of parameters. Several injector design parameters can be associated with the combustion rate and, consequently, the stability characteristics of the combustor. For example, there is some indication that longitudinal instability may be promoted if the times for propellant to travel from the injector face to the point of impingement is close to the half-period (or an odd multiple of the half-period) of the longitudinal-mode oscillations. Also, liquid-liquid injectors show strong indications that increasing the injection pressure drop to too great a value may cause unstable combustion in the transverse acoustic modes. Injection pressure drop has opposite effects on longitudinal feed-system-coupled acoustic modes and on hydrodynamic instabilities, for which stability improves as injection pressure drop increases. Other injector design parameters that may affect stability include propellant injection velocities, flow areas, and mass distribution across the injector face.

Propellant Combination and Mixture Ratio

Control tests with various propellants have shown that some oxidizers or fuels can be triggered into instability more easily at certain mixture ratios. In LO_2/LH_2 systems, reducing the hydrogen temperature tends to trigger instability.

Engine-System Operating Characteristics

In some cases, combustion instability can be avoided by modification of engine-system operating characteristics. For instance, an excessively long chamber-pressure buildup during engine start may give a chugging instability time to develop. A start sequence with a faster chamber-pressure buildup may eliminate this instability.

Application of Damping Devices

Special damping devices can enhance stability margin in the combustion chamber and engine system. Baffles, divergent wall-gap, and acoustic cavities have been applied with good results.

Injector Baffles

Injector baffles have been found to be effective in suppressing transverse acoustic modes of combustion instability. This effectiveness has been demonstrated with various propellant combinations in full-scale thrust chambers and small-scale models. Such baffles are usually designed to be secured to the injector face (Fig. 4-51). The major components of the baffles are the radial blades and the hub. The radial blades begin near the center of the injector and extend radially outward. The baffle hub is the

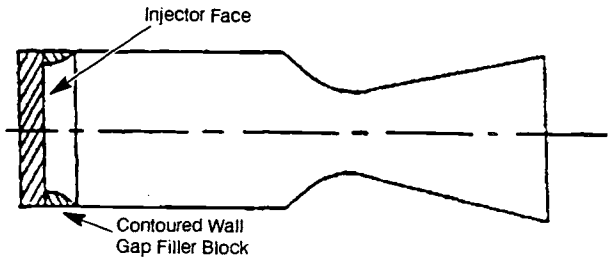

Fig. 4-79 Combustion chamber divergent wall gap.

constant-radius portion of the baffle. As shown in Fig. 4-51, the radial blades may extend outward from the baffle hub. A simple rule may be applied to determine the number of baffles needed to inhibit transverse-wave motion. This rule states that (2n + 1) blades are required to inhibit the n^{th} tangential mode. For a radial mode, n hubs are required to inhibit the n^{th} radial mode. No longitudinal-mode stability enhancement can be gained by use of baffles. Adequate cooling should be provided to keep the baffles from burnout. The height of the baffles is related to the distance of the flame front from the injector face and to the chamber diameter.

Chamber Divergent Wall Gap

It has been found experimentally that, for liquid-liquid injectors, a blank annular portion of the injection area adjacent to the combustion-chamber wall (Fig. 4-79) improves the ability of the combustion chamber to recover from triggered instabilities. It was further determined that, in many cases, filling this wall gap with a contoured filler block drastically improved stability. The exact shape of the contour is critical. Experimental evaluations are required to determine the most effective design configuration.

Acoustic Cavities and Liners

Another device effective in eliminating organized combustion noise has been the acoustic cavity. Arrays of Helmholtz resonators (a particular type of acoustic cavity) were first incorporated into air-breathing combustors, such as turbojet engines, to eliminate combustion and turbomachinery noise. These arrays, also known as acoustic liners, extend axially from the injector around the radial periphery of the combustor. Because of high heat-transfer rates, single-cavity rings tuned to specific chamber modes have seen wider use. Unlike baffles, acoustic cavities are not necessarily mode-dependent devices, but can be tuned to specific frequencies. The cavities typically have a radial or axial orientation (Fig. 4-80). The required resonant frequency and the sound speed in the cavity dictate its physical dimensions. The local sound speed in the cavity, however, is difficult to predict and usually requires experimental fine-tuning. Quite often, cavity tuning includes more than one frequency. If the combustion process has a wide bandwidth, several acoustic modes may be eliminated with a multiple-tuned cavity configuration. One drawback of using acoustic cavities is that they may be too large physically for some combustors. In this case, a combination of acoustic cavities and baffles may be required to obtain stable combustion.

Stability Rating

It is desirable to establish the combustion-stability characteristics of a particular engine system or combustor without an excessive number of tests. In most cases, it is possible to accomplish this by perturbing and observing the response of a normally stable combustor. In other cases, combustion stability may prove sensitive to the injector operating conditions, and so the combustor will be operated over a wide range of conditions to determine its spontaneous stability characteristics.

"Dynamic stability rating" is defined in NASA publication SP-194 as a methodology aimed at determining the response of a combustor to a transient in system operation. Dynamic stability is demonstrated when the combustor returns to stable, nonoscillatory combustion after such a transient. A transient may consist of some artificial variation in the propellant flows or a pulse directly applied to the combustion process.

Feed-System Disturbances

Two methods have been used to produce a transient in one or both propellant flows: continuous-oscillation generators and single-pulse devices:

Continuous-oscillation generators. This category includes piston-type pulsers and sirens that produce continuous, relatively-low-amplitude pressure perturbations. Generally, this method has been applied to evaluate low-frequency-stability characteristics of engine systems.

Single-pulse devices. The single-pulse device generates high-amplitude pulses in the feed system, typically by a gas- or explosive-driven single-pulse piston. Like the continuous oscillation technique, the single-pulse device has been applied to evaluate low-frequency feed-system-coupled stability characteristics.

Combustion-Chamber Disturbances

The principal methods used directly to perturb the combustion process are directed explosive pulses, nondirected explosive pulses (also known as stability-rating "bombs"), and directed nonexplosive gas-flows (Fig. 4-81). The first two approaches have seen the widest application.

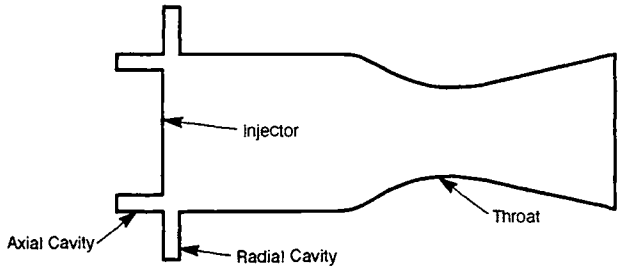

Fig. 4-80 Radial and axial acoustic cavities in combustion chamber.

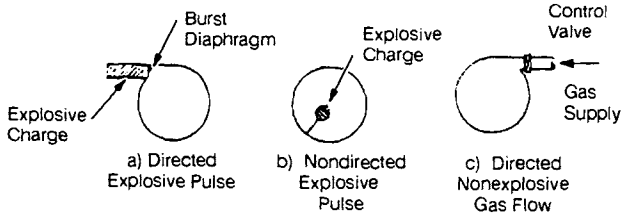

Fig. 4-81 Combustion chamber perturbation methods.

Criteria have been proposed for the range of pulse overpressures required to demonstrate combustion-stability characteristics. CPIA Publication 247 recommends stability rating with pulses of 10-100% of chamber pressure. Test experience indicates that instabilities can be successfully induced with overpressures significantly lower than 100% of chamber pressure.

Directed pulses. The directed-pulse method of inducing instability, as shown in Fig. 4-81a, mounts a solid-propellant- or high-explosive-loaded shock tube to the combustion chamber in such a way that the shock wave enters the chamber with any desired orientation.

Nondirected explosive pulses. A nondirectional explosive pulse (Fig. 4-81b) gives the closest simulation of localized, random detonation that can occur during normal operation because of accumulation of unburned propellants. A high-explosive charge assembled into a composite ablative case designed to withstand the combustion-chamber environment through the period of the start transient and into mainstage forms the pulse device. It is mounted in the desired place and detonated during chamber operation. It can be designed to be initiated electrically or by heat that is generated by the combustion process. Electrically-initiated devices can precisely control the pulse-sequence time. This is important for combustors sensitive to pulsing during engine start or at a particular operating condition. Thorough stability rating may involve use of a variety of charge sizes installed at several radial and longitudinal locations within the chamber.

Figure 4-82 shows a bomb-induced instability during a test of a coaxial injector. Note that the disturbance initially decays before growing to full amplitude. Unstable liquid-liquid injectors often exhibit full amplitude at and after the bomb pulse.

Directed nonexplosive gas-flows. In this method (Fig. 4-81c), a fast-acting valve controls a flow of gas from a regulated high-pressure source. This valve is placed as near to the chamber as possible.

Spontaneous-Instability Methods

As stated earlier, dynamic-stability rating may not be feasible with some engine systems. Other situations may arise in which the combustor appears to be more sensitive to naturally-occurring, finite-amplitude disturbances or exhibits a tendency to spontaneous instability. In such cases, a test program can be developed to demonstrate the statistical (spontaneous) stability of the engine or combustor. The test matrix should include a large number of tests at the widest possible range of operating conditions. Additionally, stability aids such as baffles and cavities may be systematically modified or removed to determine the margin of stability of the unmodified combustor. Pulsed engines are typically rated in this fashion, since, the cost per test being low, a large number of tests can be carried out during development.

A method efficient from the standpoint of the number of tests required involves fuel-temperature ramping, until either the combustor develops a high-frequency instability or the facility-limited minimum fuel temperature is reached. This stability-rating technique has been applied to coaxial injectors with gaseous fuels. It exhibits a high degree of repeatability with respect to the temperature at which the combustor goes unstable. Hardware ranging from research combustors to full-scale thrust chambers has been successfully rated by this technique, which may require modifications of the test facility to control the fuel temperature.

A stability-rating program often will be conducted with hardware of various size and configuration. Rather than risk loss of full-scale, flight-type combustors or engine systems in the event of an instability, lower-thrust, subscale combustors can be used during initial testing. Typically, the injector-element configuration and the number of elements per unit area are close to the full-scale design. The combustor may be cylindrical or two-dimensional (slab-type). The stability characteristics of a low-thrust cylindrical combustor can be used to develop stability correlations and anchor stability analyses, as well as to verify combustion performance. The width of a two-dimensional combustor can be adjusted so that it will support transverse instabilities in a range of frequencies characteristic of the full-scale design.

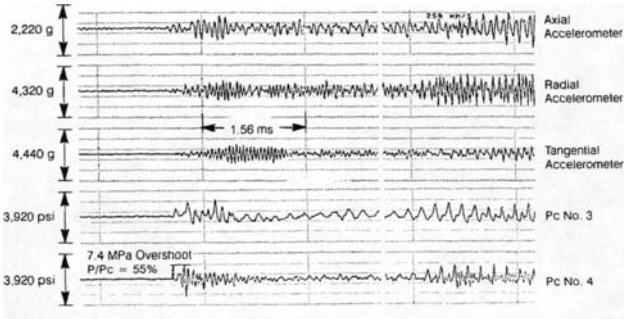

Fig. 4-82 Bomb-induced instability data, coaxial injector.

Instrumentation

High-frequency instrumentation characteristics and locations critically affect prompt combustor shutdown in the event of an instability and the attempt to determine the nature of the instability. Generally, the sensitive bandwidth of the high-frequency transducers and the recording system should permit determination of the frequency and amplitude of oscillation over the first few high-frequency modes.

High-frequency pressure transducers provide definitive evidence of the stability of the combustor. Pressure transducers should be installed to permit identification of at least the first few modes of acoustic instability in the chamber. Consideration should also be given to the fact that these modes may occur in any orientation. In general, transducers should not be installed diametrically opposite one another, because a pressure nodal line of a standing-wave instability could orient itself at the transducer,

so that little or no pressure oscillation would be measured. High-frequency pressure transducers should also be mounted in the combustor manifolds to permit assessment of feed system coupling.

Accelerometers are useful in providing backup to chamber-pressure transducers. In some cases it may not be possible to install high-frequency pressure transducers on the chamber because of chamber-cooling requirements. "Rough-combustion cutoff" control methods frequently depend on oscillation level and duration measurements by accelerometers. Ideally, accelerometers that can sense all three axes of motion should be installed on the combustor to measure the full response of the hardware to propellant flow and combustion disturbances.

Although accelerometers are quite useful for measurement of instability, some care is required in interpreting the indicated results. The sensitivity of accelerometer measurements to the structural dynamics of the combustor system and to mounting locations makes it difficult to establish the level of oscillation that corresponds to an instability. In addition, care must be taken in determining whether the observed spectra are the direct result of an instability or simply of hardware structural resonances. In some extreme situations, accelerometers may not sense the occurrence of an instability. Most often, however, a large-amplitude instability will be obvious on all accelerometer channels at a frequency matching that of the pressure oscillations.

In addition to high-frequency transducers, thermocouples should, if possible, be installed in the backing volumes of acoustic cavities to permit verification of the assumed cavity temperatures used to size the cavities. This information is useful for retuning (resizing) the cavities to improve stability.

Chapter 5

Design of Gas-Pressurized Propellant Feed Systems

Transfer of the rocket propellants from the tanks to the thrust chamber at the needed flow rates and pressures, requires a suitable feed system. Its selection will depend on the vehicle's accelerations, maneuvers, and weight, the thrust level and duration, vibration levels, the envelope available, the type of propellants, reliability, and cost. There is no simple rule for the choice between a gas-pressurized and a turbopump feed system. Typically, systems with small propellant quantities have gas-pressurized propellant tanks because the weight penalty to design the propellant tanks at a high pressure is not significant compared to the complexity of a turbopump feed system. Alternatively, weight considerations require that large systems utilize low-pressure propellant tanks with the propellant pressure increased downstream by pumps. With advancements in the state of the art of high-strength propellant tank materials and small, reliable turbopumps, the upper limit of gas-pressurized propellant tanks has been expanded and the lower limit of pump-fed systems has been reduced, resulting in considerable overlap of their applicabilities. It should be noted, however, that even pump-fed systems normally require some type of low-level pressurization of the propellant tanks to minimize pump requirements.

Classified according to source of gas, four major types of pressurized feed systems can be distinguished:

- Stored gas
- Propellant evaporation
- Nonpropellant evaporation
- Chemical reactions

The following factors must be considered when selecting a pressurization gas:

- Mission requirements
- Compatibility of pressurant gases with propellants and tank materials, considering chemical interactions, temperature, and solubility
- Pressurization-system reliability
- Pressurization-system cost
- Pressurization-system weight and size

5.1 DETERMINATION OF PRESSURANT REQUIREMENTS

The physical and chemical processes which take place during the expulsion of a liquid propellant from a tank by a gas or gas mixture are numerous and difficult to analyze. Even the simplest systems require simultaneous, time-dependent modeling of the fluid flow and heat transfer. Applicable experimental data for a selected system are often limited. Thus, the basis for the analytical approach is frequently narrow and uncertain. As a result, the initial design calculations of the quantity of pressurant gas required must be considered approximate until verified experimentally. The refinement of the analytical approach to minimize discrepancies between theoretical predictions and actual test results is an art requiring experience and thorough understanding of the physical processes. Basic considerations and necessary procedures for the calculation of pressurant requirements are described below.

Required System Data

Before starting calculations of pressurant requirements, the following operating parameters must be known or assumed:

- Operating temperature ranges of the feed-system components and fluids
- Propellant properties, weights, and corresponding volumes at the extremes of the operating temperature range and loading accuracy
- Tank volumes: nominal values, tolerances, and variations due to temperature and pressure
- Initial ullage. ("Ullage" means portion of a propellant tank not occupied by liquid.)
- Trapped-propellant volumes at the end of expulsion
- Operating propellant-tank pressure: nominal value and variations
- Mission duration and engine firing times

To avoid later marginal conditions, calculations should assume worst-case parameter values.

Factors Influencing Pressurant Requirements

Several important factors that will influence the final state of the pressurant gas, and thus the required quantity, may be summarized as follows:

1) Propellant vaporization. Propellants evaporate to various degrees from the gas-liquid interface within the tank. The amount depends upon the volatility of the propellant, the temperature of the pressurant gas, the turbulence of the gas, the sloshing of the liquid, the tank's internal structural geometry, and the rate of propellant expulsion. To the degree that vaporization takes place, it lowers the temperature of the ullage gas and adds propellant vapor as a component of the pressurant gas. Also, as the propellant level recedes, a film of liquid may be left on the tank wall, further contributing to propellant evaporation.

2) Tank wall temperature. If the pressurant gas is hotter than the propellant-tank walls, it will cool and the wall will heat up. Alternatively, aerodynamic heating of the propellant-tank walls may cause heating of the pressurant gas. It may also heat the propellant and thus increase vaporization effects and raise NPSH requirements in turbopump-feed systems.

3) Vapor condensation. Certain components of the pressurant gas, such as water vapor, may condense. Even if the bulk of the gas remains above the dew point for the condensible component, local condensation may occur at the tank walls or at the propellant surface.

4) Solubility of the pressurizing gas. If the pressurant gas contains components soluble in the propellant, these components may diffuse into it. Solubility usually will be affected by temperature and pressure.

5) Ullage-gas compression. If, before pressurization of the propellant tank, the ullage space is filled with low-pressure gas, pressurization will cause adiabatic compression. This can raise the ullage-space temperature considerably during the initial few seconds of operation.

6) Chemical reaction. If any components of the pressurant gas are chemically reactive with the propellant, the reaction products may become a component of the gas.

7) Pressurant-gas turbulence. The heat exchange between the pressurant gas and propellant can be extremely large if the gas is permitted to agitate the liquid-propellant surface. This effect can be prevented through the use of a diffuser that spreads the gas in a gentle flow at the top and sides of the tank.

Design Calculations of Pressurant Requirements

If the system operating duration is relatively short, or if the pressurant temperature is close to the propellant and hardware temperatures, heat transfer and pressurant/propellant mass-transfer effects can be neglected. The required pressurant weight in the propellant tanks can then be calculated, as follows:

$$W_g = \frac{P_T V_T Z}{R_g T_g} \qquad (5\text{-}1)$$

where—

W_g = required pressurant weight in the propellant tanks, lb
P_T = maximum propellant tank pressure, lb/ft^2
V_T = max. volume of propellants expelled, ft^3
R_g = gas constant of the pressurant, ft-lb/lb-°R
T_g = mean temperature of entering pressurant, °R
Z = compressibility factor

However, in cases where longer system durations and higher pressurant temperatures are involved, the pressurant requirement can best be determined by the following procedure, keeping in mind the limitations set forth at the beginning of section 5.1.

Consider first a single-start operation (not requiring coast periods and restarts) and neglect heat transfer from the tank walls. The total heat transferred from the pressurant gas to the vaporized propellant can then be approximated by Eq. (5-2):

$$Q = HAt(T_u - T_e) \qquad (5\text{-}2)$$

where—

Q = total heat transferred, Btu
H = experimentally determined heat-transfer coefficient at the gas-liquid interface, Btu/s/ft^2-°R
A = area of the gas-liquid interface, ft^2
t = operating duration, s
T_u = temperature of gas at end of expulsion, °R
T_e = temperature of the propellant, °R

Both T_u and T_e are treated as constant values at the interface between liquid and gas.

This heat, Q, is assumed to have heated and vaporized the propellant according to the following equation:

$$Q = W_v[C_{pl}(T_v - T_e) + h_v + C_{pv}(T_u - T_v)] \qquad (5\text{-}3)$$

where—

W_v = total weight of vaporized propellant, lb
C_{pl} = specific heat of liquid propellant, Btu/lb-°R
h_v = heat of vaporization of the propellant, Btu/lb
C_{pv} = specific heat of propellant vapor, Btu/lb-°R
T_v = vaporization temperature of propellant, °R

The value of W_v can now be obtained from Eq. (5-2) and (5-3) with an assumed value for T_u. The partial volume occupied by the vaporized propellant will be as follows:

$$V_v = \frac{W_v Z R_p T_u}{P_T} \qquad (5\text{-}4)$$

where V_v = total volume occupied by the vaporized propellant, ft^3; Z = compressibility factor evaluated at the total pressure P_T and the temperature T_u of the gaseous mixture at the end of expulsion; R_p = gas constant of the propellant vapor, ft-lb/lb-°R.

The propellant-tank volume remaining at the end of expulsion can be assumed to be occupied by the pressurant gas:

$$V_g = V_T - V_v \qquad (5\text{-}5)$$

where V_g = volume of pressurant gas at the end of expulsion, ft^3. The weight of pressurant will be calcu-

lated as follows:

$$W_g = \frac{P_T V_g Z}{R_g T_u} \tag{5-6}$$

To maintain the heat balance, the value for Q should satisfy the following equation:

$$Q = W_g C_{pg}(T_g - T_u) \tag{5-7}$$

where C_{pg} = specific heat at constant pressure of pressurant gas, Btu/lb-°R. From Eq. (5-7) the required value of T_g for the assumed T_u can thus be calculated. If, however, T_g is a predetermined fixed value, then the values of W_g, W_v, and T_u must satisfy the following as well as other correlated equations:

$$W_g C_{pg}(T_g - T_u) = W_v[C_{pl}(T_v - T_e) + h_v + C_{pv}(T_u - T_v)] \tag{5-8}$$

Thus far, heat transfer from the tank walls has been neglected. However, if there is a considerable temperature differential between pressurant gas, propellants, and tank walls, the total heat transferred between them during the mission must be taken into consideration to determine the quantity of vaporized propellant at the end of expulsion. Equation (5-3) can be rewritten as—

$$Q \pm Q_{W_1} = W_v[C_{pl}(T_v - T_e) + h_v + C_{pv}(T_u - T_v)] \tag{5-9}$$

where Q_{W_1} = total heat transferred between tank walls and liquid and gaseous propellant during the mission, Btu. The positive (+) or negative (-) sign indicates whether Q_{W_1} is from, or to, the tank walls. Furthermore, Eq. (5-7) becomes this:

$$Q = W_g C_{pg}(T_g - T_u) \pm Q_{W_2} \tag{5-10}$$

where Q_{W_2} = total heat transferred between pressurant gas and tank walls during a mission, Btu. Again the positive or negative sign indicates whether heat is from, or to, the tank walls.

Combining Eq. (5-9) and (5-10), the heat balance considering heat transfer from the tank walls can be written as follows:

$$[W_g C_{pg}(T_g - T_u)] \pm Q_{W_2} = W_v[C_{pl}(T_v - T_e) + h_v + C_{pv}(T_u - T_v)] - (\pm Q_{W_1}) \tag{5-11}$$

If the vehicle mission includes several powered-flight and coast periods, the calculation of the heat transfer across the gas-liquid interface should take the total mission time into consideration. Then Eq. (5-2) can be rewritten as follows:

$$Q = HAt_m(T_m - T_e) \tag{5-12}$$

where t_m = total mission time including powered flight and coast periods, s, and T_m = mean temperature of pressurant gases during the entire mission, °R. This is a function of many factors such as length of coast periods and heat transfer between gas and tank wall.

Other effects such as vapor condensation, solubility of the pressurant gas in the propellant, and chemical reactions of the pressurant gas with the propellant can be included; but, because of the complexity of the processes, it is usually necessary to make gross assumptions or use experimental data. Vapor condensation depends on gas-circulation patterns and contact with cooler surfaces. Solubility depends upon how vibration affects diffusion into the propellant. Chemical reactions depend on the fluids involved.

It is important to be conservative in determining the required pressurant. Inadequate pressurant will prematurely end the mission. If a cold gas is used, there may be significant cost and schedule impact to redesign the pressurant-tank volume or wall thickness for a higher pressure. The penalty for this conservatism is weight associated with a larger or thicker-walled tank.

In some cases, the uncertainties in pressurant system design can be reduced by providing adjustability of the pressurant temperature at the propellant-tank inlet. In this approach, the temperature of the pressurant gas at the end of expulsion is assumed or targeted from the beginning. Based on this and other given or assumed data, the values of required pressurant quantity and inlet temperature can be calculated by Eq. (5-1) through (5-11). If the required pressurant quantity based on test data deviates from the calculations, an adjustment of the pressurant temperature at the propellant-tank inlet can often be made to correct for this difference, such as through an adjustment of the pressurant supply from a heat exchanger or from a gas generator. The following sample calculation demonstrates this design approach:

Sample Calculation 5-1

Table 3-5 presents the following data for the oxidizer tank of the A-4 Stage propulsion system: oxidizer, N_2O_4; pressurant, gaseous He; tank volume V_T, neglecting the volume of residual propellant, = 119 ft^3; average tank cross-sectional area A = 20 ft^2; tank pressure P_T = 165 psia, or 23,760 psfa; and propellant temperature T_e = 520°R.

Problem

Calculate two cases, as follows:

(a) The total pressurant weight W_g and required temperature T_g at the propellant-tank inlet, for a single operation time t of 500 s, with an experimentally determined heat-transfer coefficient H at the gas-liquid interface of 0.002 Btu/s-ft^2-°R. Assume that the ullage-gas temperature T_u at the end of expulsion will be 700°R and that there is no heat transferred at the tank walls.

(b) The required pressurant weight W_g and temperature T_g at the tank inlet, for a mission consisting of several powered-flight and coast periods, with a total mission duration t_m of 18,000 s. The following conditions obtain: mean temperature of the pressurant gas during the mission T_m, 526°R; total heat transferred between the propellant and tank walls (Q_{W_1}), -2000 Btu; total heat transferred between the pressurant gas and tank walls (Q_{W_2}), -600 Btu; temperature (T_u) of the ullage gas at the end of expulsion, 660°R.

Solution 5-1

(a) Standard propellant references give the following data for N_2O_4 at a pressure of 165 psia: vaporization temperature T_v = 642°R, heat of vaporization h_v = 178 Btu/lb, mean value of specific heat in liquid state C_{pl} = 0.42 Btu/lb-°F, mean value of specific heat in vapor state C_{pv} = 0.18 Btu/lb-°F, compressibility factor Z = 0.95, and molecular weight = 92. The specific heat of helium, C_{pg}, is 1.25 Btu/lb-°F and its molecular weight is 4. From Eq. (5-2) total heat transferred at the gas-liquid interface will be—

$$Q = HAt(T_u - T_e)$$

$$= 0.002 \times 20 \times 500(700 - 520) = 3600 \text{ Btu} \quad \text{(bs-1)}$$

Substitute this into Eq. (5-3):

$$3600 = W_v[C_{pl}(T_v - T_e) + h_v + C_{pv}(T_u - T_v)]$$

$$= W_v[0.42(642 - 520) + 178 + 0.18(700 - 642)]$$

$$= W_v \times 239.6 \quad \text{(bs-2)}$$

Total weight of vaporized propellant W_V = 15. 1 lb. Substitute into Eq. (5-4) to obtain the volume occupied by the vaporized propellant:

$$V_v = \frac{W_v Z R_p T_u}{P_T}$$

$$= \frac{15.1 \times 0.95 \times \frac{1544}{92} \times 700}{23{,}760}$$

$$= 7.13 \text{ ft}^3 \quad \text{(bs-3)}$$

Substitute this into Eq. (5-5) to obtain the volume occupied by pressurant gas:

$$V_g = V_T - V_v = 119 - 7.13 = 111.87 \text{ ft}^3 \quad \text{(bs-4)}$$

Equation (5-6) then gives the required pressurant weight:

$$W_g = \frac{P_T V_g}{R_g T_u}$$

$$= \frac{23{,}760 \times 111.87}{\left(\frac{1544}{4}\right) \times 700}$$

$$= 9.79 \text{ lb} \quad \text{(bs-5)}$$

Substitute results into Eq. (5-7):

$$Q = 9.79 C_{pg}(T_g - T_u)$$

$$3600 = 9.79 \times 1.25(T_g - T_u) \quad \text{(bs-6)}$$

The required pressurant temperature at tank inlet will be as follows:

$$T_g = \frac{3600}{9.79 \times 1.25} + 700 = 995° \text{ R} \quad \text{(bs-7)}$$

(b) From Eq. (5-12) find the total heat transferred at the gas-liquid interface:

$$Q = HAt_m(T_m - T_e)$$

$$= 0.002 \times 20 \times 18{,}000(526 - 520)$$

$$= 4320 \text{ Btu} \quad \text{(bs-8)}$$

Substitute into Eq. (5-9):

$$4320 - 2000 = W_v[0.42(642 - 520) + 178$$

$$+ 0.18(660 - 642)]$$

$$W_v = 10.0 \text{ lb} \quad \text{(bs-9)}$$

Substitute into Eq. (5-4):

$$V_v = \frac{10.0 \times 0.95 \times \left(\frac{1544}{92}\right) \times 660}{23{,}760}$$

$$= 4.45 \text{ ft}^3 \quad \text{(bs-10)}$$

Substitute into Eq. (5-5):

$$V_g = 119 - 4.45 - 114.5 \text{ ft}^3 \quad \text{(bs-11)}$$

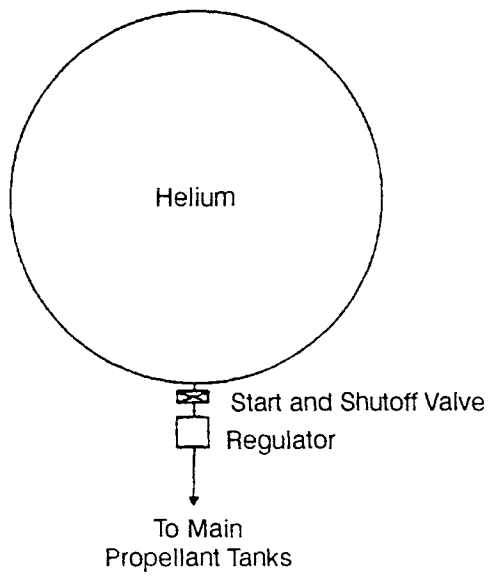

Fig. 5-1 Helium pressurization system without heating.

Substitute into Eq. (5-6):

$$W_g = \frac{23{,}760 \times 110.76 \times 1}{\left(\frac{1544}{4}\right) \times 660}$$

$$= 10.65 \text{ lb} \qquad \text{(bs-12)}$$

Substitute into Eq. (5-10):

$$4320 = 10.65 \times 1.25(T_g - 660) - 600$$

$$T_g = \frac{4320 + 600}{10.65 \times 1.25} + 660 = 1030^\circ \text{ R} \qquad \text{(bs-13)}$$

5.2 STORED-GAS SYSTEMS

Stored-gas pressurization systems are widely used. The gas is usually stored in a tank at an initial pressure ranging up to 10,000 psi and supplied to the propellant tanks at a specified pressure controlled by a regulator. These systems have achieved a high level of reliability. In early systems, nitrogen or even air (German V-2) was frequently used, mainly for logistics reasons. As it became more readily available, helium found increased usage because of its substantially lower molecular weight and thus reduced total pressurant weight. For hydrogen-fueled engines, reliable hydrogen systems have been successfully developed. In general, the most important design requirements for a stored-gas system are low molecular weight of the gas, high gas density at storage conditions, minimum residual-gas weight, and high allowable stress-to-density ratio of the pressurant-tank material. The following discussions will be based on helium systems, since they are now the most widely used.

Commonly Used Configurations

Helium system without heating. This pressurization system is shown schematically in Fig. 5-1. It consists of a high-pressure storage tank, a start and shutoff valve, and a pressure regulator. Regulated helium is ducted directly to the propellant tanks. This has the advantage of great simplicity. However, the weight of the system is relatively high because of the low temperature and specific volume of the gas.

Helium system using thrust-chamber heat exchangers. This system, which is used in the design for the A-3 and A-4 Stage propulsion systems, consists of a high-pressure helium storage tank, a start and shutoff valve, manifolded thrust-chamber heat exchangers, and a pressure regulator. Figure 5-2 shows a typical schematic. The heat exchangers are part of the thrust-chamber divergent nozzle section and absorb heat from the combustion process. From overall performance and weight considerations, it is considered preferable to locate the heat exchanger in the high-pressure portion of the system. Volume increase of the gas due to heating reduces the mass required for tank pressurization. However, a considerable quantity of cold, high-density helium still remains in the storage tank at the end of expulsion.

Helium cascade system. The cascade system shown schematically in Fig. 5-3 is an all-helium pressurization system designed to minimize the weight penalty resulting from cooling of the helium during expansion. System components include helium-storage tanks of equal pressure but of different sizes (two of which are divided internally by a flexible diaphragm), three thrust-chamber heat

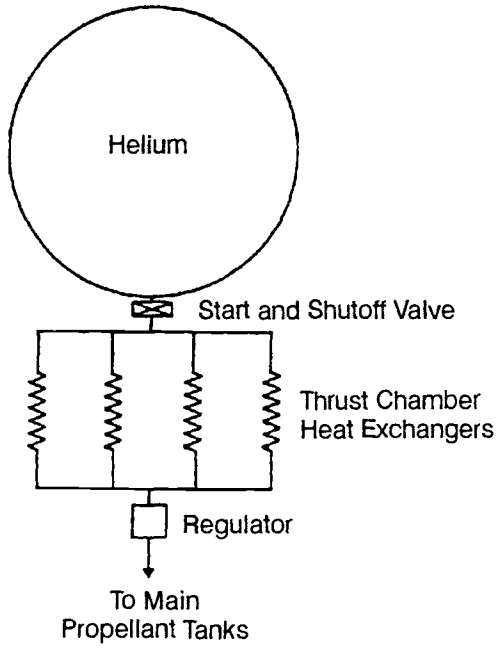

Fig. 5-2 Helium pressurization system using thrust-chamber heat exchangers.

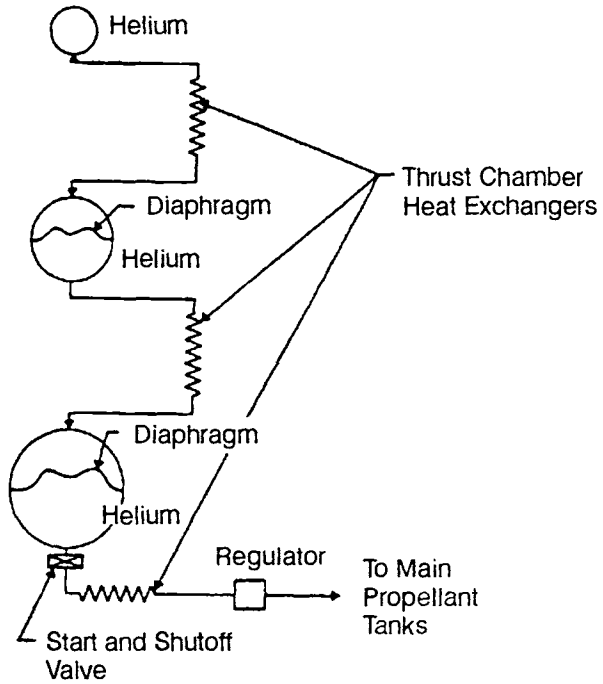

Fig. 5-3 Helium cascade system.

exchangers, a start-and-shutoff valve, and a pressure regulator. During operation of the system, helium flows from the first and smallest tank, through a heat exchanger, and displaces the helium in the intermediate tank. The helium in the intermediate tank in turn flows through a second heat exchanger and displaces the helium in the last and largest tank. The latter flows through a third heat exchanger and pressurizes the propellant tanks. At the end of the operation, only the small storage tank contains low-temperature, high-density helium, while the two larger storage tanks contain relatively warm, low-density helium. This contrasts with the preceding systems in which one large tank remains partially filled with low-temperature, high-density helium. The disadvantages of cascade systems are high weight and complexity.

Helium system with heating inside storage tank. Shown schematically in Fig. 5-4, this system consists of a high-pressure helium storage tank containing a heat exchanger or other heat-generating device mounted internally, a start-and-shutoff valve, and a pressure regulator. This system provides higher-temperature helium to the propellant tanks, simultaneously assuring relatively warm residual gas in the storage tank. Disadvantages are the need for larger and more complex high-pressure storage tanks and the possibility of control problems during operation.

For the pressurization of liquid-hydrogen propellant tanks, stored hydrogen gas can be used in place of helium for the systems described above.

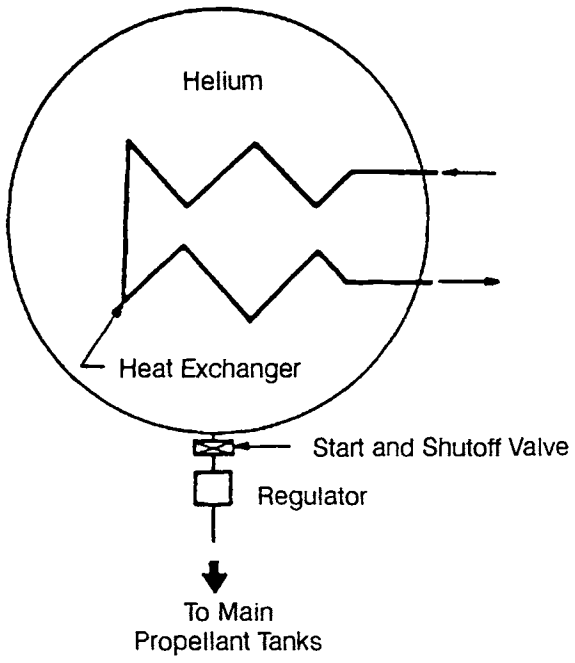

Fig. 5-4 Helium pressurization system using heaters in storage vessel.

Calculations for Stored-Gas Requirements

The design calculations discussed in section 5.1 applied only to the quantity of gas required to pressurize the propellant tanks. However, the gross weight of the stored gas required for a given system depends also on the system design, on the expansion process during operation, and on the environmental temperature range within which the system must function. Based on conditions at the end of expulsion, the total stored-gas requirement can be expressed by the following correlation:

$$\text{Stored-gas requirement} = \text{Propellant tank requirement} + \text{Residual gas in pressurant tank} + \text{Residual gas in other components} \qquad (5\text{-}13)$$

A parameter to define these additions is the "pressurant-use factor," the ratio of stored-gas requirement or initial gas weight in the storage tank to the net weight of pressurant utilized:

$$\text{Pressurant use factor} = \frac{\text{Stored-gas requirement}}{\text{Propellant tank requirement}} \qquad (5\text{-}14)$$

The lowest pressure level in a storage tank required to safely operate the pressurization system will be determined by the individual system pressure-drops. Figure 5-5 shows estimated pressure drops for the stored-helium pressurization system with thrust-chamber heating that was selected for the A-4 Stage engine's oxidizer tank. In addition, a safety margin is usually provided. In this case, the mission is assumed to be completed when the storage-tank pressure decays to 400 psia.

If a heating source is provided inside the tank, as shown in Fig. 5-4, the expansion process of the gas within would be polytropic. For a system without heating inside the storage tank, the expansion process of the gas can be assumed to be isentropic; i.e., no heat is transferred between gas and tank walls. From Eq. (1-13) the following correlation can be derived to calculate the final gas temperature in the storage tank:

$$\frac{T_2}{T_1} = \left(\frac{P_2}{P_1}\right)^{\frac{n-1}{n}} \qquad (5\text{-}15)$$

where—

T_1 = initial helium temperature in the tank, °R
T_2 = final helium temperature in the tank, °R
P_1 = initial helium pressure in the tank, psia
P_2 = final helium pressure in the tank, psia
n = exponent for the polytropic expansion process

The exponent n is estimated during analytical treatment and verified experimentally. For isentropic expansion of helium, n = 1.67.

For most analyses, it has been found adequate to assume an adiabatic flow process through regulator and lines. It is a characteristic of this process that the total (or "stagnation") temperature remains constant. Since the gas essentially comes to rest in

the propellant tank and no further compression takes place following initial propellant-tank pressurization, it is assumed that the propellant-tank temperature equals the heat-exchanger outlet temperature.

If an operating temperature range is specified for a system, the lower temperature limit must be used to calculate the weight of pressurant required, while the upper limit determines the volume of the gas storage tank for a given storage pressure. Thus, for a stated propellant tank net pressurant gas requirement, a wider environmental temperature range results in a heavier pressurization system, regardless of the expansion process of the gas.

Sample Calculation 5-2

The following data characterize the stored-helium pressurization system of the A-4 Stage oxidizer tank: temperature range in the storage tank at system start, 500-560°R; storage-tank pressure at system start, 4500 psia; pressure in the storage tank at the end of expulsion, 400 psia; volume of the helium lines downstream of regulator, 0.4 ft^3; volume of heat exchangers, 1.0 ft^3; volume of lines between storage tank, heat exchangers, and regulator, negligible; and pressurant reserve, 2%.

Problem

Assuming an isentropic expansion process, calculate the following:

(a) Oxidizer-tank pressurant weight, storage-tank volume, and use factor, for case (a) of Sample Calculation (5-1).
(b) Oxidizer-tank pressurant weight, storage-tank volume, and use factor, for case (b) of Sample Calculation (5-1).
(c) Oxidizer-tank pressurant weight, storage-tank volume, and use factor for single-start operation, but without heat exchangers.
(d) Same as (c), but assuming a polytropic expansion process with n=1.2 in the storage tank.

Solution 5-2

The following calculations establish the requirements for the oxidizer tank, which in the A-4 Stage has the higher minimum-storage-pressure requirement. To this required pressurant mass and volumes for fuel-tank pressurization must be added purges and valve actuations.

(a) A net pressurant requirement of 9.79 lb is obtained from Sample Calculation 5-1, Case (a). Temperature and pressure of the residual pressurant in the lines downstream of the regulators are assumed to be the same as those of the propellant-tank ullage gas at the end of expulsion (700°R and 23,760 psfa). Residual-gas weight in these lines then will be—

$$\frac{0.4 \times 23{,}760 \times 1}{\left(\frac{1544}{4}\right) \times 700} = 0.035 \text{ lb} \qquad \text{(bs-14)}$$

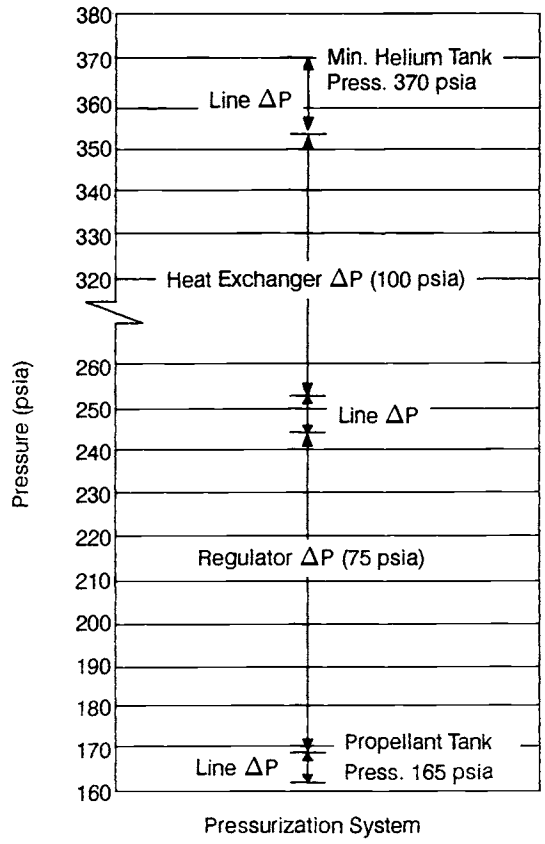

Fig. 5-5 Estimated pressure drops for A-4 Stage oxidizer-tank pressurization system.

It is further assumed that the temperature of the residual pressurant in the heat exchangers have propellant-tank inlet conditions, or 995°R, and that the pressure is that of the residual helium in the pressurant-storage tank, or 400 psia. That produces the following value for these residuals:

$$\frac{1 \times 400 \times 144 \times 1}{\left(\frac{1544}{4}\right) \times 995} = 0.15 \text{ lb} \qquad \text{(bs-15)}$$

Substituting the lower limit of the system operating temperature and the initial and final helium pressures into Eq. (5-15) yields the temperature of the residual helium in the pressurant tank at the end of expulsion:

$$T_2 = 500 \times \left(\frac{400}{4500}\right)^{\frac{1.67-1}{1.67}}$$

$$= 500 \times (0.089)^{0.4} = 191\,°\text{R} \qquad \text{(bs-16)}$$

Using Eq. (5-13), the pressurant volume V_L required for oxidizer-tank pressurization can now be calculated, based on the lower storage temperature-limit of 500°R:

$$\frac{4500 \times 144 \times V_L \times 1}{\left(\frac{1544}{4}\right) \times 500} = 9.79 + \frac{400 \times 144 \times V_L \times 1}{\left(\frac{1544}{4}\right) \times 191}$$

$$+ 0.035 + 0.15$$

$$V_L = \frac{9.957}{0.374 \times 6.9} = 3.78 \text{ ft}^3 \qquad \text{(bs-17)}$$

Pressurant weight:

$$\frac{4500 \times 144 \times 3.78 \times 1}{\left(\frac{1544}{4}\right) \times 500} \times 1.02 = 12.95 \text{ lb} \qquad \text{(bs-18)}$$

including 2% reserve.

Using the upper start temperature limit (560°R), the required volume of the pressurant tank for oxidizer pressurization will be—

$$V_u = \frac{\left(\frac{1544}{4}\right) \times 560 \times 12.95}{4500 \times 144 \times 1} = 4.3 \text{ ft}^3 \qquad \text{(bs-19)}$$

From Eq. (5-14), LOX tank pressurant use factor:

$$\frac{12.95}{9.79} = 1.325 \qquad \text{(bs-20)}$$

(b) From Sample Calculation 5-1, Case (b), the net pressurant requirement is given as 10.65 lb. Assuming temperature and pressure in the lines are the same as those in the propellant tank at the end of expulsion (660°R and 23,760 psia), the residual gas in these lines will weigh

$$\frac{0.4 \times 23{,}760 \times 1}{\left(\frac{1544}{4}\right) \times 660} = 0.037 \text{ lb} \qquad \text{(bs-21)}$$

The temperature of the residual pressurant in the heat exchangers is assumed to be at the propellant tank inlet level, or 1030°R, and that the pressure is that of the residual helium in the pressurant tank, or 400 psia. The gas weight in the heat exchangers then amounts to—

$$\frac{1 \times 400 \times 144 \times 1}{\left(\frac{1544}{4}\right) \times 1030} = 0.145 \text{ lb} \qquad \text{(bs-22)}$$

From Eq. (5-13), pressurant volume V_L and mass are obtained, using the lower temperature limit:

$$\frac{4500 \times 144 \times V_L \times 1}{\left(\frac{1544}{4}\right) \times 500} = 10.65 + \frac{400 \times 144 \times V_L \times 1}{\left(\frac{1544}{4}\right) \times 191}$$

$$+ 0.037 + 0.145$$

$$V_L = \frac{10.832}{2.58} = 4.2 \text{ ft}^3 \qquad \text{(bs-23)}$$

Pressurant weight including 2% reserve:

$$\frac{4500 \times 144 \times 4.2 \times 1}{\left(\frac{1544}{4}\right) \times 500} \times 1.02 = 14.45 \text{ lb} \qquad \text{(bs-24)}$$

Required volume of the pressurant tank:

$$V_u = \frac{\left(\frac{1544}{4}\right) \times 560 \times 14.45}{4500 \times 144 \times 1} = 4.82 \text{ ft}^3 \qquad \text{(bs-25)}$$

Pressurant-use factor:

$$\frac{14.45}{10.65} = 1.36 \qquad \text{(bs-26)}$$

(c) Without heat exchangers, the bulk temperature of helium in the propellant tank at the end of expulsion can be expected to be the average of the initial and final helium temperatures in the pressurant tank:

$$T_g = \frac{500 + 191}{2} = 346°\text{R} \qquad \text{(bs-27)}$$

Since this temperature is lower than the propellant temperature, no heat loss from pressurant to propellant is assumed. The net pressurant weight required may then be calculated by Eq. (5-1):

$$W_g = \frac{23{,}760 \times 119 \times 1}{\left(\frac{1544}{4}\right) \times 346} = 21.2 \text{ lb} \qquad \text{(bs-28)}$$

The weight of residual helium in the lines at the end of expulsion will be as follows:

$$\frac{0.4 \times 23{,}760 \times 1}{\left(\frac{1544}{4}\right) \times 346} = 0.071 \text{ lb} \qquad \text{(bs-29)}$$

Equation (5-13) gives pressurant volume V_L and mass, based on the lower ambient-temperature limit:

$$\frac{4500 \times 144 \times V_L \times 1}{\left(\frac{1544}{4}\right) \times 500} = 21.2$$

$$+ \frac{400 \times 144 \times V_L \times 1}{\left(\frac{1544}{4}\right) \times 191} + 0.071$$

$$V_L = \frac{21.27}{2.58} = 8.25 \text{ ft}^3 \qquad \text{(bs-30)}$$

Pressurant weight will equal the following, including 2% reserve:

$$\frac{4500 \times 144 \times 8.25 \times 1}{\left(\frac{1544}{4}\right) \times 500} \times 1.02 = 28.2 \text{ lb} \qquad \text{(bs-31)}$$

The required volume of the pressurant tank is—

$$V_u = \frac{\left(\frac{1544}{4}\right) \times 560 \times 28.2}{4500 \times 144 \times 1} = 9.4 \text{ ft}^3 \qquad \text{(bs-32)}$$

Pressurant use-factor will then be—

$$\frac{28.2}{21.2} = 1.33 \qquad \text{(bs-33)}$$

(d) The expansion process of helium in the pressurant tank is assumed to be polytropic, with n = 1.2. Equation (5-14) gives the temperature of residual helium in the tank at the end of expulsion:

$$T_2 = 500 \times \left(\frac{400}{4500}\right)^{\frac{1.2-1}{1.2}}$$

$$= 500 \times \frac{2.73}{4.07} = 336°\text{R} \qquad \text{(bs-34)}$$

The helium bulk temperature in the propellant tank at the end of expulsion:

$$T_g = \frac{500 + 336}{2} = 418°\text{R} \qquad \text{(bs-35)}$$

The required net pressurant-weight:

$$W_g = \frac{23{,}760 \times 119 \times 1}{\left(\frac{1544}{4}\right) \times 418} = 17.5 \text{ lb} \qquad \text{(bs-36)}$$

The residual helium weight in the lines at the end of expulsion:

$$\frac{0.4 \times 23{,}760 \times 1}{\left(\frac{1544}{4}\right) \times 418} = 0.059 \text{ lb} \qquad \text{(bs-37)}$$

Pressurant volume and mass, based on the lower ambient-temperature limit:

$$\frac{4500 \times 144 \times V_L \times 1}{\left(\frac{1544}{4}\right) \times 500} = 17.5$$

$$+ \frac{400 \times 144 \times V_L \times 1}{\left(\frac{1544}{4}\right) \times 336} + 0.059$$

$$V_L = \frac{17.56}{2.92} = 6.01 \text{ ft}^3 \qquad \text{(bs-38)}$$

Pressurant weight including 2% reserve:

$$\frac{4500 \times 144 \times 6.01 \times 1}{\left(\frac{1544}{4}\right) \times 500} \times 1.02 = 20.6 \text{ lb} \qquad \text{(bs-39)}$$

The required volume of the pressurant tank will be—

$$V_u = \frac{\left(\frac{1544}{4}\right) \times 560 \times 20.6}{4500 \times 144 \times 1} = 6.88 \text{ ft}^3 \qquad \text{(bs-40)}$$

Pressurant use factor:

$$\frac{20.6}{17.5} = 1.178 \qquad \text{(bs-41)}$$

Design of Stored-Gas System Components

Since system components can be expected to require relatively extensive development effort to achieve satisfactory performance and reliability, they require very careful design thought. This is especially true for large, high-pressure, lightweight, pressurant storage tanks, pressure regulators, and thrust-chamber nozzle heat exchangers.

Tanks

Because of the combined requirement of high pressure and lightweight, pressurant tanks are generally spherical in shape and made of high-strength-to-weight materials. Stainless steel, titanium, and thin metallic liners filament-wound with matrix materials of glass, Kevlar, or graphite-and-resin systems have been successfully employed as construction materials for tanks. Design details for pressurant tanks will be further discussed in Chapter 8.

For weight estimates in preliminary design of large tanks, it is assumed that they are made of two hemispherical shells and that the thickness of the weld lands can be accounted for by assuming a 3-in.-wide band of one-half the wall thickness placed over the weld seam. Hence, the total weight of the tank can be estimated as follows:

$$W_v = \pi d^2 \rho_m (pd/4s) + 3\pi d \rho_m (0.5pd/4s) \qquad (5\text{-}16)$$

where W_V = weight of the tank, lb; d = inside diameter of the tank, in.; p = maximum storage pressure, psia; s = allowable working stress of the material, psi; and ρ_m = density of the material, lb/in.^{3}.

It is of prime importance in the design of stored-gas systems that the tank be capable of containing the gas at high pressure for long periods without leakage. Frequent checking of the storage pressure or recharging is undesirable in most applications. Experimental data indicate that gases of low molecular weight, such as helium and hydrogen, will not leak through homogeneous metals such as good-quality, hot-rolled stock or forgings. However, they can leak through porous metals such as may exist in castings and in welded joints. Good welding workmanship and effective leakage inspection are very important in the fabrication of sound tanks.

Pressure Regulators

Most pressurization systems need a high-accuracy regulator. Regulation becomes particularly difficult if the system requires high-temperature gas, high flow rate, large variation in inlet pressure, or large variation in downstream volume. Design detail of pressure regulators will be discussed in Chapter 7. For some applications, a control system combining a pressure switch, a solenoid valve, and an orifice may be preferred.

Thrust-Chamber Heat Exchangers

For helium systems using thrust-chamber heat exchangers, as shown in Fig. 5-2, the heat exchanger should be designed as an integral part of the thrust-chamber expansion nozzle. As a rule, the heat exchanger will be made of coiled tubing formed to fit the nozzle contour (see Fig. 5-6).

The combustion-gas-side heat-transfer coefficient can be determined by methods described in Chapter 4. The heat conducted through the wall of the heat exchanger is assumed to be totally absorbed by the helium pressurant, raising its temperature. The determination of the helium-side heat-transfer coefficient and the design of the heat exchanger tubing follow the analyses for the regeneratively-cooled tubular-wall thrust chamber. The number of tube turns for the heat exchanger is a function of the helium temperature rise required and of the heat exchanger location at the nozzle. The various operating parameters of a thrust-chamber heat exchanger can be correlated by the following equation:

$$\dot{W}_h C_p (T_o - T_i) = A \left(\frac{1}{\frac{1}{h_g} + \frac{t}{k} + \frac{1}{h_h}} \right) \times \left(T_{aw} - \frac{T_i + T_o}{2} \right) \qquad (5\text{-}17)$$

where—

- $\dot{W}_h$ = helium flow rate, lb/s
- C_p = specific heat at constant pressure of helium, Btu/lb-°F
- T_i = mean He temp. at heat-exchanger inlet, °R
- T_o = mean He temperature at heat-exchanger outlet, °R
- A = effective area of the heat exchanger, in.^{2}
- h_g = combustion-gas-side heat-transfer coefficient, Btu/in.^{2}/s-°F
- h_h = helium-side heat-transfer coefficient, Btu/in.^{2}/s-°F
- t = heat-exchanger-tube wall thickness, in.
- k = thermal conductivity of the tube material, Btu/in.^{2}-s-°F/in.
- T_{aw} = combustion-gas-side adiabatic wall temperature, °R

Heat-exchanger design must consider that the temperature of the helium leaving the heat exchanger at any given time depends on the tank exit-temperature. The choice of heat-exchanger tube material must be made with consideration of its brazing compatibility with the thrust-chamber nozzle wall. The heat exchanger must be firmly attached to the nozzle wall, because its efficiency depends on intimate contact. Selection of tube thickness must be based on pressure and thermal-stress conditions.

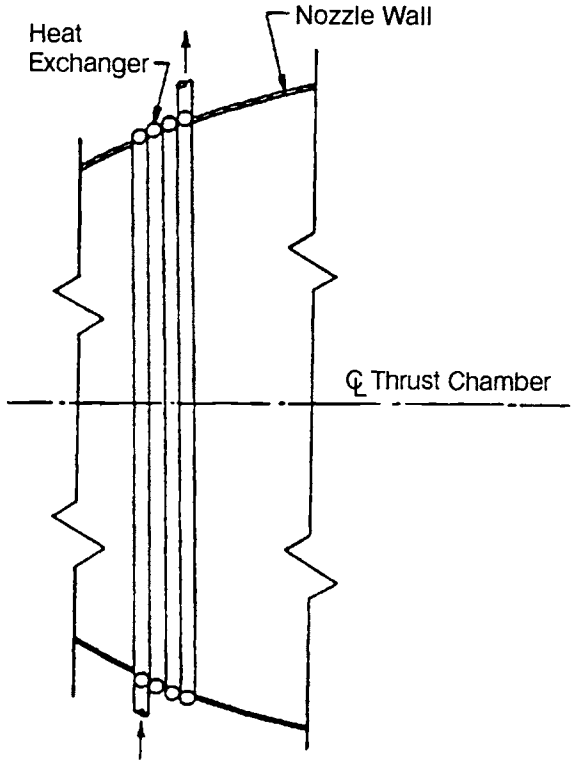

Fig. 5-6 Thrust-chamber heat exchanger.

Sample Calculation 5-3

The following data characterize the design of the pressurant heat exchangers for the A-4 Stage engine-thrust-chamber nozzle extension, when located at an area ratio = 10 and used in parallel: helium flow rate through each heat exchanger $\dot{W}_h$ = 0.024 lb/s (considers requirements for both tanks and for other uses); helium specific heat ratio γ = 1.67; helium specific heat at constant pressure C_p = 1.25; mean temperature of helium at heat exchanger inlet T_i = 346°R; mean temperature of helium at heat-exchanger outlet T_o = 1030°R [from Sample Calculation (5-1), Case (b)]; combustion-gas-side adiabatic wall temperature T_{aw} = 4900°R; and combustion-gas-side heat-transfer coefficient $h_g = 5.7 \times 10^{-5}$ (Btu/in.^{2}-s-°F).

Problem

Calculate the following:

(a) Heat-exchanger-tube dimensions, assuming tube to be made of 13V-11Cr-3Al titanium alloy with the following physical characteristics, at a recommended maximum working temperature range of 1400-1550°R:

minimum yield strength S_y = 40,000 psi; modulus of elasticity E = 12 x 10^6 psi; thermal conductivity k = 2.04 x 10^{-4} Btu/in.^{2}-s-°F/in.; coefficient of thermal expansion a = 5.0 x 10^{-6} in./in.-°F; and Poisson's ratio, v = 0.33.

(b) Number of turns of the heat-exchanger tubing.

Solution 5-3

(a) The wall temperature at given sections of the heat exchanger will vary directly with the bulk temperature of the helium in these sections. Maximum wall temperature occurs at the heat-exchanger outlets. A mean combustion-gas-side wall temperature T_{wg} at the outlets of 1400°R is allowed. Equation (4-10) gives the heat flux at that section:

$$q = h_g(T_{aw} - T_{wg}) = 5.7 \times 10^{-5} \times (4900 - 1400)$$

$$= 0.2 \text{ Btu/in.}^2\text{-s} \qquad \text{(bs-42)}$$

A stipulated tube wall-thickness t of 0.05 in. will be checked below for compatibility with pressure and thermal stresses. From Eq. (4-19) the mean helium-side wall temperature will be—

$$T_{wc} = T_{wg} - \frac{tq}{k} = 1400 - \frac{0.05 \times 0.2}{2.04 \times 10^{-4}}$$

$$= 1350°\text{R} \qquad \text{(bs-43)}$$

Using Eq. (4-20), the helium-side heat transfer coefficient will be calculated as—

$$h_h = h_c = \frac{q}{(T_{wc} - T_{co})} = \frac{0.2}{(1350 - 1030)}$$

$$= 6.25 \times 10^{-4} \text{ Btu/in.}^2\text{-s-deg F} \qquad \text{(bs-44)}$$

Equation (4-15) permits determination of the Prandtl number of the flowing helium:

$$P_r = \frac{4\gamma}{9\gamma - 5} = \frac{4 \times 1.67}{9 \times 1.67 - 5} = 0.665 \qquad \text{(bs-45)}$$

The viscosity of the helium according to Eq. (4-16) is—

$$\mu = (46.6 \times 10^{-10}) \times \mathfrak{M}^{0.5} T^{0.6}$$

$$\mu = 46.6 \times 10^{-10} \times 4^{0.5} \times (1030)^{0.6}$$

$$= 60.2 \times 10^{-8} \text{ lb/in.-s} \qquad \text{(bs-46)}$$

From Eq. (4-25):

$$h_h = \frac{0.029 C_p \mu^{0.2}}{P_r^{2/3}} \left(\frac{G^{0.8}}{d^{0.2}}\right) \left(\frac{T_{co}}{T_{wc}}\right)^{0.55}$$

$$6.25 \times 10^{-4} = \frac{0.029 \times 1.25 \times (60.2 \times 10^{-8})^{0.2}}{(0.665)^{2/3}} \times \frac{\left(\frac{4\dot{W}_h}{\pi d^2}\right)^{0.8}}{d^{0.2}} \times \left(\frac{1030}{1350}\right)^{0.55}$$

$$d^{1.8} = 0.235 \qquad \text{(bs-47)}$$

Inside tubing diameter d = 0.44 in.

Check for combined pressure and thermal stresses at the heat-exchanger outlet (neglecting bending stress) using Eq. (4-27) and assuming bending stress caused by discontinuities to be negligible, as follows:

$$S_t = \frac{(P_{co} - P_g)r}{t} + \frac{Eaqt}{2(1 - v)k}$$

$$= \frac{4500 \times \left(\frac{0.44}{2}\right)}{0.05}$$

$$+ \frac{12 \times 10^6 \times 5.0 \times 10^{-6} \times 0.2 \times 0.05}{2(1 - 0.33) \times 2.04 \times 10^{-4}}$$

$$= 19{,}800 + 2200 = 22{,}000 \text{ psia} \qquad \text{(bs-48)}$$

The combined pressure and thermal stresses at the heat exchanger inlet are now checked. It can be assumed that the difference between the combustion-gas-side wall temperature and the helium bulk temperature remains approximately constant throughout the heat exchanger. Then:

- T_{wg} at the inlet = 1400-(1030-346) = 716°R (mean temperature)
- Heat flux q at the inlet = 5.7 x 10^{-5} (4900-716) = 0.239 Btu/in.^{2}-s

Combined stress S_t at the inlet will then be—

$$= 19{,}800 + 2200 \times \left(\frac{0.239}{0.2}\right)$$

$$= 19{,}800 + 2630 = 22{,}430 \text{ psia} \qquad \text{(bs-49)}$$

Therefore, it is safe to use the selected tube size of 0.440-in. inside diameter and 0.050-in. wall thickness, with sufficient margin for the fact that the heat-exchanger helium inlet temperature will be higher than the maximum at the beginning of the process.

(b) Equation (5-17) gives the required effective area for each heat-exchanger element:

$$A = 0.024 \times 1.25(1030 - 346) \times \frac{\left(\frac{1}{5.7 \times 10^{-5}} + \frac{0.05}{2.04 \times 10^{-4}} + \frac{1}{6.25 \times 10^{-4}}\right)}{4900 - \frac{1030 + 346}{2}}$$

$$= 95 \text{ in.}^2 \qquad \text{(bs-50)}$$

The nozzle diameter at area ratio = 10 of the A-4 chamber will be—

$$D = D_t \times \sqrt{10} = 7.18 \times \sqrt{10} = 22.7 \text{ in.} \qquad \text{(bs-51)}$$

Assuming 40% of the internal surface of the tube as the effective heat-exchanger area, the number of heat-exchanger tube turns required will be as follows:

$$V = \frac{A}{\pi D \times \pi d \times 0.4} = \frac{95}{\pi^2 \times 22.7 \times 0.44 \times 0.4}$$

$$= 2.42 \text{ turns} \qquad \text{(bs-52)}$$

5.3 PROPELLANT-EVAPORATION SYSTEMS

This concept is practical only for thermally stable, low-normal-boiling-point propellants, such as cryogenics and near-cryogenics, for which it is widely used, particularly for cryogenics of low molecular weight, such as hydrogen.

Pump-Fed Propellant Feed Systems

Propellant-evaporation systems for pump-fed engines usually employ propellants tapped off downstream of the pump and vaporized in a heat exchanger, after which they are used to pressurize the main propellant tank from which they were withdrawn. Figure 5-7 shows a typical heat-exchanger design used in an LOX/RP-1 pump-fed engine system. The turbine exhaust gases are used as the heat source. Sometimes the vaporized propellant is bled directly from the manifold downstream of the chamber-cooling passage if it is the coolant in a regeneratively cooled thrust chamber. As shown schematically in Fig. 3-3 and 5-8, the pressurant for the A-2 Stage main oxidizer tank receives oxygen tapped off downstream of the oxidizer pump and vaporized in a heat exchanger located at the turbine-exhaust duct of the oxidizer turbopump. The main fuel tank of this stage is pressurized by bleeding hot hydrogen from the thrust-chamber fuel manifold downstream of the thrust-chamber cooling tubes. The pressure of both tanks can be regulated by pressure-switch/solenoid-valve combinations, as shown in Fig. 5-8, or by regulators. The latter are often preferred, particularly if a narrow band of regulation is essential. In both cases, flow-limiting orifices may be used in series for increased reliability with valve or regulator design-biased to fail open.

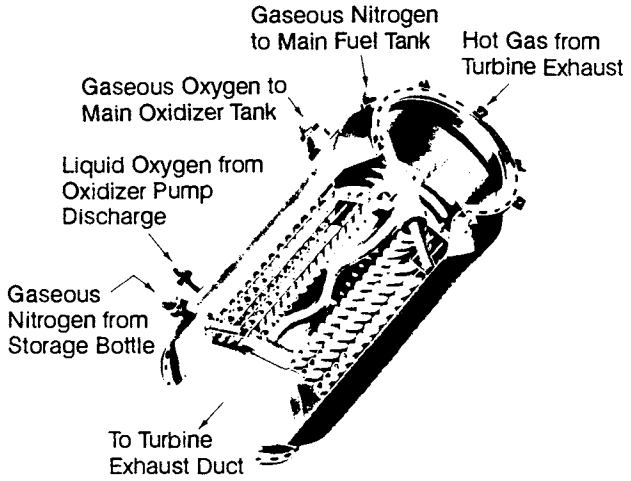

Fig. 5-7 Typical heat-exchanger design.

The required propellant flow rate bled for vaporization and main-tank pressurization will be determined by the main propellant flow rate at the pump inlet (or tank outlet) and by the heat- and mass-transfer processes within the main propellant tank, which in turn are influenced by pressurant and environmental temperatures. For a given rate of evaporation of the propellant in the tank, average flow rate through the tank vent, and tank ullage gas or vapor condition, the following steady-state correlation can be established:

$$\dot{W}_p = \frac{\dot{W} P_T}{\rho R T} - \frac{(\dot{W}_e - \dot{W}_v)}{N} \qquad (5\text{-}18)$$

where—

- $\dot{W}_p$ = required flow rate per engine bled off for propellant-tank pressurization, lb/s
- $\dot{W}_e$ = rate of propellant evaporation in the tank, lb/s
- $\dot{W}_v$ = average flow rate through the tank vent, lb/s
- $\dot{W}$ = main propellant flow rate (per engine) at pump inlet, lb/s
- ρ = density of the liquid propellant, lb/ft^3
- P_T = propellant tank pressure, lb/ft^2
- R = gas constant of the propellant vapor, ft-lb/lb-°R
- T = temperature of the tank ullage gas, °R
- N = number of engines in the system

Sample Calculation 5-4

The following data were established for the A-2 Stage engine and vehicle systems during steady-state operationing conditions:

- Number of engines in the vehicle system, 4
- Main oxidizer flow rate at pump inlet (Table 3-3), per engine, 290.5 lb/s
- Main oxidizer-tank pressure, 45 psia
- Rate of oxidizer evaporation in the tank, 1.6 lb/s
- Average flow rate through the oxidizer-tank vent, 1.64 lb/s

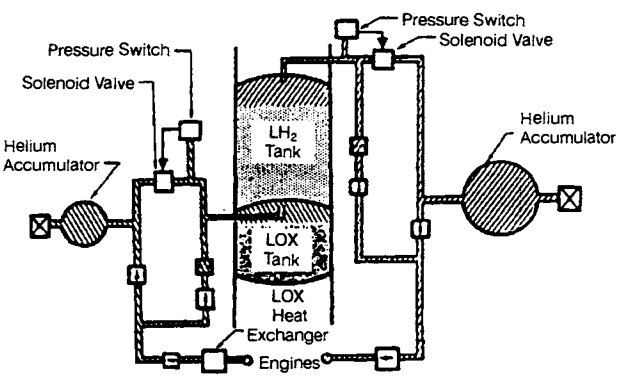

Fig. 5-8 A-2 Stage propellant-tank pressurization system (schematic).

- Temperature of the oxidizer-tank ullage gas, 220°R
- Main fuel flow rate per engine (Table 3-3), at pump inlet, 59.8 lb/s
- Main fuel tank pressure, 38 psia
- Rate of fuel evaporation in the tank, 4.2 lb/s
- Average fuel flow rate through the fuel-tank vent, 6.6 lb/s
- Temperature of the fuel-tank ullage gas, 120°R

(Concerning venting, note that, for fire-hazard reasons, vehicle design very likely will require provisions to prevent venting during first-stage boost. Also, during regulated A-2 Stage operation, venting should normally not occur, as it would be a performance loss. However, as a pressurization-system performance margin, it is well to lay out the system on the basis of some vent losses. Also, in cryogenic systems it may be desirable to increase the tank pressures toward the end of stage operation to improve pump NPSH conditions, when the upper-tank layer, in which somewhat warmer liquid may have accumulated, is about to reach the pump pass around the regulator, using the vent-valve liftoff pressure as the regulating factor. This can be simply done by opening an orificed bypass around the regulator, using vent-valve liftoff pressure as the regulating factor.)

Problem

Calculate the following:

(a) The required steady-state flow rate per engine bled off for oxidizer-tank pressurization.

(b) The required steady-state flow rate per engine bled off for fuel tank pressurization.

Solution 5-4

(a) The density of liquid oxygen is 71.38 lb/ft^3, and the gas constant of the gaseous oxygen is 1544/32=48.2 ft-lb/lb-°R. Substitute this and data given above into Eq. (5-18) to obtain the required steady-state flow rate of evaporated oxidizer pressurant:

$$\dot{W}_p = \frac{290.5 \times 45 \times 144}{71.38 \times 48.2 \times 220} - \frac{(1.6 - 1.64)}{4}$$

$$= 2.50 \text{ lb/s} \qquad \text{(bs-53)}$$

(b) The density of the liquid hydrogen is 4.42 lb/ft^3, and the gas constant of the gaseous hydrogen is 1544/4=386 ft-lb/lb-°R. Substitute this and data given above into Eq. (5-18) to obtain the required steady-state flow rate of evaporated fuel-pressurant:

$$\dot{W}_p = \frac{59.8 \times 38 \times 144}{4.42 \times 386 \times 120} - \frac{(4.2 - 6.6)}{4}$$

$$= 2.2 \text{ lb/s} \qquad \text{(bs-54)}$$

Some engine specialists prefer to use slightly lower propellant densities; for instance, 71.0 for liquid oxygen and 4.4 for liquid hydrogen. These values reflect the fact that storage and vehicle containers, even when vented to atmosphere, have small positive pressures because of vent-valve resistance, resulting in slightly increased propellant temperatures. However, since later engine-calibration-run evaluations will require corrections for a number of run-to-run engine input deviations, consistent usage of design parameters is probably more important than their absolute value. Tank pressure regulation through venting, it should be noted, particularly if used throughout the systems duration, is not efficient, since onboard gas storage must allow for the maximum vent rate anticipated.

Gas-Pressurized Propellant Feed Systems

Propellant-evaporation systems have limited application to gas-pressurized propellant feed systems. Evaporation systems can lower pressurant-tank weight, as compared to stored-gas systems, because of higher storage densities and lower storage pressures. However, this advantage can be offset by the higher molecular weight of some propellants. For hydrogen, the principal propellant with low molecular weight, another limitation exists because of the low critical pressure. To obtain reasonable volume increases due to vaporization, the tank pressure must be kept sufficiently below the critical pressure.

Furthermore, the propellant-evaporation concept, when applied to pressure-fed systems, requires a pressurization system within a pressurization system, since a separate stored gas expels the liquid pressurant from its tank, after which it is vaporized in a heat exchanger. This system comprises a relatively complicated array of components, lines, heat exchangers, and support structures. It is further complicated because of the auxiliary pressurization system required to initiate the main propulsion system operation. As shown schematically in Fig. 3-6, the main fuel tank of the A-3 Stage propulsion system is pressurized by evaporated hydrogen supplied from a separate liquid-hydrogen tank, which in turn is pressurized by helium gas. The hydrogen pressurant is vaporized in the heat exchangers, located at the thrust-chamber nozzle extensions.

For the various reasons stated, the propellant-vaporization principle will be used only for the fuel tank of the A-3 stage, for which it still appears attractive because of the relatively low pressure selected and the low molecular weight of hydrogen. The A-3 oxidizer tank will be pressurized by helium gas. This decision was further influenced by the difficulty in handling gaseous fluorine and by its toxicity.

5.4 INERT-GAS-EVAPORATION SYSTEMS

Inert-gas pressurization has not been employed frequently. Two types of inert cryogenics could be considered applicable: liquid nitrogen and liquid helium. Both have definite disadvantages that would generally preclude their use in nonpropellant evaporation systems, such a solubility in the propellants (nitrogen in liquid oxygen) and storage temperature significantly lower than that of the propellants (liquid

helium). The system design for this concept is similar to that of a propellant-evaporation system.

5.5 CHEMICAL-REACTION SYSTEMS

Pressurization systems using hot-gas products generated from solid or liquid propellants or catalytic-reacted gases have been successfully developed for storable liquid-propellant engine systems. Another technique used with noncryogenics is the main-propellant-tank injection pressurization system. Here a hypergolic fluid is injected into the tank and pressurization is provided by the products of the reaction occurring within the tank.

These methods are not applicable to cryogenic propellants because the products of reaction, such as water, will solidify and because the heat of combustion will undesirably raise the bulk temperature of the cryogenic propellant. Especially in the case of liquid hydrogen, bulk heating cannot be tolerated because of its limited liquid range (normal boiling point to critical point).

Two important considerations for the application of combustion products for pressurization are propellant compatibility and gas temperature. Except for very short operating durations (a few seconds), fuel-rich hot gases are used for fuel tanks to prevent reactions. Similarly, oxidizer-rich hot gases are applied to oxidizer tanks.

Solid-Propellant Gas Generators

Several effective solid-propellant gas generators have been developed to pressurize prepackaged, storable liquid propulsion systems. Gas temperatures up to 3000°F and tank pressures up to 2000 psia have been proven successful for short-duration applications. This pressurization method is primarily employed for its inherent simplicity, low production cost, long-term storability, relatively light weight, and compactness. The system is usually composed of two electrically fired initiators, or squibs, a charge of igniter pellets, safety and arming devices, a pressure-relief regulator, and the propellant grains. A device to cool the hot gas may be required in specific applications.

Figure 5-9 shows a typical design. The gas-generator assembly is enclosed in an insulated steel housing within an aluminum casing, which in turn is an integral part of a propellant tank constructed of aluminum alloy. The gas-generator unit is completely integrated into a compact package ready, with minimum effort and maximum safety, for acceptance testing, storage, and installation into the propulsion system. All of the gas outlets are hermetically sealed with burst diaphragms to maintain system reliability even after long storage.

The ignition train starts the propellant grains burning and producing the pressurization gas. The burning rate of the grain, and in turn the pressure of a solid-propellant system, is affected by the grain bulk temperature. The grain is designed to produce the required gas pressure and flow rate at the lower initial environmental temperature-limit. When operating at a higher initial temperature, the pressure is maintained by a regulator that vents all excess gas overboard. The required grain charge is sized for the full operating duration at the upper temperature limit, which corresponds to the maximum grain burning rate.

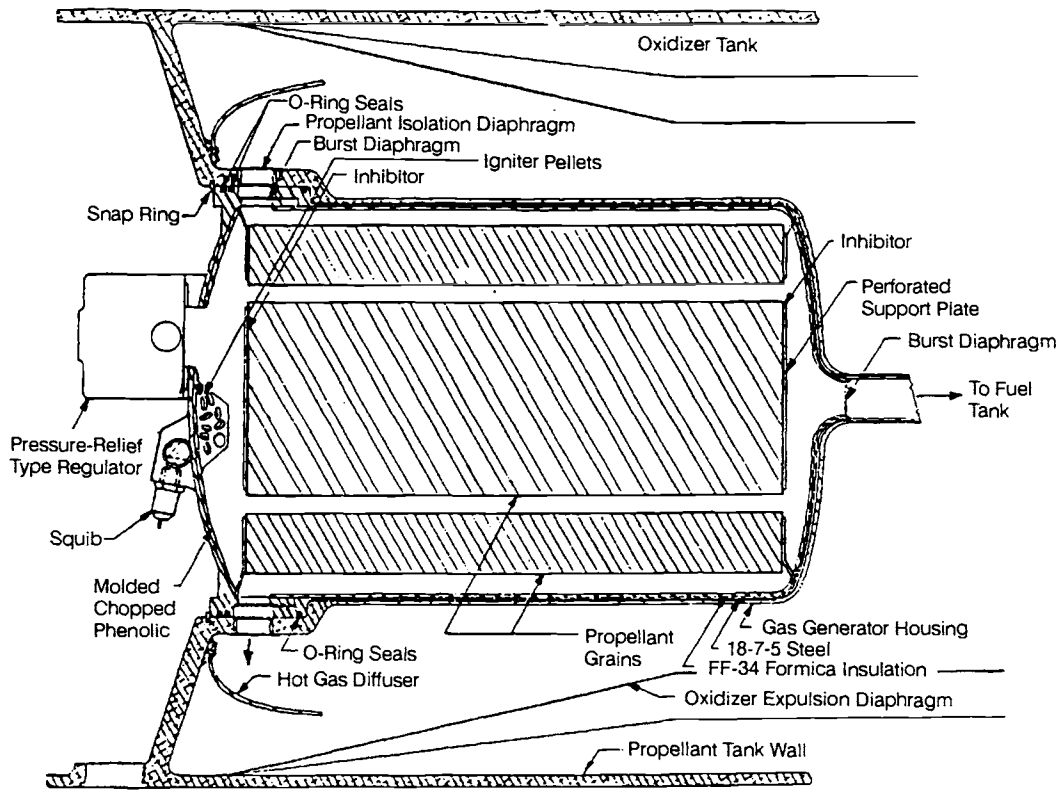

Fig. 5-9 Typical solid-propellant gas generator (GG) pressurization system.

The selection and design of solid-propellant gas-generator pressurization systems must consider potential problem areas, notably the following: chemical and temperature compatibility of the gas with the propellants; pressure-regulation difficulties; solid particles carried by the gas clogging the system; lack of restart capability; and requirement to vent gas rapidly in the event of premature engine cutoff.

Several commonly used solid-propellant systems may be described in brief as follows:

1) Gas generator without cooling, as shown schematically in Fig. 5-10, consists of a solid-propellant grain, igniter, filter, and hot-gas regulator or orifice. This system is mainly suitable for relatively short durations. Upon ignition, hot gas is fed through the filter, regulated, and ducted to the propellant tanks. The regulator dumps excess gas overboard, for which a vent line must be provided. As an alternate, an orifice may be installed in place of the regulator. In the latter case, the propellant-tank pressure and engine thrust level are functions of the gas-generator pressure, which in turn is a function of environmental temperature.

2) Gas generator with solid coolant, as shown in Fig. 5-11, consists of a solid-propellant grain and igniter, a sublimating solid coolant, a filter, and a regulator. In operation, the hot gas is cooled as it passes through a bed of solid material, subjecting it to decomposition or sublimation. Thus, the cooling process simultaneously results in additional pressurization gas. The gas then passes through a filter, is regulated, and is ducted to the propellant tanks.

A typical design might use an ammonium nitrate-base propellant with a theoretical flame temperature of 2320°F. Oxalic acid pressed into pellets—the solid coolant—decomposes endothermically at temperatures above 250°F, producing a mixture of CO, CO_2, and H_2O. The desired temperature level of the mixed gas is achieved through selection of the propellant-to-coolant ratio. Final gas temperatures as low as 400°F have been obtained.

3) Gas generator with azide cooling pack, as illustrated in Fig. 5-12, cools hot gas by passing it through a bed of azide material that decomposes and yields essentially pure nitrogen. However, the gas leaving the azide pack is often contaminated with metal particles from the decomposition of the azide. These have to be removed in a cyclone separator. The gas is filtered to remove any remaining particles, regulated, and then directed to the propellant tanks. This pressurization system provides relatively pure nitrogen gas at a reasonable temperature (as low as 600°F).

4) Helium system with gas-generator heating, as shown in Fig. 5-13, consists of a high-pressure helium tank with a solid-propellant gas generator mounted internally, a filter, and a pressure regulator. The solid-propellant grain provides both heat and additional pressurant gas. This system needs a relatively large high-pressure storage tank.

Liquid-Propellant Gas Generator

Both liquid-monopropellant and liquid-bipropellant gas generators have been used successfully for generating pressurant gas in systems with relatively long operating times. The selection and design of a gas-generation system must consider propellant compatibility, operating temperature limits of propellants and tank materials, and molecular weight of the gas.

Among monopropellants, hydrazine is considered the most satisfactory with respect to chemical characteristics and molecular weight of the product gas. The decomposition products of hydrazine can

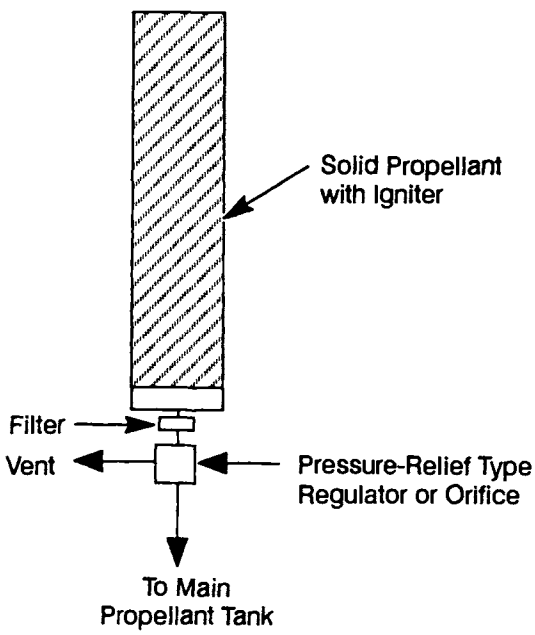

Fig. 5-10 Solid-propellant gas generator without cooling.

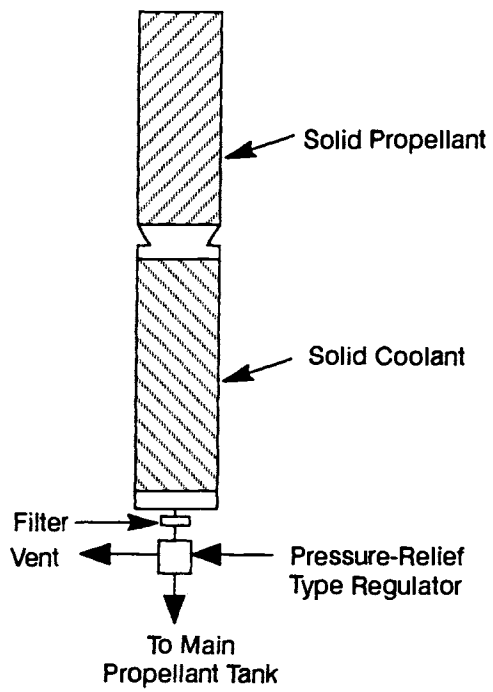

Fig. 5-11 Solid-propellant gas generator with solid coolant.

be made even lighter by catalytic decomposition of the ammonia. The gas contains no carbon, deposits of which could lower the heat transfer rate of a heat exchanger. The theoretical gas-decomposition temperature of pure hydrazine is 1800°F. Additives can be used to reduce the temperature.

To meet the requirement for compatibility with the propellant, bipropellant gas generators possess the flexibility of operation at either fuel- or oxidizer-rich conditions. Thus, the same propellant combination can be used to produce both a fuel- and an oxidizer-compatible pressurant gas. For instance, nitrogen tetroxide in combination with hydrazine, UDMH, and various other amine fuels permits hypergolic starting and stable operation in either fuel- or oxidizer-rich modes.

Several avenues are open to meet the temperature requirement of the pressurant gas. Both fuel- and oxidizer-rich mixtures burn at values far from stoichiometric, resulting in lower temperatures. A limitation exists if one of the bipropellants is also a monopropellant, which continues to decompose exothermically. The cooling effect can also be obtained by injecting a given amount of noncombustible liquid, which absorbs heat when evaporating, into the hot gas. A third method of cooling, transfering heat with one of the liquid propellants in a heat exchanger, can be applied with essentially any propellant combination, provided the cooling liquid can safely absorb the heat transfer from the gas.

The requirement of low molecular weight can be met by most fuel-rich gases if they are at approximately 1000°F, where the complex organic compounds composing most fuels are cracked into simple gases of low molecular weight. If excess fuel is injected to lower the temperature to well below 1000°F, however, this benefit will not be obtained, resulting in a gas with high molecular weight that readily condenses.

Liquid-propellant gas generators require relatively complex components and controls. The selection and application of these will be determined mainly from mission requirements, such as long operating time and need for restarts. The following systems give an idea of applications.

1) Single gas-generator system with injection cooling provides pressurant gas for both the fuel and oxidizer tanks. The liquids employed consist of either a monopropellant and a nonreacting injection coolant or a bipropellant with cooling achieved by injecting an excess of one propellant. As shown in Fig. 5-14, system components include a small high-pressure helium storage assembly (including a tank and start, relief, and fill valves), a pressure regulator,

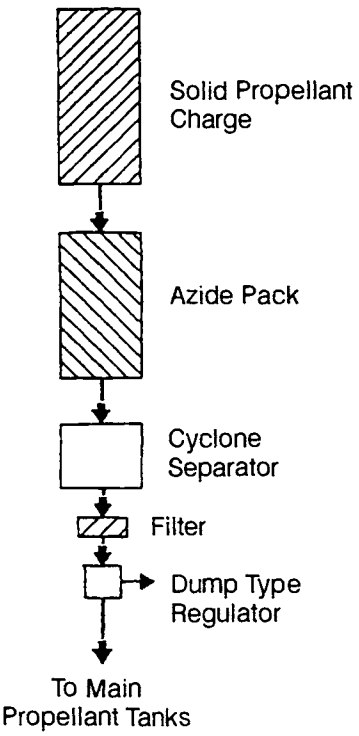

Fig. 5-12 Solid-propellant gas generator with azide cooling pack.

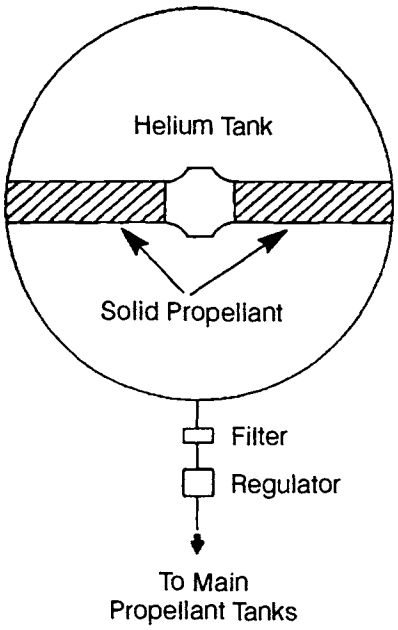

Fig. 5-13 Helium system with heating by solid-propellant gas generator.

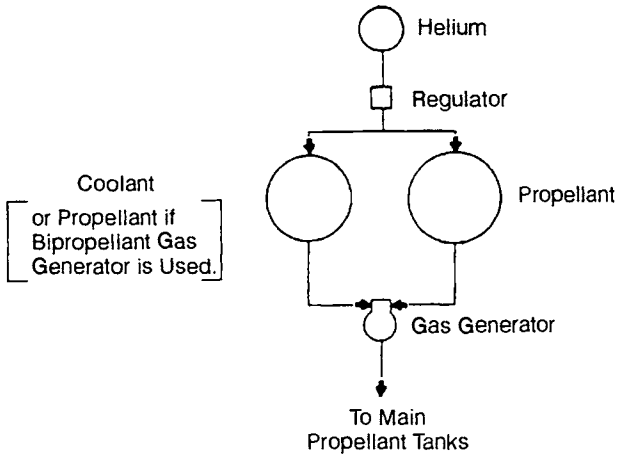

Fig. 5-14 Single liquid-propellant gas generator with injection cooling.

two liquid-storage tanks, and a gas-generator assembly (including controls).

This system is potentially simple and reliable. The product gas is cool enough for use in the propellant tanks. The difficulty is to find a combination of liquids that will produce a product gas meeting all requirements, including compatibility with both propellants. It has been demonstrated, however, that a fuel-rich gas can be used to pressurize storable oxidizers. For instance, ammonia-rich, ammonia-nitrogen tetroxide gas-generator products and hydrazine-decomposition products with either water or ammonia injection have been successfully applied as the pressurant for storable oxidizers.

2) Single gas-generator helium system has the main components shown in Fig. 5-15. The number of propellant tanks depends on use of a monopropellant or bipropellant gas generator. The hot gas-generator products are ducted to a heat exchanger where heat is transferred to the cold helium. The heated helium pressurizes the main oxidizer tank, while the gas-generator gas pressurizes the main fuel tank. While the system efficiently uses the available heat for both tanks, it has the disadvantages of requiring a moderate-size, high-pressure helium tank and of regulating the pressures and flows.

3) Dual bipropellant gas-generator system with injection cooling, as shown in Fig. 5-16, feeds fuel and oxidizer to the gas generators by pressurizing the auxiliary propellant tanks with helium. One gas generator operates with excess fuel to produce

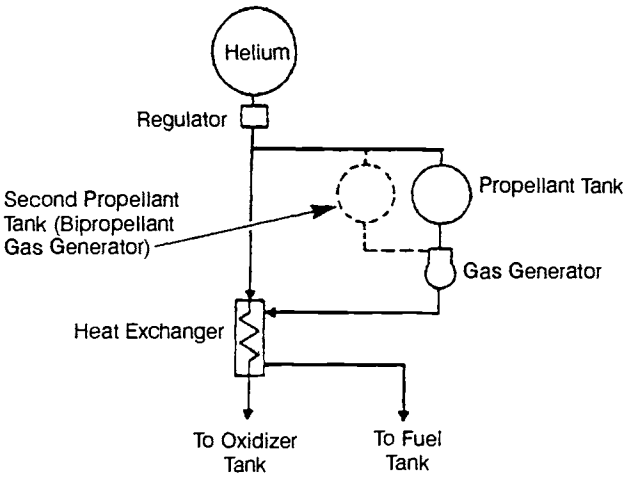

Fig. 5-15 Single liquid-propellant-gas-generator helium system.

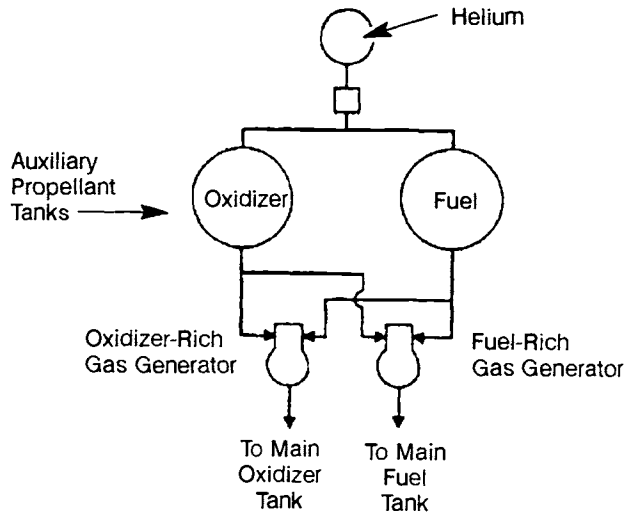

Fig. 5-16 Dual bipropellant gas-generator system with injection cooling.

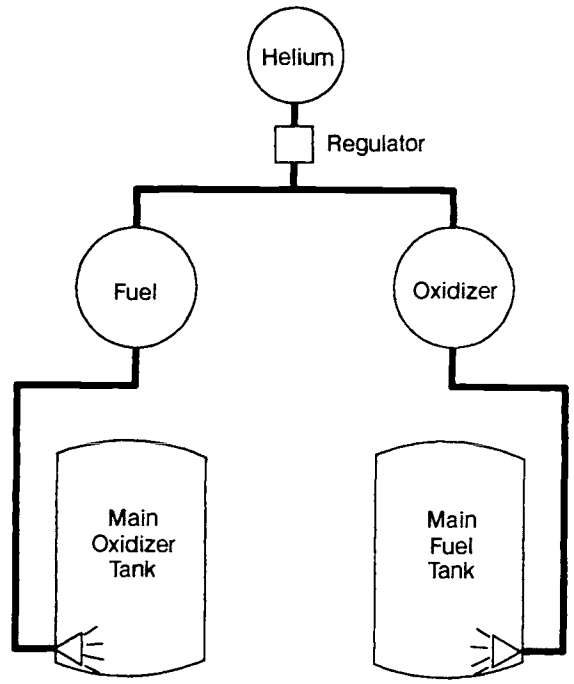

Fig. 5-17 Main-propellant-tank dual direct-injection system.

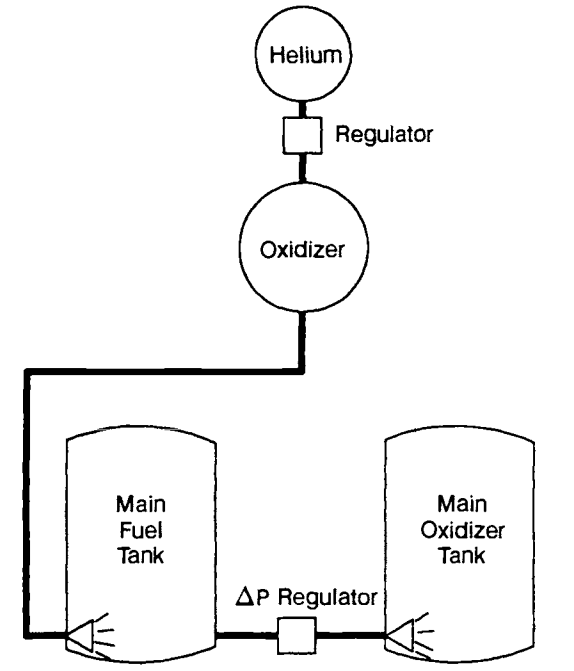

Fig. 5-18 Main-propellant-tank series direct-injection system.

relatively-cool, fuel-rich gases that directly pressurize the main fuel tank. The second gas generator operates with excess oxidizer to produce relatively cool, oxidizer-rich gases that directly pressurize the main oxidizer tank. A design problem arises from the need to balance the output of the two gas generators and to provide proper pressure control in both tanks. Gas temperatures as low as 600°F have been successfully generated with these systems.

Direct Injection into Propellant Tank

The direct-injection systems employ injection of small quantities of fuel and oxidizer into the main oxidizer and fuel tanks, respectively. Hypergolic reaction produces the pressurizing gases within the main propellant tanks themselves. The fuel system (Fig. 5-17) includes a small high-pressure helium-storage tank, a helium-pressure regulator, and two small auxiliary propellant tanks from which propellants are injected into the main tanks. The series injection system (Fig. 5-18) consists of only one auxiliary oxidizer tank for main-fuel-tank pressurization, or vice versa, instead of two separate auxiliary tanks. The series system takes advantage of the situation where one of the main propellant tanks can operate at a slightly lower pressure than the other. In the case shown in Fig. 5-18, a small quantity of the main fuel supply is fed through a regulator to the main oxidizer tank. Although these systems appear to offer the lightest and simplest method of pressurization by number of components, they present the designer with questions of system safety, reliability, and ability to produce steady, regulated tank-pressures.

Table 5-1 Comparisons of various tank pressurization systems for the A-4 Stage propulsion system.

System	Stored Gas and Generants	Gas Produced	Total Quantity of System Components	Number of Complex Component Designs	System Overall Weight, %	System Overall Volume, %
Helium with thrust chamber heating (fig. 5-2)	Helium	Helium at 995°R average	11	3	100	100
Helium--no heating (fig. 5-1)	Helium	Helium at 354°R average	9	2	182	183
Helium cascade (fig. 5-3)	Helium	Helium at 1000°R average	17	7	81	75
Solid propellant gas generator heating helium (fig. 5-13)	Helium, ammonium nitrate base grain	[a]Mixed helium and solid propellant products at 1000°R average	15	4	79	72
Solid propellant gas generator with solid subliming coolant (fig. 5-11)	Ammonium nitrate base grain, oxalic acid pellets	[a]Solid propellant products at 1000°R	9	3	53	12
Solid propellant gas generator with azide cooling (fig. 5-12)	Viton azide propellant, lithium azide coolant	Nitrogen at 1000°R	11	4	70	11
Single liquid propellant gas generator--helium (fig. 5-15)	Helium, hydrazine	[b]Helium at 1000°R on oxidizer, hydrazine products at 1200°R on fuel	11	4	63	51
Dual liquid propellant gas generator with injection cooling (fig. 5-16)	Helium, nitrogen tetroxide, ammonia	[a]Ammonia-rich gas generator products at 1000°R on fuel; N_2O_4-rich gas generator products at 1000°R on oxidizer	16	6	48	16

[a]Questionable compatibility of pressurant with propellants.
[b]Marginal pressurant temperature level on fuel.

5.6 SELECTION OF PRESSURIZATION

The inception of pressurization-system design begins with a preliminary study of the various design approaches. Although providing a technical basis for selection, this study can become a relatively complex task in view of the great number of tank-pressurization techniques that have been developed. The study will gather all information pertinent to the wide range of systems. The vehicle configuration and requirements for performance, structural materials, and other factors affecting the pressurization system design will likewise be accumulated to permit valid weight and size comparisons of the various systems.

The five principal selection criteria are mission and vehicle requirements, fluid and material compatibility, system reliability, cost, and system weight and size. Mission and vehicle requirements include storability, system start and restart, and pressure and flow tolerances. Compatibility includes chemical inertness, freedom from excessively condensible and soluble gas products, and proper pressurant temperature level. Reliability is evaluated on the basis of system complexity and failure modes. Components that can be expected to require considerable development effort to achieve satisfactory reliability include gas-generator assemblies, thrust-chamber heat exchangers, and regulators. The gross weight of the pressurization system is treated as inert weight, since the pressurant gas is part of the vehicle weight at the end of the expulsion cycle.

A sample preliminary-design study was conducted for the tank-pressurization system for the A-4 Stage propulsion system. The vehicle mission was assumed to require single-start, constant-thrust, full-duration operations. The study compared eight different pressurization systems (Table 5-1). The column "Complex Component Designs" refers to parts requiring relatively long development time and high production cost.

Design of Turbopump Propellant Feed Systems

For high-thrust, long-duration liquid-propellant rocket engines, the use of turbopump-fed systems usually lowers system weight and raises performance as compared to pressurized-gas fed systems. Turbopump-fed systems require only relatively low pump-inlet pressures, and thus propellant-tank pressures, while the major portion of the pressure required at the thrust-chamber inlets is supplied by the pumps. This saves considerable tank weight, particularly in large vehicles.

As the overall trend toward higher chamber pressure for liquid-propellant rocket engines continues, the role of turbopumps in an engine system becomes of greater importance, particularly with the high-performance hydrogen-fueled engines. The advantage of pump-fed over pressure-fed engines increases as mission velocity requirements increase, and becomes very substantial as orbit-insertion velocities are approached.

Figure 6-1 shows a representative range of pump operating parameters for various liquid-propellant rocket engine applications. Figure 6-2 depicts an envelope of power requirements for a number of actual turbine designs.

6.1 ELEMENTS OF TURBOPUMP-FED SYSTEMS

The vehicle designer must insure that propellants go to the inlet of the pumps at required minimum pressures. The turbopump feed system raises the pressure of the propellants received from the vehicle tanks and delivers them to the main thrust chamber, through ducts and valves, at pressures and flow rates commensurate with rated engine operation. A turbopump feed system may consist of the following basic elements:

- Propellant pumps.
- Turbine(s) to drive them.
- Power source for the turbine(s) (during engine start as well as main stage).
- Speed-reduction gear transmissions (if any).
- Lubrication system for bearings and gears.
- Accessory drives.
- Propellant inlet and discharge ducts.
- Turbopump mounts.

Propellant Pumps

The principal requirements of a rocket-engine propellant pump are high reliability, low cost, light weight, stable flow for the required operating range, high efficiency, adequate suction performance, and long life. The relative importance of these factors and their resulting influence on the design will vary depending on the application. The most widely used pump types are centrifugal (or radial), axial, or mixed flow. Centrifugal pumps are usually designed with a single stage; axial pumps, multistage. However, multistage centrifugal pumps with crossover-type diffusion systems have also been used effectively. Various pump configurations are shown schematically in Fig. 6-3.

Centrifugal pumps. Almost all operational rocket propellant pumps are of this type. They can handle large flows at high pressures efficiently as well as economically in terms of weight and size. The elements of a centrifugal pump are shown in Fig. 6-4 and 6-16. Centrifugal pumps, like other steady-flow rotating machinery, consist essentially of two basic elements: the rotor and the stator. These accelerate the fluid flow by imparting kinetic energy to it in the rotor and then decelerating, or "diffusing," it in the

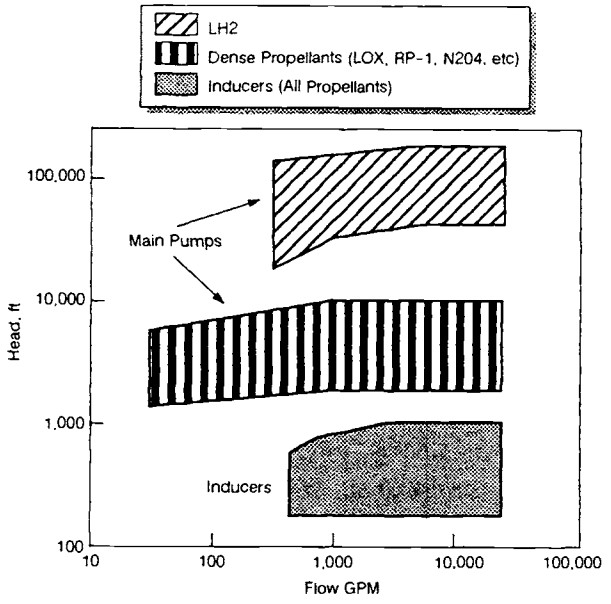

Fig. 6-1 Range of operation for typical propellant pumps.

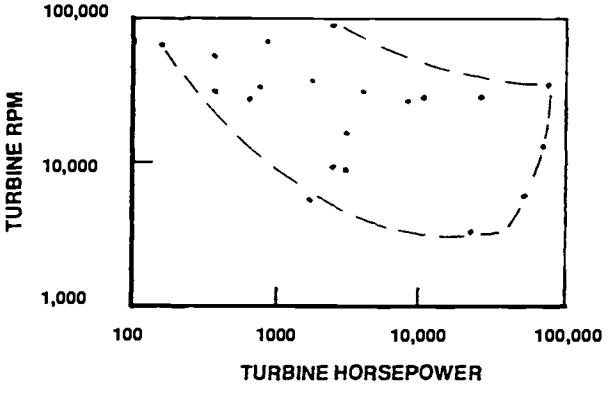

Fig. 6-2 Rocket-engine turbine design envelopes.

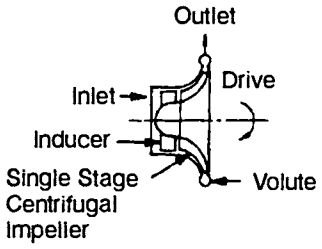

Single Stage Centrifugal Pump

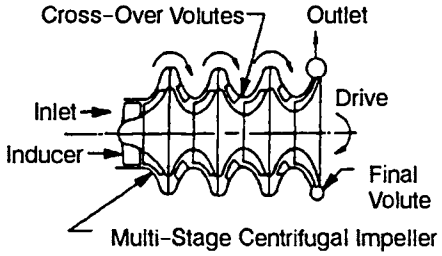

Multi-Stage Centrifugal Pump

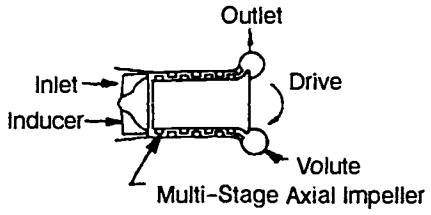

Multi-Stage Axial Pump

Fig. 6-3 Pump configurations.

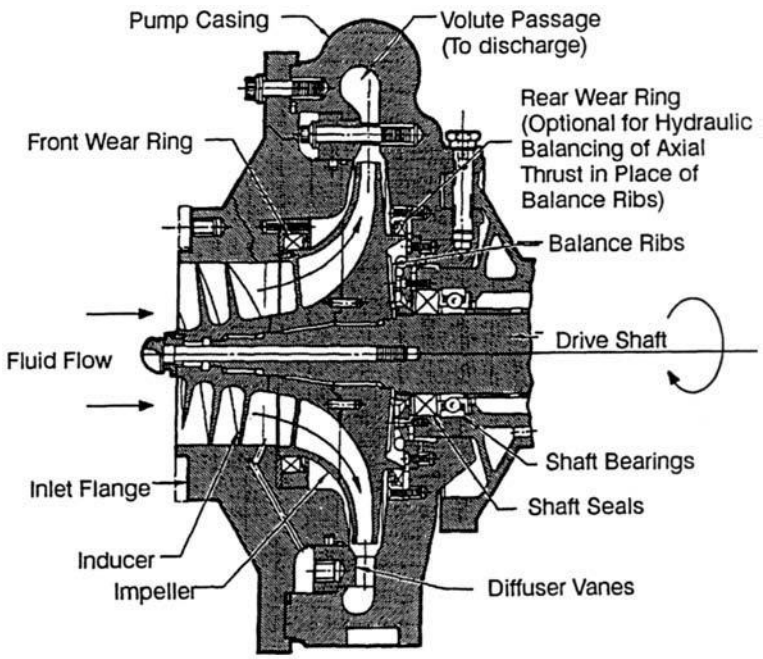

Fig. 6-4 Elements of a centrifugal-flow pump.

stator. This results in increased fluid pressure head. The rotor assembly usually includes an inducer, an impeller, bearings, and a shaft. The stator assembly consists of a casing with stationary diffuser vanes, a volute with discharge outlet, and seals.

An inducer, an axial-flow rotor, increases total pressure of the entering fluid sufficiently to permit noncavitating operation of the main impeller. An inducer can reduce the pump-inlet-pressure net positive suction head (NPSH) requirements substantially. The impeller of a centrifugal (or radial) pump basically is a rotating wheel with blades that discharge the flow in a radial direction. Fluid is admitted axially to the impeller that, when rotating in an enclosure, ejects it at the periphery with increased absolute velocity (Fig. 6-4).

As primary functions, the pump stator assembly diffuses (i.e., decelerates) the fluid to convert the velocity head into pressure head, collecting and redirecting the fluid to the pump discharge outlet, and provides structural support and a pressure enclosure for the pump. Wear rings (see Fig. 6-4) provide axial-thrust control and minimize internal leakage—circulation of the fluid between the high-pressure (discharge) and the low-pressure (inlet or suction) zones. Dynamic shaft seals prevent external leakage along the shaft.

Multistage centrifugal pumps. For higher pressure rises, multiplestage centrifugal pumps can be designed if a single stage proves limited. A multistage pump basically resembles a single-stage pump, except that it requires proper channeling of

the fluid between stages. Figure 6-5 shows such a design used on the Space Shuttle Main Engine (SSME) high-pressure fuel turbopump (HPFTP).

Multistage axial pumps. This design permits achieving high head through multiple staging with smaller-diameter pumps. It has been used for liquid-hydrogen pump applications. It is not as well suited for wide-flow-range operation, as will be discussed below, but can be more efficient in applications requiring relatively high ratios of flow vs. head (or at high "specific speeds," a term to be defined below). Elements of an axial-flow pump are shown in Fig. 6-6. The rotor assembly consists of an inducer, a cylindrical rotor with multiple rows of rotating blades, and a rotor shaft. The stator assembly includes a cylindrical casing with rows of stationary blades spaced between inducer and rotating blades, a volute casing, bearings, and seals.

An inducer placed at the pump inlet supplies the fluid to the main-pump section at the required pressure and velocity. Both rotor and stator blades have a hydrofoil shape. The rotor blades accelerate the flow relative to the stator and thus increase the kinetic energy of the fluid, while the stator blades, acting as diffusers, convert the velocity head of the fluid into pressure head. However, the velocity vector of the fluid in the axial direction is kept essentially constant throughout the various stages of the pump.

Inducer pumps. The simplest axial-flow pump consists of a single rotor designed as an inducer to achieve good suction, as shown in Fig. 6-7. The inducer can consist of either a single- or double-blade row, an example of the latter being shown in Fig. 6-8. These pumps are used as low-speed "boost pumps" to raise the pressure sufficiently to permit the main pump to operate at much higher speeds to reduce its size and cost. The inducer design for this pump is similar to those used in either centrifugal- or axial-flow pumps.

Turbines

The turbines (see Fig. 6-9 and 6-16) that provide shaft power to the propellant pumps typically derive their energy from the expansion of a high-pressure, high-temperature gas to lower pressures and temperatures. Turbines can be divided into two major types: impulse and reaction. Impulse turbines can be either single- or multiple-stage. Reaction turbines are usually multistage. Impulse turbines are most frequently used for high-pressure-ratio, low-flow applications. Reaction-bladed turbines are more frequently used for low-pressure-ratio, high-flow designs.

Single-stage, single-rotor impulse turbine. This turbine consists of a single-rotor disk or turbine wheel to which is attached a row of turbine blades or buckets. Gas is fed to the rotating blades through stationary nozzles (Fig. 6-10). In the nozzles, the gas pressure is converted into kinetic energy (velocity head) with attendant static-pressure drop. The gas flow reaches maximum velocity upon entering the rotating blades, where the kinetic energy of the gas is imparted to the turbine rotor as mechanical energy of rotation. Ideally, the static pressure of the gas remains constant when it passes through the rotating blades (except for the effects of friction).

Velocity-compounded impulse turbine. In this type of turbine, as shown schematically in Fig. 6-11, two separate rows of rotating blades instead of one transfer the kinetic energy of the gas discharged from the set of stationary nozzles. A row of stationary blades between the wheels guides the gas into the

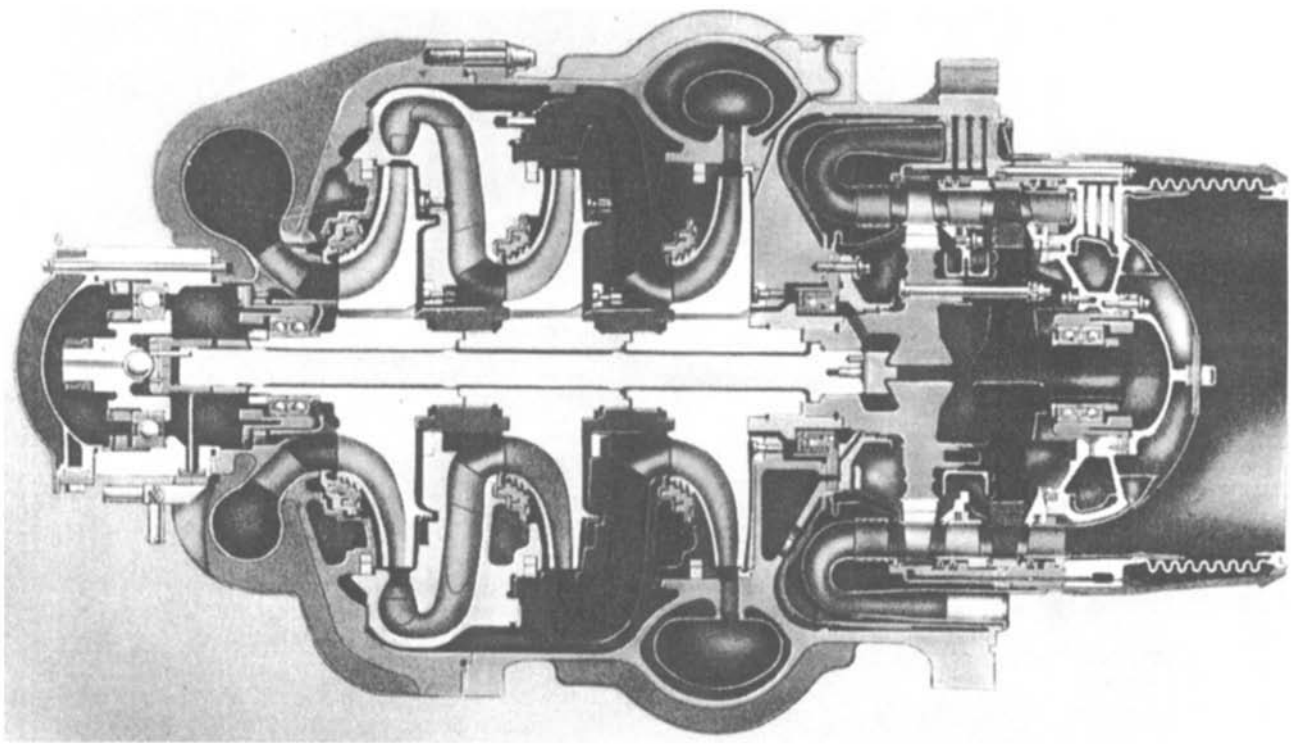

Fig. 6-5 SSME *HPFTP*.

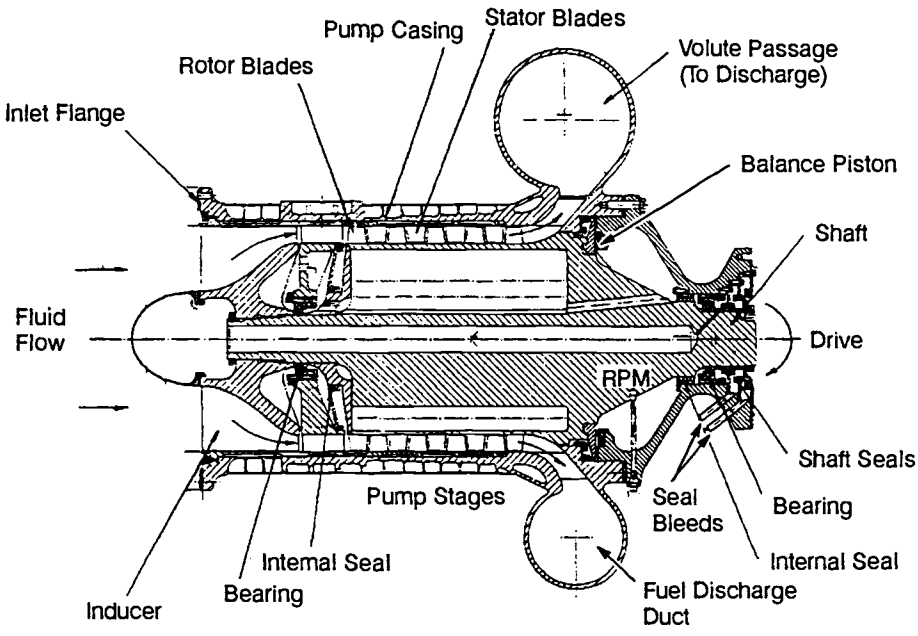

Fig. 6-6 Elements of an axial-flow pump.

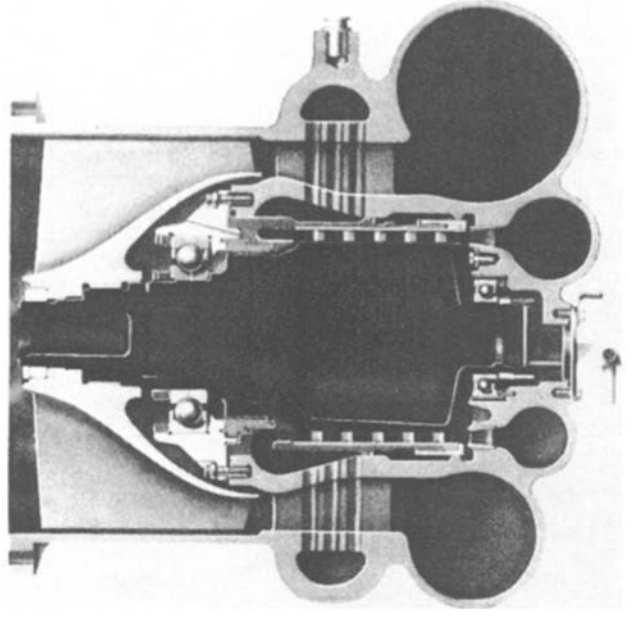

Fig. 6-7 SSME *LPOTP.*

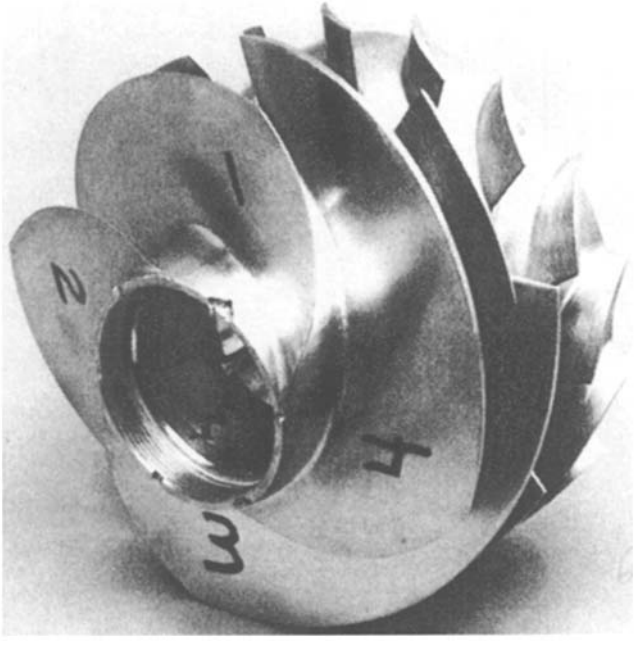

Fig. 6-8 Two-blade-row inducer.

second set of moving blades. Ideally, the entire pressure drop occurs in the stationary nozzles. The gas velocity decreases during passage through the first row of rotating blades, remains constant through the stationary blades, and decreases further as it passes through the second row of rotating blades. Velocity-compounded turbines are considered single-stage because they involve only one pressure step.

Pressure-compounded impulse turbine. As shown schematically in Fig. 6-12, this turbine expands the gas in steps, through two or more rows or stages of stationary nozzles, each set being followed by a row of rotating blades. A designer wants velocity, and thus the kinetic energy, of the gas flow to be the same at the entrance of each row of rotating blades. This results in equal energy transferred to each rotating-blade row, while the pressure drop in each stationary nozzle row will vary. Since the pressure is greater in region A than in region B, it is necessary to separate the stages by a sealing diaphragm to prevent bypass flows (Fig. 6-9). Because of clearances required at the rotating seal between diaphragm and turbine shaft, however, some losses do occur at this point due to leakage from stage to stage.

Reaction turbine. An impulse and a reaction turbine (shown schematically in Fig. 6-13) have this main difference: an impulse turbine sees no static-pressure drop (no expansion) while the gas passes

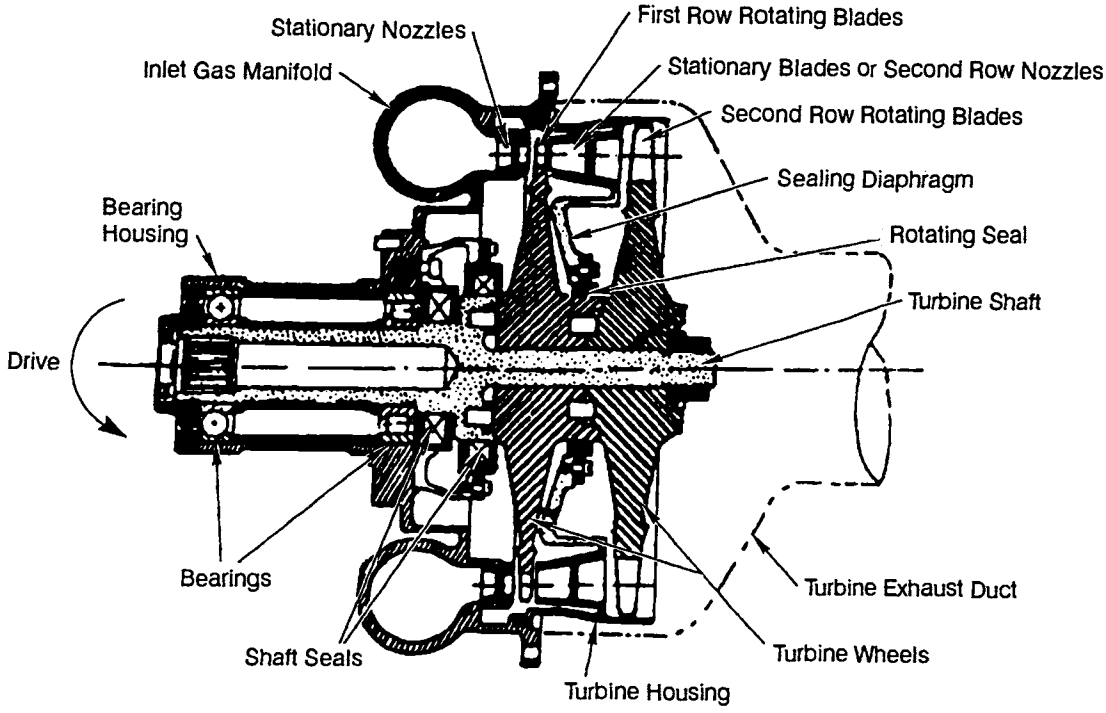

Fig. 6-9 Turbine elements.

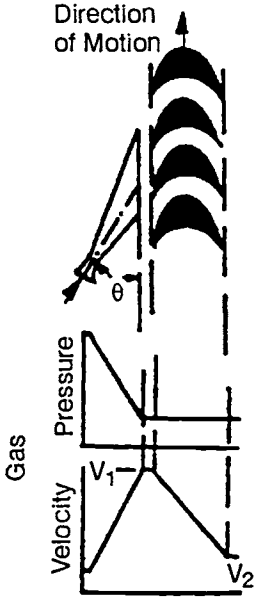

Fig. 6-10 Single-stage, single-rotor impulse turbine.

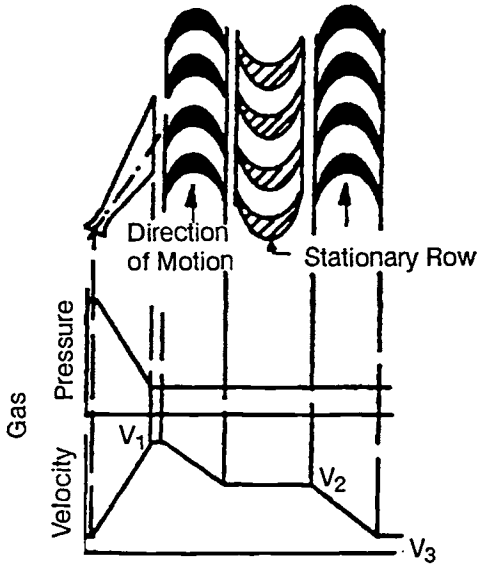

Fig. 6-11 Single-stage, two-rotor, velocity-compounded impulse turbine.

through the rotating blades, whereas the pressure does drop (expansion occurs) in a reaction turbine. Both impulse and reaction wheels are driven by a change in momentum of the gas. In a pure reaction-type turbine, the driving force is derived entirely from the reaction due to gas expansion within the rotating blades (similar to the gas expansion in a rocket nozzle). In actual reaction-turbine designs, however, a portion of the driving force comes from gas impingement on the rotating blades. The percent reaction is the ratio of the static-pressure decrease across the rotor divided by the pressure drop across both the nozzle and rotor expressed as a percentage. Thus, a 50%-reaction design has equal pressure drops across the rotor and the nozzle. Any magnitude of reaction can be designed, but typically values of 50% or less are more efficient.

Hydraulic turbines. Occasionally it will be more economical in the engine system to use the high-pressure liquid from the pump discharge to drive a hydraulic turbine which derives its energy from the pressure drop across the turbine rather than the temperature of the driving gaseous fluids. The turbine shown in Fig. 6-7 does this to simplify sealing requirements by using liquid oxygen as the

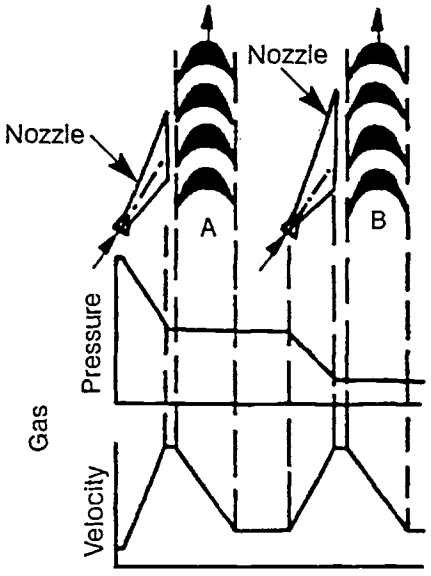

Fig. 6-12 Two-stage, pressure-compounded impulse turbine.

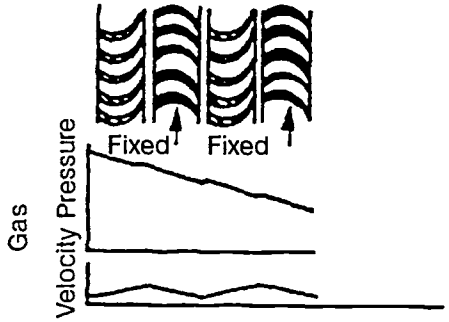

Fig. 6-13 Reaction turbine.

drive fluid in the turbine as well as in the pump. Such turbines are typically of the reaction type.

Turbine Power Sources

Several different types of engine cycle are available and can be classified primarily based on where the turbine-drive fluid originates and where it is discharged after leaving the turbine. The typical turbine power sources shown in Fig. 6-14 are described briefly here.

Bipropellant gas generator. This was the most widely used system before 1970 since it has the advantage of using the engine main propellants, and the turbine circuit is in parallel with the thrust chamber flow. The turbine-drive fluid consists of hot gas from the combustion process in the gas generator. The turbine flow is subsequently dumped overboard or to some low-pressure point. This system obviously operates with a high pressure ratio and low flowrate to minimize impact on engine specific impulse. The turbine for this system will typically be an impulse supersonic design.

Monopropellant gas generator. This provides the simplest gas-generating system, but it

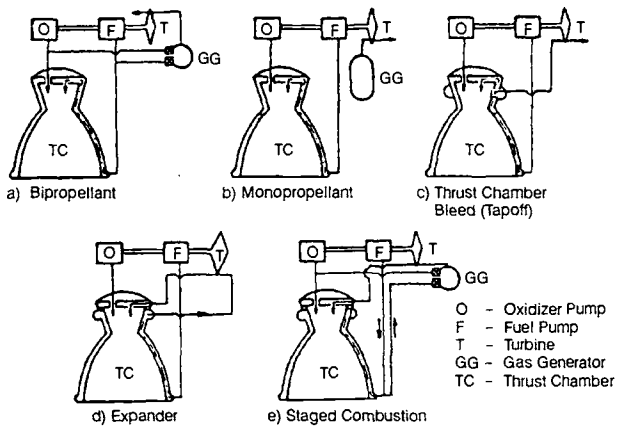

Fig. 6-14 Typical turbine power sources.

requires a third propellant if neither one of the main propellants is suitable for monopropellant application.

Thrust-chamber bleed. As applied in "tapoff" engine systems, gases will be bled off directly from the main combustion chamber to drive the turbine. The gas has an elevated temperature from the combustion process in the main chamber. Since the turbine-drive fluid is dumped overboard after leaving the turbine, this type of design is similar to those used for the gas-generator system.

Expander. In an expander cycle, such as with a hydrogen-fueled engine system, the heated hydrogen gas emerging from the thrust-chamber cooling jacket is used as the turbine working fluid before being injected into the main combustion chamber. In systems using a mono-propellant as one of the main propellants, the monopropellant can be decomposed and used to drive the turbine prior to injection into the main combustion chamber.

Dual (staged) combustion. Here the entire fuel flow reacts with a portion of the oxidizer in a bipropellant gas generator and thus provides the gas to drive the turbine. The usually fuel-rich exhaust gas is then ducted into the main combustion chamber and reacts with the balance of the oxidizer. The turbine-discharge flow goes to the thrust chamber, resulting in a similar turbine design as the expander cycle, but at higher temperature. Staged-combustion-cycle efficiency equals that of the expander cycle. The SSME engine is of this type. A variation of this cycle is to use an oxidizer-rich gas turbine for the oxidizer pump and a fuel rich turbine for the fuel pump.

Most systems require an auxiliary power source during engine start to drive the turbine until the main power source takes over. Evaluating start methods on a new engine usually calls for comparison between a spin and a tank-head start. A spin start uses an auxiliary power source to provide the initial buildup of turbine speed. A tank-head start uses propellants out of the main tanks for initial turbine power. As the speed increases, pump-discharge pressures increase, and the turbine flow and available power increase, resulting in the engine bootstrapping itself to mainstage. The primary fac-

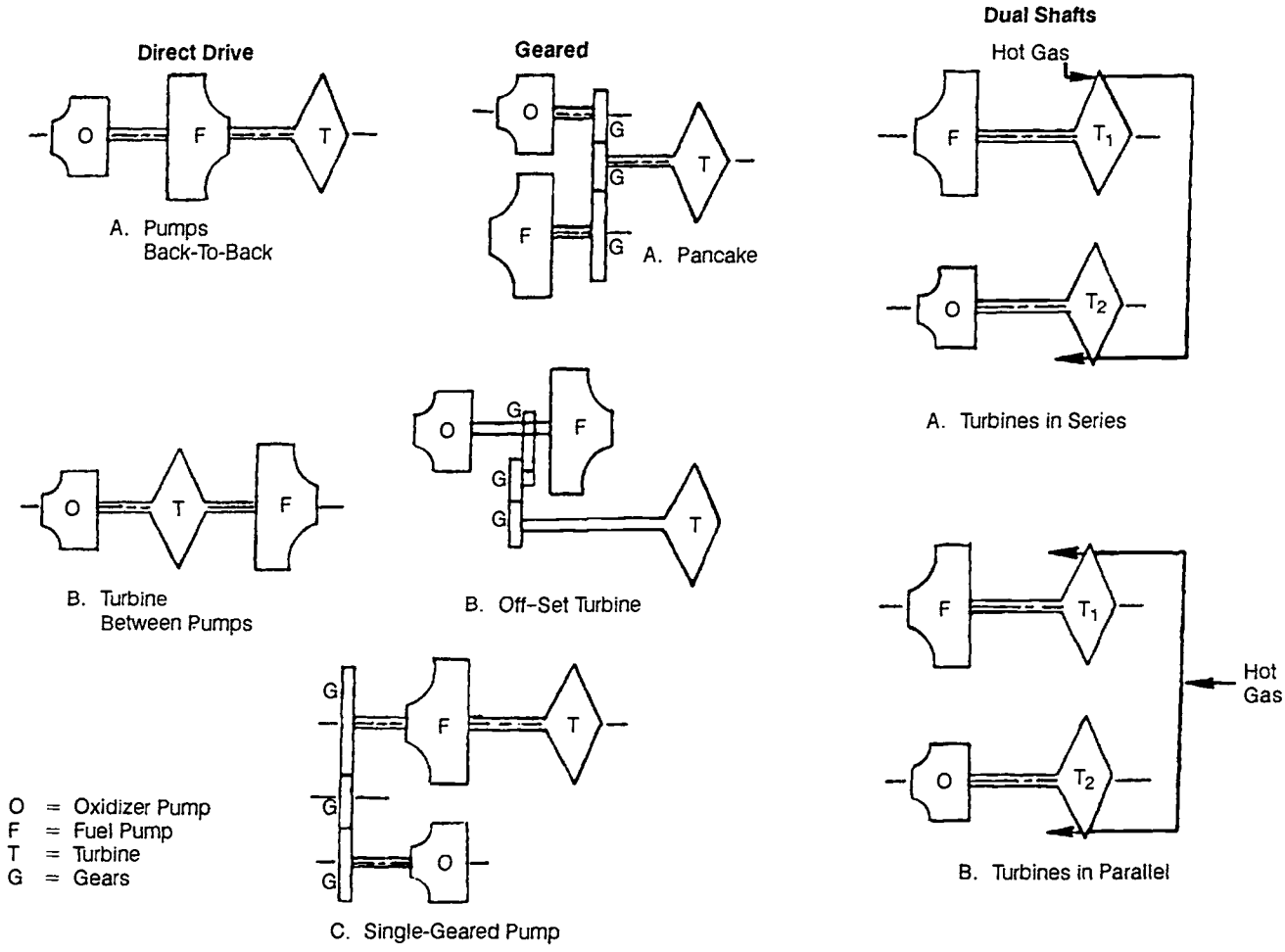

Fig. 6-15 Principal turbopump drives.

tors affecting the start method are the type of fuel used and the engine cycle. Whether the oxidizer is cryogenic or storable is not a major factor.

Storable fuel. A storable fuel will be a liquid at ambient temperature and pressure, such as RP-1 (kerosene) and the hydrazines. Since storables do not gasify at low pressures, relatively high initial flowrates can be obtained under tank-head conditions. This makes a tank-head start a reasonable option. Spin starts have also been used where stored high-pressure gas, a solid-propellant gas generator, or bipropellant start tanks generate the initial turbine power. Using a spin start will usually require less development but at the expense of the additional components.

Cryogenic-fuel; gas-generator cycle. All cryogenic pump-fed engines have used hydrogen for the fuel. The following discussion concerns using hydrogen, but would also apply for other cryogenic fuels. At mainstage, a gas-generator cycle tends to have a high turbine pressure-ratio. For a tank-head start, the initial turbine pressure-ratio will be lower than mainstage because the initial pressure driving the turbine has to be lower than the engine fuel-inlet pressure. This results in a relatively low initial power and a slow rate of bootstrap. Also, because hydrogen vaporizes easily at low pressure, it is difficult to get enough hydrogen flow to prevent temperature spikes in the gas generator. This makes a tank-head start very difficult. The gas-generator cycle does lend itself fairly easily to a spin start because only a small portion of the total hydrogen goes to the gas generator. During the spin portion of start, the main fuel valve will be open, providing a path for the main fuel flow to prevent stalling of the main fuel pump. Initial combustion for a spin start will be at a significantly higher pressure than a tank-head start, and will therefore reduce the likelihood of turbine-inlet temperature spikes. Thus, a spin start will usually be recommended for hydrogen-fueled engines with a gas generator.

Cryogenic fuel; expander cycle. An expander-cycle engine has a relatively low turbine pressure-ratio at mainstage because the turbine flow goes into the main combustion chamber. During start, prior to main-chamber prime, there is very low back-pressure. As a result, a tank-head start will be a turbine pressure-ratio equal to or higher than mainstage. This produces a high turbine power for a relatively rapid speed-buildup. Also, the expander does not have any combustion upstream of the turbines, so temperature spikes are not a problem. This cycle should therefore be fairly easy to tank-head start. It is also difficult to spin start because a significant

portion of the fuel-pump flow goes through the turbine. Therefore, a high turbine-inlet pressure generated by a spin system restricts the fuel-pump flow, resulting in a low flow-coefficient. Because a hydrogen pump is very susceptible to stall and boil-out at low flow, this cycle should use a tank-head start.

Cryogenic fuel; staged-combustion engine. In the staged-combustion engine, most of the fuel flow is used by the turbines; therefore it has the same potential fuel-pump stall problem (for a spin start) as the expander cycle. The tank-head start has the difficult problem of preventing turbine-inlet temperature spikes at low flowrates. Even though difficult, tank-head start is used for the staged-combustion cycle, but start temperature spikes can lead to turbine-blade damage. They can force use of coatings for thermal protection.

Turbopump-Drive Arrangements

The specific type of coupling between turbine and pumps depends not only upon the propellants being pumped but also on the design of the overall engine system. Various turbopump-drive arrangements are shown schematically in Fig. 6-15. Where a single turbine directly drives both propellant pumps through a common shaft, it can be located either on the shaft end (with back-to-back pump arrangement) or between pumps. Then both pumps and turbine will operate at the same shaft speed. Gear-driven turbopump arrangements include the pancake type, which uses different reduction gears and is applied where there are speed differentials between pumps and turbine; the offset turbine, with both pumps on one shaft but driven through a gear train; and the single-geared pump where one pump is mounted with the turbine on the same shaft, while the other is driven through a reduction gear. Dual-shaft turbopump arrangements with pump and turbine for each propellant on separate shafts include two gas turbines in series, with the discharge gas from the first turbine driving the second turbine, and two gas turbines in parallel, both receiving gas directly from the power source.

Description of Developed Turbopump Systems

Figure 6-16 shows the major elements of a typical geared liquid-bipropellant turbopump system for a rocket engine. Developed for a 188,000-lb-thrust LOX/RP-1 booster engine, this dual-pump unit consists of oxidizer pump, fuel pump, reduction gearbox, accessory drive adapter, and a turbine. The turbine is started by hot gases from a turbine spinner (solid-propellant gas generator) and powered from a liquid-propellant gas generator during mainstage. The turbine shaft drives a series of reduction gears, which in turn drive the pump shaft. The turbopump gears and bearings are cooled and lubricated either by a separate oil-supply system or by a fuel-additive subsystem. During mainstage operation, the turbopump supplies oxidizer and fuel to the main thrust chamber as well as to the gas generator at the required pressures and flow rates. Table 6-1 lists operating characteristics and materials of construction for this turbopump.

Both oxidizer and fuel pumps are of single-entry, centrifugal-flow type. They are mounted back-to-back on a common shaft, one on each side of the gearbox. The fuel pump is bolted to the gearbox,

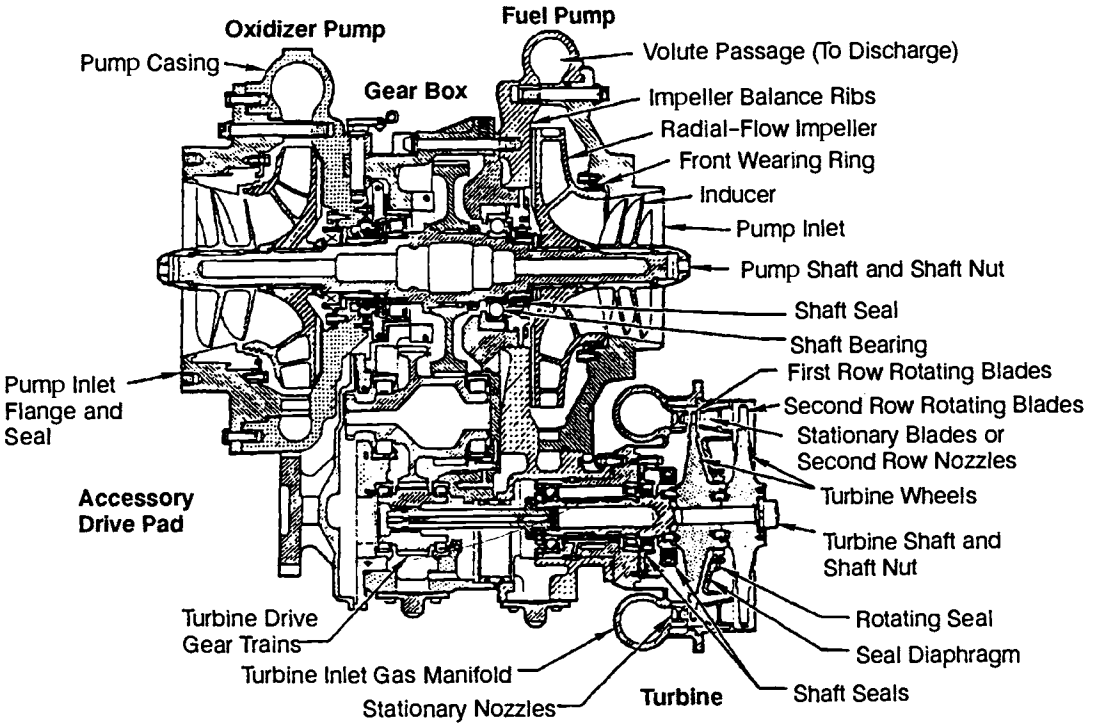

Fig. 6-16 Major elements of a geared turbopump.

Table 6-1 Operating characteristics and construction materials for turbopump shown in Fig. 6-16.

	Oxidizer	Fuel
Pumps:		
Fluid	Liquid oxygen	RP-1
Inlet density	71.38 lb/ft^3	50.45 lb/ft^3
Inlet pressure (total)	80.0 psia	57.0 psia
Discharge density	70.95 lb/ft^3	50.55 lb/ft^3
Discharge pressure (total)	915.2 psia	1,023.0 psia
Pressure rise in pump	835.2 psi	966.0 psi
Pump developed head	1,696.2 ft	2,751.0 ft
Volume flow	3,257.4 gpm	2,007.6 gpm
Flow rate	518.0 lb/s	225.7 lb/s
Shaft speed	6537 rpm	
Efficiency	75.5%	72.1%
Shaft power	2,117 bhp	1,585 bhp
NPSH required	35.0 ft	35.0 ft
Casing material	TENS 50-T6 aluminum alloy sand casting	
Inducer material	7075-T6 aluminum alloy die forging	2024-T351 aluminum alloy plate
Impeller material	TENS 50-T6 aluminum alloy sand casting	9669-48230-3 aluminum alloy sand casting
Shaft material	4340 alloy steel	
Bearing material	9310 alloy steel	
Turbine:		
Inlet gas pressure (total)	597.6 psia	
Exit gas pressure (static)	32.86 psia	
Pressure ratio: Total inlet/static exhaust	18.21	
Inlet gas pressure (static)	517.8 psia	
Inlet gas temperature	1200°F	
Exit gas temperature	938°F	
Gas flow rate	17.34 lb/s	
Brake horsepower	3,793 hp	
Shaft speed	31,740 rpm	
Efficiency	66.2%	
Housing material	Hastelloy "B"	
Nozzle block material	Hastelloy "B"	
Wheel material	Timken alloy 16-25-6 AMS-5727 steel	
Shaft material	4340 alloy steel	
Bearing material	9310 alloy steel	
Gearbox:		
Reduction speed ratio	1/4.855	
Gearbox material	TENS 50-T6 aluminum alloy sand casting	
Gear and shaft material	9310 alloy steel die forging	
Bearing material	9310 alloy steel	

while the oxidizer pump is secured to it by radially inserted steel pins. These pins allow the oxidizer-pump housing to expand and contract during extreme temperature changes without distortion and misalignment. Each pump has an axial-flow inducer, a radial-flow impeller with backward curved vanes, stationary diffuser vanes, and a volute. The diffuser vanes and volute are designed to achieve uniform pressure at the outer diameter of the impeller to minimize radial loads. Balance ribs on the back side of the impellers neutralize pump-shaft axial thrust.

The gearbox includes a series of full-depth reduction spur gears with integral-bearing inner races, gear carrier and main-shaft bearings, accessory drives, pump-shaft bearing seals, and a bearing heater on the oxidizer-pump shaft. A drain manifold handles horizontal drainage. The gears reduce the speed of rotation between turbine and pump shaft by an overall ratio of 4.88 to 1. Details of typical turbopump gears and bearings are shown in Fig. 6-17. The pump shaft turns clockwise as viewed from the oxidizer pump. The sequence of power transmission goes from turbine to high-speed pinion gear then and to pump-shaft gear. Power is also transmitted to a main accessory-drive gear from a drive pinion gear mounted on the intermediate gear shaft.

The turbine—an impulse-type, two-stage pressure-compounded unit (Fig. 6-12) bolted to the fuel-pump housing—consists of a hot-gas inlet manifold, stationary nozzles and vanes, first- and second-stage turbine wheels, a turbine shaft, and a splined quill shaft connecting the turbine shaft to the high-speed pinion gear. The turbine shaft is supported on the inboard side by a ball bearing; on the outboard side, by a roller bearing. Carbon-ring shaft seals prevent hot-gas leaks. The turbine-inlet manifold distributes the gases to the first row of stationary nozzles. They, in turn, distribute the gases to the first row of rotating blades. When leaving these, the gases again increase velocity when passing through the second row of stationary nozzles. They finally pass through the second row of rotating blades and leave the turbine through an exhaust duct. A sealing diaphragm between the first and second turbine wheel prevents the hot gas from bypassing the second row of stationary nozzles.

Figure 6-18 shows a direct-drive liquid-oxygen turbopump for a dual-shaft turbopump system. The main pump element, a double-suction design, has a rotor consisting of mirror-image inducers and back-to-back centrifugal impellers. The flow splits equally in the inlet, flows through the inducers and impellers, and is rejoined at the impeller outer diameter, subsequently flowing through the vaned diffuser and volute. As can be seen in Table 6-2, this pump has a discharge pressure at rated power level of 4100 psi, but 9.3% of the oxygen flow is tapped off downstream of the main pump and sent through the small centrifugal "kick" pump, which raises the pressure to 6952 psi. The shaft system rotates on duplex ball bearings, which are cooled by a positive flow of the liquid oxygen from the pump.

The turbine-drive gas comes from a preburner system, the turbopump being used on a staged-combustion-cycle engine. The turbine, a two-stage axial-flow reaction design, has a small reaction rate to help minimize axial loads. A mixture of liquid hydrogen and hot gas cools the turbine disks and housing to attain structural integrity. The turbine-drive fluid is prevented from mixing with the liquid oxygen by a complex seal package consisting of a main LOX seal, double-floating-ring intermediate seal with an interior helium purge, and a double-

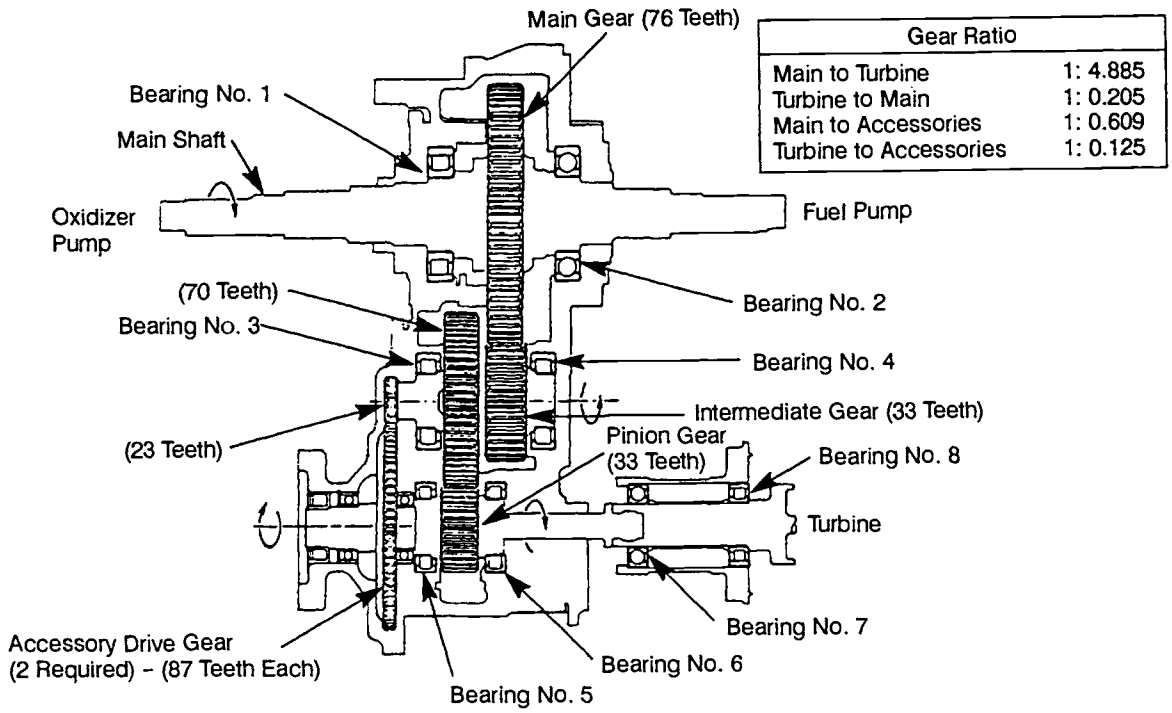

Fig. 6-17 Typical turbopump gears and bearings.

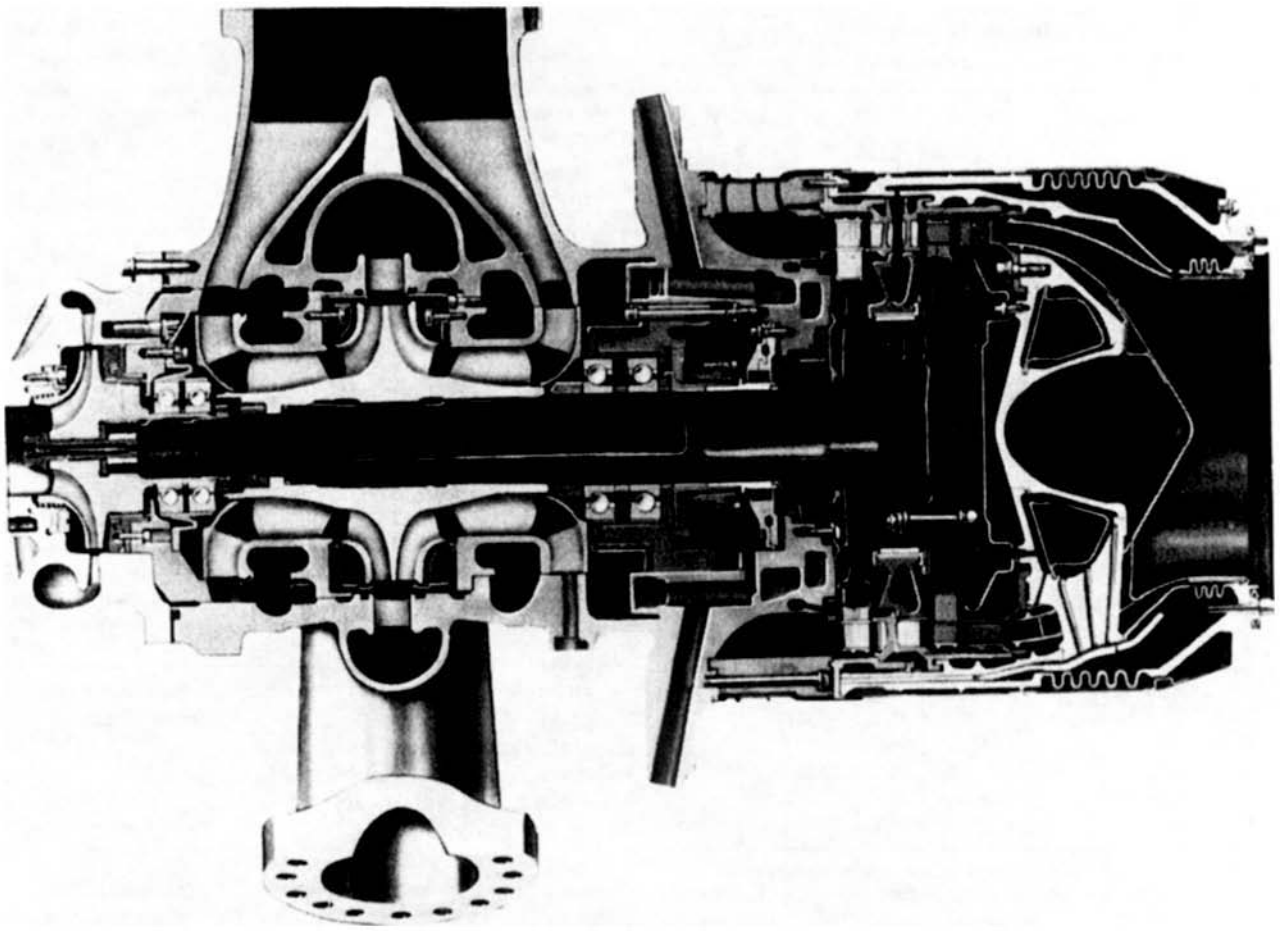

Fig. 6-18 SSME *HPOTP*.

floating-ring hot-gas seal. Overboard drains minimize the required helium-supply flowrate.

Axial thrust is controlled by a double-acting balance piston located on the front shrouds of the back-to-back main impeller.

6.2 TURBOPUMP SYSTEM PERFORMANCE AND DESIGN PARAMETERS

Being closely related, variation of the turbopump design and operating parameters will contribute to the optimization of both turbopump and engine system performance. The design procedure for the turbopump system includes evaluation of all possible design approaches and mechanical configurations that can satisfy engine system specifications. From this will be selected the best design with respect to overall systems reliability and performance. Further discussion of this subject can be found in Ref. 6-1.

Turbopump System Performance

Turbopump performance affects the vehicle payload in three ways:

1) Turbopump component weight. Since the turbopump components form part of stage burnout weight, they directly affect stage payload.

2) Required pump-inlet suction pressure. Required suction pressure directly translates into required main-propellant-tank pressure level. Suction pressure raised, tank and pressurization-system weights increase and thus reduce the stage payload for a given burnout weight.

3) Turbine-gas flowrate. For gas-generator cycles, the turbine-drive gases are usually ejected at a lower specific impulse than the thrust-chamber gases. Their flowrate decreases the overall I_s of the engine system and thus for a given velocity increment it decreases the allowable stage-burnout weight. For a fixed weight of engines, tanks, guidance, and other equipment, a decrease in allowable stage-burnout weight decreases payload weight.

Turbopump System Design Parameters

In the design of turbopump systems, the following parameters, often interdependent, are considered paramount: propellant properties, pump-developed heads and flowrates, pump specific speeds, pump net positive suction head (NPSH), pump efficiencies, overall performance and operating efficiency of turbine, turbopump-system cycle efficiency, and turbopump-system calibration and off-design characteristics. No simple rules are available for optimizing the correlations of these parameters when designing a specific type of turbopump for a given engine

Table 6-2 Operating parameters for turbopumps on the SSME at rated power level.

Turbopump Figure Reference	LPOTP 6-7	HPFTP 6-5	HPOTP Main 6-18	HPOTP Boost
Pump:				
Fluid	LOX	LH_2	LOX	LOX
Inlet density, lb/ft^3	71.03	4.32	70.28	70.28
Total inlet pressure, psia	100.0	250	374.8	4,031
Total discharge pressure, psia	408.8	6,024.8	4,129.8	6,952.2
Pump developed head, ft	625.9	168,920	7,591	5,934
Flow rate, lb/s	890.3	148.5	1,067	101.2
Volumetric flow at inlet, gpm	5,626	15,436	6,814	594.7
Shaft speed, rpm	4,961	33,974	27,039	27,039
Efficiency, %	68.6	77.3	67.3	82.5
Shaft power, bhp	1,476	58,970	21,882	1,330
Turbine[a]**:**				
Fluid	LOX	Hot gas	Hot gas	
Inlet total pressure, psia	3.961	4,933	4,924	
Discharge total pressure, psia	408.8	3,376	3,286	
Isentropic velocity ratio	0.465	0.356	0.286	
Pressure ratio, T-T	--	1.461	1.498	
Inlet temperature, °R	191.3	1835.9	1430	
Discharge temperature, °R	189.7	1698.3	1314.9	
Flow rate, lb/s	176.9	145.6	60.6	
Horsepower	1,476	58,972	23,212	
Shaft speed, rpm	4,961	33,974	27,039	
Efficiency, %	63.1	79.6	78.1	

[a] The turbine for the LPOTP is a hydraulic turbine, and the two high-pressure turbines are two-stage pressure compounded designs using O_2-LH_2 combustion products.

systems application. Generally speaking, however, available pump suction pressure together with the basic pump flow characteristics will determine the maximum shaft speed at which the unit can operate. The higher this shaft speed, the lower the turbopump weight will likely be. Once the pump speed is determined, turbine type, turbine driving arrangement, and turbine power source will be selected on the basis of efficiency, weight, simplicity, and other factors.

Propellant properties. General data for some propellants used in liquid-rocket engines are given in Tables 1-3 to 1-5. Table 6-3 lists properties of commonly used liquid propellants that have specific significance in the design of pumps. These propellants include earth-storable liquids such as RP-1 and N_2O_4, cryogenics such as LO_2 and LH_2, and liquids having a wide range of physical and chemical properties.

The low temperature of cryogenic liquids imposes design limitations that must be addressed in the selection of materials, seals, bearings, and lubricants. For example, the temperature is low enough to freeze any water vapor present, creating ice that can damage parts or cause them to malfunction. The total temperature range to which the structural elements of a cryogenic turbopump may be exposed varies from -300 to -430°F at the pumps to 1200 to 1700°F at the turbine. This induces temperature gradients between the various turbopump components that must be accommodated, and requires structural flexibility or suitable devices to

Table 6-3 Fluid properties of commonly used liquid propellants.

Liquid	[a]Data at Normal Conditions					
	Temperature, °F	Vapor Pressure, psia	Density lb/ft^3	Conversion Factors: Head ft/ Pressure, psi	Conversion Factors: gpm/ lb-s	Viscosity, $lb\text{-}s/in^2$
N_2O_4	60	11.1	90.7	1.59	4.96	0.637×10^{-7}
H_2O_2 (90%)	60	0.026	87.8	1.64	5.12	1.868×10^{-7}
N_2H_4	60	0.158	63.3	2.28	7.12	1.49×10^{-7}
RP-1	60	0.031	50.8 (max)	2.83 (min)	8.84 (min)	3.22×10^{-7}
			49.8 (min)	2.89 (max)	9.00 (max)	
Ethyl-alcohol (95%)	60	0.062	50.4	2.85	8.91	2.22×10^{-7}
UDMH	60	1.83	49.66	2.90	9.06	0.842×10^{-7}
50% UDMH/N_2H_4	60	1.77	56.66	2.54	7.94	1.378×10^{-7}
LO_2	-297.6	14.7	71.17	2.02	6.32	0.2765×10^{-7}
LF_2	-307	14.7	94.21	1.54	4.79	0.353×10^{-7}
[c]LH_2	-422.9	14.7	4.43	32.5	101.5	0.0208×10^{-7}
[b]LN_2	-320.4	14.7	50.44	2.86	8.92	0.226×10^{-7}
[b]water	60	0.256	62.37	2.31	7.2	1.64×10^{-7}

[a] Normal conditions do not necessarily imply standard conditions, if tank pressures have been applied.
[b] Included here because these fluids are frequently used as pump calibration media.
[c] Conversion factors are affected by thermodynamic effects for large pressure changes.

permit the required thermal expansion and contraction. Radial connecting pins are often employed to permit a cryogenic pump to contract independently of a turbine and of a normal-temperature pump.

The vapor pressure of the propellants under normal engine operation conditions directly influences total suction-pressure requirements at the pump inlet. This will be further discussed in conjunction with the pump-inlet net positive suction head (NPSH).

The density variations of different propellants produce substantially different pump headrise requirements, as well as large differences in volume flow. The power required per unit weight flow and pressure rise of a pump is inversely proportional to the density of the fluid—dramatically evident in the case of liquid hydrogen, which has a density of less than 10% of that of other propellants. For the same weight flow and pressure rise, a liquid-hydrogen pump requires more than 10 times the volume flow and driving power of other propellant pumps. Thus the design of liquid-hydrogen pumps requires specific considerations.

The viscosity of the pumped fluids effects a boundary layer along the surface of the flow passages within the pump. There is a minimum size of the impeller cross-section below which pump performance will fall off rapidly. As the passage clearances in the impeller are decreased, a point will be reached where the flow is predominantly boundary layer, and viscous forces rather than turbulent forces become predominant. This completely changes the performance of a pump. The drag effect of the boundary layers, together with the rotation of the fluid in certain pump passages (such as in the impeller of a centrifugal pump), results in secondary flows being set up. These flows, together with friction losses (also in direct proportion to the viscosity of the fluid) and leakage losses, constitute a major portion of the energy losses in a pump. A high propellant viscosity tends to lower pump efficiency.

Some liquid propellants, such as LF_2 and N_2H_4, are highly reactive chemically and are thermally unstable beyond certain temperature limits. In the design of turbopumps for these propellants, special consideration must be given to the selection of compatible materials as well as to the construction of mechanical parts. Seals, bearings, and the protection (insulation) of the pump section against heat influx from the turbine section following engine shutdown are typical problem areas.

Pump-developed heads and flow rates. The pump adds energy to the fluid preferably in the form of higher discharge static-pressure. The term "pump-developed head" (DH), defined as the difference between pump-discharge total head and pump suction head, represents the energy added per pound of pumped fluid expressed as a change in enthalpy with units of ft-lb/lb, which is typically shortened to units of "ft." For an incompressible fluid, developed fluid pressure [Δp (psi)] and fluid head [ΔH (ft)] have this relationship:

$$\Delta H = 144\ \Delta p/(\text{fluid density}) \qquad (6\text{-}1)$$

where Δp is in units of psi and density is in units of lb/ft^3. For a fluid like hydrogen that has a degree of compressibility, the head is typically defined as the isentropic enthalpy rise from inlet conditions to the discharge pressure. The specific head/pressure relationship is dependent on the fluid-thermodynamic state conditions. For small pressure changes (e.g., less than 1000 psi), the incompressible relationship shown above can generally be used as a first approximation.

The required pump-developed head at the design propellant flowrate (i.e., engine thrust level) is dictated by the sum of the hydraulic resistances within the engine's propellant-flow system. These resistances include the pressure drops across injector, thrust-chamber manifold, cooling jacket, propellant valves and ducts, as well as the thrust-chamber pressure. In addition, for the staged combustion cycle and the expander-cycle engine, pressure differential across the turbine must be provided for in the pump-discharge pressure. Figure 6-19 shows an engine propellant-flow-system hydraulic-resistance curve representing the resistance head to flowrate relationship at various pump operating levels.

The head is developed by the rotating members imparting energy to the fluid primarily in the form of kinetic energy. This kinetic energy is then converted by the stationary members into pressure energy. The magnitude of the developed head for a given design is a function of both the pump speed and flow. The head is generally expressed by a head-flow (H-Q) characteristic at one or more constant values of speed, as shown in Fig. 6-19. At high flows, the pump-drive energy is consumed by internal flow losses, and the head rise decreases to zero. At the other extreme, as flow decreases the head continues to increase, at least at first. It can then level off, begin slowly to decrease, or, in some cases, drop off dramatically due to phenomena known as stall. That unstable condition, discussed below, must be avoided to achieve constant pump

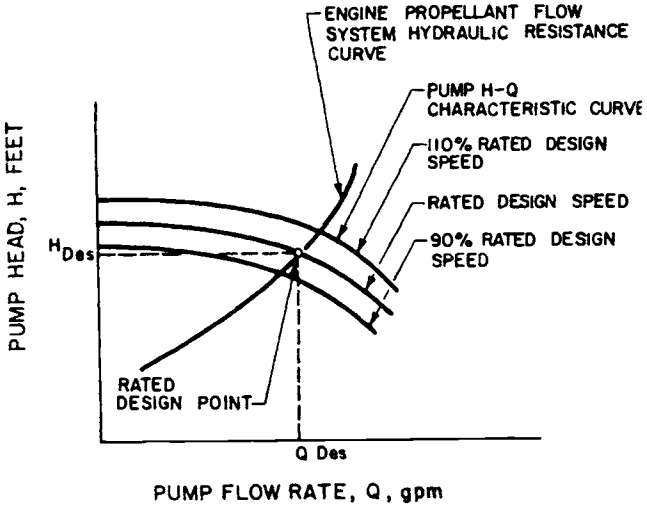

Fig. 6-19 Engine system resistance and pump characteristics.

operation. Increasing speed increases the head by the speed-squared relationship provided the ratio of flow/speed can be maintained constant. This is strictly true only for an incompressible fluid, but approximately valid even for a compressible liquid like hydrogen.

Two dimensionless coefficients are frequently used to indicate the head and flow characteristics of a given pump: pump head coefficient ψ and pump flow coefficient ϕ. The pump head coefficient is the ratio of rated pump head (ft) to the maximum theoretical head at zero flow for meridional (axial) inlet (no prerotation), expressed as follows:

$$\psi = \Delta H/(U_2^2/g) \qquad (6\text{-}2)$$

where—

- ψ = overall pump head coefficient at rated design point (range is 0.4 to 0.7 for a single-stage centrifugal pump and 0.2 to 0.4 for a single-stage axial pump)
- ΔH = pump rated developed head, ft
- U_2 = mean tip velocity of pump impeller at rated design rotating speed, ft/s
- g = gravitational constant, 32.2 ft/s^2

The pump flow coefficient ϕ can be defined based either on inlet or discharge conditions, each as a ratio of the average meridional velocity (cm) in ft/s divided by a tip speed U in ft/s (that is, ϕ = cm/U). The inlet flow coefficient uses inlet velocity based on the flow and the geometric area from the first rotor-inlet tip to the hub. The value of U is based on the inducer tip diameter, if present, or the impeller eye diameter (tip diameter at the inlet of the blade). For the discharge flow coefficient, the average meridional velocity at the impeller discharge is used together with the tip speed at the impeller exit. Inlet flow coefficients for rocket-engine pumps typically range from 0.07 to 0.30. Discharge flow coefficients range from 0.01 to 0.15.

Pump specific speeds. For any given pump design, the relation between fluid flow rate Q, developed fluid head ΔH, required driving power hp, and rotating speed N can be defined by three expressions called the *affinity laws* of a pump. These laws state:

1) *Pump volume flowrate varies directly with speed:*

$$Q_1/Q_2 = N_1/N_2 \qquad (6\text{-}3a)$$

2) *Pump-developed head varies directly as the square of the speed:*

$$\Delta H_1/\Delta H_2 = N_1^2/N_2^2 \qquad (6\text{-}3b)$$

3) *Pump driving power varies directly as a cube of the speed:*

$$hp1/hp2 = N_1^3/N_2^3 \qquad (6\text{-}3c)$$

The affinity laws are based on the assumption that the pump efficiency is independent of the rotating speed. Actual pump operation has shown, however, that pump efficiency *does* change with speed. The degree depends on the individual pump design and the pumped fluid. Most rocket-engine propellants are basically incompressible and show less than 2 or 3% change in efficiency over a wide speed range. Thus the pump affinity laws hold quite well in most cases. Because much more strongly affected by speed, hydrogen pumps need efficiency calculated by a thermodynamic model of the pump system at the desired speeds.

The relationships established in Eq. (6-3a), (6-3b), and (6-3c) permit deriving a useful pump-design parameter, the pump stage specific speed, NS:

$$N_S = N(Q)^{0.5}/(\Delta H)^{0.75} \qquad (6\text{-}4)$$

where—

- N_S = pump specific speed
- N = pump rotating speed, rpm
- Q = pump flowrate, gpm
- ΔH = pump-developed head in a given stage

Pump specific speed is a characteristic value typically defined at the point of maximum efficiency, which is usually the design point. In pump design, this term is very useful to classify inducers or impellers on the basis of both performance and geometric proportions regardless of the actual size or speed at which they operate. N_S, a function of design configuration, does not vary significantly for a series of geometrically similar impellers (having the same angles and proportions), or for a particular impeller operating at any speed.

Figure 6-20 indicates typical pump specific speeds for various impeller geometries. For a given speed, a low value of specific speed is characteristic for low-volume flow, high-headrise pumps. Higher specific speed indicates a higher-volume-flow, low-head-rise pump.

Radial-type impeller. The head is largely developed by action of centrifugal force. This radial type is used for specific-speed from 500 to 1200. Geometric proportion (r_2/r_1) varies from 2 to 3.

Francis-type impeller. This type has an axial inlet and a radial discharge, and is used for lower heads. Specific speed generally ranges from 1000 to 2400. Geometric proportion (r_2/r_1) varies from 1.3 to 1.8. The Francis type is most representative of rocket-engine pumps.

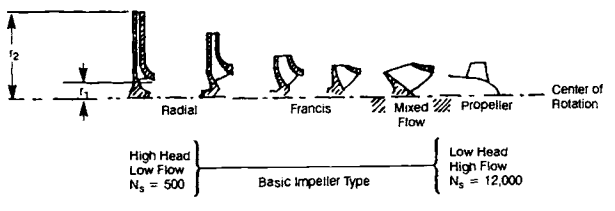

Fig. 6-20 Relationship between the pump specific speeds and pump-impeller geometries.

Mixed-flow-type impeller. The head developed in this impeller is due partly to change in tangential velocity and partly to change in fluid velocity relative to the rotor. Discharge is partly radial and partly axial. The impeller blades are doubly curved. Specific speed varies from 2200 to 3500.

Propeller-type impeller. The head developed by this type is through push of the vanes only. Flow direction is axial. Specific speeds range from 3000 to 6000 for multi-stage impellers, and from 6000 to 12,000 for inducers.

Sample Calculation 6-1

The following data characterize the propellant pumps of the hypothetical A-1 Stage engine at the rated design point:

Pump	***Oxidizer***	***Fuel***
Fluid density, lb/ft^3	71.38	50.45
Inlet total pressure, psia	55	45
Pump discharge pressure, psia	1505	1720
Pump flowrate, lb/s	1971	892
Pump speed, rpm	7000	7000

Problem

Determine the pump specific speeds.

Solution 6-1

For the oxidizer pump:

developed pressure	= 1450 psi
developed head	= 2930 ft
volumetric flowrate	= 12,420 gpm
specific speed	= 1980

For the fuel pump:

developed pressure	= 1675 psi
developed head	= 4790 ft
volumetric flowrate	= 7960 gpm
specific speed	= 1083

Pump net positive suction head (NPSH); cavitation. Allowing the static pressure of the fluid at the pump inlet or any regions within the pump to drop below the local fluid vapor-pressure level will cause these regions to cavitate; i.e., the fluid will pass from liquid to vapor and form bubbles. The formation of vapor alters the effective flow passages of the fluid and can seriously affect normal pump performance. The subsequent collapse of these vapor regions creates local pressure forces that can cause flow instabilities and/or substantial damage.

To avoid cavitation during operation of a propellant pump, the pump-inlet available net positive suction head $(NPSH)_a$, furnished by the propellant-feed system upstream of the pump, must be higher than the suction head above the propellant vapor pressure at which cavitation would begin. $(NPSH)_a$ is the difference between the propellant inlet total pressure head and the propellant vapor pressure, expressed as follows:

$$(NPSH)_a = (144/\rho)\,[P_t - \Delta p_f - p_v] + Z \qquad (6\text{-}5)$$

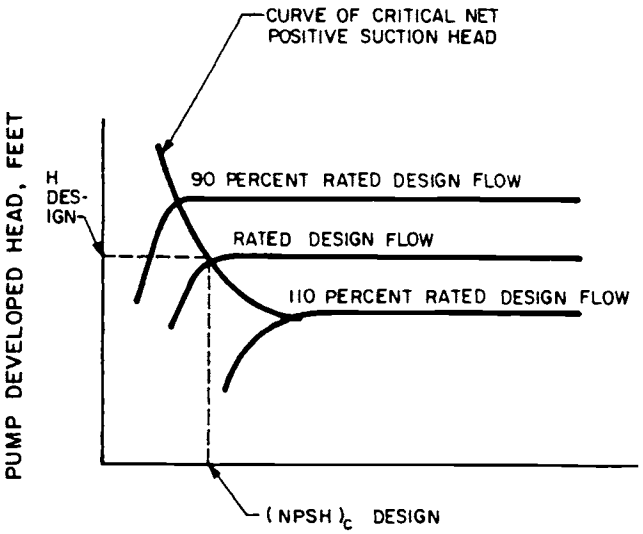

Fig. 6-21 Typical cavitation characteristics of a pump operated at rated design speed.

where—

$(NPSH)_a$ = available net positive suction head, ft
P_t = propellant-tank pressure, psia
ρ = density of propellant, lb/ft^3
Z = height of propellant above the pump inlet and within the tank (corrected in flight for vehicle acceleration and gravity effects), ft
Δp_f = pressure drop due to friction losses within the propellant suction ducts, psi
p_v = propellant vapor pressure for the propellant temperature at the pump inlet, psia

Alternatively, total pressure at the pump inlet given by P_{t1}, NPSH can be simply expressed as—

$$NPSH_a = (P_{t1} - p_v)144/\rho \qquad (6\text{-}6)$$

In design practice, the term "critical net positive suction head" $(NPSH)_c$ defines the NPSH value that will result in a 2% head-generation loss at the rated design speed and flow rate of a given pump. (Some references use a 3% head falloff rather than 2%.) Usually further reduction in inlet NPSH below the (NPSH)c point results in rapidly increasing cavitation. In turn, the developed head is further reduced, bringing on nonsteady flow. Figure 6-21 represents the cavitation characteristics of a typical pump operated at rated design speed. Although the head produced by the pump remains relatively constant down to the critical NPSH, there may be significant cavitation occurring in the pump that can produce other effects. This is particularly true of inducers, which are designed to operate with cavitation. However, the cavitation can produce physical damage to the hardware and increase oscillations of both flow and pressure in the pump. It is not uncommon to be able to visually see cavitation in inducers at NPSH values that are several times the

critical, and the oscillations are typically noticeable in the range from one to two times the critical. These effects are dependent on the design, and it is not necessary, in general, to eliminate all cavitation to achieve a good design even for applications requiring long life. In fact, most rocket-engine pumps operate with cavitation to minimize weight. Below the critical NPSH, surging flow can occur or pump speed can run away due to the loss of head in the pump. Operation below this value must be carefully monitored.

To ensure a margin of safety for pump operation, the $(NPSH)_a$ supplied by the vehicle must be larger than the $(NPSH)_c$ of the propellant pumps. The margin to be used will depend on the application. General guidelines are presented in the section on inducer design.

It is useful to compare the suction characteristics of various pump designs on the basis of a design parameter called suction specific speed N_{SS}, which is defined as follows:

$$N_{SS} = N(Q)^{0.5}/(NPSH)_c^{0.75} \qquad (6\text{-}7)$$

where—

N_{SS} = pump suction specific speed
N = pump rated design speed, rpm
Q = pump rated design volume flow rate, gpm
$(NPSH)_c$ = pump critical net positive suction head, ft

Suction specific speed is related to the critical net positive suction head in the same manner the specific speed is related to overall pump-developed head. Design values of suction specific speeds for rocket-propellant pumps range from 10,000 without inducers to values over 100,000 for certain propellants with inducers.

Another coefficient describing pump suction characteristics, the Thoma parameter r, is the ratio of critical net positive suction head $(NPSH)_c$ and rated pump-developed head ΔH:

$$r = (NPSH)_c/\Delta H = (N_S/N_{SS})^{1.333} \qquad (6\text{-}8)$$

This parameter is not commonly used today because it does not represent a common pump characteristic.

For a given vehicle $(NPSH)_a$, the pump suction characteristics N_{SS} determine the maximum permissible rpm at the design flowrate. A high pump N_{SS} capability or a high vehicle $(NPSH)_a$ permits a higher pump rpm, lower turbopump weight, and possibly higher turbine performance. It is desirable to operate a pump at the highest practical speed. Figure 6-22 represents the results of a parametric turbopump-system design study for a typical $LO_2/RP\text{-}1$ booster-stage rocket, such as the A-1 Stage engine. The study reflects the effects of N, $(NPSH)_c$, and N_{SS} on the selection of turbopump configuration.

In addition to the pump $(NPSH)_c$ values during steady-state operation, the engine starting transient pump $(NPSH)_c$ must be determined and specified to permit satisfactory pump acceleration from zero to nominal design speed and flow rate in the desired time and manner. The starting $(NPSH)_c$ depends on the rate of acceleration and on the control system of the engine, as well as on vehicle acceleration, gravity effects, and propellant-suction-duct geometry. Therefore, sufficient tank pressure must be provided to accelerate the propellant and to overcome the hydraulic resistance in the suction duct, as well as to supply the necessary pump $(NPSH)_c$ during all phases of system operation. Similarly, the NPSH during shutdown transients must be sufficient to permit a safe shutdown without a turbopump-overspeed condition.

Pump operational efficiency; losses. Several types of energy loss occuring during pump operation affect efficiency.

Hydraulic losses. These include friction losses in the passages and flow-turbulence losses. The friction losses are a function of the "wetted areas" in the passages and of the roughness of their surfaces. The turbulence losses are caused by disturbances in certain regions of the pump, such as at the inlet and outlet edge of the vanes of both impeller and diffuser and in the return guide-vanes. Flow in pump components is essentially always diffusing (lower *relative* velocity at the exit plane than at the inlet for a given blade row), which has associated losses. Tip-clearance flows contribute losses in unshrouded regions. Cavitation in flow passages can increase these losses by causing local accelerations plus adding the losses associated with the cavitation-collapse mechanism.

Disk-friction losses. The energy required to rotate a disk, such as an impeller or inducer, in a fluid is known as disk-friction loss. The disk-friction losses are due to two actions: the actual friction of fluid on the disk, which is relatively minor, and a pumping action on the fluid in contact with the disk, whereby the fluid is circulated locally by centrifugal action. The energy loss due to disk friction is transformed into heat and can appreciably increase the temperature of the fluid.

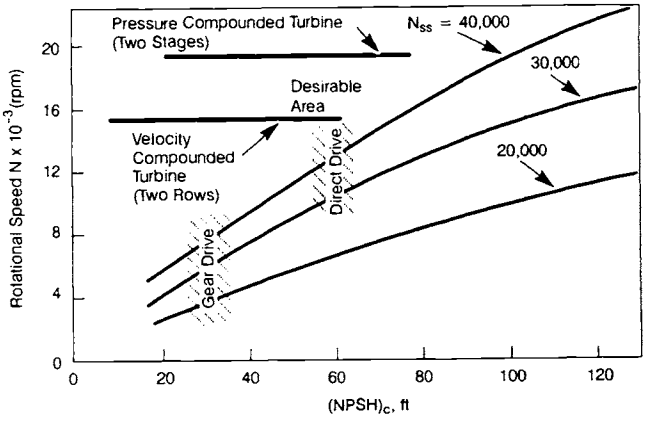

Fig. 6-22 Effects of N, $(NPSH)_c$ and N_{SS} on turbopump selection for a typical $LO_2/RP\text{-}1$ booster-stage rocket engine system.

Mechanical losses. These are losses in bearings and seals caused by mechanical friction.

Leakage losses. To prevent the pumped fluid from leaking back to the inlet after it has exited the impeller and is at outlet-pressure levels, close-clearance seals or wearing rings are provided. Increases in leakage require pumping power and introduce heat into the inlet fluid; both contribute to a loss in efficiency.

The overall efficiency of a pump (η_p) can be expressed by the ratio of pump fluid-horsepower output, fhp, to brake-horsepower input by the pump drive, bhp:

$$\eta_p = \text{fhp}/\text{bhp} \tag{6-9}$$

The pump fluid horsepower—the actual usable output delivered by the pump—is the product of delivered propellant weight flow [w_p (lb/s)] times the actual head ΔH(ft) developed by the pump, divided by a conversion factor:

$$\text{fhp} = w_p \Delta H/550 \tag{6-10}$$

The brake horsepower represents the mechanical horsepower delivered to the pump by the drive. It is consumed in the pump as fluid horsepower and as the various losses:

$$\text{bhp} = \text{fhp} + (\text{hp})_h + (\text{hp})_{df} + (\text{hp})_m + (\text{hp})_l \tag{6-11}$$

where—

- bhp = brake horsepower
- fhp = fluid horsepower
- $(\text{hp})_h$ = horsepower required to overcome hydraulic losses
- $(\text{hp})_{df}$ = horsepower required to overcome disk friction losses
- $(\text{hp})_m$ = horsepower required to overcome mechanical losses
- $(\text{hp})_l$ = horsepower required to overcome leakage loss

The efficiency of a pump is related to the volume flow rate Q and the pump specific speed N_S. There is a definite trend toward increased efficiency with higher pump capacities primarily because the resulting larger size of the pump permits operation with smaller relative clearances, reducing leakage losses, and surfaces that are hydrodynamically smoother, reducing the skin-friction losses. The low-specific-speed pumps have less efficiency because they typically have disk-friction and leakage losses that are relatively higher. This can be seen from Fig. 6-23, which shows the efficiency as a function of both the specific speed and the volumetric flowrate. (All rocket-engine pumps do not fall exactly on these curves, but they show the correct trends.) The overall efficiency of rocket-engine propellant pumps of high developed head and rotating speed ranges from 60 to 85%. This is up to 10% lower than that of high-performance industrial pumps. For a typical centrifugal pump, Fig. 6-24 shows the correlation between pump flowrate and the following three parameters: developed head, efficiency, and required brake horsepower.

Turbine overall performance and operating efficiency. The turbine generates the power needed to rotate the pump at the desired speed. The turbine derives its energy from the working fluid. The power generated equals the product of the flow times the available energy of the working fluid times the turbine efficiency. To achieve the desired power, the turbine designer will typically try to achieve the maximum efficiency within the constraints imposed, and the tradeoff between flow and available energy will depend on the particular cycle.

The available energy content of the turbine working fluid is defined as the enthalpy drop per pound of working fluid in the turbine:

$$\Delta H_t = H_o - H_e \tag{6-12}$$

where—

- ΔH_t = available energy content of the working fluid, Btu/lb
- H_o = enthalpy per unit weight of the working fluid at turbine inlet, Btu/lb
- H_e = enthalpy per unit weight of the working fluid at exhaust pressure (assuming isentropic expansion), Btu/lb

Using Eq. (1-10) and (1-13), Eq. (6-12) can be rewritten for an ideal gas as follows:

$$\Delta H_t = C_p(T_o - T_e) = C_p T_o \left[1 - \left(\frac{p_e}{p_o} \right)^{\frac{\gamma - 1}{\gamma}} \right] \tag{6-13}$$

where—

- C_p = working-fluid specific heat at constant pressure, Btu/lb-F
- T_o = working-fluid total temperature at turbine inlet, °R
- T_e = working-fluid static temperature at turbine exhaust, °R
- p_o = working-fluid total pressure at turbine inlet, psia
- p_e = working-fluid static pressure at turbine exhaust, psia
- γ = working-fluid specific heat ratio

The ratio of turbine-inlet and exhaust pressures p_1/p_2 can be expressed as the turbine pressure ratio R_t, which is a frequently used parameter in turbine design. Substituting this into Eq. (6-13) yields—

$$\Delta H_t = C_p T_o \left[1 - \left(\frac{1}{R_t} \right)^{\frac{\gamma - 1}{\gamma}} \right] \tag{6-14}$$

It can be seen that the available energy in the turbine working fluid is a function of gas properties, inlet temperature, and the turbine pressure ratio.

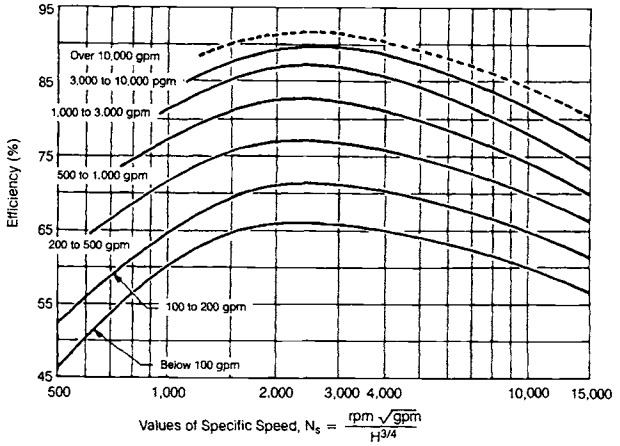

Fig. 6-23 Variation of pump efficiency with specific speed.

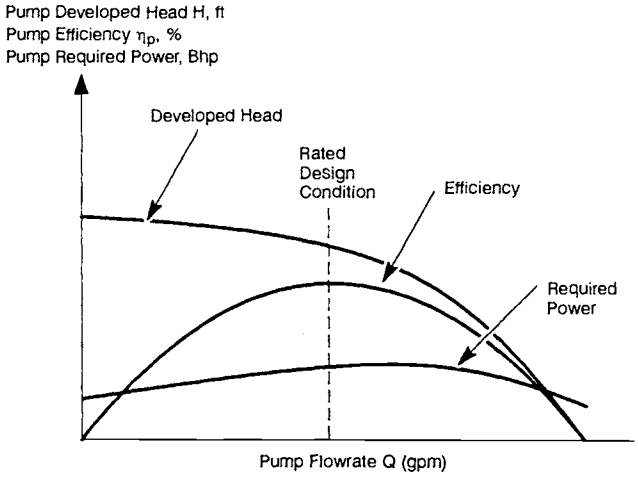

Fig. 6-24 H-Q, efficiency, and required power characteristic curves of a typical centrifugal pump.

Most of the turbine working fluids for rocket-engine application are fuel-rich product gases generated by bipropellant combustion. Typical working-fluid properties are listed in Table 6-4. Precaution: these working fluids do not behave exactly as perfect gases; real fluid properties must be used to assess accurately a turbine's performance.

Figure 6-25 shows the relationship between turbine-inlet temperature and available working-fluid energy for a turbine pressure ratio of 20 for the two propellant combinations, LO_2/RP-1 and LO_2/LH_2. Turbine-inlet temperatures are limited by the high-temperature properties of the turbine materials. State-of-the art uncooled metallic designs have a practical design limit of about 1600°F. Above certain levels, the gain from a higher turbine-inlet temperature will be offset by the turbine efficiency losses (see "blade losses" in following paragraphs) resulting from higher gas-jet speed (spouting velocity Co), which is proportional to the turbine-inlet temperature.

Table 6-4 Properties of typical fuel-rich combustion product gases.

Fluid	Inlet Temperature °F	C_p, Btu/lb °F	γ	R, ft/°R	Mixture Ratio, O/F
LOX/RP-1	1100	0.635	1.097	43.3	0.308
	1150	0.639	1.100	45.1	0.320
	1200	0.643	1.106	47.1	0.337
	1250	0.646	1.111	58.6	0.354
	1300	0.648	1.115	50.4	0.372
	1350	0.651	1.119	51.8	0.390
	1400	0.653	1.124	53.6	0.408
	1450	0.655	1.128	55.4	0.425
	1500	0.657	1.132	58.0	0.443
	1550	0.659	1.137	59.0	0.460
	1600	0.660	1.140	60.7	0.478
	1650	0.661	1.144	62.4	0.497
	1700	0.662	1.148	64.0	0.516
N_2O_4/CH_2(UDMH)	1400	0.380	1.420	87.5	0.110
	1500	0.398	1.420	91.6	0.165
	1600	0.416	1.420	95.7	0.220
	1700	0.434	1.420	99.9	0.274
	1800	0.452	1.420	104.0	0.328
	1900	0.470	1.420	108.2	0.382
LOX/LH_2	1000	2.05	1.374	434	0.785
	1200	1.94	1.364	403	0.908
	1400	1.86	1.354	378	1.025
	1600	1.80	1.343	358	1.143
	1800	1.73	1.333	336	1.273
	2000	1.69	1.322	320	1.410

Figure 6-26 shows the relationship between turbine pressure ratio and available energy of the working fluid for a turbine-inlet temperature of 1200°F, again for the propellant combinations LO_2/RP-1 and LO_2/LH_2. Although a large amount of energy may be available in a working fluid, it may be difficult to convert it efficiently into turbine shaft horsepower because of the severe weight limitations on rocket-engine turbopumps. Thus the available pressure ratio of a turbine often cannot be fully used.

The overall efficiency of a turbine η_t is defined as the ratio of turbine shaft horsepower thp to enthalpy drop rate, or the available energy-delivered rate of the working fluid:

$$\eta_t = \frac{550\text{thp}}{778\dot{w}_t\Delta H_t} \tag{6-15}$$

Again, for an ideal gas, this can be expressed using Eq. (6-14) to show the relationship to fluid properties, as follows:

$$\eta_t = 0.707\frac{\text{thp}}{\dot{w}_t C_p T_o\left[1-\left(\frac{1}{R_t}\right)^{\frac{\gamma-1}{\gamma}}\right]} \tag{6-16}$$

In turbine operation, efficiency can be affected by the following losses:

- *Nozzle losses.* Similar to those in thrust-chamber

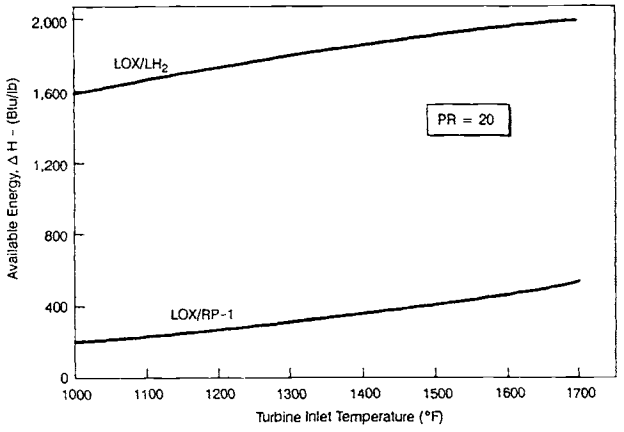

Fig. 6-25 Effect of turbine-inlet temperature on working-fluid available energy.

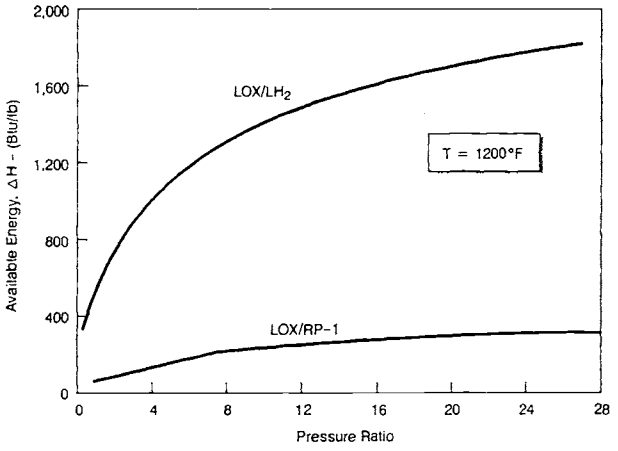

Fig. 6-26 Effect of turbine pressure ratio on working-fluid available energy.

nozzles, these losses are due to the gas leaving the nozzle at a lower velocity than it would an ideal nozzle. The losses are due to flow turbulence, fluid friction, fluid turning, and loss of heat to and through the turbine nozzle-blocks.

- *Blade losses.* These are caused by residual velocity of the gas as it leaves the rotor blades, the obliquity of the nozzle (i.e., the nozzle angle in Fig. 6-10 cannot be made zero), flow turbulence, and fluid friction. Losses due to residual gas velocity can be reduced by optimizing the turbine blade-to-gas velocity ratio U/Co, where U is the pitch speed of the rotor blades and Co is the ideal spouting velocity of the gas based on available energy and isentropic expansion. These conditions can be analyzed quantitatively by means of turbine-gas-flow velocity diagrams (to be discussed in section 6.6). Flow turbulence can be reduced through improved blade shape and through full turbine nozzle admission.
- *Leakage or clearance losses.* The clearance required between rotor-blade tips and casing permits some gas to leak past the blades without doing work, thus causing energy losses. The gas leakage from stage to stage in a multistage pressure-compounded turbine due to required clearance between shaft and sealing diaphragm results in similar losses.
- *Disk-friction losses.* Fluid friction occurs at the interface of gas and rotor-disk surfaces. Also, centrifugal action of the rotor disk causes some of the gas to flow radially to the casing and to be dragged along the face of the casing by the rotor blades, causing friction.
- *Mechanical losses.* These result from the mechanical friction in bearings and rotating seals.

Efficiency. The design of turbines for rocket turbopumps tends toward the simpler and lighter impulse-types, with most of the expansion occurring in the stationary elements. Figure 6-27 shows the typical efficiency curves of various impulse-type turbines. The design problem becomes one of balancing efficiency (optimum velocity ratio U/Co), weight (number of stages or rows), and structural considerations. A higher performance can be achieved by employing a working fluid with high

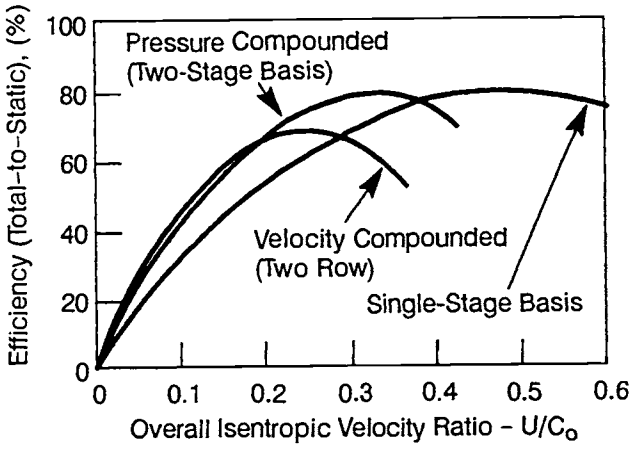

Fig. 6-27 Typical efficiency curves of impulse-type turbines.

available energy, and by matching its high gas-spouting velocity Co with a high rotor-blade pitch speed U. However, the blade speed is often limited by the required pump rpm, by the practical size of the rotor wheel, and the strength of materials. The optimum velocity ratio (or optimum value of blade speed for a given gas-spouting velocity) is reduced by the use of velocity or pressure-compounded arrangements (shown schematically in Fig. 6-9 and 6-11). However, these designs increase weight and complexity.

In general, a direct-drive configuration (Fig. 6-15) with an rpm lower than ideal produces a low value of U/Co, and a velocity-compounded turbine will be used because of its low overall weight and simplicity. Where a reduction gear is provided between pumps and turbine, a higher value of U/Co is possible and a more efficient pressure-compounded turbine can be used.

Since the turbine pressure ratio has only a small effect upon available energy content of the working fluid (Fig. 6-26), the power level of a turbine will usually be regulated by controlling the inlet pressure (po) and in turn the flow rate (w_t) of the turbine.

System calibration and off-design characteristics. Before the 1970s, rocket-engine systems operated at a single set of conditions, specifically, at rated thrust and mixture ratio. Each of the components in turn were designed for optimum functioning at that rated thrust level. However, most of the engine components, notably pumps and turbines, were also required to operate satisfactorily within a certain range different from the design point. Such a need may be caused by system and component calibration characteristics, system operational deviations, system start and shutdown transients, and special system requirements, such as throttling.

Owing to tolerance requirements on engine and component performance, and to correct for hydrodynamic variations within the components, it is sometimes necessary to calibrate a turbopump before its integration into an engine system. The performance of each pump will be determined experimentally. By modifying the pump geometry (impeller trimming) and varying the discharge hydraulic resistances, the desired operating characteristics required by the engine system can be achieved. For turbopumps with both pumps driven by a single turbine (as shown in Fig. 6-15), the calibration procedure begins with the experimental determination of the shaft speed at which one of the pumps (usually the oxidizer pump) develops the required head and flow. Simultaneously, the suction characteristics of this pump are determined at this speed. The other pump is then operated at the same speed and the discharge adjusted for the required flow. Based on the pressure readings, the diameter of the pump impeller will then be trimmed on a lathe until the desired head is produced at rated speed and flow. The pump suction characteristics at these conditions are also determined. Figure 6-28 shows the trimming effects of a typical pump. The trimming procedure requires that the pump impellers to be made sufficiently large initially, since addition of material is not feasible. The calibrated pumps are then combined with a turbine.

The turbine calibration requires either an adjustment of the flow to achieve the required power or, if the flow is limited, an adjustment of the fluid operating condition (e.g., temperature). This procedure considers the influence of turbine variations resulting from fabrication variations. The turbopump is then matched with the remaining engine system in complete-engine system calibrations. Adjustments in engine mixture ratio can be made by installing an orifice in the discharge of one of the pumps. Orifice installation considerations and type of propellant often make it desirable to ensure that the orificing is always installed for the same propellant; in LOX/RP systems, usually the fuel. For this reason, the pump for that system is trimmed for a slightly excess head. Adjustments in engine thrust level are made by varying the turbopump speed.

More recent engine designs (e.g., the SSME) require operation over a throttling range that forces the pumps to operate at off-design conditions. This requires an active control system that adjusts the respective pump parameters to achieve the desired operation. For the SSME, the oxidizer and fuel pumps are on separate shafts so that a separate adjustment of their respective speeds is achievable as well as an adjustment of flowrate.

One of the most significant pump off-design characteristics, the pump stall point, usually occurs in the low-flow region. The pump operation tends to be erratic at this point, resulting in the abrupt loss of developed head and the danger of overspeeding. Stall is the result of a boundary-layer separation at some point in the pump system. The first blade row to stall could be either a rotor or stator, depending on the particular design. The magnitude of the head falloff due to stall will also vary from pump to pump; but in general, axial-flow pumps tend to have a much more severe stall characteristic than centrifugal pumps, as illustrated in Fig. 6-29. Because of this, applications requiring a wide operating range typically use centrifugal designs rather than axial. It is the responsibility of the pump designer, of course, to establish the required operating range for a pump and to produce a design that will be satisfactory over this range.

During the start and shutdown transients of an engine system, propellant flow and pressure characteristics will be determined by the engine's system-design characteristics. Figure 6-30 shows the propellant flows and chamber-pressure buildup history for a typical gas-generator engine start transient (note temporary oxidizer-flow drop as a result of LOX-dome priming). A rocket turbopump must attain full power in substantially less time than conventional turbomachinery. Frequently, full-power operation must be attained in less than 1 s—dictated by the need for propellant-consumption economy in flight and for avoiding the possibility of flow instability in the thrust chamber and other compo-

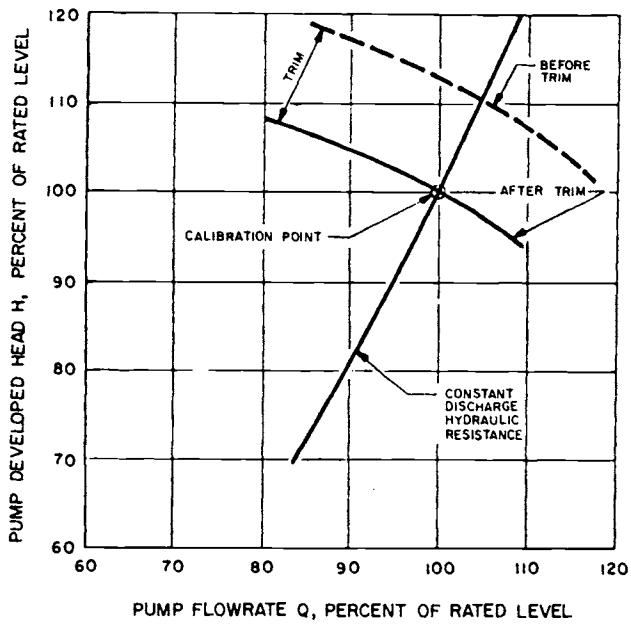

Fig. 6-28 Trimming effects of a typical pump.

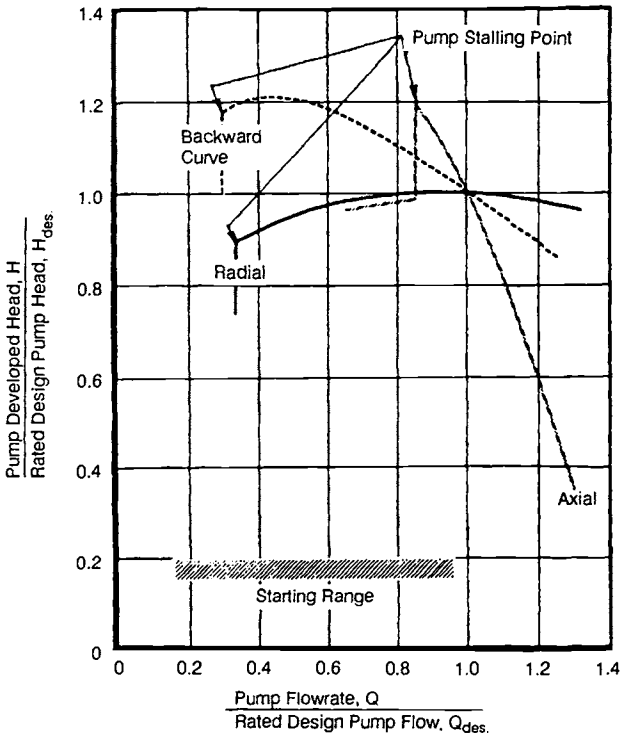

Fig. 6-29 Typical off-design characteristics of various types of pump.

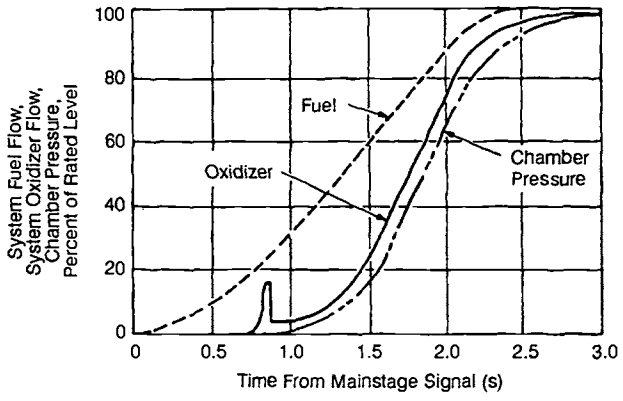

Fig. 6-30 Propellant-flow and chamber-pressure transient characteristics during engine-system start.

nents. This, together with other transient requirements, such as throttling, must be satisfied by the off-design characteristics of a turbopump. Throttling substantially influences selection of pump type. Basically, the problem involves coupling the pump characteristics with those of the rest of the engine system under off-design operating conditions.

Relative-velocity concepts. Before discussing the details of pump and turbine design, the concept of relative-velocity vectors must be understood because of the rotating blade rows. The rotating components have a velocity U in the circumferential direction that is independent of flow. The velocity of the fluid relative to the rotor (W)

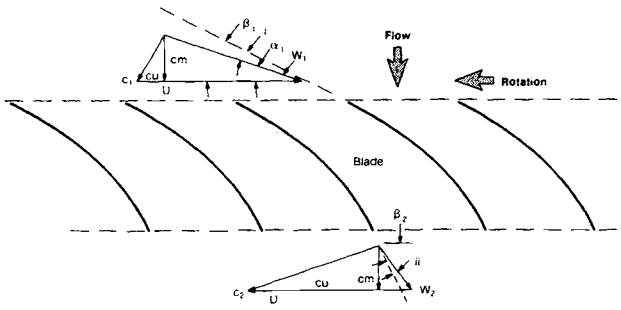

Fig. 6-31 Velocity diagrams for a pump.

plus the rotational velocity (U) equals the fluid velocity in the absolute reference plane. For example, Fig. 6-31 shows the absolute velocity at the inlet of a pump blade row as c with components cm in the through-flow direction and cu in the tangential direction (cu could be zero or even negative). The velocity W_1 is the inlet velocity relative to the blade that establishes the blade loading and performance. Similarly at the discharge, W_2 is the relative vector experienced by the pump blade, but c_2 is the resulting absolute velocity. Note that, in the absolute plane, the velocity was increased ($c_2>c_1$), i.e., the pump added energy to the flow. In the relative plane, however, the velocity is diffused (decreases, $W_2<W_1$). The boundary layers on the pump blade are based on the relative vectors, not the absolute vectors. These vector relationships will be used in further discussions of pump design.

6.3 INDUCER DESIGN

The rocket-engine industry has been the primary contributor to the development of inducer technology (Ref. 6-2). The inducer's axial-flow rotors can operate with a low inlet pressure without significant decrease in the discharge head. The inducer typically operates with some amount of cavitation, which may occur in the tip vortex flow or along the blade element itself as the inlet pressure is decreased. However, the technology has progressed to the point that long life can be achieved even with cavitation occurring. Inducers used in the initial rocket engines produced very low headrise with head coefficients that were typically less than 0.1; the inducer was operated in series, and generally was close-coupled to the main impeller. As the technology improved, inducer designs became more complex, with increased head coefficients (up to 0.25 with a single row of blades and in some cases over 0.5 with a double row of blades, as shown in Fig. 6-8). These larger head coefficients made it possible to use the inducer as a boost pump where the inducer is the only rotor on the shaft (e.g., LPOTP—see Fig. 6-7, and LPFTP pumps on the SSME). In some commercial applications, inducer pumps have been used where the only rotor is an inducer.

The need for an inducer is based on the required minimum NPSH, or alternatively, the maximum suction specific speed. Generally, an inducer will be required if the suction specific speed exceeds

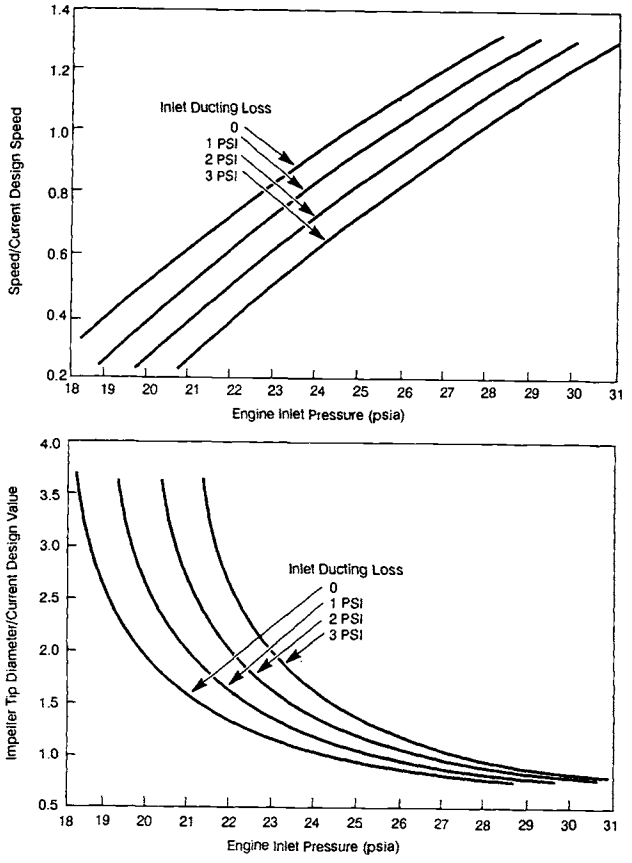

Fig. 6-32 Pump speed and diameter as a function of supplied inlet pressure.

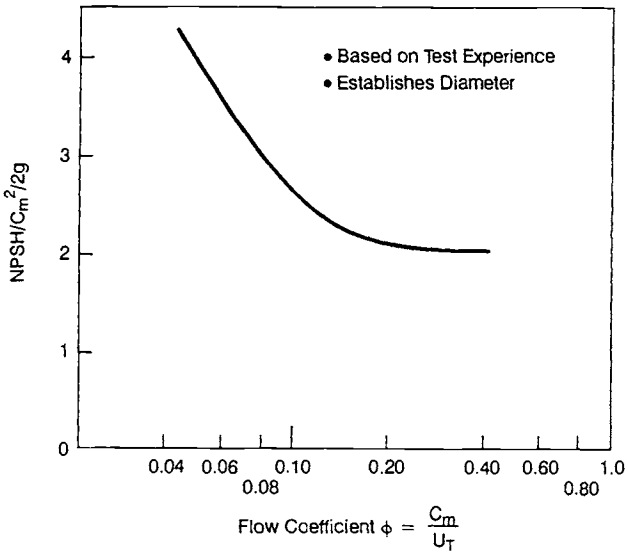

Fig. 6-33 Suction-specific-speed capability with no thermodynamic suppression head benefit.

10,000. For rocket-engine pumps that require suction specific speeds from 20,000 to 50,000 or higher, inducers are almost invariably used; and in fact, the suction performance will dictate the allowable speed of many turbopumps. This will in turn determine the size of the pump, number of stages, and general configuration to a large degree. Figure 6-32 shows the impact on speed and diameter of a given design as inlet pressure is reduced assuming constant head coefficient and number of stages for the pump.

Experience has shown that the suction of a pump strongly depends on its inlet flow coefficient. Figure 6-33 shows this effect for an inducer operating in a fluid with low vapor pressure (e.g., water). In cryogenics, the capability is even further improved because of the localized decrease in temperature and vapor pressure in the vicinity of the cavitation on the blade surface (an effect known as "thermodynamic suppression head"). This can be seen in Fig. 6-34, which shows actual data acquired from numerous pumps used in fluids with high vapor pressure, such as liquid hydrogen and oxygen. Some of the hydrogen pumps fall on the ($NPSH/cm^2/2g$) curve of 1.0, reaching corrected suction-specific-speed values of up to 140,000. Some of the LOX pumps fall on the curve of 2.0.

Capabilities as expressed in Fig. 6-33 are based on some defined percentage of head loss in the pump. Common values used in industry are either 2 or 3% head falloff from the "noncavitating" head. If the inducer is producing a small percentage of the overall head, as in a centrifugal or multi-stage axial pump, the total head lost by the inducer can be 15 to 30% when the pump head drops by 2%. For boost pumps consisting of only the inducer, the head loss in the pump is equivalent to that for the inducer itself. The NPSH at which the defined head falloff occurs is called, as mentioned earlier, the critical NPSH ($NPSH_C$).

To design an inducer, the margin relative to the critical NPSH must be established based on the required use, life, and conservatism desired in the pump. For example, a pump designed for a nonmanrated expendable launch vehicle that only experiences the minimum NPSH at end of flight might be desired to operate at $NPSH_C$ at the end of the flight. For a reusable vehicle requiring long life and consistent operation at a given NPSH, however, a margin would be required, where the margin M is expressed as a percentage using the relationship:

$$M = 100 \text{ (min. operating NPSH} - NPSH_C)/ NPSH_C \quad (6\text{-}17)$$

Typical values used in design would be M = 100% for long life at a given NPSH = 20% for short life at the minimum condition but ability to handle reasonable part-to-part and flight-to-flight variations.

To initiate an inducer design after defining the required margin, an experienced-based capability curve, as in Fig. 6-33 or 6-34, must be used. As was indicated above, fluids with a substantial vapor pressure (like liquid oxygen and liquid hydrogen) offer additional benefits. It has been shown that hydrogen inducers can operate at a critical NPSH equal to one inlet-velocity head, and liquid-oxygen inducers can operate with two inlet-velocity heads. That is, $NPSH_C$ = $cm^2/2g$ liquid hydrogen = $2cm^2/2g$ liquid oxygen. However, this is only true when the inlet-velocity head is small compared to the vapor head.

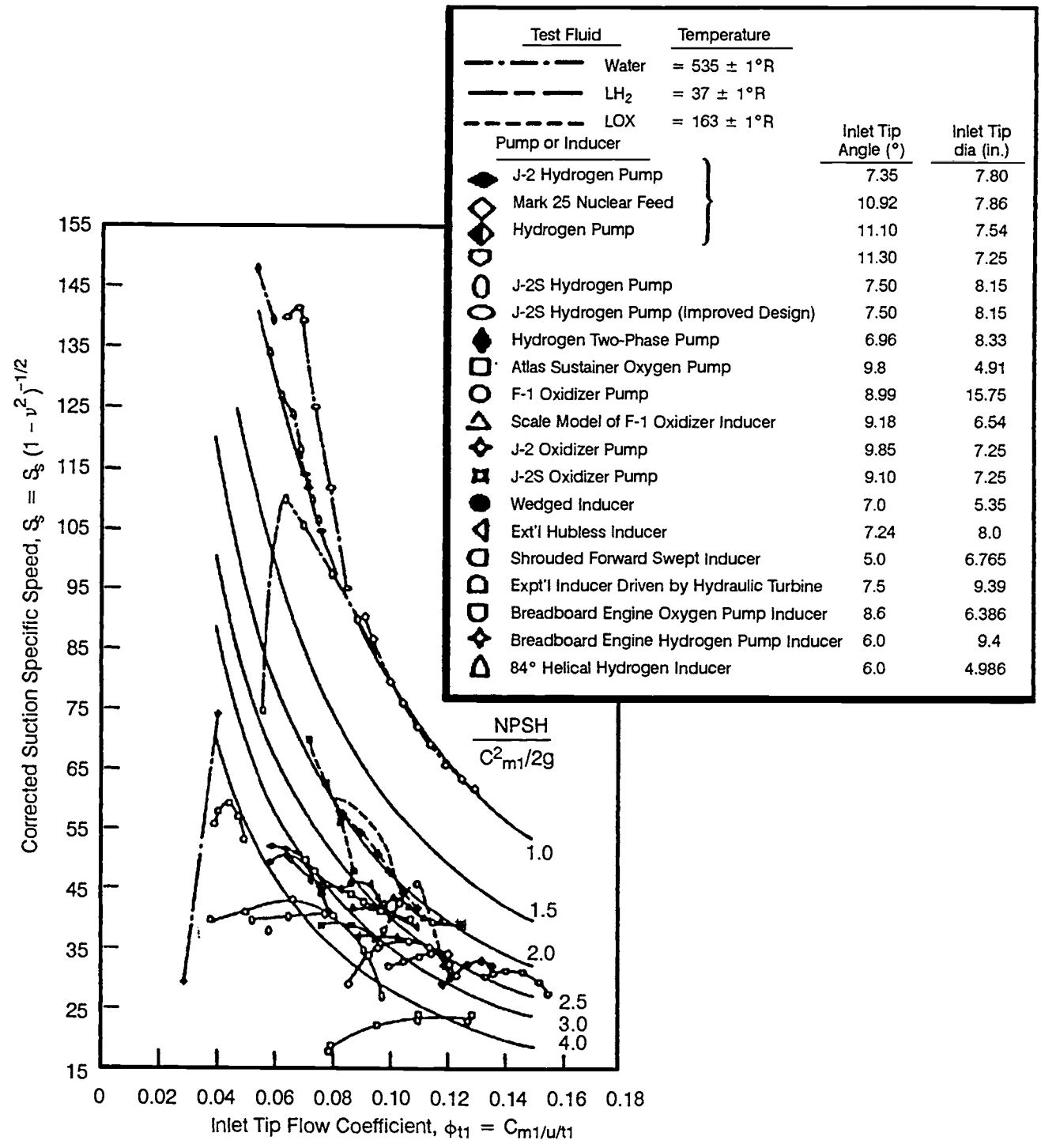

Fig. 6-34 Suction specific speed achieved in cryogenics.

As a general limit, the thermodynamic suppression head TSH of a fluid cannot exceed 50% of the vapor head.

To illustrate a typical design process, assume that an engine is being designed to deliver 25,000 gpm of liquid oxygen with a minimum required total inlet pressure of 25 psia and a vapor pressure of 15 psia. Assume the design only operates at minimum conditions for a short time, nominally operating at much higher inlet pressure.

Let M = 20%
NPSH minimum = (25-15) 144/70 ~20.6 ft
$NPSH_c$ = 20.6/1.2 = 17.1 ft

Assume the inlet hub-diameter of the inducer is 30% of the tip diameter. For some high-speed inducers in a dense fluid like liquid oxygen, a larger value of 40% may be required for structural reasons. Calculate cm:

cm = $(2g\ NPSH_c/A)^{0.5}$ (A = 1,2,3 dependent on fluid; for LO_2 use 2)
cm = (2g [17.1]/2)0.5 = 23.5 fps

Verify that inlet velocity head is less than 0.5 times vapor head to get full TSH benefit:

$cm^2/2g = 8.55$ ft
50% of vapor head = 0.5 (15)(144)/70 = 15.4 ft

Calculate the tip diameter of the inducer inlet:

$$cm = Q/A$$
$$A = (\pi/4)Dt^2 (1 - [D_h/D_t]^2)/144 \text{ ft}^2$$
$$= 4.96 (10^{-3}) D_t^2$$

where D_t is in units of inches and Q must be in units of cfs. Substituting from the above values yields:

$D_t = 21.86$ in.
$D_h = 6.56$ in

At this point, a flow coefficient must be assumed. For optimum suction performance, values in the range of 0.06 to 0.10 are used; the lowest values are more sensitive to fabrication tolerances and more limited in flow range. For long-life values higher than 0.15 are used. Inducers with values up to 0.3 have been tested. Assume:

$\phi = 0.1$
$U_t = cm/\phi = 235$ ft/s

This is a reasonable value for structural limits. The pump speed is then N = 2464 rpm. Check suction specific speed:

$$N_{SS} = N (Q)^{0.5}/(NPSH_c)^{.75} = 46{,}300$$

Based on Fig. 6-34, this is an achievable suction specific speed in liquid oxygen.

The head generated by the inducer usually will be selected to enable the following impeller to operate with essentially no cavitation. For example, the impeller might be designed for a maximum suction specific speed of 5000 to provide some margin in the impeller design. Thus, the head produced by the inducer must be sufficient to increase the NPSH from its inlet value to the value needed for the impeller. Using the numbers from the above example and letting $NPSH_I$ equal the NPSH at the impeller inlet yields—

$$N_{SS} = 5000 = 2464 (25{,}000)^{0.5}/NPSH_I^{0.75} NPSH_I$$
$$= 332.8 \text{ ft}$$

Therefore, the required inducer head rise will be ΔH = 332.8 -20.6 = 312.2 ft.

With the tip speed of the inducer previously calculated, the inducer head coefficient will be ψ = 312.2/([235]^2/32.2) = 0.182. This is an achievable head coefficient with a single row of blades. However, to achieve this it will be necessary to increase the diameter of the hub at the discharge.

The hub diameter of inducers for current rocket-engine pumps will usually be larger at the discharge than at the inlet. This reduces the amount of diffusion being done along the hub streamline—a critical factor in preventing discharge recirculation and thereby providing a relatively uniform head and velocity into the impeller eye or into a downstream stator. The design objective is to achieve the head in the inducer, provide a relatively uniform discharge condition, avoid any recirculation at the inducer discharge, and avoid any cavitation on the leading edge of the downstream blades. The exact diameter selected will be based on analyses of the flow in both the inducer and impeller (or stator) using either a quasi-3D or full-3D approach.

Approximate selections can be based on velocity-vector diagrams at the inlet and exit of each blade row using simple radial-equilibrium equations at the discharge to account for variations from tip to hub. The resulting profile would appear as shown for the inducer in Fig. 6-7.

The number of blades for the inducer is kept small at the leading edge to minimize blockage and thus improve suction performance. Previous designs have used *3* to *7* inlet blades, but *3* to *4* is preferable for suction performance. Some inducers with three blades experience larger radial loads under partial cavitating conditions. In view of that, four blades are more frequently used in current designs. Larger flow coefficients ($\varphi > 0.2$) allow a larger number of blades. To increase head rise, partial-length blades are sometimes introduced downstream of the blade-overlap region at the point where all cavitation is collapsed. Thus, the inducer exit would have twice the number of blades as the inlet. This is recommended if head coefficients must exceed 0.25.

The inlet-velocity angle at the tip is established by the flow coefficient, assuming no inlet prewhirl. That is, letting a_i equal inlet flow angle from tangential at the tip:

$$\alpha_i = \tan^{-1} cm/U_t = \tan^{-1} \phi \qquad (6\text{-}18)$$

With ϕ being generally less than 0.15 for rocket-engine inducers, α_i is generally less than 8.5 deg. Inducers are designed to operate with an incidence angle i that varies from approximately 3 deg up to a maximum of approximately one-half of the inlet blade angle. The effect of incidence angle on the design is discussed in detail in Ref. 6-2 through 6-5. The exact incidence chosen at the design point will depend on the required flow range of the part and the life characteristics. The inlet blade angle β_{1t} equals the inlet flow angle plus the incidence angle, as shown in Fig. 6-31. The length of the blade is much longer in the tangential than in the axial direction because of the small blade angle. At the inlet, the blade angle varies from tip to hub according to the relationship—

$$r \tan \beta = \text{constant} \qquad (6\text{-}19)$$

The discharge blade angle is set to achieve the desired head. This head can be expressed as—

$$\Delta H = \eta \Delta(Ucu)/g \qquad (6\text{-}20)$$

where η is the inducer efficiency and the velocities cu are as illustrated in Fig. 6-31. The discharge axial velocity is calculated to satisfy continuity and radial equilibrium. The resulting velocities enable calculation of the discharge vector diagram. This establishes fluid velocities, but because of the blade loading the flow typically exits the inducer at an angle less than the blade angle. This difference (deviation angle) must be accounted for based on experience or an accurate Navier-Stokes solution of the inducer flow-field.

The distribution of blade angle between the inlet and discharge is designed to provide for both suction performance and efficiency. To improve suction performance, the inlet region to the point of overlap of the blades is typically designed with less camber than would be obtained, for example, from a circular-arc-blade profile. Final profiles are usually established based on quasi-3D or 3D analyses of the flow field.

The structural integrity of the blades must be evaluated over the full range of operation, including any transients. The blade loading due to partially cavitating conditions can be very different from the loads noncavitating. Typically, as inlet pressure decreases, more of the blade loading shifts to the back of the blading, owing to cavitation on the suction surface, which provides a minimum pressure limit.

6.4 DESIGN OF CENTRIFUGAL PUMPS

Because of its specific needs, the rocket industry has developed its own pump design approaches, which may differ from those for conventional applications. In addition, designers may employ their individual methods of analysis and calculation. However, the broad underlying principles are quite similar. The range of speeds, proportions, design coefficients, and other mechanical details for rocket-engine pumps has been well established by earlier designs as well as through experiments (Ref. 6-6).

General Design Procedures

As a rule, rated pump head capacity (H-Q) requirements and expected available NPSH at the pump inlets will be established by engine system design criteria. The first step then is to choose a suitable suction specific speed Nss and the type of inducer that will yield the highest pump speed N at design conditions [Eq. (6-7)]. The pump specific speed (N_S) or type of impeller can now be established from the chosen pump speed and required head-capacity characteristics. Owing to its relatively light weight and simplicity of construction, a single-stage centrifugal pump may be given first consideration.

With suction specific speed and specific speed of the proposed pump design established, the designer can now look for a suitable "design model" among comparable existing pumps that approximate the desired performance (i.e., a pump with the same specific speed and suction specific speed). If a suitable model is available, the new pump design can be scaled from the previous design. Letting "f" equal the ratio of the scaled dimension, that is—

$$f = D_2/D_1 \tag{6-21}$$

makes the following correlations valid for pumps with like specific speed, based on the pump affinity laws [Eq. (6-3a) and (6-3b)]:

$$Q_2 = Q_1 f^3 (N_2/N_1) \tag{6-22a}$$

$$DH_2 = DH_1 f^2 (N_2/N_1)^2 \tag{6-22b}$$

where—

N_1, Q_1, and DH_1 = rotating speed (rpm), flow rate (gpm), and developed head (ft) of the existing model at rated conditions

N_2, Q_2, and DH_2 = rotating speed (rpm), flow rate (gpm), and developed head (ft) of the new pump at rated conditions

D_1 = impeller diameter of the existing model, ft

D_2 = impeller diameter of the new pump, ft

To achieve the same performance, all dimensions in the pump must be scaled by the scaling factor, including parameters such as surface finish and seal clearances. When scaling up, this is easily done, and usually the larger pump will achieve even better performance because of lower relative surface finish and clearance values. When scaling down, however, this works against the performance.

If a suitable model is not available for the design of a new pump, the designer can use "design factors" established experimentally by other successful designs. These may permit establishing relations between rated pump-developed head and flow rate and such parameters as velocity ratios. However, best results are obtained through experimental testing of the proposed design itself. The test results can then be used for design revisions and refinements. The discussion below uses the following basic symbols:

c = flow velocity, absolute (relative to ducts and casing)

v = flow velocity, relative to inducer or impeller

u = velocity of points on inducer or impeller

Subscript:

0 = inducer inlet

1 = inducer outlet and impeller inlet

2 = impeller outlet

3 = pump casing exit

(prime) ' = actual or design

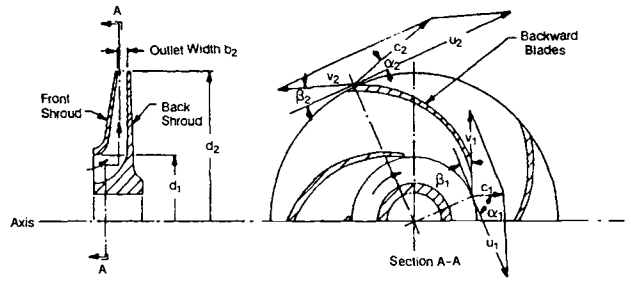

Fig. 6-35 Typical shrouded centrifugal impeller with backward-curved blades.

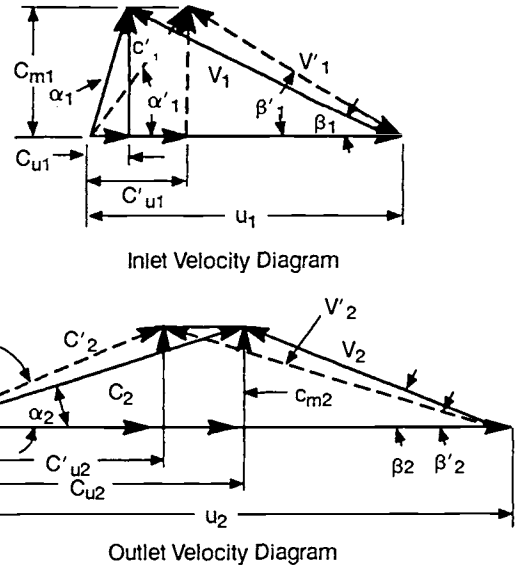

Fig. 6-36 Flow-velocity diagrams for the impeller shown in Fig. 6-35 (drawn in a plane normal to the impeller axis).

Operating Principles of the Centrifugal Impeller

In its simplest form, the impeller of a centrifugal pump can be regarded as a wheel with blades, rotating in an enclosure, with the fluid being admitted axially and ejected at the periphery, as shown schematically in Fig. 6-35. The tangential velocity component of the fluid increases as it moves out radially between the blades. The centrifugal force acting on the fluid therefore increases as the fluid moves out radially. For optimum performance, most impellers in high-speed centrifugal rocket-engine pumps have shrouded, backward-curved blades. The impeller width is tapered toward the periphery to keep the cross-sectional area of the radial flow path nearly constant, as shown in Fig. 6-35.

Velocity diagrams may be constructed to analyze the fluid flow vector correlations at various points of an impeller. Assume the following ideal conditions: no losses, such as fluid-friction losses, impeller passages completely filled with actively flowing fluid at all times, flow axisymmetrical (velocities at similar points on the flow lines are uniform), and fluid leaves the impeller passages tangential to the vane surfaces (complete guidance of the fluid at the outlet).

The ideal inlet- and outlet-flow velocity diagrams of the impeller described in Fig. 6-35 are shown in Fig. 6-36. With corresponding fluid velocities u, v, and c (as identified above), α is the angle between c and u, and β is the angle enclosed by a tangent to the impeller vane and a line in the direction of vane motion. The latter is equal to the angle between v and u (extended). Based on these velocity diagrams, the following correlations have been established:

$$\Delta H_{ip} = [u_2^2 - u_1^2 + v_1^2 - v_2^2]/(2g) \qquad \text{Eq. (6-23)}$$

$$\Delta H_i = [u_2^2 - u_1^2 + v_1^2 - v_2^2 + c_2^2 - c_1^2]/(2g) = (u_2\, cu_2 - u_1\, cu_1)/g \qquad \text{Eq. (6-24)}$$

$$Q_{imp} = 448.8\, cm_1\, A_1 = 448.8\, cm_2\, A_2 \qquad \text{Eq. (6-25)}$$

$$cu_2 = u_2 - cm_2/(\tan b2') \qquad \text{Eq. (6-26)}$$

where—

ΔH_{ip} = ideal static-pressure-head rise of the fluid flowing through the impeller due to centrifugal forces and to a decrease of flow velocity relative to the impeller, ft

ΔH_i = ideal total-pressure-head rise of the fluid flowing through the impeller = the ideal developed head of the pump impeller, ft

Q_{imp} = impeller flow rate at the design point (rated conditions), gpm

A_1, A_2 = area normal to the meridional flow at the impeller inlet and outlet, ft^2

d_1, d_2 = blade diameter at the impeller inlet and outlet, in.

u_1, u_2 = impeller peripheral velocity at inlet and outlet, ft/s

v_1, v_2 = flow velocity relative to the impeller at the inlet and outlet, ft/s

c_1, c_2 = absolute velocity of the flow at the inlet and outlet, ft/s

cu_1, cu_2 = tangential component of the absolute velocity at the inlet and outlet, ft/s

cm_1, cm_2 = "meridional" or (by definition for radial-flow impellers) radial component of the absolute inlet flow velocity at the inlet and outlet, ft/s

β_1, β_2 = impeller blade angle at the inlet and outlet, deg

For centrifugal pumps of the noninducer type (now rarely used in rocket pumps), proper selection of the impeller inlet vane-angle β_1 or the provision of guide vanes at the inlet minimizes the absolute tangential component of fluid flow at the inlet cu_1, which for best efficiency should be zero. This is defined as no prerotation, where $\alpha_1 = 90$ deg. Thus, Eq. (6-24) becomes—

$$\Delta H_i = u_2\, cu_2/g \qquad (6\text{-}27)$$

This discussion has assumed ideal conditions. For most rocket applications, centrifugal pumps are designed with an inducer upstream of and in series with the impeller. The flow conditions at the impeller inlet thus are affected by the inducer's discharge flow pattern. In addition, two types of flow usually take place simultaneously in the flow channels, namely, the main flow through the passages and local circulatory (vortex) flows. It is preferable to keep these secondary flows small, but they are always strong enough to significantly affect the overall flow field. As a consequence, the fluid is caused to leave the impeller at an angle β_2' less than the impeller discharge vane angle β_2 and to increase the absolute angle α_2 to α_2'. This and the hydraulic losses in the impeller correspondingly change the relative flow velocities v_1 and v_2 to v_1' and v_2', the absolute flow velocities c_1 and c_2 to c_1' and c_2', and the absolute tangential components cu_1 and cu_2 to cu_1' and cu_2'. Since the radial-flow areas A_1 and A_2, and the impeller flow rate Q_{imp} remain constant, the absolute radial or meridional components cm_1 and cm_2 also remain unchanged. The inlet- and outlet-flow velocity diagrams in Fig. 6-36 may now be redrawn as represented by the dotted lines. The correlation established in Eq. (6-24) may be rewritten as follows:

$$\Delta H_{imp} = (u_2 cu_2' - u_1 cu_1')/g \qquad (6\text{-}28)$$

where—

ΔH_{imp} = actual developed head of impeller, ft
cu_1 = tangential component of the design absolute-inlet-flow velocity, ft/s
cu_2' = tangential component of the design absolute-outlet-flow velocity, ft/s

The ratio of the design flow velocity cu_2' to the ideal flow velocity cu_2 can be expressed as—

$$e_v = cu_2'/cu_2 \qquad (6\text{-}29)$$

where e_v = impeller vane coefficient; typical design values range from 0.65 to 0.75. Referring to Fig. 6-36, Eq. (6-26) may be rewritten:

$$cu_2' = u_2 - cm_2/(\tan \beta_2) \qquad (6\text{-}30)$$

By definition, the required impeller-developed head can be determined from—

$$\Delta H_{imp} = \Delta H + H_e - \Delta H_{ind} \qquad (6\text{-}31)$$

where—

ΔH = rated-design pump-developed head, ft
ΔH_{ind} = required inducer head at the rated design point, ft
H_e = hydraulic head losses in the diffusion system including the volute, ft. Typical design values of H_e vary from 0.10 to 0.30 ΔH. The required impeller flow rate can be estimated from—

$$Q_{imp} = Q + Q_e \qquad (6\text{-}32)$$

where—

Q_{imp} = required impeller flow rate at the rated design point, gpm
Q = rated delivered-pump-flow rate, gpm
Q_e = impeller leakage losses, gpm. Most of these occur at the clearance between impeller wearing rings and casing. Typical design values of Q_e vary from 1 to 5% of Q_{imp}. (Oxidizer pumps may be higher.)

Centrifugal-Impeller Design Elements

After general pump-design parameters, such as developed head ΔH, capacity Q, suction specific speed N_{ss}, rotating speed N, and specific speed N_s have been established, a centrifugal (radial) pump impeller may be designed in two basic steps. The first will be selection of velocities and vane angles that are needed to obtain the desired characteristics with optimum efficiency. Usually this can be done with the help of available design or experimental data such as pump-head coefficient ψ, impeller vane coefficient e_v, and leakage loss-rate Q_e. The second step, design layout of the impeller for the selected angles and areas, requires considerable experience and skill of the designer to work out the best-performing configuration based on the given design inputs. This can be done graphically or numerically, but either approach will require a flow analysis to confirm the design using at least a quasi-3D analysis. Codes capable of solving the 3D full Navier-Stokes equations in the complex flow field of a centrifugal impeller are being used but have not yet demonstrated that they are qualified to optimize the design. Three-dimensional Euler codes are used with success in analyzing the flow fields at least near the maximum efficiency point.

The following are considered minimum basic design elements required for proper layout of a radial-flow impeller:

1) The inlet flow coefficient $\phi = cm_1/U_e$, where U_e is the velocity of the impeller at the eye. A typical design guideline imposes constant meridional velocity from the inducer discharge to the impeller eye. Thus the inlet flow coefficient is primarily set by the inducer discharge, the hub and tip diameters of the impeller inlet being set to achieve an area equal to, or larger than, that at the inducer discharge. The eye diameter of the impeller frequently is increased relative to the inducer discharge tip-diameter to account for added flow through the wear rings of the impeller. These leakage flows can be relatively large in small pumps, and if the pumped fluid is cryogenic the density of the leakage fluid may be lower, thereby increasing the volumetric flowrate. These leakage flows will be mixing with the core flow from the inducer, but complete mixing will not occur before entering the impeller eye. Thus, the area must be increased to maintain a constant inlet meridional velocity. In the early phases of the design, the leakage flows will not be known but must be estimated based on

Table 6-5 Allowable impeller tip speeds for different materials.

Material	Approxmiate tip-speed limit, FT/S				
	Forged Inco 718	Cast Inco 718	Cast Al 357	Forged Ti-5-2.5	Cast Ti-5-2.5
LOX	900	760	N/A	N/A	N/A
Hydrogen 1650	1400	1400	1190	2000	1870
Methane	1490	1260	600	1240	1200

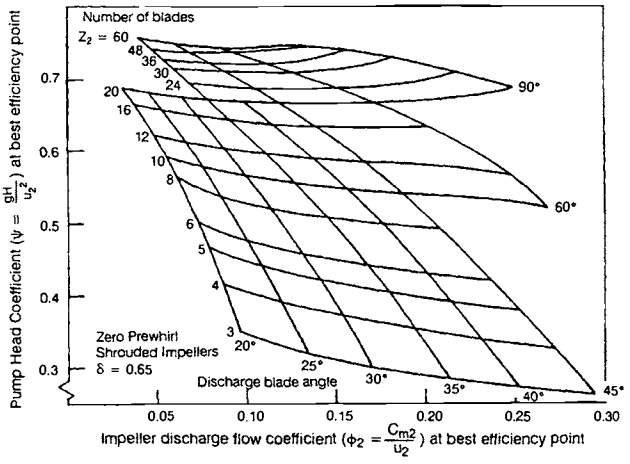

Fig. 6-37 Impeller head coefficient as a function of discharge flow coefficient, blade number, and blade angle.

experience. The flow coefficient for the impellers usually will be higher than for the inducer inlet, but values from 0.08 to 0.4 have been used. Setting this parameter will set the inlet diameters.

The impeller hub diameter must of course be large enough to fit over the shaft. The required shaft diameter can be estimated using the relationships:

$$S_S = 16\ T/(\pi d_S^3) \qquad (6\text{-}33)$$

$$S_t = 32\ M/(\pi d_S^3) \qquad (6\text{-}34)$$

where—

- d_S = impeller shaft diameter, in.
- T = shaft torque, in.-lb
- M = shaft bending moment, in.-lb.
- S_S = shear stress due to torque, lb/in.^{2}
- S_t = tensile stress due to bending moment, lb/in.^{2}

2) The discharge flow coefficient $\phi_2 = cm_2/U_2$, where U_2 is the velocity of the impeller at the tip. The discharge meridional velocity cm_2 should be approximately 1.0 to 1.5 times the inlet meridional velocity cm_i. The flow coefficient will then be set by the impeller tip speed selected to meet the head requirements. Values of discharge flow coefficient from 0.05 to 0.3 have been used.

3) Ratio of impeller eye to tip diameters. This ratio should be maintained below 0.70 to avoid efficiency penalties. Larger values have been used, up to 0.8, but a mixed-flow impeller will usually give a better efficiency for these higher values.

4) The impeller peripheral velocity at the discharge U_2. The value of U_2 can be calculated by Eq. (6-2) for a given pump-developed head H and a selected overall pump head coefficient ψ. The maximum design value of U_2 depends on the material strength, which determines the maximum developed head that can be obtained from a single-stage impeller. Typical maximum values of U_2 range from 600 to 2000 ft/s, as shown in Table 6-5. With U_2 and N known, the impeller discharge diameter d_2 can be calculated readily.

5) The inlet blade angle β_1. Because the value of β_1 will be affected by the inlet flow conditions, β_1 should ordinarily be made equal or close to the inlet flow angle β_1' so that the incidence angle is a small positive value. The incidence may be varied from hub to tip because of the velocity gradients; therefore, it is usually best to select the tip incidence because the tip has the highest relative velocity, which makes it more prone to cavitation. Also, if the pump must operate over a wide flow range, the incidence at the "design point" may be adjusted to enable noncavitating and nonstalled performance over the full required range. Typical design values for β_1 range from 2 to 8 deg, with the smaller values at the tip.

6) The discharge blade angle β_2. In the special case of radial-bladed impeller designs, β_2 equals 90 deg. Backward-curved impellers, with β_2 less than 90 deg, are usually more efficient and more stable, and these are used on almost all modern designs. Usually the selection of β_2 is the first step in determining the other impeller design-constants, since most of them depend on β_2. Pump efficiency and head-capacity characteristics are also important considerations for the selection. For a given U_2, head and capacity increase with β_2. Figure 6-37 shows the rela-

tionship between β_2, the discharge flow coefficient ϕ_2, and the number of impeller blades. Typical design values for β_2 range from 17 to 40 deg for backward swept blades.

7) Number of blades. Figure 6-37 has shown the relationship of the number of blades to other key design parameters. The figure shows the minimum number of blades needed to achieve a given head coefficient for an impeller with a ratio of eye-to-tip diameter (δ) of 0.65. The number of blades derived from the figure is the number required for the discharge of the impeller. Fewer blades will usually be required at the inlet to avoid cavitation. It is not uncommon, therefore, for a rocket-engine impeller to have partial blades (also known as splitters) which begin partway through the impeller and continue to the exit. Impellers have been successfully used with more than one set of partials; e.g., the SSME HPFTP (Fig. 6-5) has 6 blades at the inlet and 24 blades at the exit. The impeller has a set of long partials and then a set of short partials. The placement of the partial leading edge in the blade passage is critical; it must be chosen by an adequate flow analysis to avoid leading-edge cavitation and to achieve a relatively uniform flow-split. The discharge blade characteristics will usually be identical for full and partial blades, the objective being to achieve a uniform velocity field in each exit passage. As an alternative to Fig. 6-37, the designer can use other published slip factors to calculate the blade angle required to achieve a given fluid angle. (The slip factor is a ratio of the discharge fluid's tangential velocity compared to the ideal velocity obtained if the flow followed the blade.)

8) The width of the impeller at the exit can be calculated by the following correlation:

$$\beta_2 = Q_{imp}/(3.12\ \pi d_2\ cm_2\ \varepsilon_2) \qquad (6\text{-}35)$$

where—

β_2 = impeller width at the discharge, in.

ε_2 = contraction factor at the discharge. Typical design values range from 0.85 to 0.95. This nondimensional factor accounts for the blockage due to the blades and the boundary layers. Smaller pumps may require a smaller value.

Q_{imp} = impeller flowrate at the rated design point, gpm

After the blade angles and other dimensions at inlet and discharge have been established, no set rule guides designing the backward-curved blades. The blade profile must be smooth and avoid steep gradients along the suction surface to avoid boundary-layer separation. The blade shape is typically generated using smooth profiles, and then analyzed using an appropriate code (quasi-3D or better). The blade will then be adjusted to attain a smooth variation of velocity from inlet to discharge, with no local areas of large diffusion on the suction surface and no potential for cavitation along the blade. It is also desirable to minimize the length of the passage to reduce friction losses, but this must be balanced by the requirement to control the diffusion rate. The flow-passage shape should be as close to square as possible. It is also desirable to have the blade at the exit be at a relatively constant angular location from tip to hub shroud to avoid corner angles that can increase boundary-layer blockage. The blades should be as thin as the material strength and manufacturing processes will permit. They may be of constant thickness, but the leading-edge profile will be contoured to avoid cavitation and reduce incidence losses. This leading-edge contour may require an appropriate ellipse rather than just a simple circular arc.

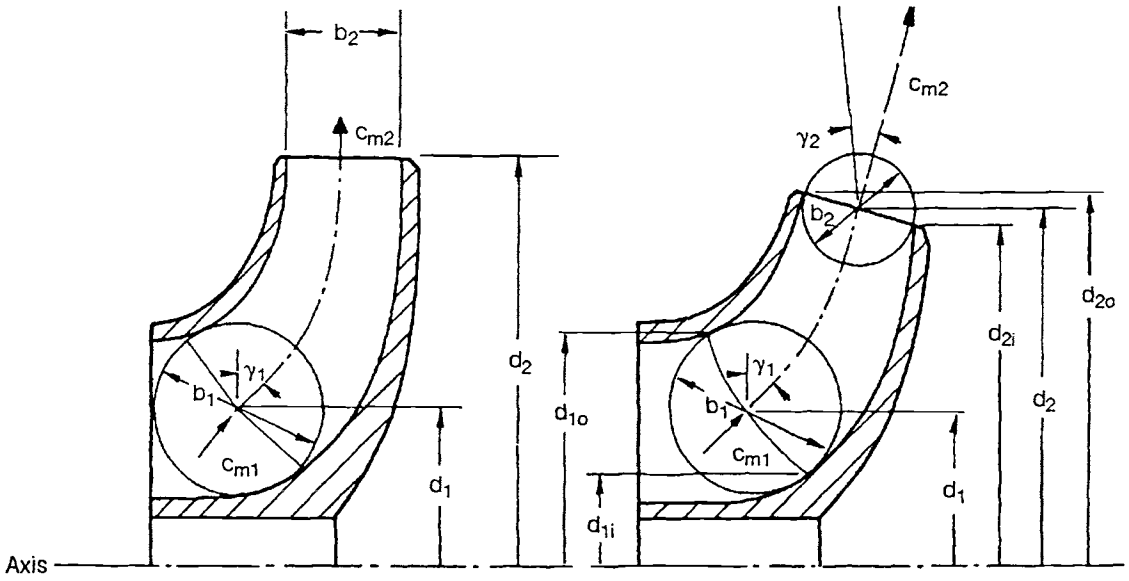

Fig. 6-38 Impeller designs.

Mixed-flow-type vanes that extend into the impeller entrance or eye (shown in Fig. 6-38a) are frequently used in rocket-engine centrifugal pumps. This is done to match the impeller-inlet flow path with the inducer-discharge flow pattern, to provide more efficient turning of the flow, and to provide structural support to the shrouds.

The mixed-flow-type impeller (shown in Fig. 6-38b) is used when the impeller needs a large ratio of eye-to-tip diameter. The velocity correlations and design constants of a mixed-flow impeller are essentially the same as those of a radial-flow impeller. Mean effective impeller diameters are used in the calculations for head rise, flow velocities, etc.

Design of Casings

The pump casing must have the structural integrity to carry loads from the pump to the engine-support system. Internally it must provide hydrodynamic passages efficiently to collect the high-velocity fluid exiting the impeller and convert this kinetic energy into pressure while minimizing the imposed radial load on the rotating members. It does not contribute to the generation of head, but a poor design can significantly reduce both head and efficiency. The construction of a typical centrifugal-pump casing is shown in Fig. 6-4. The front section of the casing, which provides the pump inlet and houses the inducer, is called the suction nozzle. The rear section of the casing, which collects the fluid from the impeller and converts the velocity head into pressure before the discharge, is called the volute. There may be an additional set of stationary vanes called a vaned diffuser between the impeller and the volute.

Since the flow path in a suction nozzle is short and the flow velocities are relatively low, the head loss in a suction nozzle due to friction is very small. The contour of the suction nozzle is designed to suit the inducer configuration. A tapered suction nozzle (as shown in Fig. 6-16) has the area gradually decreasing toward the impeller eye, which steadies the flow and ensures uniform feed to the impeller. However, many pumps cannot efficiently use a tapered inducer because of the need for axial motion of the shaft to balance axial loads. In liquid-oxygen pumps, frequently a liner made of a material such as Kel-F or silver is inserted between the inducer and suction-nozzle wall. This eliminates the possibility of metal-to-metal rubbing in the presence of narrow inducer-tip clearances. Rubbing in liquid-oxygen pumps may cause dangerous explosions.

Pump inlets are not always configured to permit an axial inlet flow. In such cases the inlet must be designed to provide a relatively uniform inlet-velocity field at the inducer inlet and to minimize the losses which reduce the available NPSH for the inducer. These design requirements can be met by using either vaned elbows, a volute scroll with vanes (Fig. 6-5), or a manifold inlet that enters radially on one side and divides the flow into two circumferential flow paths wrapped around the pump and feeding radially inward. Vanes are used in all of these designs to preserve a uniform velocity field at the inducer inlet.

Two basic types of discharge casing are used in rocket centrifugal pumps: the plain volute and the vaned-diffuser volute (see Fig. 6-39). In the first, the impeller discharges into a volute channel of gradually increasing area. Here, the major part of the conversion of velocity to pressure takes place in the conical pump-discharge nozzle at the volute exit. In the latter, the impeller first discharges into a diffuser provided with vanes. A major portion of the diffusion takes place in the channels between the diffusing vanes before the fluid reaches the volute channel. The main advantage of the plain volute is its simplicity. However, the vaned diffuser plus volute can usually provide a higher degree of point efficiency, particularly in high-head pumps. Head losses in pump volutes are relatively high. Approximately 70-90% of the flow kinetic energy is converted into pressure head in either volute type.

The hydraulic characteristics of a plain volute are determined by several design parameters, such as volute throat area a_v and flow areas a_θ, included angle θ_s between volute side walls (Fig. 6-40), volute tongue angle α_v, radius r_t at which the volute tongue starts, and volute width b_3. Pump specific speed Ns somewhat influences the design values. All of the

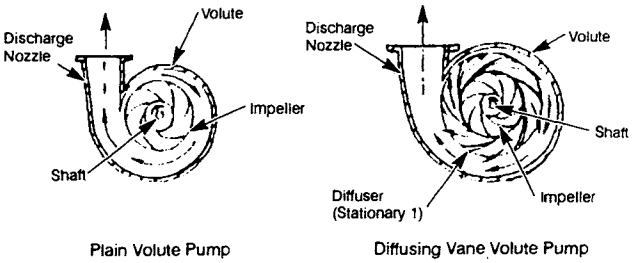

Fig. 6-39 Plain-volute and vaned-diffuser-volute centrifugal pump casings.

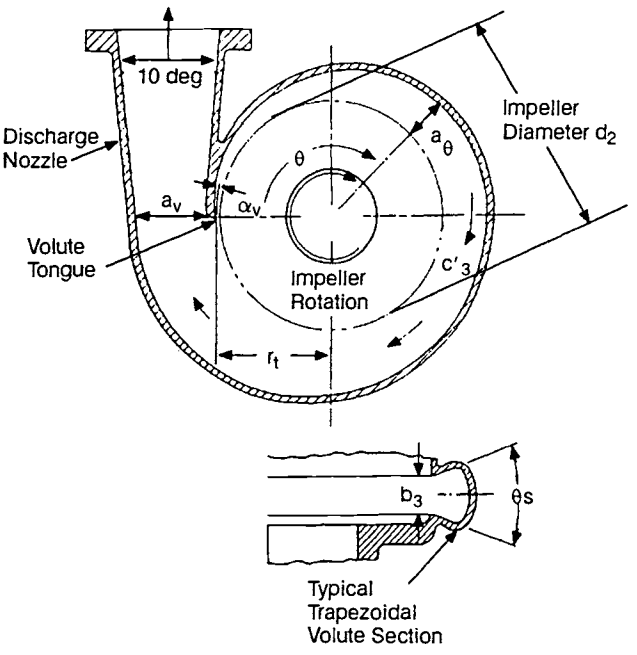

Fig. 6-40 Plain volute casing of a centrifugal pump.

pump flow Q passes through the volute throat section a_v, but only part of it passes through any other section; the amount depending on the location away from the volute tongue.

As its primary design requirement, the volute must provide a uniform pressure boundary at the impeller outer diameter at least at the design point. That is, the single discharge introduces an asymmetry to the pump that at off-design conditions produces a pressure gradient at the impeller discharge, causing a radial load acting on the rotating member that must be carried by the bearings. At the design point of the volute, these radial loads are theoretically zero. This design condition approximates a linear area distribution with circumferential angle, but is not exactly linear for two reasons. First, the friction forces acting on the volute walls affect the velocity/pressure field. Second, the decrease in velocity because of the change in radius (conservation of angular momentum) must be included.

To avoid impact shocks and separation losses at the volute tongue, the volute angle α_v is designed to correspond to the direction of the absolute velocity vector at the impeller discharge. The radius r_t at which the tongue starts should be 5-10% larger than the outside radius of the impeller to minimize dynamic loads on the impeller blades and the volute tongue.

The dimension b_3 at the bottom of a trapezoidal volute cross-section will be chosen to minimize losses from friction between impeller discharge flow and volute side-walls. The width b_3 is generally set between 1.0 and 1.25 times the impeller width at the discharge for pumps without a vaned diffuser; low-specific-speed pumps could be even higher. The shape of the volute shown in Fig. 6-40 results in a symmetric design that will generate a double vortex, as shown in Fig. 6-41. An asymmetric cross section is preferred because it produces a single vortex that is more stable and improves overall efficiency. For designs with diameter limits, a folded volute can be used (also shown in Fig. 6-41). For the symmetrical volute, the maximum included angle θ_s between the volute sidewalls should be about 60 deg. For higher-specific-speed pumps or for higher impeller-discharge flow angles, the value of θ_s should be made smaller.

The pressure at the outer diameter of the impeller cannot always be kept uniform, especially under off-design operating conditions. This results in a radial thrust on the impeller shaft. To eliminate or reduce the radial thrust, both double-tongue and double-discharge volute designs have been used (Fig. 6-42). Here, the flow is divided into equal streams by two (or more) tongues set 180 deg apart. Although the volute pressure unbalances may be the same as in a single-volute casing, the resultant of all radial forces may be reduced to a reasonably low value because of symmetry.

Vaned diffusers have also been used extensively, particularly in higher-pressure pumps. The diffuser vanes serve as structural members to maintain the integrity of the volute under hoop stresses induced by internal pressures. Also, they are sometimes used as the primary path for structural loads carried through the housing. Hydrodynamically, the use of the diffuser improves efficiency, at least near the design point ,and tends to reduce radial loads at the off-design conditions by significantly reducing the velocity in the volute and maintaining a more nearly constant velocity angle. Figure 6-43 shows a vane-island diffuser that is desirable when the diffuser is in the structural-load path. Diffuser vanes with aerodynamically shaped discharges as well as inlets are used for peak efficiencies where the vanes do not

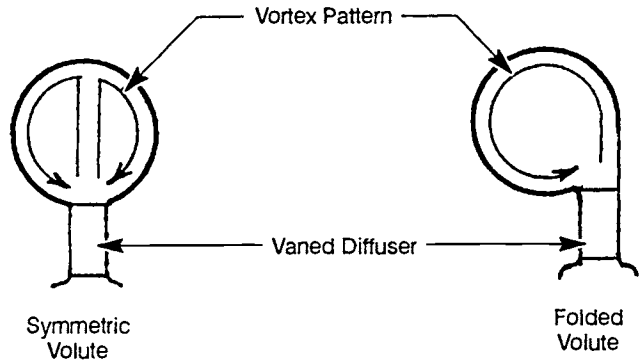

Fig. 6-41 Potential volute configurations.

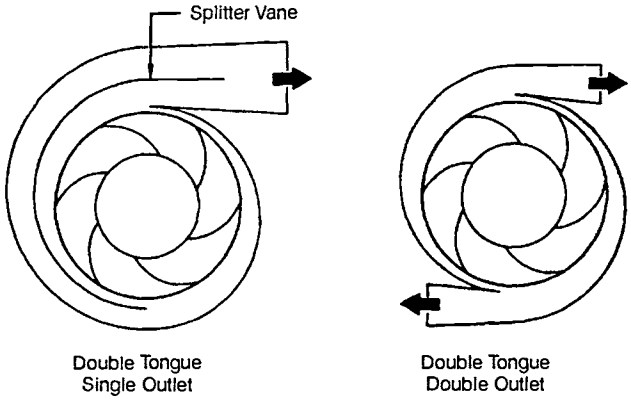

Fig. 6-42 Typical double-tongue and double-discharge volute configurations.

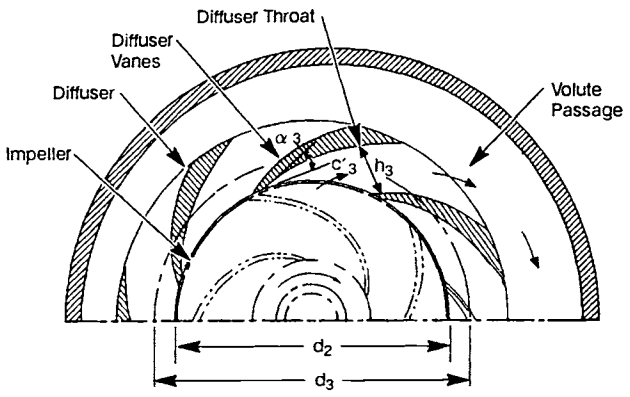

Fig. 6-43 Typical layout of the diffuser for a pump.

have to carry large loads. The radial clearance between impeller and diffuser-inlet vane tips must be sufficiently large to avoid large dynamic stresses on the impeller blades and diffuser vanes because of dynamic interaction. The preferred ratio of diffuser-inlet to impeller-discharge diameter is in the range of 1.07 to 1.10. However, for peak efficiencies and to reduce size and weight, smaller values are sometimes used, e.g., 1.05, particularly in low-density fluids such as liquid hydrogen. The width of the diffuser at its inlet should be similar to or up to 10% smaller than the width of the impeller's discharge flow.

The design of the vane shapes requires careful flow analysis to achieve efficiency and avoid inlet stall or cavitation. Typically, the design-point incidence angle of the inlet will be kept small unless the desired operating flow range allows the design be biased in one direction to minimize stall over the whole range. At the low-flow condition it is not uncommon for the vaned diffuser inlet to be the first location to experience stall, although the head loss due to the stall may be relatively small (e.g., less than 5% of the overall head).

The number of diffuser vanes (z) should be kept to the minimum, consistent with good performance, and to avoid resonances should have no common factor with the number of impeller vanes. If possible, the cross section of the passages in the diffuser should be made nearly square (i.e., $b_3 = h_3$). The shape of the passage below the throat should be diverging, with an angle between 10 and 12 deg. The flow leaving the diffuser should have velocity kept slightly higher than the velocity in the pump-discharge line.

Multistage centrifugal pumps require crossover channels to direct the flow from the discharge of one stage to inlet of the next. Crossovers can be external using a volute collector at the discharge of one stage and a duct routed to the inlet manifold of the next. However, this leads to a much larger, heavier, more-costly design as compared with an internal-crossover system.

Internal-crossover design involves conversion of kinetic energy into pressure, turning the flow 180 deg to the inlet of the next stage, and distributing the flow uniformly at the inlet to the next impeller. Crossover requirements can best be met in separate steps. The continuous-passage crossover (as found in the SSME HPFTP, Fig. 6-5) is a good example. The majority of the pressure recovery is achieved in the upcomer, which is a passage diffuser with design features similar to a vaned diffuser's. Flow will be turned in a constant-area turnaround duct, designed to minimize secondary flows and their associated losses. The remaining pressure recovery takes place in the downcomer, which is also designed to provide the desired inlet velocity vector at the next stage inlet. The flow is discharged from the downcomer in an annular channel long enough to provide some mixing of the wakes and boundary-layer growth developed in the crossover passage. The flow then enters the eye of the next impeller.

Balancing the Axial Thrust of Centrifugal Pumps

The pressures generated in these pumps and the areas of the rotating members are sufficiently large that the designer must hydrodynamically balance the axial loads acting on the rotating components. This balance must be sufficient to maintain low axial loads on the bearings throughout operation—for transient operation as well as steady state. If the pump is required to throttle, the balance must be adequate throughout the throttle range to protect the bearings from overload. Various techniques are available to achieve a balance design. For the turbopump in Fig. 6-16, the two impellers are mounted back-to-back with balance ribs on the back of the impeller that can be adjusted to achieve a reasonable balance at a fixed operating condition. The discharge pressures attained in this pump and the single-point operation yielded an acceptable design, requiring no self-adjusting control system.

The pressure forces acting on the surface of the rotating members are strongly affected by the magnitude of the rotational velocity of the fluid in the cavity between the rotating and stationary walls.

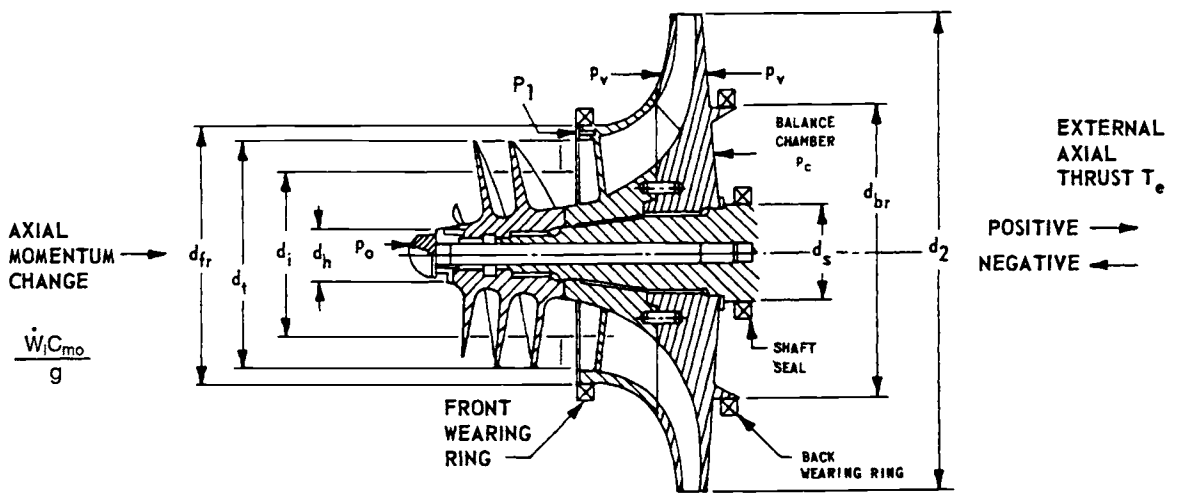

Fig. 6-44 Balancing axial thrusts of a centrifugal pump by the balance-chamber method.

Frequently, the velocity in the cavity can be approximated by a forced-vortex type of flow (velocity linearly dependent on radius). With such an approximation, pressure at any point along the rotating surface is given by—

$$p_r = p_1 - \rho k^2 (U_1^2 - U_r^2)/2g \qquad (6\text{-}36)$$

where p_1, p_r are the pressures at the tip and at any other radius, respectively; U_1 and U_r are the corresponding rotational speeds of the wheel; ρ is the fluid specific weight, and g is the gravitational constant; k is the ratio of the average fluid tangential velocity c divided by the rotational velocity of the wheel U at any radius. Note that if k is large, the pressure gradient is large, and the pressure force is less as the diameter decreases. Placing balance ribs on the rotating wheel increases the fluid velocity; that produces a higher k value and reduces the force. As another option, placing antivortex ribs on the stationary surface tends to decrease the k value and increase the fluid force. For two smooth surfaces with no appreciable through-flow, the average value of k will be 0.5.

Rather than ribs, seals can be used to achieve a balance, as illustrated in Fig. 6-44. A balance chamber is provided at the back shroud of the impeller, between back wearing-ring diameter d_{br} and shaft-seal diameter d_s. Proper selection of the projected chamber area and of the admitted fluid pressure balances axial loads. The pressure level pc in a balance chamber can be controlled by careful adjustment of the clearances and leakages of the back wearing ring and the shaft seals. The required p_C can be determined by integrating the pressure forces over the respective areas to achieve the necessary balance.

The high-pressure pumps on the SSME operate over a throttle range and involve such large pressures that more sophisticated balancing techniques were required. To illustrate the techniques available to the designer, consider the SSME HPFTP of Fig. 6-5. The pump and turbine being on the same shaft, both must be included in the axial-thrust model. The turbine thrust was designed to oppose the pump thrust to help achieve an overall balance. The labyrinth seals on the back side of the impellers were given a diameter that would improve overall balance. Finally, to provide some self-adjusting ability, a balance piston (Fig. 6-45) was incorporated on the back side of the third-stage impeller. The complete rotating assembly is free to move over a limited range, in the axial direction, to respond to any unbalanced loads. As the assembly moves it opens one of the two orifices of the balance piston and closes the other. This adjusts the pressure on the back side of the impeller that changes until arriving at a balanced force. The total available travel is typically small (e.g., 0.020 in.), and the balance piston is designed to operate at the middle of the force range at the operating point with the highest speed.

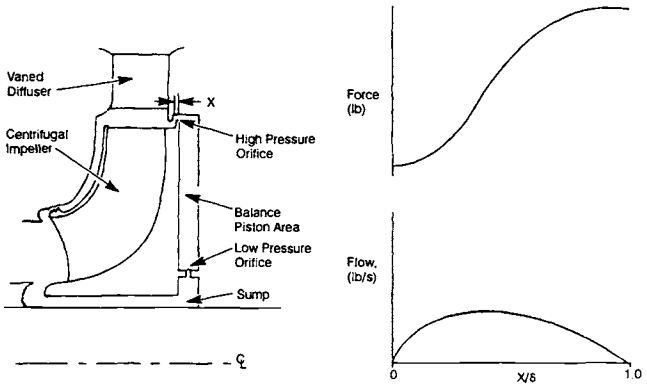

Fig. 6-45 Balance-piston concept.

6.5 DESIGN OF AXIAL-FLOW PUMPS

Except when used as inducers, axial-flow pumps for rocket engines have essentially been limited to liquid-hydrogen systems in a multistage configuration where the required flow range of operation was limited (Ref. 6-7). Multistage axial-flow hydrogen pumps are used in applications going beyond the capability of a single-stage centrifugal pump, since the multistage construction is comparatively simple (Fig. 6-3). As shown in Fig. 6-6, the fluid in an axial-flow pump flows from one stage to the next with a minimum of connecting passages.

The head coefficient of a typical single-stage centrifugal hydrogen pump falls in the range of 0.45-0.65. For an axial pump, however, the head coefficient for a single stage will usually be limited to the range of 0.2-0.4. Thus, more stages will be

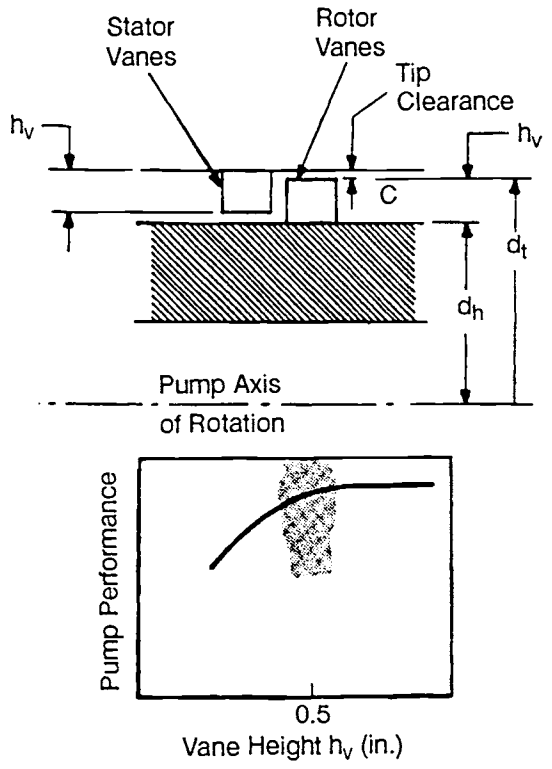

Fig. 6-46 Effect of vane height on the performance of an axial-flow pump.

required to get the same head for the axial pump, but the staging is much easier to achieve. Typically, the axial pump will have a lower flow-limit because of the minimum practical height h_v of the vanes (Fig. 6-46). For heights below 0.5 in., the tip clearance required for efficient performance becomes critical, causing manufacturing problems or increased risk of operation. Each axial stage should preferably have a flow coefficient in the range of 0.25 or higher and the stage hub/tip diameter ratio should generally be less than 0.9 for efficient operation. Using these guidelines, the designer can parametrically evaluate the relative design features, such as diameter and blade height, to meet requirements. Also, a reduction in rotor diameter below certain values will not be practical because of the high rpm required for proper blade speed.

Axial pumps typically are used where specific speeds per stage are in the range of 3000 to 6000. An area of overlap allows either a multistage axial or centrifugal pump. The better solution will be dictated by other considerations, such as space envelope, mounting and ducting arrangement, required flow range, etc. Probably the major limit of axial pumps is their tendency to stall at low-flow conditions. This stall involves separation of the boundary layers on the blades, and it significantly reduces both pump head and efficiency. This can be seen in Fig. 6-47, which presents actual data of a multistage axial flow pump. The pump operation must be maintained at some comfortable margin (e.g., 10%) of flow above the stall condition.

Basic Assumptions for Axial-Flow Pumps

During operation of an axial-flow pump, it is assumed that the meridional or axial component cm of the absolute flow velocity remains constant throughout all stages of the impeller rotor and the stator. This approximation assumes that the thermodynamic conditions do not change sufficiently to require adjusting the density of the fluid in the stages. If the density changes are significant, they should be accounted for at least in the interstage planes. (There is seldom enough density change to require analyzing the pump flow as a compressible fluid in a given stage. However, the pump designer must be aware of the potential for cavitation and design to avoid it.) To satisfy the flow-continuity equation, the cross-sectional areas of the various flow passages at right angles to cm must also remain constant. This assumption is reasonable, except for the effects of frictional drag at the casing walls and the vanes. Again, where significant boundary layers develop it may be desirable to increase the blade heights in successive stages to maintain an approximately constant cm in the core flow.

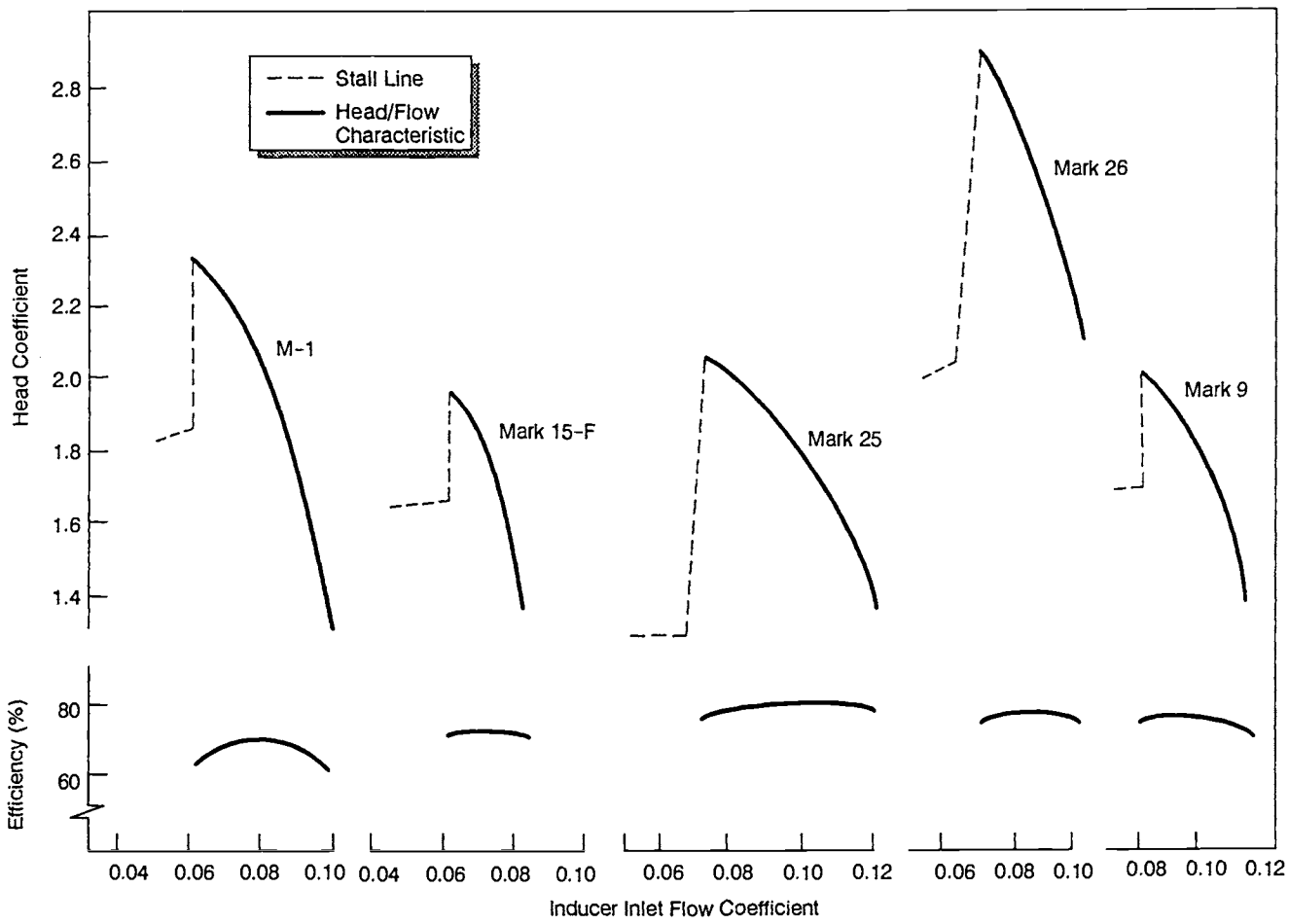

Fig. 6-47 H-Q, η-Q data for axial pump with stall.

Operation of the Impeller Rotor

As its main function, the impeller rotor of an axial-flow pump—by the action of airfoil-shaped rotor vanes (Fig. 6-48 and 6-49—imparts kinetic energy to the fluid by increasing the tangential component of the absolute flow velocity. It is convenient to describe the vanes on several developed cylindrical sections. Three sections are of particular interest: at the impeller tip diameter d_t, at the impeller hub d_h, and at its mean effective diameter d_m (inches). The mean effective diameter is defined by—

$$d_m^2 = 0.5(d_t^2 + d_h^2) = 0.5\, d_t^2(1 + r_d^2) \quad (6\text{-}37)$$

where r_d = impeller hub ratio, or d_h/d_t. For simplicity, vane characteristics and flow conditions are discussed here only with respect to the mean effective diameter d_m. The vanes are equally spaced at a circumferential distance P_r:

$$P_r = \pi d_m/z_r \quad (6\text{-}38)$$

where—P_r = pitch or rotor vane spacing at the mean effective diameter d_m, in., and z_r = number of rotor vanes. The ratio of the rotor-vane chord length C_r to the pitch P_r is called rotor-vane solidity S_r:

$$S_r = C_r/P_r \quad (6\text{-}39)$$

where S_r = rotor-vane solidity at the mean effective diameter d_m. The solidity generally increases from rotor-tip diameter d_t to hub diameter d_h for structural reasons.

The profile of the vane can be represented by the vane mean line (Fig. 6-49), which determines most of the important hydraulic properties of the vane. The thickness of the vane varies along the mean line for better performance and for structural strength. To effectively impart the driving action to the fluid, the angle of the vane mean line, or rotor-vane angle, is gradually increased from β_2 to β_3. The difference between the two, $\beta_3 - \beta_2$, gives a measure of the vane curvature (camber) along any particular vane section. Mean-line geometries developed for axial compressors and airfoils are generally applicable to pumps, but the potential for leading-edge cavitation must be evaluated and avoided for a good design. In axial-flow pump designs, all vane mean lines can often be approximated by a circular arc. For this case, the following correlations can be established:

$$\beta_c = 0.5(\beta_2 + \beta_3) \quad (6\text{-}40)$$

$$C_r = 2R_r \sin [0.5(\beta_3 - \beta_2)] = L_r/\sin\ \beta_c \quad (6\text{-}41)$$

where—

β_c = chord angle of the rotor vane, deg
β_2 = vane angle at the rotor inlet, deg
β_3 = vane angle at the rotor outlet, deg
C_r = chord length of the rotor vane, in.
R_r = radius of the rotor vane curvature, in.
L_r = axial length of the rotor vane, in.

An angle of attack (incidence angle) "i" between rotor-inlet vane angle β_2 and the direction of the relative velocity of the flow entering the rotor β_2' allows more effective driving of the fluid. Also, an angle "ii' allows deviation of the flow from the rotor-outlet vane angle β_3, the direction of the relative velocity of the flow leaving the rotor being β_3'. For the design of impeller rotors, velocity diagrams of the flows at the inlet and outlet of rotor vanes can be constructed (Fig. 6-49) with the following

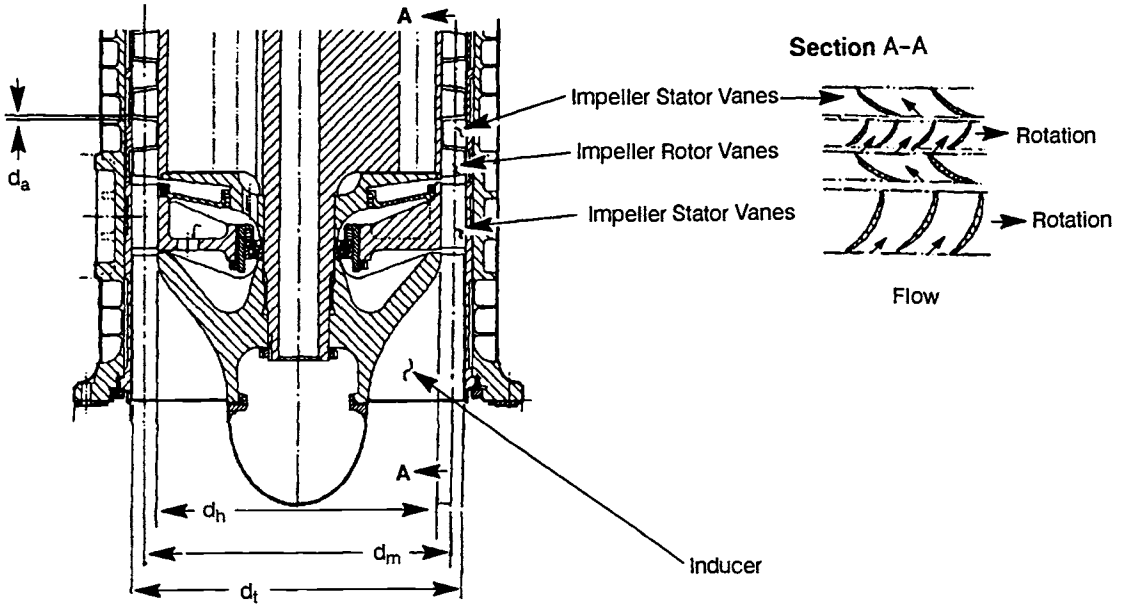

Fig. 6-48 Inducer, inducer stator, impeller rotor, and impeller stator of an axial-flow pump.

correlations:

$$\beta_2 = \beta_2' + i \quad (6\text{-}42)$$

$$\beta_3 = \beta_3' + ii \quad (6\text{-}43)$$

$$c_m = Q_{imp}/[3.12\ p(d_t^2 - d_h^2)\varepsilon/4] \quad (6\text{-}44)$$

$$Q_{imp} = Q + Q_e \quad (6\text{-}45)$$

$$u_m = \pi N d_m/720 \quad (6\text{-}46)$$

$$\Delta H_{imp} = (\Delta H)_1 + H_e = [u_m c_{u3}' - u_m c_{u2}']/g \quad (6\text{-}47)$$

$$(\psi)_1 = (\Delta H)_1/u_m^2/g \quad (6\text{-}48)$$

$$c_m = c_{u2}' \tan \alpha_2' = c_{u3}' \tan \alpha_3' = c_2' \sin \alpha_2' = c_3' \sin \alpha_3' = v_2' \sin \beta_2' = v_3' \sin \beta_3' \quad (6\text{-}49)$$

where

- i = angle of attack, deg
- ii = discharge deviation angle, deg
- β_2', β_3' = relative flow angles at the rotor inlet and outlet, deg
- α_2', α_3' = absolute flow angles at the rotor inlet and outlet, deg
- cm = meridional or axial component of the absolute flow velocities, ft/s
- u_m = rotor peripheral velocity at mean effective diameter dm, ft/s
- c_2', c_3' = design absolute flow velocities at the rotor inlet and outlet, ft/s
- cu_2', cu_3' = tangential components of the design absolute rotor inlet and outlet flow velocities, ft/s
- v_2', v_3' = design relative flow velocities at the rotor inlet and outlet, ft/s
- Q_{imp} = required impeller flowrate at the rated design point, gpm
- Q = rated design pump flowrate, gpm
- Q_e = impeller-leakage loss rate (2 to 10% of Q), gpm
- ε = contraction factor of vane passage (0.85 to 0.95)
- H_{imp} = developed head required per impeller stage, ft
- $(\Delta H)_1$ = rated design developed head per axial-flow-pump stage, ft
- H_e = hydraulic-head losses per stage of impeller stator, ft
- $(\psi)_1$ = head coefficient per axial-flow pump stage

At various cylindrical sections between vane tip diameter d_t and hub diameter d_h, the following correlations between vane angles and flow velocities have been established:

$$d_m \tan \beta_2 = d_t \tan \beta_{2t} = d_h \tan \beta_{2h} = d_x \tan \beta_{2x} \quad (6\text{-}50)$$

$$d_m \tan \beta_3 = d_t \tan \beta_{3t} = d_h \tan \beta_{3h} = d_x \tan \beta_{3x} \quad (6\text{-}51)$$

$$u_m/d_m = u_t/d_t = u_h/h = u_x/d_x \quad (6\text{-}52)$$

$$c_{u2}'/d_m = c_{u2t}'/d_t = c_{u2h}'/d_h \quad (6\text{-}53)$$

$$c_{u3}'/d_m = c_{u3t}'/d_t = c_{u3h}'/d_h \quad (6\text{-}54)$$

where—

- β_{2t}, β_{2h} = rotor-inlet vane angles at tip and hub diameter, deg

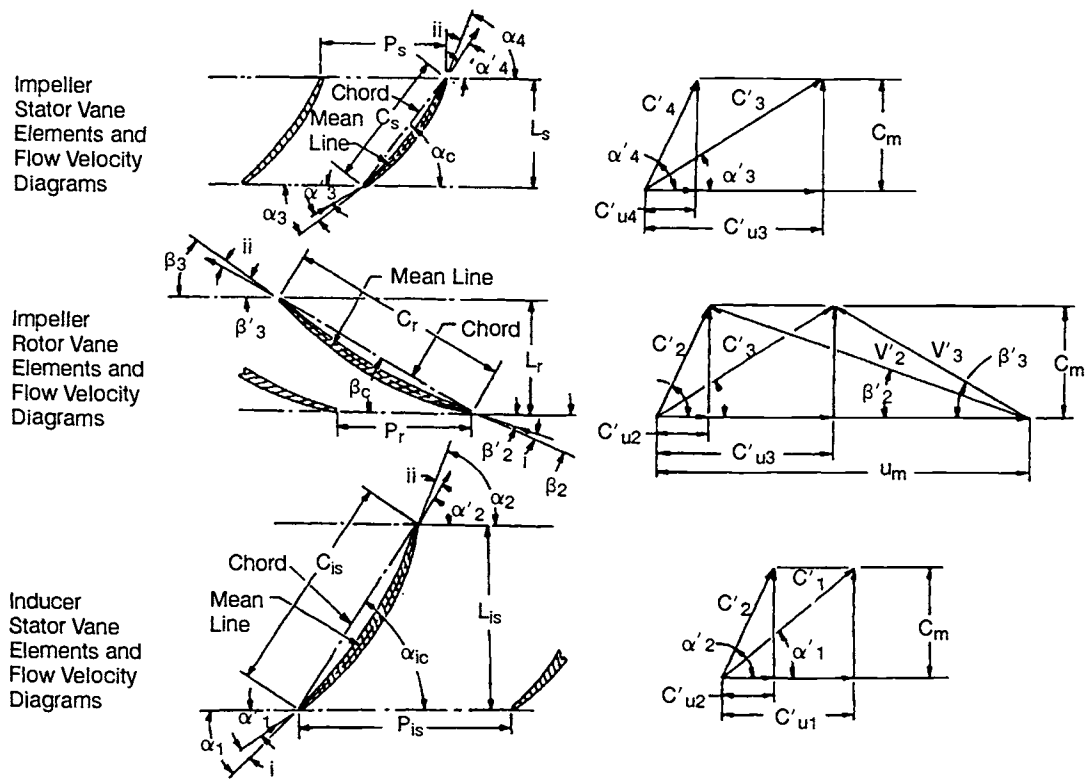

Fig. 6-49 Vane elements and flow-velocity diagrams of axial-flow pumps.

β_{3t}, β_{3h} = rotor-outlet vane angles at tip and hub diameter, deg
u_t, u_h = rotor peripheral velocities at tip and hub diameter, ft/s
c_{u2t}', c_{u2h}' = tangential components of the design absolute rotor inlet-flow velocities at tip and hub diameter, ft/s
c_{u3t}', c_{u3h}' = tangential components of the design absolute rotor outlet-flow velocities at tip and hub diameter, ft/s

Some parameters in the equations above require further definition. The parameter ε represents the ratio of effective flow area to the geometric area—a parameter introduced to express the blockage caused by the buildup of boundary layers, particularly at the hub and tip-shroud. Thus, this parameter will usually be smaller at stages further downstream. Estimation of this parameter is usually based on an empirical database, although solutions to the Navier-Stokes equations with an adequate turbulence model are also acceptable. The parameter Q_e is used to account for any leakage introduced at the various points in the flow path. Calculation of leakage flows is generally done independently and successively iterated with the pump design. The incidence angle is chosen by the designer considering the efficiency, cavitation potential, and the required flow-range. The deviation angle "ii" must be calculated in terms of the real fluid effects or estimated using some empirically based estimating technique. One such technique that has been widely used, the "Carter's Rule" or "modified Carter's Rule", can be found in various references (e.g., Ref. 6-2 and 6-7). As can be seen from Eq. (6-47), calculation of the deviation angle to design a blade to get the correct discharge velocity is absolutely critical to obtaining the correct head.

Function of the Stator

The stator of an axial-flow pump converts a major portion of the tangential component of the absolute flow velocity leaving the rotor into static pressure by "straightening" the flow after it leaves the rotor. The stator-vane curvature is designed so that the fluid enters the vanes with minimum loss and leaves the stator with a reduced tangential component of the absolute flow velocity. The cross-sectional areas of the stator flow passages normal to the axial direction equals those of the rotor, thus maintaining the axial component of the absolute flow velocity. The dimensions d_t and d_h of the stator, (Fig. 6-48) can be treated as equal to the tip and hub diameters of the rotor. The solidity of the stator vanes generally increases from hub diameter (d_h) to tip diameter (d_t) because the vanes are supported structurally at the tip. The axial length (L_S) of the stator vane at the mean effective diameter is usually made equal to that of the rotor (L_r), but it is governed by the solidity and the required number of vanes.

Regarding Fig. 6-49, the velocity diagrams for the stator inlet and outlet are constructed with the assumption that the absolute flow velocities and angles at stator inlets and outlets equal the corresponding ones at the rotor outlets and inlets. This facilitates the design of multistage axial-flow pumps using uniform rotor and stator stages.

To deflect the fluid effectively, the inlet-vane angles (α_3) of the stator should be greater, by a few degrees, than the inlet absolute-flow angles (α_3'); i.e., an angle of attack "i" should be allowed. Also, an angle "ii" should be allowed between outlet-vane angle (α_4) and outlet absolute-flow angle (α_4') for the deviation angle. The following correlations can be established for the vane and flow velocity diagrams of the stator (Fig. 6-49):

$$P_S = \pi d_m / z_S \quad (6\text{-}55)$$

$$S_S = C_S / P_S \quad (6\text{-}56)$$

$$\alpha_C = 0.5 (\alpha_3 + \alpha_4) \quad (6\text{-}57)$$

$$C_S = 2 R_S \sin [0.5(\alpha_4 - \alpha_3)] = L_S / \sin \alpha_C \quad (6\text{-}58)$$

$$\alpha_3 = \alpha_3' + i \quad (6\text{-}59)$$

$$\alpha_4 = \alpha_4' + ii \quad (6\text{-}60)$$

$$c_m = c_{u3}' \tan \alpha_3' = c_{u4}' \tan \alpha_4' = c_3' \sin \alpha_3' = c_4' \sin \alpha_4' \quad (6\text{-}61)$$

$$d_m \tan \alpha_3 = d_t \tan \alpha_{3t} = d_h \tan \alpha_{3h} = d_x \tan \alpha_{3x} \quad (6\text{-}62)$$

$$d_m \tan \alpha_4 = d_t \tan \alpha_{4t} = d_h \tan \alpha_{4h} = d_x \tan \alpha_{4x} \quad (6\text{-}63)$$

where—

P_S = pitch or stator-vane spacing, in.
z_S = number of stator vanes
S_S = stator-vane solidity
C_S = stator-vane chord length, in.
α_C = stator-vane chord angle, deg
α_3, α_4 = vane angles at stator inlet and outlet, deg
R_S = radius of the stator-vane curvature, in.
L_S = axial length of the stator vane, in.
i = angle of attack, deg
ii = angle allowed for circulatory flow at the outlet, deg
α_3', α_4' = absolute-flow angles at stator inlet and outlet, deg
cm = axial component of the absolute-flow velocities, ft/s
c_3', c_4' = design absolute-flow velocities of stator inlet and outlet, ft/s
c_{u3}', c_{u4}' = tangential components of the design absolute velocities at stator inlet and outlet, ft/s
$\alpha_{3t}, \alpha_{3h}, \alpha_{3x}$ = stator-inlet vane angles at tip, hub, and any intermediate diameter, deg
$\alpha_{4t}, \alpha_{4h}, \alpha_{4x}$ = stator-outlet vane angles at tip, hub, and any intermediate diameter, deg

Design of Impeller Rotors and Stators

A number of design factors directly affect the performance characteristics of an axial-flow pump. Evaluation of test information, on the basis of specific speed per stage $(N_S)1$, shows the following definitive correlations:

Impeller-hub ratio r_d. The ratio of impeller hub diameter d_h to tip diameter d_t (Fig. 6-48) has a direct bearing on the specific speed per stage $(N_S)_1$. Higher-specific-speed pumps have higher relative flows and therefore smaller hub ratios that result in greater free-flow area; but they also have lower head (H/Q) characteristics. However, a higher hub ratio tends to yield a higher head coefficient per stage $(\psi)_1$. Typical values of r_d in rocket-engine hydrogen pumps range from 0.75 to 0.86. Typical design values for $(N_S)_1$ and $(\psi)_1$ range from 3000 to 5000 and from 0.25 to 0.40, respectively. A key factor that sets the head coefficient, the diffusion factor, will be discussed more fully below.

Vane solidities S_r, S_s. The vane solidities or chord-spacing ratios of the rotor and stator—important design parameters—are selected on the basis of previous experience. A higher pump specific speed is linked with lower solidity primarily because the required head is smaller and so gives the higher specific speed. Typical design values for vane solidities for the rotor and stator at the mean effective diameter (d_m) range from 1 to 1.34 and 1.5 to 1.8, respectively. Lower values are generally more efficient when the diffusion factor and head generated are lower.

Number of vanes z_r, z_s. A lower pump specific speed usually results in a larger number of vanes. Design values of z_r range from 14 to 20. Design values of z_s are typically higher, up to a factor of approximately 2. To minimize the potential for dynamic interaction, the number of stator vanes should have no common factor with the number of rotor blades.

Vane curvature and setting. Experiments indicate that the head developed by the rotor is essentially determined by vane curvature, i.e., $\beta_3 - \beta_2$. Changes in vane settings (i.e., outlet-vane angle β_3 and inlet-vane angle β_2) by the same amount will not affect head rise and efficiency significantly.

The design procedure for the impeller rotors and stators of a multi-stage axial-flow pump is essentially the same as that for a single-stage centrifugal pump, except for the determination of the number of pump stages. Design parameters and coefficients established experimentally using prior successful designs should be utilized to the fullest. Special development tests will still be required to verify the characteristics of a new design. The design procedure should include the following steps:

1) To meet a given set of engine system requirements such as rated design pump-developed head H, flow rate Q, and rated pump (NPSH)c, the pump rotating speed N is determined first through selection of a suitable inducer of a given suction specific speed $(N_{SS})_{ind}$.

2) With N established, selection of impeller rotor and stator of a given specific speed per stage $(N_S)_1$, combined with a determination of the number of pump stages, can proceed with the aid of the following correlations:

$$(N_S)_1 = N\,(Q)^{0.5}/(\Delta H)_1^{0.75} \qquad (6\text{-}64)$$

$$\Delta H = \Delta H_{ind} - H_{ee} + n(\Delta H)_1 \qquad (6\text{-}65)$$

where—

- $(N_S)_1$ = specific speed per axial-flow-pump stage
- N = rated design pump rotating speed, rpm
- Q = rated design pump flow rate, gpm
- $(\Delta H)_1$ = rated design pump-developed head per axial-flow pump stage, ft
- ΔH = rated design pump-overall-developed head, ft
- ΔH_{ind} = inducer rated head rise, ft
- H_{ee} = hydraulic-head loss at the inducer stator, ft
- n = number of axial-flow pump stages

3) For the specific speed per stage $(N_S)_1$ thus obtained, various design factors and coefficients such as impeller hub ratio r_d, vane solidities S_r and S_s, number of vanes z_r, and z_s, head coefficient per stage $(\psi)_1$, etc., will be selected based on past designs with comparable $(N_S)_1$ values.

4) The required impeller rotor and stator diameters, velocity diagrams, and vane profiles can now be derived from Eq. (6-37) through (6-63).

Impeller rotor and stator vanes are usually machined from forgings of aluminum alloys or nickel-base alloys such as K-Monel. In view of the relatively low head produced by an individual axial-flow-impeller stage, reduction of skin-friction and flow-turbulence losses prove more important than with centrifugal pumps. High efficiency demands a high degree of vane streamlining and polishing.

The axial distance d_a between impeller rotor vanes and stator vanes (Fig. 6-49) has some bearing on performance. Typical design values of d_a range from 0.02 to 0.05 d_t, where d_t equals the impeller-tip diameter. This spacing is also expressed as a function of the chord of the upstream blade. In general, the spacing should not be less than 10% of this chord to avoid large dynamic stresses because of the interaction of the rotor-stator blades. As improved CFD codes are being developed, the dynamic stresses can be calculated to give guidance to the design. Design values for tip clearance c for both the rotor and stator (Fig. 6-46) should be no more than approximately 2% of the blade or vane height. Smaller values can be used depending on the manufacturing tolerances and the dynamic behavior of the pump that controls the rotor's radial motion.

The vane thickness along the mean line will mainly be determined by structural considerations because experiments indicate that there is very little effect on performance from variation of vane thickness as long as the leading and trailing edges

are kept at a small radius and the thickness is developed along the meanline in an efficient manner. The problems with calculating stresses for pump rotor vanes are similar to those with turbine blades. The methods given in section 6.6 for turbines can also be applied here. Vanes experience centrifugal, bending (due to lift and drag loading), and vibrational stresses.

Diffusion and Retardation Factors

In designing the axial pump, it is desirable to increase the head per stage to reduce the total number of stages. However, the head per stage is limited by the ability of the blading to turn the flow without inducing a separation that causes pump stall, an undesirable operating condition. Usually the peak efficiency of the design will be maximum as the head per stage is increased, but design margins must be maintained to avoid stall. To assess the stall potential and the losses in an axial stage, a "parameter-diffusion" factor has been developed; it has been shown to be a reliable indicator. Using the vector diagrams of Fig. 6-49, the diffusion factor for the rotor can be expressed as follows:

$$DF_r = 1.0-(v_3'/v_2') + (cu_3'-cu_2')/(2S_r v_2') \quad (6\text{-}66)$$

Similarly, for the stator:

$$DF_S = 1.0-(c_4'/c_3') + (cu_4'-cu_3')/(2S_S c_3') \quad (6\text{-}67)$$

Good efficiencies at reasonable stall margins have been achieved with the diffusion factors in the range of 0.45 to 0.55. Diffusion factors above this range have been successfully used, but require a more sophisticated analysis to assure that stall will be avoided. Designs have been achieved that push the stall up to a diffusion factor of 0.75; obviously, the higher the diffusion factor, the smaller will be the unstalled flow range.

Also used to estimate the stall condition has been a "retardation" factor. Using again the vectors of Fig. 6-49, the retardation factor for the rotor is given by (v_3'/v_2') and for the stator by (c_4'/c_3'). The designer should assume that stall will occur whenever the retardation factor reaches 0.5. Successfull designs have been achieved with this factor as low as 0.63.

Design of Casings for Axial Pumps

As shown in Fig. 6-6 and 6-50, the casing of an axial-flow pump consists of a cylindrical section housing the inducer and impeller stages. It also includes a volute section with radial guide vanes situated behind the last rotor stage of the impeller. In addition to converting the tangential-flow-velocity component into pressure, the volute section also serves to reduce the axial-velocity component by gradually increasing the flow area toward the volute discharge.

The radial guide vanes of the volute section are designed so that the fluid enters them with minimum losses and leaves them in a radial plane, analogous to a centrifugal pump (Fig. 6-43). The number of radial guide vanes will be chosen to achieve the desired turning with a reasonable diffusion factor in the space provided. They should have no common factor with the number of impeller rotor blades.

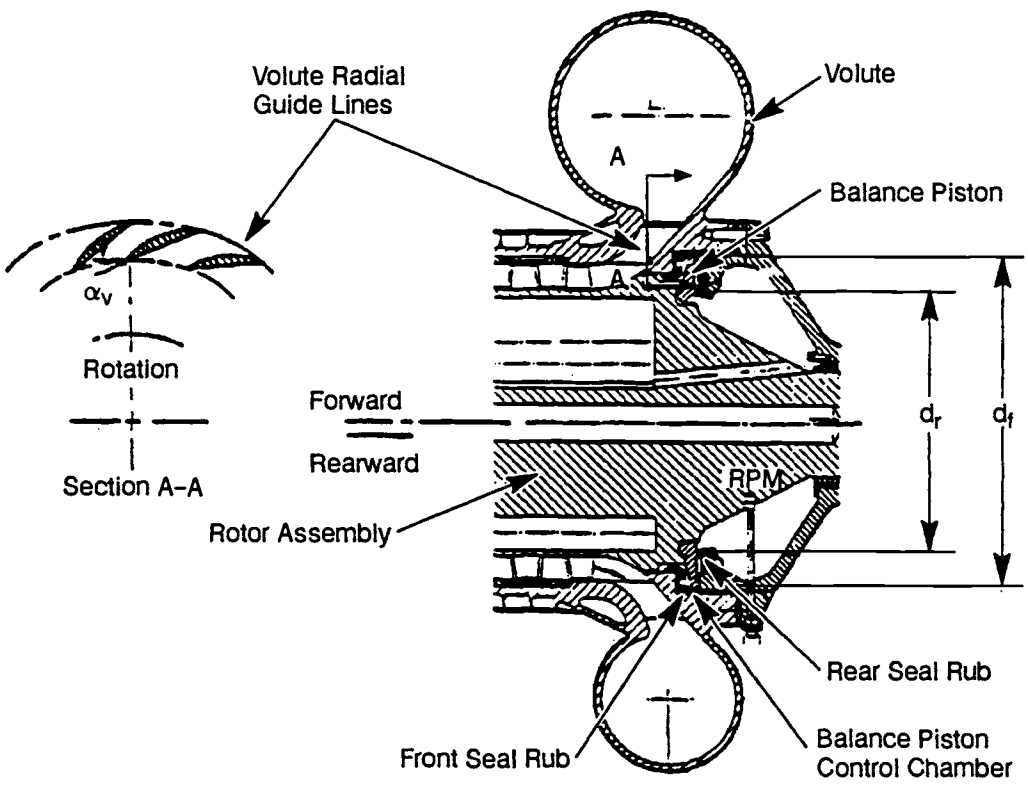

Fig. 6-50 Axial-flow pump volute casing and balance-piston arrangement.

Vane angle (a_V) can be determined by constructing the flow velocity diagram for that section.

The design calculations for the volute are the same as for a centrifugal-pump volute. This includes the area distribution, cross-sectional shape, and the volute tongue angle.

Balancing the Axial Thrust of MultiStage Axial Pumps

Balancing of the combined axial thrust of a multistage axial-flow pump is an important function because of the high pressures involved. Special balancing devices, such as automatic balance pistons, are frequently used. Secured to the rotor assembly, as shown in Fig. 6-50, the balance piston operates on the same principle as the balance piston of a centrifugal pump, consisting of a disk with small clearances and a pair of seal rubs located on either side of the disk. The balance piston has a forward movement (toward the inlet) of the rotor assembly. That reduces the clearance at the front-seal rub, simultaneously increasing clearances at the rear-seal rub. As a result, the pressure drops in the control chamber between front and rear seal rubs. This effect counteracts the forward hydraulic axial thrust of the rotor assembly. Similarly, a pressure increase in the control chambers counteracts a rearward movement (reverse thrust) of the rotor assembly. The volume to the rear of the control chamber communicates with the low-pressure region of the pump inlet through cavities in the rotor.

With the smaller diameter of the axial-flow pump, the available area for axial thrust control will usually be smaller, and thus requires higher pressures to achieve similar thrust ranges. The higher pressures also lead to higher leakage rates, which can penalize the pump efficiency. Thus, the final performance comparison of axial- vs. centrifugal-pump design must include evaluation of the effects of the balance-piston design.

6.6 TURBINE DESIGN

Gas-generator-cycle rocket engine applications will favor impulse turbines for their simplicity, high power-to-weight ratio, and low axial thrust (Ref. 6-8). Figure 6-51 shows the general arrangement of a typical single-stage, two-rotor, velocity-compounded impulse turbine. Gas-generator-cycle turbines are characterized by relatively high pressure ratios (e.g., as high as 20 for a single stage) with supersonic velocities and low flowrates. Turbine flowrate is minimized in a gas-generator cycle to maximize engine specific impulse because the turbine flowrate bypasses the engine thrust chamber and produces a relatively low thrust. In some cases the turbine flowrate may be low enough to require partial-admission turbine nozzles (nozzles flowing around only part of their circumference) for higher performance.

Staged-combustion-cycle and series-expander-cycle rocket engine applications will use low-reaction turbine stages to maximize turbine performance. Figure 6-52 shows the two-stage reaction turbine in the SSME HPFTP. Staged-combustion and expander-cycle turbines are characterized by relatively low pressure ratios (e.g., less than 2 for two stages) with subsonic velocities and high flowrates. Turbine pressure ratio will be kept as low as possible to minimize the pump-discharge pressure required to achieve a given main-chamber pressure and pump power requirements. The low-reaction staging minimizes the maximum velocities in the stage, resulting in maximum efficiency. In high-chamber-pressure rocket engines, the low pressure ratios still result in high turbine-rotor pressure drops and high axial thrust of the turbine.

A turbine stage consists of an expanding stationary-vane row (nozzle) followed by a single row or multiple rows of rotating blades. Low expansions may occur in the rotating-blade rows and redirecting stator. A second expanding nozzle begins another stage. The total available energy is divided between the stages based on the desired power split.

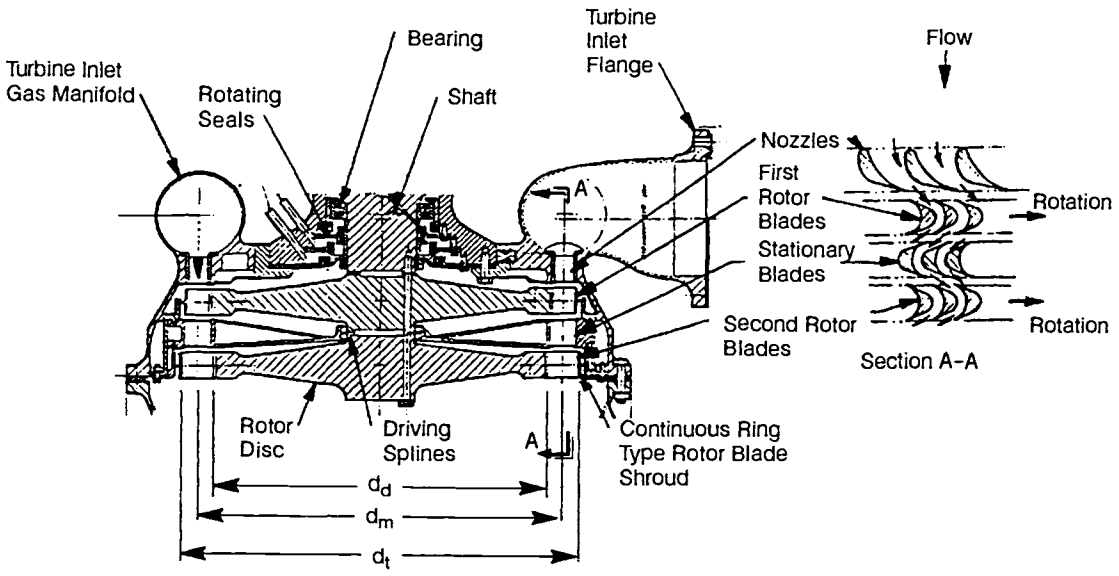

Fig. 6-51 Typical single-stage, two-rotor, velocity-compounded impulse turbine.

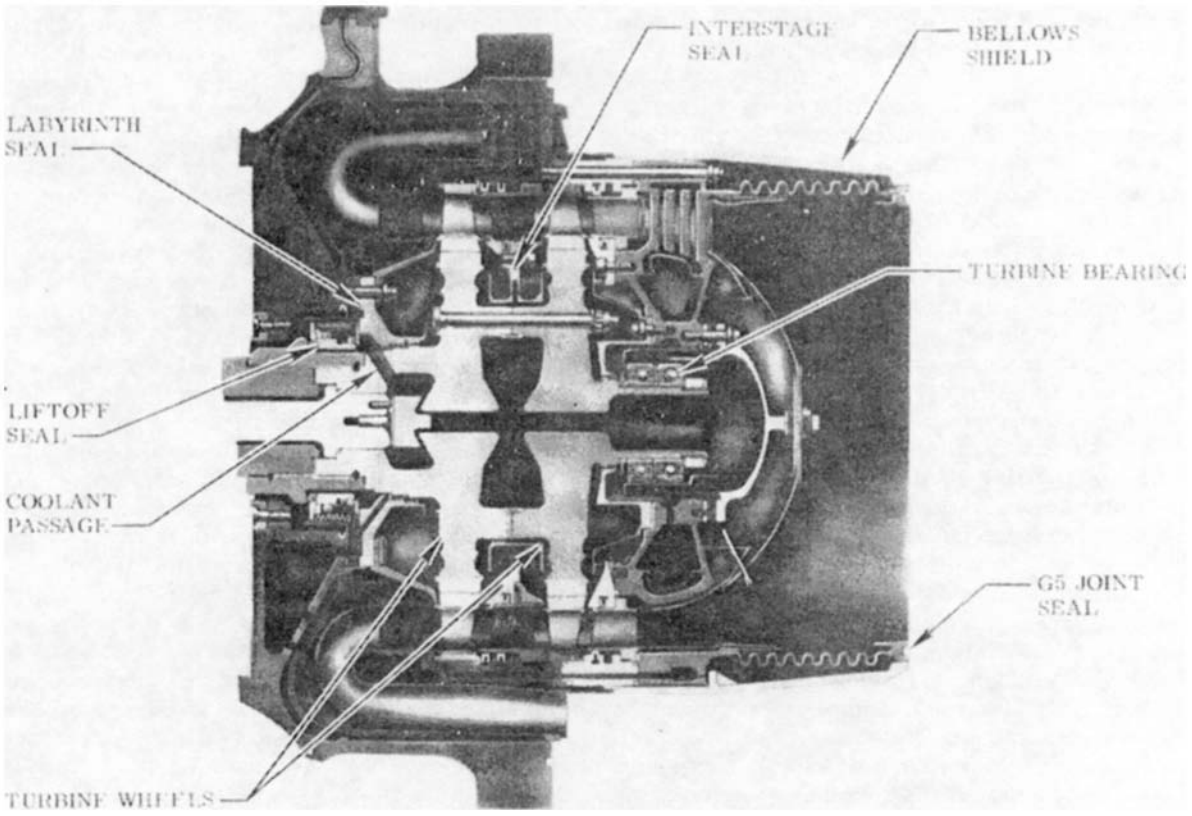

Fig. 6-52 Two-stage reaction turbine for SSME *HPFTP*.

General Design Procedure

An integrated turbine aerothermodynamic design will have overall requirements specified by a rocket-engine balance calculation. The following steps (Fig. 6-53) are essential in the design of a rocket-engine turbine.

Selection of turbine type. The first item of importance is the selection of the proper type. A single-stage rotor turbine (Fig. 6-10) will be used if the required turbine power is low, if the efficiency of the turbine has less effect on overall engine system performance, or if the pressure ratio is high and partial admission is required for high performance. When the available energy of the turbine working-fluid, and therefore the gas spouting velocity Co is relatively low, a higher turbine velocity ratio U/Co may be achieved with a moderate turbine rotor-blade speed U. As shown in Fig. 6-27, this suggests the use of a relatively simple single-stage, single-rotor impulse turbine. This type was selected for the A-2 Stage oxidizer turbopump, at the same time taking advantage of its overall simplicity.

In most direct-drive turbopump configurations (such as the A-1 Stage engine turbopump, Fig. 6-79), where the turbine rotating speed N and consequently turbine velocity ratio U/Co is lower than peak efficiency, a single-stage, two-rotor, velocity-compounded impulse turbine (Fig. 6-11 and 6-51) will be

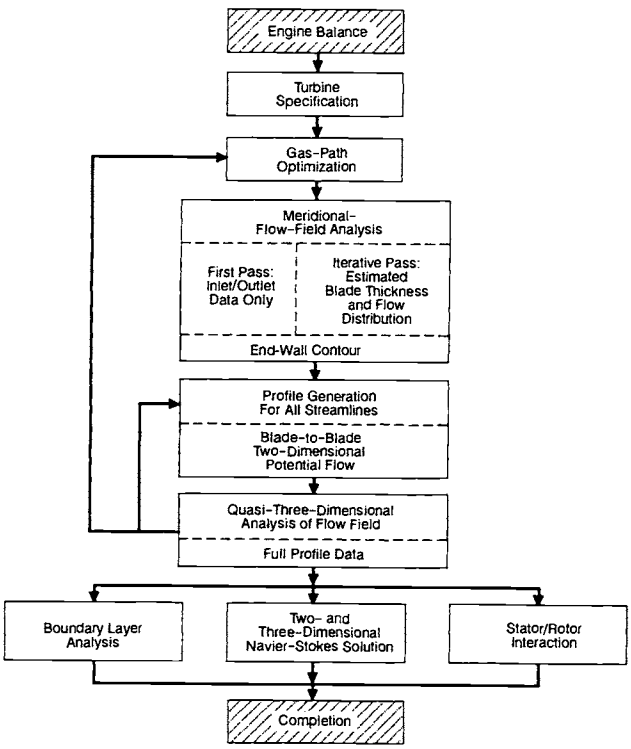

Fig. 6-53 Typical steps in the turbine design process.

selected for best results. Figure 6-27 indicates that the optimum efficiency of a velocity-compounded turbine can be achieved at a relatively low U/Co value.

The turbine can operate at a much higher rotating speed (over 25,000 rpm) if a reduction gear train couples the pump and the turbine (Fig. 6-16). A higher value of U/Co can be achieved with reasonable turbine rotor size. Then a higher-performance, two-stage, two-rotor, pressure-compounded impulse turbine (Fig. 6-12) may be used.

Low-reaction staging (about 25% reaction) enables low turbine pressure ratios to maximize efficiency. Stage velocity ratio U/Co and efficiency can be increased and blade loading reduced by using two low-reaction stages. The power split between stages typically has been about equal.

Size of turbine. After selecting the type of turbine, the designer determines the turbine-rotor size. Once the characteristics of the turbine working fluid, the turbine pressure ratio R_t, and the pump or turbine rotational speed N have been established, choosing a larger diameter for the turbine rotor tends to result in a higher velocity ratio U/Co, and thereby higher efficiency. However, the larger-diameter turbine rotor also spells higher assembly weight, larger envelope, and higher working stresses. Final selection of the turbine-rotor size, and consequently the U/Co ratio, often entails a design compromise.

Determine flowrate and pressure ratio. The required power output from the turbine must be equal to the net input to the propellant pumps, plus the mechanical losses in the bearings, seals, gears (if any), plus the net power required to drive any auxiliary drives. The required flowrate of the turbine working fluid can be calculated using Eq. (6-15) after the required power, available energy of the working fluid [Eq. (6-13)], and the overall turbine efficiency (from Fig. 6-27 in the initial phases of design) have been estimated.

Dimensions of blade rows. The initial dimensions of the stationary nozzles and of the rotating blades can be calculated using a preliminary-design pitch-line, gas-path program. The pitch-line analysis includes the selected staging, pressure distribution, and flow angles as well as representative losses due to friction and turning for each blade row, tip-clearance losses, partial-admission losses, rotor-disk windage losses, and shaft- and interstage-seal leakage losses. The blade-row outlet flow area can be calculated using continuity for the outlet conditions. Stage power, efficiency, and reaction are calculated from the Euler equation, pressure distribution, and the losses. The interactive program allows the designer to alter the various design parameters to achieve the optimum configuration within the design constraints. Computer graphics can display the resulting velocity-vector diagrams and blade-path geometry.

When blades are relatively short (height-to-radius ratio less than 0.10) and when turbine efficiency does not have a strong effect on engine cycle performance, constant-section blading can be used to lower cost and gain good performance. The radial-pressure variation is determined for constant-flow-angle blading to determine axial thrust. Constant-section blading usually employs relatively-short, high-pressure-ratio supersonic blades.

For longer turbine blades (usually in subsonic turbine stages), a free-vortex radial distribution with twisted blades may be selected. Higher efficiency results from twisted blades due to reduced-incidence losses and more uniform flow from hub to tip. The ideal characteristics of a free-vortex design are constant axial velocity and rotor work from hub to tip. (Actual operation with efficiency gradients hub to tip cause variations in both velocity and work.) The tangential absolute velocity out of each blade row from hub to tip can be calculated assuming that the product of the mean radius and the mean absolute tangential velocity is a constant. The rotor reaction at the mean diameter should be set to provide positive reaction at the hub. Inlet-blade angles are set to minimize incidence losses for the calculated flow-angles.

Efficiency can be increased to the maximum by using a forced-vortex radial work distribution. Increased work is performed in the lower-loss mid-height of the blade and reduced work is done in the higher-loss hub and tip ends of the blade, resulting in higher stage efficiency. The reduced tip work also reduces the unshrouded-blade tip clearance loss. Figure 6-54 shows an example of a forced-vortex design rotor blade.

CFD analyses. The design and analyses of forced-vortex-stage 3D blading requires extensive computer graphics and computational fluiddynamics (CFD). Computer-aided engineering (CAE) graphics must define, stack, and display the three-dimensional

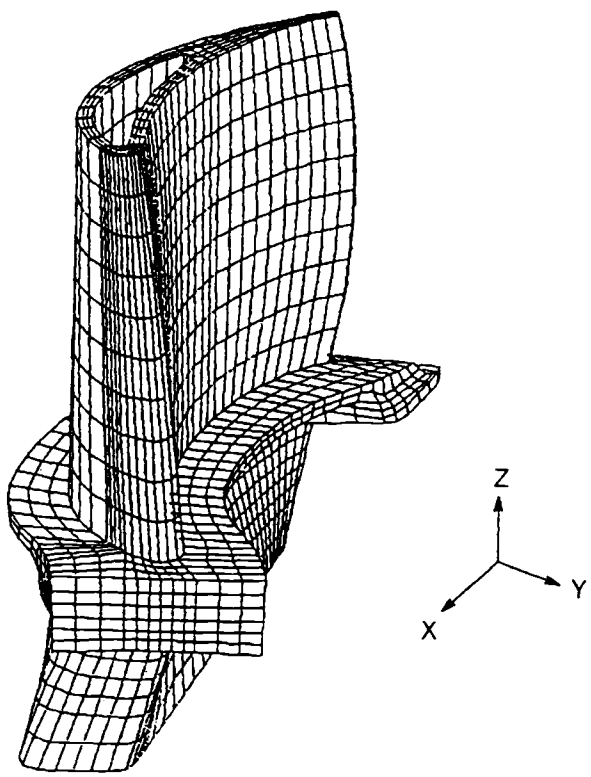

Fig. 6-54 Example of a forced-vortex-design rotor blade.

blade shapes and establish the input data to the three-dimensional analysis programs. The detail design analysis that establishes the flowpath elevation and blade-profile dimensions may be done using an inviscid quasi-3D or full-3D analysis. The vane and blade surface distributions of velocity, Mach number, static pressure, and temperature are calculated from hub to tip for each blade row. The surface boundary layers are calculated assuming turbulent flow for the high-Reynolds-number combustor products of the rocket engine. The blade shapes are modified until the surface distributions and boundary layers have acceptable diffusion levels and minimum loss and separation potential.

Blade-profile designs finalized, the viscous-flow solvers may be executed to verify the viscous effects. When the stage design is completed, the nozzle/rotor interaction should be analyzed to establish the blade integrity under dynamic loading.

Design of Turbine Nozzles

Turbine nozzle designs are classified as convergent-divergent for high-pressure-ratio, supersonic, single-stage turbines, convergent for subsonic and transonic stages, and partial admission when the rotor-blade height would be too small for full admission.

Supersonic convergent-divergent nozzles. The nozzles of most gas-generator-cycle rocket-engine turbines are basically similar to those of rocket thrust chambers. They are of the conventional converging-diverging De Laval type with supersonic outlet velocities. In the main, the nozzles of an impulse-type turbine efficiently convert the major portion of available energy of the working fluid into kinetic energy or high gas-spouting velocity. The gas flow processes in the thrust-chamber nozzles are directly applicable to turbine nozzles. However, the gas flow in an actual nozzle deviates from ideal conditions because of fluid viscosity, friction, boundary-layer effects, etc. In addition, the energy consumed by friction forces and flow turbulence will cause an increase in the static temperature of the gases flowing through a nozzle, above that of an isentropic process. (This effect is known as "reheat.") As a result of the above effects, the actual gas-spouting velocity at the turbine nozzle exit tends to be less than the ideal velocity calculated for isentropic expansion (from stagnation state at the nozzle inlet to the static pressure at the rotor-blade inlet). Furthermore, the effective flow area of a nozzle will usually be less than the actual area because of circulatory flow and boundary-layer effects. The following correlations have been established for the design calculations of turbine nozzles:

Nozzle velocity coefficient k_n:

$$k_n = C_1/Co \tag{6-68}$$

where C_1 = actual gas spouting velocity at the nozzle exit, and Co is the ideal gas velocity calculated for isentropic expansion from the stagnation state at the nozzle inlet to static pressure at the rotor blade inlet.

Nozzle efficiency η_n:

$$\eta_n = k_n^2 \tag{6-69}$$

Nozzle throat area coefficient e_{nt}:

$$\epsilon_{nt} = \text{(effective area of the nozzle throat)/(actual area)} \tag{6-70}$$

Actual gas-spouting velocity at the nozzle exit, ft/s:

$$C_1 = k_n C_o = k_n \sqrt{2gJC_pT_o\left[1 - \left(\frac{p_1}{p_o}\right)^{\frac{\gamma-1}{\gamma}}\right]} = k_n\sqrt{2gJ\Delta H_{o-1"}} \tag{6-71}$$

Amount of nozzle reheat:

$$q_{nr} = \frac{(1 - k_n^2)C_1^2}{k_n 2gJ} = \frac{(-\eta_n)C_1^2}{\eta_n 2gJ} \tag{6-72}$$

Required total nozzle throat area, in.^{2}:

$$A_{nt} = \frac{\dot{w}_t}{\epsilon_{nt}p_o\sqrt{\dfrac{g\gamma\left[\dfrac{2}{\gamma+1}\right]^{\frac{\gamma+1}{\gamma-1}}}{RT_o}}} \tag{6-73}$$

where—

- C_p = turbine-gas (working-fluid) specific heat at constant pressure, Btu/lb-°R
- γ = turbine-gas specific heat ratio
- R = turbine-gas constant (1544/molecular weight), ft/°R
- T_o = turbine-gas total (stagnation) temperature at the nozzle inlet, °R
- W_t = turbine-gas mass flow rate, lb/s
- p_o = turbine-gas total pressure at the nozzle inlet, psia
- p_1 = turbine-gas static pressure at the rotor-blade inlet, psia
- $\Delta H_{o-1"}$ = isentropic enthalpy drop of the gases flowing through the nozzles, due to expansion, Btu/lb

The performance of a turbine nozzle, as expressed by its efficiency or velocity coefficient, will be affected by a number of design factors, such as; exit velocity of the gas flow, properties of the turbine gases, angles and curvatures at nozzle inlet and exit, radial height and width at the throat, and pitch (spacing) and number of nozzles. Design values for the efficiency and velocity coefficients of a given turbine nozzle may be determined experimentally or estimated from past designs. Design values of nozzle efficiency η_n range from 0.80 to 0.96. Design values of nozzle velocity coefficient k_n vary from 0.89 to 0.98. The nozzle-throat area coefficient (ϵ_{nt}) generally will increase with nozzle radial height, design values ranging from 0.95 to 0.99.

Rocket-turbine nozzles have rectangular cross section (Fig. 6-55). Nozzle vanes are closely spaced

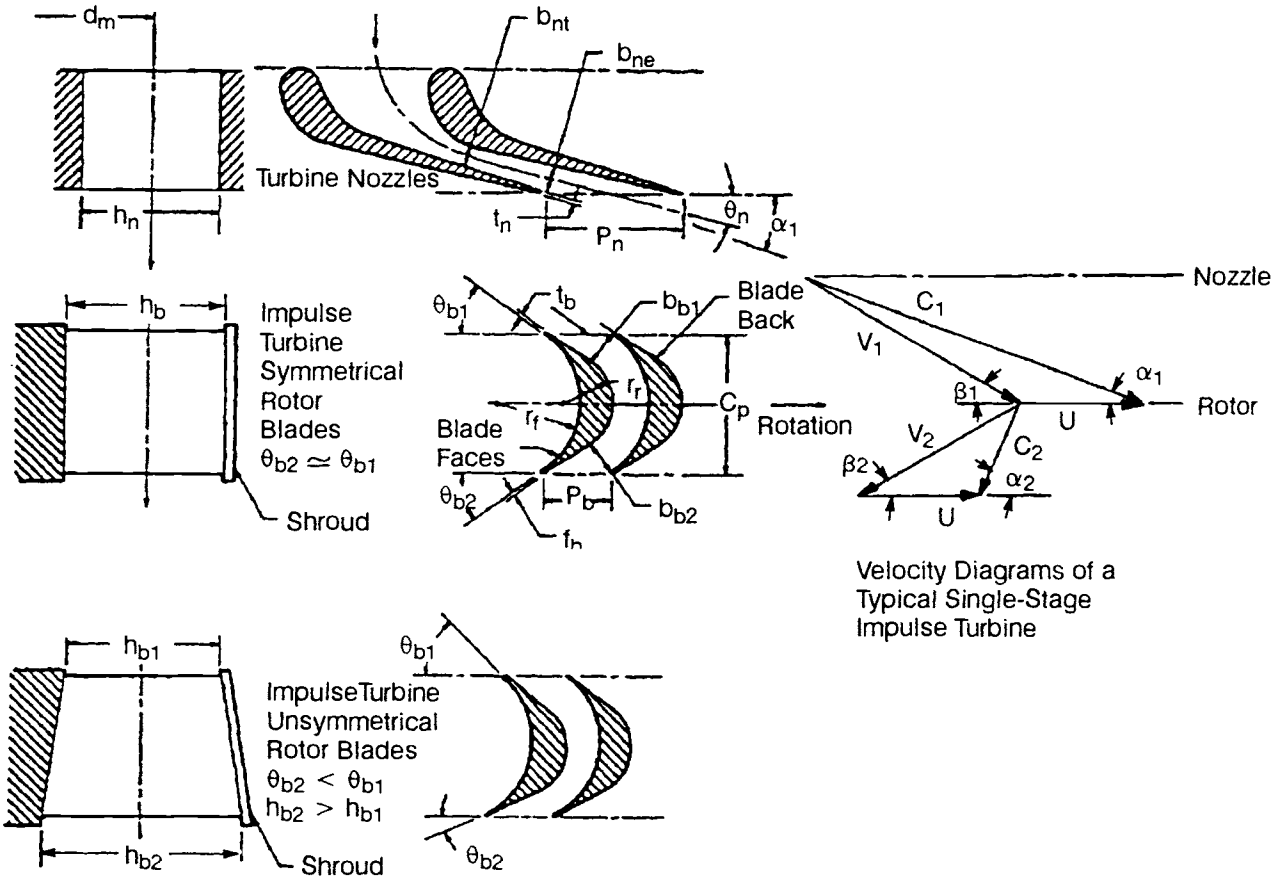

Fig. 6-55 Nozzles, rotor blades, and velocity diagrams of a typical single-stage impulse turbine.

on a circular arc extending over a part of (partial admission) or all of (full admission) the circumference. Most high-power turbines use full admission for better performance.

While the gases are passing through a nozzle and expanding, the direction of flow is changing from an approximately axial direction to one forming the angle α_1 (Fig. 6-55) with the plane of rotation, at the nozzle exit. Therefore, the turning angle is $90\text{-}\alpha_1$ deg. The angle (θ_n) of the nozzle centerline at the exit usually represents a design compromise. Theoretically, a smaller nozzle-exit-angle yields better efficiency, since the rotor blading work is larger and the absolute flow velocity at the rotor-blade exit is smaller. However, a smaller nozzle-exit-angle means a larger angle of flow deflection within the nozzle, which causes higher friction losses. Design values of θ_n range from 15 to 30 deg. The actual effective discharge angle α_1 of the gas jet leaving the nozzle tends to be greater than θ_n because of the unsymmetrical nozzle shape at the exit.

A sufficiently large nozzle passage aspect ratio h_{nt}/b_{nt} is desirable for better nozzle efficiency. For a given nozzle height, an increase in aspect ratio can be secured by decreasing the nozzle pitch P_n. However, a small pitch and consequently a large number of nozzles (z_n), with attendant increase in wall surface, tends to increase friction losses.

Determination of nozzle pitch also requires a design compromise. The following correlations have been established for calculation of nozzle-flow areas:

Total nozzle throat area, in.^{2}:

$$A_{nt} = z_{nt} b_{nt} h_{nt} \tag{6-74}$$

Total nozzle exit area, in.^{2}:

$$A_{ne} = 144\, \dot{w}_t/(\rho_1 C_1\, \varepsilon_{ne}) = z_n\, b_{ne}\, h_{ne}$$

$$= z_n h_{ne}(P_n \sin\, \theta_n - t_n) \tag{6-75}$$

Pitch or nozzle spacing:

$$P_n = \pi\, d_m/z_n \tag{6-76}$$

where—

$\dot{w}_t$ = turbine-gas mass flowrate, lb/s
ρ_1 = density of the gases at nozzle exit, lb/ft^3
C_1 = gas-spouting velocity at nozzle exit, ft/s
ε_{ne} = nozzle-exit-area coefficient
h_{nt} = radial height at nozzle throat, in.
h_{ne} = radial height at nozzle exit, in.
b_{nt} = width normal to flow at nozzle throat, in.
b_{ne} = width normal to flow at nozzle exit, in.

z_n = number of nozzles
θ_n = angle between nozzle-exit centerline and plane of rotation, deg
t_n = thickness of nozzle partition at exit, in.
d_m = mean diameter of nozzles and rotor blades, in.

Subsonic convergent nozzles. Staged-combustion and series expander-engine-cycle-drive turbines use subsonic convergent nozzles. The nozzle turns and accelerates the flow to the desired outlet Mach number from the inlet conditions. The nozzle passage converges with the minimum flow area at the outlet of the control channel (the throat). Additional expansion and turning may occur downstream of the throat. Nozzles with relatively short vanes can have constant section from hub to tip. The minimum passage width may be set by manufacturing constraints that would also affect the number of nozzle vanes. The height-to-throat opening ratio has typically been between 3.5 to 8. The trailing-edge thickness typically varies between 5 to 15% of the throat opening. The fillet radius at the endwalls usually will be less than 30% of the throat opening. The number of subsonic nozzles used in rocket turbines has varied from 25 to 61. Nozzle efficiency values range to 0.97. Radial variations from hub to tip become significant for longer nozzles. The nozzle-outlet flow angle and area distributions are set to achieve the desired work distribution.

Laid out using computer graphics and CFD analyses, nozzle profiles are designed to achieve the required acceleration and turning for the desired stage distributions. Numerous profiles are defined from hub to tip and analyzed as two-dimensional vanes, including the effects of streamtube thickness to determine the suction and pressure surface distributions of velocity, Mach number, static pressure, and static temperature. The vane loading, diffusion, and boundary layers are evaluated for acceptability, and the resulting 3D vane shape compared with the stage requirements.

Cylindrical endwalls ordinarily will be used with low-pressure-ratio turbine nozzles; contoured outer endwalls will be used on some first-stage nozzles. The preliminary subsonic-nozzle calculations for nozzle efficiency, outlet velocity, reheat, nozzle exit area, and tangential spacing use the same equations as the section for supersonic nozzles. The factors that affect supersonic nozzle performance, as discussed in the section above, apply to subsonic convergent-nozzle performance as well.

Partial-admission nozzles. Partial-admission nozzles are open for flow over only a fraction of the circumference of the turbine. The nozzles may be supersonic or subsonic, depending on the application. The minimum number of nozzles is one, but generally two or more nozzles will be used with an equal sector 180 deg apart and opposite each other, for structural and dynamic symmetry. As the number of sectors increases, losses are incurred due to the increasing number of transitions from the active to inactive arc of admission, as shown in Fig. 6-56.

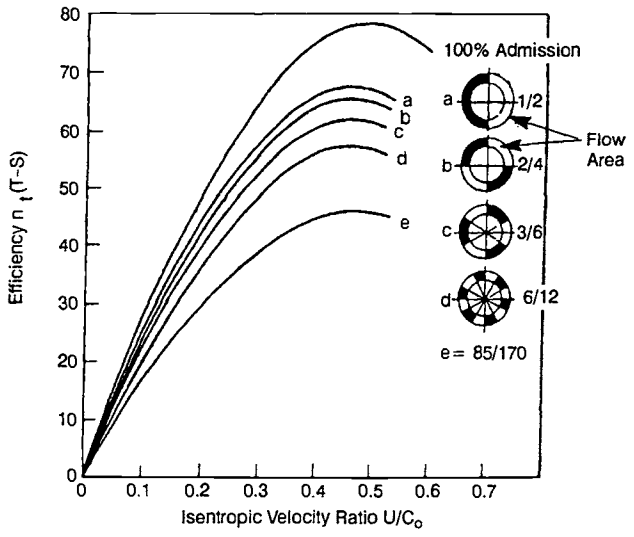

Fig. 6-56 Effect of number of active arcs on partial-admission turbine efficiency.

If the second-stage nozzle also has partial admission, the second nozzle can be set to capture the kinetic energy out of the first rotor at the design condition to maximize performance. An axial space upstream of the second nozzle will aid circumferential flow out of the first rotor into the second nozzle for off-design operation, such as startup and shutdown transients.

Design Of Turbine Rotor Blades

Turbine rotor blades used in rocket-engine turbines can be classified as supersonic impulse blades and subsonic impulse and reaction blades.

Supersonic impulse rotor-blades. Rotor blades in an impulse turbine (Fig. 6-51 and 6-55) transform a maximum of the kinetic energy of the gases from the nozzles into useful work. Theoretically, there should be no change of gas static pressure, temperature, or enthalpy in the rotor blades. In actual operation, however, some gas expansion (i.e., reaction) usually occurs. Furthermore, the actual gas flow through the rotor blades deviates from ideal flow because of friction, eddy currents, boundary layers, and reheating.

The velocity-vector diagram shown in Fig. 6-55 describes graphically the flow conditions at the rotor blades of a single-stage, single-rotor turbine at the mean diameter d_m. The gases enter the rotor blades with an absolute velocity C_1 and at an angle α_1 to the plane of rotation. The rotor blades have tangential or peripheral speed U at the mean diameter. The relative velocities at the blade inlet and outlet differ (i.e., $V_1 > V_2$) due to friction losses. Ideally, the gas should leave the blades at very low absolute velocity C_2 and in a direction close to axial for optimum energy conversion in the blades. The forces generated at the rotor blades are a function of the change of momentum of the flowing gases. The following correlations can be established for design

calculations of the rotor blades of a single-stage, single-rotor turbine.

Tangential force acting on the blades (lb/lb of gas flow/s):

$$F_t = (C_1 \cos \alpha_1 + C_2 \cos \alpha_2)/g = (V_1 \cos \beta_1 + V_2 \cos \beta_2)/g \quad (6\text{-}77)$$

Work transferred to the blades (ft-lb per unit of gas flow/s):

$$E_b = U(C_1 \cos \alpha_1 + C_2 \cos \alpha_2)/g = U(V_1 \cos \beta_1 + V_2 \cos \beta_2)/g \quad (6\text{-}78)$$

$$U = \pi d_m N/720 \quad (6\text{-}79)$$

For subsequent calculations, the following relation will be useful:

$$\tan \beta_1 = C_1 \sin \alpha_1/(C_1 \cos \alpha_1 - U) \quad (6\text{-}80)$$

Axial thrust at blades (lb per unit of gas flow/s);

$$F_a = (C_1 \sin \alpha_1 - V_2 \sin \beta 2)/g \quad (6\text{-}81)$$

Blade velocity coefficient:

$$k_b = V_2/V_1 \quad (6\text{-}82)$$

Blade efficiency:

$$\eta_b = E_b/(C_1^2/2g) \quad (6\text{-}83)$$

Ideally, η_b will be a maximum for a single-rotor impulse turbine when the turbine velocity ratio is—

$$U/C_1 = \frac{\cos \alpha_1}{2}$$

i.e., when $U = 0.5\ C_{1t}$ where C_{1t} is the tangential component of C_1. This yields a maximum ideal efficiency:

$$\eta_b = 0.5 \cos^2 \alpha_1 (1.0 + k_b \cos \beta_2/\cos \beta_1) \quad (6\text{-}84)$$

If there is some reaction or expansion of the gas flowing through the blades, the relative-gas-flow velocity at the rotor-blade outlet can be calculated as follows:

$$V_2 = (k_b^2 V_1^2 + 2gJ \eta_n \Delta H_{1\text{-}2'})^{0.5} \quad (6\text{-}85)$$

Amount of reheat in the rotor blades (Btu/lb of gas flow):

$$q_{br} = (1.0\text{-}k_b^2) V_1^2/(2gJ) + (1.0\text{-}\eta_n) \Delta H_{1\text{-}2'} \quad (6\text{-}86)$$

where—

α_1, α_2 = absolute-gas-flow angles at the inlet and outlet of the rotor blades, deg

β_1, β_2 = relative-gas-flow angles at the inlet and outlet of the rotor blades, deg

C_1, C_2 = absolute-gas-flow velocities at the inlet and outlet of the rotor blades, ft/s

V_1, V_2 = relative-gas-flow velocity at the inlet and outlet of the rotor blades, ft/s

U = peripheral speed of the rotor, ft/s

d_m = mean diameter of the rotor, in.

η_n = equivalent nozzle efficiency applicable to the expansion process in the blades

$\Delta H_{1\text{-}2'}$ = isentropic enthalpy drop of the gases flowing through the rotor blades due to expansion or reaction, Btu/lb; $\Delta H_{1\text{-}2'}$ equals 0 if only impulse is exchanged

All parameters refer to the mean diameter d_m unless specified otherwise. The turbine overall efficiency n_t defined by Eq. (6-15, 6-16) can be established for a single-stage, single-rotor impulse turbine in the following form:

$$\eta_t = \eta_n \eta_b \eta_m \quad (6\text{-}87)$$

where—

η_n = nozzle efficiency

η_b = rotor-blade efficiency

η_m = machine efficiency, indicating the mechanical, leakage, and disk-friction losses

Equation (6-84) shows that the blade efficiency (η_b) improves when β_2 becomes much smaller than β_1. Reduction of β_2 without decreasing the flow area at the blade exit can be achieved through an unsymmetrical blade (Fig. 6-55), in which the radial blade height increases toward the exit. In actual designs, the amount of decrease of β_2, or the increase of radial height, will be limited by incipient flow separation and centrifugal stresses. Generally, the β_2 of an unsymmetrical blade will be approximately β_1 - (5 to 15 deg). Equation (6-84) also indicates that η_b improves as $\alpha 1$ is reduced. Design values of k_b vary from 0.80 to 0.90. Design values of η_b range from 0.7 to 0.92.

Referring to Fig. 6-55, the radial height at the rotor inlet h_b will usually be slightly larger (5 to 10%) than the nozzle radial height h_n. This height, together with the blade peripheral speed U, will determine the centrifugal stress in the blades. The mean diameter of the rotor blades is defined as $d_m = d_t - h_b$ where d_t is the rotor tip diameter. Pitch or blade spacing P_b is measured at the mean diameter d_m. There is no critical relationship between blade pitch P_b and nozzle pitch P_n. There should be a sufficient number of blades in the rotor to direct the gas flow. The number of blades z_b to be employed is established by the blade aspect ratio h_b/C_b and the solidity C_b/P_b, where C_b is the chord length of the rotor blades. The magnitude of the blade aspect

ratio ranges from 1.3 to 2.5. Design values of blade solidity vary from 1.4 to 2. Best results will be determined by experiment. The number of rotor blades should have no common factor with the number of nozzles or of stator blades for the purpose of minimizing dynamic loading.

The blade face is concave, with radius r_f. The back is convex, with a circular arc of small radius r_r concentric with the face of the adjoining blade ahead. Two tangents to this arc to form the inlet; and outlet-blade angles θ_{b1} and θ_{b2} complete the blade back. The leading and trailing edges may have a small thickness t_b. Unsymmetrical-impulse-blade profiles have also been defined using tangent parabola curves and combinations of straight lines, circular arcs, and parabolas.

The inlet-blade angle θ_{b1} should be slightly larger than the inlet relative-flow angle β_1. If $\theta_{b1} < \beta_1$ the gas stream will strike the backs of the blades at the inlet, exerting a retarding effect on the blades and causing losses. If $\theta_{b1} > \beta_1$ the stream will strike the concave faces of the blades and tend to increase the impulse. The outlet-blade angle θ_{b2} is usually made equal to the outlet relative-flow angle (β_2).

The mass flow rate w_t through the various nozzle and blade sections of a turbine is assumed constant. The required blade flow areas can be calculated by the following correlation (Note that the temperature values used in calculating the gas densities at various sections must be corrected for reheating effects from friction and turbulence):

$$\dot{w}_t = \rho_1 V_1 A_{b1} \varepsilon_{b1}/144 = \rho_2 V_2 A_{b2} \varepsilon_{b2}/144 \quad (6\text{-}88)$$

Total blade inlet area, in.^{2}:

$$A_{b1} = z_b b_{b1} h_{b1} = z_b h_{b1} (P_b \sin \theta_{b1} - t_b) \quad (6\text{-}89)$$

Total blade exit area, in.^{2}:

$$A_{b2} = z_b b_{b2} h_{b2} = z_b h_{b2} (P_b \sin \theta_{b2} - t_b) \quad (6\text{-}90)$$

where—

- P_b = pitch or rotor-blade spacing
- ρ_1, ρ_2 = density of gases at inlet and outlet of the rotor blades, lb/ft^3
- V_1, V_2 = relative gas velocities at inlet and outlet of the rotor blades, ft/s
- $\varepsilon_{b1}, \varepsilon_{b2}$ = area coefficients at inlet and outlet of the rotor blades
- z_b = number of blades
- h_{b1}, h_{b2} = radial height at inlet and outlet of the rotor blades, in.
- b_{b1}, b_{b2} = passage widths (normal to flow) at inlet and outlet of the blades, in.
- θ_{b1}, θ_{b2} = rotor blade angles at inlet and outlet, deg
- t_b = thickness of blade at inlet and outlet, in.

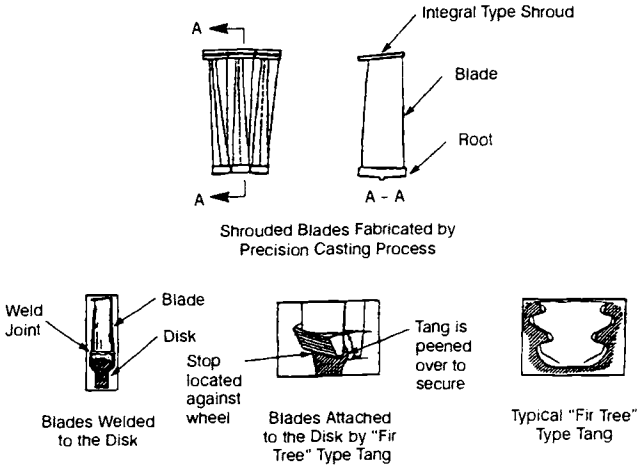

Fig. 6-57 Typical rotor-blade construction.

Typical construction of turbine rotor blades and disks are shown in Fig. 6-52, 6-51, 6-55, and 6-57. Usually, blades are designed with a shroud to prevent leakage over the blade tips and to reduce turbulence and thereby improve efficiency. The shroud also limits blade vibration amplitudes and increases rotor dynamic stability. Frequently the shroud forms an integral portion of the blade, the shroud sections fitting closely together when assembled. In other designs the shroud may form a continuous ring (Fig. 6-51) attached to the blades by tongues at the blade tip or by rivets. It can also be welded to the shrouds. The blades may be either welded to the disk or attached to it using "fir-tree" or other dovetail shapes.

The main loads experienced by a rotor blade can be divided into three types:

- *Tension and bending due to centrifugal forces.* The radial component of the centrifugal forces acting on the blade body produces a centrifugal tensile stress that reaches a maximum at the root section. As a remedy, blades are often hollowed and tapered, with the thinner section at the tip, to lower centrifugal root-stresses. The centroids of various blade sections at different radii generally do not fall on a true radial line. Therefore, the centrifugal forces acting upon the offset centroids will produce bending stresses that also are at maximum at the root section.
- *Bending due to gas loading.* The tangential driving force and the axial thrust produced by the momentum change of the gases passing over the blades produce bending stresses. These forces are sometimes integrated and treated as acting at the midheight of the blade to determine the amount of bending induced. Otherwise, distributed pressures on the blade are defined from a 3D flow analysis.
- *Bending due to vibration loads.* Gas does not flow uniformly in the blade passages, as assumed in theory, but varies cyclically from minimum to maximum. The resultant loads represent a dynamic force on the blades, having a corresponding cyclic variation. The frequency of this force coming equal to the natural frequency of the blades may cause deflections that will induce bending stresses of considerable magnitude. Therefore, the primary

forcing functions acting on the blades are designed so as not to correspond in frequency with any blade natural frequency.

Detail stress analyses for rotor blades can be rather complex. A basic approach counteracts a major portion of the bending moments from gas loading with the bending moments induced by the centrifugal forces at nominal operating speeds. This can be done by careful blade design. Thus the centrifugal tensile stresses become a first consideration in blade design, while other details such as centroid location and root configuration are established later to fulfill other design requirements. The following correlations have been established at the blade-root section where stresses are most critical:

Centrifugal tensile stress at the root section of blade of a uniform cross section, psi:

$$S_c = 0.00548\, \rho_b\, h_b\, d_m\, N^2/g \qquad (6\text{-}91)$$

Centrifugal tensile stress at the root section of tapered blade, psi:

$$S_{ct} = 0.00548 \frac{1}{g} \rho_b h_b d_m N^2 \times \left[1 - \frac{1 - \left(\frac{a_t}{a_r}\right)}{2} \left(1 + \frac{h_b}{3 d_m} \right) \right] \qquad (6\text{-}92)$$

Bending moment due to root-section gas loading, in-lb:

$$M_g = h_b\, \dot{w}_t\, (F_t^2 + F_a^2)^{0.5}/2 z_b \qquad (6\text{-}93)$$

where

- g = gravitational constant, ft/sec^2
- ρ_b = density of the blade material, lb/in.^{3}
- h_b = average blade height, in.
- d_m = mean diameter of the rotor, in.
- N = turbine speed, rpm
- a_r = sectional area at the blade root, in.^{2}
- a_t = sectional area at the blade tip, in.^{2}
- $\dot{w}_t$ = turbine gas flow, lb/s
- z_b = number of blades
- F_t = tangential force acting on the blades, lb/lb/s (6-77)
- F_a = axial thrust acting on the blades, lb/lb/s (6-81)

The bending stresses at the root can be calculated from the resultant bending moment and the blade-root section properties. The vibration stresses can be estimated from past design data. A shroud added to a blade increases stresses at the root. The total stress at the root section adds these stresses to those caused by the centrifugal forces acting on the blades.

The stresses in a turbine-rotor disk are induced by the blades and the centrifugal forces acting on the disk material itself. In addition, torque causes shear stresses. As seen in Fig. 6-51, turbine disks are generally quite thick at the axis, but taper off to a thinner disk rim to which the blades are attached. In single-rotor applications it is possible to design a solid disk so that both radial and tangential stresses are uniform at all points, shear being neglected. In multirotor applications, it is difficult to do this because of the greatly increased axial length and the resulting large gaps between rotor and stator disks.

Equation (6-94) may be used to estimate the average tangential stress in any turbine disk, neglecting rotor-blade effects:

$$S_d = 0.00137\, (\rho_d/g)\, d_d^2\, N^2/[\log_e (t_o/t_r)] \qquad (6\text{-}94)$$

where—

- S_d = average tangential tensile stress of a constant-stress turbine disk, psi
- ρ_d = density of the disk material, lb/in.^{3}
- d_d = diameter of the disk, in.
- N = turbine speed, rpm
- t_o = thickness of the disk at the axis, in.
- t_r = thickness of the disk rim at dd, in.
- g = gravitational constant, ft/sec^2

Equation (6-95) permits estimation of the stresses in any turbine disk, neglecting effects of the rotor blades:

$$S_d = 0.00548\, W_d\, r_i\, N^2/(a_d g) \qquad (6\text{-}95)$$

where—

- S_d = centrifugal tensile stress of the turbine disk, psi
- W_d = weight of the disk, lb
- r_i = distance of the center of gravity of the half disk from the axis, in.
- a_d = disk cross-sectional area, in.^{2}
- N = turbine speed, rpm
- g = gravitational constant, ft/sec^2

For good turbine design, it is recommended that at the maximum allowable design rotating speed the S_d, calculated by Eq. (6-95), be about 0.75 to 0.8 the material yield-strength.

Turbine rotor blades and disks are made of high-temperature alloys of three different base materials: iron, nickel, and cobalt, with chromium forming one of the major alloying elements. High tensile strength and fatigue resistance at the operating temperature are important criterion for material selection. Other required properties include resistance to hydrogen embrittlement, low creep rate, and oxidation and erosion resistance. Astroloy, Waspaloy, Mar M-246, A 286, and Inconel 718 are alloys frequently used. The rotor blades are fabricated either by precision casting or by precision forging. Rotor disks are best made of forgings for optimum strength. Integrally-bladed disks ("blisks") are also used, but blade damping is more difficult to achieve, requiring more care to avoid fatigue damage.

Subsonic Blades. The design of subsonic rotor blades uses extensive, interactive computer graphics and computer-aided engineering (CAE). The design

process, depicted in Fig. 6-53, sets the basic requirements of each blade row by a meanline-gas-path analysis. The turbine-configuration optimization follows various constraints. The rotor profile will be defined by a multistage meridional-flow-field analysis for the specified blade-path elevation. The results of the meridional analysis establish the acceleration and turning characteristics of each rotor-profile section from hub to tip. Initial rotor profiles are generated on the computer at several radial locations. The initial profile surface-velocity and static-pressure distributions can be checked using estimated streamtube thicknesses for adverse pressure gradients based on established guidelines. The rotor profiles are stacked from hub to tip, as can be seen in Fig. 6-54, including an estimate of the lean and tilt that may be required from the structural design to establish the 3D blade profile.

The 3D geometry is used in an inviscid multistage quasi-3D or full-3D analysis program that determines the streamline and blade-to-blade flow-field characteristics. The multistage capability being required, a complete evaluation can be made of potential changes of individual blade surfaces, including the effects on the other turbine-blade rows. The profile geometry along a specified streamline will be determined so that detailed suction and pressure surface distributions can be calculated using a suitable flow-code. These distributions will be used in the boundary-layer code to determine the boundary-layer characteristics that are assessed for losses and separation potential. Solid modeling of the defined 3D blade path that can be viewed from any orientation allows an early look at the turbine blading for mechanical, structural, and thermal design analyses.

Design of Single-Stage, Two-Rotor, Velocity-Compounded Impulse Turbines

Most impulse turbines will have only one or two rotors. It is assumed that a single-stage, two-rotor, velocity-compounded impulse turbine expands gases completely in the nozzle, and that no further static-pressure change occurs during gas flow through the moving blades. As mentioned earlier, the two-rotor, velocity-compounded arrangement provides high efficiency at low velocity ratios. In this case, the gases ejected from the first rotor blades still possess considerable kinetic energy. They are therefore redirected by a row of stationary blades into a second row of rotor blades that extract additional work from them. The gases usually leave the second rotor-blade row at a moderate velocity and in a direction close to axial.

The velocity diagrams of a single-stage, two-rotor, velocity-compounded impulse turbine are based on a mean rotor diameter, as shown in Fig. 6-58, the peripheral speed of the rotor blades at the diameter being U. The gases leave the nozzles and enter the first rotor blades with an absolute velocity C_1, at an angle α_1 with the plane of rotation; V_1 and V_2 are the relative flow velocities in ft/s at the inlet and outlet of the first rotor blades. The gases leave the first rotor blades and enter the stationary blades at an absolute flow velocity C_2, and at an angle α_2. After passing over the stationary blades, the gases enter the second rotor blades at an absolute flow velocity C_3, and at an angle α_3; V_3 and V_4 are the relative inlet and outlet flow velocities at the second rotor blades. Angles β_1, β_2, β_3, and β_4 represent the flow directions of V_1, V_2, V_3, and V_4.

As with single-rotor turbines, the exit velocity from any row of blades (rotary or stationary) will be less than the inlet velocity because of friction losses. It can be assumed that the blade velocity coefficient k_b has the same value for any row of blades:

$$k_b = V_2/V_1 = C_3/C_2 = V_4/V_3 \tag{6-96}$$

In a multirotor turbine, the total work transferred will be the sum from the individual rotors:

Total work transferred to the blades of a two-rotor turbine, ft-lb/lb of gas flow/s:

$$E_{2b} = \frac{U}{g}(C_1 \cos\alpha_1 + C_2 \cos\alpha_2 + C_3 \cos\alpha_3 + C_4 \cos\alpha_4)$$

$$= \frac{U}{g}(V_1 \cos\beta_1 + V_2 \cos\beta_2 + V_3 \cos\beta_3 + V_4 \cos\beta_4) \tag{6-97}$$

Combined nozzle and blade efficiency of a two-rotor turbine:

$$h_{nb} = E_{2b}/(J\,\Delta H) \tag{6-98}$$

where ΔH = overall isentropic enthalpy drop of the turbine gases (Btu/lb) = total available energy content of the turbine gases (Eq. 6-13). Equation (6-87) can be rewritten for the turbine overall efficiency η_t of a two-rotor turbine as follows:

$$\eta_t = \eta_{nb}\,\eta_m \tag{6-99}$$

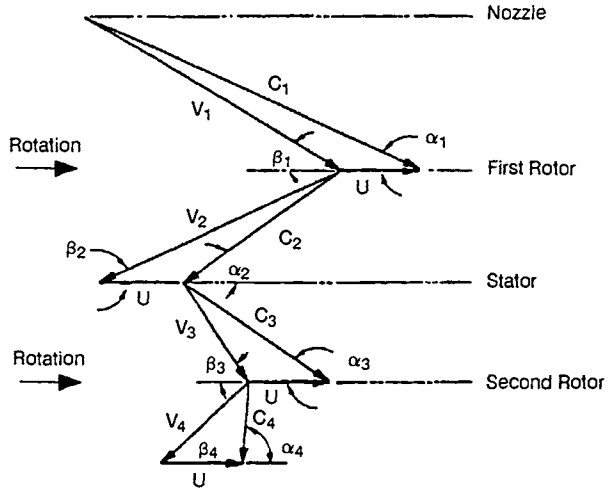

Fig. 6-58 Velocity diagrams of a typical single-stage, two-rotor, velocity-compounded impulse turbine.

Ideally, η_b would be a maximum for the single-stage, two-rotor, velocity-compounded impulse turbine velocity ratio:

$$U/C_1 = 0.25 \cos \alpha_1$$

i.e., when $U = 0.25\ C_{1t}$. The workload for the second rotor of a two-rotor, velocity-compounded turbine is designed at about one-fourth of the total work.

The design procedures for the gas-flow passages of the rotor and stationary blades of a single-stage, two-rotor turbine are exactly the same as those for a single-rotor turbine. However, velocities and angles of flow change with each row of blades. As a result, the radial height of symmetrical blades increases with each row, approximately as shown in Fig. 6-51. The effects of reheating (increase of gas specific volume) in the flow passages must be taken into account when calculating the gas densities at various sections. Equation (6-86) may be used to estimate the amount of reheat at each row of blades.

In the calculations for multi-row unsymmetrical blades, the radial heights at the exit side of each row are determined first by Eq. (6-90). The radial heights at the blade inlets are then made slightly larger, by approximately 8%, than those at the exit of the preceding row.

Design of Two-Stage, Two-Rotor Pressure-Compounded Impulse Turbine

An operational schematic of a typical two-stage, two-rotor, pressure-compounded impulse turbine and its velocity diagrams at the mean diameter are shown in Fig. 6-12 and 6-59. Each stage of a pressure-compounded impulse turbine may be regarded as a single-stage impulse turbine rotating in its own individual housing. Most of the design characteristics of a single-stage turbine are applicable to the individual stages. The gas-spouting velocities C_1 and C_3, at flow angles α_1 and α_3, of the first- and second-stage nozzles are designed to be approximately the same; V_1, V_2, V_3, and V_4 represent the relative flow velocities at inlets and outlets of the rotor blades; β_1, β_2, β_3, and β_4 are the corresponding flow angles for V_1, V_2, V_3, and V_4. The second-stage nozzles are designed to receive the gas flow discharged from the first-stage rotor blades at an absolute velocity C_2, and to turn it efficiently to a desired angle α_3. Simultaneously, by expansion to a lower pressure, the gases are accelerated to a desired velocity C_3. Flow at the outlet of the second rotor has an absolute velocity C_4 and flow angle α_4; U is the rotor peripheral speed at the mean effective diameter d_m.

The total work performed in the turbine sums the separate stages. These may be designed to divide the load equally (i.e., the velocity diagrams of each stage will be identical: $C_1 = C_3$, $C_2 = C_4$, $\alpha_1 = \alpha_3$, $\alpha_2 = \alpha_4$, etc.). The friction losses occurring in the first stage are passed on in the gas stream as additional enthalpy and increase the available energy for the second stage. Also, the kinetic energy of the gases leaving the first stage will not be entirely lost, as with

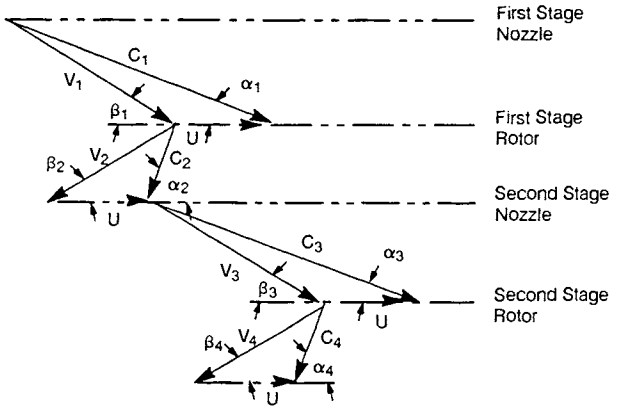

Fig. 6-59 Velocity diagrams of a typical two-stage, two-rotor, pressure-compounded impulse turbine.

a single-stage turbine. The carryover ratio r_c—i.e., the ratio of the kinetic energy actually utilized as inlet energy by the second-stage nozzles to the total kinetic energy of the gases leaving the first stage—can vary from 0.4 to close to 1.0. The axial distance between the first-stage rotor and the second-stage nozzle, as well as the leakages through the sealing diaphragm between stages, should be minimized for optimum carryover.

Determining the correct enthalpy drop resulting in equal work for each stage may require a trial-and-error approach, in relation to the effects of reheating, or the proper enthalpy drop may be estimated from previous designs and test data. With the velocity coefficients for nozzles and blades given by past or concurrent experiments, Eq. (6-72) and (6-86) can be used to estimate the amount of reheating.

Most equations established for the single-stage turbines may be used in the design calculations for two-stage turbines. The following additional correlations are available for the design of choked second-stage nozzles:

$$T_{2t} = T_2 + r_c \frac{C_2^2}{2gJC_p} \tag{6-100}$$

$$P_{2t} = P_2 \left(\frac{T_{2t}}{T_2}\right)^{\frac{\gamma}{\gamma-1}} \tag{6-101}$$

$$C_3 = k_n \sqrt{2gJC_pT_{2t}\left[1 - \left(\frac{p_3}{p_{2t}}\right)^{\frac{\gamma-1}{\gamma}}\right]}$$

$$= k_n \sqrt{r_c C_2^2 + 2gJ\Delta H_{2\text{-}3'}} \tag{6-102}$$

$$(A_{nt})_2 = \frac{\dot{w}_t}{\epsilon_{nt} p_{2t} \sqrt{\dfrac{g\gamma\left[\dfrac{2}{\gamma+1}\right]^{\frac{\gamma+1}{\gamma-1}}}{RT_{2t}}}} \tag{6-103}$$

where—

T_{2t} = turbine gas total (stagnation) temperature at second-stage nozzle inlet, °R

T_2 = turbine gas static temperature at second-stage nozzle inlet, °R

p_{2t} = turbine gas total pressure at second-stage nozzle inlet, psia

p_2 = turbine-gas static pressure at second-stage nozzle inlet, psia

C_2 = absolute-gas-flow velocity at first-stage rotor-blade outlet, ft/s

C_3 = gas-spouting velocity at second-stage nozzle exit, ft/s

r_c = second-stage carryover ratio of kinetic energy

C_p = turbine-gas specific heat at constant pressure, Btu/lb-°F

γ = turbine-gas specific heat ratio

$\Delta H_{2\text{-}3'}$ = isentropic enthalpy drop of the gases flowing through the second-stage nozzles due to expansion, Btu/lb

$(A_{nt})_2$ = required total 2nd-stage nozzle area, $in.^2$

k_n = nozzle velocity coefficient

ε_{nt} = nozzle-throat-area coefficient

Design of Two-Stage, Two-Rotor, Low-Reaction Turbine

Two-stage, two-rotor, low-reaction turbines are used in staged-combustion-cycle or series-expander-cycle rocket engine systems to provide the highest turbine efficiency. In these engine systems, the turbine pressure ratio is low (1.5 to 2.0) and the stage velocity ratio is high (0.4 or higher). In high-chamber-pressure oxygen/ hydrogen engines like the SSME, using two stages increased blade height, gave higher efficiency, and divided the high power between two rotating blade rows, lowering blade stresses in comparison with a single-stage turbine

The design calculation and resulting vector diagrams of a two-stage, low-reaction turbine (see Fig. 6-13) are similar to those for the two-stage, pressure-compounded impulse turbine (Fig. 6-12) discussed in the previous section (6.6.5), except for greater stage reaction (increased rotor-static-pressure drop fraction) and lesser nozzle and rotor turning. Two-stage, low-reaction turbines usually optimize for nearly equal power split between the rotors, with the first stage producing the slightly higher power. The blading is usually twisted to minimize inlet incidence losses for the significant radial-flow-angle variations from hub to tip. Rotor-outlet absolute velocities are usually near axial (zero swirl). Reaction turbines have higher rotor axial thrust due to the higher static-pressure drop across the rotor.

Figure 6-60 shows the mean diameter velocity vector diagram for the SSME HPFTP turbine at full power level. Note the proportions of blade speed to nozzle-outlet velocity and relative velocity increase across the rotors compared with Fig. 6-59 for the pressure-compounded impulse turbine.

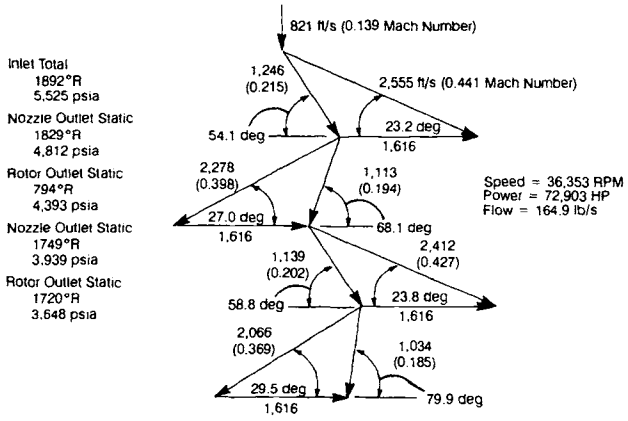

Fig. 6-60 SSME *HPFTP* turbine velocity diagram at full power.

6.7 TURBOPUMP ROTORDYNAMICS AND MECHANICAL ELEMENTS

Rotordynamics

The rotor structure will resonate when excited at its natural frequency. With the pump propellants used, the amount of damping obtained in a rocket engine turbopump is typically too small to critically damp the system. Therefore, at the resonance, large vibration amplitudes can be experienced and generally must be avoided. The rotating-assembly natural frequency will be dictated by the rotor mass and bending stiffness distribution coupled with the bearing-support-structure stiffness, and will include the gyroscopic effect of the spinning disks. "Rotor synchronous motion" means rotation with the shaft spin speed and precessional speed equal in direction and magnitude. The most common cause of forward synchronous motion is rotor unbalance. Rotor vibration amplitude is determined by the proximity of the natural frequency to the synchronous excitation and the amount of damping present in the system. Figure 6-61 shows how these factors influence the behavior of a simple rotor.

Operation of turbomachinery at or near a natural frequency causes excessive response, increases wear, and reduces reliability. Synchronous motion coincident with the rotor natural frequency is defined as operation at a critical speed. The dynamic response can be reduced by increasing the effective damping or designing the rotor to locate its natural frequencies far from the shaft-spin-speed excitation.

In dynamic analysis of the rotating assembly—an essential part of the turbopump design process—critical speeds, rotor-stability margins, bearing loads, shaft loads, and shaft deflections will be calculated to ensure that rotor-dynamic characteristics will be compatible with operating speed and transient-response requirements when traversing critical speeds. Additional analyses are performed to investigate potential problem areas due to nonlinearities resulting in nonsynchronous shaft whirl or shaft loads and deflections due to steady-state hydrodynamic sideloads. Turbopump rotors are designed

so that the critical speeds are well separated from the operating range. The rotor bearing supports are designed to provide the stiffness required to separate the critical speeds from the operating range and minimize the dynamic bearing loads and shaft deflections. The most desirable situation is to design the rotating assembly to operate below the first critical speed; that produces minimal bearing loads and shaft deflections even in the transients. A 20% separation margin between calculated critical speeds and operating speeds follows standard design practice, as demonstrated successfully in pump-fed rocket engines. Torsional vibration is not normally a problem in direct-drive turbopumps due to lack of a significant forcing function and sufficient damping.

Most turbomachinery rotors are a complex arrangement of components mounted on a shaft of variable diameter. The relationship between the rotor stiffness, mass, and damping distribution combined with gyroscopic effects determines the rotor-damped natural frequencies and associated mode shapes. The mode shape is the relative rotor deformation present when operating at a natural frequency. Every natural frequency has a unique mode shape associated with its resonant vibration. Rotor mode shapes provide valuable information that graphically indicate factors that are influential in determining its characteristics, and, thus, provide guidance as to what design changes would be most effective in changing the natural frequencies away from the operating point.

Figure 6-62 graphically displays how physical change to the rotor supports can alter rotating-machinery critical speeds and associated mode shapes. It is apparent from this data that support stiffness is a very important rotor-dynamic parameter. Design revisions will be necessary if inadequate critical-speed margins are present. Review of the rotor mode shapes can identify design modifications. In general, modifications to bearing and seal stiffness and damping can be effective if significant relative motion exists at that location. Modifications to the shaft bending stiffness can be effective if sufficient shaft angulation exists at the change location for the mode in question. Modifications to the mass distribution will only be effective when significant relative motion exists at the mass location to be relocated. Common practice maximizes the stiffness and damping and locates the bearings as close as possible to large rotor masses.

In addition to bearing and seal stiffness and damping as a function of shaft speed, damped-natural-frequency analyses include variable hydrodynamic influences. The damped critical speeds are identified as the coincidental occurrence of these natural frequencies and the shaft spin speed, as shown in Fig. 6-63.

These damped critical speeds and associated mode shapes are not only important in defining the safe-operating-speed margin, but also in predicting rotor stability. Most rotor-dynamic motion will either decay with time or maintain a constant level after application of an external excitation (perturbation)—evidence of a stable system. Unstable rotor

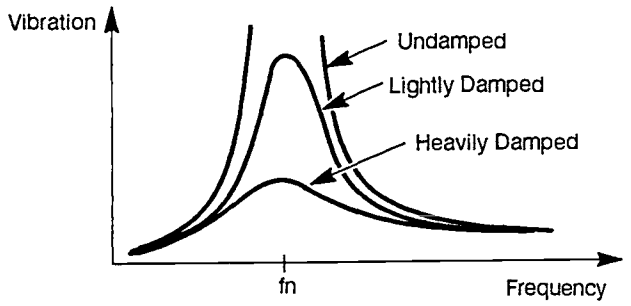

Fig. 6-61 Dynamic response of a simple system.

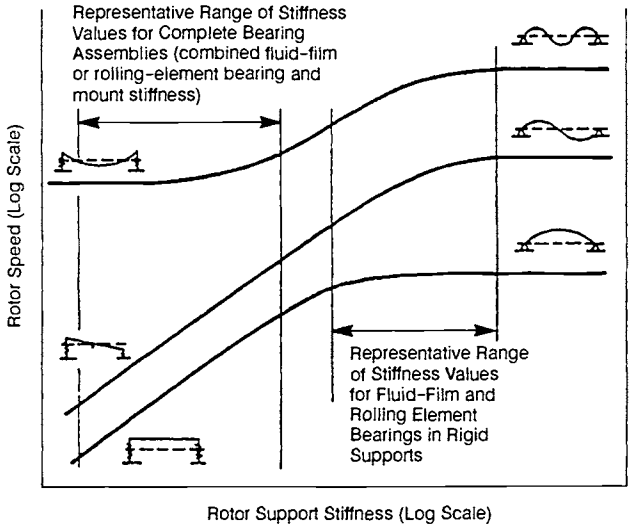

Fig. 6-62 Effect of rotor supports on critical speeds.

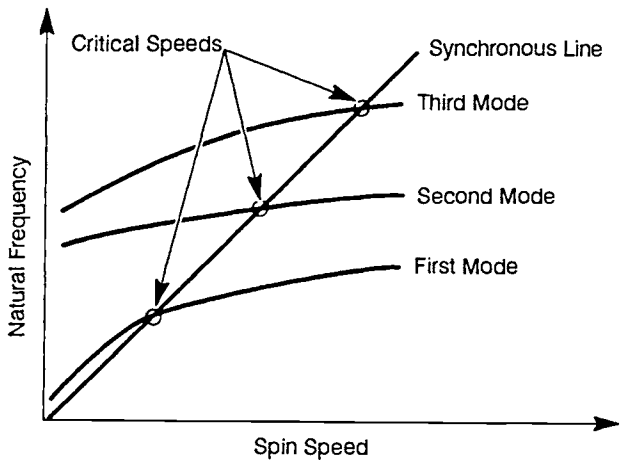

Fig. 6-63 Damped critical speed map.

assemblies will increase in response amplitude without bound after a perturbation, as shown in Fig. 6-64.

The most common form of rotor-dynamic instability, subsynchronous whirl, finds the rotor precessional speed less than the spin speed and coincident with a rotor natural frequency. This situation without sufficient damping can produce a vibration that may result in destruction or catas-

trophic failure. Rotor instability exhibits a threshold spin speed at which the normal rotor response will increase without bound. The design goal is to maintain the threshold speed above the operating speed with a large margin.

Rotordynamic stability is controlled by providing an abundance of damping to suppress the destabilizing whirl drivers. These instability drivers produce tangential forces to the radial motion that oppose the damping between the rotor and housing. The tangential forces—commonly referred to as "cross-coupling" forces—can be in the direction of shaft rotation or counter to the rotation.

The most common destabilizing tangential forces that excite nonsynchronous rotor motion are the following:

Hydrodynamic forces under pump partial-cavitation
Tangential blade-tip forces
Annular seal forces due to Couette flow
Nonlinear load-deflection characteristics in bearings
Frictional forces between shafts and shrink-fit parts
Tangential rubbing forces acting on the rotor
Hydrodynamic loads on the rotor that rotate relative to the rotor
Hysteresis forces within the rotor
Coupling of unbalance forces from one rotor through the engine structure to another rotor

Common design techniques minimize cross-coupling forces and enhance support stiffness and damping. Hydrodynamic forces are primarily functions of blade and flow-path design, but rotor-dynamic performance is generally improved by the addition of shrouds. Friction forces can be controlled by avoiding the use of long-length shrink fits on the shaft. For instance, if a long spacer is required, it should not be shrunk-fit on the shaft along its entire length. Coupling of unbalance forces through the engine structure is not normally a problem and can be controlled by proper turbopump mount-design. Close-clearance annular shaft seals can be detrimental, but can also be used to significant rotor-dynamic benefit. Labyrinth seals provide minimal stiffness and damping, and under certain conditions can provide negative stiffness and stability concerns. Rotor-dynamic characteristics of these seals can be improved significantly by converting to smooth annular seals, possibly with a slight convergent taper to the stator bore. The seal coefficients can also be further enhanced generally with the addition of fluid anti-rotation ribs at the seal entrance or roughening the seal bore relative to the shaft journal. The bearings provide a relatively large source of stiffness as the main rotor support. Rolling-element bearings tend to provide a nonlinear support stiffness, because clearance between the bearing outer diameter and housing will be made to meet other functional requirements during transient axial-shaft excursions. This nonlinearity might produce nonsynchronous rotor motion at a limited amplitude, which is usually not detrimental. Hydrostatic bearings can provide superior stiffness and damping as a rotor support and, when located optimally along the rotor, can critically damp the rotor-dynamic response.

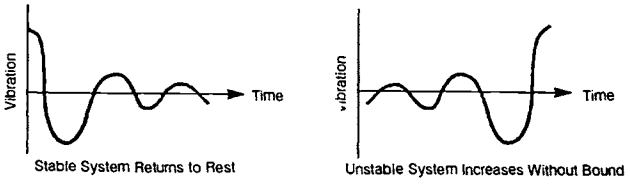

Fig. 6-64 Stability of a simple rotor system.

The rotor stability is controlled by designing significant margin into the design. Rotor-dynamic analysis, including the various instability drivers and dampers along the rotating assembly, will predict the most unstable rotor mode. It usually will be the lowest mode because it usually has the least damping. Operating at twice the lowest mode is a common concern because seal tangential forces are near half shaft speed and are therefore potentially coincident with the lowest mode in this situation. Sufficient damping is required to preclude instabilities, and adequate margins should be maintained. Normal design practice avoids operation within 20% of the calculated stability-threshold speed. Additionally, rotor stability is controlled by providing sufficient damping at the operating speed to ensure a rapid vibration decay after a perturbation as a measure of the system safety margin. The "log-decrement" parameter quantifies the relative rate of vibration decay as a dimensionless number, allowing turbopumps of different size, weight, performance, etc. and different rotor modes all to be compared on an equal basis. The larger the log-decrement number, the more stable the system. At the threshold speed the log decrement equals zero, and a critically-damped rotor mode has a log decrement of 0.7. It is debatable what log decrement should be maintained as suitable; but successful turbopump rotor experience dictates the log decrements for all modes at all rotational speeds within the operating range be at least 0.05. Physically, this means that a vibration response after a perturbation will decay to half the initial response amplitude in 20 revolutions of the shaft because the reciprocal of the log decrement indicates the number of cycles decayed in one time-constant. For clarity, Fig. 6-65 shows a graphical representation of the rotor-stability evaluation.

In general, the rotor-dynamic analysis guides the mechanical arrangement of the various rotor components on the shaft to provide a rotating assembly with minimal dynamic response, thus arguing a long service life.

Turbopump Bearing Design

A turbopump shaft is supported by two or more bearings designed to transmit all the loads acting on the rotating members to the housing (Ref. 6-9). The loads acting on the rotating members can be divided into two classes: radial acting normal to the

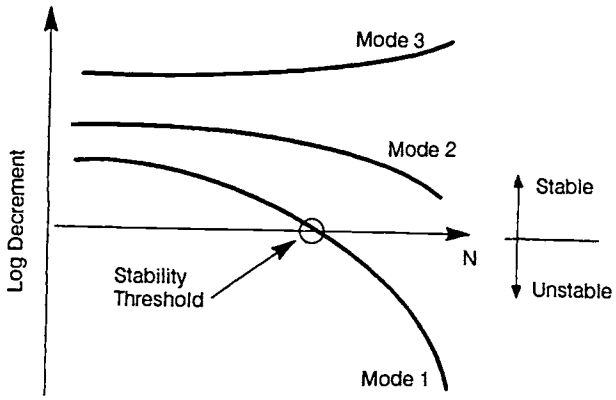

Fig. 6-65 Graphical representation of rotor stability.

shaft axis and axial acting parallel to the shaft axis. In some cases, the radial loads also act to produce a tangential moment on the shaft that can be either in the direction of rotation (e.g., the tip-seal forces on turbines) or opposite the direction of rotation (e.g., the damping achieved by certain seal designs). The objective of the turbopump designer is to define any resultant loads that must be carried by the bearings and to minimize these over the operating range.

Rolling-element bearings have been used most extensively in rocket-engine turbopumps. These include both ball bearings, as seen in Fig. 6-4, and roller bearings, as seen in the turbine end of Fig. 6-9. The ball bearings can also be used as duplex pairs, as shown in Fig. 6-5. Rolling-element bearings have been used because of their high load capability independent of speed, high radial stiffness, ability to start and shut down reliably, and compatibility with the propellant fluids being used. Normally, these bearings operate directly in the propellant medium, the propellant serving to cool the bearing by a positive controlled flow. However, some propellants

Table 6-6 Comparison of turbopump rolling-element bearings.

Type of Bearing	Advantages	Disadvantages	Primary condition for use
Conrad-type ball	Any combination of radial and thrust direction; large misalignment capability; moment-load capacity	Limited number of balls; two-piece cage necessary	Combined load; two-direction thrust loads
Angular-Contact ball	Thirty percent more capacity than similar-size Conrad; one-piece cage	Predominant thrust required; one-direction capacity; lower misalignment tolerances than Conrad	High speed, high-load single-direction thrust; can be used in duplex pairs for two-direction thrust
Split-ring	Thirty percent more thrust capacity than similar-size Conrad; one-piece cage; two-direction thrust capability; lower axial clearance through use of Gothic arch	Predominant thrust required; lower misalignment tolerance than Conrad	Two-direction thrust
Cylindrical	Much higher radial capacity than ball bearing; provides axial freedom of shaft; higher radial stiffness than ball bearings; one-piece cage	No axial load capacity; roller ends wear in nonlubricating coolants; lower misalignment tolerance than ball bearings; requires negative internal clearance	High radial capacity without axial restraint; higher radial stiffness

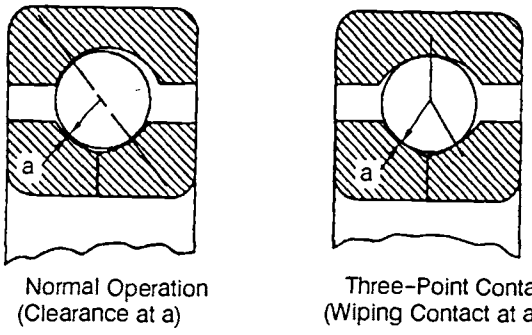

Fig. 6-66 Typical ball-bearing designs.

do not provide lubrication to the bearing and, as a result, allow bearing wear or surface distress. For many turbopump applications, the wear rate is sufficiently low that the resulting life of the rolling-element bearing more than adequately meets the turbopump requirements. Such bearings have been used very successfully in turbopumps for expendable launch vehicles.

To overcome the limitations of rolling-element bearings for long-life high-speed turbopumps, hydrostatic bearings are being introduced. These bearings operate on a fluid film and derive their ability to sustain loads and provide required rotor-dynamic stiffness through a high-pressure supply of the propellant from the pump discharge. These bearings also offer basically unlimited speed and positive damping to the turbopump rotor. There-fore, they are of particular value when high speeds are desirable and operation above one or more critical speeds is desired. Primary limitation: they must start and shut down in a rubbing contact. The ability to do this successfully has been demonstrated for certain applications and is the subject of ongoing technology developments.

Hybrid systems consisting of both rolling element and hydrostatic bearings can also be used where the rolling-element bearing carries the loads at start and shutdown when the hydrostatic pressure for the bearing is low. As pump speed increases, the hydrostatic pressure increases, and the hydro-static bearing begins to take an ever-increasing percentage of the applied loads because of its larger stiffness. Thus, the life of the rolling-element bearing is extended because it carries low loads at speed, and the life of the hydrostatic bearing is extended because it does not experience contact at start and shutdown. The hybrid system, of course, requires more axial length and must be designed to prevent the two bearings from fighting each other to avoid overload.

The primary types of rolling element bearings are listed in Table 6-6 along with advantages and disadvantages. Figures 6-66 and 6-67 show examples of such bearings. Various arrangements of duplex pairs of angular-contact ball bearings can be used, as shown in Fig. 6-68, to provide bidirectional axial-load capability and overcome their main disadvantage. Springs are typically used to maintain axial preload of the bearings to remove internal clearance and control the radial stiffness. The springs also provide axial compliance to accommodate thermal effects. In order to provide roller guidance without end wear, some roller bearings are preloaded radially by negative internal clearance achieved through a thin-flexible outer race.

Rolling-element bearings are speed-limited due to parasitic loads from ball or roller inertia. This is typically expressed as a DN limit, defined as the product of the inner-race bore diameter D (in mm) and the pump rotational speed N (in rpm). A practical DN limit for Conrad-type and cylindrical roller bearings is 1.6 million, while angular-contact bearings have shown reliability up to 2.1 million. However, the life of the bearings at even lower DN values may be limited because of the lubrication available and the load combinations experienced. The higher DN values lead to higher centrifugal forces, higher sliding velocities, and increased fluid churning. The propellant will also affect the DN limit; e.g., the maximum values just cited have been achieved in liquid hydrogen, but liquid-oxygen bearings have not typically been used at these limits. Note that for a given transmitted horsepower, the shaft diameter based on allowable stress does not decrease proportionally with the increase of shaft speed. Thus, the required bearing DN value rapidly increases for high-speed turbopumps. As a result, the turbopump rpm may be limited by the bearing DN value.

Ball-bearing radial stiffness ranges from 0.2-1.5-million ft^{-1} depending upon bearing size, contact angle, speed, mounting compliance, and applied load. As an example, the stiffness of a particular 45-mm ball bearing with 750-lb axial preload will be approximately 500,000 ft^{-1} at 30,000 rpm if the outer ring is allowed to tilt, but will be significantly stiffer if the outer ring is rigidly mounted. Roller-bearing stiffness is typically higher, ranging up to 2.0-million ft^{-1}. To achieve a given stiffness, bearing design is critical to the successful control of rotor-dynamic response.

During the turbopump design phase, computer programs are used to predict bearing characteristics and to optimize bearing geometry to meet design goals. Stiffness is calculated to support rotor-dynamic analysis of critical speeds and unbalance response. Ball excursions determine required cage pocket-clearance and structural criteria. Fatigue life, local stresses, and sliding-velocity calculations are used to assess the effects of variations in bearing geometry and operating conditions. Although the rolling bearing is a dynamic system, it is most often

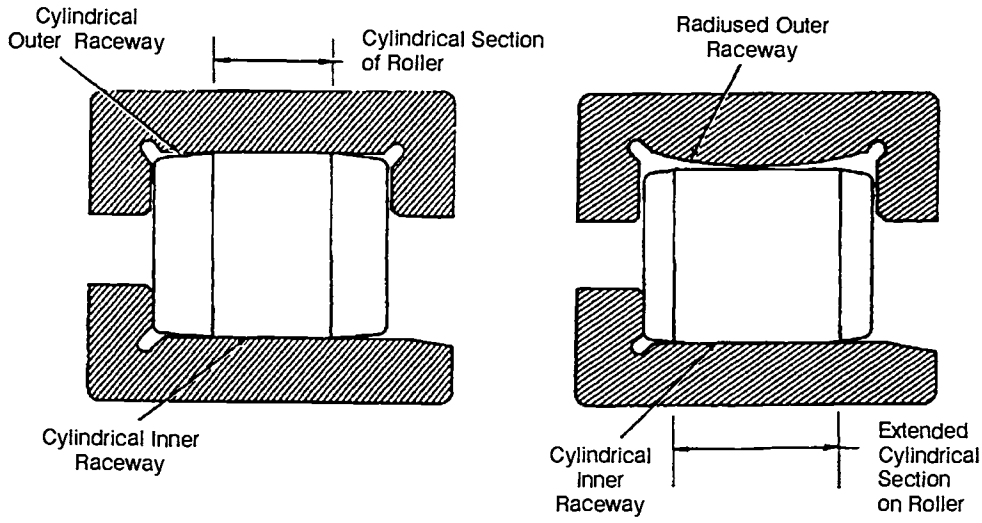

Fig. 6-67 Typical roller-bearing designs.

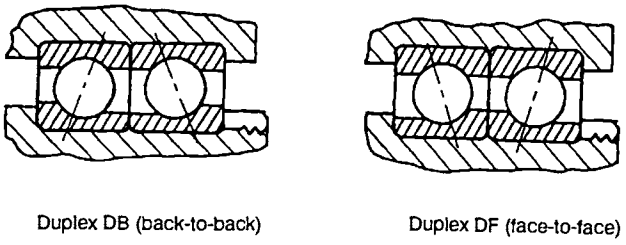

Fig. 6-68 Typical duplex-pair arrangements of ball bearings.

analyzed in a quasi-static manner; the forces and moments due to motion are determined for the assumed design configuration (speed, load, number and size of rolling elements, internal clearance, and material properties), and then the bearing-system equilibrium is established by treating the forces and moments as static quantities. These solutions are contained in commercially available computer codes. Several of the first were written by A.B. Jones, based upon his high-speed bearing analyses (Ref. 6-12). SHABERTH (SKF Technology Services, Ref. 6-13) includes options for automatically adjusting fits and clearances in response to temperature effects on shaft and bearing materials. The ADORE computer code by Pradeep Gupta (Ref. 6-14) performs a true dynamic analysis by solving the equations of motion for the interaction of the cage with the balls and rings, and can be used to assess the effects of cage clearances and mass and geometry on cage stability.

The axial loads generated by turbopump rotors at mainstage often exceed the load capacity of ball bearings, so the function of rotor axial-position control is performed by a balance piston operated by pump internal pressure. Ball bearings with axial-travel stops can limit axial motion during start and shutdown transients when loads are of short duration and within ball-bearing strength. Relatively compliant springs permit the balance piston to position the rotor without loading the ball bearings excessively.

The most commonly used material for bearing rings and balls, vacuum-melted 440-C steel, although not superior in either category, combines hard-enability and corrosion resistance better than most other materials. Since short bearing life is a major constraint on engine utility, several alternative materials have been identified which may enhance life and reliability. These include CRB-7 and BG-42 steels, which have higher hardness, and the ceramic silicon nitride (Si_3N_4), which is harder and 60% less dense than steel. In addition, the failure mode of the silicon nitride is generally fatigue-spalling rather than fracture. It thus appears to be a better material for the balls of a high-speed turbopump, but further demonstration of this is required. The most widely used cage material for propellant-cooled bearings is Armalon™, a fiberglass-reinforced polytetrafluoroethylene (PTFE), or Teflon™. The glass fabric, impregnated with PTFE, gets mandrel-wrapped under heat and pressure into a tube of near net size, and then machined to final shape. Its advantages include light weight and high strength at cryogenic temperature, and resistance to ignition in LO_2. Although the Teflon™ provides some friction reduction through film transfer, the glass fibers may promote wear. Friction-reducing treatments for Armalon™ include phosphate-bonded MoS_2 (which is quickly worn away) and a fused coating of fluorinated ethylene propylene (FEP), which has shown good improvement in bearing wear-life.

To maximize propellant-cooled-bearing life potential, a positive flow of propellant must be provided, and coolant temperature and pressure should be controlled to avoid vaporization of the fluid in the bearing. This may require maintaining high pressure in the bearing area by throttling flow downstream of the bearing. Coolant may be jet- or flood-fed, preferably to each bearing individually rather than in series. Particulate matter should be excluded by filter or traps to avoid bearing-surface damage.

A most important consideration in bearing design concerns the required operating life of the

rocket engine. The bearings must have adequate statistical probability of exceeding this. One accepted life rating for rolling-element bearings, the "B-1 life," denotes the operating life in hours at which 1.0% of a set of bearings at a fixed load and speed will have failed by contact fatigue. B-1 life is often used to show life potential, but it is recognized that the calculation methodology evaluates the fatigue life under ideal lubrication. By contrast, the bearing environmental conditions in rocket-engine turbopumps frequently lead to wear rather than fatigue. Therefore, adequate B-1 life is necessary but *not sufficient* to assure meeting bearing-life needs.

Hydrostatic bearings offer an attractive means of overcoming limitations of rolling bearings, as they are theoretically speed-limited only by the centrifugal shaft stress, and thus can operate at journal speeds to approximately 5,000,000 DN. Additional benefits include increased stiffness and load capacity (with sufficient fluid pressure and flow available) and significant damping, which is minimal with rolling bearings. Since external pressurization must develop the significant load capacity, hydrostatic bearings are subject to rubbing during start and shutdown. Means of avoiding wear during these periods include auxilliary rolling bearings, wear-resistant materials, and "prepressurization" before start. Two types of radial hydrostatic bearings are used in turbopumps: orifice-compensated and axially-fed.

Figure 6-69 illustrates a recessed, orifice-compensated radial hydrostatic bearing. Its load capacity arises from fluid pressure responding to two flow restrictions in series. The pressure drop across the bearing has approximately equal steps: the first in the compensating orifice and the second in the close clearance between the journal and the lands defining the recess boundaries. A radial motion of the journal reduces the flow area on the side of the approach, increasing the local flow-restriction, causing the fluid pressure to rise in the associated recess. Simultaneously, the land flow restriction opposite is reduced, with a resultant decrease in the associated recess pressure. The relative pressure change, acting over the projected bearing area, provides a force tending to restore the journal to its original position.

Fluid forced through an annular space can generate significant stiffness across the radial gap. With the large pressures available in turbopumps, stiffnesses of over a million lb/in. can be produced. Converging clearance assures positive stiffness and enhances load capacity with minor increases in leakage flow.

Hydrostatic bearings differ from rolling bearings because the fluid film introduces significant damping and cross-coupling. The importance of these characteristics must be assessed based on rotor-dynamic response. High values of direct stiffness can be obtained by adjusting size, pressure available, and bearing geometry, somewhat independent of the fluid used, while the cross-coupling and damping generally increase with the fluid viscosity.

Hydrostatic bearings permit additional flexibility in selecting the basic turbopump configuration; the restrictions associated with the rolling-bearing DN and stiffness limits often result in a rotor configuration that operates between critical speeds and, therefore, has significant operating-speed restrictions to maintain safety margins. By increasing the shaft and bearing stiffness, subcritical designs with less

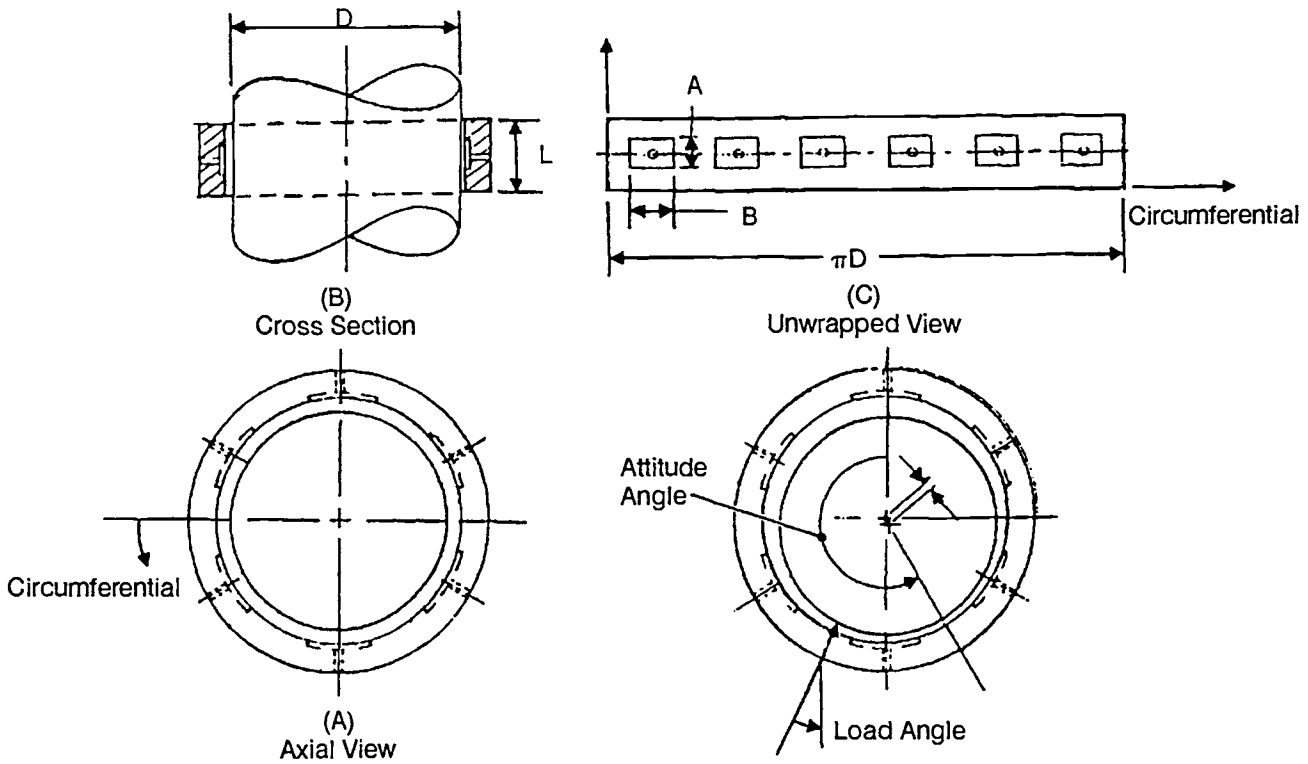

Fig. 6-69 Typical hydrostatic-bearing features.

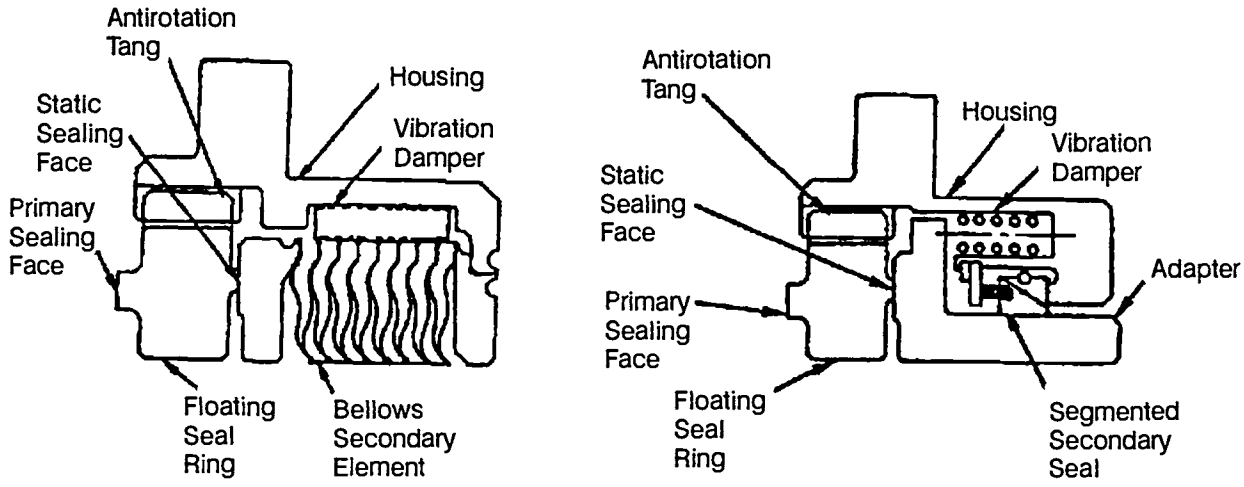

Fig. 6-70 Face contact seals.

restriction of operating speeds are more attainable.

The approximate load capacity of an orifice-compensated hydrostatic bearing is 25% of the product of the projected area (length x diameter) and the available pressure drop, and this rough rule may be used in preliminary size-selection. However, the minimum journal diameter will often be determined by other considerations, such as shaft strength and stiffness.

Bearing radial clearance has a significant effect upon the bearing stiffness, damping, crosscoupling, and leakage flow. As a general rule, there should be at least 0.001 in. of radial clearance per inch of journal radius. Sometimes a larger value is used for manufacturing economy, but the relative benefit of larger tolerances must be traded off against the consequent increase in leakage flow and lesser stiffness.

The hydrodynamic relations describing flow and pressures in a hydrostatic bearing are complex, and analyses are performed with computer programs specifically developed for this purpose. For orifice-compensated bearings, analysis is generally based on Reynolds' equations with corrections applied to approximate the effects of high levels of turbulence. Improved codes are being developed that use the more basic Navier-Stokes relations. Analytic methods used for axially-fed hydrostatic bearings is based upon work initially performed to determine the characteristics of seals.

Dynamic-Seal Design

Turbopump dynamic seals have two main purposes: to prevent or minimize the leakage of propellants or fluids between the rotating components, and thus improve efficiency, and to prevent mixing of incompatible fluids, e.g., fuel and oxidizer, for reliable, safe operation. A secondary purpose has proven to be of value in high-speed turbopumps: ability of seals through proper design to provide significant damping and stiffness to the rotor-dynamic system. The seal system, i.e., the arrangement of seals, drains, and purges, must seal reliably at all extremes of operation and allow a single seal failure without destructive failure of the turbopump (Ref. 6-10).

The type of seal for each application will be selected to satisfy the pump operating conditions and the seal limitations. The seal system design and the seal performance limits are iterated in terms of pressure capability, temperature limits, speed limits, wear life, leakage, space requirements, and cost. The principal types of seal used in turbopumps are face-contact, segmented shaft-riding, floating-ring,

Table 6-7 Relative leakage of seals.

Type of Seal	Leakage	Typical radial gap, in.	Fluid
Face contact	Minimum	0.0003	Liquid/Gas
Segmented shaft-riding	Low	0.0005	Gas
Hydrostatic/hydrodynamic	Low	0.0003-0.0005	Liquid/Gas
Floating ring	Medium	0.002-0.003	Liquid/Gas
Labyrinth	High	0.005-0.010	Liquid/Gas

Table 6-8 Face-contact-seal speed and PV limits for typical propellants.

Fluid	Max. Speed, ft/s	Max. PV, psi X ft/s
LH_2	500	50,000
LOX	200	25,000
RP-1	300	25,000
GH_2	400	20,000
Hot gas	200	10,000

hydrostatic/hydrodynamic, and labyrinth. Table 6-7 gives a relative comparison of their effectiveness.

The face-contact seal (Fig. 6-70) provides the lowest leakage and generally will be used when the pressure-speed-life limits are consistent with reliable operation. The sealing comes through rubbing contact between a rotating mating ring attached to the shaft and the seal face. The mating ring is generally plated with a wear-resistant hard plating and is lapped flat. The seal ring is generally a self-lubricating carbon material with a flat sealing face. The seal ring can be floating to minimize thermal distortions or can be press-fitted into a metal adapter. The seal ring is loaded against the mating ring with either a welded-metal-bellows secondary element or compression springs. The sealing dam is established to balance the pressure-induced closing forces to maintain a satisfactory face load at high pressure. The secondary sealing element can be a welded bellows, piston ring, segmented ring, or elastomer, depending on the operating requirements. Welded metal bellows are ordinarily used for temperatures below -65 or above 500°F.

Face-contact seals are speed-limited by heat generation at the rubbing face and cooling capacity of the environment. The heat generation rate is a function of the contact load and velocity of the rubbing surface. The limit is given as a PV factor, where P is the unit contact load in psi and V is the rubbing velocity in ft/s. The PV limit is based on the cooling capacity of the environment. Table 6-8 gives PV limit for typical propellants. Clearance-type seals, such as labyrinth, floating-ring, or hydrostatic/hydro-dynamic, are used for higher speeds.

The segmented shaft-riding seal (Fig. 6-71) consists of segmented sealing rings that are loaded against the shaft with a garter spring and the pressure differential to form a radial dynamic seal. An axial static seal is formed by loading the segments against a flat surface on the seal housing using springs and the pressure differential. The segmented rings may consist of three rings with overlapping joints or single rings with tongue and groove joints. Having the segmented rings in rubbing contact minimizes leakage. The segments are loaded by the pressure differential and are generally limited to approximately 100 psi.

The floating-ring seal (Fig. 6-72) consists of a solid sealing ring that is free to float in the radial direction for minimum operating clearance. The radial dynamic seal is formed by the close clearance to the shaft; the axial static seal, by loading the ring against the seal housing. The ring is partially pressure balanced in the axial direction to control the axial load and the radial friction force. The centering force is provided by the pressure profile in the clearance gap. The force increases on the side approaching contact and decreases on the opposite side to give a centering force when the ring moves off center relative to the shaft. The centering force is increased by a factor of approximately 3 when a convergent taper is utilized on the seal-ring bore. The optimum taper ratio of inlet clearance to exit clearance is approximately 1.5 to 2.0 for most fluids.

Hydrostatic and hydrodynamic geometry may be utilized on face seals, segmented seals, and floating-ring seals to provide a lift force proportional to the operating gap at the sealing surface. The lift force increases as the sealing surface approaches rubbing contact and decreases for larger gaps to form a very small (0.0005-in.) self-adjusting

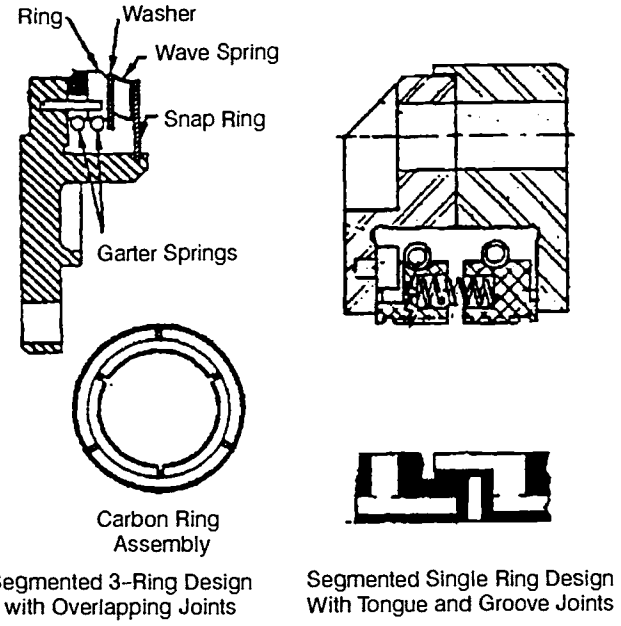

Fig. 6-71 Segmented shaft-riding seals.

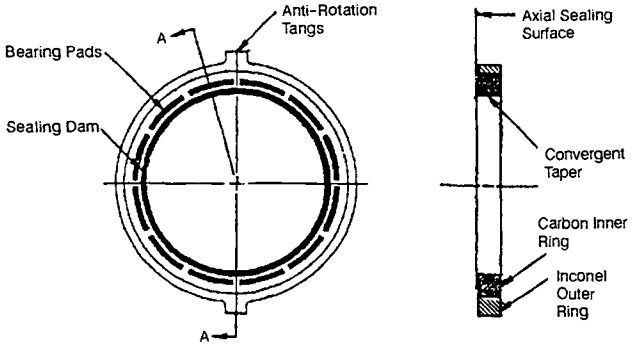

Fig. 6-72 Floating-ring seal.

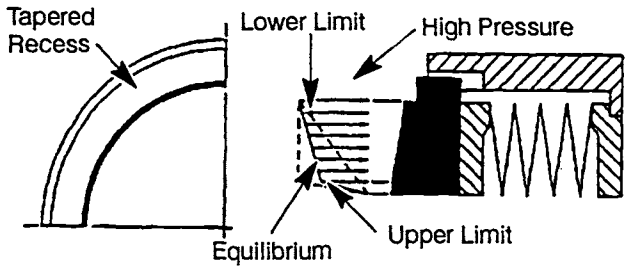

Fig. 6-73 Convergent tapered-face hydrostatic face seal.

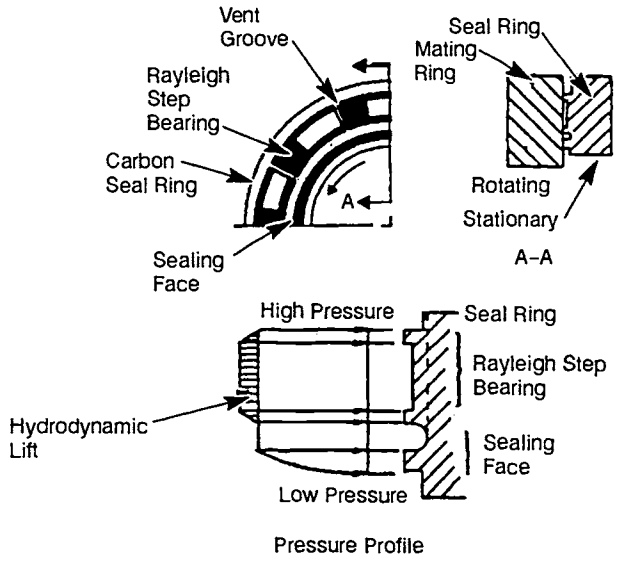

Fig. 6-74 Rayleigh-step hydrodynamic face seal.

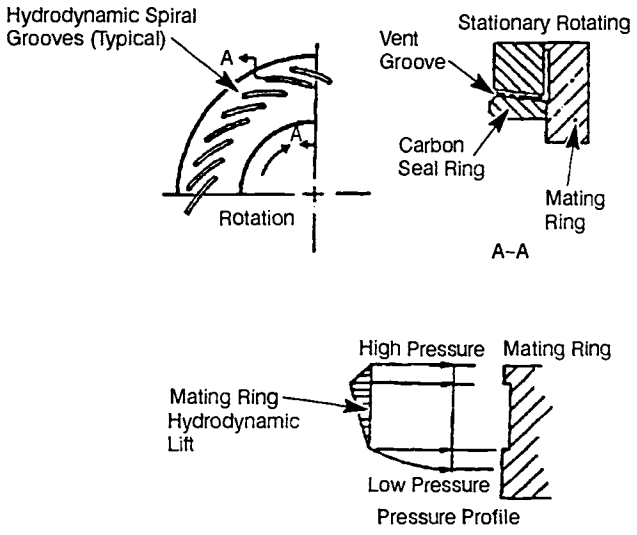

Fig. 6-75 Spiral-groove hydrodynamic face seal.

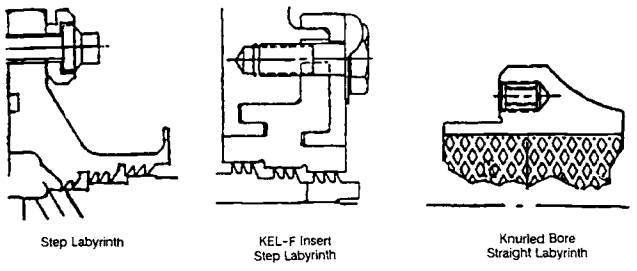

Fig. 6-76 Labyrinth-seal designs.

clearance yielding minimum leakage and no steady-state rubbing contact. A convergent tapered face (Fig. 6-73) may be used to provide hydrostatic lift. Hydrodynamic lift may be provided by Rayleigh step pads (Fig. 6-74) or spiral grooves (Fig. 6-75). The Rayleigh step pads provide hydrodynamic lift by viscous pumping of the sealed fluid in the recessed pads. The spiral grooves develop hydrodynamic lift by viscous pumping the sealed fluid in the spiral grooves. Both concepts are pressure-balanced by locating the sealing dam inside of the hydrodynamic geometry. Both the hydrostatic and hydrodynamic-lift seals, as successfully tested in the laboratory, have demonstrated positive control of the quality of the sealed fluid. To date, these seals have not been used in flight turbopumps and are not as reliable if the fluid is susceptible to vaporization in the seal.

The labyrinth seal (Fig. 6-76) can be used when low cost and reliability are the primary consideration or when the pressure and speed limits of other types of seal are exceeded. Typically, the wear rings on the rotating impellers are labyrinth seals because of the higher velocity due to the required diameter. Since the clearance gap must be large enough to allow for mislocation tolerances and shaft radial motion, the leakage is significantly higher than for the other types. Step-labyrinth seals are used to reduce the leakage by creating barriers to reduce the velocity head. The number of teeth, tooth pitch, and height will be optimized to give minimum leakage. Figure 6-77 shows typical data on the effectiveness of the labyrinth design for reducing leakage with a liquid propellant. Kel-F plastic inserts are used for oxidizer seals to allow rubbing contact without the hazard of ignition. A straight or convergent labyrinth with a knurled bore and smooth shaft provides additional dynamic stability by reducing the circumferential velocity relative to the axial-leakage velocity.

Table 6-9 gives pressure and temperature limitations for the principal types of seal. The seal type will be selected to satisfy the pressure-speed-life limits with minimum leakage and maximum reliability.

Oxidizer and fuel on a rotating shaft will usually be separated by a primary oxidizer seal, an inert-gas-purged intermediate seal, and a fuel seal with separate drains for the oxidizer and fuel. The purged intermediate seal provides a pressure barrier between the drain cavities to prevent mixing of the propellants. For reliable operation, high-pressure propellants may require staged sealing to reduce the pressure at the intermediate seal. Figure 6-78 shows a representative seal system incorporating these

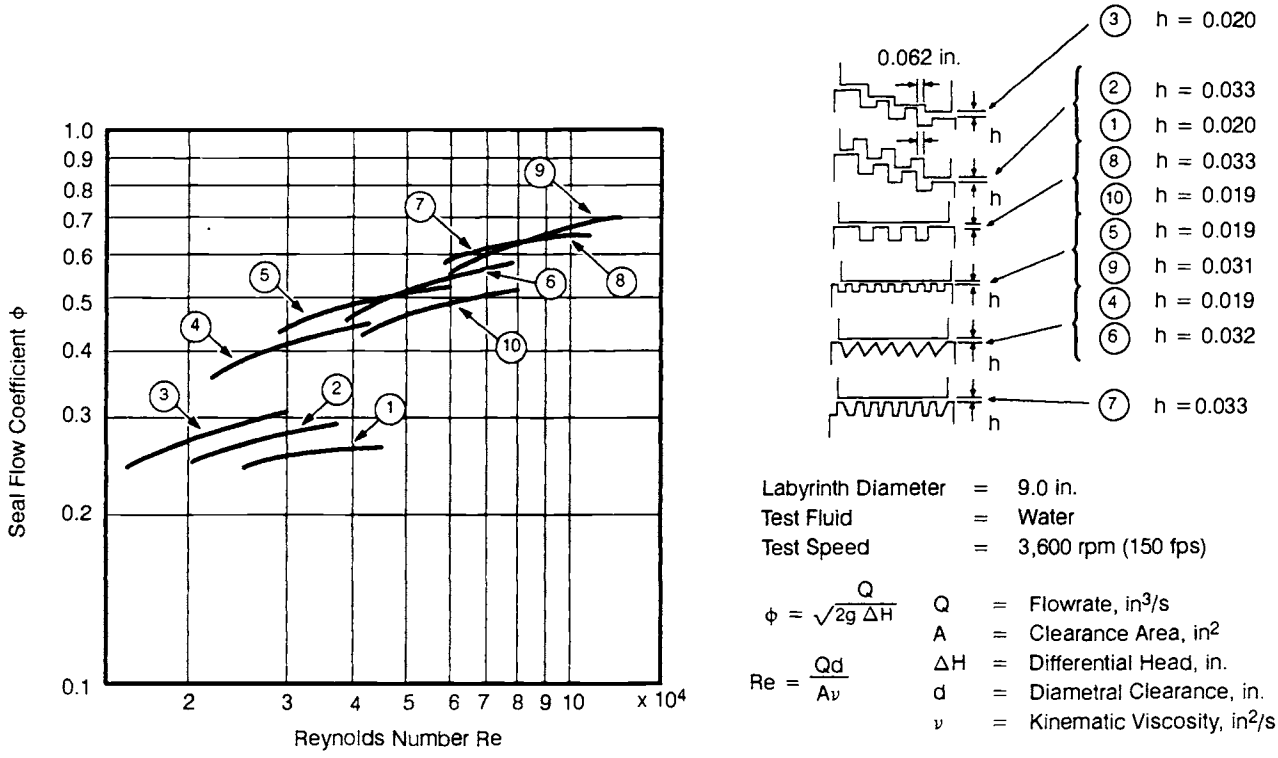

Fig. 6-77 Effect of labyrinth design on leakage.

Table 6-9 Seal pressure and temperature limits.

Seal Type	Recommended Max Pressure (psig)	Temperature Limit (°F)		Remarks
		Min	Max	
Face Contact				
Metal bellows	500	-423	1500	Cryogenic or reactive fluids
Piston ring	750	-423	1500	Hot gas or cryogenic
Elastomeric	1,000	-65	500	Lubricated
Circumferential				
Segmented	100	-423	1000	Hot gas and purge gas
Floating ring	5,000	-423	1200	Hot or purge gas, long life
Labyrinth	Unlimited	-423	1800	All fluids, reliable
Hydrostatic/hydrodynamic	500			

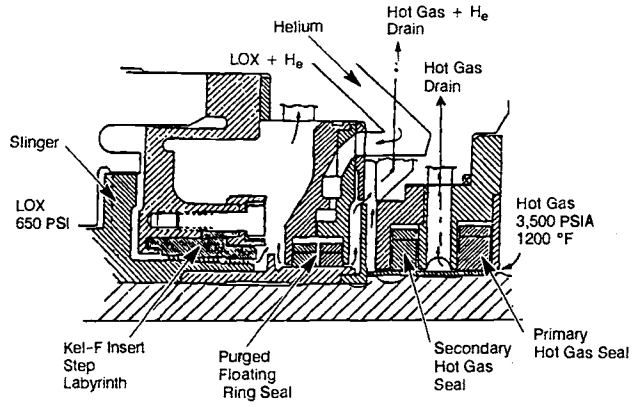

Fig. 6-78 Typical seal system for separating high-pressure propellants.

concepts. The leakage drains are sized to accommodate the maximum leakage while maintaining a pressure at the intermediate-seal discharge that does not exceed the purge pressure between the intermediate-seal rings. This assures a positive separation of the fluids at all times.

Some applications require a positive seal during prestart conditioning but an open seal during operation. For such cases, static liftoff seals are typically used that close by spring forces until internal pressures increase with rotation to provide a force large enough to completely open the seal. Typically, the seal will open at a shaft speed of 20-30% of the mainstage speed.

Turbopump Gear Design

Gear drives for rocket-engine turbopumps are used to achieve maximum efficiency in low-to-medium power applications (100-5000 hp). The need to operate the rocket-engine pumps at low inlet-pressure frequently limits the allowable operational pump speeds. In general, the optimum turbine speed will differ from that of the pumps; and if there are significant differences in oxidizer and fuel density, it is desirable to operate the pumps at different speeds as well. Geared systems provide a means of operating all components at optimum speed (Ref. 6-11).

Geared turbopumps find application in gas-generator cycles for both storable and cryogenic propellants because of the high turbine speed required for the high pressure ratio and low mass flow. Upper-stage liquid-hydrogen-fueled engines are also

candidates because the large difference in density between fuel and oxidizer causes different optimum pump-speeds, and the low power level results in a geared pump being lighter than separate, direct-driven fuel and oxidizer pumps.

Several major U.S. launch vehicles (Atlas, Delta, and Titan) utilize geared turbopumps for boost stages of flight, as does Japan's N-2, which is similar to the Delta. The European Ariane and the U.S. Centaur use a gear-driven LOX-LH_2 turbopump.

Lubrication. The method used for lubrication and cooling has a fundamental influence on the design of the gear system. Lubrication schemes are often categorized by use of oil or propellant, but the design will be most influenced by the degree of good or poor lubrication.

For small LOX/LH_2 pumps (the Centaur RL10, for example), gaseous hydrogen can be used to cool the gears and bearings with lubrication supplied by dry film coatings, such as molybdenum disulfide, applied to contacting surfaces. Such coating gives poor lubrication, but allows a workable design by keeping contact loads and speeds low. Design emphasizes minimize wear.

Higher-power applications (typically above several hundred HP) demand good lubrication. This generally means oil; but, with RP-1 (kerosene)-fueled engines, equal success has been obtained using kerosene with an extreme pressure additive (EPA) to minimize scoring of the gear. With good lubrication, turbopump gear design follows conventional practice, but gives special emphasis to factors significant at high pitchline speeds and tooth loadings.

Although fluid lubricating properties are important, flowrates and method of application are dictated by cooling requirements. Frictional heating in the gear mesh takes roughly 0.5% of the power transmitted. As pitchline velocity increases, tooth cooling becomes critical. Directing jets of lubricant at the disengaging side of the mesh, where the working flanks of the teeth are first exposed, provides efficient cooling if high jet velocities (velocities at least as large as the pitchline velocity) can overcome windage flows.

Both recirculating and single-pass oil systems are being used on larger turbopumps. The lubricant systems must be capable of meeting both gear and bearing flow-requirements. Inert-gas purges may also be used to control gearbox pressure in order to reduce lubricant foaming and to improve drainage or oil scavenging.

Gearbox arrangement. Figure 6-16 shows a cross section of the turbopump used on the Delta first-stage engine. It illustrates several factors that influence the overall turbopump and gear-train layout. The pumps and turbine are usually significantly larger than the gears and must interface with large fluid ducts. Therefore, packaging requirements usually force the impellers or turbine wheels to overhang the end of the shafts. It is often necessary to use idler gears or multiple reductions (even when the required speed reduction ratio could be obtained with a single mesh) to obtain sufficient spacing between pump and turbine shafts.

Gear alignment (shaft parallelism) is critical to obtaining maximum gear capacity. Highly loaded gears should, therefore, be centrally mounted between two bearings to minimize the deflection caused by the large transverse loads arising in the mesh. Gear alignment as well as the need to isolate the hot turbine housing and cold pump housing (in the case of cryogenic propellant) usually requires the gearcase structure be isolated from pump and turbine structures.

Rotor-dynamic and shaft bending limit the mass of discs, particularly on a high-speed shaft. To avoid this constraint, the turbine may be supported by its own set of bearings and linked to the high-speed pinion by means of a quill shaft that will accommodate misalignment and isolates loads.

Gear geometry. The factors that differentiate turbopump power gears from other high-speed aerospace power gears are higher tooth-face loads (tangential force per unit tooth width) and short life. Tooth loads may be as high as 5000 lb/in. for a turbopump power gear, but life requirements are seldom longer than a few hours. These factors, along with the need for minimum weight and extremely high reliability, determine the design of the gears.

Involute spur gears have been used exclusively because of their high efficiency and simplicity. Although helical gears offer advantages by somewhat higher load capacity and smoother operation, they introduce axial loads that complicate bearing and casing design, and therefore have been avoided.

The critical concerns in gear performance are tooth-bending fatigue life, pitting fatigue life, and scoring resistance. Gear design must balance the sometimes competing parameters that affect these concerns to achieve the desired life.

Tooth bending strength is related to tooth size (diametral pitch), pressure angle, number of teeth, and face width. Face width is generally limited to 0.5 to 0.7 times the pitch diameter of the pinion (smaller gear) because unavoidable misalignment tends to load the tooth ends as width increases. Relatively high pressure angles (angle between a normal-to-the-tooth surface and the tangent-to-the-pitch circle), typically 25 deg, are used because they allow a wider tooth base for strength and a larger radius of curvature at the point of contact to reduce hertzian contact stress.

Tooth size and number of teeth are related to the gear diameter. Smaller diameters reduce pitchline velocity and weight at the expense of higher tooth-loads. For a given pitch diameter, the larger the teeth, the smaller the contact ratio (i.e., the average number of teeth in contact at one time). High contact ratios give smoother operation (for reduced dynamic loads, especially at high pitchline velocities) and lower contact loads at the tooth tips where sliding velocity is a maximum. Contact ratio must be traded against tooth size (larger teeth provide greater bending strength). A contact ratio of 1.5 has proven near-optimum for turbopumps.

Standard tooth proportions can be modified to improve gear performance further. Pinions are frequently made with long addendums and gears made with short addendums to reduce sliding at the

pinion tip, where wear tendencies are greatest, and to strengthen the pinion, which experiences a larger number of stress cycles than the gear. Pinion teeth can be further strengthened by increasing thickness at the expense of the mating gear. The involute profile may be relieved near the tip and root to account for large elastic deflections of teeth as they enter and leave the mesh. Crowning or end-easing is also employed to prevent maximum loads from occurring at the tooth ends.

Gear materials, processing, and quality. Materials, processing, and quality control are as essential as the basic design and geometry in meeting life requirements. For highly loaded power gears, life is generally limited by bending fatigue and wear. Deep-carburized, case-hardened steel provides high surface hardness (58-62 Rc) to gain wear resistance and fatigue life. Vacuum-melted and forged materials can further improve fatigue properties.

Tight control of tooth-form tolerances proves critical for minimizing dynamic loads from tooth spacing errors and ensuring uniform load distribution across the width of the teeth. To obtain the desired tooth-form accuracy without introducing detrimental machining effects in the critically stressed fillet region at the base of the teeth, the following process may be used:

- Teeth are rough-cut before heat-treatment, leaving a slight undercut below the working-flank surface.
- After heat treatment, the root area may be shotpeened to improve fatigue resistance further.
- Working flanks are finish-ground, taking particular care to avoid grinding in the fillet and root.

6.8 DESIGN LAYOUT OF TURBOPUMP ASSEMBLIES

Figure 6-79 presents the design layout of the A-1 Stage engine turbopump assembly. Logical packaging and arranging of the basic mechanical elements of the turbopump are among the considerations in preparing the layout. For instance, ease of development will be one of the more important criteria that influences the selection or arranging of the turbopump mechanical elements. Standard or proven mechanical detail should be extensively adopted in the layouts. Important turbopump design-layout considerations include these:

- Compatibility with engine systems packaging and plumbing
- Structural integrity
- Material selection (e.g., for weight and fluid compatibility)
- Control of system critical speeds and dynamic response
- Control of axial and radial loads on the rotating members
- Positive sealing of fluid mediums
- Control of fits and deflections
- Compensation for thermal expansion and contraction
- Ease of development
- Ease of assembly
- Ease of manufacturing

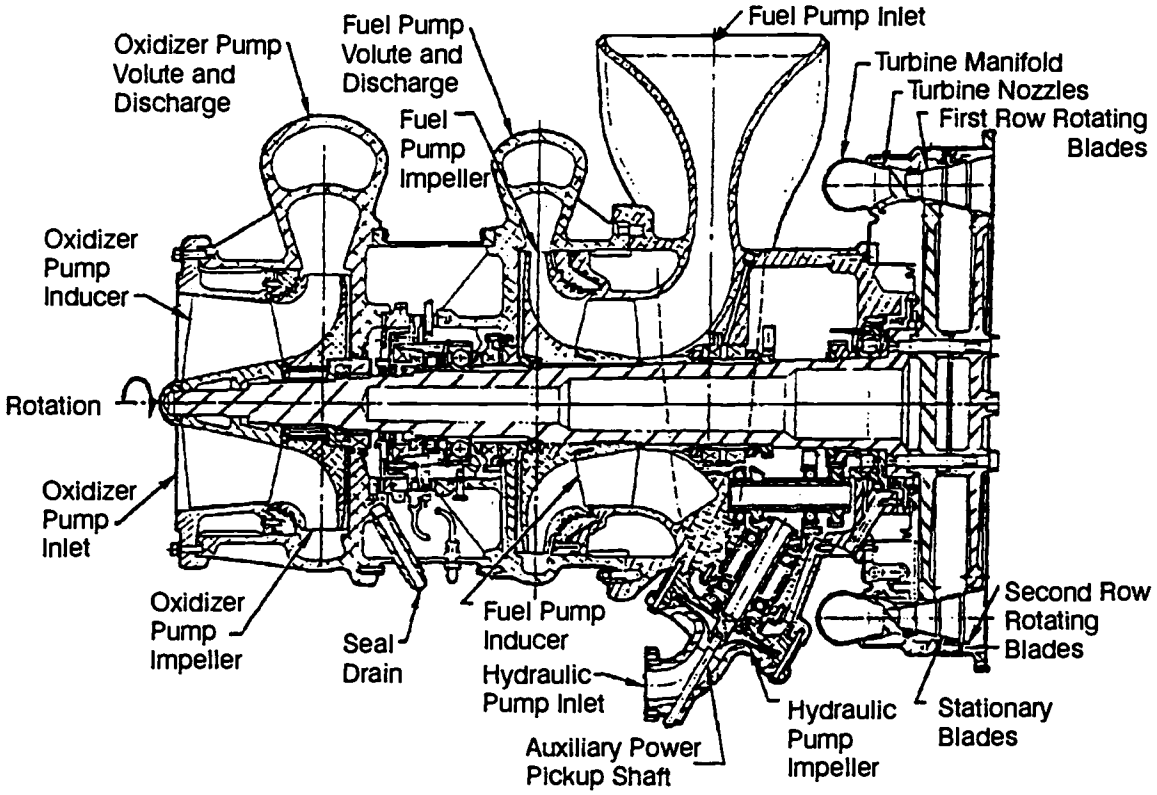

Fig. 6-79 Assembly design layout of the hypothetical A-1 Stage engine turbopump.

Turbopump design layout demands considerable experience and skill. To illustrate the influence of some of these parameters, consider the SSME HPFTP of Fig. 6-5. The use of a scroll inlet to the first stage was driven by an engine system arrangement that would not permit an axial inlet. Also, the way the turbopump was mounted to the hot-gas manifold and the structural backbone of the engine led to a decision to limit the turbine-pitchline diameter, thereby giving up several points of turbine efficiency to reduce weight and provide better structural margin. In selecting materials for the turbine disks, no material was available that provided the structural integrity at the temperature of the hot-gas turbine drive fluid. As a result, the turbine disks had to be cooled with liquid hydrogen. However, this created an incompatibility; the hydrogen embrittled the disk material. Gold-plating the disks eliminated this problem.

One of the key ways to control the critical speeds is through the selection of the bearing locations. For the SSME pump in Fig. 6-5, the bearings were placed outboard, but this was driven by bearing DN limits that prevented placing the bearings over the part of the shaft that was carrying the torque. At the outboard locations the shaft diameter can be reduced because there is no shaft torque. To improve the dynamic response with these bearing locations, the pump must operate between the second and third critical-speed, and the seals must be designed to provide additional stiffness and damping. The ball bearing at the centerline of the shaft at the pump end was added after the original design to serve as a transient axial-thrust-control device (rather than using rubbing seal surfaces within the pump). This is a clutching ball bearing that carries the loads until the balance-piston pressure can take control. This usually results in the bearing being engaged until the pump speed reaches approximately 7000 rpm. Another favorable design feature of this pump is that every external seal is only required to seal the pump-inlet-pressure, which is close to 300 psi, rather than sealing the discharge pressure of 7000 psi. This was achieved by providing internal piston-ring seals to seal the high pressures and venting the area under the external casing back to the inlet pressure of the pump.

In laying out the pump, it is necessary to plan the complete turbopump for assembly and, as well, disassembly with a minimum loss of parts. However, the fits required sometimes dictate that parts be assembled by selective heating/cooling of adjacent parts that prevents disassembly without destruction of one of the parts. Another consideration in the design layout is the requirement for instrumentation and/or inspection. For example, it is frequently desirable to be able to inspect bearings between tests, but it is hard to do this without taking the turbopump off the engine. With duplex bearing pairs, some of the bearings are generally not inspectable without turbopump disassembly. Future turbopumps will likely rely more heavily on advanced instrumentation to measure bearing condition, rather than visual inspection.

The decision to design for ease of fabrication will depend on the relative importance of other parameters. For example, in the SSME pump (Fig. 6-5) welds were used extensively rather than bolted joints, even though this significantly increased the cost and difficulty of fabrication. This was done because in the design phase of this turbopump the emphasis was on weight and performance to assure meeting all projected mission requirements.

6.9 REFERENCES

6-1. "Turbopump Systems for Liquid Rocket Engines," NASA Monograph SP-8107, Aug 1974.

6-2. "Liquid Rocket Engine Turbopump Inducers," NASA Monograph SP-8052, May 1971.

6-3. Stripling, L. B., and Acosta, A. J., "Cavitation in Turbopumps – Part 1," *Journal of Basic Engineering*, Vol. 84, Sep 1962, pp. 326-338.

6-4. Stripling, L. B., "Cavitation in Turbopumps – Part 2," *Journal of Basic Engineering*, Vol. 84, Sep 1962, pp. 339-350.

6-5. Furst, R., and Desclaux, J., "A Simple Procedure For Prediction of NPSH Required By Inducers,"ASME Pumping Machinery – 1989. FED Vol. 81, July 1989.

6-6. "Liquid Rocket Engine Centrifugal Flow Turbopumps," NASA Monograph SP-8109, Dec 1973

6-7. "Liquid Rocket Engine Axial Flow Turbopumps," NASA Monograph SP-8125, April 1978.

6-8. "Liquid Rocket Engine Turbines," NASA Monograph SP-8110, Jan 1974.

6-9. "Liquid Rocket Engine Turbopump Bearings," NASA Monograph SP-8048, Mar 1971.

6-10. "Liquid Rocket Engine Turbopump Rotating-Shaft Seals," NASA Monograph SP-8121, Feb 1978.

6-11. "Liquid Rocket Engine Turbopump Gears," NASA Monograph SP-8100, Mar 1974.

6-12. Jones, A. B., "A General Theory for Elastically Constrained Ball and Radial Roller Bearings Under Arbitrary Load and Speed Conditions," *Journal of Basic Engineering*, Jun 1960, pp. 309-320.

6-13. Hadden, G. B., Kleckner, R. J., Ragen, M. A., and Sheynin, L., "Steady State and Transient Thermal Analysis of a Shaft Bearing System Including Ball, Cylindrical and Tapered Roller Bearings," NASA CR No. 165365 (SKF Rept. No. AT810040) submitted to NASA Lewis Research Center, May 1981.

6-14. Gupta, P. K., *Advanced Dynamics of Rolling Elements*, Springer-Verlag, New York, 1984.

Chapter 7

Design of Rocket-Engine Control and Condition-Monitoring Systems

7.1 CCM—INTO A NEW ERA

The past several years have seen sophistication increasing for rocket propulsion systems. Stricter mission requirements and the demand for "smart systems" have placed more emphasis on propulsion control system analysis, design, and implementation. To obtain the required performance characteristics and meet the tougher demands, modern control approaches have been developed to supplement the classical. In addition, artificial intelligence (AI) techniques, particularly expert (knowledge) systems, are expanding the methodology for enhancing control and condition-monitoring (CCM) system designs. The ability of today's microprocessors rapidly to gather, process, and analyze tremendous quantities of data provides the necessary capability to implement increasingly complex CCM designs.

A control system interconnects components designed to yield a desired response or output based on a command or reference input. Two general categories of control approach enable the desired output. An open-loop (no-feedback) system does not measure the output or use it to modify the commanded input. As a result, owing to system disturbances, the controlled output can deviate from the command input by a large error. Systems that require minimal variations of the measured output from the commanded input usually embody one of many forms of *closed-loop* control. A closed-loop (feedback) control system uses a comparison, or error, of the commanded input with the controlled output to influence continuously the commanded input. By minimizing the measured error, the system can be made to respond with the desired accuracy. Both of these control-system approaches will be discussed later in the chapter.

Selection of the control method best suited for the propulsion system—an important first step in CCM system design—will be influenced by the requirements analysis, required accuracy, dynamic characteristics of the engine being controlled, and particularly by engine reaction-time constraints. With the control method chosen, the basic elements for the proposed system must be selected, such as type of component for the power supply and working fluid (electric, hydraulic, or pneumatic) and the operating mechanism for specific control devices.

Basic Liquid-Propellant-Engine Control Systems

Most engine systems require several or all of the basic control systems summarized in the following paragraphs.

Engine system start control. A start-sequence control brings the engine system safely from start signal to main-stage operation. A typical sequence may consist of systems preconditioning (purging, chilldown); application of start energy, if required (by means of propellant tank-head pressure, solid-gas-generator turbine spinner, gas-blowdown start bottle, etc.); and introduction and ignition of the propellants in the main combustion chamber. Secondary sequences may be required for certain subsystems such as the gas generator. A reliable engine-start sequence may be computer-controlled and maintained by monitoring during each functional step of engine operation during the start transient. The propellant-valve operating sequence effects either an oxidizer-lead or a fuel-lead start, usually as dictated by propellant type and chamber ignition and cooling methods. During the start transient, high-temperature spikes in the turbines and the thrust chamber can be avoided by proper sequencing of the turbine-feed circuit valves and the main-chamber control valves. Early engines used timing signals or pressure-ladder sequencing, in which valve sequencing was controlled by propellant pressure rise during the start transient. Figures 2-21, 3-5, 3-8, and 3-11 present typical engine-system start and cutoff sequences.

Engine-system cutoff control. Rapid and safe engine shutdown, during normal operation as well as in an emergency, allows minimum and repeatable cutoff impulse and enhances reliable systems operation. The cutoff sequence usually consists of shutoff of subsystems power (gas generator, etc.), shutoff of main-chamber flowrate, and, in the case of test firings, postfiring securing (purges, flushes). As a rule, the propellant-valve-closing sequence will be adjusted to provide a fuel-rich cutoff in the main combustion chamber. This prevents damaging temperature spikes and results in smooth and rapid thrust-termination.

Duration control of engine main stage. Important considerations governing engine firing duration have been discussed in section 2.1. The signal for in-flight cutoff, unless registering a malfunction, will be supplied by the vehicle and fed directly into the cutoff control system just discussed. For lower stages, where optimum utilization of the propellants is desired, a tank low-level sensor is often employed. In final stages, where precise cutoff velocity is essential, an integrating accelerometer or equivalent device will signal cutoff.

Engine-system safety controls. Special monitoring devices, such as monitors for detecting combustion instability, gas-generator overtemperature sensors, or turbopump-overspeed trips, are frequently employed to prevent undesired or unsafe conditions by effecting prompt, automatic, nonhazardous, fail-safe system shutdown during all phases of engine operation. In addition, most engine control systems are designed so that an interruption of electrical power supply will cause the system to shut

down safety. (For certain missions it may be desirable to switch to an emergency power source, or prevent shutdown by mechanical latching, to continue operation.) Mechanical and electrical interlock devices may be used in the control system to assure the reliability of the safety control systems.

Propellant-tank pressurization control. Various propellant-tank pressurization systems have been discussed in Chapter 5. Most propellant-tank systems employ closed-loop control of pressurization. Design requirements for the control of these systems must consider—

- Means to maintain the required tank pressure level within an allowable range during all phases of vehicle and engine systems operation, including steady-state engine mainstage; start or dynamic throttle-transients; and vehicle coasting periods between restarts.
- Effective safety devices such as pressure-relief valves to prevent overpressurization and rupture of the propellant tanks.
- Compatibility with other subsystem controls, such propellant-utilization-control and thrust-control systems.

Engine-system control calibration. Control systems described in the preceding paragraphs require proper adjustment and calibration to produce the desired engine operating characteristics and performance. This includes the programming of control computers, setting of timing devices, pressure switches, position switches, and sizing of orifices. The correct values for each of these will be verified during engine-calibration and checkout firings. For engines with fixed sea-level thrust, orifices may be placed in propellant lines for performance-parameter calibration, others in pneumatic or hydraulic lines as timing and restricting devices.

Engine-systems checkout and test controls. To verify operational readiness of the engine system and its subsystems, suitable controls must cover postassembly and prefiring checkouts. These permit simulation of engine operation and its critical control components, without actually firing the engine system. Utilizing suitable ground-support equipment (GSE), an engine checkout control system should include—

- Provisions to conduct leak and electrical-continuity checks of the entire engine system.
- Provisions for verifying proper operation of all instrumentation pickups, such as dc bus voltage and sparkplug firing monitors, and open, closed, and continuous-position signals for valves, propellant flowmeters, and pressure transducers.
- Provisions for verifying the proper function and operating range of all control devices and subsystems, such as flow-control valves, pressure regulators, and thrust and mixture-ratio control devices.
- Provisions to simulate vehicle signals for "cold" checkout of the engine system's operating sequence, such as for start and cutoff.

In addition to the checkout equipment, the engine GSE must include equipment to permit control of static-test firings.

Engine Thrust-Level Control

The significance of the thrust level of a liquid-propellant rocket engine (sea level or vacuum) has been explained in section 2.1. Fixed-thrust engines usually have this level specified with a tolerance, for instance, "±3%." Throttleable engines have it specified as a tolerance band across the thrust range. It is possible for "fixed-thrust-level" engines to guarantee this band with simple orifice calibrations in the various propellant subsystems of the engine, without resort to closed-loop systems, and with a minimum of calibration firings. However, thrust regulators or controllers may be employed in vehicle systems that require a higher degree of precision and repeatability, such as in single-stage vehicles starting at sea level, or in final stages of a multistage system. Thrust regulators are actually chamber-pressure regulators; and at altitude (vacuum) they in effect act identically to thrust regulators, since, at altitude, thrust for a given engine and mixture ratio is solely a function of chamber pressure. The same is essentially true for systems starting at sea level, because the relationship of thrust to chamber pressure as a function of altitude is predictable with high accuracy.

Occasionally, vehicle missions will require in-flight thrust control over a wider range. Usually, in such cases, the need is for a planned reduction of thrust, or "throttling," during the last portion of propelled flight. This can be done by one or the other of two basic procedures—stepwise reduction of chamber pressure (pc) or continuous reduction of pc. Each can be accomplished by control of—

- Turbine power (in the case of turbopump-fed systems), through regulation of gas-generator propellant flow rate or hot-gas flow rate.
- Main-propellant-flow rate.
- Variation of main-tank pressures (in the case of pressure-fed systems).

Additionally, in multiple (clustered) engine systems, stepwise thrust reduction can be effected by shutoff of one or more engines of the subsystems.

Propellant-Mixture-Ratio and Propellant-Utilization Control

The significance of propellant mixture ratio and its control have been discussed in section 2.1. Mixture-ratio control will be needed principally to gain optimum engine performance (vs. mixture ratio) and good propellant utilization; i.e., minimum residuals. Both goals are closely interrelated and essentially inseparable.

Open-loop mixture ratio control. Installation of properly sized calibration orifices in the main propellant lines forms the simplest mixture-ratio control. Other factors affecting engine mixture ratio during flight, such as propellant-density changes due

to heating and acceleration, can be calculated for their effect on mixture ratio, and an averaging of flight mixture ratio can be used to reduce propellant residuals. Selection of the corresponding orifice size reduces mixture-ratio deviations over the duration of flight to a level acceptable for optimum total propellant utilization in many missions. Open-loop mixture-ratio control can often be further refined by the following procedures:

- Weighing of the propellants loaded; i.e., accurate determination of the tanked-propellant mixture ratio. The vehicle to be launched rests on load cells, thus permitting weighing of the propellants actually loaded. In mixed systems, the noncryogenic component is loaded and weighed first. The cryogenic component follows and is subsequently maintained at level through a topping line. The mass of both propellants will be determined from on-the-spot temperature and ambient pressure readings during the tanking procedure.

- Use of adjustable, rather than fixed, orifices in one or both propellant lines. As close to vehicle takeoff as possible, and as a function of tanked weight and temperature readings, a hand or remotely ground-controlled orifice adjustment is made. This method is usually confined to noncryogenic fluids.

For systems where engine operation closely follows that obtained during final calibration, remarkable accuracy, approaching that of a closed-loop system (single stages, first stages), of targeted mixture ratio and thus propellant utilization can be obtained with the open-loop method.

In certain applications, however, the variation of mixture ratio as a function of increasing acceleration may exceed tolerable limits. Acceleration in most vehicle arrangements affects predominantly the propellant in the forward tank. Because of the long supply line, acceleration continues to act upon a relatively large fluid column, even near the end of powered flight (tank depletion). By comparison, the effect on the fluid in the rear tank is often nearly completely offset by the simultaneous decrease in fluid head (short liquid-column).

To offset excessive acceleration effects on the fluid from the forward tank and thus on mixture ratio, head-suppression valves are sometimes used at the pump inlet of turbopump-fed systems. Here, pump inlet-pressure increase is sensed as a function of acceleration. Corresponding signals are fed through a logic device to the head-suppression valve, gradually closing it and thus acting as a inlet-pressure throttling device.

Closed-loop mixture-ratio control. Certain cases may require a closed-loop system—such as high-velocity-increment upper stages or missions requiring engine restart following extensive cruising periods involving propellant boiloff. In a closed-loop system, the mixture ratio is controlled and compared to a command or reference mixture-ratio by a feedback system that minimizes the difference between the command signal and the mixture ratio at which the engine is operating. Figure 7-1 shows the A-4 Stage engine-mixture-ratio control loop; it uses continuous sensing of propellant mass flow to establish the ratio of propellants consumed. The mixture-ratio feedback $(MR)_b$ can then be compared with a command reference mixture-ratio input $(MR)_r$ in the propellant-utilization control computer. The resulting error signal $(MR)_e$ is fed to the mixture-ratio-control vernier position actuator for the oxidizer valve. The actuator forms a link in the mechanical coupling between the two main propellant-control valves. The oxidizer flow rate can thus be modified to eliminate the error. In high-thrust turbopump-fed engine systems, such as the A-2 Stage engine, where the propellant valves are independently actuated, the system's propellant-mixture ratio can be controlled by varying the main oxidizer flow in a similar manner. For instance, a propellant-utilization servo control valve, which regulates the pneumatic pressure to the main oxidizer-valve actuator, may control the oxidizer flow by adjusting the angular position of the oxidizer valve during mainstage operation of the engine.

It can readily be seen that control systems, based on propellant-flow-rate measurements, are basically still mixture-ratio controls and thus merely "assume," but do not measure directly, the amount of propellants actually remaining in the tanks and their unbalance. To accomplish this "propellant utilization" PU, additional control elements must be employed in the form of vehicle tank-level sensors. Numerous means for this are known: point-sensing, sonar, acoustic, radiation-sensing, differential-pressure, and capacitance probes.

Figure 7-2 presents the PU control system for the A-4 Stage propulsion system. The residual propellant

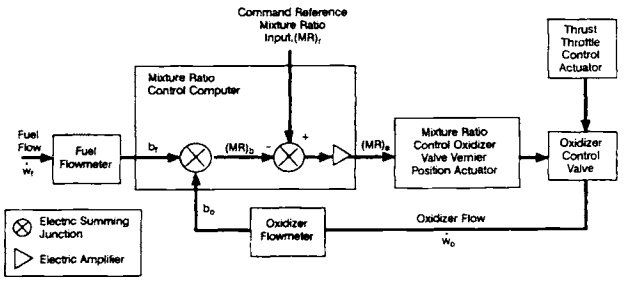

Fig. 7-1 Propellant-mixture-ratio control loop for the A-4 Stage engine.

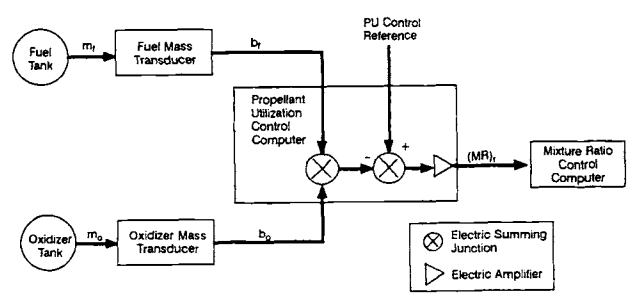

Fig. 7-2 Propellant-utilization-control system for the A-4 Stage propulsion system.

quantities in the main tanks are continuously monitored, summed, and compared with a PU-reference in the PU-control computer. Any error detected is used to modify the command reference mixture-ratio input $(MR)_r$ to the mixture-ratio-control computer. This method isolates the mixture-ratio control from the PU control, and thus prevents interaction between them. The bandwidth of the PU control system is made narrower than the mixture-ratio control system's, because residual-propellant errors may be expected to develop slowly; i.e., initial tanking errors can be corrected over the entire duration of engine operation.

The sensors used in the vehicle tanks may serve additional purposes. In combination with suitable ground equipment, they may permit an automatically controlled loading, high-level limiting and topping procedure. In static firings and flight, they may serve as redundant low-level sensors to initiate engine cutoff.

A closed-loop mixture-ratio- and PU-control system may be used not only for accurate maintenance of a fixed mixture ratio; it also has the potential for programmed mixture-ratio control (PMR) during flight, either continuously or in steps. It must be kept in mind that the average mixture ratio still must be equal to the tanked mixture ratio to assure simultaneous propellant depletion. However, by programming a mixture ratio in favor of the heavier component during the early portion of flight, and then switching it in favor of the lighter one, the accelerated vehicle mass will be reduced faster. Also, mixture ratio may be programmed to provide a higher thrust level during the steeper portion of a trajectory. This provides a better thrust-to-weight ratio in the presence of gravitation, with attendant velocity benefits. These methods, possibly in combination, may substantially increase stage payload, since the effects of mixture ratio on performance (I_s) are usually small within a reasonable range (see Table 7-1).

General design considerations. The precision with which a desired mixture ratio can be obtained or maintained will be affected considerably in open-loop systems, and to some extent in closed-loop systems, by—

- Instrumentation accuracies (in particular, flow and tank-level metering).
- Machining tolerances of orifices.
- Operating tolerances of regulators.
- Temperature influences on orifices and regulators.
- Density tolerance of the propellants, as a function of temperature and of purity (composition according to specifications; contamination and dilution).
- Acceleration effects during flight.
- Propellant-tank pressure deviations.
- Turbopump speed deviations.
- Differences between fuel and oxidizer pump characteristics as a function of speed.
- Line-resistance changes as a function of temperature and for miscellaneous mechanical reasons.

Each of these factors must be considered first evaluating the need for a closed-loop PU system as well as the mixture-ratio control range required to properly minimize residuals.

Table 7-1 Effect of mixture ratio on performance

	Mixture Ratio, O/F	Thrust	NPSH	I_s	Flow Rates	
					Fuel	Oxidizer
Change, percent	+10 -10	+11 -11	+12 -12	-1.3 +1.3	+4 -4	+14 -14

Thrust-Vector Control

Steering a vehicle over the desired trajectory employs thrust-vector control (TVC). The following methods have found application:

1) Gimballed thrust chamber or engine assembly (widely used).
2) Gimballed thrust-chamber nozzle (rare with liquid propellants).
3) Jet vanes in the nozzle section of the thrust chamber (obsolescent).
4) Secondary injection (into the thrust chamber).
5) Auxiliary jets.

The first method is used most frequently, due to its inherent reliability and performance. The first three systems require actuators that may be operated by hydraulic, pneumatic, or electric means. The remaining systems are controlled by flow regulation.

TVC systems using actuators. Figure 7-3 presents a simplified schematic for a TVC system employing hydraulic or pneumatic actuators. It can serve to explain the fundamentals of closed-loop TVC, even through the systems used in practice may differ significantly in detail. The actuators are controlled by commands, originating in the vehicle's guidance system, the commands being a function of the vehicle's deviations from a prescribed path and of its response to corrective steering action. The command signals are fed through an electronic TVC logic to servovalves. In the system shown in Fig. 7-3,

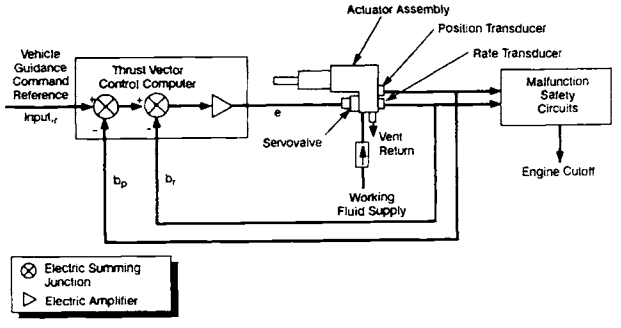

Fig. 7-3 Typical schematic of a thrust-vector-control system using hydraulic or pneumatic actuators.

each servovalve modulates the fluid flow to its respective actuator assembly in response to an electrical error signal proportional to the difference between desired actuator position and its actual position. Feedback of the actual position is obtained through a transducer attached to the actuator. Additionally, a rate transducer senses the actuating speed and applies it to the control computer to stabilize the closed-loop control through adequate damping. Instead of a rate transducer, electronic differentiation of the position transducer output may serve the same end. Malfunction safety circuits make engine cutoff in the event of erratic operation.

Figure 7-4 shows a typical schematic for a TVC system using electromechanical actuators powered by a reversible 28-volt dc motor. The control computer consists of summing junctions and an amplifier, as in the case of hydraulic actuators. The dc motor driving the actuator is controlled by the error signal generated by comparing the guidance-command reference input with systems-position feedback. To provide adequate systems damping, a rate generator or differentiation of the position signal gives the actuating speed.

Engine-to-vehicle interfaces with actuator systems. Many factors affect efficient actuator performance.

Engine installation and alignment. To keep demands to the minimum on the vehicle's guidance and engine-actuation systems, the engine thrust vector must be properly prealigned with respect to the vehicle attachment point in all three planes. Typical specified tolerances are ±0.25 in. laterally and ±0.5° vertically.

The significance of good thrust alignment can be seen from the fact that in an engine cluster, at the randomly distributed maximum of these tolerances, a trim deflection of close to 0.5° would be required from all engines to offset the misalignment.

For larger (looser) alignment tolerances, the trim deflection would be further increased. Even if the trim deflections seem to reduce effective thrust and guidance capability only slightly, the need to apply them for the full duration of powered flight would appreciably reduce payload.

It is customary to align the engine thrust vector to the upper face of the gimbal bearing before shipment. Both optical and dynamic methods (load cells) are used. The optical (cold) alignment establishes the geometrical location of the thrust vector in the shop, by finding the centers of nozzle throat and nozzle exit and aligning their connecting line perpendicular to the gimbal plane. A simple plumb attached to the injector center can aid this operation. Subsequently, during engine firing, this measurement may be confirmed dynamically using side-load cells in lieu of gimbal actuators. As a rule, after a few engines have been aligned in this manner, experience will permit meeting specification by optical means alone. The vertical alignment can be documented simply as the eye-to-eye distance of the actuator attach points or as the line through two index points (Fig. 7-5). Lateral dimensions can be marked in a suitable manner at or on the gimbal bearing face. If the mating vehicle face has been properly aligned to

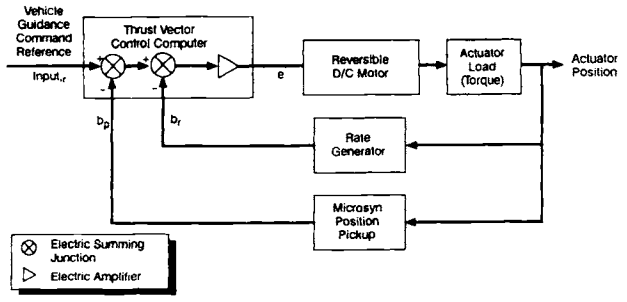

Fig. 7-4 Typical schematic for a thrust-vector-control system using electromechanical actuators.

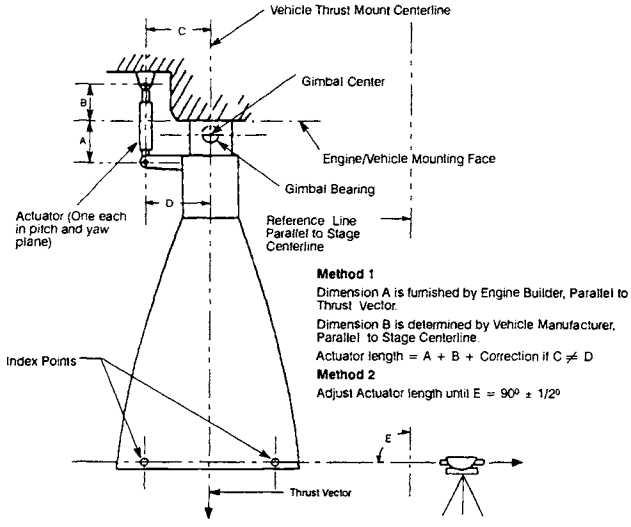

Fig. 7-5 Engine alignment.

the vehicle axes, installation of the engine then simply consists of attaching it and observing the engine logbook specifications. Figure 7-5 shows installation methods of a prealigned engine into the vehicle. For the first vehicles of a new type produced, it is advisable to specify verification of engine alignment following transportation to the launching site.

Actuators, loads. Actuators can be of the hydraulic-piston, hydraulic-rotary, or electromechanical type. Gimbal actuators are attached to the engine at one end and to the vehicle at the other (Fig. 7-5). They may be procured by the vehicle builder or by the engine builder, but must be properly dimensioned. The attachment points at either end must be capable of absorbing, with an adequate reserve, the forces encountered. As a rule, two actuators will be required for each engine. Together, they permit deflection of the engine in all directions. It is important to note that, if an individual actuator produces a maximum deflection of, say, 7 deg, the consequence will be approximately 10 deg of maximum angle ("corner deflection") from a pair of actuators. The ducts, flex lines, gimbal bearing, and possibly other components affected must be able to "take" this deflection.

Selection and design of the actuators is based on the gimbal forces required. In a typical case, the ac-

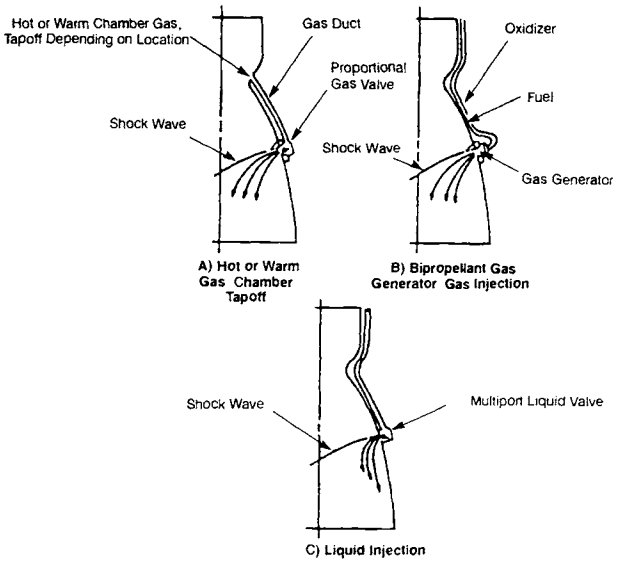

Fig. 7-6 Secondary injection systems.

tuator force may be as high as 25% of the engine thrust level. The force is determined by considering inlet-duct reactions, flexible serviceline reactions, gimbal bearing friction, heat-shield reaction (if any), correction for misalignments, aerodynamic loading (if any), vehicle acceleration effects, inertia of gimballed mass, and miscellaneous minor effects.

The engine design must reduce these forces to a minimum for the smallest size and lightest weight of the actuators and associated equipment. Recognition of this need and careful design can do much toward this goal. The system must be capable of stable, well-damped response when cold gimballed, such as during prelaunch checkout, even though the loads encountered there may be quite different from those occurring during engine firing. This dual-load situation may pose serious problems.

During startup of the engine, brief peak side-loads, in excess of those occurring during normal gimballing, can be generated by the thrust chamber itself, especially with high-expansion-area nozzles being developed at sea level. Unless these loads can be eliminated or at least reduced, they must be considered in the design of actuators and attach points at both ends.

Crosstalk and spring rate. Since the engine and vehicle designers are not entirely independent regarding actuator installation, a situation may exist wherein motion of the actuator in one plane affects the other actuator it its plane. This is referred to as "crosstalk." Excessive crosstalk may develop control instabilities. The engine designer and vehicle builder need close coordination to minimize crosstalk.

The actuator must be able to translate its motion without delay into engine deflection. If the control loop formed by actuator, engine structure, and vehicle thrust-structure is "soft,"—if it has a low spring rate (lb/in.)—the engine will not react promptly to an actuator motion as called for by the guidance system, but rather delay, with subsequent overshoot and continued oscillation. The natural frequency of this oscillation is a function of actuator stroke per degree of engine deflection, feedback gains, and compensation-network parameters.

Secondary injection. Thrust vector control through secondary injection of matter into the thrust-chamber nozzle ("SITVC") has been successfully applied to solid motors. It has found only limited, and then predominantly experimental, application in liquid-propellant propulsion systems, where it appears promising for upper-stage engines, in which the lateral forces required are smaller than with boosters. Secondary injection employs, principally, gas injection using inert stored gas, thrust-chamber tapoff [Fig. 7-6(a)], or a gas generator [Fig. 7-6(b)] or liquid injection [Fig. 7-6(c)] using inert fluid or propellants.

In a gimballed thrust chamber, the side force acts approximately at the injector end. With an SITVC system, the applied side force acts downstream of the nozzle throat and approximately at the point of injection, resulting in a longer moment arm, which decreases the required side force.

Performance evaluations. The performance of any type of secondary injection system is based upon two performance factors: amplification K and axial-thrust augmentation K_1, defined as follows:

$$K = \frac{Is_s}{Is_p} = \frac{F_s/\dot{w}_s}{F_p/\dot{w}_p} = \frac{F_s/F_p}{\dot{w}_s/\dot{w}_p} \tag{7-1a}$$

$$K_1 = \frac{Is_a}{Is_p} = \frac{\Delta F_a/\dot{w}_s}{F_p/\dot{w}_p} = \frac{\Delta F_a/F_p}{\dot{w}_s/\dot{w}_p} \tag{7-1b}$$

where—

$\dot{w}_s$ = secondary flow rate, lb/s
$\dot{w}_p$ = primary flow rate, lb/s
F_s = side force, lb
F_p = undisturbed axial primary-thrust, lb
ΔF_a = axial-thrust increase, lb
Is_p = undisturbed axial specific impulse of the primary chamber F_p/w_p, s
Is_s = side specific impulse Fs/w_s, s
Is_a = secondary axial specific impulse $\Delta F_a/w_s$, s

Essentially, the K factor determines the quantity of fluid required to obtain the side force, and the K_1 factor determines the penalty on the overall system I_s to obtain the required side-force. Both of these factors known, the total effect of a given secondary-injection system on a propulsion system may be determined. The K factor determines the quantity of secondary injectant fluid required (for a known duty cycle). The K_1 factor evaluates the I_s penalty on the propulsion system. If K_1 equals 1, the specific impulse of the secondary fluid will equal that of the primary fluid, and therefore the propulsion system will suffer no Is penalty due to the SITVC system.

Both the amplification factor K and the thrust-augmentation factor K_1 are influenced by the secondary-injection orientation. For each application, a tradeoff must be made between the two factors to de-

termine the optimum injection orientation for maximum propulsion efficiency. Side forces for a given w_s are increased if injection is made through a series of holes arranged on a horizontal arc, rather than through a single orifice. Note that the manifolds required in this case may adversely affect response, however. In a typical tapoff SITVC system, the gas flow rate may be 1.5 to 2.5 percent of the primary flow rate, the upper value indicating the situation of maximum force required between two injection stations (two jets operating).

The performance of a gas generator SITVC system is comparable to that of a tapoff system, probably slightly better. This if offset by higher complexity (valves, injectors, ignition, cooling).

Liquid injection systems (inert fluid or propellants) offer the simplest arrangement. This is offset by their lower performance, K-factors being in the order of unity, at flow rates from 5 to 6 percent of the primary flow. However, in systems with low-duty cycles, they may still be very attractive.

As a rule, four injection elements are required for a given system, equally spaced on the main chamber circumference, of which no more than two adjacent ones would be operating at a given time. The control of the required valves is accomplished through a logic and a servosystem analogous to that of a hydraulic gimbal actuator system.

CCM Concept and Preliminary Design Development

Before actual control-system logic development, mission requirements must be defined and functional analyses performed. Developing and selecting the most suitable CCM system and components for a particular application will be aided by the methodology shown in Fig. 7-7. It covers both classical and modern control-system design, and is representative of current usage in government and aerospace organizations for CCM system selection (Ref. 7-1).

Requirements generation and analysis. Basic CCM requirements are generated by the customer with contractor participation. Typically, technical requirements for a CCM system flow down from the mission, vehicle, and engine requirements. Figure 7-8 outlines sample CCM system-requirement considerations based on this flow-down. The level and scope of requirement considerations for any particular application vary widely, depending on the customer and magnitude of the program.

Functional analysis/allocation. Performed in the concept and preliminary-design phases after the complete set of requirements has been generated, functional analysis consists of determining what must be done by the CCM system to meet the mission requirements. Figure 7-8 outlines representative functional-analysis considerations. Functional flow diagrams usually aid an analysis. Figure 7-9 shows an example of a functional flow diagram for a typical orbital-transfer-vehicle (OTV) engine. The functional analysis will define the major components and internal and external interfaces of the CCM system.

Synthesis. Functional-analysis allocations will be used in the synthesis of several candidates for CCM architecture—the fundamental organization of the CCM system. The following must be accounted for in defining an architecture configuration: hierarchical levels of control, distributed processing vs. centralized processing, functional emphasis, subsystem partitioning, software architecture, and redundancy configurations.

Once defined, candidate CCM systems can be modeled and simulations run to define their performance in terms of meeting the system requirements. Trade studies between the candidate systems will use the simulation results. Evaluations are usually conducted in terms of selected system-parameter values or performance characteristics as defined in the requirements phase of the analysis. The CCM concept that best satisfies the mission needs goes into development.

Figure 7-10 shows a representative example of a modern control-system architecture, the SSME Block 11 controller. It is a dual redundant system with cross-strapping between the three major subsystems—input electronics, data processor, and output electronics—designed so that no single-point failure will ever cause the system to malfunction. A first failure causes switchover to an alternative channel of electronic hardware/software. A second failure in the alternate channel causes electrical/hydraulic lockup (engine valves and controls maintained in position) or safe shutdown (depending on the operational profile). This redundancy approach is termed *fail-operate/fail-safe.*

Control Methods

As mentioned earlier, control systems may be generally classified as either open-loop or closed-loop.

Open-loop control. Figure 7-11 shows a generic example of this type of control system along with its advantages and disadvantages. This system uses preset controls, such as orifices and on-off command devices.

A typical example of open-loop control, an engine propellant-flow system calibrated to a fixed set of conditions, has the propellant flows controlled simply by opening and closing the propellant valves. Thus, minor deviations from the design mixture ratio or propellant flow rates, such as from fabrication tolerances of engine components, can be corrected beforehand by insertion of accurately sized orifices into the propellant-flow lines to effect the desired pressure drops. The extent of correction would be determined from preflight-calibration test data. Open-loop control has the advantage of simplicity, but it is limited to a specific set of operating parameters, and is unable to compensate for variable conditions during operation.

Accurate sequencing of an open-loop control system as may be used for engine start and stop, usually with the aid of interlocks. For example, the propellant valves of many small engines or gas generators are mechanically linked and are operated by a single actuator. Adjusting the relative positions of the valve gates or poppets, with respect to the mechanical linkage, will properly sequence fuel and oxidizer valves.

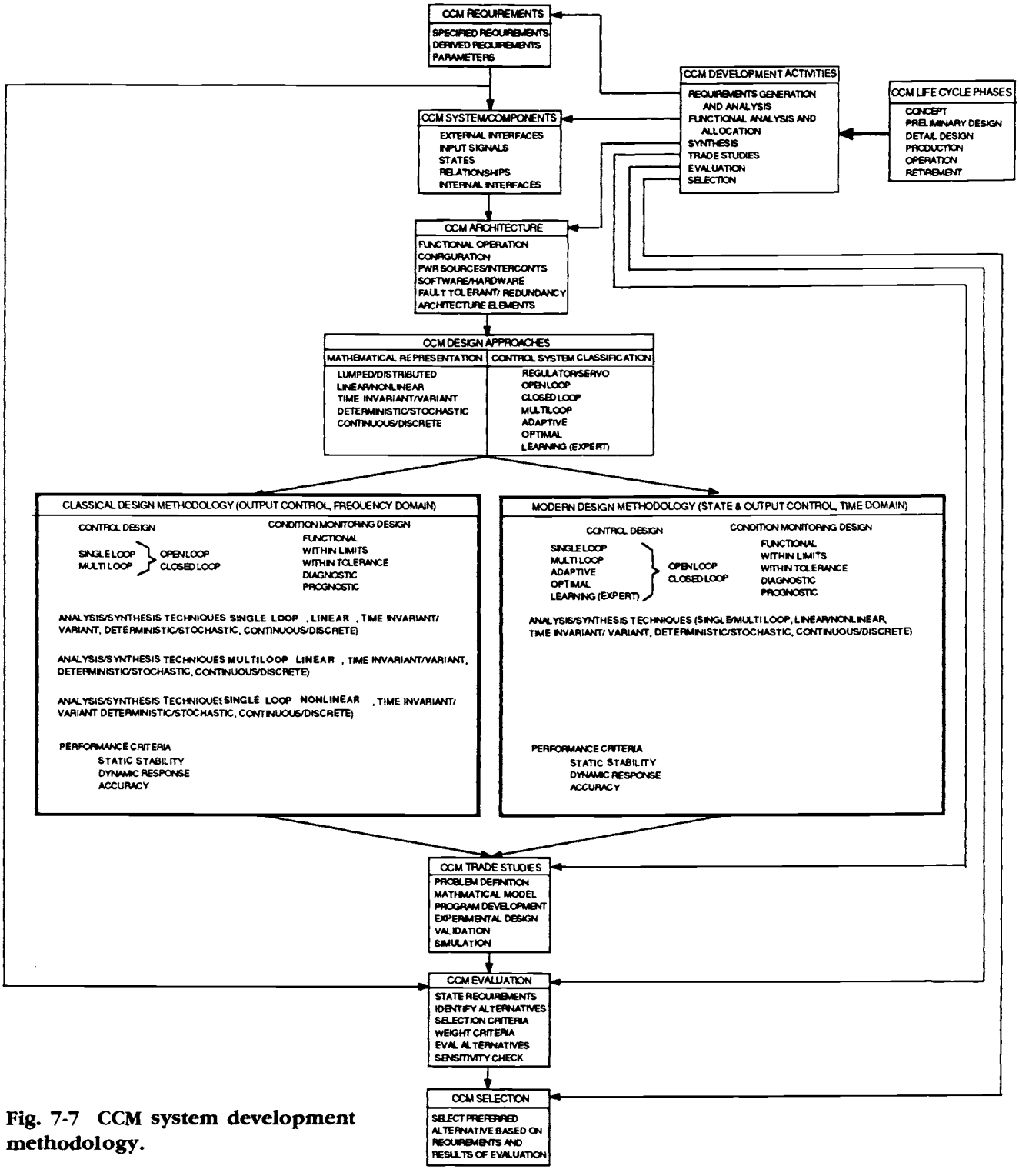

Fig. 7-7 CCM system development methodology.

Closed-loop control. Also called feedback control, this type of system usually includes sensors to measure control or engine-operating parameters, microprocessors to analyze the sensor data, and effectors to implement the control strategy. Unlike open-loop control, closed-loop control depends on the magnitude of an error signal (deviation of desired output from measured output) to bring about a correction. In general, closed-loop control aims to minimize errors during operation and reduce system sensitivity to environmental changes and changes in component characteristics. It is applied to areas such as engine thrust control and/or throttling, propellant mixture-ratio control, and thrust-vector control. Figure 7-12 shows a generic closed-loop control system and points out the advantages and disadvantages of this type of system.

A desire to make rocket-engine control more robust and stringent has brought about enhancements to the classical closed-loop diagram of Fig. 7-12.

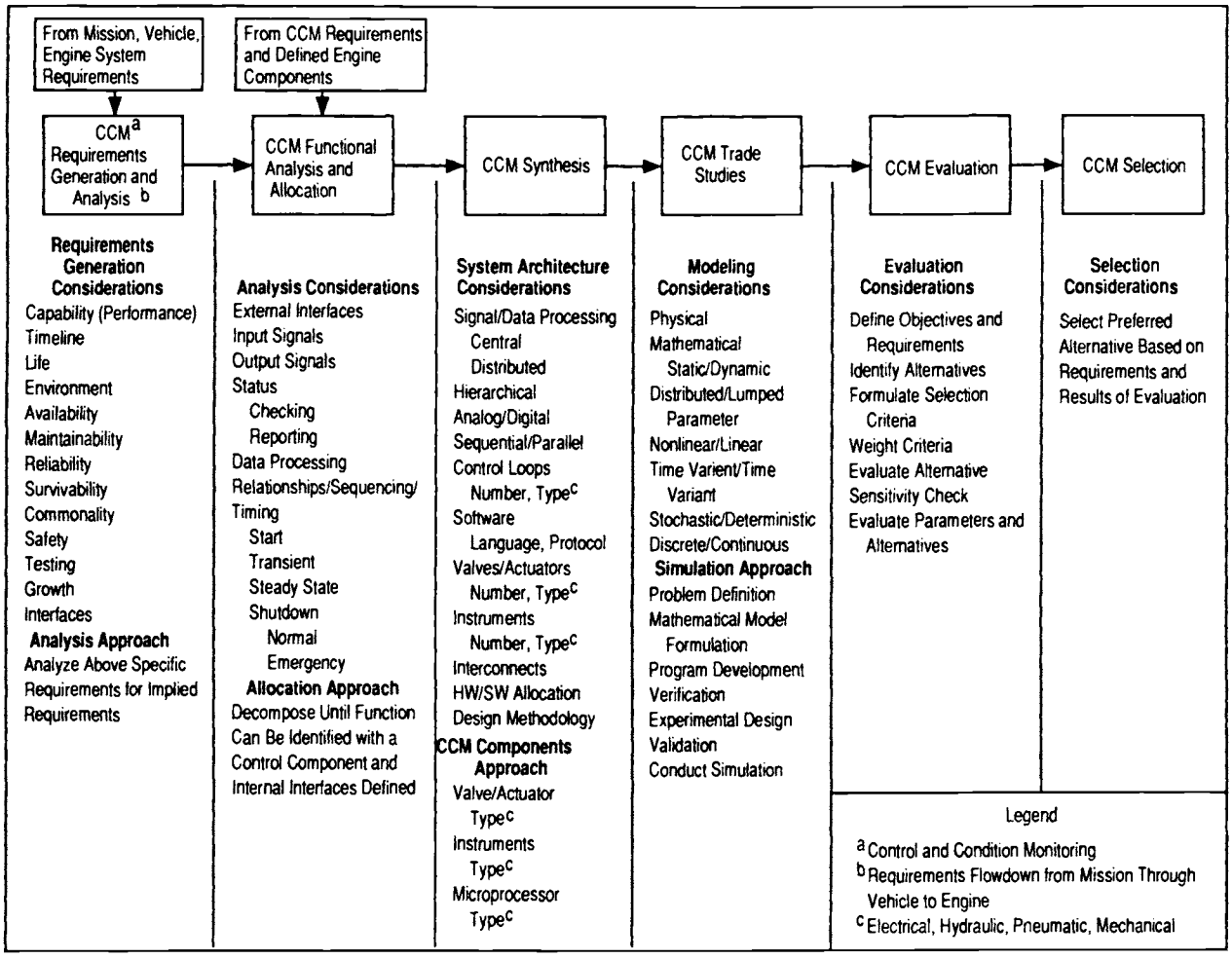

Fig. 7-8 CCM system development considerations.

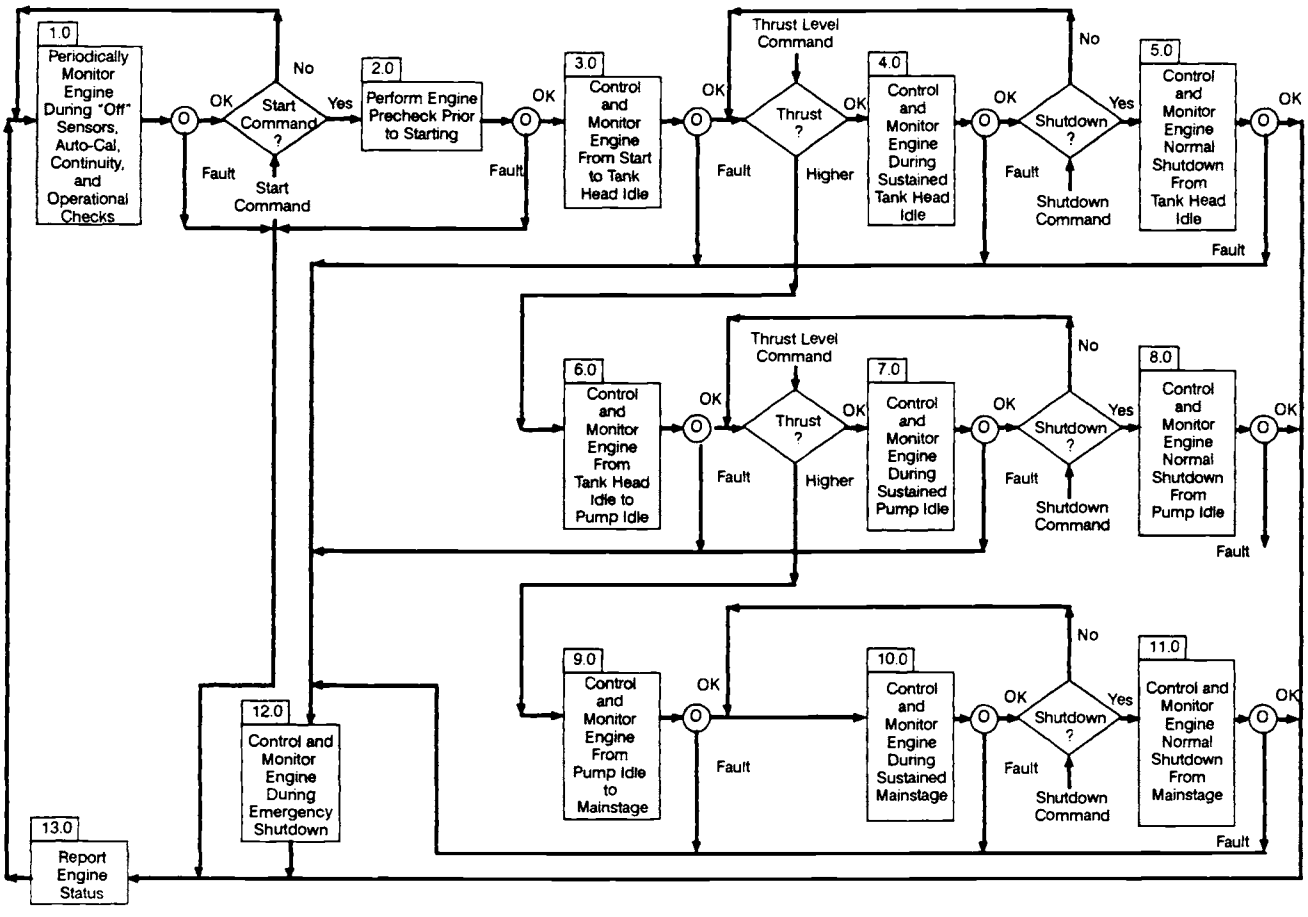

Fig. 7-9 Orbital transfer vehicle (OTV) engine control system—top-level-function flow diagram.

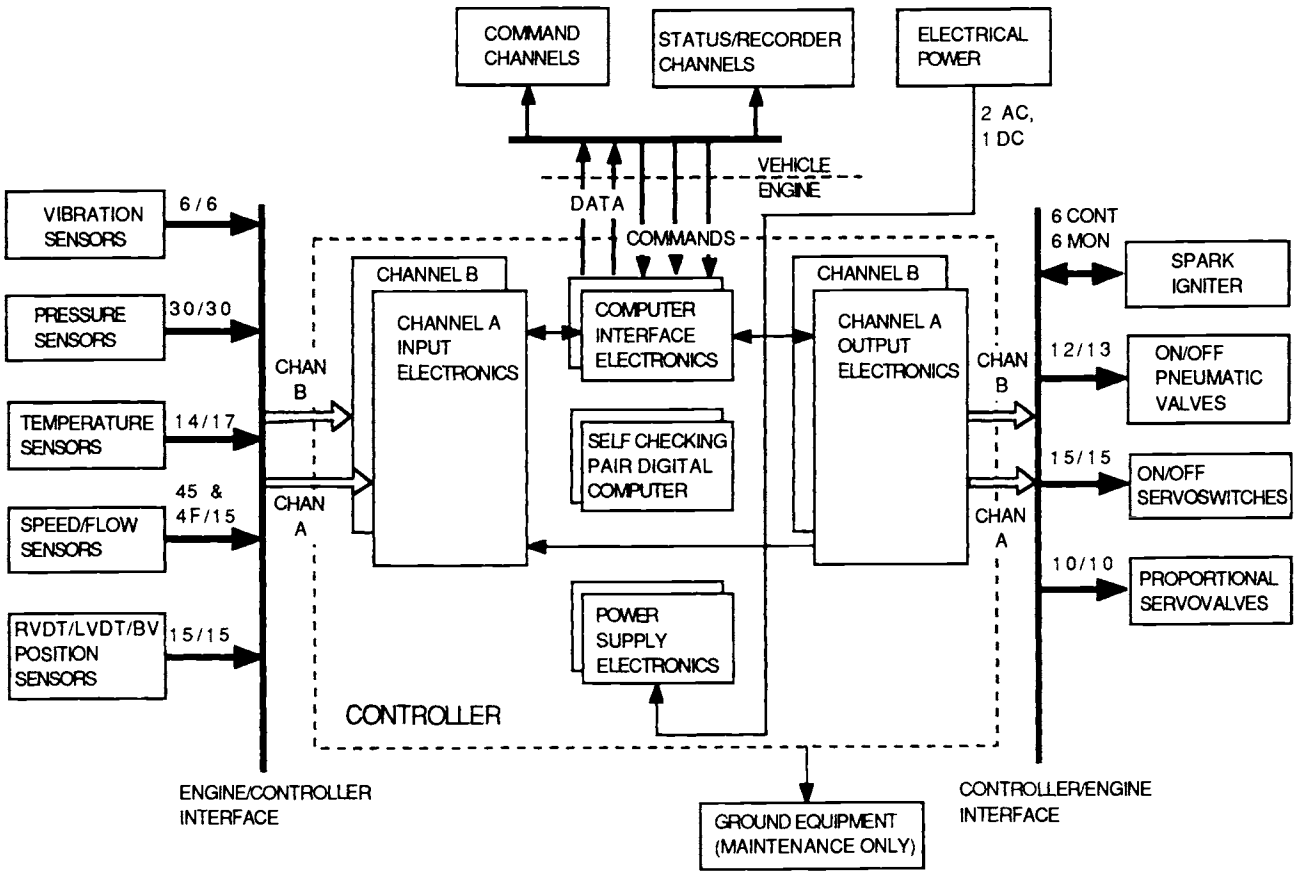

Fig. 7-10 SSME block 11 controller.

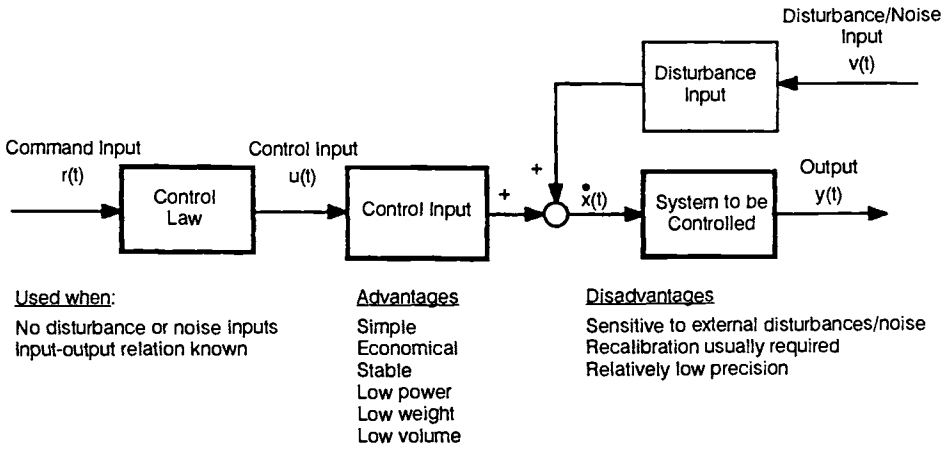

Fig. 7-11 Block diagram of an open-loop control system.

Optimal control strategies try to optimize the system with respect to a chosen operating parameter. In an adaptive-control approach, loop operating characteristics are changed to maintain control for predictable departures from the normal control mode. Closely related to the adaptive strategies are the knowledge-based (expert system) control approaches. Here, the control system has the ability to change loop operating characteristics to maintain control for unpredictable departures from the normal control mode. An onboard, real-time computerized system performs operating-system identification, develops a revised set of control laws, and then uses the adaptive component of the system to control the engine or vehicle. Figure 7-13 shows a schematic diagram of a CCM system design using an expert system with adaptive control.

Control-law Development

The previous two sections have focused on the fundamental aspects of defining the requirements of the

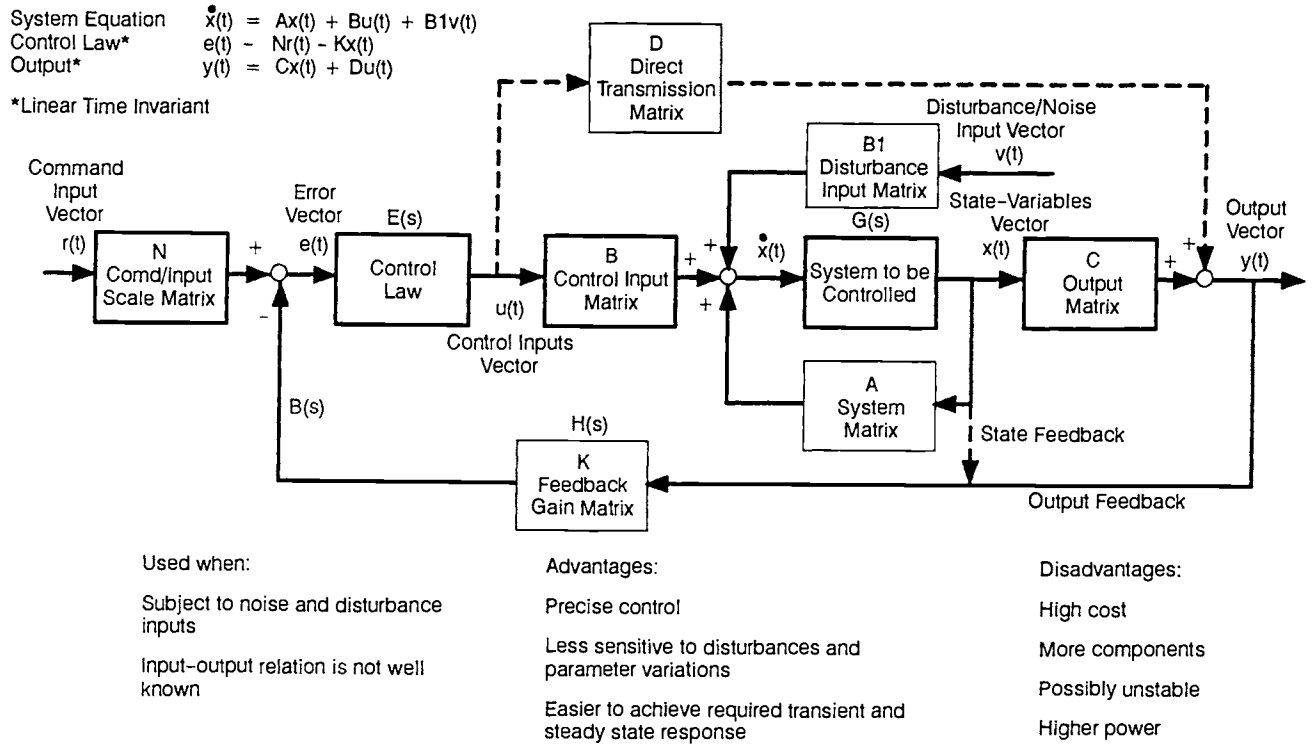

Fig. 7-12 Block diagram of a closed-loop control system.

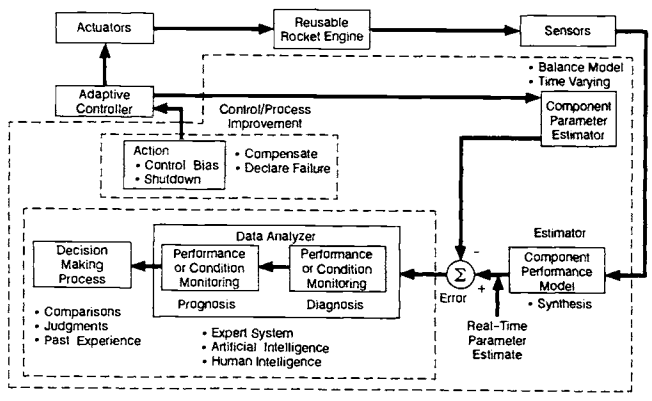

Fig. 7-13 CCM design of an expert/adaptive control system.

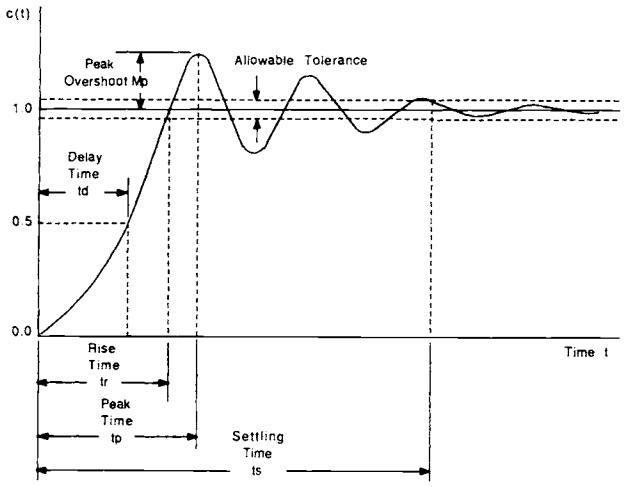

Fig. 7-14 Time-response specifications.

control system and have given an overview of the different types of control methods available to meet the mission objectives. This section discusses approaches that can be used in the design and development of a control system.

Classical control. Classical control methodology is applicable to control design problems in which the characteristics of the system to be controlled are not precisely known or in which simplifying assumptions can be made if the system is complex. Classical control views each system component as a block in which the input and output are related by a transfer function. This approach simplifies the solution by combining the behavior of the internal components of the system to be controlled into one system block (transfer function) to provide a relatively quick-and-easy design tool for control-system development. It has the disadvantage, however, of not revealing the *internal* behavior of the system.

Classical control is applicable to both open- and closed-loop designs. Being a single input-single output (SISO) approach, it does not have the ability of multiloop control system design in the strictest sense; but, some classical quasi-multiloop techniques have been developed. Classical control methodology must confine itself in practice to a lumped-parameter, linear, time-invariant modeling representation, with either stochastic, deterministic, or discrete time-capability.

The usual classical approach to a single-loop system designs the control loop on an individual basis by using one of the techniques mentioned below. For multiloop control systems, the loops are designed on an individual basis, normally resulting in various degrees of cross-coupling between them. The remainder of the system design consists of enhancing or eliminating the cross-coupling between the loops (using the methods described here under "Classical Multiloop Design Techniques") to achieve the best possible compromise design for the intended application. Classical control design can also be used to design both single and multiloop adaptive systems (i.e., when control operating regime changes can be predicted) by providing for gain changes (gain scheduling). This type of approach has been used on the SSME. Recently, classical control methodology designs, incorporating learning (expert) capability (i.e., when control operating regimes are used to define a "knowledge-base") have been receiving great attention.

Classical linear design techniques. The primary design approaches used in linear, classical control are the time- and frequency-response techniques. In the time-response approach, a step, ramp, parabolic, or impulse signal is used as an input into a control system to define its output characteristics in terms of a mathematical model of the system. Analytically, the Laplace transform is often used to transform the model from the time domain to the complex S-Plane domain. The problem is therefore transformed from a set of time-dependent differential equations to a set of time-independent algebraic equations. The solution to the algebraic set is then transformed back into the time domain by using the inverse Laplace transform.

In the time domain, system response characteristics and requirements can be specified in terms of delay time td, rise time, tr, peak time tp, peak overshoot Mp, settling time ts, and steady-state error. Figure 7-14 shows a representative time-response wave.

Performance indices may also be used to evaluate CCM performance during system development. Frequently used performance indices for a control-law development in the time domain are the following:

Integral square error ISE

$$= \int_0^{00} e^2(t)dt \qquad (7\text{-}2)$$

Integral of the absolute magnitude of error

$$IAE = \int_0^T |e(t)|\,dt \qquad (7\text{-}3)$$

Integral time-absolute error

$$ITAE = \int_0^T t\,|e(t)|\,dt \qquad (7\text{-}4)$$

Integral time-square error

$$ITSE^2 = \int_0^T te^2(t)dt \qquad (7\text{-}5)$$

Complimentary to the time-domain response technique, the frequency-response approach uses sinusoidal signals as inputs to determine the output characteristics of the system in the frequency domain. The output is displayed by means of Bode plots, root-locus diagrams, Nyquist diagrams, Nichols charts, and/or inverse Nyquist diagrams. Lengthy discussions of both the time- and frequency-domain approaches can be found in basic control textbooks (Ref. 7-2 through 7-6).

Classical nonlinear design techniques. Two additional techniques in classical control can aid the design of nonlinear systems: the describing function and the phase plane.

Describing function. The describing function, essentially a generalized transfer function for nonlinear systems, based on a restricted mathmatical foundation, is easy to apply, gives reasonable results, and can be used for systems of any order. The analysis assumes that a sinusoidal signal input to a nonlinear element has an output signal with the same fundamental period as the input. It is further assumed that all harmonics, subharmonics, and dc components can be neglected (a reasonable assumption for most feedback situations). And it is assumed that the feedback control system has only one nonlinear component, and that time-invariant. Describing functions are generated from Fourier series analysis of the output waveform. Once the nonlinearity has been characterized, various methods of compensating for it, such as reducing system gain, adding a phase-lead network, or introducing rate feedback, can be examined. Nyquist diagrams and Nichols charts are the most revealing techniques for stability analysis for the describing-function approach

Phase plane. Although associated with the classical approach, the phase-plane method, a state-space analysis, specifically concerns the solution of a second-order, nonlinear, time-invariant differential equation. It is a technique for analyzing the transient response of a feedback control system to a step input or for solving an initial-condition problem. Different curves of displacement vs. velocity, called trajectories, are generated for a series of step functions. The resulting family of curves defines the phase portrait. If the trajectory approaches infinity, the system is unstable. If the trajectory circles the origin continuously in a closed curve, a sustained oscillation (limit cycle) results. If the phase trajectory approaches the origin, the system is stable.

There are three procedures to construct the phase portrait of a system. Two are analytical: direct solution of the differential equation and transformation of the second-order differential equation to a first-order one. The remaining, a graphic method, isoclines, is the most useful of the three.

Classical multiloop design techniques. In recent years, the classical approach has been ex-

tended for certain limited cases to multi-input, multi-output (MIMO) systems. A transfer-matrix approach is used to diagonalize or decouple the system representative with a shaping-function matrix. The decoupled-loops can then be designed with such SISO techniques as the direct or inverse Nyquist array or direct or inverse characteristic-locus methodologies.

Control laws. The following equation expresses the most general and standard control law—the proportional-integral-differential (PID) control:

$$\underset{\{P\}}{} \qquad \underset{\{D\}}{} \qquad \underset{\{I\}}{}$$

$$p = K_c\varepsilon + K_c\tau_D\frac{de}{\delta\tau} + \frac{K_c}{t_I}\int_0^t edt + p_s \qquad (7\text{-}6)$$

where—

K_c = gain, τ_D = derivative time (min), τ_I = integral time (min), ε = error, and p_s = constant

Generally, it will be preferable to use the simplest procedure possible in designing the control system. However, using only the proportional mode results in degraded static accuracy caused by inherent offset-error. Adding integral control eliminates the offset but may cause large overshoot. The addition of derivative control achieves more rapid transient response and tends to decrease initial errors. Various combinations, such as proportional integral (PI) and proportional differential (PD), can meet the control requirements. If the controller cannot meet the control requirements, it will be necessary to design a compensator to move the control design into a region where the system design can provide accurate transient-and-stable operation.

Classical control system examples. An example, a multiloop system, will demonstrate the modern approach to classical control-system design. By showing how the system is modeled and control laws written, both single input/output and multiple input/output type problems can be covered simultaneously.

Multiloop-output-control example (Ref. 7-7). A two-input, two-output regulator system (Fig. 7-15) is required to control the temperatures T_1 and T_2 of a propellant in two interconnected tanks. The desired temperatures T_{r1} and and T_{r2} are set on input potentiometers that supply the command voltages E_{r1} and E_{r2}. The tank temperatures are sensed by thermistors whose outputs E_{01} and E_{02} are compared to the command voltages to obtain the errors e. The controller uses these to synthesize a control law u. The controller output signals u_1 and u_2 are boosted by thyristor amplifiers that supply power to resistance heaters (Fig. 7-15). Let w denote the product of the volumetric flowrate, density, and specific heat of the propellant and T_d the entrance temperature. Let C_1 and C_2 denote the thermal capacitances of the tanks, and q_1 and q_2 be the heat per unit-time generated by the heaters. Then conservation of energy for each tank yields—

$$C_1\frac{dT_1}{dt} = w(T_d - T_1) + q_1 \qquad (7\text{-}7)$$

$$C_2\frac{dT_2}{dt} = w(T_d - T_2) + q_2 \qquad (7\text{-}8)$$

For small deviations about equilibrium, q_1 and q_2 are related linearly to u_1 and u_2, respectively, as follows:

$$\dot{q}_1 = c_3u_1 \qquad (7\text{-}9)$$

$$\dot{q}_2 = c_4u_2 \qquad (7\text{-}10)$$

where the constants c_3 and c_4 include the power-amplifier gains. Letting $x_1 = T_1$, $x_2 = T_2$, $\tau_1 = C_1/w$ and $\tau_2 = C_2/w$. Using Eq. (7-9) and (7-10) in Eq. (7-7) an (7-8), respectively, with $b1 = c_3/C_1$ and $b_2 = c_4/C_2$ yields—

$$\frac{dx_1}{dt} = -\frac{1}{t_1}x_1 + b_1u_1 + \frac{1}{t_1}T_d \qquad (7\text{-}11)$$

$$\frac{dx_2}{dt} = \frac{1}{t_2}x_1 - \frac{1}{t_2}x_2 + b_2u_2 \qquad (7\text{-}12)$$

where the inlet temperature deviation T_d is the disturbance. The power and speed of modern microprocessors and associated software have made it more convenient to formulate the system equations in matrix form. Therefore, Eq. (7-11) and (7-12) can

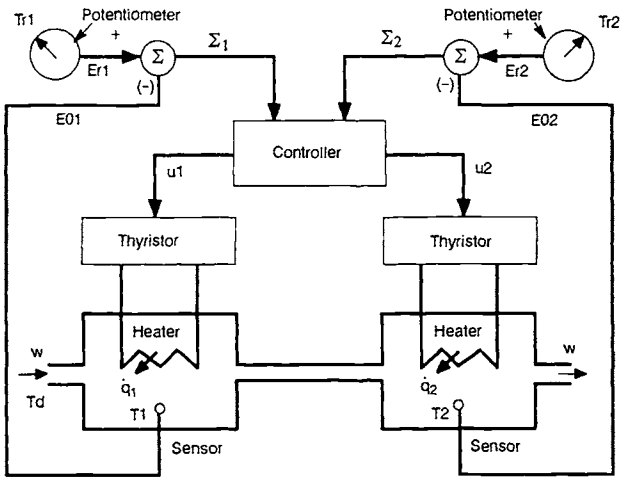

Fig. 7-15 Multiloop system.

be expressed as the matrix equations:

$$\frac{dx}{dt} = Ax + Bu + B_1T_d \qquad y = Cx$$

The relevant matrices will be defined by—

$$A = \begin{bmatrix} \frac{-1}{t_1} & 0 \\ \frac{1}{t_2} & \frac{1}{t_2} \end{bmatrix} \quad \mathbf{B} = \begin{bmatrix} b_1 & 0 \\ 0 & b_2 \end{bmatrix}$$

$$\mathbf{B}_1 = \begin{bmatrix} \frac{1}{t_1} \\ 0 \end{bmatrix} \quad \mathbf{C} = \begin{bmatrix} 1 & 0 \\ 0 & 1 \end{bmatrix} \qquad (7\text{-}13)$$

The transfer-function matrices, relating the outputs to the control inputs and the disturbances, will be given as follows:

$$Y(s) = C\,(sI\text{-}A)^{-1}\,BU(s) + C(sI\text{-}A)^{-1}\,B_1T_d \qquad (7\text{-}14)$$

After proper substitutions, the inverse matrix reduces to—

$$(s\,I - A)^{-1} = \frac{1}{\left(s + \frac{1}{t_1}\right)\left(s + \frac{1}{t_2}\right)} \begin{bmatrix} s + \frac{1}{t_2} & 0 \\ \frac{1}{t_2} & s + \frac{1}{t_1} \end{bmatrix} \qquad (7\text{-}15)$$

Substituting Eq. (7-13) and (7-15) into Eq. (7-14), it follows that—

$$Y(s) = \b\bc\[(\a\co2\vs10\hs10(\f(b\s(,1),s + \frac{1}{t_1}),$$

$$0, \frac{\frac{b_1}{t_2}}{\left(s + \frac{1}{t_1}\right)\left(s + \frac{1}{t_2}\right)}, \frac{b_2}{s + \frac{1}{t_2}})) \mathbf{U}(s) + \begin{bmatrix} \frac{1}{t_1} \\ \frac{1}{s + \frac{1}{t_1}} \\ \frac{1}{t_1t_2} \\ \frac{}{\left(s + \frac{1}{t_1}\right)\left(s + \frac{1}{t_2}\right)} \end{bmatrix} T_d \qquad (7\text{-}16)$$

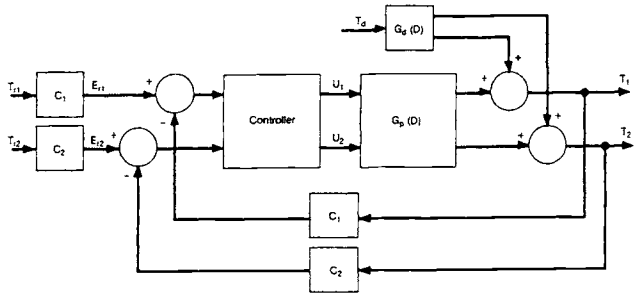

Fig. 7-16 Multivariable feedback control.

Equation (7-16) has the form—

$$Y(s) = G_p(s)U(s) + G_d(s)T_d(s) \qquad (7\text{-}17)$$

where $G_p(s)$ is the 2x2 plant matrix and $G_d(s)$ is the 2x1 disturbance matrix defined in Eq. (7-16). Figure 7-16 shows a block diagram of the control system.

Having formulated the mathematical representation of the system, a control scheme must be chosen. In this example, a PI controller was designed for each of the outputs. The system and disturbance matrices are given by Eq. (7-16). Assume that $t_1 = t_2 = 10$ and $b_1 = b_2 = 100$. With these parameter values the matrices become—

$$G_p(s) = \begin{bmatrix} \frac{100}{(s+0.1)} & 0 \\ \frac{10}{(s+0.1)^2} & \frac{100}{(s+0.1)} \end{bmatrix} \quad G_d(s) = \begin{bmatrix} \frac{100}{(s+0.1)} \\ \frac{10}{(s+0.1)^2} \end{bmatrix} \qquad (7\text{-}18)$$

A matrix, the decoupling compensator matrix, will make the plant matrix Gp(s) relating output (Y(s)) to the control U(s) become a diagonal matrix. This greatly simplifies the solution procedure. The decoupling compensator matrix is chosen as—

$$G(s) = \begin{bmatrix} 1 & G_{12}(s) \\ G_{21}(s) & 1 \end{bmatrix} \qquad (7\text{-}19)$$

Post-multiplying Gp from Eq. (7-18) by G(s) yields—

$$G_pG = \begin{bmatrix} \frac{100}{s+0.1} & \frac{100G_{12}}{s+0.1} \\ \frac{10}{(s+0.1)^2} + \frac{100G_{21}}{s+0.1} & \frac{100}{s+0.1} \end{bmatrix} \qquad (7\text{-}20)$$

We want this matrix to be diagonal; therefore, set—

$$G_{12}(s) = 0 \quad G_{21}(s) = -\frac{0.1}{s+0.1}$$

In this case the diagonal elements of Eq. (7-20) are identical to the diagonal elements of the system matrix in Eq. (7-18). Now individual PI controllers can be designed for the two uncoupled systems by employing the techniques of single-input, single-output systems. Figure 7-17 shows the resulting control system. Each of the two uncoupled systems is designated as second-order, and the two controller gains can be set to yield the desired natural frequency and damping ratio.

Modern control. As just shown, classical control theory uses input-output relationships, principally the transfer function. After being written, the differential equations describing the system are linearized and subjected to constraints to allow for useful input-output relationships. In contrast to the classical approach, modern control theory makes direct use of the differential equations in the solution approach.

Modern control theory system representations do not obscure the internal behavior of the system, as classical theory may do with the transfer function, and are not limited to linear stationary systems. In theory, there are no limitations to the applicability of modern control theory; but practical limitations do exist. Although it may be possible to represent the system as a set of simultaneous differential equations, it may prove impossible to find solutions. Therefore, the modern approach makes frequent use of digital computers and numerical solutions.

A great deal of research is being done in modern control theory to make its powerful techniques more convenient and practical. Whichever version of the modern approach is chosen, extensive use will be made of the concept of *state space.*

State-variable representation. The "state" of a system means the smallest set of variables that must be known at some time t_0 to predict *uniquely* the future behavior of the system for any specified input. Although the state of the system is unique at any instant of time, a set of state variables is *not.* The individual set of state variables chosen must be linearly independent.

For example, the second-order differential equation for a mass-spring-damper system with an external forcing function may be written as follows:

$$md^2x/dt^2 + Bdx/dt + kx = f_a(t) \qquad (7\text{-}21)$$

Replacing x by x_1 and dx/dt by x_2 allows the second-order differential equation to be written as a set of two first-order equations:

$$dx_1/dt = x_2 \qquad (7\text{-}22)$$

$$dx_2/dt = -(k/m)x_1 - (B/m)x_2 + (f_a/m) \qquad (7\text{-}23)$$

The variables x_1 and x_2 are called the state variables since they define the state of the system (they are just another form of writing the differential equation of motion of the system). These two variables may then be considered to be the components of a state vector x. *State space is then defined as the two-dimensional space with x_1 and x_2 as the coordinates.* For larger systems with more defining equations, the number of state variables will grow accordingly.

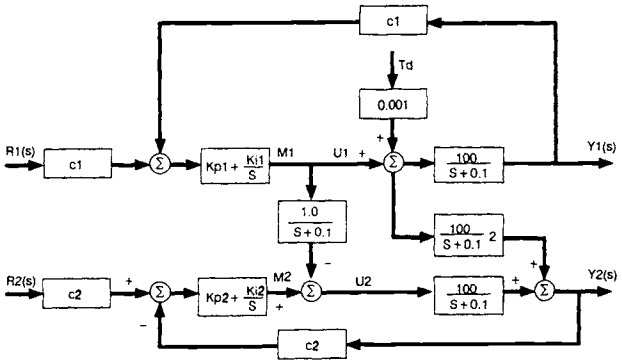

Fig. 7-17 Control system for multiple output.

For a linearized system, it is always possible to write generalized vector equations relating the output vector y to the state vector x and control vector u as follows:

$$dx/dt = A(t)x + B(t)u + B_{1v} \qquad (7\text{-}24)$$

$$y = C(t)x + D(t)u \qquad (7\text{-}25)$$

where A(t) is the plant or system matrix and B(t) is the control matrix. The C and D matrices relate the output variables y to the state x and control u variables. Modern control theory deals broadly with solving and manipulating these two equations. How does this system treat a control law of the following form?

$$u = -Kx + Nr \qquad (7\text{-}26)$$

where r is the command input vector, K the gain matrix, and N a scaling matrix. As formulated, the problem is not well-posed: there are more unknowns than equations. To circumvent this, set—

$$K = pk^T \qquad (7\text{-}27)$$

where the elements of p will be chosen arbitrarily and the elements of k^T will be the roots to be specified. After substituting, the defining equation becomes—

$$dx/dt = (A - Bpk^T)x + BNr + B_{1v} \qquad (7\text{-}28)$$

The resulting closed-loop characteristic equation becomes—

$$|sI = A + Bpk^T| = 0 \qquad (7\text{-}29)$$

which is identical to the characteristic equation of a single-input system. Continuation of the example

presented above for multiloop control will demonstrate how these concepts are applied in the design of a control system.

State feedback control example. A controller was considered in the example "Multiloop Output Control" for a two-input, two-output temperature-control system. With the parameter values used in that example, state equations (7-22) and (7-23) for the system become—

$$\frac{dx_1}{dt} = -0.1x_1+100u_1+0.1T_d$$

$$\frac{dx_2}{dt} = 0.1x_1-0.1x_2+100u_2$$

while the A and B matrices of Eq. (7-13) become—

$$A = \begin{bmatrix} -.01 & 0 \\ 0.1 & -0.1 \end{bmatrix} \qquad B = \begin{bmatrix} 100 & 0 \\ 0 & 100 \end{bmatrix}$$

In the example, the desired temperature values are set by the potentiometers; and if they remain fixed, there will not be a change in the command input vector so that r = 0. We wish to design a regulator for the system. In Eq. (7-26), u = -Kx, arbitrarily select $p_1 = p_2 = 1$. That then gives —

$$Bp = \begin{bmatrix} 100 \\ 100 \end{bmatrix} \qquad Q = [\ \mathbf{Bp} \quad \mathbf{ABp}\ ] = \begin{bmatrix} 100 & -10 \\ 100 & 0 \end{bmatrix}$$

The characteristic Eq. (7-29) of the closed-loop system becomes—

$$\left| \mathbf{sI-A+Bpk}^T \right| = \begin{vmatrix} s+0.1+100k_1 & 100k_2 \\ -0.1+100k_1 & s+0.1+100k_2 \end{vmatrix}$$

$$= s^2+(0.2+100k_1+100k_2)s+0.01+10k_1+20k_2=0 \qquad (7\text{-}30)$$

For this second-order system, the desired roots will be made so that the natural frequency will be 5 rad/sec and the damping ratio 0.7. The desired characteristic equation will then be—

$$s^2 + 7s + 25 = 0 \qquad (7\text{-}31)$$

Matching the corresponding coefficients of Eq. (7-30) and (7-31) gives $k_1 = 12.363$ and $k_2 = 2.431$. Figure 7-18 shows the structure of this regulator. The transfer function relating the output vector to the disturbance is obtained from—

$$Y(s) = X(s) = \left(\mathbf{sI-A+Bpk}^T\right)^{-1}\begin{bmatrix} 0.1 \\ 0 \end{bmatrix} T_d$$

$$= \frac{1}{s^2 + 7s + 25}\begin{bmatrix} s+243.2 & -243.1 \\ 236.4 & s-236.2 \end{bmatrix}\begin{bmatrix} 0.1 \\ 0 \end{bmatrix} T_d$$

From that will be obtained—

$$Y_1(s) = \left(\frac{0.1(s+243.2)}{s^2+7s+25}\right)T_d \qquad Y_2(s) = \left(\frac{23.64}{s^2+7s+25}\right)T_d \qquad (7\text{-}32)$$

For a step change in the disturbance T_d of magnitude H, the final value theorem yields the limits as t-> ∞ of y_1 and y_2 as 24.32H/25 and 23.64H/25, respectively; these are the steady-state errors.

This example gives some indication of the power of modern control theory. With the block diagram of the system (Fig. 7-18) and the governing equations, the designer can define a controller to eliminate the steady-state errors. It is also possible to experiment mathematically with different system parameters and input conditions.

This brief overview of control-system analysis and design has presented examples to demonstrate the application of the theory to an engineering problem. Complete development of all of the concepts introduced along with numerous examples can be found in Ref. 7-2 through 7-8.

7.2 DESIGN OF FLUID-FLOW-CONTROL DEVICES

Design Considerations for Fluid-Flow-Control Components

Liquid-propellant rocket engines use valves and pressure regulators for controlling fluid flow. Fluids con-

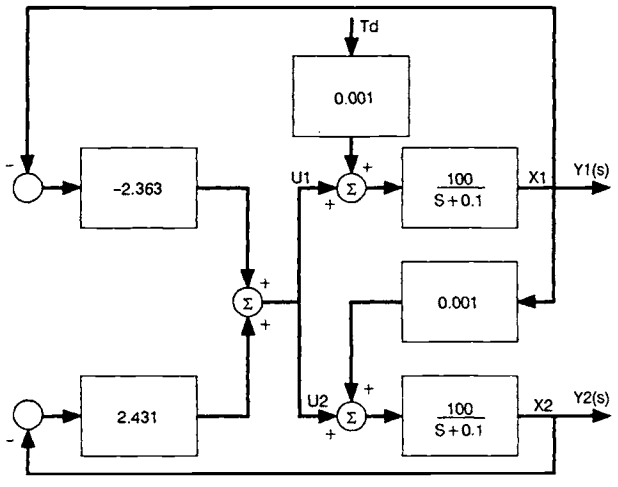

Fig. 7-18 Multiloop regulator.

trolled include propellants, pressurants, and control-system fluids (hydraulic or pneumatic). This section discusses some of the design considerations and analyses governing these components.

Flow and pressure-drop equations for sizing valves. Determining the flow area of a valve from the given flow-rate and pressure-drop data employs equations that contain empirical coefficients. These coefficients are established from test data on the specific type of valve and are specified by various methods. Several of these equations, each containing a unique empirical coefficient, are described in this section. The equations not only provide a basis for computing the required valve flow-area, but also a ready reference for converting from one method of specifying the valve size (flow capacity) to another. Table 7-2 gives nomenclature and units used in this section.

Incompressible-fluid-flow equations are used for fluids having relatively constant density with respect to operating pressure. At moderate pressures, most liquids can be considered incompressible fluids.

The orifice coefficient C together with the incompressible orifice equation defines the flow capacity of valves as well as orifices ("A" is the orifice flow area or valve minimum-flow area, which usually occurs at the seat), as follows:

$$w = \frac{CA}{12}\left[2g\rho\,(P1 - P2)\right]^{1/2} \qquad (7\text{-}33)$$

For orifices, the flow coefficient C is a function of various parameters, including the following:

- The Reynolds number, a dimensionless quantity—a function of line size, fluid velocity, and viscosity. An equation for the Reynolds number appears in Table 7-3.
- The ratio of the line inside diameter to the orifice diameter.
- The geometry of the orifice; i.e., whether or not the orifice has a sharp (or rounded) inlet and the relative length of the orifice.

A large collection of empirical data on orifice coefficients that include the effects of the above parameters will be found in Ref. 7-9.

Use of the incompressible orifice equation for valves is commonplace. Specific values for C are influenced by many of the same parameters that apply to straight orifice flow. However, valves usually have flow paths that are much more complex than orifices, often involving many changes in flow areas and flow direction throughout the valve flow-path. As a result, valve C values can be accurately defined only from flow test-data. Each valve type has its own characteristic value for C. Additionally, within each valve type other factors may cause a variance in C values. For example, consider a pilot valve that has not been designed to minimize pressure drop and has a C of 0.4. On detailed examination of the valve flow-path, one might find that all of the flow areas come close to the value of the minimum-flow area, which occurs at the seat. For this reason, all of the flow velocities within the device will be high, contributing to high differential pressure and thus a low value for C. Another pilot-valve design having an identical seat flow-area might have a higher actual flow capacity, perhaps a C of 0.6, because flow areas in series with the seat are designed to yield lower flow velocities.

The range of orifice coefficients for valves can vary from less than 0.4 for small pilot valves, with

Table 7-2 Nomenclature for flow equations

Symbols

AA	=	arithmetic average surface roughness, in.
A	=	flow area normal to flow direction, in^2
a	=	velocity of sound, ft/s
C	=	flow coefficient for nozzles, orifices, and valves
d	=	hole or hydraulic diamter, in.
D	=	seat mean diameter, in.
e	=	peak to valley surface roughness, in.
f	=	Darcy friction factor
g	=	gravitational constant, 32.174 ft/s^2
h_e	=	equivalent parallel plate gap, in.
h_p	=	parallel plate channel height (gap), in.
k	=	ratio of gas specific heats
K_f	=	resistance factor
K_l	=	pressure loss coefficient
K_N	=	Knudsen No.
K_p	=	permeability constant, $in^3/in^2/s$
L_m	=	channel length, in.
L	=	mean molecular free path, in.
M	=	Mach number
P	=	pressure, psia
ΔP	=	pressure drop, psi
Q	=	volumetric flow at 70°F and 14.7 psia, in^3/min
r	=	resistance, $s^2/ft^3/in^2$
R	=	gas constant, ft/°R
Re	=	Reynolds' number
S	=	incompressible flow function, $ft^{1/2}/s$
T	=	temperature, °R
v	=	volume, in^3
V	=	velocity, ft/s
w	=	weight flowrate, lb/s
W	=	channel width or perimeter, in.
w_m	=	mass weight, lbm

Greek Symbols

μ	=	viscosity, $lb\text{-}s/in^2$
ρ	=	density, lb/ft^3

Subscripts (other than those used above)

a	ambient conditions
1	inlet or entrance conditions
2	downstream conditions
o	stagnation conditions
*	choked conditions (M = 1)
E	exit conditions
S	standard conditions
L	liquid
G	gas

many sharp edges and changes in flow direction, to values higher than 2.0 for ball valves with a smooth flow path and with a minimum-flow area that is the same as the inlet and outlet lines. Conversely, a ball valve (which ideally has a large value of C) can also have a much lower value if the minimum-flow area through the valve is much smaller than the inlet- or exit-line diameters, which will incur expansion and contraction losses.

There are two common methods of using the orifice coefficient and flow equation to specify valve size:

- Effective area A_e, the product of the orifice coefficient and the minimum-flow area for the valve, $A_e = CA$.
- Equivalent sharp-edged orifice diameter (ESEOD). This diameter can be used in the orifice-flow equation as effective area when converted to area and multiplied by a specified orifice coefficient (usually 0.65), as follows:

$$A_e = CA = \frac{\pi}{4} ESEOD^2 \times 0.65$$

The empirical pressure-loss coefficient K_1 accounts for pressure losses in contractions, expansions, and bends in the flow path. Specific values for many cases can be found in Ref. 7-9. This coefficient is also used to characterize valve flow-capacity, based on the flow area of the upstream line. The relationship between K_1 and the flow rate is—

$$w = \frac{A_1}{12}\left[\frac{2g\rho(P_1 - P_2)}{K_1}\right]^{1/2} \qquad (7\text{-}34)$$

By equating Eq. (7-33) and (7-34) the effective area can be found:

$$A_e = CA = \frac{A_1}{K_1^{1/2}}$$

Another factor useful in measuring and analyzing pressure loss, resistance r, helps most in analyzing a system where resistances can be added algebraically in much the same way as they are added in an electrical circuit. The fluid-resistance analogy, however, requires flow as a squared function, replacing the linear current in the electrical circuit. The defining equation is—

$$w = \left[\frac{\rho(P_1 - P_2)}{r}\right]^{1/2} \qquad (7\text{-}35)$$

By equating Eq. (7-33) and (7-35), the effective area can be computed from a given resistance value, as follows:

$$A_e = CA = \frac{12}{(2gr)^{1/2}}$$

A common industrial practice relates valve flow capacity to water flow at a specific differential pressure. The C_v value becomes the number of gallons of water per minute that a valve will flow with a differential pressure of 1.0 psi. A useful form of this equation relates C_v to flow capacity for any fluid with known density:

$$w = \frac{C_v}{56.8}[r(P_1 - P_2)]^{1/2} \qquad (7\text{-}36)$$

Equating Eq. (7-33) and (7-36) yields the effective area:

$$A_e = CA = \frac{C_v}{38}$$

Many of the same equations used for incompressible-flow analysis can be used for compressible flow if the pressure drop will be less than 10% of upstream pressure. More accurate results can be obtained by using the compressible-fluid equations that are applicable over the complete range of operating pressures and pressure drops.

The following converging-nozzle equations are derived from thermodynamic considerations for isentropic flow:

$$w = \frac{CAP_1S}{(RT_1)^{1/2}}$$

where if $\frac{P_2}{P_1} \le \left[\frac{2}{k+1}\right]^c$, flow is sonic and—

$$S = \left[gk\left[\frac{2}{k+1}\right]^{c1}\right]^{1/2}$$

where if $\frac{P_2}{P_1} > \left[\frac{2}{k+1}\right]^c$, flow is subsonic, and—

$$S = \left[\frac{2gk}{k-1}\left[\left[\frac{P2}{P1}\right]^{c2} - \left[\frac{P_2}{P_1}\right]^{c3}\right]\right]^{1/2}$$

where—

$$c = \frac{k}{k-1},\ c1 = \frac{k+1}{k-1},\ c2 = \frac{2}{k} \text{ and } c3 = \frac{k+1}{k}$$

The flow coefficient for nozzles depends on nozzle geometry and the ratio of line to nozzle diameters (as detailed in Ref. 7-9). Applying this equation to sharp-edged orifices yields a flow coefficient that is nearly constant with respect to pressure ratio P_2/P_1. However, this same equation, applied to nozzles, yields a flow coefficient that depends on pressure ratio (Fig. 7-19).

The average-density orifice equation is derived from the incompressible orifice [Eq. (7-33)] and the average gas density, based on upstream and downstream pressures at constant temperature, assuming

perfect gas. The perfect gas law states:

$$P v = \frac{w_m RT}{144}$$

The resulting flow equation is:

$$w = CA \left[\frac{g}{RT_1}\left[P_1^2 - P_2^2\right]\right]^{1/2} \qquad (7\text{-}38)$$

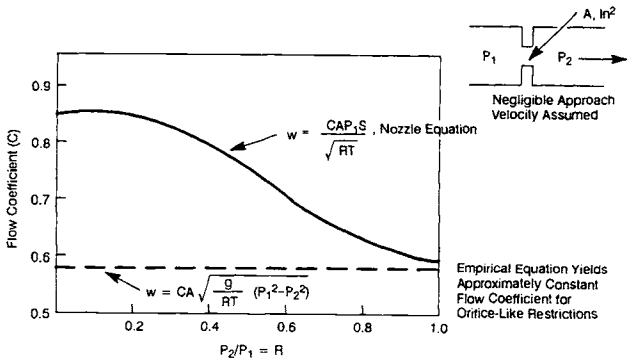

Fig. 7-19 Compressible orifice flow.

This flow equation is frequently used for sizing valves, where the flow coefficient is based on experience with similar flow devices.

Leakage flow equations. Leakage flow equations are essential tools for the design of fluid-control components. An understanding of these equations permits the prediction of propellant leakage, based on test results with referee fluids. For example, it is not practical or economical to perform component leakage tests with a cryogenic fluid, such as liquid oxygen, because of associated hazards and the difficulty of handling and measuring leakage from a fluid that changes phase from liquid to gas. In addition to leakage correlation of one fluid to another, these equations make possible the estimation of leakage from known leak-path surface geometry, such as might exist between the poppet and seat of a valve. The following discussion has been extracted from Ref. 7-10.

Leakage of fluids can occur through one or more of the following mechanisms: permeation, molecular flow, transition flow, laminar flow, turbulent flow, and nozzle flow. Each of these mechanisms will be discussed in following paragraphs. Equations and boundary conditions are summarized in Tables 7-3

Table 7-3 Gas-leakage equations

Flow Regime	Flow Equations		Boundary Parameters
Permeation	$w = \frac{k_p A(P_1 - P_a)}{L}$, k_p is a function of seal material, fluid, and temperature		No boundary; leak rate varies exponentially with temperature
Molecular flow	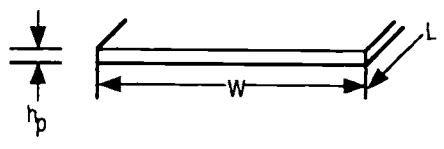 $w = \frac{4}{3}\sqrt{\frac{2g}{\pi RT}}\ \frac{Wh_p^2}{L}(P_1 - P_a)$	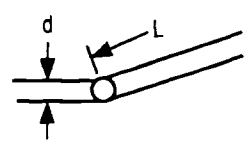 $w = \frac{1}{6}\sqrt{\frac{2\pi g}{RT}}\ \frac{d^3}{L}(P_1 - P_a)$	$K_N = \frac{Lm}{h_p}$ or $\frac{Lm}{d} > 1.0$ $Lm = \frac{43.2\mu}{P_1 + P_2}\sqrt{RTg}$
Laminar flow	$w = \frac{Wh_p^3\left(P_1^2 - P_E^2\right)}{288\mu LRT}$	$w = \frac{\pi d^4\left(P_1^2 - P_2^2\right)}{3{,}072\mu LRT}$	$K_N < 0.01$, $Re < 500$ $Re = \frac{2w}{12\mu Wg} = \frac{4w}{12\pi d\mu g}$
Choked turbulent flow	$w = AP_1M_1\sqrt{\frac{kg}{RT_1}}$, $\beta_1 = 1 + \frac{k-1}{2}M_1^2$ $T_1 = T_0/\beta_1$; $T^* = 2\beta_1 T_1/(k+1)$; $P_1 = P_0/\beta_1 \text{EXP}\frac{k}{k-1}$ $P^* = M_1P_1\sqrt{\frac{T^*}{T_1}}$, $f = \left\{2\text{LOG}\frac{d}{e} + 1.14 - 2\text{LOG}\left[1 + \frac{9.28}{Re\left(\frac{e}{d}\right)\sqrt{f}}\right]\right\}^{-2}$ $d = 2h_p$ in f equation for plate flow, $e \cong 3$ (AA) $A = Wh_p = \pi d^2/4$, Re (see above) $L \equiv L^* = \frac{2h_p}{f}\left[\frac{1 - M_1^2}{kM_1^2} + \frac{k+1}{2k}\text{LN}\frac{(k+1)M_1^2}{2\beta_1}\right]$, $(2h_p = d$ for hole)		(1) $500 < Re < 2{,}000$ For plates, $f = 96/Re$ For hole, $f = 64/Re$ (2) $Re > 2{,}000$ f = function e/d (3) L/d or $L/h_p > 10$
Choked nozzle flow	$w = \frac{CAP_o}{\sqrt{RT_o}}\sqrt{gK\left(\frac{2}{k+1}\right)\text{EXP}\frac{k+1}{k-1}}$, C is function of entrance geometry and L/d		L/d or $L/h_p < 10$

Table 7-4 Liquid-leakage equations

Flow Regime	Flow Equations	Boundary Parameters
Laminar flow	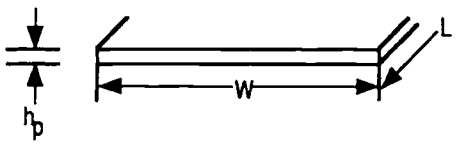 $w = \frac{\rho W h_p^3 \Delta P}{20{,}736\,\mu L}$ 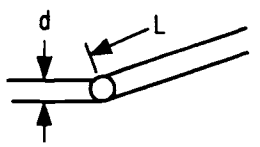 $w = \frac{\pi \rho d^4 \Delta P}{221{,}184\,\mu L}$	Re < 2,000 $Re = \frac{2w}{12\mu Wg} = \frac{4w}{12\pi d\mu g}$
Turbulent flow	$w = \frac{A}{12}\sqrt{\frac{2\rho g \Delta P}{k_{f1} + fL/d + k_{fE}}}$ $f = \left\{ 2LOG\frac{d}{e} + 1.14 - 2LOG\left[1 + \frac{9.28}{Re\left(\frac{e}{d}\right)\sqrt{f}}\right]\right\}^{-2}$ $d = 2\,h_p$ in f equation for plate flow, $e \cong 3$ (AA) $A = Wh_p = \pi d^2/4$, Re (see above)	Re > 2000 L/d or $L/h_p > 10$
Nozzle flow	$w = \frac{CA}{12}\sqrt{2g\rho\Delta P}$ $A = Wh_p = \pi d^2/4$ C is function of entrance geometry and L/d	L/d or $L/h_p < 10$

and 7-4. These equations are derived for a circular hole of diameter d and a parallel plate leak-path model of width W and gap hp, with pressure drop over length L for each path.

Permeation, turbulent flow, and nozzle flow are proportional to the flow area; thus, circular or other flow paths can be substituted. The hydraulic diameter d is used to determine the applicable Reynolds number and friction factor. However, molecular flow and laminar flow are integrated equations, involving the path geometry. The noted constants will therefore differ as shown in the tables.

Permeation flow occurs by a process of gas absorption on a surface film, diffusion through the bulk, and desorption on the low-pressure side. It usually takes large surface areas and organic materials to produce significant leakage. Natural rubber, a typical example of material with high permeability, will be easily penetrated by helium and water vapor. Metals are not permeable to the rare gases, although hydrogen gas can diffuse into most metals, often causing loss of metal strength. Unless in the mass spectrometer range ($<10^{-5}$ scim or 10^{-2} scc/hr), permeation leakage is usually insignificant. Note, however, that other modes of flow can occur through physical openings in the permeable material in the same or opposite direction as the permeation leakage. Consequently, it is difficult in the low-leakage range to differentiate between leak modes.

Molecular flow occurs when gas pressure is sufficiently low and/or the leak path is small enough that gas molecules encounter the walls more frequently than other gas molecules. This type of flow results when the mean-free path L_m exceeds the leakage gap h_p, a condition defined by the Knudsen number as follows:

$$K_N = \frac{L_m}{h_p} > 1.0$$

Molecular flow results from a greater concentration of molecules on one side of a barrier than on the other. The driving force for flow is therefore the partial-pressure differential existing across a given leak path. As an example, with 1.0-atm helium pressure on one side of an opening at 1.0 atm and a like pressure of nitrogen on the other side, there would be a molecular-flow transfer of each gas in opposite directions across the same leak path.

A small mean-free-path of the molecule with respect to the distance between walls induces laminar flow governed by bulk fluid properties, primarily viscosity. The Knudsen number for the lower boundary of laminar flow is $K_N < 0.01$. In this case, the channel is full, and flow prevails only from higher to lower pressure.

Between laminar and molecular flow, a transition region combines molecular- and laminar-flow characteristics. The easiest treatment simply adds the two types of flow or, if sufficiently high flow exists, ignores the molecular component (and vice versa). In laminar flow, the viscous forces between the fluid particles

govern the stream lines, resulting in a predictable velocity profile from zero velocity at the boundary to a maximum velocity between boundaries. This velocity profile is termed parabolic because it follows a second-degree curve (parabola). As the flow velocity is increased, the inertial forces between fluid particles become greater than the viscous forces, and a transition to turbulent flow begins. The defining parameter is the Reynolds number, the ratio of inertial to viscous forces:

$$Re = \frac{\rho V d}{1728 m g}$$

Tests of valve seats show gaseous laminar flow to exist for Reynolds numbers less than 500. Flow velocities are usually low enough to assume infinite heat transfer or isothermal flow. For Reynolds numbers approaching 500, gas-exit velocities become very high because of expansion and reduced density, and the isothermal assumption is not valid (although the results may be sufficiently accurate for most analyses). Published data indicate that liquid laminar flow prevails with Reynolds numbers up to 2000.

In the turbulent flow regime, laminar flow exists only in a narrow boundary near the walls. The velocity profile is nearly flat, and the flow characteristics are defined by both theoretical and empirical information. Basically, pressure drop is a function of internal and surface fluid friction over the length of the flow path. Under some conditions of incompressible flow, entrance and exit losses can exceed the friction loss, and these factors must be considered in computing the leakage flow. For gas flows, thermodynamic considerations are employed to define fluid conditions, and the flow is considered to be adiabatic; i.e., there is no heat transfer. Consequently, temperature will decrease as the gas expands to an exit pressure. The exit pressure will either be greater than the ambient for sonic flow or equal to the ambient for subsonic flow.

Nozzle flow occurs as the flow path is shortened, friction losses become negligible, and flow-pressure drop is expended in a turbulent jet. In this case, the flow rate is governed by the velocity head and an empirically defined flow-coefficient that is largely a function of the entrance geometry and length of path to gap ratio.

Compressibility effects exist in most modes of gas-leakage flow. The most significantly affected regions are the turbulent and nozzle-flow regimes. With constant-area leak paths, the exit velocity will be limited by a phenomenon known as "choking." This condition results when the exit velocity equals the acoustic velocity. Mach number, a measure of compressibility effects, and an important parameter in gas dynamics, is defined as the ratio of the average fluid velocity V to the speed of sound a at the same conditions: $M = V/a$.

Compressibility effects can usually be neglected with a Mach number less than about 0.4, corresponding to a pressure drop less than 10% of the upstream pressure. This case will seldom be seen with seal leakage because the supply pressure is usually several times greater than the ambient or downstream backpressure.

Control-fluid pressure level. The operating pressure of fluids has a major effect on the design of fluid-control components. For example, actuating forces required to control the component are affected by operating pressure on any unbalanced pressure areas. Additionally, seal friction loads will be higher at high operating pressures as a result of the increased contact load.

The magnitude of operating pressure influences the design of seats and seals. Elastomeric and plastic seals, for example, must be contained to prevent extrusion at high pressures.

Structural loads resulting from high pressure must be considered in selecting materials to meet stress requirements. Although more subtle, deflection resulting from high pressure, or from assembly loads required to contain the high pressure, must be considered in selection of clearances of precision devices, such as bearings. Deflections (which degrade surface geometry) may affect performance of such items as static seals and valve seats.

Under certain circumstances, combinations of pressure and temperature can cause deleterious effects on material properties. More detail on this subject can be found in the section on "Design of Dynamic Seals for Fluid-Control Components."

Special system operating provisions are often made to meet the stringent requirements in high-pressure applications. For example, the cutoff events in a high-pressure, turbopump-fed engine system may be sequenced so that turbine power is cut first; thus the main propellant valves will not be required to shut off against the mainstage high discharge pressures.

Fluid-flow velocity. Problems associated with high-velocity fluid flow in control components include generation of acoustic resonances, unforeseen loads resulting from differences between stagnation pressure and static pressure, and direct impingement of high-velocity flow on devices sensitive to side loads.

Components and lines that have a disruption in the flow path and a geometrical configuration that causes the fluid and the disruption to interact have developed acoustic resonance. The resultant local mechanical vibration and acceleration can cause hardware damage.

In components having a high-velocity fluid—i.e., the stagnation and static pressures are very different—caution must be taken to prevent these pressure differences from distorting or loosening hardware exposed to the high-velocity flow stream.

Fluid-flow temperature. Fluid temperature plays a major role in the selection of basic design concepts for seals and for material selection. Materials with similar coefficients of thermal expansion provide the best combination for extreme-temperature service. Additionally, the design should consider differential temperatures from point to point in the component to avoid excessive distortion, compression, or tension in critical parts. Differential temperatures can be expected to occur during transients, when, for example, the interior of a component is first exposed to a cryogenic propellant

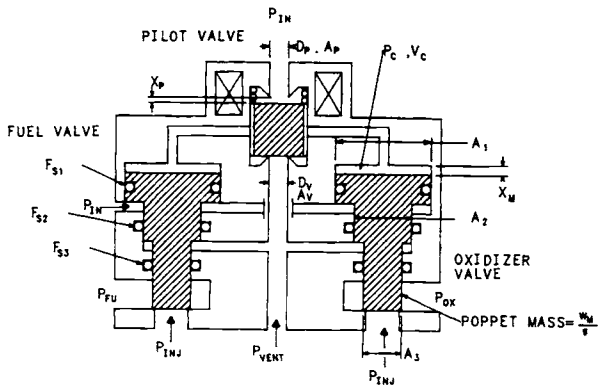

Fig. 7-20 Bipropellant-valve schematic.

and the exterior of the component is initially at room temperature.

In designing components, other considerations for temperature include selection of materials for ductility and strength (cryogenic temperatures usually lower ductility and increase strength, while high temperatures have the opposite effect).

Some pneumatic components require pressurization and venting rates to be maintained to meet certain engine-sequencing requirements. Changes in gas temperature will affect these rates. The system either should have heaters on the actuators to maintain gas temperature constant or should use thermally-compensated orifices to correct changes in temperature.

Dynamic considerations in fluid-flow control components. Dynamic analysis of fluid-flow control components often requires development of computer models. The control component to be simulated can usually be represented mathematically by a set of nonlinear differential equations. The equations can then be solved by using numerical integration techniques on a digital computer. These computer models are extremely useful in predicting and explaining component dynamic and static behavior as well as in defining performance and operation boundaries.

Transient factors, such as dynamic response, stability, pressure surge, flow noise, and induced vibration, are important design considerations in any fluid-flow control component. To obtain reliable control performance at high-fluid-flow velocities, the components must be designed to withstand the impact loading imposed upon the control surfaces by the fluid stream and also the impact force inflicted on the seat by the poppet.

The following example illustrates the use of a computer model to simulate transient characteristics of a control valve. Figure 7-20 illustrates the schematic of a bipropellant control valve. In this concept, the main valves are designed to have a differential-area piston, controlled by a three-way pilot solenoid valve (normally open). This valve alternately pressurizes and vents the control side of the piston for opening or closing. Basic equations appear below for the pilot valve and one of the main valves. Nomenclature other than that defined by the schematic may be found in Table 7-2.

Main valve force-balance and acceleration:

$$F = P_c A_1 - P_{in}(A_1 - A_2) - P_{vent}(A_2 - A_3) - P_{inj} A_3 - F_s$$

$$F = \text{mass} \times \text{acceleration} = \frac{w_M}{g} \bullet \frac{dV_M}{dt}$$

Main-valve piston velocity and position:

$$V_M = \int_o^t \frac{dV_M}{dt}\, dt + V_M(0)$$

$$X_M = \int_o^t V_M\, dt + X_M(0)$$

Pilot-valve flow area:

$$CA_P = C\,\pi\, D_P\, X_P, \quad 0 < CA_P < CA_{PMAX}$$

$$CA_V = C\,\pi\, D_P\,(X_{PMAX} - X_P), \quad 0 < CA_V < CA_{VMAX}$$

Pilot-valve flow-rate:

$$w_{IN} = CA_P \left[\frac{g}{RT}\left[P_{IN}^2 - P_C^2\right]\right]^{1/2}$$

$$w_{VENT} = CA_V \left[\frac{g}{RT}\left[P_C^2 - P_{VENT}^2\right]\right]^{1/2}$$

Main-valve variable control volume:

$$v_C = v_{CMIN} + 2\, X_M\, A_1$$

Main-valve control pressure rate and pressure:

$$\frac{dP_C}{dt} = \frac{k\,R\,T\,(w_{IN} - w_{VENT}) - 2\,k\,P_C\,V_M\,A_1}{v_C}$$

$$P_C = \int_o^t \frac{dP_C}{dt}\, dt + PC(0)$$

Seal frictional force. (Seal friction force has both a constant term, resulting from installed force, and a pressure-dependent term, where the seal-friction force is a function of the differential pressure across the seal):

$$F_s = F_{S1} + F_{S2} + F_{S3}$$

To demonstrate the analysis, a mathematical model was constructed based on the preceding equations. The computer model simulated valve opening and closing. A time-domain solution set was generated by using numerical integration. Figure 7-21 shows the dynamic response (opening and closing piston-displacement) of the bipropellant valve/pilot-valve poppets. Figure 7-22 displays the transient pressure at the valve outlet.

Plots, such as these examples, can be used during the design process to predict performance and to aid in

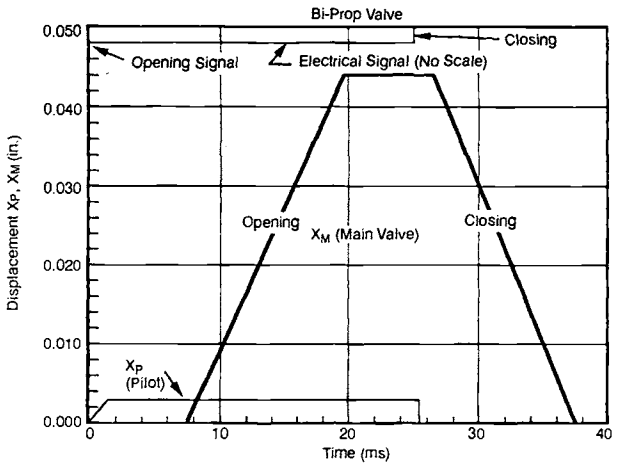

Fig. 7-21 Pilot and main-valve displacement vs. time.

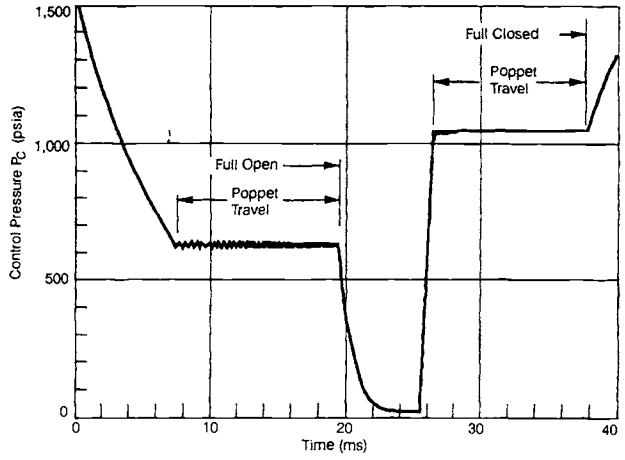

Fig. 7-22 Main-valve pressure vs. time.

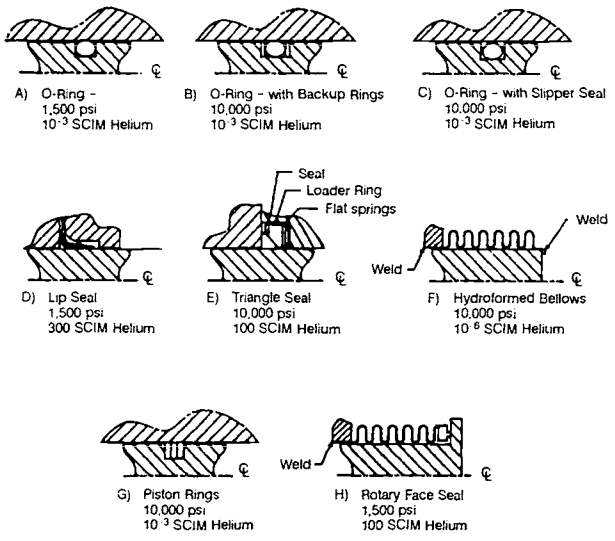

Fig. 7-23 Dynamic shaft and piston seals for fluid-control components.

ensuring that response-related requirements can be met.

Design of Dynamic Seals for Fluid-Control Components

Apart from static seals, which will be treated in Chapter 9, two basic types of seals are required for fluid-flow-control components: seals for moving (reciprocating and rotating) cylindrical elements, such as actuator pistons, shafts, and rods (referred to as dynamic seals), and seals for valve seats (seating closures).

Temperature is one of the most important considerations in the design of seals. Seals can be classified into those for medium-temperature service (-65 to 400°F), low-temperature service (-423 to 400°F), and high-temperature service (over 400°F). The selection of the configurations and the materials for these seals is based to a large extent on service conditions and the type of fluid involved. Generally, soft nonmetallic or elastomeric seals are used wherever possible. The outstanding advantage of these seals is that they function satisfactorily despite minor imperfections in the seal or the mating part.

Dynamic seals for medium-temperature services. Medium-temperature-service dynamic seals, successfully used on liquid-propellant rocket engine valves (Fig. 7-23), include O-ring packings with and without backup rings or slipper seals (Fig. 7-23a, b, and c). Plain elastomeric O-rings have been used as dynamic seals for both hydraulic and pneumatic service. For applications where the differential pressure across the seals exceeds 1500 psi, backup rings have normally been used to prevent extrusion of the O-ring between the shaft and bore.

Some applications need a plastic slipper seal in conjunction with an O-ring. As an example, a valve in which the friction accompanies an O-ring may not satisfy repeatability requirements. The plastic slipper seal, usually a Teflon-based material, then provides a nearly constant, repeatable coefficient of friction, permitting better repeatability. The slipper seal can also be useful when the available elastomers, compatible with the service fluids, show poor dynamic service because of their physical properties. The use of a slipper seal then lets the O-ring act as a static seal, while the slipper seal makes the true dynamic seal.

Dynamic seals for low-temperature service. Lip seals (Fig. 7-23d) can be used effectively as reciprocating and rotary shaft seals and as reciprocating piston seals in propellant valves for temperatures as low as -423°F and pressures up to 2000 psi. They are used to seal pressurants, such as helium and nitrogen, and propellants, such as liquid hydrogen and liquid oxygen (and RP-1 at medium temperatures). The design creates differential pressure to increase contact stress between the seal and the moving surface. This pressure enhances the contact stress already present from hoop tension in the seals. The thin sheet material used in this design furnishes the flexibility required for cryogenic operation. Mylar is the material of choice for this seal design, although KEL-F has also been used, if proven adequate in seal-fluid compatibility testing.

The triangle seal (Fig. 7-23e) serves the same applications as the Mylar lip seal, but at the operating differential pressures extending to over 8000 psi. This design is rugged and simple. Precise machining of the seal geometry permits analysis of loads required to close the gap between the seal and the mating surfaces, permits estimation of contact stress and load, and provides a means of estimating friction load from known friction coefficients. Propellant seals at high pressure use polyimide material, such as DuPont Vespel SP-211, which contains Teflon to reduce friction. Other applications, notably in lower-pressure service to approximately 1000 psid, use virgin or graphite-filled TFE Teflon, or Vespel SP-211. The wave-washer springs force the loader ring against the seal at an angle of 45 deg, which provides equal axial and radial load. Additionally, the seal contact stress and load increase with differential pressure. A major benefit of this design is the degree of lateral motion that the seal can withstand, by virtue of its ability to slide sideways, without detrimental effect on leakage or on seal stress. The lip seal, by comparison, requires hoop deflection of the seal material to accept compliance for lateral motion.

Hydroformed metal bellows (Fig. 7-23f) are used extensively as reciprocating piston and shaft seals on rocket-engine valves in applications which demand essentially zero propellant or pressurant leakage. In addition to the sealing ability, the bellows can also provide spring force to bias valve poppets to a specified position. Bellows can have either single- or multiple-ply construction. Multiple-ply construction can increase hoop strength of the bellows without the large increases in spring rate that shown by a single ply of equivalent thickness. Bellows are typically hydroformed in dies. After forming, the plies are welded together at the ends to form a solid mass for the final machining to length and for welding to the mating shaft or piston and housing. Disadvantages of bellows include high cost of the fabrication process, high spring rates, which may require additional control load to operate the component, and relatively large envelopes, which increase the size and weight of the component.

Dynamic seals for high-temperature service. Precision metal piston rings (Fig. 7-23g) are used for sealing gas at high temperatures. A typical application might have a Stellite piston ring in a nitrided-stainless-steel-bore. Piston rings are simple and effective for sealing hot gas without incurring large friction loads. However, they allow significant leakage. As a consequence, propellants must be positively separated from each other or from the atmosphere by multiple seals with vent or drain ports between the seals.

A bellows and metallic-face-seal assembly (Fig. 7-23h) can also be used for high-temperature rotary-shaft sealing. Limits on operating temperature are imposed by the allowable stress and fatigue life of the bellows material at the operating temperature. This type of seal has been used in gate valves at temperatures up to 1400°F and pressures up to 1150 psi. The illustrated seat consists of a flame-sprayed tungsten carbide surface on the shaft in contact with a Rene-41 ring.

Sealing specifications. Design requirements on leakage often dictate the seal design. For this reason, it is beneficial to have an extensive knowledge of seal capabilities. The use of inert gas for leak testing usually can circumvent the impracticalities of testing with propellants, because leakage thus measured can be analytically converted to equivalent propellant leakage.

Figure 7-24 shows typical helium-leakage for the various seal designs (maximum allowable over the range of pressure and temperature). Lower values can be achieved, but at higher cost, owing to the need to provide better hardware-geometry control and to the expected higher initial rejection rates.

Design of Seating Closures for Fluid Control Components

Seating closures used on rocket-engine control components (Fig. 7-24) include seals for propellant, pressurant, and hydraulic systems for a wide variety of operating pressures and temperatures.

Seating closures for medium-temperature service. The trapped-O-ring seat (Fig. 7-24a) is used extensively in poppet valves for medium-temperature service with gases, such as helium and nitrogen. The design employs a two-piece poppet to facilitate groove machining and to permit seal installation. Dimensions of the seal groove are selected to retain the O-ring firmly and to provide a protrusion of material that seats against a mating metal corner. This seal is used at differential pressures up to 4500 psi at 160°F with a 90-Shore-hardness O-ring. This seal design is also used for dual seating, where two seals on the same poppet must seat simultaneously, at differential pressures up to 1000 psi and temperatures of 165°F with 70-Shore-hardness O-rings. Design requirements for this seal include making certain that, to prevent blowing the seal from the groove, gas trapped between the groove and the O-ring will have been vented before applying pressure.

The bonded elastomeric seal (Fig. 7-24b) is used on certain fuel valves and pneumatic-service-control poppet valves. Leaktight to liquids, it seals less than 5 scim using helium. The bonding process used to fabricate this seal must be closely controlled, because it does not allow normal inspection, as in the case of the trapped O-ring seal. The design permits a one-piece poppet because it needs no separate retainers to hold the seal in place. Design considerations include limiting the volume of the seal protrusion above the metal-stop surface to the volume of the open section of the seal below the stop-surface cavity in order to prevent bulk compression and to ensure stopping on the metal stop.

Seating closures for low-temperature service. The plastic-disc seal (Fig. 7-24c) is but one of many configurations used in poppet valves. The primary characteristic of this seal is that it is retained mechanically, as opposed to being molded in place, and is machined from plate or bar-stock plastic, usually Kel-F. The seal does not provide the ability to conform to the mating surfaces as well as elastomer seats do; but its operating temperature extends to -423°F. Additionally, because of material compatibili-

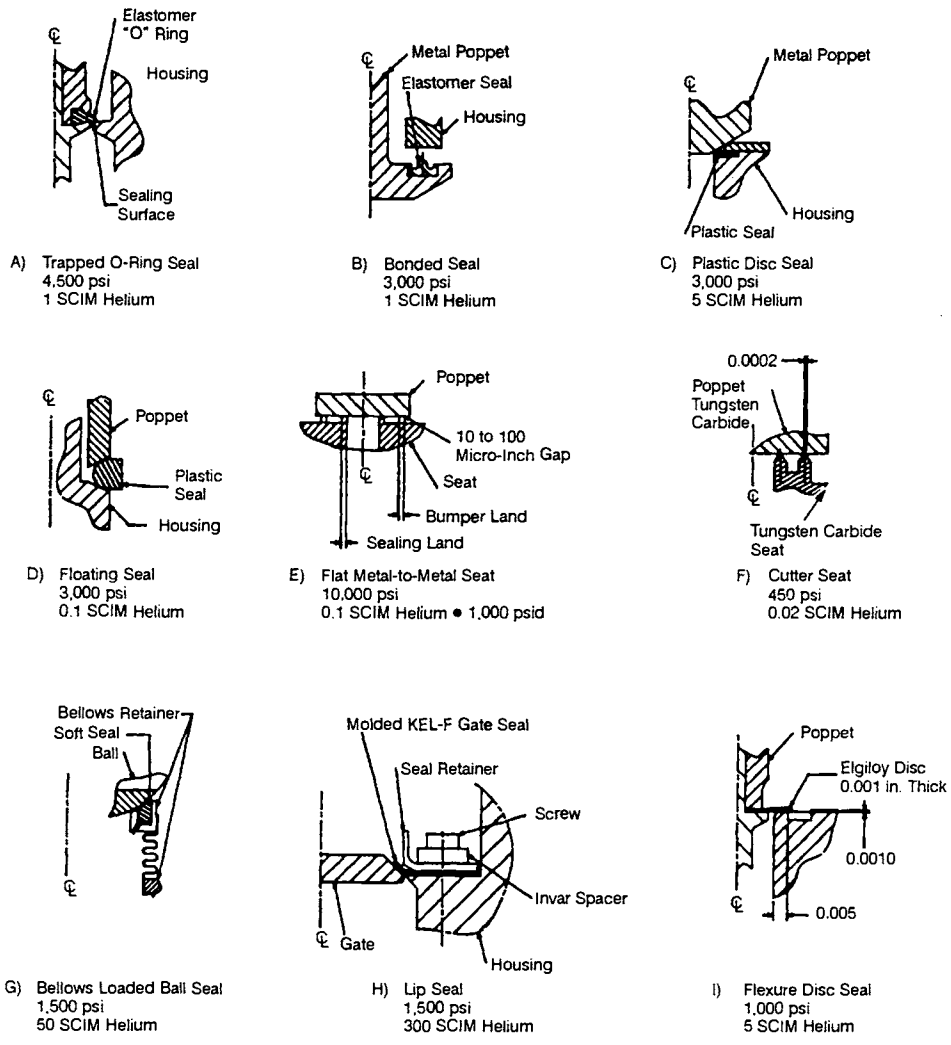

Fig. 7-24 Seating closures used in fluid-control components.

ties, the use of plastic for sealing permits service with a much wider range of propellants than elastomers have. For example, use of plastics, such as TFE Teflon, will make this design suitable for use with such exotic propellants as nitrogen tetroxide and fluorinated oxidizers. Design details that must be considered include the use of a positive stop to limit the amount of deflection imposed on the plastic. In estimating poppet stroke, material creep should be taken into account.

The floating seal (Fig. 7-24d) is used in certain poppet check-valve designs to good advantage. With a design permitting the seal (usually Teflon) to float, the seal can seek the proper geometry to achieve closure. The seal also acts as the positive stop that keeps impact-loading away from metal parts, which otherwise might create detrimental wear. Although offering the self-centering feature, this design must reseal on two faces at the end of each open-and-close cycle (whereas a more conventional seal design, retained in the poppet, has to reseat only on one face).

Flat metal-to-metal seating (Fig. 7-24e) is used extensively in small control valves where the effective unbalanced pressure area must be precisely controlled. Metal-to-metal seating is also used in components requiring service in extreme temperatures, either high or low, and with fluids not compatible with soft materials. Typical materials include tungsten carbide poppets and 440°C seats. A bumper land outside of, and slightly below, the seating land can often eliminate damage to the seating land that might result from impact of the poppet on the seating-land corner when it is not closing in true parallel fashion. Surface finishes as low as 0.1 μin. AA can be achieved with flat seats that allow practical fabrication with low leakage. Operating pressures for the metal-to-metal seat are virtually unlimited, if surface areas can limit contact stress below the yield strength. The design must take into consideration the problem of particulate contamination, which can damage the seat and cause excessive leakage. For this reason, metal-to-metal flat seats should be used only with clean fluids or with filters.

The cutter seat (Fig. 7-24f), a specialized arrangement, resists particulate contamination and keeps leakage very low. Both the poppet and the seat are tungsten carbide for extreme hardness. The seat lands are purposely kept narrow to reduce the chance of trapping a particle of contamination and to cut through particles if they do become trapped. The

narrow seating land also provides very accurate control of effective pressure area. This design is used in pneumatic service for operation at -200°F. Design considerations for this seat include sensitivity to impact damage due to the use of low-ductility materials.

The bellows-loaded ball seal (Fig. 7-24g) serves ball valves, usually employing Kel-F to gain a degree of compliance with the macrogeometry of the ball surface. The seal seats on one end in a retainer welded to a metal hydroformed bellows. The opposite end of the bellows is welded to another retainer, which is bolted in place to the valve housing and sealed by a static seal. The bellows permits the seal to seek the ball seating surface as the ball moves laterally through clearances, and also permits a degree of compliance because of ball misalignment axially in the housing. This seal design is used at differential pressures up to 1500 psi and at temperatures as low as -423°F. Careful selection of contact points between the seal and the retainer and the seal and the ball, with regard to the mean-effective area of the bellows, must be observed to establish proper seating. As a disadvantage of this method, hydroformed metal bellows are usually costly and require a lengthy lead time to procure.

A lip seal (Fig. 7-24h), similar to the dynamic seal discussed previously, typically seals butterfly valves for liquid-propellant engines, but will be one-piece Kel-F and usually much thicker than the shaft-seal designs. The additional thickness provides mechanical stiffness needed to withstand high-velocity liquid flow and the resultant differential pressure. Retainers and bolts clamp the seals to the body to effect a gasket-type static seal with the housing. Invar washers are sometimes used to provide thermal compensation, which aids in maintaining a constant gasket load as the temperature of the bolts, seal, and housing decreases to that of the propellant (as low as -423°F for liquid hydrogen). This seal design has limited differential operating pressure. Making the seal thick enough to handle high differential operating pressures would reduce its flexibility to the point that the compliance could not guarantee a good seal.

The flexible-disc seal (Fig. 7-24i) represents the low-temperature equivalent for the compliant elastomeric seal of Fig. 7-24a. This seal permits dual seating on a common shaft. It has deflections on the order of 0.001 to 0.002 in. and operating pressures under 1000 psi (owing to the hertz contact stress between the flexible disc and the seat). This seal can be used at temperatures down to -423°F.

Seating closures for high-temperature service. The metal-to-metal seat and the cutter seat (Fig. 7-24e and f) both offer satisfactory high-temperature service. Additionally, the flexure-disc seal (Fig. 7-24i), within the limits of material properties for flexure stress and hertz contact stress, also gives suitable high-temperature service.

Sealing specifications. As in the case for dynamic seals, here design must often be selected to fulfill seal-leakage requirements. For this reason, the designer needs extensive knowledge of seal capabilities. In most cases, use of inert gas for leak testing will circumvent the impracticalities of testing with propellants, because leakage thus measured can be analytically converted to equivalent propellant leakage.

Figure 7-24 shows typical helium leakage (maximum allowable over the range of pressure and temperature) for the various seal designs. Lower values increase cost, owing to the need to provide better hardware-geometry control and expected higher initial rejection-rates.

Design of Propellant Valves

Propellant valves control flow of propellants to main thrust chambers and gas generators or preburners. Other functions include control of bleed flow, spark-igniter flow, and various thermal conditionings. Although usually two-position (open/closed), normally-closed valves, to meet specific sequencing requirements, designs may include an intermediate opening position. For thrust- or mixture-control purposes, a continuously-variable opening position may be required on some propellant systems.

In addition to propellant compatibility and structural integrity, prime design considerations for propellant valves include the following objectives:

- No leakage of propellant through the valve when closed (see previous section on leakage flows for considerations to minimize potential leakage).
- Proper actuating time during opening and closing in accordance with the requirements of the control system.
- Minimum pressure-drop.
- Meet fail-safe and/or fail-operational system requirements.

Among the great variety of propellant valve types available, each has certain characteristics that make it suitable for a specific application. Frequently used propellant valves can be classified according to their design configurations: butterfly, ball, poppet, venturi, and gate.

Butterfly-type propellant valves. One of the most widely used types used in large liquid-propellant rocket engines, the butterfly valve has established a reliable operational record in LO_2/RP-1, LO_2/LH_2, storable, and other liquid-propellant services. Existing butterfly-valve designs range from 2.0- to 17.0-in. nominal diameter, for use at propellant pressures from 20 to over 1500 psia.

Figure 7-25 presents a typical butterfly-valve design. In it, a lip seal engages a spherical surface on the valve gate, similar to the one in Fig. 7-24h. The valve gate pivots on the valve shaft, the axis of which passes through the geometric center of the spherical sealing surface. In most designs, the valve gate rotates 90 deg from the closed to the fully opened position. The valve is operated by a piston-type actuator, through a connecting link and shaft crank arm. Lip seals make dynamic closure with the rotating valve shaft (Fig. 7-24d). Noncryogenic-propellant pressure, an inert gas supply, or hydraulic system pressure controlled by a pilot valve supplies the actuating power.

The valve in Fig. 7-25 is designed to be normally closed by a spring installed on the closing side of the actuator piston. Except for shaft, gate, link, lever, and

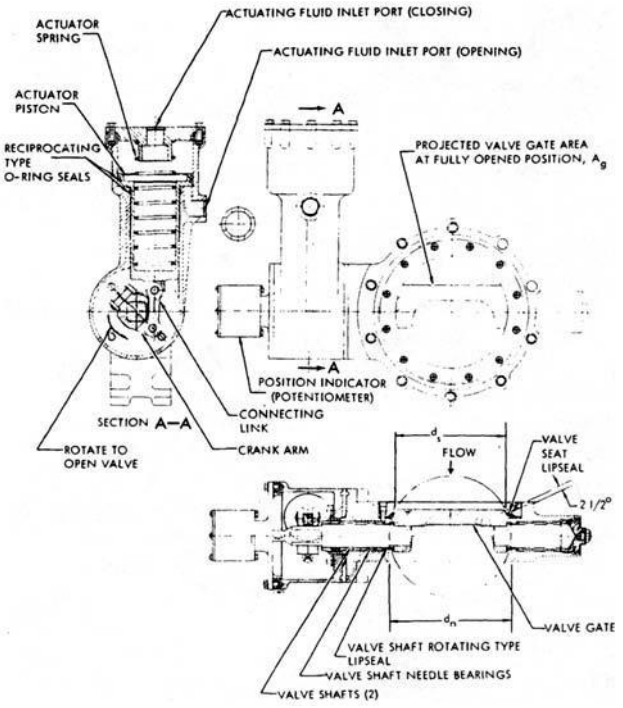

Fig. 7-25 Design of typical butterfly-type propellant valve (shown in the closed position).

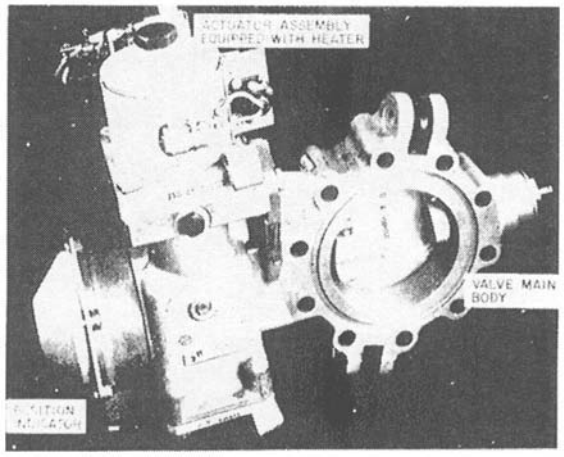

Fig. 7-26 Four-inch butterfly-type main LOX valve used on rocketdyne atlas ICBM booster engines.

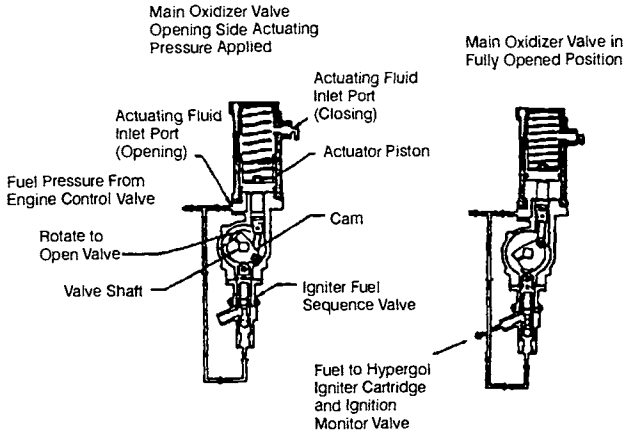

Fig. 7-27 Mechanical linkage between the main oxidizer valve and the igniter fuel-sequence valve of the A-1 Stage engine.

pins, which are made of stainless steels, most of the other parts are made of aluminum-alloy forgings. Figure 7-26 shows a 4-in., butterfly-type LOX valve used on the Atlas booster engine.

Butterfly valves have relatively low resistance to fluid flow. They are compact, light, and easy to service. And they have a high characteristic area, which can be expressed as—

$$A^* = \frac{\pi}{4} d_s^2 - A_g \qquad (7\text{-}39)$$

where (see Fig. 7-25 for dimension references) A = characteristic area of the valve, in.^{2}; d_s = inside diameter of the valve seat lip-seal, in.; and A_g = projected valve gate area at fully open position, in.^{2}. Values for A range from 65% of the duct area on a 2-in. valve to about 87% of the duct area on a 12-in.valve. A butterfly valve maintains a relatively smooth fluid-flow stream over a wide range of valve-gate angular positions. Thus, when used as a throttle valve, it has little tendency toward turbulence and its attendant adverse effects, such as local propellant cavitation.

When RP-1 is used as the actuating fluid for the LOX valve a heater may be required at the actuator to keep the fuel from freezing. The actuator and valve arrangement of the butterfly valve (Fig. 7-25) may be designed for normally-open or normally-closed operation, and position indicators may be added. Figure 7-27 illustrates the linkage between the main oxidizer valve and the igniter-fuel-sequence valve of the A-1 Stage engine. During the opening stroke, the cam attached to the main oxidizer-valve shaft actuates the igniter-fuel-sequence valve. Often a potentiometer will be attached to the shaft to give continuous indication of the angular position of the valve gate.

The torque required to turn the valve shaft and gate will be determined by the summation of hydraulic and friction torques. For most operational valve designs, hydraulic torque (imbalance of forces on the valve gate, caused by the flow of fluid around it) will be—

$$T_o = T_f + T_h \qquad (7\text{-}40)$$

$$T_c = T_f - T_h \qquad (7\text{-}41)$$

where—T_O = required opening torque, in-lb, T_C = required closing torque, in-lb, T_f = friction torque, in-lb, T_h = hydraulic torque, in-lb (assumed to act in the closing direction). The friction torque T_f varies with the pressure differential across the valve gate and with the valve-gate projected area, which is a function of gate angular position. Friction torque can be esti-

mated by—

$$T_f = K_f r_s f_m d_s^2 \Delta p \qquad (7\text{-}42)$$

where—

- K_f = friction-torque coefficient, a function of gate angular position (to be determined experimentally)
- r_s = radius of valve shaft at the bearing section, in.
- f_m = coefficient of friction between shaft and bearing (0.20 for aluminum journal and steel shaft; 0.05 for needle bearing and steel shaft)
- d_s = inside diameter of valve seat-lip seal, in.
- Dp = pressure differential across the valve gate, psi

Hydraulic torque T_h may be estimated by—

$$T_h = K_h d_s^3 \Delta p \qquad (7\text{-}43)$$

where K_h = hydraulic torque coefficient, a function of gate angular position (determined experimentally).

Figure 7-28 shows plots of required opening and closing torques vs. gate angular positions for a typical butterfly valve. In actual design practice, the actuator of a butterfly valve will provide two to three times the maximum estimated opening and closing torques. In addition, at the start of the opening stroke the actuator has to overcome the static-friction forces of all seals. Butterfly-type propellant valves are relatively fast-acting. Opening and closing times range from 20 to 200 ms.

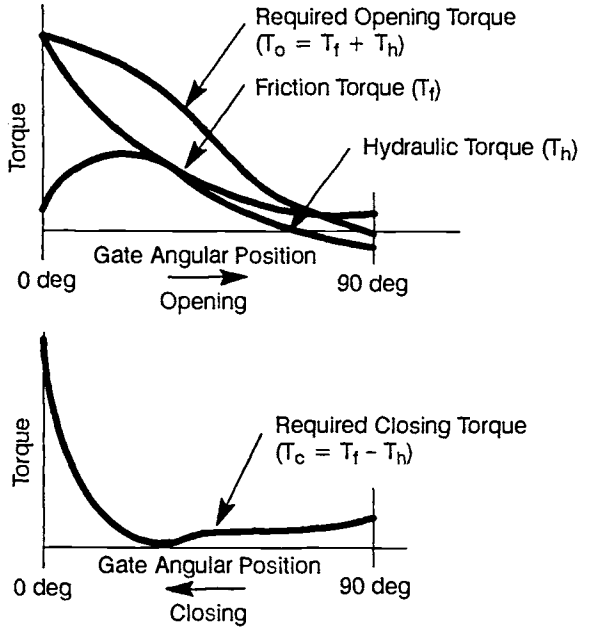

Fig. 7-28 Typical required opening and closing torques vs. gate angular position for a butterfly valve.

Ball-type propellant valves. A ball valve offers low pressure drop, since it permits in-line, unrestricted fluid flow, if it has the same flow area as the connecting lines. As an additional benefit, ball valve's spherical sealing surface can readily be fabricated with precise geometry. Ball valves have a reliable record in cryogenic and in some storable-propellant control applications for the main thrust chamber and for high-capacity gas generators.

Ball valves have actuating-torque characteristics similar to those of butterfly valves. A fluid-dynamic torque acts in a direction to close the valve, increases as the valve is opened until reaching a maximum torque value between 60 and 80 deg open, and then decreases rapidly to zero as the full, 90-deg open position is reached. This 90 deg of rotation for opening necessitates an actuator with relatively long stroke.

The SSME main LOX valve (Fig. 7-29) presents an example of a successful application. It has a 2.38-in.-diam propellant-flow passage. Flange-mounted between the main-thrust-chamber LOX dome and the high-pressure oxidizer duct, the valve controls oxidizer flow to the main-chamber LOX dome and main-chamber augmented-spark igniter. A hydraulic servoactuator, mounted to the valve housing, operates the valve. Operating pressure is 4600 psi and the flow rate is 853 lb/s. (Preburner ball valves on this engine operate at pressures as high as 8800 psi and LOX flow rates up to 83 lb/s.)

The valve has two major components, the integral ball/shaft/cams and the ball-seal retracting mechanism. The ball seal is a machined plastic, bellows-loaded design. Redundant shaft seals with an overboard drain between them prevent leakage along the shaft (actuator end) during engine operation. Inlet/outlet throttling sleeves align the flow to minimize turbulence and the resultant pressure loss. Ball-seal wear is minimized by cams and a cam-follower assembly that displaces the seal away from contact with the ball (after the initial few degrees of ball travel when it is being opened).

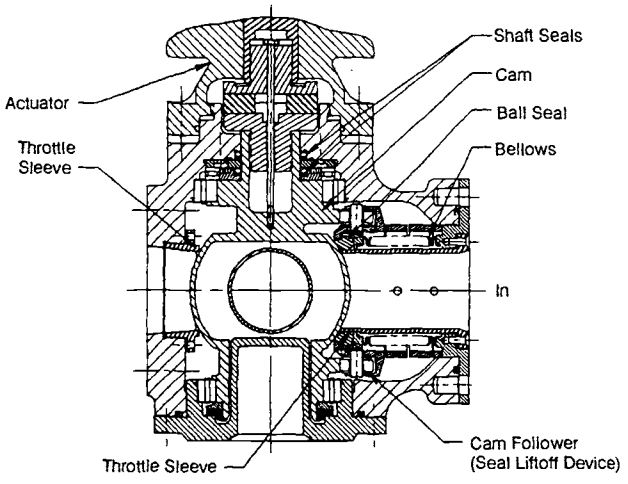

Fig. 7-29 Space Shuttle Main Engine main oxidizer valve.

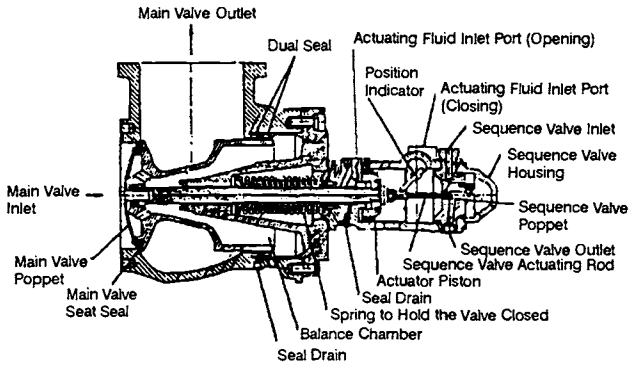

Fig. 7-30 Design of Saturn first-stage F-1 for poppet-type propellant valve.

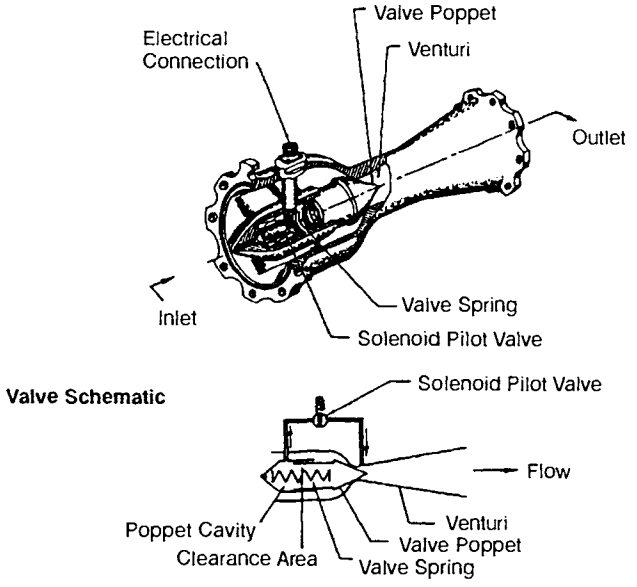

Fig. 7-31 Typical venturi-type propellant valve designed and manufactured by Fox Valve Development Co.

Poppet-type propellant valves. Poppet valves offer relative simplicity, primarily because of the reciprocating operation which permits the direct, in-line connection of an actuator. However, this arrangement requires turning the flow inside the passage, with consequent relatively high pressure-drops. Poppet valves prove satisfactory when precise throttling control is not required and when tight shutoff may be required. Throttling of poppet valves, without sophisticated contouring of some sort of plug within the flow path, results in poor control as a consequence of the high area gain when the poppet is near the seat.

Figure 7-30 presents the design of the main propellant-control poppet-type valve of a Saturn first-stage F-1 engine. The F-1 engine contains two LOX valves and two fuel valves of similar design. The displayed valve has a seat diameter of 8 in. and a 2.34-in. stroke. These valves are hydraulically actuated to either of two positions, open or closed. A pressure-balancing chamber reduces the unbalanced hydrodynamic forces and thus the size of the actuator. The relationship between the dynamic-seal and seat-seal diameters, in conjunction with the propellant pressure, produces sufficient unbalanced force that, even with the loss of actuator control pressure, the valve would still retain the fully-open position. A small sequence valve mechanically attached to the main valve actuator mechanically sequences it with other engine components. This type of poppet valve is suitable for high-flow and high-pressure cryogenic and storable-propellant services.

Venturi-type propellant valves. Figure 7-31 shows a typical design for a venturi-type propellant valve. In certain installations, for various reasons, it may be desirable to use a valve of a nominal size, smaller than that of the main duct. A valve installed in the throat of a venturi offers a possible solution. The smooth contours of the venturi limit pressure-drop penalties to a few psi. With adjacent ducting permitting, it is conceivable that the venturi may simultaneously be used for flow measurements.

The venturi may be designed to operate as a cavitating venturi. Based on Bernoulli's energy equation, the minimum pressure of a liquid is made to fall below its vapor pressure. As a result, a gaseous region forms at the throat. If this gas moves through the throat at the velocity of sound, downstream pressure variations and disturbances cannot advance beyond the throat. Up to minimum pressure differentials across the venturi (for example, 20% of upstream pressure), the flow rate will then depend on upstream pressure only. When used as a throttling device, the cavitating venturi affords smaller pressure drops, because the gaseous characteristics at the throat produce a near-linear relationship between flow rate and supply pressure, rather than following a square law. The fluid-flow venturi valves have been applied successfully in cryogenic and storable-propellant units.

In fluid-flow systems that require flow limitation and a shutoff control valve as well, the venturi valve with a cavitating diffuser will provide both, at a weight of only the valve and at a pressure drop of only the venturi.

Venturi valves occupy a relatively long space in the direction of flow, between four to six times the line nominal diameter. This length imposes limitations on size and application in engine systems. However, venturi valves up to 10-in. nominal diameter have been successfully built for rocket systems.

The venturi-type propellant valve of Fig. 7-31 was designed and manufactured by Fox Valve Development Co. A pilot-operated shutoff valve, it has a venturi section with a spring-loaded poppet seated at the throat. Propellant line pressure, controlled by a solenoid pilot valve, actuates the valve, open or closed. As shown in the schematic, the normally-closed pilot valve is inserted in a passageway that interconnects the poppet cavity and an opening in the venturi throat. Normally, upstream propellant pressure fills the poppet cavity and provides additional seating force on the poppet in the same direction as the valve spring to ensure valve closure. When the pilot valve is energized to open, propellant pressure behind the valve poppet is vented out at a greater rate than it can be replaced by leakage

through the poppet clearance area. This condition reduces pressure and thus overcomes the valve spring and causes the main valve poppet to open. Because the valve body is not pierced by a shaft or actuator rod and there are no dynamic seals, no pathways exist for leakage to ambient. The small number of moving parts further enhances the reliability of venturi valves.

Gate-type propellant valves. Figure 7-32 displays a typical design of a propellant gate valve. Its unrestricted fluid flow, resulting in low-pressure drop, is a major advantage. It also provides a relatively short distance between the valve inlet and outlet in the direction of the flow. This design uses elastomer O-rings as the valve-seat seal; these are suitable only for medium-temperature services. Cryogenic application requires other seal types. Gate valves are designed for propellant line pressures up to 3000 psi. Because of relative bulkiness, gate valves are limited to low-propellant-flow applications, including gas-generator control and ground-support services.

Design of Control Pilot Valves

A pilot valve controls a fluid, which in turn controls or actuates other fluid-flow-control components, such as propellant valves, or controls engine-sequence events, such as the admission of igniter fuel. A great variety of control pilot valves serves liquid-propellant rocket engines. Basically, they can be grouped into two categories, on-off and proportional (servo). This discussion concerns only the on-off type. Since the proportional-type pilot valves are used widely in closed-loop control systems, they will be treated as regulating devices and thus discussed in another section.

A pilot valve may be operated electrically or by fluid pressure or through a mechanical connection with other control components. Requirements for fast response, minimal leakage of control fluid through the valve when closed, and actuating power source compatible with systems design—all receive close attention in the design of pilot valves.

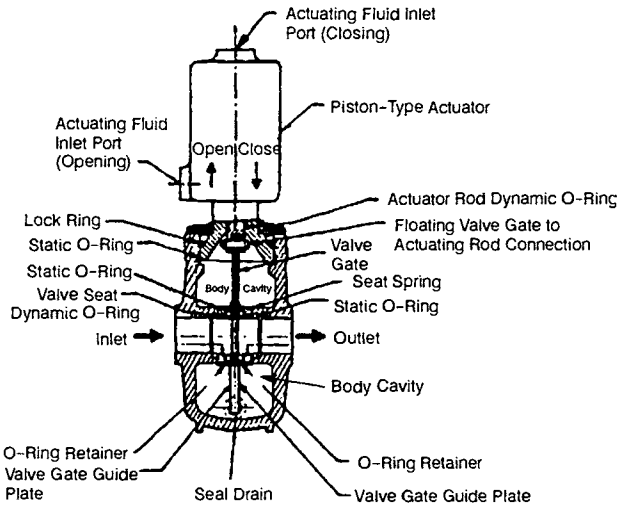

Fig. 7-32 Typical gate-type propellant valve.

The most frequently used on-off pilot valves may be classified according to design configuration into the two-way, three-way, or four-way type.

Two-way-type pilot valves. The term *two-way* refers to the number of ports. A two-way pilot valve is basically a two-port, open-close-type shutoff valve. The sequence valves shown in Fig. 7-27 and 7-31 are typical examples of two-way-type pilot valves. Both kinds use mechanical actuation from the main propellant valves. Solenoid or fluid-pressure-operated two-way pilot valves are also used frequently.

Three-way-type pilot valves. A three-way pilot valve (Fig. 7-33) has three ports: the inlet or pressure port, the outlet or cylinder (actuator) port, and the vent or return port. If the valve is designed normally closed (NC), the fluid path between inlet and outlet ports will be closed when no actuator power is applied, while the path is open between outlet and vent ports. Actuation of the valve closes one fluid path and opens the other. The reverse is true for a normally open (NO) valve; i.e., the fluid path between the inlet and outlet ports is normally open.

The design illustrated in Fig. 7-33 contains a hard metal-to-metal seat, restrained from radial motion during vibration by a flexure disc, which also serves as a spring to open the valve at low inlet pressures. Metal seating permits precise analysis of the unbalanced seating area and results in the minimum-size actuator. The poppet is made of a fine-grain tungsten carbide, and the seats are hardened 440C stainless steel. Filters are built into the inlet and outlet ports to protect the seats from particulate contamination. The valve is held closed against the inlet pressure by a spring that acts through the armature and the pushrod. Both armature and pushrod have Teflon bushings, which eliminate metal-to-metal sliding motion and the resultant need for lubrication. The solenoid is completely potted to restrain lead wires, coil wires, and solder joints during vibration. The solenoid is hermetically sealed by weld joints between the case, electrical receptacle, and base and by a glass compression seal within the electrical receptacle. In the construction of the solenoid magnetic path, 430 stainless steel eliminates need for protection from the operating fluid or from the atmo-

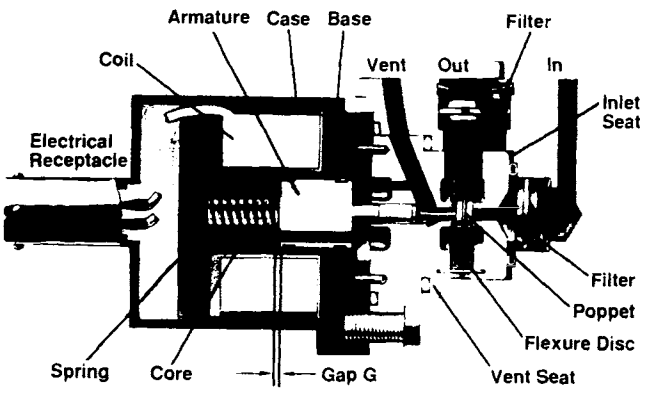

Fig. 7-33 Normally cosed solenoid-operated three-way valve.

sphere, and provides a high electrical resistivity for fast-response time.

Four-way-type pilot valves. A four-way-type pilot valve can replace two three-way valves for control of double-acting (two-directional) actuators. Figure 7-34 presents the basic schematic of a four-way pilot valve. The schematic shows a solenoid actuator; but mechanical or pressure actuators are also common. A four-way valve has two outlet ports, one normally closed and one normally open. The normally-open port is connected to the inlet port when the actuator is not energized. Likewise, the normally closed port is connected to the vent. When the actuator is energized and the poppet is moved to a second stop, the outlet ports reverse their function; i.e., the normally closed port is connected to the inlet and the normally open port is connected to the vent. Figure 7-34 shows a poppet-type four-way valve. Slide and sleeve four-way valves are also common but usually only in hydraulic systems.

Design of solenoid actuators. Solenoid actuators are usually applied to the sliding stem of pilot-valve poppets to give on-off, two-position operation. Solenoids (electromagnets) contain an armature or plunger that moves in a coil of wire. Energizing the coil exerts a magnetic force on the armature, the force's magnitude proportional to the cross-sectional area of the armature, the number of the coil turns, the electric current applied to the coil, and the gap between armature and core. The force of attraction increases as the gap narrows.

Figure 7-33 shows a typical dc solenoid actuator. Its magnetic circuit consists of a stationary core, case, base, and armature. Energizing the coil pulls the armature toward the core against a compression spring. The spring pushes the armature back to the normal position when the coil is de-energized.

The following equations are used for preliminary design of flat-faced (plunger-type) armature solenoids of the type shown in Fig. 7-33.

$$F = \frac{B^2 A}{72} \qquad NI = \frac{B\,G}{0.7\,P}$$

where—

- B = magnetic flux density in the air, kilomaxwells/in.^{2}
- A = armature cross-sectional area, in.^{2}
- P = factor comprising constants and the permeability of the fluid in gap G between core and armature; a value of 0.00319 applies for an air gap
- N = number of coil turns
- I = electric current to the coil, amp
- G = gap between core and armature, in.

The numerical value of 0.7 shown in the ampere-turns equation implies that 30% of the ampere-turns developed by the coil will be used in the fixed air-gaps and in the magnetic material, leaving the remainder to do the useful work across the variable air-gap G. More precise estimates of the distribution of the ampere-turns used within the magnetic circuit require analysis of all flux paths and are usually accomplished by numerical analysis of all fringing, leakage, and series flux-paths.

Solenoid actuators (particularly if energized for extended periods) must be designed with sufficient heat-transfer radiating-and-conducting surfaces to prevent temperature from becoming excessive. To provide the required current, the resistance of the coil should be based on its maximum temperature. Suitable protection, such as weld or braze joints, should be provided to prevent the solenoid from becoming contaminated with operating fluids.

Fast response in solenoids depends on magnetic materials with high resistivity, which reduces the eddy currents that produce flux opposing the direction of intended motion. Additionally, drop-out current may be high if gap G is permitted to go to zero. This problem can be avoided by use of nonmagnetic shims or by undercutting the face of the armature by a small amount (0.0005-0.0015 in.), leaving only a small surface area to contact the mating face.

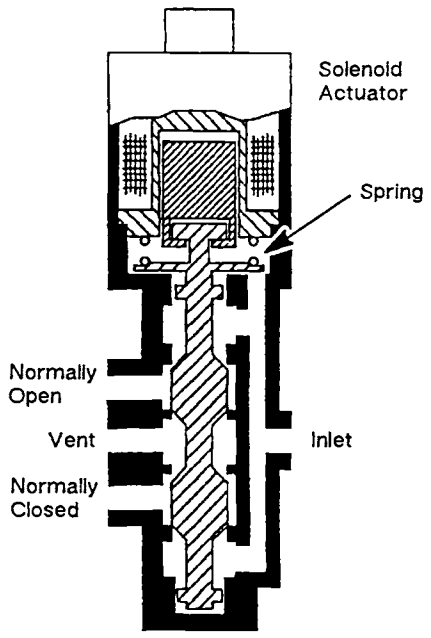

Fig. 7-34 Four-way solenoid valve schematic.

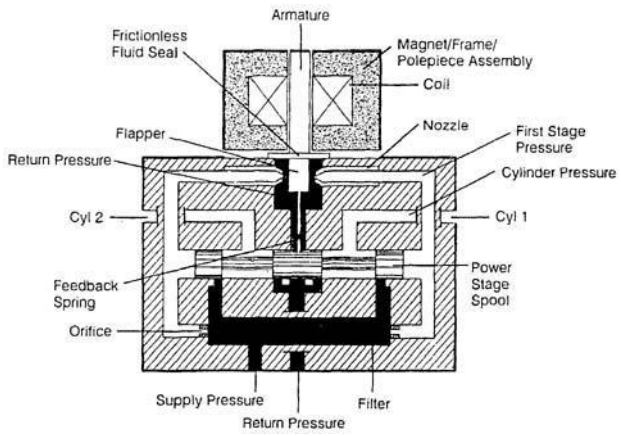

Fig. 7-35 Two-stage nozzle/flapper electrohydraulic flow-control servovalve.

Design of Servovalves

Servovalves, in general, are electrohydraulic devices that will control fluid flow or pressure applied to a load in response to an electrical signal. Valves are staged to fit the horsepower requirements of the application. A single-stage valve may be suitable for low-horsepower needs; two-stage valves are necessary for higher flow rates and pressure. The electrohydraulic interface takes place in the first stage, which incorporates a permanent-magnet torque motor and either a single-inlet (jet-pipe) or nozzle/flapper hydraulic servovalve.

Nozzle/flapper servovalve. Figure 7-35 shows a nozzle/flapper (first stage) combined with a purely hydraulic second stage. The sliding-spool valve arrangement displayed supplies the second-stage function of most servovalves for flight and engine-control applications. Proportional flow or pressure control is achieved through balance of electromagnetically-produced torque against moments produced by linear deflection of springs in the first and second stages.

The torque motor converts electrical input signals into mechanical motion of the armature. The magnets, frame, and armature form a magnetic circuit. Current applied to the torque motor coils creates an additional magnetic field which, when summed with the permanent field, produces a net torque on the armature. This magnetic torque, in a single-stage valve, is balanced by the motion of the armature, resulting from deflection of the flexure tube; in a two-stage valve, the feedback torque from spool motion is also summed.

Armature motion translates directly into displacement of the flapper between the nozzles and production of hydraulic forces on the spool. The motion of the flapper between the two opposed nozzles varies the pressure in the two branches of the hydraulic circuit. The hydraulic circuit constitutes a bridge network with four flow restrictions; two fixed orifices and two variable restrictions are formed by the nozzle/flapper clearances. Motion of the flapper increases restriction at one nozzle and decreases flow area in the other. Motion of the spool results from connecting these pressures to the ends of the spool and balancing the resulting force against the feedback spring.

The spool-and-sleeve valve represents a four-way design, with a pressure, a return, and cylinder 1 (CYL1) port and cylinder 2 (CYL2) port. Although pneumatic-service four-ways have a seat and poppets for positive sealing, hydraulic spool-and-sleeve valves rely on tight diametral clearances (on the order of 0.0002 in.) between the spool and sleeve to limit leakage flow to manageable values. The leakage through these lapped clearances is herein referred to as *lap leakage*.

Displacement of the spool from a neutral null position instigates flow from one of the two load ports (CYL1 or CYL2). Spool movement varies the flow areas of the load flow-metering slots in the second stage. Flow proportional to input current is achieved by using rectangular metering slots, in which the flow area is directly proportional to spool

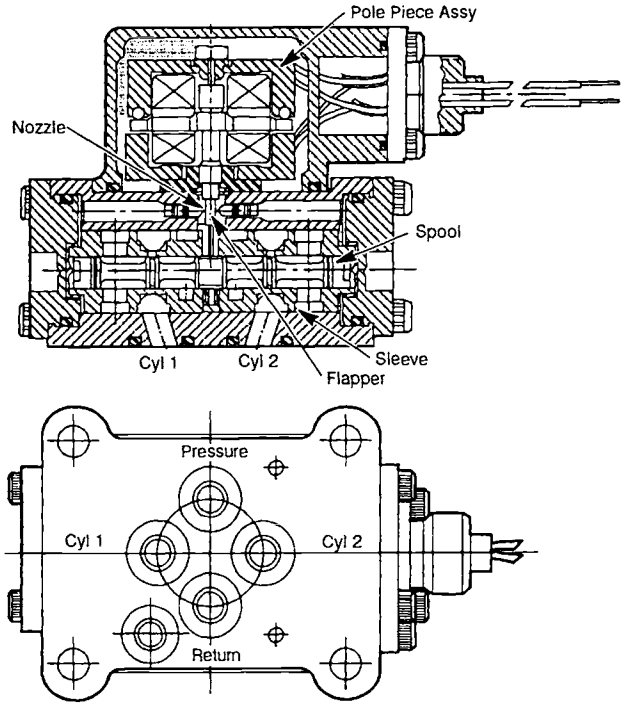

Fig. 7-36 Servovalve cross section.

displacement, and by restraining the spool with a feedback spring, referenced directly to the armature. The balance of the torque, created by spool motion with the torques produced by the electromagnetic circuit and angular deflection of the flexure tube, yields a linear relationship between input current and load flow.

Figure 7-36 shows the servovalve used on the SSME hydraulic-actuation system. The torque motor consists of coils, frame, and an armature assembly. Typical values for coil resistance and rated current are 1000 Ω and 8 mA, respectively. The frame assembly surrounding the coils closes the permanent-magnetic circuit of the torque motor. The frame is designed to minimize stray magnetic flux, so that the torque motor will neither react to, nor magnetically influence, other electrical equipment.

The armature assembly—motor armature, flapper, feedback spring, and flexure-tube support—is mass-balanced to provide minimum susceptibility to shock and vibration. The armature, which extends through the center of the coils, is mounted on a tube that acts both as a fluid barrier and a cantilever spring. The flapper extends below the assembly on the "wet" side of the joint to control the hydraulic circuit.

The first-stage orifices and filter are combined into one assembly to allow the filter to be washed with the second-stage flow. The filter is sized to ensure protection of the small restrictions in the first stage. Because any pressure drop is identical for both orifice circuits, use of a single filter element for both orifices eliminates the influence of filter pressure drop on valve null bias. Materials used in this assembly will be chosen for high structural strength, corrosion resistance, and minimum differential thermal expansion.

Servovalve performance requirements are typically defined by the following characteristics: rated flow, pressure gain, frequency response, internal leakage, hysteresis, threshold, and linearity. Typical values for the type of valves used on the SSME-HAS are as follows:

Rated flow	7.5 gpm at 3000 psid
Pressure gain	14,000 psi/mA
Frequency response	-3 db, -90° at 100 Hz
Internal leakage	0.20 gpm at 3000 psid
Hysteresis	3% rated current
Threshold	0.5% rated current
Linearity	±10 %

A basic understanding of the mechanics of a two-stage servovalve can be gained by examining simplified expressions for servovalve performance. The primary static-performance measurements will be seen in internal leakage, pressure gain, and second-stage flow. Internal leakage results from first-stage quiescent flow and lap leakage from the second stage; in equation form:

$$Q_{lk} = Q_{lk1} + Q_{lk2}$$

where—

Q_{lk} = Total internal leakage (total flow from pressure to return ports with no control flow demand, usually measured with cylinder ports blocked), $in.^3/s$
Q_{lk1} = First-stage quiescent flow, $in.^3/s$
Q_{lk2} = Second-stage lap leakage, $in.^3/s$

The following expression describes the first-stage flow:

$$Q_{lk1} = \frac{8.886\, X_{f0}\, C_{dn}\, D_n\, [P_s - P_r]^{1/2}}{p^{1/2}\left[1 + c_o^2\, X_{f0}^2\right]^{1/2}}$$

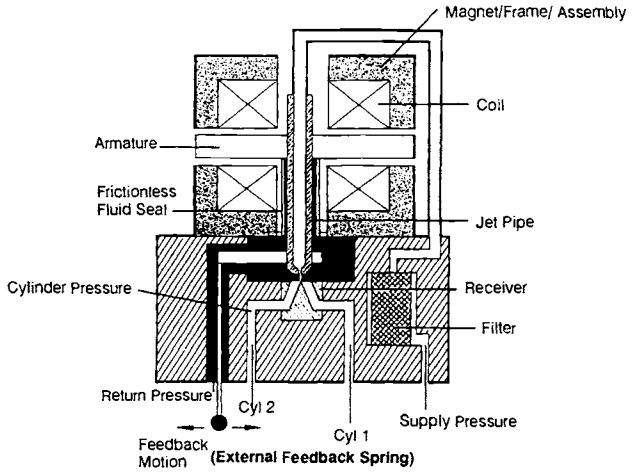

Fig. 7-37 Single-stage "jet pipe" electrohydraulic servovalve with mechanical feedback.

where—

A_o = Orifice area, $in.^2$
C_{dn} = Discharge coefficient for nozzle/flapper flow
C_{do} = Discharge coefficient for orifice flow
$C_o = \dfrac{\pi\, C_{dn}\, D_n}{C_{do}\, A_o}$
D_n = Nozzle diameter, in.
P_r = Return pressure, psi
P_s = Supply pressure, psi
p = Fluid density, $lb\text{-}s^2/in.^4$
X_{f0} = Nozzle/flapper spacing at null, in.

Second-stage leakage proves a more difficult quantity to predict because of the difficulty encountered in measuring dimensions such as diametral clearance and metering-edge radii. However, the following expression provides a reasonable estimate of the leakage through the overlap region of a spool valve:

$$Q_{lk2} = \frac{2wc}{p}\left[- \frac{3\mu C_{dm}^2 L}{c^2} + \left[\frac{(3\mu C_{dm}^2 L)^2}{c^4} + 2pP_c C_{dm}^2\right]^{1/2}\right]$$

where—

c = Radial clearance, in.
C_{dm} = Discharge coefficient for flow through spool/sleeve metering area (at null)
L = Spool/sleeve overlap (per edge), in.
P_c = Neutral cylinder pressure, psi
w = Total slot width, in.
μ = Fluid absolute viscosity, $lb\text{-}s^2/in.$

This expression holds for sleeves with two diametrically-opposed slots. Because the condition of the spool/sleeve metering edges for parameters C_{dm} and L must be taken into account, the designer must depend on previous experience in developing a two-stage servovalve.

First-stage pressure gain, an important factor in dynamic performance, normally will be measured in the development of a servovalve to verify first-stage sizing. It can be calculated using the following expression:

$$PG_1 = \frac{-4\, C_o^2\, S_{f0}\, (P_s - P_r)}{(C_o^2\, X_{f0}^2 + 1)^2}$$

Note that, in a two-stage servovalve, the spool must be locked in the null position to obtain a meaningful first-stage pressure-gain measurement.

Second-stage flow can be accurately calculated by using the turbulent-flow "orifice equation":

$$Q = C_{d2}\, w\, X_{sp}\left[\frac{P_s - P_r}{p}\right]^{1/2}$$

where C_{d2} = discharge coefficient for metered flow (out null region) and X_{sp} = spool stroke from null, in.

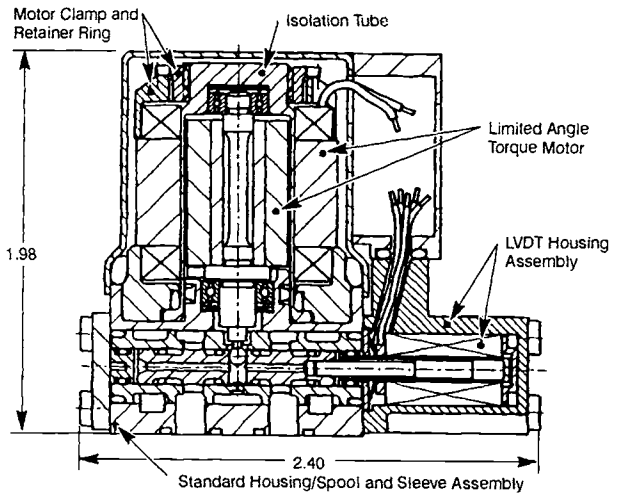

Fig. 7-38 Direct-drive servovalve.

Nozzle/flapper valves have been used as the first stage of dual-stage servovalves for at least 30 years. More recently, fluidic or completely electromechanical designs have been replacing nozzle/flapper valves on many applications.

Jet-pipe servovalves. In one type of fluidic valve design, the "jet pipe" configuration produced by HR/Textron, movement of the torque-motor armature deflects the dominant portion of a high-velocity jet into one of two "receivers," transferring the kinetic energy of the moving oil into differential pressure across a load (Fig. 7-37).

Direct-drive servovalves. In the last decade, significant work has been done in developing designs to replace the traditional electrohydraulic first stage with a completely electromechanical configuration. These "direct-drive" valves (Fig. 7-38) apply modern rare-earth magnet materials to generate the forces required to move the second-stage load and protect against contamination. The particular concept displayed employs a rotary, limited-displacement dc torque motor and an eccentric ball to impart axial motion to the second-stage spool. A LVDT provides position feedback to the control circuit.

Direct drive significantly reduces quiescent leakage, and the direct mechanical coupling of the motor to the valve also minimizes the effects of vibration, shock, and impulse loads on the null stability and accuracy of the device. The direct-drive valve currently sees favor in systems requiring great reliability, experiencing large thermal transitions and high vibration and shock loading, and needing better dynamic performance.

Design of Gas-Pressure Regulators

Basically, gas-pressure regulators are variable-area-type pressure-reducing valves. They maintain constant pressure at an outlet or in a downstream region, even though the pressure at the inlet may vary (decrease). Gas-pressure regulators may be operated independently, or in conjunction with pressure-relief devices, under either dynamic or static conditions.

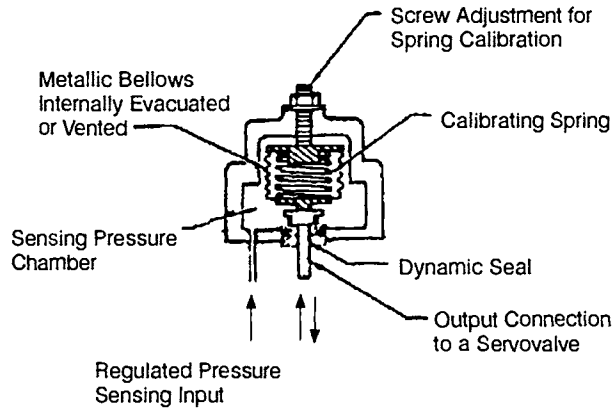

Fig. 7-39 Schematic of a typical gas-pressure-regulator controller.

For example, the gas-pressure regulator for the A-4 Stage propulsion system (Fig. 3-13) maintains a constant main-oxidizer-tank pressure of 165 psia, while the helium gas pressure at the regulator inlet varies from 4500 to 245 psia. If the tank pressure should continue to rise with the regulator completely closed because of such effects as aerodynamic heating, a tank relief valve gives additional protection.

Elements of gas-pressure regulators. Most pressure regulators include two basic elements, regulator controller and regulator valve. The controller controls opening of the regulator valve, which then meters the gas flow through the regulator.

The regulator controller, essentially a sensing and computing unit, measures the difference between actual and desired pressure. Its output, called the *error signal*, can be directly applied as a mechanical force, or it can control pressure output to a servovalve. Figure 7-39 shows the schematic of a typical gas-pressure regulator controller, the regulated pressure being sensed externally by a bellows, which is internally evacuated, or vented, to atmosphere. The vacuum establishes an absolute pressure reference, while the vented bellows uses ambient pressure for reference (gage pressure). As the regulated pressure (the sensing pressure) changes, the bellows deflects against a calibrated internal-spring load, simultaneously positioning a directly connected servovalve (Fig. 7-40), which in turn regulates a control-pressure output.

A regulator valve consists of the control valve and an actuator. If only limited accuracy is required, or if very small capacities are involved, the regulator controller can develop the error signal directly as a mechanical force to position the regulator valve. Such a directly spring-loaded pressure regulator is represented schematically in Fig. 7-41a. For greater accuracy, the regulator valve actuator can be positioned by controlled pressure from a servovalve connected to the regulator controller.

Figure 7-40 presents schematically the principle of operation of typical single-bleed, poppet-type, pneumatic servovalves (as used in gas-pressure-regulating services). Two basic configurations are in use. The first (Fig. 7-40a) regulates output control pressure p_C through variation of the bleed-port-flow area. The

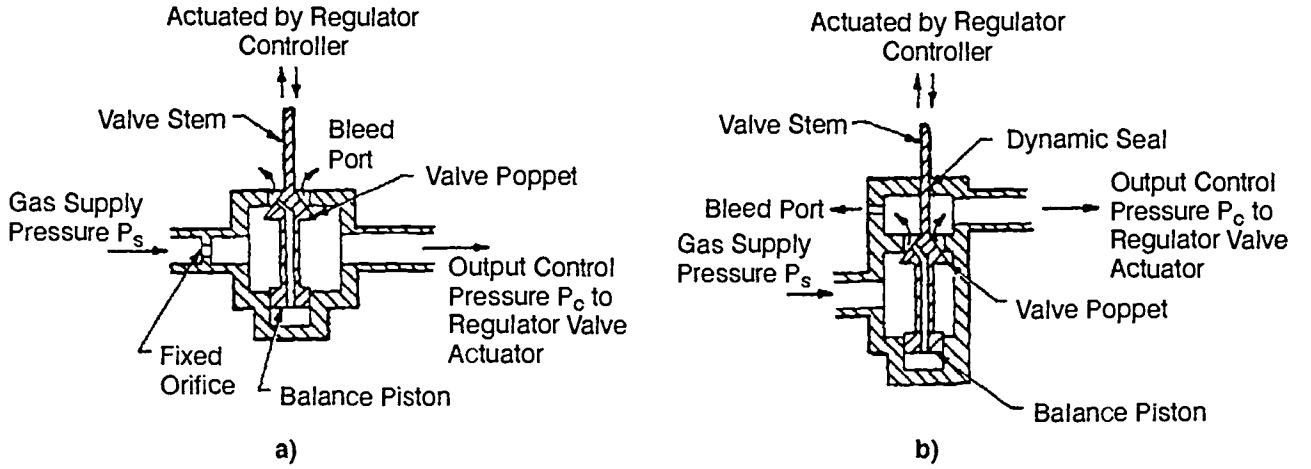

Fig. 7-40 Schematics of typical single-bleed, poppet-type, pneumatic servovalves used in gas pressure regulators.

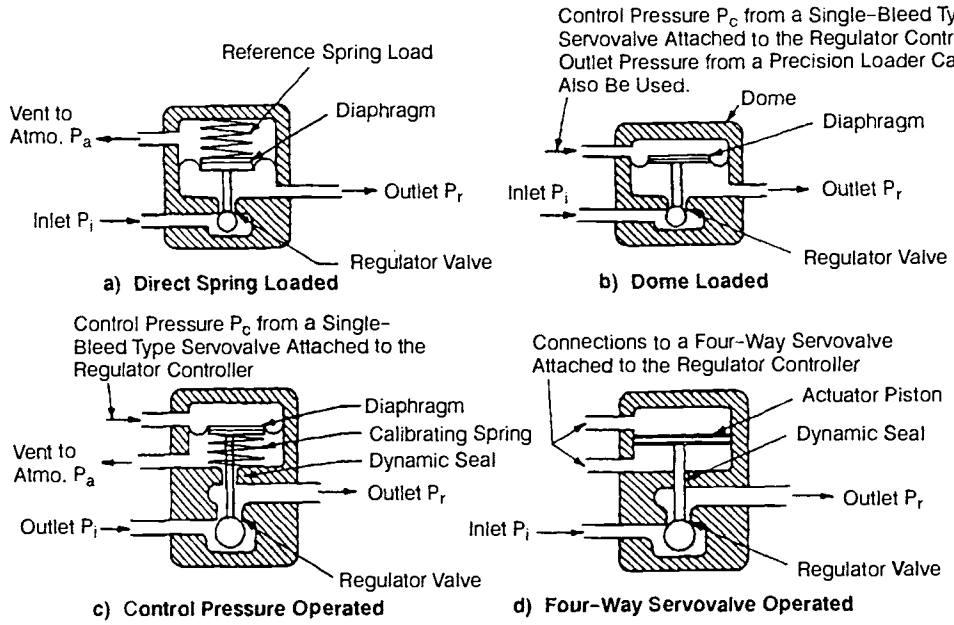

Fig. 7-41 Schematics of various gas-pressure-regulator designs.

second (Fig. 7-40b) fixes the bleed-port area , p_c being regulated by varying the gas-flow rate.

Because the servovalve amplifies them, small errors in regulated pressure will cause large changes in control-pressure output. This control pressure p_c can then be applied to control the regulator-valve position in the following ways:

1) Control pressure p_c serving as the loading pressure for a simple dome-loaded pressure regulator, as shown schematically in Fig. 7-41b. A large-capacity, dome-loaded pressure regulator can also be loaded by a separate, small-capacity precision pressure regulator (precision loader).

2) Control pressure p_c serving as the input to a mechanism that positions the regulator valve as a linear function of control pressure. In its simplest form, this mechanism, consists of a spring and a diaphragm (Fig. 7-41c).

When a single-bleed servovalve is used with the regulator controller, the supply pressure p_s to the control servocircuit must be isolated from the inlet pressure p_i to the main regulator valve, because of the steady-state error that would be introduced by the often extreme variation of p_i. A simple, (directly) spring-loaded, low-capacity regulator, similar to the one in Fig. 7-41a, will be required to reduce p_i to a reasonably constant supply of pressure p_s for the control servocircuit. This regulator, commonly called the "bleed regulator," can be a part of the main regulator controller.

Design considerations for gas-pressure regulators. Basic considerations for the design of gas pressure regulators include the following:

1) Principal causes of error in a pressure regulator: variation of inlet pressure, flow demand, and temperature; mechanical hysteresis, friction, and

creep of stress members; variation in effective length of members because of angular displacement; variation in vehicle acceleration, and vibration. Also, the fact that pressures are not sensed at the desired point of pressure control (influence of pressure drops caused by flow through downstream systems). Whether or not these errors have been held within allowable tolerances, without mechanisms (including diaphragms and springs) of unreasonable complexity and size, makes the basic test of a good regulator design.

2) Proven usage. Where feasible, proven concepts and control mechanisms of previous designs should be utilized—especially for dynamic characteristics, stability and transient response and for mechanical details, such as poppets, seals, diaphragms, and springs.

3) Balance of the regulator-valve poppet. It should minimize the forces imparted to the valve by inlet pressure p_i. This balance may be achieved by attaching a balance piston, similar to the one of the poppet servovalves (Fig. 7-40). However, this procedure will require some type of dynamic seal, and dynamic seals are known to be trouble sources. In certain applications, therefore, an unbalanced valve may be preferred.

4) Alternative mode. In most cases, the regulator must lend itself to the alternate mode of operation as a shutoff valve, until the opening of a start pilot-valve.

5) Lockups. The various gas-pressure-regulator designs in Fig. 7-41 control pressure by admitting additional gas, as required, to the regulated pressure region. If the flow demand on the regulator is reduced to zero (dead-end conditions), the regulator valve shuts off. However, the pressure in the regulated region may increase above the design point, even with the regulator valve closed, because of a time lag in closing, following reduction of demand to zero; inevitable regulator-valve leakage; and thermodynamic effects, such as increase in temperature of the gas in the regulated pressure region or vaporization of a pressurized liquid. The condition of zero flow, known as a lockup, often poses problems. Lockup can be eliminated by incorporating a relief valve downstream of the regulator valve as part of the regulator assembly. In the A-4 Stage propulsion system, individual relief valves for the main propellant tanks prevent possible intermixing of propellant vapors.

6) Miscellaneous design considerations for gas-pressure regulators: type of regulated gas; gas inlet-pressure and temperature range; regulated-gas outlet pressure level with respect to ambient or vacuum, its tolerance or accuracy of regulation, and range of adjustment; required maximum flow capacity; required response time and allowable overshoot; type of line connections; environmental conditions (temperature, vibration, humidity, etc.).

Figure 7-42 presents the dynamic-response characteristics of a typical pneumatic pressure regulator upon initiation of a demand. The regulator was set at a regulated outlet pressure of 400 psia. The gas used (helium) was discharged into a system of approximately 60-in.^{3} volume.

Sizing of the gas-pressure regulator. Required flow area across the regulator valve when it is fully open, i.e., the characteristic flow area of a pressure regulator, may be calculated for required flow capacity and regulated outlet pressure at minimum allowable gas-inlet pressure. The isentropic-nozzle-flow equation (Table 7-4) is typically used for sizing regulators.

Dome-loaded pressure regulators. The dome-loaded type of regulator (Fig. 7-41b), one of the most frequently used regulators, normally employs a metallic diaphragm in the main actuator to keep friction low. The dome pressure p_c, which determines the force to the actuator diaphragm and thus regulates valve position and outlet pressure, can be regulated either internally by a pressure controller or externally by a low-capacity pressure regulator or loader. There are many variations of dome-loaded regulators.

The typical dome-loaded gas pressure regulator, shown in Fig. 7-43, has an alternate mode of operation as a shutoff valve. The regulator chiefly maintains a regulated outlet pressure at a preselected value called the "set point." The regulator is composed of four elements: start pilot-valve, bleed regulator, sensing control unit, and main regulator valve. The combination of bleed regulator and sensing control unit forms the main regulator controller.

The start pilot valve—a solenoid-actuated poppet valve normally held closed by a spring—in the closed position locks up the outlet pressure of the bleed regulator. The bleed regulator—a normally-

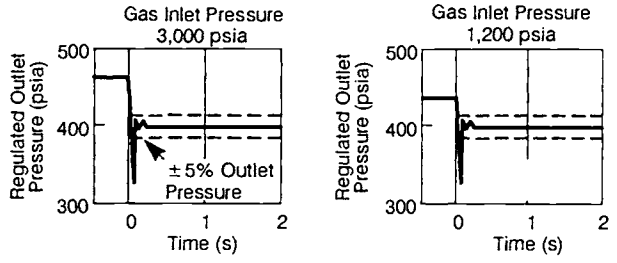

Fig. 7-42 Dynamic response characteristics of a typical pneumatic pressure regulator.

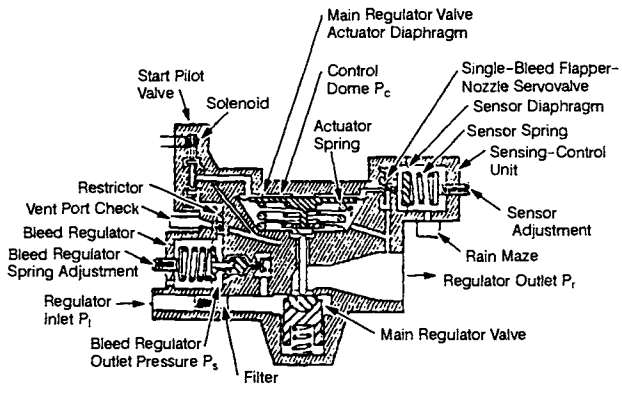

Fig. 7-43 Schematic of a typical dome-loaded, negative-gain-type gas regulator with an alternate mode of operation as a shutoff valve.

Table 7-5 Principal design parameters of a typical dome-loaded, negative-gain-type gas-pressure regulator (see Fig. 7-43).

Parameter	Design Data
Regulated gas	Helium
Inlet gas pressure, pi	4,500 psia nominal, 5,800 psia maximum, 500 psia minimum
Inlet gas temperature, T	110° to 360°R
Regulated outlet pressure, p_r	500 psig ±25 psi
Flow demand	a. Maximum: 0.1 lb/sec at 500 psia inlet pressure and 160°R inlet temperature b. Minimum: zero
Modes of operation	a. Start pilot valve solenoid deenergized: regulator remains shut off. outlet pressure = 0 b. Start pilot valve solenoid energized: regulator functions normally
Controller bleed	a. None when start pilot valve solenoid deenergized b. 0.002 lb/sec at 530°R when solenoid energized
Main regulator valve	Seating diameter, 0.205 in; characteristic area, 0.0281 in^2
Main regulator valve actuator	Effective area, 7.55 in^2; bias spring preload, 75.5 lb; rate 500 lb/in.
Start pilot valve	Seating diameter, 0.025 in; characteristic area, 0.000437 in^2
Bleed regulator valve	Seating diameter, 0.028 in; characteristic area, 0.000301 in^2
Bleed regulator sensor	Effective area, 0.185 in^2; reference sprig preload 93.5 lb; rate 1,500 lb/in.
Bleed flow restrictor	Diameter, 0.0116 in.; area, 0.000105 in^2
Main regulator controller sensor	Effective area, 0.315 in^2; reference spring preload, 126 lb, rate 702 lb/in.
Flapper-nozzle servovalve	Seating diameter, 0.043 in. (2 holes; maximum stroke, 0.0011 in.; maximum flow area, 0.003 in^2; bias spring preload, 1.0 lb; rate, 5.0 lb/in.

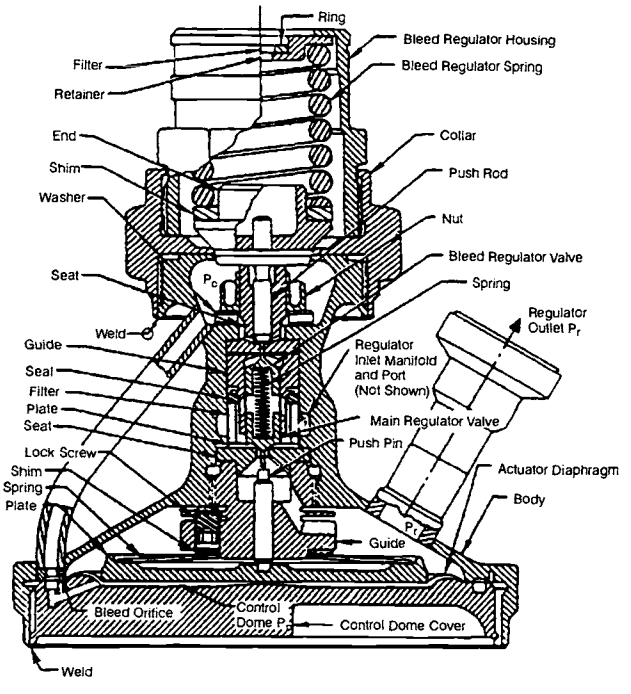

Fig. 7-44 Typical dome-loaded, zero-gain type gas-pressure regulator loaded by a bleed regulator.

closed, directly-spring-loaded type of pressure-reducing valve—supplies an approximately constant preset pressure to the sensing control unit. This preset pressure exceeds the main-regulator outlet pressure p_r. It is the sensing control unit, then, that establishes the main-regulator outlet pressure. It detects small deviations from the set point and magnifies the error signals by means of a single-bleed, nozzle/flapper servovalve linked to a sensor diaphragm by increasing or decreasing the control pressure p_c that operates the actuator diaphragm of the main-regulator valve, a normally-closed, dome-loaded pressure-reducing device.

Operations follow this sequence of events. Gas enters the regulator through a filter located at the regulator inlet port, but is prevented from entering the main-regulator-control pressure dome by the closed start-pilot valve. Upon opening the start-pilot valve by energizing its solenoid, gas flows through the bleed regulator and is reduced to pressure p_s, as determined by the preset reference-spring force. The gas then enters a fixed restrictor and passes into the control dome, where the flow tends to open the main-regulator valve against the actuator spring. Dome pressure p_c is controlled by varying the flow area of the nozzle/flapper servovalve, which bleeds the loading gas into the main-regulator outlet manifold. Equilibrium between the sensed regulated-outlet pressure p_r and the sensor-spring force positions the servovalve flapper a sufficient distance off the nozzle seat and maintains a steady-state control pressure p_c—a pressure always greater than p_r, as determined by the set of the main-regulator-valve actuator spring. Under these steady-state conditions, gas continues to flow from the bleed regulator through the servovalve at a rate determined by the restrictions and out to the outlet manifold. The regulator-controller circuitry has what is called a negative gain. A sensed increase in pressure p_r causes an amplified decrease in control pressure p_c, with attendant decrease of the main-

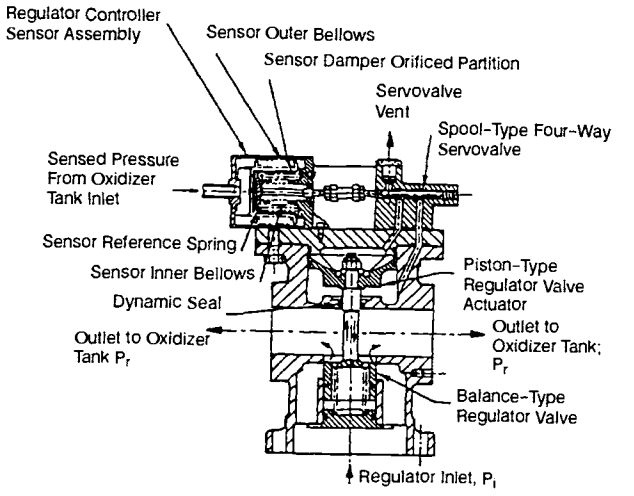

Fig. 7-45 Integrating-type gas-pressure regulator with spool-type, four-way servovalve.

regulator-valve opening. Similarly, a decrease in p_r causes an increase in valve-opening. The controller gain can be defined as follows:

$$G = -\frac{\Delta p_c}{\Delta p_r} \qquad (7\text{-}44)$$

where G = controller gain, Δp_C = change in control pressure, psi, and ΔP_r = change in sensed pressure, psi. Table 7-5 lists the principal design parameters of the gas-pressure regulator displayed in Fig. 7-43.

Figure 7-44 presents the design layout of a typical dome-loaded, zero-gain type of gas-pressure regulator. The main-regulator controller consists of a spring-loaded bleed regulator and a fixed-area bleed orifice, which gives a constant bleed from the control dome to the regulator outlet. The bleed regulator maintains the control-dome pressure p_c at a constant level. Here, too, control pressure p_c exceeds the regulated outlet pressure p_r by an amount determined by the main-regulator-valve actuator-spring preload. This regulator has been designed to maintain an outlet pressure p_r of 282 psig ±5 psi at inlet pressures ranging from 5000 to 375 psig. The actuator diaphragms are made of a 0.0025-in., 17-7 PH high-strength stainless-steel sheet. All sliding members, such as regulator-valve poppets and guides, use 440C stainless steel to eliminate surface galling. The regulator main body and housing are made of aluminum-alloy forgings.

Integrating-type pressure regulators. Figure 7-45 presents the design of a typical integrating-type gas-pressure regulator that controls the propellant-tank pressures of a pressurized-gas propellant feed system such as the A-4 Stage propulsion system. Main-oxidizer-tank pressure is sensed through a relatively short external line. Fuel-tank pressure is maintained at 10 psi below the oxidizer-tank pressure by different pressure settings of line check-valves and tank-relief valves. A spool-type, four-way servovalve, which is directly connected to the sensor of the regulator controller, controls the regulator-valve actuator. Supply pressure p_s of the servovalve is taken from the regulator-outlet pressure p_r (i.e., $p_s = p_r$). The sensor contains two bellows with an oil-filled damper between them. The damper consists of a partition with a properly sized orifice. The outer bellows (exposed to the propellant vapors) is hydroformed from thin 321 stainless-steel tubing, because the pressure differential across it is small and because it contains fluid. The inner bellows must withstand a pressure differential equal to full tank pressure, since the interior of this bellows vents directly to the atmosphere. For this reason, the bellows is machined from 17-4 PH stainless-steel stock. This regulator is called an integrating type because a constant-tank pressure error will produce a constant actuator-piston velocity (neglecting extraneous forces). This velocity, in turn, gives a constant regulator-valve opening (or closing) velocity and a constantly increasing (or decreasing) gas-flowrate. Tank pressure is then the integral of tank pressure error vs. time. The integrating type of pressure regulator provides the constantly increasing regulator-valve flow area required for decreasing supply pressures, with minimum error in tank pressure, but may be unstable if the gain of the servovalve and actuator combination gets too high. A suitable gain value should be determined by computer studies of the regulator dynamic characteristics.

Design of Liquid-Flow and Pressure Regulators

Liquid-flow and pressure regulators basically are variable-area-type, pressure-reducing valves. A liquid-flow regulator maintains a constant rate of flow or limits the maximum rate of a flow. A liquid-pressure regulator, like a gas-pressure regulator, maintains a constant fluid pressure at its outlet under variable-flow conditions. Design considerations for liquid-flow regulators and pressure regulators are similar to those for gas regulators.

Design of liquid-flow regulators. Liquid-flow control can be obtained with a venturi. The pressure at the throat is proportional to the velocity of the (incompressible) fluid and thus the flowrate. The pressure differential between throat and inlet can be used to control the position of a butterfly valve, and thus the flowrate, by means of a servocontrol circuit. Figure 7-46 shows the schematic of a regulator of this type.

Figure 7-47 presents the principle of another type of flow regulator that frequently gets used in rocket-engine systems because of its simplicity. It consists of two restrictors, one of fixed and the other of variable area. This combination automatically maintains a constant pressure drop across the fixed restrictor, providing a constant flow. The fixed restrictor consists of a disk containing a number of orifices and mounted in a piston. The variable restrictor is formed by variable throttle ports located around the piston periphery. The pressure differential across the fixed orifices causes the piston to move against the regulator reference-springs. Piston throttle ports and reference-spring rate are designed to maintain a constant pressure drop across the orifice disk.

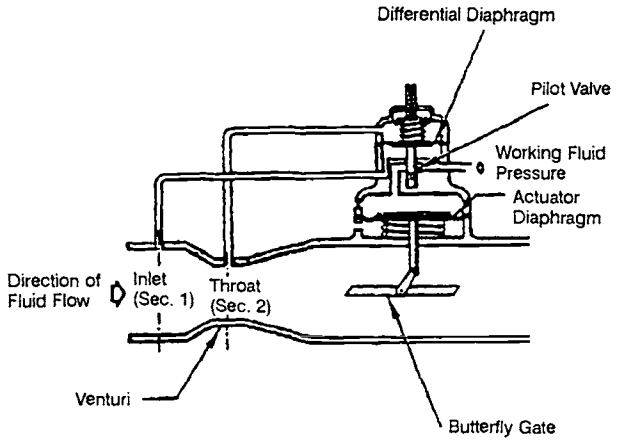

Fig. 7-46 Schematic of a typical closed-loop, fluid-flow control system.

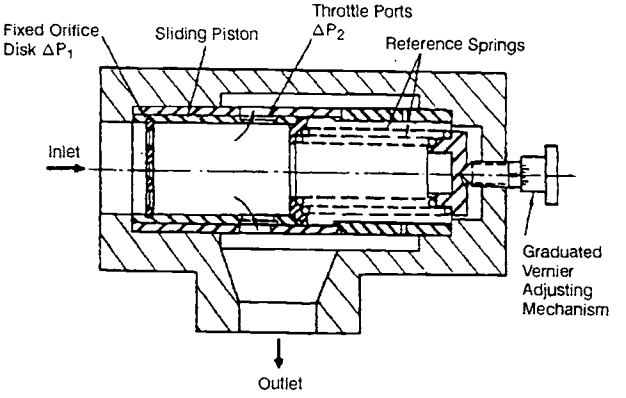

Fig. 7-47 Schematic of a typical sliding-piston-type liquid-flow regulator.

As the fluid inlet-pressure increases, or the back-pressure decreases, the flowrate tends to increase also. However, the attendant increase is pressure differential; i.e., pressure force on the piston moves it against the reference springs, simultaneously increasing the flow restriction. A new equilibrium is achieved as the inlet-pressure increase is absorbed by an increase in pressure drop across the piston throttle port. The following design correlations have been established for this flow regulator:

$$F_s = (\Delta p_1 + \Delta p_2)A_p \qquad (7\text{-}45)$$

$$K_s = \frac{\Delta p}{\Delta l} A_p \qquad (7\text{-}46)$$

where—

F_S = regulator reference-spring preload, for a given flowrate, lb

ΔP_1 = pressure drop across the fixed orifice disk at that flowrate, psi

Δp_2 = pressure drop across the piston throttle ports at that flowrate, psi

A_p = effective piston area, in.^{2}

K_S = regulator reference-spring rate, lb/in.

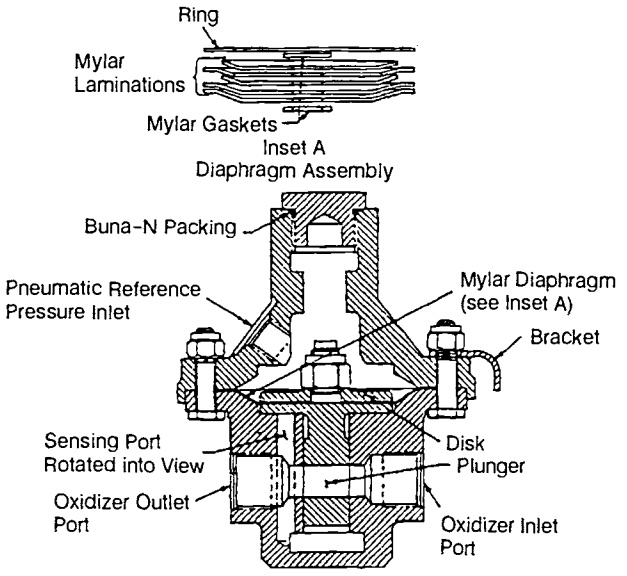

Fig. 7-48 Typical liquid-pressure regulator design for LOX service.

$(\Delta p/\Delta l)$ = change of pressure drop across the piston throttle ports per inch of movement of piston, lb/in.^{2}-in.

Adjustment of the regulated flowrate is made by adjusting the reference-spring force, using a vernier mechanism.

Design of liquid-pressure regulators. Figure 7-48 presents a liquid-pressure regulator design frequently used in rocket-engine systems. The actuator diaphragm of the regulator valve (plunger) can be loaded either by a pneumatic reference pressure (as shown) or by a reference spring. Regulated outlet pressure is sensed directly. An increase in outlet pressure tends to reduce the flow area of the regulator valve until an equilibrium is reached between outlet and reference pressures. The actuator diaphragm is made of Mylar laminations, which are compatible with cryogenic propellants, such as liquid oxygen.

Design of Pressure-Relief Valves

Pressure-relief valves protect fluid systems and pressure vessels from being over-pressurized. There are two basic types, the direct-operated and the pilot-operated. In the direct-operated, the valve poppet is loaded directly by a properly calibrated reference spring. The valve opens as the pressure force acts against the spring force. In the pilot-operated valve, the main-relief-valve actuator is controlled by a pilot valve calibrated for the desired relief-pressure setting. The direct-operated relief valves are used for large tolerance, low-capacity services. For large-flow requirements, pilot-operated relief valves are used for quick response and to avoid excessive size. Most pressure-relief valves are used in gas-pressure systems. Important design considerations include type of gas and its conditions; pressure-relief level, its tolerance and range of adjustment; required response

time, dead-band (differential between actuation or opening, and deactuation or closing pressure), and other dynamic characteristics; required maximum-flow capacity; simplicity of construction and line connections; and environmental conditions, such as temperature, humidity, acceleration, and vibration.

The required flow area for a gas-pressure relief valve at a maximum-opening position, i.e., its characteristic flow area, can be calculated from the isentropic nozzle equation of Table 7-4.

Direct-operated gas-pressure relief valves. Figure 7-49a shows the design of a typical low-capacity, direct-operated gas-pressure-relief valve. Its poppet is loaded directly by a coil spring. This valve is one of the simplest designs, but it may become dynamically unstable under externally introduced vibration.

Figure 7-49b gives the schematic of an improved design of a direct-operated relief valve, one assuring a predictable deadband and eliminating chatter under vibration. This design employs coned-disk-type (Belleville) springs, operating between positive stops, in the negative-rate portion of the force-deflection curve of the spring. As shown in Fig. 7-49b and 7-50, the spring remains against pretravel stop C until the applied force (valve-inlet pressure p_i x valve-poppet seat area) reaches level A. The spring then snaps from C to the post-travel stop D, with no further increase in applied force. Reduction of the applied force to B will cause the spring to snap back from D to C. The positions of the pretravel/posttravel stops can be adjusted for constant actuation and deactuation forces, independent of spring-manufacturing tolerances. The coned-disk spring washers are usually made of beryllium copper or 17-7 PH stainless steel. This type of relief valve suits high-pressure-helium storage bottle services, such as in the A-4 Stage propulsion system.

Pilot-operated gas-pressure relief valves. Figure 4-51 presents the schematic of a typical high-capacity, pilot-operated tank-gas-pressure relief valve. Normally, both main and pilot valves are held closed by valve spring forces F_{sm}, F_{s3}, and pressure p_c. The pilot-valve controller also senses the tank pressure p_t. When the pressure reaches or exceeds the preset level, the pilot valve is actuated to open (cracking pressure). The open valve vents the main-relief-valve-actuator control pressure p_c and, in turn, permits the main valve to open. The main-valve poppet position is a function of the control pressure, which then is controlled by the position of the pilot-valve poppet and by the tank pressure.

Design of Miscellaneous Fluid Flow Control Components

Check valves. Check valves allow fluid flow to go in only one direction. There are two basic check-valve types, the poppet and the swing-gate. Valve selection depends to a great extent on application. General design requirements for check valves include type of fluid and its pressure and temperature, required flow capacity, allowable pressure drop, allowable rate of reverse leakage (including zero leakage), space envelope and line connection, and simplicity of construction.

Figure 7-52 pictures the design of a typical poppet-type check valve. A light, compression-return spring normally holds the poppet in the closed position, preventing any possibility of fluid leaking back. When fluid pressure is introduced upstream, the poppet will open against the return spring. Because of their relatively high-pressure drop, check valves of this type are used only in low-capacity service, with either elastomer O-rings or metal-to-metal seals.

Figure 7-53 illustrates a swing-gate-type check valve. It consists of two elements, inlet body and outlet body. The swing gate is secured to the inlet body. A torsional-type return-spring holds the gate in closing position. Swing-gate check valves minimize pressure drop. However, positive sealing against reverse flow is more difficult. In some applications, orifice holes are drilled in poppets or swing gates to allow a regulated reverse flow for specific control purpose.

The tendency for check valves to oscillate during operation can be overcome by three methods:

1) Design the check valve to be fully open against a stop for the required flowrate and never reduce flow below the design flowrate during service.

2) Provide coulomb (friction) damping.

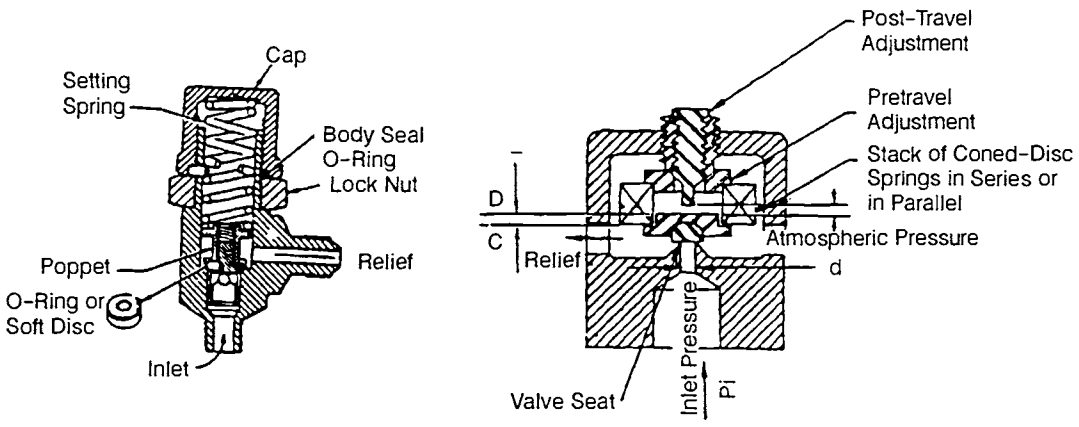

a) Coil-Spring-Loaded, Direct-Operated Relief Valve

b) Snap-Action, Coned-Disk, Spring-Loaded, Direct-Operated Relief Valve

Fig. 7-49 Low-capacity, direct-operated gas-pressure-relief valves.

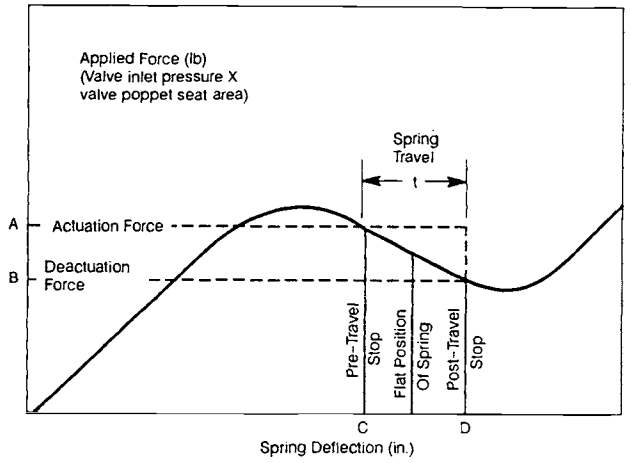

Fig. 7-50 Coned-disk-spring, force-deflection curve.

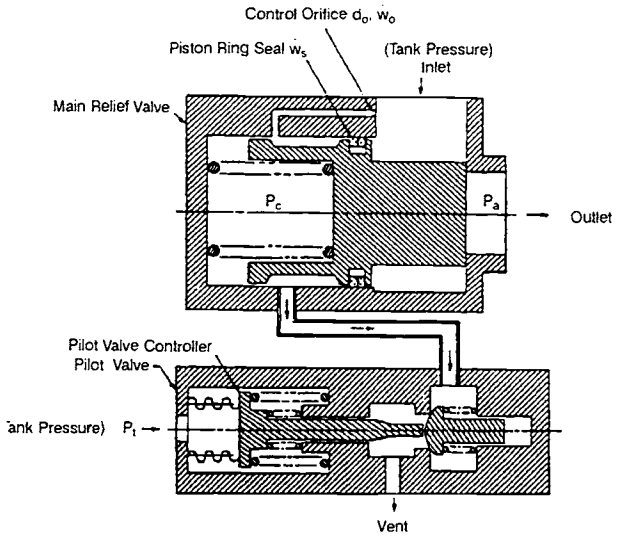

Fig. 7-51 Schematic of a typical high-capacity, pilot-operated tank-gas-pressure relief valve

3) Provide an augmented force to hold the poppet on an open stop at reduced flowrates.

Often, it is not possible to control the actual range of flowrates the check valve will be exposed to, once it is in service. As a result, preventing poppet oscillation by means of method (1) is usually impractical. Method (2), friction damping, has been used successfully; but hysteresis introduced by the friction causes cracking and reseating pressures to become less predictable. Method (3), augmenting the poppet force, can extend the range of flow rates over which oscillation does not occur. This range will be somewhat narrower than for coulomb damping; but problems associated with hysteresis will not develop.

Augmented-force check valves (Fig. 7-54) in the purge lines on the SSME isolate the pneumatic purge system from propellant systems. Force augmentation is achieved by placing a restriction (B) downstream of the seat adjacent to the poppet head area (C). As

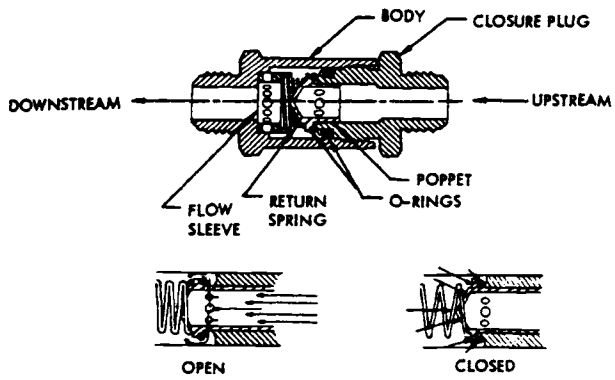

Fig. 7-52 Typical poppet-type check valve.

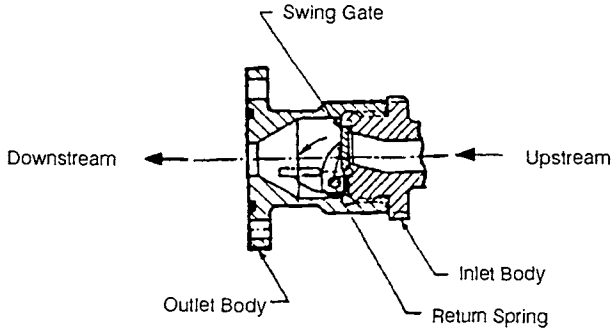

Fig. 7-53 Typical swing-gate-type check valve.

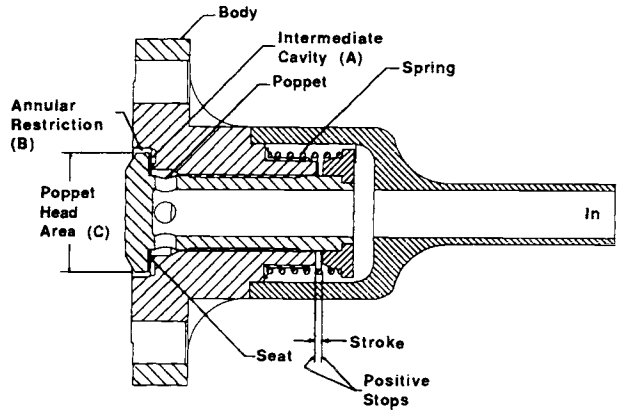

Fig. 7-54 Augmented-force check valve used in the SSME purge system.

inlet pressure is increased, pressure acting over the seat area overcomes the spring force and the poppet begins to open. As the poppet moves open, pressure builds up in a cavity (A) intermediate of the seat and the restriction (B). This intermediate pressure provides an augmenting opening force by acting against the poppet-head area (C). The poppet in this design will move to a fully-open position and rest on the positive stops at differential pressures lower than the initial cracking differential-pressure, thus extending the range of flow rates with no oscillation.

The check valve in Fig. 7-54 has metal-to-metal seating with a hard facing on both poppet and seat. This arrangement permits service with back pressures

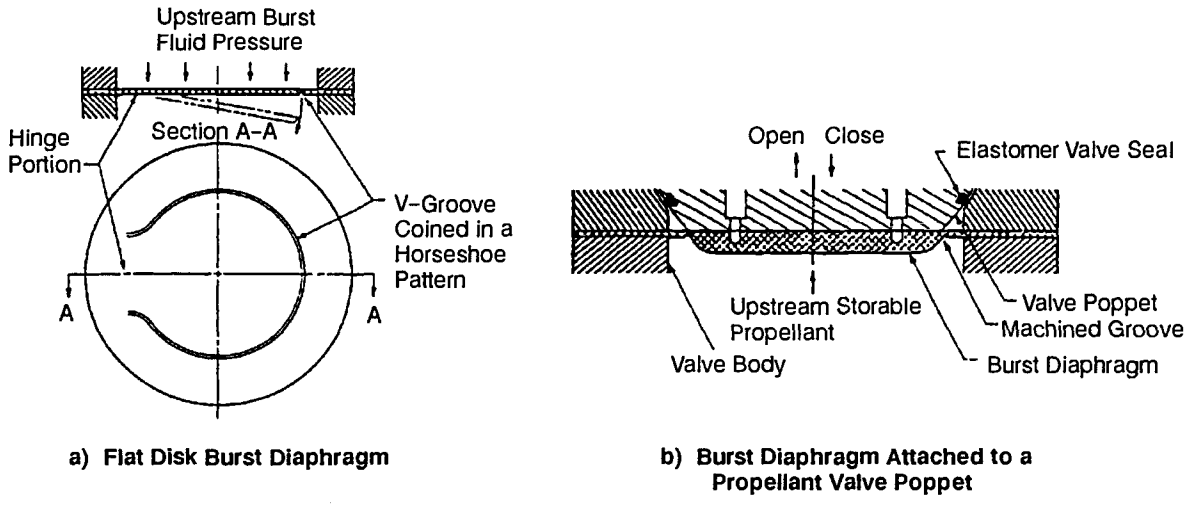

a) Flat Disk Burst Diaphragm

b) Burst Diaphragm Attached to a Propellant Valve Poppet

Fig. 7-55 Typical burst-diaphragm designs.

up to 8500 psi with both liquid-hydrogen and liquid oxygen propellants. This specific design flows up to 130 scfm of nitrogen at 750 psi and 70°F.

Burst diaphragms. To gain positive, hermetic sealing, the designer will often use burst diaphragms, especially in storable-liquid-propellant engine systems. They also serve as safety valves to prevent excessive pressures or to initiate flow at a predetermined pressure. Burst diaphragms can be ruptured either by the upstream fluid pressure or by mechanical means. General design considerations for burst diaphragms include these important points:

- The type of fluid and corrosive characteristics of it.
- Duration of storage (especially with corrosive storable liquid propellants).
- Method of diaphragm installation in duct or valvebody.
- Method of rupture (upstream fluid pressure or other means).
- Burst-pressure level (if upstream fluid pressure is used) and its tolerance; environmental temperature effects.
- Retention of the diaphragm after rupture (no metal particles are to be ejected).
- Allowable pressure drop across the burst diaphragm.

Figure 7-55a shows a typical flat-disk-type burst diaphragm. A V-groove has been coined into it in a horseshoe pattern. The depth of the groove will determine the burst pressure. The uncoined section serves as a hinge during rupture and as a retainer. The diaphragm can be jointed to the duct by welding, brazing, or bolting. This design has been satisfactory for many applications.

Figure 7-55b shows a poppet-type storable-propellant valve with a built-in burst diaphragm, that assures a positive, hermetic seal of zero leakage during long storage periods. It also protects the elastomer seal of the valve seat. Rupture of the diaphragm occurs during valve opening, either from valve actuation or from upstream propellant pressure. When closing, satisfactory valve sealing is provided by the elastomer seal only.

Burst diaphragms are made from a wide variety of metals. Annealed aluminum alloys such as 1100-0 and 6061-0, are among the alloys most easily controlled. Burst diaphragms rupture in a combination of shearing, bending, and tearing. The exact burst pressure of a specific diaphragm design can be evaluated only experimentally. Variations of the material's ultimate strength have a pronounced effect. The consistency of the desired diaphragm burst-pressure level will be greatly enhanced by the following precautions in manufacturing and quality control:

- Grinding the raw sheet or diaphragm to ensure uniform, accurate thickness.
- Close control of groove depth, by precision coining or machining, and by stress-relieving before and after coining.
- Continuous testing of the diaphragm material for hardness.
- Close control of the clamping pressure with bolted diaphragms.
- Close control of the welding or brazing processes to minimize heat effects.
- Proper dimensioning of diaphragm thickness and groove depth to allow for corrosive effects of the propellant during storage.

It is possible to hold burst-pressure variations of a specific diaphragm design to within 2% for diaphragms of over 1-in. diameter and design burst-pressures greater than 300 psi. For diaphragms of smaller size and lower burst-pressure, this tolerance may increase up to 5%. Because deliverable burst diaphragms cannot be tested, a number of samples are drawn from each manufacturing lot for testing. The number of samples is determined statistically to meet specific reliability requirements.

Explosive-actuated valves. For a device that may be required to operate only once (either to open or to close), an explosive-actuated valve provides the smallest possible size and weight. Because the power of the explosive actuation is virtually unlimited, a rigid, hermetic, zero-leakage-type seal can be used with this type of valve.

Figure 7-56 displays a typical explosive-actuated pilot valve (developed and produced by the Conax

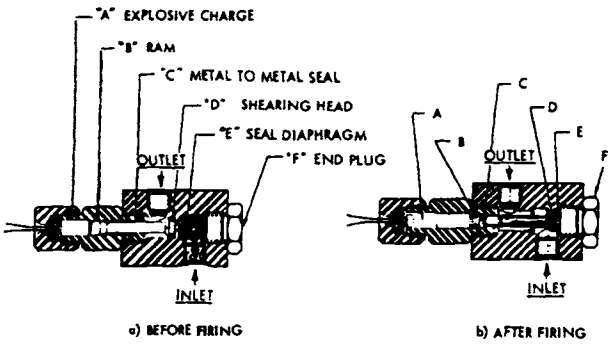

Fig. 7-56 Typical explosive-actuated pilot valve.

Corp). The actuator of this normally closed valve consists of an explosive charge "A" and a ram "B," including a shearing head "D." The seal of the valve has a solid metal diaphragm "E," machined as an integral part of the valve body. Upon an electrical signal the explosive charge detonates and drives the ram forward to cut out the seal diaphragm as a single piece of metal and hold it firmly against the end plug "F." The tapered head of ram "B" plunges into the guide-hole edge and causes a perfect metal-to-metal seal at point "C." This seal prevents contamination of the working fluid with gases from the explosive charge. The input current required for this valve is about 0.5 A, and actuation of the valve takes about 0.002 s.

7.3 DESIGN OF INSTRUMENTATION AND HARNESSES

Engine Instrumentation

For high-performance liquid rocket engines to meet demanding mission objectives, all component subsystems must be designed to operate at peak performance levels. All of the components are monitored continuously during the construction and hot-fire testing phases to ensure that reliable performance characteristics will be maintained throughout development and delivery. It is only through the use of highly specialized instrumentation and dedicated computing capability that closed-loop control, condition monitoring, and engine safety requirements can be met.

To successfully instrument a rocket-engine system, the designer must understand the intricacies of normal engine operation. This understanding should then be followed by instruction in instrumentation basics and control theory tempered by a meaningful treatment of rocket-engine failure mode data. Before instrumentation can be installed on an engine, detailed analyses must be performed to define fatigue factors, vibration levels, and heat-transfer characteristics. From a purely functional standpoint, individual sensor designs can range from the relatively simple to the highly complex. Selecting the right sensor for the job directly impacts the performance and reliability characteristics of an engine system.

Typical rocket-engine systems contain a large array of instrumentation for specific measurement tasks, in four main categories reflecting the criticality of the control system: engine ready (blueline), safety (redline), control, and condition monitoring. Some of these tasks require redundant measurements using either multiple sensors or multiple-channel sensors.

Five essential parameters must be monitored in an engine: temperature, pressure, flow rate, pump/turbine speed, and vibration. Measurements will be made during the engine design-verification or development stages plus condition-monitoring evaluations of roller bearings, coolant liners, turbine blades, etc. Sensors such as strain gages and heat-flux calorimeters are generally used for such measurements.

Proper instrumentation requires that a sensor or sensor system satisfy a wide range of operating parameters. A good rule of thumb sets a target for each sensor of using a third to two-thirds of its total range. This will be particularly important for pressure sensors because they tend to be more accurate within this range.

A thorough sensor evaluation is especially important when designing or specifying sensor components to be used in close proximity to engine hardware, due primarily to the violent nature of the engine environment. A shallow knowledge of rocket-engine behavior can produce disastrous results. Material compatibility is a major issue where liquid oxygen is concerned. Many non-metallic materials are not tolerated by the liquid-oxygen environment and can produce a violent, sometimes explosive reaction. Hydrogen on the other hand, interferes with the intergranular structure of certain nickel-chromium alloys (17-4pH for example), leading to material degradation. Special consideration should be given to the thermal properties of materials (thermal range and thermal expansion) since these effects can compound structural weaknesses.

Most importantly, once a sensor has been selected for use in an engine, proof that it functions properly over the specified temperature range will be essential to its eventual acceptance into established sensor inventories. Although a given temperature sensor might not be rated for use at liquid-oxygen or liquid-hydrogen temperatures, it is often possible to "extend" thermal ranges by performing a calibration at the "new" operating temperature.

Principal Types of Instrumentation

Temperature sensors. There are three common sensors used for measuring temperature: thermocouples, resistance temperature detectors (RTDs), and thermistors (Table 7-6).

Two dissimilar metal wires joined at one end forms a thermocouple. It generates an electromotive force (EMF) proportional to its bulk temperature. Thermocouples are simple, rugged, and have fast response time, 100 ms for very small wire diameters. They can readily be installed into most engine designs. Thermocouples are available in a variety of types for specific applications (Table 7-7).

As a disadvantage, a thermocouple has very low output voltage (Fig. 7-57), approximately 60 mV, thus

necessitating a signal amplifier. In addition, thermocouple output tends to drift over time, and that, depending on the usage time-frame, may create a problem. There are other design factors to take into account before selecting a specific thermocouple for a given application. Grounded-type thermocouples have a faster response time than ungrounded, but a shorter useful life due to mechanical strain induced during thermal cycling (Fig. 7-58 and 7-59).

Thermoelectric elements should also be matched to the physical environment in which they will be used. For example, iron-constantan thermocouples rust when exposed to moist environments. For this reason, sealed sheaths normally protect thermocouple wires. Whenever possible, thermal-expansion coefficients of the thermoelectric materials should be matched to those of the sheath material to minimize thermally-induced-strain effects.

The resistance temperature detector (RTD), a wound coil made of platinum or nickel wire whose resistance varies with temperature, gives stable performance over long periods and is highly accurate, especially while sensing at cryogenic temperatures. The coil RTD often forms the fourth leg of a wheatstone bridge that converts variable resistances into voltages. Like the thermocouple device, the RTD output is nonlinear, but can be characterized through the use of a polynomial-fit equation. Unfortunately,

Table 7-6 Temperature sensors and response times

	Thermocouple	RTD	Thermistor
Repeatability	2° to 15°F	0.05° to 0.1°F	0.22° to 2°F
Stability	1° to 2°F drift/yr	less than 0.10% drift in 5 yr	0.2° to 5°F drift in 1 yr
Sensitivity	10 to 15 μV/°C	0.2 to 10 Ω/°C	100 to 1000 Ω/°C
Interchangeability	+/- 0.75%	+/- 0.5%	+/- 0.75%
Temperature range	-400° to +5000°F	-200° to +1600°F	-150° to +550°F
Comments	Low voltage output requires low drift signal conditioning	Requires bridge or other network for typical interface	Highest sensitivity, inherently nonlinear

Table 7-7 Temperature limits for thermocouple wire

Thermocouple	ISA Type	Wire Gauge (AWG)				
		8	14	20	24	28
Copper-constantan	K	--	700°F	500°F	400°F	400°F
Iron-constantan	J	1400°F	1100°F	900°F	700°F	700°F
Chromel-constantan	E	1600°F	1200°F	1000°F	800°F	800°F
Chromel-alumel	K	2300°F	2000°F	1800°F	1600°F	1600°F
Platinum-platinum rhodium	R and S	--	--	--	2700°F	--
Platinum 6% Rhodium-platinum Rhodium 30%	B	--	--	--	3100°F	--
Tungsten Tungsten rhenium	G D C	--	--	--	4200°F	--

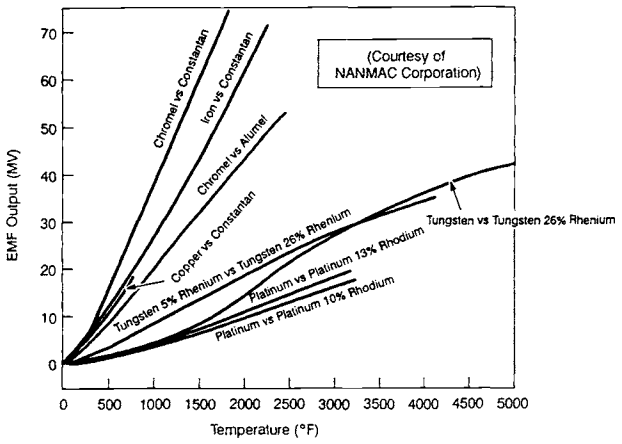

Fig. 7-57 Temperature-vs.-EMF curves.

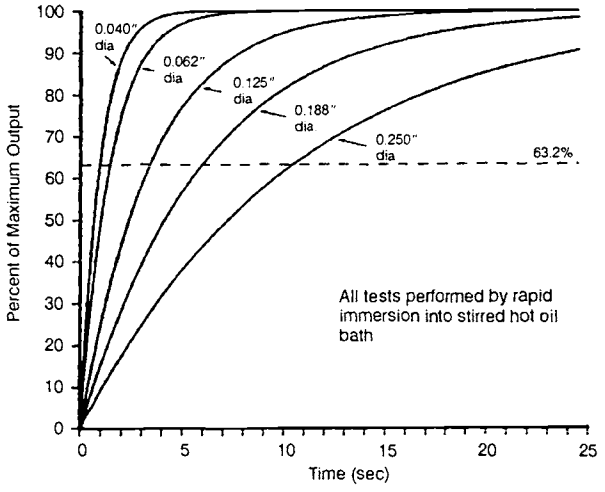

Fig. 7-58 Response times of sheathed, grounded thermocouples.

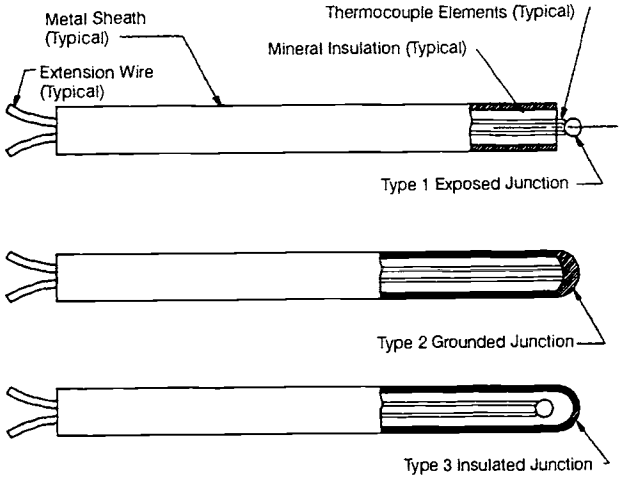

Fig. 7-59 Conventional thermal junctions.

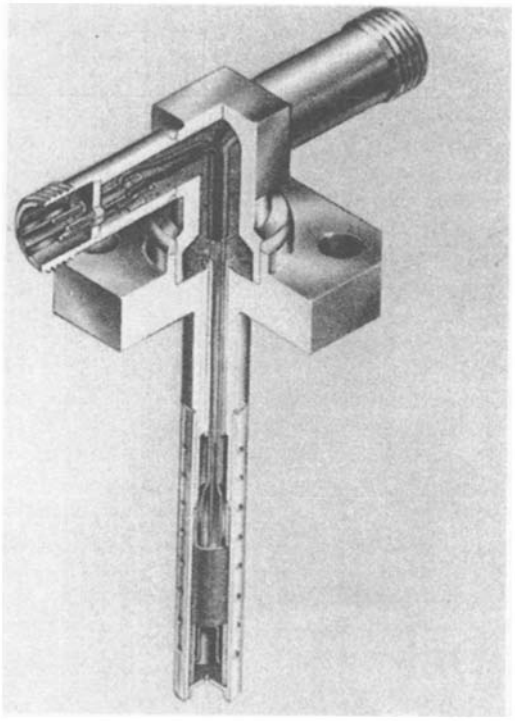

Fig. 7-60 Cryogenic temperature sensor.

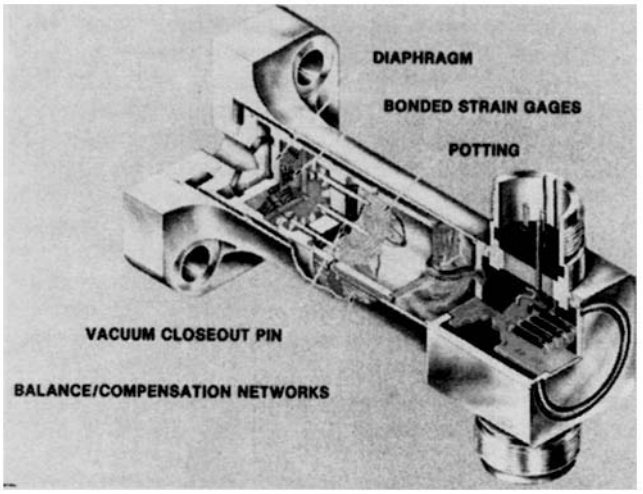

Fig. 7-61 SSME pressure transducer (manufactured by C.C.C.).

RTDs tend to be fragile and must be packaged for the environment of a specific application. Second, an "area"-sensitive device, the RTD has a slower response than the thermocouple. Figure 7-60 shows a two-element RTD used for measuring cryogenic temperatures.

The third type of temperature sensor, called a thermistor, a semiconductor device with a limited operating range, primarily has been used for monitoring the temperature of other electronic equipment. Thermistors have a fast response time and are very nonlinear. They must use a linearization circuit to provide a linear voltage-to-temperature relationship. They are also easily damaged; thus packaging requirements are an important design consideration.

Pressure sensors. Pressure measurements frequently require that sensors operate over a wide temperature range at high vibration levels. Two types of pressure measurements concern rocket-engine designers: static and dynamic. Static-pressure measurements can be performed with sensors having low frequency response, typically less than 1000 Hz. These sensors can be installed some distance from the pressure port with a small-diameter tube connecting the port to the sensor. In cases where the pressure media will experience very high temperatures (>600°F)—in the combustion chamber, for example, this type of measurement is preferable because the sensors can be installed in a more-benign thermal environment.

Dynamic pressure measurements require sensors to be installed near the pressure media. For a high-frequency-response sensor (>5 kHz), the sensing element (i.e., diaphragm) should be in almost immediate contact with the pressure media or flush to the surface of the pressure chamber.

Piezoelectric pressure sensors are used primarily for measuring dynamic-pressure components, extensively in the development phase. The term *piezo* means "to squeeze," and conveys the principle upon which these sensors operate. A quartz crystal is packaged inside a hermetically sealed container. In its equilibrium state the sensor reads "zero." But acted upon by an external pressure wave, the crystal produces a static charge on its surface proportional to the applied pressure. As the pressure stabilizes, however, the charge dissipates and the sensor's output returns to zero.

The most common type of pressure transducer utilizes a standard resistance gage to measure strain on an object and convert it to a pressure value (Fig. 7-61). Such a sensor has a metal diaphragm or force collector that employs strain gages at the areas of minimum and maximum strain. When connected to a Wheatstone-bridge network, the sensor produces a full-scale output of approximately 3 mV per volt of excitation. Pressure sensors utilizing foil-gage technology are limited to a bulk temperature of approximately 250°F.

The term "piezoresistive" is reserved for pressure transducers embodying semiconductor measuring elements. Small pieces of P- and N-type silicon (processed specifically for transducer applications) are bonded to a central diaphragm. The P-type material increases its resistance with an applied load; N-type material, the opposite. Connected to a standard Wheatstone bridge, this circuit makes an effective pressure-measuring device. These sensors are used in many high-temperature applications and are not as prone to the sensitivity and linearity shifts often associated with other pressure-sensing devices.

Pressure switches are used when it is not necessary to monitor the absolute analog pressure of a given media. Like the other pressure sensors, pressure switches use diaphragms as the force collector, which in turn actuates a switch at a predetermined pressure level. That level can be preset at the factory or set in the field.

Accelerometers. Accelerometers measure the acceleration of an engine component that has been subjected to shock and vibration. Most accelerometers utilize the same piezoelectric technology as dynamic pressure sensors. A single quartz crystal is packaged together with a seismic mass and spring mechanism. Variations in pressure on the piezoelectric element change its electrostatic charge in proportion to the vibration/shock load. This sensor has a very high natural frequency, making it ideal for shock and vibration measurements. Piezoelectric accelerometers can be used from -450 to 1400°F and are available in single- or multiple-axis configurations. Figure 7-62 shows a miniature accelerometer used for measuring engine-component vibration.

Flowmeters. Flowmeters are fundamental to propellant/oxidizer mixture-ratio determinations in the main combustion chamber. Flowrates are expressed in volumetric units or weight per unit time. Flowmeter selection criteria depend on the fluid environment and the data type required by the engine controller. Turbine and venturi are two common flowmeter types.

The turbine flowmeter has been used in rocket engines very successfully for years (Fig. 7-63). A relatively simple device, it has a turbine wheel suspended in a duct. The turbine rotates freely driven by the gas or liquid flowing past. The rotational speed of the turbine is proportional to the velocity of the fluid. Since flowrates are usually constant, the turbine's rotational speed is also a true representation of the volumetric rate of fluid moving through the flowmeter. Turbine rotation is sensed through the flowmeter body by an external pickup mounted on the surface directly above the flowmeter rotor. The rotation produces a train of electrical pulses in the pickup. The frequency of these pulses can then be transmitted to the appropriate readout electronics in the engine controller. The output characteristics of the flowmeter are quite linear. Accuracies to 0.5% full scale (FS) can be obtained. Repeatability is a respectable 0.1% FS or less.

Rocket-engine test stand facilities frequently use differential-pressure flowmeters to measure fluid flow. Either venturis or orifice plates are used as the primary restrictive elements limiting fluid flow in a localized region. Differential pressure sensed near the restriction can be related to the actual fluid flowrate. The output of this flowmeter is nonlinear (a square root function) and the dynamic range is limited to 4:1. Orifice plates and venturis cause a permanent static-pressure loss in the flow system. However, venturis can measure approximately two-thirds more flow at the same differential pressure than the sharp-edge orifice of the same size.

Speed sensors. Turbopump shaft speed needs monitoring to verify its performance while confirming that redline shaft speeds are not being exceeded. The typical speed sensor is a variable-reluctance type consisting of a permanent magnet and an independent pole piece surrounded by a coil winding of thin-filament magnet wire (Fig. 7-64). The speed sensor is installed through the turbopump case in close proximity to the speed-nut assembly mounted on the pump shaft. The speed nut has a collection of equally sized and spaced teeth around its outer diameter. Each tooth passing through the magnetic field produced by the permanent magnet induces an ac voltage in the coil winding. This voltage pulse is transmitted to the engine controller,

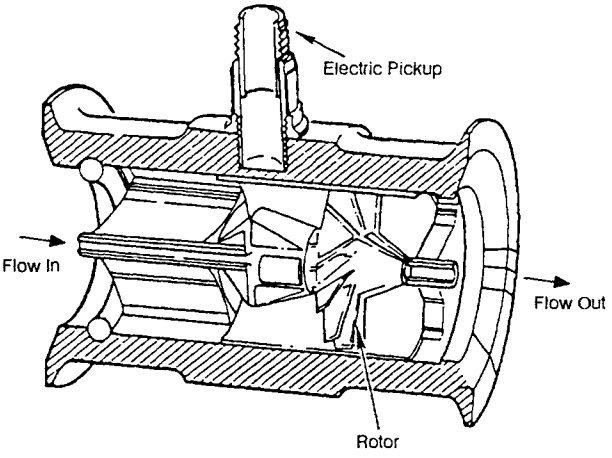

Fig. 7-63 Turbine-type flowmeter.

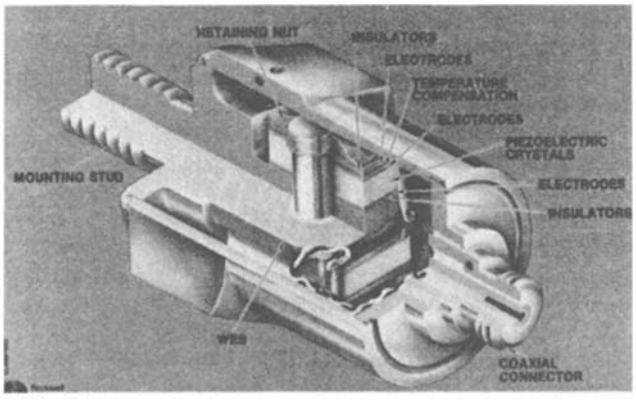

Fig. 7-62 SSME flight accelerometer.

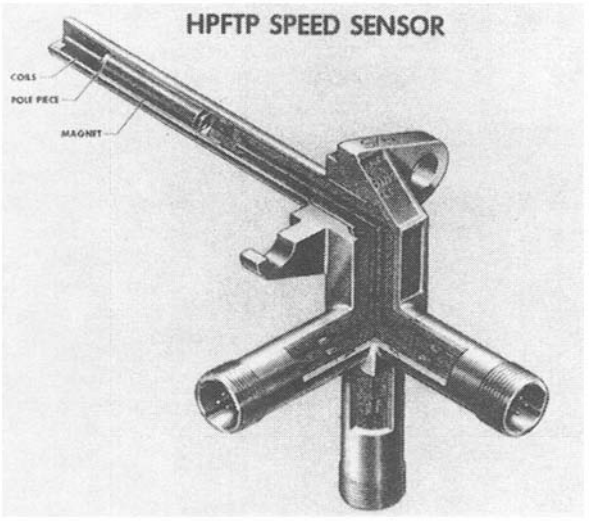

Fig. 7-64 HPFTP speed sensor.

which converts the signal frequency to a voltage proportional to the shaft speed.

Strain gages. Strain gages help to quantify strain levels in various engine components for design verification or failure investigation. Although strain gages are simple devices, to properly employ them requires the user to understand the selection criteria explicitly in terms of precision, strain magnitude, temperature extremes, cyclic endurance, and other test variables including the availability of desired gage types. Technical support provided by the strain-gage manufacturer contributing importantly to the success of strain-gage selection and installation.

Three main types of strain gage are commercially available: nickel-chromium (also known as nichrome), semiconductor, and foil. All are available as single units or in gage combinations called rosettes. Three-gage rosettes are widely used in stress analysis where magnitude and direction are totally unknown.

Temperature fluctuations represent an important source of error for strain gages because resistance changes with both strain and temperature. Compensating for temperature-induced error can be done in a number of ways. A "dummy" gage, identical to the active gage, can be attached to an unstrained coupon of the same material as the active gage and subjected to the same temperature conditions. Both active and dummy gages then connected to adjacent legs of a Wheatstone bridge will cause the resistance changes due to temperature to cancel. Another approach is to measure the temperature at the gages; this requires that the strain-gaged assembly be calibrated before use. The calibration will provide the necessary characteristic curve(s) to correct for thermal error. In either case, it is advisable to use temperature-compensated strain gages.

Position sensors. Control-system feedback loops depend heavily on the use of position sensors, particularly when modulating components such as valves and actuators are involved. These devices literally translate the mechanical position of a device (valve position 90% OPEN, for example) into an electrical output. This information can then be used for throttling control of the propulsion system. System safety or start enable/inhibit parameters are other possible commands. As a unique feature, this sensor type can be readily built into valve or actuator hardware.

Many methods can be employed to measure position. Only three types will be discussed here: LVDTs, potentiometers, and limit switches.

The linear variable differential transformer (LVDT)—a popular choice when it comes to position sensing in a valve or actuator—operates from an ac source and provide an ac signal proportional to the position sensed. In addition, the direction traveled can be defined by observing the phase characteristics of the output; that is, whether or not the output is in phase with the input. LVDTs have one particularly agreeable trait: there is little or no noise associated with their operation. In addition, by following proper design practices, LVDTs can be adapted to a wide range of temperatures (-423 to 1000°F), moderate vibration, and severe electromagnetic interference/radio frequency interference (EMI/RFI) environments.

Potentiometer displacement sensors have been used in various capacities for reporting valve and actuator position. They are cost-effective and require no specialized signal-conditioning equipment to be incorporated into a control system. They do suffer the disadvantages, being a variable-resistor type, of necessarily experiencing mechanical wear of the wiper and coil. Second, these sensors are extremely noisy when vibrated. Third, like the LVDT, they can be a bit large. It should be noted that if cost is important and long life is not an issue, this type of sensor may well be worth considering.

Certain valve and actuator applications require only that the home positions (full-open or full-close) be reported. If it will not be cost-effective to incorporate a high-priced, customized sensor, requiring extensive signal conditioning, then limit switches make an ideal choice, especially when the engine does not need throttling. Limit switches have been used in many rocket-engine applications with a high degree of success. They are extremely cost-effective and, even when used in redundant systems, maintain a high degree of reliability.

Instrumentation Installation

Temperature sensors. Sensor chosen for a particular measurement, the designer should direct attention to the selection of an appropriate sensor *port* before beginning any support hardware designs. Selecting a commercially available temperature sensor will make installation design considerably easier. Otherwise, further analyses will be required to define the structure that best facilitates the sensor installation. Sensors should be compatible with propellent and engine-hardware requirements, both internally and externally. Equally important, the designer must assure himself that the installation does not put the sensor in a position to cause measurement errors (stem conduction, velocity errors, inadequate immersion into the flow, etc).

Pressure sensors. Pressure-sensor installation procedures depend on the designer's understanding of the pressure media to be measured and also whether static or dynamic pressures are to be sensed. Pressure sensors will be installed either directly or remotely from the pressure media depending on the environmental conditions at the pressure port and/or the characteristics of the media. Sensors installed directly have the advantage of requiring no extra hardware, thus reducing engine weight.

In ducts carrying propellants, static-pressure measurement ports must be distanced from connecting elbows or other transitions that produce turbulence. In certain situations, shields are recommended in front of the pressure ports to minimize the dynamic effects of the media. Installing the sensors remotely requires a careful examination of the type of hardware available to connect sensor and the pressure port. If the pressure media is water vapor (LOX-hydrogen combustion byproducts), provisions must be made to purge the sensing line pre, post, and sometimes during testing periods. Supercooled lines

may produce an ice obstruction in the line, resulting in faulty or loss of measurement. Connecting lines must be also be designed with adequate diameters and lengths. The lines must be fastened to the structure to withstand severe vibration levels. Again, it is equally important that the installation not put the sensor or pressure-pickup point in a position to cause measurement errors (velocity errors, total pressure, etc).

In designs requiring dynamic pressure measurements, sensors should be installed as close to the pressure media as possible. In applications where the frequency response desired runs above 4 kHz, it is advisable to have the pressure-sensing element (diaphragm) in close proximity with the media. The diaphragm should never protrude into the flow.

For a dynamic response from 100 Hz to 4 kHz, the pressure-sensing element may be located several inches away from the pressure media. This is convenient if the sensor cannot be installed directly or the surrounding environment prevents it from being located in close proximity. It is always recommended to analyze the pressure cavity to ensure that the cavity resonant modes combined with the tap-transducer cavity come well above the measured pressure frequency range.

Figure 7-65 shows a typical sensor installation in the thrust chamber of a rocket engine—pressure transducer and acoustic-cavity equivalents, plus associated equations.

Accelerometers. To gain accurate and useful information, special care must be taken to couple the sensors properly to the test component. Attachment methods must not introduce any distortion and the sensors must be mounted rigidly to a base structure that responds to the frequency range of interest. Whenever possible, the accelerometer should be mounted on a stud base. The accelerometer base must be in good contact with the test object and care should be taken to ensure a flush mating with a smooth, flat surface. Standard machine screws should be avoided because, since they lack a flange or shoulder, it is possible to bottom them in the accelerometer, thereby changing its dynamic response and possibly causing damage to the unit. For an electrically insulated installation, special care must be taken to isolate the accelerometer from the electrical ground, thereby preventing ground loops.

Making accelerometer attachments to surfaces that cannot be drilled or tapped present a unique problem. As one way to resolve it, the sensor can be cemented directly into the test object. Adhesives should not be scraped or sanded from the accelerometers; this creates a rough mounting surface and can cause poor frequency response and a possible increase in transverse sensitivity.

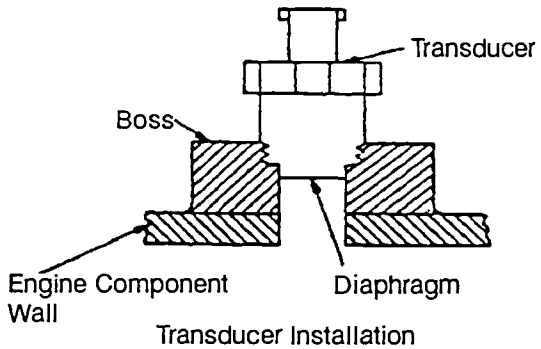

$$f_n = \frac{2n-1}{4}\left(\frac{C}{L}\right)$$

where:

- n = Any whole number (1, 2, 3 . . . etc)
- n = I for the fundamental frequency
- C = Acoustic velocity of the medium (13,550 in/s for air at 68°F)
- L = Length of tube in inches

a) Acoustic Equivalent

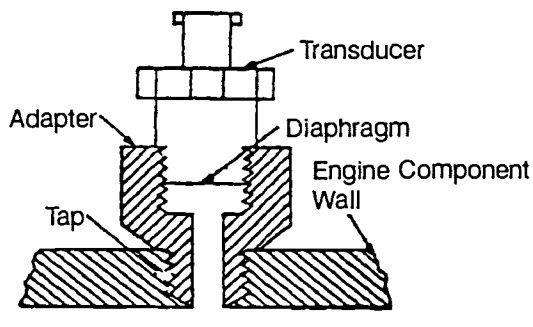

$$f_n = \frac{C}{2\pi}\sqrt{\frac{S}{L'V}}$$

where:

- C = Acoustic velocity
- S = Cross-sectional area of tube, in^2
- V = Volume of cavity at the end of the tube, in^3
- L′ = Effective length of tube, in.
- L′ = L + 1.7a

where: L = Actual length
a = Radius of tube

b) Acoustic Equivalent

Fig. 7-65 Acoustic equivalents of pressure-transducer mounting cavities.

In certain applications, mounting the accelerometer on the test object may effect the system being measured and thus the nature of the data obtained. With piezoelectric accelerometers, this occurs for one of two reasons: (1) the fixture required to couple the accelerometer to a flexible structure may introduce local stiffening, thus changing the structural response, or (2) the added mass of the fixture/transducer may change the system characteristics. Effects due to either can be reduced or eliminated by choosing the smallest and lightest accelerometer possible.

Flowmeters. The turbine-type flowmeter can be installed in a simple fashion between available flanges in existing ducting (Fig. 7-63). This type of transducer is very sensitive to velocity-profile disturbances in the flow stream. The line configuration should therefore minimize or eliminate flow disturbances during calibration and use. The line should be straight for a minimum of 10 diameters upstream and 5 diameters downstream. The presence of major flow disturbances caused by turbopumps, valve inlets/outlets may require even greater straight sections.

If swirl is present in the line ahead of the flowmeter installation, a longer straight section may be required or flow straighteners may need to be installed. Flow straightening should conform to industry standards and specifications. Piping and system components should be arranged to minimize pulsations entering the turbine meter. Pulsations may cause the meter to read high, and excessive pulsations may cause permanent bearing damage. Pulsations should be kept below 10% of flowrate at the meter location.

Pickup installation. The magnetic pickup output, a low-level signal, will range from 10 mv to several volts peak-to-peak. The following rules govern proper installation:

- Do not mount the pickup close to electrical equipment producing large electrical fields (motors, relays, etc).
- Use twisted and shielded cable for the pickup/amplifier connection.
- Hard or flexible conduit for the pickup cable must not be shared with other cabling carrying high-level power sources.
- Use a #14 AWG or larger-diameter ground wire connected from the amplifier ground to the pickup body or pipe to reduce the incidence of electrical noise.

Strain gages. The installation of strain gages is by itself a considerable science. Each application deserves special care and study. The selection of valid gage characteristics is very important to optimizing performance, taking into account the operating environment while obtaining accurate and reliable strain measurements.

Strain gages can be bonded satisfactorily to almost any solid material if the material surface is prepared properly. Cleanliness is vital. Throughout the surface-preparation process, it is wise to guard against contamination. The optimum surface finish for strain-gage bonding depends upon the nature and purpose of the installation. The recommended surface finishes for several classes of gage installation are summarized as below.

Surface Finish RMS

Class of Installation	Micro-inches	Micro-meters
General stress analysis	63 / 125	1.6 / 3.2
High elongation	> 250	> 6.4
Transducers	16 / 63	0.4 / 1.6
Ceramic cement	> 250	> 6.4

The normal method to locate and orient a strain gage accurately on the test surface first marks the surface with a pair of crossed reference lines at the point where the strain measurement will be made. The lines are made perpendicular to one another, with one oriented in the direction of the strain measurement. The lines should be made with a tool that "burnishes" rather than scores or scribes the surface (ballpoint pen or a round-pointed brass rod). Graphite pencils should never be used on high-temperature alloys where the operating temperature might cause carbon embrittlement. All residue from the burnishing operation should be removed by scrubbing with conditioners used on cotton-tipped applicators. Cleaning solutions should never be allowed to dry on the surface. The final step in surface preparation brings the surface condition back to an optimum alkalinity of 7.0 to 7.5 pH. Preparations to achieve the right alkalinity are available from strain-gage suppliers.

Several adhesives are available for bonding strain gages for use at temperatures ranging from -452 to 700°F. Special bonding materials—notably ceramic "paints" and flame-sprayed ceramics—are available for temperatures up to 1200°F.

The weldable gage, a precision foil sensor bonded to a metal carrier, can be spot-welded to structures and other surfaces. Spot welding proves convenient, particularly where bonding conditions are not ideal. It can be done with a stored-energy handprobe spot welder.

Position sensors. Most position sensors in rocket engines are specifically designed for measuring a mechanical displacement within a subsystem/component normally used for closed-loop controls (i.e., fuel/oxidized valves, actuators). The sensor installation concepts should be integrated in the earlier stages of the subsystem/component development. This will avoid unnecessary costs in developing a radical design. Furthermore, the engine designer must come to understand the operation and function of all mechanisms involved in the design. This will aid the integration of sensor and other mechanisms. In general, the designer will follow good engineering practices to achieve a successful installation.

Engine Harnesses

The various subsystems of the engine electrical system must be connected by suitable wiring, which, for proper mounting and clean routing, will be com-

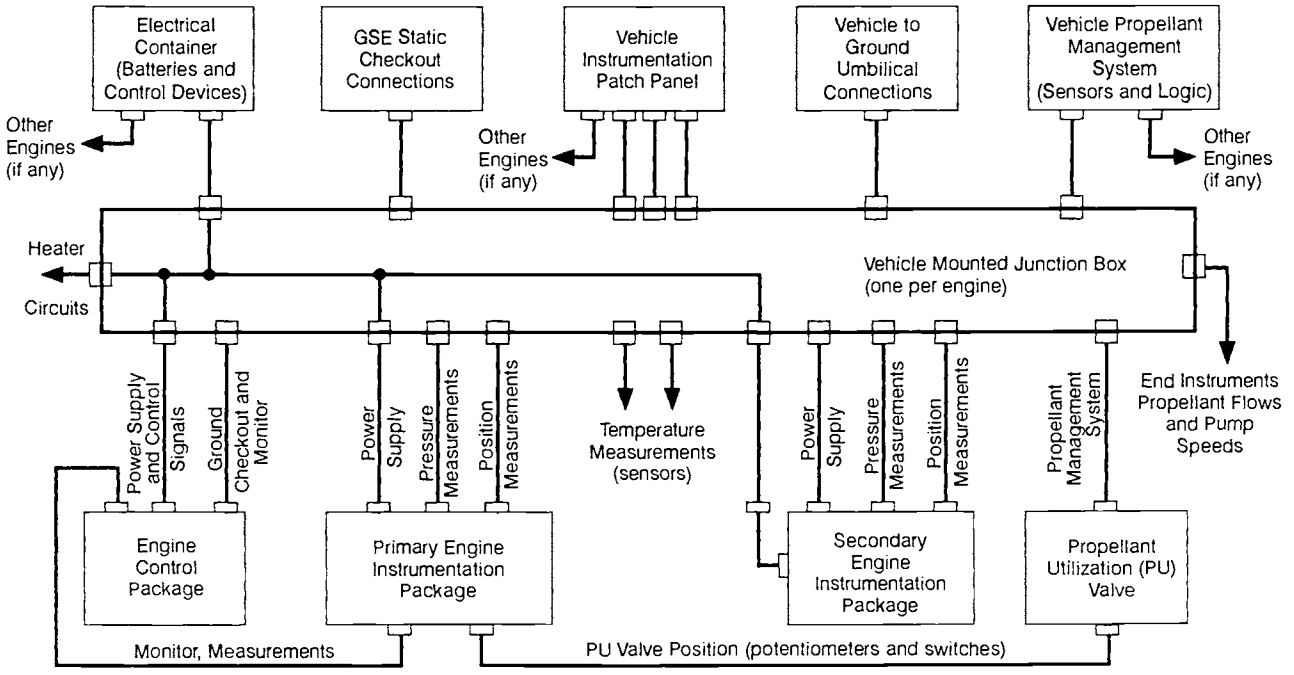

Fig. 7-66 Typical block diagram of engine-to- vehicle electrical connections.

bined into one or several wire harnesses. These components must be designed and manufactured to the same standards as any other engine component or subsystem. In addition to the cabling required to interconnect the various engine electrical subsystems, other cables are required to link the subsystems to the vehicle systems. This includes wiring for power supply, controls (start and stop, power up, throttling, etc.), instrumentation, and checkout circuits. To facilitate engine installation and line connections, these wires will be combined into trunks, each terminating in connectors that must have a mating counterpart on the vehicle. The vehicle-to-engine interface connections use a "J-Box" (junction box) into which are plugged both the engine and the connectors to vehicle systems. The "J-Box" permits easy and environment-protected redistribution of incoming and outgoing wires to assigned connectors.

The typical block diagram in Fig. 7-66 depicts the principal electrical connections between engine subsystems and vehicle.

Requirements. Proper design of a rocket-engine wire harness must consider the following:

- Working environment
- Importance of signal transmitted
- Materials
- Harness-construction type
- Routing (minimum distance, interference)
- Secure clamping (safety, avoidance of wire chafing)
- Selection of attachment points (avoidance of special brackets)
- Adequate support (harness weight, vehicle acceleration)
- Moisture protection (potting, sheathing)
- Heat protection (routing, wrapping)
- Arching protection (corona & dead shorts)
- Flexibility (installation, stiffness vs. bending load)
- EMI requirements/protection
- Redundancy
- Maintenance of harness and engine

For manufacture, the designer must supply certain information, this is best combined into a single assembly drawing containing the following information:

1) Wire list. This list (Fig. 7-67) calls out each harness wire by number, color, and conductor size, and defines its termination hardware. It also specifies the wire routing between end points (plugs and/or receptacles) and shield-termination schemes.

2) Harness schematic. For clarity, the schematic repeats in pictorial form most of the information supplied in the wire list, together with additional information. Signal names, logic names, grounds, voltages, and functions may be specified. Use of a schematic is optional.

3) Physical routing diagram. This diagram (as shown in Fig. 7-68) defines the branch points and their relative distance from the primary connector, clocking (if required) all part numbers used in assembly, identification, nomenclature, wire size, and type. Each connector will have its shell size, contact arrangement, polarity, application name, and reference designation on a hard callout (field note).

Design Considerations

Design considerations span a wide range of diverse factors.

Thermal. Thermal environments fall generally into six categories: ambient, sub-zero, hot gas, plasma gas, cryogenic and combinations of those. Each environment establishes its own parameters. Ambient

Wire List						
Wire			From		To	
No.	Color	Type	Item & Terminal	Tie Shield to	Item & Terminal	Tie Shield to
1	White	(A)	J202-E	21	P213-1	
2	Black		J202-F		P213-4	
3	White		J202-G		P213-2	
4	Black	(B)	J202-H	21	P213-3	
5	Red		J202-J		P213-5	
6	White	(A)	J202-K	21	P214-1	
7	Black		J202-L		P214-4	
8	White		J202-M		P214-2	
9	Black	(B)	J202-N	21	P214-3	
10	Red		J202-P		P214-5	
11	White	(A)	J202-A	21	P215-1	
12	Black		J202-B		P215-4	
13	White		J202-C		P215-2	
14	Black	(B)	J202-D	21	P215-3	
15	Red		J202-E		P215-5	
16	White	(A)	J202-F	21	P216-1	
17	Black		J202-G		P216-4	
18	White		J202-H		P216-2	
19	Black	(B)	J202-I	21	P216-3	
20	Red		J202-J		P216-5	
21	White	(C)	J202-HH		J202 Shield	

Wire Coded to Hard Callout on Field of Drawing
Primary Connector and Contact
Primary Shield Termination
Secondary Connector and Contact
Secondary Shield Termination

Fig. 7-67 Wire list.

conditions can often be harnessed with almost any available approved flight materials and of course may use the special materials, and designs used in hostile applications.

When harnessing in sub-zero conditions, care should be used in finding proper materials. Many soft goods will not perform well at such thermal levels. Fast freezing makes good protection from water an essential. Cryogenic conditions occur when normal atmospheric gases liquify. Insulations, soft goods, and resins will become brittle or fractured. Thermal coefficients of expansion for connectors become a factor as well as sealants in hermetic connectors. Hot gas and plasma environments also require special material; insulations are usually woven glass or ceramic.

Vibration. Vibration can have a detrimental effect on all engine harnesses. Harnesses for high-vibration areas require the use of stress/strain relief, good clamping techniques, potted backshells, and thicker insulation. High-reliability connectors should be used for interconnection.

Humidity. Humidity can be a serious problem if not handled correctly. Humidity causes short-circuit failures, corrosion failure, and water/ice damage. When harnessing in extreme humidity it is important to avoid trapping moisture in harness or connector areas. Braided harnesses and non-potted backshells tend to trap moisture and should be avoided if possible. Dual wall (glue-wall) sleeving should be used. Rigid sleevings should be avoided due to the cracking problems associated with them.

Material compatibility. Candidate materials for harness use need to be scrutinized, because incom-

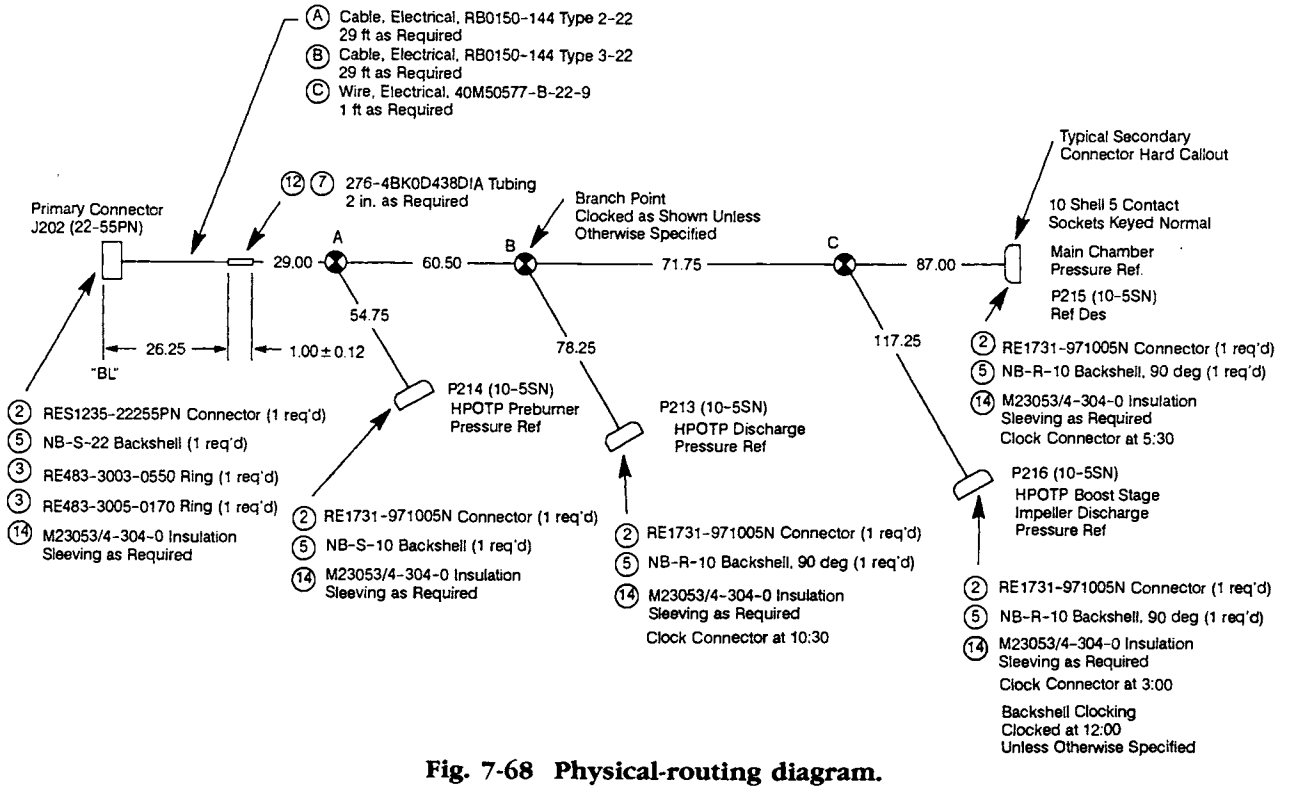

Fig. 7-68 Physical-routing diagram.

patible materials are a leading cause of harness failure. Metallic materials need to be compared on the galvanic scale to avoid galvanic corrosion. Materials selected (especially soft goods and platings) must be compatible with specified flight requirements. Flammability and outgassing requirements require definition.

Weight. Minimum-weight requirements are always important in space vehicles; but integrity, survivability, reliability and service life should never be sacrificed for less weight.

Bend radii. Bend radii fall into two categories: bend radius at connector/termination and routing-bend radii. When harnesses exit connectors, the initial bend will exhibit the most critical element on the life of a harness. Care must be taken to limit the amount of bend transmitted to the relief and harness-configuration connector. As a general rule, 10X diameter of harness is considered optimum, 3X minimum, for bend radius. Care must be taken to avoid sharp objects, corners, and other damaging parts as well as hot ducts and moving parts when routing harness and determining bend radii. It is important to maintain adequate clamping always.

Harness routing. Harnesses should be routed in a manner that prevents damage to harness or the connector. When clamping next to the connector, an effort should be made to eliminate side play (especially on angled backshells). Side play tends to loosen backshells and connectors, causes birdcaging in braided harnesses, and can cause conductor breakage. The first clamp should be located within 6-in. of the backshell exit. Harness clamps should be located in a manner that will prevent the harness from contacting sharp edges and other surfaces that can cause damage. The maximum distance between clamps should be 15 in. Multiple hamesses may be secured in a single clamp. Bend radii should be maintained by proper clamping. Routing on fuel lines should be avoided. Loops should not be left that maintenance personnel can use as hand or foot holds.

Shielding. It is sound practice when designing harnesses to provide shielding to eliminate noise, crosstalk, EMP, and RF interference and to provide a good ground connection. When designing shielding, care should be taken not to produce ground loops.

Harnesses that need protection from electromagnetic pulse (EMP), fire, or lightning strikes must be designed in a manner that will allow a high energy pulse to be absorbed and directed to the ground without degradation of signal. Most designs use a flexible or rigid outer sheath that will carry the high-energy pulse to engine ground. Flexible sheath materials are generally woven into a fabric or braid configuration around the conductor bundle. Materials used in braiding include copper with nickel plate, stainless steel, and Inconel. Rigid sheaths are usually copper and are supplied only as coax. Braided harnesses need special connector backshells to terminate the sheath mechanically and electrically. Care should be exercised to prevent ground loops when mechanically terminating secondary harness ends.

Signals. Signals usually are ac or dc and analog or digital. Input signals to the engine controller originate from the instrumentation, and output signals are transmitted to the engine control valves. Proper engine function depends upon good signal quality. Proper shielding will help guide unwanted electronic signals to ground. Power signals should be run in separate cables from data signals on the same harness leg. Shielded twisted pairs and triples should be used for most signals.

Noise. Unwanted impulses absorbed into the signal carrier create noise. There are two kinds of noise, spurious and common-mode. Spikes from other electronic carriers either near or around the signal carrier cause spurious noise. Common-mode is primarily ac noise induced by radio frequency (RF) waveform or magnetic fields. Proper shielding practices will help block spurious but not common-mode noise; it must be attenuated through the use of properly designed signal-conditioning equipment.

Electromagnetic interference. Electromagnetic interference (EMI) is caused by magnetic fields penetrating the outer shield. That changes the amplitude and RF waveform. Since 90 deg to the electronic field, a strong, dynamic magnetic (e) field creates a disturbance in the electron flow. EMI can best be eliminated by a complete shield sized to attenuate the energy in the greatest e-field found (or expected) and good conduction to ground.

Crosstalk. Two analog ac signals running parallel to each other can cause crosstalk (signal crossover). The waveforms transmitted tend to increase in amplitude and frequency as they interact with each other. Running signals in twisted pairs and triplets help reduce cross talk. Further, power should be isolated from data signals whenever possible by the use of shielded cabling and segregation.

Conductors. When choosing wire it is important to look at a current vs. resistance. As a rule, aircraft use 600-V RMS wire with resistance selected by choice of an AWG. Resistance is usually kept to less than 1 ohm over the engine-harness conductor length.

Conductor insulation. Rocket engines, owing to the severe environments in which they operate, need special insulation, the best of which are in the Teflon series TFE, PTFE, PFA. Teflon is basically limited to an operation temperature of 200°F. The insulation should be heavier than standard military wire for protection against high vibration. It is always better to use a solid insulation rather than braided insulation unless nothing else is available (such as ceramic braid in hot-gas environment).

Conductor assemblies. The standard wire used for harnessing, multi-conductor cable grouped in sets of two or three, can be shielded or unshielded (shielded preferred), twisted (preferred) or non-twisted, stranded (preferred) or solid. Groups of multi-conductors are bundled to make a harness run. When implementing a redundant harness, the backup will usually be routed in the opposite direction and never tied into the primary assembly.

Conductor construction. Solid conductor wire normally will not be used in harnessing since it should not be crimped, is not flexible, and will break upon repeated bending. In special cases, solid conductor can be used (wire welds, transitions, etc.). Stranded conductor wire is considered to be the best

choice for harnessing. It is crimpable and flexible, and has a long fatigue life. Preferred strand configurations are bundles of seven or nine conductors regardless of individual strand AWG.

Conductor material. Conductor material should be high-strength copper alloy. High-strength alloy gives excellent pull and crimp strength with little sacrifice to higher-resistance values. Pure copper should be avoided except under special circumstances. Other materials include nickel wire, thermocouple-harness wire, fiberoptic cable, and stainless steel. Aluminum should not be used due to galvanic corrosion.

Conductor plating. Plating will normally be used to prevent corrosion on copper-alloy conductors. Nickel plating is used extensively due to its excellent properties. Silver plate is to be avoided due to oxide growth and bad galvanic relationship with copper. Unplated copper wire should never be used except in noncorrosive conductors (such as nickel, nickel alloys, and stainless steel).

Coaxial conductors. Coax is commonly used for RF signals. The "RG" series is recommended due to its inherent ability to mate with existing connector systems. When choosing coax, impedance must be matched as well as voltage standing-wave ratio (VSWR) in the selected connectors. Careful attention must be made to verify that all components of coax to cable are matched: center conductor AWG, dielectric ID and OD, braid and braid type (foil, braid, etc.), and outer sheath OD. If required, low-noise coax may be used; it incorporates a second outer conductor to shunt EMI and noise to ground.

Connectors. Connector assemblies can be very versatile as long as the design stays within the chosen series. When choosing parts, threads, contacts, shell sizes, and materials must be compatible. The choice of connector series should be based upon these parameters:

- A qualified standard part
- Flight-rated and certified
- Reliability failure history based upon in-house experience and industry alerts
- Available standard materials (pins, sockets, shells, platings)
- Electronic characteristics (attenuation, current, VSWR)
- Available pin sizes
- Backshell accommodations
- Density of contacts
- Shape (bulkhead, firewall, etc.)
- Hermetic availability
- Scoop-proof (no bent pins)
- Connector shell-type (circular, "D", miniature, etc.)
- Interconnect type (threaded, bayonet, breech lock, etc.)
- Availability
- Self-locking, non-locking

Self-locking connectors can lock themselves in position after being assembled and do not loosen in working environments. Locking schemes can be ratcheting, wire bales, jam nuts, or screw posts. Self-locking connectors are preferred over non-locking types.

Non-locking connectors require help to stay installed while in use. Lockwire, locktite, or Torque stripe can be used to keep connectors tight.

High reliability. High reliability, as the name implies, means withstand severe environments without degradation or loss of electrical signal. High-reliability connectors are designed primarily for high-vibration and high-moisture environments.

Hermetics. Hermetic connectors are normally used on assemblies that require a gas-tight seal. Hermetic-connector assemblies are inseparable (contacts cannot be removed or replaced). Most hermetic connectors have a shell with a permanent dielectric (glass) insulator around the pins. The glass insulator can be a small bead or can cover the whole insert area. Hermetic connectors are usually circular.

Mechanical retention. Bayonet connectors are used in applications where side loading and vibration are not present. Bayonet connectors are fully engaged in less than one turn. Threaded connectors come in two main series, standard thread and tri-start thread. Standard thread uses English or metric threads to retain the connector; this style is used less in new designs. Most new designs now use tri-start connectors. Tri-starts become fully engaged in about one full turn and require low hand-torque to lock and seal. The thread-form type has three lead-in circular threads with a modified acme form in either English or metric pitch.

Scoop-proof. Scoop-proof connectors should be used whenever possible because they prevent bent pins, a major cause of connector failure.

Connector clocking. When two or more of the same connectors are used in one place, clocked connectors can prevent accidental/incorrect hookup. Clocked connectors use polarized keys on the connector to prevent mismating. Polarized connectors make interconnection "fool-proof" by eliminating the possibility of improper connector mating. In addition, the harness design should avoid placing two or more of the same connectors close enough to be cross-connected.

Pins and sockets. The national electric code requires that power supplied by sockets and that mating pins be the correct size for the intended service. This philosophy—intended to stop accidental shorting across unprotected pins with a foreign conductor—should be used unless precluded by other requirements. Contact materials are usually gold-plated alloy 52 (iron-nickel) with a crimp socket for connector interconnection.

Crimp terminations are preferred because they are stronger in tensile strength than the conductor used and provide true electron-exchange bonding. The drawbacks are that only one conductor may be crimped in a single well and solid-conductor wire should not be crimped. Pull tests must verify crimp integrity as well as correct tooling. Crimps must be sized by conductor size vs. crimp-well size (see military or commercial specification). A conductor may never be doubled over to increase its size for proper crimping.

Four types of solder terminal will normally be available (Fig. 7-69): spade, turret, solder-well, and wire-wrap post. The spade lug is preferred since its two sides and hole relieve the most strain. Spade

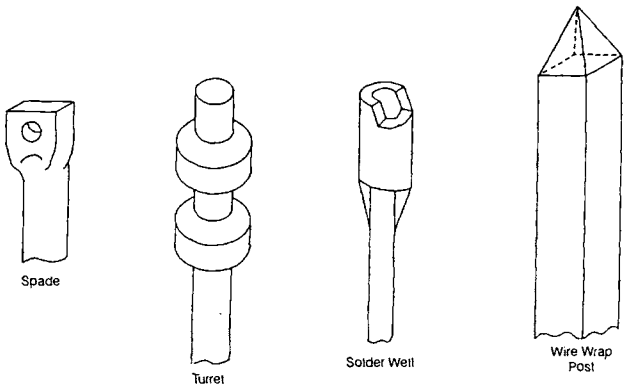

Fig. 7-69 Typical solder terminals.

terminations without holes should not be used. Turrets are good for multi-conductor solder termination but are more susceptible to strain failure. Solder well, the standard design available in most military-type pins, can be used to accommodate multi-conductor termination, but need good strain relief and possibly potting boots to ensure fatigue life. Wire-wrap posts should only be used with solid conductors, with minimum of four wraps on each post. It should be noted, however, that solder terminals should be avoided if possible.

Contact insertion and extraction. Contacts must be inserted using only the approved tool. Unapproved or wrong-size tools will cause grommet damage and destroy sealing. All contacts must be inserted into the connector (used or unused contacts). Unused contacts should have sealing plugs inserted behind the contact; test done with a proper tool after insertion to verify seating of the contact; contacts extracted using an approved tool. Unapproved or wrong-size tools will cause grommet failure and seal damage. Special tools are required to remove contacts from unused holes.

Specialized hardware. In most applications, hardware must be added to protect harness and connector. Protective caps, strain reliefs, and backshells all must be checked for compatibility. Shrink sleeving, strain-relief boots, and part-number tags must be added in proper order and be made of pliable materials. All end-points must have a readable reference-designator tag. Other special hardware may be added—EMI backshells, potting boots, etc.

Redundancy. Redundant signals should always be carried through separate harnesses and separate primary connectors. A good block diagram will always show single-point failure areas which negate redundancy principles.

Identification methodology. There are two types of identification methodology—system style and assembly style. System identification uses distinct reference designation (REF DES) for each interconnection. The REF DES is broken into two parts, class letter and unique numeral (for example, J78). The class letter (per ANSI Y 32,2) is usually "P" for plugs or movable connector and "J" for jack/receptacle or more-primary (closer-to-source) movable connector. P&J should not be confused with pins and sockets, which do not influence reference designations. The numeric identifier is individually numbered. Numbers should not be used twice or reused if a REF DES is cancelled. In system methodology all P&J prefixes may or may not match the mating-connector reference designator. When using system identification, a permanent log must be kept with the system to assign REF DES, to prevent errors, and to assign future REF DES.

In assembly-style methodology, each assembly will have its own series of REF designators starting with numeral one. Each connector will have a unique numeral regardless of prefix (for example: J1, P2, J3, J4, P5, etc.). Most organizations prefer assembly style to identify connections.

Harness types. Conventional harnesses are used in areas that are not usually vital to engine function. Most expendable engines use conventional harnesses because of cost-effectiveness and ease of fabrication. Conventional harnesses are constructed of insulated conductors in braided shielded cable available in groups of 1,2,3,5, etc., with 2 and 3 being most common. Conductor groups are laced together with twine or sleeving and terminated in normal strain-reliefs or backshells.

Coax harnesses serve all kinds of high-frequency data cabling. Normally they are connected to accelerometers and high-frequency pressure transducers. Coax cabling is available in two forms, rigid and flex, the more common being flex. Normally, low-noise coax will be the common flex form. It is almost always triaxial-type cable, constructed with two outer conductors in common to attenuate noise. Coax harnesses can be point-to-point or ganged into a common connector/harness configuration.

Specialized harnesses. Harsh environments may include water or salt spray/ice, vibration, hot or cold working-temperature, high electrical loads, dynamic movements, high "delta" temperature over working temperature, and harsh or hazardous working medias. It is the designers responsibility to determine the extent of the working environment and choose suitable hardware (Fig. 7-70).

Armored harnesses. Armored braided harnesses provide lightning protection and allow an engine system to shut down in the event of a failure/fire. An armour harness must survive a fire that is present in a reducing environment (oxidizer rich). Armored harnesses are usually constructed with multiple layers of braided sheath, with the outer braid typically made of Inconel and the inner braids of stainless steel and/or copper (with nickel plate).

Lightning harnesses. Lightning braid, on the other hand, is used to prevent lightning strikes on the engine or vehicle from affecting engine function A good rule of thumb is to carry the impulse to ground as soon as possible. Lightning protection should conform to MIL-B-5087 or other specifications.

Harness construction methods. Most harnesses are made on a wire board created on the basis of the wiring document (usually assy drawing). A good assembly drawing will show branch points with clocking (if none specified, it will be constructed as drawn) and the connector clocking (if none shown, it will be 12:00 to master keyway) so that the wire board will be made correctly.

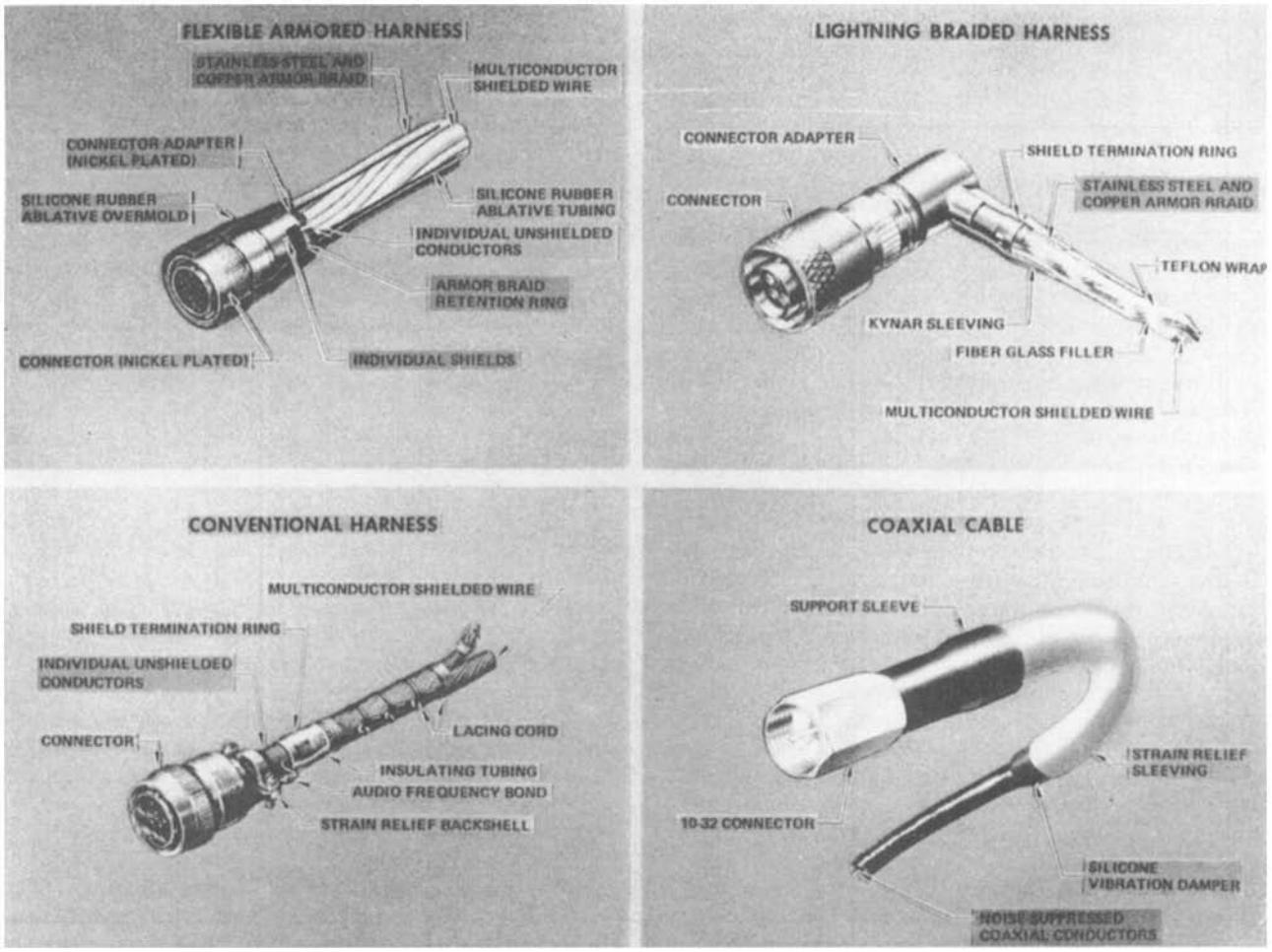

Fig. 7-70 SSME harness configurations.

Mockup hardware should imitate the final product, ordinarily using rope of the same approximate OD, but sometimes cable for more complex mockups. Mockups should have realistic tolerances and dimensions from connector face-to-face. Also, when locating branch points, short branch points (break out before intended branching point) will be preferable to long ones since long branch points will cause the harness to double back on itself.

Splicing should be avoided in harnessing. Splices should be crimp splices with shrink-sleeving covers. Sleeving should be multi-layered dual wall under flexible single wall for moisture protection. When splicing conductors in a leg or run, the entire area should be covered with a separate shrink sleeving to provide strain relief. Individual splices must be clamped to prevent tensile loads from pulling on the splice.

Connector mating. Circular connectors should be mated and torqued down according to the connector series. Before mating, threaded connectors should be inspected for cleanliness, bent pins, deplated contacts, and corrosion. Ionized air should be blown on each connector face. If ionized air is not available, clean gaseous nitrogen should be used. Torquing should be performed with strap wrench and torque wrench.

Bayonet connectors should be inspected, air-gunned, and then installed by hand until clicked into position. Use turning to demate the connectors. Inspect and install the protective cap on the mating connectors.

Coax connectors should be inspected, air-gunned, installed, torqued, and then potted to keep out moisture and lock the connector. Potting needs to be removed for demating. Remove the connector, inspect, and cap.

7.4 AVIONICS ARCHITECTURE

The early rocket engine might have been compared to the carbureted internal-combustion engine in that mixture ratio was controlled by orificed openings and control sequences were programmed by a pressure-ladder process. As engine complexity evolved, the control sequencing became more critical and a rudimentary control unit, the relay controller, came into use. Two significant changes in the SSME made the electronic controller a necessity. The first involved achieving the required performance by means of closed-loop control and safety monitoring of critical parameters. To do this and optimize start, run, and stop sequences, as well as manage redundancy and accommodate changes, the general-pur-

pose computer was essential. The second significant change was the concept of a reusable engine. This required measurement, processing, and recording of data relevant to health of the engine so that its condition could be determined before the next flight.

Requirements Definition

The foremost requirements for a control system are reliability, response, accuracy, and stability. The preliminary design of the engine determines what must be controlled, how it is to be controlled, and control accuracy. As the engine design progresses into the detail phase, the number of sensors and control valves will be further defined. From this, an engine-to-controller interface can be defined and initial processing requirements established. After initial sizing of the hardware, a preliminary reliability analysis determines the required redundancy to achieve the mission goal. The requirements can be divided into four areas: converting sensor inputs to a usable form, processing sensor data to perform safety monitoring and process control, converting computed results into a form suitable for driving the necessary effectors, and performing necessary prelaunch and in-flight tests to ensure safe engine operation.

Sensor-Input Requirements

Parameters that must be monitored include combustion temperatures, fuel and oxygen temperatures, combustion chamber and pump pressures, valve positions, pump speed and flow, and engine vibration. Resistance temperature devices (RTDs) and thermocouples will usually be employed to measure temperatures. For each temperature to be measured, the type of device must be determined, and required response times, device impedance, accuracy, and the maximum and minimum temperature range must be defined. Calibration and linearity characteristics must also be specified.

The principal type of pressure sensor employed—a strain-gage unit connected in a balanced bridge configuration (see Fig. 7-61 in section 7.3)—must have specified its characteristics such as impedance, frequency response, excitation voltage, voltage sensitivity (in volts per unit of pressure), and maximum and minimum pressure ranges as well as calibration requirements.

Typical instruments for measuring speed and flow use a moving ferromagnetic-pole piece and pickup coil to sense shaft rotation (of either the pump shaft or flow-measuring turbine shaft). A counter circuit measures the interval between successive pulses. Electrical characteristics such as coil resistance, inductance, output voltage versus frequency, and the maximum and minimum frequency range to be measured are also considered. One often-used testing technique employs a second coil that is inductively coupled to the primary coil, which in turn applies a test frequency to the primary coil. This signal is then measured through the pulse-interval counter and verified. Where two coils are provided for redundancy, the test signals can be cross-coupled.

The position of the main fuel and oxidizer valves, as well as valves used for thrust and mixture-ratio control, must be measured accurately to ensure proper engine performance. The position of other valves (such as anti-flood and bleed valves) must be known to determine whether the engine can be safely operated. For valve-position sensing, the rocket-engine control will employ the rotary variable differential transformer (RVDT) for measuring angular motion and the linear variable differential transformer (LVDT) for measuring linear travel. Optical encoders and ratiometric techniques, such as the tracking resolver-to-digital converter, offer better accuracy and should be specified in new valve designs. Parameters that should be specified are minimum and maximum values of position to be measured, resolution, accuracy, and excitation source (if required). Techniques that are sensitive to cable length or capacitance should be avoided. For on-off indications, the LVDT has been employed instead of limit switches because of the unreliability of switches in the rocket-engine environment. New proximity switches that use magnetic or capacitive effects offer adequate accuracy with lower cost but are as yet unproven in the rocket-engine environment.

The reusable rocket engine has made it necessary to monitor vibration during flight to detect bearing wear or failure. Radial accelerometers located on the pumps are fed to bandpass amplifiers that record the real-time signal on tape for postflight analysis; if required, the rms value of the vibration will be available as an engine-shutdown control (redline). The requirement to protect the vehicle from the effects of bearing failure is leading to the development of new bearing-wear detectors and use of real-time tracking filters to provide precise vibration data. Parameters that should be specified include frequency range of interest, signal-processing bandwidth and range, and a complete definition of vibration amplitude over the entire frequency range that the transducer is capable of detecting. Piezoelectric accelerometers are capable of outputting signals in the high-frequency range up to 5000 g. Electronics must be designed to filter and amplify without signal distortion. To minimize the effects of random vibration, a narrow-band tracking filter should be employed that can measure synchronous or harmonic vibration only. Accuracy and response time need to be specified.

Certain general requirements apply to all sensors: tolerance to faults (such as open or shorted connections), sensitivity to electrostatic discharge, and protection from electromagnetic interference (EMI). Interface design should prevent any external failure from causing an in-range parameter failure. Sensor lines coming into the controller should have EMI filters to prevent radiation from within the controller as well as entry of external EMI and electrostatic charges. (See section 7.3 for a more detailed discussion of engine instrumentation.)

Data-processing Requirements

Determining the data-processing requirements necessitates an assessment of the tasks necessary to control the engine. That calls for an in-depth

analysis of the engine operation. The following task list illustrates the approach:

- Sensor processing requirements can be estimated from the engine measurements list. Processing tasks for sensors include a reasonableness test, comparison to other sensors, curve fitting, scaling to engineering units, and reporting the data to a health-monitoring system.
- Control processing requirements include redline monitoring, control of thrust and mixture ratio, and receipt and acknowledgment of vehicle commands. Algorithms should be developed and processing requirements should be estimated from them. A state table should be maintained that defines engine and controller status. During prelaunch, launch, and postlaunch activities.
- Control of output devices requires command output and verification that the device responded.
- Continual self-testing of the controller must verify that input and output data paths are functioning correctly. The processors themselves must be tested, either by doing a preprogrammed problem with known answers or by some other technique such as parallel processors that compare computed results. Redundancy management of the controller and engine resources requires maintaining a fault table. The complexity of the fault table can affect processing requirements and execution time dramatically. Typical software requirements for redundancy management exceed those required for control. After the tasks are defined, an estimate of processing time can be made. Experience from similar programs can be used, and representative tasks can be coded and then extrapolated to the total requirements. Because of the uncertainty of the process, a safety factor of two or more is prudent.

Control of Effectors

The engine is controlled simply by the opening and closing of valves: for control of flow paths, solenoid on-off valves; for engine performance, proportional valves controlled by several methods. In one method in current use, an electrical current controls the flow of fluid in a hydraulic servovalve. The hydraulic circuit has power amplification to drive the valve. Position feedback to the electrical circuit allows closed-loop control of commanded valve position. (See section 7.2 for a more detailed discussion of engine valves.)

Proportional and on-off valves both employ inductive coils for control, but the resistive and inductive characteristics of the solenoids must be defined. The power levels required to activate the coils and the response time for each valve must also be determined. Power levels should be kept as low as practical and where practical, should use existing voltage forms. Solenoids and drivers must be designed with built-in fault detection that monitors solenoid voltage and/or current. Solenoid drivers should be designed to give high-side switching and to withstand shorts to ground or other voltages in the harness without overstress. The driver circuits should be unconditionally stable for any load impedance. EMI filters should be provided on each output line, and self-induced voltages in the solenoid should be suppressed at the output loads of the inductor to prevent spark-gap emissions from intermittent cables.

Engine and Controller Self-test

To reduce prelaunch checkout time and to perform health monitoring, self-test capability must be designed into the controller, sensors, and effectors. All functional elements such as analog-to-digital converters, digital-to-analog converters, effector drivers, computers, and memories must be verified as functioning before launch and periodically checked during flight. All analog and digital data-paths should be checked in the same manner by monitoring transfer of known data through each path.

For each element required in real-time engine control, a watchdog timer monitors the control function and has the ability to switch to the backup control after a failure. Where redundant elements or backup functions such as watchdog timers are required, all elements must be verified as functional before a launch. Controller circuits calibrate pressure and temperature sensors and verify sensor continuity for voltage-source devices such as speed or flow components.

Before launch, software-controlled automated checkout will be required on engine and control components to ensure a successful mission. Control valves, sensors, and the electronic controller must be exercised in a mode that simulates flight. Control valves should be opened and closed with response checks in the controller. Sensor accuracy should be verified at ambient conditions and at simulated near-full-scale readings. All controller interface circuits must be verified to be operating properly, and all redundant elements of the controller must be verified as functional; likewise, all circuitry required to perform self-test, such as data comparators, watchdog timers, and self-generated test signals.

Because it is not possible to perform self-tests on sensors and valves during flight without interrupting their control function, other techniques must be used. "Reasonableness" testing of all sensors is currently employed; for example, during main-stage engine operation, an abnormally low or high chamber-pressure reading would indicate that the sensor or sensor interface circuit had failed. Choosing the limits for a reasonableness test requires analysis and historical-data evaluations. Future engine-control-system designs may incorporate mathematical models of engine performance to predict all measured parameters and to monitor engine performance more closely.

Environmental Requirements

The requirements imposed upon rocket-engine electronics are unique: vibration levels may be 100 *g* or greater across a wide range of frequencies, temperatures may go below -55°C, or above 100°C, and the environment may be saturated with water. Of course, it is necessary to protect electronics from these extremes. Hardware that cannot be designed to withstand these environments must be enclosed in her-

metically sealed containers and mounted on vibration isolators. Because both heating and cooling may be required at different phases of engine operation, all controls are centrally located in a single unit to minimize the cost and weight penalties of providing isolation from the environment. The advent of highly integrated electronics offers the possibility of locating circuits such as valve drivers and sensor processors directly on the component to save harness weight and cost; but the environmental concerns must be addressed as a design trade-off.

Vehicle Interface

Engine interface with the vehicle consists of commands such as start, stop, and thrust-level changes, as well as health-monitoring data sent back to it. Certain data such as engine commands, critical to operation, are encoded in some form of error-checking code. The SSME makes use of Bose, Chaudhuri, and Hocqeuenghem (BCH) polynomial encoding for command data transmission. Health-monitoring data that are not mission-critical may be transmitted with no more than parity-bit encoding, but any data transmitted in a noisy environment or through the atmosphere requires some level of encoding to achieve an acceptable reliability.

In addition, multiple sets of command lines are necessary to maintain engine control after one or more data-transmission failures. A typical system would employ three command lines and remain fully operational after one data-path failure. Response after the second failure would depend on the nature of the failure and criticality of the command data.

Additional interfaces such as power and cooling may be required and should be defined with the same care. For example, for power, maximum and minimum voltages under all operating conditions, conditions for power loss, transient response, and power requirements should be defined.

Controller Architecture

The design of a high-performance engine such as the SSME required precise control of start sequences, thrust, and mixture ratio, which could only be realized with an electronic control system. Fuel and oxygen flow, pressure and temperature, must be measured and in many cases averaged or compared with other similar measurements for additional resolution. This requires the use of high-speed, precision analog-measurement circuits and a digital computer to process measurement data. The computer will also provide mixture-ratio and thrust control and management of self-test and redundancy. The identification of these requirements and their breakdown by task description mark the first steps in defining a hardware configuration (or architecture) to accomplish the task.

Function Allocation

Controller functions can be divided into three areas (Fig. 7-71): input of engine sensor data (input electronics), processing of data (digital computer), and control of engine valves (output electronics). The interface between the engine sensors and the controller forms part of the input electronics (IE). Temperature sensors include thermocouples (TCs) and resistance temperature devices (RTDs).

Each RTD needs a bridge termination network with noise filtering, and each TC requires additional gain. These RTD or TC outputs must be converted from analog to digital for use by a digital computer, and there are numerous approaches to performing this conversion. Figure 7-72 shows one approach: conditioning all temperature and pressure signals and multiplexing them onto a single analog-data bus, and thence converting them to a digital value for data processing. This approach features minimum hardware but imposes high-frequency response requirements on the multiplexing and analog-to-digital (A-D) converters. Pulse-interval counters measure the period of the speed and flow waveforms. The period is then converted to a flowrate in the computer. Other functions include sensor testing and calibration, which are controlled by the computer as part of preflight testing.

Engine data require a variety of operations for control and monitoring:

- Comparison of engine parameters to stored data for reasonableness as a sensor fault-detection technique.
- Comparison against stored data that define safe operating limits.
- Conversion of all input data into engineering units for recording and/or real-time display.

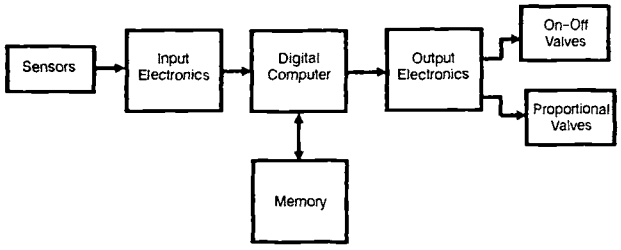

Fig. 7-71 Functional diagram of an engine controller.

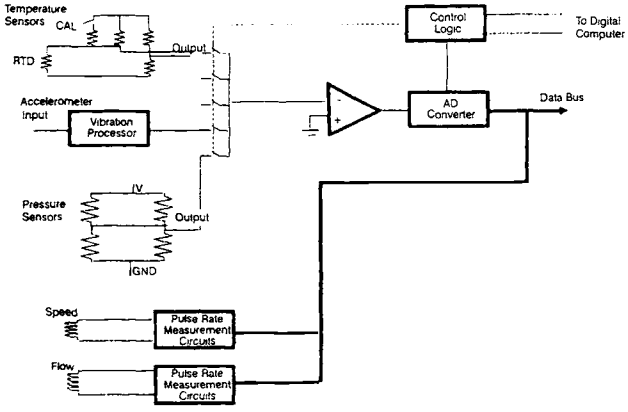

Fig. 7-72 Functional diagram of input electronics.

- Solution of all control equations related to engine control.
- Communication to and from the vehicle.
- Verification that engine components respond to commanded inputs, valve position, etc.
- Scheduling of input, computation, and output within the controller sampling-cycle.

These tasks can be performed by a general-purpose digital computer. Its design should be based on the data-processing needs identified in the requirements analysis, but the nature of the computing task should also be considered. For example, since the dynamic range of sensor and control-output data will be limited, fixed-point data processing proves adequate and results in a faster and less-complex computer than a floating-point machine. Should a single, powerful processor perform every task or multiple processors share a task? Because of the microprocessor, distribution of the processing task may now be the preferred method. Should special-purpose data buses be tailored to the specific needs of this controller or industry standard buses employed? The tradeoffs are lower performance and additional hardware if industry standard buses are used. However, the flexibility to incorporate new functions in the future may offset the disadvantages of a standard bus. The selection and sizing of the memory should also relate to the system-requirements analysis and support the necessary data-processing rates. Issues that must be considered are memory volatility, data integrity, and size.

As to the valve-control driver circuits, valve and valve-driver design will be affected by response time, power levels, electromagnetic noise, and reliability. Since a valve that uses low power has high inductance and, therefore, poor response time, a tradeoff must be made between response time and power level. To minimize system-interconnect noise, power and ground circuits associated with valve drivers should be isolated from the input and computer electronics. Where high current levels are employed, such as in motor-driven valves, the power electronics may be collocated with the motor. The goal of valve and valve-driver design should be to use standard voltage forms wherever possible on the vehicle. Monitoring the valves for confirmation that the command was executed should also be done in the output-electronics area. Monitoring of voltage and current for each valve can check for associated open and shorted cables. Valve position must be monitored to verify that the valve has responded to the command.

The selection of a system architecture, then, becomes a series of tradeoffs featuring cost, weight, performance, and reliability as the principal factors. For example, whether a motor driver circuit is located on the motor or in the controller chassis would determine environment (vibration and temperature), harness design, and packaging design in addition to electrical design considerations.

Failure Detection and Response

Because failures in electronic hardware are random, the minimum requirement for fault tolerance is to be operational after the first failure and to shut the engine down safely after the second failure (fail-op; fail-safe). The first problem is to detect when a failure has occurred and the second is to be able to switch control of the engine to the backup hardware. Of the many approaches to fault detection, two representative selections are discussed here.

The first approach has been used on the SSME—diagnostic testing by built-in-test (BIT) hardware. Sensors are tested by switching in a BIT signal that simulates an input. Analog circuits are tested by inserting precision test voltages in the analog-data path and checking for correct analog-to-digital conversion. Digital-data paths are exercised by transmitting known data patterns and checking for proper data-transfer. Digital computers can be checked by a series of operations to verify correct arithmetic and data-transfer operations. When a microprocessor is used, it is not possible to predict the scope of fault coverage of self-test software. Therefore, a scheme employed in a number of high-reliability applications uses self-checking processor pairs. Two identical microprocessors are operated in lockstep and their output compared on a bit-by-bit basis. Data sent from one unit to another can be looped back to the sending unit for verification.

Valve-driver response can be checked by measuring coil voltage and current and by monitoring the valve position. The portion of failures that can be detected in this manner is referred to as *fault coverage*, and it is critical to mission success.

A second approach employs multiple channels of independent hardware to solve the problem and then compare the answers. If an output is incorrect, switching logic prevents that channel from controlling the engine. This approach can provide 100% fault coverage for all the controller electronics except the output comparator and switching logic. Multiple comparators and redundant switching logic can circumvent these problems.

The second part of the problem involves switching control from a failed unit to any unit still operating properly. For most failures, the built-in selftest hardware detects the problem and the unit takes itself out of service. A minority of failures cannot be self-diagnosed; for example, if the processor should halt, it can no longer control the engine and, in addition, cannot relinquish control.

Figure 7-73 illustrates one method for switching control. Both channels can control the valve, but

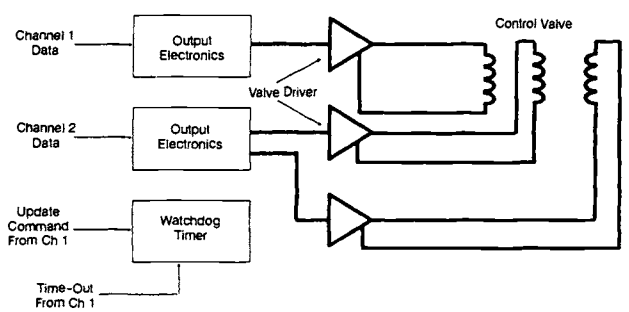

Fig. 7-73 Output-electronics redundancy diagram.

channel 2 has an additional control coil that, when enabled, allows the channel 2 valve driver to control the valve. In one servoactuator design, each control coil modulates an independent hydraulic circuit and the channel-enable coil selects which of the two independent circuits is active. For the design shown in Fig. 7-73, if channel 1 detects a failure, it would force a time-out of the watchdog timer, allowing channel 2 to assume control. If channel 1 halted, no channel 1 updates would be received by the watchdog timer, which would allow channel 2 to assume control by default. This diagram, a simplistic concept of only one redundancy management scheme, only serves to illustrate the principle.

Finally, as part of the design process, a failure mode and effects analysis (FMEA) would be conducted to determine if the design contains undetected failures, improper failure responses, or single-point failure modes.

Hardware Design Rules

The following guidelines are to be used for analog-digital circuit design, EMC/EMI requirements, component placement, standard-parts usage, and component derating.

Analog-design guidelines. The guidelines for analog-circuit design can be divided into four areas of concern: verifying that the circuit meets requirements by using a circuit-analysis program such as SPICE; selectiing parts whose parameters permit the circuit to perform over the environment and life of the unit; derating component parameters to ensure the reliability of the circuit; and seeing that the packaging and layout constraints of decoupling, signal routing, and component placement retain the performance inherent in the design. These design steps should be followed:

1) Select a circuit topology (mechanization) that performs the required function with minimum error sources and minimum number of parts.

2) Select parts, considering standard parts, part availability (qualified parts lists, STD-Parts list, multiple sources), stress, and parameter stability—initial tolerance, temperature, and time stability.

3) Analytically determine that the circuit requirements meet design centering and worst-case conditions as a design goal. Root-sum squared (rss) analysis should be used only on circuits unable to meet worst-case conditions. Breadboard, brassboard, or prototype tests should be used to show that the circuit requirements will be met under temperature extremes and power-supply variations.

4) Consider mechanical constraints, including power dissipation, grounding/shielding, signal routing, and error coupling (component placement).

Digital-design guidelines. The ground rules to control the digital logic design cover fan-out, propagation delays, termination, unused logic gates and pins, component and board decoupling, signal line lengths, and multiple-loaded signal paths for various logic elements.

Propagation-delay calculations. A worst case timing consideration of logic implementation is necessary to ensure that adequate timing margins exist in the design. In addition to intrinsic propagation delay of a logic device, other timing delay contributors must be included in the analysis. These contributors account for the effects of voltage, temperature, aging, external loading, and interconnect media. For high-speed devices with subnanosecond delays, it is necessary to treat most circuit paths as transmission lines.

Digital interfaces. The quality of digital signals and system noise generated by signal distortions should be considered in the design, interconnection, and physical layout of digital elements. To ensure that the desired signal characteristics are achieved, the following should be given consideration:

- Interface line impedance and various discontinuities.
- Source- and load-impedance management to control reflection on lines.
- Electrical line lengths and relationship to signal rise/fall time.
- Configuration of multiple-load connections.
- Separation and parallel run length of adjacent signal paths.

Unused gates and pins. Unused logic gates (spares) should be forced into their lowest power-dissipation state by grounding or pulling up their inputs. Of unused input pins on logic gates, those required to be logically low must be grounded, and those required to be logically high must be returned to 5 Vdc through a pull-up resistor.

Decoupling. The following procedure will decouple simultaneously digital logic components and logic boards: For low-frequency board decoupling, each printed wiring board (PWB) uses one 15-μF +/- 20%, 30-V tantalum capacitor, CLR79 type, located near the main connector. For high-frequency board and component decoupling, CKR05 or CKR22 ceramic capacitors are distributed around the board. For each group of logic or digital elements, the amount of capacitance follows this rule: a minimum of 0.20 mF of capacitance for every group of elements totaling a change in power supply current (state to state) of 100 mA.

EMI/EMC design guidelines. The most important step in achieving electromagnetic compatibility will be to define the EMC system, that is, decide how to separate electrically noise from electrically sensitive areas and where to put EMI filters and shields. The Space Shuttle main engine controller (SSMEC), a complex system, employs high-level transient output signals, low-level analog input signals, high-speed digital signals, and a complex, multi-output power supply. In general concept, the SSMEC should enclose the circuitry in a metal box with the power supply isolated in a separate compartment within the box, and the EMI filters should be placed on power-supply inputs and outputs, noisy boards, physically separated from sensitive boards and high-level and low-level signals routed separately.

The power supply should be isolated in a separate compartment with prime power entry on one side of the compartment through bulkhead-mounted

EMI filters. Power-supply outputs should be routed through bulkhead-mounted EMI filters on another power-supply wall. Output signal cables, digital-signal cables, and input analog-signal cables should be physically separated and should not have shields terminated at the same point. Back-plane interconnects should be via multilayer boards. If wire wrap is used, sensitive signals should be placed in the first two layers adjacent to the ground plane, with the less-critical signals further away.

Mechanical considerations. The SSMEC must be electromagnetically compatible with the remainder of the Shuttle. To this end, the integrated EMC design requires that the metal box or cabinet housing the SSMEC circuitry provide on the order of 60-dB attenuation of electromagnetic fields over the frequency range of 14 kHz to 1 GHz. This is not difficult to achieve with any of the common aluminum alloys. Thickness of the material is not critical, since thickness is usually driven by structural requirements rather the EMI requirements and any thickness greater than about 0.020 in. is satisfactory for EMI protection.

Particular attention must be paid to seams and joints in the areas of fastener spacing, material finish, and joint evenness to prevent unacceptable degradation of attenuation. All metal structural parts should be electrically bonded together and ultimately to the housing ground-lug. Small covers should be bonded with silver-filled silicone rubber radio-frequency-interference (RFI) gaskets to avoid bowing of joints.

Power distribution and grounding. Prime power should be brought into the power-supply compartment through tubular bulkhead-mounted EMI filters. If the power cable passes through the controller before going through the EMI filters, it must be shielded. A "doghouse" is preferred for power entry; that is, a small enclosure is used to mount the power connector on the outside of the controller housing so that the EMI filters are outside of the controller.

Both the high- and return-power lines must be isolated from the chassis and signals made common within the controller. Transformer isolation is preferred, even on dc power lines. In this case, the dc is chopped before application to the transformer. Providing a control signal across the transformer, if necessary, will best be done with fiber-optic techniques or transformer coupling.

Secondary power should be distributed on flat planes placed adjacent to power/signal common planes. Power connections to digital-logic PWB should be made by multiple pins spaced across the connector. Output-electronics (OE) driver power should be carried to the OE PWB by twisted pairs. If made through multilayer boards, power and returns must be routed together and carried through connectors on adjacent pins. OE power returns/common should be connected to logic common or analog common only on the OE PWB. Input electronics (IE) power/signal common should be connected to logic common only on a PWB.

Interconnects. Printed wiring boards should have multilayer construction with no more than two signal layers between ground planes. As a design goal, PWB paths should have a characteristic impedance of 50-75 L. PWB-to-PWB signal paths should tend toward 50 L to minimize cross-coupling. PWB-to-outside-world signal paths should tend toward 75 L to minimize reflections. On a logic PWB, parallel paths should be limited to minimize crosstalk.

Thermal overlays should be isolated from signal common on PWB. Provisions should be made for grounding the thermal overlays to the chassis, where the overlays are clamped to the chassis sidewalls, so that the overlays function as shields.

Clock signals should be routed only where absolutely necessary and should be distributed at as low a frequency as possible. Clock lines should not be routed around the edge of a PWB and should not go off of a PWB if at all possible. Clocks leaving the daughter board should be distributed differentially, and clock signal paths should be surrounded by grounds (signal common) on both sides, top and bottom. Cables should be as short as possible and yet consistent with maintainability. Digital signals may be routed on etched flex tapes with ground planes above and below.

Postflight Data Analysis

An essential development requirement will be to measure parametric data for determination of engine performance. Typical required measurements include vibration, pressure, temperature, turbine speeds, fuel and oxidizer flow rates, and valve positions. Engine design parameters such as thrust and flow rates must be verified by engine testing. Temperature and pressure measurements must be taken to confirm design safety-margins. These measurements will first be made during engine-development ground testing and become a set of baseline data that define nominal engine-operating parameters.

Measurement of various engine temperatures ensures that cryogenic propellants are not leaking into the engine, subjecting its components to temperature overexposure. During engine start and shutdown, turbine temperatures, speeds, and pressures indicate whether transients have damaged engine components. Rotor unbalance, bearing wear, and pump-inlet cavitation can be evaluated from vibration measurement.

For the case of the expendable rocket engine, these measurements were of primary importance during development and acceptance testing of the flight hardware. Many of the measurements were of secondary importance during flight in determining causes of failure. However, the amount of data taken during flight was limited by how much data could be downlinked from the vehicle.

The advent of the reusable rocket engine, however, required acquisition of data that can indicate hardware conditions during operation. The engine controller for a reuseable engine must measure, process, and report engine data. As each engine builds operating time, a database is established. After each

engine run, the data are examined by each discipline within the engine team and a data review made before the engine is flown again. The instrumentation group examines the data for indications of sensor or sensor-processing failures. Most instrumentation failures are usually caused by shorted or open connections in the harness or sensor, and these can be detected by tests performed automatically by the electronics. However, intermittent or parameter-shift failure may require more analysis. The data-analysis group, using statistical analysis, compares the most recent run to the existing database and identifies components that may be indicating premature failure. Long-term trends sometimes indicate more subtle failure modes. Research on the SSME indicates that these long-term trends exist and suggests that additional data taken during flight may reduce flight turnaround-time through more accurate prediction of component failure.

Software Requirements

When the electronic controller was introduced to pace and monitor the engine operation, software became an important element in rocket-engine control, supporting optimum engine performance, safety and health monitoring, redundancy management, etc. It enables the controller to use many complex control algorithms and a close monitoring scheme. For a reusable engine, the historical data can be used for the next flight as well as real-time health monitoring.

The beginning of the engine-controller design process sees software requirements defined as one of the controller components. Hardware/software trade studies determine the best balance to meet the fundamental control-system requirements, including functional performance, reliability, accuracy, and stability. In addition to the hardware interface, the software requirements normally include the following areas: engine control requirements, engine and controller performance and status monitoring, failure detection and recovery, and communication and data-gathering requirements.

Engine control. One of the primary functions of the software, engine control, will be based on the overall engine-performance requirements. Software may be used in both open-loop and closed-loop control. In future systems, adaptive control will be made possible with advanced software architecture in the control loop.

During control-algorithm development, a computer program simulates control models to determine necessary sensor data, actuator output, and other engine parameters. These parameters, along with the control algorithm, will be included in the software functional requirements.

Engine control includes start, run, and stop phases with engine-thrust, propellant-mixture, and igniter-control outputs. The control requirements also include timing requirements of the control loop, startup sequence, shutdown sequence, and post-shutdown operation.

Engine and controller performance and status monitoring. The software performs various checks, validation, and monitoring before, during, and after engine operation to determine status and performance of the engine and the controller hardware. These operations normally include the following items: controller self-test, sensor validation, sensor check and monitoring, valve monitoring, engine-ready and ignition monitoring, actuator and pneumatic checkout, communication check and monitoring, and power-supply check and monitoring.

Failure detection and recovery. Software monitoring and controlling of the engine makes possible early detection of failure and smooth switching to an alternate component. The software may compensate for temporary hardware errors and some hardware degradation to support safe operation. Certain critical parameters must be monitored to be within specified limits (redlines) to ensure engine, vehicle, and mission safety. These parameters, which are determined by the type of engine, controller, and vehicle, normally include main combustion pressure, turbine-discharge temperatures, turbopump-seal purge pressures, turbopump coolant-liner pressures, preburner purge pressures, and pump-vibration sensors. The software should also include failure-mode analysis and diagnostic routines to determine the cause of failures.

Communication. The processor communicates with the vehicle to accept commands and report engine and controller status. This communication depends on the amount of data traffic and response-time requirements. Reliability of the communication link is just as important as any other part of the system. Communication protocol and error-detection and recovery methods will be part of these requirements.

Data gathering. Software will gather pertinent data for use in postflight analysis and health monitoring. These data are especially useful for reusable engines, new engine design, and improvements in existing engine designs.

Fault tolerance. The system requires at least fail-operational/fail-safe operation, which includes redundancy management, tolerance of hardware degradation, and recovery from temporary errors. If the controller is used for critical operation, software redundancy should also be considered to detect any bugs.

Software architecture. Primarily the engine controller controls and monitors the engine within specified times required in its operation. To be efficient, the software structure must reflect this real-time requirement. The architecture design must also consider software-development efficiency, which affects software integrity, maintenance, cost of development, expansibility, and reusability.

Real-time operating systems are more flexible and easier to use both for run-time system and software development. However, the resulting software programs tend to be larger than other architectures. "Real-time executive," an efficient run-time system, requires careful planning and design to be flexible and maintainable. The software development requires another operating system or compatible development environment.

Embedded software, a customized architecture, yields the most efficient run-time program for the

real-time system. It is the most time-consuming system to develop and is not easy to maintain without careful planning and a well-structured development methodology.

Multitasking operations will be determined at the time of requirements definition. Number of tasks, response time, interrupts, and task priorities, among other factors, affect the decision.

Software development. Although not a large-scale task, development of the engine-controller software will be a complicated and critical operation. Success demands proper design methodology along with efficient project management.

Design methodology. Engine system design will see many requirement changes and improvements. The popular waterfall method is not well suited for changing requirements or design. The following three methods best suit this design task:

Incremental. The incremental method, a variation of the waterfall method, may be applicable if the requirements are fairly well established. The software is divided into a number of modules of manageable size and is designed one module at a time. Since each module is small, normal changes are easily accommodated.

Evolutionary. The evolutionary method can be used when the major requirements are known. The design starts with only the major requirements implemented and evolves to the final configuration. For the engine-controller software, normally the major requirements will be known and the refinements may change from time to time. This methodology well suits this type of software.

Prototyping. The prototyping method is best used when the customer says, "I know what I want when I see it." It develops functional elements closest to the estimated requirements as a feasibility model and evaluates this prototype to generate prototype requirements. The process is repeated until the final requirements are established. This process creates a product most desirable for the system; but it can be very time-consuming and costly.

Design tools. Establishing the software-development environment entails the greatest capital investment in this area. It must be carefully chosen so that proper software tools will be available for design. Computer aided software engineering (CASE) tools can facilitate this work throughout—from requirement analysis, software design, and design analysis to all documentation and the configuration management.

Design language. Selection of design language or method will reflect the software complexity and coding requirements. Figure 7-74 graphically represents the control flow of the program. This type of detailed design is easy to code and modify; but data flow can not easily be shown in the computer-generated diagram and documentation. Using the computer for graphical design is cumbersome compared to the program design language (PDL), as shown in Fig. 7-75. Many other types of graphic software design charts are available with CASE tools. PDL offers the advantages of ease of writing the detailed design and documentation on the computer, but the disadvantage that the designer tends to code in PDL, rather than concentrating on design—and that lapse may cause more design errors.

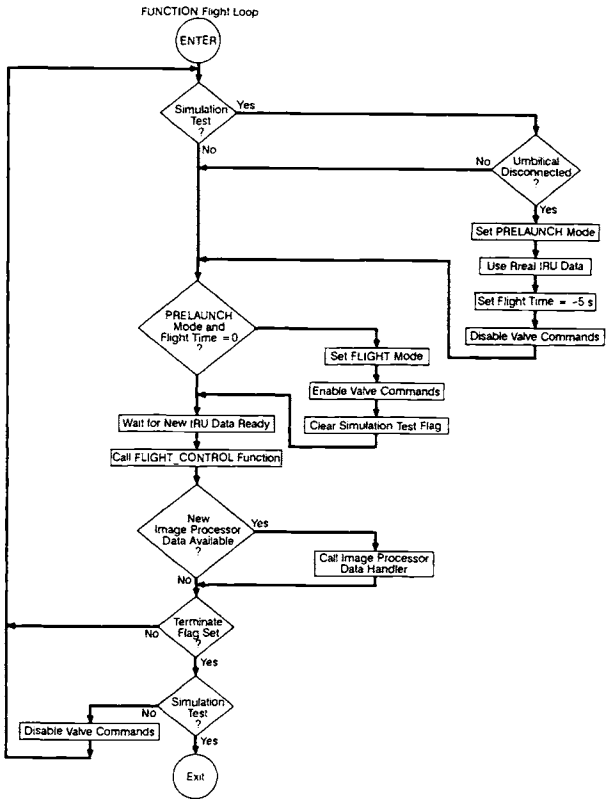

Fig. 7-74 Flow diagram

```
DO UNTIL terminate flag is set and simulation test flag is set
   IF simulation test flag is set
      IF umbilical is disconnected
         set prelaunch mode
         use real IRU data
         set flight time to -5 seconds
         disable valve commands
      ENDIF
   ENDIF
   IF prelaunch mode
      IF flight time is 0
         set flight mode
         enable valve commands
         clear simulation test flag
      ENDIF
   ENDIF
   DO UNTIL new IRU data ready
      null process
   ENDDO
   IF new image processor data is available
      call image processor data handler
   ENDDO
   IF terminate flag is set
      IF simulation test flag is clear
         disable valve commands
      ENDIF
   ENDIF
ENDDO
```

Fig. 7-75 Program design language.

Implementation language. For most of the controller software, any language may be used for implementation; but assembly language is used to code the most efficient software. The "C" language is widely used because of simplicity and flexibility. The Ada language is suited for complex software to minimize coding errors. Another disadvantage of high-order language (HOL) is that compiler efficiency, in many cases, determines the code efficiency of the program. On the other hand, assembly-language programming, although complicated, produces the fastest code if programmed properly. In many case, HOL and assembly language are mixed to get the best results.

Testing. The final phase of software development is testing. The software is tested as a module (unit testing), together with the other modules (integration testing), and finally as a total system. The thoroughness of these tests determines the quality of the final product. The final test must include all real conditions such as faults and noise. Since the engine cannot be fired for all the software tests, simulated engine tests are performed until the product is sufficiently proven. Therefore, these tests depend highly on the quality of the engine-simulation program.

Independent validation and verification. Independent validation and verification (IV&V) of software development has proven highly desirable in creating a quality software product. The IV&V process may cover the entire software-development cycle, from the requirements-analysis phase to the final test, or it may be limited to the test phase only, depending on the criticality of the software.

Other software-design considerations. Basic software requirements for the controller will be established during the initial engine-system design through a careful hardware-vs.-software tradeoff. At the time the software functions are defined, related hardware functions, inputs, and outputs must be clearly and unambiguously defined. These items include hardware accessibility by the software, memory-size limitation, communication and bus speed, data traffic, timing requirements, etc. The trade study also evaluates hardware/software efficiency in terms of size, cost, complexity, and ease of maintenance. Other software design considerations are as follows:

- Software response time to any critical event.
- Software system modularity for ease of development and maintenance.
- Robustness to tolerate hardware degradation and noise and temporary errors.
- Maintainability to reduce cost of maintenance and improvements.
- Testability to improve testing and quality of the software product.
- Reusability to improve software quality and reduce development cost and time.
- Flexibility in both software structure and design to adapt to any engine system improvement.

Summary. The primary ingredients of any high-quality software design will be the *software engineers*, followed by proper development methodology, efficient software tools, and software environment suited to the development. Since the engine-controller software design requires a team effort and close coordination with hardware design, efficiency in project management greatly affects the final software product.

The most important phase of the development cycle will be the requirements analysis and definition, followed by the testing regimen. Erroneous requirements are the hardest to find and most costly to repair. Good documentation is another important factor in maintaining the software.

The controller software development does not different from any other software development in that it must follow good software-engineering practices. As critical tasks pile on the software, its quality becomes aa ever more dominant factor in the overall engine system.

7.5 REFERENCES

References 7-1 through 7-8 cover material for design of rocket-engine control and monitoring systems. References 7-9 through 7-11 cover material for design of fluid-flow-control components. These reference materials prove invaluable in the design of fluid flow control components.

7-1. *Systems Engineering Management Guide*, Defense Systems Managment College, United States Government Printing Office, Washington, D.C. 20402, 1986

7-2. Ogata, K., *Modern Control Engineering*, Prentice-Hall, New York, 1970

7-3. Brewer, J., *Control Systems Analysis, Design, and Simulation*, Prentice-Hall, New York, 1974

7-4. Shinners, S., *Modern Control System Theory and Application, 2d Ed.*, Addison-Wesley, Reading, Mass., 1978

7-5. Kuo, B., *Digital Control Systems*, Holt, Rinehart and Winston, Inc., 1980

7-6. Borrie, J., *Modern Control Systems*, Prentice-Hall International, 1986

7-7. D'Souza, A., *Design of Control Systems*, Prentice-Hall, New York, 1988

7-8. Brogan, W., *Modern Control Theory*, Quantum Publishers, Inc., 1974

7-9. *Flow of Fluids Through Valves, Fittings, and Pipe*, Engineering Division, Crane Inc., New York, NY

7-10. Tellier, G., "Space Shuttle Prototype Check Valve Development," NASA-CR-150991, Sep 1976

7-11. *Engineering Guide to Spring Design, Associated Spring*, Barnes Group Inc., Bristol, CT

The following additional references will aid the reader who needs more in-depth information on subjects related to fluid-flow-control component design. A more complete listing of useful reference material can be found in the bibliography of Ref. 7-11.

Howell, G. W., and Weathers, T. M., *Aerospace Fluid Component Designer's Handbook*, RPL-TDR-64-25, TRW Systems Group, TRW, Inc., Redondo Beach, CA

Materials Selector, published annually by Materials Engineering, Cleveland, OH

Parker O-Ring Handbook, Parker Seal Group, O-Ring Division, Lexington KY

Roters, H. C., *Electromagnetic Devices*, John Wiley and Sons, New York, NY

Young, W. C., *Roark's Formulas for Stress and Strain*, McGraw-Hill, New York, NY

Electrohydraulic Flow-Control Servovalves, Society of Automotive Engineers, Pittsburgh, ARP 490D, Rev. 11/1/78

Merritt, H., *Hydraulic Control Systems*, 1967, John Wiley and Sons, New York, NY

"Two-Stage Servovalve," Model 25C, HR/Textron Report HR72100112, 14 May 1987

Design of Propellant Tanks

Liquid-propellant rocket engines and propellant-feed systems form the propulsion system. Since propellant tankage and its arrangement have a large effect upon liquid propellant rocket engine design and propulsion systems integration, a detailed discussion of propellant tank design is presented in this chapter. Much of the information also applies to pressurant tank design.

8.1 DESIGN CONFIGURATIONS

The configuration of propellant tanks depends largely on vehicle mission and size. In many designs, the tanks form an integral part of the vehicle structure. Propellant tanks can be nonexclusively categorized, according to vehicle application, as prepackaged storable-liquid, booster-stage, and upper-stage systems.

Prepackaged Storable-liquid Systems

Figure 8-1 presents the configuration of a typical prepackaged storable-liquid propulsion system. The tanks, arranged in tandem, have a common bulkhead. This system is designed for long storage periods, perhaps 5 to 10 years. A main characteristic of these systems: propellants will be loaded and contained in the tanks by burst disks or isolation valves. Both the tank and containment component construction materials must be compatible with the propellants for the storage duration. In the example, the propellants are expelled by a pressurization gas produced by a solid-propellant gas generator. The tank walls form an integral part of the vehicle structure and are designed to withstand the internal pressure loads as well as the vehicle dynamic loads. In some designs the tanks are further stabilized by the internal pressure against buckling; i.e., the walls are always kept under tension loads by a specified pressure level maintained during storage and handling. In smaller units, the walls are usually capable of taking external loads without being pressurized internally. Operational tank pressures range from 400 to 2000 psia. Prepackaged storable-liquid systems are usually employed in relatively short-duration, low-thrust applications.

Booster-stage Systems

Figure 8-2 presents the propellant-tank configuration of a typical propulsion system used in the booster stages of a large launch vehicle such as the Saturn V. The system shown can be used for either storable or cryogenic propellants. The tanks, arranged in tandem, form walls of the vehicle structure. For booster

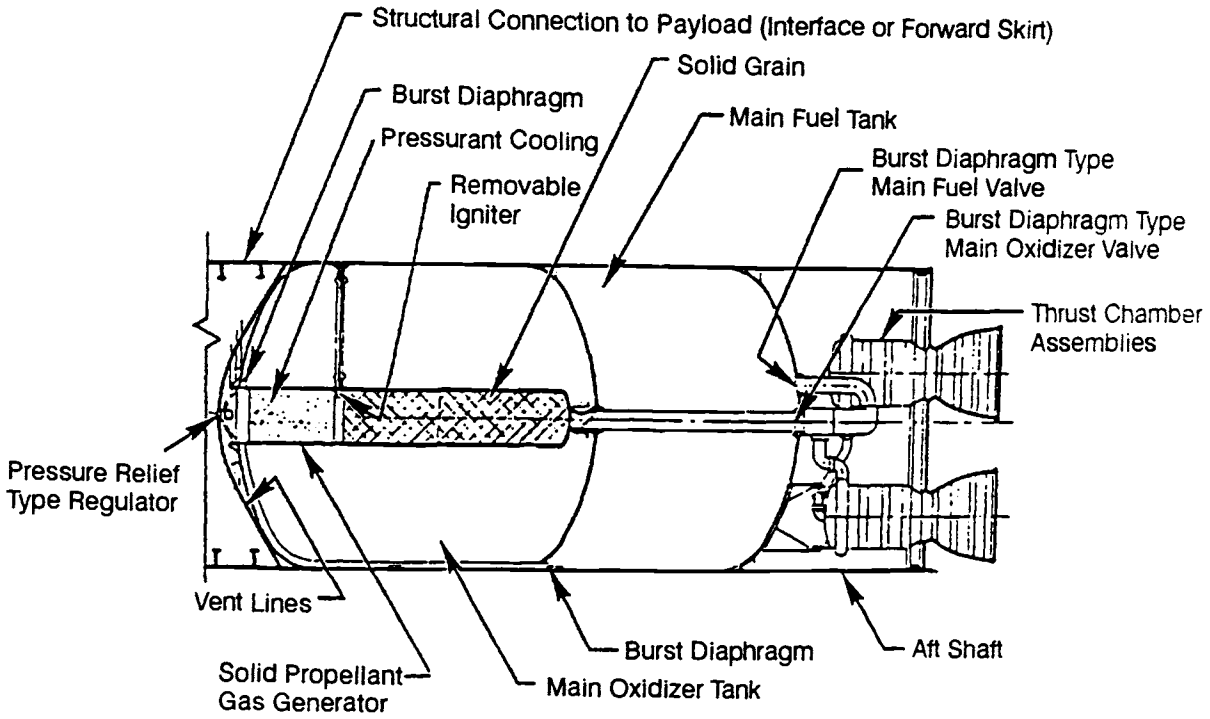

Fig. 8-1 Propellant-tank design configuration of a typical prepackaged storable-liquid propulsion system.

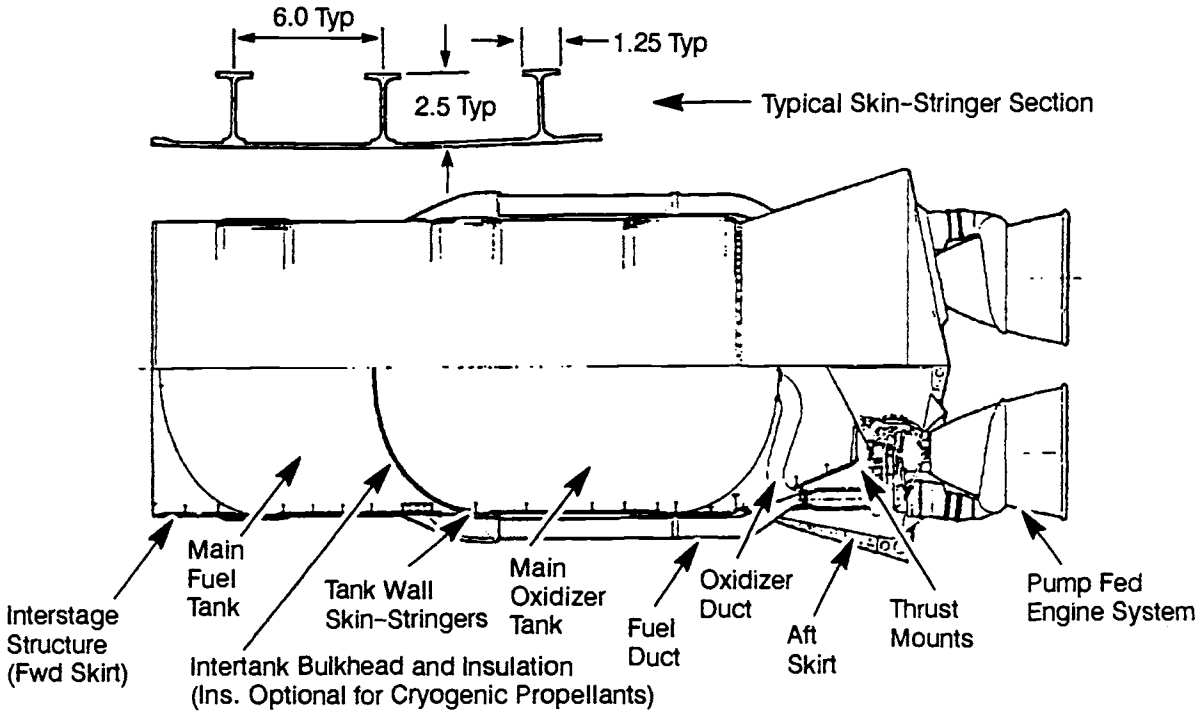

Fig. 8-2 Propellant-tank design configuration of a typical booster-stage propulsion system.

application, overall vehicle systems optimization usually dictates use of a turbopump-fed engine system. This permits relatively low operational tank pressures, ranging from 30 to 100 psia.

The tanks represent a large percentage of the vehicle structural (inert) weight. Low pressure levels allow constructing the tanks with extremely thin walls. However, the often huge tank structures thus become sensitive to external buckling loads. To stabilize the tank structures of large booster-stage systems, two basic design avenues are open: pressure-stabilization and self-supporting structures. In pressure-stabilized systems, such as the Atlas ICBM, tank pressures must be constantly maintained above a specific minimum by elaborate controls. Atlas's tank structure, basically a thin-wall monocoque, requires special handling procedures. In most booster-stage systems, the propellant tanks are self-supporting, with tank walls reinforced by skin stringers (Fig. 8-2) or by other structural means, such as waffle-grid patterns.

Cryogenic propellants may require tank insulation. It will be mandatory in a liquid hydrogen system to prevent ambient-air liquefaction, which causes high heat-transfer rates, with attendant high boiloff rates, and safety hazards.

Upper-stage Systems

Figure 8-3 presents the propellant-tank design for a typical pressure-fed upper-stage propulsion system. An outer cylindrical shell, designed to withstand all anticipated boost and flight loads, contains the tanks. The propellant tankage consists of two individual welded aluminum-alloy tanks, modified spheres, faired into conical sections at the bottom for propellant discharge. The tanks are bolted to the shell structure around their support ring.

Many upper-stage vehicles employ a gas-pressurized propellant feed system. Tank pressures range from 100 to 400 psia. The system shown in Fig. 8-3 uses helium gas for pressurization. The gas is stored at an initial pressure level from 4500 to 5500 psia at -300°F in two liquid-nitrogen-jacketed, high-pressure spherical tanks located between the two main propellant tanks.

The following discussion treats directly only upper-stage propulsion systems; but many of the design principles presented apply equally to booster-stage tanks.

8.2 DESIGN CONSIDERATIONS

Systems optimization within the overall vehicle design greatly influences tank design. A principal vehicle-design objective will be highest payload and/or velocity increment with maximum possible reliability. Design details depend largely upon type of propellants, mission requirement and configuration, propulsion-system design, and available construction materials and fabrication techniques.

Propellant Properties

Propellants affect tank design mainly by their physical and chemical characteristics. The boiling point or storage temperature of a propellant determines the operating temperature range of the tank assembly. Cryogenic propellants cause tank design problems due to thermal gradients, the need for insulation, and need for construction materials ca-

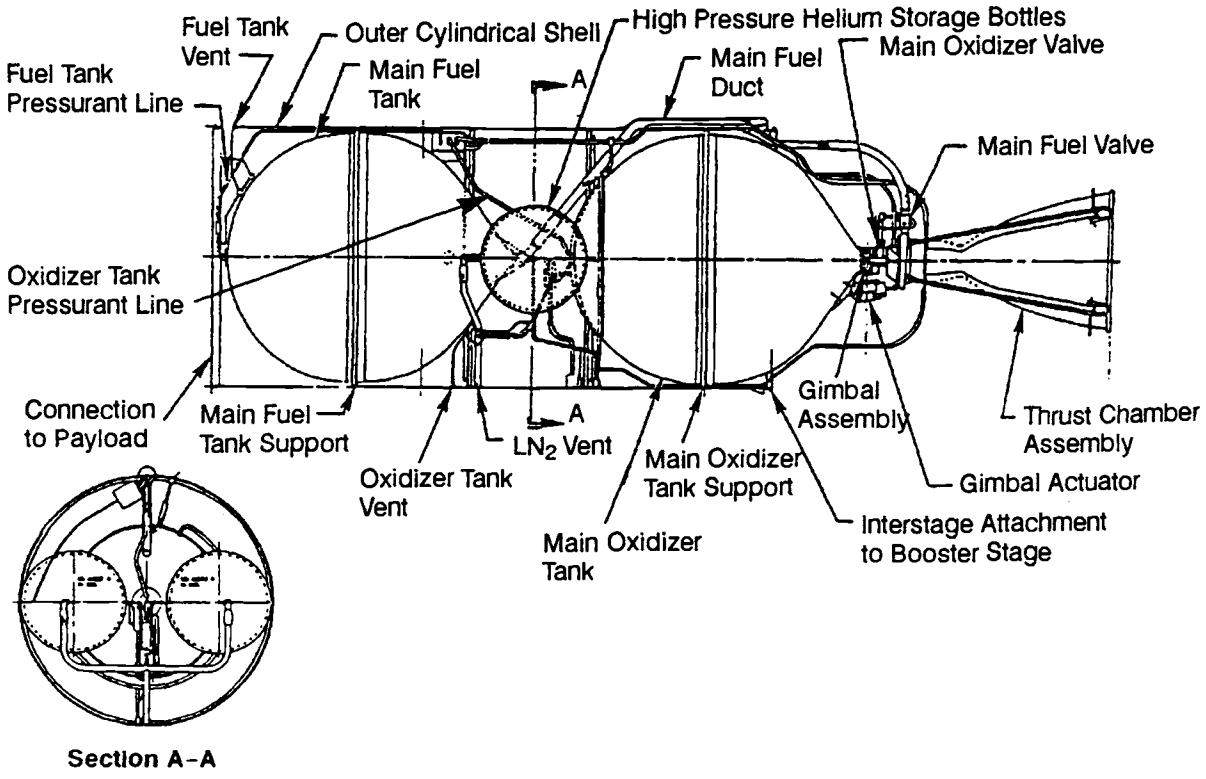

Fig. 8-3 Propellant-tank design configuration of a typical upper-stage propulsion system.

pable of remaining ductile at very low temperatures. The low density of some propellants, such as liquid hydrogen, necessitates tanks of considerable volume. The highly corrosive and reactive properties of other propellants severely limit the selection of tank materials.

Shape and Size of Propellant Tank

As a propellant tank, a sphere offers the smallest surface-to-volume ratio and the smallest shell stress for a given internal pressure, but the combination of several spheres into the generally cylindrical envelope typical for most rocket vehicles causes sizable weight and volume penalties. Furthermore, a sphere precludes use of the tank wall as a load-carrying member of the vehicle structure (Fig. 8-1 and 8-2), resulting in further weight and volume penalties.

Thus, both vehicle configuration and tank pressure will determine the shape of propellant tanks. Vehicles of relatively large length-to-diameter ratios and of limited space envelopes will use cylindrically-shaped tanks. Relatively high tank pressures and less-stringent space conditions may favor spherical tanks (Fig. 8-3). The ends of cylindrical tanks can have either spherical or ellipsoidal shapes. The basic cylindrical tank with spherical ends weighs less than one with ellipsoidal ends; but overall, an ellipsoidally-ended tank may weigh less owing to shorter interstage structure. In some designs, the propellant-tank ends will have special shapes to accommodate structural loads, minimize residual propellants, and utilize available envelope.

The required volume of a propellant tank will be the sum of usable propellant volume and other volume requirements:

$$V_t = V + T + B + U \tag{8-1}$$

where—

- V_t = propellant-tank design volume, ft^3
- V = usable propellant volume calculated from propulsion-system requirements, ft^3 (may include a "usable residual" term representing design reserves, loading uncertainty, and mixture-ratio-shift effects)
- T = trapped-propellant volume, a function of system configuration; includes propellants trapped in tank and components down to the engine valves, ft^3
- B = boiled-off propellant volume (applicable only to cryogenic propellants), ft^3
- U = tank ullage volume, ft^3

The calculation of propellant volume takes propellant density at specific temperatures. The tank ullage-volume calculations should allow for propellant volume changes due to temperature change of the tanked propellant and for tank deformation under pressure. This is especially important for prepackaged storable-liquid systems to prevent excessive tank pressures when the system is exposed to a specified upper temperature limit during storage. The weight of the trapped propellant will be greatest, however, at the lowest operating temperature.

Sample Calculation 8-1

The following data characterize the A-4 Stage propulsion system, including two engines:

- Oxidizer (N_2O_4) density, 90.12 lb/ft^3
- Oxidizer weight-flowrate, 12.78 lb/s per engine
- Fuel (N_2H_4) density, 63.17 lb/ft^3
- Fuel weight-flowrate, 10.65 lb/s per engine
- Nominal engine-firing duration at full thrust, 410 s
- Trapped oxidizer volume T_O = 0.9 ft^3
- Trapped fuel volume T_f = 1.8 ft^3
- Tank ullage volume U = 2.5% of propellant volume

Problem

Determine the volume of the propellant tanks.

Solution 8-1

The required usable oxidizer volume:

$$V_o = \frac{12.78 \times 2 \times 410}{90.12} = 116.2 \text{ ft}^3 \qquad \text{(bs-1)}$$

The oxidizer-tank ullage volume:

$$U_o = (V_o + T_o) \times 0.025$$

$$= 117.1 \times 0.025 = 2.9 \text{ ft}^3 \qquad \text{(bs-2)}$$

From Eq. (8-1), the required design volume of the oxidizer tank:

$$V_{to} = V_o + T_o + U_o$$

$$= 116.2 + 0.9 + 2.9 = 120 \text{ ft}^3 \qquad \text{(bs-3)}$$

The required usable fuel volume:

$$V_f = \frac{10.62 \times 2 \times 410}{63.17} = 138.2 \text{ ft}^3 \qquad \text{(bs-4)}$$

The fuel-tank ullage volume:

$$U_f = (V_f + T_f) \times 0.025 = 140 \times 0.025 = 3.5 \text{ ft}^3 \qquad \text{(bs-5)}$$

From Eq. (8-1), the required design volume of the fuel tank:

$$V_{tf} = V_f + T_f + U_f$$

$$= 138.2 + 1.8 + 3.5 = 143.5 \text{ ft}^3 \qquad \text{(bs-6)}$$

Propellant-tank Arrangement

Most vehicle systems have the propellant tanks in tandem, but other arrangements can be used for specific design reasons. Figure 8-4 presents various propellant-tank configurations for a typical vehicle system using helium for tank pressurization. A design analysis will determine the best solution for a given propellant-storage volume and vehicle envelope. General considerations include minimum overall weight, maximum storage volume in a given envelope, least possibility of propellant mixing, aerodynamic vehicle shape, ease of installation of ducts and lines, ease of insulation, ease of fabrication and handling, and a minimum of trapped (unusable) propellants.

Arrangement "a" in Fig. 8-4 is taken as standard. Arrangement "b", combining tandem propellant tanks with an integrated helium bottle in between, gives lowest weight, but poses design problems in the routing of pneumatic lines and controls. Arrangement "c" with concentric tanks eases the installation of propellant ducts, but has the possibility of simultaneous puncture of both tanks, and subsequent mixing of the propellants. Arrangement "d" with multiple tanks has the highest weight, but is easier to fabricate and handle, especially for very large vehicles.

Structural Loads

As structural members, propellant tanks must be designed to withstand a combination of the following

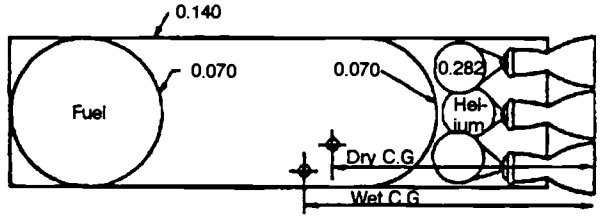

a) Tandem Propellant Tanks with Common Bulkhead and Separate Helium Bottles - Tankage Weight, 100%

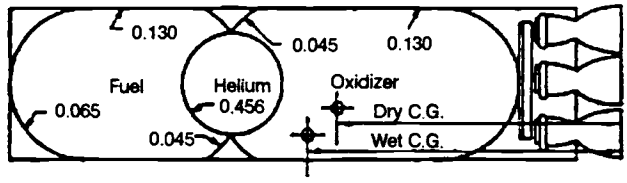

b) Tandem Propellant Tanks with Integrated Helium Bottle in the Middle - Tankage Weight, 93%

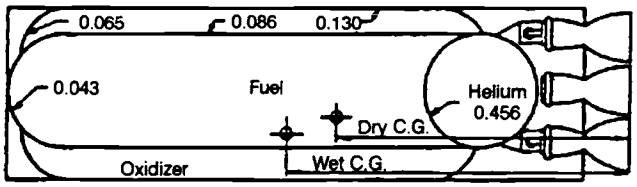

c) Concentric Propellant Tanks with Integrated Helium Bottle at Aft End - Tankage Weight, 118%

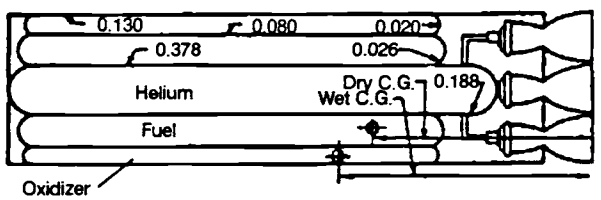

d) Multiple Propellant Tanks and Helium Bottle in Cluster - Tankage Weight, 162%

Fig. 8-4 Various propellant-tank arrangements of a typical vehicle system.

probable structural loads:

- Internal pressures and their dynamic effects
- Axial thrust loads and their dynamic effects
- Bending moments due to vehicle transverse accelerations, wind loads, and shifting of the center of gravity
- Aerodynamic forces
- Thrust-vector-control forces
- Vibration and shock loads
- Loads produced by mounting arrangement
- Loads caused by thermal transients and gradients
- Loads produced during ground handling

In most vehicle systems, internal tank pressure loads and axial-thrust loads are the principal ones. These and other loads require careful evaluation, including experimental testing.

Safety Factors

The recommended criteria for structural loads presented in Chapter 2 (Eqs. 2-4 through 2-7) generally apply to propellant-tank design. However, when calculating allowable operating stresses from tank internal pressure, Military Standard MIL-STD-1522A (USAF), Standard General Requirements For Safe Design And Operation Of Pressurized Missile And Space Systems, is frequently imposed. It requires minimum proof test and burst factors of 1.25 and 1.5, respectively. If MIL-STD-1522A is not specified, the following correlations are recommended minimums for various situations:

1) No hazard to personnel or vital equipment:

$$S_w = \frac{F_y}{1.1} \qquad (8\text{-}2)$$

or

$$S_w = \frac{F_u}{1.25} \qquad (8\text{-}3)$$

2) Special safety devices provided for personnel (example: the booster for a manned upper stage which has an ejection device with an exceptionally high degree of reliability):

$$S_w = \frac{F_y}{1.15} \qquad (8\text{-}4)$$

or

$$S_w = \frac{F_u}{1.35} \qquad (8\text{-}5)$$

3) Hazard to personnel or vital equipment:

$$S_w = \frac{F_y}{1.25} \qquad (8\text{-}6)$$

or

$$S_w = \frac{F_u}{1.5} \qquad (8\text{-}7)$$

where—

S_w = maximum allowable operating stress, psi; i.e., the stress due to maximum tank pressure under normal transient and steady operating conditions

F_y = yield strength, psi, of the tank construction material, at operating-temperature conditions

F_u = ultimate strength, psi, of the tank construction material under operating-temperature conditions

Maximum allowable operating stress S_w gets calculated for both F_y and F_u. The lower value should then be used. All propellant tanks are subjected to hydrostatic-pressure tests before acceptance. For case (1), the proof-test pressure equals 110% of the maximum tank working pressure. For cases (2) and (3), the proof-test pressures should be 115 and 125% of the maximum tank working pressure, respectively.

Sample Calculation 8-2

The start transient of a prepackaged storable-liquid propulsion system for an aircraft-launched missile is programmed not to attain main-stage level until the missile reaches a specified distance from the aircraft.

Problem

Calculate the maximum allowable operating stresses for propellant tanks made of—

(a) Aluminum alloy 6061-T6, F_y = 35,000 psi, F_u = 45,000 psi

(b) Aluminum alloy 6066-T6, F_y = 50,000 psi, F_u = 57,000 psi

Solution 8-2

(a) *Tank made of aluminum alloy 6061-T6.* Since the system involves personnel safety during start transient, Eq. (8-6) and (8-7) will be applied, as follows:

$$S_w = \frac{F_y}{1.25} = \frac{35{,}000}{1.25} = 28{,}000 \text{ psi} \qquad (\text{bs-7})$$

or

$$S_w = \frac{F_u}{1.5} = \frac{45{,}000}{1.5} = 30{,}000 \text{ psi} \qquad (\text{bs-8})$$

Maximum allowable operating stress during start transient = 28,000 psi.

During mainstage operation, personnel are considered safe and Eq. (8-4) and (8-5) can be used:

$$S_w = \frac{F_y}{1.15} = \frac{35{,}000}{1.15} = 30{,}435 \text{ psi} \qquad (\text{bs-9})$$

or

$$S_w = \frac{F_u}{1.35} = \frac{45{,}000}{1.35} = 33{,}360 \text{ psi} \qquad (\text{bs-10})$$

Maximum allowable operating stress for mainstage = 30,435 psi.

(b) *Tank made of aluminum alloy 6066-T6.*

During start transient:

$$S_w = \frac{F_y}{1.25} = \frac{50{,}000}{1.25} = 40{,}000 \text{ psi} \qquad \text{(bs-11)}$$

or

$$S_w = \frac{F_u}{1.5} = \frac{50{,}000}{1.5} = 38{,}000 \text{ psi} \qquad \text{(bs-12)}$$

Maximum allowable operating stress during start transient = 38,000 psi.

During mainstage operation:

$$S_w = \frac{F_y}{1.15} = \frac{50{,}000}{1.5} = 43{,}478 \text{ psi} \qquad \text{(bs-13)}$$

or

$$S_w = \frac{F_u}{1.35} = \frac{57{,}000}{1.35} = 42{,}222 \text{ psi} \qquad \text{(bs-14)}$$

Maximum allowable operating stress during mainstage = 42,222 psi.

Material and Fabrication Considerations

In addition to considerations of propellant compatibility and operational-temperature ranges, selection of construction materials for propellant tanks will be based on strength-to-density ratio at a given temperature and on ductility. Properties will often be specified from Military Standardization Handbook MIL-HDBK-5E, "Metallic Materials and Elements for Aerospace Vehicle Structures." For a given working pressure, the lightest tank structure will be the one made of the material with the highest ratio of ultimate strength-to-density. The following construction materials have frequently been used for propellant tanks:

- Aluminum alloys, such as 2000 and 6000 series. Room temperature properties: average density ρ = 0.1 lb/in.^{3}, F_y up to 60,000 psi, F_u up to 70,000 psi, F_u/ρ= 70 x 10^4.
- Steel alloys, such as AISI 300 series, A286, 17-7 PH, PH 15-7 Mo and Inconel 718. Room temperature properties: average density ρ = 0.285 lb/in.^{3}, F_y up to 200,000 psi, F_u up to 220,000 psi, F_u/ρ = 77.2x 10^4.
- Titanium alloys, such as 6Al-4V. Room temperature properties: average density ρ = 0.16 lb/in.^{3}, F_y up to 155,000 psi, F_u up to 170,000 psi, F_u/ρ =106x10^4.
- Filament-wound graphite/resin composites. Room-temperature composite properties: average density ρ = 0.059 lb/in.^{3}, F_u = 600,000 psi. F_u/ρ = 1020 x 10^4.

Compatible with most storable and cryogenic propellants, aluminum alloys may be used for operating temperatures up to 350°F. Stainless steels and titaniums qualify for storable and cryogenic propellants, and can serve at higher temperatures (800°F maximum). Epoxy resins used with graphite will ordinarily be limited to temperatures less than approximately 300°F, but other resins may be used up to approximately 500°F.

Fabrication methods for propellant tanks depend largely upon the type of material used. The most important considerations for tank fabrication are dimension control, heat treating, and welding. Tank-stress calculations must consider the lower limit of wall-thickness variation, but the upper limit will be used for weight calculations. The strength of a metal may fall into a band, too, the variation of which depends on the heat-treating process. Stress calculations will be based on the minimum expected strength. The quality of the welding process or the efficiency of a welded joint may require extra wall thickness as calculated from separate operating stresses. Assuming a weld efficiency of 90-95% will be reasonable. Depending on the alloy, welds are frequently subjected to a heat cycle to relieve residual stresses due to welding. Figure 8-5 presents the construction of a welded propellant tank. Note the segmented tank end, which is typical for large tanks.

Design Problems

Many other design and analysis problems have to be carefully considered before a successful propellant tank can be produced. The relatively thin, highly stressed shells make it difficult to attach concentrated loads. The loads must be spread out in a suitable way to prevent localized overstresses. Cryogenic propellants may create thermal transient and gradient problems. While the empty portion of a tank may be subject to aerodynamic heating, the filled portion

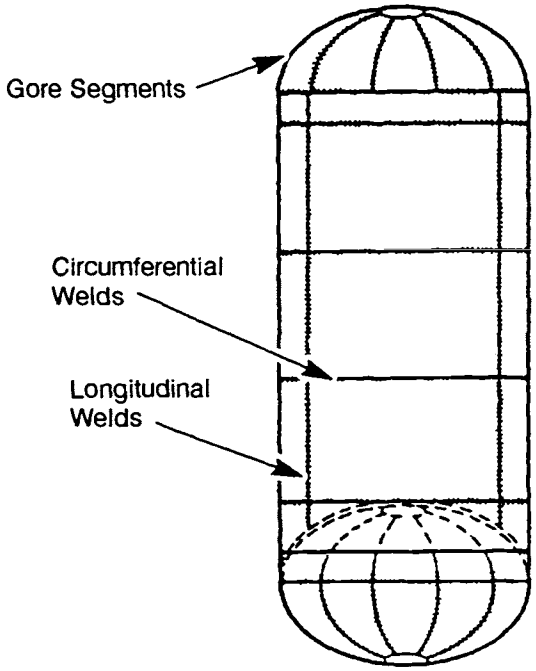

Fig. 8-5 Typical welded propellant-tank construction.

may be at a very low temperature. Additional thermal problems may arise in outer space, such as from solar heating of one tank side and radiation cooling of the other. Other problems associated with the management of the propellants within the tanks include uniform dispersion of the entering tank pressurant, sensing of propellant quantities (PU), prevention of propellant sloshing, expulsion of propellants under adverse conditions, and fill, drain, vent, and pressure relief of the propellant tanks.

8.3 STRUCTURAL DESIGN

As a rule, the wall thickness of propellant tanks will first be calculated from stresses caused by internal-pressure loads and discontinuities. Then the design will be checked for other loads. If small in thickness compared to the radii of curvature ($t/r \leq 1/15$) and offering no resistance to bending, the wall will be subjected only to direct or hoop-membrane stresses, which are assumed to be uniformly distributed over the thickness. However, any discontinuity along the wall, such as an abrupt change in radius of curvature or wall thickness, will introduce discontinuity and bending stresses. At a sufficient distance from the juncture between the tank ends and the cylindrical shell, where interaction does not occur, the maximum stress in the tank wall due to internal pressure should be calculated using the hoop-membrane-stress formula only.

Figure 8-6 identifies the major tank elements. In an optimum tank design, the wall thickness varies according to a combination of local membrane, bending, and discontinuity stresses, especially for spherical and ellipsoidal tank-ends. The following methods can be used to calculate volume, wall thickness, wall surface area, and weight of various tank shapes. The following general terminology is used:

- p_t = maximum tank operating pressure, psig
- S_w = maximum allowable operating stress of the tank construction material, psi
- ρ = density of the tank construction material, lb/in.^{3}
- E = modulus of elasticity, psi
- v = Poisson's ratio
- e_w = weld efficiency

Spherical Tanks

1) *Volume*, in.^{3}:

$$V_s = \frac{4\pi a^3}{3} \tag{8-8}$$

where a = nominal radius of the tank, in.

2) *Wall thickness*, in., required to withstand membrane stresses from internal tank pressure:

$$t_s = \frac{p_t a}{2S_w e_w} \tag{8-9}$$

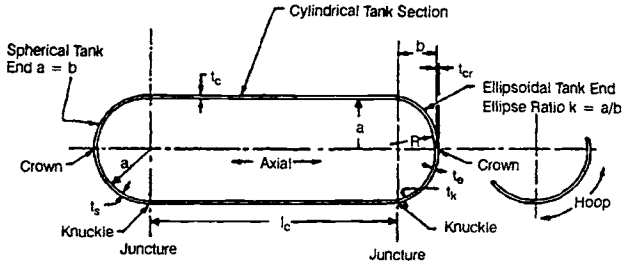

Fig. 8-6 Nomenclature of principal tank elements.

3) *Wall surface area*, in.^{2}:

$$A_s = 4\pi a^2 \tag{8-10}$$

4) *Weight*, lb:

$$W_s = 4\pi a^2 t_s \rho \tag{8-11}$$

5) *Critical pressure due to external loading*, psi. External pressure higher than the internal tank pressure may create a pressure differential across the wall that can buckle the tank.

$$p_{cr} = \frac{2Et_s^2}{a^2}\sqrt{3(1-v^2)} \tag{8-12}$$

Ellipsoidal and Spherical Ends (Fig. 8-6)

The spherical end, a special case of ellipsoidal end, has the major half-diameter, a, equal to the minor half-diameter, b.

1) *Volume*:

Ellipsoidal-tank-end volume, in.^{3}:

$$V_e = \frac{2\pi a^2 b}{3} \tag{8-13}$$

Spherical-tank-end volume, in.^{3}:

$$V_s = \frac{2\pi a^3}{3} \tag{8-14}$$

where a = elliptical-tank-end major half-diameter, in. = radius of the cylindrical tank section; b = elliptical tank end minor half-diameter, in.

2) *Wall thicknesses* considering combined membrane, discontinuity, and local bending stresses caused by internal tank pressure p_t. An equivalent wall thickness—an average value of knuckle-and-crown thickness—may be used to calculate the weight of the tank ends:

$$t_k = \frac{Kp_t a}{S_w e_w} \tag{8-15}$$

$$t_{cr} = \frac{p_t R}{2S_w e_w} \tag{8-16}$$

$$t_e = \frac{(t_k + t_{cr})}{2} = \frac{p_t a\left(K + \frac{k}{2}\right)}{2S_w} \qquad (8\text{-}17)$$

$$t_s = \frac{p_t aK + \left(\frac{1}{2}\right)}{2S_w} \qquad (8\text{-}18)$$

$$\frac{t_e}{t_s} = \frac{\left(K + \frac{k}{2}\right)}{\left(K + \frac{1}{2}\right)} \qquad (8\text{-}19)$$

$$\frac{t_e}{t_c} = \frac{\left(K + \frac{k}{2}\right)}{2} \qquad (8\text{-}20)$$

where—

- k = tank-end ellipse ratio=a/b; k = 1 for a spherical end
- R = tank-end crown radius, in. = ka; R = a for a spherical end
- K = stress factor, a function of the ellipse ratio k. Figure 8-7 presents a K-vs.-k curve for combined membrane, discontinuity, and local-bending stresses
- t_k = wall thickness at the knuckle, in.
- t_{cr} = wall thickness at the crown, in.
- t_e = equivalent wall thickness of an ellipsoidal tank-end, in.
- t_s = equivalent wall thickness of a spherical tank-end, in.
- t_c = wall thickness of a cylindrical tank section, in.

3) *Wall surface area*:

Ellipsoidal-tank-end surface area, $in.^2$:

$$A_e = a^2 + \frac{\pi b^2 \ln\left[\frac{(1+e)}{(1-e)}\right]}{2e} \qquad (8\text{-}21)$$

Spherical-tank-end surface area, $in.^2$:

$$A_s = 2\pi a^2 \qquad (8\text{-}22)$$

where—

$$e = \text{eccentricity} = \frac{\sqrt{a^2 - b^2}}{a} = \sqrt{1 - \frac{1}{k^2}} \qquad (bs\text{-}15)$$

4) *Weight*:

Ellipsoidal-tank-end weight, lb:

$$W_e = \frac{\pi a^2 t_e E' \rho}{2k} \qquad (8\text{-}23)$$

Spherical-tank-end weight, lb:

$$W_s = 2\pi a^2 t_s \rho \qquad (8\text{-}24)$$

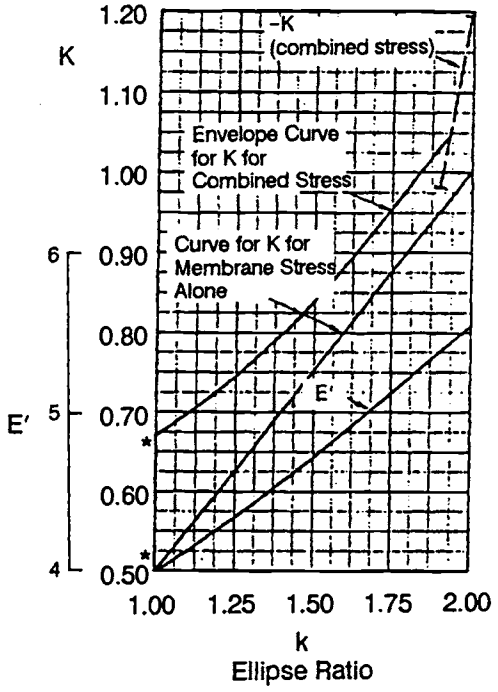

*For spherical tanks use K = 0.50 at k = 1.0
For spherical heads use K = 0.67 at k = 1.0

Fig. 8-7 Ellipse ratio k vs. knuckle factor K, compression stress -K, and parameter E'. (From ARS paper, "Design Criteria and Analyses for Thin-Walled Pressurized Vessels and Interstage Structures," by T. J. Hart)

where—(see Fig. 8-7)

E' = design factor

$$= 2k + \frac{1}{\sqrt{k^2 - 1}} \ln \frac{k + \sqrt{k^2 - 1}}{k - \sqrt{k^2 - 1}} \qquad (bs\text{-}16)$$

5) *Critical pressure* due to external loading, psi:

For an ellipsoidal tank end, approximated as:

$$P_{cre} = \frac{C_b 2Et_e^2}{R^2} \qquad (8\text{-}25)$$

For a spherical tank end:

$$P_{crs} = \frac{0.342Et_s^2}{a^2} \text{(approximately)} \qquad (8\text{-}26)$$

where C_b = buckling coefficient, a function of R/t_e, ranging from 0.05 to 0.10.

Cylindrical Section

1) *Volume*, $in.^3$:

$$V_c = \pi a^2 l_c \qquad (8\text{-}27)$$

where a = radius, in., and l_c = length, in.

2) *Wall thickness*, in., required to withstand membrane stresses due to internal tank pressure:

$$t_c = \frac{p_t a}{S_w e_w} \tag{8-28}$$

3) *Discontinuity stresses.* The discontinuity at the juncture between the cylindrical tank section and the tank ends will cause bending and shear loads along the cylindrical circumference at the juncture and the adjacent areas. These discontinuity stresses will superimpose upon the membrane stresses axial bending stress, hoop bending stress, additional hoop stress due to the shear load, and shear stress. Discontinuity stresses fade out rapidly, becoming negligibly small a short distance from the juncture. Detail analyses of discontinuity stresses can be found in standard textbooks. In general, buildup of wall thickness of less than 0.5 t_c, near the juncture, will suffice for most designs, with only small weight penalty.

4) *Wall surface area*, in.^{2}:

$$A_c = 2\pi a l_c \tag{8-29}$$

5) *Weight*, lb:

$$W_c = 2\pi a l_c t_c \rho \tag{8-30}$$

6) *External-loading critical pressure*, psi:

For a short tank (i.e., *BS-17*):

$$l_c < 4.9a\sqrt{a/t_c}$$

$$p_{crc} = 0.807\frac{Et_c^2}{l_c a}\sqrt[4]{\left(\frac{1}{1-\nu^2}\right)^3\frac{t_c^2}{a^2}} \tag{8-31}$$

For long tanks (i.e., *BS-18*):

$$l_c \geq 4.9a\sqrt{a/t_c}$$

$$p_{crc} = \frac{Et_c^3}{4(1-\nu^2)a^3} \tag{8-32}$$

where E = modulus of elasticity.

Sample Calculation 8-3

The following design data characterize the A-4 Stage propulsion system, which employs a cylindrical propellant-tank section with ellipsoidal ends (preliminary layout shown in Fig. 3-10):

- Required design volume of the oxidizer tank, V_{to} = 120 ft^3
- Maximum oxidizer tank operating pressure, p_{to} = 180 psia
- Required design volume of the fuel tank, V_{tf} = 143.5 ft^3
- Maximum fuel-tank operating pressure, p_{tf} = 170 psia
- Internal radius of the cylindrical section, a = 41 in.
- Tank construction material, aluminum alloy 6066-T6: F_y = 50,000 psi; F_u = 57,000 psi; ρ = 0.101 lb/in.^{3}; E = 10.4 x 10^6 psi; ν = 0.36
- Weld efficiency, e_w = 100%

Problem

Determine the following:

(a) Required internal dimensions of tank.
(b) Required thickness of the tank walls at various sections, considering internal pressure loads, discontinuity, and local bending stresses.
(c) Approximate weight of the tankage.
(d) Critical external loading pressures, using a buckling coefficient C_b = 0.10 for the tank ends.

Solution 8-3

(a) Since the oxidizer tank consists of two ellipsoidal ends without a cylindrical section, Eq. (8-13) may be applied:

$$v_{to} = \frac{2 \times 2\pi a^2 b}{3} \tag{bs-19}$$

Rearrange to obtain the minor elliptical half-diameter of the tank ends:

$$b = \frac{3 \times V_{to}}{2 \times 2\pi a^2} = \frac{3 \times 120 \times 1{,}728}{4 \times \pi \times (41)^2} = 29.4 \text{ in.} \tag{bs-20}$$

The tank-end ellipse ratio:

$$k = \frac{a}{b} = \frac{41}{29.4} = 1.395 \tag{bs-21}$$

Using an ellipsoidal end of the same proportion at the fuel-tank top, the fuel-tank volume may be treated as the volume of a cylindrical tank section with the length l_c. Equation (8-27) gives the volume of the fuel tank:

$$V_{tf} = \pi a^2 l_c$$

$$l_c = \frac{V_{tf}}{\pi a^2} = \frac{143.5 \times 1{,}728}{\pi \times (41)^2} = 46.9 \text{ in.} \tag{bs-22}$$

To summarize the internal dimensions of the tankage:

$$a = 41 \text{ in.} \quad b = 29.4 \text{ in.}$$

$$k = 1.395 \quad l_c = 46.9 \text{ in.} \tag{bs-23}$$

(b) Assuming that certain missions of the A-4 vehicle require it to be man-rated., the maximum allowable operational stresses can be derived from Eq. (8-6) and (8-7):

$$S_w = \frac{F_y}{1.25} = \frac{50{,}000}{1.25} = 40{,}000 \text{ psi}$$

$$S_w = \frac{F_u}{1.5} = \frac{57{,}000}{1.5} = 38{,}000 \text{ psi} \tag{bs-24}$$

Use the lower value of 38,000 psi.

Figure 8-6 gives the tank-end stress factor K of the combined stresses as 0.80 for an ellipse ratio k of 1.395. Then, from Eq. (8-15), the required wall thickness at the knuckle of the oxidizer tank end will be as follows:

$$t_{ko} = \frac{Kp_t a}{S_w} = \frac{0.80 \times 180 \times 41}{38{,}000} = 0.155 \text{ in.} \quad \text{(bs-25)}$$

From Eq. (8-16), the required wall thickness at the crown of the oxidizer-tank end:

$$t_{cro} = \frac{p_t R}{2S_w} = \frac{180 \times 1.395 \times 41}{2 \times 38{,}000} = 0.135 \text{ in.} \quad \text{(bs-26)}$$

From Eq. (8-17), the equivalent wall thickness of the oxidizer-tank end:

$$t_{eo} = \frac{(t_{ko} + t_{cro})}{2} = \frac{(0.155 + 0.135)}{2} = 0.145 \text{ in.} \quad \text{(bs-27)}$$

Some designs "save" weight by taking advantage of the fact that the bulkhead common to both tanks experiences a relatively small differential pressure in operation. Such systems, however, require more elaborate pressurization and loading systems including interlocks. In case of malfunction, the common bulkhead may suffer serious damage.

The required wall thickness at the knuckle of the fuel-tank end:

$$t_{kf} = \frac{t_{ko}p_{tf}}{p_{to}} = \frac{0.155 \times 170}{180} = 0.146 \text{ in.} \quad \text{(bs-28)}$$

The required wall thickness at the crown of the fuel-tank end:

$$t_{crf} = \frac{t_{cro}p_{tf}}{p_{to}} = \frac{0.135 \times 170}{180} = 0.128 \text{ in.} \quad \text{(bs-29)}$$

The equivalent wall thickness of the fuel-tank end:

$$t_{ef} = \frac{(t_{kf} + t_{crf})}{2} = \frac{0.146 + 0.128}{2} = 0.137 \text{ in.} \quad \text{(bs-30)}$$

From Eq. (8-28), the required wall thickness of the cylindrical tank section:

$$t_c = \frac{p_{tf}a}{S_w} = \frac{170 \times 41}{38{,}000} = 0.183 \text{ in.} \quad \text{(bs-31)}$$

To provide a buildup of 0.4 t_C on the cylindrical-tank-section wall near the juncture to allow for discontinuity stresses:

$$t_{cj} = t_c + 0.4t + 0.183 + 0.4 \times 0.183 = 0.256 \text{ in.} \quad \text{(bs-32)}$$

To summarize:

$$t_{ko} = 0.155 \text{ in.}, \quad t_{cro} = 0.135 \text{ in.}, \quad t_{eo} = 0.145 \text{ in.}$$

$$t_{kf} = 0.146 \text{ in.}, \quad t_{crf} = 0.128 \text{ in.}, \quad t_{ef} = 0.137 \text{ in.}$$

$$t_c = 0.183 \text{ in.}, \quad t_{cj} = 0.256 \text{ in.} \quad \text{(bs-33)}$$

(c) From Eq. (8-23), the weight of the oxidizer-tank end:

$$W_{eo} = \frac{\pi a^2 t_{eo} E' \rho}{2k} \quad \text{(bs-34)}$$

Figure 8-7 gives E' = 4.56 for k = 1.395:

$$W_{eo} = \frac{\pi(41)^2 \times 0.145 \times 4.56 \times 0.101}{2 \times 1.395} = 126.4 \text{ lb} \quad \text{(bs-35)}$$

The weight of the fuel-tank end:

$$W_{ef} = \frac{W_{eo}t_{ef}}{t_{eo}} = \frac{126.4 \times 0.137}{0.145} = 119.4 \text{ lb} \quad \text{(bs-36)}$$

From Eq. (8-30), the weight of the cylindrical tank section:

$$W_c = 2\pi a l_c t_c \rho = 2 \times \pi \times 41 \times 46.9 \times 0.183 \times 0.101 = 223.3 \text{ lb} \quad \text{(bs-37)}$$

Add 4% of overall tankage weight to allow for local wall-thickness buildups, welded joints, discontinuity stresses, etc., and for tolerances during fabrication. Approximate overall weight of the tankage:

$$W_t = 1.04(2 \times W_{eo} + W_{ef} + W_c) = 1.04(2 \times 126.4 + 119.4 + 223.3) = 596 \text{ lb} \quad \text{(bs-38)}$$

(d) From Eq. (8-25), the critical external loading pressure for the oxidizer ends:

$$P_{creo} = \frac{C_b 2Et_{eo}^2}{R^2} = \frac{0.10 \times 2 \times 10.4 \times 10^6 \times (0.145)^2}{(1.395 \times 41)^2} = 13.4 \text{ psi} \quad \text{(bs-39)}$$

The critical external loading pressure for the fuel-tank end:

$$P_{cref} = \frac{C_b 2Et_{ef}^2}{R^2} = \frac{0.10 \times 2 \times 10.4 \times 10^6 \times (0.137)^2}{(1.395 \times 41)^2} = 11.9 \quad \text{(bs-40)}$$

This leads to the following:

$$l_c < 4.9a\sqrt{a/t_c} \quad \text{(bs-41)}$$

Thus, Eq. (8-31) applies, yielding the following external-loading critical pressure for the cylindrical tank section:

$$P_{crc} = \frac{0.807 \times 10.4 \times 10^6 \times (0.183)^2}{46.9 \times 41} \times \sqrt[4]{\left(\frac{1}{1-(0.36)^2}\right)^3 \left(\frac{0.183}{41}\right)^2} = 10.8 \text{ psi} \quad \text{(bs-42)}$$

Axial Compressive Loading on the Cylindrical Section

In integrated propellant tank designs (Fig. 8-2 and 8-3) the cylindrical tank section must withstand large axial compressive loads during vehicle handling and operation. If the tank is not pressurized, i.e., if tank pressure = ambient pressure, the critical axial compressive stress for an unstiffened cylindrical tank may be calculated as follows:

$$S_c = \left[9\left(\frac{t_c}{a}\right)^{1.6} + 0.16\left(\frac{t_c}{l_c}\right)^{1.3}\right]E \qquad (8\text{-}33)$$

where S_C = critical axial compressive stress, psi.

This is the axial compressive stress that will cause the tank to buckle.

Internal pressure can increase the axial load-carrying ability of a cylindrical tank section with minimum weight penalty. This is known as pressure stabilization. Internal pressure will raise the critical buckling stress of a tank; or it may be used to counterbalance an axial compressive load F_a where—

$$F_a = \pi a^2 p_t \qquad (8\text{-}34)$$

Pressurization will also reduce tank failures from very large bending loads. If the pressure is ever permitted to drop below a value necessary to carry the axial and bending loads, however, the tank will collapse and the vehicle will probably be damaged beyond repair.

An alternative method of increasing the external load-carrying ability of a cylindrical tank is to make it self-supporting. This involves stiffening the cylindrical skin by means of longitudinal and circumferential members, or honeycomb structures. The members may be either separate stiffeners welded to the tank wall, or may be made integral with the wall by machining or chemically milling a thicker wall.

Sample Calculation 8-4

Problem

For the A-4 Stage tankage, calculate:

(a) Critical axial compressive load of the cylindrical section with no internal pressure.
(b) Required internal tank pressure to offset an axial compressive load of 100,000 lb with no compressive stress on the cylindrical section.

Solution 8-4

(a) From Eq. (8-33), the critical compressive stress of the cylindrical section:

$$S_c = \left[9\left(\frac{0.183}{41}\right)^{1.6} + 0.16\left(\frac{0.183}{46.9}\right)^{1.3}\right] \times 10.4 \times 10^6$$

$$= 17{,}476 \text{ psi} \qquad \text{(bs-43)}$$

The critical axial compressive load of the cylindrical section:

$$F_c = S_c \times 2\pi a t_c = 17{,}476 \times 2\pi \times 41 \times 0.183$$

$$= 823{,}900 \text{ lb} \qquad \text{(bs-44)}$$

From the results it is obvious that the A-4 Stage tankage can withstand a substantial axial compressive load without internal pressurization.

(b) From Eq. (8-34), the required internal tank pressure:

$$P_t = \frac{F_a}{\pi a^2} = \frac{100{,}000}{\pi \times (41)^2} = 18.95 \text{ psi} \qquad \text{(bs-45)}$$

Water-hammer Effects Due to Impact

Impact on a loaded propellant tank will cause a water-hammer effect within it—a surge of the tank internal pressure. For very short impacting times (less than 1.2×10^{-3} s), the following correlations have been established for cylindrically-shaped propellant tanks:

$$P_s = \frac{cw}{\pi a^2 g} \qquad (8\text{-}35)$$

$$c = \frac{c'}{\sqrt{1 + \dfrac{2.5E_p a(1 - 0.8v)}{Et_c}}} \qquad (8\text{-}36)$$

where—

- p_s = pressure surge due to the impact, psi
- w = equivalent flow rate of the propellant due to the impact, lb/s
- a = radius of the cylindrical tank, in.
- t_c = wall thickness of the cylindrical tank, in.
- g = gravitational constant, 32.2 ft/s^2
- c = acoustic velocity of the restrained propellant, in./s
- c' = free acoustic velocity of the propellant, in./s
- E_p = compressive modulus of elasticity of the propellant, psi
- E = modulus of elasticity of the tank construction material, psi
- v = Poisson's ratio of the tank construction material

In many prepackaged liquid applications, the propellant tankage must withstand certain impact loads, as specified by the height of drop tests. The following sample calculation illustrates details of estimating tank pressure-surges from a free-fall impact.

Sample Calculation 8-5

The following data characterize the cylindrical fuel tank of a prepackaged storable-liquid propulsion

system:

Fuel, N_2H_4
Fuel density ρ_p = 63.17 lb/ft^3
Compressive modulus of elasticity of the fuel, E_p = 6.06 x 10^5
Free acoustic velocity of the fuel, c' = 80,100 in./s
Tank construction, aluminum alloy 6066-T6
Modulus of elasticity of the tank construction material, E = 10.4 x 10^6
Poisson's ratio of the tank construction material, v = 0.36
Radius of the cylindrical tank, a = 4 in.
Length l_c of the cylindrical tank = 50 in.
Wall thickness t_c of the cylindrical tank = 0.167 in.

Problem

For a tank falling in the direction of its longitudinal axis, estimate—

(a) Tank pressure surge due to the impact after a 6-ft free drop.
(b) Tank pressure surge due to the impact after a 20-ft free drop.

Solution 8-5

(a) *For a 6-ft free drop the final velocity at impact:*

$$V = \sqrt{2gh} = \sqrt{2 \times 32.2 \times 6} = 19.65 \text{ fps} \qquad \text{(bs-46)}$$

This yields an equivalent propellant flow rate due to impact of—

$$\dot{w} = \rho_p \pi a^2 V = 63.17 \times \pi \times \left(\frac{4}{12}\right)^2 \times 19.65$$

$$= 434.5 \text{ lb/s} \qquad \text{(bs-47)}$$

From Eq. (8-36), the acoustic velocity of the restrained fuel:

$$c = \frac{80{,}100}{\sqrt{1 + \left[\dfrac{2.5 \times 6.06 \times 10^5 \times 4(1 - 0.8 \times 0.36)}{10.4 \times 10^6 \times 0.167}\right]}}$$

$$= 43{,}100 \text{ in./s} \qquad \text{(bs-48)}$$

Impact time delay in the tank:

$$\frac{l_c}{c} = \frac{50}{43{,}100} = 1.16 \times 10^{-3} \text{ s}$$

$$\text{(i.e., } < 1.2 \times 10^{-3} \text{ s)} \qquad \text{(bs-49)}$$

Equation (8-35) yields the tank pressure surge due to impact after a 6-ft free drop:

$$p_s = \frac{c\dot{w}}{\pi a^2 g} = \frac{43{,}100 \times 434.5}{\pi \times (4)^2 \times 386} = 964 \text{ psi} \qquad \text{(bs-50)}$$

(b) *After a 20-ft free drop, the final velocity at impact:*

$$V = \sqrt{2gh} = \sqrt{2 \times 32.2 \times 20} = 35.9 \text{ fps} \qquad \text{(bs-51)}$$

The equivalent propellant flow rate due to impact:

$$\dot{w} = \rho_p \pi a^2 V = 63.25 \times \pi \times \left(\frac{4}{12}\right)^2 \times 35.9$$

$$= 792.5 \text{ lb/s} \qquad \text{(bs-52)}$$

The tank pressure surge due to impact after a 20-ft free drop:

$$p_s = \frac{c\dot{w}}{\pi a^2 g} = \frac{43{,}100 \times 792.5}{\pi \times (4)^2 \times 386} = 1{,}765 \text{ psi} \qquad \text{(bs-53)}$$

8.4 STORABLE-LIQUID-PROPELLANT TANK DESIGN

The design of tanks for storable liquid propellants uses the same general design practices applied to other propellant tanks, except in the area of compatibility. Most storable propellants will remain stable for long periods if stored in tanks constructed of compatible materials. To minimize propellant decomposition and tank-material corrosion, the surface of tank walls in contact with the propellants must be smooth and clean.

Tank-material Compatibility

Final selection of tank material requires a study to determine compatibility of it and its fabrication processes with the propellants. Two major considerations should be kept in mind: the required storage life and the applicability of available data. Several material/propellant compatibility test programs have been conducted; but some have reported results at variance, possibly as a consequence of the way material coupons were processed before the test, the testing of material coupons vs. fabricated tanks, using techniques to achieve "long-term" results with short-term tests, and differing environmental conditions.

The Air Force Astronautics Laboratory (formerly Air Force Rocket Propulsion Laboratory) has conducted extensive long-term-compatibility tests of coupons and tanks using numerous combinations of alloys and propellants. A series of reports have documented the results, one of the latest being "Metallurgical Analysis of Liquid Rocket Tankage," by E.J. King and H.G. Kammerer, AFRPL TR-84-054.

Tank Construction

Eliminating maintenance during storage and prelaunch activities represents one of the prime design objectives for storable-propellant tankage. All-welded construction permits this. To achieve isolation, leakproof burst diaphragms or pyrotechnic valves are installed at the inlets and outlets of the tanks. Propellant fill ports are capped and welded after tanking. Tandem tanks are favored over concen-

tric tanks, since they separate propellants more positively during storage, transportation, and adverse conditions. Some applications have the common bulkhead between two propellant tanks designed to withstand a differential pressure in either direction that may result from nonsimultaneous pressurization. However, the diaphragm at the pressurant inlet to the oxidizer tank of the A-4 Stage system, being designed to a lower burst pressure than the pressurant inlet diaphragm for the fuel tank, keeps the oxidizer-tank pressure always higher.

Full-penetration welds should be used in the construction of all propellant tanks, and especially tanks for storable propellants. A full-penetration weld shows complete fusion to the root of the joint. All such welds which cannot be dye-penetrant-inspected at the root must be x-rayed to ensure full penetration. Figure 8-8 presents the design detail of a typical full-penetration, single-weld butt joint.

If possible, interpropellant welding (i.e., the fuel and oxidizer separated by only one welded joint) should be avoided in tank designs. A double-weld design will prevent the mixing of propellants due to a single failure of welded joints. Figure 8-9 presents the design of a typical storable propellant tank with a forged one-piece common bulkhead. A double-weld design is used on the center-hold joint for the oxidizer duct.

Wall Surface Requirements

The tank must be cleaned with a solvent or, in some instances, with an alkaline or acid solution to eliminate contamination that may cause corrosion or be reactive with the propellant—a process called "passivation." In extreme circumstances, it can be achieved by application of a propellant rinse before loading the propellant.

8.5 CRYOGENIC-LIQUID-PROPELLANT TANK DESIGN

Design of cryogenic-propellant tanks presents several potential problem areas that may affect proper functioning and reliability: properties of the tank construction materials at the cryogenic propellant service temperature range, thermal stresses induced in the tank structure by temperature gradients, the relief of tank pressure caused by boiloff of the cryogenic propellants, and thermal insulation of the tank walls.

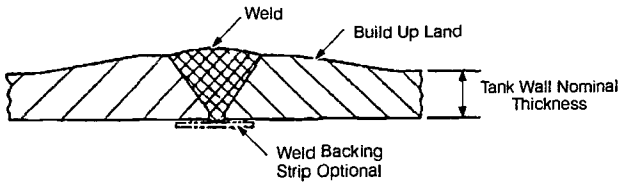

Fig. 8-8 Design detail of a typical full-penetration, single-welded butt joint for propellant tanks.

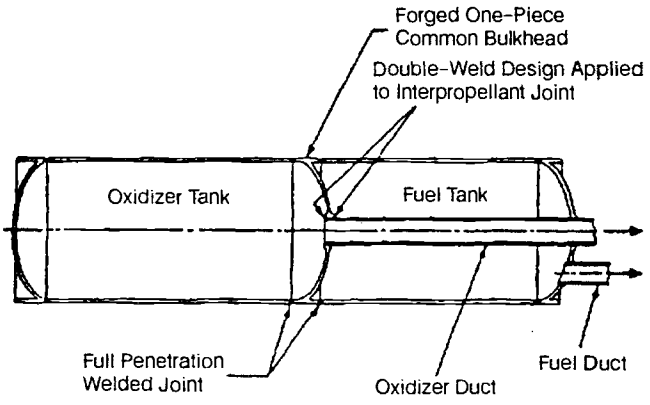

Fig. 8-9 Design of a typical storable-propellant tank with a forged one-piece common bulkhead.

Knowledge of the precise strength characteristics, degree of brittleness, and notch sensitivity of the tank construction materials at cryogenic temperatures (as low as -423°F for liquid-hydrogen service) is a prerequisite for their selection. In general, most of the aluminum alloys and the austenitic and semiaustenitic stainless steels possess good mechanical properties at cryogenic temperatures (also see Chapter 2). The thermal stresses can be analyzed by determining the temperature profile at various regions of the tank and may be minimized by discrete design approaches. The capacity of the tank relief valve should be based on the maximum anticipated propellant boiloff rate during ground hold and actual operation of the vehicle systems.

Among the cryogenic propellants, liquid hydrogen imposes the most serious tank-design problems, mainly due to its very low service temperature and its relatively large specific volume. Design problems are especially acute with the hydrogen-tank insulation. It often becomes one of the most critical design factors in a hydrogen-fueled vehicle system. The difficulties arising in hydrogen systems in connection with heat transfer may be dramatically illustrated as follows.

Assume two tanks of equal size, subject to the same heat influx per unit time, one filled with liquid oxygen and the other with liquid hydrogen. The ratio of heat of vaporization per unit weight O/H = 0.48, but density ratio O/H = 14.3. Thus the volume rate of vaporization in the hydrogen tank will be 6.85 times faster than in the oxygen tank. In reality, the heat influxes would not be equal for two uninsulated tanks, because of the higher temperature differential across the wall, and especially because of the greatly increased heat-transfer rate from air liquefaction on the hydrogen-tank surface. This may further accelerate the hydrogen boiloff to approximately 70 times that of oxygen. In an actual oxygen/hydrogen system operating at a weight mixture ratio O/H = 5, the tanked mixture ratio by volume H/O = 3.23. Depending on the shape of the tanks (surface ratio), this may again double or triple the relative boiloff of hydrogen. Insulation, it is clear, must drastically reduce heat influx into a hydrogen system.

Boiloff rate is not the only problem caused by the physical properties of hydrogen. Near the ambient boiling temperature, the gradient of vapor pressure is 2.4 psi/°R, as compared to 0.78 psi/°R for liquid oxygen. Moreover, this gradient increases rapidly with increasing temperature, which would be experienced following tank pressurization. Figures 8-10 and 8-11 show the trend for both liquid oxygen and hydrogen. The data have great significance to pump NPSH. As may be seen, just one degree of liquid-hydrogen temperature rise requires a 3-psi increase in tank pressure to maintain proper NPSH. In a large vehicle, the required increase in tank-wall thickness may affect payload noticeably. The situation is further aggravated by the high heat influx into hydrogen, for reasons mentioned in connection with boiloff. Even for relatively short boost periods, rapid warm-up may create a problem more severe than boiloff, and place further emphasis on adequate insulation. The following discussion of tank insulations therefore emphasizes hydrogen service.

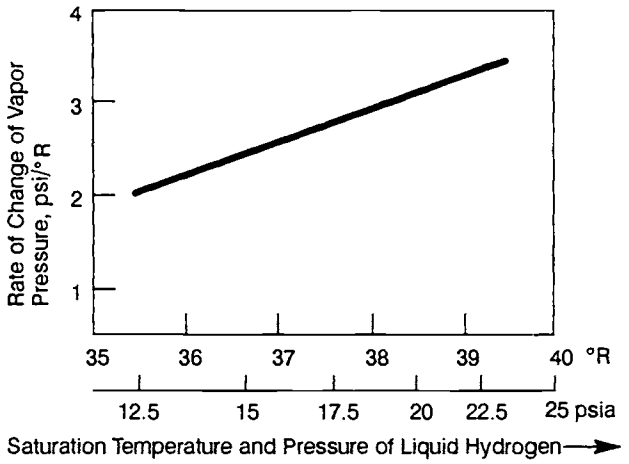

Fig. 8-10 Rate of change of saturation vapor pressure to temperature for liquid hydrogen.

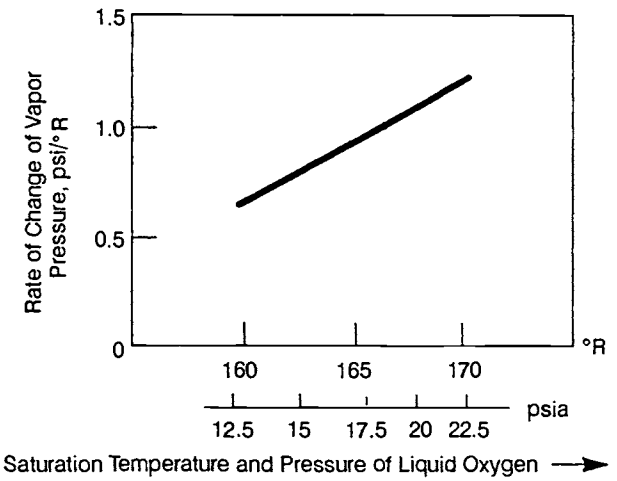

Fig. 8-11 Rate of change of saturation vapor pressure to temperature for liquid oxygen.

Insulation Requirements for Cryogenic-Propellant Tanks

Most vehicle missions include three distinct phases calling for effective insulation of cryogenic-propellant tanks: ground hold, boost phase, and coast in space. The propellant-tank insulation design will primarily be based on flight-performance criteria. However, propellant evaporative losses during long hold periods on the ground requiring continuous topping may become a significant cost item. Then it may be economical to provide an insulating blanket on the tank, and remove it just before liftoff. The boost phase sees high temperatures from aerodynamic heating and large aerodynamic forces. Although of short duration, this phase dictates the structural elements of the insulation. During coast in space, the principal source of thermal energy, radiation from the sun and planets, can be blocked by radiation shields surrounding the basic tank insulation, thereby effectively controlling the heat flux across the tank wall. Very important will be the properties of the materials used in a solar shield, such as the absorptivity and emissivity of the surface when subjected to various types of radiation and body temperatures. The amount of shielding required depends on the duration of the coast and on optimization of shield weight vs. propellant-boiloff weight.

Basic Insulation Types

Major desirable design features of an insulation include light weight, uniform and repeatable insulation characteristics, ease of application, low cost, low hazard, reasonable ruggedness, ease of repair, good reliability, and, above all, low heat-conductivity.

Excellent results can be achieved with a laminated-type insulation—an aluminum foil and a structural material, often in multiple layers. The aluminum foils act as reflectors, effectively rejecting radiative heat, while the evacuated space in between prevents conductive heat transfer. This insulation can be applied to single-curved and to large-diameter, double-curved surfaces. The laminar insulation can fairly easily be damaged, however, possibly resulting in loss of vacuum (cracks and infiltration of gas, for instance). Use of this type of insulation in atmospheric applications has therefore been infrequent.

Honeycomb-supported structures are finding wide application. Figure 8-12 shows typical externally-applied hydrogen-tank insulation. A 1/2- to 3/4-in.-nominal-size plastic honeycomb goes between an inner and outer facing sheet. The cells may or may not be filled with an isocyanate-type foam, depending on weight limitations. The foam bubbles or the properly sealed cells will form individual vacuum spaces when cold (cryopumping). However, because of the possibility of vacuum degradation by infiltration of air (outer insulation), or hydrogen (inside insulation), it is often preferred to purge the cells with helium, for which lateral passage ways must be provided. The purge also serves as a leak-detection device, in conjunction with gas analyzers, to detect contamination of the helium from leaks. Figure

8-12 shows a separate gap purged with helium, rather than the honeycomb cells. Thermal conductivity of the insulation shown is about 3.8×10^{-7} Btu-in./in.^{2}-s-°F (0.2 Btu-in./ft^2-h-°F).

Thermal conductivities of various types of insulation vary from 0.05×10^{-7} to 6.0×10^{-7} Btu-in./in.^{2}-s-°F. Densities range from 2.0 to 20 lb/ft^3. Since the quality of an insulation will affect cost and weight, an optimization study will have to be made, based on mission characteristics.

Sample Calculation 8-6

Problem

Determine heat-transfer rates in Btu/in.^{2}-s across the tank insulation shown in Fig. 8-12 during—

(a) Ground hold, with temperature of the insulation surface near the tank wall approximately -360°F and the outer surface 70°F.
(b) Boost phase, with inner insulation-surface temperature reaching -210°F and the outer insulation temperature 800°F.

Solution 8-6

(a) During ground hold, the temperature differential across the insulation $\Delta T = 70-(-360) = 430$°F. The overall thickness of the insulation $t = 2 \times 0.03 + 0.75 = 0.81$ in. Equation (4-19) gives the heat-transfer rate:

$$q = \left(\frac{k}{t}\right)\Delta T = \left(\frac{3.8 \times 10^{-7}}{0.81}\right) \times 430$$

$$= 2.02 \times 10^{-4} \text{ Btu/in.}^2\text{-s} \qquad \text{(bs-54)}$$

(b) During the boost phase, $T = 800-(-210) = 1010$°F. The heat-transfer rate:

$$q = \left(\frac{k}{t}\right)\Delta T = \left(\frac{3.8 \times 10^{-7}}{0.81}\right) \times 1010$$

$$= 4.74 \times 10^{-4} \text{ Btu/in.}^2\text{-s} \qquad \text{(bs-55)}$$

Selection of Tank-insulation Designs

Many factors will influence the selection of a tank-insulation design. The insulation may be located internal or external to the tank wall. It can be integral or disposable during boost; i.e., it can be bonded in place or mechanically retained. Basically, any insulation applied to a tank must be justified with respect to advantages of performance and/or economy.

Locating the insulation inside the propellant tank has the obvious advantage of protecting the insulation from handling damage. The tank structure is isolated from the severest low-temperature effects of the propellant and is thus subjected to only moderate thermal cycling from its source. Internal insulation also minimizes propellant loss when chilling the tank during filling. However, if a crack or leak should occur in internal insulation of a hydrogen tank, gaseous hydrogen would enter the crack and gradually increase the heat transfer. Other undesirable features of internal insulation include difficulties in installation, in locating and repairing of leaks, and in cleaning the tank. Internal insulation is also subject to higher pressures and more severe temperature effects, which tend to impair the insulation sealing.

External insulation has the advantage of isolating the tank structure from the extreme temperature of aerodynamic heating during boost. Installation, repair, and sealing of the external insulation can all be done without special consideration of access, ventilation, and curing techniques in closed areas. However, special consideration will be required for tank-leak detection, especially with integrally insulated areas. A crack in the external insulation will allow liquefaction of air and cryopumping, resulting in a significant rise in heat transfer.

Insulation for Common Bulkheads

When a common bulkhead is used between propellant tanks and cryogenics are involved, insulation is required to prevent freezing of the propellant with the higher boiling point. Figure 8-13 shows the equatorial area of a typical insulated common bulkhead. A fiberglass honeycomb is located between a forward and an aft facing sheet. In the equatorial area, where the facing sheets have to be faired into the cylindrical tank portion, they are reinforced by waffle grid ribs. This design also requires special insulation on the inside of the LOX

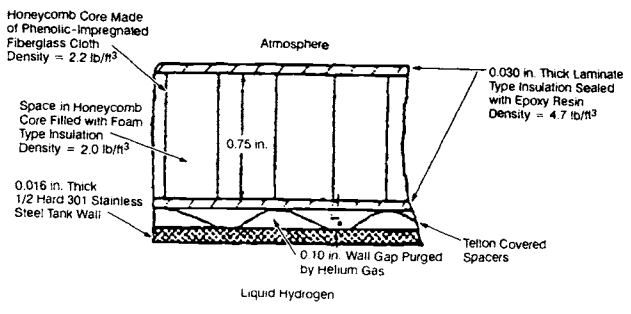

Fig. 8-12 Construction elements of a typical liquid hydrogen tank insulation design (external type).

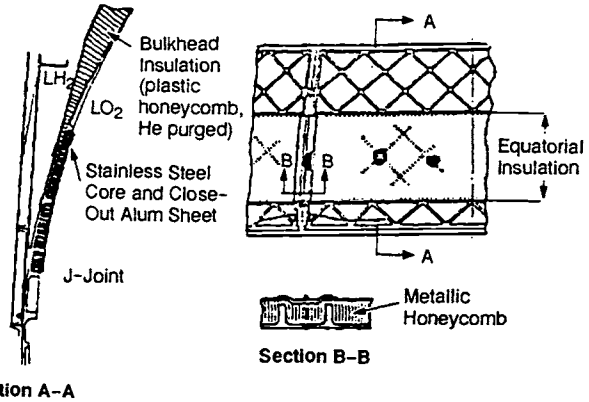

Fig. 8-13 Design of a typical insulated common bulkhead separating LH_2 and LO_2 tanks.

tank in the equatorial region. No foam filler was used in this particular example.

8.6 COMPOSITE LIQUID-PROPELLANT TANK DESIGN

Most tanks with surfaces of revolution can be fabricated as a continuous filament wrapped in a specific pattern, impregnated with resin, and then cured. Compared to metals, such composite has relatively high strength-to-weight ratio, owing to the intrinsically higher strength of uniform filiaments and the ability to vary directional properties in the wrapping process.

The progression of filament material technology has been from fiberglass (E-Glass and S-Glass) to aramid (Kevlar) to graphite. The strength-to-density ratio advantage for composites has increased from 2:1 for E-Glass to 10:1 for graphite, compared to metal tanks. An additional weight advantage can be achieved by design efficiency. For example, loads in the cylindrical section of a tank are twice as great in the circumferential direction as in the meridional direction. Fibers in a composite structure can be oriented to correspond to the directional variability, but metal tanks must be designed for the circumferential loads, leaving a large excess in the meridional direction. Uniform properties and good reliability require the use of numerically-controlled winding machines to orient the fibers precisely. Figure 8-14 shows a typical filament-wound tank.

Being relatively porous and incompatible with propellants, composites must be separated from the contained fluid by a liner, either elastomeric (for pressurant-gas storage) or metallic. Elastomeric liner materials, such as chlorobutyl or acrylonitrile rubber, are formed over a rigid, water-soluble mandrel, the composite overwrap applied and cured, and then the mandrel washed out. Such a liner, for tanks less than 4 ft. in diameter, will typically have a leakage rate of 10^{-4} scc/s.

Metallic liners can either be thin and carry essentially no load or relatively thick and carry as much as 20% at operating pressure. The design and fabrication of metallic liners are similar to metallic tanks, but being relatively thin can cause design problems at thickness-transition regions, fabrication problems in meeting tolerances, and welding problems. Leakage rates, for tanks less than 4 ft. in diameter, are typically less than 10^{-7} scc/s.

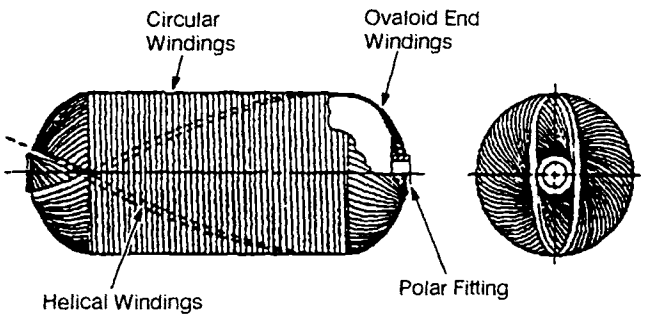

Fig. 8-14 A typical filament-wound tank.

Since the cyclic fatigue of the composite will far exceed that of a metallic liner, liner design becomes critically important. In a typical design, the liner plastically deforms during proof testing, while the composite does not exceed its elastic limit. Upon venting of the proof pressure, the composite returns to its original shape and causes the liner to be in compression. During subsequent operating pressure cycles, the liner is subjected to compressive and tensional stresses that are not always in the elastic range. Ductility and toughness are therefore important parameters in the selection of a liner material. Alloys that have been used include 2219, 5086, 6061 and 6351 aluminum, 321 stainless steel, 6Al-4V and 15-3 titaniums, and Inco-718.

Another consideration in the design of composite tanks will be useful life at pressurized conditions, usually referred to as "static-fatigue life." This drops as the operational pressure conditions, expressed as a percentage of ultimate strength, increase. Because of scatter in experimental data, a reliability value is normally expressed along with the static-fatigue-life requirement.

8.7 DESIGN OF PROPELLANT-TANK PRESSURANT DIFFUSERS

A pressurant diffuser introduces the pressurant gas evenly into the propellant tank at a desired direction and velocity. The gas is usually injected in a plane near the forward end, at a right angle to the tank and vehicle axes. This will minimize disturbances at the pressurant/propellant interface. Figure 8-15 presents some typical designs for a propellant-tank pressurant diffuser. A radial-type diffuser, located at the tank axis, serves the fuel tank. This arrangement permits a simple, lightweight diffuser design. However, the reversed ellipsoidal common bulkhead at the forward end of the oxidizer tank requires a ring-type diffuser, consisting of many individual diffusing nozzles at the circumference of the tank.

The pressurant enters the tank at a temperature depending on the source, such as a LOX heat exchanger. In some cases, because this may not be the optimum temperature for critical structural members, a separation tube (Hilsch tube) may be combined with the diffuser. Without moving parts, it operates on the principle of separating the higher-energy from lower-energy molecules. Temperature spreads of 100°F or more can be obtained, depending on construction and available pressure-drop. In a LOX/hydrogen system with common bulkhead, the device may be used to direct the cold stream toward the bulkhead, thus lowering the temperature differential and heat transfer across it.

8.8 PROPELLANT EXPULSION UNDER ZERO-GRAVITY OR OSCILLATORY g-LOADING CONDITIONS

Under zero or oscillatory g-loading conditions typical of many vehicle trajectories, the propellant's location in a tank becomes uncertain and thus requires a means to prevent gas from being expelled with the propellant. The propellant must be sub-

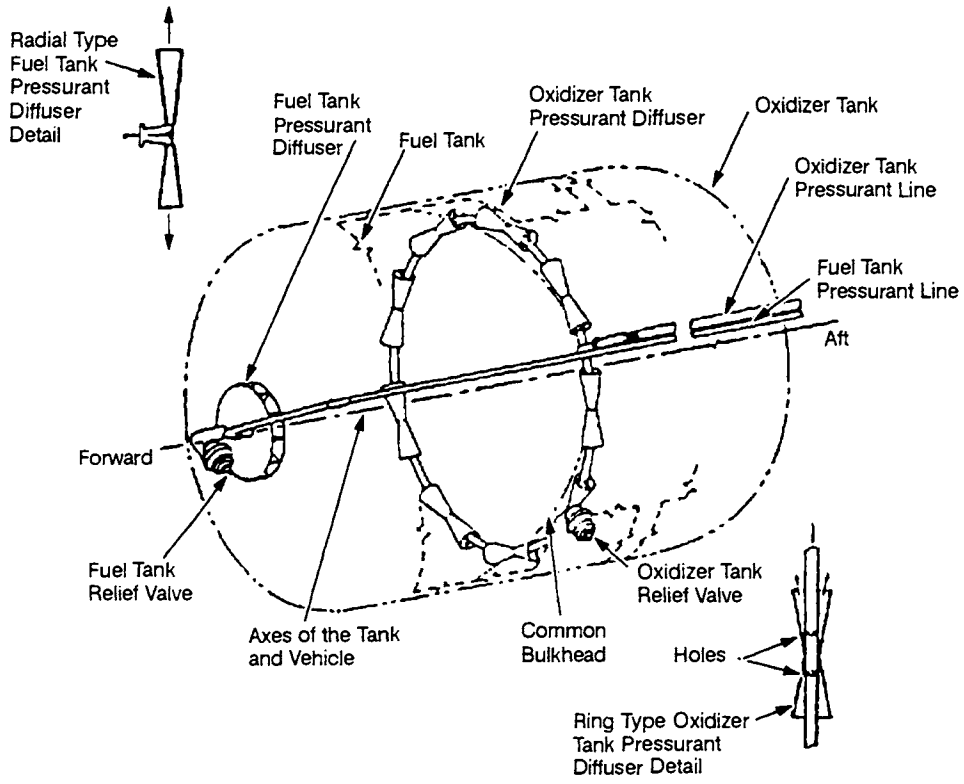

Fig. 8-15 Typical designs of propellant-tank pressurant diffusers.

jected to an acceleration to settle it immediately before usage, or at least a portion of it must be continuously confined to the vicinity of the tank outlet. The two approaches can be defined as "impulse settling" and "propellant management."

Settling

This method employs a small propulsive force directed axially, parallel to the vehicle center line of thrust. This acceleration forces the propellant to the tank outlet before initiation of main-engine operation. This approach especially suits most space vehicles, because their low-thrust reaction control units can also provide the thrust for propellant settling.

Although this method would eliminate the need for propellant-management devices for the main propellant tanks, it would necessitate them in separate tanks for the sole use of the reaction-control system. This settling method has the possible disadvantages of no control of vehicle center-of-gravity shifts and low thrust-to-weight ratio under these conditions, which may increase response time beyond tolerable limits.

For single-start upper stages, jettisonable short-duration solid-propellant settling rockets may also be applied to advantage.

Propellant Management

The other method of achieving proper propellant orientation within the tanks is by continuously confining the propellant to the vicinity of the tank outlet. This may be accomplished by positive displacement of the propellant with a moving surface or by using the surface tension properties of the propellant with a porous plate or screen.

A positive-expulsion propellant tank consists of an outer structural shell and an inner movable expulsion device, such as metallic diaphragm or bladder, elastomeric diaphragm or bladder, bellows, and pistons. A surface-tension propellant tank consists of an outer structural shell and an inner compartment that confines a small portion of the propellant at the outlet at all times. The inner compartment may be very simple or extremely complex, depending on the possible orientations of propellant within the tank when flow to the engine is required.

There are three important factors in the selection of a method of propellant management: the impulse on the vehicle generated by propellant movement, variation in the propellant center of gravity, and available tank envelope. Positive expulsion may be the only alternative if the impulse generated by propellant sloshing inside a tank with a surface-tension device cannot be controlled adequately with reasonably sized baffles. Positive expulsion may also be required if the center-of-gravity shift caused by propellant movement during vehicle maneuvers with a surface tension device causes excessive attitude-control-system requirements. Finally, bellows and pistons are not applicable if propellant volume requirements cannot be packaged into cylindrical tanks in the available envelopes.

Metallic Diaphragms

Metallic diaphragms (half shells) or bladders (full shells) can be used with spheroidal, cylindrical or conospheroidal tank shapes. Dual-wall containment of propellant uses a bladder, half of it normally thick (stiff) enough to keep it from deflecting. As its

primary design goal, a diaphragm or the movable half of a bladder makes complete reversal (i.e., from being nestled in the inlet tank-half to being nestled in the outlet, stationary bladder tank-half) in a smooth, controlled manner.

Diaphragms can be designed to start reversal at either the apex or the girth. A flat or slightly dimpled area at the apex can control the initiation at the apex. A small amount of prereversal is normally formed into the girth region of a girth-initiated reversal.

Once reversal has been initiated, the goal is to continue in a rolling mode, rather than buckling, by designing for a small force to roll the material compared to the force to buckle it. This can be done by the shape of the tank, the diaphragm alloy and heat treatment, variations in diaphragm thickness, prestressing the diaphragm, and bonding the diaphragm to the shell with a low-strength adhesive. Figure 8-16 shows the progression of an apex-initiated diaphragm during expulsion.

To achieve a volumetrically efficient propellant tank and to provide structural support for the diaphragm, which supports part of the propellant mass, the diaphragm and tank shell should be in contact until reversal. Diaphragms are usually made from a low-strength annealed alloy. To avoid corrosion problems associated with dissimilar metals wetted with propellant for a long storage period, diaphragms are usually made from a material within the same class as the tank, i.e., an 1100 aluminum diaphragm would be used with a 2219 aluminum tank, but not with a stainless-steel tank. Similar materials permit conventionally welded joints but avoid heavy flanges with mechanical fasteners and seals. Diaphragm membrane thickness can be varied by thinning during spin-forming, machining, or chemical milling of step changes. Another technique to preclude buckling locally stiffens the diaphragm by mechanical attachment or integral machining of rings, which must be positioned to avoid interference with one another during reversal.

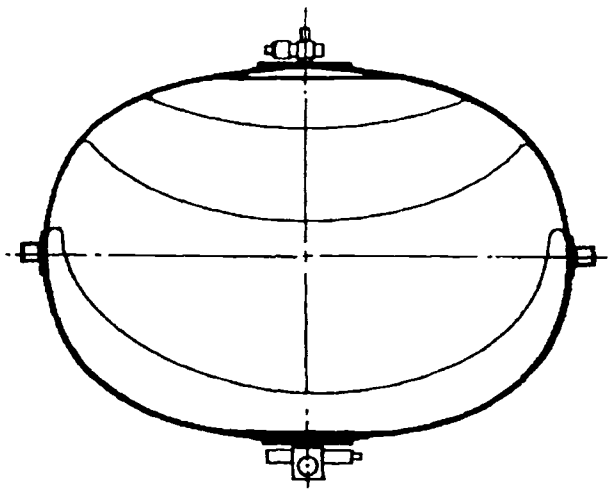

Fig. 8-16 Progression of an apex-initiated diaphragm during expulsion.

In addition to promoting rolling and inhibiting buckling, variations in diaphragm thickness can control reversal symmetry. Normal variations in thickness, due to forming or machining the diaphragm to shape, and lateral external loads such as acceleration can cause nonsymmetrical reversal, nonrepeatable shifts in the center of gravity during expulsion, reduced volumetric expulsion, and greater risk in cracking the material. This can be controlled on an apex-initiated reversal, for example, by increasing the thickness from the apex to the girth. As a result, if one side of the diaphragm starts to reverse ahead of the other, it encounters greater resistance to rolling because of the increased thickness, which helps to correct the nonsymmetry.

Diaphragms as thin as 0.010 in. are used to minimize wrinkling, increase expulsion efficiency (reversed volume divided by propellant-wetted volume), and reduce the differential pressure across the diaphragm. As long as the tank-outlet half-shell (or rigid bladder half) has the same shape as the natural shape of the reversed diaphragm, there is little risk from cracks due to wrinkles, unless a high-vibration environment can cause fatigue failure. Because wrinkling is inevitable and cold-working during rolling degrades the elastic properties, metallic diaphragms are not ordinarily considered to be reusable. Expulsion efficiencies usually range from approximately 95% for small tanks to 99% for large ones. The pressure differential across the diaphragm during reversal typically runs 5 to 25 psi.

Development testing of diaphragms in a transparent tank or attached to only the tank-inlet half-shell conveniently allow observing the diaphragm during reversal. Test results can then be used to optimize the design.

Elastomeric Diaphragms

An elastomeric diaphragm (or bladder) can be applied to most tank configurations. However, because not as stiff as the metallic, elastomeric diaphragms do not provide as much resistance to propellant movement and the impulses imparted on the vehicle or variations in the center of gravity. Elasticity does, however, increase the expulsion efficiency compared to metallic diaphragms and allows reuse.

An elastomeric diaphragm does entail a design complication: the leak-free mechanical joint required where it attaches to the tank shell. Elastomers have not been developed for all of the propellants being used or for hot-gas pressurization. Some propellants, such as nitrogen tetroxide, degrade the properties of existing elastomeric materials to the extent that affects the reliability. But there are solutions to the leak-free-joint problem.

Bellows

Another metallic device for positive expulsion of propellant, bellows can be used in cylindrical tanks and may be either of the expanding or contracting type. In the expanding type, the propellant resides in the tank, ahead of the compressed bellows, which on

expansion ejects it. In the contracting type, the bellows contains propellant and when compressed expels it.

Pistons

An alternative method of obtaining positive expulsion in cylindrical tanks, a piston actuated by pressurant gas requires seals to prevent leakage during operation. The seals may be piston-type rings or some type of wiper. In either case, the dimension and surface finish of the tank inside diameter should be maintained relatively accurate and smooth. In some designs a concentric center post guides the piston, requiring an additional seal. In other designs the surface in contact with the tank wall will be made long enough to prevent cocking of the piston. Figure 8-17 presents the design of a piston guided by a center post.

The pressure differential across the piston required to overcome friction during operation increases the required pressurant pressure and the tank structural loads for a given propellant pressure at the tank outlet. The pressure differential may be estimated as follows:

$$\Delta p A_p = f_s F_n L_s \qquad (8\text{-}37)$$

where—

- Δp = pressure differential across piston, psi
- A_p = cross-sectional area of the piston, in.^{2}
- f_s = coefficient of friction of the piston seals
- F_n = unit normal force reacted by the piston seals on tank wall and guide post, lb/in. of seal
- L_s = total length of all piston seals, in.

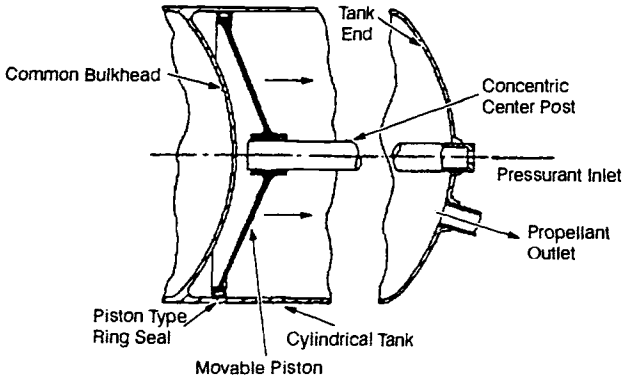

Fig. 8-17 Movable piston used in a cylindrical propellant tank for positive expulsion.

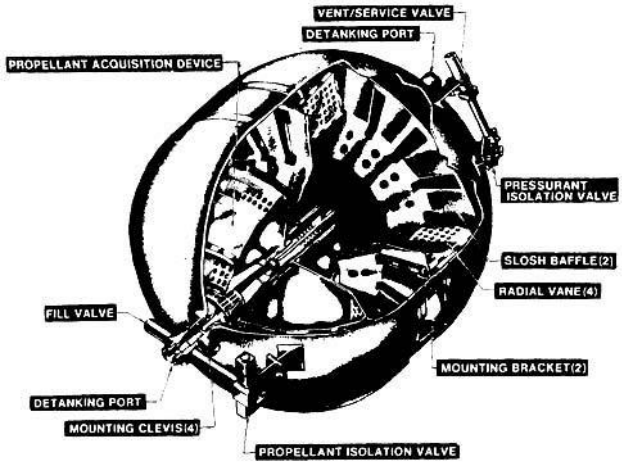

Fig. 8-18 Surface tension propellant storage assembly.

Sample Calculation 8-7

The following data characterize a cylindrical positive-expulsion tank with a movable piston as shown in Fig. 8-17: inside diameter of the tank, 20 in.; diameter of the guide post, 1.5 in.; coefficient of friction f_s of the piston seals = 0.1; and unit normal force F_n reacted by the seals = 500 lb/in.

Problem

Estimate the pressure differential across the movable piston.

Solution 8-7

The cross-sectional area of the piston:

$$A_p = \frac{\pi \times (20)^2}{4} - \frac{\pi \times (1.5)^2}{4} = 314.16 - 1.76$$

$$= 312.4 \text{ in.}^2 \qquad \text{(bs-56)}$$

The total length of piston seals:

$$L_s = \pi \times (20 + 1.5) = 67.54 \text{ in.} \qquad \text{(bs-57)}$$

Substituting this into Eq. (8-37) gives the pressure differential across the piston:

$$\Delta p = \frac{f_s F_n L_s}{A_p} = \frac{0.1 \times 500 \times 67.54}{312.4} = 10.8 \text{ psi} \qquad \text{(bs-58)}$$

Surface-tension Devices

Unlike a positive-expulsion device, a surface-tension device maintains propellant at the tank outlet without any moving parts by relying on the surface tension of the propellant. The principle may be quite simple, but the mechanical design can be complicated. The objective is to keep the surface-tension "compartment" at the tank outlet filled with propellant while the rest of the tank is emptied. It is necessary to know where the propellant will be located during each type of maneuver, and that depends on the acceleration vector. Means of flowing propellant from its locations into the compartment, i.e., porous plates or wire screens, must then be positioned where the propellant is.

In the Peacekeeper Missile Stage IV cylindrical tank (Fig. 8-18) the surface-tension compartment—

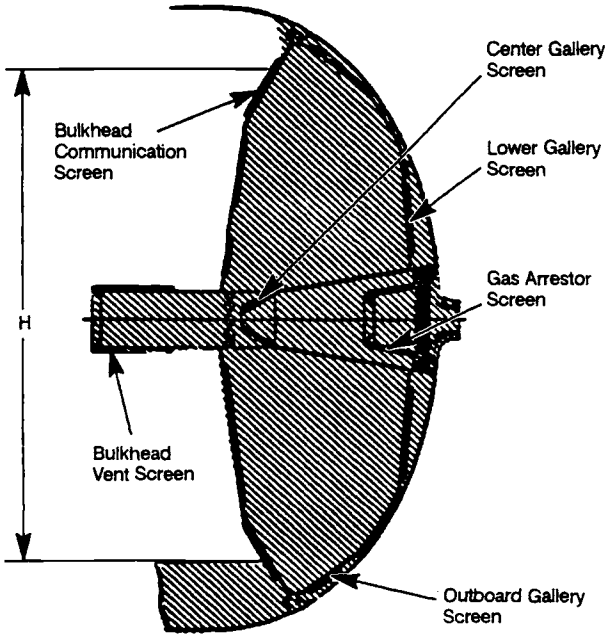

Fig. 8-19 Propellant acquisition device screens and bulkhead communication screen operation.

called the propellant-acquisition device (PAD)—was designed for forward, lateral, and backaway maneuvers, and thus includes six screens (see Fig. 8-19). During a lateral maneuver, propellant is contained within the PAD and along the wall on one side of the tank in its forward section. Propellant in the forward section and aft compartment is separated by a bulkhead and a circumferential "communication" wire-mesh screen (Fig. 8-19). As propellant flows out of the tank (and PAD), it is preferable to flow propellant rather than pressurant gas through the communication screen into the PAD.

As long as propellant wets a *portion* of the screen, the propellant will wick and wet the *entire* screen. When wetted, the screen will preclude the flow of gas up to a certain differential pressure, called the "bubble point." The "breakdown" differential pressure can be increased by reducing the pore size of the screen (increasing the mesh wires per inch). The differential pressure is created by height (Fig. 8-19), the vehicle acceleration, and the propellant velocity through the screen. The screen must be designed so that the bubble point exceeds the pressure differential.

Design of Interconnecting Components and Mounts

9.1 INTERCONNECT COMPONENTS

Interconnect components are defined here as fluid-carrying conduits—lines or ducts along with integral elements such as bellows, flexible joints, flexible hoses, flanges and seals, tube fittings, and engine-gimbal mounts. Except for the gimbal mounts, all of the above components also connect other rocket-engine system components together.

Line Assemblies

As the first requirement, interconnect components and lines must remain leak-tight under the extreme conditions found within an engine system during rocket operation. Second, under all expected conditions, movement in one end of a line (or duct) must not unduly stress either components fastened to the other end or line components. Once a design meets these two requirements, then reliability enhancement, weight/cost reduction, and other features can be optimized. This methodology was followed in designing the LH_2/LO_2 turbopump-fed engine system shown in Fig. 9-1.

Over the years, requirements keep increasing. The engines used on the Saturn vehicle and the associated propellant-feed systems had severe design requirements. Line sizes, operating pressures, flow velocities, and gimballing life all exceeded previous engine requirements. More recently, the Space Shuttle Program specification for hardware design included the new requirement of reusability. That introduced the need for longer low- and high-cycle fatigue life, improved long-term corrosion resistance, a greater number of gimballing cycles for articulating ducts, and ease of maintenance and refurbishment. Another new requirement was the high chamber pressure of the engine (3000 psi, three times greater than previous operational man-rated rocket engines) and very high pump-discharge pressures (as high as 8500 psi), forcing the use of stronger materials.

Propellant-supply Ducts

Principal interconnections between engine and vehicle include the propellant-supply ducts that operate at relatively low pressure. Since every psi of propellant-tank pressure above the minimum required for proper engine performance adds weight to the tank walls and gas pressurants, it is desirable to keep the pressure losses between tank outlets and engine inlets to a minimum.

The task of designing these ducts, or at least the flexible portion of them immediately upstream of the engine, frequently falls to the engine designer. The designer must find an optimum balance between low pressure-drop (by making the duct diameter as large as possible) and flexibility and structural integrity, which in general becomes more difficult with increasing duct diameter. The designer must further consider the fact that the ducts, because of their location off the engine gimbal center, experience torsional loads in addition to bending. Furthermore, the ducts are subjected to internal pressure, frequently in a stringent cryogenic and vibration environment. The many forces acting upon the ducts call for restrainers

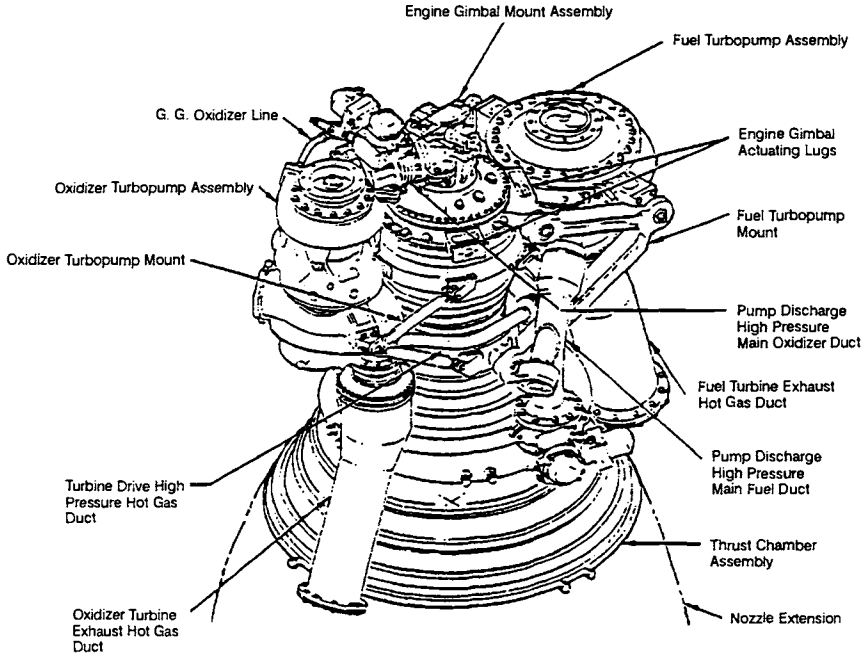

Fig. 9-1 Various interconnecting components and mounts in a typical LH_2/LO_2 pump-fed engine system.

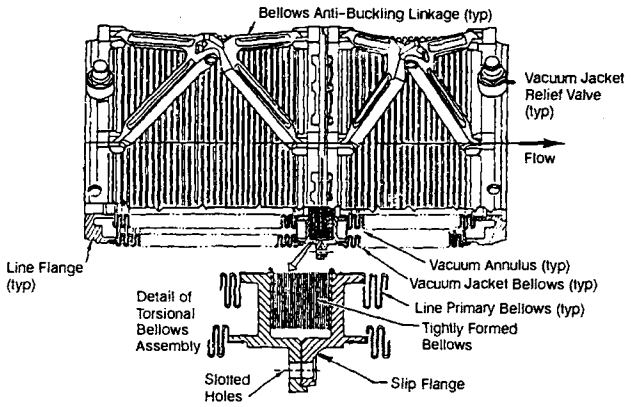

Fig. 9-2 Tightly formed bellows subassembly used to absorb torsional deflection of primary bellows in inlet line of pump on J-2 engine.

against buckling. These may be located inside the ducts, thus adding to undesired pressure drop; or they may be applied externally, which increases the duct envelope and may cause interference with other vehicle systems.

Figure 9-2 shows a typical flexible propellant-supply duct that has outer restraining linkages for stabilizing the bellows. At the vehicle end, these ducts will connect to longer or shorter ducts, the length of which depends on the tank being connected, fore or rear. It is important that the engine designer inform the vehicle builder not only of connecting-flange dimensions and types of gasket being used, but also of the forces transmitted by the engine duct to the vehicle during gimballing. In most pump-fed systems, the working pressure of propellant-supply ducts usually does not exceed 50 psig. In upper stages, during lower-stage boost, however, pressures may temporarily be substantially higher as a result of combination of high accelerations and full tanks (100 psig and over).

The compression-type duct system (Fig. 9-3) uses free bellows (i.e., no tension-tie linkage across the bellows) to absorb the deflections imposed on the duct during operation. The pressure-separating loads on the bellows react to the supporting engine or vehicle structure. Brackets may be required to offset column buckling if the ducting has a large length-to-diameter ratio; i.e., > 1 (Fig. 9-3a). The compression-type system, although widely applied, will usually be limited to low-pressure applications such as the inlet ducts of the engine propellant pumps to avoid unnecessarily heavy restraining structures.

A line containing flexible joints will be given a centerline geometry that will minimize the number of flexible joints. Since a flexible joint (bellows) is complex, costly, and not as reliable as a hard line, the necessity for each flexible joint receives careful scrutiny in the design phase. System considerations that must be kept in mind during the centerline routing and locating of flexible joints include provisions for line deflection and clearance under vibration, thermal contraction and expansion, and engine gimballing; accessibility for installation inspection and removal; wrench clearance around bosses and fittings; accessibility for in-place welding or repair; consideration for clearance if the line needs insulation; and accessibility to other major components. Whenever critical components become integral parts of a line, such as a flowmeter, reliability must be weighed against the replaceability of the component.

A classic configuration adhering to the minimum-number-of-flex-joints principle (believed to have originated with pump-discharge ducts for the Atlas-booster engines)—the wraparound duct arrangement for gimballing engines shown in Fig. 9-4 places a flex joint centered on each of the two gimbal axes. This geometry has been used for the Atlas, Thor, and Jupiter engine pump-discharge ducts, the pump-inlet ducts of the H-1 engine, the gimballing feedlines of the Apollo Service Module engine, and the descent engine for the Lunar Excursion Module (LEM). It was used for all of the vehicle-to-engine interface lines of the F-1 engine except the main propellant lines.

The SSME uses the wraparound concept extensively—seven articulating ducts and six braided-metal hose assemblies crossing the engine-gimbal plane. Each of the ducts has three tension-type bellows joints with one of the joints centered as closely as

Fig. 9-3 Compression-type flexible line configurations.

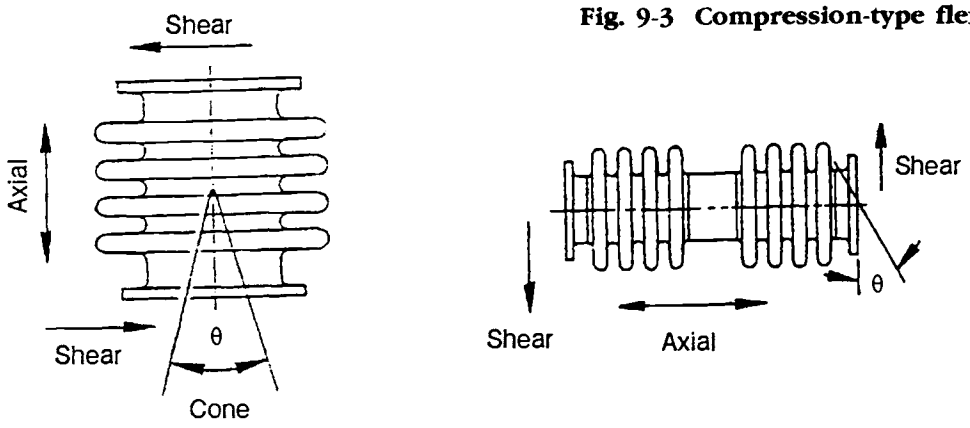

a) Single Bellows **b) Double Bellows**

possible on each of the gimbal axes. The ducts are arranged in parallel routing around the gimbal in a plane perpendicular to engine thrust line (Fig. 9-5).

The second important consideration in duct routing, the location of flexible joints, calls for a kinematic analysis to determine the optimum location for flexible joints in the system. Each will be positioned in the duct assembly to maximize the deflection capability of the assembly. Further, each joint will be placed and designed to accommodate as few modes of deflection as possible and to minimize any deflection of the joint, thus imposing minimum strain. Torsional deflections and "Hooke's Joint" effect may also impose significant restrictions.

Pump-discharge, high-pressure propellant ducts. In turbopump-fed engines, the pump-discharge, high-pressure propellant ducts connect the oxidizer and fuel pump discharges to the main oxidizer and main fuel valves attached to the thrust chamber. The ducts contain bellows sections that permit the degree of movement required between thrust chamber and turbopump to accommodate tolerance buildups, misalignments, and motion due to temperature change and acceleration loads. In some engine designs, however, rigid, in-place welded ducts have been successfully applied. Therefore, the separating pressure loads acting on the two components connected by a flexible member must be absorbed by restraining links attached to the bellows or by other compensating means.

Figure 9-6 presents a typical pump-discharge, high-pressure propellant duct with external restraining links. It is used for the main LOX duct of the system shown in Fig. 9-1.

The high-pressure propellant lines between pump discharge and gas generator usually can be made of

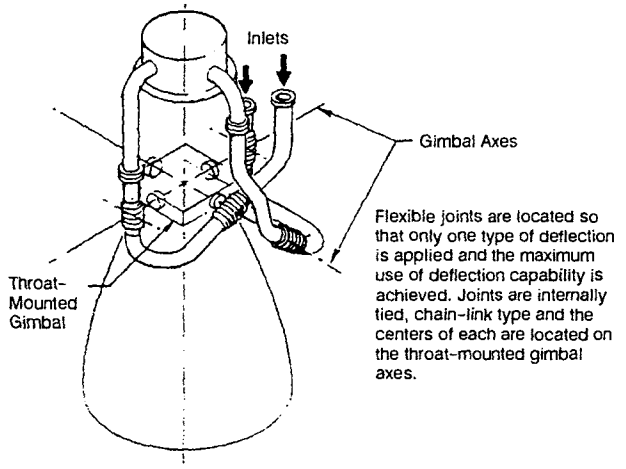

Fig. 9-4 Propellant feeding arrangement on the LEM descent engine

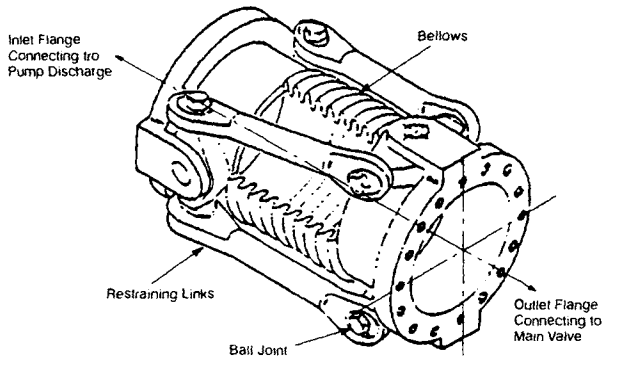

Fig. 9-6 Typical pump-discharge, high-pressure propellant duct with restraining links.

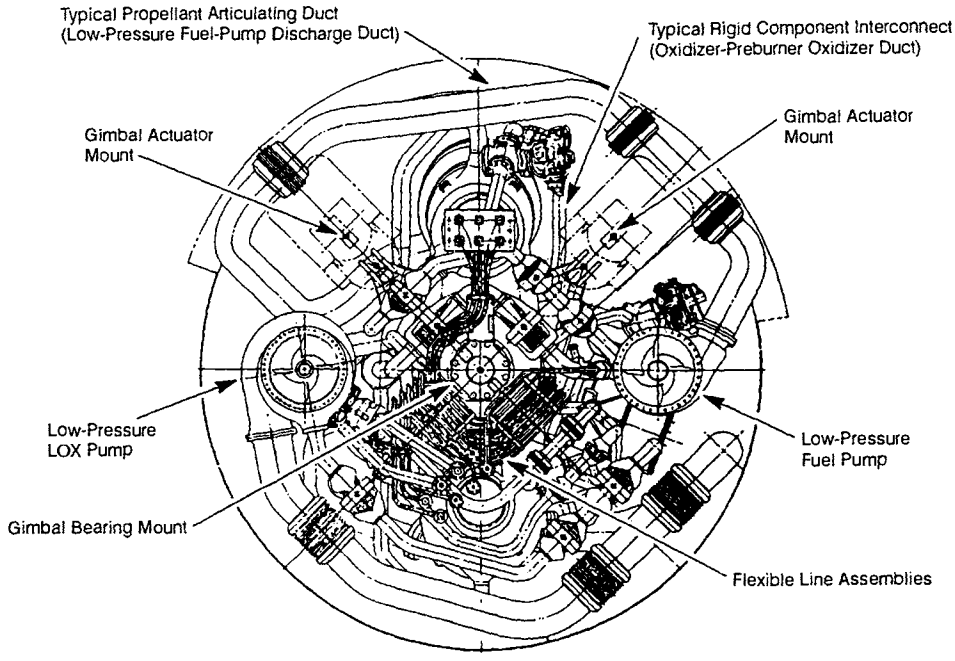

Fig. 9-5 Plan view of articulating-duct arrangement in gimbal plane of Space Shuttle Main Engine.

wire-braided flexible hoses or tubing, because of their relatively small size (often less than 1 inch).

Propellant-tank-pressurization lines. These lines connect the main propellant tanks to the pressurant sources such as stored-pressurant-gas systems (including storage bottles, heat exchangers, pressure regulators), gas generators, cryogenic-propellant heat exchangers, etc. High-pressure hoses and tubings are used.

Seal drain lines. It is difficult to achieve perfect dynamic sealing at the shafts of turbopumps and other components. Seal drains are therefore often provided between two dynamic seals placed in series. The required seal drain-lines, including flexible hoses and tubings, are routed away and overboard. For LO_2/RP-1 systems, this can be done by routing the drain lines along the thrust chamber wall to the chamber exit. Propellant combinations that can form highly explosive mixtures require routing to sufficiently spaced vent ports at the vehicles periphery. Figure 9-7 shows a schematic of a typical pump-seal drain line for an upper-stage system. The seal drain-lines are routed to the vehicle periphery during boost flight and to chamber exits in stage operation.

Pneumatic supply lines. Liquid-propellant rocket engines usually have one or more pressure vessels to supply pneumatic pressure for valve actuation, turbine start, sequenced purges, and other purposes. The vessels must be charged before a test run or flight, requiring high-pressure flexible line connections to the vehicle and disconnects at the vehicle periphery. The design of these not only must consider the mating counterpart on the vehicle side but also the type of fluid and its temperature and pressure.

Cryogenic-propellant bleed lines. Cryogenic-propellant engine systems with turbopump feed may experience difficulties during start if the metal parts containing cryogenic fluid are at ambient or insufficiently low temperatures, and if the fluids in the volumes below the tank outlet are superheated and form gas pockets. Since the pressure upon opening of the main valves and start of the turbopumps will further reduce the static pressure at the pump inlet, gas production will accelerate and, in turn, may cause pump cavitation and starving of the gas generator. To prevent this, a continuous bleed from a point farthest downstream from the pump inlet is applied until shortly before engine start. In this manner, fresh liquid at tank bulk temperature will continuously replace the warming fluid and cool the containing metal parts. To avoid hazardous conditions at the launch site, the bleeds, particularly if they can form combustible or explosive mixtures, are ducted away, through a line connection from the engine to the vehicle and beyond. Such lines are usually made of wire-braided flexible hose and tubings.

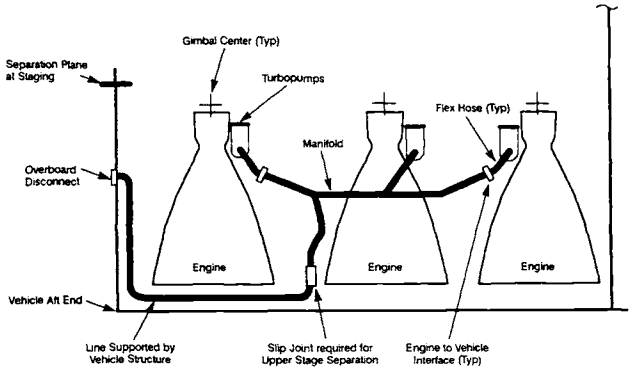

Fig. 9-7 Typical pump seal drain schematic.

A special case is presented by cryogenic engines in upper stages that will not start until some time after the bleeds have been closed at liftoff or that have to start after prolonged cruising periods. For them will be preferred a recirculation system that returns the fluids to the tanks rather than dumping them overboard. Lines across the interface between engine and vehicle are required.

Bleed and recirculation flows can be minimized if the vehicle builder will provide the means, such as subcooling, insulation, avoidance of temperature stratification, maximum economic tank pressure to keep the temperature of the bulk sufficiently below the boiling temperature at operating tank pressures. In some cases, prechilling of metal parts exposed to cryogenic fluids may be advantageously done by cooling media supplied from ground through a vehicle disconnect to the engine. Routing of all lines mentioned will be similar to drain lines (Fig. 9-7).

Purge lines. During the start and shutdown sequences, and for prerun and postrun servicing, inert-gas purges are frequently required to keep a system dry, to prevent combustible mixtures from forming, or to expel residual propellants. If they are continuous during ground hold, it is advantageous to feed them from ground to avoid increased flight weight. This requires connecting lines from the engine to the vehicle. It is strongly recommended that entirely separate purge systems for each propellant be employed to avoid backup of one fluid into the system of the other. Check valves are not considered as reliable as strict separation. For engine design, we are concerned here only with purges that connect directly to an inlet port of an engine part, such as the thrust-chamber cooling jacket or injector manifold. From the viewpoint of the environment in which the engine must operate, the engine designer should additionally specify the purges to be provided by the vehicle building to condition the engine compartment as needed. All purge lines can be made of wire-braided flexible hoses and tubings and may be routed as are the drain lines.

Hydraulic lines. Various high-pressure hydraulic lines are used in a liquid-propellant rocket engine for hydraulic actuating, lubrication, etc. All lines must permit flexure and must be of the proper size and pressure rating. Most of the hydraulic lines are made of wire-braided flexible hoses and tubings.

Turbine-drive, high-pressure, hot-gas ducts. In most turbopump-feed engines, the gas generator connects directly to the turbine inlet; thus, there is no need for ducting. In some designs, however, high-pressure hot-gas ducts must make the connection between gas generator and turbines (in systems with two individual turbopumps) or between main-thrust-chamber bleedoff ports and turbines (tapoff gas-turbine-drive systems). These ducts usually consist of

rigid and flexible sections made of stainless steels and nickel-based alloys, for service temperatures up to approximately 1700°F. The ducts must be capable of absorbing considerable deflections from thermal expansion, in addition to deflections due to misalignments and dynamic loads.

Turbine-exhaust, hot-gas ducts. The hot gases from the turbine exhaust may be ducted to near the main-chamber nozzle exit or into a thrust-chamber exhaust manifold. Most turbine-exhaust ducts are of welded-stainless-steel or nickel-alloy sheet-metal construction. Bellows sections permit the degree of movement required by the system for thermal expansion, misalignments, and tolerances. In most cryogenic propellant systems, a heat exhanger in the exhaust-duct assembly vaporizes one of the propellants, usually LOX, for tank pressurization.

Sizing

Flow area. After the centerline routing of the duct has been established, the inside diameter (ID) must be determined. The ID will represent a compromise among tolerable system pressure-drop, available space, weight, spring rate and pressure thrust reaction of bellows, system dynamic considerations, and cost.

Any prediction of system energy loss based on the test data for individual elements will likely be very conservative. Flow tests on pressure loss of a particular component usually are run to evaluate the maximum component loss. The maximum loss is realized when the installation incorporates a long straight run downstream of the test component; only part of the loss chargeable to the component actually occurs within its confines, the remainder arising from flow disturbances downstream of it. Obviously, if another component closely follows the first, part of the effect of the first will cancelled. Thus, a 180-deg return bend causes no more than four-thirds the loss of a 90-deg elbow, or slightly over twice the loss of a 45-deg elbow. Calibration of a particular component, will subtract test-setup tare (i.e., basic pressure drop of the test setup only, with the component under test removed) from total differential pressure. References 9-1 through 9-2 provide detailed procedures. References 9-3 through 9-7 treat pressure losses in duct components.

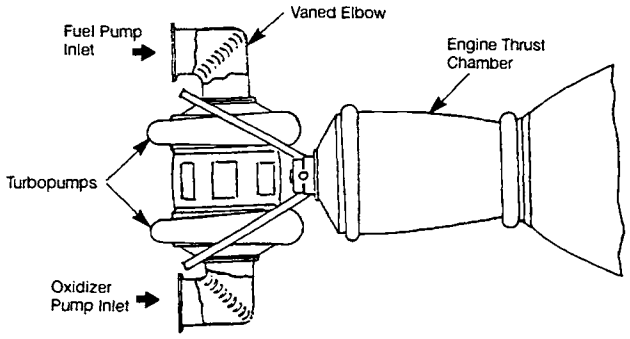

Fig. 9-8 Flow guide vanes in sharp elbows of pump inlet lines.

Wall thickness. After the duct flow area has been sized, the duct wall thicknesses can be established through a stress analysis, in which the magnitudes of the stresses produced by fluid pressure, fluid flow, thermal gradients, external forces, and acceleration forces are evaluated so that the optimum thickness for reliability, fabricability, and weight minimization can be selected.

Determination of hard-line wall thickness must be carefully assessed because the lack of flexible sections requires that the line itself and its attachment points be capable of handling any applied load. The structural analysis of hard lines is based on the maximum envelope resulting from tolerance stackups. The minimum wall thickness, developed from basic thin-shell theory, is based on maximum operating pressure at the critical operating temperature and includes the effect of thinning in the bends. The flanges are designed to develop the axial yield strength of the line at operating temperature. Maximum misalignment, thermal, and discontinuity loads must be determined.

Life considerations for hard lines include both high- and low-cycle fatigue. High-cycle fatigue will limit the effective alternating stress due to pressure and vibration enough to provide a given minimum safety factor on the material-endurance limit. For low-cycle fatigue, the effective peak strain resulting from both primary stresses (pressure and vibration) and secondary stresses (misalignment, thermal, and discontinuity) typically will be limited to provide a minimum given factor on cycles. The strain levels of hard lines can be up to twice the yield strain. Yielding during the initial installation will permit operation in the elastic region for subsequent loadings.

Control of Pressure Drop

Elbow flow losses. When engine vehicle interfaces do not permit a straight approach, flow must be directed into the engine (or pump) through elbows. For flow in a given Reynolds number regime, the loss coefficient for an elbow attains a minimum value and then increases as the ratio of bend radius to inside diameter (R/D) decreases. Pressure drop can be minimized by selecting an optimum R/D value for the elbow; otherwise, pressure drop can be minimized by addition of flow guide vanes. (See Ref. 9-8.)

In an elbow having a small R/D value, guide vanes provide parallel-flowing elbows of more nearly optimum R/D. Flow guide vanes as shown in Fig. 9-8, are utilized in sharp elbows at the pump inlets for the Centaur (RL10), Thor, Atlas, and Saturn S-IC (F-1) engines, and have also been used in the pump discharge ducts of the Thor and Jupiter engines. Minimization of pressure drop in all these applications directly enhances engine performance. (References 9-9 and 9-10 provide design data on pressure loss for flow guide vanes). Because vanes can be excited by fluid oscillations in the system, vane frequencies must be calculated to avoid potential vibration.

Branch or takeoff duct centerlines are aligned with mainline flow directions to capture mainline velocity pressure. This alignment yields higher available pressure at the branch inlet than would be avail-

able at a flush wall tap at a right angle to the main-line flow. Minimum tapoff-pressure drop figures importantly in applications such as tapoffs from main propellant ducts to gas-generator bootstrap lines. Reference 9-11 provides information on optimum takeoff angle.

Bellows flow loss. The flow loss in a bellows exceeds considerably—10 to 15 times—that of a smooth pipe of the same diameter. Pressure loss in straight lengths of unsleeved bellows can be calculated using the following expressions from Ref. 9-8:

$$\frac{f}{NDi} = 0.4\left(hDi\right)^{1.6} \qquad (9\text{-}1)$$

where N = number of convolutions per in., f = Darcy-Weisbach friction factor, h = height of convolution, and D_i = inner diameter of bellows. After determining f, the following formula can be used to determine the total pressure loss:

$$\Delta P = \frac{L\rho V^2}{Di2g} \qquad (9\text{-}2)$$

where ΔP = total pressure loss, ρ = fluid density, V = average fluid velocity through bellows, g = gravitation constant, and L = line length.

Figure 9-9 may be used to determine the pressure-loss factor for 90-deg bends in convoluted metal hoses, using K in place of f in the above formula for the total pressure loss in the elbow. Bellows flow liners frequently can minimize the high friction losses in the convolutions.

Flow-area change. Almost every interface where a line begins or terminates involves an area change to or from the line. The shape of these transitions requires consideration to avoid excessive pressure loss from abrupt flow-area changes. Flow-

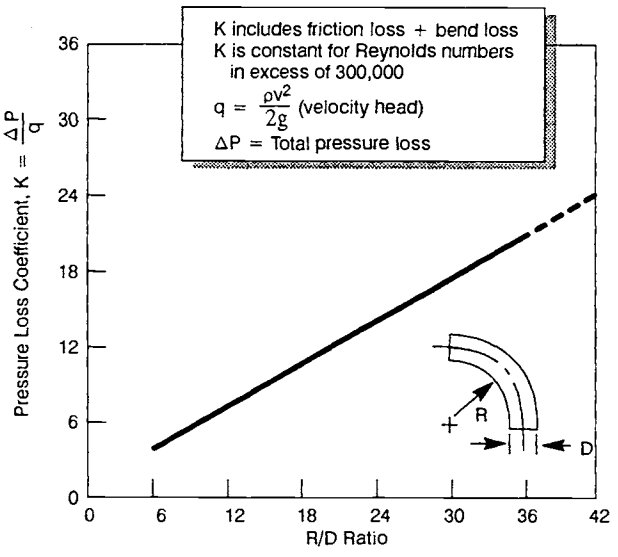

Fig. 9-9 Pressure-loss coefficient for 90-deg bends in convoluted metal hose, annular or helical.

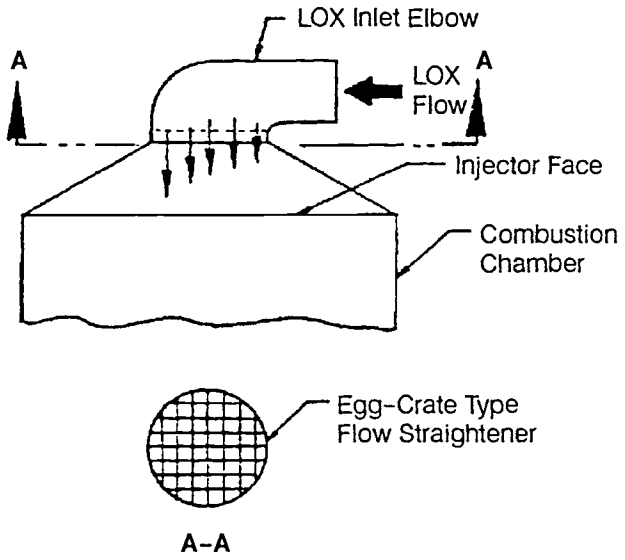

Fig. 9-10 Flow-distribution device incorporating an "egg crate" type of flow straightener.

contraction pressure losses can be reduced by about 90% if the edges of the contraction are radiused rather than sharp. Radii larger than 0.15 times the contracted diameter add little improvement. For expanding sections, little reduction in pressure loss for a given area ratio can be expected unless the divergence cone angle is kept small (total included angle near 10 deg).

In small-diameter lines with threaded fittings, care must be exercised in calculating the line losses, because standard fittings (unions, tees, elbows, and crosses) usually have a smaller ID than the tubing itself. Reference 9-12 presents data on loss factors for fittings.

Flow distribution. The flow distribution (to maintain equal pressure drop) at the exit of engine-feed ducting importantly affects duct design. For example, the flow profile at pump, valve, and injector entrances can have a great effect on the performance of these components. In pumps having dual opposed discharge-ports, the attached ducts must have equal pressure loss to ensure equal flow out of each port. Flow distribution has been improved with vaned elbows (Fig. 9-8) and with "egg crate" straighteners (Fig. 9-10) downstream of elbows. This latter design evolved as a solution to the uneven flow distribution of LOX from the inlet elbow to the injector on the Atlas and Thor engines.

The splitter in the propellant feedlines of the Lunar Excursion Module (LEM) descent engine (Fig. 9-11) represents another flow-directing device for achieving even distribution. The engine utilizes redundant shutoff valves; in normal operation, both valves open and close simultaneously. In a partial failure, however, either of the valves can be closed. Flow into the valves therefore must be evenly distributed for minimum effect on engine performance. That can be done with the flow splitter in the duct elbow immediately upstream of the valves.

Flow straighteners or splitters, or any other structures that rigidly span the diameter of a duct, cause

structural loading by differential thermal expansion or contraction. In a duct, the vane usually heats or cools during thermal transients at a faster rate than the restraining duct wall. When this happens, the vanes try to move farther than the duct will allow. Differentials large enough can distort or destroy the vanes or duct. This can be prevented by an expansion element in the duct-to-vane connection that will slide or flex, absorbing thermally-induced motion while transmitting minimum loads to the wall. One effective solution has been a sliding clevis joint, which allows sliding normal to the wall but adequately carries the flow loads on the vane to the wall. A different approach was used on the SSME low-pressure fuel duct to avoid the thermal expansion and contraction problem. This duct had the egg crate machined into a tube section that was then welded into the duct.

Flow resistance. Surface friction between rough duct walls and the flowing fluid can produce large pressure losses. As the ratio of roughness-height to duct diameter increases, so does the pressure loss. Castings generally have undesirably rough walls and are smoothed to improve flow efficiency. Drawn-tubing and sheet-metal ducts have been adequately smooth for all applications, but weld protrusions into the flow stream have to be controlled when they contribute sufficient disturbance to the flow stream. Weld protrusions contribute much more to large contraction ratio in small lines than they do in large.

In flexible-joint assemblies with internal ties (e.g., chain link, tripod with ball-and-socket bearing, internal gimbal ring), the linkages protrude into the flow stream and cause head losses. Reference 9-13 presents data on pressure-loss factors for some of these bellows restraints.

Control of Pump-inlet-line Vibration

Virtually every pump-fed liquid-propellant rocket developed in the United States has experienced some form of vibrational instability during flight. Such an instability first caused real concern in the Titan II in 1962. A significant longitudinal instability occurred late in first-stage flight. Analysis showed that the vibration was caused by a regenerative-feedback interaction between the vehicle's propulsion and structural systems. This lengthwise oscillation was named "Pogo," after the motion of a pogo stick (Ref. 9-14). The incorporation of a simple hydraulic suppression device into the first-stage propellant feedlines solved Titan's Pogo problem; the oscillation amplitude at the payload was maintained within ± 0.25 g, a level tolerable to the astronauts in the Gemini spacecraft. Although Pogo is a system-design problem, duct designers need to be aware of the phenomenon because it can influence their designs, particularly for pump-inlet ducts of a pump-fed system. (For a more complete discussion of Pogo, see section 10.7.)

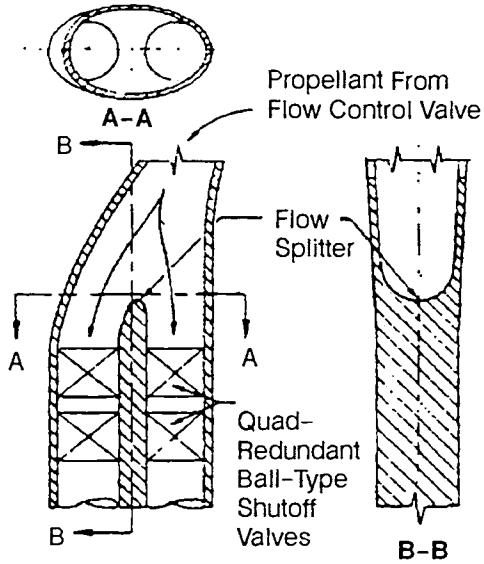

Fig. 9-11 Flow splitter in propellant-feed system of LEM descent engine.

Insulation

Insulation of propellant lines may be required on cryogenic lines to prevent condensation of liquid air or nitrogen on liquid-hydrogen lines, to reduce chill-down recirculation flow rates, and to minimize propellant-subcooling requirements. Nitrogen or liquid air should be kept from dripping because the liquid falling on critical components can easily make them inoperative. On the SSME, the fuel lines have been insulated using two different methods: vacuum jackets and polyurethane-foam insulation. A combination of the two was used on the low-pressure fuel duct and a fuel-bleed duct. The bellows flex joints have an outer bellows and air-tight supporting structure that provide a vacuum around the flex joints, and the rigid duct section has a 1/2-in.-thick polyurethane molded-foam case with an outer cover of nickel to protect it. Damage has been known to occur on the nickel-plated cover due to handling and by abuse from ground-support personnel working in the area. A vacuum cover with a stronger outer tube could prevent some of this type of damage. The liquid-oxygen lines were not insulated since the chill-down recirculation flow rates and sub-cooling requirements were acceptable without insulation.

9.2 DESIGN OF TUBING ASSEMBLIES

Interconnect tubing assemblies are made up of tubing, in-line fittings, and threaded fittings or flanges on the tube ends for installation purposes. Tubing ordinarily will be made of corrosion-resistant steel or aluminum; but nickel-base alloys or titanium may be used for special applications. Design considerations include material, tube size, separable tube fitting or flange, and the engine-installation requirements.

Design Working Pressures for Tubing

Tubing normally used on rocket engines is corrosion-resistant steel (18-8), annealed and pressure tested. Where weight is critical, aluminum may be used. The term "tube" refers to lines up to 2 in. in outside diameter (OD). Flanged joints are the preferred method of attachment for tubing, although threaded coup-

Table 9-1 Corrosion-resistant-steel (18-8) annealed (MIL-T-8504 ASG) tubing. Allowable working pressure in psi at 100°F; safety factor of 4.

Maximum Working Pressure, 3,000 psi									
Tube OD in.	1/4	3/8	1/2	5/8	3/4	1	1-1/4		
Wall thickness, in.	0.022	0.035	0.042	0.058	0.065	0.083	0.109		
Maximum Working Pressure, 2,400 psi									
Tube OD in.	1/4	3/8	1/2	5/8	3/4	1	1-1/4	1-1/2	
Wall thickness, in.	0.020	0.028	0.035	0.049	0.058	0.072	0.095	0.109	
Maximum Working Pressure, 1,500 psi									
Tube OD in.	1/4	3/8	1/2	5/8	3/4	1	1-1/4	1-1/2	2
Wall thickness, in.	0.020	0.028	0.032	0.035	0.042	0.049	0.058	0.065	0.095

Table 9-2 Aluminum-alloy: 5052 round, seamless drawn WW-T-78a, temper H34. Allowable working pressure in psi at 100°F; safety factor of 4.

Maximum Working Pressure, 1,500 psi									
Tube OD in.	1/4	3/8	1/2	5/8	3/4	1	1-1/4		
Wall thickness, in.	0.025	0.042	0.049	0.058	0.072	0.095	0.120		
Maximum Working Pressure, 750 psi									
Tube OD in.	1/4	3/8	1/2	5/8	3/4	1	1-1/4	1-1/2	2
Wall thickness, in.	0.020	0.028	0.032	0.035	0.042	0.049	0.065	0.072	0.095

Table 9-3 Minimum bend radii for stainless-steel and aluminum-alloy tubing. All measurements in inches.

Tube OD	Wall Thickness	Inside Bend Radii	Radii to Center of Tube
3/16	Any	5/8	23/32
1/4	Any	3/4	7/8
5/16	Any	3/4	29/32
3/8	Through 0.022	1-1/2	1-11/16
	Over 0.022	1	1-3/16
1/2	Through 0.028	1-3/4	2
	Over 0.028	1-1/2	1-3/4
5/8	Through 0.028	2-1/2	2-13/16
	Over 0.028	1-3/4	2-1/6
3/4	Through 0.028	3	3-3/8
	Over 0.028	2-1/2	2-7/8
7/8	Through 0.035	3-1/4	3-11/16
	Over 0.035	2-3/4	3-3/16
1	Through 0.035	3-1/2	4
	Over 0.035	3	3-1/2
1-1/8	Through 0.035	4	4-9/16
	Over 0.035	3-1/4	3-13/16
1-1/4	Through 0.035	4-1/2	5-1/8
	Over 0.035	3-1/2	4-1/8
1-1/2	Through 0.035	6	6-3/4
	Over 0.035	4	4-3/4
1-3/4	Through 0.035	7	7-7/8
	Over 0.035	5	5-7/8
2	Through 0.035	7	8
	Over 0.035	6	7
2-1/2	Through 0.049	9	10-1/4
	Over 0.049	7	8-1/4
3	Through 0.049	11	12-1/2
	Over 0.049	9	10-1/2
4	Through 0.065	12	14
	Over 0.065	10	12

lings have been used on a number of engine programs.

Tables 9-1 and 9-2 present pressure ratings for various tube sizes for corrosion-resistant and aluminum-alloy tubing. A factor of safety (i.e., the ratio of the ultimate strength of the tubing material to the maximum allowable working stress) of 4 may be used for most rocket-engine applications. Higher values (6 to 7) should be used in applications involving hazard and excessive vibration. For high-pressure applications, aluminum tubing should be avoided. Other alloys are available for high-pressure use, such as Inconel 625 with ultimate strength of 120,000 psi and yield strength of 60,000 psi and Inconel 718 with ultimate strength of 180,000 psi and yield strength of 150,000 psi.

Tubing Installations in Engine Systems

Installations requiring bends must be made with minimum distortion and constriction of the tubing. A satisfactory bend decreases tubing OD less than 6%. Table 9-3 lists recommended minimum bend radii for stainless-steel and aluminum-alloy tubing. The stainless-steel radii can also be used for Inconel materials. More severe forming is feasible but incurs increased cost owing to special tooling requirements.

Tubing assemblies must be properly supported to prevent stresses and consequent weakening of the system under vibration. In addition, proper support minimizes the danger of recoil and live whip in event of tube failure. Where tube fittings are employed, support spacing should be reduced by 20% to account for the added weight. Supports should be placed as close as practical to each side of fittings, valves, and other components. Overhang should be minimized by placing supports as close to bends as conditions allow. Table 9-4 presents the recommended maximum bracket spacing for common-size tubing assemblies in engine systems. Where tubes of different diameters are connected, average spacing may be used.

General design practice requires no detail drawings for tubing assemblies less than the 3/8-in. size. They are shop-fitted according to an engine mockup during the assembly of the engine system.

Separable Tube Fitting

The flared-tube fitting coupling (Fig. 9-12a) was developed for aircraft hydraulic systems before World

Table 9-4 Recommended support-bracket spacing for tubing assemblies in engine systems. Maximum support spacing in inches.

Tube Size (OD) in.	Aluminum Alloy	Stainless Steel and Inconel Material
1/4 through 1/2	12	14
5/8 through 3/4	17	20
1 and over	21	24

War II and was carried over on the early rockets. These fittings have several disadvantages, which in most cases result in system leakages. Aluminum connectors have limited strength to contain the system fluid in high-temperature or high-vibration environments and are subject to seizing under high torque. Stainless-steel connectors proved difficult to seal because of poor yield characteristics at the seal surface, difficulty in controlling the tube flare, tube cracking during flaring operation, and torque relaxation of the coupling due to temperature changes and vibration environment.

A machined flare sleeve (Fig. 9-12b) was developed to overcome some of the tube-flare problems. Put into service on the Saturn program, the flare sleeve provided the following advantages over the flared tube:

1) Tolerances in the conical-tube sealing surface can be closely controlled.

2) Increased rigidity of the machine flare resists distortion at the sealing surface.

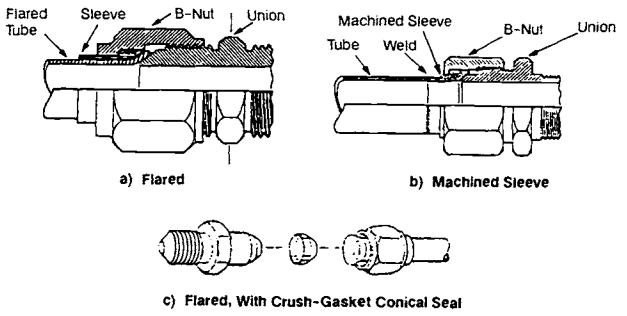

Fig. 9-12 Flare types of threaded couplings.

3) The weak point of the tubing at the base of the flare is eliminated.

4) Seizing eliminated between tube and sleeve.

5) Greater hoop strength helps prevent seizing between sleeve (now the tube end) and coupling nut.

6) Stronger couplings permit higher torque, which improves sealing and resists nut relaxation.

Another approach for achieving a seal on the flared connector, use of a soft material, generally copper or aluminum, between the steel interfaces (Fig. 9-12c), raised the likelihood of making a leak-free-coupling; but some of the above problems still exist (e.g., torque relaxation due to vibration, tube cracking during flaring operation). This seal created new problems, including improper seal installation (which orificed the flow) and galling of the seal, which introduced metal particles into the fluid system.

Due to the leakage problems with the flared-tube coupling, the Air Force issued a directive that requires separable tube connectors to have redundant seals for new designs in space and launch vehicles. This requirement has been met by a dynamic beam connector per MIL-F-85421 (Fig. 9-13). Tests by users and manufacturers have demonstrated that the connector has redundant seals in series and good sealing characteristics.

The dynamic beam connectors contain the following desirable features: all-metal construction, integral redundant seals in series, seals in most fluid systems, seals in cryogenic and elevated temperature units, seals in vacuum, low-pressure helium and fluids to 8000 psi, small envelope, light weight, high strength, low torque values, numerous attaching methods, availability in various materials, and less protrusion for easier component removal.

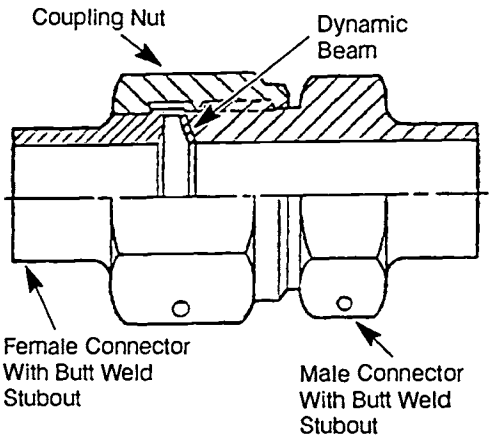

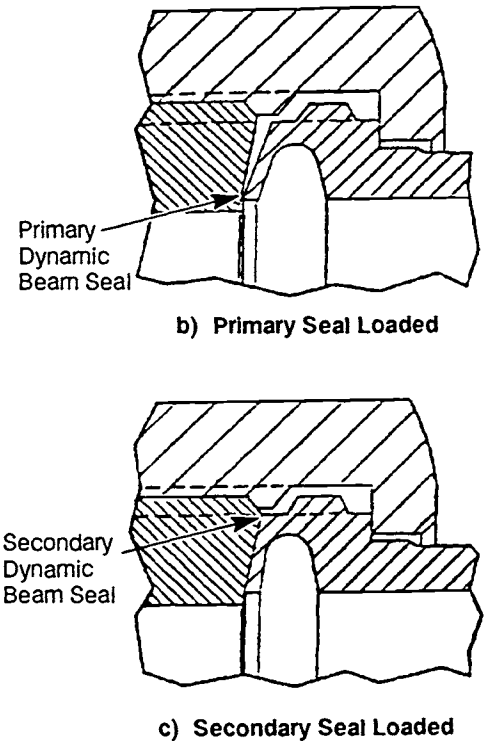

Fig. 9-13 Dynamic-beam fluid fitting.

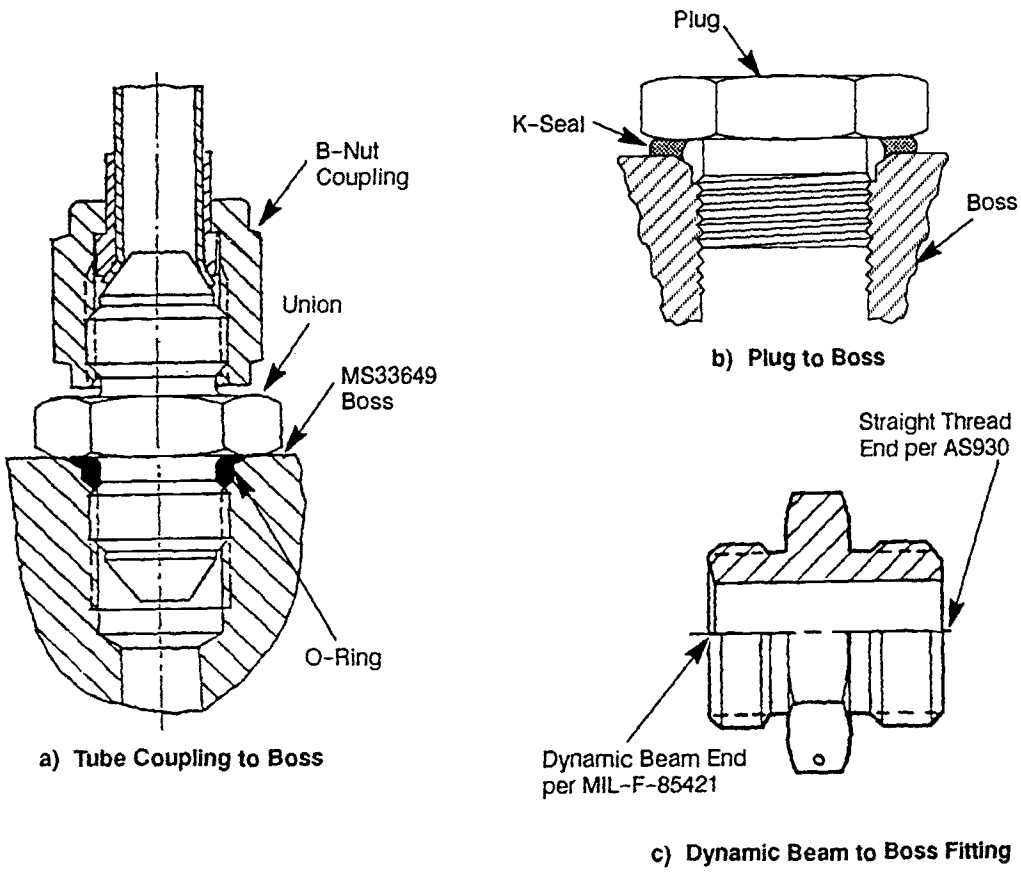

Fig. 9-14 Typical installations of fittings into MS33649 bosses.

Small lines may be required to connect to components or larger lines. For this purpose a threaded fitting and boss connection offers an alternative to a bolted flange. Figure 9-14a shows a line with a B-nut, union, and elastomer O-ring installed in a MS33649 boss and figure 9-14b shows a plug with a metallic seal (K-seal) installed. Section 9.3 describes seal selection. It must be based on the service conditions. A special fitting available has a dynamic-beam-coupling interface on one end and a straight thread on the other (Fig. 9-14c) that can be installed in the MS33649 boss. The tube fittings should be made of the same material type as the tube when possible to avoid coefficient-of-expansion/contraction problems and to prevent metal distortion during the torque operation. A fitting will be designed to be as strong as the strongest tubing of like material that would be used with it. Design details and dimensions of tube fittings can be found in AF, AS, and MS specs.

9.3 DESIGN OF FLANGED JOINTS

The interconnecting lines of a rocket-engine system must retain various fluids at a wide range of pressures and temperatures. Each of these lines may have one or more mechanical flanged joints requiring a static seal to prevent leakage. These flanged joints must satisfy the following requirements: "zero leakage" for man-rated systems (a philosophy that developed through the Saturn vehicle development and flights and continued during the Shuttle Program), high reliability and low weight (a consideration often in conflict with high reliability), and low cost. The joint as an assembly must be capable of maintaining intimate conformance of seal and sealing surfaces throughout the joint's life, regardless of all strains, loads, and thermal gradients. Such design can also be applied to other components, such as thrust chamber, injector, dome, turbopump, and valve-housing flanges.

Typical flanged-joint configurations, shown in Fig. 9-15, can be modified as required to mate with the various types of seal. Flanged joints are used where loads require the type of restraining force provided by bolts or vee clamps or where joint reliability dictates the use of more than one threaded clamping fastener. Failure of a threaded coupling by thread disengagement can be catastrophic, whereas failure of one of a number of bolts on a flanged joint may have less impact. This factor was one of the reasons that threaded couplings on the F-1 engine were limited to zero-pressure drain systems. The joint configurations used on this engine consisted primarily of flat-face flanges, flat face with seal cavity, and flat-face flanges with swivel ring. The swivel-ring design was used where alignment of bolt patterns presented a problem. Leakage monitoring was provided on joints that were considered critical or were representative of a family of joints of similar design and operational environment. On the J-2 engine, flat-face flanges, flat face with swivel ring, and threaded-boss couplings were used, with leakage monitoring at each joint. On the SSME, the high-pressure flanged joints used a raised flange with a seal cavity (Fig. 9-15h). A

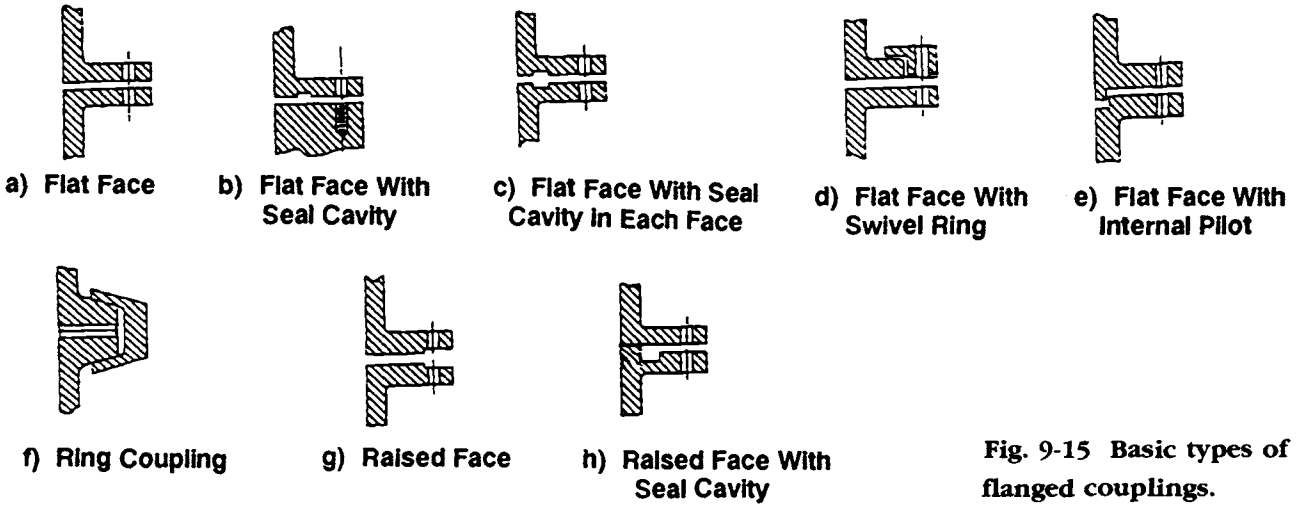

Fig. 9-15 Basic types of flanged couplings.

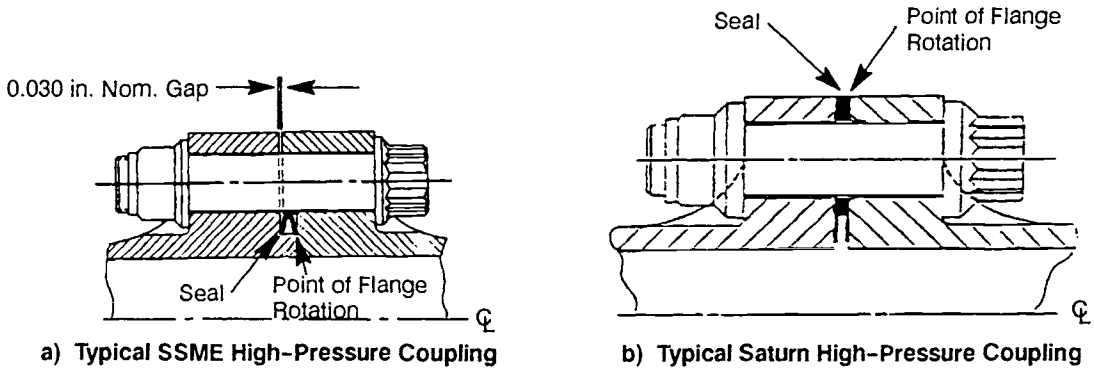

Fig. 9-16 Comparison of flanged-coupling designs used on SSME and Saturn engines.

design study showed this design to have a significantly smaller envelope and to be lighter in weight than the flat-face flange. In addition to the raised-face flange, bolt sizes on the SSME joints were kept small by using a larger number of bolts, and the bolt load per bolt was increased by using bolt elongation rather than a torque measurement. Figure 9-16 compares typical SSME and Saturn joints. The SSME flange concept saved some 500 lb on the engine as compared to flat-face flanges.

Flange-Joint Design Integration

The flange joints normally consist of three elements—the flanges, the fasteners (bolts and nuts), and the seal. Proper integration of these elements must provide a leak-tight joint. In addition to the structural needs, other considerations for flange joints include seal contact surfaces, rigidity, restraining mechanism, temperature, degree of sealing, leakage monitoring, and seal drainage.

Seal-contact surface on flanges. The success of the flanged joint in limiting leakage depends on its ability to make the necessary seal contact. The interface requirements involve the seal housing on the flanges, surface finish, machine lay, and surface flatness and waviness. The sealing surface for aerospace-type seals, including elastomeric O-rings, requires a 32-μin. finish and, for pressure-assisted seals, also a circular lay (phonograph-record profile).

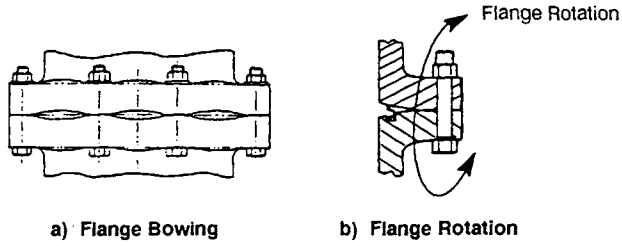

Fig. 9-17 Two kinds of flange deflection resulting from lack of rigidity.

Rigidity. Flange rigidity enables the coupling to resist deflections and distortions due to mechanical or thermal loading. The degree of rigidity required for a flange relates directly to the seal element that must compensate for deflections and distortions. Figure 9-17 shows typical deflections and distortions that can cause leakage problems with flanged joints.

Flange bowing, the tendency for flanges to separate between bolts as a consequence of thinness or an inadequate number of bolts, can be prevented by increasing the flange thickness or the number of

bolts or both. Flange rotation denotes the tendency of the joint to separate at the seal surface as a consequence of thin duct walls that have too little resistance to the rotating moment, flanges that lack sufficient rigidity and consequently deflect under high separating loads, insufficient flange contact outside the bolt circle, insufficient flange thickness, and an adverse thermal gradient that prevents the flange from expanding without constraint. The flange-rotation problem normally will be resolved either by increasing the flange rigidity or by increasing the ability of the seal to follow the flange separation. The current flange design practice permits deflections within the capability of one of the high-resilience type of seals (metal or elastomer), so that flange size and weight are kept to a minimum.

In the flange-joint design concept used on the SSME, the point of rotation is placed just on the pressure side of the seal and as near to it as possible, with a gap between the two flanges (Fig. 9-16a). Any rotation of the flange, therefore, has little effect on the seal. Figure 9-16b shows the design widely used on the large Saturn engines. The two figures illustrate the difference in size that can be achieved in sealing the same fluid pressure by using the SSME design with high strength material (Inconel 718) for the flanges and the bolts and by measuring the fastener preload with an ultrasonic instrument that measures a change in bolt length.

Restraining mechanism. The restraining device provides the force required to keep the flanges together under all operating loads, internal and external. Internal loads, due to the system pressure, include the effects of surges generated by operation of components in the system and by the system operation itself. External loads include vibration and misalignment loads transmitted through the lines or components, torque from rotating machinery, thermally-induced loads, seal loads, acceleration loads, and the load from the joint-restraining mechanism itself.

To provide the required restraint, a preloaded device seats the seal and exerts a compressive load greater than the separating loads. Insufficient preload will result in leakage if the resilience of the seal can not compensate for the separation that occurs in operation. Also, a gap between the flanges can result in seal abrasion in an installation subjected to high vibration. Joint restraining problems have occurred on both cryogenic and hot-gas applications as a result of installation preload, loss of preload because of a thermal gradient, and bolt yielding at high temperatures. Such problems are resolved by analyzing the joint and specifying the proper bolt loading.

The restraining mechanisms for flange joints consists of bolts or ring clamps. Most liquid-propellant rocket engine joints are restrained by bolts because of high clamping-load requirements and the large duct diameters, which prohibit the use of threaded couplings. Ring clamps have not been used extensively on rocket engines.

A significant problem with bolted systems has been the inherent inaccuracies in the common methods for preloading bolts. The usual method of torquing with the standard torque wrench is considered to be only about 50% accurate because of frictional variations from unit to unit. This variation limits the design bolt-load to the minimum expected value and does not permit the optimum utilization of the bolt ultimate strength. As a consequence, the joint requires thicker flanges, larger bolts, and more bolts than if a more accurate preload method were used. The high pressures required on the SSME necessitates large, heavy joints, and these became a significant weight problem. As noted, the joint design was changed as shown in Fig. 9-16a. In addition, preload for the SSME joint bolts was determined by measuring bolt-length change with an ultrasonic device. In this method, a transducer mounted on the bolt head sends a sound pulse down the length of the bolt. The wave reflects from the bolt end back to the transducer. The time for the wave to traverse the length of the bolt and return is determined. The instrument is calibrated to read changes in length as a function of time. The method, however, involves more than bolt-length change, since material density due to strain, bolt bending, and twist also affect the ultrasonic wave travel through the bolt material.

Temperature. The temperature of the fluid greatly affects the type of seal selected and the joint material. Also, the problem of maintaining a leak-tight flange joint is compounded by temperature effects. Temperature differentials at the flange joints of rocket engines may be large, because of steep heating and flow transients. They introduce thermal stresses and strains that may disturb the sealing. When designing an elevated-temperature or cryogenic flange joint, the temperatures of the various parts should be analyzed to assess their effect on the sealing load. Ideally, thermal effects should neither loosen nor tighten the joint. In actual design the flange joint must be sufficiently elastic to maintain sealing loads within acceptable limits.

Degree of sealing. Most applications require sealing to prevent mass flow under operating conditions. Joint design integrity can be verified by simulated operating tests and measuring leakage. Once the joint integrity has been proven, soap-solution leak tests are performed at the assembly levels to verify the joints free of leaks. When sealing the lighter gases (H_2 and H_e), diffusive flow through openings of molecular size may become significant.

Seal. Effectively sealing at the flange surfaces usually requires a material that will readily conform to them, or that as coated with a soft material will form a barrier at the flange interfaces. Seals which damage the flange sealing surfaces are usually unsatisfactory, since they prevent resealing. Sealing load at installation must be maintained so that the seal compressive load will withstand internal fluid pressure without leaking.

Leakage monitoring and seal drainage. A requirement for monitoring joint leakage was implemented early on the Saturn program. Joint leakage could be monitored on bench, subsystem, static-engine-firing tests, and, if desired, even on critical joints in flight. Leakage monitoring introduced a low-pres-

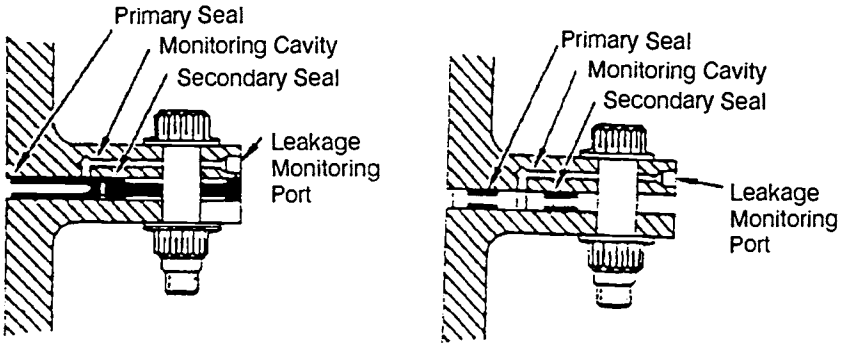

a) Flanged Joint With Spacer Seal

b) Flanged Joint With Molded-in-Place Spacer Seal

Fig. 9-18 Provisions for monitoring leakage at a joint.

sure secondary seal concentric with the primary seal and a bleedoff passage in one of the mating flanges between the two seals. The secondary seal gives sufficient resistance to leakage past the primary seal to force flow out through the bleed passage and an attached flowmeter. These flow passages may also be used to collect leakage past the seal, so that combustible fluids may be separated and drained to a suitable venting area. Figure 9-18 shows typical monitoring provisions for joints. The SSME did not have leakage-monitoring provisions.

Leakage monitoring entails design penalties. The coupling diameter must be increased to permit a secondary seal inside the bolt circle, enlarging it, thus requiring larger bolts (increased weight).

Flange-Joint Structural Design

Figure 9-19 presents the structural design configuration of a typical flat face flange joint as frequently used in rocket engines. The flange ring, under various working loads, is subject to bending as shown exaggerated by the dotted lines. The bending moments may become quite large; the resulting stresses reach their maximum at corner Z, where the flange joins the wall of the duct.

The basic approach to the design of a flange joint is to prestress the flange bolts in tension so that a gasket compressive stress or seal compression is maintained to seal effectively against fluid leakage, under maximum working pressure and other loads. Defining a flange ring segment of unit length (i.e., 1 in. along the arc of a circle passing through the flange cross-section centroid) as a free body, the correlations between all forces acting on that segment, and the minimum required design flange bolt loading, are established as follows:

$$F_1 = F_2 + F_3 + F_4 + F_5 \tag{9-3}$$

$$F_2 = \left(\frac{pD_1^2}{4D}\right) + \frac{W_e}{\pi D} \tag{9-4}$$

$$F_3 = \frac{p(D_2^2 - D_1^2)}{4D} \tag{9-5}$$

$$F_4 = \frac{S_g(D_3^2 - D_2^2)}{4D} \tag{9-6}$$

$$S_g = mp \tag{9-7}$$

$$F_5 = nF_1 \tag{9-8}$$

$$W_b = F_1 \pi D \tag{9-9}$$

where (refer to Fig. 9-19)—

- D = diameter of the circle passing through the centroid of the flange-ring cross section, in.
- D_1 = inside diameter of flange and duct, in.
- D_2 = inside diameter of the gasket, in.
- D_3 = outside diameter of the gasket, in.
- p = internal fluid pressure, psi (the maximum working pressure should be used)
- F_1 = force per unit length of the flange ring from bolt loading, lb/in.
- F_2 = force per unit length of flange ring from longitudinal tension of duct, lb/in.
- F_3 = force per unit length of the flange ring from internal pressure p, lb/in.
- F_4 = force per unit length of the flange ring from gasket loading, or seal loading, lb/in. Load ranges (F_4) for several types of seals are:

  O-rings:
  - Elastomer O-ring: 5-150 lb/in.
  - Metal O-ring (See Table 9-6)

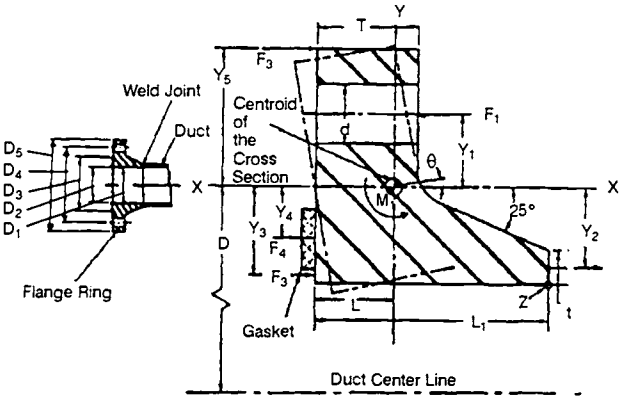

Fig. 9-19 Structural design configuration of a typical flange joint.

Pressure assisted seals:
- Teflon-coated: 75-150 lb/in.
- Metal-plated: 100-500 lb/in.

F_5 = force per unit length of the flange ring from compression load at the flange outside diameter, lb/in.

S_g = required average gasket compressive-stress, for proper seating against an internal fluid pressure p, psi

m = gasket factor, a function of gasket design to be determined experimentally; design values range from 0.8 to 10

n = flange factor, a function of flange configuration and its rigidity; design values range from 0.1 to 0.8

W_e = end loads on the duct due to inertia and thermal effects (tension or compression), lb

W_b = min. required design bolt-loading, lb

Sample Calculation 9-1

The following design data characterize the flange joint of the flexible duct for oxidizer-pump discharge in the A-1 Stage engine:

Working pressure under normal steady, operating conditions, 1505 psia
Maximum fluid working pressure under occasional transient conditions, 1750 psia
Inside diameter D_1 of the duct = 8 in.
Inside diameter D_2 of the gasket = 8 in.
Outside diameter D_3 of the gasket = 8.5 in.
End loads on the duct due to thermal contraction, W_e = 2400 lb
Gasket factor m = 0.8
Flange factor n = 0.3

Problem

Determine the minimum required bolt loading of the flange joint.

Solution 9-1

Maximum working pressure p equals 1750 psia. Equation (9-5) gives the required average gasket compressive-stress, as follows:

$$S_g = mp = 0.8 \times 1750 = 1400 \text{ psi}$$

Combine Eqs. (9-3) and (9-8):

$$F_1 = \frac{(F_2 + F_3 + F_4)}{(1 - n)} \tag{9-9a}$$

Combining this and Eq. (9-4), (9-5), (9-6), and (9-9) yields the minimum required design bolt loading of the flange joint:

$$W_b = \frac{[p\pi D_i^2 + 4W_e + p\pi(D_2^2 - D_i^2) + S_g\pi(D_3^2 - D_2^2)]}{4(1 - n)}$$

$$W_b = \frac{[1{,}750 \times \pi \times 8^2 + 4 \times 2{,}400 + 1{,}400 \times \pi(8.5^2 - 8^2)]}{4(1 - 0.3)} = 141{,}000 \text{ lb} \tag{9-9b}$$

After the required design bolt loading has been determined, the number, size, and torque value of the bolts needed to produce that load must be chosen. Use of small-diameter, high-strength bolts will be desirable to gain tensile elasticity. Bolts should be placed sufficiently close to ensure a reasonably even distribution of the load around the gasket circumference. The following empirical correlation is recommended for maximum spacing to produce a tight joint:

$$P_S = 2d + T \tag{9-10}$$

where P_S = maximum bolt spacing, in.; d = nominal bolt diam, in.; and T = flange thickness, in. The general proportion of the flange ring may be determined by the following empirical equations (Fig. 9-19):

$$T = At \tag{9-11}$$

$$L_1 = Bt \tag{9-12}$$

where t = thickness of the duct wall as determined by a hoop-stress calculation, in.; L_1 = overall axial length of the flange ring, in.; A = design factor, ranging from 4 to 10; and B = design factor, ranging from 10 to 14. A taper angle of 25 deg is generally used for the hub portion of the flange ring.

The stress-and-strain analysis of the flange ring may be treated as the twisting of a thick circular ring of uniform cross section under the influence of turning couples uniformly distributed along a circle passing through the centroid of the ring cross-section. The following correlations approximate the maximum working stress and strain of a flange ring (see Fig. 9-19):

$$M_t = F_1Y_1 + F_2Y_2 + F_3Y_3 + F_4Y_4 - F_5Y_5 \tag{9-13}$$

$$y_1 = \frac{(D_4 - D)}{2} \tag{9-14}$$

$$y_2 = \frac{(D - D_1 - t)}{2} \tag{9-15}$$

$$y_3 = \frac{(2D - D_2 - D_1)}{4} \tag{9-16}$$

$$y_4 = \frac{(2D - D_3 - D_2)}{4} \tag{9-17}$$

$$y_5 = \frac{(D_5 - D)}{2} \tag{9-18}$$

$$\theta = \frac{M_t D^2}{4EI_{y-y}} \tag{9-19}$$

$$S_z = \frac{M_t D^2 (L_1 - L)}{2D_1 I_{y-y}} \tag{9-20}$$

where Y_1, Y_2, Y_3, Y_4, Y_5 = distances between the ring cross-section centroid and forces F_1, F_2, F_3, F_4 and F_5 in inches and—

D_4 = diam of bolt circle, in.
D_5 = outside diameter of the flange ring, in.
M_t = resultant twisting couple per unit length of flange ring, in.-lb/in.
I_{yy} = the moment of inertia of the ring cross-section about the Y-Y axis, $in.^4$
E = modulus of elasticity of the flange material, psi
θ = angular displacement of the flange ring under maximum working pressure and loads, rad
S_z = flange-ring maximum tensile stress, which occurs at the corner Z and is normal to the plane of Fig. 9-19, i.e., in the hoop direction, $lb/in.^2$

Figure 9-16 presents the structural design configuration of a flanged joint used throughout the SSME in the high-pressure system. A modified ASME flange, this design has been optimized for minimum joint weight. The design maintains contact between a surface on one flange and the mating surface on the other flange under all operating conditions by proper use of bolt loads. The design offers nearly constant fastener loading under pressurized and nonpressurized condition and minimum flange deflection at the sealing surface, which results in maintaining the sealing load. The flange size is kept small by positioning the bolts on the smallest practical bolt circle and making the flange outside diameter tangent to the bolt heads.

The flanges have been structurally verified with proven structural computer-programs. This includes determining stress levels, bolting requirements, and flange deflections. The flange joint carriers all applied loads through the load pilot, which is the only contact between mating flanges. When the bolts are installed, the contact point is compressed and the outside diameters of the flanges rotate toward each other. The seal contact surface, being adjacent to the load contact-point, keeps flange rotation low and produces a negligible effect on seal deflection and seal load. Flange deflection is under 0.002 in. for each flange and within the seal-deflection capability of 0.006 in. for the pressure-assisted seal. When external loads are applied, the flange contact load decreases to a minimum of 10% of the installed load. The maximum bolt load occurs at installation and remains nearly constant during operation, thus reducing bolt fatigue.

Preliminary flange-joint sizing criteria have been developed for the SSME-type flange shown in Fig. 9-20. Listed below are the ground rules used for sizing this type of joint:

1) Flange deflections at the sealing diameter due to pressure will not exceed 0.002 in. (maximum) per flange.

2) Seal groove dimensions (pressure assisted seal) will be as follows:

0.163 depth (axial) $\begin{cases} +.002 \\ -.000 \end{cases}$

0.210 width (radial) $\begin{cases} +.005 \\ -.000 \end{cases}$

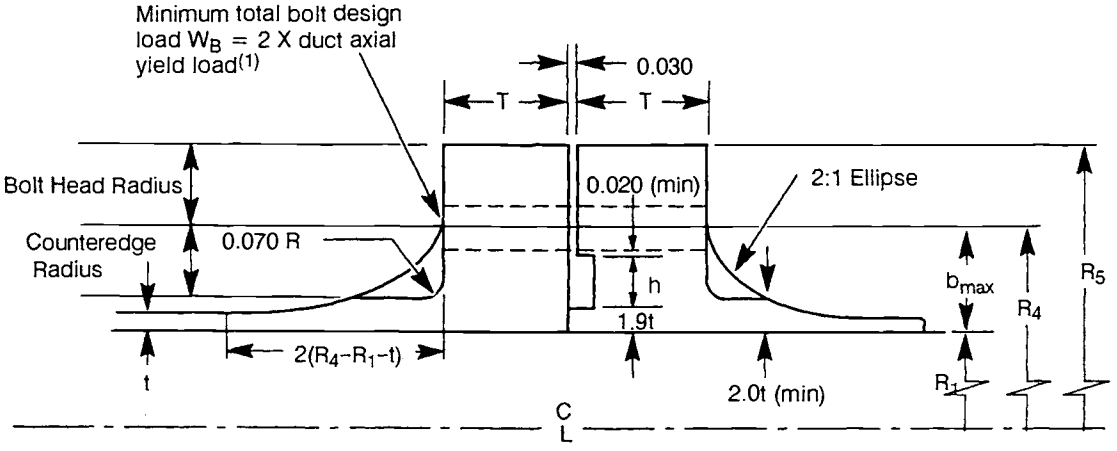

(1)Axial yield load will be based on room temperature properties for ambient and high temperature ducts and cryogenic properties for cryogenic operation.

Nomenclature

t = Nominal duct thickness (in.)
R_1 = Inner duct radius (nom.) (in.)
h = Seal groove width (in.) (0.215 in. used in this study)
W_b = Minimum total bolt design load = $4\pi RtF_y$
F_y = duct yield stress as defined above(1)
R_4 = Bolt circle radius = $R_1 + b_{max}$ (nom.) (in.)
where b_{max} = larger of:
(1) 1.9t + h + 0.020 + radius bolt hole
(2) 2.0t + $R_{counterbore}$
S = Minimum bolt spacing = 2 X bolt dia.
R_5 = Outer flange radius = $R_4 + R_{bolt\ head}$
T = Flange thickness = $1.9\ R_1^{1/3}\ t^{1/2}$

Fig. 9-20 Preliminary flange sizing-criteria for SSME type of flange joint.

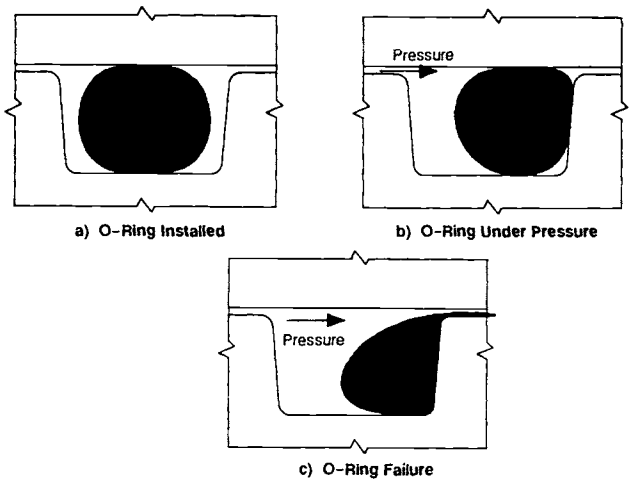

Fig. 9-21 Elastomer O-ring installation.

3) Under all load conditions, the axial contact at the flange I.D. (Load Pilot) will be maintained (see Fig. 9-20).

4) When rigid ducts are used, the flange joint will be capable of taking the allowable yield load of the duct.

5) The flanges will be sized for 200-ksi bolts.

6) The preload will be known within ± 10%.

7) The bolts will be installed with a minimum factor of safety on ultimate of 1.4.

8) The strain at the maximum point in the flange will not exceed two times the yield strain, and no more than 20% of the maximum cross section of the flange will exceed the yield strain.

9) The bolt-circle diameter, as well as the outer-flange diameter, will be a minimum.

Sample Calculation for SSME Flange 9-2

The following design data characterize the fuel high-pressure-pump discharge line for Inconel 718 duct and flange: duct design pressure P = 6600 psi, duct inside radius R_1=2.5 in., operating temperature T= -320°F, seal groove width of 0.300 in., and material properties, Inconel 718:

T, °F	Fy, psi	Fu, psi
70	145,000	175,000
-320	163,000	215,000

Problem

Design the flange.

Solution 9-2

Duct thickness $t_{min} = \dfrac{P \times R_1}{F_{allowable}}$

For operation at -320°F, $F_{allowable}$ = 163,000/1.1 or 215,000/1.5 = 148,000 psi or 143,340 psi. Then:

$$t_{min} = \frac{6{,}600 \times 2.5}{143{,}340} = 0.115 \text{ in.}$$

Proof pressure P_{proof} (at LN2 temperature) = 1.2 (6600) = 7920 psi.

$$s_{proof} = \frac{7920\ (2.50)}{0.115} = 172{,}000 \text{ psi}$$

$$\text{Factor safety}_y = \frac{163{,}000}{172{,}000} = 0.948$$

$$\text{Factor safety}_u = \frac{215{,}000}{172{,}000} = 1.25$$

Now calculate the minor yielding acceptable based on flange-joint sizing criteria of item 8 above. Assuming a duct with a 2D bend radius that results in a 20% wall thinning, weld efficiency of 100%, and disregarding tolerance:

$$t_{nom} = \frac{t_{min}}{0.8} = 1.44 \text{ in.}$$

The minimum design total bolt load Wb for this engine will be twice the duct axial yield-load with a safety factor of 1.4 on ultimate for the bolt:

$$Wb = 2\ (2p\ R_1 t)\ Fy = 4\pi\ (2.5)(0.144)(163{,}000)$$
$$= 738{,}000$$

Bolt Size	Min. Ult. Bolt Load (# Bolt)	No. Bolt Req'd (N)	Min. Bolt Spacing S, in.	NS/2 π, in.
9/16	37,240	20	1.13	3.597
5/8	47,396	16	1.25	3.183
3/4	69,464	11	1.50	2.626
7/8	95,102	8	1.75	2.226

S=2 times bolt diameter. Based on Inconel 718 bolts, with 220,000-psi F_u, bolt-circle radius R_4 and outer-flange radius R_5 will be—

$$R_4 = R_1 + b \text{ max}$$

Then b max will be the greater of calculation (1) or (2) below:

1) b = 1.9 (0.144) + .300 + .020 + R of bolt hole + .030 oversize hole = 0.624 + R of bolt hole.

Column	1	2	3	4	5	6
Bolt Size	1.b	2.b[a]	R+ (>Col. 1 or 2)	NS/2π	R Bolt Head	R_5[b]
0.562	0.905	0.840	3.405	3.597	0.482	4.079
0.625	0.936	0.883	3.436	3.183	0.525	3.961
0.750	0.999	0.983	3.499	2.626	0.625	4.124
0.875	1.061	1.077	3.577	2.228	0.719	4.296

[a] R of counterbore = R of bolt head + 0.70
[b] R_5 = (larger of col. 3 or 4) + col. 5

2) b = 2.0 (0.144) + R of counterbore = 0.288 + R of counterbore.

Static Seals for Flange Joints

Early rocket engines used seals available from industrial applications. These included elastomeric O-rings, flat-sheet gaskets of asbestos fibers with rubber binder, spiral-wound gaskets of asbestos, and preformed steel ribbons. Over the years, operating conditions on engines have become much more severe—seeing pressures up to 10,000 psi and temperatures from -423 to 1400°F—and thus created the need for development of new metal seals, including metal O-rings and pressure-assisted seals. Flat-sheet and spiral-wound gaskets are no longer recommended for use on rocket engines since they are prone to leakage at all pressures, the leakage increasing at higher pressures and at temperature extremes. Asbestos fibers are avoided because of their environmental impact. In spiral-wound gaskets, the metal ribbons can mar the flange surfaces on aluminum and corrosion-resistant steels, forcing a refinishing of the flange sealing surfaces or even component replacement.

Considerations in seal selection or seal design include resilience (spring back), installation load, environment of media to be sealed (including temperature, pressure, and fluid compatibility), and cost. Ideally, a universal seal for a rocket engine would be very resilient so it could conform to flange-surface waviness and accommodate flange separation and deflection; have low installation load to minimize impact on bolt and flange designs; be effective at both low (-423°F) and high (1400°F) temperatures; be operational at pressures to 10,000 psi; be compatible with all engine fluids such as propellants, hydraulic fluids, and combustion gases; and be low in cost.

The importance of trouble-free and leak-free static-seal joints in spacecraft cannot be overemphasized. The consequences of leakage include fire and explosion hazards, freezing of fluid or equipment adjacent to a leak, overpressurization of an engine compartment on the vehicle, and degradation of engine performance because of loss of specific impulse.

Elastomer seals. The elastomer O-ring, the simplest seal, has proven the most reliable when the flanged joint is properly designed. The inexpensive O-ring will usually be the first seal choice if the elastomer is compatible with the environment.

Elastomer O-rings have been used with good results in rocket-engine joints in the temperature range between -30 and 400°F. At temperatures lower than room temperature, the elastomers become hard and at -60°F all of the various elastomer compounds lose the resilience that permits them to conform to the flange surfaces. For low-temperature service (below 0°F), elastomers should be selected by an evaluation of the different compounds for low-temperature properties, such as flexibility, resilience, compression set, and hardness. The upper temperature limit for elastomers is based on heat deterioration of the elastomer. Selection of an elastomer compound for high-temperature service should be based on properties at the service temperature and should include volume reduction, increase in hardness, and compression set.

In O-ring sealing, a two-step operation, compression of the O-ring by the dimensional control of the groove (Fig. 9-21a) makes the initial seal at installation. Then, under system pressure, the elastomer acts as a viscous fluid with a high surface tension and is forced to the side of the groove and blocks off the leak path (Fig. 9-21b). An O-ring fails when the gap between the two flanges becomes greater than the O-ring can block (Fig. 9-21c). Failures can be eliminated by one or more of the following: reduce pressure, increase flange stiffness, or use a harder O-ring material.

Satisfactory results have been experienced at pressure levels as high as 3000 psi. Higher pressures are possible if joint design can control the deflections that support the O-ring from extrusion. The information in figure 9-22 should be used to select hardness of the O-ring material with respect to working pressures. Table 9-5 gives typical elastomer O-ring flange-joint design data for use in groove-type flanges, as shown in Fig. 9-23.

Metal O-rings. Properly designed, the metal O-ring, a tube formed into a circle with ends welded together, can be used at cryogenic temperatures and up to 1200°F or higher when made of high-temperature metal. It can be used at high pressures by drilling vent holes on the pressure side of the tube when used with rigid flanges. The metal O-ring operates differently than an elastomer O-ring. The metal O-ring is compressed by the flange load into a groove which controls the deflection, and this deflection produces an interface load sufficient to seal at low pressures. The vent holes permit pressure into the tube, which

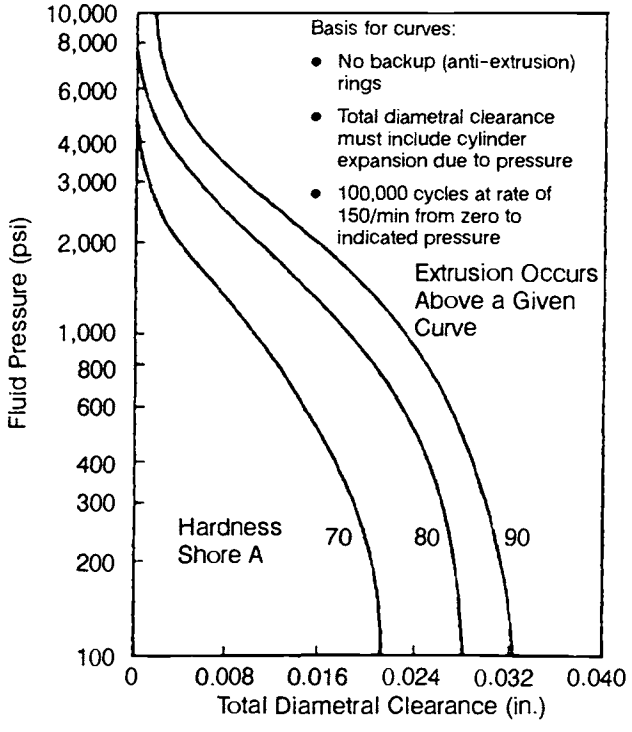

Fig. 9-22 O-ring extrusion related to diametral clearance, fluid pressure, and O-ring hardness.

Table 9-5 Recommended elastomer O-ring flange-joint design data. All dimensions in inches.

Nominal O-ring Cross Section	Actual O-Ring Cross Section	Minimum Squeeze	Depth of Groove, a	Width of Groove, b	Bottom Radius, r	Seal Surface Finish, f_1	Seal Surface Finish, f_2
1/16	0.070 ± 0.003	0.013	0.052 ± 0.002	0.101 to 0.107	0.005 to 0.015		
3/32	0.103 ± 0.003	0.020	0.077 ± 0.003	0.136 to 0.142	0.005 to 0.015		
1/8	0.139 ± 0.004	0.028	0.104 ± 0.003	0.177 to 0.187	0.010 to 0.025	32 rms	64 rms
3/16	0.210 ± 0.005	0.043	0.157 ± 0.005	0.270 to 0.290	0.020 to 0.035		
1/4	0.275 ± 0.006	0.058	0.206 ± 0.005	0.342 to 0.362	0.020 to 0.035		

provides a pressure-assist load for sealing high-pressure systems (Fig. 9-24).

The industry has established standard tube sizes ranging from 0.032 in. for small-diameter rings up to 0.625 in. for very-large-diameter rings (32 in. and larger). Recommended tube diameters for normal engine applications are 0.062, 0.093, 0.125, 0.188 and 0.250 in. Aerospace static joints normally must be gas-tight due to the hazardous fluid and high operating pressure in the system as well as the required gas-leak checking procedure. To achieve a gas-tight joint,

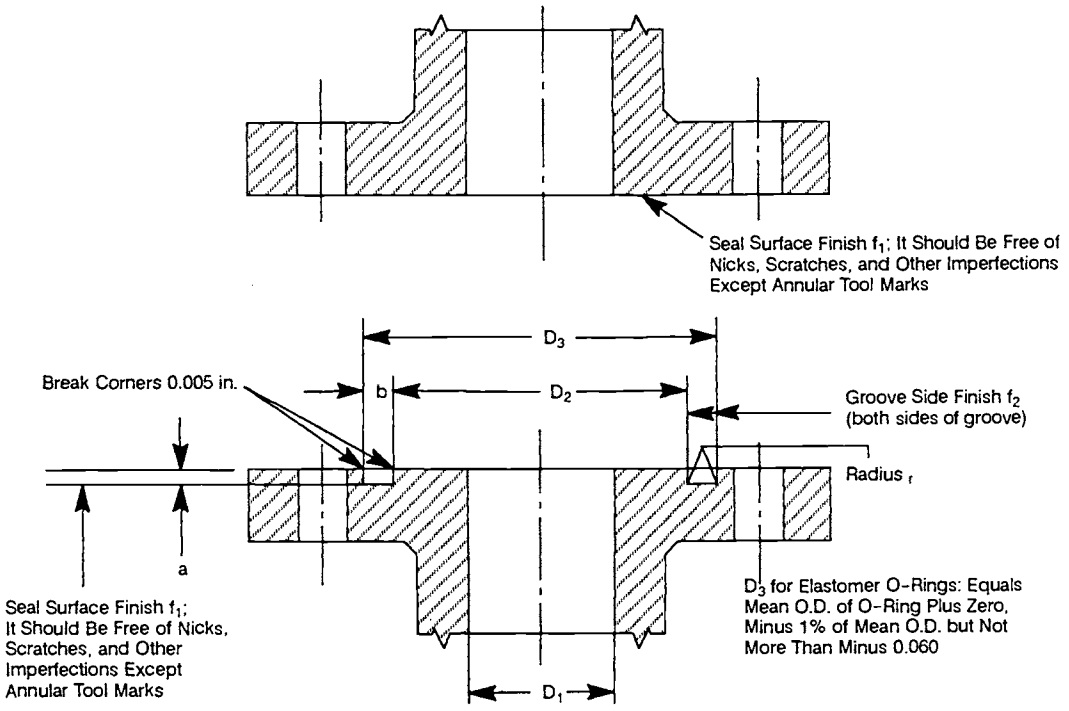

Fig. 9-23 Flange seal groove design

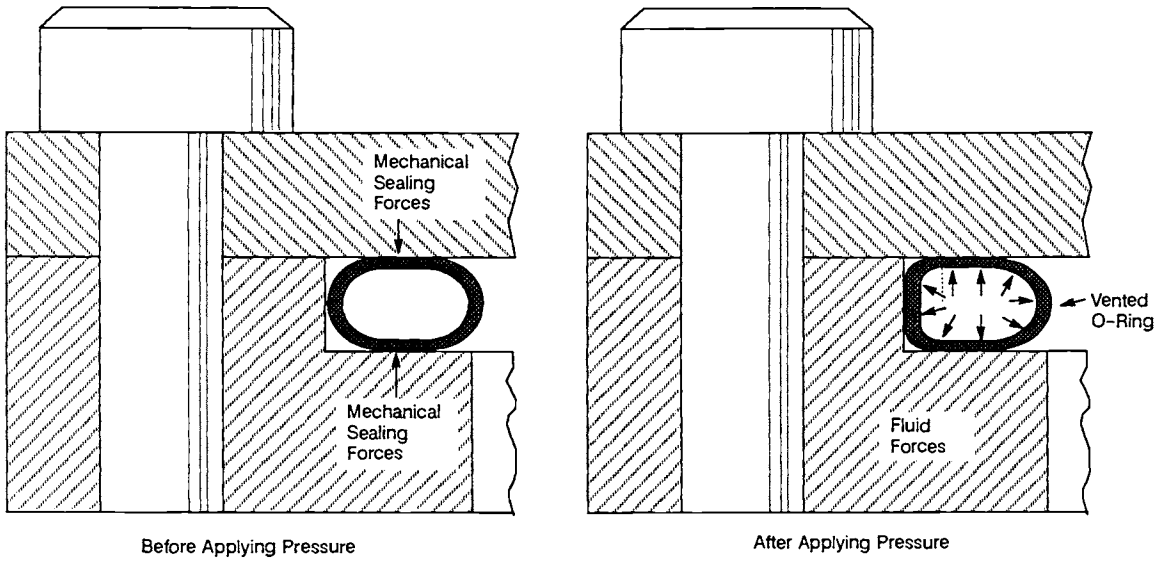

Fig. 9-24 Metal O-ring installation.

the O-ring must be sized to obtain an installation load of 700 lb/in. of length or higher. This requires an O-ring selection based on diameter, tube thickness, and material properties. Table 9-6 shows the variables required for O-ring sizing plus data on elastic spring-back (point no seal load if the flange joint has deflection equal to the spring-back). As the flange deflection approaches the spring-back, the joint will be prone to leakage. Metal O-rings must be coated with Teflon, silver, or gold for cryogenic service and silver, gold, or nickel for high-temperature service. Table 9-7 shows typical metal O-ring tube sizes for various O-ring diameters and flange-groove dimensions.

Pressure-assisted seals. The pressure-assisted seal was developed to attain a deflection that would better handle deformation of the flange joint under working loads. Figure 9-25 shows two different seal types. The spring effect is achieved by a metal circular seal having a U-shaped cross section. The tapered legs provide a nearly uniform stress in the material. Compressed between the surfaces of the flange joint, the seal tips at the open ends make contact with the flange surfaces and deflect until the flanges make contact. This type of seal permits the seal legs to follow the flange deflections. The open end of the seal is oriented toward the pressure side of the flange joint. Thus the system pressure generates a considerable portion of the seal's contact load at the higher pressures. Seals have been designed and are in service on the SSME with the legs extending outward for sealing an external pressure. Pressure-assisted seals are installed in a concentric groove cut into one of the flanges. This limits the amount of total flange preload transmitted through the contact points of the seal. The following correlations have been established for the seal designs to determine the appropriate seal-contact load.

$$F_{s1} = \frac{E\,J^3\,d}{8\,K^3\,C_1} \qquad F_{s2} = F_{s1} + \frac{pK}{2}$$

where—

F_{s1} = Seal-contact load per inch of seal circumference without internal fluid pressure, lb/in.
F_{s2} = Seal-contact load per inch of seal circumference with internal fluid pressure, lb/in.
E = Modulus of elasticity of seal material, psi
J = Ave. thickness of seal leg, $\frac{D+L}{2}$ in.
K = Length of seal leg F-G in Fig. 9-25, in.
d = Seal deflection in the flange joint (i.e., difference between initial seal width E_s and flange-groove depth), in.
p = Internal fluid pressure, psi
C_1 = Design factor; a function of seal leg configuration and seal diameter, its value ranging from 0.5 to 1.0

Contact surfaces of pressure-assisted seals will usually be coated with a material with a lower elastic modulus than the seal material. The seal structural material will be chosen for the good spring-like properties to gain maximum deflection, while the

Table 9-6 Metal O-ring design installation loads.

Basic Tubing OD, in.	Wall Thickness, in.	Tubing Metal	Installation Load, lb/lineal in.	Elastic Springback, in.
0.062	0.012	Stainless steel	800	0.002
	0.014	Stainless steel	1,300	0.0025
	0.016	Stainless steel	1,500	0.003
	0.006	Inconel	300	0.002
	0.010	Inconel	420	0.002
	0.012	Inconel	550	0.002
	0.014	Inconel	1,100	0.002
	0.010	Inconel X-750	550	0.002
	0.012	Inconel X-750	700	0.002
0.093	0.016	Stainless steel	1,100	0.0035
	0.007	Inconel	150	0.0025
	0.010	Inconel	250	0.0025
	0.012	Inconel	350	0.002
	0.018	Inconel	1,000	0.0025
	0.010	Inconel X-750	300	0.0025
0.125	0.020	Inconel	1,000	0.0035
	0.025	Inconel	1,400	0.004
	0.020	Inconel X-750	800	0.004
	0.025	Inconel X-750	1,600	0.004
0.155	0.025	Stainless steel	1,000	0.003
	0.025	Inconel X-750	950	0.002
0.186	0.032	Stainless steel	2,300	0.005
	0.020	Inconel	600	0.004
0.250	0.035	Stainless steel	1,100	0.006
	-0.049	Stainless steel	2,500	0.007

Table 9-7 Typical metal O-ring flange-joint design data.

Nominal O-Ring, OD	Actual O-Ring Size		Flange Groove Dimensions			
	O-Ring OD +0.005 -0.000	Tube OD +0.003 -0.000	D_2 Maximum	D_3 +0.005[b] -0.000	a +0.005 -0.000	A
1	1.000	0.061	0.857	1.005	0.042	32 r ms, circular lay
1-1/2	1.500	0.061	1.357	1.505	0.042	
2	2.000	0.061	1.857	2.005	0.042	
2-1/2	2.500	0.061	2.357	2.505	0.042	
3	3.000	0.061	2.857	3.005	0.042	
4	4.000	0.094	3.777	4.005	0.075	
5	5.000	0.094	4.777	5.005	0.075	
6	5.000	0.094	5.777	6.005	0.075	
8	8.000	0.124	7.705	8.005	0.105	
10	10.000	0.124	9.705	10.005	0.105	
15	15.000	0.124	14.705	15.005	0.105	
20	20.000	0.124	19.705	20.005	0.105	
30	30.000	0.124	29.705	30.005	0.105	

[a] See figure 9-32 for flange design. Duct diameter D_1 may be equal to D_2.
[b] Increase diameter to compensate for coatings or platings.

coating material provides the properties needed to establish the intimate contact required to prevent leakage between the seal and flange surfaces. To prevent leakage, sufficient compressive stress must be developed in the coating to make it flow into imperfections on the flange surfaces.

The seal-tip load will be limited by the coating applied to the seal. Teflon coating will extrude to the point of cutting through and causing leakage if the load exceeds approximately 150 lb/in. of seal circumference at installation and 450 lb/in. when pressurized with a cryogenic fluid for the configuration. Silver and gold plating require higher seal-tip bearing pressures to cause it to flow, and can withstand a much larger load when pressurized. Seal-tip load runs approximately 300 lb/in. of seal circumference at installation and can be over 1000 lb/in. when pressurized.

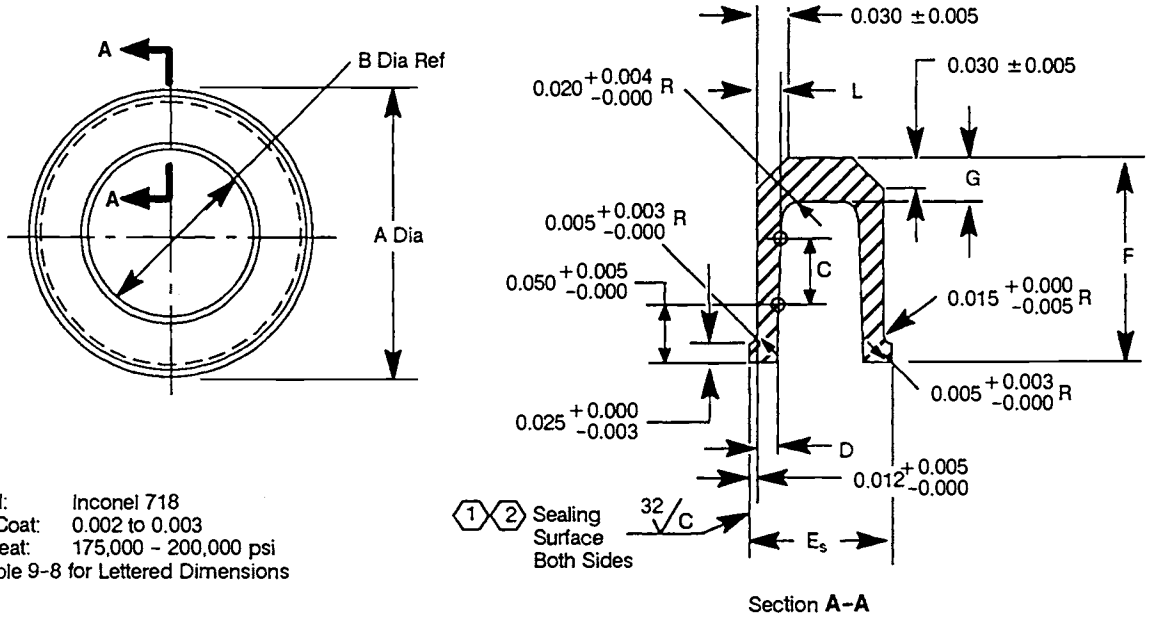

Material: Inconel 718
Teflon Coat: 0.002 to 0.003
Heat Treat: 175,000 - 200,000 psi
See Table 9-8 for Lettered Dimensions

(1) Sealing surfaces shall be free of nicks, scratches, or other imperfections which would impair the sealing function

(2) Flatness and waviness within 0.0003 in. when restrained against a surface plate

a) Cryogenic Pressure-Assisted Seal, Teflon Coated

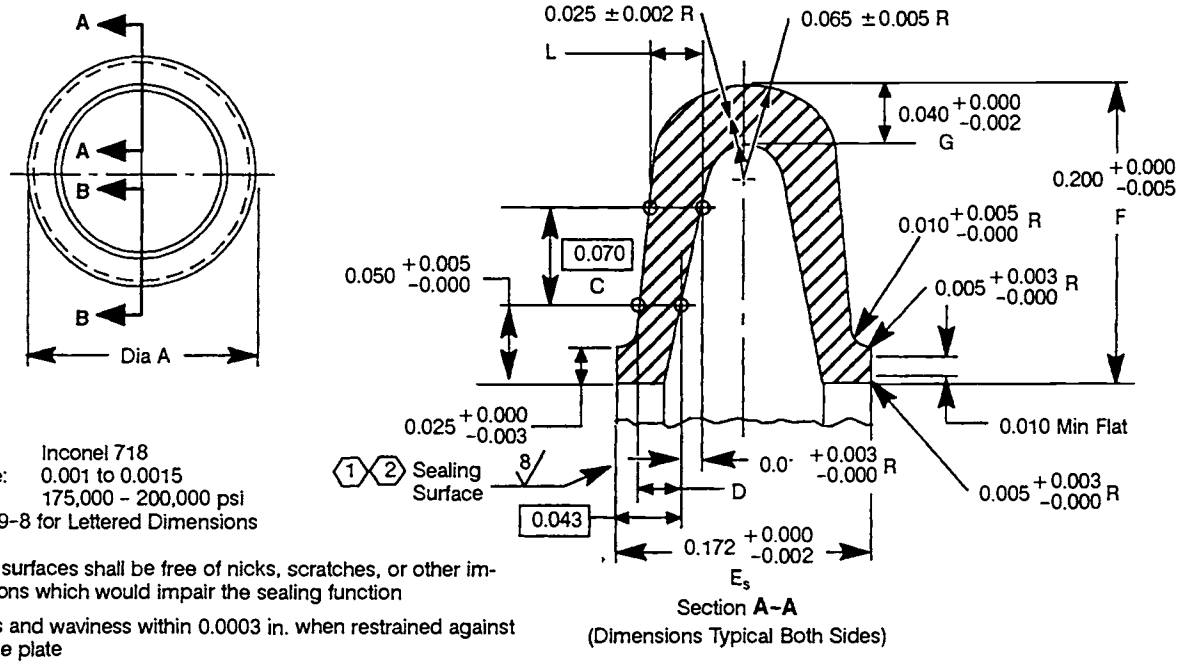

Material: Inconel 718
Silver Plate: 0.001 to 0.0015
Heat Treat: 175,000 - 200,000 psi
See Table 9-8 for Lettered Dimensions

(1) Sealing surfaces shall be free of nicks, scratches, or other imperfections which would impair the sealing function

(2) Flatness and waviness within 0.0003 in. when restrained against a surface plate

b) Cryogenic and Hot Gas Pressure Assisted Seal, Silver Plated

Fig. 9-25 Pressure-assisted seals.

To prevent leakage, the surface finish on the flanges must have a 32 (rms) roughness with a circular lay (approximately circular relative to the center of the surface, similar to a phonograph record). If the flange configuration does not permit this type of finish, an 8 rms multi-directional lay has been determined to be an acceptable alternate. The sealing surfaces must be free of defects such as machine steps, tool gouges, scratches, material tears, and pits for the seal to function without leakage. Teflon coating is softer and more forgiving of defects on the flanges than silver, and Teflon-coated seals have a lower installation load, which translates into lower flange loading.

Many versions of pressure-assisted seals have been used on rocket engines. Rocketdyne developed the Naflex-type pressure-assisted seals with the early seal designs made of alloy steel, nickel-plated and coated with a layer of Teflon. Later designs used Inconel 718 with Teflon, silver, or gold. The Teflon-coated seals are effective for cryogenic service (-430°F). Silver- and gold-plated seals are used for cryogenic and hot-gas service (1700°F). The Teflon-coated seals are limited to 3000 psi; the silver- and gold-plated seals are effective at pressures greater than 10,000 psi. Design details and data for typical cryogenic and hot gas seals and flange joints are given in Fig. 9-25 and table 9-8.

9.4 DESIGN OF FIXED JOINTS

Fixed joints are nonseparable connections of fluid-system components. Since it is impractical to make line assemblies in one piece from end to end because of requirements to insert specially formed or machined parts such as elbows, tees, bosses, and valves, fixed joints are a necessary design element. Complexity, cost, and the effect on reliability keep the number of such joints to a minimum within a line. Fixed joints can be made by welding, brazing, diffusion bonding, and soldering. However, welding is the preferred method. Problems that make brazed joints a second choice to welding include close dimensional tolerances of component parts, inadequate cleaning, which reduces braze wettability (ability of braze alloy to adhere to the surface), built-in crevices that can trap contamination and act as stress concentrations, intergranular carbide penetration of line material, and inability to inspect for proper braze coverage with non-destructive testing. Diffusion bonding—a unique method for joining some widely different metals by the use of controlled temperature and pressure—does not have many applications in rocket-engine ducting to date. Soldered joints have very low strength and some of the same problems associated with brazing.

Welding, the most common and recommended method of joining the various duct components, produces joints with mechanical properties and environmental and propellant compatibility characteristics similar to the components being joined. A butt weld does not contribute to the system contamination and does not have a built-in crevice. Welded joints are usually made on a bench, but they can be made as final-installation joints. The type of welded joints which have been used in fluid-system lines are illustrated in Fig. 9-26. The butt, fillet, and sleeve welds—the most common—sometimes are used in combination, as shown in Fig. 9-26f. Butt welds are bench-fabrication joints and are the recommended

Table 9-8 Typical design data of Naflex pressure-assisted seals and flange joints. All dimensions in inches.

Seal Dimensions								Flange Groove Dimensions[1]					
A Diameter +0.000 -0.005	B Diameter (Ref)	C Basic	D +0.000 -0.003	E_2 +0.000 -0.002	F +0.000 -0.005	G	L +0.000 -0.003	D_2 +0.000 -0.010	D_3	a +0.002 -0.000	r_i	r_o	Sealing Surface Finish f
Cryogenic Pressure-Assisted Seals (figure 9-25a)													
				a		+0.000 -0.004			+0.010 -0.000		± 0.005	± 0.005	
0.943	0.513	0.075	0.024	0.157	0.215	0.049	0.026	0.433	0.948	0.148	0.020	0.020	32 rms
1.943	1.513	0.075	0.024	0.157	0.215	0.049	0.026	1.433	1.948	0.148	↕	↕	Circular
2.005	1.525	0.100	0.026	0.158	0.240	0.048	0.031	1.445	2.010	0.148			Lay
5.005	4.525	0.100	0.026	0.158	0.240	0.048	0.031	4.445	5.010	0.148			↕
5.130	4.650	0.100	0.024	0.183	0.240	0.052	0.031	4.570	5.135	0.173			
23.505	23.025	0.100	0.024	0.183	0.240	0.052	0.031	22.945	23.510	0.173	0.020	0.020	↕
Cryogenic and Hot Gas Pressure-Assisted Seal (figure 9-25b)													
				b		+0.000 -0.002			+0.005 -0.000		+0.005 -0.000	+0.010 -0.020	
1.000	0.600	0.070	0.028	0.172	0.200	0.040	0.034	0.560	1.005	0.163	0.005		32 rms
1.450	1.050	↕	0.028	↕	↕	↕	0.034	1.000	1.455	↕	↕	↕	Circular
1.500	1.100		0.028				0.036	1.060	1.505				Lay
2.950	2.550		0.028				0.036	2.510	2.955				↕
3.000	2.600	↕	0.031	↕	↕	↕	0.036	2.560	3.005	↕	↕	↕	
46.000	45.600	0.070	0.031	0.172	0.200	0.040	0.036	45.560	46.005	0.163	0.005	0.020	↕

[a]Dimension increases 0.005 in. after Teflon coating
[b]Dimension increases 0.003 in. maximum after silver plating
1. See figure 9-32 for flange design
2. Duct diameter D_1 may be equal to D_2

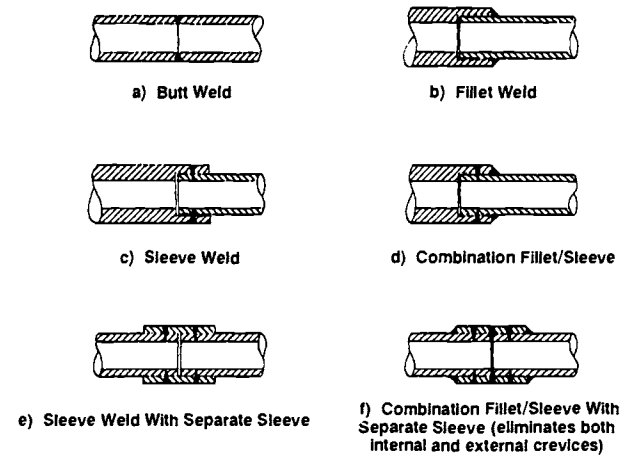

Fig. 9-26 Types of welded joints used in fluid systems.

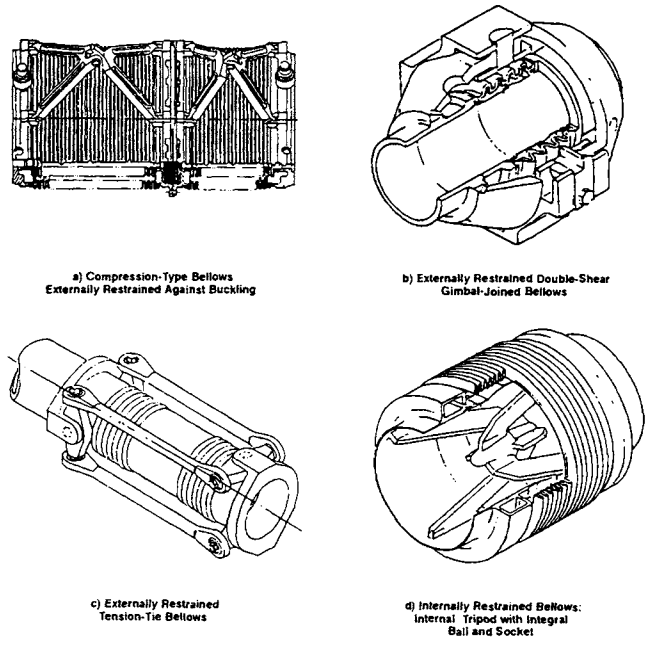

Fig. 9-27 Four examples of bellows joints.

type because of the ease of bench welding, ability to perform thorough nondestructive testing (surface penetrant inspection and X-ray), and the lack of built-in crevices. Butt-weld joints are used extensively on rocket engines including the J-2, F-1, and the SSME.

In-place joints normally used on small tube lines (< 1 in.) have the sleeve-weld configuration shown in Fig. 9-26e because of the self-aligning feature of this type joint. Sections of tubing can be cut out of a line assembly for tube repair or for installing different components or fittings by use of the in-place sleeve joint. Sleeve welds are used to join thin-wall tubing where the sleeve must be added to achieve the thickness for practical welding. They entail the following disadvantages:

- Unless all crevices can be eliminated by design, as in Fig. 9-26f, the resulting built-in crack will act as a stress raiser and lower fatigue life.
- The longitudinal forces in the tube will load the weld in shear.
- Unless all can be eliminated by design, as in Fig. 9-26f, crevices provide a collector for contaminants and corrosive materials.
- Radiographic inspection of the weld proves relatively difficult.

The F-1 engine used the combination fillet/sleeve weld (Fig. 9-26d) extensively on tube sizes of 1-in. in diam or less. The fillet was added because of line failures due to the high vibration experienced on this engine. The sleeve weld with separate sleeve (Fig. 9-26e) was predominant on the J-2 tube lines and the combination fillet/sleeve (Fig. 9-26f) was used in some instances of high vibration. When the B-nut type of coupling was used (for instrumentation lines), machined sleeve-tube stubs were attached to tubing with the welded-sleeve design of Fig. 9-26e. Weld joints are located in low-vibration areas when possible. Welds with vibration normal to the tube axis should be avoided. Clearance around the exterior of the joint must be provided for in-place welding equipment. The number of joints should be kept to a minimum consistent with overall system requirements.

9.5 BELLOWS AND FLEX JOINTS

Introduction

Bellows joints are the critical design and performance members of the flexible-line assembly. A bellows section in a line usually consists of three parts: a flexible pressure-carrying convoluted tube (the bellows), a restraint on the bellows to handle the pressure-separating load, and a provision for attaching the bellows to the line. Straight-sidewall, annularly-convoluted bellows with tension-type, pressure-separation, load-restraint linkages are the most commonly used designs. Typical bellows joints are shown in Fig. 9-27. References 9-15 through 9-25 provide recommended information on the design and use of bellows.

Different deflection modes (i.e., axial, angular, and shear) produce the same type of bending stresses in the bellows convolutions. If a bellows must deflect in all of these modes simultaneously, the sum of the deflections for all modes must be kept within acceptable stress limits. (Reference 9-26 presents methods for converting different types of bellows deflection into equivalent axial deflection.) Therefore, the duct system will be routed so as to keep all accumulated deflection stresses within the safe working stress value of the material and meet the required fatigue life.

Torsional loading (twist about the duct longitudinal centerline) should be avoided in the design and application of a duct system. When, because of design constraints, torsional loading is unavoidable, the torsional effects should be minimized by appropriate design, such as introduction of slip plates and torsional bellows or slip-limiting flanges.

If space limitations force a duct to be designed relatively short and straight, so that torsional deflections cannot be absorbed through angulation of bel-

lows joints in dog-legs of the duct, other means of permitting torsional deflection must be provided. Figure 9-27a shows a device designed to absorb torsional deflection. A tightly-formed bellows assembly, it was incorporated into the pump-inlet ducts of the J-2 engine (used on the Saturn S-II and S-IV stages) when the torsional movement of the ducts was found to be too high for the pump casings to resist.

The bellows is thin-walled (0.010 in.) and has 40 deep convolutions stacked in a 1.25-in. height. Flanges encompass the bellows and permit the application of only torsional deflections. The joint constitutes, in effect, a low-spring-rate torque tube that can absorb torsional rotation while maintaining a leak-tight enclosure.

A bellows joint in ducting can absorb motions with much smaller reaction loads than those developed in a hard line. A free bellows can absorb four kinds of motion applied to its ends: axial (extension or compression), offset (with end-planes parallel), angular (about its center), and torsional (about its axis). Typical applications may impose one, all, or any combination of these end-point motions (deflections) on a bellows. Various restraining devices or linkages are designed to limit a bellows to absorb only certain motions (e.g., a gimbal-ring linkage allows a bellows to receive only angulation). These end-point motions and the number of motion cycles that a bellows joint is designed to absorb must be specifically defined *before* the design phase.

Table 9-9 Bellows restraint-linkage selection chart.

Types of Restraint Linkages					
Type	**External Gimbal Ring**	**Internal Gimbal Ring**	**External Hinge**	**Internal Chain-Link**	**Internal Tri Pod Ball & Socket**
Design	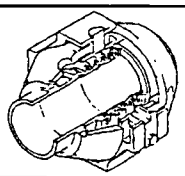	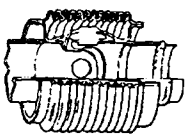	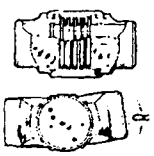	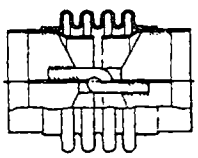	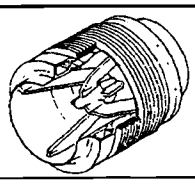
Movement Capability	Angulation in any plane	Angulation in any plane	Angulation in plane of hinge only	Angulation in any plane	Angulation in any plane
Load to Deflect	Spring rate of bellows plus bearing friction of gimbal	Spring rate of bellows plus bearing friction of gimbal	Spring rate of bellows plus bearing friction of hinge	Spring rate of bellows plus bearing friction of link	Spring rate of bellows plus bearing friction of ball and socket
Weight	Tends to be heavy due to twisting moments applied to gimbal ring	Lighter than external gimbal for a given application	Lighter than hinge	Lightest type of restraint for low pressure application	
Envelope Size	Larger than with internal gimbal ring	Bellows O.D. but must be increased slightly to allow for internal restraint	Smaller than hinge ring	Bellows O.D. itself since there is no external linkage	Bellows O.D. itself since there is no external linkage
Pressure Drop	Bellows can be fully sleeved so that loss no greater than smooth bore mitered elbow when angulated	Restraint linkage can be integrated into flow sleeve; loss factor is in 0.04 to 0.08 range	Bellows can be fully sleeved so that loss no greater than smooth bore mitered elbow when angulated	High loss factor is a function of percentage of blocked area and is in the 0.2 to 0.5 range	High loss factor is a function of % of blocked area and is in the 0.2 to 0.5 range
Principal Advantages	Affords some damage protection to bellows	Cools linkage of cryogenic joints in radiation environment	Same as gimbal ring joints except can absorb single plane motions only	Low cost; simple construction	Permits efficient tie across long line length bellows
	1. Inherently restrains pressure thrust, no guide or anchor requirements 2. Gimbal carries dead weight of ducting and other external loads 3. Transmits shear loads 4. Provides for close control of movement 5. Prevents torsion loads from being applied to bellows			1. Suitable for low velocity flow applications where pressure loss is not a factor 2. Provides lightweight tension system for low pressure applications	
Principal Uses	1. Used in pairs or sets of three to absorb large complex, multi-plane motion without imposing pressure thrust on ducting or equipment 2. Transmits weight and other loads to available support points		Same as gimbal ring joints except for single plane motion usage only	1. Used in pairs or sets of three to absorb large, complex, multi-plane motion without imposing pressure thrust on ducting or equipment 2. Transmits weight and other loads to available support points	

Table 9-9 (Cont'd) Bellows restraint-linkage selection chart.

Types of Restraint Linkages				
Type	**External Ball and Socket**	**Internal Ball and Socket**	**Braided Wire Sheath**	**PVC; External Tie Rods**
Design	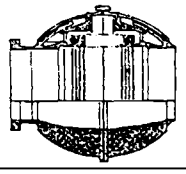	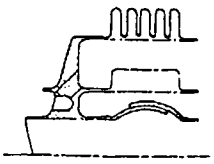		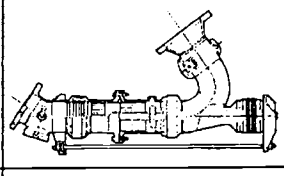
Movement Capability	Angulation in any plane	Angulation in any plane	Angulation and lateral offset	Axial movement, lateral and angular deflection
Load to Deflect	Spring rate of bellows plus bearing friction of ball and socket, large radius arm on bearing friction torque	Spring rate of bellows plus bearing friction of ball and socket	Spring rate of bellows inner core plus high friction of braid wire	Combined spring rates of bellows and linkage bearing friction
Weight	Lighter than an external gimbal ring	Lighter than an external gimbal ring	Low weight, light test tension tie device	Very low weight for a PVC type duct
Envelope Size	Smaller than external gimbal ring for a given application	Smaller than external gimbal ring for a given application	Small, only slightly larger than bellows O.D.	Smallest envelope of PVC type duct
Pressure Drop	Bellows can be fully sleeved	Restraint linkage can be integrated into flow sleeve, loss same as smooth bore mitered elbow when deflected	High, 10 to 15 times that of same ID smooth tube. No practical flow sleeve yet devised	Bellows can be fully sleeved to minimize pressure drop
Principal Advantages	1. Permits an even distribution of pressure separating load over full circumference of attaching duct 2. Offers smaller envelope than gimbal restraints		1. Angulation pivot point does not have to be carefully aligned 2. Can absorb lateral offset combined with angulation 3. Small envelope, light in weight 4. Bellows not susceptible to squirm due to braid enclosure, consequently long sections may be used when needed	1. Only externally tied-type expansion joint to absorb axial movement while still restraining pressure thrust
Principal Uses	1. Same as gimbal ring joints		1. Small diameter (< 2 in.) applications with large installation misalignments	1. To absorb axial or combined axial/lateral/angular movement where pressure thrust on equipment or anchors cannot be tolerated

These requirements largely determine the type of joint needed.

Selecting a restraint calls for weighing such factors as motion capability (modes and moments), pressure drop, weight, and envelope size. Table 9-9 gives a list of such factors. It shows ratings assigned for each of 12 restraint linkages. The table may be used as a guide in selecting, designing, or modifying a restraint mechanism. Figure 9-28 shows the configurations more clearly.

Restraints

Hinge joint. This type of joint suits applications requiring angular deflection in only one plane. The design may be of the internal- or external-hinge type and can be either single- or double-shear. Bellows sizing can be kept to a minimum with this type of restraint; flow obstructions will be minimal in the hinge design. Weight is generally low.

Table 9-9 (Cont'd) Bellows restraint-linkage selection chart.

Types of Restraint Linkages				Accessories	
Type	PVC; Concentric Bellows	PVC; Axial and Externally Pressurized Bellows	PVC; Concentric and Externally Pressurized Bellows	Type	Uses and Advantages
Design	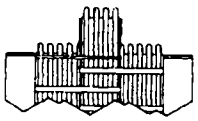	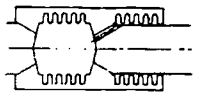	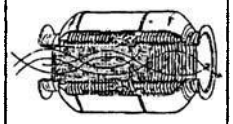	Internal Flow Sleeves	Uses 1. Have been used successfully on all of listed joints except braided wire sheath Advantages 1. Reduces pressure drop through bellows joint 2. Prevents flow induced vibration of bellows by high velocity impingement 3. Prevents erosion of bellows in abrasive service, e.g., turbine exhaust duct downstream of J-2S solid propellant turbine starter 4. Internally insulates bellows in high temperature service
Movement Capability	Axial movement only	Axial movement only	Axial and angular movement		
Load to Deflect	Combined spring rates of bellows	Combined spring rates of bellows	Combined spring rates of bellows, ball bearing friction on angulating bellows		
Weight	Heavy due to concentric bellows design	Lighter than concentric bellows design due to use of axial balancing bellows	Heavy due to concentric bellows design		
Envelope Size	Large due to concentric bellows design	Large due to annular flow path requirement	Large due to concentric bellows design	Vacuum Jackets	Uses 1. Bellows concentric to primary bellows forms vacuum jacket cavity to insulate primary line fluid Advantages 1. In cryogenic service, limits boil-off of propellant during filling operation 2. Prevents formation of liquid air on outer surface of liquid hydrogen and helium lines 3. Minimizes recirculation flow required to maintain propellant quality in cryogenic systems
Pressure Drop	High due to long unsleeved bellows	High due to changes in flow direction through annulus	Angulating bellows unsleeved causes high loss in that area		
Principal Advantages	1. Deflection cycling of duct will not produce possible performance degrading pressure surges in system because of pressure-volume compensation feature		1. Since pressure thrust is inherently restrained, the need for heavy structural reaction members is eliminated		
Principal Uses	1. To absorb large axial deflections in proportion to bellows live length where pressure thrust on equipment or anchors cannot be tolerated		1. To absorb large axial and angular deflections in a relatively short overall length	Travel Limit Stops	Advantages 1. Prevents overdeflection and possible fatigue or interference damage during processing and handling
				External Cover	1. Protect bellows against mechanical damage during installation and in service 2. Protect personnel in hazardous service 3. Serve as support for external insulation

Gimbal joint. Sometimes referred to as a universal joint, the gimbal joint may be of internal- or external-restraint design. Gimbal-jointed assemblies are used predominantly in high-pressure systems that require angular deflection in all planes and will withstand imposed torsional loads. Although the pressure drop of either design will be relatively low, internal flow sleeves should be considered in the external-restraint configuration. Both designs impose a weight penalty and the external design requires a larger envelope. Stops to prevent excessive angulation are readily adaptable to the external-restraint design. The external-restraint assembly offers the bellows excellent external protection.

Chain links. Chain-link joint has application similar to the gimbal joint, but it is recommended for use in medium-pressure systems where flow loss is not critical. It typically sees use in low-pressure, low-velocity, hot-gas exhaust systems not needing high torsional strength. Centering of the bellows with respect to the internal link joint is critical in this design. Some offset deflection may be the product of the linkage center of rotation and may generate addi-

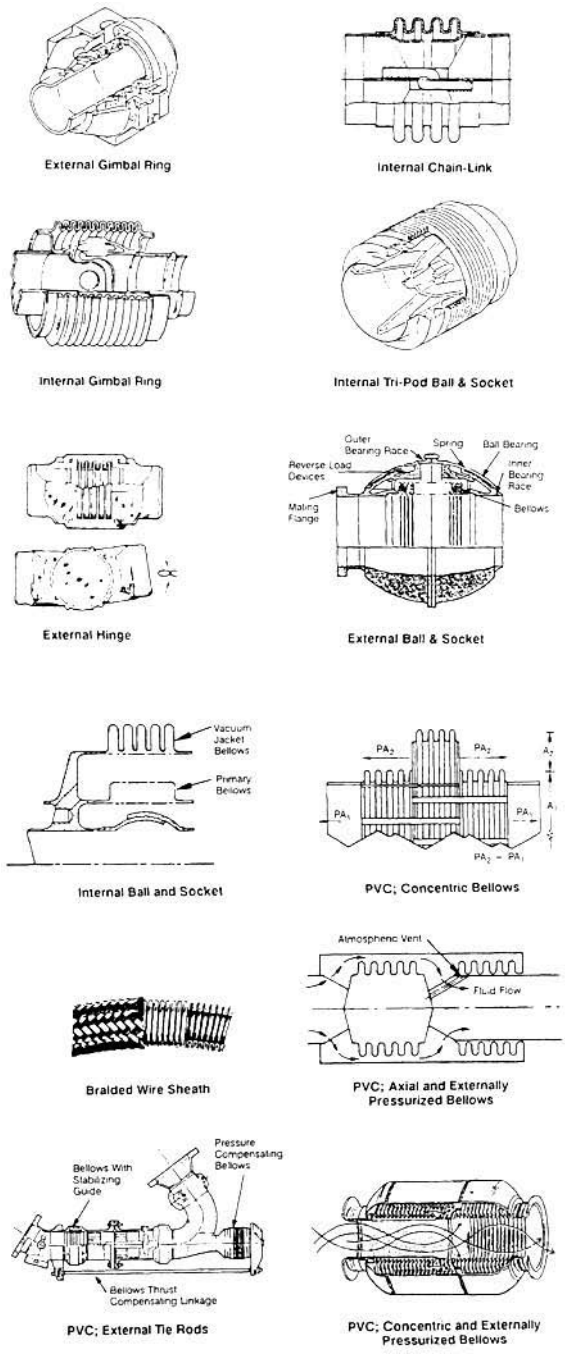

Fig. 9-28 Bellows restraint-linkage configurations.

tional loads on the bellows that must be accounted for in the joint design.

Ball joints. This type of joint design provides a gimbal-type restraint and motion while applying a uniform circumferential load in the mating assembly. The bellows in this design is enveloped with a spherical inner and outer race separated by ball bearings. The bellows can receive excellent external protection by the external-restraint assembly.

Braided-wire sheath. A braided flexible hose—an inexpensive method for a tension tie restraint—can accommodate both angular and shear deflections, and the braid acts as a vibration damper for the bellows inside. Friction between the braid and the bellows can be minimized by applying solid-film dry lubricant to the outer surface of the bellows and the inner (or all) surfaces of the braid. Care must be exercised in the selection of the dry lubricant to ensure compatibility with the end-use fluids. Flex hoses are acceptable for use in both high and low temperature and pressure extremes.

Slide joint. A slide joint is a variation of a bellows with an internal flow sleeve except that the bellows is isolated from the flow media and undergoes an external pressure differential. Flow loss with this design is negligible; and since bellows pressure is external, this type of joint is far less susceptible to squirming. It can absorb axial deflection, shear, and bending forces and can be designed to accommodate angular deflections.

Basic Types

Bellows have been used successfully in vehicle and rocket-engine ducting in a wide range of sizes under a variety of operating conditions. However, success depends on careful design, as bellows generally operate in the plastic range of the bellows material. This condition is necessary so that the wall thickness can be reduced sufficiently to produce acceptable end-restraint reaction loads with the bellows in a deflected position and to reduce weight.

The pressure-separating load on a bellows in a duct system is developed, as if the bellows were a pressure vessel with end caps, by the duct pressure reacting against a projected area across the duct bore (e.g., an elbow, an injector face, or any other reaction point in the system). Bellows have low spring rates and thus cannot withstand very-high-pressure separating loads without changing length. Therefore, restraint mechanisms to prevent this change must be used to enable the bellows to perform its function in a duct assembly.

Formed, straight sidewall bellows predominantly see use in aerospace ducting. Welded-disk bellows, the other major type, are not used in any aerospace ducting.

There are four basic types of bellows manufactured: formed, welded, machined, and deposited—the formed being by far the most predominant. Table 9-10 describes typical applications of each type. Convolution shapes are many and varied.

Table 9-10 Typical applications for bellows.

Formed	Welded	Machined	Deposited
Flexible joints for ducting	Loading element for rotary face seals	Sensory bellows	Instrumentation systems
Positive expulsion tank bladders	Surge suppressors in fluid flow systems	Servo-actuator balancing bellows	
Valve seals	Positive expulsion tank bladders	Bearing preload springs	
Innercore for braided wire restrained flexible hose	Valve seals	Check valve seal and spring	
Pressure sensing elements for regulator controls	Accumulators		
Flexible drive shaft couplings	Aneroid systems		
	Volume compensators in hermetically sealed instruments such as gyros and accelerometers		

	Convolution Shape	Axial Spring Rate	Long Stroke Capability	Resistance to Diff. Pressure
Formed				
Semitoroidal		Very high	Very poor	Very good
U-shaped		Medium	Fair	Fair
U-shaped, ext. ring support		High	Fair	Very good
U-shaped, int. ring support		High	Fair	Very good
U-shaped, ext. T-ring support		High	Fair	Very good
S-shaped		Medium	Fair	Fair
S-shaped, ext. ring support		High	Fair	Very good
Toroidal, ext. pressure		Very high	Poor	Excellent
Toroidal, int. pressure		Very high	Poor	Excellent
Welded				
Flat		Medium	Fair	Good
Stepped		Low	Good	Fair
Single sweep		Medium	Good	Good
Nested ripple		Very low	Excellent	Poor
Deposited				
U-shaped (can be varied)		Low	Good	Fair
Machined				
Rectangular		High	Fair	Excellent

Fig. 9-29 Major bellows convolutions and characteristics.

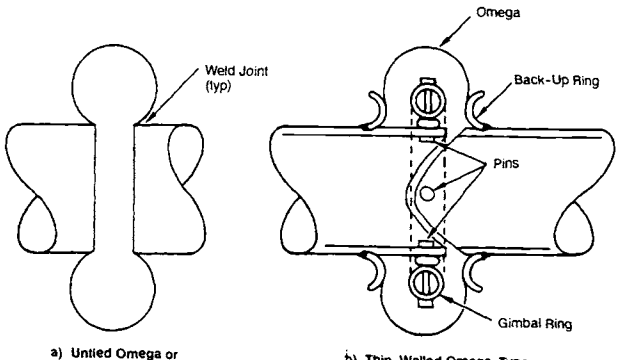

Fig. 9-30 Typical omega joints.

Figure 9-29 shows the major shapes and methods of fabrication, and gives a brief description of characteristics.

Omega joints. Omega or toroidal joints are not used extensively in aerospace ducting systems because of the difficulty in incorporating some means of selfrestraint against the unbalanced pressure force. Figure 9-30a depicts an untied omega joint; the pressure force must be restrained by the mounting structure. It has the attractive characteristic of hoop stress being a function of the omega cross-sectional and not its full diameter (Ref. 9-27).

The joint shown in Fig. 9-30b is used on the relatively low pressure (<400 psi) propellant-feed systems

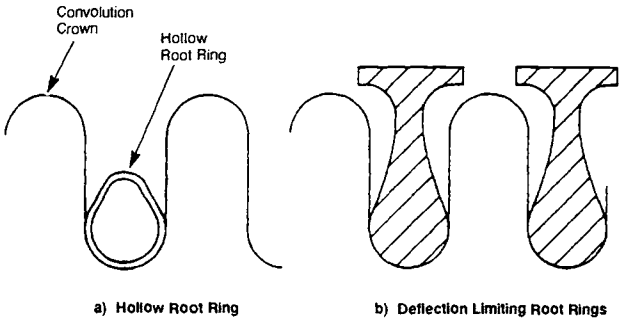

Fig. 9-31 Deflection-limiting root rings.

of the Atlas vehicle (Ref. 9-28). When using very-thin-gauge material, on the order of 0.005 to 0.010 in., it offers low deflection forces but is highly susceptible to damage.

Welded-disc bellows. In rocket engines, welded disc bellows have been limited to rotary-face-seal applications as a low-axial-travel loading element. This mechanical face-type seal incorporates a welded metallic bellows in place of the more commonly used spring and elastomeric packing. The bellows can be made from any weldable material and usually has low spring-rate, negligible hysteresis, and great compactness. It can be designed for pressure systems up to 2000 psig and temperature extremes ranging from -425 to 1500°F. The major disadvantage of welded disc bellows is that by nature of fabrication each ID and OD weld has a built-in notch that is susceptible to premature failure unless kept to low magnitudes of stress. These welds have lineal length 30 to 40 times that of a bellows made from a tube with a single butt weld. At present, no nondestructive methods can examine and verify the integrity of the ID and OD welds.

Formed bellows. Extensively used in aerospace systems, convoluted bellows serve both high- and low-pressure liquid and gas systems at high- and low-temperature extremes. They maintain positive sealing characteristics and can be designed to deflect axially, angularly, or laterally. They can be made from most available materials and in unlimited sizes and wall thicknesses. The bellows can be either single- or multiple-ply depending on the application. This type of bellows may be restrained internally or externally, or may be of the free type.

Root rings. When design pressures are high, it may be impractical to design the root of the convolution to resist the effects of pressure. Thicker bellows walls, required to resist high pressure, produce higher spring rates and attendant lower fatigue life when exposed to repeated flexings. In such cases, root rings (Fig. 9-31) are sometimes used to assist in carrying the pressure load.

The root ring must have sufficient area to carry the hoop tension loads and, if hollow, must also resist the bending loads applied to the ring wall by pressure. The deflection-limiting root rings (Fig. 9-31b) are sometimes used in aerospace ground facilities. They permit thin-wall bellows and, thereby, low

Table 9-11 Bellows design reference stresses.

Material	Sheet Thick. (in.)	Max. Bulging Stress (psi)	Max. Bending Stress (psi)	
			1,000 Cycle Life	10,000 Cycle Life
321 & 347 CRES	≤0.012 >0.012	140,000 120,000	120,000	74,000
A286	≤0.012 >0.012	200,000 160,000	200,000	120,000
Alloy 718	≤0.012 >0.012	200,000 160,000	210,000	135,000
Inconel 750	≤0.012 >0.012	200,000 160,000	165,000	105,000
Hastelloy C-276	≤0.012 >0.012	150,000 130,000	185,000	105,000
Inconel 625	≤0.012 >0.012	140,000 120,000	133,650	74,250
Inconel 903	≤0.012 >0.012	200,000 160,000	190,000	125,000

deflection forces, and prevent overdeflection by use of the rings as excursion limiters.

Machined bellows. Typically applied in instrument systems and check valves and as null-balance springs in servo-mechanisms, this kind of bellows can be machined from most materials, including aluminum, and can be designed for use at high- and low-temperature extremes and high and low pressures. Made in sizes ranging from 5/16 in. to 3 ft in diam, it can be used with an internal or external gimbal. Fatigue life will usually be high due to the absence of forming stresses and the low spring rates achieved through deep convolution machining. Wall thickness can be varied in given areas to suit design requirements.

Deposited bellows. This type of bellows usually serves the need for extremely-low spring rates. Wall thicknesses of deposited bellows can be as low as 0.0003 in. They are used mainly for instrument systems.

Rigidized tubing. This type of "bellows"—what might by termed a partially formed bellows—typcially stiffens a spool piece that separates a double-bellows joint; and it can be used in a rigid-tube assembly to accommodate slight misalignment. It has been used with great success in thin-walled double-bellows assemblies where the line assembly is subjected to handling damage.

Pressure Capability

A bellows must withstand several kinds of operational pressure: normal operating, surge, proof [(normal operating pressure + surge pressure) times safety factor], and burst (proof pressure times safety factor)

These pressures produce both hoop stresses in the bellows and stresses that tend to bulge the convolution sidewalls. The bellows must be stable and resist column buckling under the proof-pressure application.

The calculated operational stresses are very high, exceeding the yield strengths of the materials, but in reality are only index stresses and must be treated as such. Table 9-11 gives the limiting bulging stresses and allowable motion stresses (bending stresses) of frequently-used bellows materials. Cycles-life tests apply full-stress reversals at a frequency of 30-60/min.

The following expression can be used to determine additive bending stresses in the convolution crowns and roots caused by simultaneous application of pressure and deflection, assuming the maximum stress to be the one from only one of the effects:

$$\left(\frac{J_b}{J_{b,max}}\right)^2 + \left(\frac{J_B}{J_{B,max}}\right)^2 \leq 1$$

where J_b = bending stress (motion stress) and J_B = bulging stress.

The major problems with bellows in ducting on large liquid-propellant rocket engines have been the following: fatigue failures (due to mechanical and flow vibration and possibly contributed to by handling abuse), buckling stability (internal and external), corrosion, manufacturing difficulties, handling damage, and, less frequently, implosions in LOX, hydrogen, or high temperature service and bursting due to pressure surge.

Fatigue Life

The end-point motions of a flexible-duct assembly impose the largest deflections on the bellows joints within the duct. These motions, like the anticipated duty cycle, can be predicted in the design phase. With the use of this information and the S-N (alternating stress vs. number of cycles) properties for the particular materials involved, the bellows then can be designed for an adequate low-cycle fatigue life while operating under very high stresses. Since aerospace design emphasizes light weight, thin walls characterize bellows. They reduce the weight of the bellows itself and also reduce spring rates, so that the reaction loads on attaching members stay low and thus keep weight to a minimum. This thin-wall feature dictates that the bellows operate under stresses near or in the plastic range; i.e., in the low-cycle range affecting fatigue life.

Other motions imparted to the bellows come from vibrations induced mechanically or by the fluid flow. The bellows must be designed so that stresses stay below the endurance limit of the material (i.e., no reduction in fatigue life caused by vibration).

Methods for predicting flow-induced vibration inputs—as presented in Ref. 9-29 through 9-36—enable the designer to develop a bellows completely free from vibration or at least free from unacceptable levels of vibration.

Vibration susceptibility. Structural integrity must be maintained during and after the operational periods, when many types of dynamic loads may be applied to a bellows. The types of loads include those generated by the enclosed fluids (e.g., pressure surging such as Pogo, water hammer, pump oscillations, and flow-induced vibration) and those imposed by mechanical environments (e.g., sinusoidal vibration, random vibration, shock, noise, and steady-state acceleration).

Bellows experience three primary modes of vibration (Fig. 9-32): the axial or accordion mode, the lateral mode, and the mode in which the individual convolutions rotate back and forth at the inner diameter while pivoting about the outer diameter. The individual convolution mode (Fig. 9-32c) is especially noticeable in flow-induced vibration of braided hoses, where the convolution outer diameter is restrained by the braid friction and thus provides a fixed pivot point for the convolution being excited by flow forces.

For a given bellows design, the frequencies of these modes can be predicted with reasonable accuracy. The difficult problems concern determining the frequencies and amplitudes of flow or mechanical vibratory forces that may excite these modes and the possible response characteristics of the bellows to these forces.

Flow-induced vibration. Flow-induced vibration of flexible-line bellows, with resultant fatigue failure, frequently plagues lines containing fluids flowing at high velocity. In bellows, an internal flow liner has always resolved the problem by preventing impingement of the flow stream on the convolutions. However, the installation of the liner usually presents complications in design and fabrication and makes the bellows more difficult to clean. The liners themselves have sometimes failed, apparently as a result of vibration. Flow liners appear to be the best solution to flow-induced vibration, particularly if incorporated early in the design, to avoid "quick fixes" or "add-ons" that are more difficult to integrate once the duct configuration has been established.

Flow-induced-vibration analysis determines the dynamic response and fluid excitation required to cause fatigue failures associated with the individual convolution vibration-mode. The essential dynamic fact concerns the response characteristics for the individual convolution mode being the consequence of a coupling of the structural dynamics of the convolutions and the dynamics of the fluid within the convolutions. The excitation due to fluid flow within the flexible line can excite a band of response frequencies having the boundaries of the excitation frequencies proportional to velocity. The low-frequency excitations generally are associated with vortex shedding within the turbulent boundary layer. The high-frequency (and potentially much stronger) excitation is associated with a convection frequency in the turbulent boundary layer. The convection frequency is defined as the characteristic frequency associated with the fluid velocity past equally-spaced wall irregularities (the convolutions).

Acoustic loading can increase the number of degrees of freedom of a bellows system by coupling the bellows to the acoustic modes. That can propagate very significant pressure fluctuations throughout the fluid system. These acoustic resonances, in addition to producing noise, significantly increase the flow-induced stress levels, apparently owing to the acoustics resonance flow and pressure fluctuations coupling with the vortex-shedding process to produce a force amplification (see Ref. 9-31 and 9-35).

If a resonance can exist, the analysis provides a technique for estimating the energy levels associated with the resonance; and the energy available can then be translated to a stress level in the part. When the expected stress level is known, a quantitative evaluation then can be made to determine if the stress level exceeds the alternating stress that the part can withstand without high-cycle fatigue failure.

The detailed analytical methods for determining flow-induced vibration excitation and response dynamics are presented in Ref. 9-29 and 9-36. The analytical methods allow determining, with a high confidence level, the flow-induced vibration susceptibility of a given flexible-line design for a given set of operating conditions while still in the design phase. These techniques thus eliminate the need for expensive cut-and-try flow testing of prototype hardware.

Mechanically-induced vibration. The vibration-response characteristics for a given mechanical excitation input can be calculated just as for flow-induced vibration. It is relatively simple to predict flow-induced-excitation inputs, but extremely difficult to predict the mechanical-excitation amplitudes and frequencies of the components or system in which the bellows will be installed.

Double-bellows spoolpiece arrangements (Fig. 9-27c) with an undamped or unsupported span show vulnerability to vibration of the long unsupported mass from both flow-induced and mechanical excitation. The initial design of the discharge duct on the pump for a particular engine incorporated this configuration; and fatigue cracks attributed to vibration occurred in its bellows. The condition was intensified by stress raisers in the form of wrinkles found on the inside radius of the convolutions. These wrinkles were attributed to an overly small ratio of bellows convolution radius to thickness.

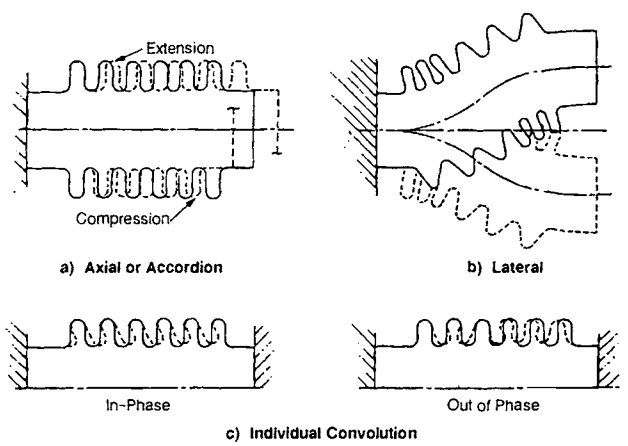

Fig. 9-32 Three primary modes of bellows vibration.

Table 9-12 Effect of parameter adjustment on bellows performance.

Parameter	To Increase/Decrease Parameter		Consequence
	Increase	Decrease	
Spring rate	Thickness of ply		Increased bending stress. Decreased bulging and hoop stress.
	No. of plies		
		Convolution height	Increased bending stress, Decreased hoop stress.
		No. of convolutions	
	Elastic modulus (other material)		Changes in other material properties. Increased bending stress.
Buckling stability	Spring rate	Live length	Increased bending stress.
Fatigue life		Bending stress	Decreased spring rate and buckling stability
		Bulging stress	
	Material fatigue resistance (other material)		Changes in other material properties
Axial deflection capacity	Live length	No. of plies	Decreased spring rate, buckling stability, and bending stress. Increased hoop stress and bulging stress.
		Thickness	
		No. of convolutions	Increased spring rate, buckling stablity, bending stress, and hoop stress.
Angular deflection capacity and offset deflection capability	Axial deflection capability		Increased spring rate, buckling stability, bending stress, and hoop stress.
		Mean diameter	Decreased spring rate, buckling stability, and hoop stress.
Bending stress	No. of convolutions, convolution height		Decreased spring rate, buckling stability, and hoop stress. increased bulging stress.
		Thickness	Decreased spring rate and buckling stability. Increased bulging stress and hoop stress.
	No. of plies		
		Thickness (without changing total thickness)	Increased bulging stress. Decreased spring rate, and buckling stability (no hoop stress change).
		Elastic modulus (other material)	Changes in other material properties. Decreased spring rate and buckling stability.
Bulging stress		Convolution height	Increased bending stress. Hoop stress and spring rate.
	Thickness of ply		Increased bending stress and spring rate. Decreased hoop stress.
	No. of plies		Increased spring rate. Decreased hoop stress.
	Thickness (without changing total thickness)	No. of plies	Increased bending stress and spring rate (no hoop stress change). Decreased bulging stress.
Hoop stress	Convolution height		Decreased bending stress, spring rate, and buckling stability. Increased bulging stress.
	No. of convolutions		
	Thickness of ply		Increased bending stress and spring rate. Decreased bulging stress.
	No of plies		Increased spring rate. Decreased bulging stress

Design of Bellows for Flexible Ducts

There are many acceptable approaches to the design of bellows, and the majority of them can reasonably predict characteristics, the most significant being the spring rate and the ability to perform for a given number of cycles, or "life." Many other factors must be taken into account as stated before, such as susceptibility to flow-induced vibration and fabricability limits.

Spring rates for multiple bellows prove particularly difficult to predict due to friction forces between plies and effects of forming techniques on the actual convolution shapes. Convoluted bellows can be made from most available materials and in an almost unlimited number of sizes and wall thicknessess. The bellows can be of single or multiple ply depending on application. To adequately design a bellows for a particular application requires knowledge of some basic elements: operating pressures, temperatures, flow rates, deflections, operating fluids (and characteristics), and a reasonable idea of the number of "safe" cycles required. The envelope limitations must be defined. One of the most significant problems will be simply identifying the governing parameters. Generally speaking, envelope will be a major concern, with the available length in a pipe and the adjacent structures dictating maximum envelope. Since ideally it will not add to the overall constraints of the engine design, the bellows will be small and light, and generate low reacting loads—in most designs. Table 9-12 offers guidance on various effects bellows geometry may have on aspects of reacting loads, life, and envelope.

Structural fatigue due to cyclic stressing—the most common mode of failure for metal-bellows expansion joints used in ducting—usually takes the form of circumferential cracks in the roots or crowns of the convolutions with consequent leakage of the contained fluid. Most bellows will have relatively short fatigue life because they are designed to operate in the plastic stress range to minimize spring rates and attendant reaction loads on connecting ducts and structure. This is specially true in missile and space vehicle applications where weight is at a premium. Low-cycle fatigue life, primarily a function of bending stress in the convolutions, will be relatively independent of steady-state stresses, such as bulging stress in side wall of convolution and hoop stresses due to internal pressure. Thus, the expected life of a new design can be approximated before fabricating and testing the part.

The envelope decided (life length and inside diameter), other parameters will have to be manipulated to conform to the desired requirements: (as a minimum) performance of the bellows and deflections to be absorbed (axial, angular, or offset). Considerations of weight and life will often dictate the material to be used, and cost and producibility of the bellows will also be factored out on the final design. In general, multiply bellows made of thick material will tax most forming equipment and methods. Reasonable lengths will prevent special material-joining techniques, which at best will add unpredictable discontinuities and increased nondestructive-testing costs. The detailed methods and examples for calculating spring rate, pressure-separating loads, friction forces, stress analysis, fatigue life, damage analysis, buckling instability, and vibration susceptibility go beyond the scope of this presentation. Publications dealing with these subjects can be found in the literature (e.g., Ref. 9-37 and 9-38.)

Bellows Restraint

Mechanical linkages. The most commonly used restraint employs the gimbal-ring joint (or universal). Other concepts include the hinged joint, ball joint, and braided sheath. Referring back to the opening section, Table 9-9 describes a broad spectrum of design.

The gimbal ring joint, the "workhorse" of bellows restraints, can be designed to withstand extremely high pressures and temperatures, allows angular deflection in all planes, and will withstand torsional loads. Stops to prevent excessive bellows angulation are readily adaptable to this design. The load-carrying pivot pins may be designed for either single- or double-shear support, the choice depending on the separating load. The same comments apply to the hinged joint, which provides angulation in one plane only.

A subtlety of gimballed bellows, sometimes overlooked even by experienced duct designers, is the fact that a gimbal (or universal) joint, when deflected about both of its axes simultaneously, produces a torsional deflection. Motion is not transmitted with a constant angular-velocity ratio unless the intersection of driving and driven components lies in a homokinetic plane. Gimbal-ring linkages do not have this type of geometry, and therefore induce a torsional deflection. The normal rigidity of gimballed bellows in torsion produces high torsional stresses.

One of the most popular and inexpensive methods for an external, tension tie restraint—the use of a braided-wire sheath, as in the case of a flexible hose—can absorb both angular and shear deflections, and acts as a vibration damper for the bellows inside. The braid restricts angular deflection under high pressure by off-center pivoting, which increases bending moments.

Friction between the braid and bellows can be minimized by an adapter, which provides clearance at the end convolutions, and by the application of solid, dry-film lubricant on the outer surface of the bellows and inner surface of the braid. Excessive friction and possible eventual galling of the journal-type pin bearings on the linkages present a problem that also can be alleviated with solid, dry-film lubricants. LOX-compatible lubricants should be used between bellows plies and on the bearings of restraint linkages in LOX systems. Data on LOX compatibility of lubricants aid a selection. If data are not available, as on a new product, LOX impact tests are performed.

Once a gimbal-ring type of bellows restraint has been selected, the question of internal vs. external mounting (Fig. 9-28) must be resolved. In general, the design will have the option of an internal or external gimbal *after* design tradeoffs have been made

on the particular application. Each type has advantages and disadvantages. The internal gimbal will be more difficult to clean, because all of the mechanisms come in contact with the flowing fluid and therefore require cleaning. Both gimbals can be "sleeved" to reduce flow losses; but the conventional internal gimbal ring design has a higher flow-loss coefficient than the external-ring, sleeved-bellows design.

If the diameter of an internal gimbal ring at least equals the duct ID, a larger-diameter bellows must encompass the linkage. The larger bellows causes a greater separating load and consequently an increase in linkage weight to carry it. A comparison of the weights of internal and external gimbal designs for a given diameter and pressure cannot be generalized, but rather must be evaluated for each individual design case.

The internal chain-tie-link joint, an economical version of the gimbal joint for small or medium pressure-separating loads, weighs less than the equivalent gimbal, but has the disadvantage of high-flow-loss factors due to the frontal area's restriction to flow. Although not suitable for use in systems with high-velocity fluids, this joint has frequently been used in the low-pressure, turbine-gas-duct systems of rocket engines. Link joints also have low torsional strength.

The chain-link joint (Fig. 9-33) does not have a fixed pivot point of the linkage. That peculiarity depends on the plane in which the joint is angulated. Since the angular deflection is evenly distributed over the live length of the bellows only when that length is centered about the pivot point, this change in pivot-point location with plane of angulation will reduce fatigue life.

With bellows restraints, both gimbal and hinge types, the bellows pressure-separating load often produces reaction in highly localized areas of the duct. Loads concentrated in a point on a member will span the cross section of the member, as described by a 30-45-deg half-angle. When the joint adjoins a flange, the duct will not have the length to allow the concentrated loads to redistribute circumferentially into the walls of the duct. Consequently, localized loads applied to the bolted flange can overload the bolts in the load area or cause deflection in the flange, possibly allowing static leakage of the joint.

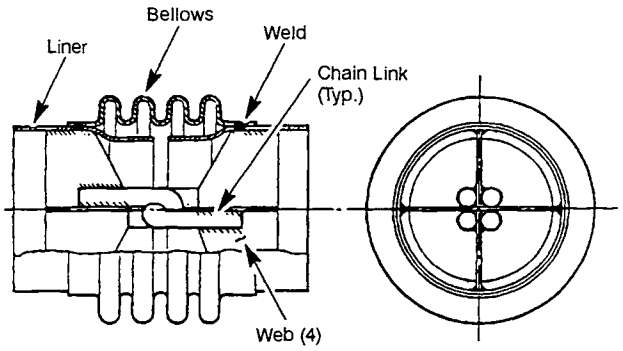

Fig. 9-33 Chain-link restraint joint with internal tie.

The SSME flexible joints incorporate internal tripod and external gimbal-ring linkages. The internal type (Fig. 9-34) serves the low-pressure pump-discharge ducts, where the pressure loss can be tolerated and the overall joint envelope must be kept as small as possible. The external type (Fig. 9-35) serves small-diameter (2.0-2.7-in.), high-pressure ducts, where the pressure losses associated with internal ties are not acceptable. The extremely high pressures and gimbal angles (up to ±13.5°) of the externally tied joints required the use of bellows' live lengths that were unstable in column buckling. This difficulty necessitated the development of a novel linkage that provided lateral support at the midspan of the bellows' live length and thereby eliminated a potential buckling instability. The geometry of the design in Fig. 9-35 ensures that the angular deflection of the joint assembly will be distributed equally between the two bellows.

The bending-moment loads required to angulate flexible-joint assemblies can be a significant factor in the design of a duct assembly and the load reactions at the installation and attach points of the duct. A gimballing duct, for example, can add a considerable force requirement to the actuators that apply the moments to gimbal an engine.

Thrust-compensating linkages. The use of a thrust-compensating bellows to offset the thrust of a primary bellows in a duct system (Fig. 9-36 and 9-37) can be considered as a form of pressure-separating,

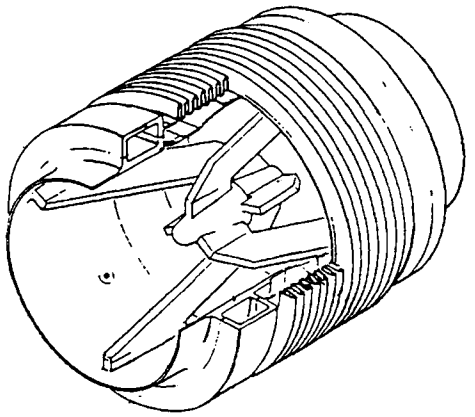

Fig. 9-34 Internally-tied tripod flex joint used on discharge duct of SSME low-pressure pump.

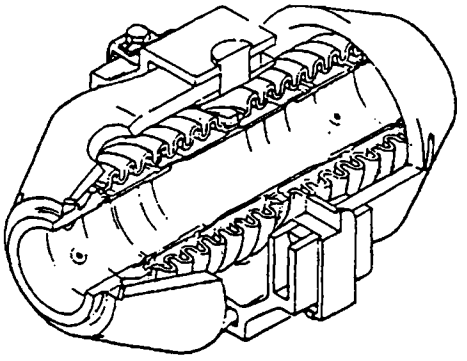

Fig. 9-35 Externally-tied gimbal-ring flex joint used on SSME high-pressure lines.

load-restraint mechanism (i.e., a thrust-compensating linkage). This type of bellows assembly allows axial deflection in the same manner as an unrestrained bellows.

The term "pressure volume compensating" (PVC) duct has come into use in describing this type of joint. This terminology is misleading, since the duct makes no pressure compensation. A more nearly correct description is "thrust compensating," because it is the axial thrust caused by the pressure separating force that is balanced by the compensating bellows. It is axiomatic that, in order to compensate for thrust, the volume must also be compensated; so this portion of the PVC description is correct. The compensating joint chiefly serves to retain a tension-type system in limited space where axial travel cannot be absorbed by angulation. By proper selection of the cross-sectional area of the balance bellows, the thrust force may be undercompensated, fully compensated, or overcompensated, so that a compressive, balancing, or tensile load gets imposed on the installation restraints.

The large (± 50%) volumetric changes incurred in straight-run gimballing ducts correspondingly incur pressure perturbations that could be detrimental to engine operation. The thrust-compensating design eliminates these pressure variations. This design concept was used in all ducts to the pump inlets of the five F-1 engines of the Saturn S-IC vehicle. As the engines respond to thrust-vector control, these ducts must deliver an axial stroke of as much as ±50% of the live length of the compensator bellows. Without the PVC feature, the volume change of the system could cause corresponding pressure pulses and variable loading on the pump inlets. Consistent engine performance depends on uniform supply of propellants to the pumps. The PVC design maintains a constant system volume under all engine-gimballing conditions.

The thrust-compensating design shown in Fig. 9-38 has axial bellows of the same cross-sectional area, with operating pressure applied to the outside surfaces of both. The internal volume of the bellows second from the left in the figure is vented to atmosphere. The outer shell over both center bellows acts as the linkage that restrains the forces separating the two. The joints on either end of the duct are of the internally-tied, angulating type and complete the utility of the duct assembly. This externally pressurized configuration permits the use of axial bellows with lower spring rate than can be used with pressure applied internally to bellows, because a given bellows design will have higher critical buckling pressure with external pressure than with internal.

Compression system. A compression system has free bellows, without tension tie linkages, that absorb the operational deflections in a duct system. The pressure-separating and spring-rate forces of the bellows then must be reacted by the mating attachment of the engine or airframe; this reaction places the ducting in compression.

In ducting systems with compression-restrained bellows (e.g., low-pressure systems), the engine or vehicle-support structure can be overloaded with moments (in bellows, shear deflections) caused by eccentric pressure-separating loads from the bellows. This problem can be minimized by aligning the thrust vector of the bellows with the reaction points of the attaching structure. If the operational deflections of the bellows are predictable and repeatable, the bellows can be installed in an opposite deflection position so that it moves toward a neutral (and lower-stress) position while in operation. Fig. 9-39 shows this type of installation.

Bellows-to-duct Attachment

The present practice of joining bellows made of thin, sometimes laminated, and often dissimilar materials to adjacent, more-massive parts requires careful manufacturing techniques. Weld fixturing for proper fitup, use of chill blocks, and automatic welding where possible must all be carefully planned, designed, and

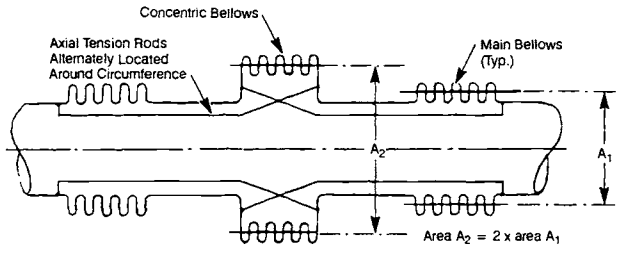

Fig. 9-37 Internal pressure on thrust-compensating linkage of F-1 pump-inlet line.

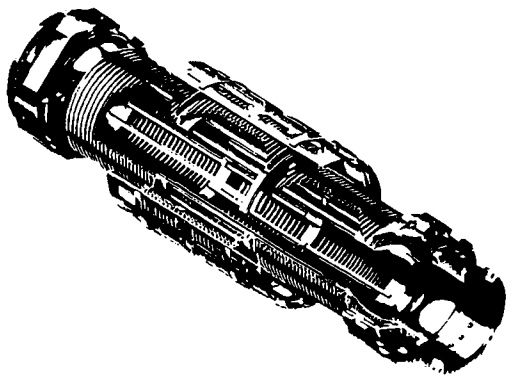

Fig. 9-36 Thrust-compensating linkage employing thrust-compensating bellows (PVC joint).

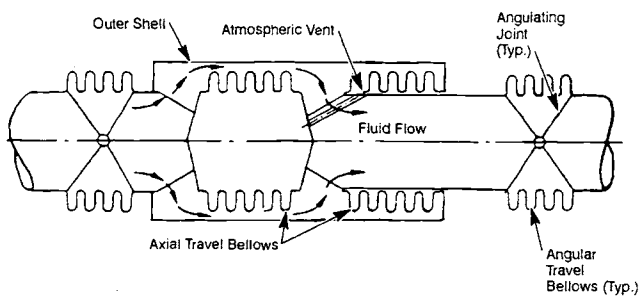

Fig. 9-38 External pressure on thrust-compensating linkage.

applied. Electron- or laser-beam welding and diffusion bonding offer advantages for joining dissimilar metals and widely different wall thicknesses in addition to minimizing the effect on heat-treat properties because of confined heat input. Heat-treatable alloy bellows can be welded to non-heat-treatable alloy ducts without disturbing the heat-treat condition in the bellows material. This attachment can be made by welding a transition section of the duct alloy to the bellows before heat treating so that the final weld to the duct involves identical alloys.

The welded junctions of bellows to ducts (usually thicker walled than the bellows) can cause high discontinuity stresses. Butt-welded connections, which are as thick as the bellows wall at the weld and gradually taper to the tube thickness, appreciably reduce stresses resulting from thermal shock. This type of welded connection also reduces discontinuity stresses resulting from radial pressure. The cobra-head hood (Fig. 9-40a) of the H-1 turbine exhaust demonstrated fatigue failure in a weld joint from thermal cycling with mechanical vibration superposed. Fatigue cracks and eventual leakage repeatedly occurred in its sandwich-joint design (Fig. 9-40b). Thermal and stress analyses of the design indicated that high cyclic thermal stresses at engine start and cutoff, due to the large temperature gradient across the laminated structure, were causing the failures. The butt-welded forged Y-ring design (Fig. 9-40c), in which laminations of material in a high-heat-flux region are eliminated (to reduce the thermal gradient) and all welds are Class I, proved to be the design solution, as demonstrated by successful test evaluation.

Resistance seam welding, although the least expensive and quickest way to join thin-wall bellows to thin-wall ducts (<0.090-in. wall), does present some problems. During the circumferential seam-welding operation, the clearance between the mating parts is gathered into a single large gap as the roller electrodes approach the 360-deg closeoff point (Fig. 9-41). Too large a gap will prevent the electrodes from forcing the two parts together for an adequate weld. Close fitup (i.e., careful sizing of the parts to be joined) and intermittent resistance spot welding around the circumference of overlapping parts before welding constitute a fundamental requirement for a structurally acceptable joint. Lap resistance welds also lack a conclusive nondestructive-test method for proving adequacy. Radiography can be used, but the film is difficult to interpret because of the built-in cracks adjacent to each side of the weld nugget.

Fusion butt-welds (burndown) welds are preferable to resistance welds, but require very accurate jigging and tooling to align the butting edges. Butt welds can be inspected radiographically, and they are structurally superior to resistance welds, since the weld is loaded in tension, not in shear, as in the resistance type.

Joining bellows to ducting sometimes unavoidably must employ induction brazing, a useful method when the joint otherwise proves inaccessible.

Flow Liners

Internal liners (sleeves) for bellows solve the problem of fatigue failure brought about by flow-induced vibration. Liners also can reduce the pressure loss of a bellows joint. They have been used as structural members supporting tube coils in the engine heat-exchangers. The liners themselves are not without problems, however. Liners must be designed such that, with the bellows at the maximum limits of excur-

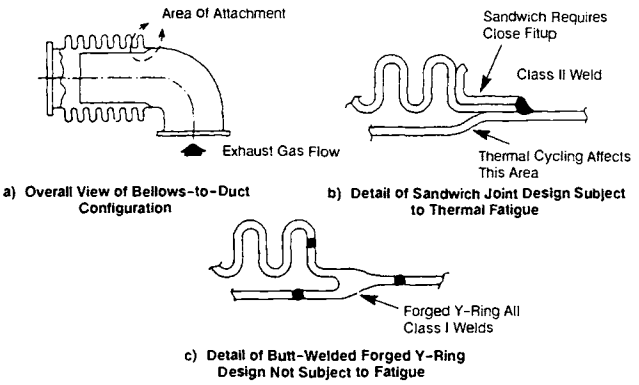

Fig. 9-40 Design change to preclude fatigue failure of bellows-to-duct attachments on H-1 turbine exhaust.

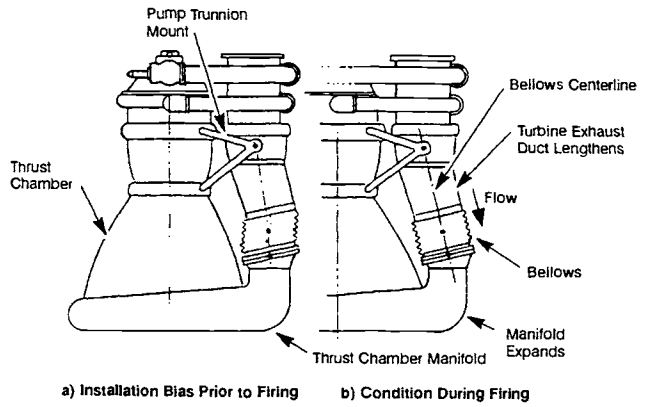

Fig. 9-39 Installation of compression bellows to minimize loading on support structure.

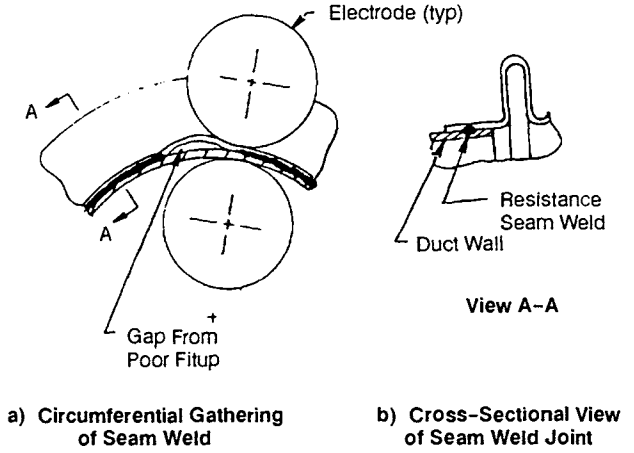

Fig. 9-41 Fitup problem with resistance seam welding of thin-wall ducts.

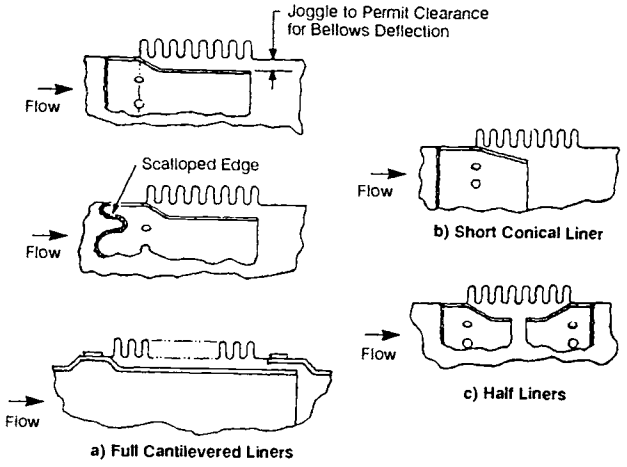

Fig. 9-42 Typical flow-liner configurations.

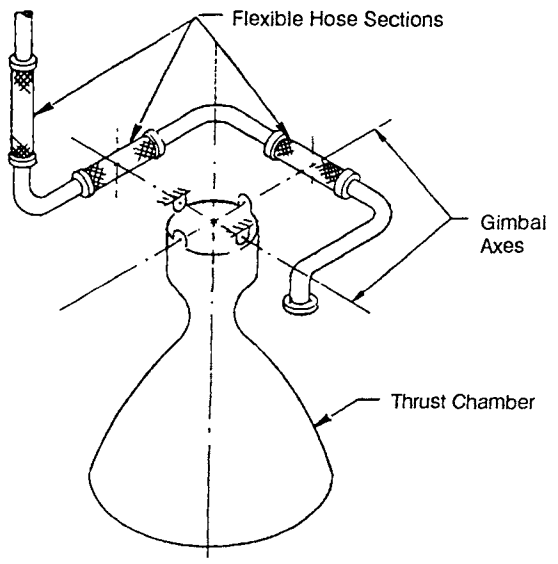

Fig. 9-43 Gimbal-plane wraparound hose configuration.

sion, they will not bottom out or bind on the bellows or ducting; and they also should be designed with drain holes located as near as possible to the weld attachment to allow the removal of cleaning fluids and contaminants. Figure 9-42 shows typical flow-liner configurations.

Liners in which cracks appeared in the trailing edge and in the weld joint have exhibited fatigue failure attributed to vibration modes of the cantilevered end of the sleeve. Increasing the wall thickness, which increased the rigidity of the liner, solved this problem.

Liners have collapsed from pressure on the outer diameter exceeding that on the inner diameter. Collapse was attributed to sudden changes in flowrate that cause a differential static pressure across the liner wall. Since liner usually has a diameter smaller than the attaching duct's, the liner section behaves like a venturi, and rapid changes in flowrate cause static-pressure changes in the liner section. If the static pressures on either side of the liner do not stabilize quickly, a momentary differential can be induced on the liner wall and cause collapse. Vent holes in the liner can relieve some of this pressure differential, or the liner can be strengthened to withstand the applied load.

9.6 FLEXIBLE HOSE

The industrial experience in braided flexible hose provided a starting point for advancing the technology to the state required for space-vehicle applications. However, as in the case of bellows joints, pressure ratings in the sizes needed were unheard of—for example, the procurement of commercial braided metal hose of 3.0- and 3.5-in. diam made of 321 CRES for 750-psi operational pressure in the original Atlas-booster engine design. This pressure level greatly exceeds the commercial rating and left little or no margin of safety. These hoses, however, were used for initial engine tests, and pressure ratings eventually were increased by modifying the design to meet aerospace requirements. Thousands of hoses in this size have now been used for both cryogenic-oxidizer and hydrocarbon-fuel applications in rocket engines.

Routing

The same practices for routing ducts or lines generally apply to assemblies of braided flexible hose, except that all systems are of the tension type. The designer wants a minimum number of flexible sections in an assembly, and positions them to achieve the maximum line motion possible with minimum motion of the flexible section.

Figure 9-43 shows a typical configuration for flexible-hose assembly that displays sound design practice. The assembly is for a rocket engine with a thrust-chamber head-mounted gimbal used for thrust vector control. The entire wraparound lies in the gimbal plane. For two of the three flexible sections, the longitudinal centerlines lie in the gimbal plane. The center of the live length of each of these two flexible sections is located on each of the gimbal axes. A third flexible section is located in the vertical leg to provide universal motion of one end of the line with respect to the other. When the gimbal motion is fixed and limited to two planes normal to each other (including corner angle), the third (vertical) hose may be omitted, with consequent savings of weight and reduction of envelope. This method of locating the flexible sections limits their motions to the gimbal angle only, thereby minimizing bending stresses and attendant fatigue.

Hoses not inherently stiff enough to resist motions imparted by mechanical vibration or undesirable displacements due to acceleration loads can be given clamps and support brackets, strategically located, as dampers.

Other configurations have been used for crossing the gimbal plane when lack of available installation space prevented the wraparound approach. The engine-to-vehicle interface flex lines of the J-2 engine are a case in point. These lines were arranged in L-shaped routing configurations with a section of braided flexible hose in each leg of the L shape.

A considerable amount of test data has been accumulated on the flow losses through flexible metal hoses (Ref. 9-39 through 9-41) and used in the design phase of a new application. The pressure drop in a convoluted inner core is 10 to 15 times as much as for a hard tube of comparable diameter. Bends in flexible hose elements are avoided where possible. The references show that, for comparable geometries, the ratio of the pressure-loss factor for a convoluted elbow to straight convoluted section greatly exceeds the ratio of pressure loss factor for plain tube elbow to straight tube. In addition to the pressure-drop disadvantages, the bent flexible configuration maintains a steady-state deflection stress on the part in an installed position that can adversely influence fatigue life.

Sizing

Current practices in sizing flexible hose involve the same general considerations used for sizing lines. Analyses of pressure loss (Ref. 9-39 through 9-41) and flow-induced vibration (Ref. 9-30 through 9-36) are better methods for avoiding problems with either phenomenon.

As standard design practice, manufacturers of flexible metal hose make the innercore ID greater than the attaching tube's ID. This procedure introduces expansion and contraction losses that must be traded off against hose pressure losses for an acceptable total loss.

Inner-core Behavior

Analysis of flexible-hose innercore for flow- and mechanically-induced vibration follows the attack for bellows, with the exception that the braid restrains the convolutions to vibrate individually. Other considerations for flexible hoses, such as pressure capability and corrosion resistance, are similar to those for bellows.

Temperature extremes experienced by components in a rocket-engine system usually will exempt a nonmetal hose from consideration. Even if the hose qualifies otherwise to convey a particular fluid, proximity to hot or cold running components, placement in view of the exhaust plume, exposure to exhaust blowback, a test stand fire, or exposure to cryogenic temperature could cause failure of a nonmetal hose. These adversities seldom pose problems with metal hoses.

The methods of stress analysis for bellows also apply to annularly-convoluted metal innercore, the predominant type of pressure-carrying member in aerospace flexible hoses. However, it cannot be assumed that the total live length will be active in bending. The "Chinese finger trick" effect of the braid, which causes a compressive load on the innercore OD, plus the bottoming out of the braid wires in bending, do not permit a smooth arc (constant-radius) deflection of the innercore.

The moment required to bend a flexible hose may affect adjacent components. For example, lowering the bending moments of flexible hoses that cross the engine gimbal plane reduces the actuator

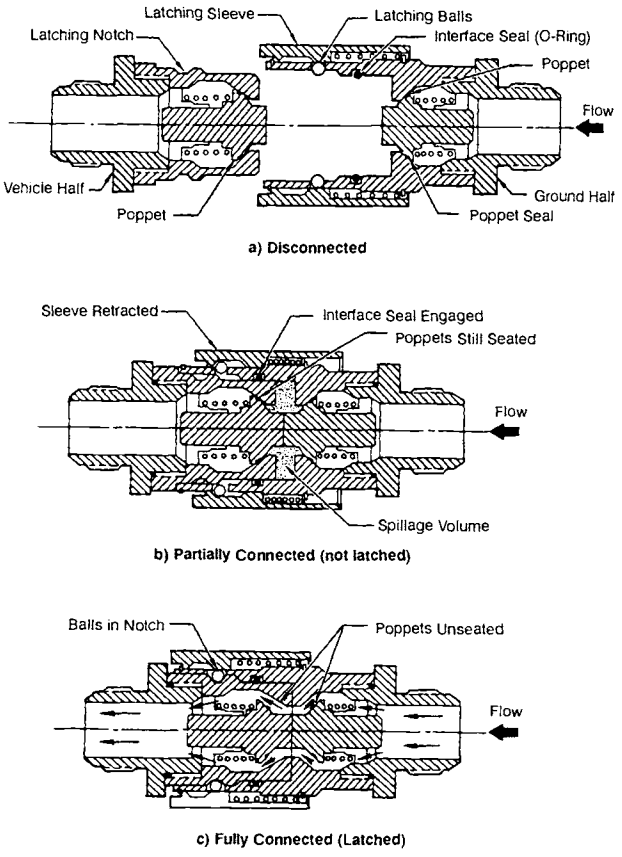

Fig. 9-44 Three stages of operation of a typical manually-operated disconnect.

loading needed to gimbal the engine. Lubricants applied to braid wires and the outer surfaces of the innercore reduce bending moments. Compressing the innercore axially before installing the braid results in more convolutions per inch and a lower bending stiffness at the expense of increased weight and material cost. Innercore compression also improves the ability of the hose to withstand pressure impulses.

Buckling stability in the design of flexible hose does not draw the concern it does for bellows. The support that the braid provides for the innercore prevents buckling unless end attachments (on installation) prevent the braid from pulling taut when the hose is pressurized.

Manually operated disconnects normally contain a check or shutoff valve in each half; the valve is forced open mechanically by the connecting operation. Figure 9-44 illustrates this action. In some applications (e.g., purging from the ground) a pressure-actuated valve may be used in the vehicle half. Figure 9-44 shows the spillage volume in a typical manually-operated disconnect design.

9.7 GIMBAL-MOUNT ASSEMBLIES

Gimbals permit the engine to be angulated for thrust-vector control of the vehicle. Most turbopump-fed engine systems (Fig. 3-2, 3-4, and 9-1) have gimbals that are universal joints with provisions for mounting

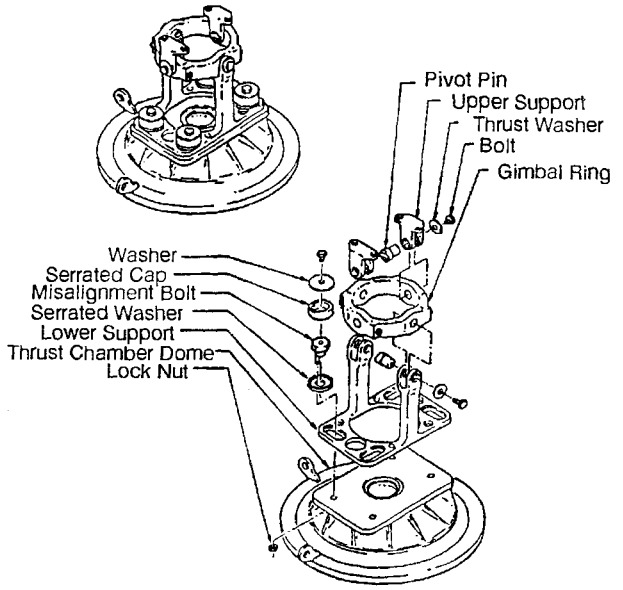

Fig. 9-45 Typical ring-type gimbal mount designed for low-thrust, upper-stage engine.

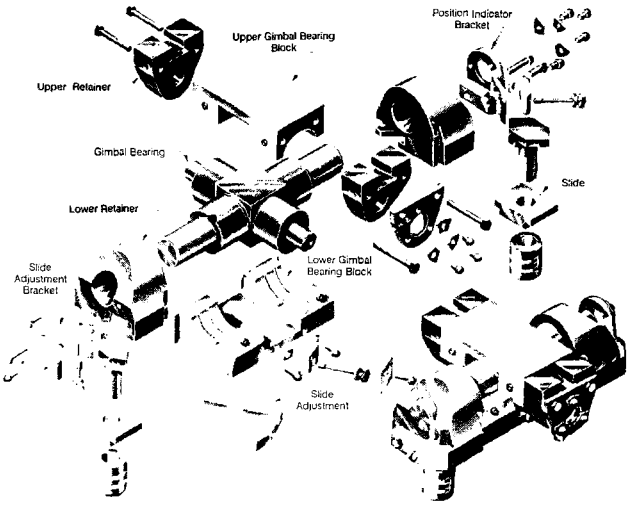

Fig. 9-46 Typical cross-type gimbal mount designed for medium-thrust engine.

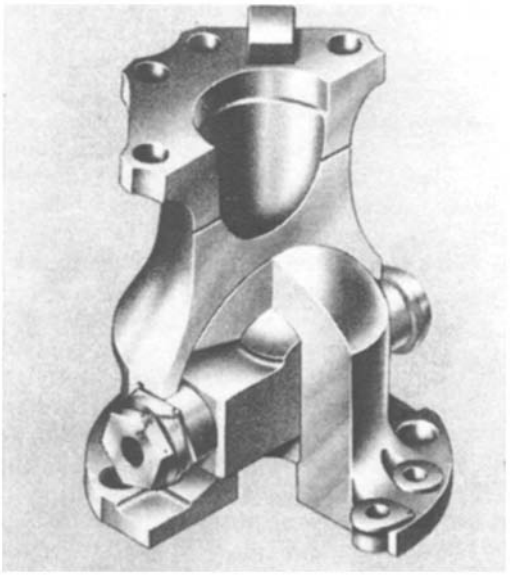

Fig. 9-47 Spherical-type gimbal bearing assembly.

normally at the vehicle interface on one side and the engine on the other side. In addition to the angulation function, the gimbal must transmit engine thrust and all resulting loads to the vehicle. The angulation is accomplished through the incorporation of bearing surfaces within the gimbal. Common types of gimbals are ring type, as shown in Fig. 9-45, cross type, as shown in Fig. 9-46, and spherical type, as shown in Fig. 9-47.

Design of Gimbal Mounts

The following primary design considerations affect gimbal mounts:

1) Angulation. Pivotal movement will be required of engine assembly or thrust chamber for thrust-vector control, generally ranging from ± 4 to ± 12 deg.

2) Thrust alignment. Design features must enable lateral offset at the gimbal-engine interface for thrust-vector alignment with respect to the engine centerline. Adjustment capability normally ranges from $\pm$ 0.10 to $\pm$ 0.4 in.

3) Loads. As derived from engine thrust requirements and engine configuration, side loads and moments must be transmitted through the gimbal to the vehicle.

4) Operation life. Generally 1000 complete cycles will be made at maximum angle, i.e., total of 40-deg excursion for a 10-deg gimbal angle. Reusable engines have higher cycle requirements.

5) Bearing surfaces. The designs must have minimum deflection of bearing surfaces and adequate bearing area to prevent bearing-surface damage.

6) Propellant-duct installation. Some gimbal designs require a propellant duct to pass through the gimbal.

7) Maintenance of the gimbal. Some gimbals require reapplication of a lubricant to the bearing surfaces; others have antifriction bearings or bearing inserts that are maintenance-free. Gimbal boots may be required to protect the bearing surfaces from dust, water, and foreign materials.

8) Weight. High-strength-to-weight materials help lessen the weight impact on the vehicle.

Ring-type gimbal mount. The ring-type gimbal shown in Fig. 9-45 was designed for a low-thrust, upper-stage engine. The design has a closed-yoke, flow-through, ring-type gimbal with plain-bearing pivot joints. This configuration allows the main oxidizer duct to pass through the assembly in the longitudinal axis to the thrust-chamber dome. The gimbal mount was designed to connect the vehicle on one interface and the engine thrust-chamber dome on

the other interface. The lower support of the gimbal mount provides an adjustment mechanism for thrust-vector alignment. Except for the steel pivot pins and the alignment bolts, all other parts can be made of either aluminum or titanium alloys for minimum weight. The bearing surfaces of the pivot pins should be chromium or electroless-nickel-plated. Solid, dry-film lubricant or grease coatings are applied to all bearing surfaces. The design bearing pressure of this gimbal type runs about 10,000 psi of bearing projected area. The bearing coefficient of friction is about 0.08.

Cross-type gimbal mount. Figure 9-46 shows the design of a typical cross-type gimbal mount used on medium-thrust engines (up to 200,000 lb). Here, the gimbal mount secures the engine assembly to the vehicle thrust frame and is mounted to the thrust-chamber dome and elbow assembly. It consists of a cross-shaped unit incorporating bearing surfaces, upper and lower gimbal-bearing blocks, upper and lower retainers, and thrust-vector-aligning slides. All parts of this design are made of 4340 alloy steel. The bearing surfaces of the cross unit are chromium or electroless-nickel-plated. The bearing surfaces of the blocks and retainers are phosphate-treated. Solid-film dry-lubricant coatings are applied to all bearing surfaces, with grease providing supplemental lubrication. The design bearing pressure of this type gimbal mount ranges from 15,000 to 27,000 psi of bearing projected area. The bearing coefficient of friction varies between 0.06 and 0.10.

Spherical-type gimbal mount. Figure 9-47 shows a spherical gimbal mount designed for the SSME; and similar designs have been used on engines with thrust up to 1,500,000 lb. The gimbal is bolted to the vehicle on one side and to the engine powerhead on the other. The unit consists of a lower body with a spherical protrusion and an upper seat with a spherical socket. A center block and shaft transmit side and torsional loads. Spherical bearing surfaces receive the engine-thrust load. All parts are made of 6 AL-6V-25n titanium heat-treated to provide an ultimate strength of 175,000 psi. A Teflon-fiberglass-composite insert bonded to the spherical socket provides a low-friction bearing surface. The shaft and block bearing surfaces are coated with a dry-film lubricant. With the bearing insert and dry-film lubricant, the gimbal does not require additional lubrication. The design bearing pressure for the bearing insert extends to 28,000 lb/in.^{2} and for the dry-film lubricant, to 20,000 lb/in.^{2} of bearing projected area. The coefficient of friction varies between 0.06 and 0.10 for the dry-film-lubricant coating and between 0.02 and 0.10 for the Teflon-fiberglass insert at 75°F. The coefficient of friction increases to 0.20 at -100°F and lower temperatures. Friction at low temperature can be a concern if the gimbal is mounted on a component carrying a cryogenic propellant that produces a temperature soak-back condition or if operation occurs in a cold space environment.

The lateral adjustment for thrust alignment can be done by eccentric bushings with the required offset machined into the bushings based on engine hot-fire data. In another common adjustment, this type of gimbal will be given a tongue-and-groove arrangement between the lower gimbal body and the thrust-chamber dome.

9.8 REFERENCES

9-1. Sverdrup, N. M., "Theory of Hydraulic Flow Control," *Product Engineering*, Vol. 26, No. 4, April 1955, pp. 161-176.

9-2. Morgan, P. G., Saunders, A., and Rajah, M., "Measurement of Pressure Drop in Fluid Flow," *The Engineer*, London, England, Vol. 214, Feb 23, 1962, pp. 359-360.

9-3. Beij, K. H., "Pressure Losses for Fluid Flow in 90° Pipe Bends," Res. Paper RP1110, *J. Res. Natl. Bur. Std.*, Vol. 21, Jul 1938, pp. 1-18.

9-4. Fowler, H.S., "Design of Power Plant Ducting," Rep. ME-208, National Research Laboratory, Ottawa, Canada, May 11, 1954.

9-5. Ginzburg, I.P., *Applied Fluid Dynamics* (translated from the Russian), NASA TT F-94, 1963. (Available from OTS, U.S. Department of Commerce.)

9-6. Lamb, O. P., and Holdhusen, J.S., "Investigation of Aircraft Ducting Components at High Subsonic Speeds," WADC Tech. Rep. 56-187, Fluidyne Engineering Corp., Sep 1956.

9-7. Howell, G. W., and Weathers, T.M., *Aerospace Fluid Component Designers' Handbook* Vol. I, Rev. D, RPL-TDR-64-25 (AD 477995L), TRW Systems Group, Redondo Beach, Calif., Feb 1970.

9-8. SAE Aerospace Recommended Practice No. 735.

9-9. Pfleiderer, C., *Die Kreiselpumpen fur Flussigkeiten and Gas,*. Springer-Verlag, Berlin, 1955, pg. 73.

9-10. Ito, H., and Imai, K., "Pressure Losses in Vaned Elbows of a Circular Cross Section," *Journal of Basic Engineering, Transactions ASME*, Series D, Vol. 88, 1966, pp. 684-685.

9-11. Daniels, C. M., and Pelton, H. A., "Pressure Losses in Hydraulic Branch-Off Fittings," *Product Engineering*, Vol. 30, No. 29, Jul 20, 1959, pp. 60-61.

9-12. Campbell, J. E., "Fundamental Characteristics of High-Performance Hydraulic Systems," USAF Tech. Rep. 5997, USAF Air Material Command, Jun 1950.

9-13. Daniels, C. M., and Fenton, R. E., "Pressure Loss Factors for Internally Linked Bellows Joints," *Machine Design*, Vol. 33, No. 19, Sep 14, 1961, pp. 187-189.

9-14. Anon.: "Dynamic Analysis of Longitudinal Oscillations of SM-73B Stage 1 (POGO)," CR-64-71

(bsd TR65-179), The Martin Co., Denver, CO, Mar 1964.

9-15. Trainer, T. M., Hulbert, L. E., Lestingi, J. F., Keith, R. E., et al., "Final Report on the Development of Analytical Techniques for Bellows and Diaphragm Design," Tech. Report No. AFRPL-TR-68-22, Battelle Memorial Institute, Columbus Laboratories; Air Force Rocket Propulsion Laboratory, Edwards Air Force Base, CA, Mar 1968.

9-16. Gerlach, C. R., Bass, R. L., Holster, J. L., and Schroeder, E.G., "Flow-Induced Vibration of Bellows with Internal Cryogenic Fluid Flows," Interim Tech. Rep. No. 2 (Contract No. NAS8-21133), Southwest Research Institute, San Antonio, TX, Aug 1970.

9-17. Salzmann, F., "Ueber Die Nachgiebigkeit Von Wellrohrexpansionen," Schweiz Bauztg. Band 127, N. R. 11, Mar 16, 1946, pp. 127-130.

9-18. SAE SC-9D Committee, "Aerospace Vehicle Cryogenic Duct Systems" SAE ARP 735, Aug 15, 1966.

9-19. Anon., *Design of Piping Systems,* M. W. Kellogg Co. Second Edition, Wiley, New York, 1956, pp. 210-230.

9-20. Matheny, J.D., "Bellows Spring Rate for Seven Typical Convolution Shapes," *Machine Design*, Vol. 34, No. 1, Jan 4, 1962, pp. 137-139.

9-21. Howard, J. H., "Designing with Metal Bellows," *Machine Design*, Vol. 26, No. 1, Jan 1954, pp. 137-148.

9-22. Northdurft, N., "Eigenschaften von Metallbalgen," *Regelungstechnik*, Vol. 5, No. 10, Munich, Germany, Oct 1957, pp. 334-338.

9-23. Anon., "Analysis of Metallic Expulsion Bellows Design," Rep. No. 8230-933014 (Final Rep. on Contract NAS7-384), Bell Aerosystems Co., Div. of Bell Aerospace Corp., Niagara Falls, NY, Feb 1968.

9-24. Matt, Richard J., "High Temperature Metal Bellows Seals for Aircraft and Missile Accessories," Paper No. 62-WA-25, ASME, New York, NY, Nov 25-30, 1962.

9-25. Anon., "Investigation of System Components for High Chamber Pressure Engines," Rep. 5329.F, Section VIII on Bellows (NAS8-5329), Aerojet-General Corp., Sacramento, CA, May 1964.

9-26. Daniels, C. M., "Designing for Duct Flexibility with Bellows Joints," *Machine Design*, Vol. 31, No. 21, Oct 15, 1959, pp. 146-156.

9-27. Dahl, N.C., "Toroidal Shell Expansion Joints," Paper No. 53-APM-30, ASME, New York, 1953.

9-28. Kin, K. M., "Design of Bellows," Rep. No. PSD-12, GD Astronautics Div. of General Dynamics, San Diego, CA, Mar 7, 1962.

9-29. MSFC Spec 20M02540; "Assessment of Flexible Lines for Flow Induced Vibration," NASA Marshall Space Flight Center, Huntsville, AL.

9-30. Gerlach, C. R., "Study of Minimum Pressure Loss in High Velocity Duct Systems," Quarterly Rep. 2 (NAS8-21133), Dept. Mech. Sci., SRI, San Antonio, TX, Nov 3, 1967.

9-31. Gerlach, C. R., "Study of Minimum Pressure Loss in High Velocity Duct Systems," Quarterly Rep. 3 (NAS8-21133), Dept. Mech. Sci., SRI, San Antonio, TX, Feb 5, 1968.

9-32. Gerlach, C. R., "Study of Minimum Pressure Loss in High Velocity Duct Systems," Quarterly Rep. 4 (NAS8-21133), Dept. Mech. Sci., SRI, San Antonio, TX, May 3, 1968.

9-33. Gerlach, C. R., "Study of Minimum Pressure Loss in High Velocity Duct Systems," Quarterly Rep. 5 (NAS8-21133), Dept. Mech. Sci., SRI, San Antonio, TX, Aug 6, 1968.

9-34. Gerlach,C. R., and Schroeder, E. C., "Study of Minimum Pressure Loss in High Velocity Duct Systems," Interim Tech. Rep. 1 (NAS8-21133), Dept. Mech. Sci., SRI, San Antonio, TX, Jul 16, 1969.

9-35. Gerlach, C. R., et al., "Bellows Flow-Induced Vibrations and Pressure Loss," Final Report (NAS8-21133), Dept. Mech. Sci., SRI, San Antonio, TX, April 1973.

9-36. Sack, L. E., "Avoiding Fluid-Line Failure in Bellows and Convoluted Tubing," *Machine Design*, Vol. 43, No. 13, May 27, 1971, pp. 68-71.

9-37. Anon., "Liquid Rocket Lines, Bellows, Flexible Hoses, and Filters," NASA Space Vehicle Design Criteria Monograph, NASA SP-8123, April 1977.

9-38. Anon., "Liquid Rocket Disconnects, Couplings, Fittings, Fixed Joints, and Seals," NASA Space Vehicle Design Criteria Monograph, NASA SP-8119, Sep 1976.

9-39. Daniels, C. M., "Pressure Losses in Flexible Metal Tubing," *Product Engineering*, Vol. 27, No. 4, April 1956, pp. 223-227.

9-40. Daniels, C. M., and Fenton, R. E., "Determining Pressure Drop in Flexible Metal Hose," *Machine Design*, Vol. 32, No. 21, Oct 13, 1960, pp. 195-198.

9-41. Hawthorne, R. C., and von Helms, H. C., "Flow in Corrugated Hose," *Product Engineering*, Vol. 34, No. 24, Jun 10, 1963, pp. 98-100.

Engine Systems Design Integration

10.1 SYSTEMS ENGINEERING

The foregoing chapters have covered design of the major liquid-propellant rocket engine subsystems and their components. These subsystems fulfill a useful purpose only when integrated into a whole where they function as a system and generate the designed thrust. Although viewing the complete rocket engine as *the* system, the designer should not lose sight of the fact that, to the *stage* builder, the engine is again a subsystem. In fact, to the launch-vehicle systems engineer, the stage in turn becomes a subsystem, in addition to other stages, ground-support equipment, launch facilities, downrange stations, etc.

An earlier chapter defined the major engine parameters requiring optimization during rocket-engine design. Clearly the subsystems discussed will not form an optimized complete system unless they are designed for one another with this goal in mind from the beginning. The subsystems presented in the foregoing chapters have become highly specialized fields during recent years. Their designers and developers often have only a rather general feeling for the functions and peculiarities of the other subsystems. Their concentrated effort will not come about unless guided by an important function: systems engineering.

In most rocket-engine projects this function is assigned to the "systems engineer," commonly called the "project engineer" or "project manager." In conformance with user requirements, the systems engineer has the job of establishing all ground rules and performance parameters (see Chapter 2). He/she subsequently optimizes them through complete integration of all subsystems during the entire design and development period.

Because of the interaction of funding, time, and reliability (previously discussed), the project engineer must be a good manager, in addition to having engineering qualifications. The project engineer needs to have adequate authority, commensurate with his or her responsibilities, from superiors. The project engineer must have a broad and thorough understanding of the various disciplines governing the design and development of the subsystems. In view of the latter's high specialization, the project engineer cannot be expected to have a complete education in all these disciplines. However, in the words of Du Pont's Crawford H. Greenewalt, the project engineer must have "the ability to create a harmonious whole out of what the academic world calls dissimilar disciplines," and that in this respect this job may be compared to that of a "symphony conductor under whose hand a hundred or so highly specialized and very different talents become a single effort of great effectiveness."

The job of systems integration does not merely ensure that all parts physically fit together, although this certainly is a basic requirement. Wherever parts and subsystems join, an interface exists, i.e., a demarcation line between these systems. This interface may be a bolt-hole pattern; a flow of fluid, heat, or electrical current; an exchange of forces, loads, or torques; or a complex dynamic interaction.

The word "aerospace" has become synonymous with systems engineering. Over the years it has been increasingly stressed. Figure 10-1 shows the final configuration of an F-1 engine, used in the Apollo Program. Comparing this to Fig. 2-4 will reveal the progress made through good systems engineering. However, to have designed and developed a good-looking, perfectly-functioning rocket engine is not enough.

It may seem superfluous to state that the design of a rocket engine must also consider the vehicle application. Yet, in problem solving, and in engine detail design and development, this application is easily forgotten. The rocket engine/component designer and developer who can think and converse in terms of vehicle application will be sought after indeed, as will the company represented by that designer.

Rocket-engine design for a particular vehicle application is a consideration not only for vehicle flight or for optimum mission performance but also for the many details of integration into the flight vehicle. After the engine has been designed and developed, and long before the first flight, it must be installed. The facets of engine installation in a vehicle range from the more complex areas, such as guidance-loop compliance and prestart conditioning, to simple "nuts and bolts" problems, such as matching, connecting, fitting dimensions, and attachment-bolt sizes.

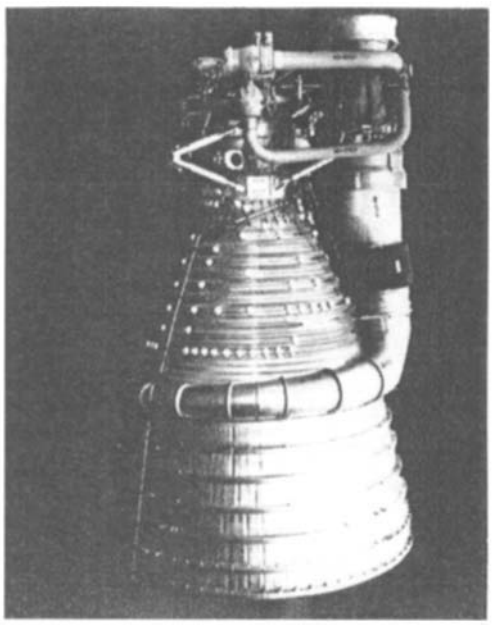

Fig. 10-1 F-1 engine.

We can easily realize the importance of continuous and close communication between the engine design team and the vehicle design team. Complete and free exchange of correspondence, documentation and progress reports, frequent design reviews, and, above all, prompt notification of changes are vital. A close simulation of the flight-vehicle configuration when performing static engine-development tests will materially reduce the possibility of later "surprises." Each vehicle type, according to its mission, will have somewhat different interface problems. Many of these problems occur, however, in almost any vehicle type.

10.2 ENGINE SYSTEM DYNAMIC ANALYSIS

System dynamic analysis looks at the behavior of the engine system as it changes with time—as opposed to the steady state of constant operation with time—such operations as start, shutdown, throttling, and pulsing. In addition, stability and control are examined and evaluated not only internal to the engine system but also between the engine and vehicle.

This dynamic analysis helps characterize the operation of the system. It thus provides a means for evaluating the feasibility of a given engine configuration, predicting its operational performance, troubleshooting as development problems arise, examining alternate operating approaches, and optimizing various aspects of operation and control.

In pump-fed propulsion systems an optimum sequence of controls is critical to a safe and reliable start, throttle, and shutdown operation. The optimization must consider but not be limited to component performance tolerances, e.g. high temperature excursions in a main combustion chamber or tubine inlet(s), or pressure surges in feed lines. Attention must also be given to operating the respective propellant pumps within a certain range relating to head (pump delta-P/density), speed, and flowrate.

Technical Approach

The basic analytical approach uses mathematical models to simulate the many aspects of engine-system operation. In the case of start, shutdown, and throttling, the models are nonlinear, with lumped and distributed parameters, and are composed of algebraic and integral-differential equations. The equations are programmed for digital-computer solution and give a time history of the appropriate parameters. The computer model becomes, in effect, an engine simulation which can be varied to evaluate different operating concepts.

Another type of system dynamic problem concerns the interaction of the propellant-feed system and the combustion process. It too will be analyzed with mathematical models. However, these models utilize linear system techniques, such as frequency-response analysis. The approach is often one of finding the appropriate resistance in the injector to damp the oscillating behavior that results from this interaction.

Combustion instability that occurs within the combustion chamber (and is of an acoustic nature) is considered a combustion-chamber design problem. Radial modes are handled by the use of acoustic cavities around the periphery of the injector. Circumferential modes are handled by the use of baffles that protrude perpendicularly from the injector face and run radially from the face center to the outside edge of the injector.

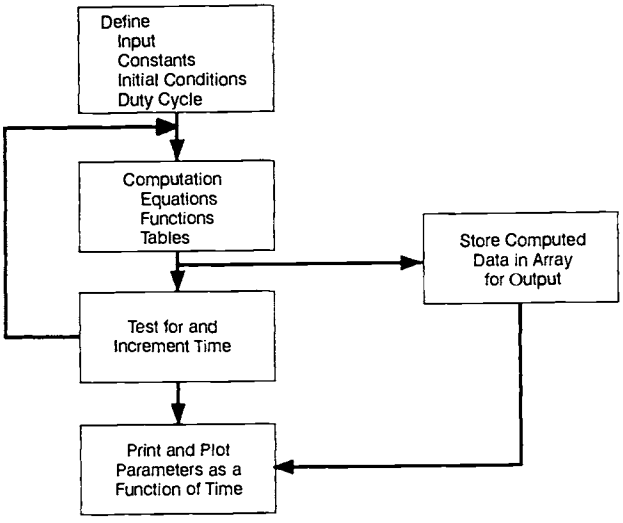

Fig. 10-2 Computer-model structure.

The interaction between the feed-system dynamics and vehicle structure (POGO) sometimes occurs in large rocket systems and is moderated by the use of an accumulator to detune the feed system. Here again, mathematical modeling is the analytical tool.

Modeling. A computer model consists of structured equations and incorporated chemical and physical data. It blends these elements with program logic. The logic framework can be represented by a diagram, as shown in Fig. 10-2. The model typcially consists of input, computation, and data-storage and output sections. The logic directs the data input, the computation process, and the generation and display of output data.

Examples of Equations, Functions, and Tables for a Mathematical Engine Model

The mathematical expressions and equations for the various physical processes and operating dynamics of a rocket engine may be derived from equations given in Chapter 1 and in other chapters for the design of the various components. In this chapter, several typical examples will be presented to illustrate the application of these equations in a mathematical model.

1. *Pressure drop of fluid flow in duct or component:*

$$P_1 - P_2 = a\dot{w}^2 + b\dot{w} - \rho h_{1\text{-}2} \qquad (10\text{-}1)$$

where a is a resistance term defined by—

$$a = K/(2g\rho A^2) \qquad (10\text{-}2)$$

and b is an inertance term defined by—

$$b = L/(Ag) \qquad (10\text{-}3)$$

where—

P_1 = pressure at the inlet, psi
P_2 = pressure at the outlet, psi
$\dot{w}$ = weight flowrate, lb/s
$\ddot{w}$ = rate change in weight flowrate, lb/s^2
$h_{1\text{-}2}$ = acceleration head of the fluid in the duct, in.
ρ = fluid density, lb/in.^{3}
K = duct or component resistance coefficient, to be obtained from flow tests
A = flow area of the duct, or flow area of the component at the design operating point, in.^{2}
L = length of the duct or component, in.
g = gravitational constant, 386.4 in./s^2

2. *Combustion process; operating dynamics:*

Figure 10-3 describes schematically the combustion process. A transportation delay, representing the time required for the propellants to pass through the injector and enter into the combustion process, can be expressed as follows:

$$\tau_O = \rho_O A_O (L_O + L'_O)/\dot{w}_O \qquad (10\text{-}4)$$

$$\tau_f = \rho_f A_f (L_f + L'_f)/\dot{w}_f \qquad (10\text{-}5)$$

For frequency-domain analysis, these can be indicated by the Laplace-transformation operators $e^{-t_O S}$ and $e^{-t_f S}$. A homogeneous combustion gas allows defining the following correlations:

$$p_C = R' (T_C/M) (w_C/V_C) \qquad (10\text{-}6)$$

$$w_C = w_O + w_f \qquad (10\text{-}7)$$

$$R_O = w_O/(w_O + w_f) \qquad (10\text{-}8)$$

$$w_o = \bar{w}_o + \int_0^t (e^{-\tau_o S}\dot{w}_o - R_o\dot{w}_c)\, dt \qquad (10\text{-}9)$$

$$w_f = \bar{w}_f + \int_0^t (e^{-\tau_f S}\dot{w}_f - (1\text{-}R_O)\dot{w}_c)\, dt \qquad (10\text{-}10)$$

In large engine time-domain models, Eq. (10-9) and (10-10) are simply used in the form:

$$w_O = \int_0^t (\dot{w}_O - R_O\dot{w}_C)\, dt$$

$$w_f = \int_0^t (\dot{w}_f - (1\text{-}R_O)\dot{w}_C)\, dt$$

$$w_C = A_t P_C g / C^* \qquad (10\text{-}11)$$

$$T_C/M = f(R_O) \qquad (10\text{-}12)$$

$$C^* = f(R_O) \qquad (10\text{-}13)$$

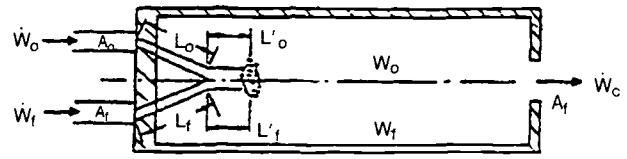

Fig. 10-3 Schematic description of the combustion process.

where—

τ_O, τ_f = time required for oxidizer and fuel to pass through injector and enter into the combustion process, s
ρ_O, ρ_f = density of oxidizer & fuel, lb/in.^{3}
A_O, A_f = injector area, oxidizer and fuel, in.^{2}
L_O, L_f = travel of injected oxidizer and fuel before impingement, in.
L'_O, L'_f = travel of impinged oxidizer and fuel before combustion, in.
t = period in consideration, s
$\dot{w}_O$, $\dot{w}_f$ = injected flowrate of oxidizer and fuel, lb/s
w_O, w_f = weight of oxidizer and fuel stored in combustion-chamber volume at the end of period "t," lb
$\bar{w}_O$, $\bar{w}_f$ = weight of oxidizer and fuel stored in combustor chamber volume at the beginning of period "t," lb
s = complex operator in a Laplace transformation
P_C = combustion-gas pressure, psia
T_C = temp. of the combustion gas, °R
V_C = volume of combustion chamber from injector to throat, in.^{3}
R' = universal gas constant, 18,528 in-lb/°R mole
M = molecular weight of the combustion gas, lb/mole
w_C = weight of the gas stored in the combustion volume, lb
$\dot{w}_C$ = flowrate of the gas emerging from the combustion chamber, lb/s
R_O = weight fraction of oxidizer stored in the combustion chamber
A_t = throat area, in.^{2}
g = gravitational constant, 32.2 ft/s^2
C* = characteristic velocity, ft/s

These equations for the combustion process can be applied to the main thrust chambers, gas generators, and other types of combustors.

3. *Turbopump operating dynamics:*

With certain components, such as pumps and turbines, it is sometimes effective to use performance

curves developed by the component-design groups rather than to use equations. For example, the relationships between pump delta-P, speed, flow, and torque are depicted in Fig. 10-4, along with the characteristic turbine curves.

To define combustion-gas properties for a given propellant combination, the characteristic velocity C*, combustion temperature T_c, molecular weight M, and ratio of specific heats γ can be plotted as a function of oxidizer fraction, as shown in Fig. 10-5. Curves can be input as a series of points, and interpolation can be used to obtain appropriate values.

Propellant properties can be obtained from reference tables and interpolated as a function of two variables. Pressure is often determined as a function of internal energy and density as depicted in the following example:

Density	Internal Energy U_1 U_2 U_3 ...
ρ_1	P_{11} P_{12} P_{13} ...
ρ_2	P_{21} P_{22} ...
ρ_3	P_{31}...
.	
.	
.	

Other commonly used functions are valve sequencing as a function of time, duty cycle as a function of time, etc.

Dynamic Analysis of Engine-System Start and Shutdown Transients

The main objectives of fluid-dynamic analysis of engine-system start transients may be summarized as follows:

- Investigation of the system's design for needed start-transient controls, such as type and quantity of control components, and sequencing and timing of their operation.
- Estimation of start energy, time, and thrust-buildup characteristics.
- Evaluation of component dynamic characteristics and interactions during start transients, such as propellant-pump stalling, combustion-chamber ignition delays, and mixture-ratio excursions within combustion devices.
- Evaluation of system dynamic stability during the start transient. The aim is to avoid prolonged operation at levels exhibiting system or thrust-chamber oscillations.
- Evaluation of various potential perturbations and their effects on start transients, such as a start lacking the propellant-settling effects of gravitation.

For some engine systems, such as the LO_2/LH_2 turbopump-feed system of the A-2 Stage engine, dynamic analyses of its start transient become rather complex. They may include effects such as waterhammer (wave equation) in the propellant-feed systems, distributed heat transfer and pressure drops throughout the high-pressure fuel-feed system, the choking of hydrogen gas in the chamber coolant passages, stall characteristics of the fuel pump, cavitation at the pump inlets, changes in fuel density in the pump caused by enthalpy changes from pumping, and many others.

Figure 10-6 presents graphically a modeled start-transient of a typical turbopump-fed engine system utilizing a gas generator for turbine drive. It indicates valve timing, as well as pressure-buildup characteristics of the gas generator, propellant pumps, and main chamber. Other parameters, such as gas-generator combustion gas temperature and propellant flowrates, can be included in the graph. The model typically will be used to simulate several engine-start methods to evaluate potential problem areas and to optimize the system's transient operation.

Dynamic analysis of engine-shutdown transients focus on the following important objectives:

- Investigation of the system's design for needed shutdown-transient controls, including operational sequencing and timing of various control valves.

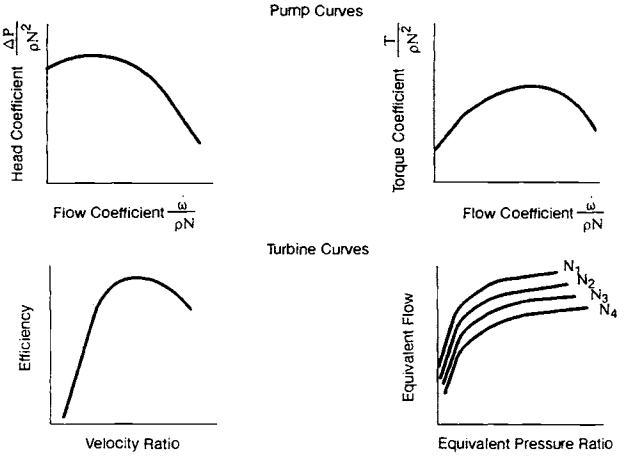

Fig. 10-4 Pump and turbine performance.

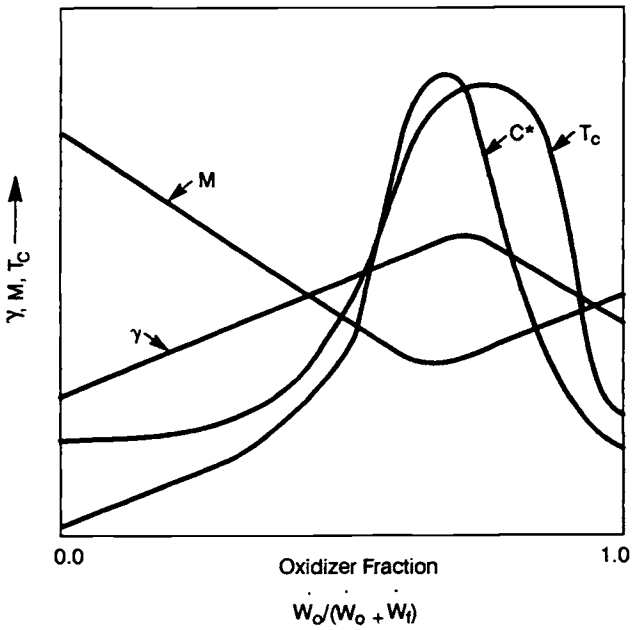

Fig. 10-5 Combustion-gas properties.

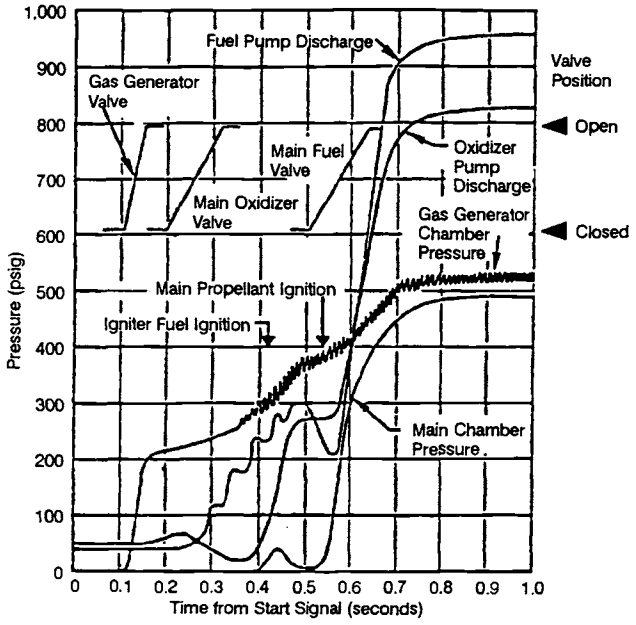

Fig. 10-6 Start-transient model for typical turbopump-feed engine system utilizing a gas generator for turbine drive.

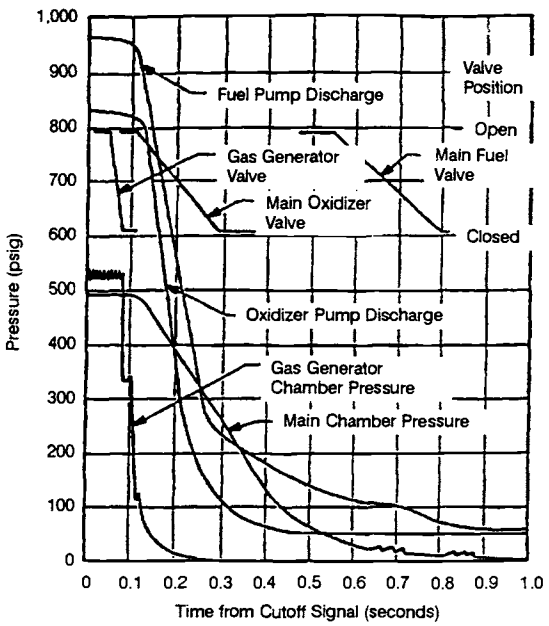

Fig. 10-7 Cutoff-transient model of the typical engine of Fig. 10-6.

- Evaluation of pressure surges and other adverse effects in propellant ducts and feed-system components during the shutdown transient.
- Evaluation of possible temperature surges in the main chamber, turbine, or gas generator during the shutdown transient.
- Evaluation and optimization of total shutdown impulse, by minimizing shutdown time and improving repeatability.
- Evaluating engine thrust-decay characteristics.

A series of shutdown sequences with modified shutoff timing of the control valves will usually be simulated with the mathematical model. The various simulated shutdown runs will be analyzed to determine potential problem areas and to investigate whether or not these problems are a function of the particular sequence used.

Figure 10-7 presents graphically the shutdown transient model of the typical engine depicted in Fig. 10-6. The engine thrust-decay characteristics are represented by the main-chamber-pressure decay curve. The integrated area under the chamber-pressure-vs.-time curve may be used to assess the engine-shutdown impulse.

Dynamic Analysis of Engine-Vehicle Interactions

Engine-vehicle interaction analyses may be performed during the initial design phase of an engine system, as well as following developmental test firings. Areas of general interest to be analyzed may include, but should not be limited to, the following:

- Engine system operation and performance requirements from a vehicle-mission point of view.
- Matching of engine propellant-supply requirements with the vehicle propellant system, including dynamic evaluation of the vehicle-propellant-tank pressurization system, propellant-utilization (PU) control system, vehicle acceleration and sloshing effects, and feed-system combustion-coupled instabilities.
- Matching the engine controls with the vehicle guidance system, including response of engine start, shutdown, thrust level, and vector controls to vehicle guidance commands.
- Simulation of the interaction between engine-system operation and vehicle dynamics. (This may involve closed-loop coupling of a simulation of vehicle guidance and trajectory characteristics with an engine system during hot-firing.)
- Simulation of the interaction between engine feed-system and vehicle structural dynamics.

Section 10.7 under the heading "Dynamic Interactions" describes the problem of and a decoupling approach to engine-vehicle interactions.

Low-Frequency Combustion Instability

Analysis of low-frequency combustion stability treats the interaction of the propellant system (pump inlet to combustion-chamber injector) and the combustion process. The term "low frequency," in this case, refers to the range of 50 to 1000 Hz. Linear-system analytical tools are used, i.e., linear differential equations to model the system and to define transfer functions and a frequency-response technique to define stability. Component characteristics accounted for in the analysis include the following:

- Resistance of the pump, propellant valve, and orifice.
- Dynamics of the feed line downstream of the pump.

• Resistance of the injector with the inertia and compliance of the injector manifold.
• Combustion chamber as an acoustic tube terminated by a sonic throat.
• Gas generated by combustion.

The liquid/gas conversion is ideally described by a linear differential equation that can be expressed as a frequency-dependent transfer function. Combustion delays and clumping, as well as a distributed burning zone, form part of the modeling.

In a low-pressure combustion chamber under steady flow, propellant droplets atomize and vaporize as they move downstream from the injector, while chemically reacting. Atomization is essentially a mechanical process while vaporization results from the feedback of a portion of the heat from the chemical reaction. In a high-pressure system, true atomization and vaporization may not be possible, but there is still mixing and energy feedback in preparation for the chemical reaction. Either case will see a change in propellant density distributed along the chamber length. The fraction of propellant burned as a function of axial distance can be calculated.

For low-frequency combustion, the combustion and feed systems can be considered to be composed of a number of sections, as shown in Fig. 10-8. Each of the blocks has a single input and output. The dashed line represents a signal path, which is actually closed. For this case, however, the stability of the system can more readily be studied by using the open-loop approach.

The thrust chamber is assumed to have an oscillatory gas flow as an input. The resulting injection end chamber pressure variation drives flow through the injector. The flow variation is attenuated somewhat by the impedance of the feed system.

The frequency response of the combustion chamber, feed system, and injector are combined and evaluated over the frequency range of interest to generate a stability plot (Nyquist). An example in Fig. 10-9 shows the stability characteristic as a system is throttled down through the 70% power level (PL) and through the 60% PL. Note that at 70% PL the system is stable in that the response curve does not enclose the +1 point on the real axis. At 60% PL the system has become unstable.

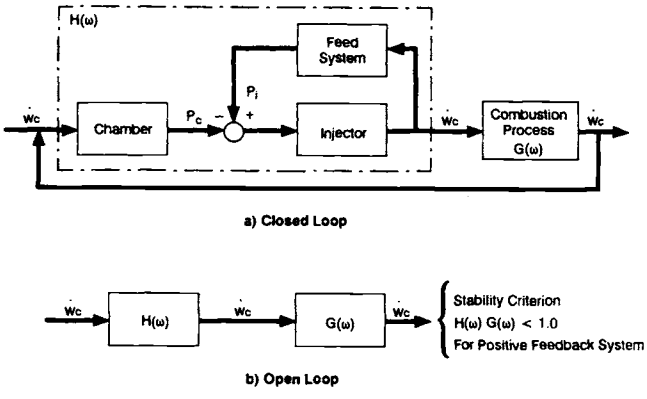

Fig. 10-8 Feed combustion system.

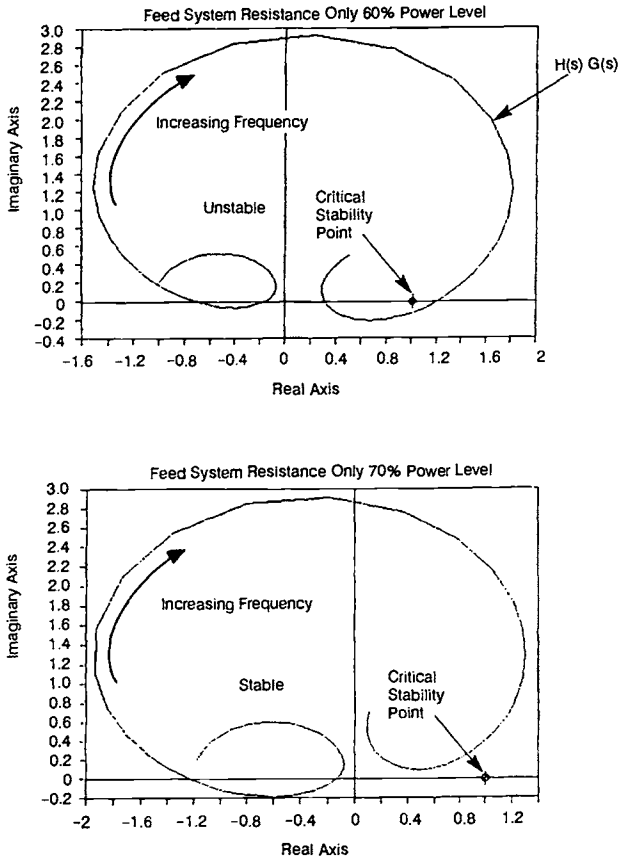

Fig. 10-9 Nyquist stability at throttled conditions.

10.3 DESIGN INTEGRATION FOR ENGINE SYSTEM CALIBRATION

Calibration Design Requirements

Because of unavoidable mechanical tolerances, it may be expected that the operating characteristics and performance of the various engine-system components will deviate somewhat from the nominal design value. A certain amount of calibration will always be required for these components, as well as the engine system as a whole, to attain the desired engine-performance characteristics within design specification. Provisions must be made in component and systems design to permit effective calibration during system integration.

The specific impulse I_s of an engine system being the ratio of thrust F to propellant weight flowrate $\dot{w}$, any deviations affecting F or $\dot{w}$ will affect system performance. I_s is also being a function of propellant mixture ratio; therefore it might be desirable and beneficial to calibrate an engine system by adjusting its propellant-feed system. Before a complete engine-system calibration, the pressure or pressure-drop-vs.-flow characteristics of each individual component should be calibrated and evaluated.

Hydraulic and pneumatic components, such as pressure and flow regulators, valves, flowmeters, ducts, and lines, can all be readily calibrated on flow benches. However, components that operate at tem-

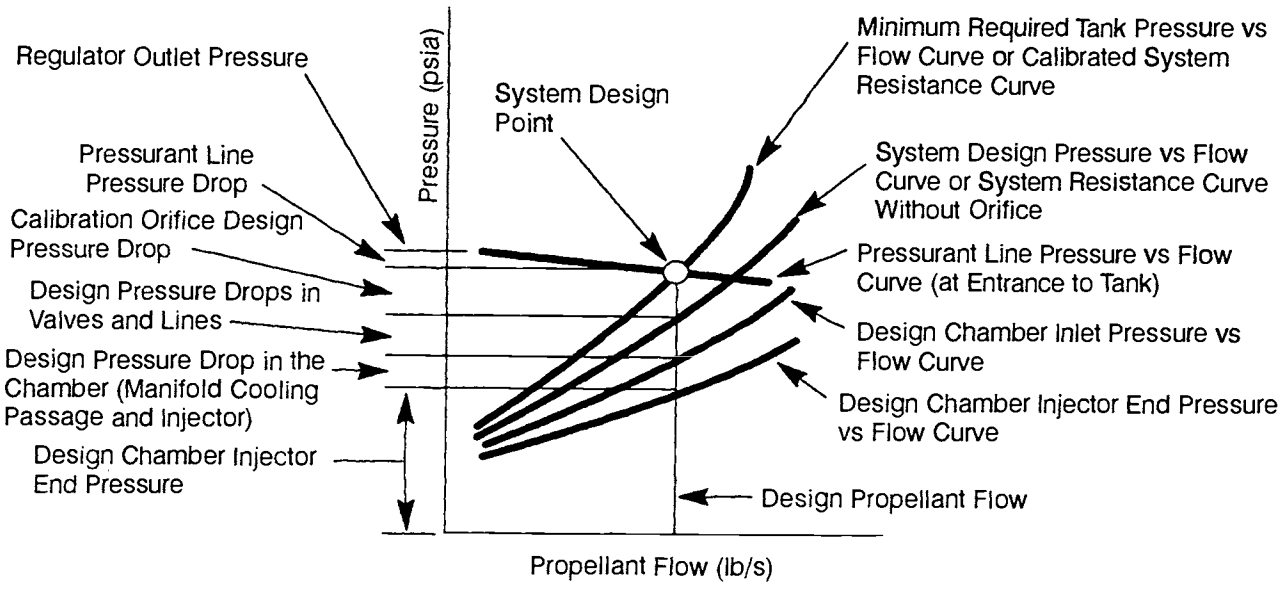

Fig. 10-10 Propellant-flow design characteristics of a typical pressure-fed engine system (oxidizer or fuel).

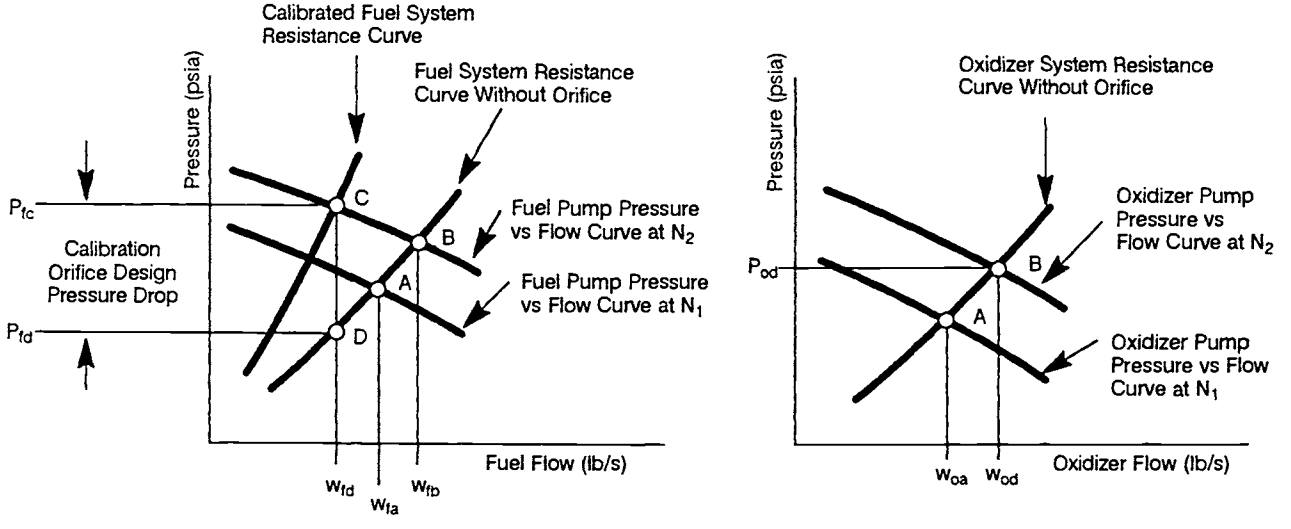

Fig. 10-11 Propellant-flow design characteristics of the A-1 Stage turbopump-fed engine system.

perature extremes, such as thrust-chamber assemblies, gas generators, and turbopumps, will best be calibrated by combining the flow tests with actual hot firings. The characteristic propellant-flow curve of an engine system will be obtained by summing the pressure or pressure-drop-vs.-flow curves of the various components (Fig. 10-10 and 10-11).

The general design approaches in calibrating an engine system (to attain its design thrust at design mixture ratio) are the following:

- The design operating point of each component should be kept within the relatively flat region of its pressure or pressure drop versus flow curve.
- The mechanical tolerances and built-in adjustments of each component should be designed so that the random deviation of its flow characteristics from its design value will be kept within a reasonable limit, in order to facilitate systems calibration, and to keep other system components in their design operating region.
- Sufficient pressure head should be set aside in each engine propellant feed system to compensate for contingencies caused by component flow resistance deviations. The propellant feed system can then be calibrated by means of orifices or other adjusting means.

Design for Calibration of a Pressure-Feed System

The first design step determines the design flowrate of each propellant, as calculated from the system's thrust, design mixture ratio, and I_s (as verified by actual thrust-chamber test firings). Based on these

flowrates, the pressure drops of the various components at the design operating point can be estimated from previous design data or as obtained from actual testing. Certain components may have to be designed for the specific design pressure drops allowed by the system.

The design-pressure-vs.-flow curve of either propellant flow system can be obtained by summation of design-chamber-pressure-vs.-flow and component design-pressure-drop characteristics, as shown in Fig. 10-10. In addition, a calibration orifice will be introduced into each propellant-flow system. These steps will yield the minimum required tank-pressure-vs.-flow curve for each propellant. In most pressure-feed systems, design orifice pressure drop for system calibration determines the maximum allowable cumulative-pressure-drop increase of the components above nominal values. A suitable tank-pressurization system can then be designed, compatible with minimum required tank-pressure-vs.-flow characteristics.

Sample Calculation 10-1

The following data from analyses and component tests characterize the A-4 Stage propulsion system at rated-thrust conditions:

- Thrust-chamber-injector end pressure range required to maintain rated thrust = 110 ± 3 psia.
- Thrust-chamber-injector pressure drop range (both oxidizer and fuel) = 25 ± 2 psi.
- Thrust-chamber oxidizer-dome pressure drop= 3 ± 1 psi.
- Oxidizer-line pressure drop = 5 ± 1 psi.
- Main-oxidizer-valve pressure drop (at the fully open position) = 4 ± 1 psi.
- Thrust-chamber fuel-manifold pressure drop= 4 ± 1 psi.
- Fuel-line pressure drop = 4 ± 1 psi.
- Main-fuel-valve pressure drop (at the fully open position) = 4 ± 1 psi.
- Pressure allowance required for mixture-ratio control by oxidizer-valve vernier positioning = ± 10 psi.

Problem

Determine the design pressure drops of the calibration orifices and the minimum required tank pressures for design flowrates.

Solution 10-1

The design pressure drop of a calibration orifice must equal the sum of the maximum pressure-drop increases of components above design values. Thus:

- The design pressure drop of the oxidizer-calibration orifice = 3 + 2 + 1 + 1 + 1 = 8 psi.
- The minimum required oxidizer-tank pressure at the design flowrate = 110 + 25 + 3 + 5 + 4 + 8 + 10 = 165 psia.
- The design pressure drop of fuel-calibration orifice = 3 + 2 + 1 + 1 + 1 = 8 psi.
- Minimum required fuel-tank pressure at the design flowrate = 110 + 25 + 4 + 4 + 4 + 8 = 155 psia.

This particular example, a worst case, assumed that all components had maximum pressure drop. It is more likely that the square root of the sum of squares would be used. In the case of the oxidizer orifice, for example, that would give about 4 instead of 8 psi for the calibration orifice. Also, it should be noted that in the early stages of a system design, most of the pressure-drop numbers represent estimates that will continually be revised as a system is developed.

Design for Calibration of a Turbopump-Fed System

The propellant-flow characteristics downstream of the pump discharge of a turbopump-fed system are similar to those of a pressure-feed system. However, the difference in turbopump pressure or head-vs.-flow characteristics from those of a pressurized system dictates a somewhat different approach to system calibration. For mechanically coupled turbopump-fed systems, such as the A-1 Stage engine, system calibration typically involves adjustment of the turbopump speed, as well as installation of an orifice in one of the propellant lines. For turbopump-fed systems with dual turbine drive, such as the A-2 Stage engine, the calibration can be made by adjusting the speeds of both turbopumps.

The design principles for calibration of mechanically-coupled turbopump-fed engine systems will best be illustrated by a typical example, as shown in Fig. 10-11. Here, the propellant-system resistance curves without orifices (representing conditions downstream of the pump discharges) are constructed based on the designs and test results of the components for the A-1 Stage engine system. Next, the discharge pressure-vs.-flow curves of both pumps are constructed from test data obtained with the A-1 Stage engine turbopump, operated at speed N_1. These pump curves intersect the corresponding system resistance curves at point A. At this speed, fuel flowrate w_{fa} exceeds, and oxidizer flowrate $\dot{w}_{oa}$ falls below, the required design flowrates, $\dot{w}_{fd}$ and $\dot{w}_{od}$. To achieve the design oxidizer-pump flow $\dot{w}_{od}$ at a desired discharge pressure P_{od}, the design operating speed of the turbopump assembly must be raised to a required level N_2 by increasing the turbine gas flow. At this speed, however, the fuel pump, which is mounted on the same shaft as the oxidizer pump, would be delivering a flowrate w_{fb} considerably above the required design flowrate w_{fd} (point B in Fig. 10-11). To reduce the fuel flow to w_{fd}, a calibration orifice is placed in the fuel line. This amounts to increasing the fuel-pump discharge pressure at constant speed N_2 to P_{fc}, where w_{fd} is reached at point C. The pressure drop across the calibrating orifice is represented by P_{fc}-P_{fd} where P_{fd} is the desired fuel pressure.

If fuel flowrate w_{fa} comes below and oxidizer flowrate w_{oa} exceeds the required design flowrates, the calibrating process would effect a speedup the turbopump to obtain the desired fuel flow, and lead to placement of an orifice in the oxidizer line. However, it will usually be desirable to place the ori-

fice in the system of the propellant with the higher boiling point. In this situation, therefore, and also when the pressure drop across a calibrating orifice tends to become excessive, it is customary to trim the pump impeller to reduce the effective speed and thus attain the required flow and pressure levels. In view of pump-efficiency effects, it is desirable to trim the pump drawing the smaller horsepower, usually the one with the lower mass flowrate, except in cases of extreme density differences. The adjustment of the turbine-gas flowrate, and thus the turbopump operating speed, can also be made by means of orifices in the turbine-inlet gas line or in the gas-generator propellant lines.

In general, turbopump-fed systems permit less-stringent requirements for the various components regarding deviations from their design steady-state flow values, because the system is inherently more flexible. However, systems dynamic characteristics under transient conditions may restrict these deviations.

Sample Calculation 10-2

The following design values and allowable deviations characterize the A-1 Stage LOX/RP-1 engine-system components at rated thrust:

- Thrust-chamber injector end pressure = 1095 + 30 psia.
- Thrust-chamber injector pressure drop (both oxidizer and fuel) = 200 ± 20 psi.
- Thrust-chamber oxidizer-dome pressure drop= 150 ± 10 psi.
- Oxidizer-line pressure drop = 25 ± 2 psi.
- Main-oxidizer-valve pressure drop = 35 ± 3 psi.
- Oxidizer-pump specific speed N_S = 1980 rpm.
- Oxidizer-pump suction (min) = 55 psia.
- Oxidizer-pump discharge pressure at 7000 rpm and a design flowrate of 1971 lb/s = 1505 + 25 psia.
- Thrust-chamber fuel jacket and manifold pressure drop = 290 ± 20 psi.
- Fuel-line pressure drop, 10 ± 2 psi.
- Main-fuel-valve pressure drop, 15 ± 2 psi.
- Fuel-pump specific speed N_S, 1090 rpm.
- Fuel-pump suction pressure, 45 psia min.
- Fuel-pump discharge pressure at 7000 rpm and a design flowrate of 892 lb/s = 1720 ± 25 psi.

Problem

Determine the location of the calibration orifice, its nominal design pressure drop, and its expected range of adjustment.

Solution 10-2 [See *Sample Calculation 6-2*]

- Required oxidizer pressure head at the design point = 1095 + 200 + 150 + 25 + 35 = 1505 psia.
- Required fuel pressure head at the design point = 1095 + 200 + 270 + 10 + 15 = 1590 psia.

Since the LOX-pump discharge pressure is 1505 psia, but the fuel-pump discharge pressure is 1720 psia, the calibration orifice must be located in the fuel system. The nominal orifice design pressure drop will be 1720-1590 = 110 psi.

Because of the effects of chamber-pressure deviations, the maximum value of fuel-calibration-orifice pressure drop will be required when the following conditions exist:

(a) Thrust-chamber-injector end pressure at its lower limit (1065 psia).

(b) All pressure drops in oxidizer passages at their higher limits.

(c) All pressure drops in fuel passages at their lower limits.

(d) Oxidizer-pump discharge pressure, 25 psi below its nominal value at the turbopump speed commensurate with the stated specific speed.

(e) Fuel-pump discharge pressure, 25 psi above its nominal value at the same speed.

The equivalent required oxidizer pump discharge pressure under these conditions:

$$1065 + 220\ \ 160 + 27 + 38 \pm 25 = 1535 \text{ psia.}$$

Required oxidizer-pump-developed head H:

$$144 \times (1535 - 55)/71.38 = 2986 \text{ ft}$$

Oxidizer-pump volumetric flowrate Q:

$$1971 \times 449/71.38 = 12{,}400 \text{ gpm}$$

Substitute this into Eq. (6-7) to obtain the required pump speed, as follows:

$$N = N_S H^{0.75}/Q^{0.5}$$
$$= 1980 \times (2{,}986)^{0.75}/(12{,}400)^{0.5} = 7182 \text{ rpm}$$

Fuel-pump volumetric flow Q:

$$892 \times 449/50.45 = 7939 \text{ gpm}$$

From Eq. (6-7), fuel-pump nominal developed head at 7190 rpm $H = (NQ^{0.5}/N_S)^{1.333} = (7182 \times (7939)^{0.5}/1090)^{1.333} = 4905$ ft or $4905 \times 50.45/144 = 1718$ psi.

The equivalent fuel-pump discharge pressure at these conditions would be 1718 + 45 + 25 = 1785 psia.

The required pressure drop for the fuel line calibration orifice thus would be 1788-1065-180-250-8-13 = 232 psi.

Similarly, a minimum fuel-calibration-orifice pressure drop must be achieved when the following conditions exist:

- Thrust-chamber-injector end pressure is at its higher limit (1125 psia).
- Conditions (b), (c), (d), and (e) above are reversed.

The equivalent required oxidizer-pump discharge pressure under these conditions = 1125 + 180 + 140 + 23 + 32 - 25 = 1475 psia. Required oxidizer-pump developed head H = 144 (1475 - 55)/71.38 = 2865 ft.

Substituting this into Eq. (6-7), the required pump speed will be—

$$N = 1980 \times (2865)^{0.75}/(12{,}400)^{0.5} = 6963 \text{ rpm}$$

From Eq. (6-7), the fuel-pump nominal developed head will be—

$$H = [(6963)\,(7950)^{0.5}/1090]^{1.333}$$
$$= 4707 \text{ ft or } 4707 \times 50.45/144 = 1649 \text{ psi}$$

The equivalent fuel-pump discharge pressure at these conditions would be 1649 + 45 - 25 = 1669 psia.

The required pressure drop of the fuel-line calibration orifice under these conditions would be 1669 - 1125 - 220 - 290 - 12 - 17 = 5 psi.

Therefore the required range of adjustment for the pressure drop of the fuel-line calibration orifice runs from 5 to 232 psi.

The preceding discussion pertains to fixed-thrust rocket engines. Engine systems that throttle under computer control automatically adjust mixture ratio.

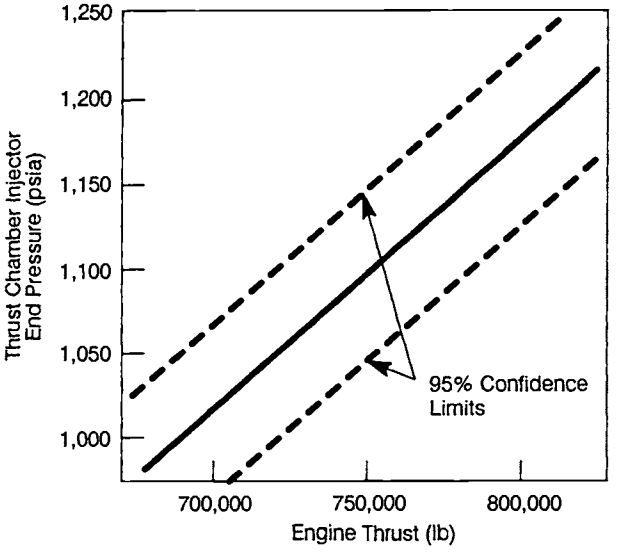

Fig. 10-12 Chamber pressure vs. engine thrust at sea level for the A-1 Stage engine.

10.4 ENGINE-SYSTEM INTEGRATED PERFORMANCE CHARACTERISTICS

Engine-system design must integrate performance characteristics. These data are prepared and compiled by the rocket-engine designer to provide the vehicle systems engineer with information necessary to integrate the propulsion system with the vehicle system. Where possible, a brief explanation of the data and its application should be included to provide clearer understanding and greater usefulness. The following data represent important aspects of integrated engine performance.

Nominal Engine-Performance Values at Rated Conditions

Usually prescribed by the engine-model specification, these data describe nominal steady-state operation of the engine system at rated conditions. Tables 3-2 to 3-5 give typical examples of nominal engine operating and performance parameters, which include nominal thrust, specific impulse, propellant combination, flowrates, mixture ratio, and various component operating data. Allowable deviations are specified for important parameters such as thrust (+3%) and mixture ratio (+2%). Engine-system specific impulse will usually be specified at its minimum value. The performance of all deliverable engine systems must exceed this minimum during acceptance tests.

In addition to tables for nominal engine-performance parameters, nominal engine performance graphs, such as chamber pressure vs. engine thrust and engine specific impulse vs. engine thrust, are often included as additional monitoring aids. Figure 10-12 presents a typical performance graph for the A-1 Stage engine system: chamber pressure vs. engine thrust at sea level.

Sample Calculation 10-3

The following data from design analyses and component tests characterize the A-1 Stage LOX/RP-1 engine system at nominal rated conditions, i.e., 750,000-lb thrust at sea level:

Thrust-chamber sea-level specific impulse at 1000-psia nozzle stagnation pressure and a mixture ratio of 2.35 O/F = 270 s
Turbine-exhaust-gas specific impulse = 32.6 s
Oxidizer-pump-developed head = 2930 ft
Oxidizer-pump overall efficiency = 70.7%
Fuel-pump-developed head = 4790 ft
Fuel-pump overall efficiency = 65.9%
Gas-generator O/F mixture ratio, 0.408
Turbine-gas available energy content = 359 Btu/lb
Turbine overall efficiency, 58.2%
Required auxiliary-drive shaft power = 500 bhp
Required oxidizer flow for vehicle-tank pressurization = 3 lb/s

Problem

Determine the following nominal performance values at rated conditions:

(a) Thrust generated by turbine exhaust gas.
(b) Thrust generated by the main thrust chamber.
(c) Engine-system propellant flowrates.
(d) Engine-system mixture ratio.
(e) Engine-system specific impulse.

Solution 10-3

A trial-and-error method solves this problem. The first step approximates engine-system and gas-generator propellant flowrates. Substitute thrust-chamber I_s

into Eq. (1-28):

$$\dot{w} = F/I_s = 750{,}000/270 = 2778 \text{ lb/s}$$

The thrust-chamber mixture ratio can now be used to approximate the corresponding oxidizer and fuel flowrates:

$$\dot{w}_O = 2778 \times 2.35/(2.35 + 1) = 1948 \text{ lb/s}$$

Oxidizer flowrate = 1948 + 3 = 1951 lb/s

Engine-fuel flowrate $\dot{w}_f$ = 2778 - 1948 = 830 lb/s

From Eq. (6-12) and (6-13) can be determined the required oxidizer- and fuel-pump drive horse power for this approximation:

- Oxidizer-pump horsepower = (1951 x 2930)/(550 x 0.707) = 14,700 hp.
- Fuel-pump horse power = (830 x 4790)/(550 x 0.659) = 10,970 hp.
- The corresponding turbine shaft horsepower T_{hp} = 14,700 + 10,970 + 500 = 26,170 hp.

From Eq. (6-19), the corresponding turbine-gas flowrate:

$$\dot{w}_t = (550/778) \times 26{,}170/(359 \times 0.582) = 88.6 \text{ lb/s}$$

This value can be used to start a new calculation cycle to separate main-chamber and gas-generator data. Thrust generated by a turbine-exhaust-gas flowrate of 88.6 lb/s = 88.6 x 32.6 = 2887 lb.

- Thus, the main-chamber thrust F_t = 750,000 - 2887 = 747,113 lb.
- Thrust-chamber flowrate w_{tc} = 747,113/270 = 2767 lb/s.
- Oxidizer-pump flowrate = (88.6 x 0.408)/(1 + 0.408) + (2767 x 2.35)/(1 + 2.35) + 3 = 25.7 + 1941 + 3=1969.7 lb/s.
- Fuel-pump flowrate = (88.6-25.7)+(2767-1941) = 888.9 lb/s.
- Turbine-shaft horsepower T_{hp} = (1969.7x2930)/(550 x 0.707) + (888.9 x 4790)/(550 x 0.659) + 500 = 27,090 hp.
- Turbine gas flowrate w_t = [(550/778) x 27,090]/(359 x 0.582) = 91.7 lb/s.

This value will serve another calculation trial:

- Thrust generated by a turbine-exhaust gas flowrate of 91.7 lb/s = 91.7 x 32.6 = 2989 lb.
- Main-chamber thrust F_t = 750,000 - 2986 = 747,014 lb.
- Thrust-chamber flowrate w_{tc} = 747,011/270 = 2767 lb/s.
- Oxidizer-pump flowrate = 91.7 x 0.408/(1 + 0.408) + (2767 x 2.35)/(1 + 2.35) + 3 = 1970.6 lb/s.
- Fuel-pump flowrate = (91.7 - 26.6) + (2767 - 1941) = 891.1 lb/s.
- Turbine shaft horsepower T_{hp} = 1970.6 x 2930/(550 x 0.707) + (891.1 x 4790)/(550 x 0.659) + 500 = 14,849 + 11,776 + 500 = 27,125 hp.
- Turbine-gas flowrate $\dot{w}_t$ = (550/778) x 27,125/(359 x 0.582) = 91.8 lb/s.

This last value closely confirms the assumptions for the last trial. Thus:

(a) Nominal turbine-exhaust-gas thrust = 91.8 x 32.6 = 2993 lb.

(b) Nominal main-thrust-chamber thrust = 750,000 - 2993 = 747,000 lb.

(c) Nominal thrust-chamber propellant flowrate = 747,000/270 = 2767 lb/s.

Nominal engine-system propellant flowrate = 2767 + 91.8 = 2859 lb/s.

Nominal engine-system oxidizer flowrate = 91.8 x 0.408/(1+0.408)+(2767x2.35)/1 + 2.35 = 1967.6 lb/s.

Nominal engine-system fuel flowrate = (91.8-26.6)+(2767-1941) = 891.2 lb/s.

(d) Nominal engine-system O/F mixture ratio = 1967.6/891.2 = 2.21.

(e) Nominal engine specific impulse I_s = 750,000/2858.8 = 262.3 s.

Engine-Performance Variations from Off-Nominal Conditions

Engine-performance characteristics at various off-nominal conditions must be available to the vehicle-systems engineer. They can be summarized in graphic form, such as Fig. 2-2 (engine-thrust- and specific-impulse-vs.-altitude curve), or by means of tabulated engine influence coefficients, as discussed below. The effects of off-nominal conditions of the following engine-system performance parameters vitally affect the design of a vehicle system: atmospheric pressure, propellant densities, pressures at the engine propellant inlets, propellant mixture ratio and vehicle PU (propellant utilization) control, vehicle acceleration, and throttling of the engine system.

Engine Influence Coefficients

Engine influence coefficients are used to convert or correct steady-state, main-stage-engine system performance parameters (dependent variables) from one condition to another of independent variables, such as atmospheric pressure, fuel temperature, oxidizer density, etc. This may be a correction to standard sea-level conditions (first-stage booster engine) or a conversion to other specified conditions. The coefficients are derived from the linearized solution of a set of steady-state equations that describe the performance of an engine system. These equations are solved by a digital computer using matrix methods and are presented in tabular form, as shown in Table 10-1 for the A-1 Stage engine system. Each influence coefficient takes the form of a percentage—the change of a dependent engine variable, such as thrust, as produced by a 1% change in an independent variable, such as atmospheric pressure. A coefficient preceded by a positive sign indicates that an increase of an independent variable produces an increase in the dependent variable. Conversely, a coefficient with a negative sign indicates a decrease in the dependent variable, as a result of an independent-variable increase. These influence coefficients are usually sufficiently accurate over the entire design operating range of an engine system.

Table 10-1 Influence coefficient for the A-1 Stage engine system.

(Value of C* correction to be obtained from the C* correction vs mixture ratio curve shown in figure 10-13)

A 1% Increase of Independent Variables Causes the Following Percentage Change of Dependent Variables	Independent Variables and Nominal Values					
	Atmospheric Pressure, 14.696 psia	Oxidizer Density, 71.38 lb/ft^3	Fuel Density, 50.45 lb/ft^3	Oxidizer Pump Inlet Suction Pressure, 55 psia	Fuel Pump Inlet Suction Pressure, 45 psia	C* Correction, 1.000
Dependent variables and nominal values:						
Engine thrust, 750,000 lb	-0.1780	1.8750	-0.7420	0.0440	-0.0066	1.1030
Engine specific impulse, 262.4 s	-0.1780	0.2650	-0.0640	0.0072	-0.0150	1.1350
Engine mixture ratio, 2.20	0.0000	1.6420	-1.3650	0.0270	-0.0020	-0.0260
Engine oxidizer flow, 1,967.7 lb/s	0.0000	2.0430	-1.1120	0.0465	0.0108	-0.0632
Engine fuel flow, 892.3 lb/s	0.0000	0.6530	0.3120	0.0207	0.0045	0.0094

Because the influence coefficients are linear, the total of several influences acting simultaneously on an engine system can be determined by summing the individual effects. For example, the change of engine thrust for the A-1 Stage engine system (without C* correction) can be expressed as follows:

$$(F - F_n)/(F_n) = C_1 (P_a - P_{an})/P_{an} + C_2 (\rho_o - \rho_{on})/\rho_{on} + C_3 (\rho_f - \rho_{fn})/\rho_{fn} + C_4 (P_{oi} - P_{oin})/P_{oin} + C_5 (P_{fi} - P_{fin})/P_{fin} \quad (10\text{-}14)$$

where—C_1, C_2, C_3, C_4, C_5 are the influence coefficients and—

F, F_n = engine-system thrust and its nominal value, lb

P_a, P_{an} = atmospheric pressure and its nominal value, psia

ρ_o, ρ_{an} = oxidizer density and its nominal

ρ_f, ρ_{fn} = fuel density and its nominal value, lb/ft^3

P_{fi}, P_{fin} = fuel-pump-inlet suction pressure and its nominal value, psia

P_{oi}, P_{oin} = oxidizer-pump-inlet suction pressure and its nominal value, psia

Sample Calculation 10-4

Problem

Estimate the thrust of the A-1 Stage engine system operated at the following conditions, without considering the effects of C* correction: atmospheric pressure P_a = 10.2 psia, oxidizer density ρ_o = 71.00 lb/ft^3, fuel density ρ_f = 50.90 lb/ft^3, oxidizer-pump-inlet suction pressure P_{oi} = 65 psia, and fuel-pump-inlet suction pressure P_{fi} = 49 psia.

Solution 10-4

From Eq. (10-14) and Table 10-1:

$(F-F_n)/F_n$ = (-0.178) x (10.2 - 14.696)/14.696 + 1.875 x (71 - 71.38)/71.38 + (-0.742) x (50.9 - 50.45)/50.45 + 0.044 x (65 - 55)/55 + (-0.0066) x (49 - 45)/45 = 0.04527, or 4.527%.

Engine-system thrust at an altitude, where Pa = 10.2 psia, will then be—

$F = 0.04527\ F_n + F_n = 0.04527 \times 750{,}000 + 750{,}000 = 783{,}950$ lb

Nonlinear Corrections

When the linear approximation is not sufficiently accurate, the usefulness of the engine influence coefficients can be extended by a technique that allows nonlinear corrections for certain parameters. An example of this method is the C* correction. For instance, a plot the change of C* correction vs. engine mixture ratio may be used in conjunction with a table of influence coefficients, such as Fig. 10-13 and Table 10-1, which are for the A-1 engine system. The change of engine mixture ratio can be computed for changes in atmospheric pressure, propellant densities, etc., as-

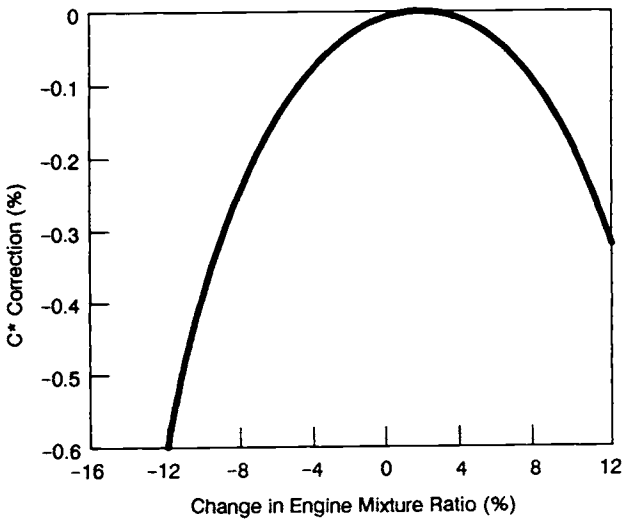

Fig. 10-13 C* correction vs. change in engine mixture-ratio curve for the A-1 Stage engine.

suming the C* correction to be initially zero. The C* correction for the resultant change in engine mixture ratio can be read from the graph, and then used with other independent variables to compute the changes in the remaining dependent variables.

Sample Calculation 10-5

Problem

Estimate the thrust of the A-1 Stage engine system operated at the conditions listed for sample calculation (10-4), adding the effects of C* correction. Also, for the same conditions, estimate the thrust, assuming an additional mixture-ratio error of +10% caused by faulty calibration.

Solution 10-5

By analogy with Eq. (10-14) and using Table 10-1, the engine system's mixture ratio change caused by the conditions of Sample Calculation 10-4 will be as follows:

$$(MR - MR_n)/MR_n = 1.642 \times (71 - 71.38)/71.38 +$$

$$(-1.365) \times (50.9 - 50.45)/50.45 + 0.027 \times (65 - 55)/55 +$$

$$(-0.002) \times (49-45)/45 = -0.0162 \text{ or } -1.62\%$$

From Fig. 10-13, the C* correction for a mixture ratio change of -1.62% is approximately -0.02%. From Table 10-1, the influence coefficient for engine-system thrust is 1.1030 for a 1% C* correction. Thus—

$$\% \text{ change in } F = 4.527 + (-0.02) \times 1.103 = 4.505\%$$

Therefore, engine-system thrust considering effects of C* correction will be—

$$F = 750{,}000 \times (1 + 0.04505) = 783{,}790 \text{ lb}$$

Adding the mixture ratio error of 10%, the total mixture ratio change = 10 - 1.62 = 8.38%. From Fig. 10-13, the C* correction will then be approximately -0.11%. Thus:

$$\% \text{ change in } F = 4.527 + (-0.11) \times 1.103 = 4.406\%$$

$$\text{Engine system thrust } F = 750{,}000 \times (1 + 0.04406)$$
$$= 783{,}050 \text{ lb}$$

10.5 MECHANICAL INTEGRATION OF ENGINE SYSTEMS

Basic Considerations

Besides combining all components and subsystems functionally and physically, the design for mechanical integration of an engine system must consider the overall envelope of the system and its weight. This includes the location of the system's center of gravity. Also, it should permit simplified maintenance and checkout practices. Judicious packaging design should be applied to minimize the number of interconnecting hydraulic, pneumatic, and electrical lines, with their attendant fittings, connectors, joints, and other potential trouble spots. Welded and brazed joints should be used as much as possible. Problems introduced by vibration, high temperatures and pressures, and leakage and space restrictions will thus be more easily handled. Engine mechanical integration being a vital part of the system-design concept, all factors related to integration and packaging of components and subsystems must receive careful consideration early in the preliminary design stage.

In general, a modular packaging approach should be selected—like those used for the A-1 (Fig. 3-2) and A-2 (Fig. 3-4) Stage engine systems, as well as for many advanced operational engine systems. This ensures engine integrity from time of manufacture through vehicle launch. It also provides a compact package for ease of handling, transportation, and installation in the vehicle. Such packaging enables ease of checkout and component accessibility.

The engine should be completely assembled in the manufacturer's plant. Subsequent acceptance testing, air transportation, and installation in the vehicle in the field should not require assembly of additional major components. Integrity of the propellant-feed and hot-gas systems, once verified in a complete system during acceptance test, will not necessarily be nullified by the need to temporarily disassemble the engine for shipment. The integrated-engine-package concept provides added assurance that static test-stand firing results have verified structural soundness of the package to a substantially greater degree than would be the case for a system in which the vehicle provides portions of the engine structure.

As an example of a special case of mechanical integration of a liquid-propellant rocket engine, the prepackaged storable-liquid-propellant propulsion system shown in Fig. 8-1 represents a completely integrated assembly, of all-welded construction, consisting of thrust-chamber assemblies, propellant tanks, pressurization system, and necessary controls. This integration provides maximum assurance of system integrity from the time of manufacture, which includes loading of the propellants, delivery, vehicle assembly, and launch. For maximum safety, hermetically sealed burst-diaphragms completely separate propellants until "systems start." Acceptance tests sample units at random from the production line and hot-fire them. In addition, destructive tests of various types are performed on prepackaged storable propellant systems.

Packaging of Rocket-engine Components

Most major rocket-engine components, such as thrust-chamber (Fig. 4-1) and turbopump (Fig. 6-16) assemblies, readily form a logical, independent mechanical unit by virtue of function and physical shape. In the case of minor components, however, such as control valves, gas generators, and igniters, packaging design principles can best be served by making them an integral part of a major component assembly or integrating them by grouping—a typical example being a gas-generator assembly externally attached to a turbine-inlet flange (Fig. 3-2). Similarly, gas-generator propellant valves and the combustor can be integrated into one unit (Fig. 4-64).

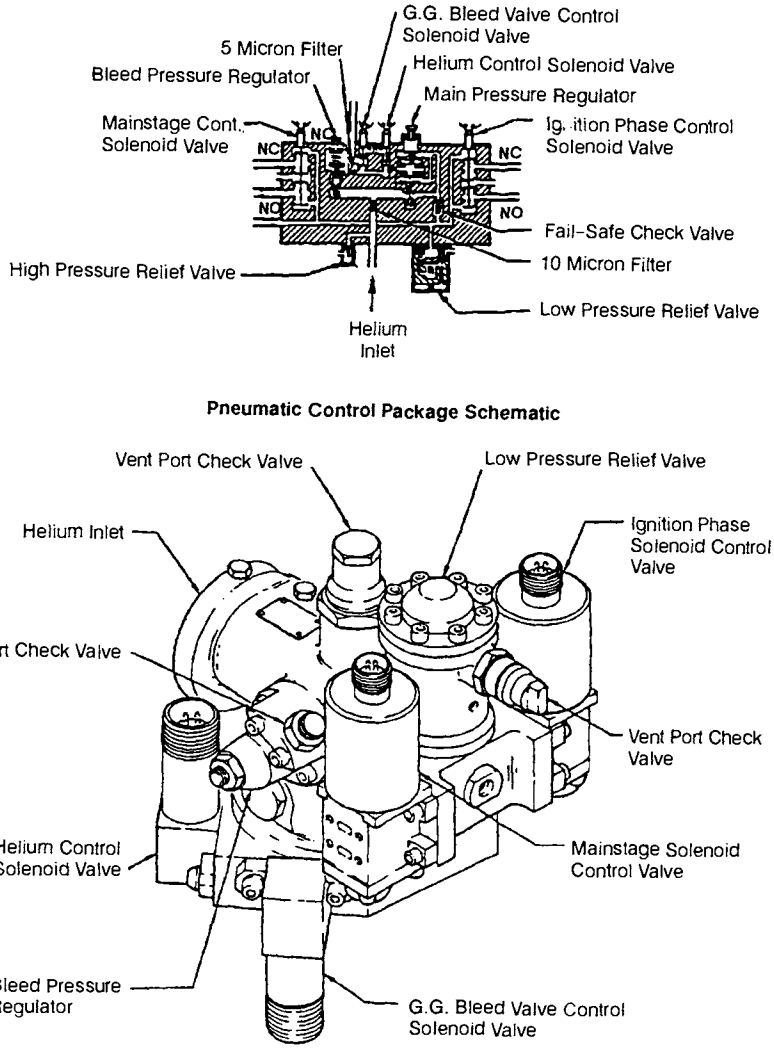

Fig. 10-14 Typical pneumatic-control package design used in liquid-propellant rocket engine systems.

Certain types of hydraulic and pneumatic rocket-engine control components lend themselves most conveniently to the packaging design, one of the main objectives with these being to reduce line runs by combining all parts and passages into one housing. Such a housing (or mounting plate) can be relatively leakproof, because trouble areas will be limited to external line connections to other components. Furthermore, if components are packaged in this manner, reductions of weight and size will be achieved through the use of common walls and through the elimination of extra mounting platforms, clamps, and fasteners. The relatively few packages required, as compared to the usually large number of individual components, greatly simplifies maintenance of such a system. Integrated packages are about as easily removed and replaced as are the separate components making up each package. However, packaged design will not necessarily be desirable for every control system. Each case must be carefully studied.

As a rule, one of the following methods, or a combination, can be used for packaging engine-control components:

Bank packaging: A group of similar flat-sided component assemblies are bolted together in a bank or stack, with common porting through the mating surfaces from one unit to the next.

Subplate packaging: Two or more individually housed components are fastened to a subplate, so that all ports of the individual component housings lead into the subplate manifold, through their mating surfaces with the subplate, and on to the systems plumbing.

Cartridge packaging: Two or more components housed individually in cylindrical cartridges are in turn assembled in a common body with suitable manifolding to the systems plumbing.

Multiple-component packaging: Detail parts for two or more components are assembled in a normal fashion in a common housing or body.

Figure 10-14 shows a typical pneumatic-control package for a large liquid-propellant rocket engine. This package combines two pressure-regulator assemblies, two relief valves, a series of solenoid valves, filter units, and check valves. It controls the flow of helium gas to various engine components. Engine start energizes the helium-control solenoid, allowing helium to flow through the main pressure regulator to the control system, and thence internally to the main control valves through a fail-safe check valve. Should the helium gas supply system fail, this check ensures

that the various engine propellant valves remain pressurized and thus open.

Packaging of Turbopump-fed Engine Systems

In earlier high-thrust rocket propulsion systems (some of which may still be in operational use), all major engine components were mounted into a cage-shaped thrust mount that was bolted to the vehicle thrust frame by lugs. Figure 2-5 shows several typical examples. With these systems, vehicle steering was done with carbon vanes protruding into the jet (V-2 and Redstone) or by swiveling the thrust chamber (Thor, Jupiter). In the latter case, the high-pressure feed lines between pumps and injector had to be much more flexible than to account for misalignments and thermal expansion and contraction alone.

Most advanced liquid-propellant rocket engines are tightly packaged. All major components are attached to the main thrust chamber, directly or by means of mounting structures, as shown in Fig. 3-2, 3-4, and 9-1. The thrust chamber serves as the principal structural member of the entire engine system. For steering, the complete engine package is gimballed from a gimbal bearing that attaches directly to the thrust-chamber dome. The other half of the bearing attaches the vehicle thrust structure. The low-pressure-propellant-supply ducts must be sufficiently flexible to accommodate gimbal motions. Note that vehicle steering by gimballing a single engine or chamber will be effective only for the pitch and yaw planes. Roll control requires at least two engines. For vehicles with a cluster of engines this poses no difficulties; but single-engine vehicles need special roll-control devices. These may be small auxiliary nozzles, possibly used simultaneously as vernier engines after main-engine shutdown. Turbine exhaust has been proposed for roll control.

The engine may attach to the vehicle thrust structure by a thrust frame or a gimbal bearing, but either must be able to transmit the full thrust forces at full gimbal deflection, yet retain an adequate reserve for normal and side loads. The bolt-hole pattern must permit adjustment for tolerance deviations. In general, engine and vehicle attachment-halves must be designed for one another.

Figures 10-15 and 10-16 illustrate packaging design details of a typical pump-fed system, a LO_2/RP-1

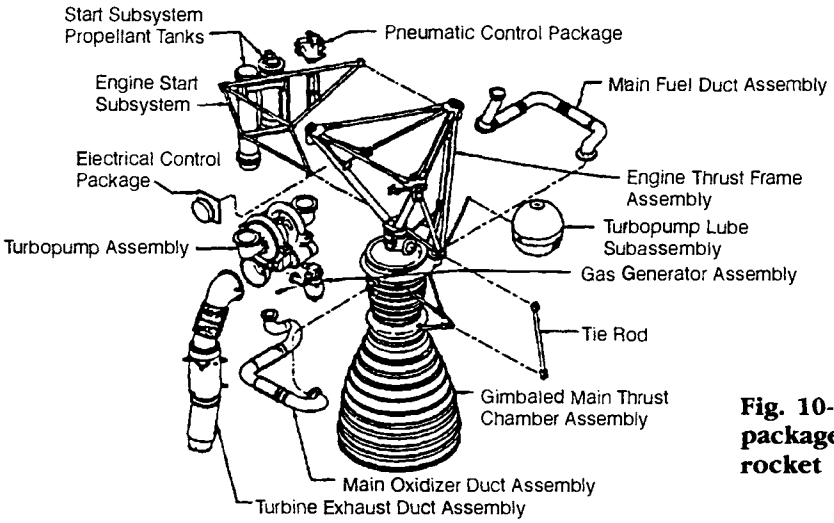

Fig. 10-15 Major component and subsystem packages of turbopump-fed liquid-propellant rocket engine.

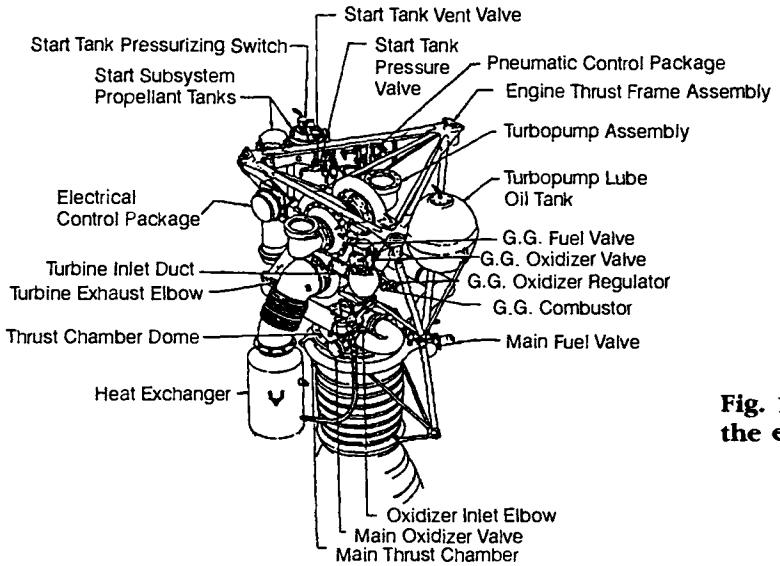

Fig. 10-16 System-packaging design detail of the engine shown in Fig. 10-15.

fixed-thrust engine with constant-chamber-pressure control. The basic engine package consists of the following subpackages: gimballed main-thrust-chamber assembly (thrust chamber, injector, dome, oxidizer elbow, and gimbal mount), turbopump assembly (propellant pumps, turbine, gearbox, lube pump, electric heater, and auxiliary drive), gas-generator assembly (combustor, control valves, regulator, and turbine-inlet duct), main-oxidizer-duct assembly (including main oxidizer valve), main-fuel-duct assembly (including main fuel valve), turbine-exhaust-duct assembly (including heat exchanger), engine-start subsystem (oxidizer and fuel tanks, control valves), turbopump lube subsystem (lube-oil tank and fittings), pneumatic-control package, electrical-control package, and engine-thrust-frame assembly. The majority of the major component and subsystem packages go within, or at the periphery of, the engine-thrust-frame assembly. The main-thrust-chamber assembly attaches to the thrust frame through a gimbal mount.

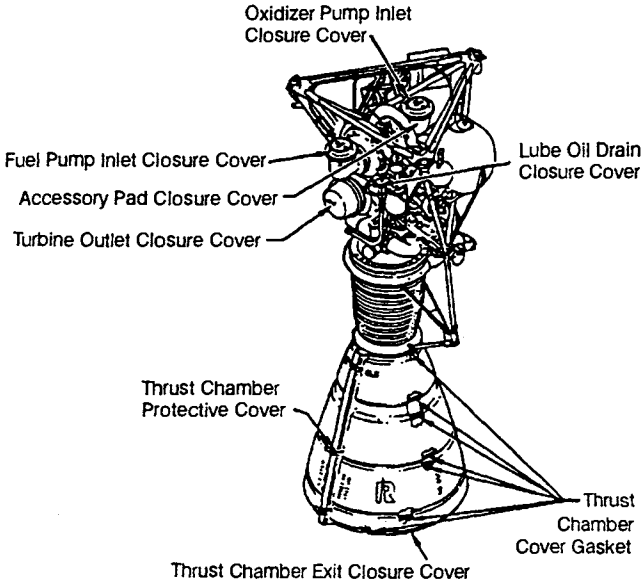

Fig. 10-17 Various protective closure covers for the engine shown in Fig. 10-15.

Mechanical Protection of Engine-system Packages

Several years may elapse between the date a liquid-propellant rocket engine is completed and accepted by the user and its vehicle flight. Design must therefore consider means to protect the engine-system package in transit or storage against moisture, dirt, and shock. Protections include simple closures, such as caps, plugs, and cover plates applied to valve and regulator vent holes, propellant inlets, and to other openings. Frequently, these closures contain desiccant bags and indicators that warn, through change of color, of the undesired intrusion of moisture. Certain lines, however, may require communication with ambient air ("breathing"). Then the closures may be equipped with desiccant filters to permit access of dry air only. Some of the covers must be removed to permit installation of the engine in the vehicle. Others will be left in place until the engine is actually operated. To prevent being left in place inadvertently, these closures must be readily accessible and clearly marked, such as with bright colors. Figure 10-17 shows locations of various protective closures for the Rocketdyne LR79-NA-11 engine.

10.6 CLUSTERING OF LIQUID-PROPELLANT ROCKET ENGINES

The idea of obtaining higher thrust levels expeditiously through the combination of several smaller rockets probably is as old as rocketry itself. The topic of clustering still provokes spirited debate among designers. Perhaps this reached a peak in March 1952 when, in a *Collier's* magazine article, Wernher von Braun described a space vehicle having a first stage powered by a cluster of 51 turbopump-fed rocket engines.

Debate invariably turns around the deceptively simple question: Will higher overall reliability be obtained through a combination of well-developed smaller engines or through one large, specially-developed unit? The question has no simple answer. The failure probability of the smaller units may be low, but it increases with the number of units clustered. Reliability will not be a fixed value for either large or small, but rather will be a function of *development effort and time*. A realistic analysis, considering all factors, *may* determine the appropriate choice; but the hard fact of the cost of going both routes for a given mission and of comparing final scores almost surely being prohibitive will preclude an absolute answer.

The clustering of liquid-propellant rocket engines—in other words, the subdivision of vehicle thrust into smaller units—may be done a number of ways. The choice, for the most part, will be based on *vehicle* considerations. Depending on the method chosen, however, engine design will be directly affected.

There are no hard-and-fast rules that will determine *optimum* cluster configurations. Liquid-engine clusters actually used in practice, however, do provide a guide for future designs.

Early Cluster Configurations

Figure 10-18 shows the cluster of two experimental LOX/alcohol engines for a planned but discontinued ballistic missile. It consisted of two units of 120,000-lb-thrust each. Both subunits had a gimballed tubular-wall thrust chamber and a geared turbopump. The turbines were powered in parallel from a single, common gas generator and also had common controls. Thus, this propulsion system was not a true cluster, because it was not possible to develop and fire each unit independently. This engine powered several successful experimental flights.

Figure 10-19 shows another experimental cluster consisting of three units that, although never flown, achieved a remarkable reliability record during static firings at thrust levels up to 500,000 lb. This cluster, too, used common controls and gas-generating sys-

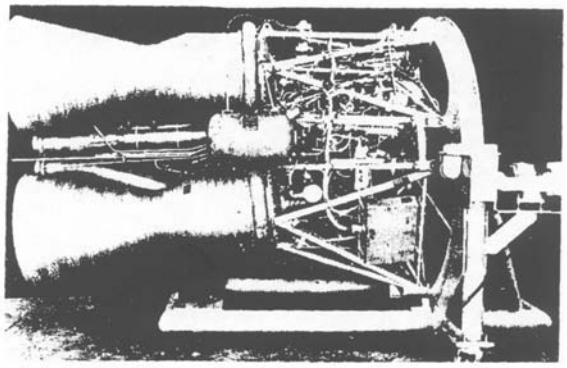

Fig. 10-18 Dual-engine cluster.

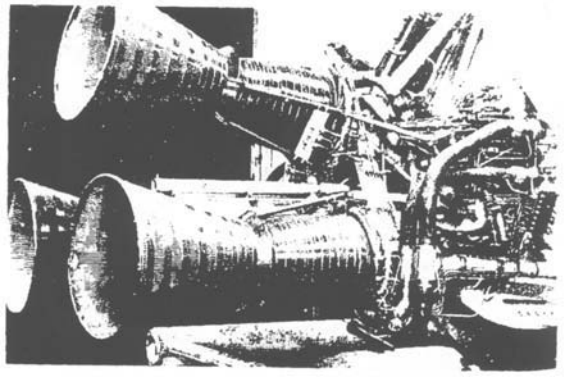

Fig. 10-19 Three-engine cluster.

tem for the three subunits. Most of its components were essentially the same as those used for the two-engine cluster, except that propellants were RP-1 and liquid oxygen.

Still another approach for ballistic missiles combines a pair of booster engines with a large-expansion-area sustainer engine. During flight, the booster engines may be jettisoned following the boost period, while the sustainer continues, fed from the same tanks. Such a configuration has been termed a "one-and-one-half-stage vehicle."

Recent Cluster Design Trends

The first U.S. clustered-engine vehicle—signifying the modern trend toward multipurpose engines—NASA's S-1 first-stage booster for the Saturn I, was powered by eight LOX/RP-1 engines, the basic elements of which were transplanted with relatively minor modifications from earlier engines. The S-1 is noteworthy for its tank arrangement—eight tanks from a precedent missile clustered around a central larger tank. This "multicellular" design, which in the case of the S-1 permitted early availability of large tank capacity without major retooling, has been recommended by some vehicle designers for still larger vehicles. The eight engines of the S-1 are grouped into four fixed inner engines and four gimballed outer engines. Except for the outer-engine actuators, all eight are identical, independent units, built and tested singly,

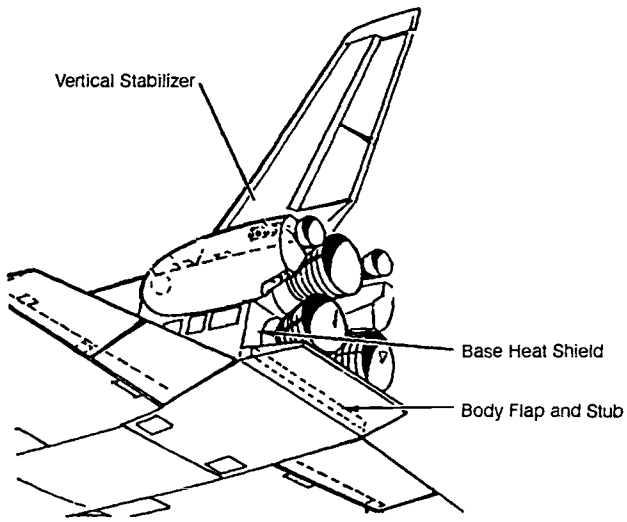

Fig. 10-20 Space Shuttle Orbiter Three-main engine cluster.

and combined for the first time on the vehicle proper.

In the S-1, the number of engines was, no doubt, almost entirely governed by the availability of existing major engine components and tankage. For subsequent vehicles, such as the Saturn V three-stage vehicle, greater freedom existed, particularly with respect to the optimization of thrust and total impulse (propellant load).

The Space Transportation System utilizes a cluster of three liquid-oxygen/liquid-hydrogen main engines installed in the Orbiter aft fuselage. These Space Shuttle Main Engines (SSMEs) run from liftoff until main-engine shutdown at approximately 510 s. Two large solid-rocket boosters, one attached to either side of the external tank, supply additional thrust for the first stage of the flight. The clustered SSMEs take the tucked-in position for reentry and landing of the Orbiter. Figures 10-20 and 10-21 depict the installation of the SSME cluster.

Assume that payload and mission of a multistage vehicle have been defined and that stage propellant loads (total impulse) and tank geometry (diameter) have been optimized. Assume further that engines are available and will not be redesigned, and that the optimum thrust for a typical stage suggests a range of four to six engines. An analysis has shown that payload performance probably increases with the larger number of engines (Fig. 10-22), but there are other considerations.

One of the most influential will be the ability of a vehicle to complete its mission with one engine inoperative (also see Chapter 2, "Thrust Level"). Engine provisions for "Engine-Out (EO) Capability" will be summarized in section 10.7. Engine-out always entails some performance loss, but it decreases with increasing number of engines because less performance reserve will be needed, likewise less correcting thrust-vector trim from the operating engines.

EO capability makes a substantial contribution to mission reliabilty, reducing cluster-failure potential by more than half.

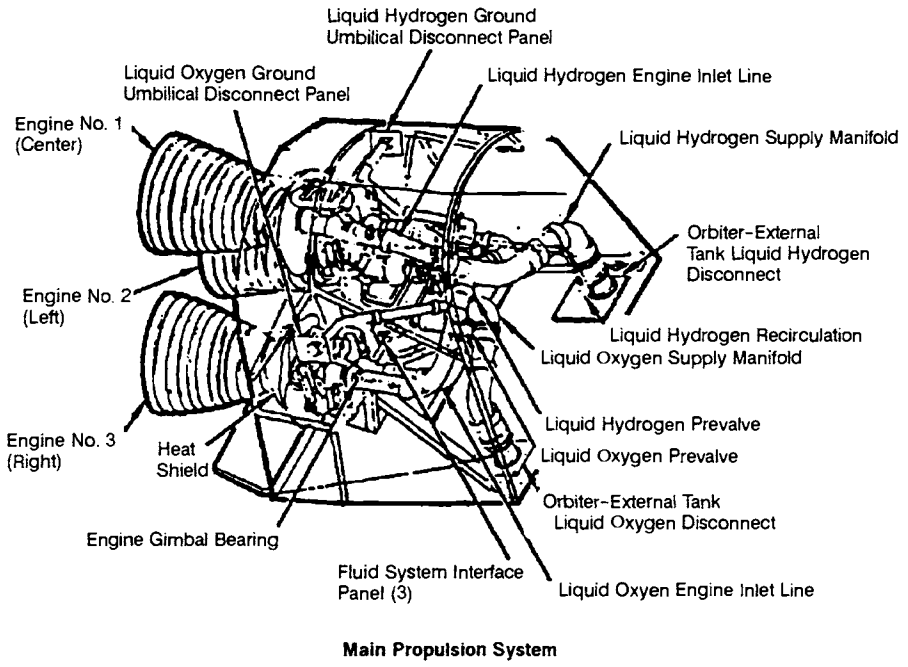

Fig. 10-21 Space Shuttle Orbiter aft fuselage.

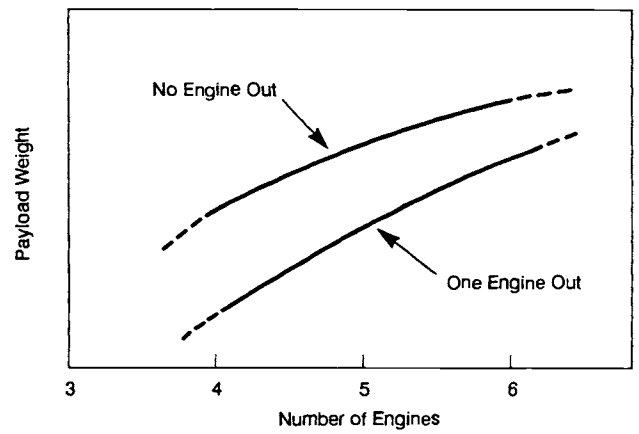

Fig. 10-22 Stage-payload weight vs. number of engines in cluster.

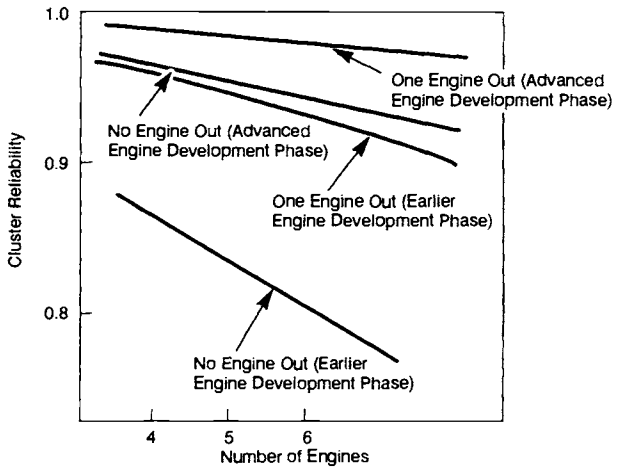

Fig. 10-23 Typical cluster reliability prediction vs. number of engines in cluster and of development time.

Figure 10-23 illustrates reliability at two points in engine overall development. As testing progresses, the difference between engine-out and no-engine-out narrows (see also Table 2-2). It may be stated that, for a given number of vehicle flights, the lower the engine reliability, the greater will be the benefits of engine-out. Figure 10-22, in combination with Fig. 10-23, shows that simultaneous addition of one engine and inclusion of engine-out capability retain about the same payload for a substantially higher cluster reliability at any single-engine reliability level.

Cluster diameter in relation to vehicle diameter raises another important consideration. As discussed in section 10.7, all engines must fit into the interstages to permit stage separation without interference. That condition does not restrict the first stage, but the degree of protrusion must be balanced against drag losses.

Specific considerations for some common engine clusters may be summarized as follows (Fig. 10-24).

Four-engine cluster. This configuration, in the groupings from four to six, offers optimum engine interchangeability. All four engines will be gimballed. Only one installation is required: all inlet ducts and other engine-to-stage connections can be made identical. The thrust vector control (TVC) mode is simplest: all engines deflect in pitch and yaw, and all actuators participate equally in roll control (Fig. 10-24a). The vehicle contractor's requirements will decide the actual gimballing requirements.

Five-engine cluster. Five engines provide greater thrust but complicate matters in other respects. Of two basic arrangements possible, as shown in Fig. 10-24b and 10-24c, designers prefer the arrangement with the center engine, mounted fixed—i.e., stiff-arms installed in place of gimbal actuators. It is advisable to install the engine with a complete gimbal bearing for standardization and ease of alignment. The remaining four engines can be gim-

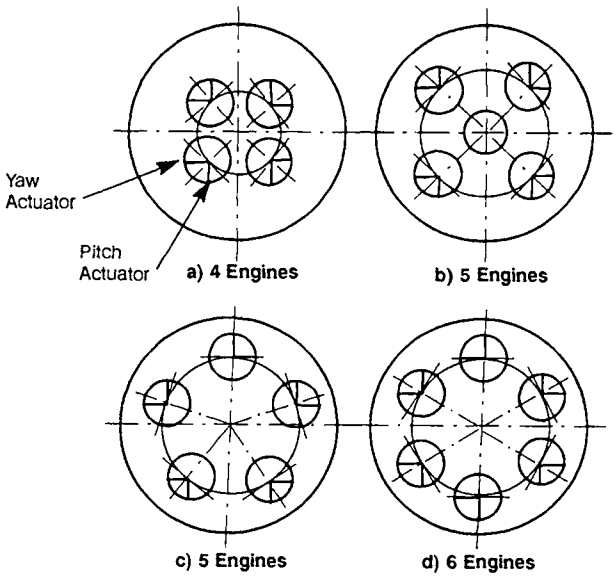

Fig. 10-24 Typical engine-cluster arrangements.

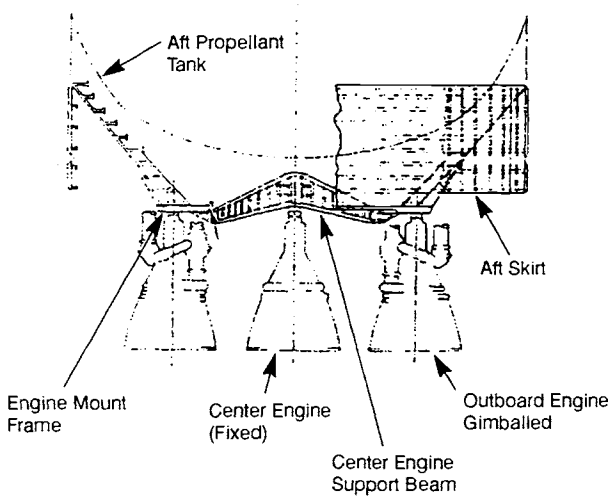

Fig. 10-25 Typical five-engine cluster configuration (center engine fixed, four outer engines gimballed).

balled and grouped as in a four-engine cluster and thus yield the same benefits. The centered engine, however, forces two installations and two sets of inlet ducts. The different length of the ducts affects pressure drop and fluid velocity profile (engine turbopump NPSH), waterhammer from closure of valves (valve timing), trapped propellants, and possibly insulation requirements (weight penalties and complexity). Figure 10-25 shows a typical five-engine installation with fixed center engine.

With all five engines arranged on a circle, the basic engine package may become more uniform, since all will be gimballed. However, the five engines will need three different installations (Fig. 10-24c), and will seriously affect systems TVC response, because of roll and yaw coupling, particularly under malfunction conditions. As to mounting-circle diameter, the two five-engine clusters are about equal.

Six-engine cluster. This combination provides the highest thrust, at the expense of a larger mounting circle. This in turn increases the effects of one-engine-out on trim required and may compound interstage and inter-engine clearance problems. In simplicity the control mode is comparable to the four-engine cluster. The six-engine cluster requires two installations, with inlet and other effects similar to those discussed with the five-engine configuration.

This cluster of six offers the potential of removing (not installing) two engines and still retaining a satisfactory four-engine combination—added flexibility at minimum scar weight (i.e., weight of components that cannot readily be removed along with the engines).

If at all possible, the engine designer should specify that the engine intended for cluster use be tested under conditions *closely simulating vehicle installation*. It may be expected that the vehicle builder will conduct a firing program of his own; but this program must be devoted to cluster behavior and performance evaluation, and should not deteriorate into continued single-engine development. A major difference between single-engine and cluster firing concerns the base conditions, i.e., the heat and pressure environment of the engines, particularly at altitude. Flame radiation effects, backwash of combustion gases, and impingement may create much more severe conditions than are present during single-engine firing. The pressure environment produced by several engines firing together may create moments on the engines that must be accounted for in the design of the gimbal system. The engine designer should be familiar with these conditions so that the claim that the engine can be clustered remains valid after delivery.

Awareness by engine designers of the considerations governing engine clustering, as presented here, will enable them to complete a systems integration with a broader view to specific applications.

10.7 ENGINE-TO-VEHICLE INTERFACE

Throughout this book, references have been made to the ultimate purpose of rocket-engine design and production: propulsion of a vehicle. Some of the principal engine-to-vehicle interfaces, such as thrust mount, pneumatic fluid, and electrical and propellant lines, have been discussed in preceding chapters. This section will summarize a number of vital engine-to-vehicle interfaces. The able engine designer will keep cognizant of them.

Design Documentation

Adequate mechanical design data, vital for the physical integration of engine into vehicle system, must be properly documented *by the engine systems designer*, the following being considered minimum requirements:

- Engine-system general arrangement drawing. This drawing defines the engine envelope and the lo-

cations and detail of various agreed-upon vehicle connect points, such as—

—Thrust or gimbal mount
—Gimbal-actuator attach points
—Fuel- and oxidizer-inlet flanges
—Hydraulic and pneumatic system connections
—Propellant bleeds
—Electrical and instrumentation connections
—Autogenous pressurization connections

- Mechanical dimensions, tolerances, seals (if any), fasteners, and loads at the vehicle connect points listed.
- Engine-system mass properties which include engine weights, gimbaled mass, center of gravity, and added moment of inertia for the basic engine, including accessories.
- Engine performance data (as in Fig. 3-1).
- Engine functional description (see Chapter 3).
- Engine handling procedures and equipment, needed for installation and maintenance.
- Engine servicing needs.
- Electrical-power requirements for both ac and dc systems; power profiles and surge limitations included.
- Command and data channels and the necessary software details for any computer-driven controller.
- Fluid requirements—purge gases, propellants, propellant-tank pressurant, hydraulic fluids, etc. Included too will be flowrates, supply pressures, temperatures, and cleanliness requirements.
- Environmental conditions, such as engine-compartment thermal conditions at prelaunch, ascent, and, if applicable, on orbit and during re-entry and landing.
- Induced loads and vibration at all mechanical interfaces and aerodynamic loads on the nozzle for ascent, re-entry, and landing.

As a rule, this information will be compiled in detailed handbooks. Several years before the engines are delivered and handbooks become available, however, the vehicle builder will need numerous engine design details in support of the stage design.

These interface-design operational details will be contained in the interface control document (ICD), a *contractual* entity that controls all of the engine/vehicle interfaces. With a new program involving a new engine and a new vehicle, the basic release of the ICD usually has many specifics defined only as TBDs ("to be determined's"). A propulsion-system-interface working group must coordinate further definition of the interfaces and properly document all interface requirements. Any drawing for either the engine or the vehicle interface must have a coded note that *prohibits* changes to mutually affected dimensions without proper coordination and subsequent changes to the ICD. A properly administered ICD has only design/operational requirements and does not contain instructional information. The "how to" and instructional information will be contained in the engine-model handbook prepared by "Logistics." Maintenance and handling information will also be defined in the various supporting logistics manuals.

The ICD will describe operational requirements and characteristics—such as prestart conditioning, thrust buildup curves, steady-state performance, and thrust-decay characteristics—and fluids requirements, interface loads, thermal environment, mass properties, and electrical and software requirements.

Space Envelope

An engine being installed in a vehicle not only must be properly bolted to the vehicle thrust mount, but also, equally important, must be impeded by no other vehicle parts. Space in the engine compartment of the vehicle must not only accommodate the engine envelope when in the neutral position (i.e., pointing straight aft) but also when fully deflected in all directions. Typical maximum engine deflections range from 4 to 10 deg. For clusters, moreover, the possibility of faulty deflection of engines must be taken into account. Because space in the engine compartment of a vehicle will usually be limited; engine designer and vehicle builder must have the closest cooperation, especially for upper-stage clusters, where large-expansion-area nozzles must be housed in a minimum interstage.

Connect Panels

All engine-to-vehicle lines, which may amount to a dozen or more per engine, must be reliably connected for each engine installation, not only in the vehicle but also in the static development and acceptance-firing stands. It has been found beneficial to define this interface clearly by combining all lines in one or several terminal-connecting panels (Fig. 10-26).

These panels, uniformly designed for all test locations, may be mounted on the vehicle (or test stand) or on the engine. For certain installations it may be advantageous to have matching panels on

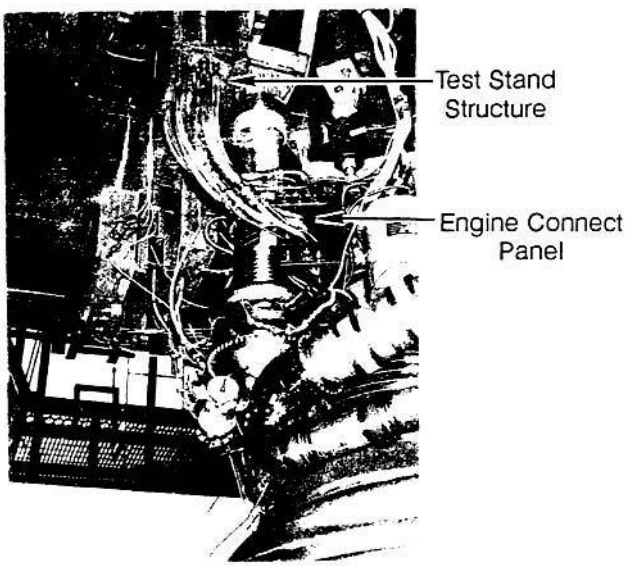

Fig. 10-26 Typical line connections on an experimental liquid-propellant rocket engine.

both the vehicle (or stand) and the engine. Aligned a short distance apart, standardized jumper lines between pairs of panels will permit rapid and reliable connections. As a possible disadvantage of the panel method, routing a line through the panels may force additional line length, as compared to individual routing of each line. Through careful design and close coordination between the engine designer and the vehicle builder, and in consideration of optimum location, subdivision, and orientation of the panels, advantages will, in most cases, far outweigh disadvantages.

Dynamic Interactions

Coupling between the propellant-feed system, the rocket engine, and the vehicle structure (as shown in Fig. 10-27) can result in a transient instability during launch commonly called "POGO." Typically it is recognized in data as a low-frequency oscillation (5-50 Hz) that grows out of the noise, levels off, and then decays back into the noise. This phenomenon was first seen in early unmanned flights of the Titan-Gemini that observers likened to the motion of a child bouncing on a pogo stick. Evidence of POGO can be seen in the inlet-pressure measurement of Fig. 10-27.

The problem (as indicated schematically in fig. 10-28) involves the vehicle structure, the columns of propellant in the feed lines, and the engines. The structure supports the engine while the engine supports the propellant mass during powered flight. During axial low-frequency vehicle vibration as the engine moves forward, (relative to the vehicle) fluid compression at the engine inlet causes the local pressure to increase. This pressure fluctuation produces an upward force on the propellant column and an equal downward force on the engine and structure. The pressure also causes an increase in flow into the engine, resulting in an upward-thrust component on the structure. If this upward-thrust component exceeds the downward force caused by the engine-inlet pressure fluctuation, the consequence will be a negative damping component on the structure. That will cause an instability, with divergent oscillations, if it exceeds the inherent structural damping of the vehicle. Circumstances resulting in an instability can tune the dominant propellant-feed line to a major vehicle structural resonance. Such tuning and detuning occur naturally during flight as propellant in the tanks is consumed.

The engine has two significant effects on the "POGO loop." It forms the lower boundary for the propellant-system and provides compliance and loss so that it helps define propellant system resonant frequencies and damping. More importantly, the engine sets the variation in upward thrust generated by a variation in inlet pressure. This so-called "engine gain" is critical to the evaluation of stability. In manned vehicles, for which 1/4 g POGO acceleration has been established as the crew limit, the frequency-dependent "engine gain" can be obtained empirically to preclude the possibility of a potentially disastrous instability. Unmanned vehicles often apply an analytical estimate, although some unmanned vehicles routinely experience peak POGO accelerations of 5-8 g.

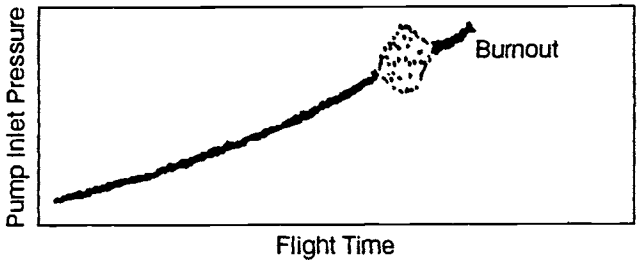

Fig. 10-27 Typical pump-inlet pressure variation of a vehicle affected by longitudinal oscillations.

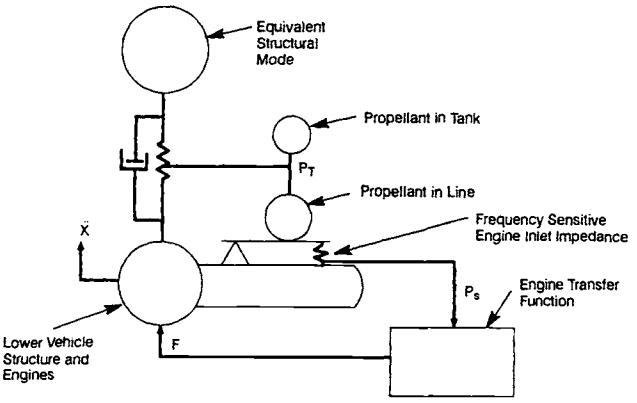

Fig. 10-28 Closed-loop coupling of propulsion system and vehicle (POGO).

When analysis predicts or flight data indicates POGO, the usual approach attempts to prevent tuning of the feed system and structure by use of a compliant device in the feed line near the engine inlet. Devices to do this detuning include helium-filled accumulators, spring-loaded piston accumulators, gas-tuned stand pipes, and compliant duct walls. The Space Shuttle used an accumulator with a gaseous-oxygen ullage and automatic level control that was contained within the engine oxidizer-feed system.

Avoiding POGO on a launch vehicle requires interaction between several disciplines. Like the flutter problem in aircraft, POGO occurs only during flight. Consequently, the dynamics of the subsystem must be mathematically described so that system stability can be estimated from simulation of in-flight coupling.

POGO-suppression devices. The devices used to attenuate the flow perturbations in the Titan II feedlines (Fig. 10-29 and 10-30) resemble in operation the surge tanks employed in the pressure regulation of large pipelines that have water-hammer problems. Surge tanks have been used as pressure-stabilizing devices in the flow lines of hydroelectric plants and pumping stations for more than 50 years; they serve as a point of pressure relief or cushion whenever there is a sudden change in flow. Vehicle feedlines, however, need suppression in a specific frequency range, and that necessitates a specially tuned surge-system. By selection of the proper damping and spring characteristics, the pressure perturbations

in the line can be absorbed by the suppression device and, in effect, uncouple the engine from the structural feedback loop.

In the Titan II, an entrapped gas bubble was incorporated in the oxidizer-line standpipe to provide a cushion or soft spring for the oxidizer mass in the standpipe to act on (Fig. 10-29); the energy due to pressure oscillations in the feedline can be transferred to this spring-mass system by judicious choice of the volume or height of the entrapped bubble. The fuel feedlines incorporated piston-type accumulators that utilize a mechanical helical spring and piston arrangement to give the desired soft spring-action (Fig. 10-30); the fixed mass of the spring and piston along with the mass of fuel in the accumulator provided the equivalent mass required for a resonant system.

The suppression devices were constructed and tuned so that their frequency responses, coupled with the appropriate feedline characteristics, would provide maximum attenuation of pump suction-pressure oscillations that were excited by tank-structure oscillations. The combined system could be optimized for maximum attenuation in a specified frequency range.

POGO oscillations also occurred in the Saturn V vehicle during boost flight. The frequency involved, 5 Hz, happened to be the natural frequency of the combustion process of the F-1 engines and of the entire Saturn V vehicle including the spacecraft. The vibration increased as propellants were consumed because the natural frequency of the vehicle increased. The frequency approached 5.5 Hz about 125 s after liftoff. While not necessarily destructive, the vibration had to be attenuated because it placed an undesirable acceleration on the crew. The design solution was to deter the two frequencies by placing a pneumatic spring in the liquid-oxygen feedline of each of the five F-1 booster engines. Cavities in the

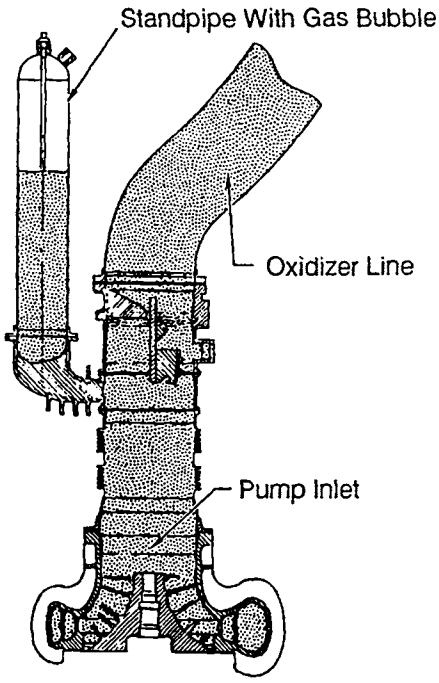

Fig. 10-29 Standpipe with bubble for POGO.

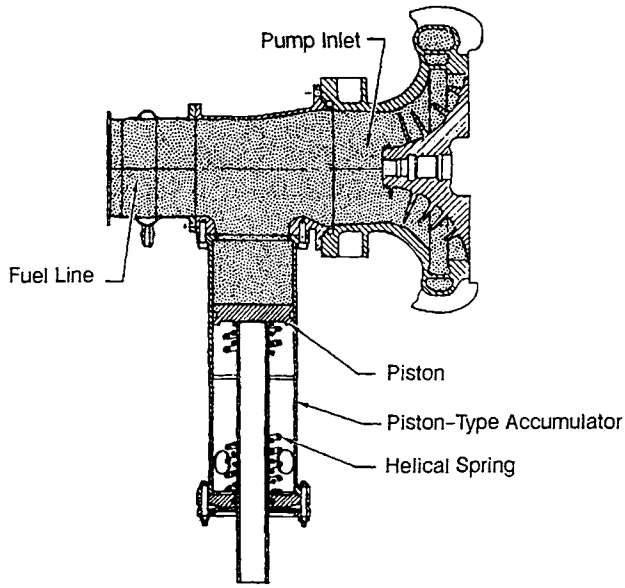

Fig. 10-30 Spring-loaded accumulator for POGO suppression, Titan II fuel-pump inlet line.

LOX prevalves for the engines provided convenient volumes for introducing gaseous helium, which does not condense at LOX temperature, to act as de-tuners.

A POGO suppression system in the LOX-feed system of the SSME at the inlet of the high-pressure oxygen turbopump (HPOTP) utilizes a gas-filled accumulator to suppress vehicle-induced flow oscillations. Gaseous oxygen tapped off the heat exchanger in the oxidizer-tank pressurization system acts as the compliant medium following an initial helium precharge. The system controls liquid level in the accumulator by means of a line that routes overflow fluids to the inlet of the low-pressure oxygen turbopump (LPOTP).

In the SSME's POGO suppression (see Fig. 10-31), the heart of the system, the gas-filled accumulator, serves as a capacitance in the LOX-flow circuit and prevents the transmission of the low-frequency (20-30 Hz) flow oscillations into the HPOTP. The system is sized to provide sufficient overflow at the maximum decreasing pressure transient in the LPOTP discharge duct. The engine controller supplies valve actuation signals and monitors system operation.

***Engine-failure sensing and shutoff system* (EFSS).** Such systems have been in use since the early days of liquid rocketry. They are especially important during engine and early cluster development. Part of them may later become a portion of flight emergency detection systems (EDS) and engine-out systems (see Chapter 2). The following list (not necessarily complete) of major engine-oriented malfunctions should be considered:

Pump-inlet pressures below safe minimum
Turbopump overspeed
Turbopump-bearing overheating
Turbopump-bearing vibration
Excessive turbopump leaks
Turbine-gas overtemperature
Combustion instability

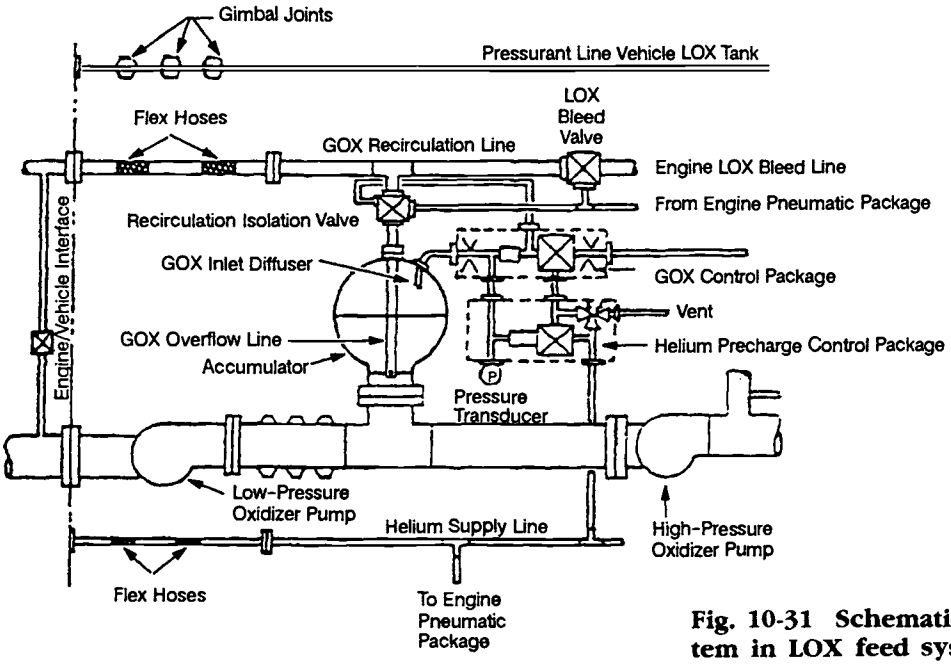

Fig. 10-31 Schematic of POGO-suppression system in LOX feed system on SSME.

Abnormal injection pressures
Ignition failure
Premature propellant depletion
Electrical-power failure
Pneumatic-pressure failure
Improper valve positions
Fires

Because of their potential for sudden destructive effects, many of the malfunctions will be sensed and the signals used to initiate immediate automatic shutdown. For others, which would not create an emergency within, say, fractions of a second, it is not uncommon to simply record their allowable minimum/maximum values using the test data computer. If the test data goes outside of the safe region, the computer can initiate shutdown.

For flight, a few highly critical parameters of the EFSS may be retained for automatic engine shutdown or mission abort. In this case, if the engine-failure sensing and shutoff system shuts down an engine yet the flight continues with the remaining engines, a vehicle-mounted electronic logic must sense the shutdown and take certain actions, including these:

- Closing emergency-shutoff valves in the ducts to the defunct engine, but not those in the others.
- Disconnecting electric power to the defunct engine only.
- Resetting or disarming backup shutdown-timers, since the reduced number of engines will consume the available propellants over a longer period of time.
- Locking the defunct engine in the neutral gimbal position.

Heat protection. The liquid-propellant rocket engine is a technological rarity, in which hot and cold temperature extremes must be handled together: insulation to maintain temperatures as low as -423°F in certain ducts, heaters to protect sensitive components against these temperatures. At the same time, in other areas at or around the engine, protection must be provided against the very high temperatures of the combustion process and the emerging gas jet, such as the cooling of the thrust chamber. The exhaust jet, at sea level, usually does not pose a major problem, unless blowback occurs from the flame deflector. At higher altitudes with vacuum or near-vacuum pressures, however, which are experienced even by first stages of a vehicle over the last portion of its flight, a substantial portion of the thrust-chamber gas jet expands sideways from the nozzle exit, forming a plume, creating considerable backwash and radiating powerfully back into the engine compartment. This endangers both engine and vehicle components—can cause surface temperatures of 1000°F or more without heat protection. In some cases it may be too cumbersome or costly in weight to provide individual insulation for each component. A protective heat-

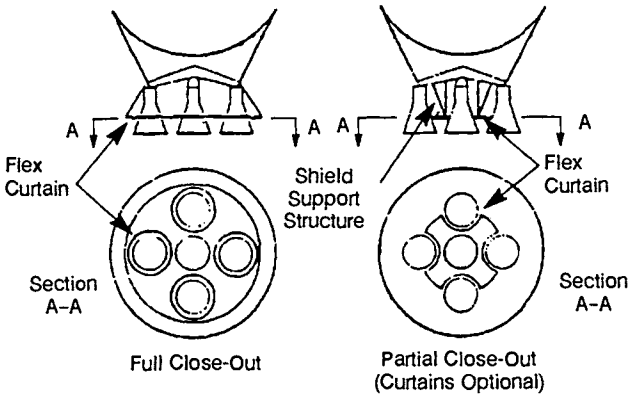

Fig. 10-32 Typical base-heating protection concepts (center engine fixed, outer engines gimballed).

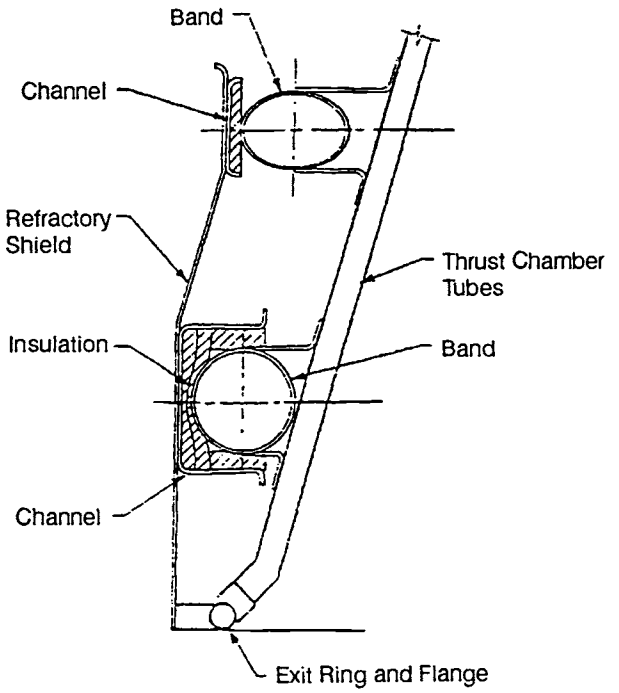

Fig. 10-33 Center-engine flame-impingement shield.

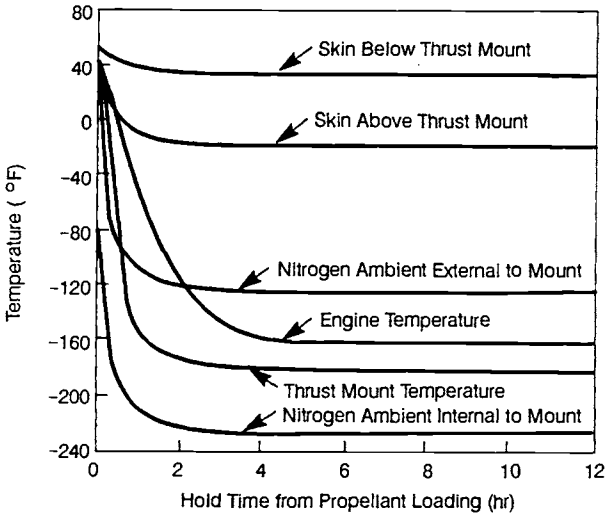

Fig. 10-34 Typical interstage temperature environment for an upper-space using cyrogenic propellants—565 SCFM (-100°F) nitrogen purge.

shield, forming a closeout diaphragm, may then be more effective (Fig. 10-32). This shield may be supported from a stationary (center) engine, if available, or from a supporting structure.

Design and installation of the base heat-shield requires the closest cooperation between engine and vehicle designer. The need for a partial or full closeout must be determined through special model tests. In most designs the shield connects to the engine nozzle. Suitable brackets must therefore be provided. During gimballing the heat shield will resist the engine motion. The forces encountered must be considered in the power budget for the hydraulic actuators. It must be taken into account that the heat-shield flex curtains may be quite cold before engine start and may still remain relatively cool at the far side, as planned, during stage operation.

In addition to backwash and radiation, which usually will not harm the internally-cooled engine nozzle itself, mutual gas-jet impingement between engines may occur from extreme deflection during gimballing. Excepting a major control malfunction, this impingement should affect the nozzle only for very brief periods near the exit. However, the heat may affect chamber structural elements, such as stiffening bands, which are not internally cooled. A heat-protective strip, a few inches wide, of ablative or other suitable material applied to the nozzle should suffice in most cases (Fig. 10-33). Obviously, single-engine vehicles do not need this type of protection.

Engine prestart conditioning and start. Functional conditions required within the engine to assure its readiness to start have already been discussed. When installed in the vehicle, the engine also requires external conditions that must be met by the vehicle builder. If prelaunch checkouts have ascertained readiness with regard to absence of leaks, correct valve positions, etc., prestart conditioning of the engine essentially refers to temperature and pressure levels around the engine and at the pump inlets. For both, early cooperation will be essential between the engine designer and the vehicle builder to arrive at a mutually feasible solution. Without this collaboration, the optimistic note in engine drawings "to be supplied by vehicle contractor" will accomplish little.

Certain engine subsystems, such as hydraulic components, control systems, and valve-actuation mechanisms, can function properly only if they come within a specified temperature range. Engine systems not employing cryogenic propellants may be dependent on heating or cooling only during prolonged coasting times in space. Engine systems that do use cryogenic propellants almost always need at least some heating. The cryogenic propellants within the engine, following start of tanking and the heat absorption of tank surfaces and lines, may rapidly lower the air temperature surrounding the engine to a few hundred degrees below 0°F.

Most vehicle systems will specify an allowable hold period, following tanking, to allow adjustments and checkout of other systems and to await optimum launch times (rendezvous missions), etc. A hold period exceeding the allowance may allow severe subcooling of engine components.

The temperature environment can be substantially improved by the vehicle builder through engine-compartment purges with warm gas (Fig. 10-34). An inert gas will bring the additional advantage of counteracting the accumulation of combustible gas mixtures from minor leaks. However, the vehicle builder's possibilities of heating through use of compartment gas purges are definitely limited. Some of the limitations stem from the engine designer's own specifications, which require avoidance of elevated temperatures around components containing cryogenic fluids to minimize boiloff and to prevent formation of gas bubbles. Also, certain structural mem-

bers must be kept below maximum temperatures because of their strength characteristics. Moreover, the purge-gas requirements and necessary heating provisions would become prohibitive if attempts were made to raise compartment temperatures above 32°F or even to 0°F. Figure 10-35 shows the effects of increasing purge flow and temperatures over those of Fig. 10-34. The analyses on which the graphs are based have shown that a further increase of the purge rate to 12,000 standard cubic feet per minute (SCFM) and 250°F barely raises the interstage temperature above 0°F. At the same time, the propellant boiloff rates in exposed ducts increased tenfold over those under the conditions of Fig. 10-34. The locations quoted are identified in Fig. 10-36.

For most applications the purges to the various areas will be made from a ground source. Once preconditioned, affected components can be expected to maintain their temperature within an allowable band after vehicle liftoff during the relatively short boost-periods. Only stages with prolonged cruising times may require an onboard purge supply system; that imposes payload penalties.

Literally a few inches away from the components requiring protection against low temperatures will be others that must be protected against warmup due to influx of heat. Here again, noncryogenic propellants pose few problems. By contrast, however, cryogenic systems, in particular those including liquid hydrogen, are very sensitive to heat influx. The effects on pump NPSH, which includes the vapor pressure of the fluid pumped, have been discussed in detail in section 8.5 in connection with tank insulation. For engine start, which involves the cryogenic fluids stored in the ducts immediately upstream of the engine and within the engine itself, insulation may become prohibitively complex. Continuous removal of superheated cryogenic fluids from the engine system and substitution of fresh liquid, therefore, has been widely used. This removal can be accomplished through continuous overboard bleeding or through recirculation back to the tank. In both cases, the liquids are tapped off at a point farthest away from the pump inlets and routed to the stage for overboard dumping or return to the tanks. A small auxiliary pump has often been required to obtain the minimum flowrates required for adequate bleeding.

During engine development, and even during vehicle static-firing programs, relatively favorable prestart conditions exist: the enclosing interstage is not in place, hold periods are under better control, and cold lower-stage tank surfaces are absent. But what worked faultlessly under these conditions may well fail in vehicle flight. A realistic recognition of this situation and close coordination between the two design teams will therefore be vital during the early phases of engine *and* vehicle design and development.

For first-stage applications, the engine builder stays relatively independent regarding start characteristics and sequence. The vehicle will not take off until thrust exceeds vehicle weight; gravity holds the propellants at the tank outlets; and all parameters are closely monitored from the ground control center. A holddown period before vehicle release and takeoff introduces an additional safety margin.

For upper-stage engine start, conditions become considerably more complicated. Absence of the propellant-settling effects of gravitation, the surrounding vacuum, temperature conditions at altitude, and remoteness from ground stations can only be crudely simulated in ground tests. Until first flights of a new vehicle have been made, therefore, the engine in-flight start sequence, which is closely interwoven with the stage separation sequence, must be based largely on analytical work. Neither vehicle builder nor engine designer can do this without consideration of, and consultation with, the other. The following principal relationships must be considered.

Starting the upper-stage engines while the lower stage is still at full-thrust level is difficult, mainly because of flame impingement and exhaust-gas dissipation from the interstage. Engine start will therefore preferably follow stage separation; but then propel-

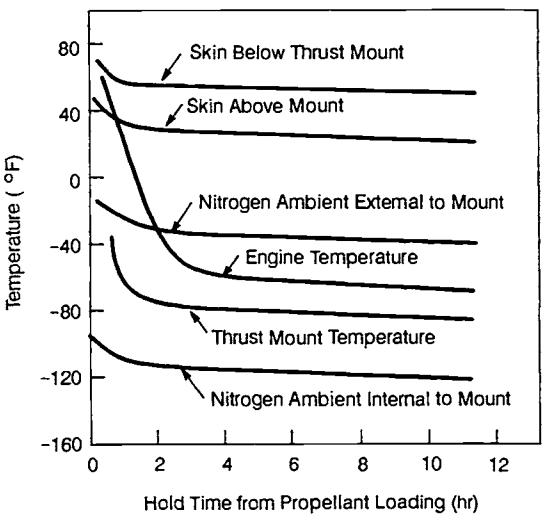

Fig. 10-35 Typical interstage environment for an upper-space using cryogenic propellants—4170 SCFM (250°F), nitrogen purge.

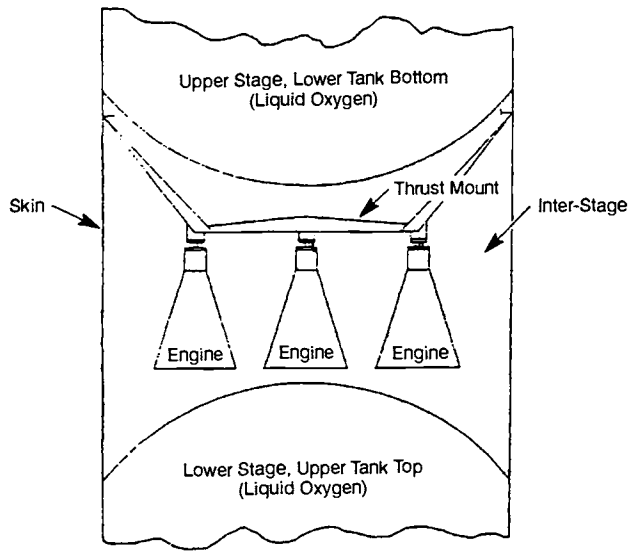

Fig. 10-36 Multistage-vehicle interstage.

lant settling from acceleration effects of the lower stage can no longer be assured. Auxiliary propellant-settling ("ullage") rockets (usually solid-propellant type) are required instead during engine starts. These add weight and drag and reduce payload. The size of the weight penalty, in turn, depends on engine-start characteristics (thrust-buildup time). For engines with relatively protracted buildup times, advanced initiation (with respect to lower-stage thrust decay and separation) of upper-stage engine start may substantially reduce the penalties. One second, lopped off the ullage-rocket burning times, may save hundreds of pounds of stage weight. The same amount of time added may not only reduce payload weight but may also pose serious control problems to the space vehicle, which floats essentially "rudderless" after separation and before the start of its own engines. From the foregoing requirements, the need for thorough mutual understanding of this important vehicle-to-engine interface becomes apparent.

Vibration environment. Even a normally or "smoothly" operating rocket engine generates a vibration pattern transmitted mechanically through the thrust mount, or acoustically through the ambient atmosphere, if present, to the vehicle structure. Neglect of these vibrations by the vehicle builder may lead to serious structural weakness or malfunction of vital control organs mounted to the vehicle structure. Means of reducing the normal engine vibrations are limited and hard to analyze. Rather, it is important that the engine developers establish, as accurately as they can, the existing acoustic and vibration pattern and inform the vehicle builder of their findings. Inability of the tiedown-firing measurements reliably to predict free-flight conditions imposes a serious handicap. However, through a thorough understanding of the potential and through specifications of static-test and flight measurements, in cooperation with the vehicle builder the engine designer can greatly help reduce the incidence of serious problems.

Nozzle expansion area ratio. From his own analyses, the engine designer may have selected a nozzle expansion area ratio that appears to be an optimum compromise among engine weight, performance, size, and producibility. When analyzed in the larger framework of vehicle performance, however, the selection may turn out not to be optimum. For stages with engine clusters, in particular, upper stages, the following factors must be considered (single-engine first stages disregarded here because least affected):

Gimbal angle. Following determination of the maximum gimbal angle required for safe vehicle guidance, including consideration of actuation malfunctions, the nozzle exit diameter will determine the attachment-point distances (mounting pattern) of the engines in a cluster.

Vehicle diameter. When mounted for proper gimbal capability, the envelope of the engine cluster must be in proper relationship to the vehicle diameter. If the cluster envelope is too large, the increase in vehicle dimensions may void all gains from a larger expansion area ratio. Engines not permitted to protrude beyond the projected vehicle plane in neutral

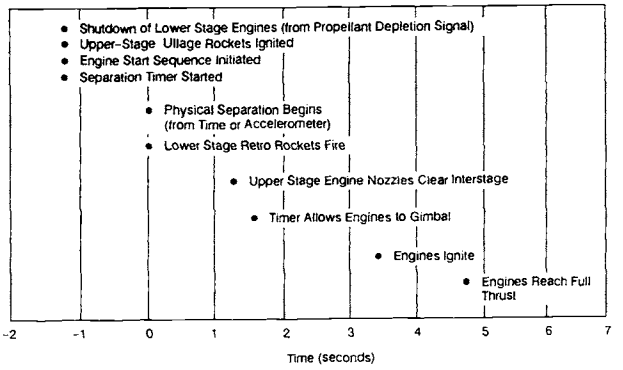

Fig. 10-37 Typical stage-separation sequence.

and/or in gimbaled position create an even more stringent situation.

Interstage length. When the upper-stage engines are mounted to the lower stage their length will determine the length of the required interstage. For a vehicle of the Saturn V class, each additional inch of interstage length will cost approximately 40 lb. Thus, here too, the added interstage weight required to accommodate a longer, better-performing nozzle may void the theoretical gains.

Stage separation. Separating the stages of a space vehicle entails three basic possibilities:

1) Leaving the interstage with the lower stage. This procedure requires the engines to pull out of the interstage cylinder during separation (Fig. 10-37). Marginal clearance between engine skirts and the interstage wall may force complicated means to avoid collisions between the separating stages. These may include a control system to tuck the engines inward and then swing them out upon separation and start them. Any such system adds complexity, lowers reliability, and may add weight. A shorter nozzle skirt of lesser diameter, although of somewhat lesser performance, may be better overall.

2) Leaving the interstage with the upper stage. To avoid the problem of stage collisions, it may appear attractive to leave the interstage attached to the upper stage. This adds inert weight to the upper stage, a penalty that may prove considerably larger than the performance loss from a somewhat shorter nozzle. A control problem may also be incurred in that the engine nozzles, in their outward gimbal deflection, still must clear the interstage wall. In joint optimization studies, the engine designer and the vehicle builder may weigh the possibility of leaving part of the interstage with either stage.

3) Leaving the interstage with the upperstage but dropping it in a second separation maneuver several seconds after first separation. In this dual-separation sequence, the second separation may consist of shedding the interstage as a complete ring, possibly in combination with guide rails, or of blowing it off to the side in segments. Either method requires some form of actuation in addition to accurate timing. Also, while the interstage is still attached, a serious base-heating

problem may develop. The requirement to overcome any difficulties may increase complexity and reduce reliability and partially neutralize nozzle-performance gains.

Whichever method is applied, the thrust-decay characteristics of the spent lower-stage engines greatly affect the separation sequence and the clearances. To optimize these, the vehicle builder needs accurate information on thrust-decay characteristics and tolerances from the engine designer. This information may take the form of a graph, as shown in Fig. 10-38.

Flame-deflector size. Engine nozzle size and arrangement on the vehicle, together with maximum gimbal angles, strongly influence the design of flame deflectors on engine and stage static-firing test stands and launcher flame-deflectors. Here, the problem is not so much one of optimizing vehicle performance, but of minimizing cost and of assuring the adequacy of these indispensable development tools.

Engine Handling, Installation, and Servicing Fixtures

For handling engine parts and assemblies during engine installation into development test stands and for various servicing functions, the engine builder requires numerous fixtures commonly referred to as ground support equipment (GSE). Some of these fixtures can be used by the vehicle contractor as designed, and others can be used for only a few minor changes or additions. GSE takes substantial funding in a typical vehicle program. Common use of as many of these fixtures as possible by the engine designer and the vehicle builder is strongly advised. To ensure this, the two must work together from the earliest design steps.

Standardization

The task of mating engine and vehicle will be substantially facilitated if the designers of both work to the same standards. This requirement applies to national, government, and company standards; to terminology and to mathematical symbols; and to the measuring system (metric or English, decimals or fractions, tolerances). Since several avenues are open, it is necessary, at the very outset, to agree on which one shall be pursued. This task requires close cooperation and full documentation.

Delivery Schedule

For the vehicle builder to deliver the stage on time, complete and equipped with engines, the engines must be available to him with sufficient lead-time. If the engine builder is directly contracted by the vehicle contractor, this schedule can be negotiated and followed up in a straightforward manner. In most cases, however, particularly with large liquid-propellant engines, these will be supplied to the vehicle contractor as government-furnished equipment (GFE). The engine supplier may not necessarily be fully cognizant, therefore, of the detailed vehicle needs. In either case, to avoid sudden unexpected compression of schedules the engine designer and developer must make sure that schedules for design, drawing release, manufacture, development, and engine delivery are in accordance with the vehicle needs.

Maintenance and Logistics

For systems not man-rated, until reliable and economic methods are developed to recover and refurbish rocket vehicles, rocket engines will ordinarily be used only once in flight, preceded by a reasonable number of checkout and acceptance firings. The engine model specification will include the total prescribed run capability (lifetime) of the engine, usually expressed in multiples of the rated flight duration. A factor of, for instance, 6, which includes a reserve for repetition of checkout runs, is typical. Because of the stringent weight considerations in rocket vehicles, engine design attempts to assure this life expectancy, but no more. Although reasonable safety factors make it most unlikely that the engine would completely collapse shortly after exceeding the allowable maximum run-time, the statistical probability of some engine part failing does increase. For this reason, most engine specifications prescribe overhauls of a stated scope whenever this limit is exceeded.

Similarly, upper limits are set for storage times. Exceeding these will trigger routine replacement of certain engine parts, notably of gaskets and seals. Rocket-engine preservation and packaging methods are well developed, permitting storage periods exceeding five years without overhaul.

During shipping, handling, installation, servicing, checkout, static firing, and launch preparation, damage of various types may be incurred by the engine because of parts failures, mishandling, oversights, or accidents. All incidents must be corrected by repair and/or parts replacements.

Any or all of the described maintenance actions may be required either while the engine remainsl with the engine builder or following its delivery to the vehicle contractor. An accurate and effective

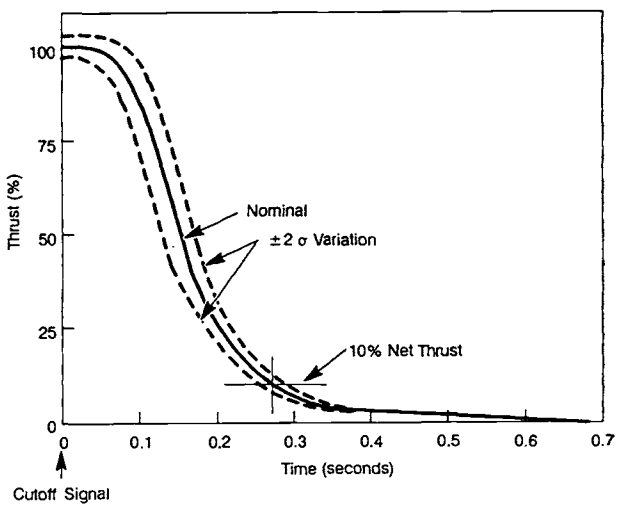

Fig. 10-38 Typical engine thrust-decay deviations.

maintenance or logistics plan must be worked out between the two contractors, or with their contracting agency, considering all handling needs at all test stations. This plan will include the conditions under which an engine should be returned to the factory for overhauls, repairs, and parts replacements. If return is not required, the correct handling fixtures and tools must be provided for each location. Above all, an adequate stock of spare parts must be planned. The engine designers will frequently be consulted for their advice in an effort to avoid both time losses due to lack of parts and costly overstocking.

Multiple-Engine Use

In view of the cost of rocket-engine design, development, and procurement, common usage of a given engine for several vehicles, or for several stages of the same vehicle, will be very desirable. Also, common usage can substantially reduce or simplify logistics, handling, checkout, launch preparation, and instrumentation requirements. Caution must be exercised, however, not to go "overboard," lest engine-to-vehicle interfaces become considerably more complicated.

Effort should be concentrated on the common usage of the major cost items and engine building blocks, such as turbopumps, injectors, combustion chambers, gas generators, valves, gimbal blocks, and high-pressure ducts. Peripheral equipment, such as instrumentation lines, servicing lines, inlet ducts, and wire connections, should be left flexible enough to adapt them to each vehicle without compromise. It is tempting for procuring agencies to warehouse just one engine model and to ship "from the shelf" to wherever the need arises. This convenience, however, may cost substantially more than the expected savings: in mission compromises, reduced reliability, increased coordination effort between engine builder and vehicle builders, substantially increased possibility of oversights and communication gaps, and cost- and time-consuming retrofits. As always, a thorough and unbiased joint analysis considering all aspects, including that of the long-range future, will readily yield information about the point of diminishing returns.

Reserves and Safety Margins

In the engine designer's negotiations with the engine user, i.e., "the customer," which quite likely is a government agency, the engine designer, like the vehicle builder, will frequently find himself under pressure to compromise. This compromise may be to cut weight or to accelerate schedules. It is then that designers will be most in need of their top management's understanding and support. But it is here also where they will be most criticized if their analyses prove incomplete, superficial, not optimized, or heavily biased by safety factor upon safety factor. Striking an optimum balance between high performance and adequate safety-factor reserves represents one of the finest arts of engineering and is directly translatable into the degree of success. Once certain that this balance has been achieved, or concerned that it may be lost, the designer should go on record. Doing so, the designer should also remember Edmund Berkeley's observation: "Thoughtful and tolerant disagreement is the finest climate for scientific progress."

Design of Liquid-Propellant Space Engines

Liquid-propellant space engines embody the same operating principles and general characteristics as the liquid-propellant rocket systems previously discussed. However, their specific missions for use in spacecraft require special design considerations, as described in this chapter.

11.1 PRINCIPAL SPACE APPLICATION

By definition, space engines supply all the forms of rocket propulsion that a spacecraft requires for various maneuvers in space, including attitude control and stabilization, coplanar and interplanar orbit changes, trajectory corrections, rendezvous maneuvers, lunar and planetary landings and takeoffs, and retrofiring (reversed thrust for deceleration) during re-entry into Earth's atmosphere. The thrust of a space engine may be a fraction of a pound or many thousands of pounds. Aside from a few solid-propellant motors (used mainly for perigee and apogee propulsion for raising orbits) and stored-gas systems (used only in applications for thrust levels less than 1.0 lb and for a total impulse of less than 5000 lb-s), the majority of space engines employ liquid propellants. Because of inherent operational advantages, liquid systems likely will continue to dominate the space-engine field for the foreseeable future.

Liquid-propellant space engine systems may be divided into two basic groups: vehicle main propulsion and reaction control. These differ not only in function and thrust level but also in the type of propellant used, the degree of required controllability and thrust variation, and system components. But common to virtually all of them will be the requirement that they be able to start and operate reliably in the cold vacuum of space.

Spacecraft Main Propulsion

The main propulsion for most spacecraft has employed pressure-fed, storable hypergolic propellants, such as the Transtage propulsion system, with a thrust level of 16,000 lb. The systems include propellant tanks and pressurization system, control valves, main thrust-chamber assembly or assemblies, and a gimbal mechanism or some other type of thrust-vector control. Most main thrust chambers are ablatively or regeneratively cooled, sometimes with radiation-cooled nozzle extensions.

A few spacecraft have used pump-fed systems, such as the 17,000-lb-thrust pump-fed engine for the Agena. As missions become more ambitious, requiring greater delta-V and higher-energy cryogenic propellants, pump-fed systems become increasingly important in spacecraft propulsion. Most space missions require multiple starts (sometimes over a long period of time) and may require throttling. These requirements usually account for the principal differences between the main propulsion systems for spacecraft and those for booster vehicles.

Reaction Control

Reaction-control systems differ from other liquid-propellant rockets in design arrangement and thrust level, which may run from 1 up to 1000 lb, with most systems falling within the 1-to-100-lb range. These systems may be used to provide attitude control, to align a spacecraft for a midcourse corrective or terminal maneuver, to rendezvous with another vehicle, and to stabilize the vehicle after separation from another stage or during Earth re-entry.

As a rule, attitude-control engines are used in opposing pairs to produce pure couples about an axis. They are often mounted in clusters to simplify plumbing and wiring. Parallel pairs of engines, or individual units, produce the translational movements along the vehicle axis, as in rendezvous and docking maneuvers.

The reaction-control engine systems are usually pressure-fed, using monopropellants or storable hypergolic propellants. Thrust level and duration must be very closely controllable. The thrust chambers may be ablatively or radiation cooled, depending on the application.

Application Example

The application of various space engine systems may best be illustrated by typical examples, such as the Space Shuttle Orbiter, which has onboard propulsion for orbital maneuvering and attitude control. The orbital maneuvering system (OMS) provides axial thrust for orbit insertion, orbit circularization, orbit transfer, rendezvous, deorbit, and various abort scenarios. The reaction control system (RCS) provides thrust for three-axis attitude maneuvers and small translation maneuvers. Both systems are pressure-fed and use nitrogen tetroxide (N_2O_4) oxidizer and monomethyl hydrazine (MMH) fuel. The propellants are earth-storable and hypergolic.

The OMS is mounted in two identical pods in the rear of the Orbiter, as shown in Fig. 11-1. Each pod contains about 12,000 lb of propellants and a single 6000-lb-thrust OMS engine. The tanks are pressurized with high-pressure helium; high-pressure nitrogen supplies engine purge and valve operation. After each engine burn, nitrogen purges propellants from the engine downstream of the bipropellant valve. This procedure allows up to 10 restarts per flight. The reusable OMS has been designed for 100 missions with 1000 engine starts and up to 15 hr of cumulative firing time.

The OMS engines are gimballed in the pitch and yaw planes. RCS operation is not required during OMS burns unless gimbal capabilities are exceeded or a single OMS engine is used. Redundancy is provided. The aft RCS thrusters can provide any of the OMS maneuvers. Propellant can be transferred from the OMS tanks to the aft RCS tanks and between the left and right OMS pods.

The RCS has both fore and aft positions, as shown in Fig. 11-2; the forward RCS, in the fuselage nose area; the rear RCS, in each of the pods containing an OMS. Each of the three systems contains about 2400 lb of propellants and a helium-pressurization system. The forward system includes 14 primary thrusters, with a thrust level of 870 lb, and two vernier thrusters with 24 lb of thrust. Each of the aft systems includes 12 primary thrusters and two vernier thrusters. The primary thrusters can perform all RCS tasks; multiple units provide redundancy. Vernier thrusters usually will be preferred for attitude control in orbit. Because primary thrusters can also be used, redundancy is not provided for the verniers.

The primary RCS thrusters can sustain 20,000 starts and cumulatively 12,800 s of firing duration. The engines can be pulsed in durations as low as 0.08 s. Continuous steady-state thrusting can run from 1 to 150 s. In the event of OMS engine failure, the aft-facing engines have a maximum single-mission firing capability of 800 s, and the forward facing engines can fire for 300 s. The vernier thrusters are capable of 330,000 starts and 125,000-s duration. They can provide steady-state burns of 1 to 125 s and pulses as low as 0.08 s.

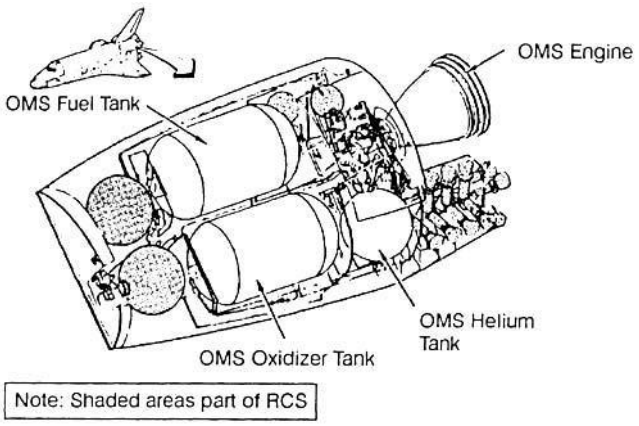

Fig. 11-1 Space Shuttle Orbiter OMS (courtesy of NASA).

11.2 GENERAL DESIGN CONSIDERATIONS

Before the actual design of a space system, it is necessary to examine the basic engine parameters to determine their influence on the spacecraft's ability to perform its intended mission. An overriding consideration will be reliability. Typical space missions include the establishment of an orbit around a planet following a transfer from Earth, which may last several months or years. The ability of a propulsion

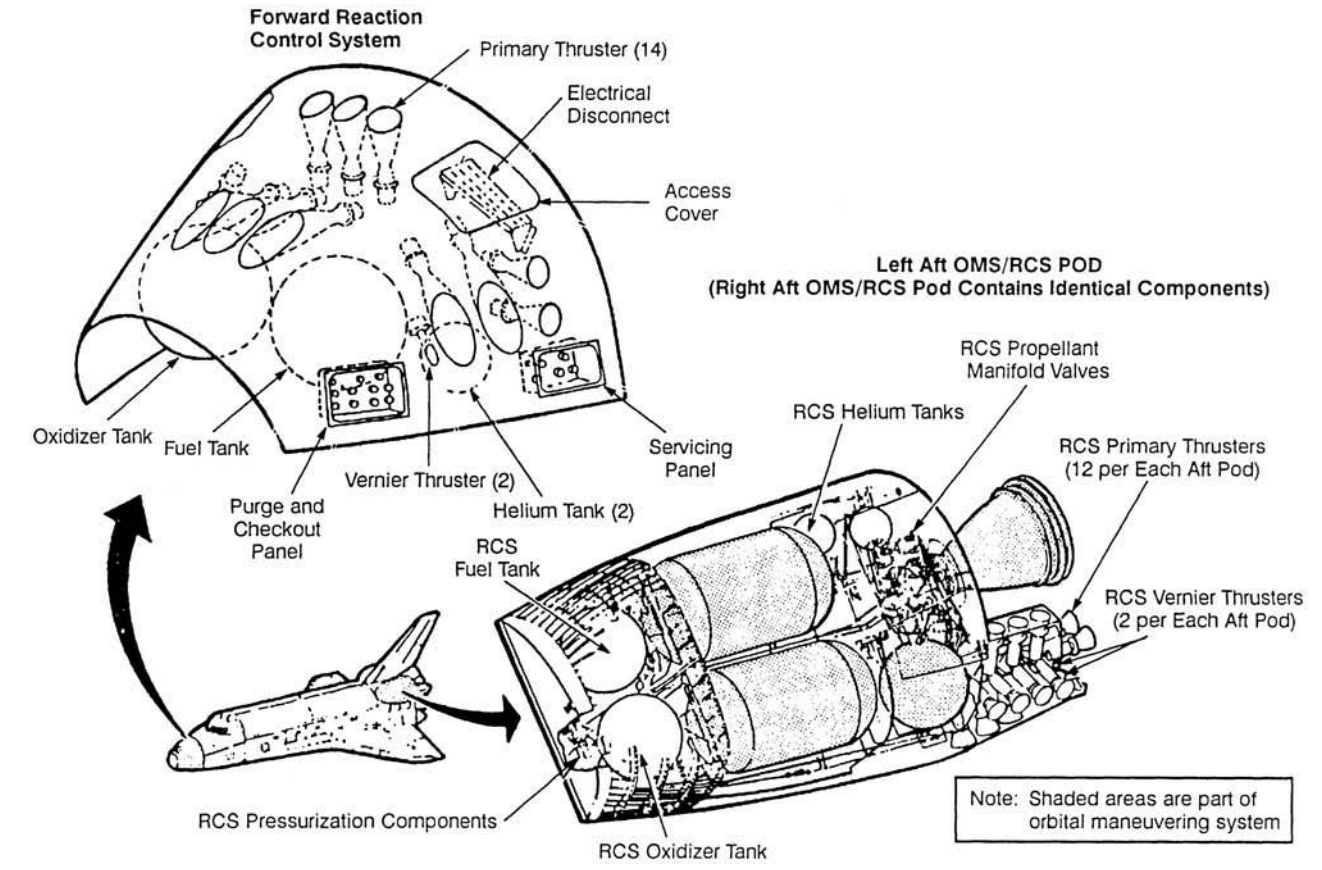

Fig. 11-2 Space Shuttle Orbiter RCS (courtesy of NASA).

system to coast in space for such long periods and then fire reliably typifies many contemplated missions. It is one of the foremost considerations in the design of a space engine.

Based on mission, trajectory, and payload requirements, optimization of one or a group of propulsion systems must examine the ramifications of propellant type, vehicle-system operational requirements, and mission environmental effects.

Several different designs (assuming various propellants, feed systems, chamber-cooling methods, etc.) may be conducted simultaneously for a given space mission. These designs must be carried far enough to evaluate their relative merits, such as reliability and performance, and establish the advantage of one design over the other. An optimum system design should thus emerge.

Selection of Propellants

Various aspects of liquid rocket propellants have been discussed in section 1.4. Here will be covered characteristics pertinent to selecting propellants for space-engine application. The reliability and performance of a spacecraft will depend greatly on the propellants. The choice ranks paramount in establishing the optimum design criteria and final operational capabilities of a vehicle. For any planned mission, the projected program time-periods, as related to the anticipated state of the art and operational reliability of propellants, should be the first criterion for selection. Propellants with undesirable characteristics and those that have no advantages over similar, more desirable types should be eliminated early in the studies. In addition, propellants will be selected on the basis of the following:

1) *Specific impulse.* Specific impulse may be the most commonly used basis for comparison in nearly all propellant evaluations. For a given initial spacecraft weight (limited by the payload capability of the launch vehicle) and required mission velocity increment, mission payload will be a function of the main engine system's specific impulse and the spacecraft inert weight, as shown in Chapter 2. Similarly, for a given spacecraft initial weight, inert weight, and payload, the mission velocity increment will be directly proportional to the main engine system specific's impulse. The specific impulse of a reaction-control engine directly affects its "system package" weight. A higher specific impulse will lower system weight for a given total-impulse requirement.

2) *Operating temperature.* In an overall vehicle-optimization study, specific impulse must not be used as the only criterion for propellant selection. Maintaining propellants at temperatures that permit effective use of the propulsion system after coast adds a major design consideration. Thus thermal control of the propellants during coast affects the selection and vehicle configuration. Heat transfer between propellants, and between propellants and other vehicle components, must be considered, as well as heat radiation out to space, in from the Sun, and between vehicle components. Studies have indicated the feasibility of insulating propellants against excessive temperature changes even during long coast periods in deep space missions. More insulation weight will be needed for cryogenic propellants than for the earth-storable. This difference becomes greater as the coasting periods last longer.

3) *Density.* The bulk density of a propellant combination also affects vehicle payload, especially in volume-limited applications. Higher bulk densities mean smaller propellant tanks and pressurization systems for a given propellant weight.

4) *Ignition characteristics.* Better hypergolic action by the propellant combination will effect a simpler and more reliable space-engine system, particularly for multiple starts.

5) *Cooling and other characteristics.* Some propellants are excellent coolants (for regenerative or film cooling), while others have little cooling ability. The propellant combination will determine the combustion temperature and the gas constituents, which vary widely as to their compatibility with chamber materials, especially with the ablative or refractory materials frequently used in space engines.

Ideally, all propulsion systems in a spacecraft should use the same propellant combination. However, in some applications the reaction-control engines will do the propellant-settling in the main system tanks. Then they must be supplied by separate tanks equipped with positive-expulsion devices. This factor likewise affects propellant choice. Table 11-1 summarizes characteristics of various propellants suitable for space-engine applications.

Vehicle-System Operational Requirements

After the vehicle-system operational requirements have been analytically established for a given space mission, many design parameters and special considerations for the engine system or systems can be derived, notably the following (besides propellant selection):

1) *Engine-system design thrust and run time.* These will be optimized by analysis of the mission trajectory, considering spacecraft operating limitations such as acceleration loads. Required mission delta-V and engine-thrust level influence, to a large extent, the choice between a pressure-fed and a pump-fed system.

2) *Engine system operating characteristics.* These include engine throttling range, thrust as a function of time, number of starts and repetition rate, cutoff impulse and accuracy, and TVC requirements—most of these determined by various projected spacecraft maneuvers. It may also be desirable for the same engine system to fulfill more than one type of maneuver or to be reused on subsequent missions. Figure 11-3 shows typical thrust-time histories for various spacecraft maneuvers.

3) *Engine power cycle.* If a pump-fed engine is selected, one of the major decisions to be made concerns the power cycle. The power cycles discussed in Chapter 2 apply to space engines as well as booster engines, the primary difference between the two being that engines that do not operate in the atmosphere do not benefit as much from high chamber pressure. Since vacuum specific impulse increases only slightly with increasing chamber

Table 11-1 Liquid-propellant combinations for space-engine applications.

Propellant Combination	[a]Specific Impulse (s)	Density Impulse (s-gm/cc)	Freezing and Boiling Points (°F), Oxidizer/Fuel (FP)(BP)/(FP)(BP)	Mixture Ratio (O/F)	Combustion Temperature (°F)	Remarks
F_2/H_2	474	241	(-364)(-307)/(-435)(-423)	9.3	6440	Hypergolic
[b]O_2/H_2	456	143	(-362)(-298)/(-435)(-423)	4.7	5110	Nonhypergolic
OF_2/B_2H_6	430	424	(-371)(-299)/(-265)(-135)	3.5	7010	Hypergolic
OF_2/B_2H_6	420	357	(-371)(-299)/(-265)(-135)	2.15	5910	Hypergolic
F_2/N_2H_4	419	551	(-364)(-307)/(35)(236)	2.4	7285	Hypergolic
OF_2/CH_4	417	451	(-371)(-299)/(-300)(-260)	5.6	6700	Nonhypergolic
O_2/B_2H_6	408	303	(-362)(-298)/(-265)(-135)	2.0	5960	Nonhypergolic
N_2H_4/B_2H_6	402	254	(35)(236)/(-265)(-135)	1.2	4085	Nonhypergolic
N_2O_4/B_2H_6	375	340	(11)(70)/(-265)(-135)	2.9	5710	Nonhypergolic
[b]N_2O_4/N_2H_4	341	409	(11)(70)/(35)(236)	1.23	5513	Hypergolic
[b]MON/EMHF	341	407	(-23)(29)/(-76)(144)	2.2	5330	Hypergolic
[b]MON/MMH	338	401	(-23)(29)/(-63)(189)	2.4	5370	Hypergolic
[b]N_2O_4/50-50	339	408	(11)(70)/(18)(170)	2.1	5175	Hypergolic
[b]N_2O_4/MMH	339	407	(11)(70)/(-63)(189)	2.3	5290	Hypergolic

Notes: MON = Mixed oxides of nitrogen, 85% N_2O_4-15% NO.
MMH = Monomethylhydrazine, $CH_3 \cdot N_2H_3$, 50-50 = 50% UDMH, $(H_3C)_2N_2H_2$ -50% N_2H_4.
EMHF = Eutectic mixture of hydrazine fuels = 87.6% MMH-12.4% N_2H_4.

[a] Based upon theoretical shifting equilibrium at 150-psia nozzle stagnation chamber pressure and 40:1 nozzle expansion area ratio in the vacuum.

[b] Propellant technology and application are well established.

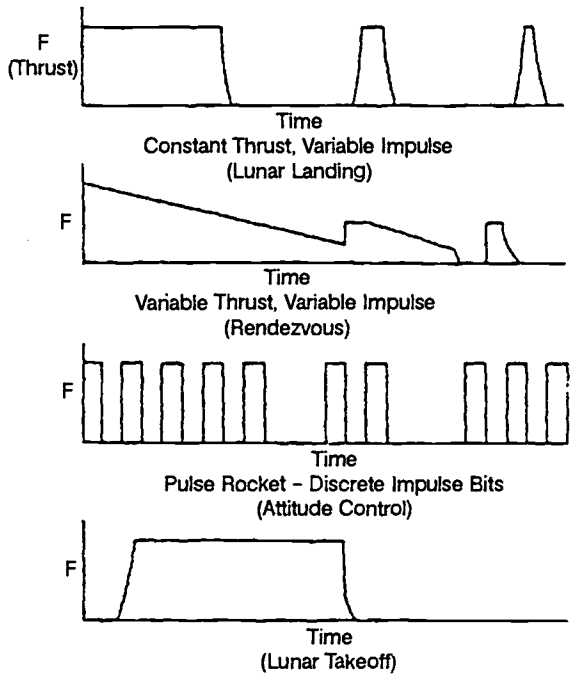

(Coulbert, C.D., "Selecting Cooling Techniques for Liquid Rockets for Space Craft," *J. Spacecraft and Rockets* 1, 129-139, 1964.)

Fig. 11-3 Typical liquid-propellant-engine thrust-time histories for various spacecraft maneuvers.

pressure, higher pressures primarily bring the benefit of smaller engine size and, up to a point, lower engine weight. Expander cycles are therefore more attractive for space engines since they are generally limited to relatively low chamber-pressures.

4) *Engine system design.* Experience has shown that multiple-start operation, as required by most space-engine systems, has a more severe effect on a rocket engine than has continuous steady-state operation of comparable firing duration. This should be expected, because continuous operation involves a minimum of control components and actuations. Multiple starts, on the other hand, require that each component responds perfectly each time it is called upon. In addition, multiple starts require much longer periods of minimum leakage by propellant and pressurant. More rigorous approaches toward improved reliability, such as component or subsystem redundancies, must therefore be considered in the design.

5) *Engine-system component design.* Besides mission environmental effects (to be discussed below), detailed design of the engine-system components will be directly affected by the spacecraft configuration. For instance, the location of the engine-system (internal in or external to the spacecraft) determines the feasibility of radiation cooling for the thrust chamber. Engine envelope limitations affect the choice of nozzle type, allowable expansion area ratio, and even the feed-system type. (In some applications a pump-fed system affords a

much higher expansion area ratio for a given envelope.) The structural design of the system components will be influenced by the maximum vehicle acceleration and by vibration loads.

Mission Environmental Effects

After the propellants have been selected and the basic propulsion-system design established (with preliminary considerations of mission environmental effects), it is possible to examine the various engine subsystems in detail to determine which components or phase of system operation will still be affected by the projected mission environment in space. Characteristics of this environment include the following:

1) *High vacuum.* The low ambient pressures experienced in space missions may cause vaporization of metals and partial or complete removal of film or adsorbed gas layers at the surface of the material. Principal problems associated with high-vacuum conditions are—

—Reduced ability of a component to perform its function, due to mass loss through material vaporization or bulk-property changes.

—Changes in the radiative-heat-transfer properties of the material, which could increase, to a destructive level, the bulk temperature of a component such as a radiation-cooled nozzle skirt.

—Possible condensation of metallic vapor on electrical components, resulting in short-circuiting.

—Changes in the fatigue, frictional, and creep properties of materials; possibility of self-welding of metals.

Design remedies against high-vacuum effects include material selection and proper location of the components within the vehicle to take advantage of nonvacuum environments.

2) *Thermal environment.* The thermal environment encountered in space missions, such as in Earth orbit or during the transfer phase in interplanetary flights, obviously will affect the design of space propulsion systems, especially the storage of propellants. Three external sources of radiant energy must be considered when evaluating the thermal environment of a spacecraft: direct-solar, albedo (solar energy reflected from a planet), and planetary-emitted radiation. Direct solar radiation, the largest external heat source, will motivate an orientation of the spacecraft for maximum protection of the vulnerable subsystems such as propellant tanks. Quantitative evaluation of thermal radiation in space indicates that excessive absorption of radiant energy may damage some components unless protected by means such as reflective surfaces or coatings.

3) *Nuclear radiation.* The two most important effects on metals of nuclear radiation in space are the production of internal heat and the dislocation of atoms within their crystalline structure. The nuclear particles of interest are fast neutrons, lower-energy protons, alpha particles, electrons, and gamma rays. The fast neutrons present the most severe problem. It is known, however, that they do not exist to a great extent in space. Generally speaking, the total radiative flux from all nuclear radiations will not cause appreciable damage to metals over a period less than two years.

4) *Meteoric bombardment.* Spacecraft will be exposed to the impact of meteoroids ranging in size from microscopic dust particles to bodies of asteroid dimensions, with a correspondingly wide distribution of kinetic energies. Collision of the spacecraft with these materials can cause surface erosion, punctures, or total destruction of the vehicle. The ideal protection for propulsion-system components would be to locate them entirely within the vehicle. This, however, will usually not be practical for parts such as the thrust-chamber nozzle skirt. Adequate consideration must be given to the design of these parts with respect to the cited effects.

5) *Effects of gravity.* The absence of gravity, as well as the presence of large acceleration forces, should, proper provisions being made in the design phase, cause no mechanical-design problems. The main problem will be with the propellant-feed system. This can be overcome by positive expulsion or by providing propellant-settling rockets (which themselves would require a positive-expulsion feed system).

11.3 DESIGN OF THE SPACECRAFT'S MAIN PROPULSION SYSTEMS

System Design

The reliability requirements for space missions have led to simple, stored-inert-gas pressure-fed main propulsion systems using conventional hypergolic earth-storable propellants and redundant control components. Recent development of a high performance pump fed space engine (the 3750 lb thrust XLR132, N_2O_4/MMH propellants) can lead to future application of pump fed systems for space missions.

For tube connections, the trend is to welded or brazed joints, with flexibility provided either by braided metal hoses or metal bellows. Beside meeting thrust and performance specifications, a spacecraft main engine will have the following principal system design requirements:

- High reliability and crew safety (through redundancy in the control system; use of proven design concepts, materials, and fabrication techniques; and extended-life and overstress testing).
- High combustion-stability rating with respect to perturbations during start and throttle transients.
- Ability to make numerous starts, with repeatable cutoff impulse.
- Deep throttling (optional, not required by all missions) with simple controls.
- Propellant utilization that exhausts both propellants simultaneously.
- Effective isolation of the propellants from the system during long coast periods (use of propellant-isolation valves).
- System growth potential and flexibility for mission modifications.
- Sufficient protection against heat, nuclear radiation, and meteoric bombardment.

In some applications, the propulsion system can be operated on a propellant-tank-ullage-gas blowdown principle during the latter portion of the mission. This could reduce the required amount of pressurant (and pressurant-tank volume) by as much as one-half of that for a regulated, constant-pressure system.

The critical start of the main thrust chamber will not need ignition devices if the system uses hypergolic propellants. However, careful sequencing of the propellant flows during start will usually be required to avoid pressure spikes and instabilities.

Nonhypergolic propellants typcially employ augmented spark igniters (ASI)—essentially spark plugs recessed into a cavity in the combustion chamber. Propellants fed into the ASI ignite and light the main combustion chamber.

Various schemes have been considered and developed for the deep throttling often required by spacecraft main propulsion systems. For instance, the Apollo LEM descent engine was required to vary thrust continuously over a range from 1050 to 10,500 lb to permit hovering, selection of a landing site, and the landing itself.

The most straightforward means of throttling—valves in the main propellant lines—can give throttling ratios of about 3:1. Other components must also be designed to accomodate the throttling. The injector pressure drop must be high enough to promote good mixing and atomization of the propellants as well as to prevent dynamic instabilities between the combustion chamber and feed-system components. Since the injector pressure drop varies with the square of the flowrate for liquid propellants and directly with the flowrate for gaseous and supercritical propellants, the design point pressure drops will typically be higher for a throttling engine than for a fixed-thrust design. Similarly, the turbopumps (in a pump-fed system) must be able to accommodate a wider operating range without experiencing stall or unstable operation, and control valves must provide adequate control margins over a wider operating range. If the thrust chamber is regeneratively cooled, the heat flux will fall off more slowly than the coolant flow as the thrust is reduced, so the cooling margins must be greater than with a fixed-thrust engine.

Some means of varying the injector area will allow higher throttling ratios—such as two or more manifolds with separate valving so that only some of the injector elements will be used during throttling; but this method adds complexity to the hardware and control system and will usually lower combustion efficiency. Another method makes use of pintles to change the injector flow area, which allows control over injector pressure drop with drop in the flowrate, again adding complexity.

Figure 11-4 presents the schematic of the propulsion system for Transtage, an upper stage used with the Titan launch vehicle to make orbit insertion, orbit modification, and rendezvous maneuvers. A pressure-fed system with multiple-restart capability, it uses about 23,000 lb of N_2O_4/50-50 propellants.

The Transtage has two engines that share propellant tanks, pressurization system, and electrical and mounting systems. Two interconnected spherical helium tanks, initially at 3600 psia, hold pressurant to maintain the tanks at a regulated 160-psia pressure. When restarting in space, attitude-control engines settle the propellants in the main tanks preparatory to engine start. Each Transtage engine develops 8000 lb of thrust and operates at a chamber pressure of 105 psia with an area ratio of 40:1, for a delivered specific impulse of 310.6 s. The thrust chamber has ablative cooling and a radiation-cooled extension made of aluminide-coated columbium. Propellants are fed to the combustion chamber through a bipropellant valve controlled by an electrically-actuated pilot valve.

In a complete space-vehicle system, performance gains of the spacecraft stages will effect increasing weight savings for each succeeding lower booster stage, as described in Chapter 2. Plans for future spacecraft missions usually consider high-performance liquid propellants, such as O_2/H_2. For high mission delta-V, these propellants in pump-fed systems usually give a considerable performance edge over pressure-fed systems. A pump-fed system for these applications must reliably supply high-pressure propellants to the combustion chamber, under vacuum and zero-gravity conditions and after long periods of coasting. All pumps must be fully primed before starting the engine system to prevent delays in pump buildup and overspeeding. This may require ullage-settling rockets, before and during main engine start, or positive-propellant-expulsion devices. In addition, the systems should be able to restart (if possible from available tank-pressure energy, without auxiliary starting devices) and to throttle (for some applications over a wide range). Major design concerns associated with turbopumps under space environmental conditions (other than material considerations) include: vacuum, temperature, and radiation effects on exposed high-speed bearings and dynamic seals; micrometeorite penetration of fluid passages; and absence of the effects of gravitation on pump operation.

An example of an advanced, high-performance pump-fed space engine, the RS-44 (Fig. 11-5), has undergone detailed design and component testing. A 15,000-lb-thrust regeneratively-cooled O_2/H_2 engine intended for orbit-transfer stages and lunar and interplanetary flight, it employs an expander cycle and, due to the excellent properties of the hydrogen working fluid, operates at the relatively high chamber pressure of 1540 psia, which improves performance and reduces the size and weight of the engine. Its reliability has been raised by eliminating the hydraulic system, a step made possible by operation of the control valves and gimbal actuators by electric motors. Pneumatic override on the actuators provides redundancy. Low-pressure-drop ball valves are used in the major propellant lines. The engine can be continuously throttled from 100 down to 10% thrust and can also be operated at about 3% of full thrust in a pressure-fed tank-head idle mode to settle propellants in the tanks and to chill the engine efficiently before a start.

High-performance partial-admission turbines drive the centrifugal pumps. A single-stage turbine

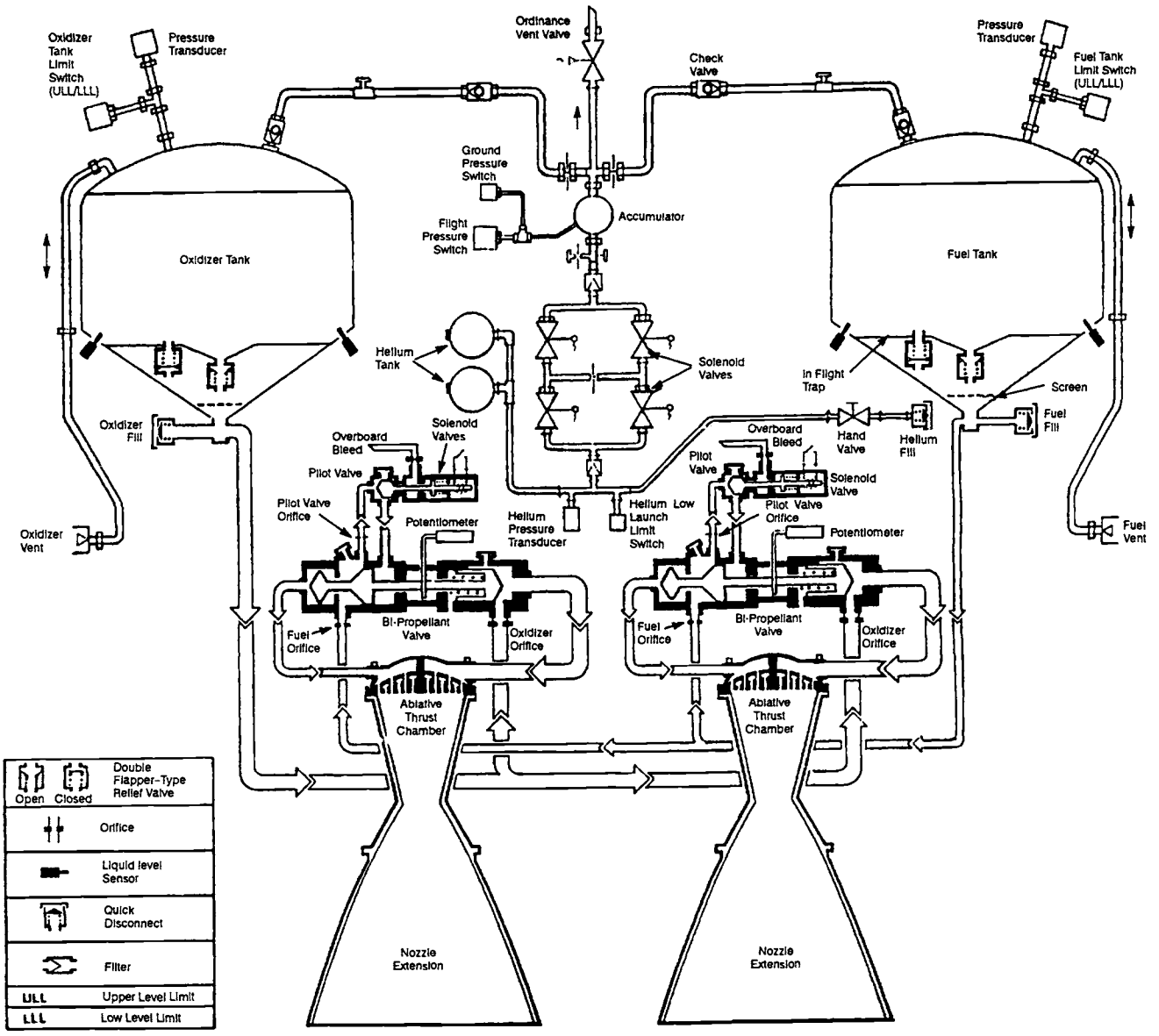

Fig. 11-4 Schematic of the Transtage propulsion system (courtesy of Aerojet Tech Systems Co.).

and single-stage pump are used for the O_2; the fuel side uses a two-stage turbine and three-stage pump.

The RS-44 thrust chamber, a channel-wall design made of Narloy copper-alloy material, has regenerative cooling to an area ratio of 225:1. A radiation or dump-cooled extension can be added and can be fixed or extendible, depending on the application. Figure 11-5 shows an extendible nozzle with an overall area ratio of 625, which will produce a vacuum specific impulse of over 480 s. The injector uses concentric elements with a transpiration-cooled rigimesh face for long life. An electric spark igniter provides restart capability, and the design life is 10 hours total run time.

Another advanced pump-fed engine design, the XLR-132 (Fig. 11-6), delivers 3750 lb of thrust using N_2O_4/MMH propellants. Currently under development for the Air Force by both the Rocketdyne Division of Rockwell International and the Aerojet Tech Systems Co., it will support a wide variety of space missions. (The following paragraphs describe the Rocketdyne version of the engine.)

Rocketdyne's design for the XLR-132 operates on a gas-generator cycle, shown schematically in Fig. 11-7. The gas generator feeds a single partial-admission turbine that drives two single-stage centrifugal pumps, one mounted on each end of the turbine. The turbine-exhaust gases are collected in a manifold and injected through supersonic nozzles into the main nozzle and further expanded to provide thrust. The combustion chamber is regeneratively cooled with oxidizer to an area ratio of 50:1 and a radiation-cooled columbium nozzle extension is attached for an overall area ratio of 400:1. The low-temperature-turbine-exhaust gases provide additional film cooling for the forward portion of the extension. The engine operates at a chamber pressure of 1500 psia and produces a specific impulse greater than 340 s.

The XLR-132 is designed for multiple starts and an operating life of 10 yr in orbit. The start/cutoff

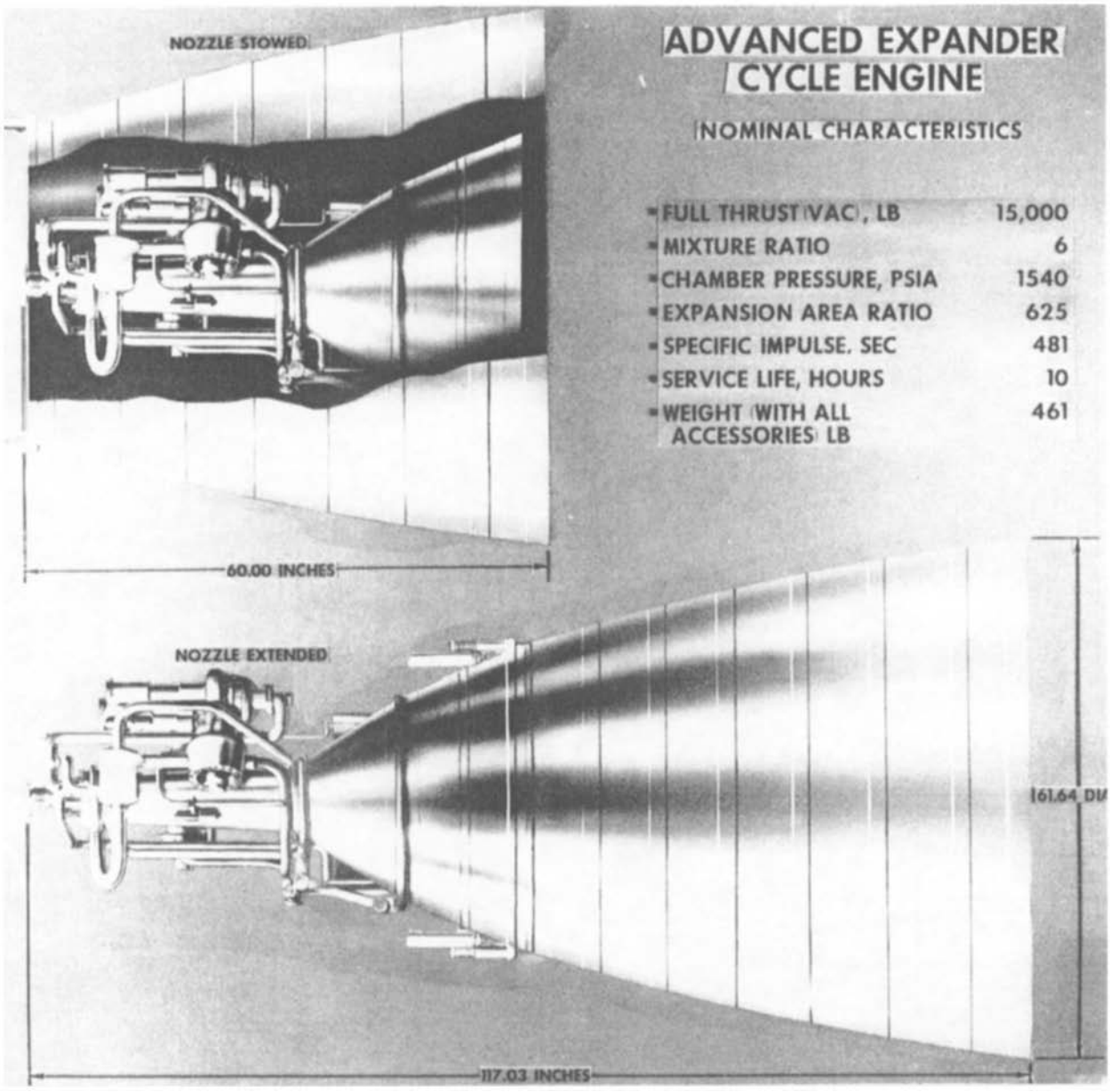

Fig. 11-5 RS-44 pump-fed cryogenic-propellant rocket engine (courtesy of Rocketdyne).

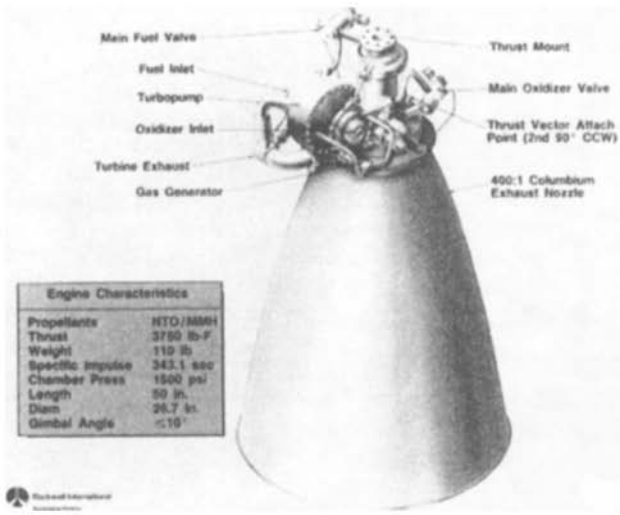

Fig. 11-6 XLR-132 pump-fed storable-propellant rocket engine (courtesy of Rocketdyne).

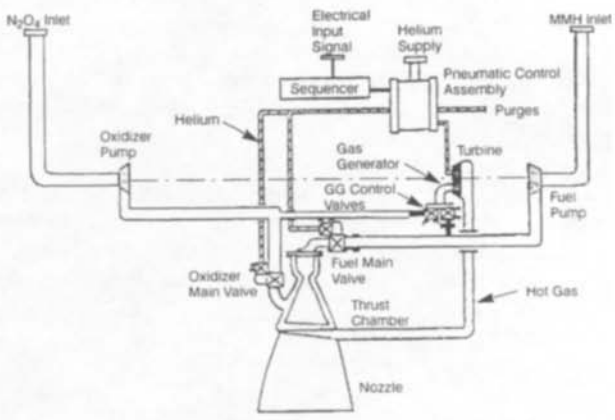

Fig. 11-7 XLR-132 schematic (courtesy of Rocketdyne).

sequences are simplified to allow immediate restart and high reliability. The propellant valves, designed for long life, incorporate propellant filters, gas-generator supply ports, trim orifices, and ports for propellant purging.

Main-Thrust-Chamber Design

In addition to the design elements presented in Chapter 4, primary requirements for thrust chambers of spacecraft main propulsion systems may include optimum steady-state cooling methods, with due consideration of application in space; ability to withstand postrun soakback, intermittent operation, and storage in the space environment; and ability to enter planetary atmospheres at high velocities.

Many of the thrust-chamber cooling techniques described in Chapter 4 can be applied to space engines, especially ablative cooling of thrust chambers. Ablative-cooled chambers offer the inherent advantage of simplicity, ruggedness, and independence of propellant coolant flows (including their pressure drops), and thus offset the factors of limited total life and relatively heavy weight. They are suitable for most pressure-fed space engine systems using earth-storable propellants at chamber pressures of less than 150 psia. In some applications, ablative cooling can be supplemented by one or a combination of refractory throat-inserts, radiation-cooled nozzle extension skirts, and propellant film cooling.

Selection of ablative material will be influenced by the propellants due to potential rapid reactions between the combustion products and the thrust-chamber materials. With oxygen-based oxidizers (e.g., oxygen, nitrogen tetroxide, nitric acid, etc.), an oxide-based or silicon-carbide fiber reinforcement must be used for laminated ablative liner and nozzle materials. Suitable materials include quartz, high-silica glass, asbestos, and some ceramic fibers. Fluorine-based oxidizers (e.g., fluorine, chlorine trifluoride, chlorine pentafluoride, etc.) require carbon fibers as the laminate reinforcement. Fuels containing carbon are not recommended with fluorine-based oxidizers due to build-up of pyrolitic graphite in the throat and throat-entrance region.

Ablative cooling changes the dimension of the chamber due to erosion during burning. Nozzle-throat erosion, if predictable and controlled, may be acceptable for some engine systems; it becomes proportionally less significant in larger thrust-chambers. For fixed-area injectors and fixed propellant-supply pressures, propellant flow and engine thrust would increase with time, while specific impulse would decrease, due to throat enlargement. However, for a 40:1 expansion nozzle operated in vacuum, the specific impulse loss would be only 0.5%, for as much as a 10% increase in throat area, if the aerodynamic characteristics of the nozzle contour did not deteriorate.

A refractory nozzle-throat insert represents one remedy against excessive throat erosion with oxygen-based oxidizers. A ceramic, silicon carbide, has been used extensively for throat inserts in space-engine applications. It has a high melting point (4400°F), excellent thermal-shock characteristics, relatively high thermal conductivity (115 Btu/h-ft^2-°F/in.), low coefficient of thermal expansion (2.4×10^6 in./in.-°F), excellent oxidation resistance, and high abrasion resistance. Sometimes, a molybdenum backup sleeve is used when the silicon carbide insert cannot conduct heat sufficiently. This material has good thermal-shock resistance for a ceramic, but the design of the throat must keep the cross-section thicknesses as thin and as constant as possible to prevent the insert from thermally cracking. Such throats are limited to about 2 in. in diam at the throat portion of the insert. Even then, throat diameters exceeding 1 in. are recommended only for steady-state firing conditions, because large inserts usually will crack and thus must be kept in place only by mechanical restraints imposed by the way the material cracks and interlocks. Throat erosion in larger thrust chambers can be reduced through the use of laminated silicon carbide-reinforced phenolic.

Throat erosion in engines using fluorine-based oxidizers can be minimized by the use of graphite or carbon-carbon throat inserts. The graphite inserts, however, have given mixed results and are not generally recommended, especially for pulsed operation. Carbon or graphite-fabric-reinforced phenolic ablative can protect chambers at low pressures (less than about 150 psia) with minimal erosion.

High-silica glass in the ablative material of the combustion chamber section may become fluid enough to be swept downstream and deposited in the throat section. This causes thrust variances and promotes an unsymmetrical velocity profile in this area. This danger may be prevented by a liner of JTA (45% graphite, 45% zirconium diboride, and 10% silicon) inserted in the combustion zone. The liner is usually segmented to provide a path for the gases from the pyrolyzed ablative (and reduce the pressure drop across the liner) and prevent cracks that would develop in an expanding unsegmented liner.

Following the firing of an ablative thrust chamber, the heat stored in the chamber walls soaks into the unburned virgin material. This postrun soakback promotes further thermal degradation, which might also be affected by the vacuum conditions, for 100 s or more, until the mean temperature of the char drops to about 500°F. Gas generated and expelled by soakback charring will constitute about 15% of the weight of ablative material charred. This gas could cause a postrun residual impulse exceeding the desired minimum cutoff-impulse. However, this effect will be small for larger systems. For long-duration space missions, the temperature effects from solar radiation may cause vaporization of the ablative chamber material during coasting, and thus should be prevented if possible.

Ablative thrust chambers for space engines should be designed to permit many restarts. At the end of a specified total firing-duration (design values: 400-2000 s), sufficient insulation material must remain between char and structural shell to limit the adhesive-bond temperature between the ablative and shell to a specified maximum (typical design values are 350°F for repeated firings and 500°F for steady-

state single firings). Any heat soakback during intervals between firings should not affect total chamber duration. For high-silica-fabric-reinforced phenolic thrust chambers operated at pressures of 100-125 psia, using N_2O_4 and hydrazine-type fuels, the following empirical equations may be used to estimate char depth, including the effects of charring due to soakback:

For the combustion zone and the throat section (with or without liner and/or insert):

$$a = 0.0415t^{0.5} \tag{11-1}$$

For nozzle sections downstream of the throat:

$$a = 0.0335t^{0.5}e^{-0.0247\epsilon} \tag{11-2}$$

where a = char depth, in.; t = thrust chamber cumulative firing duration, s; e = base of natural logarithms, 2.718; and ϵ = nozzle expansion area ratio at the section under consideration. Knowing the char depth based on design duration, including effects of soakback, the designer can calculate the thickness of the insulating layer needed to keep the outer wall at the required temperature.

Thrust chambers cooled only by radiation will be limited in application due to the high temperatures and thrust loads in the combustion zone and throat region. In contrast, the radiation-cooled nozzle skirt experiences lower heat flux and lower thrust loads, which can be accommodated by high-temperature materials. Radiation-cooled devices must "see" space. Thus a radiation-cooled skirt should face outboard, and not radiate undesirable heat to vehicle components. Clustered engines magnify this problem.

Nearly all radiation-cooled and ablatively-cooled thrust chambers employ some degree of film cooling, fuel being injected near the wall to provide some protection against the hot temperatures in the core flow. The fuel coolant can reduce the heat flux to the walls in the combustion chamber and on through the throat. This also reduces the problem of oxidizer impingement on the wall, which can occur if injector fabrication has not been controlled very closely. Oxidizer impingement can cause severe erosion and key-holing of the throat, which will cause thrust misalignment. The degree of film cooling ranges from a few percent, which has an unmeasurable effect on engine performance, to as high as 40%, which can reduce specific impulse by several percent.

For pump-fed space engines operated at relatively high chamber pressures, or engines having long-life requirements, regeneratively-cooled thrust chambers are more suitable in terms of heat transfer. As a possible disadvantage, response time from start signal to full thrust may be substantially higher than with other cooling techniques. Spacecraft main propulsion systems usually do not, however, require rapid response.

Heat-transfer characteristics during throttling also may present problems; and coolant passages may be more susceptible to meteoroid damage than solid walls. In some applications, an optimum overall design may combine regenerative cooling with film cooling and a radiation-cooled nozzle extension skirt.

An example of a pump-fed, regeneratively cooled space engine, the RL10 (see section I), powers the Centaur upper stage of Atlas and Titan IV launch vehicles. First flown in 1963, the current RL10 (designated RL10A-3-3A) uses O_2/H_2 propellants and delivers 16,500 lb of thrust. The thrust chamber, constructed primarily of stainless-steel tubes, is regeneratively cooled with hydrogen, which is then used to drive the turbine in an expander cycle. The turbine drives a two-stage fuel pump directly and a single-stage oxidizer pump through a gearbox. The engine operates at a chamber pressure of 475 psia, has an area ratio of 61:1, and produces a specific impulse of 444 s at a mixture ratio of 5:1.

The Space Shuttle Orbiter OMS engine is an example of a pressure-fed regeneratively-cooled engine using Earth-storable propellants. The 6000-lb-thrust engine is fuel cooled to an area ratio of 6:1 with a radiation-cooled extension to the final area ratio of 55:1. Channel-wall construction is employed in the regenerative portion and the extension is made of Columbian alloy.

Solenoid-operated bipropellant ball valves control fuel and oxidizer flows. Following engine shutdown, gaseous nitrogen purges the fuel circuit downstream of the propellant valve for 2 s to clear the coolant jacket and injector of fuel, permitting safe engine restart. The engine uses a platelet injector, consisting of a stack of plates, each with an etched pattern that controls the distribution and velocity of the propellant. The stack is diffusion-bonded and welded to the body of the injector. The engine

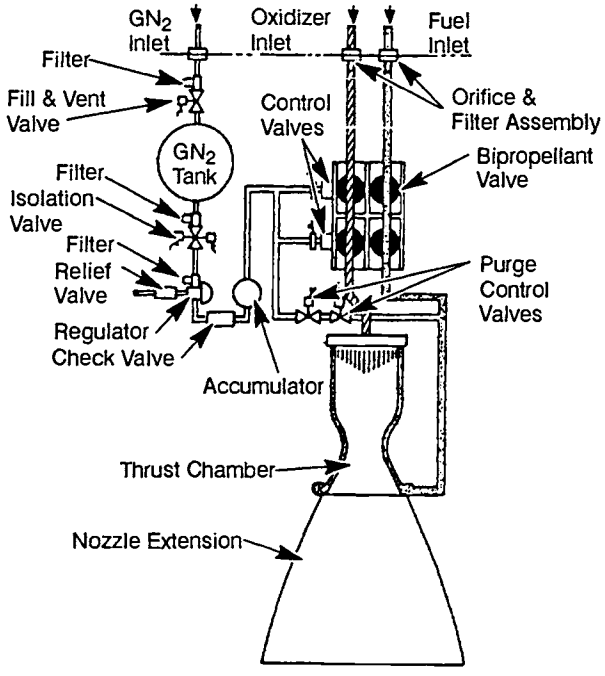

Fig. 11-8 Regeneratively cooled storable-propellant OMS engine (courtesy of Aerojet Tech Systems Co.).

operates at a chamber pressure of 125 psia and delivers a specific impulse of 313 s.

Design of Control Components

The various aspects of control-component design have been discussed in Chapter 7. The following considerations particularly apply to the design of space-engine control components in general and of propellant valves in particular:

- Maximum reliability.
- Use of bellows for dynamic sealing in view of the need for long-term operating life in a vacuum environment.
- Combination hard and soft valve-seats to minimize leakage.
- Provision of a minimum of two seals and a vent between different propellants.
- Avoidance of sliding surfaces in components operating in a vacuum.
- Mechanical linkage (where possible) of the propellant-valve actuators by a mechanism that ensures positive, consistent, and synchronized opening and closing for smooth, repeatable ignition and thrust termination.
- Minimum electrical-energy requirements.

The basic design details of the various control components for space-engine systems, such as pilot valves, regulators, and vent valves, are quite similar to those for booster-stage applications. The mechanically-linked, poppet-type arrangement shown in Fig. 11-9 typifies main-propellant or propellant-isolation valves of space engines using hypergolic earth-storable propellants. In the valve shown, placing the poppets in series causes the oxidizer poppet's motion to simultaneously move the fuel poppet. Welded-bellows seals located at both ends of the fuel poppet and at the connection end of the oxidizer poppet completely separate fuel and oxidizer. The actuation chamber needs no bellows because fluid pressure acutates the valve. The center vent chamber between valve sections is the critical area where propellant mixing must be prevented. Both bellows would have to fail, however, to cause this failure mode (reliability through redundancy). This design also incorporates all-welded static sealing joints, all-metal construction except for the Teflon dynamic-poppet-valve seals, and hermetically-sealed solenoids or torque motors.

The valve is spring-loaded normally closed, and is also held closed by pressure imbalance when inlet pressure is applied. Allowing the oxidizer fluid to enter the actuation chamber at nominal oxidizer-valve inlet pressure opens the valve and, in turn, overcomes the closing forces on the poppets. For on-off and isolation use, a three-way solenoid pilot valve actuates the fully open or closed valve positions. When energized, the valve actuation chamber is pressurized to open the poppets, and when de-energized, the same chamber is vented, allowing the pressure imbalance and springs to close the poppets.

In a bipropellant throttling valve, the position of the linked main poppets is controlled by a servo pilot spool-valve that meters the control-fluid flow (oxidizer) to the main valve-actuation chamber. The pilot spool valve, in turn, is proportionally positioned by a servo torque motor, as a function of the command signal current and its polarity supplied from a servo amplifier. By means of properly shaped valve-poppet contours, the main throttling valves control the flow of oxidizer and fuel to the main thrust chamber at constant mixture ratio, and thus regulate the main chamber pressure (thrust).

Propellant Storage for Space Missions

As previously mentioned, storage of propellants for space-system propulsion represents an important design area. Cryogenic propellants require protection against high temperatures, particularly over long storage periods. Earth-storable propellants, by contrast, require protection against low temperature, because of the danger of freezing. There are two basic design approaches to propellant storage for space missions, vented and nonvented. Selection of the optimum system design depends on mission, propellant type, and type of engine feed system.

In a vented storage system, mainly used for cryogenic propellants, the pressure and temperature of the propellant are maintained at a constant value, any heat input being absorbed by allowing a small boiloff. Since conditions will vary widely during travel, the net heat input to each propellant tank may be computed by numerical integration for the specific vehicle path, such as a complete orbit. This path can be divided into a number of intervals, and the equilibrium skin temperatures and net heat fluxes (considering both internal and external sources) to propellant tanks determined for each orbit position. By algebraically adding the net heat inputs for each, the net heat input rate for one complete orbit can then be obtained and the amount of propellant boiloff per orbit calculated.

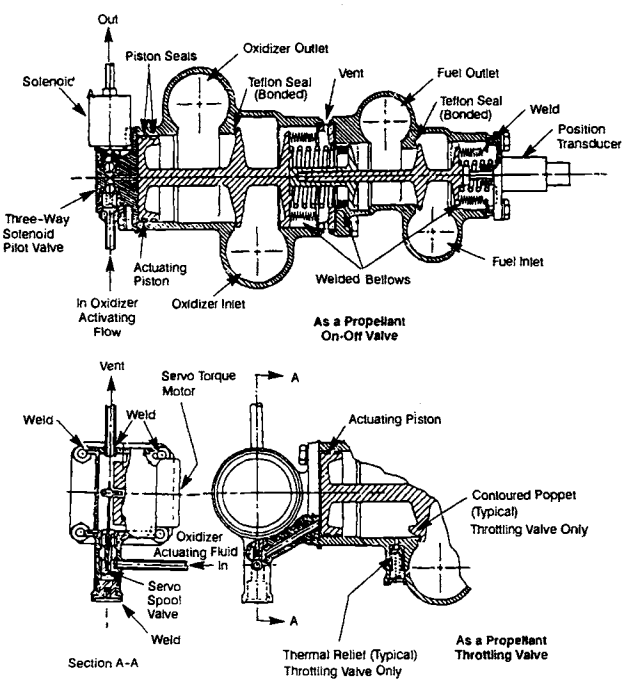

Fig. 11-9 Typical mechanically-linked poppet-type, dual-propellant on-off or throttling valve for spacecraft main propulsion systems using hypergolic earth-storable propellants.

In a system without venting, heat input causes propellant temperature rise and a corresponding increase in vapor pressure. This system can be applied to both cryogenic and earth-storable propellants. The allowable pressure rise, and consequently the maximum heat input, will be dictated by the allowable tank pressure. In this case, the storage analysis assumes an allowable vapor-pressure rise during the mission, based on initial conditions. This permits determination of the final propellant temperature, expected changes in propellant density and ullage-volume requirements, and pressure-dependent propellant tank weights. For cryogenics, insulation is usually provided to limit heat input. For earth storables, insulation may be needed either to limit heat input or heat loss (to avoid freezing the propellants).

11.4 DESIGN OF REACTION-CONTROL ENGINE SYSTEMS

Spacecraft Attitude Control Requirements

Spacecraft attitude control requires application of torques about the three axes (yaw, pitch, and roll) passing through the vehicle's center of mass. The problem of attitude control implies rotation and/or stabilization of the vehicle about these axes. Its operation consists of two main phases:

- Rotation of the vehicle over a given angle, within a specified time.
- Stabilization of the vehicle in a required position, within acceptable tolerance limits.

The position of a vehicle, if left uncontrolled, may not be the one required for efficient use of its main propulsion system. For example, a spacecraft may have to perform a series of trajectory correction maneuvers, for which it must be oriented properly. Or during separation from the launch vehicle the spacecraft may gain unwanted momentum and thus need correction for proper orientation.

Ideally, a spacecraft oriented at some attitude should remain so indefinitely; but being continuously subjected to small external and internal forces, it will drift off the desired position. An attitude-control system, either continuous or on-off, must counteract all disturbing torques. Practical considerations tend to favor the on-off operation. The attitude-control system itself contains certain nonlinearities and nonideal conditions. In actual operation these inherent nonlinearities cause the vehicle to settle into a periodic motion about a reference point—represented by a closed curve in the phase-plane and termed the "limit cycle of operation."

The problem of attitude control, then, becomes twofold:

1) What will rotate the vehicle through a given angle to some new attitude?

2) What will maintain the vehicle in this attitude?

The energy for these two basic maneuvers can be calculated, and total attitude-control requirements for any space mission can be computed, by simply determining the total number of times these two maneuvers occur.

Of the various attitude-control systems, the reaction systems have proven the most versatile, and provide a wide range of torque, up to high levels. They have been universally applied to manned spacecraft and in large unmanned vehicles.

RCS Operational Modes

In any reaction control system (RCS) the amount of thrust delivered on command must be very precisely controlled to avoid overshoot or undershoot and hunting. Three basic operational modes are available:

- *On-and-off ("bang-bang") control.* This "multiple-start" system operates intermittently as long as necessary at its rated thrust level. If the on-and-off command signals are given as a function of sensed position error only, the system would tend to be unstable because of the time lags that are present in all real systems. This situation can be corrected through the use of control systems that use both position error and rate of error change to time the on and off command signals.
- *Proportional control.* The RCS operating thrust will be varied according to the error signals.
- *Repetitive-pulse control.* This type of control needs only position-error sensing. It uses a system that delivers thrust in a continuous series of accurately reproducible impulse bits to assure orientation and stabilization of the vehicle. The optimum thrust pulse-outline should be a square wave. Control may be achieved by modulating pulse width or the frequency of a fixed pulse width, or by a combination of these.

RCS Engine Selection

Liquid monopropellants and bipropellants both have been used for reaction-control engines. Selection of an optimum system for a given mission primarily depends on total system weight (including propellants) vs. total impulse. As mission time increases, so does the propellant and tankage portion of the total system weight, while the weight of nozzles, valves, and plumbing remains fixed. A comparison of two reaction-control systems of different fixed weight and specific impulse may show the lower fixed-weight system to have an overall weight advantage despite a considerably lower specific impulse.

If total impulse is the variable and total system weight the evaluating criteria, a plot of total system weight vs. total impulse helps compare competitive systems. If thrust and number of restarts (operating cycles) are also factors, comparison will need more dimensions. Based on the selection criteria of minimum total system weight, the three major factors to be considered as independent variables for different space missions are total impulse, thrust level, and number of cycles. Selection of an RCS engine largely depends on these three requirements, and reliability considerations. Other important factors will be cost, performance tolerances, maximum impulse per cycle, space storage and environment, systems integration, and logistics.

Monopropellant reaction control systems typically use N_2H_4 (decomposed catalytically or thermally) with a vacuum specific impulse of 200-230 s. For bipropellant systems using earth-storables or cryogenics, the system vacuum specific impulse may be estimated by applying an efficiency ranging from 90 to 94% for steady state and from 80 to 86% for transient operation (less than 25-ms pulse width) of the ideal specific-impulse values given in Table 11-1. The monopropellant systems are applied up to a total impulse of about 50,000 lb-s, or somewhat higher. Beyond this level, the hypergolic earth-storable bipropellant systems take over.

Optimization of RCS Operating Parameters

Most reaction-control systems are a pressure-fed using stored inert gas as pressurant because of simplicity and reliability. After the propellants and the feed system have been selected, parametric analyses of all engine system design variables establish the minimum-weight system, within mission requirements, that satisfies other important considerations. Major operating parameters affecting systems weight include chamber pressure, pressurant-storage pressure, mixture ratio, and the nozzle expansion area ratio.

Chamber pressure and nozzle expansion area ratio are foremost optimization parameters, since the weight of major system components is directly related to and defined by them. Component weights considered in the analyses should include the pressurant and its storage tank, the fuel and oxidizer tanks, and the thrust-chamber assemblies. Optimum values for chamber pressure range from 50 to 200 psia and for nozzle expansion area ratio from 25:1 to 60:1. The optimum mixture ratio depends on propellant type and thrust chamber cooling method. Optimum design values for pressurant-storage pressure range from 3000 to 5000 psia.

Basic System Design for Reaction-Control Engines

For monopropellant systems, the propellant tank can be pressurized by a stored-inert-gas system. The propellant valves, downstream of the propellant tanks, control propellant flow to the thrust chamber. For N_2H_4 systems, catalysts or electrical heating elements can initiate the decomposition reaction. Frequently, to simplify ignition requirements in an N_2H_4 system, a common gas generator feeds several nozzles. Suitable high-temperature materials must be used for all components downstream of the gas generator.

Figure 11-10 illustrates the basic schematic of a typical reaction-control system using hypergolic earth-storable bipropellants and helium-gas pressurization. The RCS has two redundant subsystems, each physically and functionally independent. (It should be noted that this degree of redundancy is rare in actual practice.) Each subsystem is activated independently by an electrical command signal to explosive-actuated pressurant-start valves located in the helium pressurized line, and to the various solenoid isolation valves. After passing through a filter, different pressurant-isolation valves, pressure regulators, and the "quad" check-valve assemblies, the helium at the required pressure level pressurizes the positive expulsion bladders in the oxidizer and fuel tanks. Opening of propellant-isolation solenoid valves allows the pressurized propellants to flow through filters, distribution lines, and line-isolation solenoid valves to the normally-closed injector solenoid valves that control the operation of the individual reaction-control thrust chambers. Removal of the start signal shuts down the system. This closes the propellant-isolation valves and disconnects the reaction-control injector-valve solenoids from the command system.

A relief valve sealed with a burst diaphragm protects the pressurant tank against overpressurization. A high-pressure transducer monitors helium-tank pressure. In a hermetically-sealed system, this transducer could also indicate the amount of propellants remaining in the tanks. A low-pressure transducer downstream of the helium-pressure regulators detects regulator malfunctions. Relief valves sealed with burst diaphragms protect the propellant tanks against overpressurization.

Systems Redundancy in RCS

Redundancy may be provided for reaction-control-engine operation in the following three areas:

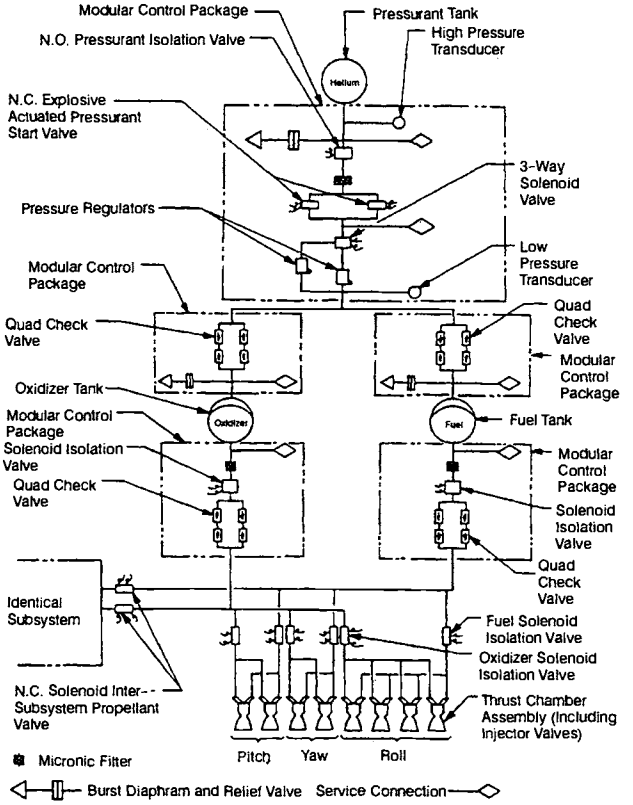

Fig. 11-10 Basic schematic of a typical reaction control system (RCS).

• *Redundancy within a subsystem.* Figure 11-10 shows several typical examples of redundancy within a subsystem. Two explosive-actuated pressurant-start valves operate in parallel; likewise, two pressure regulators are used pilot-selected by a three-way solenoid valve. In each propellant-pressurant line, a "quad" check-valve assembly ensures that propellants that may have permeated through the positive-expulsion bladders will not reverse-flow into the common pressurant line downstream of the pressure regulators. A similar "quad" check-valve assembly downstream of each propellant tank prevents reverse flow of propellants from the other propellant subsystem or from the main propulsion system.

• *Redundancy between subsystems.* Refering again to Fig. 11-10, normally-closed solenoid inter-subsystem propellant valves provide redundancy between two independent subsystems. If one propellant subsystem should fail, these valves open and connect to the propellant lines of the other subsystem. The distribution-line solenoid valves can isolate a group of thrust chambers (pitch, roll, or yaw) should one in the group malfunction.

• *Redundancy outside the system.* Redundancy outside the system may be provided by connecting to the pressurant and propellant system of the spacecraft's main propulsion system, which must be capable of supplying one or both subsystems with pressurant and/or propellants.

Packaging and Installation of RCS

As with the spacecraft's main propulsion, the control components of a reaction-control engine system can be packaged in modules. The modular packages may incorporate related control components within the same housing. Typical modular control packages for reaction-control systems are indicated schematically in Fig. 11-10. All-welded and brazed construction will prevent leakage of pressurant and propellant and minimize weight.

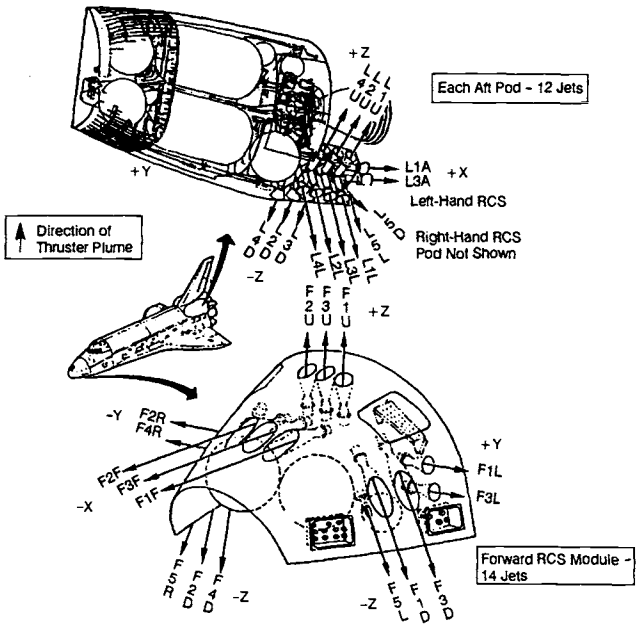

Fig. 11-11 RCS installation for the Space Shuttle Orbiter (courtesy of NASA).

Figure 11-11 presents the installation of the reaction-control engine systems used on a typical manned spacecraft, the Space Shuttle Orbiter. All systems are pressure-fed and use N_2O_4/MMH propellants. The tasks of the Orbiter's reaction-control system include attitude control in orbit and during reentry and small translational maneuvers. In the event of OMS failure, the RCS thrusters can also be used for the OMS burns.

The Orbiter's reaction-control engine systems comprise thirty-eight 870-lb-thrust primary thrusters, 14 forward and 12 in each of the rear pods, and six 24-lb-thrust vernier thrusters, two forward and two in each of the rear pods. The forward RCS module and the aft RCS pods each have five propellant manifolds to provide redundancy.

Design of RCS Thrust Chambers

For systems using hypergolic earth-storable bipropellants, reaction-control thrust chambers are generally cooled by some combination of ablative, radiation, or film cooling. The design and construction principles for ablatively-cooled RCS thrust chambers do not basically differ from those for main propulsion systems; but the small physical sizes (1-100-lb thrust) and the operational modes (such as the pulse mode) of reaction-control thrust chambers require some special considerations.

For example, a typical thrust chamber with a thrust level of 1 lb and a chamber pressure of 100 psia would have a throat diameter of less than 0.1 in. This throat diameter must be produced accurately and remain unaffected by erosion during firing. Generally, in small ablative rocket motors, the internal geometry remains essentially unchanged as ablation progresses. The thermal protection in this case, provided by the internal change from the pyrolysis or decomposition of the plastic resin, yields a porous char layer without any significant dimensional changes. The transition zone between the virgin ablative and the char is referred to as the "char front." The ablation rate, in this case, would not be governed by a surface regression, but rather by a regression of the interface between the virgin ablative and the char. For highest accuracy, however, throat inserts made of refractory ceramics, such as silicon carbide, and combustion chamber liners made of graphite or ceramics, will further reduce throat-size changes due to erosion and will prevent ablative fluid from being swept downstream from the combustion chamber and deposited in the throat section. Silicon carbide can be machined to rather close tolerances. The diameter of a throat can usually be maintained with a tolerance of +0.001 in.

Determining the char depth of ablative RCS thrust chambers employs methods similar to those for the larger-size chambers. Methods described in Chapter 4 and earlier in this chapter may be used. However, in the case of RCS thrust chambers designed for repetitive pulse, or for intermittent operation, the heat-transfer conditions may be quite different. Many studies and experiments have been

conducted in this area, and theoretical and empirical correlations have been generated.

A study by Lee and Hahn indicates that, under repetitive short-pulse operation, the char-front region in an ablatively-cooled thrust chamber does not experience appreciable temperature fluctuations, because of the attenuating effect of the low thermal diffusivity of the char layer (Lee, J. C., and Hahn, J. R., "Regression Rate of Char Front in Ablative-Cooled Rocket Motor Under Pulse Operation," AIAA Preprint 64-262, AIAA, New York, 1964.). The char-front region therefore stays at the pyrolyzing temperature during the entire period of cycling. The char regression under pulse operation can thus be treated as a case of continuous firing with effectively reduced gas-side heat transfer. The results show the char depth based on equal cumulative firing time to be a function of percentage of firing time over elapsed time. It increases with the decrease of the percentage of firing, to a maximum value several times that obtained with continuous firing. At low percentages of firing—i.e., below approximately 5% burn (pulse width/pulse cycle)—the char depth drops again, because of the increasing proportion of radiation or convection losses from the outer skin surface of the chamber to heat influx from the combustion gases. In fact, at some critical pulse mode the char regression ceases after reaching an equilibrium char-depth.

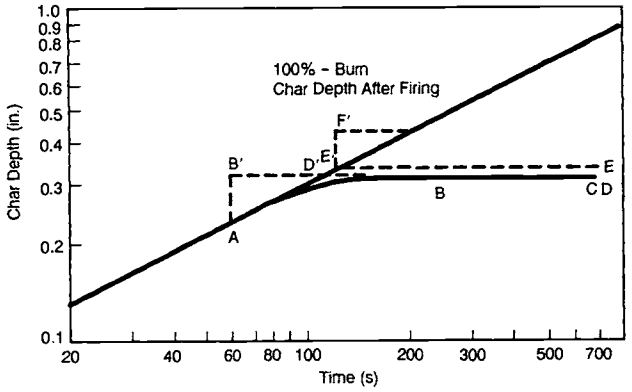

Fig. 11-12 Combustion-chamber char depth vs. cumulative firing time of a typical ablative-cooled RCS thrust chamber.

During intermittent firings, with off periods between firings of relatively long duration, the temperature at the char front does not remain at the pyrolyzing temperature all the time. Figure 11-12 shows the char-depth progression for a typical multiple-start system. The ascending straight line represents char-depth progression for a continuous firing (100% burn). Assuming that the first firing cycle was terminated at "A,"the char layer at this time reaches a higher temperature than the pyrolyzing temperature, and ablation continues until the temperature at the char front drops below the pyrolyzing temperature (point "B"). When the next cycle starts at "C," the char depth remains constant during warmup, until pyrolyzing resumes through shutoff at "E." The various events may be projected onto the 100%-burn line for convenience. The line D'-E' in this case represents the soakback char depth following the second cycle. Subsequent cycles can be treated similarly. Note that the short second cycle finds soakback charring a multiple of the charring during burning. In general, it can be seen from Fig. 11-12 that soakback usually consumes a large percentage of virgin ablative and does not contribute to the useful firing time. Even though some char-preheating time will be gained during the subsequent firing, that will hardly compensate for the loss of burn time compared to what would have been available had the chamber been fired continuously. In this respect, it is desirable to minimize the number of soakbacks, particularly toward the last portion of the virgin ablative.

Combinations of repetitive pulsings and multiple starts can be treated in the same manner as described above, except that the "on" cycles composed of repetitive pulsings will effect a different gradient of the ablation curve, based on the particular percent-burn value, instead of the continuous-firing (100%) curve.

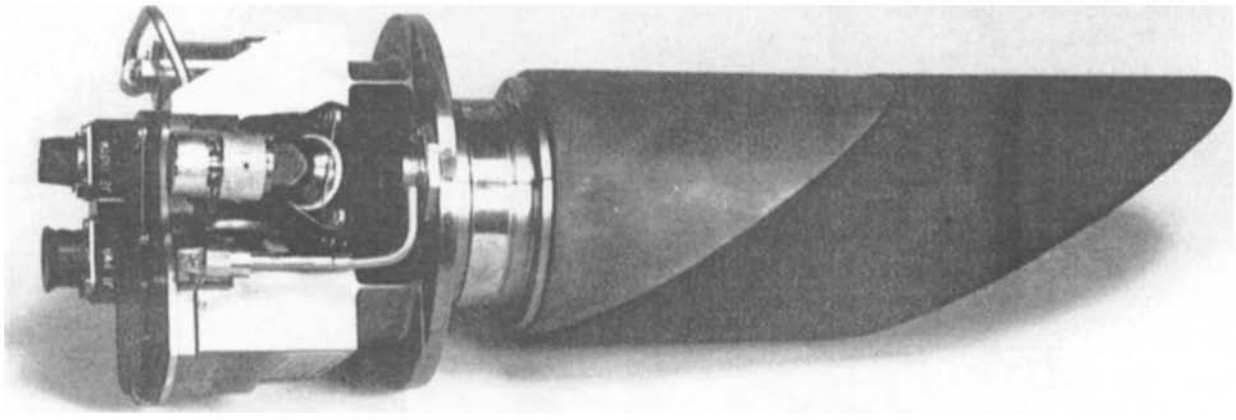

Fig. 11-13 Radiation-cooled RCS thruster (courtesy of the Marquardt Co.).

Total radiation cooling applied to RCS thrust chambers may pose the following problems:

- Difficulties with inboard installation of the thrust chamber.
- Thermal-shielding requirements for components surrounding the thrust chamber.
- Recrystallization of the chamber construction metals in multiple-start applications.
- Need for a larger thrust chamber, when operated at a relatively low chamber pressure.

If properly designed and applied, however, a radiation-cooled thrust chamber probably will prove the simplest, lightest, and relatively most reliable.

The radiation-cooled Space Shuttle Orbiter RCS vernier engine (manufactured by the Marquardt Co.) shown in Fig. 11-13 has a combustion chamber made of columbium with a columbium disilicide coating to prevent oxidation. The nozzle is scarfed to match the external contour of the forward RCS module and the rear RCS pods; and the engine has been insulated to protect the Orbiter structure from the 2000-2400°F temperatures. The injector has a single pair of fuel and oxidizer holes canted to cause impingement of the two streams. Each engine has a 10-W heater to maintain injector temperatures within an acceptable operating range. Solenoid-operated poppet valves are used for both the fuel and oxidizer.

Design of RCS Control Components

The various aspects of RCS control-component design are similar to those for spacecraft main propulsion systems, except that propellant and pressurant have much lower flowrates. For instance, the propellant flowrate of a thrust chamber may be as low as 0.004 lb/s to produce a thrust of 1.0 lb. Besides the propellant-injector valves, all other control components, such as pressure regulators, check valves, and vent valves, are similar to those of other systems.

In addition to high reliability and suitability for the space environment, the RCS injector propellant valves need fast and precise response when opening or closing, tight shutoff, with no leakage, and low power consumption.

Weight Considerations

The importance of rocket vehicle propulsion system weight to the achievement of the required velocity increment with a given payload wieght is presented in this appendix.

As was seen with residual propellants, excessive dead weight at burnout imposes penalties. Whenever rocket engines can be made lighter without compromising reliability and structural integrity, the payoff in range and payload will therefore be sizable. Engine and vehicle builders usually distinguish several types of engine weight:

Dry weight. The net weight of the engine as it leaves the factory.

Burnout weight. Engine dry weight plus residual, measurable propellants remaining in the engine at cutoff. In a typical engine design, burnout weight may be 4% higher than dry weight. Burnout weight plays importantly in vehicle mass ratio (Eq. 1-30).

Wet weight. The engine dry weight plus all propellant within it, during main stage. In a typical design, engine wet weight may be 6% higher than dry weight. Wet weight significantly affects vehicle in-flight center of gravity and moments of inertia.

Wet gimballed weight. This *portion* of wet weight represents engine mass gimballed for steering purposes. In earlier designs this meant essentially the thrust-chamber and injector wet-weight. In later designs it often refers to the entire engine less a relatively small amount of stationary parts. This weight affects gimbal actuator loads and response characteristics of the guidance control loop.

Ideally, dry weight and burnout weight should be equal; that is, no propellants should be trapped in the engine at shutdown. In practice, this will not always be possible. However, the engine designer can do much to bring it about through proper design, sizing and routing of lines, avoidance of traps, and location of valves.

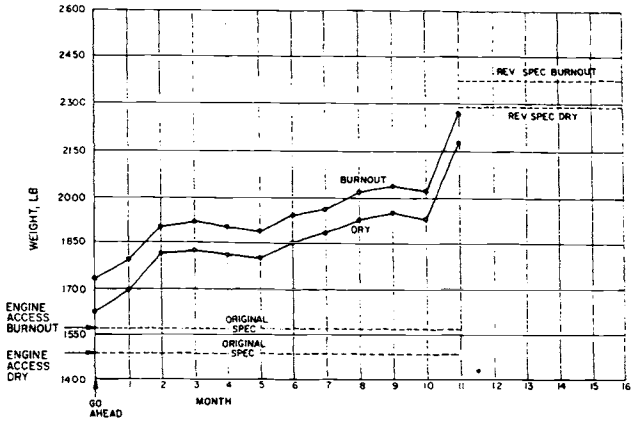

Fig. A-1 Weight history on A-2 Stage rocket engine and accessories.

Because of the importance of weight control, rocket-engine manufacturers employ engineers specifically in charge of this area. Table A-1 shows a typical weight progress form, as used by the Rocketdyne Division of Rockwell International. It is revised and reissued periodically. Thus it becomes a useful tool to raise early warnings of a trend to overweight. The arbitrary example shows a slight underweight. However, the table also shows the data to be based almost entirely on estimated and calculated figures, rather than on actual weighing results. This is characteristic for the earlier phases of design and development of a rocket engine. More often than not, the weight advantage will disappear gradually as the design firms up; then the squeeze will be on. For convenient display of the weight tendencies over time, a graph like Fig. A-1 will be useful.

The weight changes of the various components as well as of the entire engine affect centers of gravity and moments of inertia. Through issue of a data sheet like Fig. A-2, all parties concerned can be kept informed on changes as they occur.

Note that the data presented in Table A-1 and Fig. A-1 and A-2 concern the 150,000-lb A-2 Stage engine system, a part of an assumed multistage space vehicle configuration.

Consider the influence of structural weight on the performance and gross takeoff weight of a rocket vehicle, and how its magnitude varies with the design parameters of different vehicle systems. The quantitative relationships will be evaluated individually for each case.

Equation (1-30) can be rewritten for the stage-burnout velocity of a single-stage vehicle or the stage velocity increment of any individual stage of a multistage vehicle system, as follows:

$$V_{bo} = C_{vc} \cdot g \cdot (I_s)_{oa} \ln \left(\frac{\text{Stage usable propellant weight} + \text{Stage payload weight} + \text{Stage inert weight}}{\text{Stage payload weight} + \text{Stage inert weight}} \right) \tag{A-1}$$

where

$$\text{Stage inert weight} = \text{Stage residual propellant weight at burnout} + \text{Stage engine system weight} + \text{Stage structure, guidance and other weights, which are not payload} \tag{A-2}$$

Table A-1 Weight report on A-2 Stage engine.

Model: A-2 stage Contract: Issue: 1 Date: Enclosure: Page: 1 Report No.: 12	Spec. Weight per Original Design	Contractor Changes (Rev. Spec. Weight)	Current Status	Last Status (Report No. 11)	Changes Last to Current Status (Col. 4 minus Col. 5)	Basis for Current Data			Notes
						% Estimated	% Calculated	% Actual	
1	2	3	4	5	6	7	8	9	10
Rocket engine and accessories (at burnout) (A+D+E)	(1580)	(2380)	(2292)	(2112)	(+180)				
Rocket engine and accessories (dry) (B+D)	(1485)	(2280)	(2181)	(2011)	(+170)	(30)	(52)	(18)	
A. Rocket engine (at burnout) (B+C)	(1365)	(2000)	(1923)	(1763)	(+160)				
B. Rocket engine (dry)	(1300)	(1930)	(1850)	(1700)	(+150)	(24)	(59)	(17)	
Thrust chamber	500	750	730	640	+90	7	62	31	
Gimbal bearing	40	55	52	–	–	6	94	0	
Turbopump, fuel	200	260	250	217	+33	1	97	2	
Mount, fuel pump	25	30	27	–	–	1	87	12	
Turbopump, oxidizer	190	230	224	202	+22	0	33	67	
Mount, oxidizer pump	25	30	28	26	+2	3	82	15	
Fuel feed system	70	100	95	96	+1	72	28	0	
Oxidizer feed system	60	90	87	87	0	75	25	0	
Controls (ignit. elect. pneu.)	100	130	114	114	0	65	33	2	
Exhaust system	70	100	96	96	0	60	39	1	
Propellant utilization system	10	15	12	10	+2	4	96	0	
Start system	0	140	135	135	0	100	0	0	
C. Fluid at burnout (rocket engine)	(65)	(70)	(73)	(63)	(+10)				
D. Accessories	(185)	(350)	(331)	(311)	(+20)	(57)	(41)	(2)	
Inlet line, fuel pump	50	85	79	74	+5	33	65	2	
Inlet line, oxidizer pump	50	85	81	75	+6	30	64	6	
Helium bottle	0	24	21	21	0	100	0	0	
Heat exchanger, oxygen	30	34	31	27	+4	12	82	6	
Flowmeters	5	6	5	5	0	100	0	0	
Instrumentation	50	80	78	73	+5	100	0	0	
Vehicle connection provision	0	36	36	36	0	100	0	0	
E. Fluid at burnout (accessories)	(30)	(30)	(38)	(38)	(0)				

A-2 Stage Rocket Engine

Center of Gravity and Moment of Inertia Data

Issue 12 Enclosure

Date February 28 Page 1 of 1

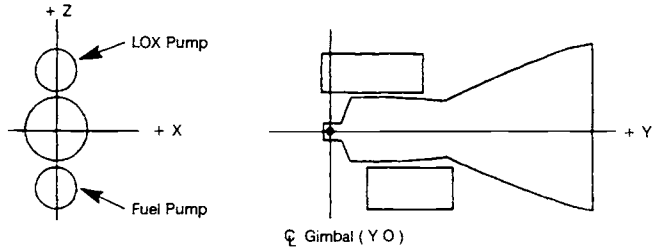

Description	Weight (lb)	Center of Gravity - Inches			Moment of Inertia - Slug ft²		
		Y - Arm	X - Arm	Z - Arm	Y - Y	X - X	Z - Z
(1) Rocket Engine + Acc. - Dry	2181	+23.3	+1.5	-0.7	176	391	362
(2) Rocket Engine + Acc. - Wet	2317	+22.5	+1.5	-0.1	185	411	379
(3) Rocket Engine + Acc. - Burnout	2292	+22.7	+1.6	-0.2	184	408	375
(4) Gimballed Mass - Dry	2061	+25.2	+1.5	-0.2	168	672	649
(5) Gimballed Mass - Wet	2086	+24.6	+1.5	-0.2	177	688	662

Note: Items (1) through (3) represent the moment of inertia about specified C.G.'s.
Items (4) and (5) represent the moment of inertia about the referenced gimbal axis.

Fig. A-2 Typical data sheet for center of gravity and moment of inertia.

For a given burnout velocity these equations show an even weight tradeoff between stage engine-system weight and stage payload weight. The weight of all other items being kept constant, a pound decrease in the stage engine-system weight will increase the stage payload capacity by one pound.

For a fixed payload, and assuming other items except engine weight to be constant, the relation between the stage velocity increment V_{bo} and stage engine-system weight for a given system can be written as follows:

$$V_{bo} = k_1 \ln \left(\frac{k_3 + \text{Stage engine system weight}}{k_2 + \text{Stage engine system weight}} \right) \quad \text{(A-3)}$$

where—

k_1 = $C_{vc} g (I_s)_{oa}$ = constant
k_2 = Stage payload weight + Stage residual-propellant weight at burnout + Stage structure, guidance and other weight = constant
k_3 = Stage usable-propellant weight + k_2 = constant

Since $k_2 < k_3$, the denominator will decrease more rapidly than the numerator, with decreasing engine weight. Thus fixed payloads increase burnout velocity, which will pay off in longer range or higher orbit.

For a given burnout velocity and for a fixed payload, the required Stage average overall specific impulse $(I_s)_{oa}$ in terms of Stage engine-system weight can be established as follows:

$$(I_s)_{oa} = k_4 / \ln \left(\frac{k_3 + \text{System engine system weight}}{k_2 + \text{Stage engine system weight}} \right) \quad \text{(A-4)}$$

where—

$$k_4 = \frac{V_{bo}}{C_{vc} g} = \text{constant}$$

Equation (A-4) shows that the overall-specific-impulse requirements decrease with decreasing engine-system weight.

The "growth factor" of a rocket vehicle also illustrates the importance of weight. If the weight of a component increases, for instance, the designer can adjust for this by increasing the propellant load and thus possibly that of other components, such as a pump, to maintain the same required vehicle performance—i.e., payload and vehicle trajectory. If one part of the vehicle system exceeds its weight allotment by one pound, the total vehicle system weight at takeoff will see a certain number of additional pounds. Growth factor is defined as the total vehicle-system (including payload) weight increase at takeoff divided by the causal increment of added inert and/or payload weight. Growth factor for a *given vehicle* system will not be a precise value, but rather vary within a band. For instance, a small weight increase of a component in an existing system may only require the addition of a corresponding small amount of propellant, but not require enlargement of the tanks, valves, etc.; then the growth factor will be small. In another case, the weight increase may be "the straw that breaks the camel's back," requiring the use of the next-larger valve, duct, or the like; the growth factor will then be large.

In general, growth factor gives the designer a useful tool during the early steps to an engine system, because it attaches a tangible value to the importance of the engine-system weight. A systems-weight increase may be considered "uninvited payload." For single-stage vehicles, and relatively small weight changes, the value of the growth factor then can be expressed with sufficient accuracy as follows:

$$\text{Growth factor} = \frac{\text{Total vehicle system weight at takeoff}}{\text{Payload weight}} \quad \text{(A-5)}$$

For any stage of a multistage vehicle, the approximate value of the growth factors against total vehicle-system weight at takeoff can be expressed as follows:

$$\text{Growth factor} = \frac{\text{Total vehicle system weight at takeoff}}{\text{Stage payload weight}} \quad \text{(A-6)}$$

The growth factors of any stage against the vehicle-system weight at ignition of the same or lower stage can be expressed as follows:

$$\text{Growth factor} = \frac{\text{Vehicle system weight at same or lower stage ignition}}{\text{Stage payload weight}} \quad \text{(A-7)}$$

Sample Calculation

A three-stage rocket has the following weight data: total vehicle-system weight at takeoff, 40,000 lb.; vehicle-system weight at second-stage ignition, 7500 lb; vehicle system at third-stage ignition, 2200 lb; payload weight, 700 lb.

Problem

For each pound increase of engine-system weight of first, second, and third stages, respectively, determine (at a constant vehicle performance) **(a)** increases of total vehicle-system weight at takeoff, and **(b)** increases of vehicle-system weight at second- and third-stage ignition.

Solution:

(a) Payload weight of first stage = vehicle-system weight at second-stage ignition = 7500 lb; payload weight of second stage = vehicle-system weight at third-stage ignition = 2200 lb; payload weight of third stage = actual system payload-weight = 700 lb.

From Eq. (A-6):

1) Growth factor of first stage against vehicle-system takeoff weight:

$$\frac{\text{Vehicle system takeoff weight}}{\text{First-stage payload weight}} = \frac{44{,}000}{7{,}500} = 5.86$$

2) Growth factor of second stage against vehicle-system takeoff weight:

$$\frac{\text{Vehicle system takeoff weight}}{\text{Second-stage payload weight}} = \frac{44{,}000}{2{,}200} = 20$$

3) Growth factor of third stage against vehicle-system takeoff weight:

$$\frac{\text{Vehicle system takeoff weight}}{\text{Third-stage payload weight}} = \frac{44{,}000}{700} = 62.9$$

Therefore:

1) For each pound increase of first-stage engine-system weight, the increase on vehicle-system takeoff weight will be 5.86 lb.

2) For each pound increase of second-stage engine-system weight, the increase on vehicle-system takeoff weight will be 20 lb.

3) For each pound increase of third-stage engine-system weight, the increase on vehicle-system takeoff weight will be 62.9 lb.

(b) Note that the weight growth of lower stages will not affect the upper-stage weight growth. For an increase of first-stage vehicle-system weight, there will be no weight changes on second and third stages; and for an increase on second-stage vehicle system weight, no weight change will be required for the third stage. From Eq. (A-7):

1) Growth factor of second stage against vehicle-system weight at second-stage ignition:

$$\frac{\text{Vehicle system weight at second-stage ignition}}{\text{Second-stage payload weight}} = \frac{7{,}500}{2{,}200} = 3.41$$

2) Growth factor of third stage against vehicle-system weight at second-stage ignition:

$$\frac{\text{Vehicle system weight at second-stage ignition}}{\text{Third-stage payload weight}} = \frac{7{,}500}{700} = 10.72$$

3) Growth factor of third stage against vehicle-system weight at third-stage ignition:

$$\frac{\text{Vehicle system weight at third-stage ignition}}{\text{Third-stage payload weight}} = \frac{2{,}200}{700} = 3.14$$

Therefore:

1) For each pound increase of second-stage engine-system weight, the increase on vehicle-system weight at second-stage ignition will be 3.41 lb.

2), 3) For each pound increase of third-stage engine-system weight, the increase on vehicle-system weight at second-stage ignition will be 10.72 lb and the increase on vehicle-system weight at third-stage ignition will be 3.14 lb.

The correctness of results can be checked by recombining the individual stage growth factors to obtain the growth factor for the entire vehicle system:

$$3.14 \times 3.41 \times 5.86 = 62.9$$

Reliability Considerations

The effort to increase reliability in rocket engines should span the entire program spectrum from conceptual design through production. The reliability effort can basically be split into three parts: prevention of failures, process assessment and control, and monitoring of performance. Reliability through prevention involves early involvement of reliability engineers in "concurrent engineering" design and development loops to identify high-risk devices and designs and catastrophic failure modes. Both before and during fabrication and fielding of hardware, potential process faults and their effects should be evaluated and controlled to assure expected reliability performance through a "Continuous Process Improvement (CPI)" approach. The continuous monitoring of performance needs to be organized in a formal way (e.g., Reliability Growth or Reliability Demonstration Test Monitoring) to assure identification and correction of possible faults.

Reliability in Design

The reliability contribution to a concurrent engineering effort should be through assessment of past performance of similar-type hardware to identify high-failure-risk components or approaches in the proposed designs, conducting reliability-optimization trade studies, and correlating past "lessons learned" in rocket-engine-specific systems. Potential process inadequacies should be addressed, with consideration for control of a process or designing in "fault tolerance." For example, process-induced contamination may be a problem largely solvable by enlargement of flow passages in the engine systems.

Another aspect of reliability in design, so-called "simplicity," usually will contribute significantly to higher reliability. Parts which do not fulfill a truly useful purpose should be omitted; this may include many so-called safety features and interlocking devices, which often cause more trouble than they prevent. Early designs of liquid-propellant rocket engines indeed often suffered from an overdose of sophistication and safety devices. Many of the more recent designs have been substantially improved in this area. Simplifications, like all other design features, must be carefully planned and evaluated. Simplification by elimination of a useful component must not become an excuse for failure to improve that component if its absence could severely penalize other subsystems or maintenance and servicing procedures.

The counterpoint to simplicity will be redundancy. Occasionally, the reliability of certain types of parts are inherently too low or the consequences of the failure effect are too great to accept. Then a redundant functional architecture may be considered, in which complexity, in terms of more parts, will be increased to achieve a higher reliability. The additional cost, weight, and failure modes must be weighed against the reduction in probability of the failure mode of concern. Man-rated systems typically have the additional requirement to isolate physically the redundant element from its sister element to assure protection from common causes of failure (e.g., contamination, heat, vibration, explosion, etc.). Additionally, the operational status of each element of the redundancy may have to be monitored to assure its existence before flight.

For instance, to avoid a troublesome sealed connection it may be decided to omit flanges and seals and to weld it. However, if one of the lines thus connected were inadvertently pinched in the field, it would be necessary to remove the entire engine from the vehicle under preparation for launch—magnifying a simple replacement into a major operation. To be sure, welding or preferably brazing may indeed be the best solution for many problem connections. The point is, this will not be true for *all* connections. The design team must carefully analyze all aspects of the system including handling and, in particular, mishandling by the user.

As another example, tests may have shown that an engine could readily be set up and calibrated to specifications by means of orifices, eliminating previously used regulators. Engines get delivered accordingly. With rocket engines, it is entirely normal that many months, if not several years, may elapse between delivery and final use. Much can happen during this period. Changes in mission plans, for instance, may have made another thrust level more desirable. Then, suddenly, an adjustment by means of orifices, in particular its verification, becomes a major operation. Omission of a strategic regulator was indeed an engine simplification, but for the vehicle system it turned out to be a complication. The point, again: careful evaluation of a planned omission must consider *all* aspects, including changes of plans.

Reliability Assurance

The emphasis on reliability must not become an empty slogan. Fortunately, the rocket-engine designer has certain means to achieve the highest degree of reliability. One of these is an effective "failure reporting and corrective action system (FRACAS)" during the monitoring of hardware test activities. Testing of all hardware should be monitored in an organized and regimented fashion to assure identification and resolution of hardware design and processing failures. The designer should, at the very least, implement a fundamental FRACAS loop. This may be supplemented with a "reliability growth" assessment program to appraise regularly the progress of the engine system toward the expected reliability performance. In many cases, a "reliability demonstration" test program may be proposed to determine, with "confidence," the final reliability performance of the engine system.

Definitions

The definitions used in rocket-engine reliability programs vary widely with individual program requirements, with the object under design and development, and with the missions contemplated. The definitions given below typify usage in actual rocket engine programs, and can be readily adapted to others. For the sake of clarity, irrelevant jargon and detail have been omitted.

Reliability. The probability that a part or system will function properly and, if necessary, repeatedly under rated operating conditions, within the specified load and time limits.

Mission success. Completion of the rocket-engine mission objectives within specified tolerances. All subsystems contribute to the success. It is an inherent characteristic of mission-success analysis and assurance that they anticipate the probability of certain part and subsystem malfunctions, offsetting them with appropriate countermeasures (such as redundancies, emergency power sources, power and propellant reserves, etc.).

Mission failure. Failure of the rocket engine to produce the required thrust for the specified time to complete the mission objectives. Mission failures can be classified as catastrophic, premature shutdown, and "deferred."

Catastrophic failure (Criticality I). An "uncontained" failure in which the effects propagate beyond the physical envelope of the engine system, with sufficient energy potential likely to propagate failure to adjacent systems. It is important to assess and discriminate this type of failure from a premature shutdown for crew safety in manned vehicles and for mission success in multi-engine unmanned vehicles (if engine out is a viable mode of operation).

Premature shutdown (Criticality II). A failure in which the effects are contained and degrade performance enough to trigger an engine shutdown. In multi-engined vehicles with "engine-out" capability, the discrimination between catastrophic failure and premature shutdown figures importantly in the criteria for vehicle mission success.

Deferred failure (Criticality III). A failure causing generally slow-acting and minor performance degradation in which continued operation of the engine is a consideration. Action to cope with the failure will be deferred to allow analysis by the pilot or an automatic logic, to decide whether corrective action can be taken or an abort sequence should be initiated. Typical example: shutting off an engine in a four-engine airplane and reaching destination safely, although with a delay. Analogous provisions are anticipated for manned rockets.

Man-rating. Design and operational provisions to assure crew survival even in case of mission failure. Thus, man-rated crew reliability typically exceeds mission reliability. For instance, overall vehicle reliability to achieve mission success may be 95%. By the addition of an escape mechanism, man-rated reliability may be increased to 99.5%. Caution is advised not to become entirely "wrapped up" in man-rating at the expense of mission reliability. A single launch of a man-carrying space vehicle costs several hundred million dollars, all told. Investment in means to save the mission as well as the man, therefore, appears to be prudent. Table B-1 illustrates this clearly. Pressing optimum reliability for spacecraft and launch vehicle, including the engines, therefore minimizes the need for a crew-escape system.

Engine out. Design and operational provisions in a multi-engine system to permit limited or complete mission continuance in case one engine fails to fire or malfunctions and gets shut down. This option can notably improve system reliability since one of the engines is a redundant element.

Failure mode. The specific manner in which a part or system malfunctions. This may be a "short" or "open" circuit, an incorrectly "closed" or "open" valve, an engine out, or similar malfunction.

Order of failure. The number of components in a system that would have to fail, regardless of their failure mode, to cause a system or mission failure. First-order failures derive from malfunction of a single component or part (i.e., "single-point" failure). Second- and higher-order failures are defined in a like manner. Typical example: a stuck pressurizing valve causing overpressure in a vessel would rupture it only if the safety valve failed to open; this would be second-order failure. However, continuous venting of a properly opening vent valve may prematurely deplete the gas supply. A thorough failure-effect analysis will reveal all ramifications. In the example, depletion would not occur instantaneously; this would be "deferred" failure. The designer can do something about it in advance, such as by giving the pilot an overriding closing valve that remains completely inactive when not needed (although—not a complete blessing—this adds weight).

Failure modes and effects analysis. An orderly, hardware-based analysis listing all credible modes in which components or parts of a system can fail, the effects of the failures on the engine's or vehicle's ability to complete the mission, and the order of the failures. Such an analysis should distinguish between the prelaunch, launch, and cutoff phases. All identified failure modes should be classified as catastrophic, premature shutdown, or "deferred." This hardware-to-effect approach assures that all notable pieces of hardware will be addressed and assessed.

Fault-tree analysis. An event-based analysis that targets specific failure-effect scenarios and then lists all the hardware malfunctions in a graphical, hierarchical "tree" (a reverse of the hardware-to-effect approach of the Failure Modes and Effects Analysis).

Table B-1 Relationship of vehicle reliability to flight safety.

Reliability		Flight Safety
Spacecraft and Launch Vehicle	Escape System	Probability of Crew Survival
0.50 0.90 0.999	0.998 0.99 0.00	0.999

***Emergency detection system* (EDS).** The EDS comprises the electromechanical devices, including sensors and discriminators, to detect an imminent malfunction. Depending on the type of failure (catastrophic, premature shutdown, or "deferred"), it may initiate immediate action, or defer but store and/or display it in a suitable manner (timer, visual gage, or light). Inputs to the EDS must be analyzed, selected, and provided by the designer (in particular, the engine designer) at the outset.

Noncomplex redundancy. The simultaneous function of identical equipment. Application depends upon the particular failure mode to be eliminated. For a typical example, see Fig. B-1 and B-2. Other examples include dual (series) seals and parallel valves.

Complex redundancy. The original function carried out by one component. Failure sensors, logic circuits, and switching devices energize an identical standby component, when needed. The advantages obtained can be completely offset by the additional complexity of sensing and switching circuitry. The potential problem area may be merely shifted from the equipment to the failure-detection components. However, this standby redundancy may be advantageous for long mission times (e.g., days or weeks) where it may be undesirable also to subject the backup equipment to prolonged operation. A typical example: electric-power emergency battery with voltage sensor and switchover circuitry.

Failure Modes of Engine Components

Failure of a rocket-engine component may be attributed to basically three causes: functional, structural, and process faults. They have the following principal modes: functional failures, fatigue failures, overstress and overstrain, failures pertaining to combustion devices, failures pertaining to electrical devices, manufacturing and material defects, unexplained failures, human error, and manufacturing of field-processing faults.

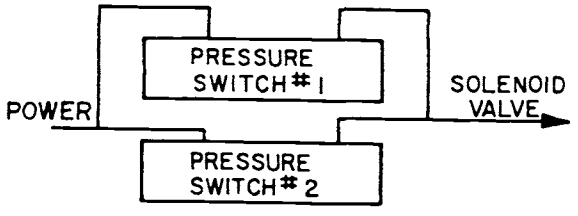

Fig. B-1 Noncomplex parallel redundancy. This type of redundancy guards against failure to close when commanded.

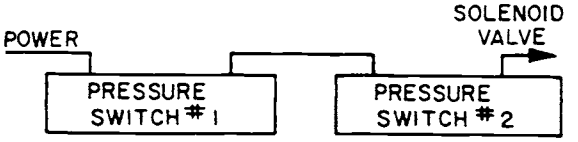

Fig. B-2 Noncomplex series redundancy. This type of redundancy guards against inadvertent closing; i.e., closing when not called upon to close.

Functional failures. Something other than structural failure can cause malfunction of parts or components. For instance, an "0" ring may fail to seal due to improper groove depth specified in the design; or a plunger may freeze in the bore of a guiding bushing, because of improper surface finish and/or noncompatibility of materials. The following precautions will minimize possible function failures in the design of engine components:

- Choose proven designs with an established service record.
- Use standard mechanical elements (bolts, nuts, threads, gears, pins, rivets, springs, seals, tube fittings, pistons, keys, shafts, bearings) wherever possible.
- Select simple designs, but without impairing flexibility. In particular, minimize the number of moving parts and sealing surfaces.
- Allow adequate functional margins in the design of components (spring forces, actuating powers, supply of lubricants, supply of coolants).
- Subject newly designed parts to extensive functional testing, under simulated working and environmental conditions, before "freezing" the final configuration.
- Provide redundancy, a "buddy plan": where one component would be sufficient, provide two of the same type. If one fails, the other takes over. This can be achieved in two ways: by noncomplex and by complex redundancy. Intelligently applied, redundancy can significantly increase reliability.
- Pursue a rigorous program of continuous product improvement.

Fatigue failures. Fatigue failures are fractures caused by repeated loading at stresses considerably lower than those causing failure by a single load. They are the most common type of mechanical failure. The ability of a part to resist fatigue failure cannot be checked without destroying the part. Checking is possible, however, through destructive endurance tests with representative samples selected at random.

Most fatigue failures start with a crack at or near an outside surface because stresses are apt to be greatest there. The actual failure will result from gradual propagation of these cracks.

The starting point for a crack will depend upon the geometry of the part and on surface conditions. Any notch or other stress-raiser, being a point of high stress concentration, may start fatigue cracks. Fillet radii too small, threads, oil holes, keyways and similar surface irregularities all present potential sources of fatigue failure. Although a part may be designed to be free of geometric irregularities, having no shoulders, grooves or the like, it may still contain a great number of minute stress-raisers—tool marks, scratches, identification stamp marks, or various inherent discontinuities in the material itself, such as inclusions of foreign matter and quenching cracks.

The design engineer should make every effort to avoid stress concentrations in a highly stressed part subject to repeated loads. In the design, rigid specifications should be called out for surface finishes. To carry repeated loads, forgings are usually preferable to castings, and ductile materials to material prone to become brittle. Welded joints see almost every type of stress concentration and fatigue failure. Wherever

possible, welded joints should be minimized in the design of parts subject to repeated loads. Rigid procedures for welding and inspection must be called out in the design.

Overstress and overstrain. Stress analysis in mechanical design to prevent overstress and overstrain was discussed in section 2.5.3. The interrelationship of stress and reliability of mechanical parts (as illustrated simplistically in Fig. B-3) can be evaluated probabilistically.

Two stress levels exist for every part in a given engine component: the working stress and the damaging stress at which failure occurs. The failure may be either a fracture or a deformation beyond allowable tolerances. Either will be a mean value of a distribution about a mean. The difference between the working and the damaging stress mean values indicates the stress reliability margin of the part.

Deviations from the mean working stress mainly reflect variations in the dimensions of the part and operational and environmental conditions. The distribution about the mean damaging stress results from variations in material properties, fabrication processes, quality control, and maintenance practices. The area P_f, where the two distributions overlap, represents the probability of failure (unreliability).

Close control of functional and environmental loads may decrease the variation of the working stress about the mean. Likewise, better materials and strict quality control should increase the damaging-stress mean value and decrease the variation about the mean. Thus, the area of overlap may be substantially reduced or eliminated, and reliability increased.

Failure of combustion devices. Under steady-state operating conditions, combustion devices in liquid-propellant rocket engines must withstand hot gases—temperatures ranging from 1000 to 6000°F. The walls of these devices either are made from high-temperature-resisting (refractory) materials or are cooled by heat-absorbtion, ablation, and propellant-film and/or regenerative effects. Structural failure may occur because of erosion from wall temperatures exceeding values assumed during design or a combination of excessive temperatures and pressures.

Under certain transient or unstable conditions, such as engine start or stop, combustion instability or abrupt pressure surges may cause a failure; see Chapter 4, "Design of Thrust Chambers and Other Combustion Devices."

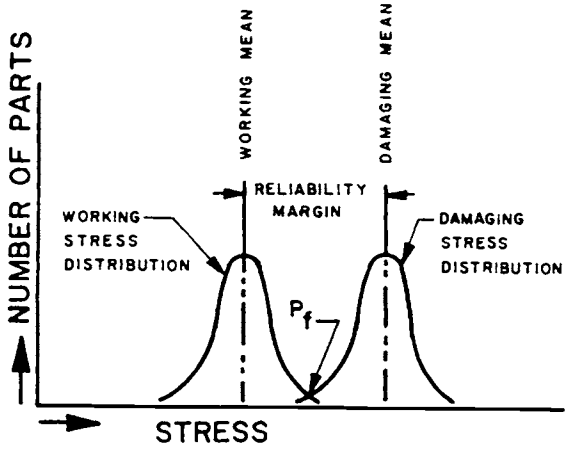

Fig. B-3 Interrelationship of stress and reliability as related to mechanical parts.

Electrical failures. Although predominantly an assembly of mechanical parts, a modern rocket engine employs a number of electrical devices without which it cannot function reliably. Electrical components used most widely include power sources (batteries), converters (dc to ac), microprocessors, tranducers, wires and harnesses, connectors, switches, relays (electromechanical and solid-state), timers, pressure switches, diodes, solenoid valves, servomotors, and position indicators.

All of these devices represent, to some degree, a potential source of failure, the consequences of which can be just as detrimental as failure of mechanical parts. By proper design and assembly instructions, by careful selection of the elements, and by Environmental Stress Screening (ESS), the designer can forestall electrical failures and thus assure overall system reliability. Common points of electrical failure include the following:

- Cold-solder spots in connectors, wirings, and electrical elements. They often cause sporadic discontinuities, particularly under vibration.
- Short circuits in wirings, connectors, and other electrical devices. This may be due to poor design, leaving insufficient separation between connector pins, lugs, and the like; or to excessive solder; or damaged insulation due to poor harness installation, chafing under vibration, and poor handling; or overload and/or overheating in solenoids, moisture in connectors, etc.
- Fused relay contacts, due to overload and/or incorrect current rating of the elements.
- Relay and switch contact-loss under vibration. This is really an electromechanical malfunction. It can be prevented by proper relay selection, shock-mounting, orientation of installation, or replacement by solid-state circuitry.
- Power failure resulting from one or more of the causes listed above. Preventions include emergency batteries and overload switches, combined with subcircuit isolation through diodes.

A liquid-propellant rocket engine usually includes additional electrical elements as required for instrumentation and telemetry—instrumentation power supplies, end organs (sensors, pickups, thermocouples, accelerometers, position indicators), signal conditioners (analog-to-digital), wiring, and the like. Although, as a rule, instrumentation does not directly effect proper functioning of the engine system, its failure may indirectly cause engine malfunction, by interfering with its operation. For instance, a pressure pickup may rupture and cause premature depletion of a gas supply; the same event in the fuel system may cause an engine-compartment fire; improper installation of a thermocouple may block a vital lubricant or other line.

The engine designer's task includes engine instrumentation. It is obvious that this peripheral system, too, will require his full attention.

Manufacturing and material defects. The producibility of parts directly affects the reliability of components. Manufacturing and material defects can be prevented only by strict process and quality control. The areas of quality control may be subdivided as follows:

- *Materials inspection.* The extent of inspection and testing of raw materials depends upon the nature of the part for which they will be used. Inspection of materials includes testing for composition, uniformity, mechanical properties, fabrication and heat-treating characteristics, and possibly other properties, as the application may demand.
- *Traceability.* By the time a materials defect is detected, many more parts may have been made from the same lot or batch of raw material. If accurate records have been kept on parts for which numbered material lots have been used, it will be possible, without a "panic," to withdraw and replace all parts made from the faulty lot. The importance of accurate and complete records is obvious.
- *Process inspection.* This refers to all shop inspections made of parts as they are being processed. It in effect checks the performance of the operators and tools or equipment, and sorts out faulty parts as soon as errors are detected.
- *Salvage.* Someone decides whether defective materials or parts can be corrected or must be scrapped.
- *Final inspection.* This inspection covers the completed component parts to ensure they come within the limits required by the design.
- *Checking of actual service performance.* This includes investigation of complaints and studies of actual service performance of the part in the engine system (see "Failure-Reporting System").

Reliability demonstration. This is a strict, reliability test series in which the "matured" engine system configuration is repeatedly tested in the same configuration and mission cycle. The primary objective is to statistically determine the reliability performance level and confidence limits for the engine configuration.

Reliability-growth monitoring. This is typically a monitoring and assessment task over engineering development test programs to continually assess the development (i.e., "growth") in the reliability performance of an engine system. Early successes and failures are plotted to continually check for the expected improvements through corrective actions and process improvements.

Human error. Experience with early manned rocket flights showed that certain functions could be performed better by trained men than by automatic devices. It appears certain that future spaceflight will employ combinations of automatic and manual systems, the ratio of the two depending on mission requirements. Even unmanned missions, ostensibly fully automatic, have people directly involved during launch preparations and through postlaunch commands for trajectory-correction maneuvers, information playback, and similar actions.

As recent nuclear powerplant catastrophes attest, even a fully trained, possible very alert individual can be subject to error. He may commit an error at a desk while using a computer, or while connecting a number of hydraulic lines, or under stress while pushing buttons. The history of rocketry is full of glaring examples. Whenever it happens, the most eloquent regrets are probably voiced by the designers of the system involved: If someone had not done something to their perfect creation, it would have worked faultlessly. The reaction is understandable, but *wrong.*

For whatever reason a system failed, it obviously was not perfect. Its designer did not consider human nature, non-ideal operating conditions, or emergency situations. Clear and complete drawings, specifications, and other written instructions are important, but they will not prevent, by themselves, human errors, because they can be misplaced, misread, or not read at all.

It is not surprising that the elimination of human error, or more positively, the perfection of the integration of man with the machine, is becoming an independent branch of engineering. It would be beyond the scope of this book to go into the details of "Human Engineering" or "Human Factors Analysis." Simply by applying mostly known methods and common sense, the rocket-engine designer can do much to prevent human error by the design of his parts and by mandatory actions during their building, checking, and handling. The following are only typical examples of a probably infinite number of ways to prevent human error by design:

- Clear marking of bolts, lines, connectors, wires.
- Use of dissimilar connectors, dissimilar threads, a variety of keyways, etc. to make incorrect electrical and mechanical connections impossible.
- Safety wiring, electrical and mechanical interlocks.
- Painting bright red and/or attaching bright red streamers to auxiliary devices that must be removed before operation.
- Storing of components and systems that have successfully passed all inspections and checkouts in locked, controlled-storage rooms.
- Simulated, mock operations—with intentional attempts at improper handling, assembly, checkout, and operation of components and systems—to assist "foolproofing" during development.

None of these and numerous similar steps will eliminate human errors. However, they will substantially reduce the likelihood of them and thus contribute to overall reliability.

Design Reviews for Reliability

The reliability of a rocket engine and its components depends on many factors. A concurrent engineering approach topped with periodic design reviews can bulwark reliability. In practice, a design review, the progressive evaluation of a design, starts with the preliminary schematics, layouts, and specifications and extends through the release of all final drawings. Those conducting reliability design reviews should include reliability specialists, design engineers, de-

velopment, test, and service engineers, and various specialists for structures, materials, manufacturing, and quality control. A minimum of three design reviews should be made for each design:

1) *Preliminary design review.* This is a preliminary review of work statements, basic concepts, schematics, layouts, and analyses. It determines development needs and results in decisions for the next design phases. This review should uncover misapplications, critical areas and marginal designs at an early stage, when changes can be effected without difficulty.

2) *Critical design review.* This is the most important review for decisions and approvals. It includes formal review of all reliability aspects of layouts, analyses, planned development tests, and procurement specifications.

3) *Final design review.* This is the final review of overall design layouts, detail and assembly drawings, analyses, process specifications, and R&D test results, before production release.

The reviews should emphasize the following points: structural integrity, function and performance, customer (vehicle) connections and envelope, materials compatibility and component interfaces, producibility and cost, reliability and repeatability, malfunction effects, environment and servicing, and "special" requirements. It is highly recommended that the agreed-to layout bear the approval signatures of the groups involved.

A reliability checklist tailored to the individual designs may be used as a guide during the various design-review phases. The "Design Check-Off Sheet" shown in section 2.5 may serve this purpose.

Design reviews are valuable and cost-saving tools for improving reliability. A group well organized and staffed will assure a meaningful review and instigate effective recommendations and actions. Complete documentation of all review details will provide valuable data for future reference.

Failures occur, from time to time, that cannot readily be isolated as having originated in a given component or part—because several causes were present simultaneously and could not be separated, because instrumentation was inadequate, recording only the ultimate effects but not the cause, or because an incomplete investigation was conducted, perhaps in the hope it would not happen again.

Classification of a failure as "unexplained" should never be done as a matter of convenience, but rather *only as a last resort* if the most thorough investigation did not establish a clear cause. Complete and accurate records must be kept of the details associated with the failure. Through special statistical methods it may be possible to isolate the cause or causes at a later date. Also, special instrumentation may immediately be added in the areas of suspected but unproven causes. But the most sophisticated explanation of a failure cannot transform it into a success.

Under "Man-rating" the cost of a single launch was mentioned. Press releases give the cost of a major space program as about 3.5 billion dollars a year—10 million a day! To save a mission, or just a single day of preparation, by improved reliability will quite clearly be worth the effort!

Likewise, the loss of a launch, or a day in the program, is very costly indeed. The rocket-engine designer must do everything he can to prevent either.

Rocket Engine Materials

Liquid propellant rocket engines utilize a wide range of materials; from steel alloys to thermoplastics and composites. This appendix presents a brief discussion of a range of material types and their general application in the design of liquid propellant rocket engines.

Plain-Carbon/Low-Alloy Steels

Plain-carbon steels alloy iron and carbon. The low-carbon grades (0.1-0.2%) have excellent ductility and toughness and are easily formed. The medium-carbon grades (0.3-0.5%) respond well to heat treatment, and thus provide a good combination of strength and toughness. The high-carbon grades (1.0-1.2%) are hard and wear-resistant, but have poor toughness and ductility.

Low-alloy steels contain up to 2.0% alloying element in addition to the iron and carbon. Adding alloying elements to steel increases hardenability (i.e., ability to harden through thick sections). Other improvements derived from alloy addition include improved elevated-temperature properties, tough-ness, and corrosion resistance.

Plain-carbon and low-alloy steels are *not* good candidates for rocket-engine hardware. Although inexpensive, readily available, easy to fabricate, and typically high in strength, steels poorly resist atmospheric corrosion and will rust in ambient environments unless protected. Also, they have a limited range of useful operating temperatures. Most steels become brittle below 0°F and, on the high-temperature side, are limited by tempering temperature, which is usually below 1000°F. Plain-carbon and alloy steels are susceptible to hydrogen-environment embrittlement, and are not resistant to stress-corrosion cracking in some heat-treat conditions.

Stainless Steels

In stainless steels—iron-carbon alloys with the addition of at least 12% chromium—the chromium provides a "passive" oxide film that protects the body from most corrosive environments. This film must be maintained to ensure corrosion protection. Oxygen shielding could cause deterioration of this passive film, rendering the steel "active"—having corrosion resistance and galvanic activity similar to those of low-alloy steels. There are four distinct classes of stainless steels—martensitic, austenitic, ferritic, and precipitation hardening.

Martensitic stainless steels (400 series except 405, 430, 446). Martensitic stainless steels resemble low-alloy steels except they have sufficient chromium to become passive. They can be heat-treated to high strengths, but have the poorest atmospheric corrosion resistance of the stainless steels. They are susceptible to stress-corrosion cracking and hydrogen embrittlement and become quite brittle at cryogenic temperatures. With the exception of 440C, martensitic stainless steels have limited usefulness on liquid propellant rocket engines. Being a high-carbon alloy, 440C attains the highest hardness of the stainless steels. It is widely used for bearings and other compressively loaded hardware requiring wear resistance.

Austenitic stainless steels (300 series). The austenitic stainless steels all contain nickel in addition to the chromium. Nickel stabilizes austenite, normally a high-temperature phase, at room temperature and below. Austenite differs from martensite in many respects. The nonmagnetic austenitic stainless steels are not heat-treatable, and cannot achieve the high strength of martensitic alloys. However, they possess good cryogenic toughness, good fabricability and weldability, excellent corrosion resistance and resistance to stress-corrosion cracking, and are compatible with oxygen and hydrogen. Relatively low cost, high availability, and good fabricability make austenitic stainless steels an excellent choice for rocket-engine components where strength-to-weight ratio is not a primary consideration.

Most austenitic stainless steels will be limited in usefulness by their low (30-ksi) room-temperature yield strength. Alloy 21-6-9, a nitrogen-strengthened modification, has about twice the yield strength at room temperature and three times the yield strength at -400°F of 300-series stainless steel. It does not require heat treatment and possesses all of the other attributes of austenitic stainless steels.

The corrosion resistance of all stainless steels can be severely diminished by denying access to a plentiful supply of oxygen. For this reason, any application which results in close faying surfaces or crevices should be avoided. Multiply assemblies, such as bellows, are therefore not ideal applications for stainless steels.

Moreover, a carbide precipitation characterizes many austenitic stainless steels when heated in the temperature range of 800-1600°F. This "sensitization" reduces corrosion resistance. Not only is this a limitation of application temperature, but also of processes which involve heating above 800°F. The problems of sensitization can be mitigated by utilizing low-arbon grades (304L, 316L) or stabilized grades (321, 347) of austenitic stainless steels.

Ferritic stainless steel (405, 430, 446). Ferritic stainless steels see use in rocket engines for magnetic effects, as in solenoids. These steels have good corrosion resistance, are resistant to stress-corrosion cracking, and are compatible with liquid fuels. They are low in strength, but have good ductility.

Precipitation-hardening (PH) stainless steels (17-4PH, 17-7PH, PH15-7MO, A286, etc.). The

precipitation-hardening stainless steels combine good corrosion resistance with high strength at temperatures up to 1100-1300°F. However, most of the PH stainless steels are martensitic, and as such are susceptible to stress-corrosion cracking, hydrogen-environment embrittlement, and loss of toughness at cryogenic temperatures. An exception, A286, austenitic steel, possesses all of the attributes of the austenitic stainless steels coupled with high strength (up to 200-ksi ultimate tensile strength in the cold-worked condition). A286 has proven to be exceptionally suitable for fasteners, and has been used for nozzle tubing. Poor weldability limits wider application of A286. JBK 75, a modification of A286, is not susceptible to weld cracking and therefore has applicability for rocket-engine hardware.

Iron-Base Superalloys

The iron-base low-expansion superalloys have extensive application in liquid-propellant rocket engines because they provide high strength, low coefficient of thermal expansion, and resistance to hydrogen-environment embrittlement (HEE). These iron-nickel-cobalt alloys retain excellent properties from -423 to 1200°F, are resistant to stress-corrosion cracking, and are readily weldable. However, lack of resistance to corrosion limits the use of them.

Incoloy 903 was the first of these alloys to find widespread application to structural components operating in gaseous hydrogen or hydrogen-rich steam. It also can be used as an overlay to provide HEE protection to welds of non-HEE-resistant alloys. Incoloy 903 can be thermomechanically processed (TMP) for improved high-temperature stress-rupture properties.

Incoloy 907 offers better stress-rupture properties without requiring the TMP procedure. Incoloy 909 offers better low-cycle fatigue life and a simplified heat-treat cycle, which is compatible with that for Inconel 718. The weldability of Incoloy 907 has been rated higher than that of Incoloy 903, and Incoloy 909 has been shown to be the most weldable of the group.

Aluminum Alloys

Aluminum alloys are low in cost, easily fabricated, and readily available, but are limited in rocket-engine usage by maximum operating temperature. The high-strength wrought alloys (i.e., 2024, 7075) are limited to 200-300°F while the cast alloys such as Tens-50 and 356 can be used in the 300-400°F range. The development of aluminum-base-metal matrix composites has extended the operational limits of wrought aluminum alloys to the 800-900°F range. However, limited availability, high cost, and difficulties in fabrication have been deterrents to the use of these composites in rocket engines. All of the aluminum alloys are light in weight, resistant to hydrogen embrittlement, and (most) have excellent cryogenic properties. Caution should be exercised with aluminum applications in oxygen systems because of low ignition temperature.

The casting alloys, low-strength wrought alloys, and moderate-strength 6061 are weldable. Corrosion resistance varies from excellent to fair; but in general the higher-strength alloys must be anodized for atmospheric- and galvanic-corrosion protection. Anodizing forms an electrically insulating layer that could preclude electrical grounding.

Copper Alloys

Copper of course has high electrical and thermal conductivity, excellent corrosion resistance, and ease of fabrication, plus immunity to hydrogen-environment embrittlement. Alloying elements improve its strength, but generally at the expense of electrical and thermal conductivity. For example, 2% beryllium can increase ultimate tensile strength of copper from 30 to 200 ksi; but the electrical conductivity of beryllium copper is only 20% of pure copper.

The more widely used copper alloys—brass (copper and zinc), phosphor bronze (copper and tin), and beryllium copper (copper and beryllium)—have strength increasing in the order listed.

The major application of copper alloys in rocket engines is for high-heat-flux applications, such as combustion chambers. Their high thermal conductivities minimize thermal gradients and resulting thermal stresses. Narloy A is a copper-silver alloy with thermal conductivity equivalent to pure copper, but with moderately high strength to 800°F. Narloy-Z, with a zirconium addition, improves ductility and fatigue life, and extends the operating range to 1000°F. These alloys are available in the cast as well as wrought form. Copper alloys also serve as electrical conductors, conductive springs, and bearings and bushings.

Nickel-Base Alloys

Nickel-base alloys comprise some 65% of the weight of the Space Shuttle Main Engine. These alloys derive their widespread usage in rocket engines from superior corrosion resistance, high-temperature oxidation resistance, retention of useful properties over a wide temperature range, and, in many cases, very unique physical properties. The nickel-base alloys can be divided into three groups, based on application.

The first group—nickel-base alloys used mainly for superior corrosion resistance—include Nickel 200, the monel alloys, Inconel 600, Inconel 625, and electro-deposited (ED) nickel. Inherently corrosion-resistant, nickel does not depend upon a metastable passive film for protection; and, being strongly electronegative, it is not susceptible to galvanic corrosion when in contact with most other metals. Monels, alloys of nickel and copper, besides having good corrosion resistance, have useful magnetic properties at cryogenic temperature and high resistance to ignition in oxygen. The Inconel alloys, composed of nickel-chromium-iron, resist oxidation at temperatures up to 1800°F.

The second group, the nickel-base superalloys, retain high strength at elevated temperatures. Alloy 718, the workhorse of this group, has high strength up to 1300°F, good cryogenic ductility, and good weldability. Fine-grained material should be specified for

parts to be electron-beam-welded. Higher-temperature applications exploit Rene' 41, Waspaloy, and MAR-M-246.

The third group, the special-application alloys, includes Nichrome (for electrical-resistance heating elements), chromel and alumel (for thermocouples), and Incoloys and Invar (for low-thermal-expansion applications).

All of the nickel-base alloys resist corrosion and stress corrosion and are oxygen-compatible, but are susceptible to hydrogen-environment embrittlement (HEE) at temperatures above -200°F. HEE in nickel-base alloys can be prevented by avoiding plastic strains or, this being impractical, by providing a protective barrier, such as electroplating with copper or gold or overlaying by weld deposition with a nonsusceptible alloy.

Cobalt Alloys

Cobalt-base alloys, like nickel alloys, offer excellent high-temperature strength and oxidation resistance. Unlike the nickel alloys, cobalt alloys are immune to HEE.

Alloy 188, a corrosion- and heat-resistant alloy, exhibits outstanding oxidation and creep resistance up to 2100°F. Although not hardenable by heat treatment, 188 has moderate room-temperature strength and good cryogenic properties. It also has good resistance to corrosion and stress-corrosion cracking and can be readily welded, including by electron-beam welding.

Elgiloy, a cobalt-base alloy, has found widespread usage for springs. The alloy has high strength and good corrosion resistance, and is nonmagnetic. Elgiloy derives its strength from a combination of heat treatment and cold work. It has a maximum use temperature of approximately 700°F.

Titanium Alloys

Titanium alloys possess high strength-to-weight ratios and good toughness, as well as excellent corrosion resistance and resistance to stress corrosion cracking. However, titanium alloys are susceptible to hydrogen embrittlement at temperatures above -110°F, and are not compatible with gaseous or liquid oxygen or with red fuming nitric acid, at any temperature. Titanium alloys also are incompatible with the products of combustion from many propellants; these factors limit their usefulness in liquid-propellant rocket engine systems. They can be applied, however, in fuel systems involving propellants such as liquid hydrogen, monomethyl hydrazine (MMH), and kerosene (RP-1). They also are compatible, under certain circumstances, with nitrogen tetroxide (NTO). Titanium alloys have found use in liquid-propellant rocket engine systems for pump impellers and inducers, valve bodies, pump housings, high-pressure fuel ducts, hydraulic tubing, pressure bottles, struts, gimbal blocks, propellant-storage bottles, and nozzles.

The most demanding applications have been for use at cryogenic temperatures, where titanium alloys offer some of the highest strength-to-weight ratios of presently available engineering materials. Two titanium alloys are most commonly used at cryogenic temperatures: Ti-5Al-2.5Sn ELI and Ti-6Al-4V ELI. In the ELI (extra-low interstitial) grade of these alloys, good cryogenic toughness is achieved by controlling the interstitial elements oxygen, nitrogen, carbon, and hydrogen, and the substitutional element iron, to much lower than normal levels. Typically, Ti-6Al-4V ELI is used to -320°F while the higher-toughness Ti-5Al-2.5Sn ELI is used as low as -423°F. However, Ti-6Al-4V ELI can be employed at -423°F if the component design compensates for its lower ductility and toughness.

Titanium and titanium alloys are classified into three major categories according to the predominant phases present in their microstructure: alpha, alpha-beta, and beta alloys. Although non-heat-treatable, alpha alloys offer high toughness, are more oxidation-resistant than alpha-beta or beta alloys, are usable up to about 1000°F, and are relatively difficult to form. Ti-5Al-2.5Sn is an example of an alpha alloy. Alpha-beta alloys, such as Ti-6Al-4V, are heat-treatable to higher-strength levels, are usable to 800°F and in some instances to 1000°F, and are somewhat more formable than alpha alloys. However, alpha-beta alloys ordinarily would not be used in the fully-heat-treated condition because its heat-treat response is limited to relatively thin sections (~1.0 in.) and its fracture toughness decreases significantly with increasing strength level. Beta alloys are generally quite formable at room temperature, are usable up to approximately 600°F, and are heat-treatable to relatively high strength (e.g., ~190 ksi) in thick sections while still retaining good toughness. The disadvantages of beta alloys are a higher density, lower oxidation resistance and lower toughness at cryogenic temperatures. Examples of beta alloys include Ti-10V-2Fe-3Al, Ti-3Al-8V-6Cr-4Mo-4Zr, and Ti-15V-3Al-3Cr-3Sn.

Most titanium alloys can be welded, although welding requires the hardware to be thoroughly clean and the operation to be performed in a high-purity inert gas (Ar, He) or vacuum. Titanium and titanium alloys are available as sheet, strip, plate, bar, forgings, extrusions, tubing, and castings.

Thermoplastic Materials

Thermoplastics, polymeric materials that can be formed or reformed by melting or softening with heat, serve well as electrical insulation and seals. They include fluorocarbons, nylon, polycarbonate, and amide-imide materials. Of these, the fluorocarbon polymers find the greatest number of applications in liquid-propellant rocket engine design. Polytetrafluoroethylene (PTFE), fluorinated ethylene propylene (FEP), and polychlorotrifluoroethylene (Kef-F) with or without fillers or reinforcing fibers find extensive use in rocket engines for seals and coatings for seals due to the compatibility of these materials with oxygen and their properties in both liquid oxygen and liquid hydrogen.

Elastomers

Elastomers—a multitude of polymers that have high elongation within the elastic range—include all of the

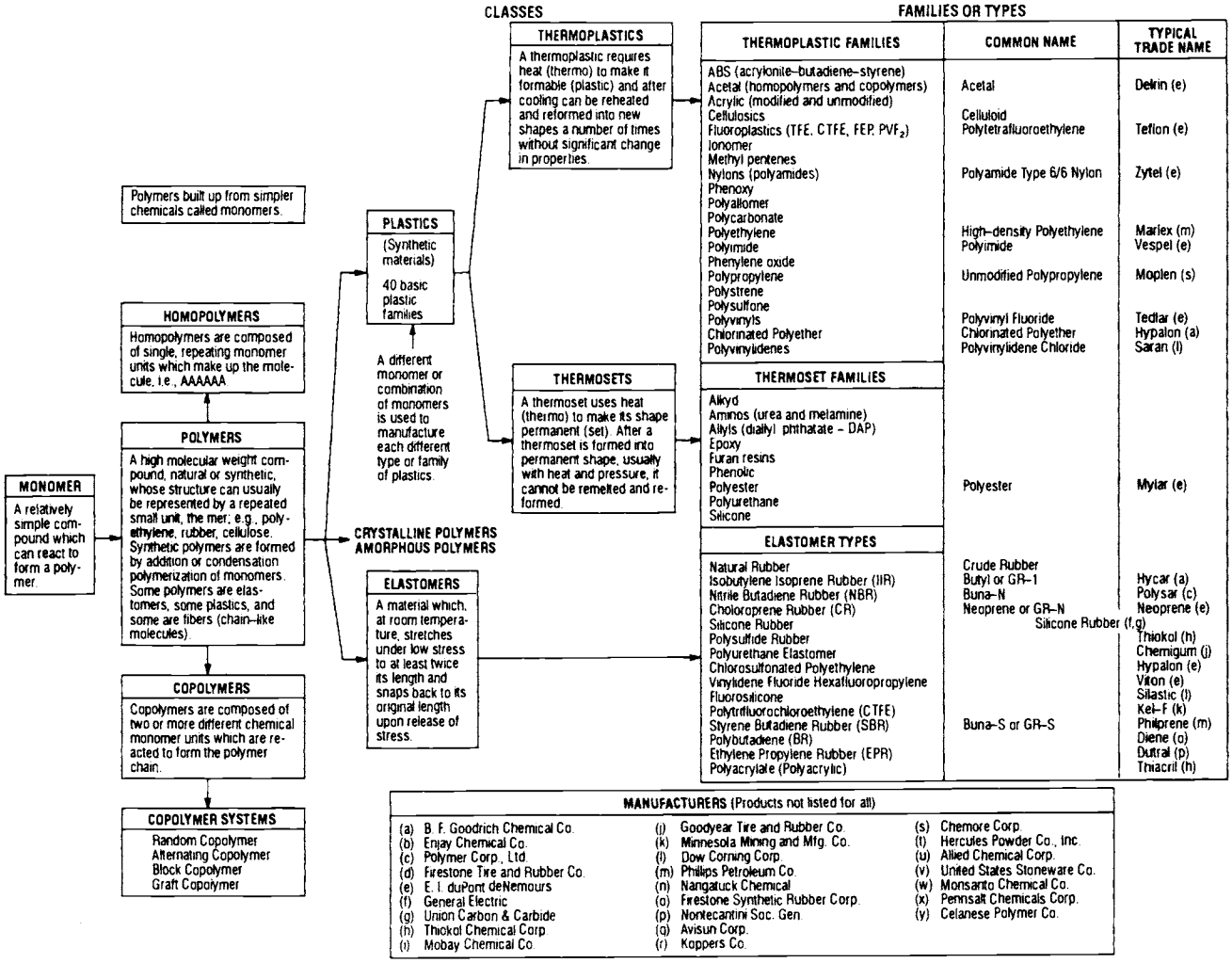

Fig. C-1 Polymeric materials—terminologies and relationships.

rubber materials noted in Fig. C-1 that find extensive use in O-ring seals, gasket-type seals, electrical insulation, vibration dampers, etc. These materials are also used for adhesives, sealants, formed-in-place seals, and potting of electrical components.

Nitrile rubbers find considerable use because resistant to oxidation and hydraulic fluids. They do not take a permanent set for long periods of time. Consequently, these rubbers find much use in O-ring seals of hydraulic and pneumatic components.

Silicone rubber, an extensively used sealant and potting compound, has been exploited primarily due to its ease of application and wide usable-temperature range of -165-500°F. Fluorocarbon rubber is used when the application requires compatibility with oxygen or when the use temperature is in the range of 300-375°F.

Special designs may call for other elastomers, with unique properties. For example, resin-cured butyl has been found to provide excellent seals in NTO and/or hydrazine for short periods (i.e., under one hour).

Carbons and Ceramics

Pressed-carbon materials and various ceramics find use in throat inserts for ablative engines, dynamic seals of gas-turbine drives of turbopumps, and coatings to protect metals from high-temperature gases.

Composites

A composite has a matrix materal reinforced in random or oriented form with a special fiber, tape, fabric, etc. Examples would be glass-fiber-filled polytetrafluoroethylene (PTFE), tape-wrapped ablative plastics, fabric-reinforced epoxy sheets, filament-wound thrust-chamber shells, etc. Composites find a wide range of uses in liquid-propellant rocket engine design, such as in seals, thrust-chamber structure, electrical printed wiring-boards, and ball-bearing separators. The matrix may be carbon, metallic, polymeric, or ceramic. Three types of composites might be distringuished: structural plastics, ablatives, and carbon-carbon composites.

Structural plastics. Choice of thermosetting resin such as an epoxy, phenolic, or polyimide for fabricating a laminate will depend upon the thermal and adhesive properties required. Epoxy resins offer high adhesive strength, but are more severely limited in maximum use-temperatures. Other resins such as the phenolics or polyimides have very good high-temperature characteristics, but at the expense of lowered adhesion and greater fabrication difficulties.

Reinforcements used in the laminated structure may take the form of layers of fabric, random placement of short fibers, or very precise placement of continuous filaments through the use of filament winding or lay-up of collimated tapes. The exact type and form of reinforcement will depend upon the mechanical properties that are to be derived from it. For example, a cover requiring low mechanical strength and rigidity might be made of random fibers of glass sprayed onto a form with the resin added simultaneously, while a structural shell for a small thrust chamber might well be produced by filament-winding a resin-preimpregnated graphite so as to produce a structure with high strength and rigidity.

Ablatives. Rocket ablatives—materials that can "sacrificially" cool a thrust chamber or nozzle—usually are fabric-reinforced phenolic or rubber-modified-phenolic laminated materials. The reinforcing fabric is placed in the formed structure at some predetermined angle to the expected flow of the hot gas. The matrix material and the reinforcing material are each selected for performance with the propellants to be used and the duty cycle of the thrust chamber or nozzle.

The phenolic or rubber-modified-phenolic resins have found the greatest use. They offer a high-temperature-resistant matrix with predictable properties when exposed to the hot gas of the rocket engine. They form a structural char and provide a cooling gas at the hot surface as they pyrolize. The use of rubber modification yields a somewhat lower ablation rate, but keeps the structure from delaminating.

Reinforcements for ablative components will usually be selected on the basis of the oxidizer. Oxygen-based oxidizers demand the use of a fiber reinforcement that will not oxidize and that has a high melting point plus high viscosity when melted, such as silica glass and quartz, which tend to protect the char from oxidizing rapidly even though there is a high percentage of water vapor in the combustion gases of the thrust chamber. A fluorine-based oxidizer develops the combustion products that rapidly attack quartz and other glass, forming fibrous materials. This propellant demands reinforcements of carbon or graphite.

Carbon-carbon composites. Carbon-carbon composites—materials with some type of amorphous-carbon matrix reinforced by fibrous carbon or graphite—find use as thermal shields and nozzle extensions. In all of the uses associated with liquid-propellant rocket engine design, these composites have been coated with some form of silicon carbide (with or without glass formers) to prevent oxidation.

Adhesives

Polymeric and ceramic materials are also used in adhesive applications on rocket engines. In general, silicones are used for sealants and bonding applications requiring good peel-strength at temperatures in the range of -165 - 500°F; epoxies for high bond shear-strength from -65°F to as high as 350°F; epoxy-phenolics for good bond shear-strength from liquid-helium temperature to 500°F; and polyurethanes when bonding must be done with contact pressure without elevated-temperature cure and the material must exhibit good peel and shear strength at a cryogenic temperature. Pressure-sensitive-adhesives having a natural rubber base find use on tapes where the adhesive must be completely removed with the tape.

Lubricants

Although some hydrocarbon lubricants used for rocket engines typify those for automotive purposes (i.e., gear cases), most will have to be selected on the basis of propellant compatibility. As a result, few greases or oils are used. If needed, a grease will usually be based on a fluorocarbon oil. Because most oils and greases become brittle at cryogenic temperatures, dry-film lubrication is most often used, the lubricant usually being pure molybdenum disulfide powder sprayed onto the component surfaces with some binding agent (usually a resin if a fuel environment or a phosphate material if oxidizer).

Platings, Surface Finishes, Coatings

Components are sometimes given a surface finish to assure corrosion resistance. It can be applied either by electroplating or by an electrolysis process, a chemical film, or a paint. Coatings are also used to give a soft chemical-resistant sealing surface to pressure-assisted seals.

Chromium and nickel are examples of plating materials commonly used. An anodized surface is an example of a chemical-conversion coating. Zinc or strontium chromate-containing paints are commonly used to protect a variety of metals against corrosion.

Many alloys protect against corrosion with an oxide film. To assure the formation of this film, the component will often be given a chemical treatment ("passivated") to assure formation of the protective oxide.

List of Illustrations

List of Illustrations (Continued)

List of Illustrations (Continued)

List of Illustrations (Continued)

List of Illustrations (Continued)

List of Illustrations (Continued)

List of Illustrations (Continued)

List of Illustrations (Continued)

List of Illustrations (Continued)

List of Tables

List of Tables (Continued)

List of Acronyms

A-D	analog to digital
ACS	attitude control system
ASI	augmented spark igniter
ASIC	application specific integrated circuits
BIT	built-in test
CAE	computer-aided engineering
CASE	computer-aided software engineering
CCM	control and condition monitoring
CFD	computational fluid dynamics
CIE	computer interface electronics
CP&T	coarse pointing and tracking
CSMA/CD	carrier sense multiple access with collision detection
CYL	cylinder
D-A	digital to analog
DCU	digital computer unit
DETA	Diethylene Triamine
DMA	direct memory access
ED	electro-deposited
EDS	emergency detection system
EFSS	engine failure sensing and shutoff systems
ELI	extra low interstitial
EMC	electromagnetic compatibility
EMF	electromotive force
EMI	electromagnetic interference
EO	engine out
ESEOD	equivalent sharp-edged orifice diameter
FEP	fluorinated ethylene propylene
FMEA	failure mode and effects analysis
FP&T	fine pointing and tracking
GFE	government-furnished equipment
GLOW	vehicle gross liftoff weight
GNC	station guidance, navigation, and control
GOX	gaseous oxygen
HAS	hydraulic actuation system
HEE	hydrogen environment embrittlement
HOL	high-order language
HPFTP	high pressure fuel turbopump
HPOTP	high pressure oxygen turbopump
I/O	input/output
IAE	integral of the absolute magnitude of error
IC	integrated circuit
ICD	interface control document
ID	inside diameter
IE	input electronics
IEEE	The Institute of Electrical and Electronic Engineers, Inc.
ISE	integral square error
It	inertia
ITAE	integral time—absolute error
$ITSE^2$	integral time—square error
IV&V	independent validation and verification
JANNAF	Joint Army, Navy, NASA, and Air Force
Kel-F	polychlorotrifluoroethylene
KKV	kinetic kill vehicle
LAN	local area network
LEM	lunar excursion module
LN	local area network
LOX	liquid oxygen
LPOTP	low pressure oxygen turbopump
LVDT	linear variable differential transformer
MCT	major cycle time
MIMO	multi-input multi-output
MIPS	mega instructions per second
MMH	monomethyl hydrazine
Mp	peak overshoot
MSLD	mass spectrometer leak detector
NC	normally closed
NDT	nondestructive testing

NO	normally open
NPSH	net positive suction head
NTO	nitrogen tetroxide
OD	outside diameter
OE	output electronics
OME	orbit maneuvering engine
OMS	orbital maneuvering system
OTVE	orbital transfer vehicle engine
P&T	pointing and tracking
PDL	program design language
PFRT	preliminary flight rating tests
PI	proportional integral
PID	proportional-integral-differential
PL	power level
PRC	pulse rate converter
PTFE	polytetrafluoroethylene
PU	propellant utilization
PVC	pressure volume compensator
PWB	printed wiring board
RCS	reaction control system
REF DES	reference designations
RFI	radio frequency interference
RISC	reduced instruction set computer
RM	redundancy management
rms	root mean squared
rss	root sum squared
RTD	resistance temperature detector
RVDT	rotary variable differential transformer
S-N	alternating stress vs number of cycles
SISO	single input-single output
SC	solar dynamic
SCC	stress corrosion cracking
SCFM	standard cubic feet per minute
SD	solar dynamic
SISO	single input-single output
SSME	Space Shuttle Main Engine
SSME-HAS	Space Shuttle Main Engine Hydraulic Actuation System
SSMEC	Space Shuttle Main Engine Controller
SSTO	single stage to orbit
TC	thermocouple
TC	thrust compensating
td	delay time
TMP	thermomechanically processed
tp	peak time
tr	rise time
ts	settling time
UDMH	Unsymmetrical Dimethyl Hydrazine
VCO	voltage-controlled oscillator
VIE	vehicle interface electronics
WDT	watchdog timer

Index